SUSTAINABLE METHODS IN C–H FUNCTIONALIZATIONS

Dissertation

for the award of the degree

“Doctor rerum naturalium”

of the Georg-August-University Göttingen

within the doctoral program of chemistry

of the Georg-August University School of Science (GAUSS)

Submitted by

Julia Rebecca Struwe

from Zürich

Göttingen, 2023

Thesis Committee

Prof. Dr. Lutz Ackermann

Institute of Organic and Biomolecular Chemistry, Georg-August University Göttingen

Prof. Dr. Konrad Koszinowski

Institute of Organic and Biomolecular Chemistry, Georg-August University Göttingen

Prof. Dr. Shoubhik Das

Department of Chemistry, University of Antwerp

Members of Examination Board

Reviewer: Prof. Dr. Lutz Ackermann

Institute of Organic and Biomolecular Chemistry, Georg-August University Göttingen

Second Reviewer: Prof. Dr. Konrad Koszinowski

Institute of Organic and Biomolecular Chemistry, Georg-August University Göttingen

Further Members of the Examination Board

Prof. Dr. Dr. h.c. Lutz F. Tietze

Institute of Organic and Biomolecular Chemistry, Georg-August University Göttingen

Jun.-Prof. Dr. Johannes Walker

Institute of Organic and Biomolecular Chemistry, Georg-August University Göttingen

PD Dr. Michael John

Institute of Organic and Biomolecular Chemistry, Georg-August University Göttingen

Dr. Holm Frauendorf

Institute of Organic and Biomolecular Chemistry, Georg-August University Göttingen

Date of the Oral Examination: 19.04.2023

LIST OF ABBREVIATIONS

A	Ampere
Ac	Acetyl
acac	Acetylacetonato
Ad	Adamantyl
AMLA	Ambiphilic Metal Ligand Activation
aq.	Aqueous
BHT	Butylated hydroxytoluene (3,5-di-*tert*-4-butylhydroxytoluene)
BIES	Base-assisted Internal Electrophilic Substitution
Bn	Benzyl
Boc	*tert*-Butyloxycarbonyl
Bpy	2,2-Bipyridine
BQ	Benzoquinone
Bu	Butyl
Bz	Benzoyl
calcd	Calculated
cat.	Catalytic
CCE	Constant Current Electrolysis
CFL	Compact Fluorescent Lamp
CMD	Concerted Metalation Deprotonation
Cp*	Pentamethylcyclopentadienyl
CPE	Constant Potential Electrolysis
CV	Cyclic Voltammetry
Cy	Cyclohexyl
d	Doublet
DCA	9,10-Dicyanoanthrachene
DCE	Dichloroethane
DCN	1,4-Dicyanonaphthalene
DDQ	2,3-Dichloro-5,6-dicyano-1,4-benzoquinone
DFT	Density Functional Theory
DG	Directing Group

DMA	*N*,*N*-Dimethylacetamide
DMF	Dimethylformamide
DMG	*N*,*N*-Dimethylglycine
DMSO	Dimethyl sulfoxide
EI	Electron Ionization
equiv	Equivalents
ESI	Electrospray Ionization
Et	Ethyl
EWG	Electron-withdrawing group
Fc	Ferrocene
GC	Gas Chromatography
GC-MS	Gas Chromatography Mass Spectroscopy
GF	Graphite Felt
GPC	Gel Permeation Chromatography
h	Hour
Hept	Heptyl
Het	Heteroatom
Hex	Hexyl
HFIP	1,1,1,3,3,3-Hexafluoroisopropanol
HMBC	Heteronuclear Multiple Bond Correlation
HR-MS	High Resolution Mass Spectrometry
HSQC	Heteronuclear Single Quantum Coherence
Hz	Hertz
i	*iso*
IR	Infrared
ISC	Intersystem Crossing
ISET	Inner-Sphere Electron Transfer
J	Coupling Constant
KIE	Kinetic Isotope Effect
L	Ligand
LED	Light-Emitting Diode
LG	Leaving Group

µ	Micro
m	*meta*
M	Metal
M	Molar
m.p.	Melting Point
max	Maximum
MBH	Morita-Baylis-Hillman
Me	Methyl
Mes	Mesityl
Mes-Acr	9-Mesityl-10-methylacridinium
min	Minute
MS	Mass Spectrometry
m/z	Mass-to-charge ratio
n	*normal*
NMP	*N*-Methyl-2-pyrrolidone
NMR	Nuclear Magnetic Resonance
NOESY	Nuclear Overhauser Enhancement Spectroscopy
nr	No Reaction
o	*ortho*
ox	Oxidation
p	*para*
PEG	Polyethylene Glycole
PC	Photocatalyst
Ph	Phenyl
Piv	Pivaloyl
PMP	4-Methoxyphenyl
ppm	Parts Per Million
ppy	2-Phenylpyridine
dtbbpy	4,4’-Di-*tert*.-butyl-2,2’-dipyridyl
Pr	Propyl
PTS	Polyoxyethanyl-α-tocopheryl sebacate

Py	Pyridine
Pym	Pyrimidine
q	Quartet
R	Rest
red	Reduction
RT	Room (Ambient) Temperature
RVC	Reticulated Vitreous Carbon
s	Singlet or second
sat.	saturated
SCE	Saturated Calomel Electrode
SDS	Sodium dodecylsulfate
SET	Single Electron Transfer
SPGS	β-Sitosteryl polyoxoethanyl succinate
t	Triplet
TAC	Trisaminocyclopropenium
t-Amyl	2-Methylbut-2-yl
TBA	Tetra-*n*-butyl Ammonium
TEMPO	(2,2,6,6-Tetramethylpiperidin-1-yl)oxyl
tert, *t*	*tertiary*
Tf	Triflate
TFA	Trifluoroacetic Acid
THF	Tetrahydrofuran
TLC	Thin-Layer Chromatography
TM	Transition Metal
TMP	3,4,5-Trimethoxyphenyl
TMS	Trimethylsilyl
TPGS	D-α-Tocopheryl polyethylene glycol 1000 succinate
Trp	tryptophan
Ts	Tosyl
V	Volt
vs.	*versus*
X	(Pseudo)halide

TABLE OF CONTENTS

1 INTRODUCTION 1

1.1 Green Chemistry 1

1.2 Transition Metal-Catalyzed C–H Activation 5

1.3 Ruthenium-Catalyzed C–H Activation Reactions 12

1.3.1 Ruthenium-Catalyzed Alkylations with *ortho*- and *meta*-Selectivity 12

1.3.2 Ruthenium-Catalyzed Arylations 20

1.3.3 Ruthenium-Catalyzed Benzylations 28

1.4 C–H Activation Reactions with other Metals 30

1.4.1 Rhodium-Catalyzed C–H Activation of Carboxylic Acids and Amides 30

1.4.2 Manganese-Catalyzed C–H Activation 34

1.5 Undirected C–H Functionalization 38

1.5.1 Trifluoromethylation Reactions 39

1.6 Sustainable Strategies in C–H Activation 44

1.6.1 Electrochemical C–H Activation 44

1.6.2 Photo-Induced Transition Metal-Catalyzed C–H Functionalization 50

1.6.3 Electrophotocatalytic C–H Functionalization 56

2 OBJECTIVES 61

3 RESULTS AND DISCUSSION 65

3.1 Rhodium-Catalyzed Electrooxidative C–H Olefination of Benzamides 65

3.1.1 Optimization for Olefination with Acrylates 66

3.1.2 Optimization for Olefination with Styrenes 70

3.1.3 Mechanistic Studies 71

3.1.4 Proposed Catalytic Cycle 72

3.2 Ruthenium-Catalyzed Regiodivergent C–H Alkylation Of Pyrazoles 74

3.2.1 Optimization Studies 75

3.2.2 Substrate Scope 76

3.2.3 Mechanistic Studies 80

3.2.4 Proposed Catalytic Cycle 83

3.3 Photo-Induced Ruthenium-Catalyzed C–H Arylations at Ambient Temperature 86

3.3.1 Optimization Studies 87

3.3.2 Substrate Scope 88

3.3.3 Comparison to Thermal Reaction Conditions 94

3.3.4 Mechanistic Studies 96

3.3.5 Proposed Catalytic Cycle 100

3.4 Photo-Induced Ruthenium-Catalyzed C–H Benzylations and Allylations at Ambient Temperature 103

3.4.1 Optimization Studies 103

3.4.2 Substrate Scope 109

3.4.3 Mechanistic Studies 116

3.4.4 Proposed Catalytic Cycle 119

3.5 Electrophotochemical Undirected Trifluoromethylation of (Hetero-)Arenes 122

3.5.1 Comparison of Photoelectrocatalysts 124

3.5.2 Substrate Scope 126

3.5.3 Kinetic Studies and Mechanistic Experiments 129

3.5.4 Trifluoromethylation of KAN0438757 133

3.5.5 Proposed Catalytic Cycle 139

3.6 Manganese(I)-Catalyzed Tryptophan Functionalization in Water 142

3.6.1 Optimization Studies with Allyl Carbonate 143

3.6.2 Optimization Studies with MBH Substrate 149

3.6.3 Substrate Scope 155

3.6.4 Kinetic Studies 156

4 CONCLUSION AND OUTLOOK 159

5 EXPERIMENTAL SECTION 163

5.1 General Remarks 163

5.1.1 Solvents and Chemicals 163

5.1.2 Experimental and Analytical Methods 165

5.2 General Procedures 168

5.2.1 General Procedure A: Electrochemical Rhodium-Catalyzed Alkenylation of Benzamides with Acrylate 168

5.2.2 General Procedure B: Electrochemical Rhodium-Catalyzed Alkenylation of Benzamides with Styrene 169

5.2.3 General Procedure C: Regiodivergent Ruthenium-Catalyzed C–H Alkylation of Pyrazoles 169

5.2.4 General Procedure D: Photo-Induced Ruthenium-Catalyzed *ortho*-C–H Arylation 169

5.2.5 General Procedure E: Ruthenium-Catalyzed *ortho*-C–H Arylation under Thermal Conditions 170

5.2.6 General Procedure F: Light-Induced Ruthenium-Catalyzed *ortho*-C–H Benzylation 170

5.2.7 General Procedure G: Electrophotochemical C–H Trifluoromethylation of (Hetero-)Arenes 170

5.2.8 General Procedure H: Manganese-Catalyzed Allylation of Tryptophan 171

5.3 Rhodium-Catalyzed Electrooxidative C–H Olefination of Benzamides 172

5.3.1 Characterization Data 172

5.3.2 Cyclic Voltammetry 174

5.4 Ruthenium-Catalyzed Regiodivergent Alkylations of Pyrazoles 175

5.4.1 Characterization Data 175

5.4.2 C–H Alkylation in the Presence of Typical Radical Scavengers 183

5.4.3 Detection of Free *para*-Cymene 185

5.4.4 Synthesis of Cyclometalated Ruthenium Complex **233** 187

5.4.5 C–H Alkylation by Ruthenacycle **233** in Stoichiometric Amounts 188

5.4.6 C–H Alkylation by Ruthenacycle **233** as Catalyst 189

5.5 Photo-Induced Ruthenium-Catalyzed C–H Arylations at Ambient Temperature 190

5.5.1 Characterization Data 190

5.5.2 Comparision to Thermal Reaction Conditions 209

5.5.3 H/D Scrambling Experiments 212

5.5.4 Competition Experiments 214

5.5.5 C–H Arylation in the Presence of Typical Radical Scavengers 219

5.5.6 On-Off Experiment 220

5.5.7 Detection of Free *para*-Cymene in Photo-Induced Arylation 221

5.5.8 Determination of Quantum Yield 223

5.6 Photo-Induced Ruthenium-Catalyzed C–H Benzylations and Allylations at Ambient Temperature 224

5.6.1 Characterization Data 224

5.6.2 Late-Stage Diversification by Ozonolysis 243

5.6.3 H/D Scrambling Experiments 244

5.6.4 Competition Experiments 246

5.6.5 Photo-Induced C–H Benzylation by Ruthenacycle **276** in Stoichiometric Amounts 250

5.6.6 Photo-Induced C–H Benzylation by Ruthenacycle **276** as Catalyst 251

5.6.7 Photo-Induced Benzylation in Presence of TEMPO 252

5.6.8 On-Off Experiment in Benzylation Reaction 253

5.7 Electrophotochemical undirected Trifluoromethylation of (Hetero-)Arenes 254

5.7.1 Characterization Data 254

5.7.2 Kinetic Studies of Caffeine (**137k**) *In Situ* Flow NMR 265

5.8 Manganese(I)-Catalyzed Tryptophan Functionalization in Water 266

5.8.1 Characterization Data 266

5.8.2 Kinetic Studies: Temperature 271

5.8.3 Kinetic Studies: Catalyst Loading 272

6 REFERENCES 273

7 APPENDIX 289

Zusammenfassung/Summary 291

Acknowledgements 293

NMR Spectra **295**

1 INTRODUCTION

1.1 GREEN CHEMISTRY

Since the beginnings in organic synthesis and the pioneering finding by Wöhler with the synthesis of urea in 1828,[1] which is nowadays considered as the inception of the organic chemistry, this discipline has evolved dramatically during the past two hundred years.[2] The chemical synthesis of a plethora of organic compounds with complex molecule architectures has been and continues to be of great importance for the modern society.[2] The development of countless small molecule drugs and their synthesis in large preparation scale has revolutionized medicinal treatments, thereby allowing for a strong increase of life expectancies.[3] The organic synthesis has affected our society not only in terms of pharmaceuticals but also in the field of material science, providing access to functional materials, such as polymers or coatings, which are indispensable in almost all industries. As a consequence, the organic synthesis can be considered as the driving force for progress and modernization of the society.[2] The great relevance of their discoveries was reflected by numerous Nobel Prizes attributed to organic chemists in the 20th and 21st century. A plethora of groundbreaking discoveries were honored, such as in the field of natural product synthesis (R. B. Woodward: 1965), retrosynthesis (E. J. Corey: 1990), catalysis (Y. Chauvin, R. Grubbs, R. R. Schrock: 2005; R. F. Heck, E.-i. Negishi, A. Suzuki: 2010) and there, more precisely, asymmetric transformations (W. S. Knowles, R. Noyori, B. Sharpless: 2001; B. List, D. MacMillan: 2021).[4]

Albeit being a key technology, the chemical sector is associated with considerable drawbacks and environmental concerns due to pollution and chemical waste formation. Moreover, despite the progress, the chemical industry is highly energy consuming. Especially nowadays, where the current energy crises is increasing, the call for a sustainable future is of utmost importance. Lengthy multistep transformations often require the use of enormous amounts of often toxic solvents, additives in stoichiometric amounts, such as bases, chemical oxidants or reductants, as well as auxiliaries, resulting in vast waste production. During the past decades, the environmental awareness in the society has strongly increased, driven by the scarcity of feedstock materials and energy resources as well as the global warming, thus inducing a rethinking of the chemical industry. Besides the cost-efficacy of the process, the environmental footprint is now taken into consideration to realize a sustainable synthesis. The claim for a greener and less-hazardous chemistry was already addressed by Anastas and Warner in 1998.[5]

They published the ’12 Principles in Green Chemistry’ as a guideline to reduce the environmental impact of chemical processes (Figure 1.1). In addition to the use of energy and feedstock materials in a responsible way, they demand for the use of benign, ideally degradable, reagents and solvents to ensure non-hazardous conditions for nature and humans.[6]

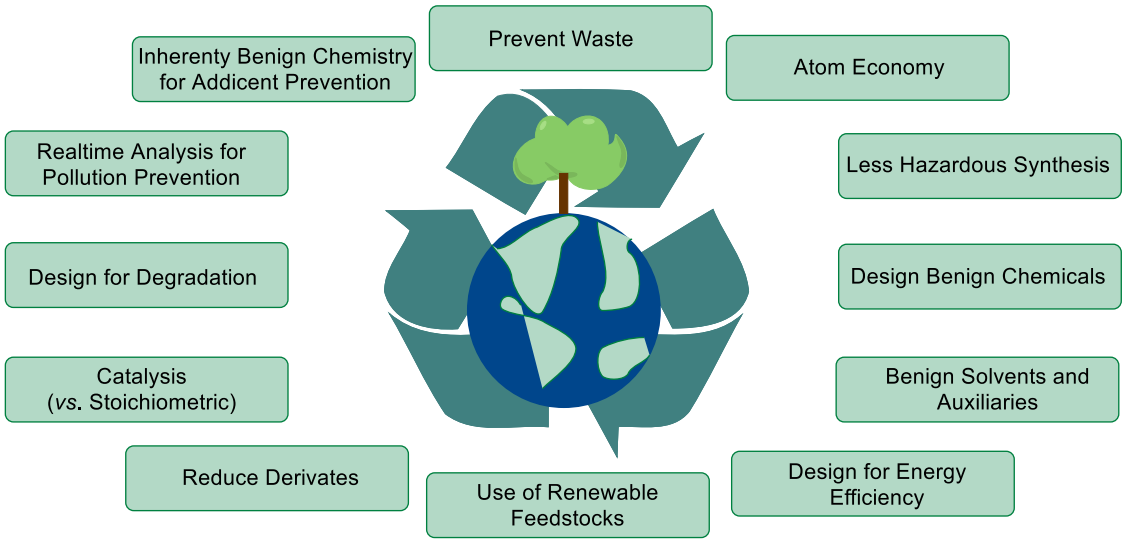

Figure 1.1: The ‘12 Principles of Green Chemistry’ according to Anastas and Warner.

Since the revolutionizing beginnings of organic synthesis in the early 19th century, significant progress has been made. Both, chemical industry as well as academia investigated procedures with improved sustainability to enable chemical transformations. A central aspect, which is extensively disclosed, is the use of catalysis.[7] With predominantly transition metal complexes as catalysts, numerous transformations were achieved under milder reaction conditions as the catalyst allows for a reduction of the activation energy barrier by accessing new reaction pathways. Not only precious metals, but also earth-abundant metal catalysts receive great attention due to their lower prices as a consequence of their high abundance as well as their often reduced toxicity.[8] In terms of enhanced sustainability aspects, the concept of heterogeneous catalysts[9] and immobilized hybrid catalysts[10] is highly attractive as they allow recyclability. Further details in terms of catalytic transformations with focus on C–H activation will be provided in Section 1.2.

Another important issue, which will be addressed in the course of this thesis, is the use of water as a sustainable reaction medium and there especially the use of surfactants and micellar catalysis.[11] Both, academic and industrial research focuses on this aspect, as water is a highly desirable reaction medium given its low toxicity and non-flammable properties as well as its

great abundance and low price, contrary to many organic solvents.[12] However, one fundamental challenge with regard to water is the in general rather low solubility of organic compounds in it, which restricts the applicability of possible substrates. This issue could be addressed by the development of surfactants, which form micelles in water if the concentration is above a critical concentration.[11a] The formation of these nanoreactors does not only allow for satisfying solubility, but also protects organometallic species involved in transformations from hydrolysis. A multitude of long-term established detergents, such as the Brij-series or Triton-X, is commercially available. However, among those classical ones, some are classified as toxic and are associated with environmental concerns due to degradation products.[13] To address this drawback, several so-called benign-by-design[14] surfactants have been developed in the past two decades (Figure 1.2).

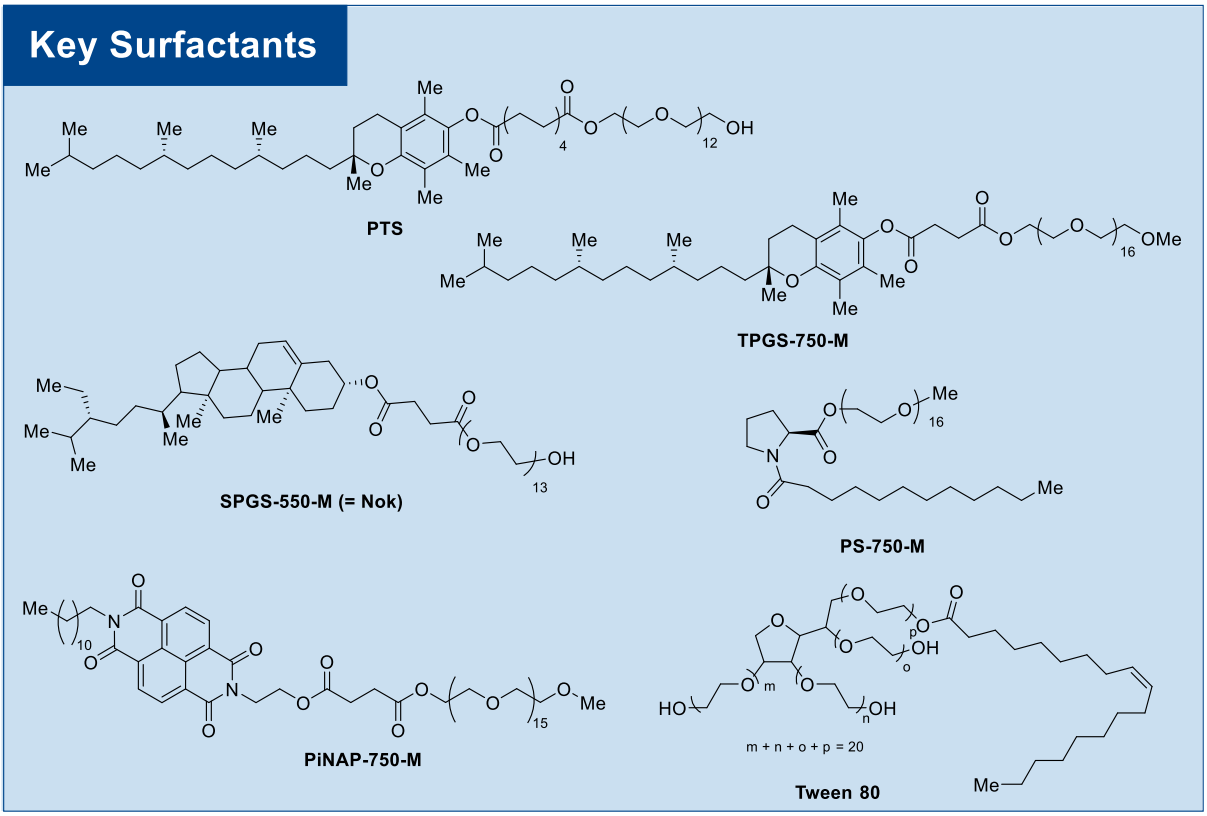

Figure 1.2: Selected examples of surfactants used in organic synthesis.

In sharp contrast to the classical ones, improved features concerning the composition characterize these benign amphiphiles. The first generation designer surfactant PTS is composed of only non-hazardous fragments, in the concrete case, racemic vitamine E, sebacic acid and PEG-600. While the second generation surfactant, the improved TPGS-750-M surfactant, still possesses a tocopherol-core, the third generation non-ionic amphiphile SPGS-550-M (Nok) bears another scaffold. The latter one can easily be obtained in a two-step

synthesis out of the readily available feedstock chemicals β-sitosterol, succinic anhydride and PEG-550-M.[15]

The beneficial effect of micellar catalysis was demonstrated for many different reaction types, such as different C–C and C–N bond forming cross-couplings,[16] among a plethora of other reaction types.[17] Given the great importance of Suzuki-Miyaura cross-couplings especially in the pharmaceutical industry,[18] many reports have focused on mild approaches for this transformation. These highlight the beneficial effect of micellar catalysis, resulting in typically milder reaction conditions when compared to conventional organic solvents. Especially, a significant enhancement of the reaction rate was often observed. Contrary to the long-term prevalent theory, where this increase in efficacy was explained by higher local concentrations, recent calculations are rather suggestive of an entropic effect. As the reaction takes place at the inner 2D-surface of the micelle, a loss of the degrees of freedom is assumed, which leads to an over-all reduced loss in entropy compared to organic solvents, causing an increased reaction rate and high efficacy at lower temperatures.[19]

Besides milder reaction conditions, the sustainability aspect could be further substantiated, as the use of surfactants often enables efficient recycling of the surfactant solution and the catalyst. Upon completion of the reaction, the product can be isolated by phase separation with an organic solvent.[20] The addition of new reactants allows for further product formation without significant loss in efficacy over several cycles. To address the limitation that an organic solvent is required for the isolation, some methods rely also on the use of polymers, which form thermoresponsive micelles above a certain temperature that behave functionally as surfactants.[21]

Apart from the use of catalysis and environmentally-benign solvents, the implementation of new strategies in synthesis and catalysis another approach that allows for more sustainable reaction procedures. Here, the use of electric current or visible light were identified as powerful strategies.[22] While the use of electricity can induce new mechanisms or replace stoichiometric chemical oxidants, metallaphotoredox catalysis is an elegant way to perform reactions under ambient conditions. As both methodologies have been frequently employed in C–H activation chemistry, they will be discussed later in detail in Section 1.6.

1.2 TRANSITION METAL-CATALYZED C–H ACTIVATION

Selective and efficient catalytic procedures for the formation of omnipresent C–C and C–Het bonds are of key importance in organic synthesis, as they allow to access complex scaffolds, such as those present in biological relevant compounds. The modification of natural products or *de novo* synthesis procedures present high relevance in pharmaceutical industry, but likewise in crop protection and material science.[23] During the last century, the new findings in transition metal catalysis have strongly progressed and impacted the molecular synthesis. They revolutionized the synthetic organic chemistry by facilitating new strategies to overcome the restriction to long-term established reactivities. Early reports from Ullmann[24] and Goldberg[25] on copper-catalyzed cross-couplings of aryl halides to facilitate the access to biphenyl scaffolds did not find considerable application in organic synthesis due to the rather harsh reaction conditions. However, this innovative strategy paved the way for the development of powerful, predominantly palladium-catalyzed, cross-coupling procedures during the second half of the 20th century. A plethora of different coupling reactions of aryl halides or aryl pseudohalides with different organometallic nucleophiles can now be considered as a breakthrough in modern chemistry. Well known and established catalytic transformations, such as the Kumada-Corriu,[26] Mizoroki-Heck,[27] Sonogashira-Hagihara,[28] Suzuki-Miyaura,[29] and Negishi cross-couplings,[30] among others,[31] afford the formation of C–C bonds in arylations, alkylations, alkenylations as well as in alkynylations. Moreover, the palladium-catalyzed Buchwald-Hartwig amination is worth to mention, although being not a cross-coupling in its traditional sense.[32] As these reactivities have evolved into an indispensable and powerful tool for chemists, these valuable contributions were honored with the Nobel Prize in Chemistry in 2010, which was attributed to R. F. Heck, E.-i. Negishi and A. Suzuki.[33]

Although transition metal-mediated cross-coupling chemistry has emerged as a notable strategy with indisputable advances which revolutionized the molecular synthesis, this approach is also associated with significant drawbacks. In general, these transformations do not only rely on the use of (pseudo)halides, but additionally necessitate the use of an organometallic reagent. These nucleophile compounds, such as organomagnesium- (RMgX) in Kumada-Corriu-, organosilyl- (RSiR'$_3$) in Hiyama- or organotin reagents (RSnR'$_3$) in Stille-coupings, require tedious and time-consuming multistep synthetic procedures to obtain them. Moreover, they are usually highly reactive and toxic, thus presenting the demand for special handling and forming hazardous metal waste in stoichiometric amounts (Scheme 1.1a). An approach which addresses these limitations, is C–H activation chemistry, which gained considerable momentum as a

sustainable alternative.[34] Through the direct functionalization of omnipresent C–H bonds by transition metal catalysis, the prefunctionalization to afford the organometallic reagents in cross-coupling chemistry can be circumvented, thus ending up with a substantially improved atom- and step-economy (Scheme 1.1b).[35] Further improvement can be achieved by efficient C–C bond formation through a twofold C–H activation strategy in a dehydrogenative manner, which is concomitated formally by H_2 as sole byproduct, thereby presenting an ideal atom-economy. However, the use of often toxic and expensive (metal)oxidants in stoichiometric amounts is required to enable the envisioned transformation with an oxidative C–H/C–H activation manifold catalytically (Scheme 1.1c)

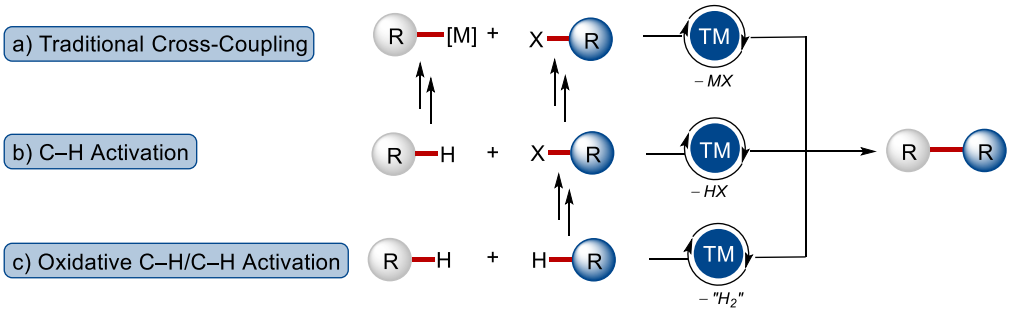

Scheme 1.1: Comparison of conventional cross-coupling reactions to C–H activation chemistry.

Due to the great interest in C–H functionalization reactions, many efforts were done to gain mechanistic insights into the central C–H bond activation step. In addition to radical-type outer-sphere manifolds,[36] five different pathways had been proposed for the C–H bond cleavage. Depending on the reaction conditions, more precisely, on the employed transition metal with a certain oxidation state and a coordination environment manipulated by potentially used ligands, the scission can proceed through oxidative addition, σ-bond metathesis, 1,2-addition, electrophilic substitution or a base-assisted metalation pathway (Scheme 1.2).[37]

C–H cleavage through oxidative addition to a metal complex is usually facilitated by electron-rich, low-valent complexes of late transition metals with vacant coordination sites, such as seen for ruthenium(0), rhodium(I) or palladium(0). Usually, a σ-complex is formed as an intermediate, which is stabilized by an agostic interaction between the C–H bond and the metal center (Scheme 1.2a). In contrast, the σ-bond metathesis follows a concerted mechanism, where two σ-bonds are cleaved in the same way as two new σ-bonds are formed, thus the oxidation state of the metal center is kept untouched. Early transition metals, especially with d^0-configuration feature C–H activations with this mechanism (Scheme 1.2b). The 1,2-addition manifold is the preferred reaction mechanism for early transition metal complexes including

certain ligands. On the other hand, a complex bearing a multiple bond between the metal and a ligand, such as observed with alkylidene- or imido-ligands or, on the other hand, those with formally anionic ligands with significant π-donation character can undergo this mechanism. The C–H cleavage is enabled by an 1,2-addition of the C–H bond onto the M=X bond, formally being a [2π+2σ] process (Scheme 1.2c). Late transition metals, usually in higher oxidation states are prone to catalyze C–H scissions following an electrophilic substitution-type mechanism. This proceeds *via* an electrophilic attack of the metal center on the carbon atom, which affords the substitution of the hydrogen by the metal (Scheme 1.2d). Another important mode of C–H cleavage is the base-assisted metalation pathway, which is the prevalent pathway for metal complexes possessing carboxylate- or carbonate-ligands in the coordination environment. Being closely related to the electrophilic substitution pathway, the major difference is that the C–H cleavage occurs simultaneously to the creation of the C–M bond, which results in a proton transfer to the coordinated base. The crucial role of a carboxylate-type ligand was already discovered in 1979,[38] which was further substantiated by experiment and calculations (Scheme 1.2e).[39]

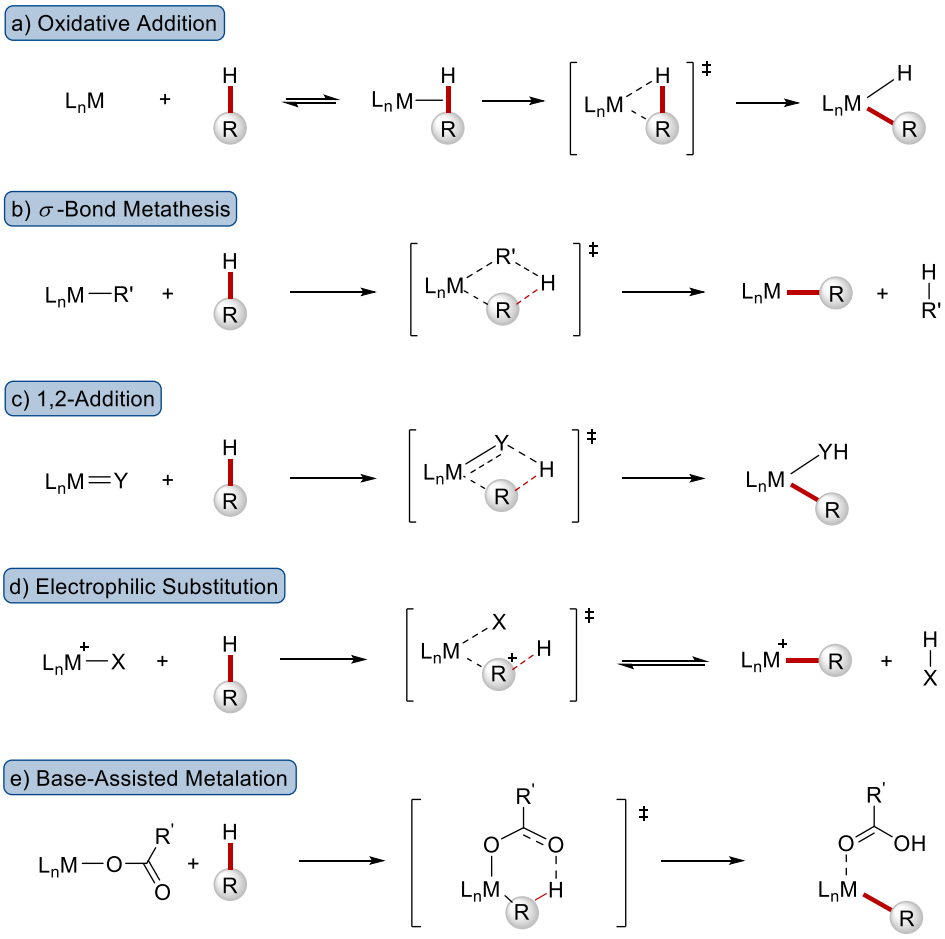

Scheme 1.2: Mechanistic scenarios for C–H scission.

The pathway of the base-assisted C–H metalation was further investigated, and different scenarios were proposed in dependence on the exact nature of the transition state and the partial charges being involved (Scheme 1.3). Fagnou/Goresky proposed a concerted metalation-deprotonation (CMD) scenario as transition state.[40] Closely related is the amphiphilic metal ligand activation (AMLA). In this proposal by Macgregor/Davies, an additional agostic interaction between the C–H bond and the metal ion is assumed in the intermediate species.[37e, 41] As in both cases a deprotonative manifold is operative and it is generally accepted that the C–H scission preferentially takes place in an electron-deficient substrate, which is controlled by the C–H acidity. Ackermann instead introduced the concept of the base-assisted internal electrophilic substitution (BIES) with the preferential activation of electron-rich substrates.[42]

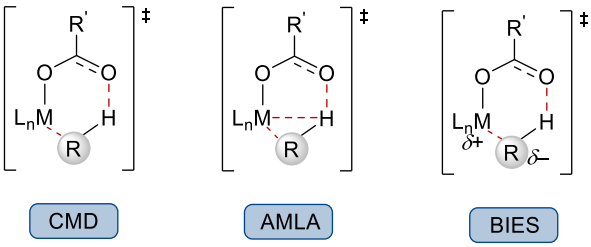

Scheme 1.3: Proposed transition states for the base-assisted C–H metalation.

Striving for a better understanding on the working modes in the C–H functionalization, the concerted metalation-deprotonation pathway was disclosed in greater detail. Echavarren illustrated with an intramolecular competition experiment of fluorinated arene **1** to access phenanthrenes **2a** and **2b** the preferential functionalization of the electron-deficient, fluorinated arene moiety in the less nucleophilic but more acidic position (Scheme 1.4a).[43] This finding is inconsistent with an aromatic electrophilic substitution pathway, which should cause a preferred formation of product **2a**. In contrast, they were suggestive of a deprotonative, assisted pathway, which was further supported by Maseras in computational studies. Independently, Fagnou described an intermolecular direct arylation of perfluorobenzene **3** with aryl bromide **4** with the same inversed reactivity (Scheme 1.4b).[44] Competition experiments revealed that electron-deficient arenes were preferentially converted. Based on calculations, a concerted metalation deprotonation was proposed, which likely involves a carbonate-assisted proton-abstraction transition state, as illustrated in **6**.

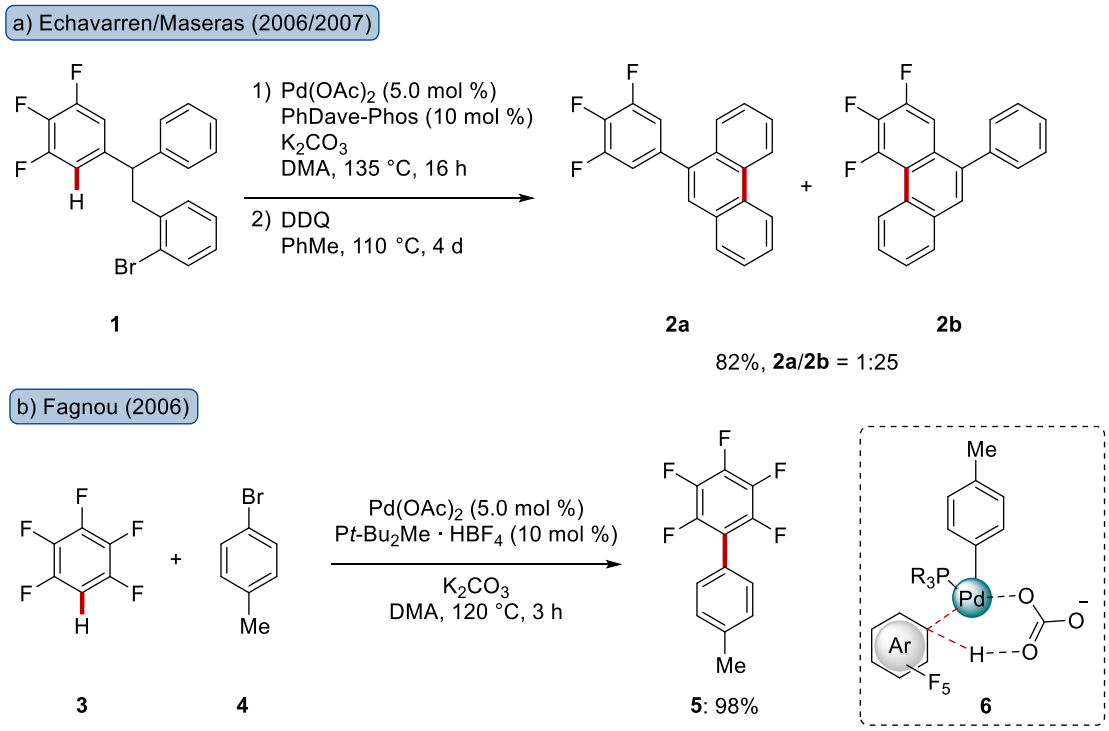

Scheme 1.4: Key experiments for the concerted metalation-deprotonation mechanism.

Due to the omnipresence of C–H bonds with similar bond dissociation energies in organic molecules, the development of efficient protocols with a controlled positional selectivity was the key challenge the C–H activation concept was faced with.[45] To address this, at least three different strategies have been emerged to ensure the site-selectivity. Concerning the undirected functionalization of heterocyclic scaffolds, differences in electronic properties and, as a consequence, in the reactivity can be exploited. An example for this electronic bias is the heterocycle benzoxazole, in which the C2–H atom has a strongly reduced pk_a value compared to its other aromatic C–H bonds. Based on the kinetic acidity, catalytic transformations lead to high selectivities (Scheme 1.5a).[46] Another approach relies on the regiocontrol by introduction of sterically demanding substituents, which prevent the C–H activation process in the neighboring positions, thus ensuring that the catalysis takes place exclusively in the less hindered position (Scheme 1.5b).[47] Although these two approaches are highly selective, they are restricted to specific substrates which fulfill the requirements, hence limiting the intended broadly applicable strategy. A more general approach in C–H activation chemistry is the use of a directing group bearing a Lewis-basic atom or moiety for chelation assistance (Scheme 1.5c).[48] By coordination of the transition metal catalyst, the complex is brought into close proximity to a specific C–H bond, typically in *ortho*-position to the directing group, therefore facilitating the C–H bond cleavage and metalation in this position. The highly selective transformation can be enabled by a broad range of Lewis-basic functional groups,

ranging from hydroxyl- to carboxylic acid-, ester- or carbonyl-substituents, among others. Remarkably, a multitude of different nitrogen-containing heterocycles was identified as suitable assisting groups for *ortho*-selective conversions. Although the employed directing group is not necessarily part of the target compound, in many cases, the Lewis-basic group can be either removed after the conversion (removable DG) or converted into another valuable group (transformable DG).[49] In addition, the temporary or reversible installation and removal of a transient directing group during the catalysis has received considerable interest.[50]

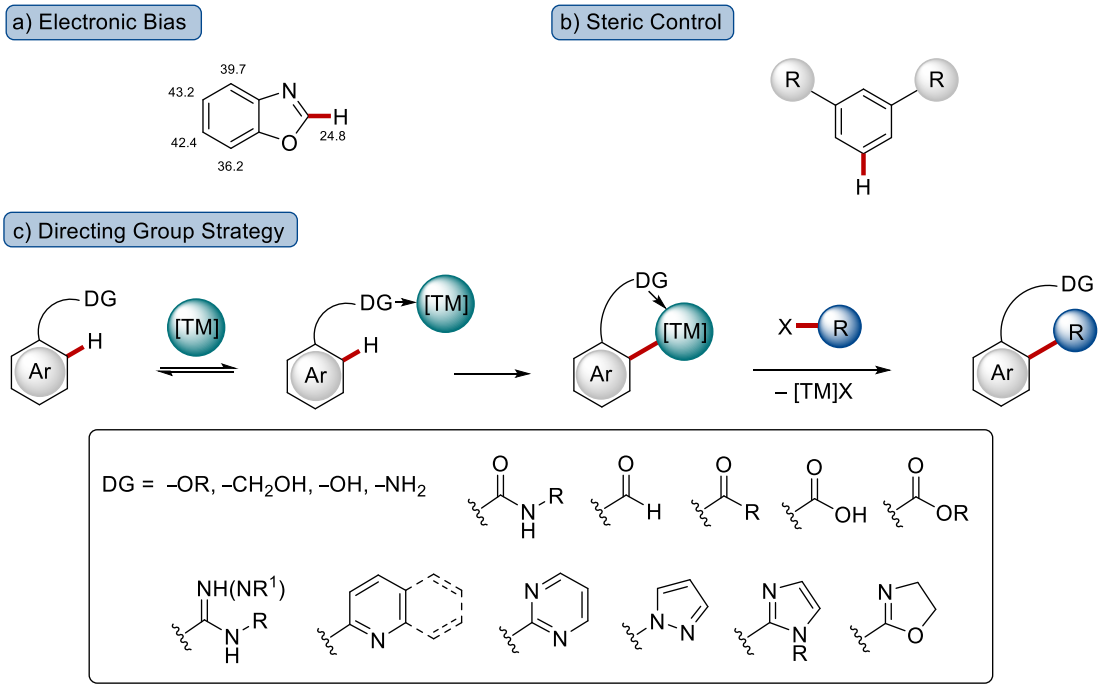

Scheme 1.5: Positional selectivity control in C–H activation by a) exploiting electronic properties, b) steric control or c) the assistance of directing groups.

Besides a plethora of *ortho*-selective C–H activation reactions realized for the atom- and step-economic modification of arenes, distal *meta*- and *para*-selective transformations were achieved, albeit these reactions in a selective manner continue to be scarce.[51] Nonetheless, several suitable strategies could be identified to enable distal C–H activations in dependence on the employed transition metal (Scheme 1.6). A previously mentioned strategy consists in the use of substrates decorated with bulky substituents. As the C–H activation and metalation is prevented at the neighboring positions, the reaction takes solely place in the non-hindered *meta*-position. However, this approach is thus far limited to iridium-enabled borylation of arenes.[52] Another, more general strategy is the use of removable directing groups, such as carboxylic acids. The implementation of a substituent in one of the *ortho*-positions next to the directing moiety is indispensable for the construction of *meta*-substituted arenes. After the chemical

transformation of the C–H bond in the close proximity and removal of the chelating substituent, *e.g.* decarboxylation, formally a *meta*-selective transformation is achieved (Scheme 1.6a).[53] Moreover, the introduction of a template or auxiliary bound to the arene is a strategy, providing access to distal C–H activation in *meta*- or *para*-positions. The auxiliary bearing a Lewis-basic moiety for coordination of the transition metal, ensures that the metal center is brought into close proximity to a specific C–H bond and enables selectively the conversion at this position (Scheme 1.6b).[54] As the covalent implementation of such a template is associated with significant drawbacks because of additional synthetic steps for the installation and the removal, attempts to employ non-covalent linkers were made. As introduced by Kuninobu and Kanai, a linker bound *via* hydrogen bonding to the carbonyl substrate enabled *meta*-selective borylation by coordination of the iridium catalyst to a bipyridine scaffold.[55] However, this approach is limited to iridium catalysis, thus diminishing the synthetic versatility of this strategy (Scheme 1.6c). In addition, also specific approaches were developed for other precious metals. Inspired by the Catallani reaction,[56] norbonene was identified as efficient transient mediator in palladium-catalyzed C–H activation reactions. Hence, *meta*-functionalized products can be obtained by an *ortho*/*ortho* C–H activation regime (Scheme 1.6d).[57] The remote *σ*-bond activation frequently employed in *meta*-selective ruthenium-catalyzed reactions should be mentioned as one of the most versatile strategies. This elegant approach is based on the chelation-assisted C–H metalation in *ortho*-position in relation to the directing group. As a consequence, the *para*-position with respect to the ruthenium is activated, and therewith features the remote functionalization in *meta* to the directing group (Scheme 1.6e).[58]

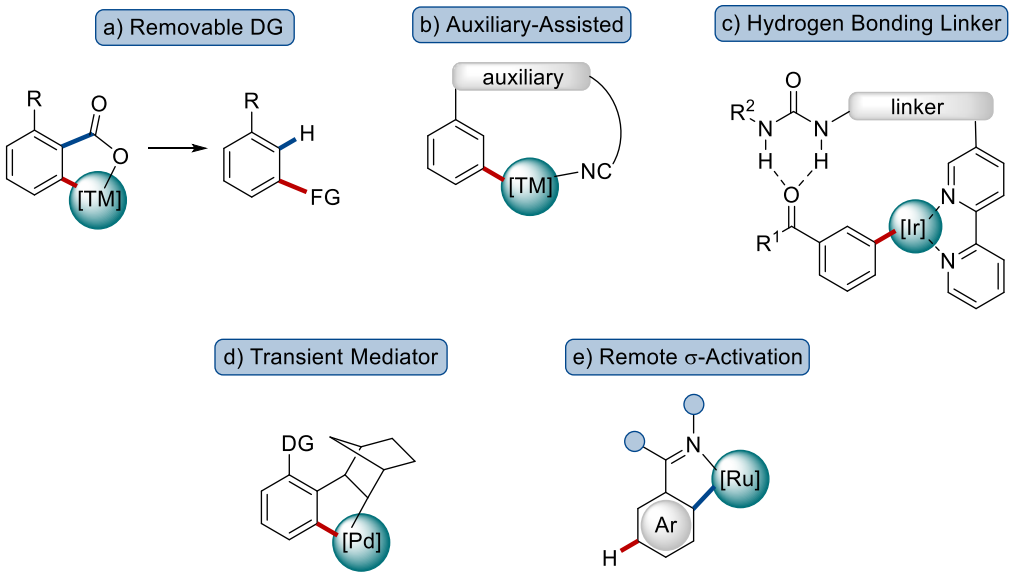

Scheme 1.6: Strategies for *meta*-selective C–H activation.

1.3 RUTHENIUM-CATALYZED C–H ACTIVATION REACTIONS

The use of ruthenium as transition metal for the activation of C–H bonds goes hand in hand with a long tradition with origin in the stoichiometric activation of naphthalene **8** reported by Chatt in 1965 (Scheme 1.7).[59] Oxidative addition to an *in situ* formed ruthenium(0)/phosphine complex yielded the complex **9**, bearing a ruthenium ion in the oxidation state +II. Based on this pioneering work, a variety of stoichiometric C–H activations relying on a ruthenium catalyst has been developed, as presented in the following section with selected examples.

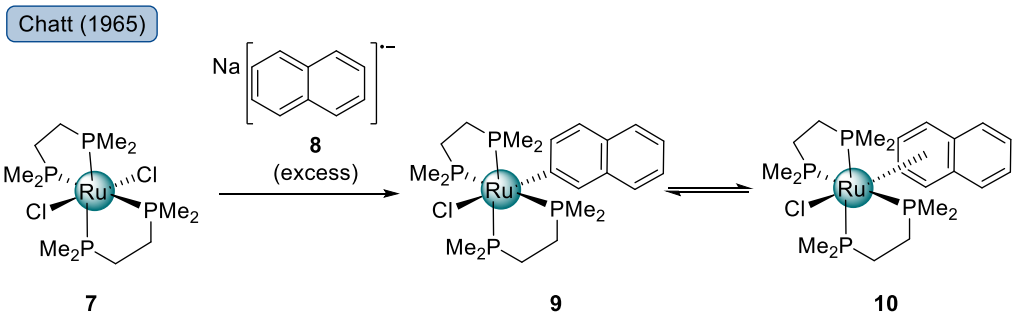

Scheme 1.7: C–H activation in naphthalene **8** with ruthenium in a stoichiometric reaction.

1.3.1 Ruthenium-Catalyzed Alkylations with ortho- and meta-Selectivity

Almost twenty years later, the C–H alkylation reaction of phenol (**11**) was disclosed by Lewis and Smith, which can be considered as the first example of a C–H activation in a ruthenium catalysis regime (Scheme 1.8).[60] The reaction of phenol (**11**) with ethene **12** allowed for the ethylation at the *ortho*-position to the hydroxy group by utilization of phosphites as transient directing groups. However, the rather harsh reaction conditions with elevated pressure and temperature, led to a mixture of the mono- and di-alkylated products **13** and **13'**. Moreover, this reaction was restricted to the ethylation and an H/D exchange of phenol. Later on, this approach was expanded by Gunnoe reporting on the undirected hydroarylation of benzene and the heteroarenes furane and thiophene under significantly milder conditions.[61]

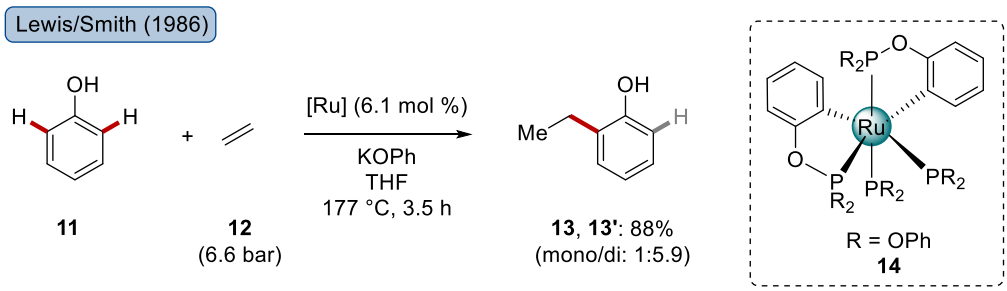

Scheme 1.8: Alkylation of phenol **11** with ethene **12** as the first example of catalytic ruthenium in C–H activation, here by a transient directing group.

Afterwards, Murai achieved another meaningful progress towards ruthenium-catalyzed alkylations in 1993 by presenting an *ortho*-selective transformation of aromatic ketones **15** with olefins **16** (Scheme 1.9 top).[62] In this case, $[RuH_2(CO)(PPh_3)_3]$ served as a suitable ruthenium precursor. A broad set of different aryl ketones **15**, among those also heteroarenes, was successfully reacted with a variety of alkenes **16**, hence representing a broadly applicable ruthenium-enabled C–H alkylation procedure. Despite the fact that experimentation was missing to elucidate the mechanistic details, the authors provided the suggestion that this reaction proceeds through a five-membered ruthenacycle by oxidative addition under chelation assistance of the carbonyl group to form a ruthenium-hydride intermediate **18**. A few years later, DFT studies on this system published by Matsubara and Morokuma were indicative of a stepwise C–H bond cleavage enabled by an *in situ* generated Ru(0) species after liberation of H_2 under thermal heating (Scheme 1.9 bottom).[63] In the first step, the C–Ru bond is formed, thereby keeping the C–H bond untouched as shown in **20**. A divalent ruthenium-center is generated, and in the second step, the scission of the C–H bond occurs and the hydrogen is transferred to the metal center.

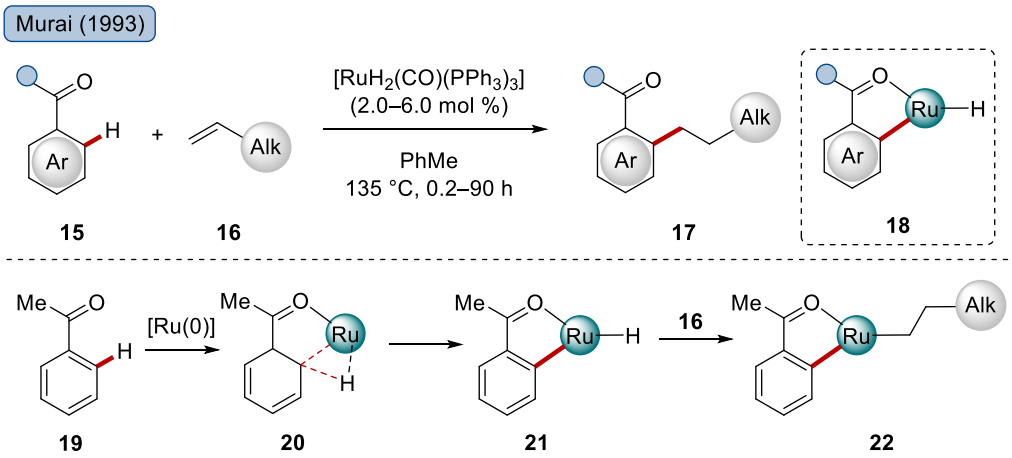

Scheme 1.9: *ortho*-Alkylation of aromatic ketones **15** as first generally applicable procedure.

Another major achievement towards robust and efficient C–H alkylation was made by Ackermann in 2009 by reporting on a carboxylate-assisted direct C–H alkylation with alkyl halides (Scheme 1.10).[64] Arenes **23** were hence smoothly converted with primary or secondary alkyl halides **24** and **25** as electrophiles. Different nitrogen-containing heterocycles ensured an excellent selectivity of the transformation in *ortho*-position. Besides pyridine and pyrazole scaffolds, ketimines were identified as compatible substrates. In a two-step procedure with a subsequent reduction, the corresponding benzylamine derivatives were obtained. The addition

of a sterically demanding carboxylic acid was essential to enable synthetically useful conversions with best results for 1-AdCO$_2$H (**28**).

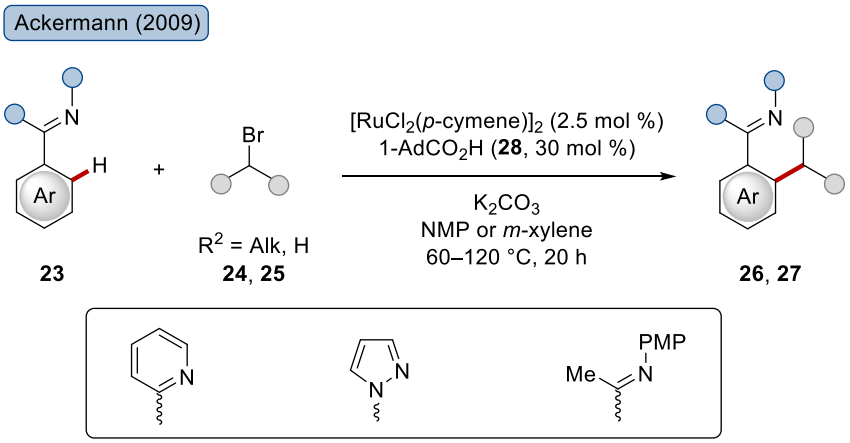

Scheme 1.10: *ortho*-Alkylation of arenes **23** by ruthenium(II) catalysis with carboxylate-assistance.

Detailed mechanistic studies disclosed the catalytic manifold of this versatile ruthenium-catalyzed C–H alkylation and were illustrated in a subsequent study by proposing a plausible catalytic cycle (Scheme 1.11).[65]

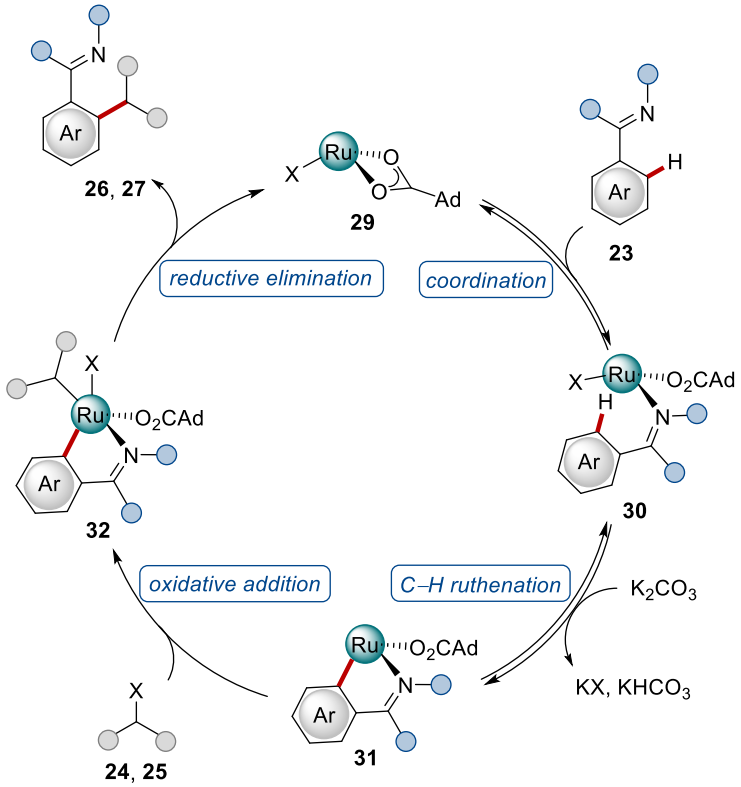

Scheme 1.11: Proposed catalytic scenario for the ruthenium-catalyzed *ortho*-alkylation.

As concluded from H/D scrambling experiments, the catalytic cycle commences with coordination of the heteroatom in substrate **23** to ruthenium(II) carboxylate complex **29** followed by reversible C–H cleavage to afford the ruthenacycle **31** through C–H ruthenation. Oxidative addition of the alkyl halogen **24** or **25** to the cyclometalated species results in the ruthenium(IV) intermediate **32**. Thereafter, reductive elimination to ruthenium(II) complex **29** allows the next turnover by closing the catalytic cycle, with the concurrent release of the desired *ortho*-alkylated product **26** or **27**.

Significant progress in terms of mild reaction conditions for ruthenium-catalyzed direct C–H alkylations was recently achieved by Larrosa (Scheme 1.12).[66] By using the cyclometalated ruthenium benzylamine complex RuBnN (**33**), initially introduced by Pfeffer,[67] efficient alkylation at the *ortho*-position was realized at ambient temperature. Key to success was the addition of a potassium phosphonate salt in substoichiometric amounts. In sharp contrast to this catalyst system, the frequently employed complex $[RuCl_2(p\text{-cymene})]_2$ did not furnish alkylation product **27** under otherwise identical reaction conditions. A broad range of different assisting heterocycles was tolerated, such as pyrimidines, benzimidazoles and ketimines. However, this procedure is limited to the use of primary alkyl bromides **25**, and among those, predominantly substrates with long alkyl chains or other hydrophobic architectures.

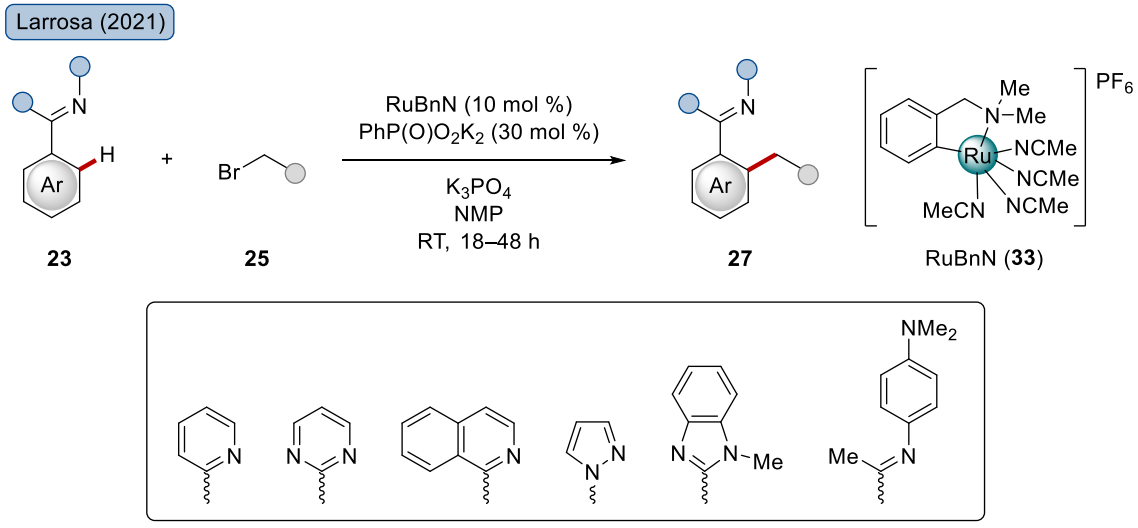

Scheme 1.12: *ortho*-Alkylation with a cyclometalated ruthenium complex at ambient temperature.

Ruthenium-catalyzed C–H alkylations of arenes are not restricted to *ortho*-selective transformations. In contrast, *meta*-selective alkylations have evolved as a remarkable tool after the first example has surfaced in 2011 (Scheme 1.13).[65] In pioneering experiments, Ackermann observed small amounts of the *meta*-functionalized product **37** formed by reaction of phenylpyridine **34** with hexyl bromide. The ruthenium/carboxylate-enabled reactivity led predominantly to the formation of the *ortho*-alkylated product **36** by using water as an environmentally-benign solvent. However, the accessibility of *meta*-alkylated arenes by ruthenium catalysis was nonetheless demonstrated as a proof of concept.

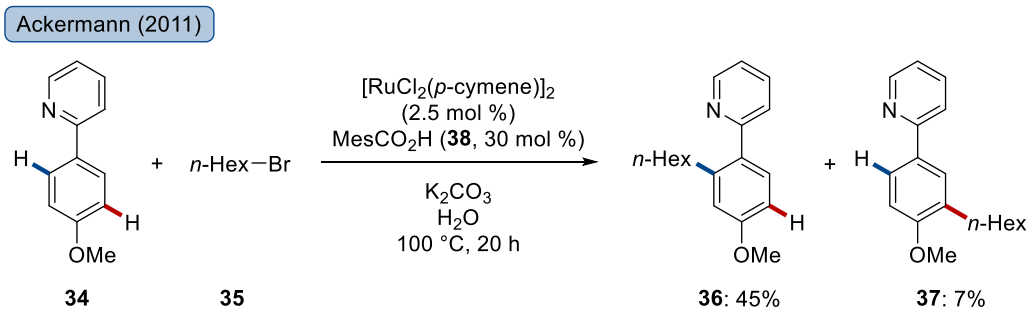

Scheme 1.13: First example for remote C–H functionalization *via ortho*-ruthenation.

In continuation of this remarkable finding, Ackermann realized in 2013 the alkylation of arenes **23** in reasonable yields and excellent *meta*-selectivity (Scheme 1.14 top).[68] The addition of $MesCO_2H$ (**38**) in catalytic amounts in combination with $[RuCl_2(p\text{-cymene})]_2$ resulted in an efficient *meta*-alkylation of arylpyridines, arylpyrazoles and arylazoles **23** with secondary alkyl bromides **24** possessing an ample scope. Detailed mechanistic studies including intramolecular competition experiments concerning the positional selectivity for *ortho*-substituted arenes **23** and the electronic bias as well as a reaction with the well-defined complex $[Ru(O_2CMes)_2(p\text{-cymene})]$ shed light on the catalyst's mode of action. In addition, a reaction with the enantiomerically enriched alkyl halide **40** led to racemization during the catalysis and furnished a racemic mixture of the alkylation product **41**, thus being indicative of a radical reaction mechanism for the remote functionalization through *ortho*-ruthenation (Scheme 1.14 bottom). Furthermore, this was underpinned by control experiments in the presence of TEMPO as a radical scavenger, whose addition completely inhibited the reactivity.

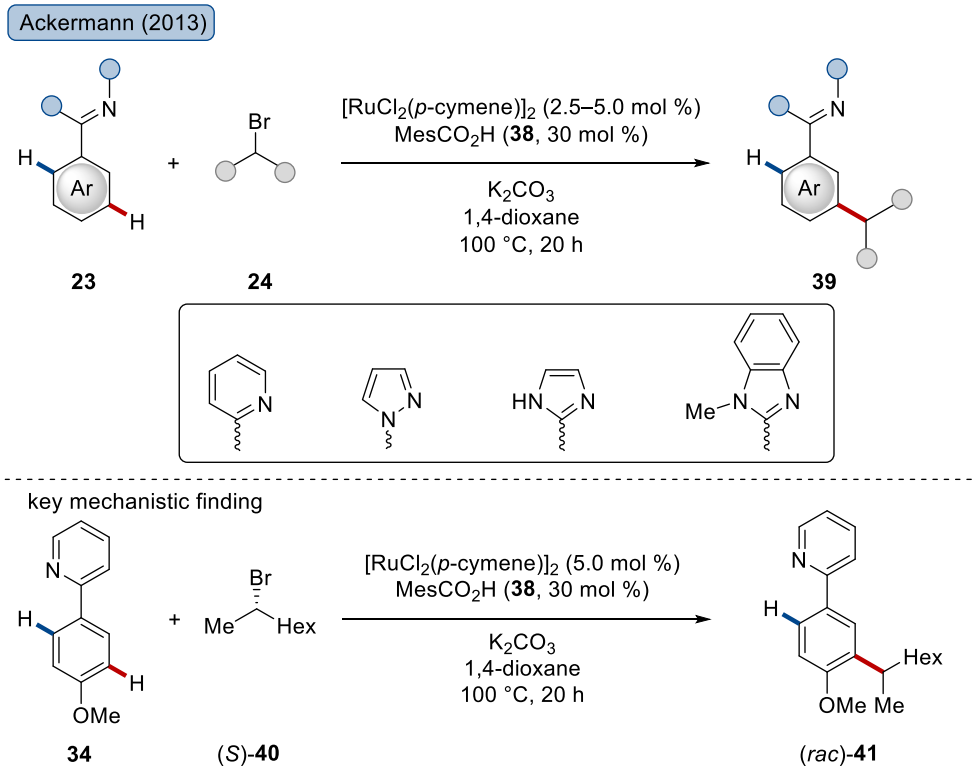

Scheme 1.14: Remote C–H alkylation with secondary alkyl bromides **24** by carboxylate-assisted ruthenium catalysis.

In 2015, Ackermann[69] and Frost[70] investigated concurrently the *meta*-alkylation using tertiary alkyl bromides **42**. Both reports focused on ruthenium catalysis with an assisting carboxylate additive, and thus, exploiting the strategy of transformation in *meta*-position induced by *σ*-bond activation in the *ortho*-position. Ackermann made use of a monoprotected amino acid as the supporting carboxylate ligand, which was here employed in ruthenium-catalyzed C–H activation for the first time (Scheme 1.15a).[69] The versatile protocol allowed efficient modification of arenes **23** bearing a diverse scope of chelating moieties, among those also *N*-pyrimidyl anilines, which can be cleaved under acidic conditions to the corresponding anilines. In contrast, Frost presented simultaneously a protocol, in which KOAc was employed as the assisting additive (Scheme 1.15b).[70] Remarkably, less reactive alkyl chlorides **45** were suitable electrophiles under these conditions, reacting efficiently with the phenylpyridine **44**.

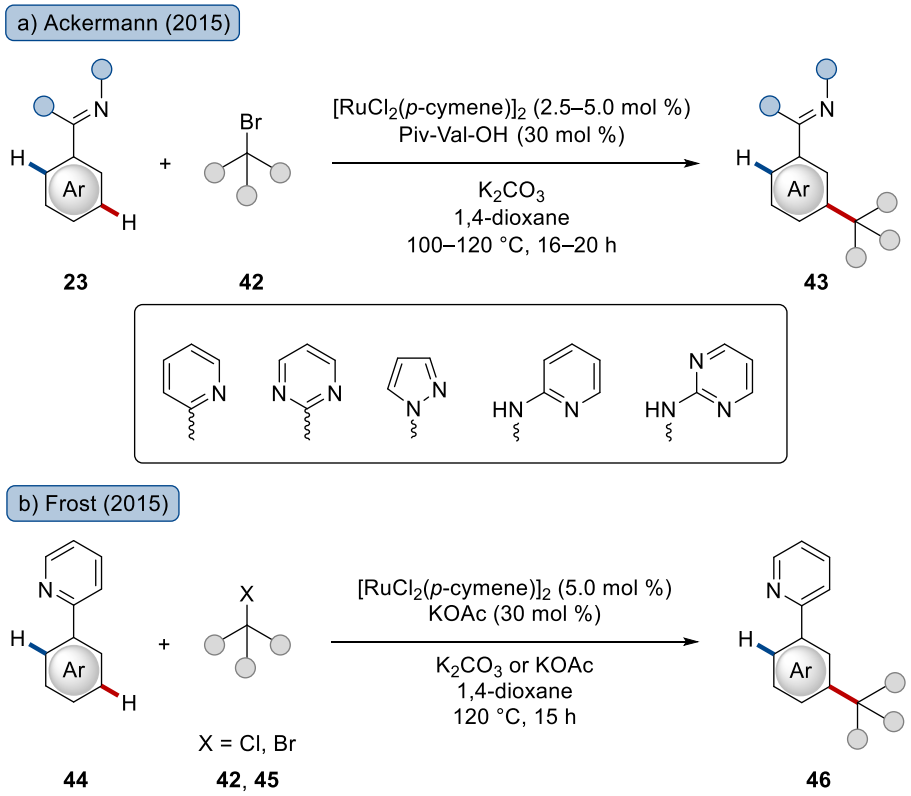

Scheme 1.15: Ruthenium-catalyzed *meta*-C–H alkylation with tertiary alkyl halogens **42** and **45**.

Both contributions included detailed experiments to disclose the reaction mechanism, which were in good agreement with a radical pathway, as was already earlier suggested by Ackermann.[68] The catalytic cycle according to the report from Ackermann was proposed as follows (Scheme 1.16).[69] Starting from the amino acid ligated ruthenium *p*-cymene complex **47**, arene **44** is coordinated and undergoes C–H ruthenation, hence leading to the formation of the cyclometalated ruthenium intermediate **48**. Thereafter, radical addition of the tertiary alkyl radical **49**, generated by single-electron transfer (SET) from alkyl bromide **42** or **45**, results in the stabilized radical ruthenium complex **50** through attack in *para*-position to the ruthenium. Subsequently, rearomatization occurs *via* electron- and proton-transfer to ruthenium(III) and the base K_2CO_3. The thus generated ruthenium complex **51** enables the liberation of the alkylated product **46** in a protodemetalation step, thus regenerating the active ruthenium catalyst **47**. Frost proposed albeit less detailed, a similar reaction mechanism.[70]

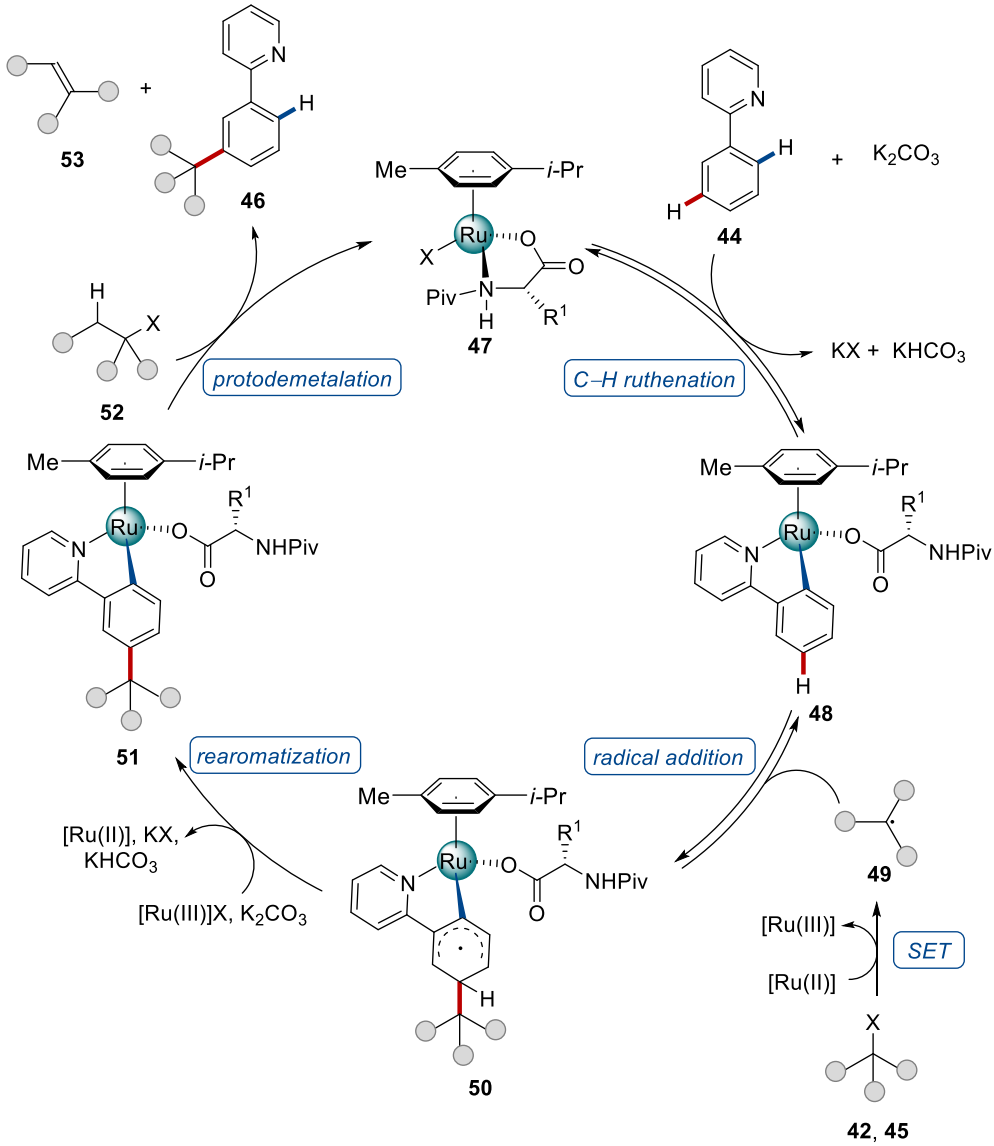

Scheme 1.16: Proposed mechanistic scenario for distal C–H alkylations *via ortho*-ruthenation.

Inspired by the catalytic modification of pyrimidyl aniline, the removable/transformable directing group approach was expanded to the *meta*-selective transformation of diazobenzenes **54**, developed from Li and Yang, thus providing access to substituted anilines after removal of the chelation-assisting group (Scheme 1.17a).[71] In the same year, Li enabled the *meta*-selective modification of phenoxypyridines **57**, furnishing phenols after removal of the pyridine moiety (Scheme 1.17b).[72]

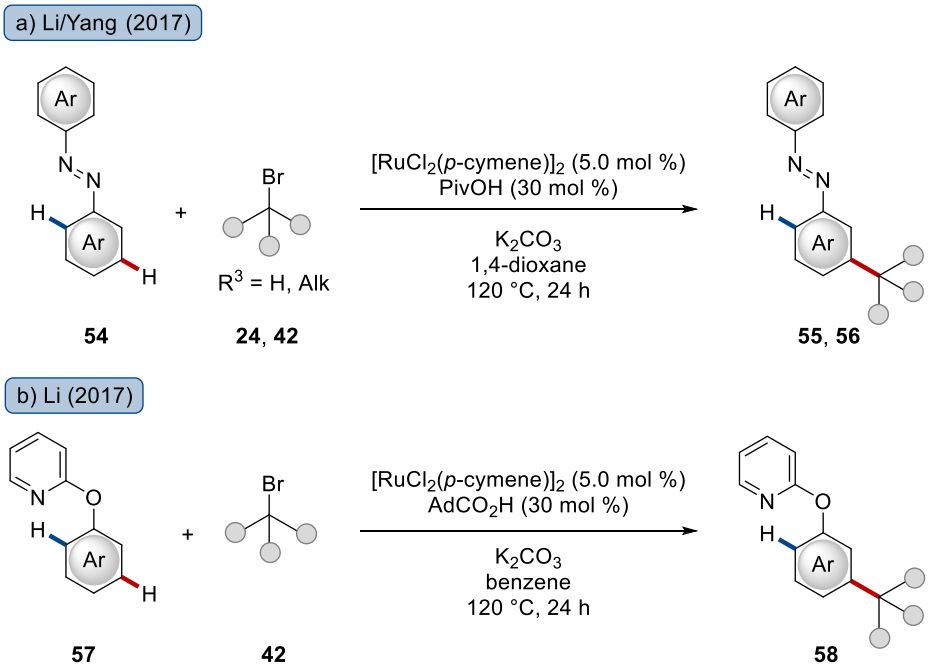

Scheme 1.17: Remote C–H alkylation with removable directing groups.

1.3.2 Ruthenium-Catalyzed Arylations

Due to the significant momentum of transition metal-catalyzed arylation reactions for efficient and sustainable C–C bond formations, extensive research has focused on this field.[73] During the past two decades, ruthenium catalysis was recognized as one of the most powerful tools to promote the molecular construction of such diaryl motifs via C(sp^2)–H activation.

Early contributions in this field were made by the group of Oi/Inoue in 2001, where they reported an efficient *ortho*-selective arylation of arenes **23** with NMP as the reaction medium (Scheme 1.18 top).[74] The catalytic system was composed of a ruthenium(II)-arene complex as precursor and a catalytic amount of PPh_3, which was employed as the additive for the first time. The initial protocol enabled coupling of phenylpyridine with various aryl bromides **59** to furnish the envisioned *ortho*-functionalized product in good yields. Likewise, a high positional selectivity was achieved, as highlighted by *meta*-substituted arenes, which exclusively reacted at the less hindered *ortho*-position. Later on, the group also applied this reaction to ketimines,[75] and synthetically useful oxazolines and imidazolines,[76] which proceeded smoothly under identical reaction conditions. The authors proposed a reaction mechanism for this scenario, which is enabled by a ruthenium(II) complex. Oxidative addition of the aryl bromide leads to a ruthenium(IV) species, which undergoes C–H ruthenation of arene **23** followed by elimination of HBr and subsequent reductive elimination. Although these pioneering works got significant attention, work by Ackermann in 2008[77] and Oullet from Merck in 2011[78] uncovered

problems in reproducibility. During their studies on the implementation of a multikilogram-scale ruthenium-catalyzed arylation step in the synthesis of the CETP-inhibitor Anacetrapib (**65**), the reaction turned out to be not reproducible (Scheme 1.18 bottom). However, the authors revealed that low levels of γ-butyrolactone as trace impurity in the solvent NMP caused a drastic difference in reaction efficacy and robustness. With the addition of the carboxylate KOAc in co-catalytic amounts, this issue was circumvented and reproducible high yields were achieved under these slightly modified reaction conditions.

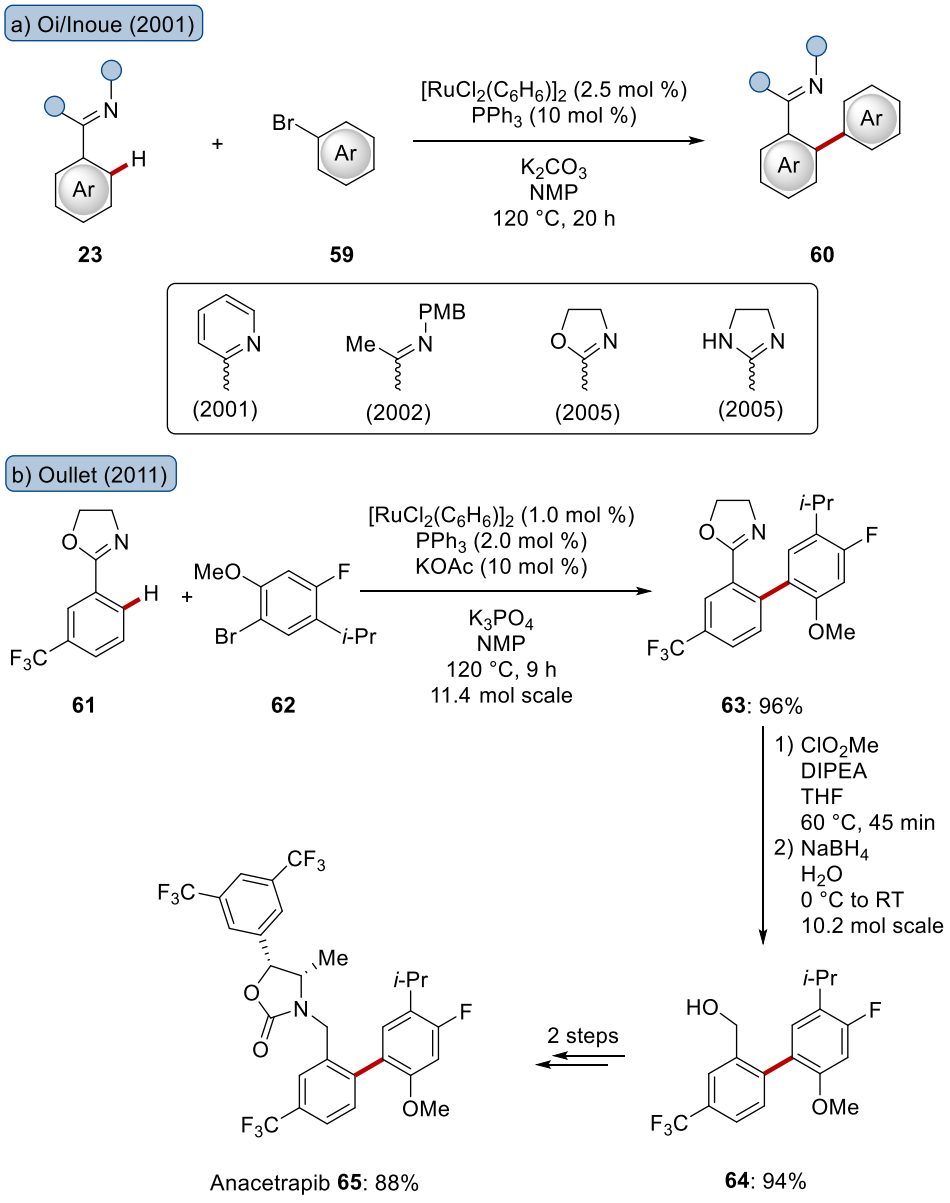

Scheme 1.18: Direct C–H arylation of arenes **23** by ruthenium catalysis and application to the synthesis of Anacetrapid **65**.

In addition to the use of a ruthenium/phosphine catalyst system, $RuCl_3 \cdot nH_2O$ was also identified as a potent and cost-efficient catalyst for *ortho*-selective arylations (Scheme 1.19).[79] As nicely illustrated by Ackermann in 2007, efficient transformation of different *N*-heterocycles **23** was achieved by the reaction with aryl bromides **59** or aryl chlorides **66**, hence representing a rare example for a ruthenium(III)-catalyzed C–H activation. Subsequently, synthetically useful ketimines and heterocyclic aryl bromides could be successfully converted under otherwise identical reaction conditions.[80]

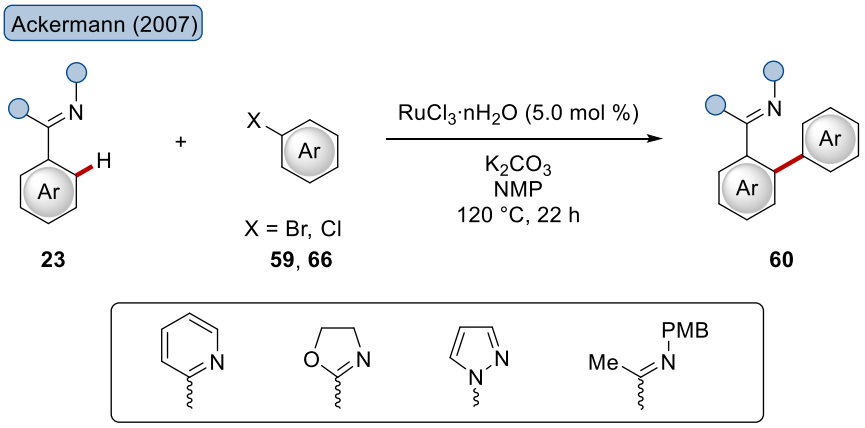

Scheme 1.19: Ruthenium(III)-catalyzed *ortho*-arylation with $RuCl_3 \cdot nH_2O$ as catalyst.

Another breakthrough in the field of generally applicable and robust ruthenium-enabled direct arylation of C–H bonds was achieved by Ackermann in 2008 (Scheme 1.20).[81] By proposing an activation of arene **23** facilitated by the carboxylate $MesCO_2^-$ in catalytic amounts, the first general strategy was disclosed for ruthenium-catalyzed C–H arylations. The functionalization of various heteroaryl arenes could be achieved, such as valuable triazoles, which are in particular of interest in medicinal chemistry and crop protection. Particularly, the superior influence of the carboxylic acid compared to *N*-heterocyclic carbene- and phosphine additives was supported by control experiments, in which the latter ones failed in good performances. Apart from the aromatic carboxylic acid, 1-$AdCO_2H$ (**28**) turned out to be a highly efficient additive. The enhancing effect of the acid as ligand was rationalized as a result of a base-assisted metalation process going through a six-membered transition state. Notably, the C–H arylation did not require NMP as the solvent anymore.

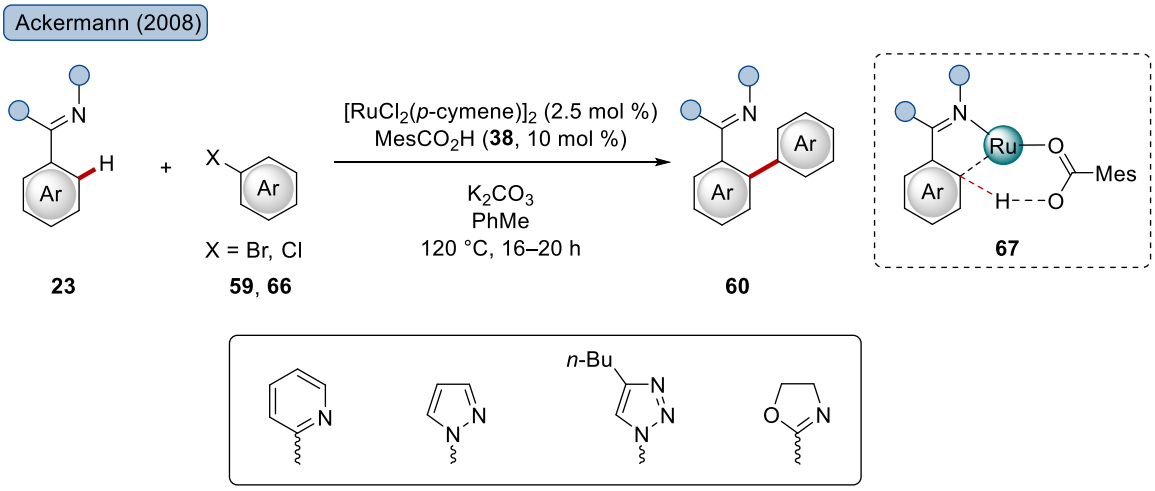

Scheme 1.20: Carboxylate-assisted arylation of different arenes **23** by ruthenium(II) catalysis.

Attracted by the remarkable properties of this catalytic approach, detailed mechanistic investigations on the carboxylate-assisted ruthenium-mediated *ortho*-arylation were performed to shed light on the mechanistic scenario.[82] By the treatment of $[RuCl_2(p\text{-cymene})]_2$ with $MesCO_2H$ (**38**), the well-defined $[Ru(O_2CMes)_2(p\text{-cymene})]$ complex was obtained, whose catalytic ability was demonstrated by employing this air-stable complex in arylation reactions. Stoichiometric reactions revealed that no transformation was observable when the ruthenium(II) complex was treated with aryl chloride **66**. In contrast, after reaction with substrate **23**, a catalytically competent cyclometalated ruthenium complex was formed, which led to the suggestion of a plausible catalytic mechanism as shown in Scheme 1.21. Starting with the ruthenium-mesityl complex **68** formed *in situ* from $[RuCl_2(p\text{-cymene})]_2$, the reversible coordination of the arene substrate **23** results in ruthenium(II) intermediate **69**. Base-assisted deprotonation and C–H ruthenation yield in the cyclometalated ruthenium species **70**. Subsequently, the oxidative addition of aryl halide **59** or **66** takes place to generate complex **71**, which was identified as the rate-limiting step in the mechanistic scenario. Finally, reductive elimination leads to the release of product **60** and the regeneration of the ruthenium carboxylate complex **68** ensures the continuation of the catalytic cycle.

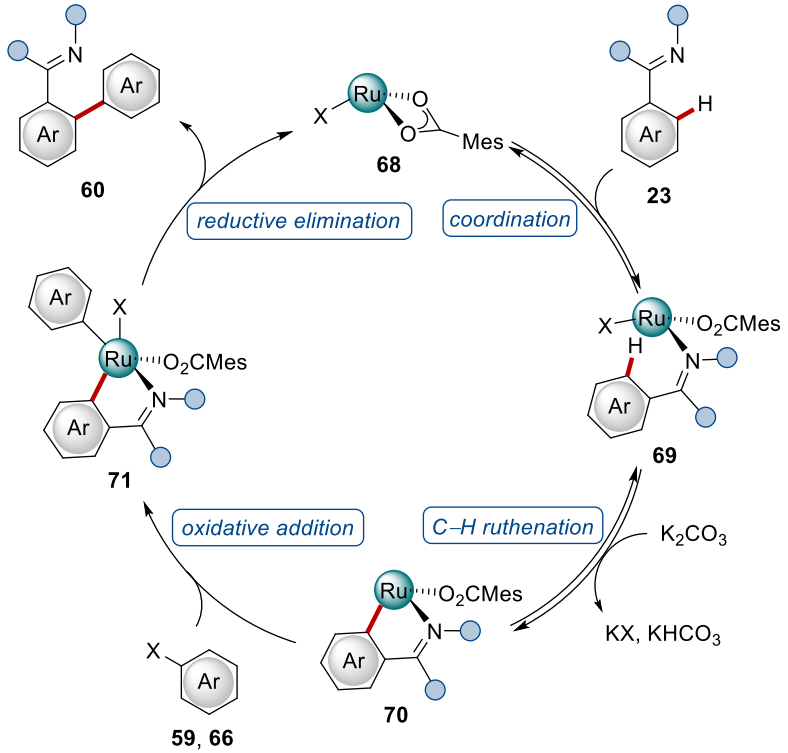

Scheme 1.21: Proposed catalytic cycle for ruthenium-catalyzed arylation *via* carboxylate-assistance.

During the next years, further research on the ruthenium carboxylate system resulted in an improved generality and applicability of this approach. For instance, the requirement of aryl halides as arylating reagents was addressed. By employing [Ru(O_2CMes)$_2$(*p*-cymene)] as the catalyst, efficient modification of arenes **23** with phenols **72** could be achieved (Scheme 1.22).[83] Key to success was the addition of *p*-tosyl chloride, which allowed for the formation of tosylates as pseudohalides *in situ*. Interestingly, this approach was not restricted to the use of toluene as organic solvent. Noteworthy, water was a highly efficient reaction medium with improved safety and sustainability.[83a]

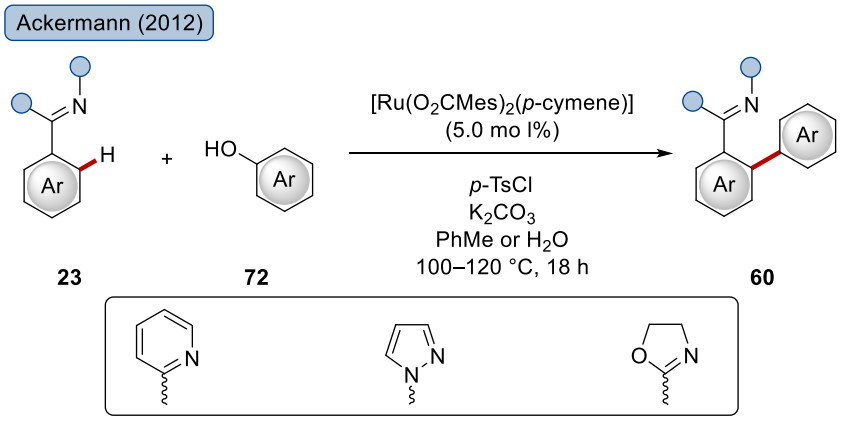

Scheme 1.22: Base-assisted direct C–H arylation with phenols **72**.

A remarkable contribution highlighting the robustness of *ortho*-arylations under ruthenium catalysis regime was the selective transformation of challenging aryl tetrazoles **73** (Scheme 1.23 top).[84] Initially achieved by the use of carboxylate assistance of mesityl carboxylate or acetate bases,[85] the arylation of tetrazoles could be strongly improved by harnessing a natural amino acid-derived ligand, with Piv-Val-OH as the most potent one. Noteworthy, the power of this exceptional procedure was nicely demonstrated by the concise synthesis of protected Valsartan (**77**) (Scheme 1.23 bottom).

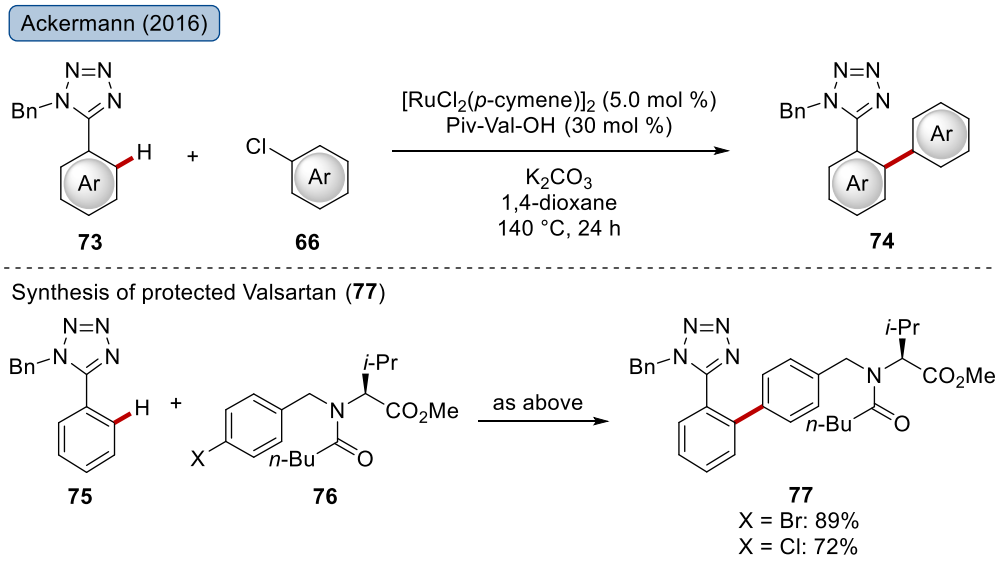

Scheme 1.23: Ruthenium-catalyzed arylation of tetrazole **73** and synthesis of Valsartan (**77**).

Recently, the addition of phosphine additives in combination with a well-defined ruthenium carboxylate catalyst was identified as a suitable approach to modify sensitive scaffolds, such as silylated triazoles **78** (Scheme 1.24).[86]

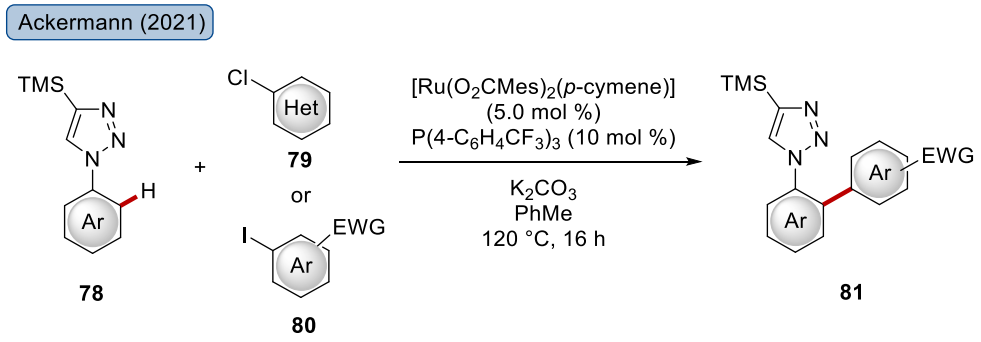

Scheme 1.24: Ruthenium-catalyzed arylation of the sensitive triazole **78** enabled by an electron-deficient phosphine.

Screening of different phosphine ligands determined the electron-deficient *para*-trifluoromethyl derivative as the most efficient ligand allowing the *ortho*-arylation.

Heterocyclic pyrimidine substrates **79** as well as iodoarenes **80** bearing valuable electron-withdrawing substituents, such as trifluoromethyl- or nitro-groups, were fully compatible.

The relevance of ruthenium-catalyzed arylations was furthermore demonstrated by Larrosa[87] in 2018 by coming back to the use of a cyclometalated ruthenium complex, after this concept was initially employed in 2010.[88] Larrosa's research was focused on mild *ortho*-arylations by direct C–H activation of areres **23** with remarkably low reaction temperatures of 35–50 °C with the aid of the cyclometalated ruthenium complex RuBnN (**33**) with carboxylate assistance in NMP as solvent (Scheme 1.25). This protocol tolerated not only a varied set of functional groups but also many Lewis-basic heterocycles for chelation assistance. Moreover, the potential of this approach in late-stage diversification was illustrated by modification of drug molecules and natural products.

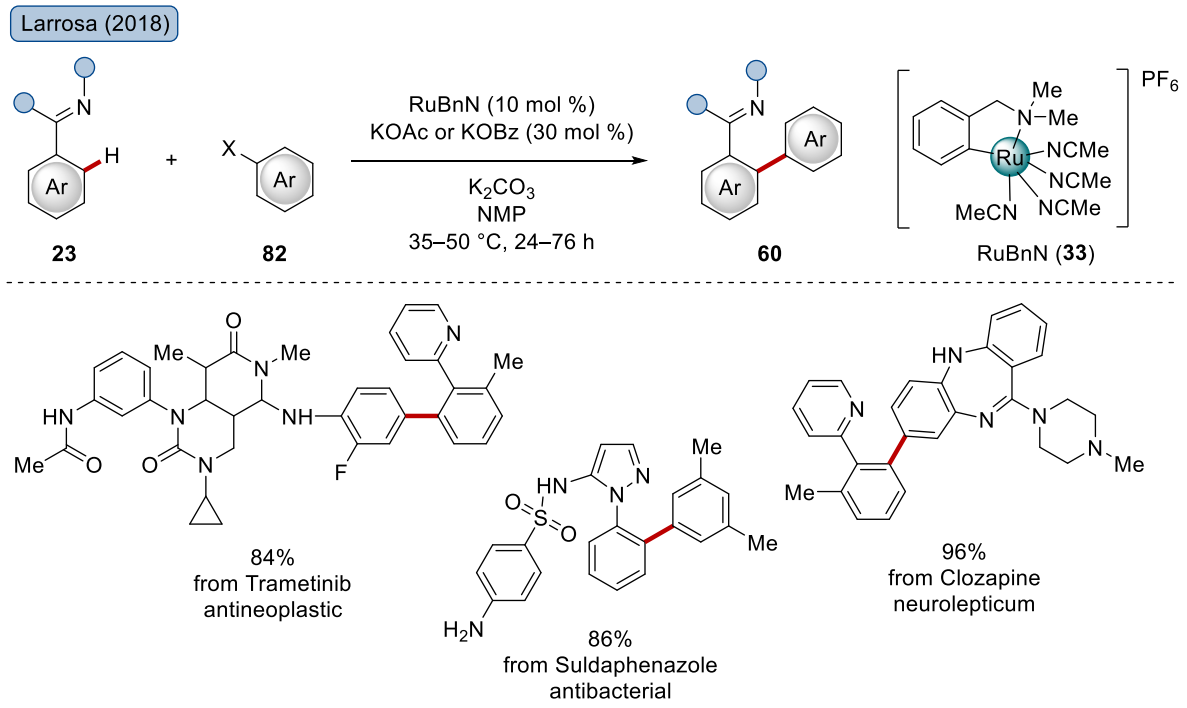

Scheme 1.25: C–H arylations with a cyclometalated complex for late-stage diversification of drugs and natural products.

Ruthenium-catalyzed C–H arylation reactions are not limited to the use of *N*-hetero arenes as assisting directing groups. In contrast, several studies illustrated the applicability to other directing groups as well as undirected transformations.

A valuable example for a commercially available substrate class allowing for chelation assistance are benzoic acids **83**. After successful realization of *ortho*-arylations with other precious metals such as palladium, rhodium and iridium, Larrosa reported in 2017 an approach

for an arylation relying on ruthenium catalysis to enable the modification of benzoic acids **83** with aryl iodides **84** (Scheme 1.26).[89] Interestingly, the addition of potassium perfluoro-*tert*-butoxide strongly improved the catalytic performance. In contemporaneous reports, also Ackermann[90] and Gooßen[91] presented the direct C–H arylation of benzoic acids with a different catalytic system.

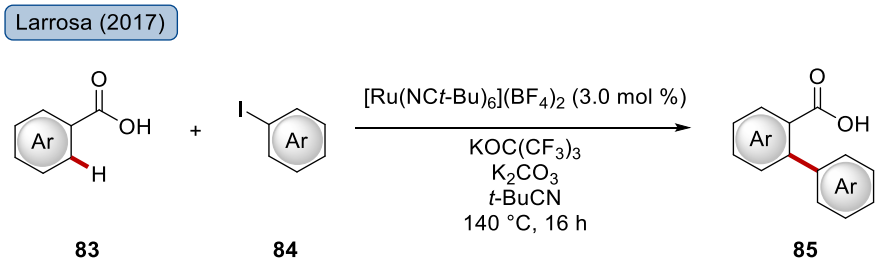

Scheme 1.26: Ruthenium-catalyzed *ortho*-selective arylation of benzoic acids **83**.

Moreover, a notable example for a heteroatom directed arylation was the ruthenium-catalyzed functionalization of ferrocenes **86** by employing a weakly coordinating thioketone as directing group (Scheme 1.27).[92] This sustainable transformation is attributed to Ackermann who presented the first example of micellar catalysis in ruthenium-catalyzed C–H activation by employing the environmentally-benign TPGS-750-M surfactant. The beneficial effect of the aqueous surfactant environment resulted in a broad functional group tolerance and, at the same time, allowed for the recyclability of the reaction medium without any loss in yield. This approach rendered a strongly decreased E-factor compared to the use of an organic solvent, thus highlighting the sustainability.

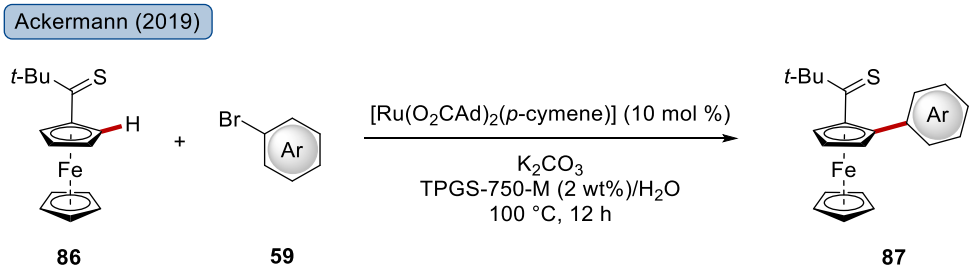

Scheme 1.27: First example of ruthenium-catalyzed C–H arylation using micellar catalysis.

Beyond these examples for the directing group strategy, an alternative method for site-selective C–H transformation is the exploiting of intrinsic properties of certain arenes, in which the modification in the most acidic position is favored. Taking the beneficial effect of carboxylate additives in earlier reports on ruthenium-catalyzed C–H activations into account, Larrosa realized the ruthenium-catalyzed arylation of oligofluorinated arenes (Scheme 1.28).[93] Using

fluoroarenes **88** or other highly electron-deficient arenes, efficient arylation with a broad range of different aryl bromides **59** furnished the corresponding products **89**, which was enabled by the *in situ* formation of a cationic ruthenium pivalate complex.

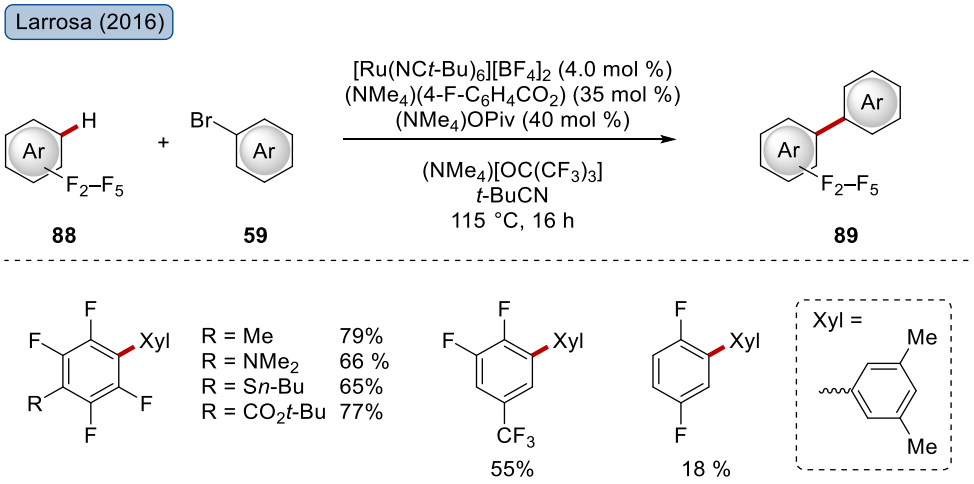

Scheme 1.28: Ruthenium-catalyzed arylation of fluoroarenes **88**.

1.3.3 Ruthenium-Catalyzed Benzylations

In addition to C–C formations for the diversification of arenes through alkylations and arylations by ruthenium catalysis, the direct benzylation was successfully developed in *ortho*- as well as *meta*-selective transformations. As the first example, Ackermann described in 2009 the efficient functionalization of a diverse set of arenes **23** using benzyl chlorides **90** as electrophile (Scheme 1.29).[94] Experimental studies suggested that a S_EAr-type mechanism is rather unlikely to be operative. In contrast, an *in situ* formed ruthenium-carboxylate complex is arguably catalytically active since the acidities of the C–H bonds turned out to be of relevance. Thus, this work is an appropriate contribution in continuation of extensive studies on this catalyst system previously introduced and employed by the same group.[64, 81]

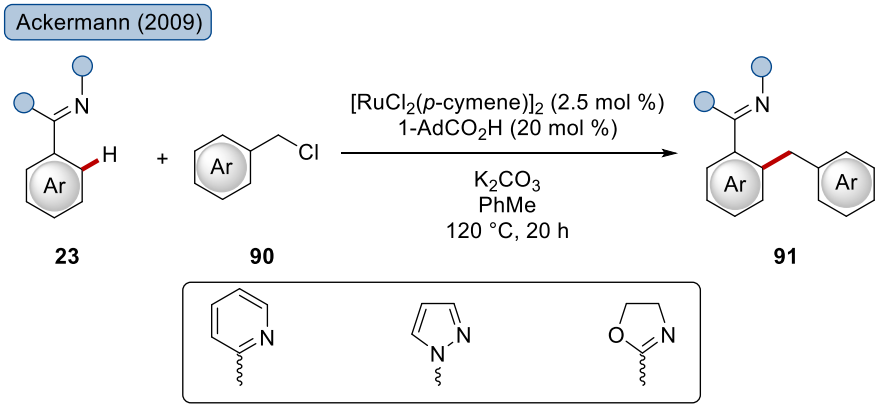

Scheme 1.29: *ortho*-Selective ruthenium-catalyzed C–H benzylation.

The following reports in this field by Shi and Zhao focused on position-controlled benzylations of arenes **23** with toluene substrates **92** (Scheme 1.30a).[95] The twofold C–H/C–H activation was enabled by an oxidative manifold. The use of di-*tert*-butylperoxide (DTBP) as a radical initiator to generate benzyl radicals was crucial to ensure efficient transformations. Therewith, the requirement of prefunctionalized benzyl halides could be circumvented, but a large excess of arene **92** was mandatory. In addition to ferrocene as mediator in co-catalytic amounts, the catalyst [$Ru(PPh_3)_3Cl_2$] furnished the *ortho*-benzylated product **91** with good efficacy. However, the use of $RuCl_3$ and *rac* BNDHP (**94**) caused a switch in selectivity, resulting in the *meta*-selective transformation to product **93**. In an independent work, Shi further illustrated the potential of this oxidative ruthenium catalysis strategy by reporting on *meta*-selective benzylations (Scheme 1.30b).[96] In this case, the use of perfluoroisopropyl iodide as a radical initiator was beneficial.

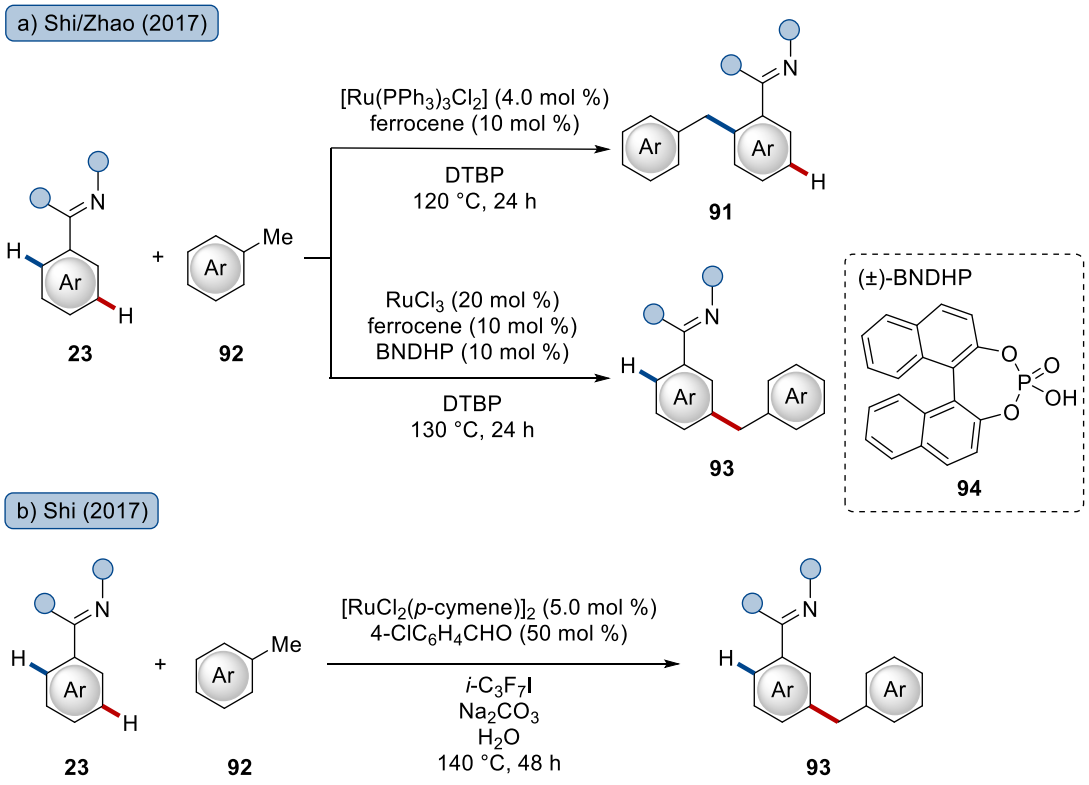

Scheme 1.30: Oxidative ruthenium-catalyzed C–H benzylation of arenes **23** with toluene derivatives **92**.

This interesting approach to control the site-selectivity of the C–H benzylation reaction was not restricted to the oxidative conditions with toluene as coupling partner. In contrast, by coming back to benzyl chlorides **90**, Ackermann also achieved a selectivity switch by using cost-efficient triphenylphosphine as ligand (Scheme 1.31).[97] Furthermore, the conditions allowed

for the late-stage diversification of purines with numerous biorelevant scaffolds, for instance with peptides, nucleosides, glycosides, drug molecules and lipids. Thus, the mildness of this catalytic approach could be highlighted in an ample scope, while the previous procedures required elevated temperatures of 100–120 °C.

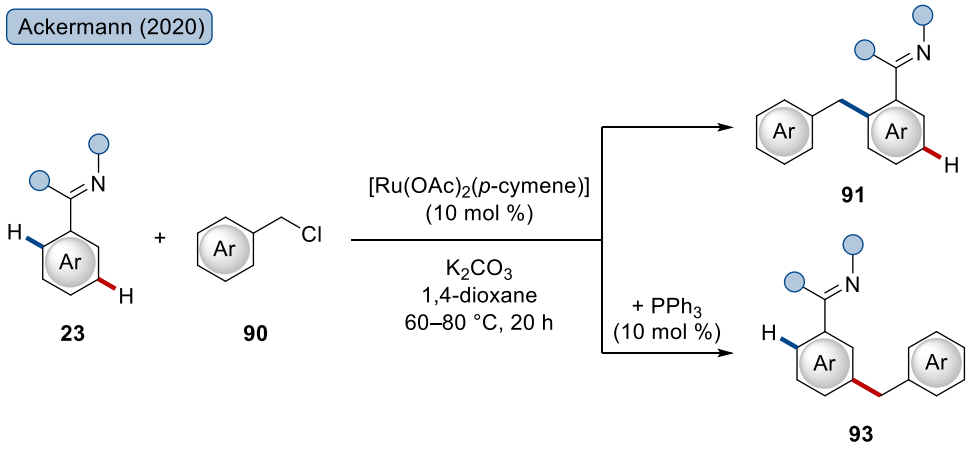

Scheme 1.31: Selectivity switch in ruthenium-catalyzed benzylation of arenes **23** by PPh_3.

1.4 C–H Activation Reactions with other Metals

1.4.1 Rhodium-Catalyzed C–H Activation of Carboxylic Acids and Amides

The use of rhodium in organic synthesis can at least be traced back to the 1960s with the introduction of the Wilkinson catalyst.[98] The importance of this homogeneous metal catalysis, which is a generally employed method in hydrogenation, hydroformylation and hydrosilylation, was appreciated with a Nobel Prize in Chemistry attributed to G. Wilkinson in the 1973.[4] Despite the fact that rhodium was early recognized as a powerful transition metal, its diverse utilization in C–H activation chemistry remained underexplored until twenty years ago.[99]

The pioneering work from Kim and Kang in 1994 set the stage for directing group-assisted *ortho*-selective C–H activation.[100] They reported on the alkylation of phenylpyridine **95** with terminal olefins **16** enabled by the Wilkinson catalyst, albeit with long reaction times up to 144 h (Scheme 1.32).

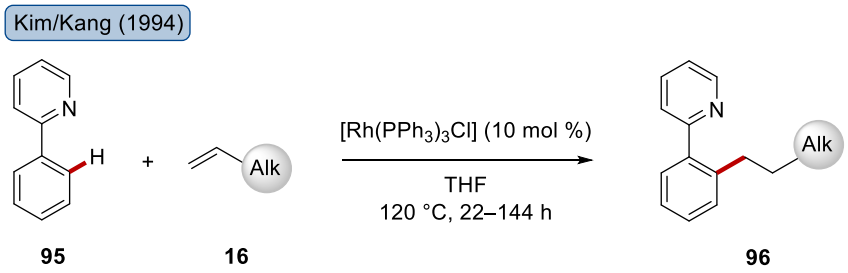

Scheme 1.32: Pioneering work on rhodium-catalyzed alkylation by chelation assistance.

Afterwards, a multitude of rhodium-catalyzed C–H activations has been realized. Among those, arylations and alkenylations usually follow an oxidative addition pathway to rhodium(I).[101] Matsumoto described the oxidative olefination of arenes by a rhodium catalysis regime.[102] Styrene could be accessed by employing different rhodium catalysts, such as $[Rh(ppy)_2(OAc)]$, $[Cp^*RhCl_2]_2$ or $[Cp^*Rh(acac)]_2(BF_4)_2$. In this reaction, O_2 and $Cu(OAc)_2$ served as the terminal oxidant, thereby representing a rare example for the rhodium-catalyzed, oxidative couplings of simple arenes with alkenes, while later examples focus on the modification of arenes bearing a chelating moiety. However, despite this early contribution, oxidative transformations remained rare until 2007 with a seminal work from Miura (Scheme 1.33).[103] He developed a rhodium-catalyzed modification of benzoic acids **83** through annulation with alkynes **97** or acrylates **99**, resulting in isocoumarins **98** and phthalides **100**. Later, these transformations were realized with less expensive ruthenium catalysts.[104]

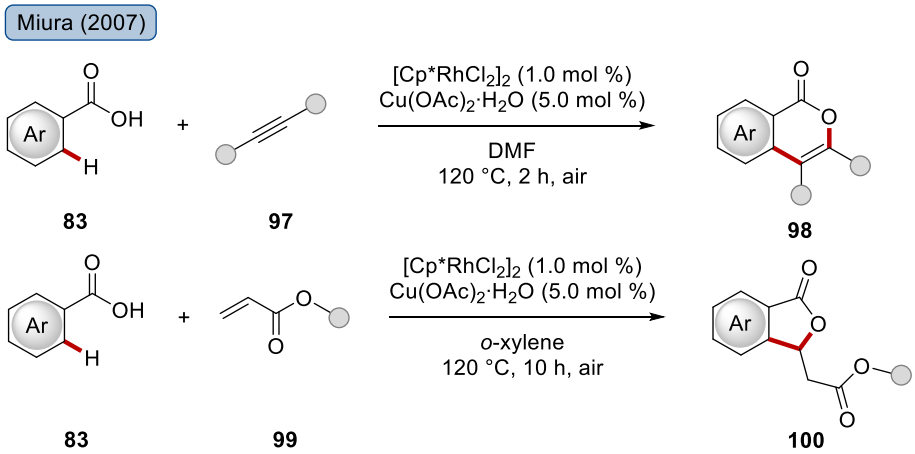

Scheme 1.33: Rhodium(III)-catalyzed annulation of benzoic acids **83** with alkynes **97** and acrylates **99**.

Miura also proposed a mechanistic scenario (Scheme 1.34).[103] In contrast to the previously reported rhodium(I) catalysis, this annulation reaction was suggested to proceed through a redox-neutral electrophilic substitution pathway on rhodium(III). Starting from rhodium(III)

species **101**, coordination of the arene substrate **83** leads to formation of a rhodacycle **103** by *ortho*-C–H activation. Coordination of the alkyne **97** and migratory insertion results in the formation of the seven-membered intermediate **104**, which generates rhodium(I) complex **105** after reductive elimination of the annulated product **98**. Subsequently, the reoxidation to rhodium(III) was ensured by the use of copper(II) in catalytic amounts with oxygen as terminal oxidant. The formation of such a seven-membered rhoda-species as intermediate was confirmed by Jones with crystal structures of stoichiometric reactions with a related system.[105]

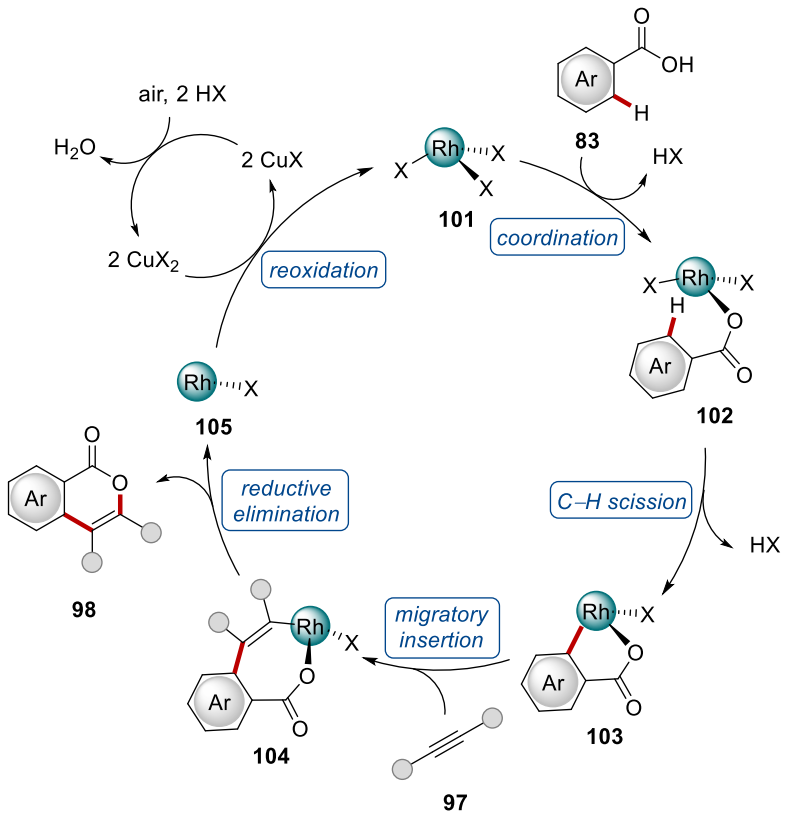

Scheme 1.34: Proposed mechanism for rhodium(III)-catalyzed annulation of aromatic acids.

Based on this oxidative rhodium(III) approach, a plethora of molecular transformations was achieved. Taking the advantages of C–C, C–N and C–O bond formations by rhodium catalysis into account, methods for the efficient construction of a variety of valuable heterocyclic architectures were developed.[99] Fagnou reported the synthesis of indole scaffolds **107** by exploiting the rhodium-mediated annulation approach using acetanilides **106** as the starting material (Scheme 1.35a).[106] The efficacy of the rhodium catalysis was strongly increased by the addition of $AgSbF_6$ as additive. In contrast to Miura's work, the reaction was performed under inert atmosphere with a copper(II) oxidant in stoichiometric amounts. Later, the efficient synthesis of isoquinolines **109** was likewise illustrated by the same group, this time with a cationic rhodium species as the catalyst (Scheme 1.35b).[107]

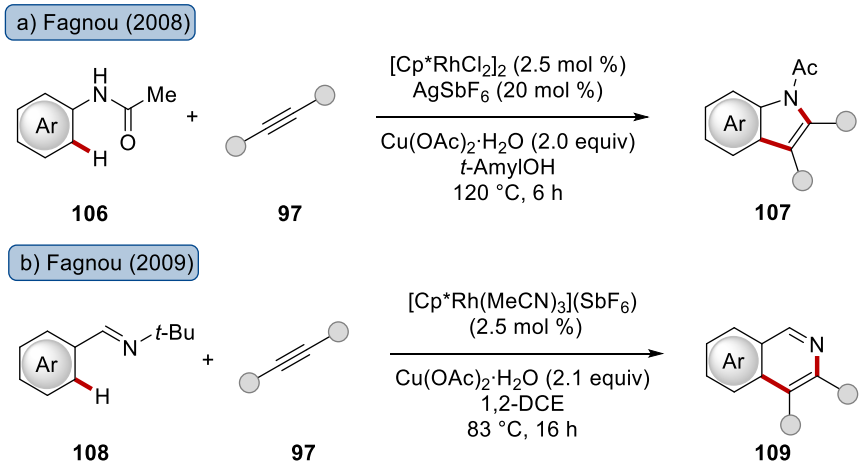

Scheme 1.35: Heterocycle synthesis by rhodium-catalyzed alkyne annulation.

In the following years, the chelation assistance could be expanded to imines[108] and naphthols.[109] Likewise, the applicability of *N*-heterocyclic directing groups was successfully demonstrated, using phenylpyrazoles,[110] phenylindoles[111] and benzoxazoles,[112] which allowed the construction of expanded π-systems with potential application as fluorescent labels.

In addition to the use of carboxylates, the use of benzamides as directing groups was disclosed by Miura[113] and Rovis[114] in independent contributions. The annulation of alkynes **97** by amides **110** was achieved by Miura for both, free *N*H and *N*-arylated benzamides **110** by rhodium(III) catalysis (Scheme 1.36a). In contrast, Rovis focused on *N*-alkylated and *N*-benzylated amides as well as the annulation of heteroarene amides as substrates under slightly different reaction conditions (Scheme 1.36b).

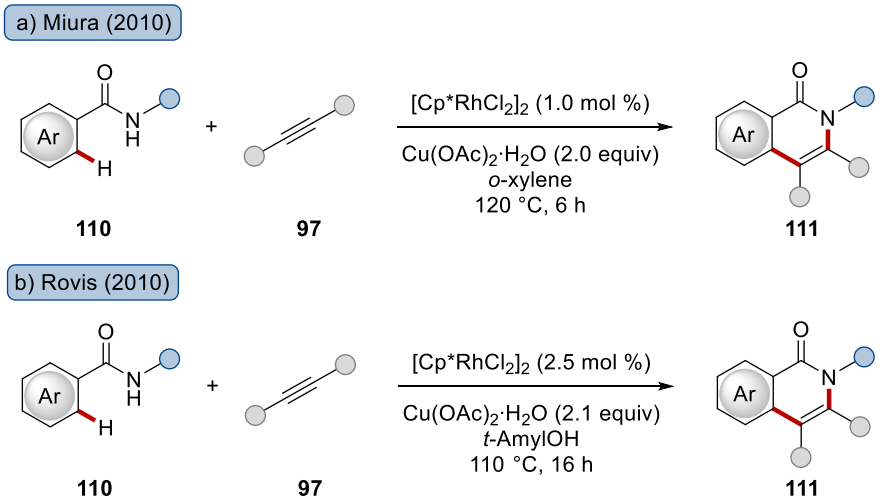

Scheme 1.36: Alkyne annulation of benzamides **110** by rhodium(III) catalysis approach.

Apart from the annulation of diverse arenes, olefination reactions were studied by means of rhodium(III) catalysis. Glorius reported on the Fujiwara-Moritani reaction of acetanilides **112**

with activated olefins, more precisely acrylates **99** and styrenes **113**, in 2011 (Scheme 1.37a).[115] As seen in Fagnou's synthesis of indoles from acetanilides, the use of $AgSbF_6$ as an additive was beneficial for efficient catalysis. Shortly after, the same group expanded their work of rhodium-catalyzed olefinations to other chelation-assisting scaffolds, such as ketones **15** and benzamides **110** (Scheme 1.37b).[116]

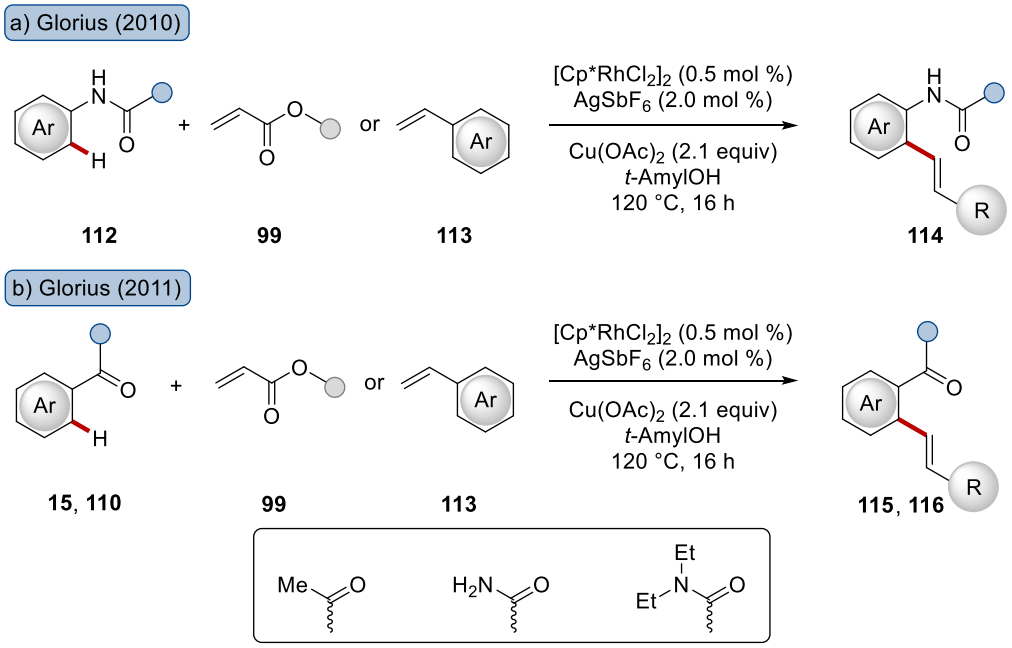

Scheme 1.37: Rhodium-catalyzed olefination reactions.

1.4.2 Manganese-Catalyzed C–H Activation

After titanium and iron, manganese is the third most abundant metal in the earth's crust, and it is also an important element in bioinorganic chemistry.[8a] This is highlighted by the fact, that this metal is part of the catalytic center in many enzymes, with manganese-superoxide dismutase as the most prominent one. Thus, manganese plays an important role in the metabolism and is classified as essential trace element for humans.[117] The use of manganese catalysts is highly attractive, not only because of its high abundancy in nature, but also because of its low toxicity.[34c, 118] With this in mind, it is understandable why the use of earth-abundant 3d-metals and especially manganese has gained significant momentum in C–H activation chemistry. Besides outer-sphere C–H functionalizations, which were often achieved by mimicking enzymes and have been applied to a plethora of chemical transformations,[119] many manganese(I)-mediated organometallic C–H activations were developed to afford C–C bond constructions, as illustrated with a few selected examples in the following section.

Groundbreaking work was presented by Bruce and Stone in 1970, in which they disclosed the stoichiometric synthesis of the cyclometalated manganese complex of azobenzene **117** through C–H activation with the manganese(I) complex [$MnMe(CO)_5$] or manganese(0) source $Mn_2(CO)_{10}$ (Scheme 1.38).[120] Afterwards, several contributions focused on the preparation of related *ortho*-metalated complexes and their investigation in stoichiometric reactions.[121]

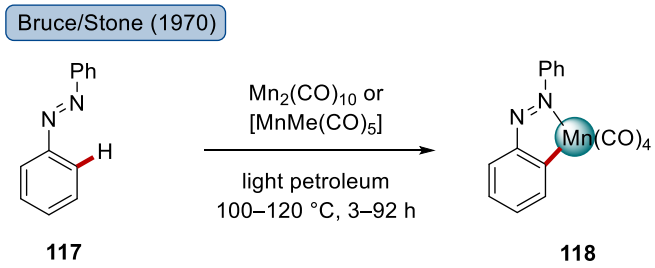

Scheme 1.38: *ortho*-Manganated cyclometalated complex **118** through C–H activation.

After this early contribution, it took almost forty years, until Kuninobu and Takai presented in their seminal work the first C–H activation with manganese in a catalytic manner.[122] The use of $MnBr(CO_5)$ or $Mn_2(CO)_{10}$ as catalyst allowed the *ortho*-functionalization of phenylimidazoles **119** with aromatic aldehydes **120** to provide access to silylethers **121** (Scheme 1.39). Interestingly, the addition of triethylsilane was indispensable to ensure catalytic turnover. Control experiments with stoichiometric amounts of manganese explained this effect by a hydrosilane-promoted reductive elimination in this Mn(I)/Mn(III) catalytic process.

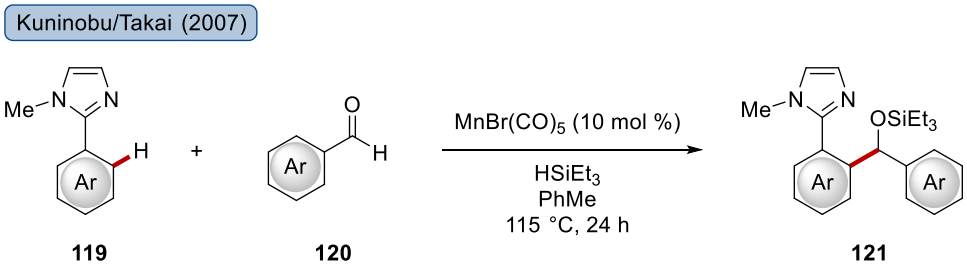

Scheme 1.39: First catalytic C–H activation with manganese.

Encouraged by this addition-type reactivity, further C–C bond forming transformations were disclosed by different groups. Several of these contributions identified the use of alkynes as suitable substrates. Wang reported on the manganese(I)-catalyzed hydroarylation of arenes **23** with terminal alkynes **122** (Scheme 1.40a).[123] An efficient synthesis of substituted alkenes **123** was enabled by $MnBr(CO)_5$ as catalyst together with substoichiometric amounts of a secondary amine base. It was proposed that a manganese-alkynyl complex was formed under these reaction conditions. Detailed computational studies were performed on related catalytic systems, being indicative of a base-promoted C–H activation manifold enabled by ligand-to-

ligand hydrogen transfer.[124] Thereafter, Lei and Li applied this approach on internal alkynes **97** with a carboxylic acid additive, which allowed for efficient construction of substituted indoles **125** (Scheme 1.40b).[125] It is noteworthy, that in the absence of the acid additive, a heterocyclic carbazole was obtained as product by the reaction with two alkyne molecules.

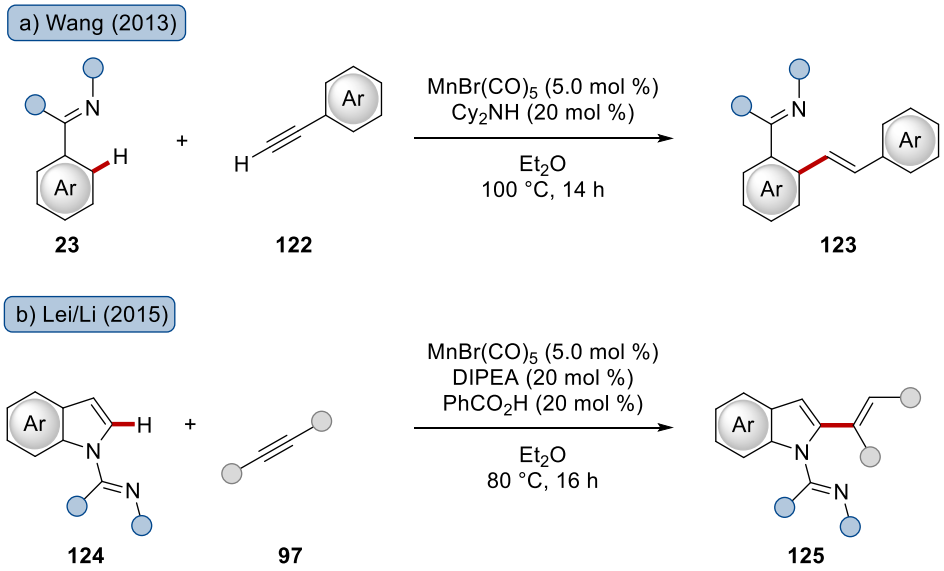

Scheme 1.40: Manganese(I)-catalyzed C–C bond formation with terminal and internal alkynes **122** and **97**.

In contrast, alkynylated indoles **127** were obtained by using bromo alkynes **126** as coupling partner, nicely illustrated by Ackermann (Scheme 1.41).[126] During the optimization of the reaction conditions, a strongly enhancing effect of the catalytic efficacy was observed by the addition of BPh_3, which was assumed to accelerate the key *β*-bromide elimination. Remarkably, this system was not only restricted to indoles but was similarly applicable to protected tryptophan derivatives and small peptides with a remarkable functional group tolerance, including azides and *NH*-free indoles under slightly modified reaction conditions. Even a cyclic peptide could be accessed by following this strategy.

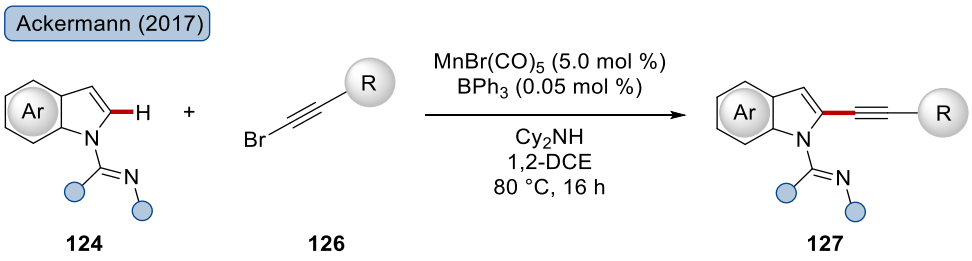

Scheme 1.41: Manganese-catalyzed alkynylation of indole **127**.

Based on this pioneering work on manganese-catalyzed peptide modification, this field was further investigated in later reports, and a protocol for tryptophan modification with terminal alkyne-containing BODIPY-labels as well as cyclization reactions to afford cyclic peptides, was presented by the same group.[127] Additionally, carborane-labelling of amino acids and peptides was achieved by manganese-catalyzed C–H activation with alkynylated carboranes as terminal alkynes.[128]

The modification of arenes by a manganese catalysis regime was not limited to alkynes. *Ortho*-allylations of different arenes were realized as well to address the limitation to an addition-type reactivity to multiple bonds. Ackermann accounted for an unprecedented substitutive allylation with $MnBr(CO)_5$ and NaOAc as catalyst system to convert transformable ketimines and indoles bearing *N*-heteroarenes for chelation assistance into the desired allyl compounds **130** or **131** upon reaction with allyl carbonate **128** or **129** (Scheme 1.42).[129]

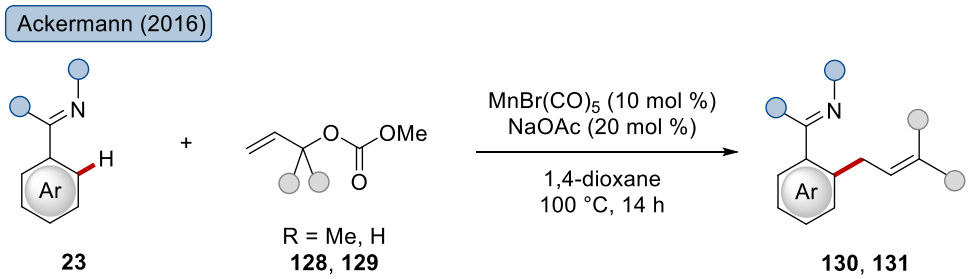

Scheme 1.42: Manganese-catalyzed allylation with allylmethyl carbonates **128** and **129**.

Mechanistic experiments were performed to investigate the mode of action, which was rationalized in the proposed catalytic cycle (Scheme 1.43). Starting from the manganese(I)-acetate species **132**, the turnover is initiated by coordination of the arene substrate **23**, followed by reversible base-assisted C–H bond cleavage to furnish the cyclometalated manganese intermediate **134**. Subsequently, allyl carbonate **129** is coordinated, thereby generating the manganacomplex **135**. Insertion of the allyl species **129** causes the formation of the new C–C bond as illustrated in intermediate **136**. Subsequent *β*-hydrogen elimination provides the allylation product **131** accompanied with CO_2 and MeOH evolution, while the coordination of CO and acetic acid regenerate the initial $Mn(OAc)(CO)_5$ species **132**.

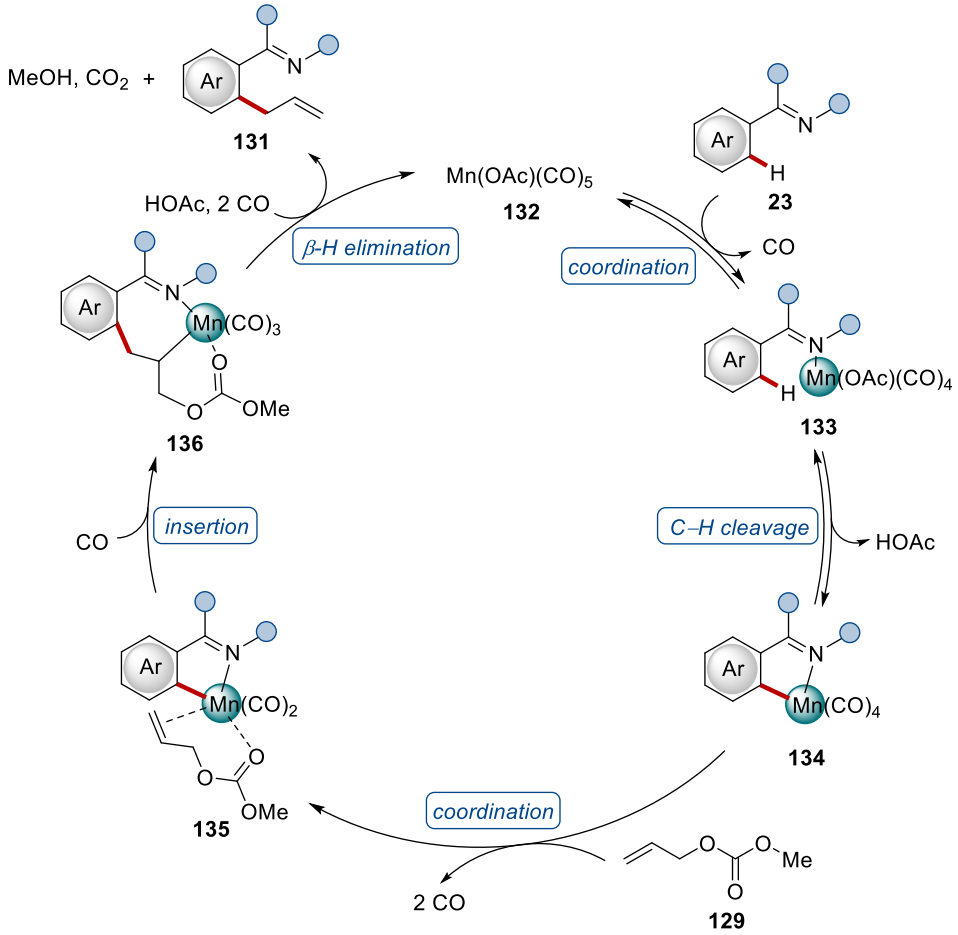

Scheme 1.43: Proposed mechanistic scenario for the manganese-mediated allylation with allyl carbonate **129**.

1.5 UNDIRECTED C–H FUNCTIONALIZATION

As previously discussed, transition metal-catalyzed C–H activation has evolved into a powerful tool in molecular synthesis, especially with enormous relevance for the modification of arenes. To ensure the transformation of complex architectures with good chemoselectivity, certain challenges need to be met with respect to the substrates. Aside from the prevalent approach to employ Lewis-basic directing groups for guidance of the metal catalyst, undirected methodologies have been developed. Usually, the selectivity is determined by inherent electronic or steric properties of the substrate, causing an "innate reactivity".[130]

A groundbreaking example made for a transition metal-med undirected transformation is the undirected olefination of arenes developed by Fujiwara and Moritani (Scheme 1.44).[131] The undirected transformation of arenes **137**, such as benzene or toluene, was realized with styrene derivatives **138** to furnish the *trans*-stilbene **139**. Gratifyingly, also ethylene could be

successfully employed, yielding predominantly *trans*-stilbene after a two-fold arylation, accompanied by minor amounts of styrene.

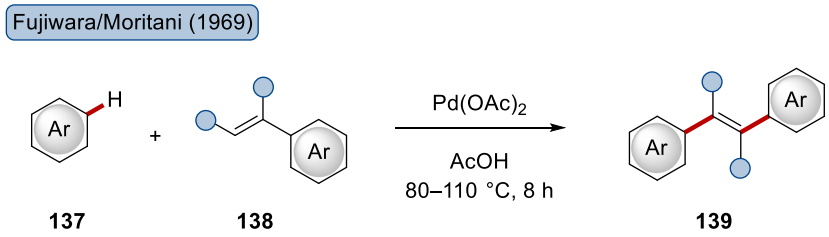

Scheme 1.44: Palladium-mediated undirected olefination by Fujiwara and Moritani.

Beside transition metal-enabled C–H functionalization reactions, many transformations involving free radicals are a prominent example for the undirected functionalization in metal-free or metal-mediated transformations.[132] The incorporation of trifluoromethyl moieties should be mentioned here as an important modification, which is usually achieved in an undirected manner.

1.5.1 Trifluoromethylation Reactions

Many pharmaceutical drugs are substituted with trifluoromethyl substituents, as they render interesting stereoelectronic properties. Trifluoromethyl groups possess a steric demand lying between the one of methyl- and *tert*-butyl groups, an electronegativity comparable to the one of oxygen and a high lipophilicity.[133] These interesting features make them highly attractive due to increased bioavailabilities or improved biological activities, which explains their exploitation in drug design.[134] Besides the addition of a trifluoromethyl radical to double and triple bonds, C–CF_3 bond constructions can be achieved *via* electrophilic or nucleophilic pathways, but also *via* a radical mechanism.[133] Although many reports focus on the trifluoromethylation of aliphatic C(sp^3) centers,[135] the following section refers to the modification of arenes and heteroarenes by presenting selected examples.[136]

The synthesis of electrophilic trifluoromethylating reagents was for a long time associated with certain challenges owing to an unfavored distribution of the charge.[133] However, several compounds have been developed with pioneering studies by Yagupolskii on different trifluoromethyl chalcogen salts.[133, 137] In continuation of this approach, Umemoto developed the dibenzothiophene-based reactive electrophilic trifluoromethylating reagent **141**, which enabled functionalization of different arenes, such as aniline (**140**) (Scheme 1.45).[138] Moreover, pyrrole was identified as a suitable substrate, thereby demonstrating the applicability

to electron-rich heterocycles. Inspired by this seminal work, other trifluoromethylating reagents were developed, such as the diarylsulfonium salts employed by Shreeve a few years later.[139]

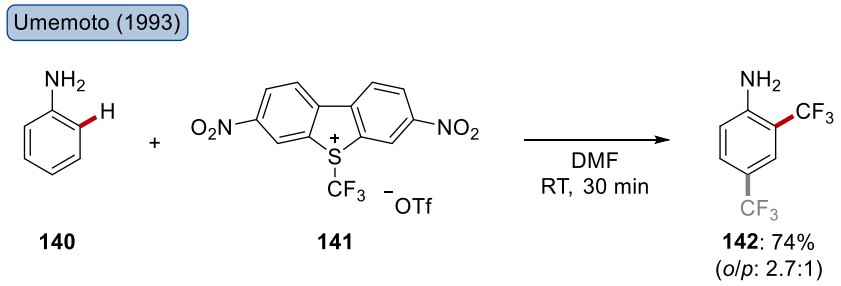

Scheme 1.45: Electrophilic trifluoromethylation with trifluoromethyl chalcogen salts.

The other important class of electrophilic trifluoromethane sources are hypervalent iodine species introduced by Togni in the 2000s,[140] which tend to be more reactive than the chalogen salts.[133] Phenolates **143** were efficiently reacted to the corresponding trifluoromethylated products **145** and **145'** by treatment with this stable and non-explosive reagent (Scheme 1.46). Moreover, this robust reagent allowed for the efficient coupling of trifluoromethyl groups to different heteroarenes, which was further analyzed by the same group subsequently.[141]

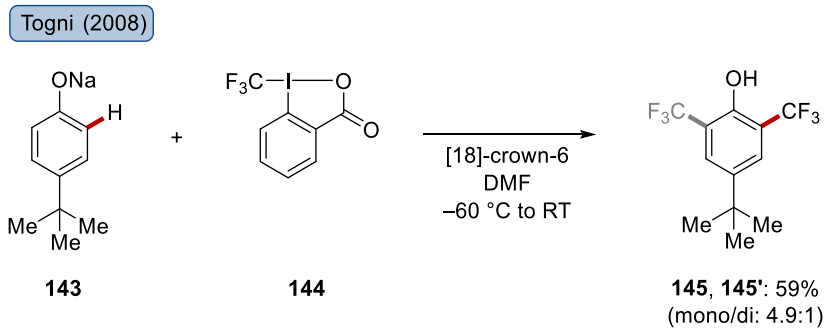

Scheme 1.46: Trifluoromethylation of phenolate **143** with hypervalent iodine reagent **144**.

In contrast to the rather recent field of electrophilic trifluoromethlyations, the nucleophilic approach was for a long time the prevalent strategy. In many cases, these transformations of aryl halides necessitate a metal, predominantly copper,[142] which allows the incorporation of valuable trifluoromethyl moieties in (hetero-)arenes with different reagents. An early example for this copper-mediated reactivity employed trifluoromethyl iodide **146** as the trifluoromethyl source, which was *in situ* converted by stoichiometric amounts of copper to $CuCF_3$. Subsequently, this enabled the transformation of aryl halides **82**, as reported by Thrower and Kumadaki in independent studies (Scheme 1.47a).[143] As this reagent is gaseous at ambient temperature, the development of more easy-to-handle alternatives was highly desirable. In

contrast, the liquid trifluoromethyltrialkylsilyl reagent **148** turned out to efficiently allow for the modification of arenes **84** with good efficacy (Scheme 1.47b).[144] Based on this strategy, a catalytic trifluoromethylation was realized by Beller later.[145] In addition, sodium trifluoroacetate was identified as a convenient reagent, which enabled not only the functionalization with stoichiometric amounts of copper(I) iodide,[146] but likewise in a catalytic manner, as illustrated in 2011 by Li and Duan for aryl iodides **84** with Ag_2O as a promotor (Scheme 1.47c).[147]

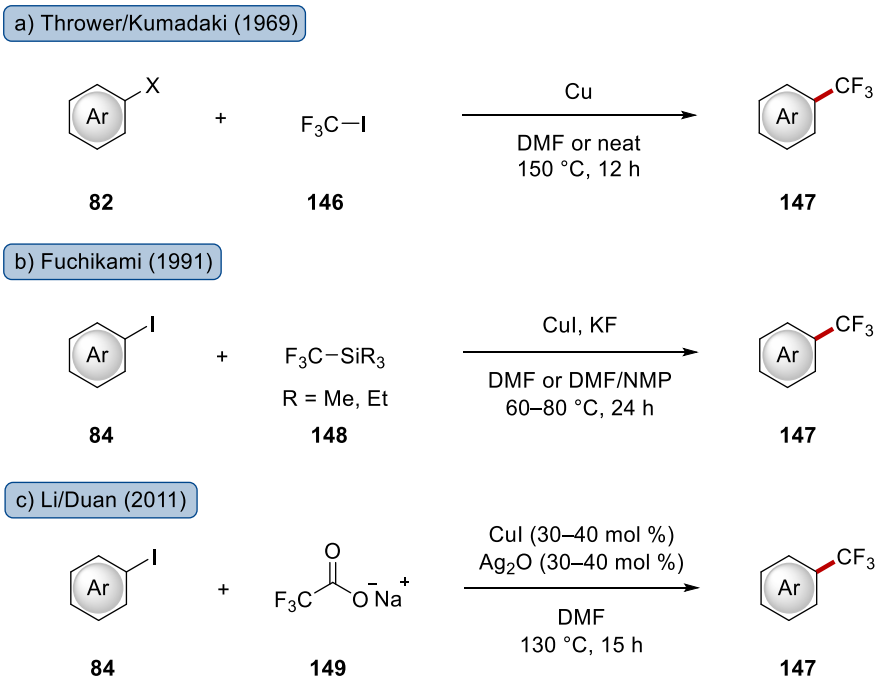

Scheme 1.47: Selected examples of copper-mediated trifluoromethylation of arenes **82** and **84**.

Expanding these approaches, especially C–H trifluoromethylations following a radical pathway have a great impact. These have been achieved with a multitude of different fluorinating reagents, among those reactions with the previously introduced Umemoto and Togni reagents **141** and **145**.[135a] A few selected examples will provide an insight into the radical trifluoromethylation with different strategies to realize the undirected functionalization by modifying C–H bonds without the necessity of prefunctionalized arenes, such as the aryl halides in case of electrophilic trifluoromethylations.

One strategy for these radical trifluoromethylations consists in transition metal-catalyzed reactions. Greaney disclosed a silver-mediated system for the modification of arenes **137** with $TMSCF_3$ (**150**) (Scheme 1.48a).[148] This versatile procedure was well appropriate to transform

different (hetero-)arenes at room temperature, such as pyrrole, furane or thiophenes. Based on mechanistic experimentations, the authors proposed that a trifluoromethyl radical is generated in the presence of the silver(I) salt and (diacetoxyiodo)benzene (PIDA). In contrast, AgF alone was not sufficiently oxidizing to form the trifluoromethyl radical, while PIDA was moderately effective. Moreover, the electrophilic Togni reagent proved to be inefficient, thereby ruling out a S_EAr mechanism. Beller achieved the palladium-catalyzed trifluoromethylation of arenes **137** with trifluoromethyl bromide **151** (Scheme 1.48b).[149] Essential to obtain good conversions was here the addition of TEMPO, which was explained with its ability to serve as single-electron reducing and oxidizing agent. The palladium catalyst enabled the homolytic cleavage of the C–Br bond under formation of the electrophilic trifluoromethyl radical.

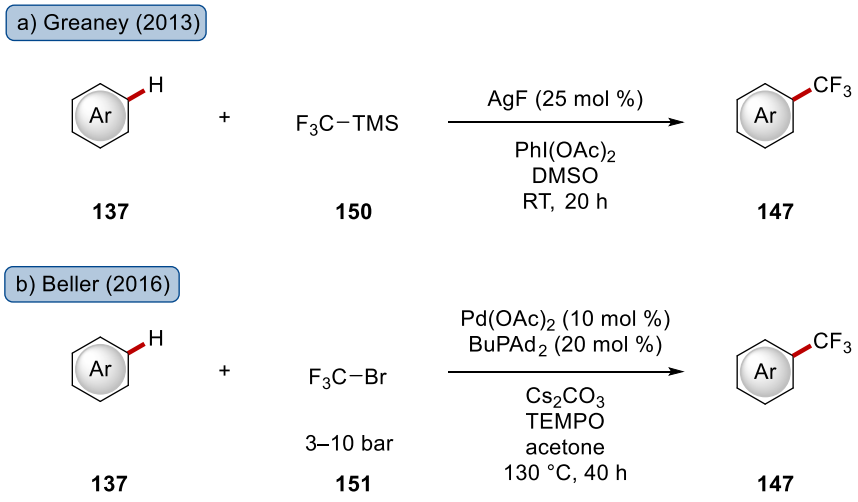

Scheme 1.48: Examples for metal-catalyzed trifluoromethylations with a radical mechanism.

Besides these metal-catalyzed systems, further research was focused on the employment of other CF_3-sources, which allow for radical functionalization of (hetero-)arenes by omitting transition metals, such as for example also trifluoromethylated thianthrene triflate ($TT–CF_3^+OTf^-$), which was recently introduced by Ritter for efficient trifluoromethylation of aryl boronic acids.[150] More desirable is the direct modification of ubiquitous C–H bonds without prefunctionalization. Langlois firstly introduced sodium trifluoromethylsulfinate (**153**) as a powerful trifluoromethyl precursor for the modification of electron-rich arenes, *e.g.* phenol, anisol or aniline under oxidative conditions (Scheme 1.49a).[151] Due to its beneficial properties, such as being non-explosive, easy to handle, bench-stable and cost-efficient, the use of this reagent was further investigated, and Baran highlighted its suitability to decorate a broad range of different valuable heteroarenes (Scheme 1.49b).[152] After extensive screening, *tert*-butylperoxide was identified as the optimal oxidant, which was suggested to fragment into

tert-butoxy radicals. Those induce the formation of trifluoromethyl radicals being subsequently captured by the heteroarene **155**. The reaction conditions were applicable to an ample scope, including several different architectures associated with biological activity. In continuation of this work, Baran developed the zinc sulfinate salt **156**, which enabled the functionalization of different *N*-containing heterocycles.[153] Inspired by these contributions, the advantageous Langlois reagent (**153**) was employed in numerous trifluoromethylation procedures following a radical pathway.[154]

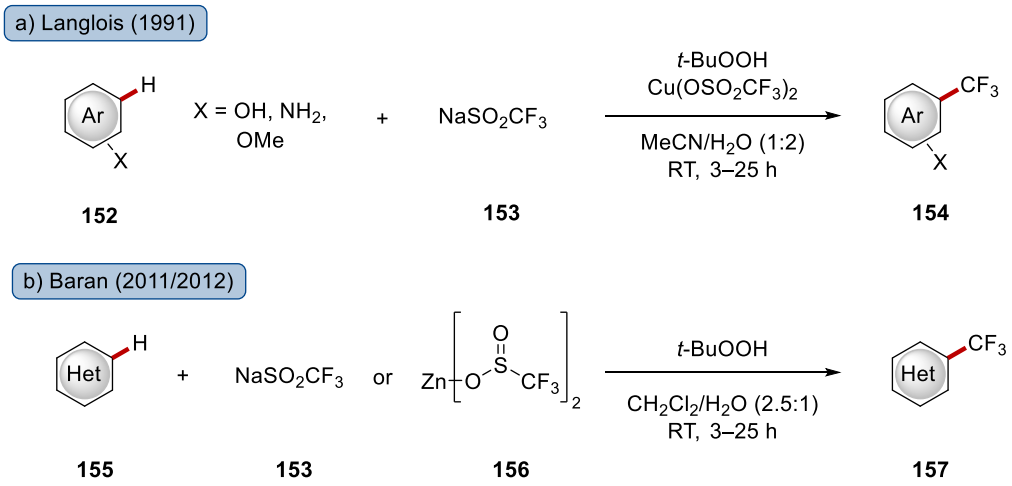

Scheme 1.49: Radical trifluoromethylation with Langlois reagents under catalyst-free conditions.

Apart from a chemical radical initiator, the use of visible light[155] and electricity[156] as external stimuli were identified as suitable methods to modify arenes by incorporating a trifluoromethyl substituent with a multitude of different reagents. Also an electrophotocatalytic procedure was accomplished.[157]

In addition to many undirected trifluoromethylation procedures, a directed methodology in palladium catalysis regime was reported by Yu, who relied on the C–H activation strategy.[158] The *ortho*-selective modification of diverse arenes **23** was achieved by chelating assistance with different heterocyclic scaffolds (Scheme 1.50). The electrophilic Umemoto reagent **158** led to excellent conversions with $Pd(OAc)_2$ as the catalyst, while the addition of TFA strongly enhanced the reactivity. Likewise, the use of $Cu(OAc)_2$, which was proposed on the one hand to act as an oxidant for regeneration of the palladium(II) species, but on the other hand also as a Lewis acid for the sulfur, was beneficial in this catalytic system, albeit the role was not fully understood. Subsequently, the same group developed *ortho*-trifluoromethylations of

benzamides[159] and benzylamines[160] by a palladium(II)/palladium(IV) manifold, as well as copper-catalyzed trifluoromethylations of benzamides.[161] In addition, Bräse contributed with an early example on directed trifluoromethylation of azides by employing a silver catalyst.[162]

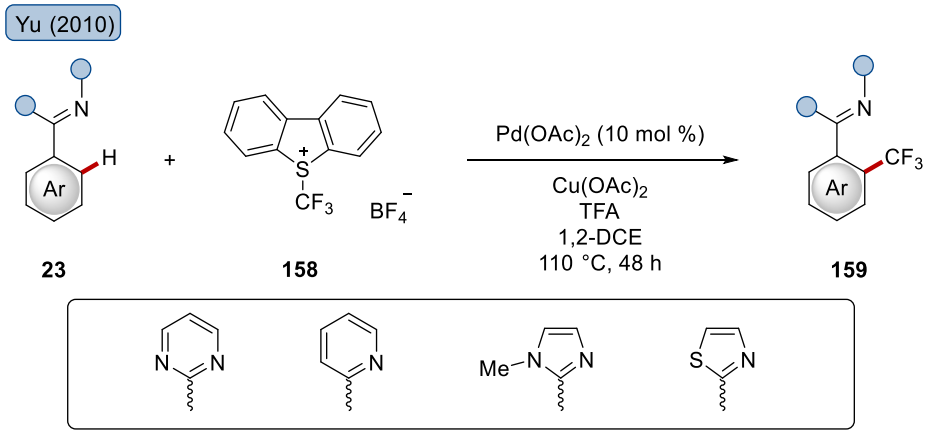

Scheme 1.50: *ortho*-Directed trifluoromethylation by palladium-catalyzed C–H activation.

1.6 SUSTAINABLE STRATEGIES IN C–H ACTIVATION

In order to circumvent the previously disclosed classical reaction design of thermal heating, innovative approaches have emerged in the past decades. Thus, they expand the possibilities for synthetic chemists as useful and sustainable approaches for the functionalization of ubiquitous C–H bonds, thereby being in good agreement with the '12 Principles of Green Chemistry'. The use of abundant visible light[163] as well as electric current[22b, 164] have matured to become attractive alternatives with numerous advantages and opportunities. More recently, the combination of photoredox chemistry and electrocatalysis has gained considerable attention.[165] These new strategies will be introduced with a brief discussion of selected examples.

1.6.1 Electrochemical C–H Activation

The use of electric current in organic synthesis has a long history in chemistry. The first electrochemical transformations can be traced back to Faraday, who attempted the first electrochemical electron transfer reactions.[166] Kolbe studied this in greater detail and proposed an electrochemical oxidative quasi dimerization of carboxylates through radical recombination to access **163** (Scheme 1.51).[167] These radicals were generated through anodic oxidation followed by decarboxylation. Despite this early example, the use of electric current remained largely underexplored during the following century. After being identified as a powerful and

environmentally-benign alternative to chemical oxidants and reductants, this method has experienced a renaissance in organic synthesis during the past two decades.[164, 168]

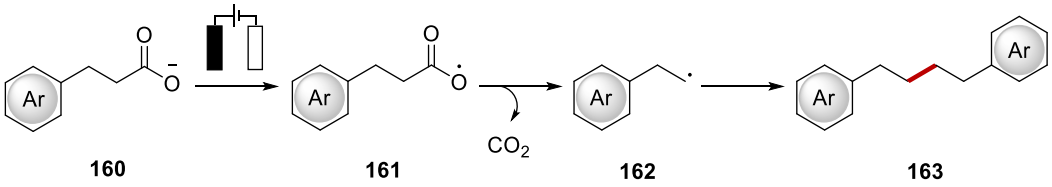

Scheme 1.51: Kolbe electrolysis of carboxylates **160**.

Besides the generation of radicals through electricity, especially the merger with transition metal catalysis has gained significant impact, more precisely in the field of C–H activation.[22b, 169] As uncountable reactions follow an oxidative reaction mechanism, stoichiometric amounts of chemical oxidants, often silver(I) or copper(II) salts, are typically required. Those are not only toxic and expensive, but also cause metal waste in stoichiometric amounts. This diminished sustainability and atom-economy can be addressed by the implementation of electricity as environmentally-benign electron donor. Even more important, the combination of electric current with a transition metal catalyst allows the modification of inert C–H bonds, which can not be directly manipulated under electrochemical conditions (Scheme 1.52). As shown for benzamide **164**, the electrolysis takes place at the most acidic C–H bonds in α-position to the *N*-atom, and treatment with a nucleophile affords product **166**.[170] In contrast, this inherent Shono-type reactivity can be avoided by addition of a transition metal catalyst, which enables an arene functionalization in *ortho*-position of the directing group, thereby illustrating the complementary chemoselectivity of electrosynthesis and electrocatalysis.[171]

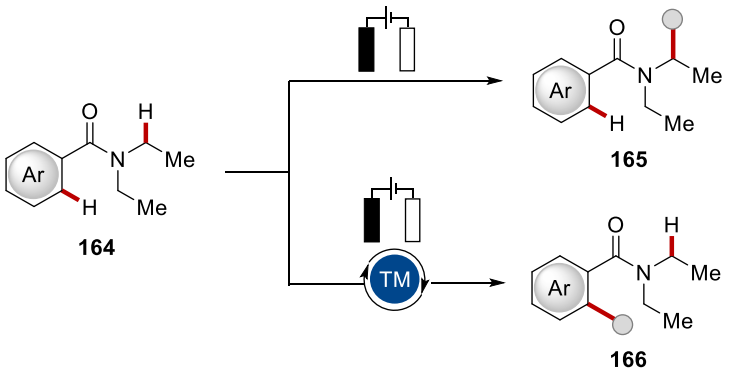

Scheme 1.52: Comparison of inherent electrochemical reactivity and transition metal-mediated electrochemical transformation.

An early and pioneering contribution on metalla-electrocatalyzed C–H activation was reported by Jutand and Amatore in 2007 (Scheme 1.53).[172] They achieved a palladium-catalyzed

Fujiwara-Moritani-type alkenylation of acetanilides **106** with acrylates **99** to obtain the decorated arene **167** as the product. This reaction required a divided cell set-up to avoid deposition of the catalyst on the electrode. By constant current electrolysis (CCE) or constant potential electrolysis (CPE), the catalytic transformation was conducted in the presence of benzoquinone as a redox mediator. This mediator ensured the regeneration of the catalytically active species palladium(II) catalyst after reductive elimination to palladium(0). 5.4 Faraday were employed under CCE conditions at 220 mA, while theoretically 2 Faraday are required.

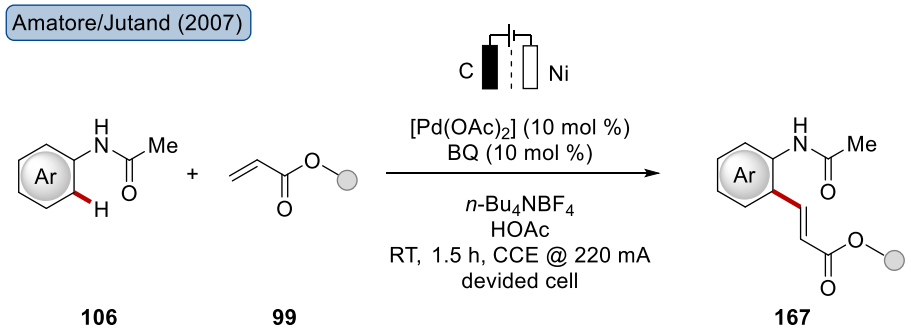

Scheme 1.53: Metalla-electrocatalyzed olefination of acetanilides **167** as pioneering example in C–H activation.

Inspired by this work, remarkable progress towards sustainable C–H activation methodologies was made. After the development of palladium-catalyzed reactions,[173] the concept was applied to other metals with significant contribution from Ackermann. Many recent examples with earth-abundant metals,[174] such as cobalt, manganese, iron and copper, but also with the precious metals ruthenium,[175] rhodium[176] and iridium[177] proved their applicability as catalysts in metalla-electrocatalysis.[178] In the following section, the progress of rhodium-mediated electro-catalyzed will be presented with selected examples.

Ackermann firstly reported in 2018 on an electrochemical, rhodium-catalyzed C–H activation reaction. Benzoic acids **83** were successfully alkenylated with acrylates **99** in a Fujiwara-Moritani-type reaction to phthalides **100** (Scheme 1.54 top).[179] This robust reaction could be conducted in a user-friendly undivided cell set-up without redox mediator and additional electrolyte due to an acetate base in a mixture of *tert*-amyl alcohol and water as solvent system. Primary experimentation indicated that the functionalization of benzamides and indoles is feasible, albeit less efficient. The authors investigated the reaction mechanism, which was summarized in a proposed mechanistic cycle (Scheme 1.54 bottom). The scenario commences with the coordination of the aromatic acid **83** to the rhodium(I) species **168** and C–H scission in a BIES-type manner, hence generating rhodacycle **169**. Subsequently, acrylate substrate **99**

coordinates to the metal center, which undergoes migratory insertion under formation of the seven-membered rhodium complex **171**. Next, the intermediate undergoes *β*-hydride elimination and reductive elimination to form the rhodium(I) sandwich complex **172**. Finally, the key anodic oxidation step of **172** regenerates the active rhodium(III) species, thus highlighting the feasibility of the reoxidation of the homogeneous catalyst, and liberates the product **100**. Moreover, cathodic proton reduction closes the electric cycle, by hydrogen generation in a hydrogen evolution reaction (HER), which was proven as the sole side-product of the reaction.[179]

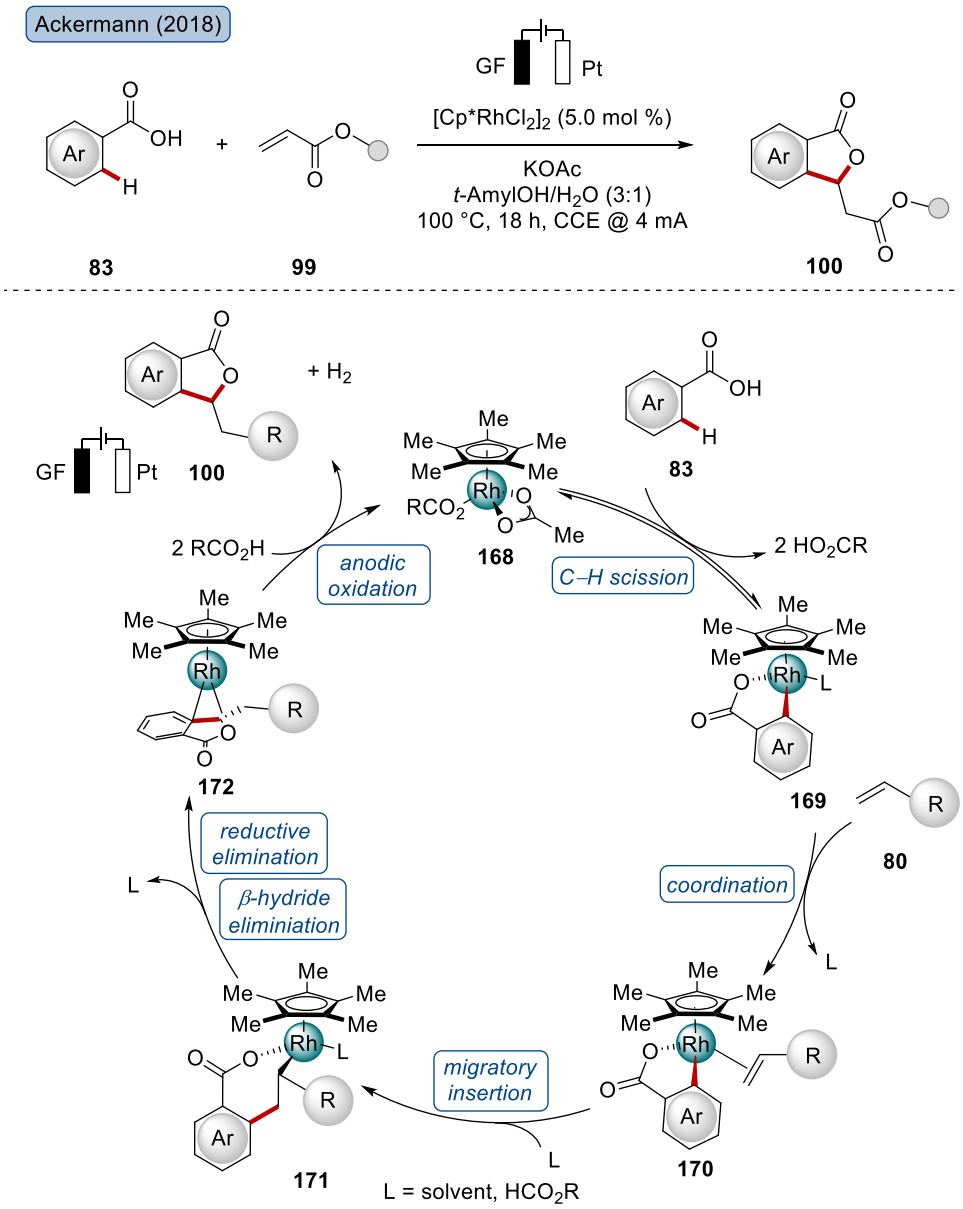

Scheme 1.54: First C–H activation with rhodium under electrochemical conditions with the proposed catalytic cycle.

After this initial report on an electrochemical, rhodium-mediated C–H activation, this concept was expanded to allow for further reactivities. As an early contribution in this field, Ackermann illustrated the broad applicability of rhodium-electrocatalysis in a formal [2+2+2] alkyne annulation of boronic acids **173** with internal alkynes **97** to furnish the construction of polyarenes **174** (Scheme 1.55 top).[180] Remarkably, a comparison of the electrocatalytic conditions to chemical oxidants demonstrated that the use of electric current did not only allow for sustainable conditions, but was much more efficient in product formation. Moreover, the authors could further diversify the products **174** to condensed the polyaromatic scaffolds **175** with extended π-systems in an electrochemical benzoquinone-mediated Scholl reaction (Scheme 1.55 bottom).[180] Subsequently, the same group achieved the synthesis of aza-polycyclic architectures under rhodium catalysis.[181]

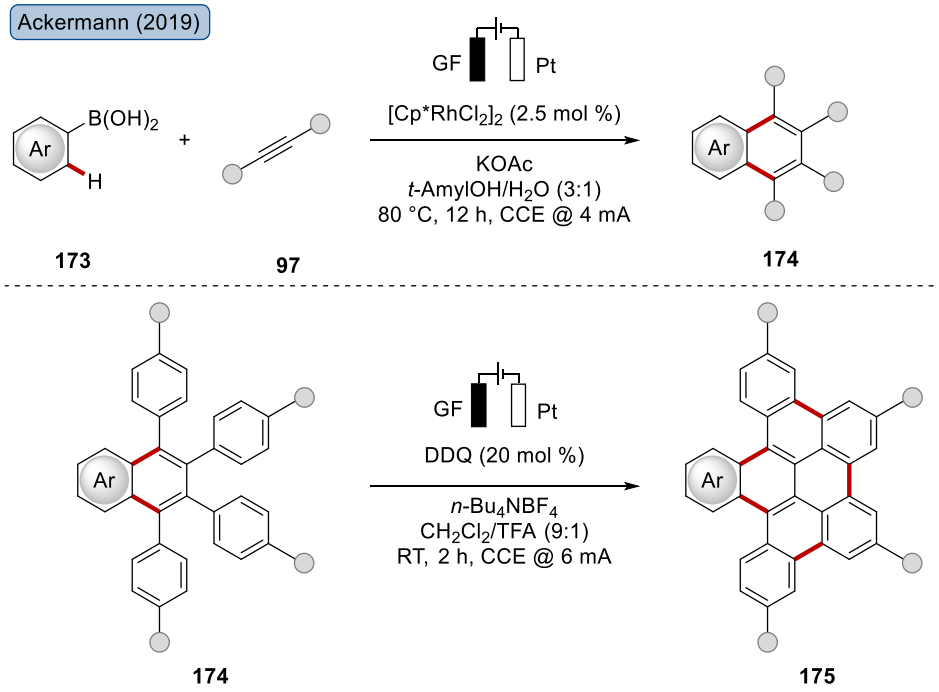

Scheme 1.55: Rhodium-catalyzed alkyne annulation of boronic acids **173** with alkynes **97**.

Furthermore, several examples highlighted the rhodium-mediated synthesis of heterocycles under electrochemical conditions. In a remarkable study, Ackermann realized the inter- and intramolecular annulation of internal alkynes **97** by chelation-assistance of weakly-coordinating imidate-motifs **176** to afford valuable isoquinolines **177** under electro-flow conditions (Scheme 1.56a).[182] Mechanistic experiments with an isolated seven-membered rhodium complex were suggestive of an oxidation-induced reductive elimination manifold being operative. In addition, Mei developed divergent alkyne annulations enabled with acrylamides **178** (Scheme 1.56b).[183] In dependence on the residual moiety on the *N*-atom, the *α,β*-

unsaturated amide **178** was converted into two different products under slightly modified reaction conditions. Either imidates **179** or α-pyridones **180** were obtained by a rhodaelectrocatalyzed manifold. DFT-calculations on this system revealed that a stepwise-ionic reductive elimination pathway is for tosylated substrates more favorable than a neutral concerted pathway, which explains the difference in chemoselectivity.

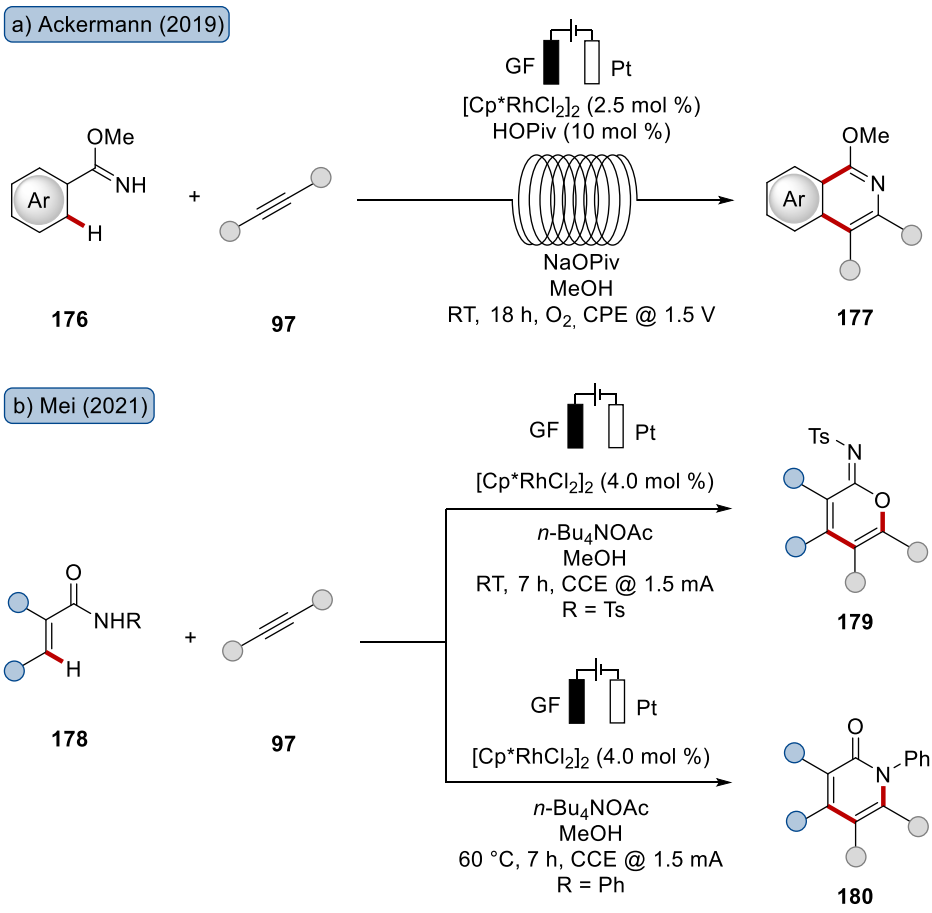

Scheme 1.56: Alkyne annulation reactions by imidates **176** and amides **178**.

Alkyne annulation reactions were likewise exploited for the synthesis of oxygen-containing heterocycles. The construction of challenging seven-membered rings was enabled by alkyne annulation of vinylphenols **181** under rhodaelectrocatalysis, as shown by Ackermann (Scheme 1.57a).[184] Remarkably, this reaction turned out to be generally applicable by tolerating numerous functional groups, and was employed for BODIPY-containing alkynes, thus furnishing fluorescent benzoxepines. Shortly afterwards, the rhodium-catalyzed annulation of hydroxybenzaldehydes **183** with asymmetric and symmetric alkynes **97** was developed to obtain valuable chromone scaffolds **184** (Scheme 1.57b).[177] This versatile electrocatalyzed annulation reaction allowed for modification of **183** with alkynes **97** bearing numerous functional groups in significantly higher yields than with $Cu(OAc)_2$ as the oxidant. Apart from

that, the robust procedure enabled the diversification of amino acids and peptides. A subsequent electrochemical Scholl reaction resulted in π-extended systems, thereby providing access to fluorescent peptide labels.

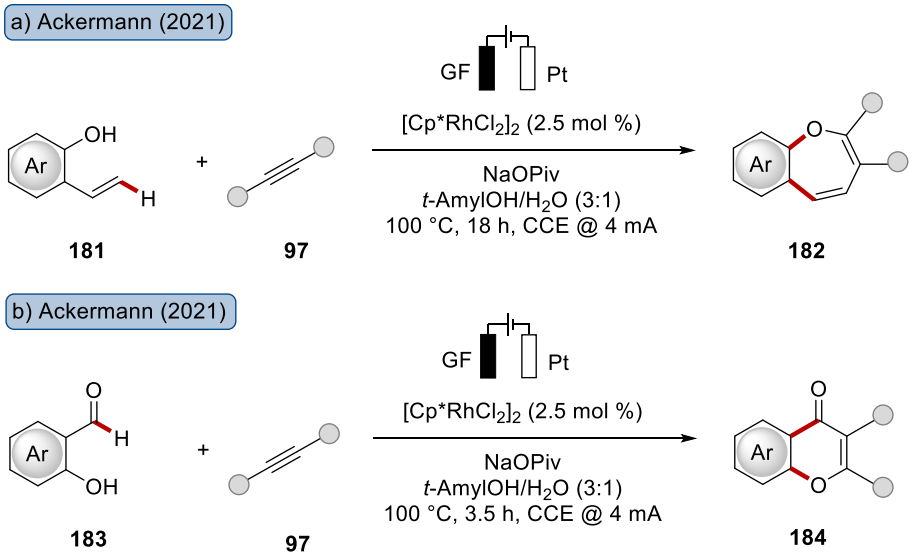

Scheme 1.57: Further rhodium-catalyzed alkyne annulations with C–O bond formation.

Moreover, also the research on C–C bond formations by olefinations was continued to be disclosed under rhodaelectro-catalytic conditions. Ackermann illustrated the C–H functionalization of weakly coordinating naphthols **185** with styrenes **113** to access the olefinated arene **186** (Scheme 1.58).[185]

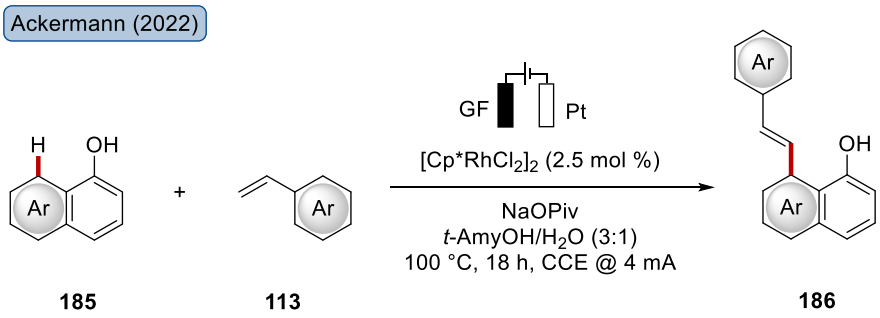

Scheme 1.58: Rhodaelectro-catalyzed alkenylation of naphthols **185**.

1.6.2 Photo-Induced Transition Metal-Catalyzed C–H Functionalization

Many chemical transformations require rather high reaction temperatures to proceed efficiently. Inspired by the photosynthesis in plants, light was recognized as potent and abundant energy source being a renewable alternative to the conventional thermochemical reaction design. Already in the early 20th century, Ciamician illustrated his vision of a chemical production relying on solar energy instead of coal.[186] An early example from Schenck and Ziegler in the

1940s employed chlorophyll as light-harvesting species, which enabled the modification of α-terpinene with molecular oxygen under irradiation of sun light for several days.[187] Since this pioneering work, substantial progress in photoredox chemistry was achieved, and during the last few decades, uncountable procedures were reported, with great impact on the organic synthesis.[163c] Predominantly, an organic dye or a metal complex serves as photosensitizer, which allows for photo-induced single-electron transfer (PET) with subsequent generation of radical species.[188] This concept is generally useful for both, C–C bond and C–Het bond constructions. Within this discussion, the focus will be set on the combination of this strategy with transition metal catalysis and selected examples, in majority directed C–H functionalizations will be discussed.[22c, 163b, 189]

The earliest contribution for the merger of light as external stimulus and traditional metal catalysis consists in a palladium-mediated Sonogashira-Hagihara cross-coupling reported by Akita in 2007 (Scheme 1.59).[190] During their studies, the authors found a remarkable impact of light while using $[Ru(bpy)_3]^{2+}$ as a photocatalyst on the formation of diarlyalkynes **187**. In sharp contrast, only trace amounts of the product were observed in the absence of one of those two elements.

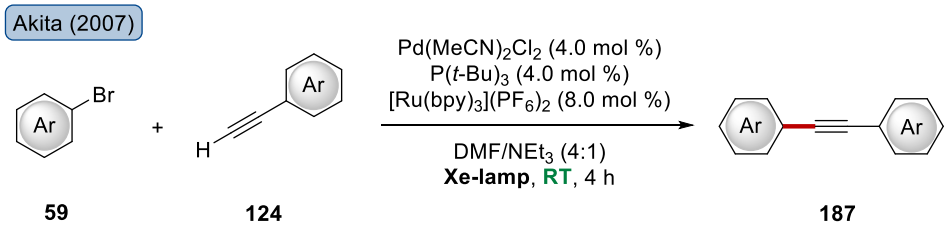

Scheme 1.59: Visible light-induced palladium-catalyzed Sonogashira-Hagihara cross-coupling.

After this seminal contribution, examples for directed C–H activations surfaced and highlighted the mild reaction conditions at room temperature instead of usually harsh conditions frequently seen in C–H activation by classical transition metal catalysis. Sanford reported in 2011 on a C–H activation merged with photoredox catalysis by describing an arylation of arenes **23** with $Pd(OAc)_2$ as mediator (Scheme 1.60 top).[191] The reactivity was enabled by $[Ru(bpy)_3]^{2+}$ under irradiation of visible light by omitting of strong bases. The reaction was not limited to a specific directing group, but was applicable to various chelating substituents. Key to success was the use of the aryldiazonium salt **188** as the arylating reagent, which was known to form aryl radicals by using $[Ru(bpy)_3]^{2+}$.[192] Interestingly, the *ortho*-arylation of arenes **23** proceeded in some cases without the exogenous photosensitizer (Scheme 1.60 bottom). Related transition

metal-catalyzed directed arylations with diazonium salts **188** were later achieved at reaction temperatures of 35 to 60 °C for iridium catalysis[193] and at ambient temperature with a palladium catalyst without light irradiation.[194]

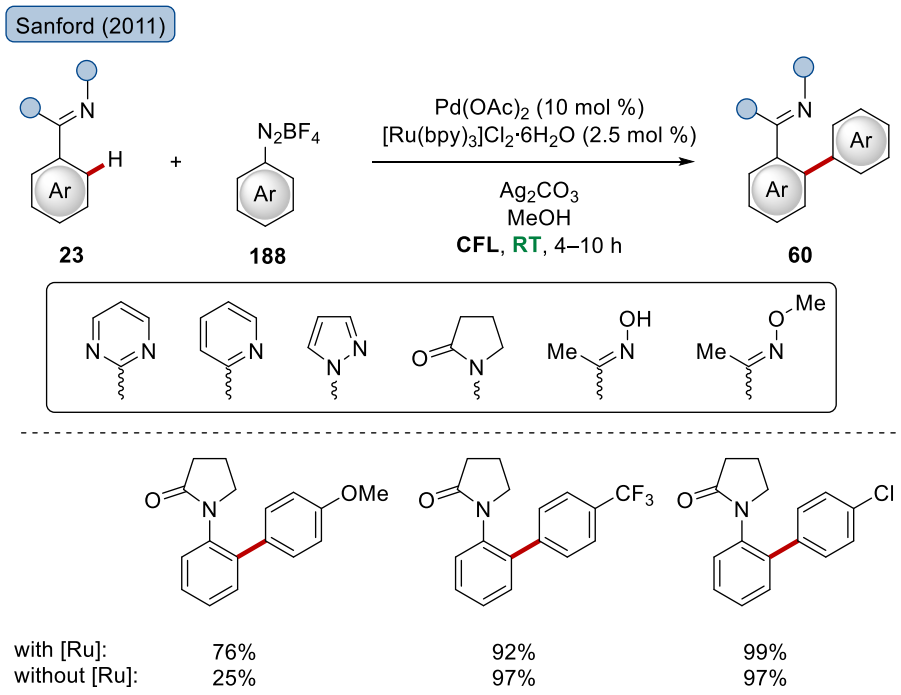

Scheme 1.60: Palladium-catalyzed arylation of arenes **23** with diazonium salts **188**.

Thereafter, other groups reported closely related systems to further demonstrate the synthetic utility of this approach. Guo developed an arylation of purines based on the powerful combination of palladium as the C–H bond-activating catalyst and $[Ru(bpy)_3]Cl_2 \cdot H_2O$ as photocatalyst.[195] Later, Xu and Balaraman disclosed the *ortho*-arylation of ketones and acetanilides under similar reaction conditions with the organic photocatalysts Acr-H_2 and eosin Y under irradiation of blue and green LED lights, respectively.[196]

In continuation of her previous work, Sanford reported one year later an arylation of arenes **23** with diaryliodonium salts **189** under palladium catalysis regime (Scheme 1.61).[197] In this case, the use of an iridium complex as photosensitizer was much more efficient than the previously employed ruthenium photocatalyst due to the more negative reduction potential of the iodonium salts **189** than for diazonium salts **188**. Again, this mild arylation procedure tolerated different functional groups and different directing groups.

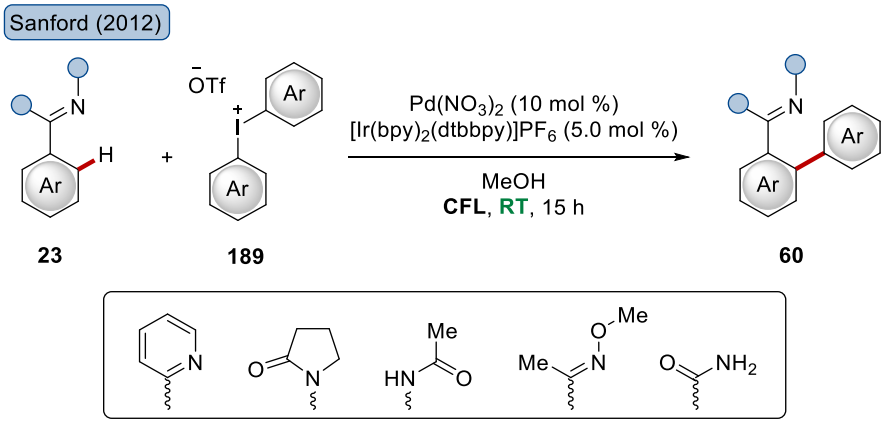

Scheme 1.61: Arylation of arenes **23** with iodonium salts **189** under dual catalysis.

Moreover, undirected arylation procedures have evolved. Thus, Lee demonstrated the undirected arylation of arenes **137** using aryldiazonium salts **188** as coupling partner (Scheme 1.62a).[198] This protocol relied on the combination of a gold catalyst with $[Ru(bpy)_3]^{2+}$ as a photoredox mediator, which allowed for the efficient conversion of differently decorated arenes **137** at ambient temperature under irradiation with blue LEDs (450 nm). One year later, Ackermann reported a manganese-catalyzed undirected arylation with diazonium salt **188** in a continuous flow set-up, which clearly outperformed the reaction in batch on larger scales (Scheme 1.62b).[199] The authors suggested the formation of a manganese-aryl complex with both aromatic substrates, which is excited with visible light under formation of an aryl radical by electron transfer to the coordinated diazonium salt and nitrogen release. Subsequently, this aryl radical undergoes radical attack on the arene, followed by oxidation and deprotonation.

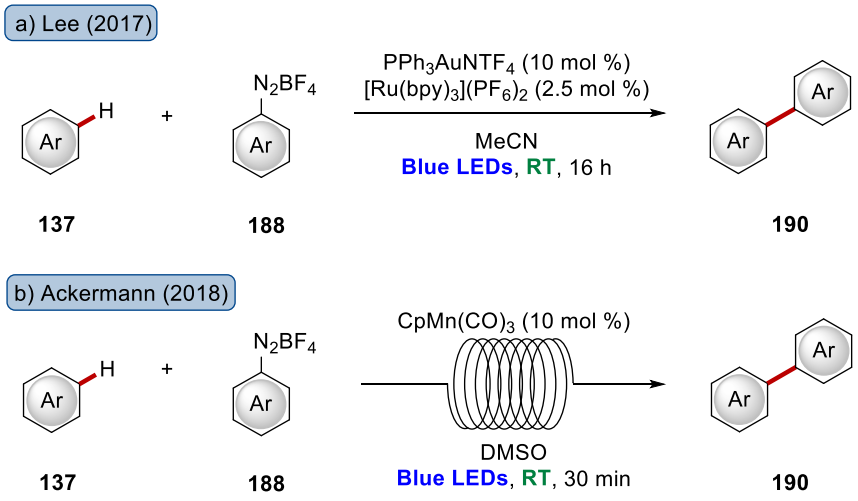

Scheme 1.62: Examples for undirected arylation with gold and manganese as catalyst.

In addition, Ackermann developed an efficient system, which allowed the direct C–H arylation of heterocyclic scaffolds **191** with aryl iodides **84** (Scheme 1.63).[200] Valuable (benzo)thiazoles

and oxazoles **191** were efficiently converted by copper catalysis using UV-light. Noteworthy, the arylation proceeded smoothly under milder conditions using blue LED with 450 nm wavelength light albeit the addition of $[Ir(ppy)_3]^{2+}$ as an exogenous photoredox catalyst was required to achieve synthetically useful conversions. Moreover, experiments with radical scavengers were conducted, being indicative of a PET mechanism. In continuation of this work, the same group realized this azole modification with a heterogenized catalyst under photochemical conditions.[10a] In this hybrid catalyst, the copper(I) center was coordinated by a bipyridine moiety, which was linked to a silica-supported heterogenous material. This system did not only hold the advantage, that more challenging benzimidazole substrates were transformed with good yields, but also allowed for recyclability of the catalyst, as nicely demonstrated over five cycles without any loss in efficacy.

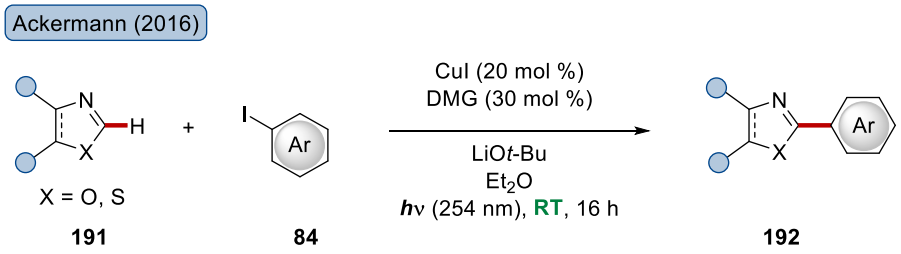

Scheme 1.63: Copper-catalyzed arylation of azoles **191** induced by light.

Besides transition metal-catalyzed C–C bond formation by means of C–H arylation reactions, further reactivities with photo-induced procedures were achieved in both, batch and flow chemistry.[201] In addition to acylation reactions,[202] many annulation reactions[203] and different alkylation reactions have been investigated. A well-established system of this dual catalysis concept is the merger with nickel catalysts with important contributions from Doyle, MacMillan and Molander focusing on cross-coupling-type transformations to modify aryl halogens in alkylation and benzylation reactions.[204] Additionally, nickel-catalyzed C(sp^3)-alkylations and arylations were reported by Martin[205] and MacMillan[206] in independent works using organic photocatalysts or an iridium complex to enable an efficient catalysis.

Alkylation of arenes by C–H activations are also known in literature. Tan and Wang developed the directed modification of benzamides **193** with perfluoroalkyl iodides **194** following a copper(I)-enabled C–H activation pathway with eosin Y as the organic photosensitizer (Scheme 1.64).[207] However, in this protocol, stoichiometric amounts of the copper(I) salt were required for the C–H activation step.

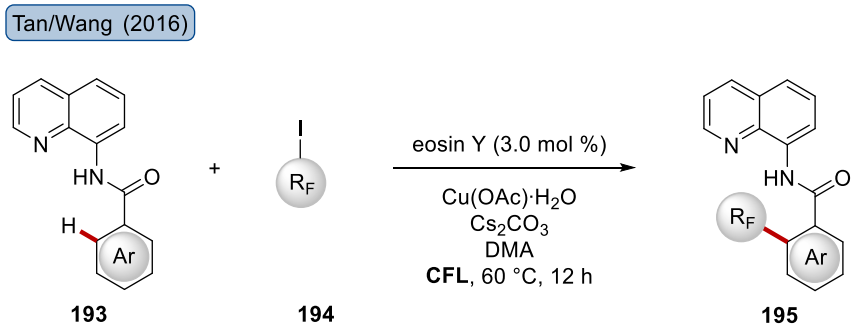

Scheme 1.64: Copper(I)-mediated directed perfluoralkylation of benzamides **193**.

Ackermann realized in the same year the adamantylation of azoles **196** in a cobalt-catalyzed system (Scheme 1.65).[208] The alkylation was achieved with adamantyl carboxylic acid **28**, which undergoes a decarboxylation process. As photoredox mediator, the cost-efficient [Mes-Acr]ClO_4 dye was employed.

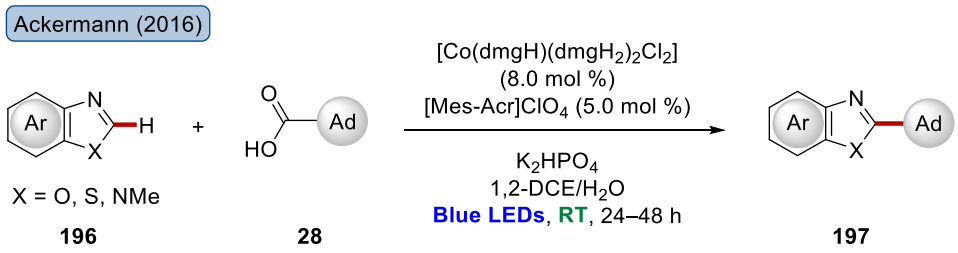

Scheme 1.65: C–H Adamantylation of azoles **196** with by cobalt catalysis.

Common for the most of the developed procedures is the requirement of a transition metal catalyst and an exogenous photocatalyst to ensure the catalytic turnover. This constraint was recently successfully addressed by Ackermann[209] and later Greaney[210] *via* a ruthenium catalysis regime. Ackermann reported in 2019 on a directed *meta*-selective C–H alkylation of arylazines **23** with tertiary and secondary alkyl bromides **24** and **42** (Scheme 1.66). In contrast to traditional catalysis, arenes **23** were efficiently converted at ambient temperature with the aid of the merger of ruthenium catalysis with visible light. In good agreement with the generally accepted pathway under thermal conditions,[69-70] the authors suggested a SET manifold for the directed *meta*-selective alkylation enabled by *ortho*-ruthenation and subsequent radical attack *para* to ruthenium. An exogenous photocatalyst was notably not required. In contrast, the authors showed that an *in situ* generated cyclometalated ruthenium intermediate undergoes an excitation process under absorption of blue LED light, thus furnishing intermediate **198** after radical attack.[209] In an independent, subsequent report, Greaney achieved a comparable reactivity by combining versatile ruthenium-catalyzed C–H activation and light-induced

reactivity albeit under slightly different reaction conditions.[210] A few months later, this concept was exploited by Baslé, who reported on a directed borylation and hydroxylation of phenylpyridines by a single rhodium/NHC catalyst, which was capable of both, to enable the scission of the C–H bond and to harvest the light.[211]

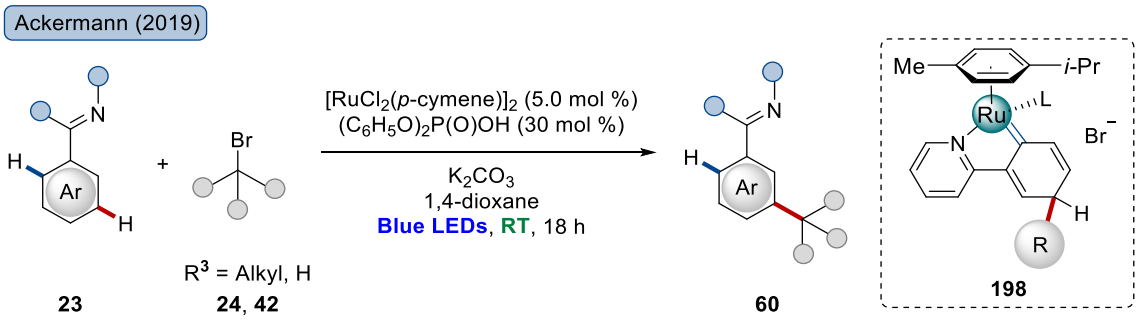

Scheme 1.66: *meta*-Selective alkylation of arenes **23** with a dual-functional ruthenium complex.

In addition to these innovative examples, the merger of ruthenium catalysis and photoredox chemistry remains scarce. Rueping has illustrated earlier an olefination of phenol ethers **57** with acrylates **99** with $[RuCl_2(p\text{-cymene})]_2$ as catalyst in the presence of a cost-intensive iridium photoredox mediator (Scheme 1.67).[212] Elegantly, oxygen was employed as terminal oxidant, which allowed for the avoidance of stoichiometric chemical oxidants usually employed in comparable reactions. In addition to the ruthenium catalysis manifold, a rhodium-catalyzed olefination of Weinreb amides was enabled by the same group.[213] In this case, a ruthenium photosensitizer enabled the transformation with air as benign oxidant.

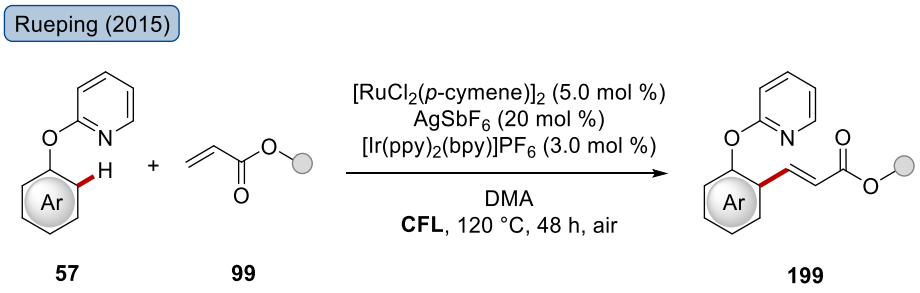

Scheme 1.67: Ruthenium- and iridium co-catalyzed olefination by visible light irradiation.

1.6.3 Electrophotocatalytic C–H Functionalization

After the notable progress which has been made in terms of photocatalytic and electrocatalytic chemistry, electrophotocatalytic methods have surfaced very recently after having recognized, which tremendous potential the combination possesses.[214] Electrophotocatalysis describes the utilization of both electric current and photons by the same catalyst.[165] Since 2019, this

innovative strategy has witnessed a remarkable progress with several reports, which employ one of two different approaches in the electrophotochemical reaction design. The first one is that the electricity is used *in lieu* of a chemical oxidant, which ensures the reoxidation of the light-harvesting photocatalyst, such as [Mes-Acr]ClO_4. The other approach comprises in the electrochemical conversion of a non-absorbing precursor, such as the tris(amino)-cyclopropenium-based [TAC]ClO_4, into a potent light-absorbing photocatalyst.[215]

Early examples of the merger of electro- and photochemistry can be dated back to at least 1979, when Moutet and Reverdy reported on the dimerization of olefin **200** (Scheme 1.68).[216] The controlled electrochemical oxidation of PTZ (**202**) to a radical cation, which is stable for hours in solution, and subsequent irradiation with a mercury lamp led to formation of product **201** through SET to **200**. Despite the fact, that in this example, PTZ was used in stoichiometric amounts and that the electrochemical and photochemical steps were conducted sequentially, this can be considered as a trendsetting idea, guiding towards future electrophotochemical transformations. A few years later, the same group also developed an advanced procedure for the oxidation of benzyl alcohols to benzaldehydes with both processes at the same time.[217] In addition, Sheffold contributed to these early examples with a conjugate addition of acyl radicals, which was catalyzed by vitamine B_{12}.[218]

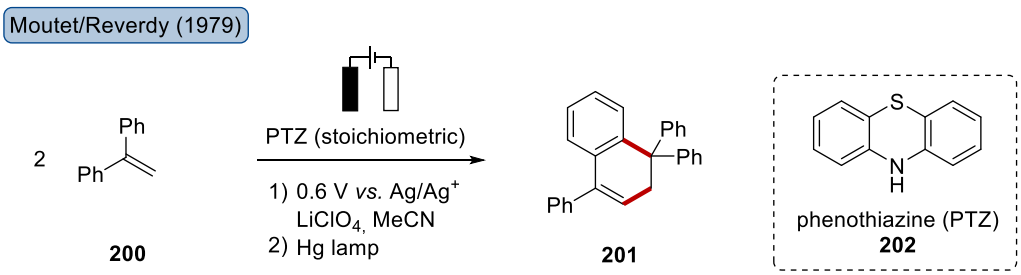

Scheme 1.68: Early example of the merger of photochemistry and electrochemistry.

After these initial pioneering reports, the first examples for modern electrophoto-catalyzed transformations were reported by *inter alia* Xu,[219] Lambert[220] and Stahl.[221] Albeit different reaction types have been achieved, among those also one enantioselective transformation,[222] only selected examples for oxidative C–C bond forming reactions on arenes will be discussed herein. Likewise, C–Het constructions[223] have been established, as well as redox-neutral[224] and reductive functionalizations,[225] which will be not further discussed herein.

In a seminal work, Xu was among the first, who demonstrated the great potential bearing in the synergy of electricity and visible light (Scheme 1.69).[219] He achieved the undirected alkylation of a broad range of different heterocycles **155** with secondary and tertiary trifluoroalkyl borates

203. The use of [Mes-Acr]ClO_4 as photosensitizer enabled efficient catalytic conditions under irradiation of blue LED light (450 nm).

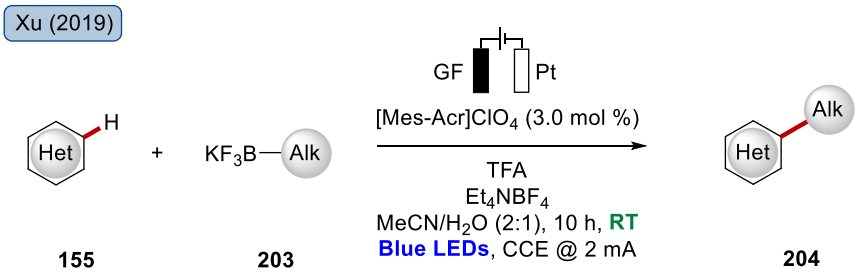

Scheme 1.69: Electrophotocatalytic alkylation of heteroarenes **155**.

In continuation on this work, the same group developed one year later another versatile alkylation procedure with broad scope.[226] The synthetically useful protocol allowed the coupling of primary, secondary and tertiary alkyl groups, arising from carboxylic acid derivatives **205**, onto different heteroaromatic structures **155**, thereby highlighting the mildness by late-stage diversifications of drugs (Scheme 1.70). The authors proposed that the cerium(III) catalyst undergoes anodic oxidation to cerium(IV), which reacts with the carboxylic acid **205**. Subsequently, a carboxyl radical is formed by irradiation of the purple LED light with 390 nm wavelength. Decarboxylation furnishes a C-centered alkyl radical, undergoing radical attack onto heteroarene **155**. Likewise, a carbamoylation of heteroarenes was achieved by exploiting the decarboxylation strategy under irradiation of blue LED light with an organic photocatalyst.[226]

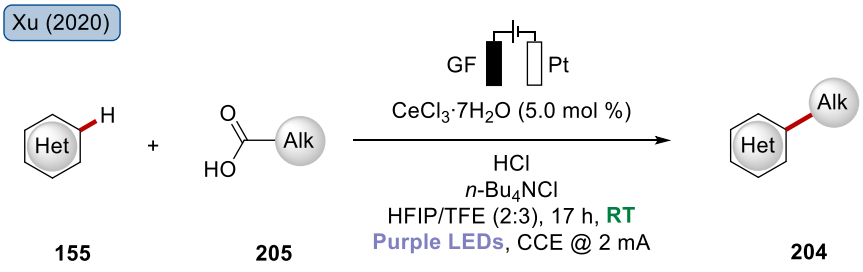

Scheme 1.70: Undirected alkylation with cost-efficient carboxylic acids **205** by irradiation with purple LEDs (390 nm).

Moreover, the alkylation of arenes **155** with simple alkanes **206** was reported by Xu (Scheme 1.71a).[227] Here, the addition of HCl was essential whereas the use of the ammonium salt TBACl in catalytic amounts enhanced the envisioned reactivity. The authors suggested that a chloride anion is the actual mediator, which is converted to Cl_2 by anodic oxidation. Under visible light irradiation, Cl_2 is cleaved homolytically to furnish chlorine radicals, which enable the formation of C-centered sp^3 radical. In contrast, Ravelli illustrated the alkylation of

benzothiazoles **207** with tetrabutylammonium decatungstate (TBADT) as photocatalyst in a divided cell set-up under irradiation with light of 390 nm wavelength (Scheme 1.71b).[228] The transfer of one electron from the excited state of TBADT enables the formation of an alkyl radical, which further reacts with arene **207**, while the reduced photocatalyst is regenerated by anodic oxidation.

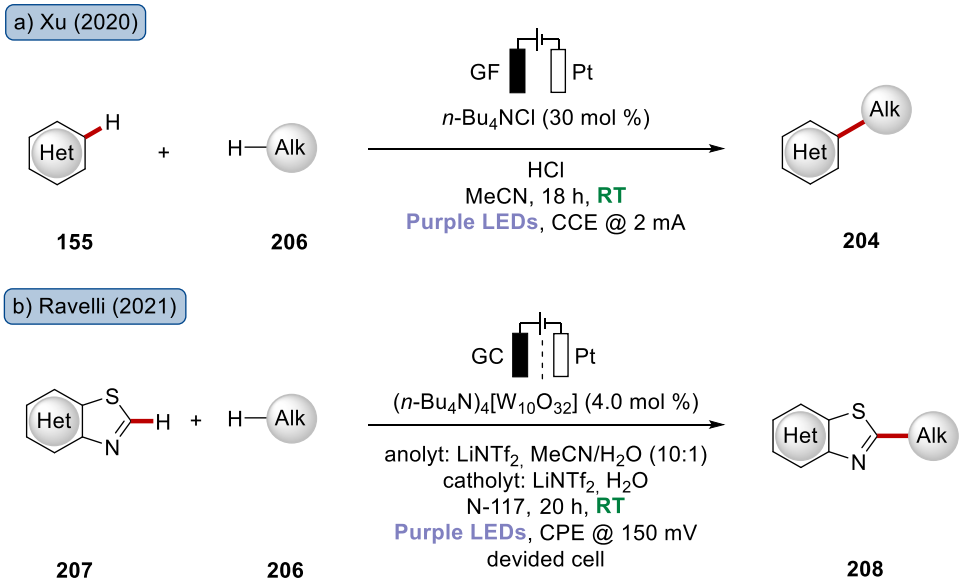

Scheme 1.71: Alkylation of heteroarenes with alkanes **206** by irradiation with purple LEDs (390 nm).

Besides the different alkylation procedures, also an electrophotochemical trifluoromethylation was described by Ackermann (Scheme 1.72).[157] The undirected C–H functionalization of arenes **137** was realized with the Langlois reagent $NaSO_2CF_3$ (**153**) under irradiation with blue LED light of 450 nm wavelength in presence of two different photocatalysts. Gratifyingly, also different heteroarenes could be modified under these conditions.

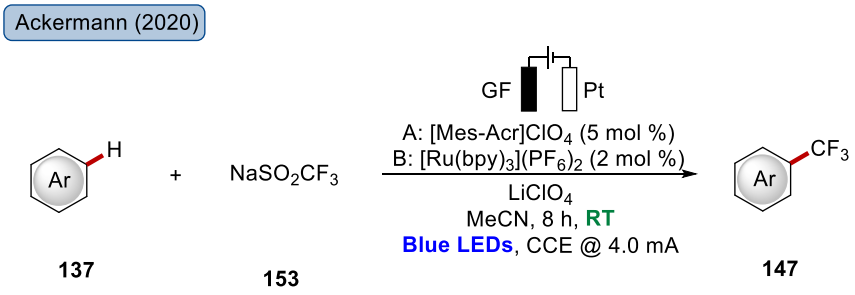

Scheme 1.72: Undirected trifluoromethylation of arenes **137** under electrophotocatalytic conditions.

Another interesting example for electrophoto-catalyzed functionalizations of arenes **155** beyond the incorporation of simple alkyl substituents was presented by Lambert in 2020 and deals with a Minisci-type reaction with ethers **209** to modify different heteroarenes **155** (Scheme 1.73).[229] As a electrophotoredox mediator, triaminocyclopropenium perchlorate ([TAC]ClO_4, **211**) was employed, which forms an photoactive species after anodic oxidation.

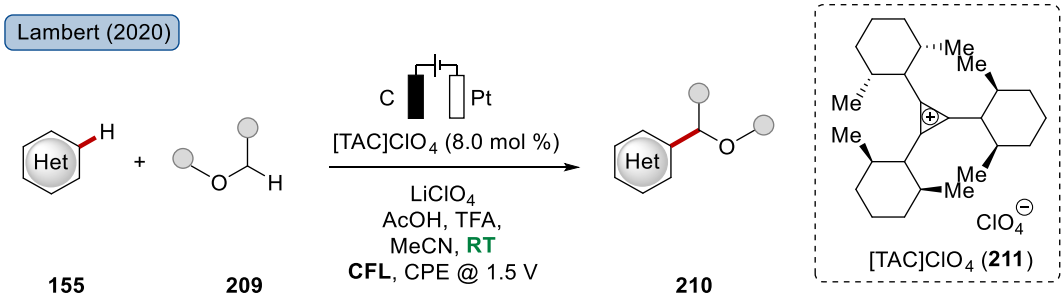

Scheme 1.73: Minisci-type functionalization of heteroarenes with [TAC]ClO_4 (**211**).

2 OBJECTIVES

During the last decades, transition metal-catalyzed C–H activation has evolved into a powerful and versatile tool in synthetic chemistry, and methods for the selective construction of C–C and C–Het bonds could be enormously expanded. To ensure the synthetic utility of the direct transformation of C–H bonds, the control of the site-selectivity in the presence of several similar C–H bonds is of key importance. Therefore, several concepts have been developed to allow for position-controlled reactivity, with the use of chelation assistance for directed *ortho*-selective modifications as the most prominent one.[34b, 34d, 48b, 174] Diverse protocols for guided ruthenium-catalyzed C–H activations resulted in the acceptance of ruthenium catalysis as a uniquely effective tool for C–H activations.[230] Furthermore, the use of readily available earth-abundant metals, such as cobalt and manganese, gains increasing importance as cost-efficient and powerful alternative.[34c]

Although significant progress has been achieved to develop sustainable strategies, they are still often associated with considerable restrictions, such as harsh reaction conditions and high temperatures as well as the use of toxic and environmental hazardous solvents. Moreover, oxidative transformations through a C–H/C–H activation strategy typically require chemical oxidants which diminishes the sustainability despite the ideal atom-economy. More recently, the merger of transition metal catalysis with electrochemistry or photoredox chemistry has been recognized as a sustainable approach to allow for mild catalysis.[22b, 22c, 163b, 169, 189] In addition, the combination of photo- and electrocatalysis was identified as a suitable methodology to realize new reactivities.[165] Taking these aspects into account, the main objective of the thesis is the exploration of sustainable C–H activation and C–H functionalization procedures with focus on the advancement of electro-catalyzed and photo-induced reactivities.

Rhodium-catalyzed C–H activations have received considerable attention for transformations guided by weakly coordinating directing groups. Moreover, a variety of protocols has proven rhodium catalysis as a remarkable tool in the assembly of heterocyclic scaffolds through annulation reactions. However, the oxidative transformations with alkynes and activated olefins usually require chemical oxidants in stoichiometric amounts. To address the compromised resource-economy, the first rhodaelectro-catalyzed reaction with electric current proved its applicability as the terminal oxidant.[179] In continuation of this work, an electrooxidative

modification of benzamides should be developed with acrylates **99** and styrenes **113** as coupling partners (Scheme 2.1). Furthermore, the catalytic scenario should be elucidated.

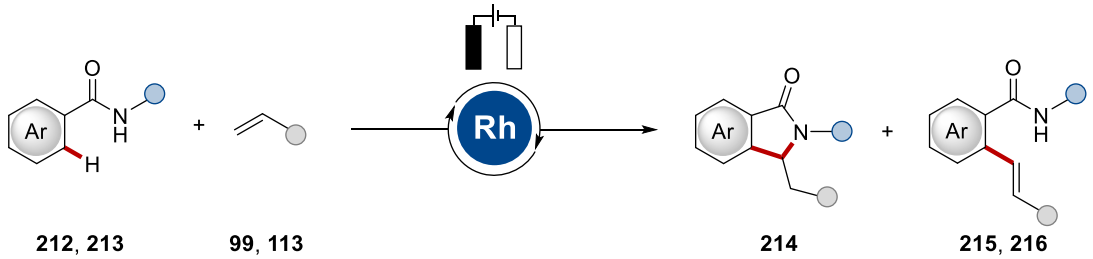

Scheme 2.1: Rhodaelectro-catalyzed C–H alkenylation of benzamides.

Another precious metal with great importance in organic synthesis is ruthenium,[231] which is frequently applied in C–H activation chemistry due to remarkable properties and the capability to catalyze a plethora of different transformations. Attracted by a so far unprecedented *ortho*-selective alkylation of arenes with secondary alkyl bromides in a decarboxylative manifold,[232] the regiodivergent alkylation of phenylpyrazoles **217** by ruthenium-catalyzed C–H activation should be explored for the first time (Scheme 2.2). The site-selectivity of this thermally-induced transformation should be studied for various secondary alkyl bromides. Moreover, the catalytic pathway is intended to clarify by detailed mechanistic experiments.

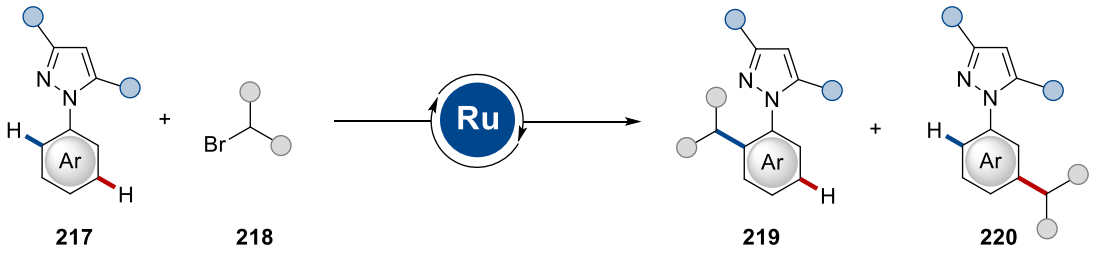

Scheme 2.2: Position-selective C–H alkylation with secondary alkyl bromides.

Inspired by reports on mild ruthenium-catalyzed remote C–H alkylations at ambient temperature enabled by irradiation with visible light without any exogenous photocatalyst,[209-210] the concept to merge powerful ruthenium catalysis with photoredox chemistry was envisioned to enable mild C–H arylations (Scheme 2.3). Thereby, the prevalent harsh reaction conditions with elevated temperatures of typically 120 °C should be circumvented by mild reaction conditions at room temperature. In addition, a comparison of the sustainable photo-induced reactivity and traditional thermal conditions should be conducted to support the synthetic utility, while mechanistic studies should disclose the working mode of the photo-induced ruthenium catalysis.

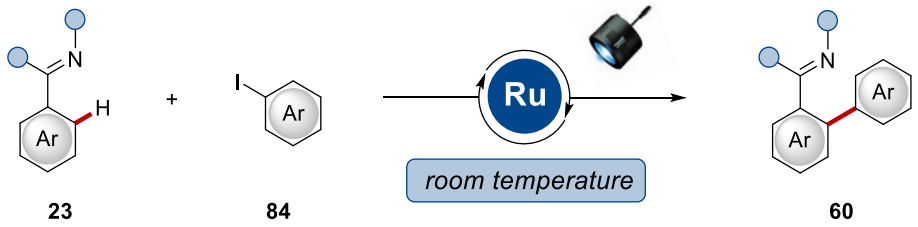

Scheme 2.3: Ruthenium-catalyzed C–H arylations under photoredox conditions.

Next, *ortho*-selective transformations of arenes, namely efficient C–H benzylations should be developed, as *ortho*-benzylations continued to require high reaction temperatures (Scheme 2.4). In addition to studies on sustainable reactions with water and surfactant solutions as reaction medium, the reaction mechanism should be devised with mechanistic studies.

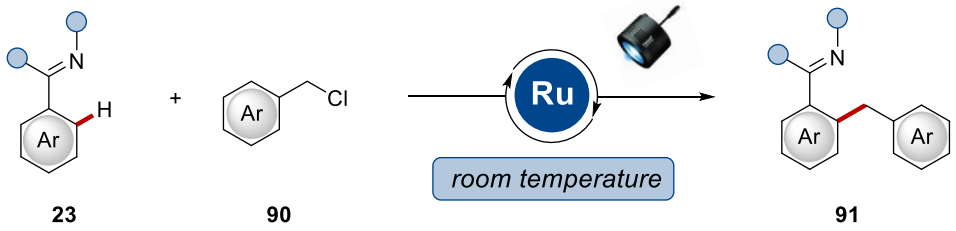

Scheme 2.4: Photo-induced ruthenium-catalyzed C–H benzylations.

Besides the previously introduced directed C–H activations with a chelating entity, a plethora of undirected C–H functionalization procedures has been established. Among those, the trifluoromethylation of arenes and heteroarenes has gained significant interest to provide access to valuable trifluoromethyl substituted compounds. Many of these rely on a radical pathway, such as the undirected electrophotocatalytic trifluoromethylation with the bench-stable Langlois reagent.[157] Based on this report, the trifluoromethylation under electrophotochemical conditions should be further analyzed (Scheme 2.5). Beyond attempts to synthesize a trifluoromethylated drug derivative, the main focus should be a detailed comparison of different photoelectro catalysts supported by kinetic, as thus far, such a comparison has unfortunately proven elusive. Given the great performances of the electrophotocatalyst $[TAC]ClO_4$,[165, 215] the use of this catalyst is in particularly of interest.

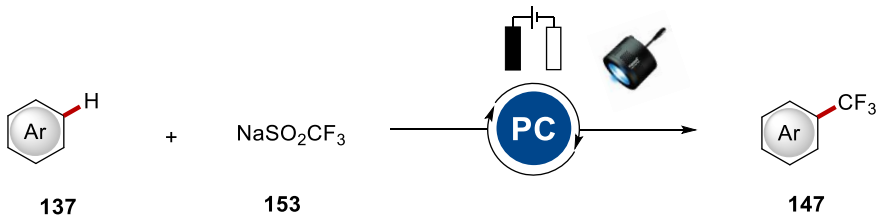

Scheme 2.5: Undirected trifluoromethylation with Langlois reagent (**153**) by electrophotocatalysis.

Although catalysis and especially C–H activation is in good accordance with the 12 principles to achieve green and sustainable chemistry due to an improved step- and atom-economy, the use of organic solvents continuous to be a major limitation, as they cause the majority of waste in large scale and have an enormous impact on the ecological footprint. For this reason, the use of water by micellar catalysis has emerged as an attractive strategy to allow for a reaction design with improved sustainability. However, examples in C–H activation chemistry remain scarce. Within this thesis and in collaboration with Novartis, the allylation of tryptophan should be devised using an aqueous reaction medium and surfactants (Scheme 2.6). Given the great potential of manganese in the late-stage diversification of peptides caused by its great robustness and low toxicity,[34c, 118] the focus should be set on manganese catalysis. Detailed kinetic studies at different reaction temperatures and with reduced catalyst loadings should be attempted also.

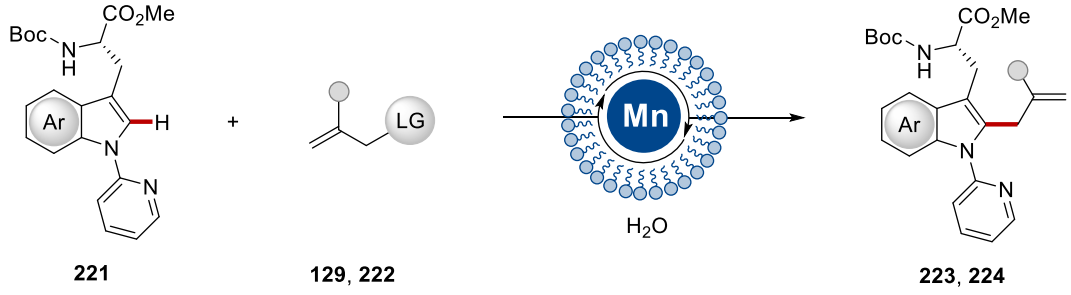

Scheme 2.6: Manganese-catalyzed C–H allylation of tryptophan **221** in water.

3 RESULTS AND DISCUSSION

3.1 RHODIUM-CATALYZED ELECTROOXIDATIVE C–H OLEFINATION OF BENZAMIDES

The occurrence of unsaturated entities coupled to arenes and heteroarenes can be observed in the architecture of several top-selling drugs (Figure 3.1).[233] Therefore, the development of efficient and sustainable procedures to build up this structural motif is of great interest.

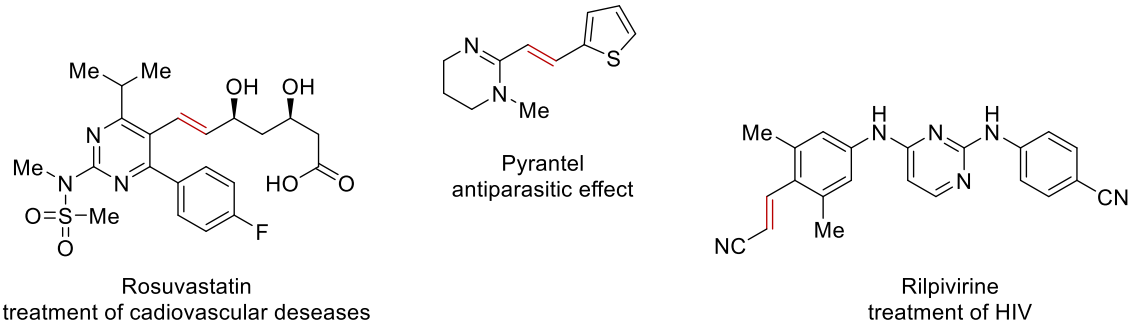

Figure 3.1: Selected examples of olefinated arenes in drug molecules.

A valuable tool to enable the modification of arenes with unsaturated coupling partners was identified in terms of rhodium-catalyzed C–H activations by directing group assistance. Besides the alkylation of arenes with olefins in rhodium-mediated hydroarylation reactions, especially numerous annulation approaches have been reported which allow the construction of precious heterocycles. In addition, the olefination with activated olefins has emerged as an accepted approach with guidance by the chelation-assistance of different directing groups.[101]

Although these approaches are versatile and useful strategies, common to these oxidative transformations is that they require stoichiometric amounts of a chemical oxidant, such as silver(I) and copper(II) salts.[169b] In addition to the associated cost of goods, in particular the sustainability is diminished owing to the formation of toxic metal waste in stoichiometric quantities. This drawback was firstly addressed by Ackermann in an electrooxidative, rhodium-catalyzed synthesis of phthalides,[179] before several reports captured this strategy and further electrochemical rhodium-catalyzed transformations were disclosed.[176] Herein, the concept of the arene functionalization with activated olefins under rhodium catalysis regime was utilized for the direct functionalization of benzamides. As this project was initialized during the master thesis, part of the results can be found in the thesis submitted by J. Struwe.[234]

3.1.1 *Optimization for Olefination with Acrylates*

During the course of preliminary experimentation[234] for the electrooxidative olefination of benzamides, the *N*-methylbenzamide (**212a**) was found to be converted into the isoindolin-1-one scaffold **214aa** by the reaction with acrylate **99a**, however, with moderate yield. In initial attempts to realize higher conversions, the addition of different salts in co-catalytic amounts has been evaluated. As the formation of a cationic rhodium complex was believed to be beneficial, additives which are supporting its formation were employed (Table 3.1). Using $NaPF_6$ or KPF_6 led to slightly increased efficacy giving more than 50% isolated product **214aa** (entries 1–3), while the addition of $AgSbF_6$ had no beneficial effect (entry 4). The best yield was obtained with AgOTf in co-catalytic amounts (entry 5).

Table 3.1: Electrooxidative olefination of benzamide **212a** with acrylate **99a**.

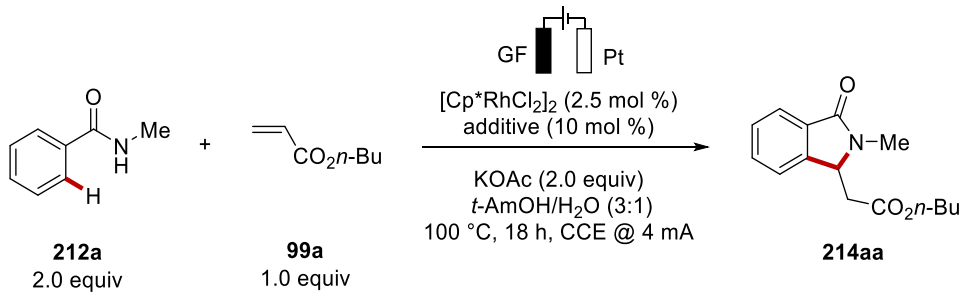

Entry	Additive	**214aa** [%][a]
1	---	49
2	$NaPF_6$	54
3	KPF_6	53
4	$AgSbF_6$	48
5	AgOTf	57

[a] Reaction conditions: Undivided cell, graphite felt anode, Pt cathode, constant current electrolysis at 4.0 mA. **212a** (1.00 mmol), **99a** (0.50 mmol), $[Cp^*RhCl_2]_2$ (2.5 mol %), additive (10 mol %), KOAc (1.00 mmol), *t*-AmylOH/H_2O (3:1, 4.0 mL), 100 °C, 18 h, under N_2. Yields refer to the isolated products.

As already discovered in initial results,[234] the change of the substituent on the nitrogen atom had an impressive impact on the reaction product. In stark contrast to the small methyl group, the bulky *tert*-butyl substituent yielded the non-cyclized olefination product **215aa** *via* a Fujiwara-Moritani-type reaction without subsequent aza-Michael reaction. Investigations of different substoichiometric additives highlighted their essential role (Table 3.2). Whereas only

traces of the product were detectable in the absence of the additive, $NaPF_6$ enabled moderate product formation of **215aa** with 43% yield (entries 1–2). Further improvement was achieved by changing the counter ion from sodium to potassium, therewith ending up with 60% isolated yield (entry 3). The addition of $AgSbF_6$ fell short in allowing for efficient catalysis, while the utilization of AgOTf furnished the product **215aa** in 57% (entries 4–5). As this yield was slightly lower than the best result with KPF_6, the latter one was employed for the further optimization.

Table 3.2: Electrochemical modification of amide **215aa** with rhodium-catalyzed olefination.

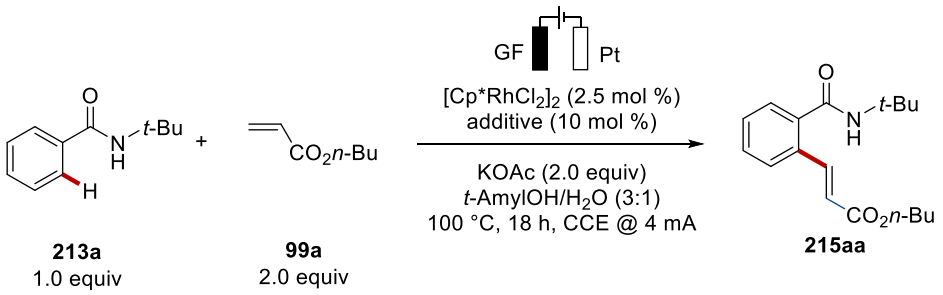

Entry	Additive	**215aa** [%][a]
1	---	traces
2	$NaPF_6$	43
3	KPF_6	60
4	$AgSbF_6$	22
5	AgOTf	57

[a] Reaction conditions: Undivided cell, graphite felt anode, Pt cathode, constant current electrolysis at 4.0 mA. **213a** (1.00 mmol), **99a** (0.50 mmol), $[Cp^*RhCl_2]_2$ (2.5 mol %), additive (10 mol %), KOAc (1.00 mmol), *t*-AmylOH/H_2O (3:1, 4.0 mL), 100 °C, 18 h, under N_2. Yields refer to the isolated products.

In continuation of the initial screening of a few solvents,[234] the optimization of the reaction medium was conducted with the *tert*-butyl substituted benzamide **213a** in the presence of KPF_6 as the additive (Table 3.3). Starting from a mixture of *tert*-amyl alcohol and water, which was identified as an appropriate solvent in electrochemical rhodium catalysis for C–H functionalization of benzoic acids,[179] the catalytic activity was strongly reduced by changing to a mixture of *tert*-butyl alcohol and water (entries 1–2). With ethanol as the sole solvent, the reactivity was completely suppressed (entry 3). Unsatisfactory results were obtained with 1,2-DCE and HFIP, resulting in low yields of 12% and 23%, respectively (entries 4–5).

However, the high boiling rather polar solvents DMSO and DMA fell short in affording the desired product **215aa** (entries 6–7).

Table 3.3: Optimization of the solvent for electrochemical transformation of benzamide **213a**.

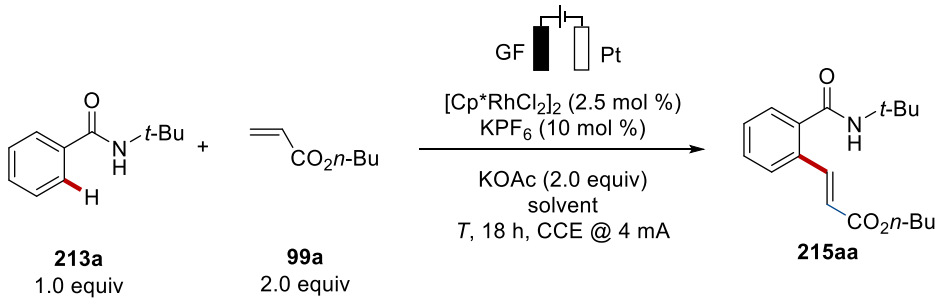

Entry	Solvent	Temperature [°C]	**215aa** [%][a]
1	*t*-AmylOH/H_2O (3:1)	100	60
2	*t*-BuOH/H_2O (3:1)	80	33
3	EtOH	80	---
4	1,2-DCE	80	12
5	HFIP	60	23
6	DMSO	130	---
7	DMA	130	---

[a] Reaction conditions: Undivided cell, graphite felt anode, Pt cathode, constant current electrolysis at 4.0 mA. **213a** (1.00 mmol), **99a** (0.50 mmol), $[Cp^*RhCl_2]_2$ (2.5 mol %), KPF_6 (10 mol %), KOAc (1.00 mmol), solvent (4.0 mL), 60–130 °C, 18 h, under N_2. Yields refer to the isolated products.

After having identified the optimal solvent, further experiments were performed to test the catalytic ability of different transition metal catalysts (Table 3.4). In contrast to the precious and expensive $[Cp^*RhCl_2]_2$ catalyst, which resulted in a satisfactory yield of 60%, the base-metal $[Cp^*Co(CO)I_2]$ complex was incapable to furnish the alkenylation product **215aa** (entries 1–2). The iridium derivative of the employed rhodium precursor allowed for the electrooxidative transformation with a low yield of 9% (entry 3). In contrast, frequently employed ruthenium and palladium catalysts in C–H activation chemistry turned out to be inefficient in this reaction (entries 4–5). Moreover, the indispensability of the rhodium catalyst was not only highlighted in comparison to the other transition metals, but also in a control experiment in the absence of a transition metal catalyst under otherwise identical reaction conditions (entry 6).

Table 3.4: Electrooxidative alkenylation of benzamide **213a** with different transition metal catalysts.

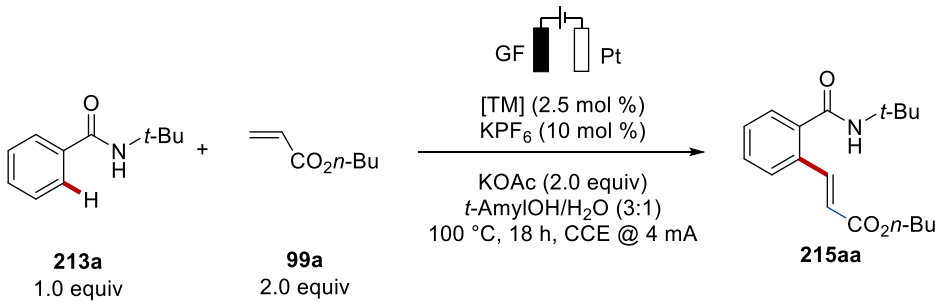

Entry	Catalyst	**215aa** [%][a]
1	$[Cp^*RhCl_2]_2$	60
2	$[Cp^*Co(CO)I_2]$	---[b]
3	$[Cp^*IrCl_2]_2$	9
4	$[RuCl_2(p\text{-cymene})]_2$	traces
5	$Pd(OAc)_2$	---[b]
6	---	---

[a] Reaction conditions: Undivided cell, graphite felt anode, Pt cathode, constant current electrolysis at 4.0 mA. **213a** (1.00 mmol), **99a** (0.50 mmol), catalyst (2.5 mol %), KPF_6 (10 mol %), KOAc (1.00 mmol), *t*-AmylOH/H_2O (3:1, 4.0 mL), 100 °C, 18 h, under N_2. Yields refer to the isolated products. [b] 5.0 mol % of the catalyst.

With the suitable reaction conditions in hand, the generality of the modification of benzamides with acrylate **99a** under sustainable electrochemical reaction conditions was elucidated by using differently substituted benzamides **110** (Table 3.5). Unfortunately, the arenes bearing other alkyl substituents on the amide moiety failed in the electrooxidative C–H modification by rhodium catalysis. With an exceptional good result for the *tert*-butyl group, the reaction with the acrylate **99a** was not successful with other sterically demanding substituents (entries 1–4). Changing to Weinreb amides or benzohydrazines did not provide the corresponding products (entries 5–6). Likewise, amides **110** being hydroxylated or tosylated could not be identified as suitable substrates under these reaction conditions (entries 7–8).

Table 3.5: Reactions with benzamides **110** bearing different substituents.

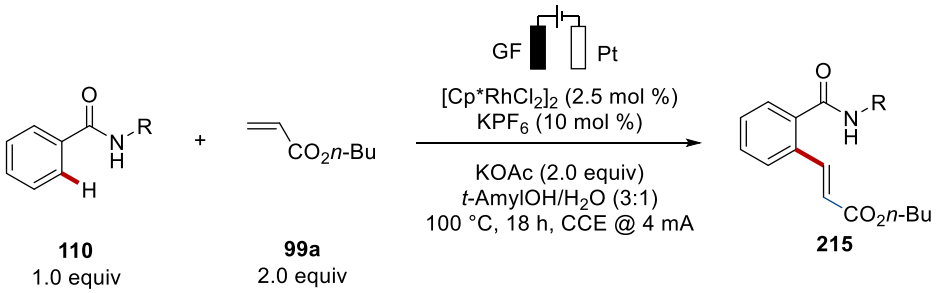

Entry	Substituent R	**215** [%][a]
1	*t*-Bu	60
2	*i*-Pr	traces
3	Cy	---
4	Ad	---
5	OMe	traces
6	NHMe	---
7	OH	---
8	OTs	traces

[a] Reaction conditions: Undivided cell, graphite felt anode, Pt cathode, constant current electrolysis at 4.0 mA. **110** (1.00 mmol), **99a** (0.50 mmol), $[Cp^*RhCl_2]_2$ (2.5 mol %), KPF_6 (10 mol %), KOAc (1.00 mmol), *t*-AmylOH/H_2O (3:1, 4.0 mL), 100 °C, 18 h, under N_2. Yields refer to the isolated products.

As also the use of other acrylates was faced with challenges and low yields, this project was stopped due to the narrow scope.

3.1.2 Optimization for Olefination with Styrenes

Interestingly, similar reaction conditions as in case of the olefination of benzamides with acrylates **99** were later recognized to enable the alkenylation with styrenes **113**.[235] Optimization studies performed by visiting Prof. Dr. Y. Zhang in the Ackermann group showed that the C–H activation and alkenylation of benzamide **212** was realized efficiently with $[Cp^*RhCl_2]_2$ complex as the precursor, along with NaOPiv as the base in a mixture of *tert*-amyl alcohol and water (Scheme 3.1).

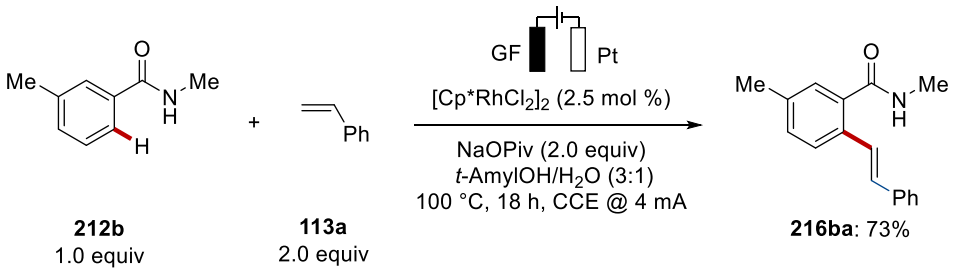

Scheme 3.1: Optimized reaction conditions for C–H alkenylation with styrene **113a** using an electrochemical rhodium catalysis approach.

With the optimized conditions in hand, Prof. Dr. Y. Zhang further examined the substrate scope of the reaction.[235] Both, electron-withdrawing and electron-donating substituents on the styrene derivative **113** were fully tolerated. Valuable functional groups, such as halogens, nitro and nitril substituents were compatible with these reaction conditions. Furthermore, the synthetic utility of this electrochemical transformation was demonstrated by the tolerance of different heterocyclic moieties. Alkyl substituted olefines were also employed as substrates, albeit proving the envisioned product **216** in minor amounts.

3.1.3 Mechanistic Studies

To elucidate the catalyst's working mode, several mechanistic experiments were performed.[235] H/D scrambling experiments performed by Prof. Dr. Y. Zhang revealed a facile deuterium incorporation in the presence of D_2O. Moreover, KIE studies were conducted, indicating that the C–H cleavage is unlikely the rate-determining step.

In addition, CV measurements of the catalytic system were performed (Figure 3.2). While the benzamide **212b** itself did not show any oxidation wave, styrene **113a** showed a strong oxidation peak of around 1.4 V *vs.* SCE, and the formed product **216ba** turned out to be easily oxidized. Likewise, the oxidation of $[Cp^*RhCl_2]_2$ was observable at the same regime. CV studies with mixtures of different components of the catalytic system showed that the presence of NaOPiv and benzamide **212b** had an impact on the oxidation of the rhodium species and the maximum of the irreversible oxidation wave was slightly shifted, while the peak current was increased. For the mixture of the complex with benzamide **212b** and NaOPiv, the onset of the peak was at 1.35 V *vs.* SCE.

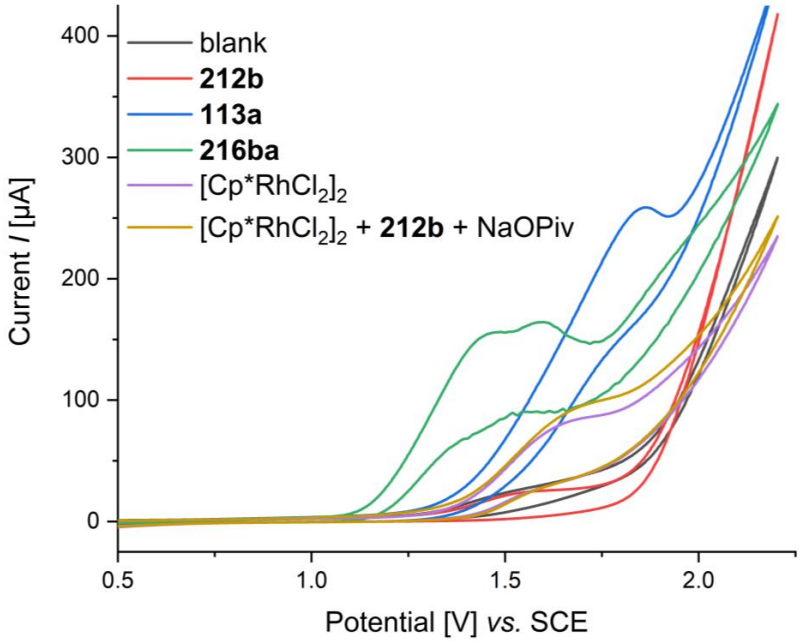

Figure 3.2: CV studies for rhodium-catalyzed olefination of arenes **212** with styrenes **113**.

3.1.4 Proposed Catalytic Cycle

With these mechanistic insights acquired and taking related literature into account,[113-116] a reasonable catalytic cycle was presented (Scheme 3.2).[235] Commencing with the employed rhodium dimer as the precursor, rhodium(III) intermediate **225** is formed by ligand exchange. Coordination of the *N*-methyl amide **212** followed by C–H activation furnishes the cyclometalated rhodium species **226**. Subsequent binding of the styrene substrate **113** provides the intermediate **227**. By migratory alkene insertion the rhodacomplex **228** is obtained. Elimination of the *β*-hydrogen and reductive elimination cause the liberation of the C–H alkenylation product **216** and the formation of the rhodium(I) intermediate **229**. Upon anodic oxidation, the catalytic cycle is closed by regeneration of the rhodium(III) complex **225**.

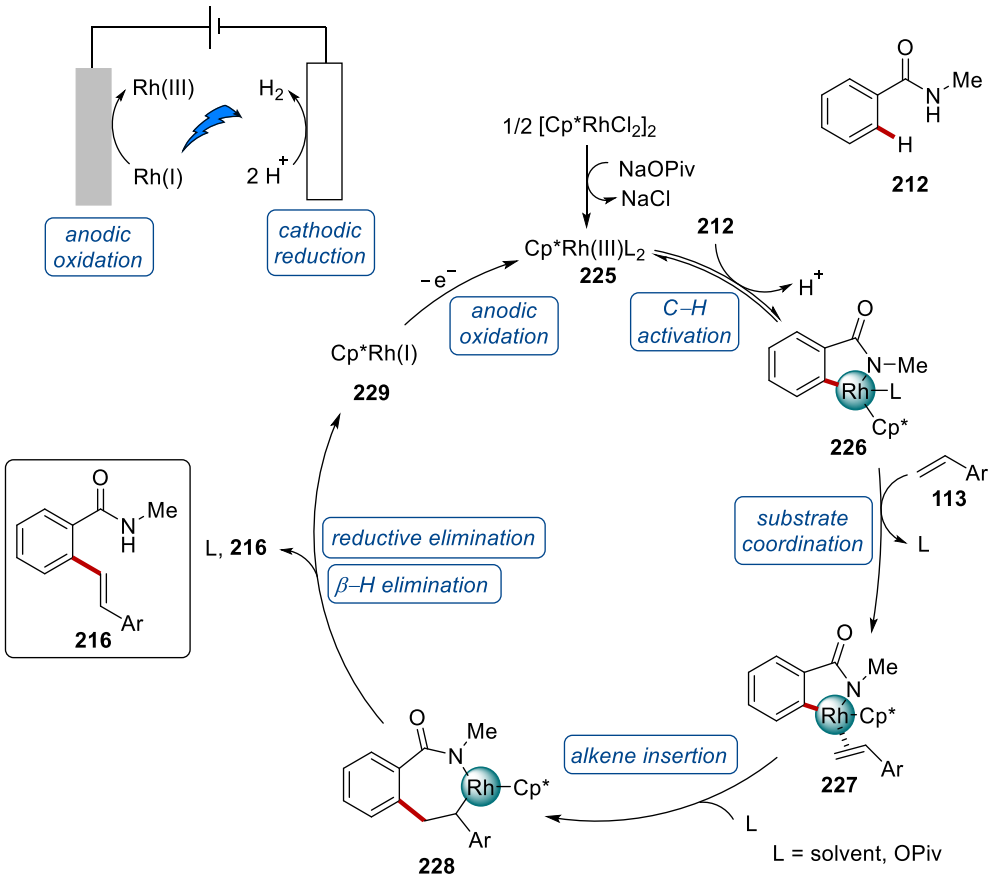

Scheme 3.2: Proposed mechanistic scenario for electrochemical rhodium-catalyzed alkenylation of benzamides **212**.

3.2 RUTHENIUM-CATALYZED REGIODIVERGENT C–H ALKYLATION OF PYRAZOLES

Alkylated arenes are frequently used as structural motifs in many important drugs (Figure 3.3).[233, 236] For this reason, sustainable and selective procedures to achieve direct C–H alkylation of arene moieties have gained significant attention.

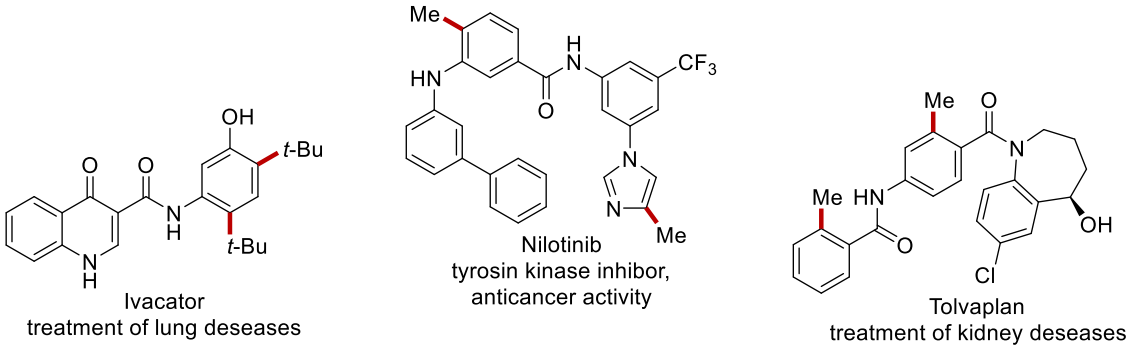

Figure 3.3: Selected examples for alkylated arenes as important scaffolds in important drugs.

During the past decades several ruthenium-catalyzed alkylations[58b, 230] have been reported. These methods highlighted that secondary as well as tertiary alkyl bromides predominantly allowed for selective functionalization in the *meta*-[68-69, 209] or *para*-position.[237] In sharp contrast, primary alkyl bromides were selectively converted into the *ortho*-alkylated products by ruthenium catalysis regime.[64-65] An exceptional behavior was observed in a ruthenium-enabled decarboxylative alkylation of phenylpyrazole **230** with bromocyclohexane (**218a**) yielding selectively the *ortho*-alkylated product **219aa** by C–C activation (Scheme 3.3).[232]

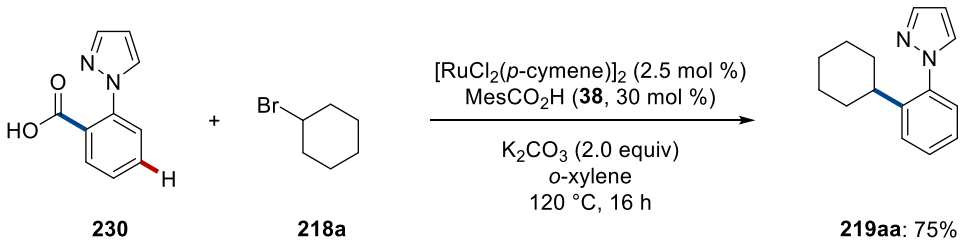

Scheme 3.3: Decarboxylative *ortho*-selective alkylation of arene **230** by ruthenium catalysis.

Inspired by this interesting example, the further investigation of the reaction mechanism of ruthenium-catalyzed *ortho*-selective C–H functionalizations was of interest. After an initial experimentation performed by Dr. K. Korvorapun with phenylpyridine as the starting material,[232] the alkylation of phenylpyrazole **217** was studied in greater detail by employing the C–H activation strategy.

During the course of the revision of this project, Larrosa concurrently reported on a ruthenium-catalyzed alkylation with high *ortho*-selectivity with secondary alkyl halides, which further supports the importance of so this thus far unprecedented reactivity.[238] Key to success for a switch in selectivity for alkylations with secondary alkyl bromides was in this case the use of a cyclometalated benzylamine complex as the catalyst.

3.2.1 Optimization Studies

Optimization studies performed by Dr. K. Korvorapun identified that the C–H alkylation of the pyrazole **217a** proceeded efficiently by employing ruthenium catalysis in the presence of a carboxylic acid, potassium carbonate as the base and *tert*-butyl benzene as the solvent.[232] However, the reaction with bromocyclohexane **219a** yielded predominantly the *ortho*-alkylated product **219aa**, accompanied by significant amounts of the *meta*-alkylated product **220aa** (Scheme 3.4). Control experiments validated the central role of the ruthenium complex and the beneficial effect of the carboxylic acid as additive.

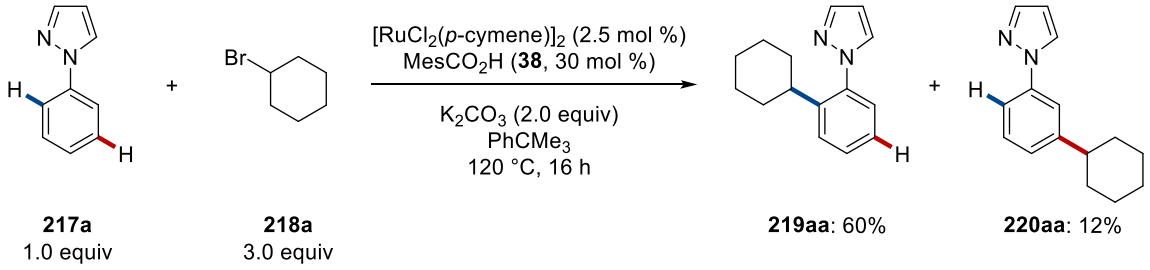

Reaction conditions: **217a** (0.50 mmol), **218a** (1.50 mmol), $[RuCl_2(p\text{-cymene})]_2$ (2.5 mol %), $MesCO_2H$ (**38**, 30 mol %), K_2CO_3 (1.00 mmol), $PhCMe_3$ (1.0 mL), 120 °C, 16 h, under N_2. Yields refer to the isolated products.

Scheme 3.4: Optimized reaction conditions for C–H alkylations under ruthenium catalysis.

Further optimization studies with respect to the ruthenium source were carried out to probe whether other complexes could serve as (pre-)catalysts (Table 3.6). The focus of these experiments was the comparison between the standard catalyst and cationic, arene-free ruthenium complexes (entries 1–4) under the same reaction conditions. They were identified to be comparably efficient, providing the alkylation products **219aa** and **220aa** with slightly increased over-all yields. Noteworthily, the reactions resulted in similar positional selectivity. In opposition to the additive-free conditions, the reactivity was completely suppressed in the presence of the $MesCO_2H$ (**38**) as additive in substoichiometric amounts (entry 5).

Table 3.6: Ruthenium-catalyzed regiodivergent alkylation with ruthenium complexes.

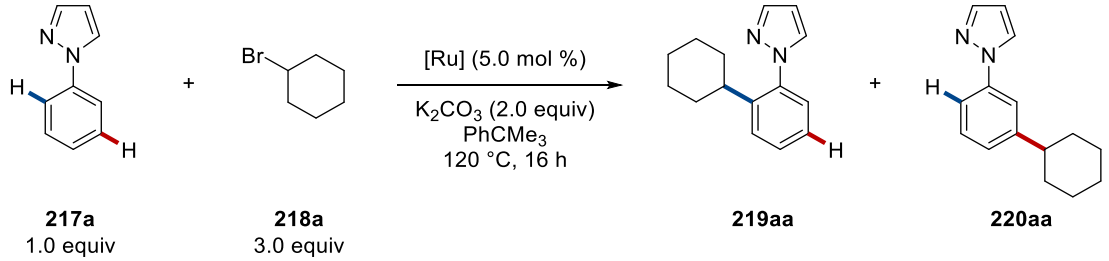

217a 1.0 equiv | **218a** 3.0 equiv | **219aa** | **220aa**

Entry	[Ru][a]	**219aa** [%]	**220aa** [%]
1	$[RuCl_2(p\text{-cymene})]_2$[b,c]	60	12
2	$[Ru(NC\text{-}t\text{-}Bu)_6](BF_4)_2$	60	8
3	$[Ru(NC\text{-}t\text{-}Bu)_6](PF_6)_2$	62	10
4	$[Ru(NC\text{-}t\text{-}Bu)_6](SbF_6)_2$	65	12
5	$[Ru(NC\text{-}t\text{-}Bu)_6](BF_4)_2$[c]	traces	---

[a] Reaction conditions: **217a** (0.50 mmol), **218a** (1.50 mmol), [Ru] (5.0 mol %), K_2CO_3 (1.00 mmol), $PhCMe_3$ (1.0 mL), 120 °C, 16 h, under N_2. Yields refer to the isolated products. [b] $[RuCl_2(p\text{-cymene})]_2$ (2.5 mol %). [c] Addition of $MesCO_2H$ (**38**, 30 mol %).

3.2.2 Substrate Scope

Since the bromocyclohexane **218a** furnished a mixture of the *ortho*- and the *meta*-alkylated products **219aa** and **220aa**, the generality of this selectivity was further elucidated by comparing the reaction outcome in terms of yield and site-selectivity for other substrates. To this end, the ruthenium-catalyzed C–H alkylation was performed with a series of different primary and secondary alkyl bromides **218** (Scheme 3.5). The C–H alkylation reaction was not restricted to the cyclohexyl moiety. In sharp contrast, smaller alkyl rings, such as cyclobutyl were introduced efficiently in 71%, thereby furnishing exclusively the *ortho*-functionalized product **219ab**. Contrarily, bromocyclopentane and bromocyclohexane **218a** and **218c** resulted in a mixture of both isomers. Whereas in case of bromocyclopentane **218c** the *meta*-alkylated product **220ac** was obtained primarily, in the reaction with bromocyclohexane **218a** the *ortho*-substituted phenylpyrazole **219aa** was predominantly formed. These results suggest that not only the steric demand of the alkylating reagent determines the site-selectivity. Upon treatment of arene **217a** with seven- or eight-membered alkyl bromides **218d** and **218e**, the corresponding products were obtained with good yields and excellent site-control for *meta*-functionalization (**220ad**, **220ae**). Additionally, the primary neopentyl bromide **218f** was converted selectively

to the corresponding *ortho*-alkylated products **219af** and **219bf**. Interestingly, in this case the change to *o*-xylene as the reaction solvent was advantageous and resulted in a slightly higher yield than in the previously employed *tert*-butyl benzene.

To further analyze the robustness of the ruthenium-catalyzed C–H alkylation, differently decorated pyrazolyl arenes **217** were used as the starting materials (Scheme 3.6). Arenes with electron-donating as well as electron-withdrawing groups furnished the corresponding products **219** in moderate to good yields. However, the yield was significantly diminished in case of the electron-deficient trifluoromethylated arene **217d** compared to the yields achieved in case of electron-rich arenes. Not only the yield, but also the position-selectivity was affected by the electronic properties. For arenes bearing an electron-donating or neutral substituent in *para*-position to the pyrazole, both, the *ortho*- and the *meta*-functionalized products **219** and **220** were obtained. Here, the *ortho*-alkylated products **219** were accessed in majority with a ratio ranging from 71:29 for the methylated substrate **217c** to 87:13 for the unsubstituted substrate **217a**. Contrarily, arylpyrazoles **217d** with electron-withdrawing functionality afforded the *ortho*-alkylated product **219da** in a completely selective manner, as also observed for other derivatives bearing electron-withdrawing substituents.

The change from pyrazole to 3,5-dimethylpyrazole as the directing group had likewise a significant impact on the site-selectivity of the reaction (Scheme 3.7). Independent on the ring size of different secondary alkyl bromides **218**, the developed reaction conditions for the ruthenium-mediated alkylation furnished solely the *meta*-substituted products **220**, accompanied by a significant amount of the dialkylation product in case of bromocycloocctane (**218e**). Equally, neopentyl bromide **218f** resulted in *meta*-alkylation to provide **220ef** as the sole reaction product.

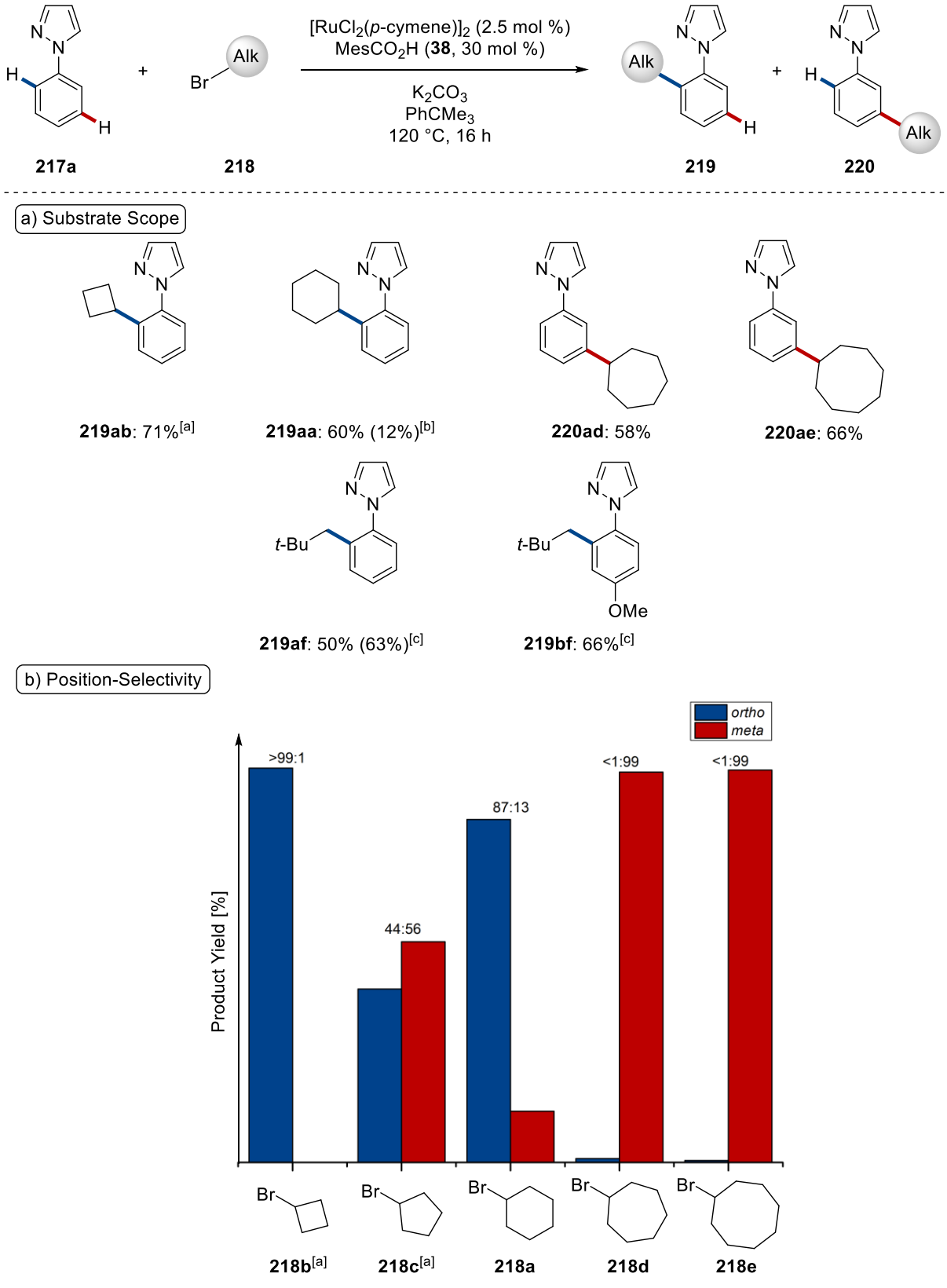

Reaction conditions: **217a** (0.50 mmol), **218** (1.50 mmol), $[RuCl_2(p\text{-cymene})]_2$ (2.5 mol %), $MesCO_2H$ (**38**, 30 mol %), K_2CO_3 (1.00 mmol), $PhCMe_3$ (1.0 mL), 120 °C, 16 h, under N_2. Yields refer to the isolated products. [a] Reaction was performed by Dr. K. Korvorapun. [b] Yield of the *meta*-alkylated product is given in parentheses. [c] *o*-Xylene as solvent.

Scheme 3.5: a) Scope and b) position-selectivity for C–H alkylation of phenylpyrazole (**217**).

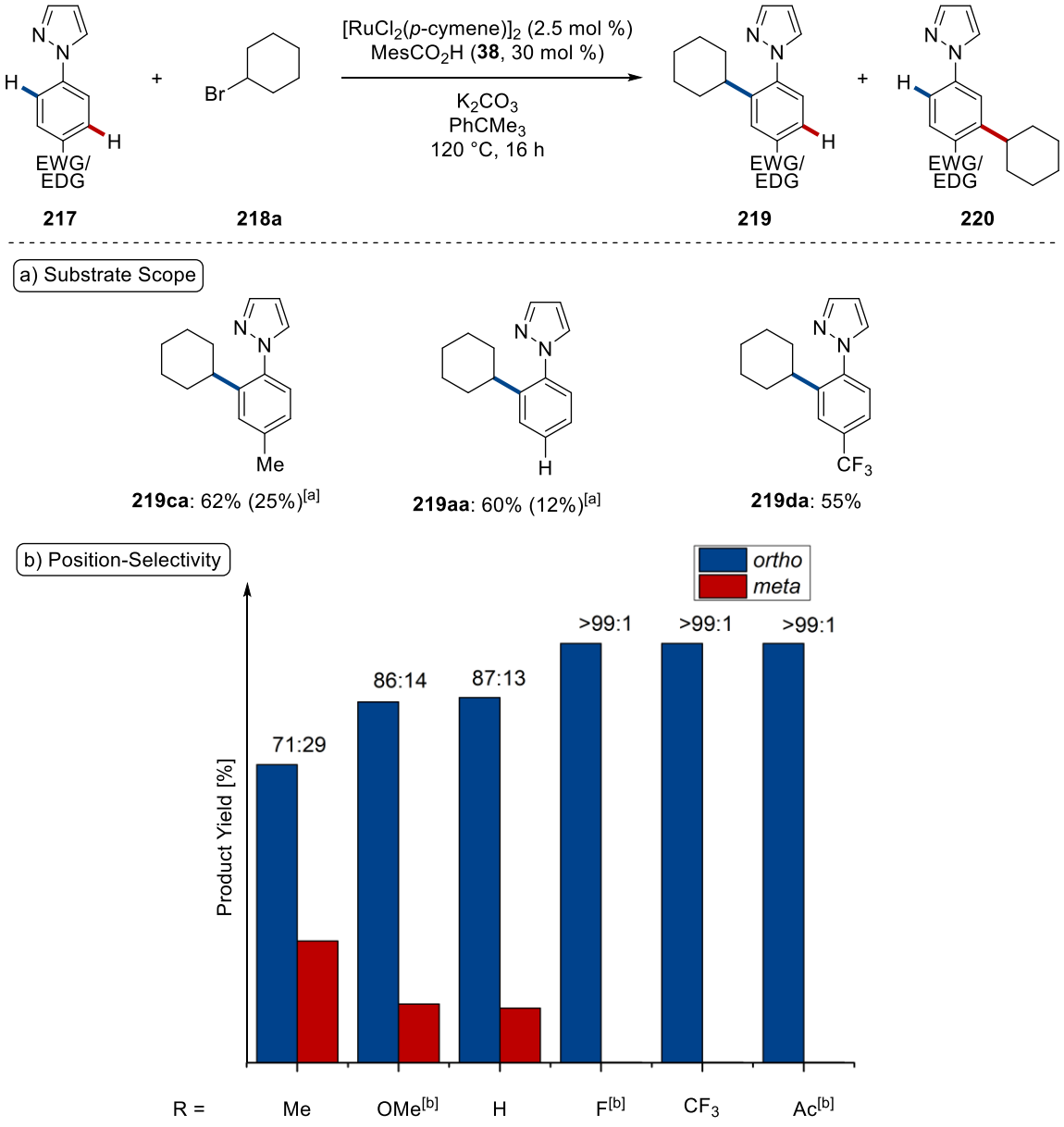

Reaction conditions: **217** (0.50 mmol), **218a** (1.50 mmol), $[RuCl_2(p\text{-cymene})]_2$ (2.5 mol %), $MesCO_2H$ (**38**, 30 mol %), K_2CO_3 (1.00 mmol), $PhCMe_3$ (1.0 mL), 120 °C, 16 h, under N_2. Yields refer to the isolated products. [a] Yield of the *meta*-alkylated product is given in parentheses. [b] Reaction was performed by Dr. K. Korvorapun.

Scheme 3.6: Electronic effect of aryl pyrazoles **217** on the a) reactivity and b) position-selectivity of the ruthenium-catalyzed C–H alkylation with bromocyclohexane **218a**.

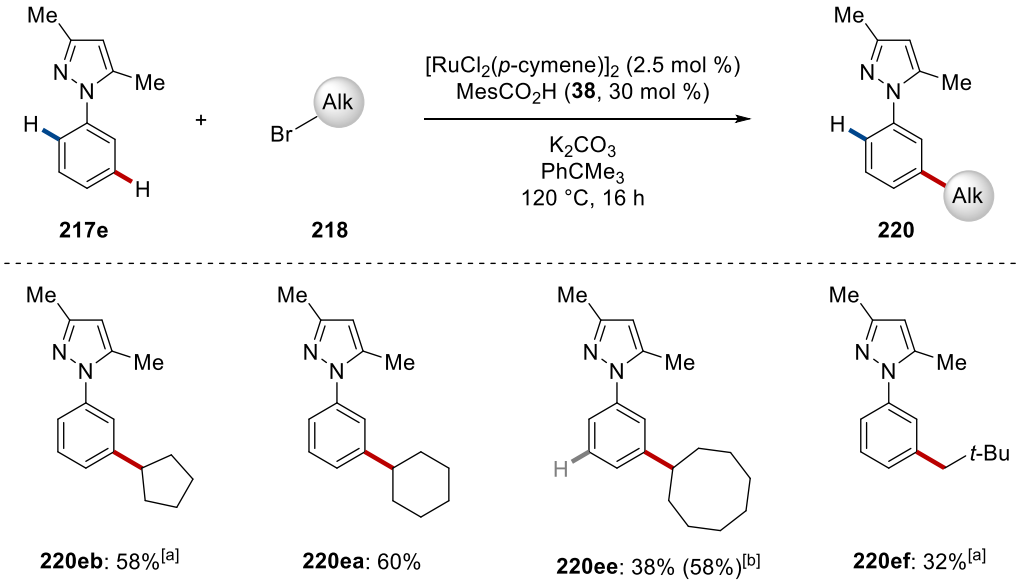

Reaction conditions: **217e** (0.50 mmol), **218** (1.50 mmol), $[RuCl_2(p\text{-cymene})]_2$ (2.5 mol %), $MesCO_2H$ (**38**, 30 mol %), K_2CO_3 (1.00 mmol), $PhCMe_3$ (1.0 mL), 120 °C, 16 h, under N_2. Yields refer to the isolated products. [a] Reaction was performed by Dr. K. Korvorapun. [b] Yield of the di-alkylated product is given in parentheses.

Scheme 3.7: Ruthenium-catalyzed C–H alkylations of dimethylated phenylpyrazole **217e**.

3.2.3 Mechanistic Studies

After having explored the applicability and the position-selectivity for the developed ruthenium-mediated C–H alkylation, several mechanistic experiments were performed to examine the catalyst's mode of action. To this end, the reaction was performed in the presence of different radical scavengers (Scheme 3.8).

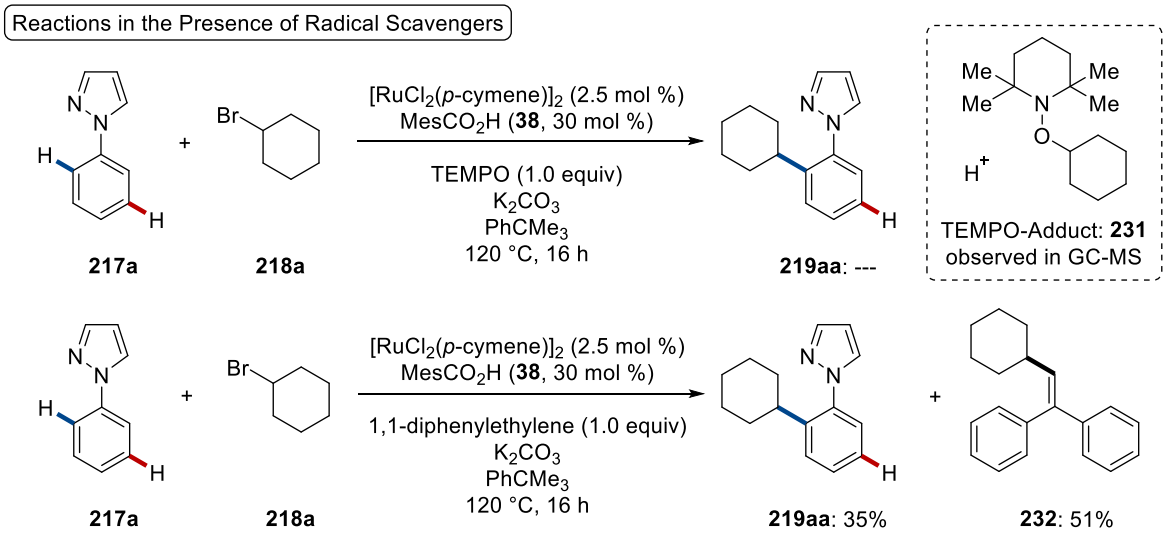

Scheme 3.8: Ruthenium-catalyzed regiodivergent alkylations in the presence of radical scavengers.

The regiodivergent alkylation was completely suppressed in the presence of TEMPO. Analysis of the crude mixture by gas chromatography analysis confirmed the formation of the TEMPO-adduct **231**. Furthermore, the catalytic efficacy was strongly inhibited by addition of 1,1-diphenylethylene in stoichiometric amounts. The reaction resulted in a significantly reduced yield of the *ortho*-alkylated product **219aa**, whereas the *meta*-alkylated product **220aa** was not formed at all. Instead, 2-cyclohexyl-1,1-diphenylethylene (**232**) was isolated in a considerable amount of 51%. The formation of this side product proposes that the alkyl bromide undergoes a homolytic C–Br cleavage.

The reaction mechanism for the regiodivergent alkylation was further studied with diastereomerically pure electrophiles *cis*-**218g** and *trans*-**218g** (Scheme 3.9).[232] The reactions performed by Dr. K. Korvorapun highlighted that the stereochemistry of the alkyl moiety remained untouched in case of the *ortho*-alkylation for both diastereomers and the corresponding products *cis*-**219ag** and *trans*-**219ag** were obtained. This finding provides support for a concerted oxidative addition/reductive elimination reaction mechanism for *ortho*-C–H functionalization. In contrast, the alkylation in *meta*-position with the single isomer *cis*-**218g** resulted in a diastereomeric mixture of **220ag**, which can be explained by the formation of an alkyl radical *via* single-electron transfer. This observation is in good agreement with the results in the experiments with radical scavengers. The site-selectivity and stereochemistry of the obtained products **219ag** could be confirmed by 2D-NMR and X-ray analysis.

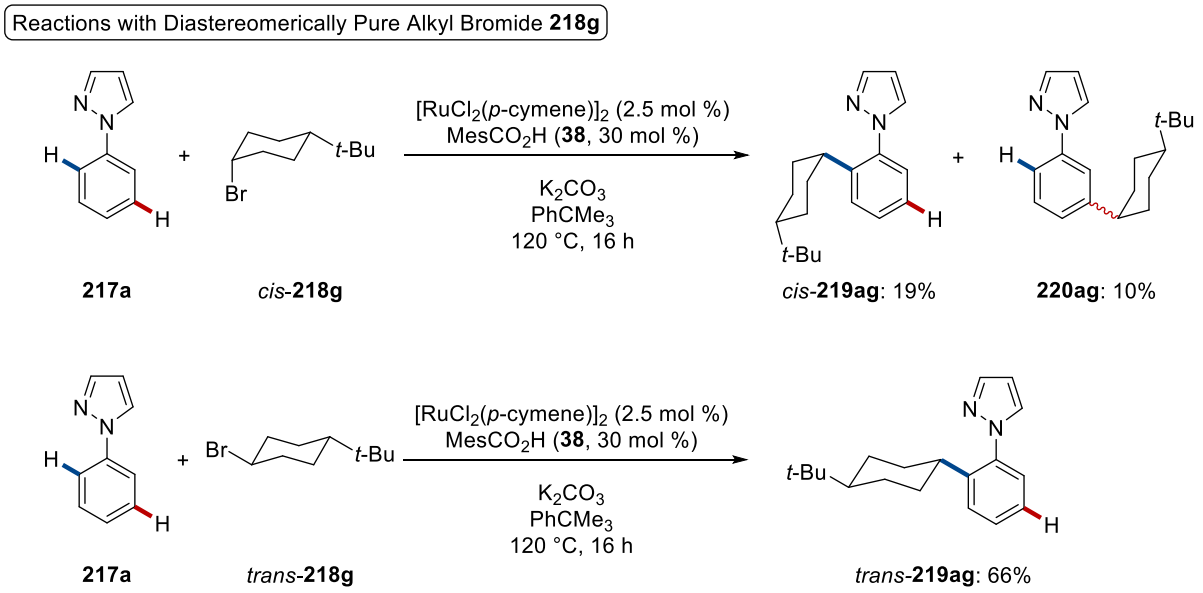

Scheme 3.9: C–H Alkylation of pyrazole **217a** with diastereomerically pure alkyl bromide **218g**.

Moreover, a careful analysis of the crude reaction mixture of phenylpyrazole **217a** and bromocyclohexane **218a** was performed by means of gas chromatography analysis (Figure 3.4). Besides a kinetic profile which monitored the formation of the *ortho*- and *meta*-alkylated products **219aa** and **220aa** in parallel, some hints on the ruthenium catalyst could be obtained. During the first period of the regiodivergent alkylation, a significant *p*-cymene ligand dissociation was observable, resulting in 62% of free *p*-cymene, which is indicative of an arene-free ruthenium complex as the active catalyst.

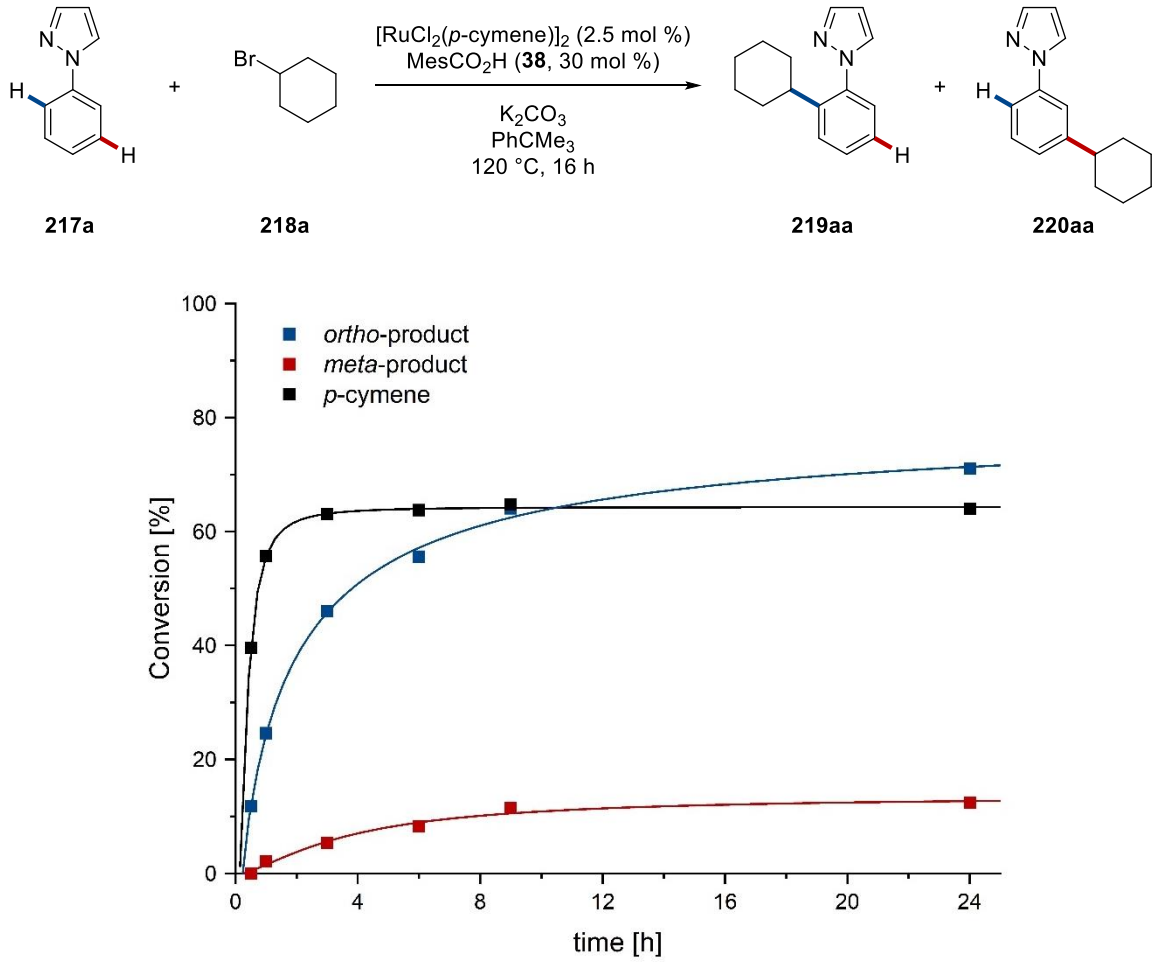

Figure 3.4: Detection of free *p*-cymene and the reaction profile for the regiodivergent C–H alkylation.

To further elucidate the nature of the active ruthenium catalyst, the well-defined cyclometalated ruthenium complex **233** was prepared to be employed under the optimized reaction conditions. Stoichiometric amounts of the ruthenacycle **233** failed to provide the alkylation products **219aa** and **220aa** in the absence of acid **38** (Scheme 3.10a). The addition of the carboxylic acid additive **38** afforded the *ortho*-functionalized product **219aa** in a low yield of 25%. Also in case of utilization of the cyclometalated complex **233** in catalytic amounts, the addition of $MesCO_2H$

(**38**) was essential for efficient catalysis (Scheme 3.10b). The well-defined arene-free complex was capable to catalyze the envisioned alkylation, thereby providing a mixture of both alkylated products 2**19aa** and **220aa** in a ratio which was similar to the one obtained in the standard reaction conditions with $[RuCl_2(p\text{-cymene})]_2$ as the catalyst. Interestingly, findings by Dr. K. Korvorapun[232] with the cyclometalated ruthenium complex with 3,5-dimethyl pyrazole (**217e**) as C–H activated ligand indicated that this complex afforded a mixture of the *ortho*- and *meta*-alkylated products **219ea** and **220ea** in the absence of the additive **38**. However, in the presence of the $MesCO_2H$ (**38**), the corresponding ruthenium complex exclusively furnished the *meta*-alkylated product **220ea**, which is in accordance with the obtained products under the optimized reaction conditions.

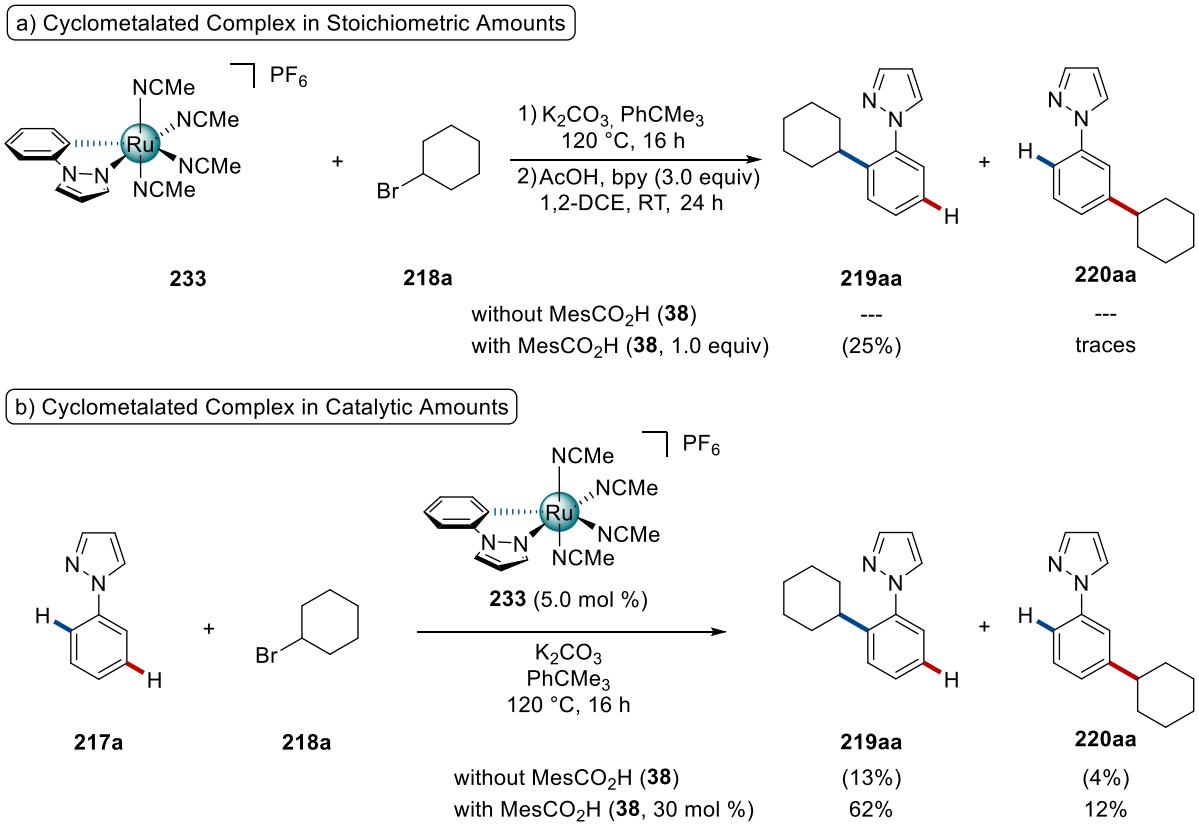

Scheme 3.10: Ruthenium-catalyzed C–H alkylations with cyclometalated ruthenium complex **233** a) in stoichiometric amounts and b) in catalytic amounts.

3.2.4 Proposed Catalytic Cycle

Based on the experimental results as well as calculations performed by Dr. T. Rogge,[232] a plausible reaction mechanism for the ruthenium-catalyzed regiodivergent alkylation was proposed (Scheme 3.11).

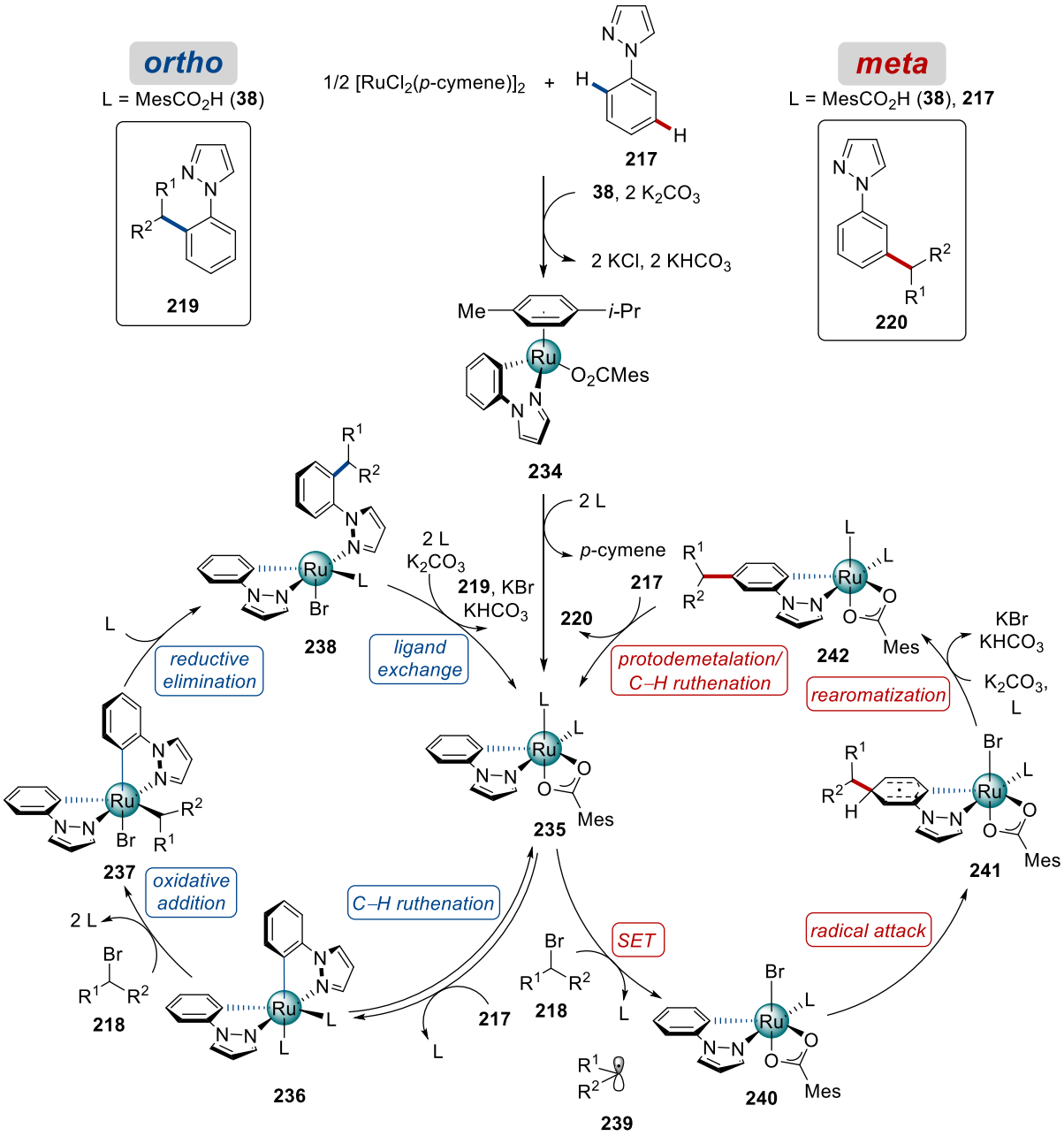

Scheme 3.11: Plausible reaction mechanism for the ruthenium-catalyzed regiodivergent alkylation of arene **217**.

The catalytic manifold is initiated by a carboxylate-assisted C–H bond activation and dissociation of the *p*-cymene ligand to provide ruthenacycle **235** (Scheme 3.11 center). *Ortho*-selective functionalization is enabled by coordination of a second molecule of the arene **217** (Scheme 3.11 left), which undergoes C–H ruthenation to furnish the biscyclometalated ruthenium intermediate **236**. Subsequent oxidative addition of alkyl bromide **218** affords ruthenium(IV) complex **237**. Next, reductive elimination along with subsequent ligand exchange closes the catalytic cycle for the *ortho*-selective alkylation by product release, thereby regenerating the monocyclometalated ruthenium(II) complex **235**. Similarly, the *meta*-selective

functionalization is realized starting from the ruthenium(II) key intermediate **235**. In this case, single-electron transfer (SET) to alkyl bromide **218** occurs, which affords the ruthenium(III) complex **240** and generates the alkyl radical **239** (Scheme 3.11 right). This stabilized radical attacks on the C–H activated arene ligand preferentially in *para*-position to the ruthenium, which is leading to the triplet ruthenium species **241**. Subsequent ligand-to-metal electron transfer and rearomatization generates ruthenacycle **242**. The catalytic cycle for the *meta*-selective transformation is closed by protodemetalation, which furnishes the *meta*-alkylated product **220**. At the same time, C–H ruthenation of a new arene substrate **217** affords the central monocyclometalated ruthenium(II) intermediate **235**.

3.3 PHOTO-INDUCED RUTHENIUM-CATALYZED C–H ARYLATIONS AT AMBIENT TEMPERATURE

Given the vast utility of diaryl scaffolds as building blocks in numerous components of biological relevance, efficient and sustainable arylation procedures are of great interest. Therefore, ruthenium-catalyzed direct C–H arylations have been identified as a valuable tool for drug discovery, crop protection and material science.[85a, 239] Ruthenium-catalyzed C–H arylations enabled the synthesis of biologically active compounds, such as Anacetrapib, the tetrazole-based block-buster drugs Valsartan and the structurally related Candesartan, which had been accomplished by Oullet at Merck,[240] Ackermann[84, 85b] and Seki at API Corporation[241] (Figure 3.5). Besides the synthesis of biorelevant compounds, ruthenium-catalyzed arylations have surfaced as a valuable methodology for the late-stage diversification of peptides[242] and nucleosides.[243]

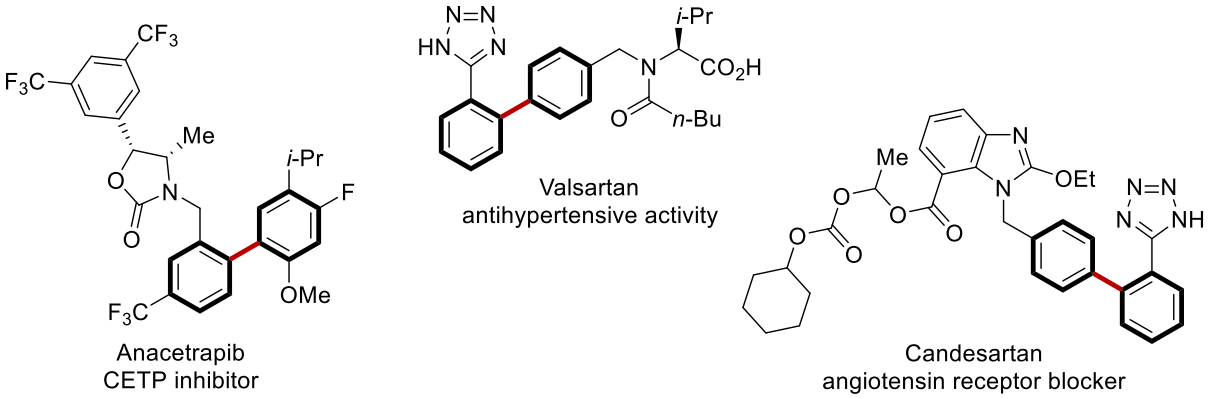

Figure 3.5: Selected examples of diaryl motifs in bioactive compounds and drugs.

Indisputable progress has been made in the past years to develop robust and general procedures for ruthenium-catalyzed arylations. In addition, the reaction mechanism was studied in greater detail, which is thus far believed to follow a ruthenium(II/IV) pathway by going through oxidative addition and reductive elimination.[82] However, the established reaction conditions come with liabilities. Despite major advances, the direct ruthenium-mediated arylation of aromatic C–H bonds continues to require harsh reaction conditions with temperatures of typically 100–140 °C.[81-82, 244]

In contrast, photoredox catalysis[22c, 188, 245] has been recognized as an indispensable alternative to enable C–H functionalizations under milder conditions and frequently at ambient temperature. Although numerous reports haven proven the applicability for several metals, the use of exogenous photocatalysts, such as light absorbing ruthenium[190-191, 246] and iridium

complexes[247] or organic dyes[248] is predominantly crucial. Ackermann and later independently Greaney addressed this drawback recently and reported *meta*-selective ruthenium-catalyzed alkylations at ambient temperature.[209-210] An *in situ* generated cyclometalated complex was suggested to have a dual function by absorbing visible light and by enabling the activation of the C–H bond. The versatility of sustainable photo-induced transformations was aimed to further investigate for arylations in ruthenium catalysis regime, as illustrated by Ackermann.[249] In an independent work, Greaney thereafter presented similarly a photo-induced arylation following the same strategy, which was published while this project was under revision.[250]

3.3.1 Optimization Studies

Detailed optimization studies performed by Dr. K. Korvorapun showed that the desired photo-induced ruthenium-catalyzed *ortho*-arylation of arene **44a** through a C–H activation was achieved most efficiently with the [$Ru(OAc)_2$(*p*-cymene)] complex as catalyst in 1,4-dioxane or DMA as solvent in the presence of K_2CO_3 as base (Scheme 3.12).[249] Considering the faster work-up with 1,4-dioxane by filtration and its easier removal, this was chosen as the solvent. In contrast to the majority of the reported transition metal-catalyzed photochemical reactions, an exogenous photocatalyst was in this case not required, as previously shown for *meta*-alkylations in ruthenium catalysis regime.[209-210] Control experiments without the ruthenium catalyst or the base confirmed their essential roles to efficiently furnish the desired arylated product **243aa**. Furthermore, the reaction fell short in providing the desired product without blue LED light irradiation.[249]

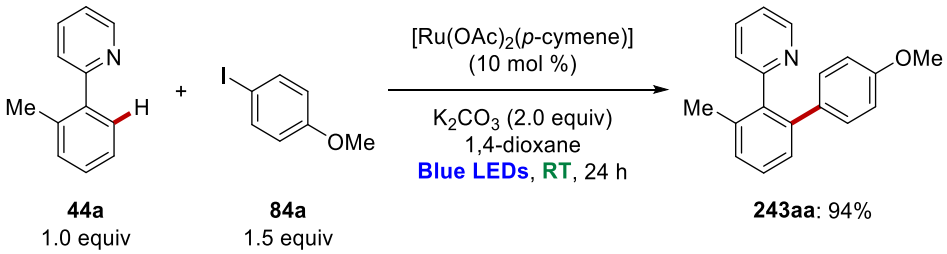

Scheme 3.12: Optimized conditions for photo-induced arylation of pyridine **44a**.

After having identified the optimized reaction conditions for aryl iodide, arenes bearing other leaving groups were subjected as substrate **82** to the arylation reaction at ambient temperature (Table 3.7). Notably, aryl bromide was likewise a compatible arylation reagent which afforded the *ortho*-arylated product **243aa** in good yield, although the reaction was less efficient than with aryl iodide (entries 1–2). In contrast, the use of aryl chloride resulted in a significantly lower yield (entry 3). In addition, employing triflate and tosylate as pseudohalides was also not

beneficial for the reaction outcome and furnished the product **243aa** with moderate efficacy (entries 4–5).

Table 3.7: Screening of the leaving group for the photo-induced arylation.

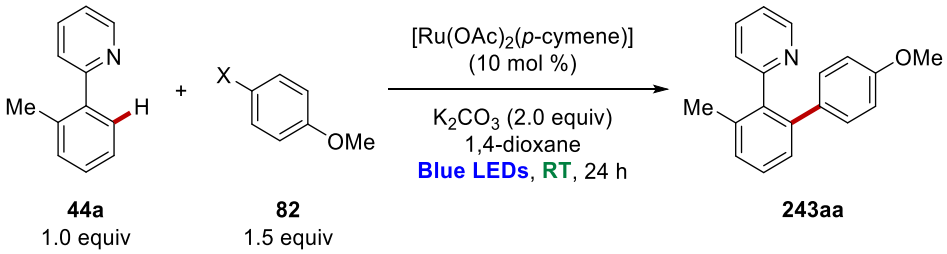

Entry	(Pseudo)halides	**243aa** [%][a]
1	I	94 (94)
2	Br	68 (69)[b]
3	Cl	(43)[b]
4	OTf	(39)[c]
5	OTs	45 (46)

[a] Reaction conditions: **44a** (0.50 mmol), **82** (0.75 mmol), [Ru(OAc)2(*p*-cymene)] (10 mol %), K_2CO_3 (1.00 mmol), 1,4-dioxane (2.0 mL), 30–33 °C, 24 h, under N_2, blue LED irradiation (450 nm). Yields refer to the isolated products. The conversion in the parentheses was determined by ^{1}H-NMR using 1,3,5-trimethoxybenzene as the internal standard. [b] Reaction was performed by Dr. K. Korvorapun. [c] Reaction was performed by A. Casnati.

3.3.2 Substrate Scope

Having identified the optimized reaction conditions, the generality of the ruthenium-catalyzed *ortho*-arylation of phenylpyridine **44a** was examined by using a broad variety of different aryl iodides **84** to obtain the corresponding products **243** (Scheme 3.13). Coupling partners bearing diverse functional groups in *para*-position demonstrated a great robustness of the C–H arylation and yielded the corresponding diaryl derivatives **243aa**–**243al**. Electron-donating and electron-withdrawing moieties were fully tolerated and the desired products **243** were obtained in good to excellent yields, while only trace amounts of the products were isolated for reactions which had been performed in the absence of light. The synthetic utility of this exceedingly mild arylation procedure could be mirrored by the broad functional group tolerance under these conditions. Among the explored substrates, several sensitive, yet valuable functional groups were fully tolerated and furnished arenes with useful substituents, such as free hydroxyl (**243ae**), chloro (**243ah**), bromo (**243ai**), ketone (**243ak**), ester (**243al**) and nitrile (**243af**) albeit

the latter one with a reduced yield. Moreover, the arylation reaction was not restricted to *para*-substituted aryl iodides **84**. In contrast, arenes **84** with substituents in *meta*- and *ortho*-position were selectively converted into the corresponding products **243am**–**243ao** with slightly diminished yield for the *ortho*-substituted one, presumably due to hindering steric reasons. Furthermore, the photo-induced arylation was applicable to heteroarenes (**243ap**–**243aq**), including (*NH*)-free indole as the substituent. Additionally, coupling partner with biorelevant scaffolds, such as menthol (**84r**) and oleic acid (**84s**) were suitable arenes in the ruthenium catalysis regime, accessing **243ar** and **243as** in moderate efficacy.

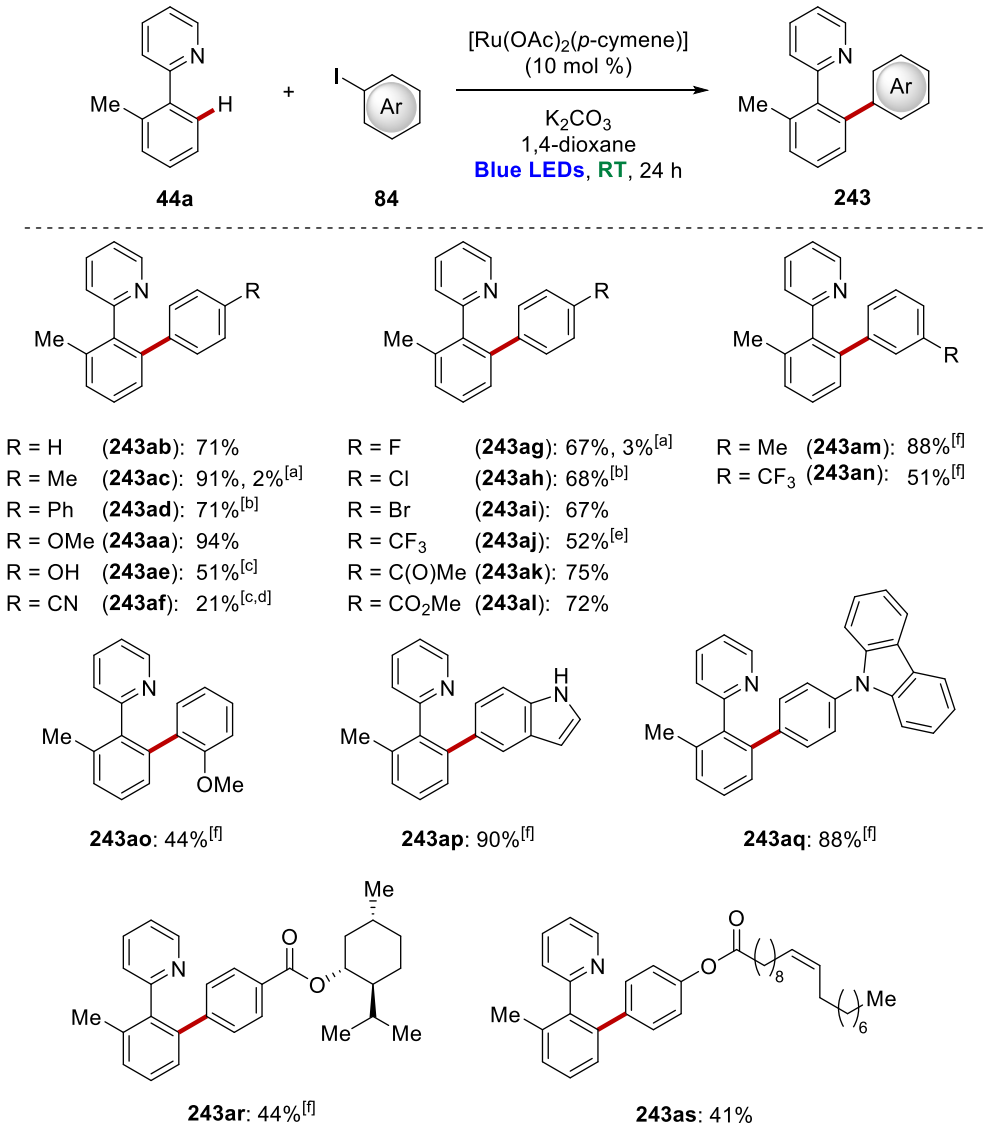

Reaction conditions: **44a** (0.50 mmol), **84** (0.75 mmol), [Ru(OAc)$_2$(*p*-cymene)] (10 mol %), K_2CO_3 (1.00 mmol), 1,4-dioxane (2.0 mL), 30–33 °C, 24 h, under N_2, blue LED irradiation (450 nm). Yields refer to the isolated products. [a] Reaction in the absence of light at 30–34 °C. [b] Reaction was performed by A. Casnati. [c] DMA was used as solvent. [d] 48 h. [e] Ar-Br was used. [f] Reaction was performed by Dr. K. Korvorapun.

Scheme 3.13: Photo-induced direct arylation of phenylpyridine **44a**.

Notably, the developed ruthenium-catalyzed arylation at ambient temperature was applicable for twofold C–H activation to afford the bisfunctionalized product **244aa** with excellent selectivity by using 1,4-diiodobenzene (**84t**) as the limiting reagent (Scheme 3.14).

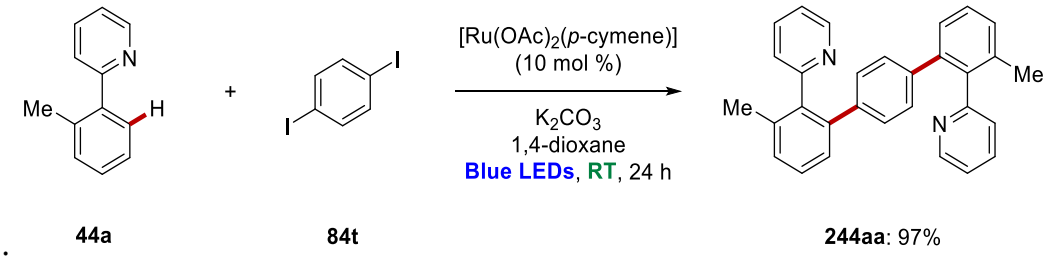

Reaction conditions: **44a** (1.10 mmol), **84t** (0.50 mmol), $[Ru(OAc)_2(p\text{-cymene})]$ (10 mol %), K_2CO_3 (2.00 mmol), 1,4-dioxane (2.0 mL), 30–33 °C, 24 h, under N_2, blue LED irradiation (450 nm). Yield refers to the isolated product.

Scheme 3.14: Twofold arylation of phenylpyridine **44a**.

The versatility of the arylation reaction was further highlighted with arenes with chelation assistance by other heterocycles (Scheme 3.15).

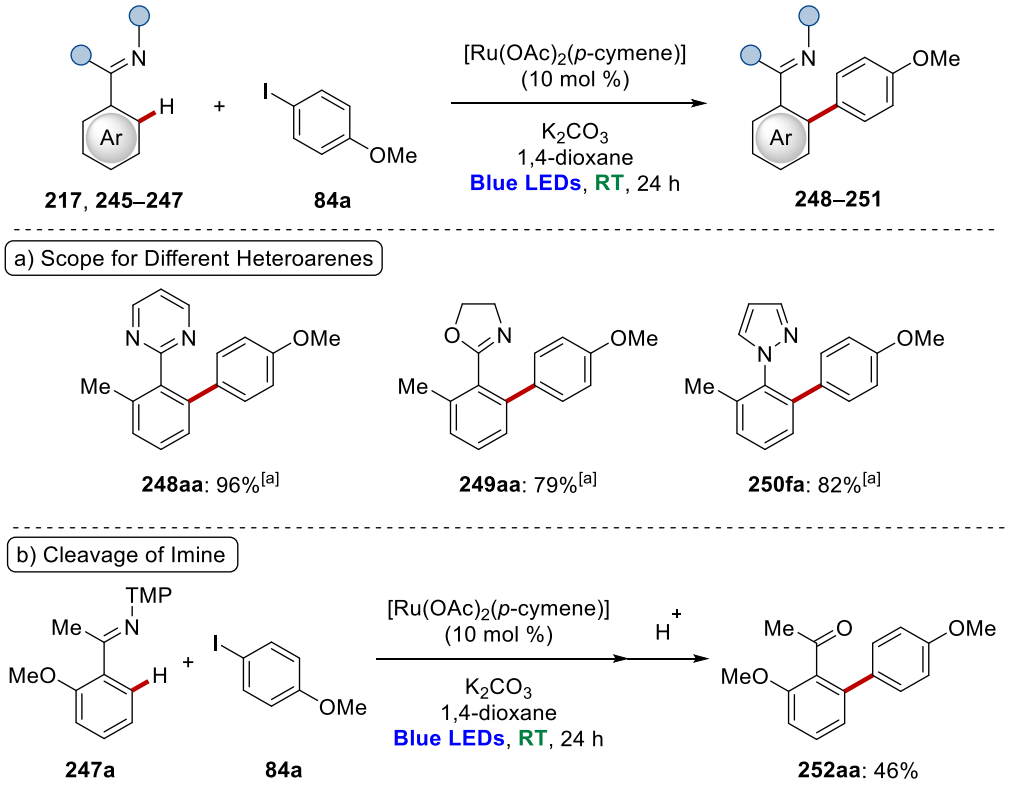

Reaction conditions: **217**, **245**–**247** (0.50 mmol), **84a** (0.75 mmol), $[Ru(OAc)_2(p\text{-cymene})]$ (10 mol %), K_2CO_3 (1.00 mmol), 1,4-dioxane (2.0 mL), 30–33 °C, 24 h, under N_2, blue LED irradiation (450 nm). Yields refer to the isolated products. [a] Reaction was performed by Dr. K. Korvorapun.

Scheme 3.15: Ruthenium-catalyzed C–H arylation a) with assistance of various heteroarenes and b) catalysis and cleavage with transformable ketimine group.

Not only pyridines, but also pyrimidines, oxazolines and pyrazoles, among others, were converted into the *ortho*-arylated products **248aa**, **249aa** and **250fa**, with excellent yields up to 96% (Scheme 3.15a).[249] Additionally, ketimine **247a** was selectively transformed into the corresponding product **251aa**. Subsequent cleavage of the imine directing group under acidic conditions provided ketone **252aa** in a moderate yield over two steps (Scheme 3.15b).

Remarkably, the transition metal-catalyzed photo-induced arylation at ambient temperature was versatile to modify valuable substituted click-triazoles[251] under slightly modified reaction conditions (Scheme 3.16). Differently substituted triazoles **253** provided the envisioned products **254** in synthetically reasonable yields (**254aa**–**254aq**). The results showed that solely the *ortho*-methyl substituted substrate **253b** resulted in lower conversions (**254bc**, **254ba**), while a methoxy functionality was beneficial (**254aa**–**254ag**). Furthermore, the *meta*-substituted arene **84m** resulted in an unsatisfactory reaction outcome with low yields of **254am** and **254bm**. Besides differently substituted aryl iodides, the arylation protocol was suitable for different heterocycles. Indole and carbazole scaffolds **84p** and **84q**, as well as 5-iodobenzo[*d*][1,3]dioxole (**84u**) exhibited good reactivity under the photochemical reaction conditions. Product **254au** was tested in cell culture studies performed by our collaboration partner Prof. Dr. W.-H. Zimmermann with the intention to identify a new target in heart failure therapy by cell culture studies with cardiac muscle cells and in an Engineered Human Myocardium (EHM) model. Preliminary results for triazole **254au** regarding the force and frequency of contraction, the contraction rhythm as well as the toxicity were promising, and a series of structural derivatives was prepared for further cell culture studies to offer derivatives for a structure-activity relationship study. Aside from differently alkylated triazoles **254cu**–**254du**, the dimethoxy analogue **254av** was prepared by the mild ruthenium arylation approach. However, the use of catechol iodide **84w** failed in delivering the desired product **254aw**.

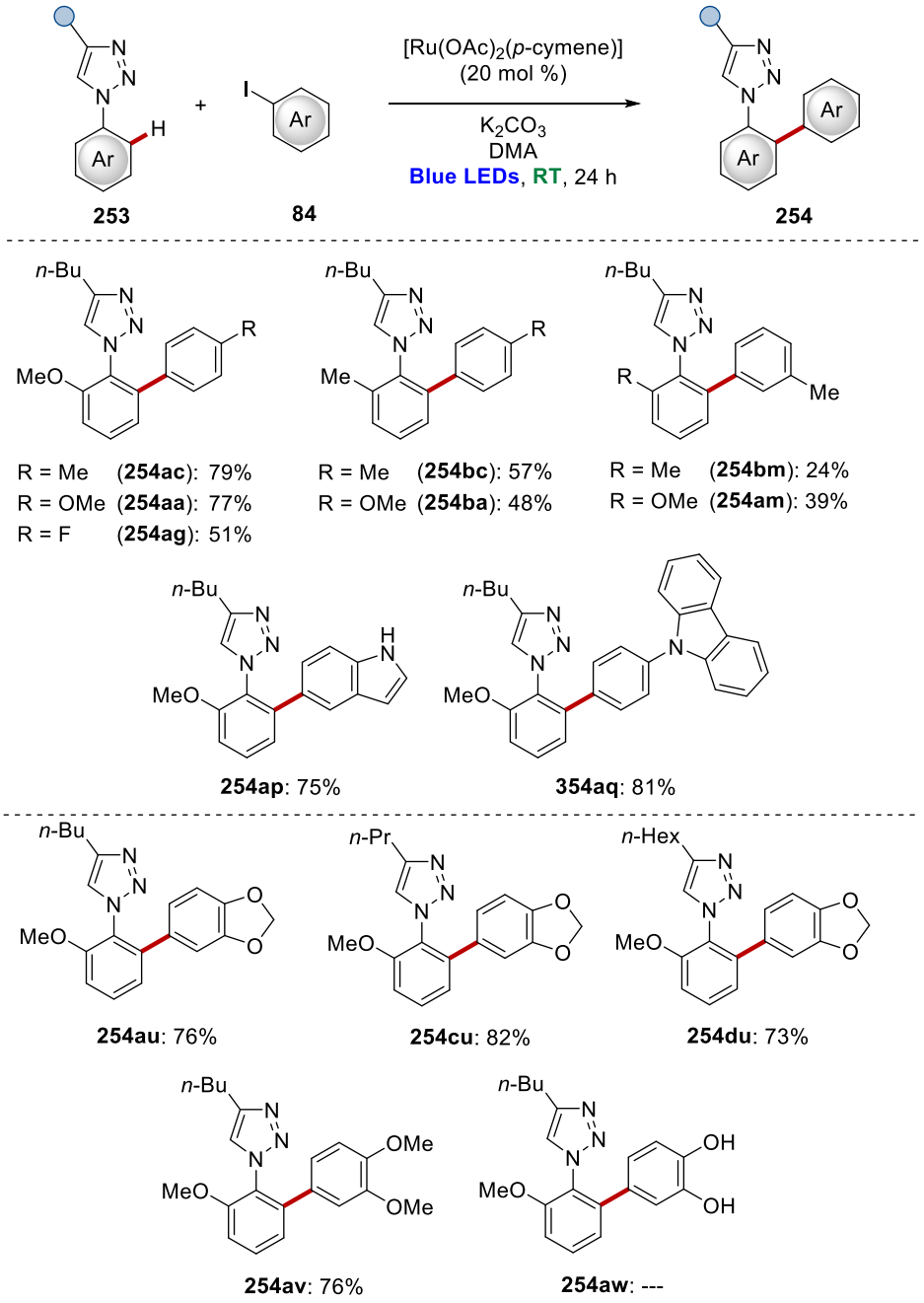

Reaction conditions: **253** (0.50 mmol), **84** (1.50 mmol), [Ru(OAc)$_2$(*p*-cymene)] (20 mol %), K_2CO_3 (1.00 mmol), DMA (2.0 mL), 30–33 °C, 24 h, under N_2, blue LED irradiation (450 nm). Yields refer to the isolated products.

Scheme 3.16: Substrate scope of photo-induced arylation for substituted triazoles **253**.

Inspired by this mild ruthenium-catalyzed arylation using visible light as external stimulus, T. Mandal developed reaction conditions which allowed the efficient arylation of styryl pyridines **255** (Scheme 3.17a).[252] In this case, the use of a solvent mixture of 1,4-dioxane and DMA was key to success to achieve high conversions. Based on the optimized photochemical conditions, different derivatives of arene **255** were functionalized to afford the product in moderate to good yields (**256aa**–**256ca**). Interestingly, and in contrast to a previously reported ruthenium-

mediated arylation procedure of this compound class at elevated temperatures of 120 °C,[251d] an isomerization of the double bond was observed. To elucidate, whether this isomerization was caused by the blue LED irradiation, the functionalization of the standard substrate **255a** was repeated under conventional heating to 120 °C, which showed comparable efficacy and resulted likewise in an isomerization of the double bond. Furthermore, a control experiment was performed to analyze the impact of the light (Scheme 3.17b). Subjecting the isolated product **256aa** to the reaction conditions in absence of the aryl iodide **84a** caused a significant change in the *E*/*Z* ratio of the modified styryl pyridine **256aa** afterwards. This indicates, that the isomerization is promoted by the ruthenium catalyst in the presence of the light irradiation, while an iodine-mediated process could be ruled out.

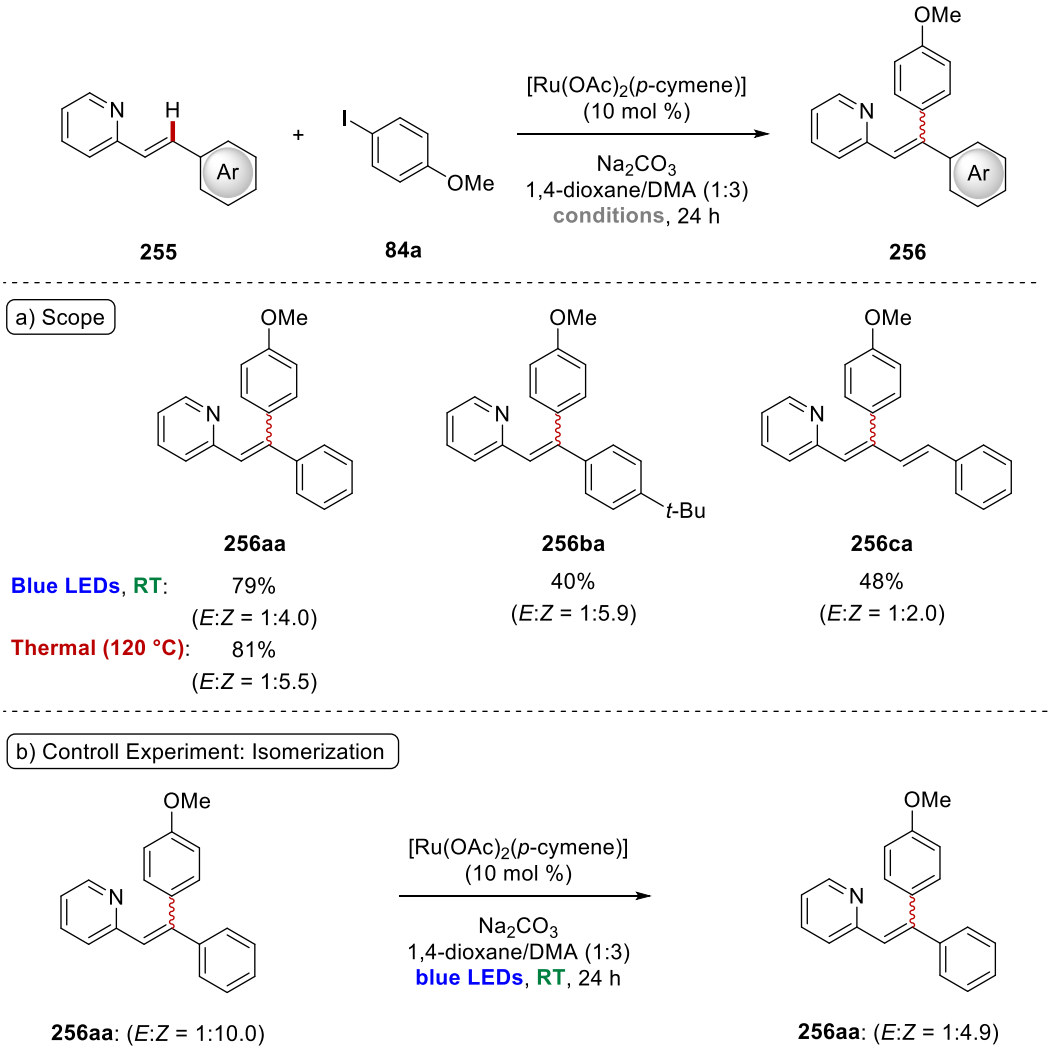

Reaction conditions: **255** (0.50 mmol), **84a** (0.75 mmol), [Ru(OAc)$_2$(*p*-cymene)] (10 mol %), Na_2CO_3 (1.00 mmol), 1,4-dioxane/DMA (1:3, 1.5 mL), 30–33 °C, 24 h, under N_2, blue LED irradiation (450 nm). Yields refer to the isolated products.

Scheme 3.17: Arylation of styryl pyridines **255** under slightly modified conditions. a) Substrate scope and b) control experiment for the isomerization of the double bond.

3.3.3 Comparison to Thermal Reaction Conditions

Besides the illustration of the broad applicability and robustness of the photo-induced direct C–H arylation through versatile ruthenium catalysis, the comparison to thermal conditions was of great interest for this project. To this end, a systematic analysis of the reaction efficacy was performed for different reaction temperatures under exclusion of light irradiation (Table 3.8).

Table 3.8: Determination of the reaction temperature for the direct arylation in thermal conditions.

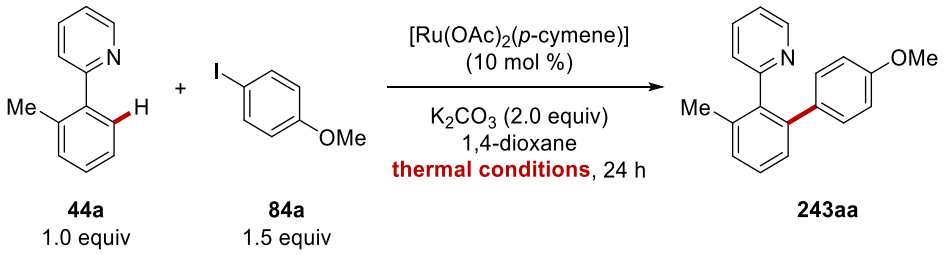

Entry	Temperature	**243aa** [%][a]
1	rt	(12)[b]
2	40 °C	(10)
3	60 °C	(15)
4	80 °C	(32)
5	100 °C	(49)
6	120 °C	91 (93)

[a] Reaction conditions: **44a** (0.50 mmol), **84a** (0.75 mmol), [Ru(OAc)$_2$(*p*-cymene)] (10 mol %), K_2CO_3 (1.00 mmol), 1,4-dioxane (2.0 mL), 30–33 °C, 24 h, under N_2, blue LED irradiation (450 nm) or heating using an oil bath. Yields refer to the isolated products. The conversions in the parentheses were determined by ^{1}H-NMR using 1,3,5-trimethoxybenzene as the internal standard. [b] Reaction was conducted in the same set-up as the photo-induced reaction. The vial was covered with aluminum foil to avoid irradiation with the light.

When the reaction was conducted under the same reaction conditions as the photochemical approach, but in the dark by shielding the vial with aluminum foil, only 12% of the product **243aa** could be detected (entry 1). Comparable outcomes were observed for thermochemical conditions at 40 °C and 60 °C reaction temperature (entries 2–3), thereby further substantiating the essential role of the visible light irradiation. A moderately efficient arylation of arene **44a** was monitored for 80 °C and 100 °C with 32% and 49% conversion (entries 4–5). Only at

120 °C, the ruthenium-catalyzed *ortho*-arylation of arene **44a** underwent highly efficient and furnished the product **243aa** in synthetically reasonable amounts (entry 6).

After having confirmed that the thermally driven reaction requires a rather harsh reaction temperature of 120 °C, several experiments were conducted to probe whether the reaction conditions have an impact on the reaction selectivity (Scheme 3.18).

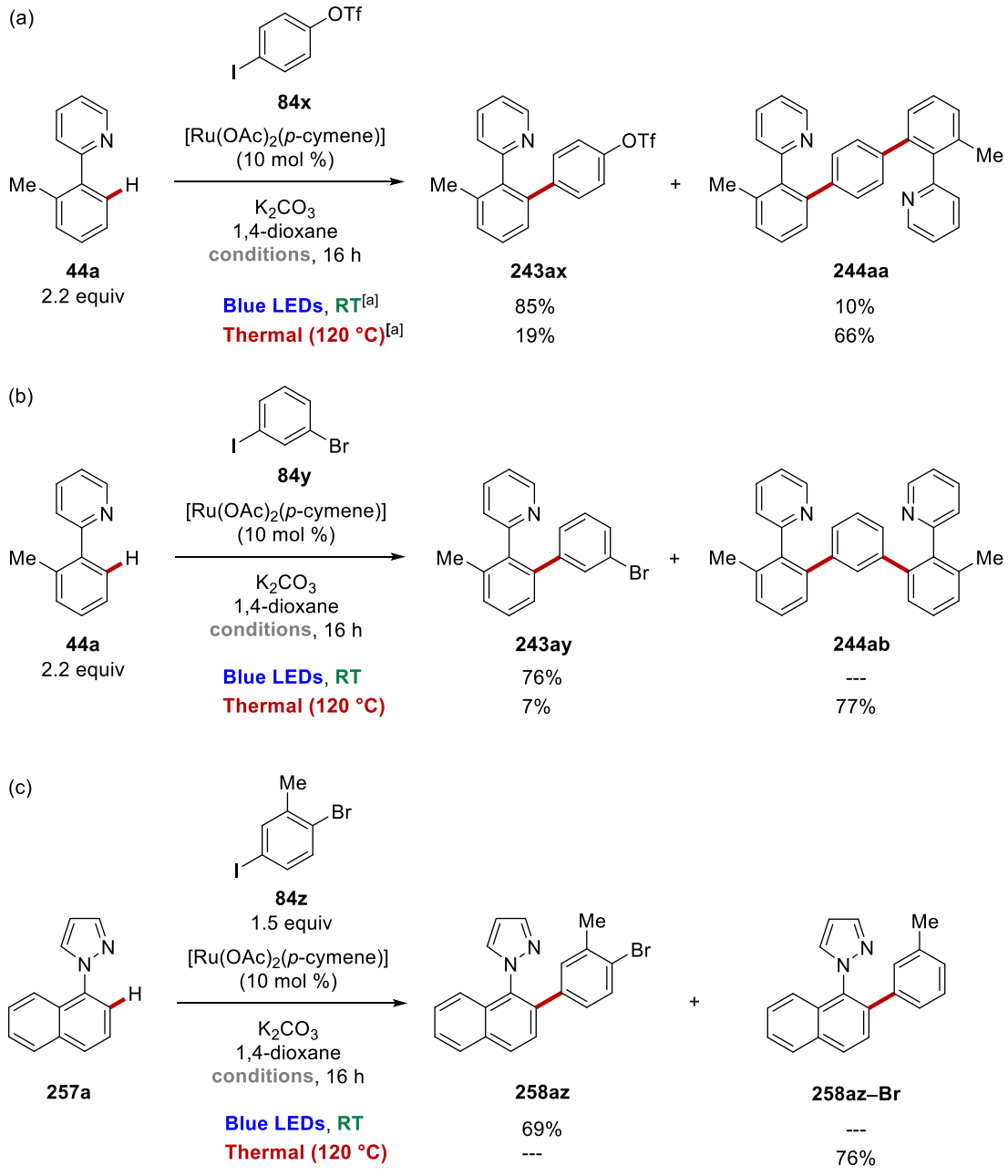

Reaction conditions: **44a**, **257a** (0.50 mmol or 1.10 mmol), **84** (0.75 mmol or 0.50 mmol), $[Ru(OAc)_2(p\text{-cymene})]$ (10 mol %), K_2CO_3 (2.00 mmol), 1,4-dioxane (2.0 mL), 24 h, under N_2. At 30–33 °C under blue LED irradiation (450 nm) or at 120 °C heating using an oil bath. Yields refer to the isolated products. [a] Reaction was performed by A. Zangarelli.

Scheme 3.18: Improved chemoselectivity under photochemical conditions compared to the conventional thermal arylation.

Using phenylpyridine **44a** as substrate in the presence of the bifunctional iodoaryl triflate **84x**, the reaction outcome differed significantly for both reaction conditions (Scheme 3.18a). The photo-induced reaction furnished predominantly the mono-arylated product **243ax**, accompanied by minor amounts of twofold C–H activation product **244aa**. An inverse behavior was observed for the thermal reaction, lacking a discrimination of the complementary aryl halides. Similar results were obtained in case of aryl iodide **84y**, which gave exclusively the mono-arylated product **243ay** under light irradiation (Scheme 3.18b). Keeping the valuable electrophilic halogen substituent untouched potentially allows for further diversification of the modified arene **243ay**, for example through cross-coupling reactions. In contrast, the thermally induced reactivity provided the twofold C–H activation product **244ab** together with trace amounts of **243ay**. Another interesting example for different obtained products in dependance of the applied conditions was achieved by using 1-bromo-3-iodobenzene (**84az**) as arylating reagent (Scheme 3.18c). The reaction with pyrazole derivative **257a** afforded the envisioned arylation product **258az** in good yield, remaining the sensitive bromo-substituent unimpaired. On the contrary, a protodebromination process took place under thermal conditions which led to product **238az**–**Br**. This nicely reflects the selectivity advantages of the mild photo-induced approach at ambient temperature.

3.3.4 Mechanistic Studies

Given the robustness and the unique chemo-selectivity of the mild photo-induced arylation, several experiments were conducted to elucidate the mechanism of the transformation. H/D scrambling experiments with deuterated methanol as cosolvent revealed a high incorporation of deuterium into the starting material **44a** under the optimized photochemical reaction conditions (Scheme 3.19a). The facile C–H ruthenation process was further supported by H/D scrambling experiments in the presence of aryl iodide **84a** as the limiting reagent, in which the reisolated phenylpyridine **44a** exhibited 93% labeling (Scheme 3.19b).

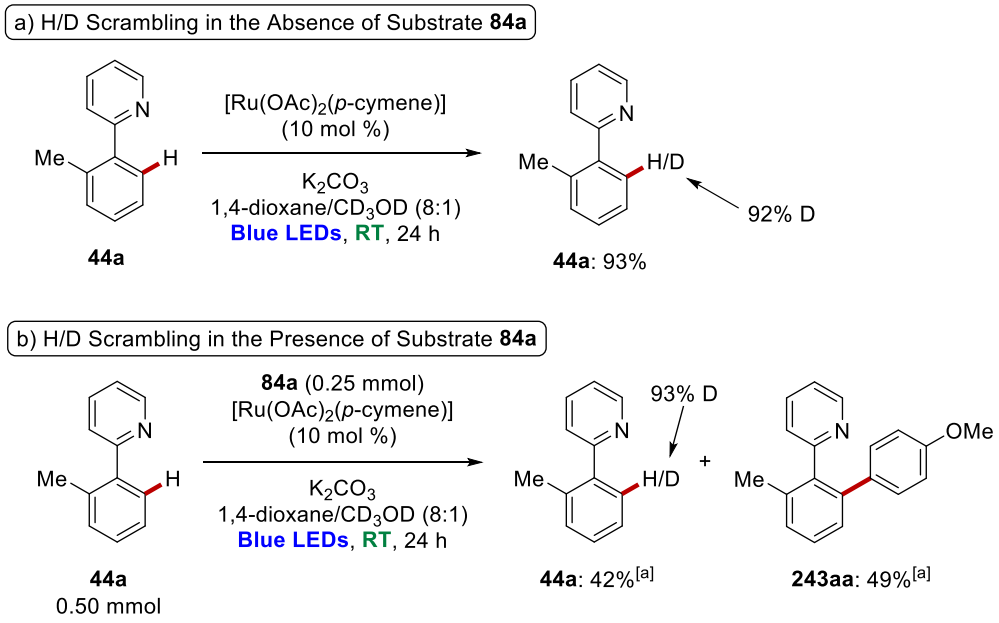

[a] Yield determined based on phenylpyridine **44a**.

Scheme 3.19: H/D scrambling experiments of the phenylpyridine **44a**.

Furthermore, intermolecular competition experiments with respect to arene **44** were performed by employing the photochemical reaction conditions (Scheme 3.20).

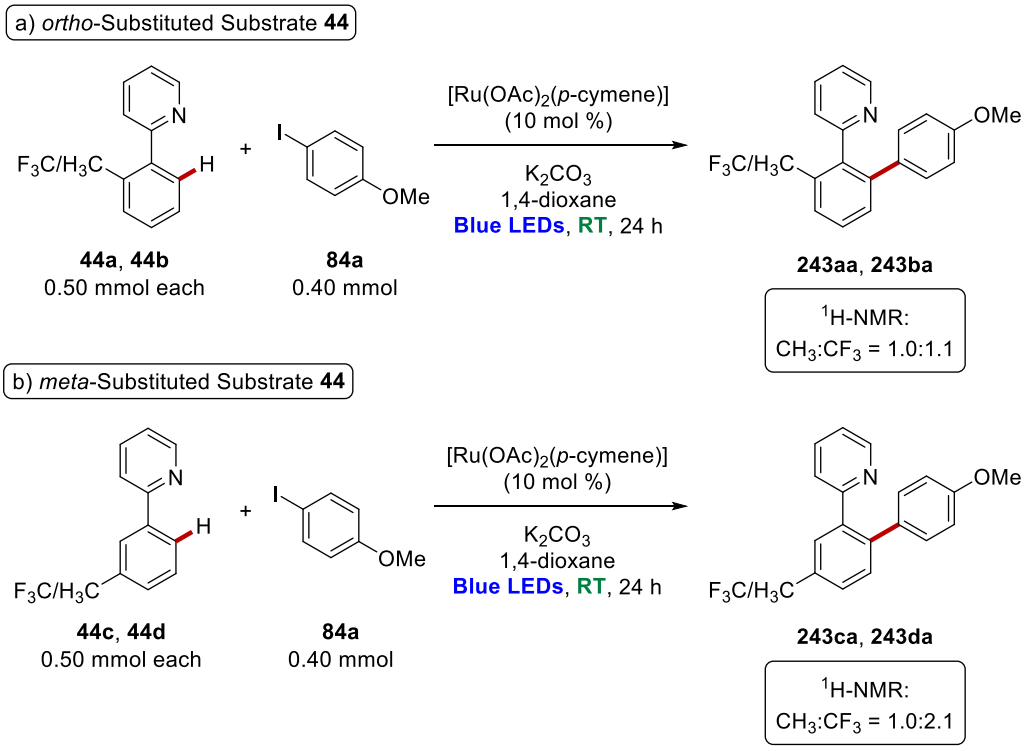

Scheme 3.20: Competition experiments for photo-induced C–H arylations of arenes **44**.

For the *ortho*-substituted substrates **44a** and **44b**, only a minor electronic bias with slightly higher reactivity of the electron-poor trifluoromethylated derivative **44b** was observable

(Scheme 3.20a). As an influence of the steric demand of the *ortho*-substituents can not be excluded, the competition experiment was repeated with the in *meta*-position decorated arenes **44c** and **44d**, whose reactivity is expected to be determined solely by the electronic properties (Scheme 3.20b). In this case, a significantly enhanced inherent reactivity could be confirmed for the electron-deficient substrate **44d**, being thereby indicative of a deprotonative CMD-type C–H activation process rather than a base-assisted BIES-type C–H activation mechanism.

Further insights into the reaction mechanism were obtained, when the reaction was performed in the presence of frequently employed radical scavengers (Table 3.9). In contrast to the standard reaction conditions, the addition of TEMPO to the reaction mixture completely suppressed the photo-induced arylation (entries 1–2). Moreover, the reaction in the presence of BHT was significantly inhibited and led to a lower yield of the arylated product **243aa** (entry 3). Both findings were in good agreement and supported the assumption that the reaction follows a radical mechanism.

Table 3.9: Direct C–H arylation in the presence of radical scavengers.

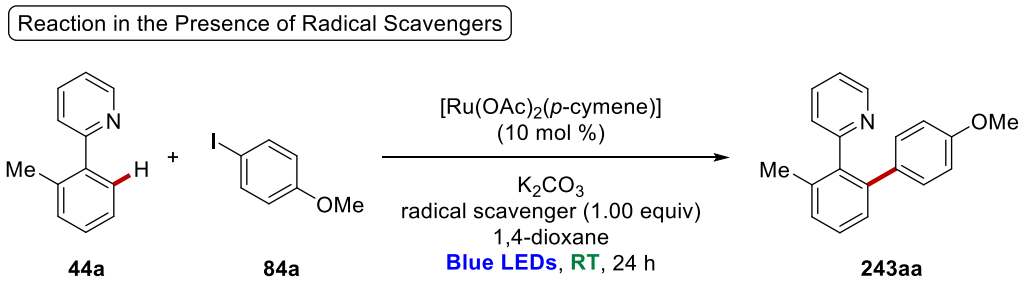

Entry	Radical Scavenger	**243aa** [%][a]
1	---	94
2	TEMPO	---
3	BHT	61

[a] Reaction conditions: **44a** (0.50 mmol), **84a** (0.75 mmol), [Ru(OAc)$_2$(*p*-cymene)] (10 mol %), K_2CO_3 (2.00 mmol), radical scavenger (0.50 mmol), 1,4-dioxane (2.0 mL), 30–33 °C, 24 h, under N_2, blue LED irradiation (450 nm). Yields refer to the isolated products.

To probe whether a radical chain mechanism was operative under the ruthenium catalysis, an on/off experiment was conducted (Figure 3.6). As the formation of the desired product **243aa** was strongly prevented in the absence of light, a radical chain process is rather unlikely for this reaction.

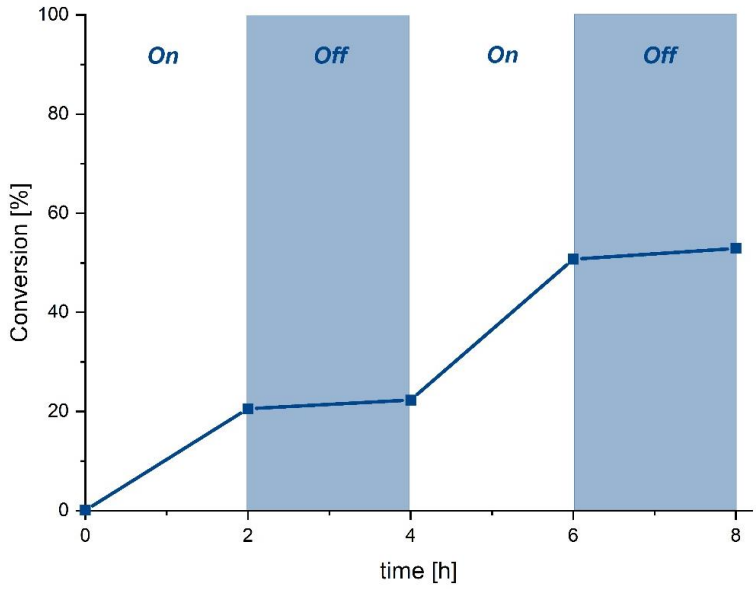

Figure 3.6: On/off experiment for ruthenium-catalyzed arylation of phenylpyridine **44a**.

In order to gain further insights into the nature of the ruthenium catalyst, the dissociation of the *p*-cymene ligand was monitored during the arylation at ambient temperature (Figure 3.7).

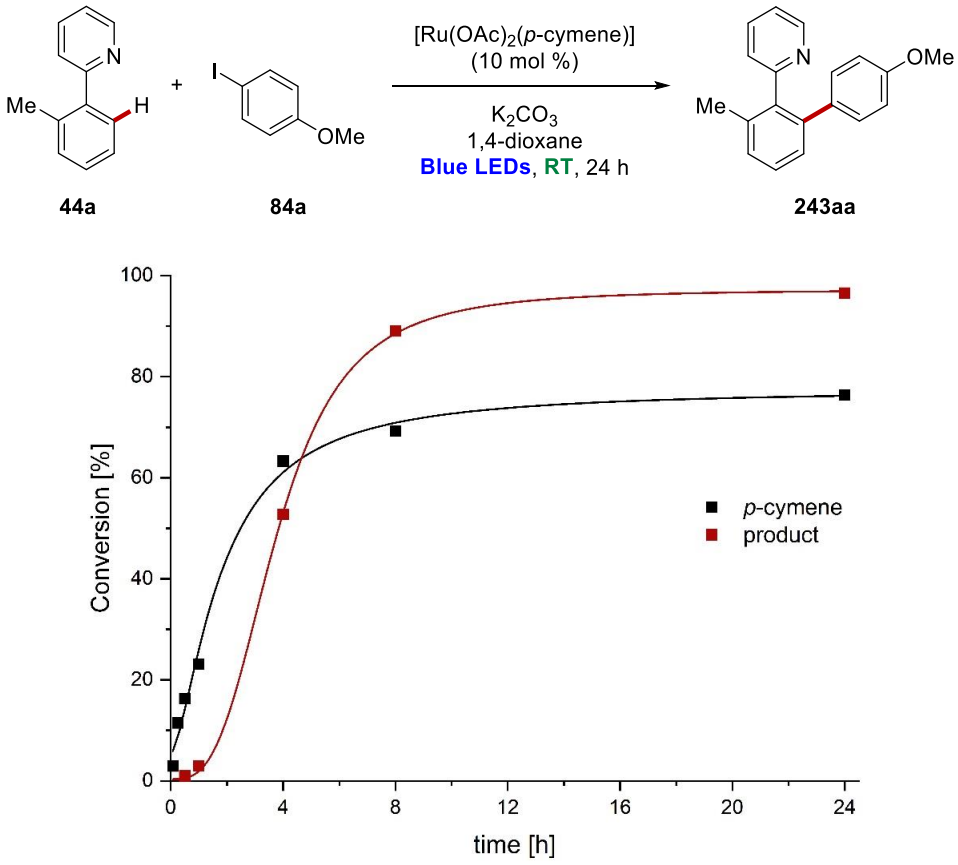

Figure 3.7: Monitoring of the dissociation of the *p*-cymene ligand from the ruthenium precatalyst.

Within the first hour of the reaction, the release of a significant amount of the free *p*-cymene was detected. As the product formation started slowly after an induction period, the monitored profile is indicative of an arene-free catalytically-active ruthenium species which is formed by decoordination of the *p*-cymene ligand from the precatalyst.

Additional insights into the catalyst's properties were gained by using a monocyclometalated ruthenium complex. Experiments performed by Dr. K. Korvorapun revealed that this ruthenacycle required the presence of an acetate base to be catalytically competent,[249] which provides support for a carboxylate-modified ruthenacycle being involved in the photo-induced C–H arylation.

Furthermore, the quantum yield for this reaction was determined to be $\Phi = 0.087$.[249] Detailed computational studies were also performed by Dr. Rositha Kuniyil, which included the computed absorption properties for different ruthenacycles. Moreover, the results suggested, that an outer-sphere electron-transfer process is unlikely as the inner-sphere one is energetically favored.[249]

3.3.5 Proposed Catalytic Cycle

Based on the detailed experimental studies and the computational results, a plausible catalytic cycle was proposed (Scheme 3.21). A reasonable mechanistic scenario for the ruthenium-catalyzed arylation induced by visible light is initiated by the decoordination of the *p*-cymene ligand from the ruthenium precatalyst and twofold carboxylate-assisted C–H activation of arene **44**, thereby providing the arene-free biscyclometalated ruthenium(II) complex **259**. Subsequent coordination of the aryl iodide **84** generates the photochemically active ruthenacycle **260**. Absorption of the blue LED light leads to photo-induced excitation to provide the singlet excited species **260***. Intersystem crossing (ISC) allows for relaxation to afford the long-lived ruthenium triplet species **260****, which undergoes an inner-sphere electron transfer (ISET) to iodoarene **84** under formation of the phenyl radical **261** and the ruthenium(III) intermediate **262**. The stable ruthenium(IV) intermediate **263** is subsequently formed by radical recombination of those. Ligand exchange and reductive elimination furnish the released product **243** in line with the formation of ruthenacycle **264**. The catalytic cycle is finally closed by C–H ruthenation to regenerate the biscyclometalated key intermediate **259**.

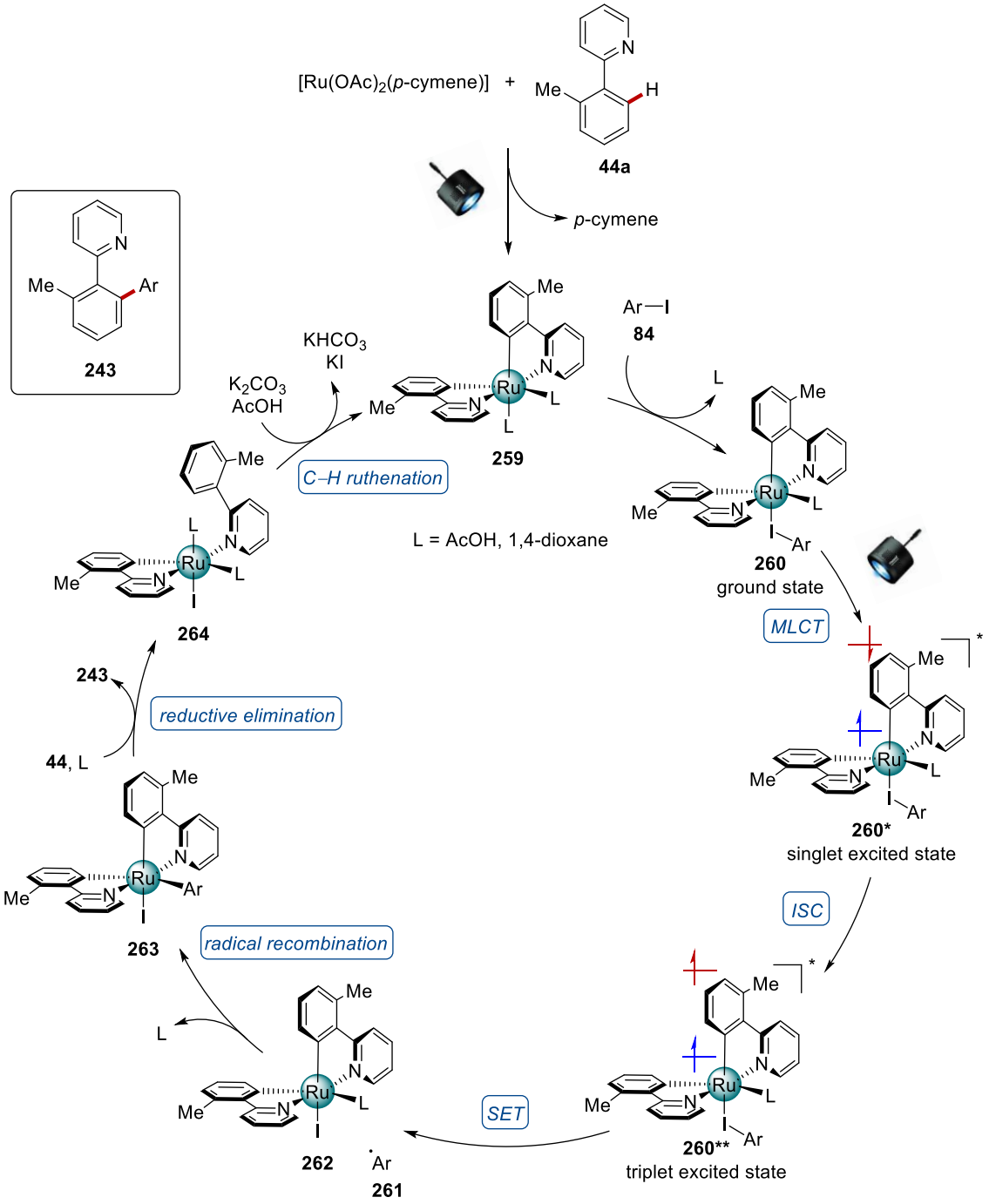

Scheme 3.21: Plausible catalytic cycle for the photo-induced ruthenium-catalyzed C–H arylation of pyridine **44**.

3.4 PHOTO-INDUCED RUTHENIUM-CATALYZED C–H BENZYLATIONS AND ALLYLATIONS AT AMBIENT TEMPERATURE

In addition to ruthenium-catalyzed C–H alkylations and arylations, ruthenium-mediated direct benzylations of arenes were developed to furnish diarylmethane compounds, a structural motif in different drug substances (Figure 3.8).[253]

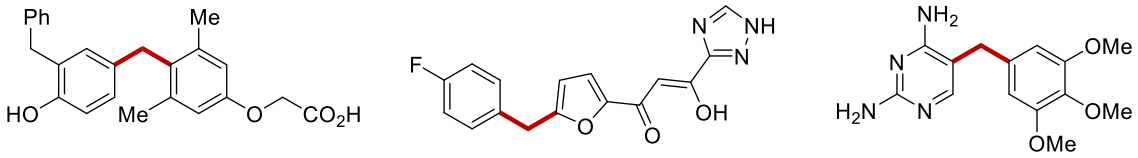

GC-24
agonist for thyroid hormone receptor ß

S-1360
anti-HIV activity

trimethoprim TMP
antimicrobial activity

Figure 3.8: Selected examples of diarylmethane structures in bioactive compounds and drugs.

Traditionally, these diarylmethane scaffolds can be synthesized by electrophilic aromatic substitution through Friedel-Crafts benzylations exploiting Lewis acid catalysis with restricted practicability as they often lead to the undesired formation of regioisomeric mixtures and overbenzylation.[254] Other approaches include nucleophilic additions of usually sensitive, organometallic reagents followed by a subsequent reduction,[255] or transition metal catalysis in cross-coupling reactions.[256] These procedures are associated with certain drawbacks, such as the formation of waste products in stoichiometric amounts and their cost- and time-intensive synthesis. As a consequence, the development of sustainable alternatives, such as direct benzylation through ruthenium-catalyzed C–H activation, is highly desirable.[94-97] Although significant progress has been made, *ortho*-benzylations required rather harsh reaction conditions with temperatures of typically 100 °C.[94]

In continuation of the research on the induction of ruthenium-mediated reactivities by visible light, this versatile strategy was expanded to *ortho*-selective benzylations. Inspired by the work on *meta*-alkylations[209-210] and the successful realization of *ortho*-arylations,[249-250] a sustainable methodology was realized to access diarylmethanes under exceedingly mild conditions at ambient temperature in the absence of an exogeneous photocatalyst.

3.4.1 Optimization Studies

The development of the mild reaction conditions for the photo-induced benzylation reaction of the methyl substituted phenylpyridine **44a** commenced with the screening of various solvents to identify suitable reaction media (Table 3.10). Starting with toluene, the yield was

significantly improved by changing to the non-aromatic solvents 1,2-DCE and 1,4-dioxane, which both resulted in good isolated yields of the product **265aa** around 75% (entries 1–3). A similar good result was obtained with water as reaction medium (entry 4), thereby allowing for an even greener and more sustainable approach in a safe and non-toxic reaction medium. In sharp contrast, the use of polar aprotic solvents, such as MeCN and DMF, was not beneficial and led to strongly decreased conversions (entries 5–6). Likewise, the biomass-derived green solvent 2-Me-THF fell short in furnishing the desired product **265aa** in good yields (entry 7). Similar reaction outcomes were observed by changing the base to NaOAc (entries 8–9). Although the result was slightly better in case of 1,2-DCE than for 1,4-dioxane, it was decided to continue the optimization with 1,4-dioxane to avoid the highly toxic, halogenated solvent.

Table 3.10: Optimization of the reaction medium for the photo-induced benzylation.

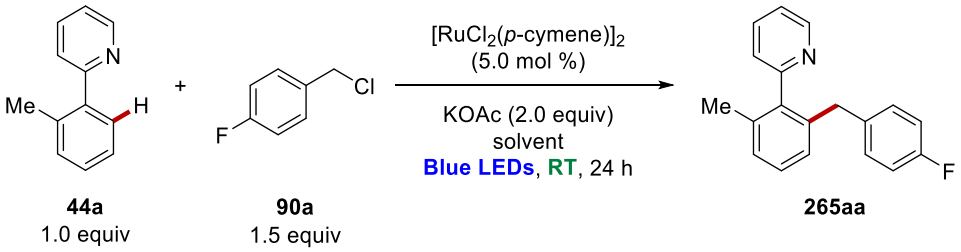

Entry	Solvent	**265aa** [%][a]
1	PhMe	41 (43)
2	1,2-DCE	75 (82)
3	1,4-dioxane	74 (76)
4	H_2O	(74)[b]
5	DMF	(25)
6	MeCN	(22)
7	2-Me-THF	(41)
8	PhMe	45 (47)[c,d]
9	1,2-DCE	76 (79)[c,d]

[a] Reaction conditions: **44a** (0.50 mmol), **90a** (0.75 mmol), $[RuCl_2(p\text{-cymene})]_2$ (5.0 mol %), KOAc (1.00 mmol), solvent (2.0 mL), 30–33 °C, 24 h, under N_2, blue LED irradiation (450 nm). Yields refer to the isolated products. The conversion in the parentheses was determined by ^{1}H-NMR using 1,3,5-trimethoxybenzene as the internal standard. [b] Another isomer and a di-functionalized product were also formed. [c] NaOAc (1.00 mmol) was used. [d] Reaction was performed by A. Casnati.

Subsequently, the most appropriate base for the envisioned reactivity towards diarylmethane **265aa** was determined (Table 3.11). Among the different acetate bases (entries 1–4), NaOAc turned out be the most efficient one and provided the desired product **265aa** with an increased isolated yield of 81% (entry 2). In sharp contrast, LiOAc gave unsatisfactory results for the desired *ortho*-benzylation product **265aa** due to formation of the *meta*-isomer and a di-functionalized species (entry 1), while no conversion was observable when CsOAc was employed (entry 4). Using substituted carboxylates did not provide better results (entries 5–7). Concerning pivaloyl bases, only slightly diminished yields were observed (entries 5–6), supporting the trend of a higher conversion with sodium as counterion. The sterically more demanding, structurally related adamantyl derivative showed even lower reactivity (entry 7). However, the use of sodium trifluoroacetate resulted in a reduced product formation as a consequence of the low selectivity and formation of the *meta*-isomer (entry 8).

Table 3.11: Optimization of the base for the photo-induced benzylation of arene **44a**.

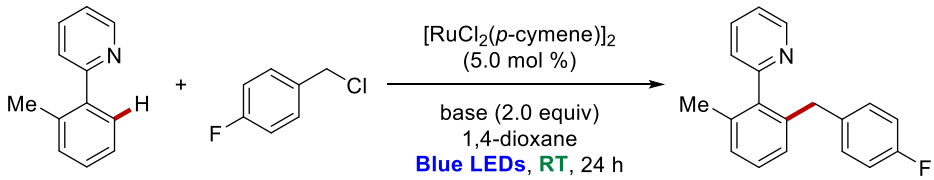

44a 1.0 equiv | **90a** 1.5 equiv | **265aa**

Entry	Base	**265aa** [%][a]
1	LiOAc	(21)[b]
2	NaOAc	81 (83)
3	KOAc	74 (76)
4	CsOAc	---
5	NaOPiv	77 (79)
6	KOPiv	61 (62)
7	1-AdCO_2Na	(59)
8	CF_3CO_2Na	(34)[b]

[a] Reaction conditions: **44a** (0.50 mmol), **90a** (0.75 mmol), [$RuCl_2$(*p*-cymene)]$_2$ (5.0 mol %), base (1.00 mmol), 1,4-dioxane (2.0 mL), 30–33 °C, 24 h, under N_2, blue LED irradiation (450 nm). Yields refer to the isolated products. The conversion in the parentheses was determined by ^{1}H-NMR using 1,3,5-trimethoxybenzene as the internal standard. [b] Another isomer was also formed.

In an effort to increase the conversion further, several ruthenium complexes were probed to catalyze the photo-induced transformation (Table 3.12). The arene-containing complexes $[RuCl_2(p\text{-cymene})]_2$ and $[Ru(OAc)_2(p\text{-cymene})]$ both showed comparable high reactivity and the *ortho*-functionalized product **265aa** was obtained in good yields close to 80% (entries 1–2). On the contrary to the C–H arylation reaction, the use of the acetate complex was not beneficial under these reaction conditions (entry 2). As the base NaOAc was in excess available in the reaction mixture for both complexes, the formation of an acetate complex seems likely to occur starting from the ruthenium dimer as precursor. In comparison, other ruthenium sources failed in catalyzing the desired reaction with the mass balance accounting for unreacted starting material **44a** (entries 3–7). The cationic *p*-cymene-free ruthenium nitrile complexes resulted only in trace amounts of the desired product **265aa** (entries 3–5). Equally, other ruthenium sources, such as $Ru_3(CO)_{12}$ and $RuCl_3{\cdot}nH_2O$, failed to furnish the benzylated product **265aa** (entries 6–7), presumably due to their low solubility in 1,4-dioxane.

Table 3.12: Optimization of the ruthenium catalyst for the photo-induced benzylation.

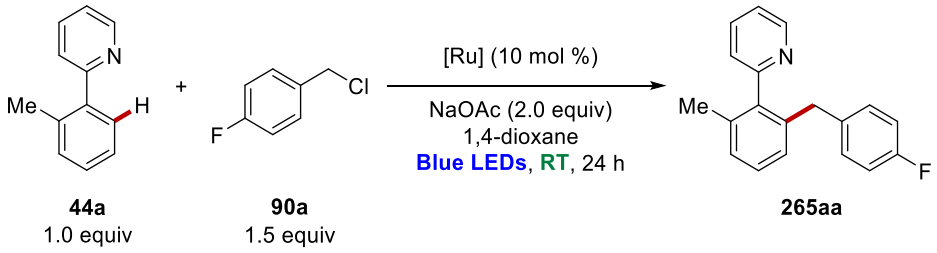

Entry	[Ru]	**265aa** [%][a]
1	$[RuCl_2(p\text{-cymene})]_2$	81 (83)
2	$[Ru(OAc)_2(p\text{-cymene})]$	77 (80)
3	$[Ru(NCtBu)_6](BF_4)_2$	(4)
4	$[Ru(NCtBu)_6](PF_6)_2$	---
5	$[Ru(NCtBu)_6](SbF_6)_2$	---
6	$Ru_3(CO)_{12}$	(2)[b]
7	$RuCl_3{\cdot}nH_2O$	(8)[b]

[a] Reaction conditions: **44a** (0.50 mmol), **90a** (0.75 mmol), $[RuCl_2(p\text{-cymene})]_2$ (5.0 mol %), NaOAc (1.00 mmol), 1,4-dioxane (2.0 mL), 30–33 °C, 24 h, under N_2, blue LED irradiation (450 nm). Yields refer to the isolated products. The conversion in the parentheses was determined by ^{1}H-NMR using 1,3,5-trimethoxybenzene as the internal standard. [b] Reaction was performed by Dr. K. Korvorapun.

Due to some promising preliminary results, the development of an optimized procedure using water as reaction medium was initiated (Table 3.13).

Table 3.13: Optimization of photo-induced benzylation with water as reaction medium.

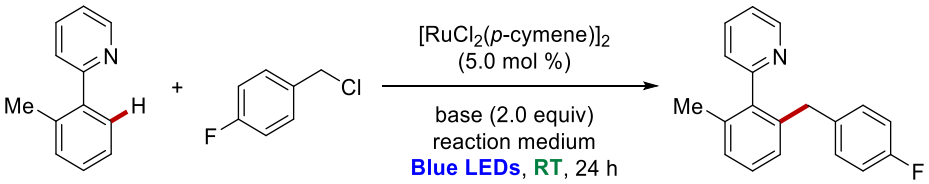

44a 1.0 equiv | **90a** 1.5 equiv | **265aa**

Entry	Base	Reaction Medium	**265aa** [%][a]
1	NaOAc	H_2O	74 (76)
2	NaOAc	SDS (10 wt%)/H_2O	35 (38)
3	NaOAc	Triton-X-100 (10 wt%)/H_2O	66 (69)
4	NaOAc	Tween-20 (10 wt%)/H_2O	75 (79)
5	NaOAc	Brij-93 (10 wt%)/H_2O	64 (65)
6	NaOAc	Brij-35 (10 wt%)/H_2O	77 (80)
7	NaOAc	SPGS-550-M (Nok) (2 wt%)/H_2O	72 (74)
8	NaOAc	TPGS-750-M (2 wt%)/H_2O	49 (52)
9	NaOAc	PTS (5 wt%)/H_2O	63 (65)
10	NaOPiv	H_2O	63 (65)
11	1-AdCO_2Na	H_2O	(42)

[a] Reaction conditions: **44a** (0.50 mmol), **90a** (0.75 mmol), [$RuCl_2$(*p*-cymene)]$_2$ (5.0 mol %), base (1.00 mmol), reaction medium (2.0 mL), 30–33 °C, 24 h, under N_2, blue LED irradiation (450 nm). Yields refer to the isolated products. The conversion in the parentheses was determined by ^{1}H-NMR using 1,3,5-trimethoxybenzene as the internal standard.

Aside from pure water (entry 1), different surfactants were taken into account to enable micellar catalysis for the benzylation reaction of phenylpyridine **44a**. The addition of SDS as amphiphile caused a considerable drop in yield, which can be explained by the formation of significant amounts of the *meta*-isomer (entry 2). Alternative surfactants enabled the photo-induced catalysis with good yields of product **265aa** and led to comparable results of approximately 70% (entries 3–6). Beyond those, a few designer surfactants frequently employed in cross-coupling reactions, were probed (entries 7–9). Among those, the β-sitosterol-derived, third

generation amphiphile Nok showed the highest efficacy with almost the same yield as in water (entry 7). In contrast, the vitamine E-derived designer surfactants TPGS-750-M and PTS, which both possess a tocopherol-moiety, turned out to be less efficient (entries 8–9). Furthermore, the effect of the base was evaluated for the aqueous reaction conditions as well (entries 10–11), clearly identifying NaOAc as the most efficient base. Although Tween-20 (entry 4) and Brij-35 (entry 6) gave slightly higher yields than the reaction in pure water, the subsequent screening of the base was performed in pure water. This was taken as the medium of choice by considering the negligibility of the improvement with surfactants and the more time-consuming work-up in the presence of a detergent into account. However, the use of the surfactant might be interesting for highly hydrophobic substrates in case of low solubility even through this was not further investigated.

Based on the best reaction conditions so far determined, a series of control experiments was conducted (Table 3.14).

Table 3.14: Control experiments for the photo-induced benzylation.

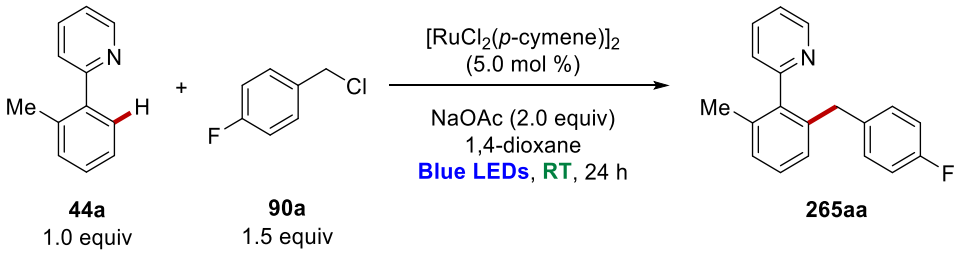

44a 1.0 equiv | **90a** 1.5 equiv | **265aa**

Entry	Deviation from Standard Conditions	**44a** [%]	**265aa** [%][a]
1	without light (dark)	(79)[b]	---
2	without base	(71)[c]	(8)
3	without [Ru]	(65)	---
4	**90a** (1.0 equiv)	(30)	(56)

[a] Reaction conditions: **44a** (0.50 mmol), **90a** (0.75 mmol), $[RuCl_2(p\text{-cymene})]_2$ (5.0 mol %), NaOAc (1.00 mmol), 1,4-dioxane (2.0 mL), 30–33 °C, 24 h, under N_2, blue LED irradiation (450 nm). The conversion in the parentheses was determined by ^{1}H-NMR using 1,3,5-trimethoxybenzene as the internal standard. [b] Reaction in the dark was performed by covering the vial with aluminum foil to avoid irradiation by the blue LED lamps under otherwise identical reaction conditions. [c] Reaction was performed by A. Casnati.

When the reaction was performed in the absence of light, the reactivity was completely suppressed, while the *ortho*-benzylated product **265aa** was detected in trace amounts in the absence of the base (entries 1–2). Furthermore, the essential role of the ruthenium catalyst could

be validated with a control experiment (entry 3). To check if the benzylation is likewise efficient with a reduced amount of the electrophile **90a**, the reaction was performed with one equivalent of the benzyl chloride, resulting in a less satisfactory conversion (entry 4).

3.4.2 Substrate Scope

With the optimized conditions in hand, the utility of the developed benzylation was investigated with a set of different benzyl chlorides **90** (Scheme 3.22).

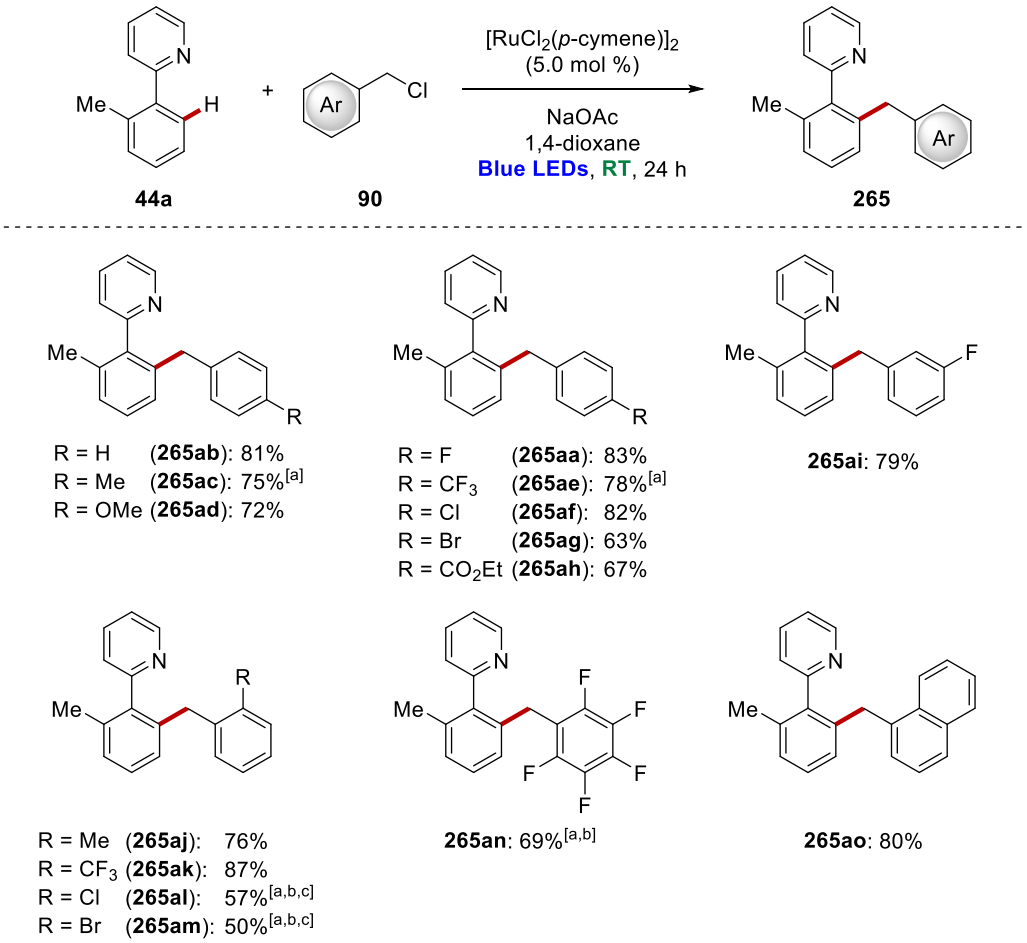

Reaction conditions: **44a** (0.50 mmol), **90** (0.75 mmol), $[RuCl_2(p\text{-cymene})]_2$ (5.0 mol %), NaOAc (1.00 mmol), 1,4-dioxane (2.0 mL), 30–33 °C, 24 h, under N_2, blue LED irradiation (450 nm). Yields refer to the isolated products. [a] Regioisomers (3–8%) were also formed. [b] $ArCH_2Br$ was used. [c] Reaction was performed by Dr. K. Korvorapun.

Scheme 3.22: Substrate scope for the photo-induced *ortho*-benzylation of phenylpyridine **44a**.

Electrophiles **90** with electron-donating as well as electron-withdrawing substituents in different positions of the arene were smoothly converted into the corresponding products **265** with moderate to excellent yields, accompanied by trace amounts of other regioisomers in some exceptional cases. For *para*- as well *ortho*-decorated arenes, the yield was slightly lower for benzyl chlorides **90** with electron-donating groups than for those with electron-withdrawing

properties. Among the tested arenes, substrates **90** bearing sensitive functional groups, such as ester (**90h**), chloro (**90f**, **90l**) and bromo functionalities (**90g**, **90m**), were fully tolerated. Although the yield of the halogen-containing product derivatives **265af**–**265ag** and **265al**–**265am** were significantly lower than for the other electrophiles, the reaction proceeded without any hints for side reactions, such as a competing arylation, which was previously reported under comparable conditions.[249] The versatile ruthenium catalysis at ambient temperature was used for the highly electron-deficient pentafluorobenzyl bromide **90n** to furnish the *ortho*-benzylated product **265an** in moderate yields. In addition, the photo-induced reaction was employed for the naphthyl derivative **90o** to access the desired product **265ao** in good yield.

Apart from the great functional group tolerance, the sustainable transformation under ruthenium catalysis regime was very efficient and enabled twofold C–H activations (Scheme 3.23). Conducting the reaction with 1,4-bis(chloromethyl)benzene (**90p**) as limiting reagent together with an excess of the phenylpyridine **44a**, the bisfunctionalized product **266aa** was predominantly obtained together with minor amounts the mono-C–H activation product **265ap**.

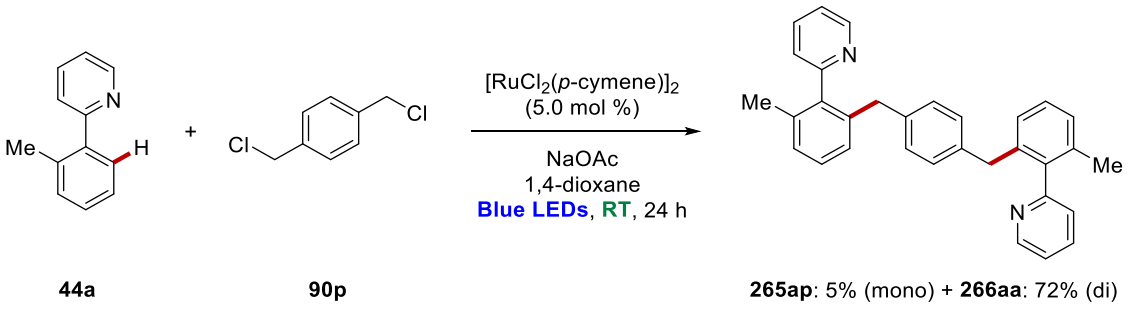

Reaction conditions: **44a** (1.10 mmol), **90p** (0.50 mmol), $[RuCl_2(p\text{-cymene})]_2$ (5.0 mol %), NaOAc (1.00 mmol), 1,4-dioxane (2.0 mL), 30–33 °C, 24 h, under N_2, blue LED irradiation (450 nm). Yields refer to the isolated products.

Scheme 3.23: Twofold benzylation of substrate **44a** under photochemical conditions.

After having demonstrated the generality of the mild light-induced benzylation, the broad applicability of the developed reaction was further substantiated by probing electrophilic substrates containing sensitive, biorelevant structural motifs (Scheme 3.24). Benzyl chlorides **90q** with a sensitive monosaccharide or **90r** bearing a monoglyceride building block were converted efficiently and the desired products were obtained in good to excellent yields (**265aq**, **265ar**). Furthermore, the sustainable ruthenium catalysis turned out to be feasible for amino acid containing benzyl chlorides **90s**–**90t**, which were reacted with good efficacies to furnish yields of 70–80% without any hints for the loss of the stereo information. The mild approach even allowed for the transformation of the tryptophan containing electrophile **90t** bearing a free

indole moiety. In addition, the nucleoside **90u** with uracil as a purine base was a suitable substrate in the room temperature ruthenium-catalyzed C–H benzylation and furnished the corresponding product **265au** in 70%. In these cases, the formation of constitutional isomers in minor amounts was observable.

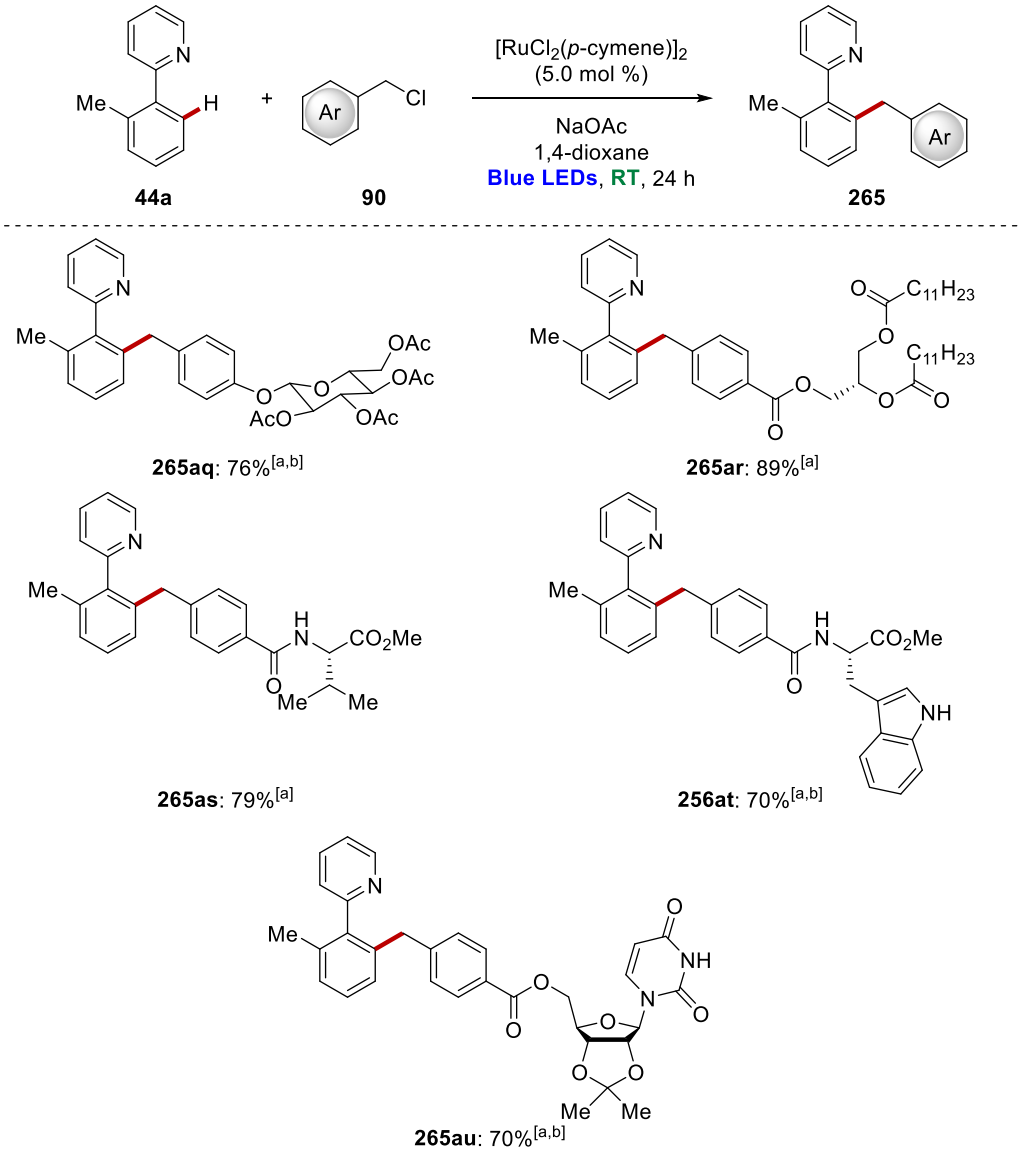

Reaction conditions: **44a** (0.50 mmol), **90** (0.75 mmol), $[RuCl_2(p\text{-cymene})]_2$ (5.0 mol %), NaOAc (1.00 mmol), 1,4-dioxane (2.0 mL), 30–33 °C, 24 h, under N_2, blue LED irradiation (450 nm). Yields refer to the isolated products. [a] Regioisomers (2–8%) were also formed. [b] Reaction was performed by Dr. K. Korvorapun.

Scheme 3.24: Ruthenium-catalyzed photochemical benzylation with biorelevant electrophiles **90**.

In addition to the *ortho*-methylated phenylpyridine **44a**, a few other arenes with an assisting pyridine heterocycle were subjected to the optimized reaction conditions (Scheme 3.25). Unsubstituted phenylpyridine (**44e**) yielded a mixture of the mono- and di-benzylated products

265ea and **265ea'** with the latter one being prominent. In sharp contrast, both, *ortho*- or *meta*-substituted arenes resulted selectively in mono-benzylation in the less hindered *ortho*-position of the heteroarene (**265aa**–**265da**). For both substitution patterns, the electron-donating methyl group and the electron-withdrawing trifluoromethyl moiety were fully tolerated und resulted in high conversions, being slightly increased for the electron deficient arenes (**265ba**, **265da**). In good agreement with this observation, arenes **44** bearing *meta*-substitution on the phenyl ring showed excellent yields which were about 10% higher than in case of the *ortho*-substituted analogue.

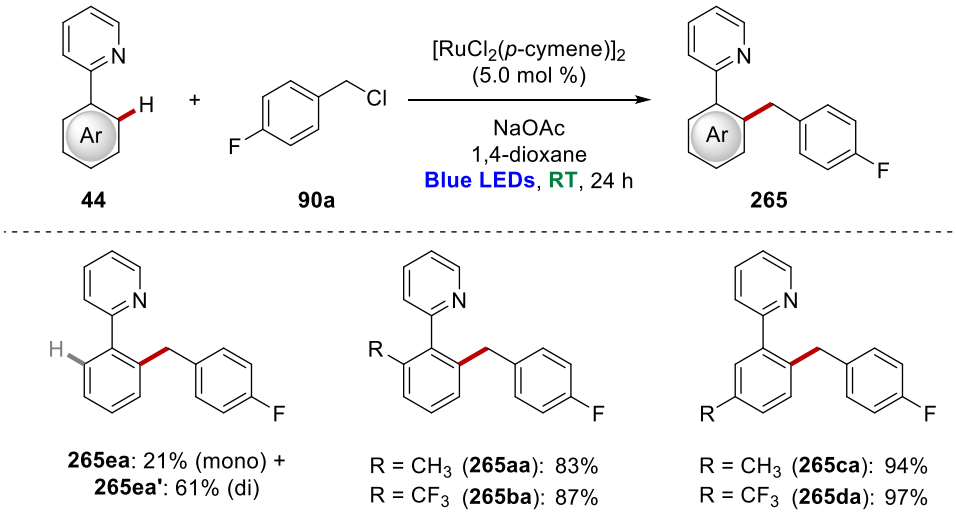

Reaction conditions: **44** (0.50 mmol), **90a** (0.75 mmol), $[RuCl_2(p\text{-cymene})]_2$ (5.0 mol %), NaOAc (1.00 mmol), 1,4-dioxane (2.0 mL), 30–33 °C, 24 h, under N_2, blue LED irradiation (450 nm). Yields refer to the isolated products.

Scheme 3.25: *ortho*-Benzylation of different phenylpyridines **44**.

The versatile light-induced ruthenium catalysis was not restricted to the assistance of pyridines as chelating moiety. In contrast, a broad range of different heteroarenes turned out to be suitable directing groups in the envisioned transformation (Scheme 3.26a). Among those, transformable phenylpyrazoles (**217e**, **217g**) were modified efficiently although with slightly diminished yields compared to the standard substrate **44a**. In addition, triazole-decorated arene **253a** was identified as capable starting material and delivered the corresponding product **269aa** in a moderate yield. The unsubstituted phenyloxazoline **246b** gave exclusively the di-benzylated product **270ba'**. Furthermore, the developed ruthenium catalysis could be expanded on the use of biorelevant purine base derivatives **267** as substrates with 1,2-DCE as solvent to ensure good solubility under otherwise identical reaction conditions. Besides the arylated purine **267a**, the nucleoside derivative **267b** was efficiently converted into the desired product **271ba**. In addition to the catalytic transformation, the diversification of the pyrazole product **268ga** was

shown by ozonolysis (Scheme 3.26b). After treatment with ozone followed by reductive work-up, the corresponding acetanilide **272ga** was obtained.

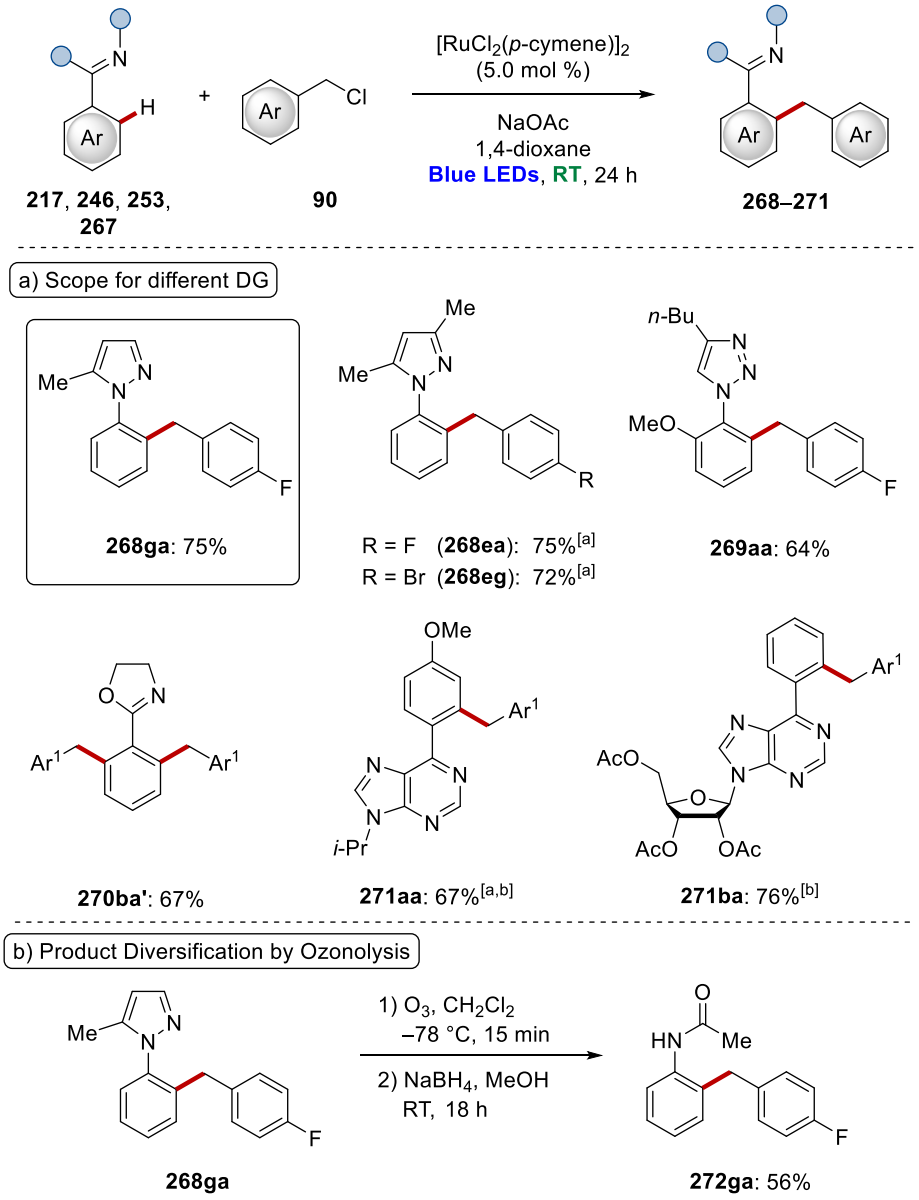

Reaction conditions: **217**, **246**, **253**, **267** (0.50 mmol), **90** (0.75 mmol), $[RuCl_2(p\text{-cymene})]_2$ (5.0 mol %), NaOAc (1.00 mmol), 1,4-dioxane (2.0 mL), 30–33 °C, 24 h, under N_2, blue LED irradiation (450 nm). Yields refer to the isolated products. Ar^1 = 4-C_6H_4F. [a] Regioisomers (2–7%) were also formed. [b] 1,2-DCE was used as the solvent.

Scheme 3.26: Photochemical ruthenium-catalyzed benzylation a) with the assistance of different heteroarenes and b) product diversification by subsequent ozonolysis.

The detailed optimization studies showed that the light-enabled benzylation was not limited to the use of organic solvents but was fully compatible with an aqueous reaction medium as a more environmentally-benign alternative. Therefore, the C–H benzylation reaction was conducted for a few examples in pure water and with addition of Brij-35 surfactant, which was

the most efficient one during the optimization studies (Scheme 3.27). Phenylpyridine **44a** and phenylpyrazole **217e** underwent the reaction in water with great efficacy and resulted in slightly higher yields in the presence of the surfactant. The yield was in a comparable range to the one observed for the organic solvent 1,4-dioxane. Noteworthily, the benzyl chloride **90g** bearing a sensitive bromo-substituent was selectively transformed into the products **265ag** and **268eg** without any side reactions.

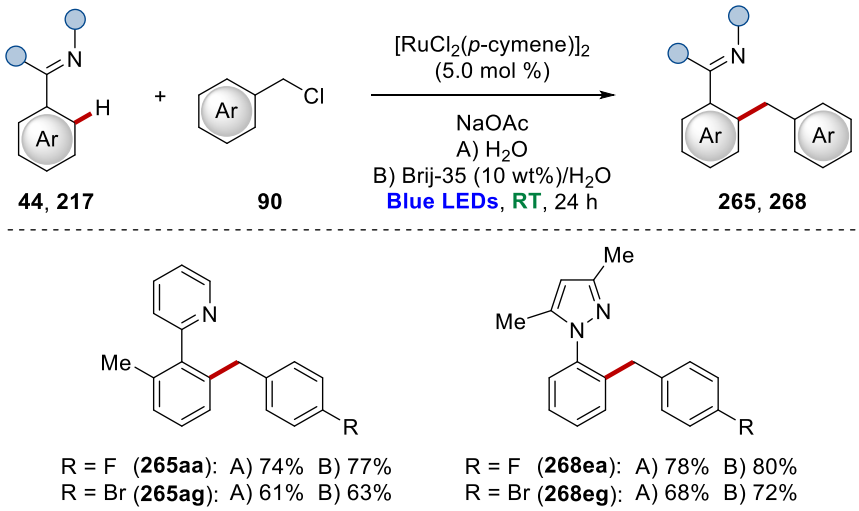

Reaction conditions: **44**, **217** (0.50 mmol), **90** (0.75 mmol), $[RuCl_2(p\text{-cymene})]_2$ (5.0 mol %), NaOAc (1.00 mmol), H_2O or Brij-35 (10 wt%)/H_2O, (2.0 mL), 30–33 °C, 24 h, under N_2, blue LED irradiation (450 nm). Yields refer to the isolated products.

Scheme 3.27: Photo-induced C–H benzylation in water or surfactant-solutions as reaction media.

Inspired by an earlier report by Ackermann on a heterogenized ruthenium catalyst realizing distal C–H alkylations,[257] the corresponding hybrid ruthenium catalyst was probed in the mild photo-induced benzylation reaction. In this heterogenized catalyst, which was shown to have a good recyclability over several cycles without significant loss in efficacy,[257] the ruthenium center is immobilized *via* a phosphine linker at the polystyrene. The use of this hybrid catalyst **273** was highly efficient for the photo-induced C–H benzylation of arene **44a** to afford the *ortho*-benzylated product **265aa** in an excellent yield (Scheme 3.28 top). In contrast to the earlier report, the reaction did not occur in *meta*-position. To further substantiate this finding, the reaction was conducted by employing the homogeneous approach in the presence of PPh_3 as co-catalytic additive to mimic the hybrid catalyst (Scheme 3.28 bottom). A previously reported procedure by Ackermann proved that the phosphine ligand can induce a selectivity switch from *ortho* to *meta*.[97] Again, careful NMR analysis of the isolated product **265aa** and comparison to the known compound confirmed the sole formation of the *ortho*-benzylated product **265aa** under the photo-induced reaction conditions.

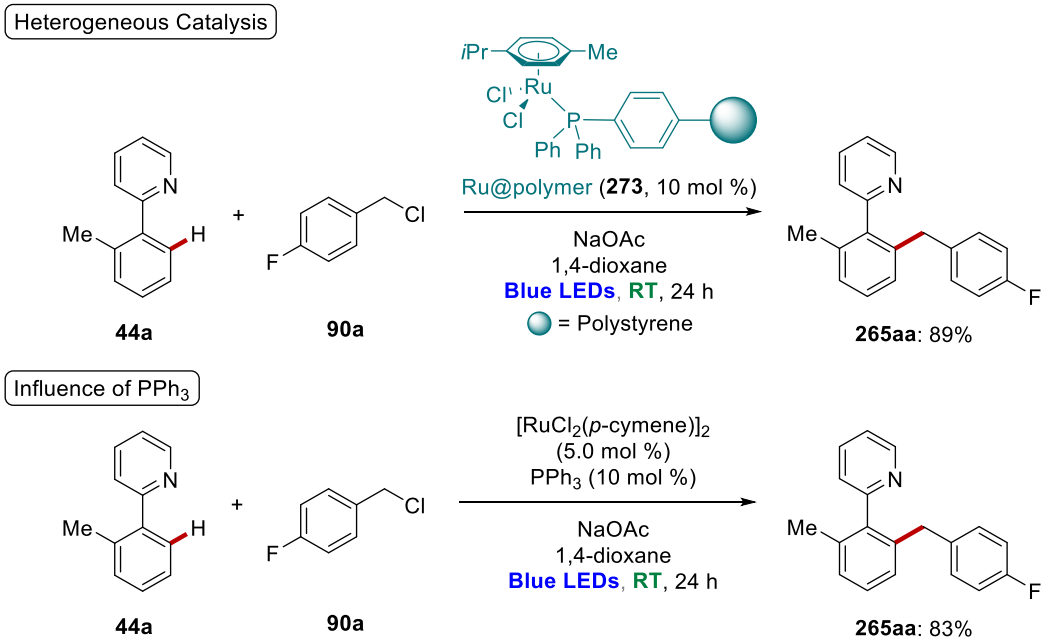

Reaction conditions: **44a** (0.50 mmol), **90a** (0.75 mmol), Ru@polymer (**273**, 10 mol %) or $[RuCl_2(p\text{-cymene})]_2$ (5.0 mol %) together with PPh_3 (10 mol %), NaOAc (1.00 mmol), 1,4-dioxane (2.0 mL), 30–33 °C, 24 h, under N_2, blue LED irradiation (450 nm). Yields refer to the isolated products.

Scheme 3.28: Benzylation of phenylpyridine **44a** using homogeneous and heterogeneous phosphine-coordinated ruthenium catalysts.

Interestingly, the developed ruthenium catalysis at ambient temperature was not restricted to benzylation reactions. The versatility of the catalytic system could be further demonstrated by allylation of arene **44e** using allylbromide **274a** as the electrophile (Scheme 3.29). Under otherwise identical reaction conditions, the envisioned *ortho*-allylated product **275ea** was obtained in a good yield.

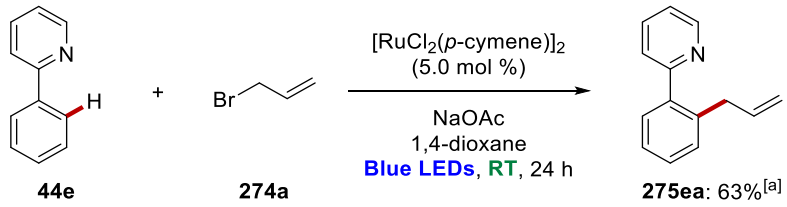

Reaction conditions: **44e** (0.50 mmol), **274a** (0.75 mmol), $[RuCl_2(p\text{-cymene})]_2$ (5.0 mol %), NaOAc (1.00 mmol), 1,4-dioxane (2.0 mL), 30–33 °C, 24 h, under N_2, blue LED irradiation (450 nm). Yield refers to the isolated product. [a] Reaction was performed by A. Zangarelli.

Scheme 3.29: Photo-induced ruthenium-catalyzed *ortho*-C–H allylation of pyridine **44e**.

3.4.3 Mechanistic Studies

Next, a series of mechanistic experiments were conducted to explore the catalysts' mode of action. To this end, H/D exchange experiments were performed by using deuterated methanol as deuterium source under the optimized reaction conditions (Scheme 3.30). For both reactions, in the absence and in the presence of the electrophile **90a**, a significant deuterium incorporation at the *ortho*-position of the starting material **44a** was observed which ranged from 85% to 92%. With this, the efficient H/D exchange is indicative of a facile C–H metalation process.

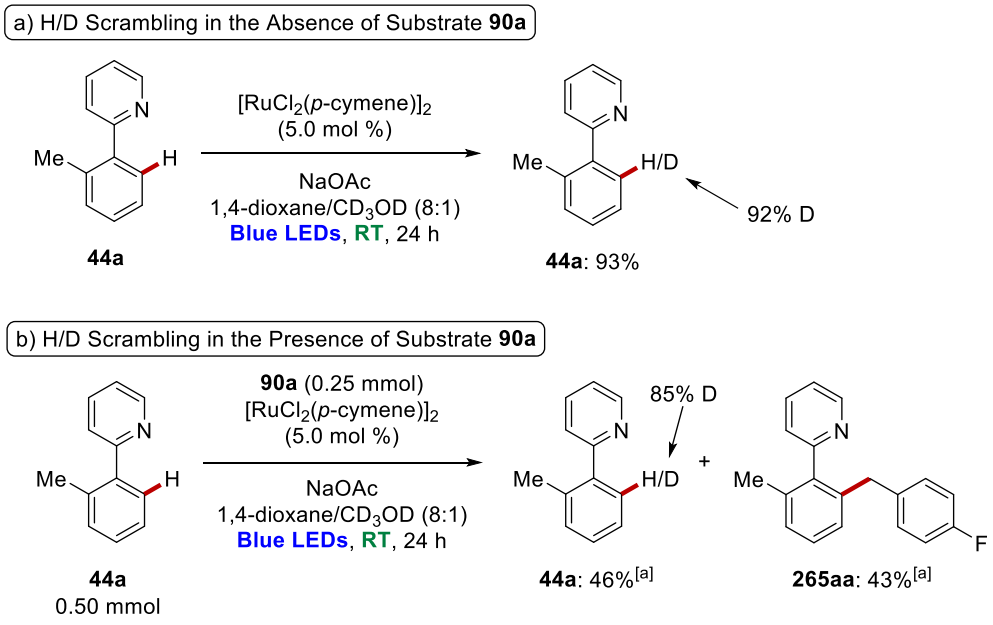

[a] Yield determined based on phenylpyridine **44a**.

Scheme 3.30: H/D exchange experiments under the photochemical reaction conditions.

Furthermore, competition experiments with *ortho*- and *meta*-substituted arenes **44** were performed. To analyze the impact of light in comparison to the conventional thermal conditions at 100 °C, the competition experiments were conducted under both conditions. In case of the *ortho*-substituted phenylpyridines **44a** and **44b**, the evaluation of the crude mixture revealed comparable reactivity for the methylated and the trifluoromethylated starting materials under both conditions (Scheme 3.31a). To avoid that the reaction outcome is not only influenced by the electronic properties, but also by the steric demand of the substituents, the competition experiment was repeated with arenes **44** bearing the differently featured substituents in *meta*-position (Scheme 3.31b). In this case, the electron-poor substrate **44d** showed a strong preference to be converted under photochemical reaction conditions. In comparison, the electron-deficient substrate **44d** reacted also more efficiently under thermochemical conditions to furnish the corresponding product **265da**, but the ratio of both products is shifted towards

the electron-donating starting material. The observed preference of the electron-poor substrate is in good agreement with a CMD-type C–H ruthenation process.

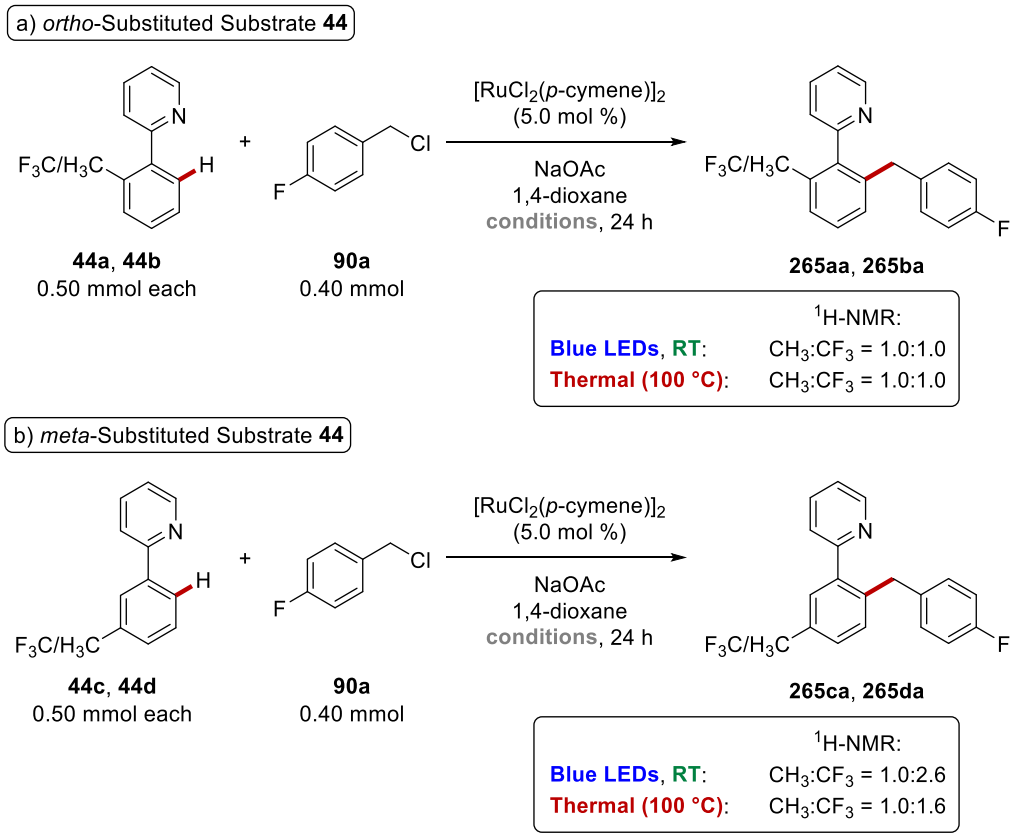

Scheme 3.31: Competition experiments for *ortho*- and *meta*-substituted arenes **44** under the ruthenium catalysis regime.

In addition, an intermolecular competition experiment with electronically different benzyl chlorides **90** was performed under light-induced and thermal reaction conditions (Scheme 3.32). Again, the electron-deficient substrate **90e** turned out to be preferentially converted than the electron-rich substrate **90c** for both conditions.

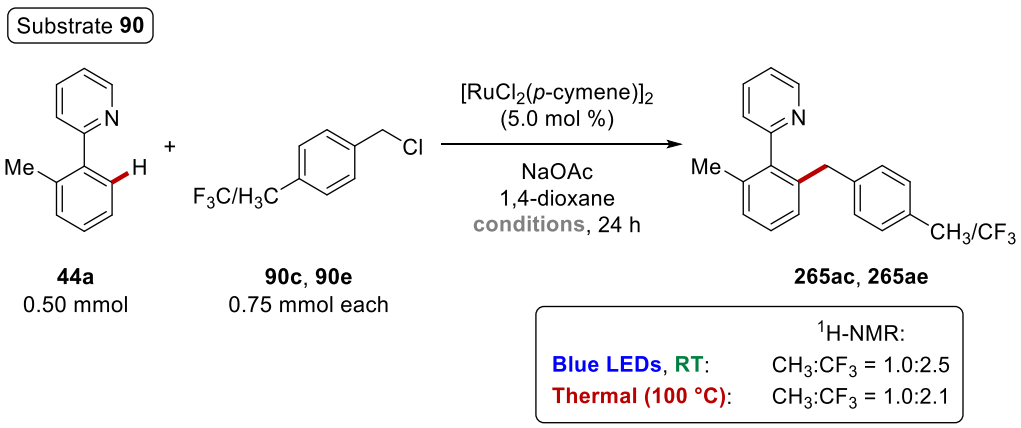

Scheme 3.32: Intermolecular competition experiments for substituted electrophiles **90**.

To gain further information on the reaction mechanism, the well-defined cyclometalated ruthenium complex **276** was prepared and employed in the photochemical C–H benzylation reaction. In a stoichiometric reaction of the complex, the desired product **265aa** was formed in good efficacy in the presence of additional arene **44a** (Scheme 3.33a), being indicative of the formation of a biscyclometalated ruthenium complex as a key intermediate. The monocyclometalated ruthenacycle **276** was a capable catalyst in the reaction and the corresponding product **265aa** was isolated in 94% yield (Scheme 3.33b), which supports that similar to the photo-induced arylation reaction, a *p*-cymene ligand-free ruthenacycle is involved in the direct C–H benzylation reaction.

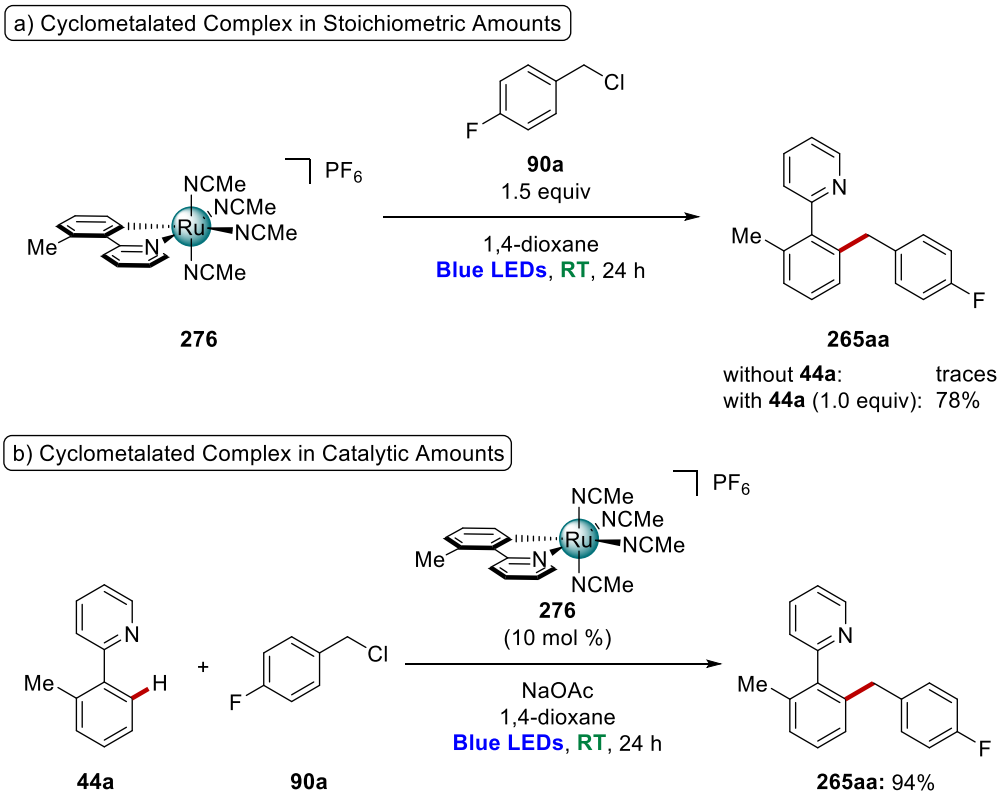

Scheme 3.33: Photochemical transformations using the cyclometalated ruthenium complex **276** a) in stoichiometric amounts and b) in catalytic amounts.

A control experiment in the presence of the radical scavenger TEMPO was performed to probe whether the photo-induced *ortho*-benzylation proceeds through a radical pathway (Scheme 3.34). The significantly reduced yield of the product **265aa** and the generation of the TEMPO-adduct **277** are suggestive of the formation of a benzyl radical under the tested reaction conditions.

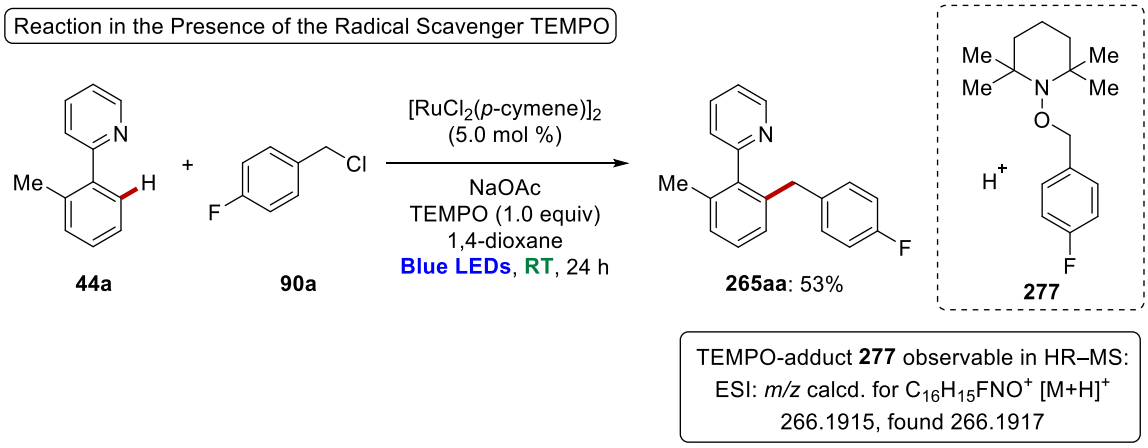

Scheme 3.34: Ruthenium catalysis in the presence of TEMPO.

To explore the role of light in greater detail, an on/off experiment was performed (Figure 3.9). In the absence of blue LED irradiation, the conversion of arene **44a** to **265aa** was strongly suppressed, which is indicative of the fact that the reaction does not proceed through a radical chain process.

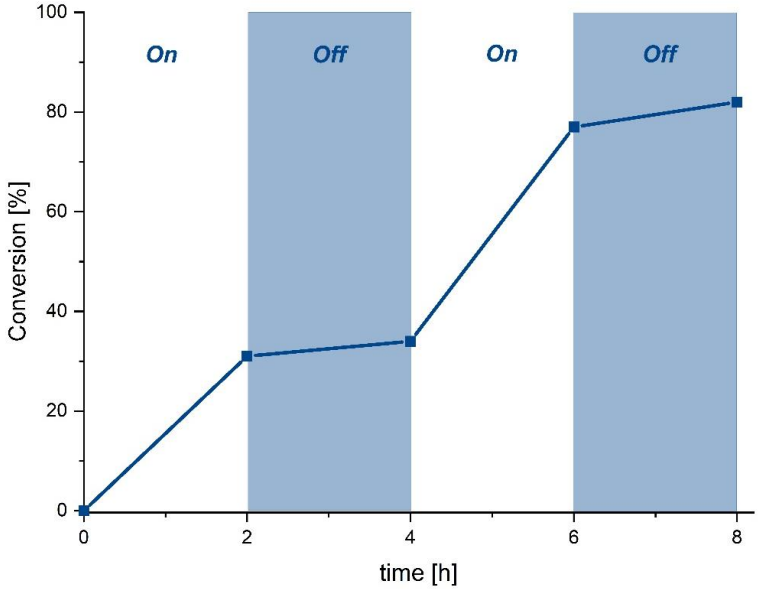

Figure 3.9: On/off experiment for ruthenium-catalyzed benzylation of arene **44a** enabled by visible light.

3.4.4 Proposed Catalytic Cycle

Based on the detailed experimental mechanistic studies and previous work,[249] a plausible reaction mechanism was suggested (Scheme 3.35).

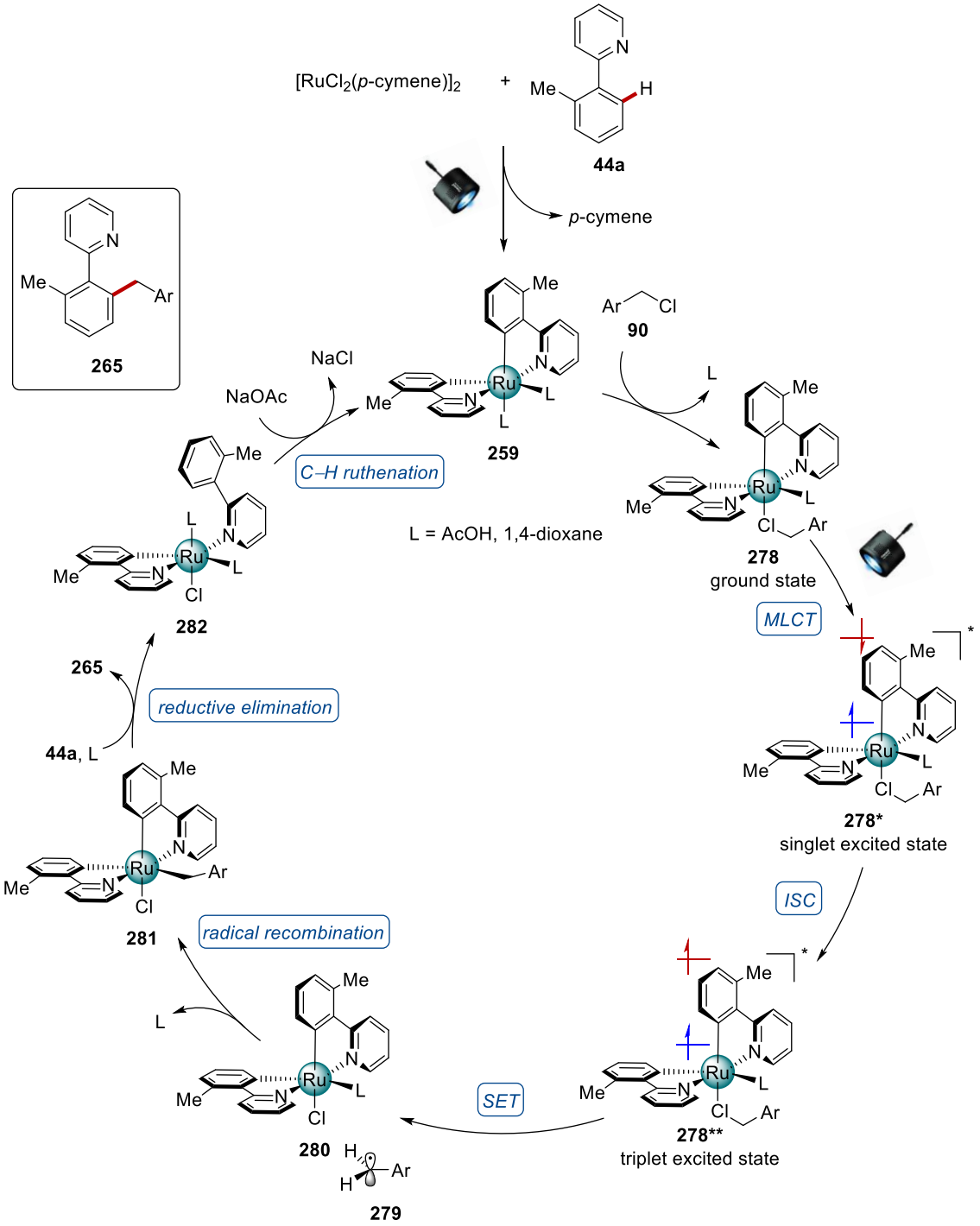

Scheme 3.35: Plausible mechanistic scenario of ruthenium-catalyzed photo-induced benzylation.

The catalytic cycle is initiated by the dissociation of the *p*-cymene ligand and the twofold carboxylate-assisted C–H activation of arene **44a** to furnish the biscyclometalated ruthenium complex **259**. The benzyl chloride substrate **90** subsequently coordinates and the ruthenacycle **278** is formed. This complex is believed to be photochemically active, and light-induced metal-to-ligand charge transfer (MLCT) results in the formation of the singlet exited state species

278*. Fast intersystem crossing (ISC) allows for relaxation furnishing the long-lived triplet complex **278****. An inner-sphere electron transfer (ISET) to benzyl chloride **90** affords the benzyl radical **279** and ruthenium(III) intermediate **280**, which readily recombine under formation of the ruthenium(IV) complex **281**. Reductive elimination and ligand exchange deliver the benzylated product **265** and ruthenium(II) species **282**, which closes the catalytic cycle by C–H ruthenation to regenerate the biscyclometalated ruthenium intermediate **259**.[258]

3.5 ELECTROPHOTOCHEMICAL UNDIRECTED TRIFLUOROMETHYLATION OF (HETERO-)ARENES

Trifluoromethylated arenes are important scaffolds in pharmaceuticals as beneficial effects on pharmacokinetic and physicochemical properties can often be observed (Figure 3.10).[259] Especially due to their increased lipophilicity and as a consequence thereof, increased bioavailability and enhanced membrane permeability, the incorporation of fluorinated groups in drugs is highly attractive.[260] Improved metabolic stability, the strong electron-withdrawing ability together with the small van-der-Waals radius and the greater stability of the C–F bond than C–H bond are further explanations for their prominent role in medicinal chemistry, not only as valuable moiety in bioactive compounds, but also as sensitive ^{18}F radio tracer.[134]

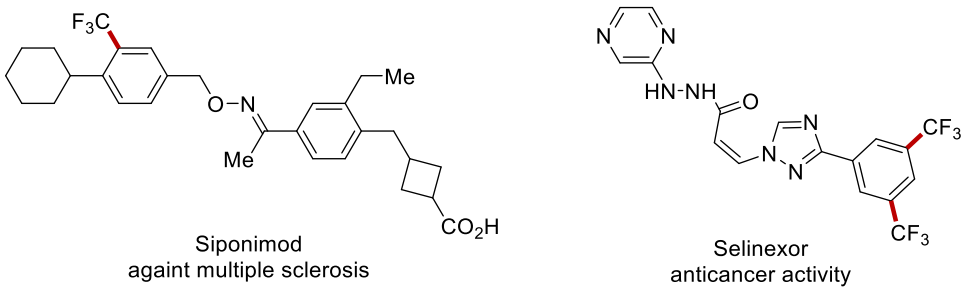

Figure 3.10: Selected examples of pharmaceuticals with trifluoromethyl substituents.

Among the different procedures for the trifluoromethylation of arenes, Ackermann reported in 2020 an electrophotochemical approach (Scheme 3.36).[157]

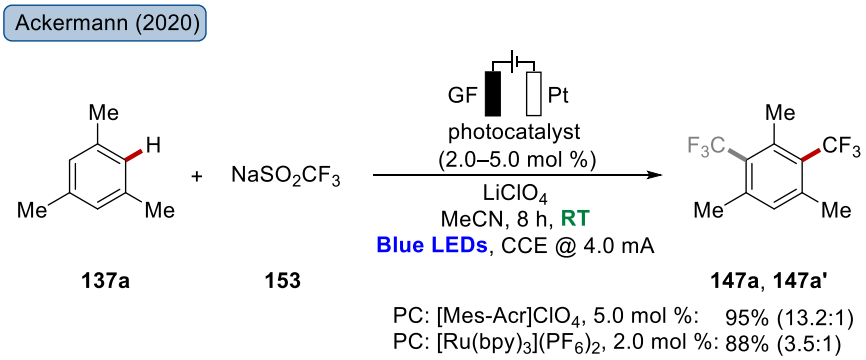

Scheme 3.36: Undirected trifluoromethylation under electrophoto-catalyzed conditions with two different photocatalysts.

The sustainable procedure relied on the use of the Langlois reagent $NaSO_2CF_3$ (**153**) as inexpensive trifluoromethyl source. The undirected C–H functionalization was realized under visible light irradiation in presence of a photocatalyst under constant current electrolysis in a user-friendly undivided cell set-up. Noteworthily, two different photocatalysts, among those,

an organic dye, could be employed in this catalysis and led to the formation of products **147a** and **147a'** in high yields.

Beyond this example, numerous electrophotochemical C–C bond forming procedures in C–H functionalization have been reported during the last two years. However, a comparison of different catalysts is missing thus far in literature. Inspired by this fact, the impact of the nature of different electrophotocatalysts was envisioned to disclose. In particular of interest was the cyclopropenium-based [TAC]ClO_4 electrophotocatalyst (Scheme 3.37).

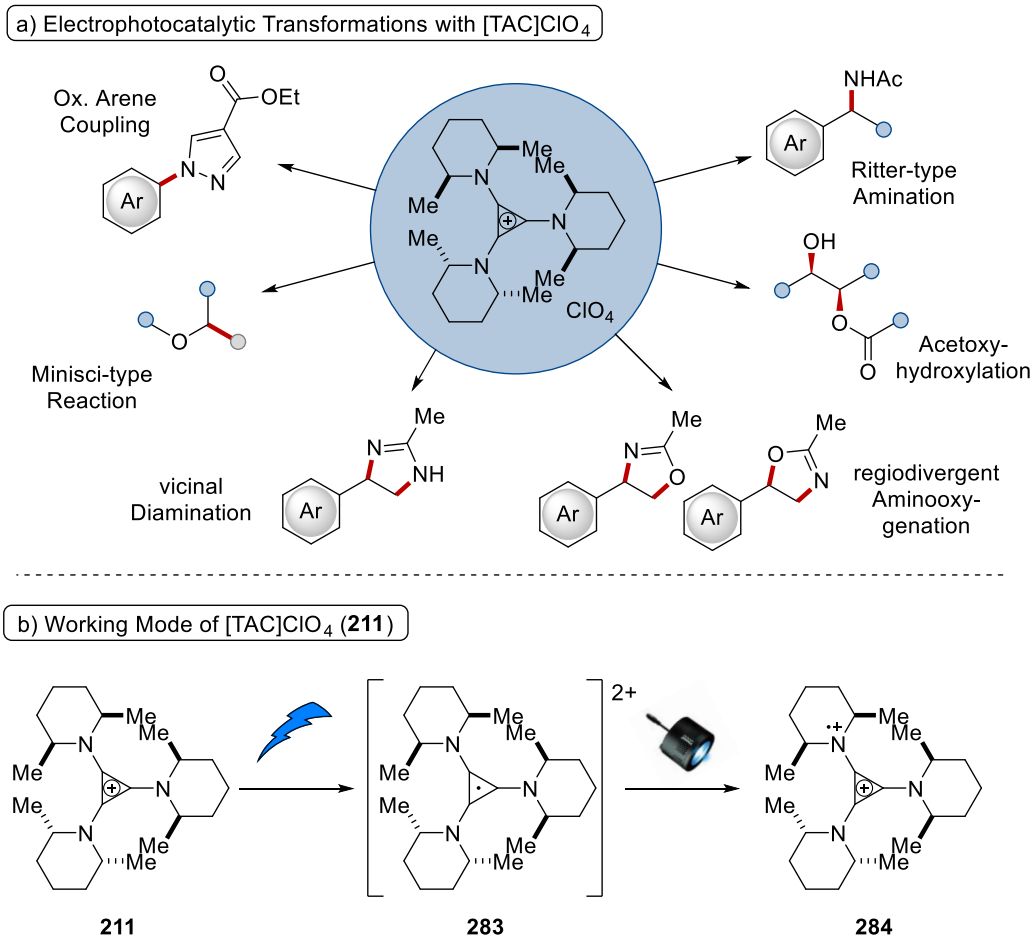

Scheme 3.37: [TAC]ClO_4 as electrophotocatalyst.

Cyclopropenium ions have been identified as versatile tool in organic synthesis with applications ranging from phase transfer catalysts to Brønsted acids and higher-order superbases.[215] The trisaminocyclopropenium derivative [TAC]ClO_4 instead possesses remarkable properties as electrophotocatalyst, which enabled a multitude of different transformations, as were shown by Lambert (Scheme 3.37a). The highly efficient colorless cationic catalyst is proposed to be oxidized by anodic oxidation, thus yielding a stable, red

colored radical dication which can be excited by visible light. Absorption of a photon affords the excited state species, which has a remarkable oxidizing ability (Scheme 3.37b).[165, 215]

Although several C–Het formations were thus far reported for this catalyst, efficient C–C bond formations for the modification of arenes continue to be elusive. Therefore, the expansion of its applicability towards the unprecedented trifluoromethylation would be highly desirable.

3.5.1 Comparison of Photoelectrocatalysts

Based on the previously reported reaction conditions which had been developed by Dr. Y. Qiu,[157] the catalytic efficacy in the envisioned trifluoromethylation was examined for a variety of different organo as well as transition metal containing (photo)redox catalysts under otherwise identical reaction conditions. To this end, the radical undirected functionalization of 1,3,5-trimethoxybenzene (**137b**) with the Langlois reagent **153** was chosen as a model reaction (Table 3.15). Noteworthily, not only the previously employed organo-photosensitizer [Mes-Acr]ClO_4 was a highly potent catalyst, but also other organic photoredox catalysts turned out to be similarly efficient (entries 1–5). The use of the earlier from Lambert exploited electrophotocatalyst [TAC]ClO_4 resulted in a slightly lower conversion than the other ones, but caused the highest selectivity for mono-functionalization to **147b** (entry 2). In contrast, the use of DDQ furnished the highest amount of the di-functionalized product **147b'** (entry 3). The undirected arene modification was not restricted to the use of organic photocatalysts. In comparison, tetrabutyl ammonium halides led to product formation in likewise excellent yields over 95% (entries 6–8). A high percentage of the di-functionalized molecule **147b'** was obtained by employing these efficient mediators. Likewise, cerium(III) chloride was identified as a viable photoredox catalyst (entries 9–10). Although this catalyst was previously known to enable efficient C–C formation under irradiation with 390 nm from purple LEDs, the absorption of both wavelengths, 390 nm as well as 450 nm, yielded the trifluoromethylated products **147b** and **147b'** with conversions higher than 90%. In case of irradiation with the shorter wavelength, the ratio of the di-functionalized product **147b'** was higher. In addition, different metal-based trisbipyridine complexes were used as light-harvesting catalysts. Besides the previously reported ruthenium complex, the more sustainable nickel- and iron-containing derivatives were highly suitable photoredox catalysts, giving product formations of close to 90% (entries 11–13). Moreover, the reaction of substrate **137b** was conducted with the decatungstate ammonium salt as photocatalyst, resulting in a high conversion of 85% with high mono-selectivity (entry 14). To prove the central role of the (photo)redox catalyst conclusively, a control experiment without catalyst was performed, which furnished the decorated arene **147b** only in minor 9%

yield (entry 15). Likewise, the use of both, electric current as well as light as external stimulus was crucial to ensure high conversions with [Mes-Acr]ClO_4 as photocatalyst (entries 16–17). Moreover, the light had a strongly enhancing effect on the efficacy with TBABr as mediator (entry 18). To summarize the comparison, the catalyst is essential to allow for reactivity. All employed catalysts resulted in excellent over all yields. However, the ratio of the mono- *vs*. di-functionalization showed to be strongly influenced by the catalyst. Exceedingly good mono-selectivity was achieved with the versatile cyclopropenium catalyst [TAC]ClO_4.

Table 3.15: Comparison of different catalysts for undirected trifluoromethylation of 1,3,5-trimethoxybenzene **137b**.

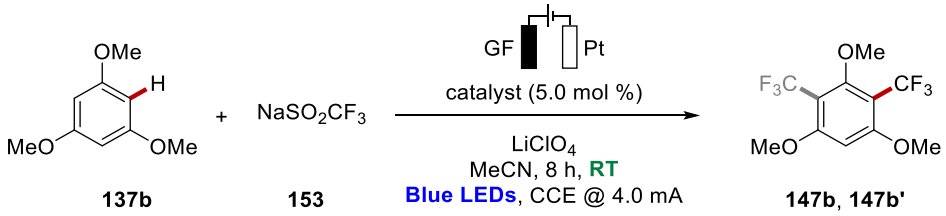

Entry	(Photo)redox Catalyst	**147** [%] (**147b**:**147b'**)[a]
1	[Mes-Acr]ClO_4	95 (4.9:1)
2	[TAC]ClO_4	89 (6.4:1)
3	DDQ	93 (1.7:1)
4	DCA	96 (5.0:1)
5	DCN	90 (4.3:1)
6	TBAI	95 (2.2:1)
7	TBABr	97 (1.5:1)
8	TBACl	95 (1.4:1)
9	$CeCl_3 \cdot 7H_2O$	90 (3.5:1)
10	$CeCl_3 \cdot 7H_2O$	93 (2.6:1)[b]
11	$[Fe(bpy)_3](PF_6)_2$	87 (3.8:1)[c]
12	$[Ni(bpy)_3]Br_2$	89 (5.2:1)[c]
13	$[Ru(bpy)_3](PF_6)_2$	91 (3.3:1)[c]

14	(n-$Bu_4N)_4[W_{10}O_{32}]$	85 (5.5:1)[c]
15	---	9 (---)
16	[Mes-Acr]ClO_4	7 (---)[d]
17	[Mes-Acr]ClO_4	4 (---)[e]
18	TBABr	39 (12.0:1)[d]

[a] Reaction conditions: Undivided cell, graphite felt anode, Pt cathode, constant current electrolysis at 4.0 mA. **137b** (0.25 mmol), **153** (0.50 mmol), catalyst (5.0 mol %), $LiClO_4$ (0.1 M), MeCN (4.0 mL), 30–33 °C, 8 h, under N_2, blue LED irradiation (450 nm). Conversion was determined by ^{1}H-NMR using dimethyl terephthalate as internal standard. [b] 390 nm wavelength. [c] Catalyst (2.0 mol %). [d] Reaction in the dark was performed by covering the vial with aluminum foil to avoid irradiation by the blue LED lamps under otherwise identical reaction conditions. [e] Reaction in the absence of electric current.

3.5.2 Substrate Scope

After having discovered that a range of catalysts enables the trifluoromethylation of arenes by electric current and visible light, the generality was examined by using different arenes and heteroarenes **137**. Encouraged by the beneficial effect of [TAC]ClO_4 on the selectivity, the substrates were subjected in transformations with the two different organic photocatalysts [Mes-Acr]ClO_4 and [TAC]ClO_4 (Scheme 3.38). Remarkably, the amount of the corresponding products was in all cases for both catalysts quite similar. The trisubstituted arenes **137b** and **137c** furnished the mono-functionalized products **147b** and **147c** together with minor amounts of the di-functionalized ones. In addition, different *N*-heteroarenes, such as quinoline (**137d**, **137e**) and pyrimidine (**137f**), were selectively converted under the reaction conditions, albeit with moderate yields in case of the sensitive dichlorinated quinoline **137e**. Moreover, furane (**137g**, **137h**) and thiophene **137i** were fully tolerated in both catalytic systems, even though a mixture of regioisomers was obtained for amides **147h** and **147i**.

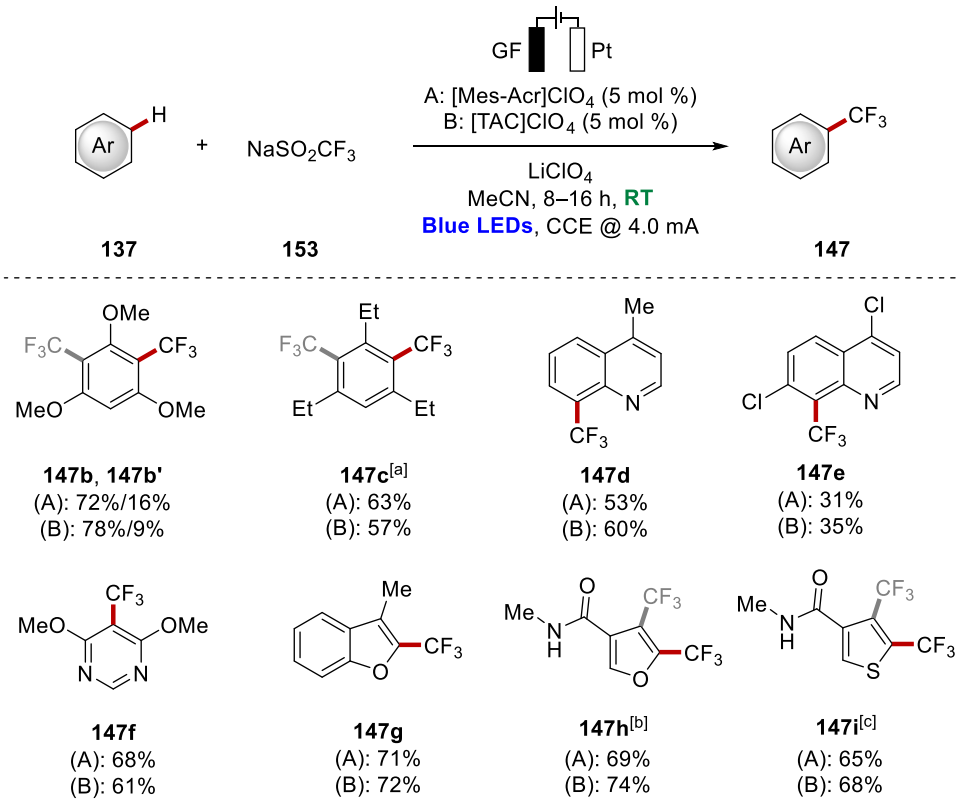

Reaction conditions: Undivided cell, graphite felt anode, Pt cathode, constant current electrolysis at 4.0 mA. **137** (0.25 mmol), **153** (0.50 mmol), A: [Mes-Acr]ClO_4 (5.0 mol %) or B: [TAC]ClO_4 (5.0 mol %), $LiClO_4$ (0.1 M), MeCN (4.0 mL), 30–33 °C, 8 h, under N_2, blue LED irradiation (450 nm). Yields refer to the isolated products. [a] Product was obtained together with the di-functionalized product (3.6:1). [b] Product was obtained as a mixture of regioisomers (3.0:1). [c] Product was obtained as a mixture of regioisomers (2.7:1).

Scheme 3.38: Undirected trifluoromethylation of different arenes **137** using [Mes-Acr]ClO_4 or [TAC]ClO_4.

To explore the different photoredox mediators, different heteroarenes **137** with biological relevance were transformed under the electrophotochemical conditions which allow for late-stage diversification (Scheme 3.39). As before, the product formation was compared for the two different photoredox catalysts [Mes-Acr]ClO_4 and [TAC]ClO_4, again resulting in very similar reaction yields. Gallic acid derivative **137j** was converted with both catalysts to furnish the trifluoromethylated product **147j** with moderate yields of close to 50% without difunctionalization. In addition, the purine alkaloids caffeine (**147k**) and pentoxifylline (**147l**) resulted for both catalytic systems in good yields of approximately 70%. Slight differences in the product yield were observed for the functionalization of purine base derivative **137m** as well as in the modification of the protected amino acid tryptophan **137n**, which were obtained in moderate yields around 50%.

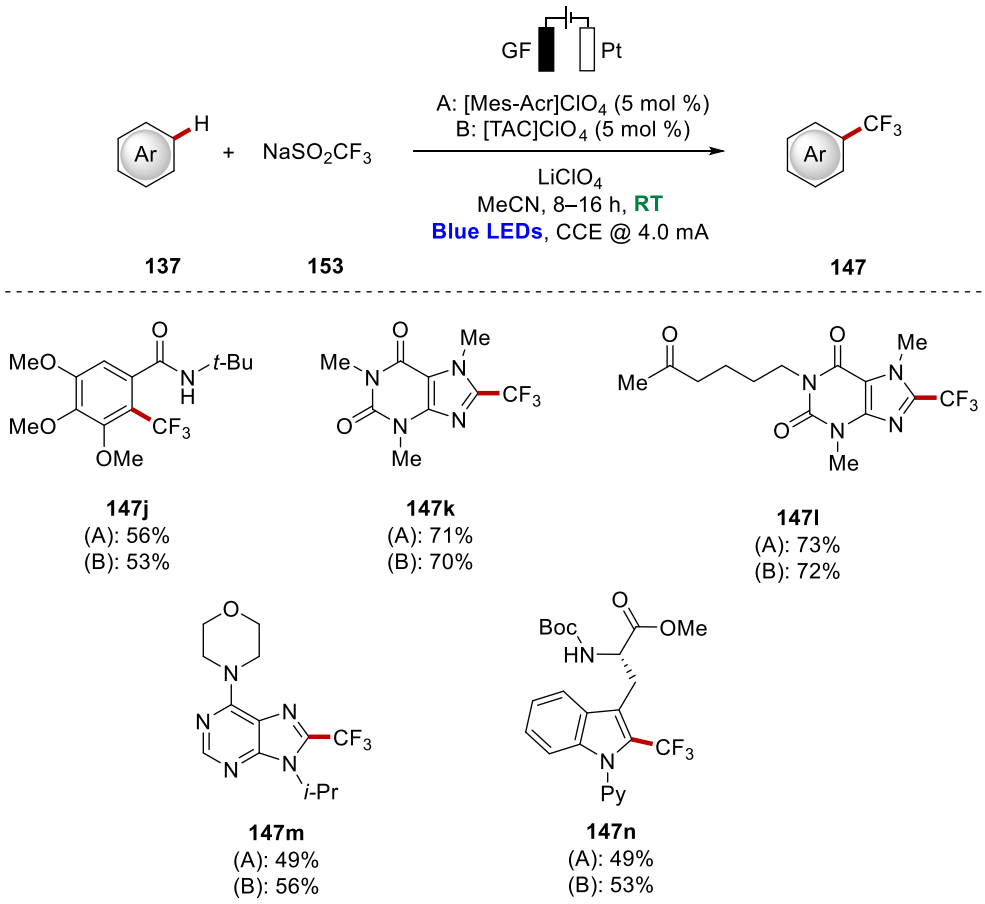

Reaction conditions: Undivided cell, graphite felt anode, Pt cathode, constant current electrolysis at 4.0 mA. **137** (0.25 mmol), **153** (0.50 mmol), A: [Mes-Acr]ClO_4 (5.0 mol %) or B: [TAC]ClO_4 (5.0 mol %), $LiClO_4$ (0.1 M), MeCN (4.0 mL), 30–33 °C, 8 h, under N_2, blue LED irradiation (450 nm). Yields refer to the isolated products.

Scheme 3.39: Trifluoromethylation of biorelevant arenes **137** with [Mes-Acr]ClO_4 or [TAC]ClO_4.

Although the applicability of the trifluoromethylation procedure is quite broad and various heterocyclic substrates were functionalized with good catalytic efficacy and positional selectivity, some substrates could not be modified under the reaction conditions (Scheme 3.40). A few substrates frequently used in C–H activation with different *N*-heterocycles as directing group as well as pivaloyl indole turned out to be challenging substrates **137** due to a lack in site-selectivity. With both catalysts, a complex mixture of regioisomers and di-functionalized products were obtained, which could not be separated. Other arenes **137** did not react at all and the incorporation of the trifluoromethyl substituent was only detectable in trace amounts.

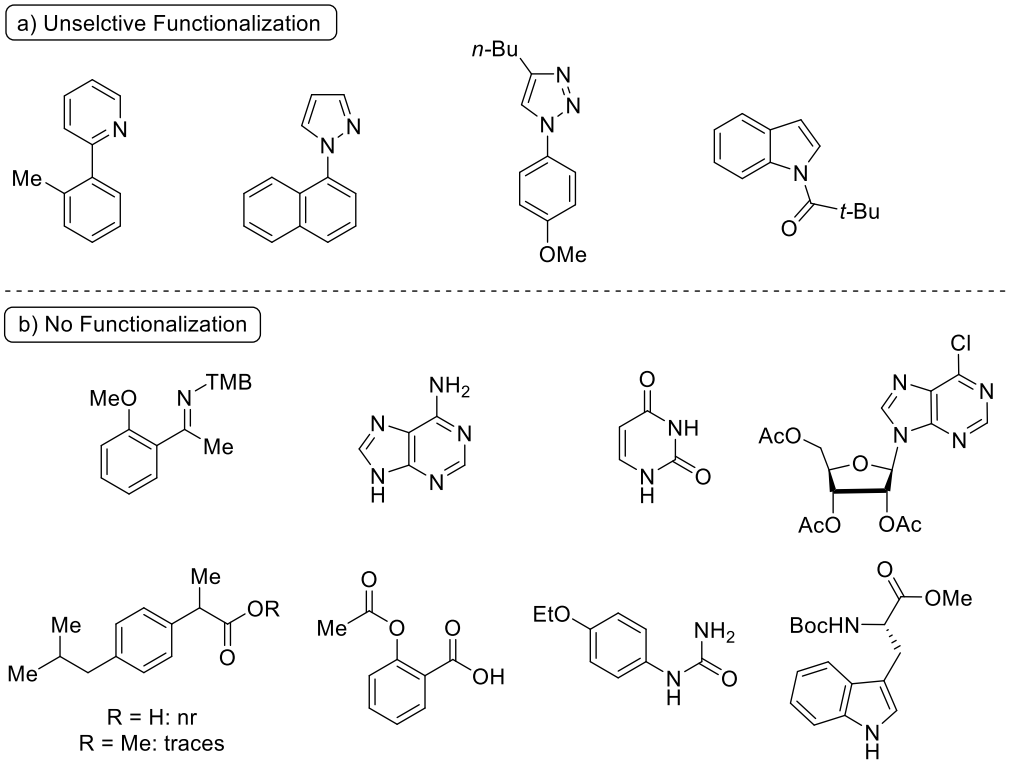

Scheme 3.40: Unsuccessful examples for undirected modification with electrophotocatalytic trifluoromethylation.

3.5.3 Kinetic Studies and Mechanistic Experiments

To gain further information on the catalytic efficacy of the different mediators, the conversions were determined after 2, 4 and 8 h to not only compare the yields after the reaction, but also to collect data during the course of the reaction (Table 3.16). In this case, caffeine (**137k**) was chosen as the model substrate to avoid difunctionalization. Among the different employed organo-catalysts (entries 1–5), [Mes-Acr]ClO_4 showed the highest efficacy after the first hours with 34% conversion. DCN overtook the other photosensitizers, resulting in an excellent yield of 95%, while for the others yields between 79% and 88% of the modified caffeine **147k** were determined by crude ^{19}F-NMR-analysis. Furthermore, the ammonium salts as mediators showed very good performances (entries 6–8). Interestingly, moving from chlorine to iodine resulted in less efficient catalysis, which caused a difference of 9% after 8 h reaction time. Reactions with cerium(III) as the photoredox catalyst highlighted the beneficial effect of the irradiation with the shorter wavelength of 390 nm, which enabled significantly higher conversions of arene **137k** than with 450 nm (entries 9–10). Additionally, several bipyridine-based transition metal photocatalysts were evaluated (entries 11–13). Despite the fact that the ruthenium complex was the most efficient one after 2 h, the conversion remained behind the base-metal ones with Fe and Ni as metal center at longer durations. In addition, the

decatungstate salt allowed for good reactivities during the whole reaction time (entry 14), while only minor amounts of the product **147k** could be measured in the absence of a photoredox catalyst (entry 15). This study, which was meant to disclose the catalytic activity, highlighted that the performance of the different mediators was rather comparable during the reaction with around 30% after 2 h, approximately 70% after 4 h and 80% to 90% after 8 h. However, slight differences were observed during the course of the reaction, which was reflected in slightly different product yields of **157k**.

Table 3.16: Comparison of different catalysts in the electrophotochemical modification of caffeine (**137k**).

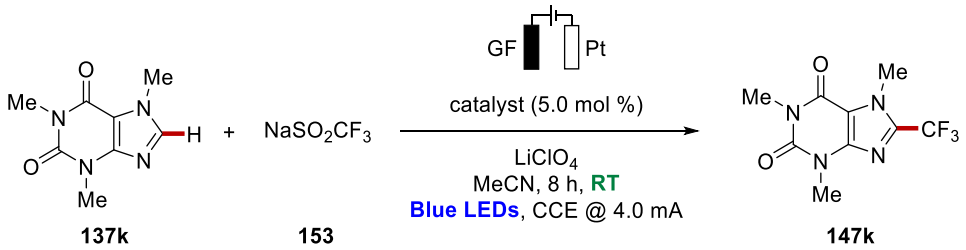

Entry	(Photo)redox Catalyst[a]	**147k** [%] 2 h	**147k** [%] 4 h	**147k** [%] 8 h
1	$[Mes\text{-}Acr]ClO_4$	34%	67%	79%
2	$[TAC]ClO_4$	27%	61%	81%
3	DDQ	28%	62%	88%
4	DCA	30%	73%	83%
5	DCN	23%	70%	95%
6	TBAI	26%	63%	83%
7	TBABr	28%	68%	90%
8	TBACl	29%	73%	94%
9	$CeCl_3 \cdot 7H_2O$	27%	61%	79%
10	$CeCl_3 \cdot 7H_2O$[b]	31%	71%	93%
11	$[Fe(bpy)_3](PF_6)_2$[c]	31%	71%	89%
12	$[Ni(bpy)_3]Br_2$[c]	30%	70%	89%
13	$[Ru(bpy)_3](PF_6)_2$[c]	33%	65%	86%

14	(n-$Bu_4N)_4[W_{10}O_{32}]$[c]	34%	67%	79%
15	---	1%	3%	8.%

[a] Reaction conditions: Undivided cell, graphite felt anode, Pt cathode, constant current electrolysis at 4.0 mA. **137k** (0.25 mmol), **153** (0.50 mmol), catalyst (5.0 mol %), $LiClO_4$ (0.1 M), MeCN (4.0 mL), 30–33 °C, 8 h, under N_2, blue LED irradiation (450 nm). Conversion was determined by ^{19}F-NMR using 1-fluorononane as internal standard. [b] 390 nm wavelength. [c] Catalyst (2.0 mol %).

A graphical presenting of these results for the catalytic efficacy of the trifluoromethylation of caffeine (**137k**) is shown in Figure 3.11.

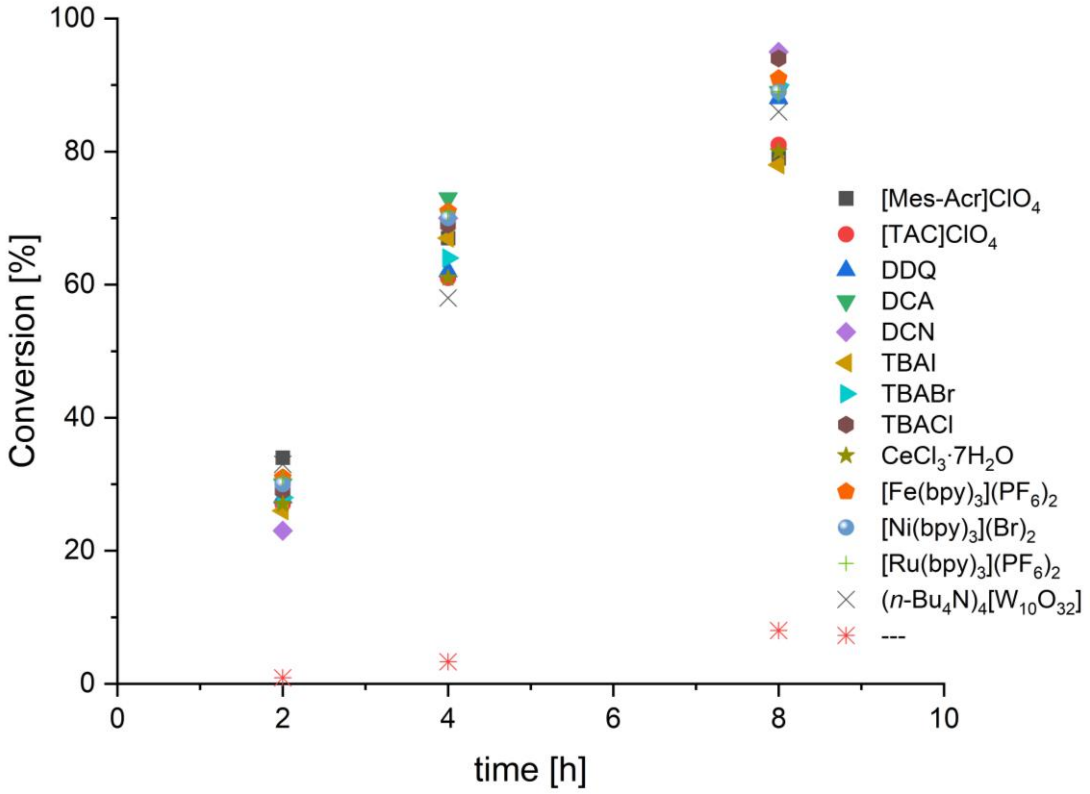

Figure 3.11: Electrophoto-catalyzed trifluoromethylation of caffeine (**137k**) with different photoredox mediators.

Moreover, the reaction progress of the caffeine modification was monitored for the three different photocatalysts [Mes-Acr]ClO_4, [TAC]ClO_4, and [Ru(bpy)$_3$]$(PF_6)_2$ by using a flow *in situ* NMR set-up (Figure 3.12). The conversions were determined by ^{19}F-NMR with 1-fluorononane as internal standard. As illustrated in the reaction profiles, only minor differences in the rates could be detected. However, the data indicates that the acridinium-based organic dye has the highest reaction rate during the first 100 min, which is in good agreement with the previous results of the catalyst comparison for the functionalization of caffeine (**137k**). In contrast, the versatile catalyst [TAC]ClO_4 has over-all the highest rate over the first 6 h,

before the conversion is staying almost constant. The ruthenium catalyst exhibited almost a linear relation between conversion and time and similar to the [Mes-Acr]ClO_4 photocatalyst, the catalyst remains active until the end of the reaction time of 8 h. A slight difference in the reaction profile was observed during the reaction progress.

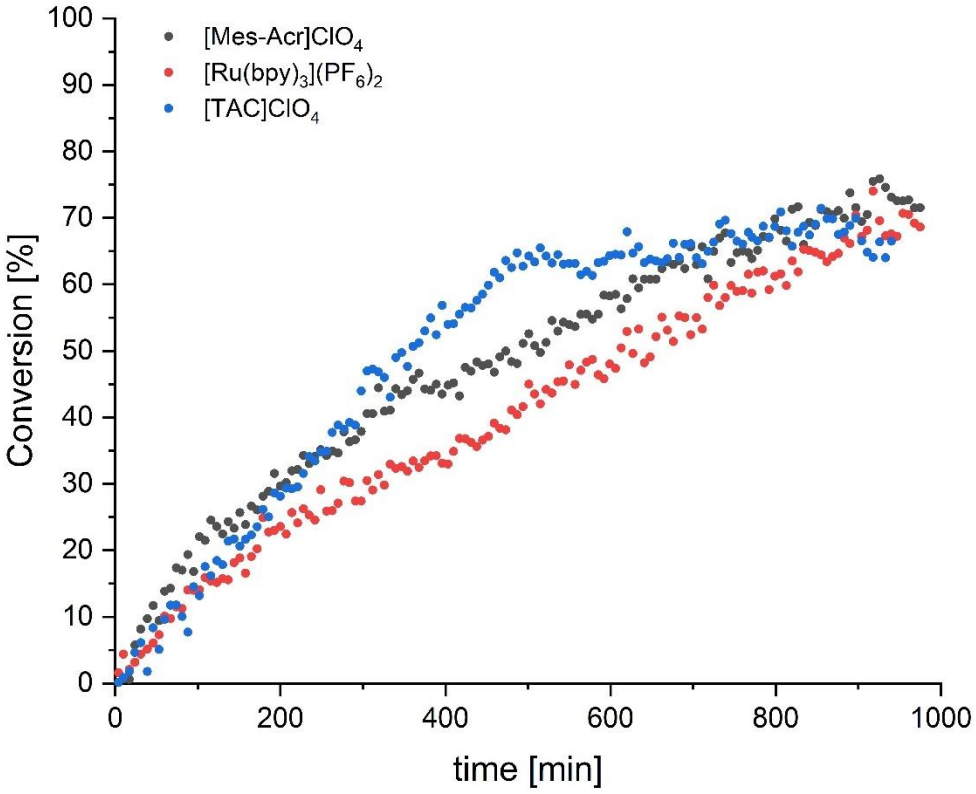

Figure 3.12: Reaction monitoring with *in situ* NMR studies with different catalysts.

To gain some more information on the role of the electricity and the light, control experiments were conducted, where the electric current, the light or both of them were switched off after an initial period of 30 mins (Table 3.17). The conversion at this moment was determined by crude ^{19}F-NMR analysis and compared to the one after full 8 h reaction time to be able to comment on the reaction progress under the modified conditions. Under standard reaction conditions with electric current and blue light irradiation, the trifluoromethylated arenes **147b** and **147b'** were formed with 14% conversion after 30 min, while 94% was detected after 8 h, with the mono-functionalized product **147b** as the major one (entry 1). If the current was switched off after 30 min at standard conditions, the conversion dropped to 46%, which suggested that the formation of products **147b** and **147b'** continued under sole light irradiation (entry 2). Even more extensive was the trifluoromethylation under electrochemical conditions, resulting in 72% yield, thus indicating that after the induction in the presence of light, the reaction can be enabled

also electrochemically (entry 3). On the contrary, when neither light nor electricity was available after 30 min, no further conversion was observed, being indicative that at least one of the parameters needs to be ensured (entry 4). A control experiment in the absence of the light and electricity for the full 8 h without the initial exposure furnished only trace amounts of the product **147b** (entry 5). Similar results were obtained with $[Ru(bpy)_3]^{2+}$ as photocatalyst.

Table 3.17: Impact of light and electricity on the undirected functionalization of trimethoxybenzene **137b** with $[Mes\text{-}Acr]ClO_4$.

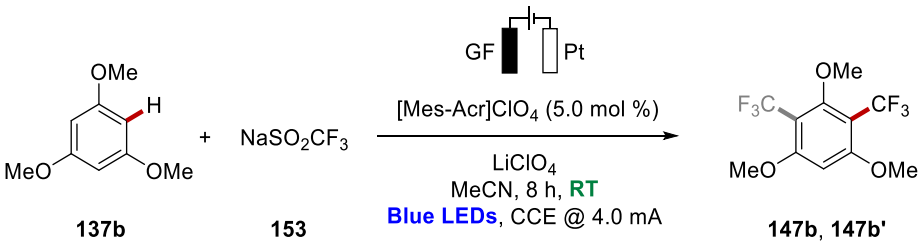

Entry	Deviation from Standard Conditions[a]	**147** [%] (**147b**:**147b'**) 30 min	**147** [%] (**147b**:**147b'**) 8 h
1	none	14% (14:0)	95% (4.9:1)
2	no electric current after 30 min, only light	17% (17:0)	46% (45:1)
3	no light after 30 min, only electricity	14% (14:0)	72% (6.9:1)
4	no light and no current after 30 min	12% (12:0)	15% (15:0)
5	no light and no current during the full 8 h	3% (3:0)	9% (9:0)

[a] Reaction conditions: Undivided cell, graphite felt anode, Pt cathode, constant current electrolysis at 4.0 mA. **137b** (0.25 mmol), **153** (0.50 mmol), $[Mes\text{-}Acr]ClO_4$ (5.0 mol %), $LiClO_4$ (0.1 M), MeCN (4.0 mL), 30–33 °C, 8 h, under N_2, blue LED irradiation (450 nm). After 30 min and 8 h, an aliquot was analyzed and the conversion determined by ^{19}F-NMR using 1-fluorononane as internal standard.

3.5.4 Trifluoromethylation of KAN0438757

Considering the importance of trifluoromethyl substituents in medicinal chemistry, the developed sustainable procedure was employed for the modification of biological relevant scaffolds. The protocol was intended to realize the late-stage functionalization of KAN0438757 (**291**), a PFKFB3 kinase inhibitor which possesses anticancer activity.[261] The synthetic route to prepare the drug compound **291** is a four step procedure (Scheme 3.41).[261b] Commencing from the commercially-available sulfonyl chloride **285** and aniline **286**, sulfonamide **288** is

formed. Subsequent Suzuki-Miyaura cross-coupling of sulfonamide **288** with boronic acid **287** by palladium catalysis furnishes the intermediate **289**. The actual biologically active drug compound is the acid **290**, KAN0438242. Due to the fact that the membrane permeability and therefore bioavailability of the free acid is not sufficient, the uptake into the cell must take place as an ester pro-drug. As the methyl ester **289** can not be cleaved under physiological conditions, the conversion into an easily cleavable ester is required to allow membrane permeabilization and assimilation of the compounds into the cancer cell. To this end, methyl ester **289** is cleaved under acidic conditions, before esterification of acid **290** with ethylene glycol, thus providing access to the desired pro-drug kinase inhibitor KAN0438757 (**291**), which is cleavable under physiological conditions

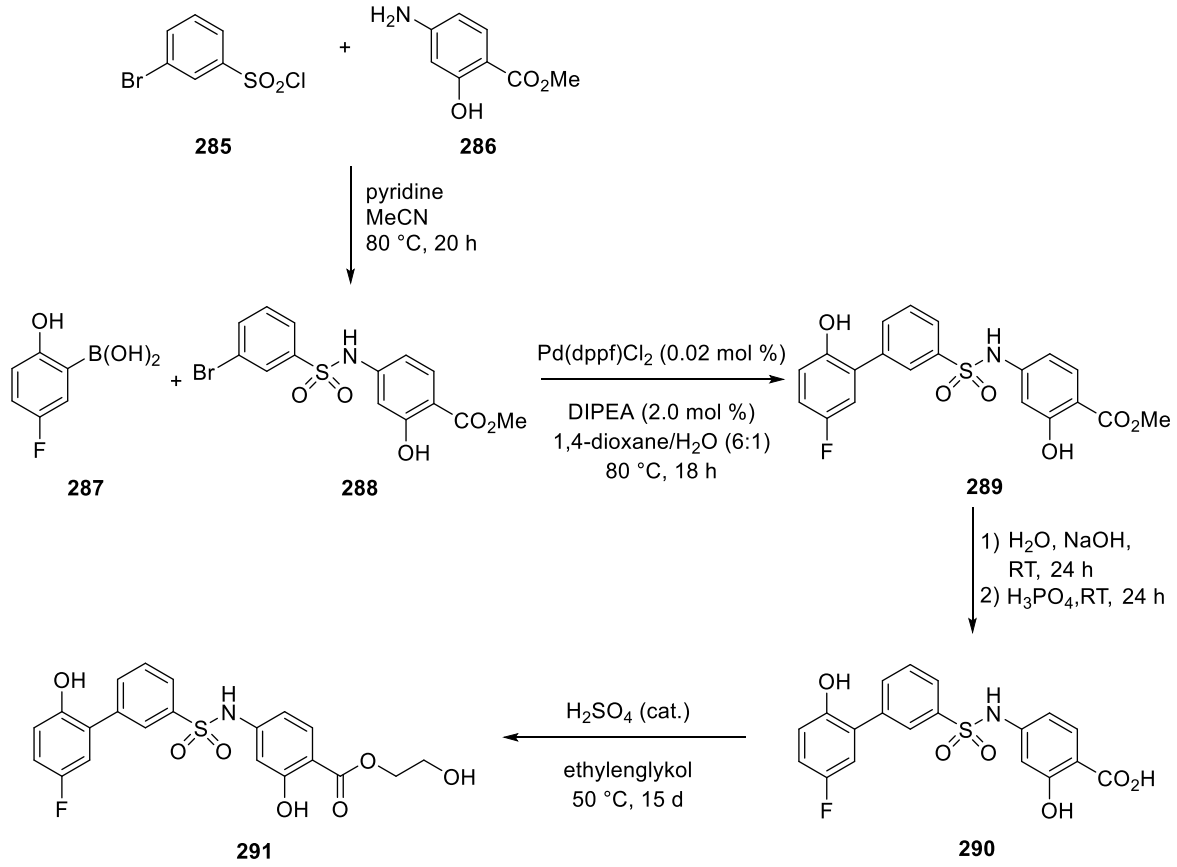

Scheme 3.41: Synthesis of anticancer pro-drug KAN0438757 (**291**).

The most convenient way to obtain the trifluoromethylated anticancer pro-drug **291** would be the direct late-stage diversification of KAN0438757 by following the electrophotochemical procedure (Scheme 3.42). Hence, attempts to functionalize the drug were made with [Mes-Acr]ClO_4, [TAC]ClO_4 and $[Ru(bpy)_3](PF_6)_2$ as the electrophotocatalyst. Although a higher catalyst loading was used for this challenging substrate **291**, the careful analysis of the crude mixture revealed that the incorporation of the valuable trifluoromethyl moiety was not

successful. In opposition, the starting material **291** was decomposed under these reaction conditions and therefore, it could not be reisolated after the reaction.

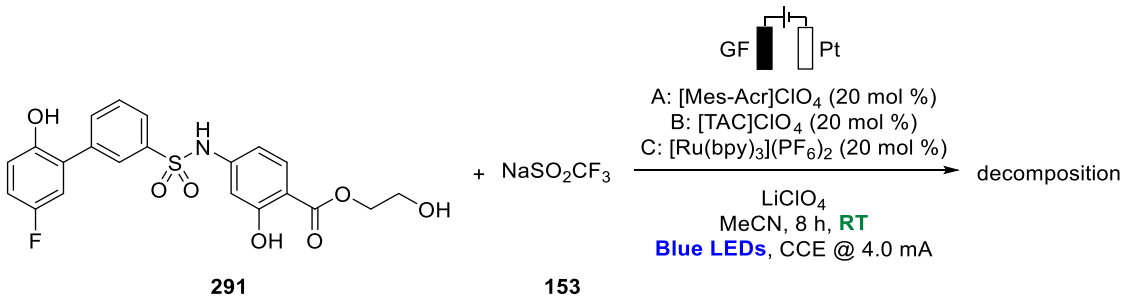

Reaction conditions: Undivided cell, graphite felt anode, Pt cathode, constant current electrolysis at 4.0 mA. **291** (0.05 mmol), **153** (0.10 mmol), A: [Mes-Acr]ClO_4 (5.0 mol %) or B: [TAC]ClO_4 (5.0 mol %) or C: $[Ru(bpy)_3](PF_6)_2$ (20 mol %), $LiClO_4$ (0.1 M), MeCN (2.0 mL), 30–33 °C, 8 h, under N_2, blue LED irradiation (450 nm).

Scheme 3.42: Late-stage diversification of anticancer pro-drug KAN0438757 (**291**).

Further attempts to functionalize the intermediates were challenging as well due to low conversions and low selectivity. Hence, the aim to prepare trifluoromethylated derivatives of the pro-drug **291** was further pursued with the small arene building blocks. Frist, the methyl ester of the sulfonic acid, arene **292**, was added to the reaction conditions to prove a possible functionalization (Table 3.18).

Table 3.18: Electrophotochemical modification of sulfonic acid derivative **292**.

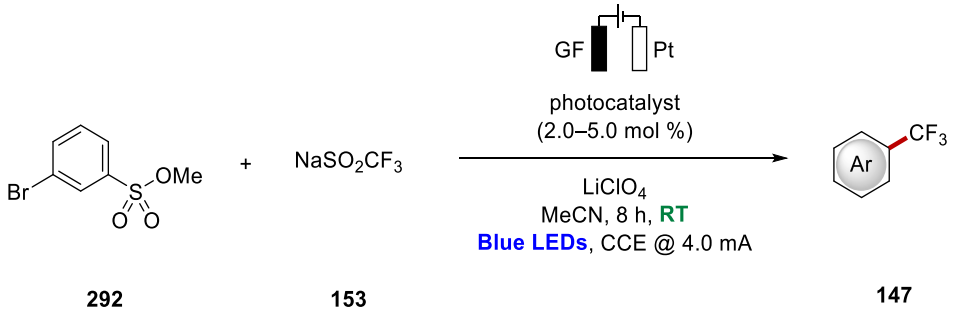

Entry	Photoredox Catalyst	**147** [%][a]
1	[Mes-Acr]ClO_4	---
2	[TAC]ClO_4	traces
3	$[Ru(bpy)_3](PF_6)_2$	---

[a] Reaction conditions: Undivided cell, graphite felt anode, Pt cathode, constant current electrolysis at 4.0 mA. **292** (0.20 mmol), **153** (0.40 mmol), A: [Mes-Acr]ClO_4 (5.0 mol %) or B: [TAC]ClO_4 (5.0 mol %) or C: $[Ru(bpy)_3](PF_6)_2$ (2.0 mol %), $LiClO_4$ (0.1 M), MeCN (4.0 mL), 30–33 °C, 8 h, under N_2, blue LED irradiation (450 nm).

Unfortunately, the modification of the arene **292** was not successful. For all three employed photocatalysts, only trace amounts of the trifluoromethylated product **147** were detected (entries 1–3).

In contrast, the electrophotocatalytic modification of the aniline derivative **286**, which is used for coupling to afford sulfonamide **288**, was indeed realized (Table 3.19).

Table 3.19: Undirected trifluoromethylation of amine **286** with different photoredox catalysts.

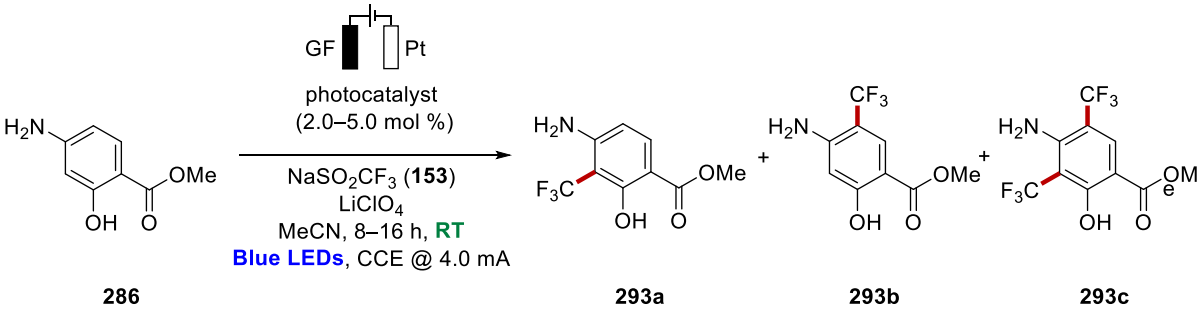

286 **293a** **293b** **293c**

Entry	Photoredox Catalyst	**293** [%] (**293a**:**293b**:**293c**)[a]
1	[Mes-Acr]ClO_4	42 (9.3:3.6:1.0)
2	[Mes-Acr]ClO_4	43 (8.2:2.6:1.0)[b]
3	[TAC]ClO_4	71 (5.5:1.8:1.0)
4	[TAC]ClO_4	72 (5.3:1.3:1.0)[b]
5	[Ru(bpy)$_3$]$(PF_6)_2$	42 (6.8:4.0:1.0)
6	[Ru(bpy)$_3$]$(PF_6)_2$	47 (6.8:2.4:1.0)[b]

[a] Reaction conditions: Undivided cell, graphite felt anode, Pt cathode, constant current electrolysis at 4.0 mA. **286** (0.20 mmol), **153** (0.40 mmol), A: [Mes-Acr]ClO_4 (5.0 mol %) or B: [TAC]ClO_4 (5.0 mol %) or C: [Ru(bpy)$_3$]$(PF_6)_2$ (2.0 mol %), $LiClO_4$ (0.1 M), MeCN (4.0 mL), 30–33 °C, 8 h, under N_2, blue LED irradiation (450 nm). Yields refer to the isolated products. [b] 16 h reaction time.

Remarkably, this arene turned out to be viable for the trifluoromethylation with any of the three tested photocatalysts, resulting in a mixture of the two mono-functionalized products **293a** and **293b** together with the di-functionalized arene **293c**. Although the yield and the ratio were influenced by the chosen photocatalyst, in all cases arene **293a** was obtained as the major product. As the different products could be easily separated from each other by column chromatography, the lack of selectivity was not seen as disadvantage as it allows in the end for preparation of three different derivatives of pro-drug **291**. The use of [Mes-Acr]ClO_4 resulted

in a moderate over-all yield of 42% with high selectivity for the predominant product **293a** (entry 1). Increasing the reaction time to 16 h did not influence the yield and only negligibly the ratio of the products **293** (entry 2). Much higher conversions were obtained by the electrophotocatalyst [TAC]ClO_4 with a good combined yield above 70% for all three arenes **293a**–**293c** and in a rather high selectivity for the minor products **293b** and **293c** compared to the other organo-photosensitizer (entries 3–4). However, $[Ru(bpy)_3](PF_6)_2$ led to similar moderate yields as [Mes-Acr]ClO_4, which only marginally increased with a prolonged reaction time (entries 5–6).

Noteworthy, this demanding arene substrate **286** being decorated with sensitive free hydroxy- and amine groups as well as the ester functionality, was the only example in which a significant impact of the photocatalyst was observed. These results highlighted that the use of the [TAC]ClO_4 might be interesting especially for sensitive arenes, such as **286**. To get deeper insights into this remarkable example, a few experiments with slightly modified conditions were conducted to analyze their influence on the reaction yield as well as the ratio of the three different products **293** (Table 3.20). A reduced reaction time of 4 h resulted in a significantly diminished conversion of 50% instead of 71%. Remarkably, the ratio of the products was changed dramatically at shorter reaction times, resulting in an exceptional high selectivity for the major mono-trifluoromethylated product **293a** (entries 1–2). Additionally, the impact of the electrochemical settings was analyzed. With a maximal voltage of 3 V instead of 5 V or a higher one with 7 V, the envisioned modification failed to appear or the decomposition of the products **293** was caused (entry 3). Changing the equivalents of the Langlois reagent (**153**) resulted in case of a decreased amount in a reduced yield of 50% and excellent selectivity to provide the major product **293a** (entry 4). An increased excess of $NaSO_2CF_3$ (**153**) had less influence and afforded in total similar conversions, albeit with a slightly increased formation of the bis-trifluoromethylation product **293c** (entry 5). Employing an increased catalyst loading of 10 mol % of [TAC]ClO_4 had limited effect on the efficacy of the electrophotochemical transformation furnishing the products **293a**–**293c** in a slightly higher yield of 81%. Moreover, control experiments were substantiating that the addition of a photoredox mediator as well as the irradiation with blue LED light is strongly enhancing the reactivity, since only 10% product formation were found in their absences (entries 7–8). Finally, the essential role of the electric current was proven in a control experiment (entry 9).

Table 3.20: Different test reactions and control experiments for electrophotochemical diversification of amine **286**.

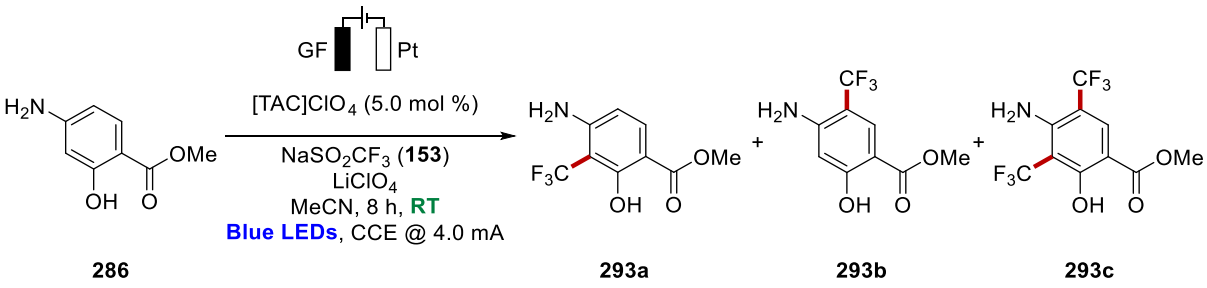

Entry	Deviation from Standard Conditions	**293** [%] (**293a**:**293b**:**293c**)[a]
1	none	71 (5.5:1.8:1.0)
2	t = 4 h	50 (21.1:3.0:1.0)
3	Max. Potential 3 V or 7 V	traces
4	**153** (1.0 equiv)	51 (19.5:5.0:1.0)
5	**153** (3.0 equiv)	70 (4.1:2.1:1.0)
6	$[TAC]ClO_4$ (10 mol %)	81 (5.3:2.3:1.0)
7	no catalyst	12 (11.0:3.0:1.0)
8	no light	10 (2.0:1.0:1.0)
9	no current	---

[a] Reaction conditions: Undivided cell, graphite felt anode, Pt cathode, constant current electrolysis at 4.0 mA, V_{max} = 5 V. **286** (0.20 mmol), **153** (0.40 mmol), $[TAC]ClO_4$ (5.0 mol %), $LiClO_4$ (0.1 M), MeCN (4.0 mL), 30–33 °C, 8 h, under N_2, blue LED irradiation (450 nm). Yields refer to the isolated products.

Attracted by the fact that the arene **286** possesses a high capability to be trifluoromethylated under electrophotocatalytic conditions, especially by using $[TAC]ClO_4$, whereas the functionalization of this arene moiety seems difficult in sulfonamide **288**, this discrepancy was disclosed in an additional control experiment (Scheme 3.43). In contrast to the assumption that the different electronical properties cause the low reactivity in sulfonamide **288**, the finding is rather supportive for an inhibition by the sulfonamide functionality itself. The best conditions for the functionalization of aniline **286** with $[TAC]ClO_4$ as a photoredox catalyst usually gave arenes **293** with an over-all yield of 70%. However, by addition of one equivalent of tosylamine

(**294**), the reactivity was completely suppressed and only trace amounts of the trifluoromethylated products **293** were detected.

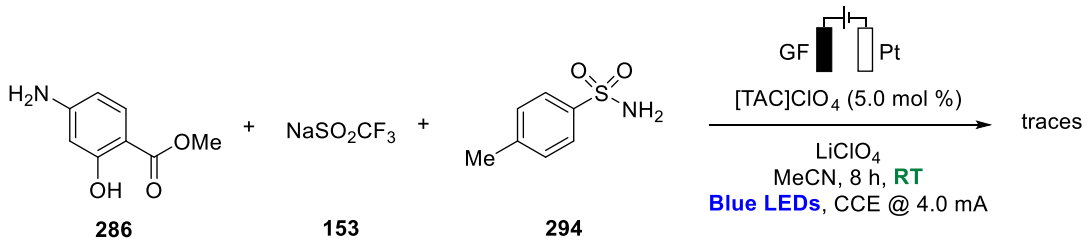

Scheme 3.43: Control experiment of undirected trifluoromethylation with $[TAC]ClO_4$ in presence of a sulfonamide **294**.

Although the initially envisioned late-stage diversification of the kinase inhibitor pro-drug KAN0438757 (**291**) turned out to be challenging due to the decomposition of the starting material and low tolerance of the sulfonamide moiety itself, an approach to realize the preparation of the modified drug candidates could be found. The electrophotochemical trifluoromethylation of the aniline building block allowed for efficient formation of three different trifluoromethylated products, which could be easily purified.

3.5.5 Proposed Catalytic Cycle

Detailed mechanistic studies were performed by Dr. Y. Qiu, Dr. L. Finger, and A. Scheremetjew to delineate the mode of action.[157] Reactions in the presence of radical scavengers were indicative of a single-electron transfer (SET) manifold, not only because the C–H functionalization was strongly suppressed by the addition of TEMPO or BHT, but also because the corresponding adducts were isolated. Stern-Volmer fluorescence quenching studies of $[Mes\text{-}Acr]ClO_4$ highlighted an efficient quenching with $NaSO_2CF_3$ (**153**), whereas the quenching with arene **137** was less intense. In sharp contrast, the emission of the alternative photocatalyst $[Ru(bpy)_3](PF_6)_2$ was not quenched in the presence of either the one or the other starting material. As a consequence, these interesting findings are suggestive of two different mechanistic scenarios in dependence on the employed photoredox catalyst. Further information on the catalytic mechanism was provided by CV experiments, which showed that the anodic oxidation with E_{onset} = 1.02 V *vs.* SCE of the Langlois regent (**153**) remained unaltered in the presence of $[Mes\text{-}Acr]ClO_4$. Contrary to this, the irradiation with blue LED light caused a consumption of the trifluoromethylating reagent, thus being indicative of the formation of a trifluoromethyl radical in the presence of the excited state species of the organic photosensitizer. Moreover, kinetic studies with flow ^{1}H-NMR suggested the formation of a Wheeland

intermediate, while headspace chromatographic analysis verified the evolution of hydrogen gas as side product.[157]

Based on these findings, a plausible catalytic cycle was proposed for the [Mes-Acr]ClO_4-mediated trifluoromethylation (Scheme 3.44). Excitation of the photocatalyst allows for single-electron transfer (SET) from the trifluoromethanesulfinate anion **153**, thus affording the radical species of the photocatalyst, which is reconverted into the cationic species by anodic oxidation. The thus generated trifluoromethanesulfinate radical (**295**) subsequently undergoes decomposition, and under irreversible release of sulfur dioxide, trifluoromethyl radical (**296**) is obtained. Radical attack on arene **137**, followed by another SET process, yields the Wheeland complex **298** as a key intermediate, which leads to the trifluoromethylated product **147** after deprotonation. The electric cycle is closed by cathodic reduction of the released protons, thereby affording H_2 by the hydrogen evolution reaction (HER).

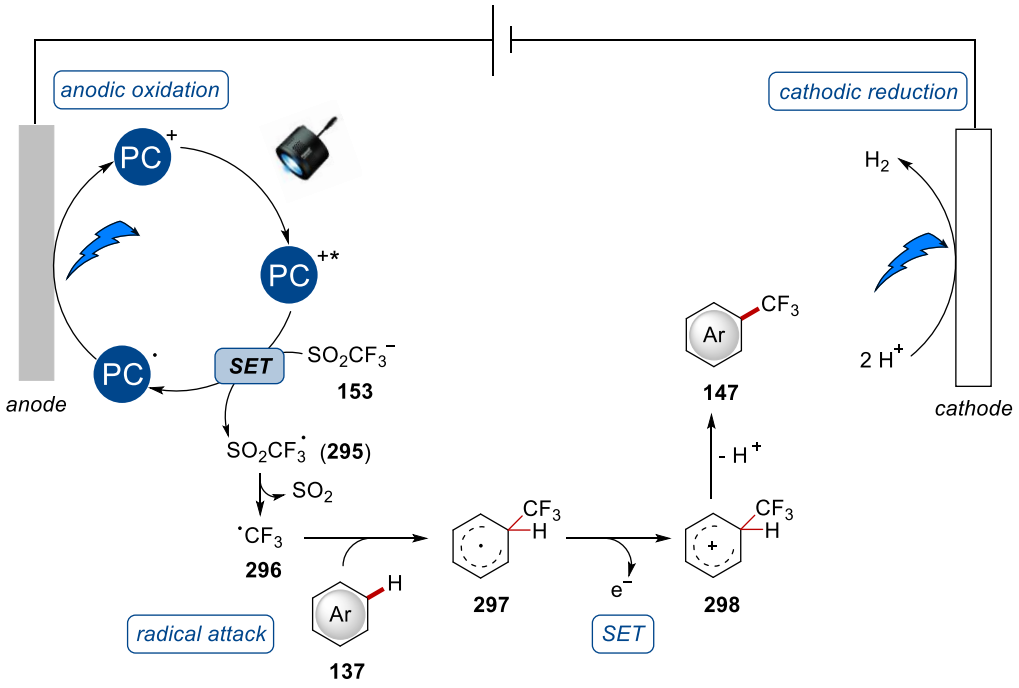

Scheme 3.44: Proposed catalytic scenario for electrophotochemical trifluoromethylation with [Mes-Acr]ClO_4 as photoredox catalyst.

Taking the different behavior of both tested photoredox catalysts during the Stern-Volmer fluorescence quenching into account, an alternative mechanistic scenario was proposed for the the $[Ru(bpy)_3]^{2+}$ photocatalyst (Scheme 3.45). In this case, the photocatalyst is converted into the excited state species by absorption of the blue LED light. Facile anodic oxidation of the excited state species results in $[Ru(bpy)_3]^{3+}$, before single-electron transfer (SET) from the trifluoromethanesulfinate anion **153** causes the reduction to $[Ru(bpy)_3]^{2+}$, thereby regenerating

the active photocatalyst. Concomitantly, the trifluoromethanesulfinate radical is therewith formed, which affords the trifluoromethyl radical (**296**) upon fragmentation. The subsequent trifluoromethylation of arene **137** occurs following the same mechanism as described before.

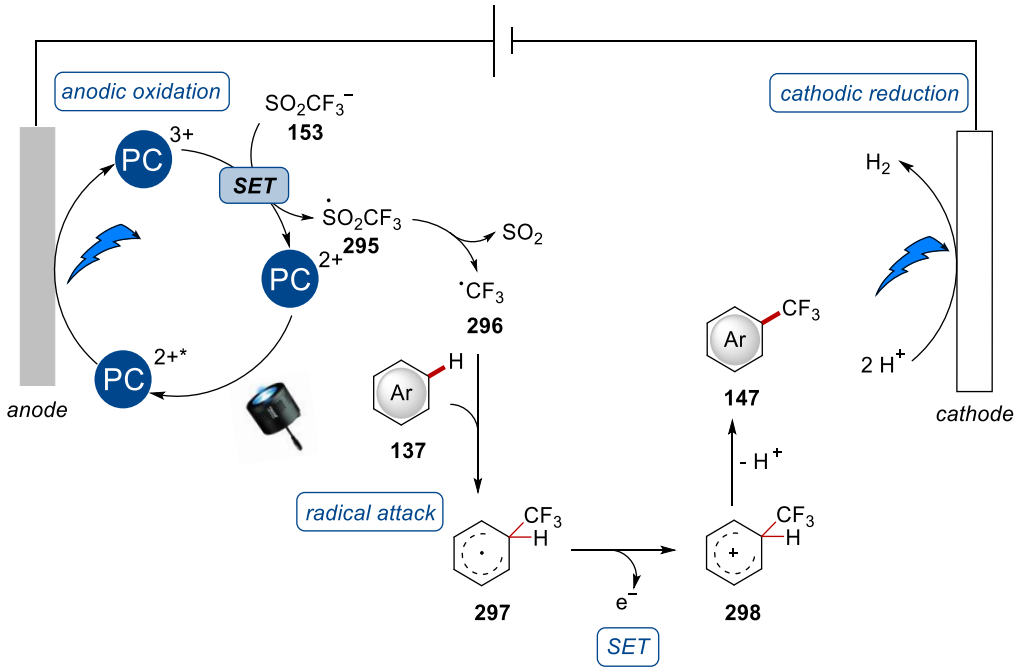

Scheme 3.45: Alternative mechanistic scenario for undirected trifluoromethylation with $[Ru(bpy)_3](PF_6)_2$ as photocatalyst.

3.6 MANGANESE(I)-CATALYZED TRYPTOPHAN FUNCTIONALIZATION IN WATER

Since the synthesis of the therapeutically used peptide Insulin in 1921, a plethora of other peptide-based therapeutics has been developed.[262] Although small molecules as pharmaceutically active ingredient are associated with several advantages compared to peptides, such as lower production costs and sales prices, often oral administration and good properties in terms of membrane permeability,[263] the modern medicinal treatments can not be imagined without the use of peptide drugs, resulting in 33 non-insulin peptide medications being approved since 2000. With a broad applicability predominantly as hormones or growth factors, as neurotransmitters and effectors on ion channels or as anti-infective agents, they offer valuable treatments through binding with high affinity and specificity to cell surface receptors, which triggers various intracellular effects.[264] Many of these peptide drugs are bearing the valuable aromatic amino acid tryptophan (Trp), such as Sandostatin and Leuprorelin (Figure 3.13).

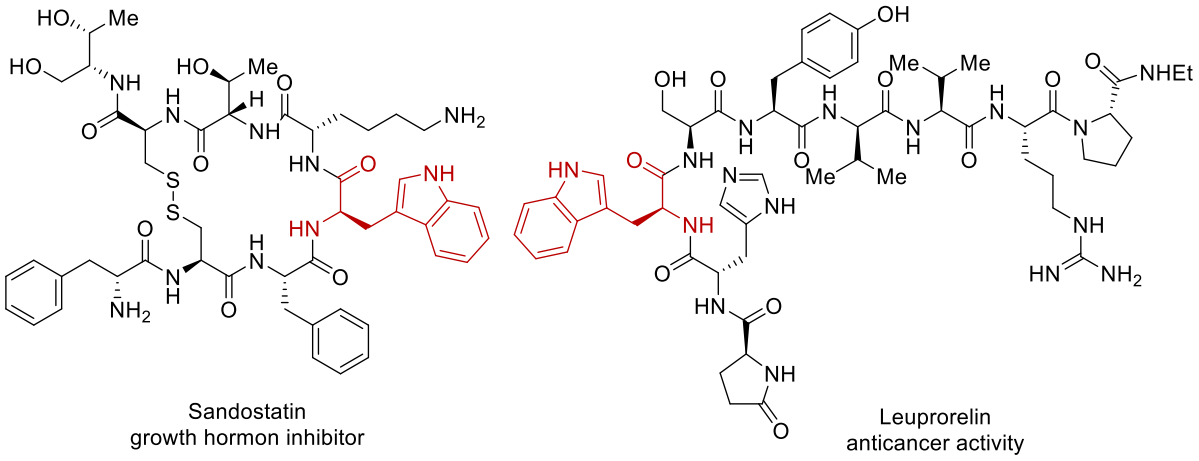

Figure 3.13: Important peptide pharmaceuticals containing tryptophan.

The modification of amino acids allows for the access to non-natural ones. The incorporation of these unusual and chemically modified amino acids was recognized as an elegant tool to affect the properties of peptides, such as increased selectivity or enhanced stability.[265] Therefore, efficient methods for their late-stage diversification to synthesize modified amino acids have gained significant momentum. Besides the predominant approach which is relying on classical cysteine ligation and palladium-catalyzed cross-coupling chemistry,[266] improved atom- and step-economy can be realized by C–H activation.[267] In addition to the use of precious and rather toxic ruthenium,[175a, 242] rhodium[268] and palladium catalysts,[269] the use of

more benign earth-abundant manganese and cobalt catalysts has emerged as a valuable alternative in the directed C–H functionalization of tryptophan.[127, 270]

Although the manganese-catalyzed allylation of tryptophan or pyridine indole is a sustainable approach in many aspects to achieve the introduction of synthetically useful allyl moieties, the reported procedures remain restricted to the use of an organic solvent as reaction medium, such as 1,4-dioxane.[123, 125-127, 129, 270b] Given the high interest in academia, but also in pharmaceutical and chemical industry, to perform chemical transformations in pure water and/or by the addition of a surfactant,[11b, 17c, 20b] the aim of this project was the realization of a mild and sustainable procedure for manganese-catalyzed C–H activations in an aqueous reaction medium. As a model reaction, the allylation of tryptophan was chosen, which was intended to be achieved by manganese catalysis. This project was conducted in cooperation with Dr. F. Gallou from Novartis Pharma AG during an internship in the department of Chemical and Analytical Development.

3.6.1 Optimization Studies with Allyl Carbonate

The previously reported manganese-catalyzed allylation of pyridine indole **299** with allyl carbonate **129** was observed to proceed efficiently by using $Mn_2(CO)_{10}$ in the presence of NaOAc in co-catalytic amounts (Scheme 3.46).[129] 1,4-Dioxane was identified as highly suitable reaction medium, enabling high conversions at elevated temperatures of 100 °C. Furthermore, also $MnBr(CO)_5$ was shown to be a potent catalyst for this reaction as well.

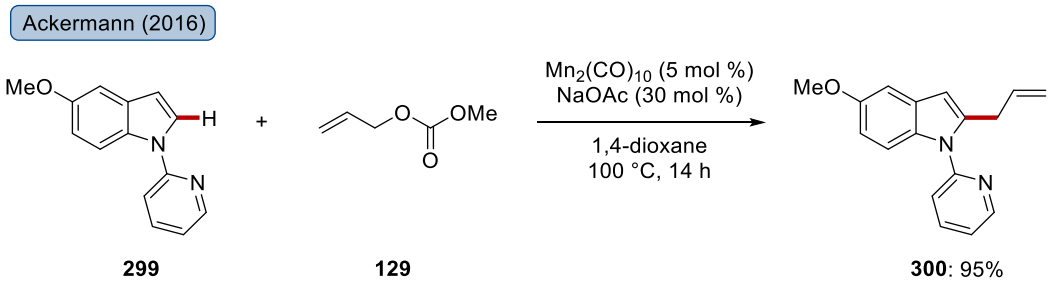

Scheme 3.46: Manganese-catalyzed allylation of pyridinyl indole **299** with allyl methyl carbonate (**129**) in 1,4-dioxane.

To achieve the manganese-catalyzed C–H allylation of the protected tryptophan derivative **221a** in an aqueous reaction medium, the optimization studies were initiated by test reactions in different reaction media and at different temperatures under otherwise comparable reaction conditions (Table 3.21).

Table 3.21: Test reactions of allylation of Trp **221a** with $Mn_2(CO)_{10}$ as the catalyst.

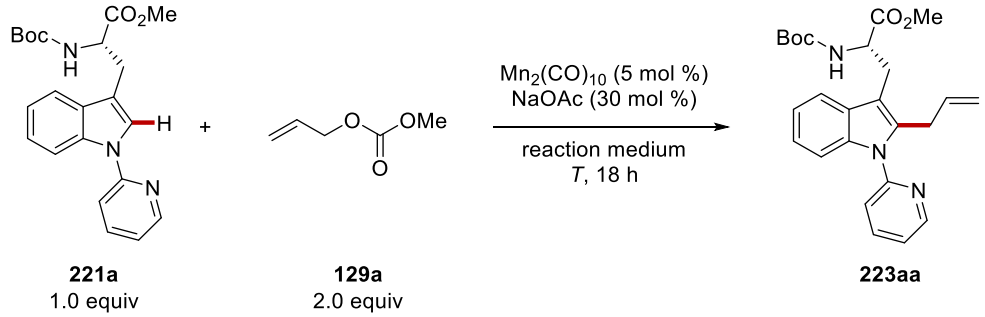

221a 1.0 equiv | **129a** 2.0 equiv | **223aa**

Entry	Reaction Medium	Temperature [°C]	**223aa** [%][a]
1	1,4-dioxane	80	---
2	1,4-dioxane	100	---
3	1,4-dioxane	120	(71)
4	H_2O	120	---
5	TPGS-750-M (2 wt%)/H_2O	120	(9)
6	PS-750-M (2 wt%)/H_2O	120	(12)

[a] Reaction conditions: **221a** (0.20 mmol), **129a** (0.40 mmol), $Mn_2(CO)_{10}$ (5.0 mol %), NaOAc (30 mol %), reaction medium (1.5 mL), 80–120 °C, 18 h, under N_2. The conversion in parentheses was determined by LC-MS.

Temperatures below 120 °C failed in furnishing the desired product **223aa** efficiently with 1,4-dioxane as solvent (entries 1–2). Only at a reaction temperature of 120 °C, the amino acid **221a** underwent the transformation to provide the allylated product **223aa** in a good yield of 71% (entry 3). However, the change to an aqueous reaction medium fell short in reasonable product formation. While no product could be detected in pure water (entry 4), the use of TPGS-750-M or PS-750-M surfactant yielded minor amounts of the allylated product **223aa** (entries 5–6).

After these initial results with low yields the catalyst was changed to $MnBr(CO)_5$ to continue the optimization studies with this complex (Table 3.22). The use of 1,4-dioxane led to the formation of product **223aa** in a moderate yield of 34% (entry 1). A slightly diminished conversion was observed in water, while the addition of the TPGS-750-M designer surfactant was beneficial and gave 35% of the C–H activation product **223aa** (entries 2–3). Besides the use of the TPGS-750-M surfactant, the effect of the more polar PS-750-M surfactant was evaluated and led to 33% conversion to the C–H activated tryptophan **223aa** (entry 4).

Table 3.22: Optimization of the reaction medium for the manganese(I)-catalyzed allylation of Trp **221a**.

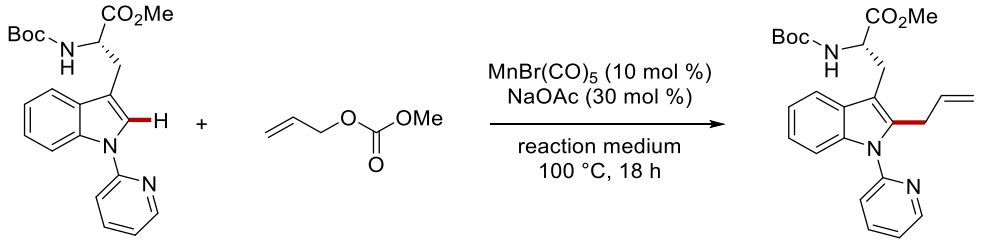

221a 1.0 equiv | **129a** 2.0 equiv | **223aa**

Entry	Reaction Medium	**223aa** [%][a]
1	1,4-dioxane	(34)
2	H_2O	(30)
3	TPGS-750-M (2 wt%)/H_2O	(35)
4	PS-750-M (2 wt%)/H_2O	(33)

[a] Reaction conditions: **221a** (0.20 mmol), **129a** (0.40 mmol), $MnBr(CO)_5$ (10 mol %), NaOAc (30 mol %), reaction medium (1.5 mL) + 0.3 mL cosolvent, 100 °C, 18 h, under N_2. Yields refer to the isolated products. The conversion in parentheses was determined by LC-MS.

Encouraged by the fact, that slightly higher conversions were obtained for the TPGS-750-M surfactant than for the other ones, attempts were made to increase the formation of the desired product **223aa** by modifying the reaction medium by adding different additives (Table 3.23). The use of various cosolvents was tested to evaluate their influence, as this is a commonly used approach in micellar catalysis to improve the solubility of organic compounds (entries 1–9). In all cases, the yield was significantly lower than the sole surfactant solution as reaction medium. The best conversions were thus obtained with PEG-200 (entry 2), the aromatic cosolvents benzene and toluene (entries 5–6) or 1,4-dioxane (entry 7), all of them furnishing the product **223aa** in 25%. Moreover, the effect of the addition of salts was analyzed, and the use of 1.2 mmol LiCl or NaCl resulted in improved yields of **223aa** over 40% (entries 10–11).

Table 3.23: Optimization of the manganese(I)-catalyzed allylation of Trp **221a** with the TPGS-750-M surfactant.

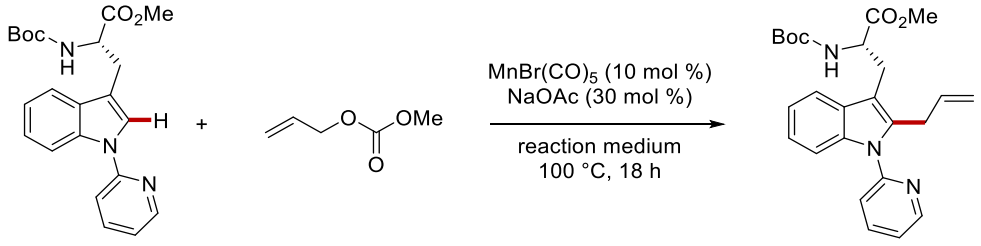

221a 1.0 equiv | **129a** 2.0 equiv | **223aa**

Entry	Reaction Medium	**223aa** [%][a]
1	TPGS-750-M (2 wt%)/H_2O	(35)
2	TPGS-750-M (2 wt%)/H_2O + 20% PEG-200	(25)
3	TPGS-750-M (2 wt%)/H_2O + 20% THF	(6)
4	TPGS-750-M (2 wt%)/H_2O + 20% acetone	(15)
5	TPGS-750-M (2 wt%)/H_2O + 20% benzene	(25)
6	TPGS-750-M (2 wt%)/H_2O + 20% toluene	(25)
7	TPGS-750-M (2 wt%)/H_2O + 20% 1,4-dioxane	(25)
8	TPGS-750-M (2 wt%)/H_2O + 20% DMA	(8)
9	TPGS-750-M (2 wt%)/H_2O + 20% *t*-AmylOH	(12)
10	TPGS-750-M (2 wt%)/H_2O, 1.2 mmol NaCl	(42)
11	TPGS-750-M (2 wt%)/H_2O, 1.2 mmol LiCl	41 (44)

[a] Reaction conditions: **221a** (0.20 mmol), **129a** (0.40 mmol), $MnBr(CO)_5$ (10 mol %), NaOAc (30 mol %), reaction medium (1.5 mL) + 0.3 mL cosolvent, 100 °C, 18 h, under N_2. Yields refer to the isolated products. The conversion in parentheses was determined by LC-MS.

After having identified the TPGS-750-M solution as a more suitable reaction medium than water or the PS-750-M surfactant solution, several bases were tested to probe the most powerful co-catalyst (Table 3.24). Using KOAc instead of NaOAc or NaOPiv had minor impact on the reaction outcome (entries 1–3). In contrast, the sterically more demanding base NaO_2CAd or the carbonate Na_2CO_3 gave unsatisfactory results for the allylation of heteroarene **221a** (entries 4–5). The use of potassium *tert*-butyl alcoholate resulted likewise in a lower conversion

(entry 6). Among the tested amine bases (entries 7–10), only the addition of NEt_3 enabled a slightly improved conversion and the allylation product **223aa** was formed in 43% (entry 7).

Table 3.24: Optimization of the base for the manganese-catalyzed allylation of amino acid **221a**.

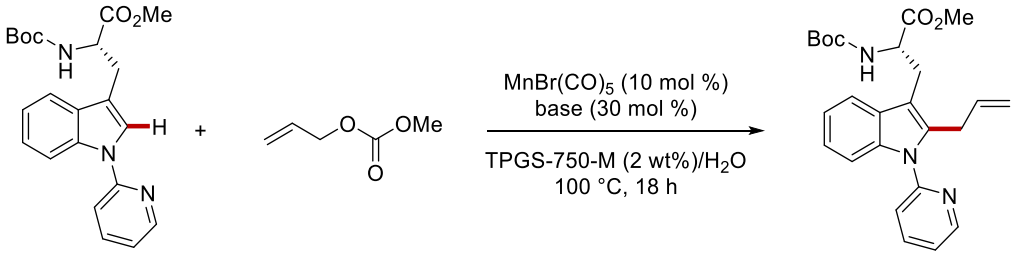

221a 1.0 equiv | **129a** 2.0 equiv | **223aa**

Entry	Base (30 mol %)	**223aa** [%][a]
1	NaOAc	(35)
2	KOAc	(35)
3	NaOPiv	(34)
4	$AdCO_2Na$	(20)
5	Na_2CO_3	(18)
6	KO*t*-Bu	(26)
7	NEt_3	(43)
8	DMEDA	(25)
9	DBU	(14)
10	NE*t*i-Pr_2	(31)

[a] Reaction conditions: **221a** (0.20 mmol), **129a** (0.40 mmol), $MnBr(CO)_5$ (10 mol %), base (30 mol %), TPGS-750-M (2 wt%)/H_2O (1.5 mL), 100 °C, 18 h, under N_2. The conversion in parentheses was determined by LC-MS.

To probe the effect of several other factors, further optimization and test reactions were performed (Table 3.25).

Table 3.25: Further optimization for the manganese-catalyzed functionalization of Trp **221a**.

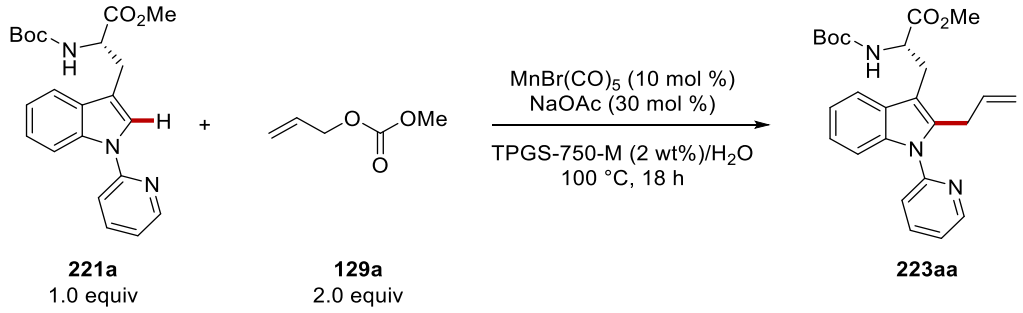

221a 1.0 equiv | **129a** 2.0 equiv | **223aa**

Entry	Deviation from Standard Conditions	**223aa** [%][a]
1	none	(35)
2	V = 1.0 mL	(47)
3	V = 0.6 mL	53 (54)
4	t = 64 h	(35)
5	under air	(29)
6	**129a** (4.0 equiv)	(45)
7	$MnBr(CO)_5$ (20 mol %)	(37)
8	NaOAc (1.0 equiv)	(29)
9	NaOAc (60 mol %)	(31)
10	NaOAc (10 mol %)	(37)
11	no NaOAc	(44)

[a] Reaction conditions: **221a** (0.20 mmol), **129a** (0.40 mmol), $MnBr(CO)_5$ (10 mol %), NaOAc (30 mol %), TPGS-750-M (2 wt%)/H_2O (1.5 mL), 100 °C, 18 h, under N_2. Yields refer to the isolated products. The conversion in parentheses was determined by LC-MS.

Although these were not the best reaction conditions so far, NaOAc was employed as the base to ensure good comparability of the results with TPGS-750-M as micellar medium. By reducing the volume of the solvent, the formation of the C–H activation product **223aa** was further improved (entries 1–3), affording a conversion of 54% **223aa** in a reduced volume of 0.6 mL. In comparison, a longer reaction time of 64 h did not influence the yield of the desired product **223aa** (entry 4). Performing the reaction under air caused a slightly reduced product formation of **223aa** (entry 5). Furthermore, an excess of the allyl carbonate **129a** of four equivalents, was employed but the effect was low (entry 6). Additionally, a higher catalyst loading had minor

impact on the catalytic efficacy (entry 7). The effect of the amount of the base as co-catalyst was also further analyzed (entries 8–11). While higher loadings afforded the product **223aa** in diminished yields (entries 8–9), a reduced amount turned out to have an enhancing effect on the yield of the allylated compound **223aa** (entry 10). Interestingly, the best result with respect to the amount of the base was obtained by omitting the additive NaOAc (entry 11).

After these detailed studies the use of water seems not be competitive with organic solvents for the envisioned allylation of tryptophan **221a** with allyl carbonate **129a** as coupling partner. Thus, the allylation in the manganese catalysis regime was focused subsequently on the more reactive Morita-Baylis-Hillman substrate (MBH substrate).

3.6.2 Optimization Studies with MBH Substrate

In the course of the long-lasting studies on late-stage functionalizations of peptides, the allylation of the tryptophan derivative **221b** was found to proceed efficiently by a manganese catalysis manifold by employing the MBH substrate **222a** as the allylating reagent (Scheme 3.47).[270b] Efficient C–C bond formation through C–H activation was successfully achieved with $MnBr(CO)_5$ as the catalyst in the presence of NaOAc in substoichiometric amounts. Again, 1,4-dioxane was a suitable solvent allowing for high conversions at 80 °C.

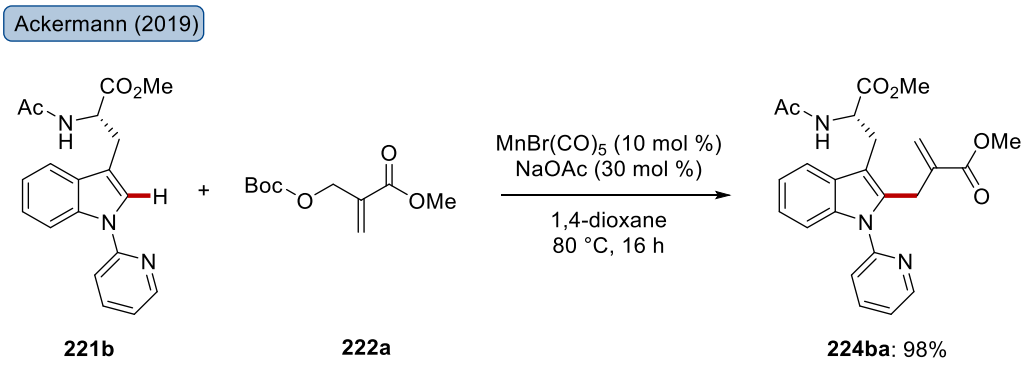

Scheme 3.47: Manganese-catalyzed allylation of tryptophan **221b** with MBH substrate **222a** in 1,4-dioxane.

Using the reaction conditions in the organic solvent developed by Dr. N. Kaplaneris as the starting point,[270b] the optimization of the allylation in aqueous conditions was initiated by probing the efficacy of the manganese catalysis in different reaction media at different temperatures (Table 3.26). Commencing with different solvents at 80 °C (entries 1–4), both, 1,4-dioxane and water, showed the formation of the desired product **224ab** in excellent yields close to 90% (entries 1–2). A slightly lower conversion was observed for the TPGS-750-M or

PS-750-M surfactant solutions (entries 3–4). An increased reaction temperature of 100 °C resulted in slightly higher conversions in 1,4-dioxane and water (entries 5–6), while decreased amounts of allylation product **224ab** were obtained for the surfactant solutions at 100 °C than observed at 80 °C (entries 7–8).

Table 3.26: Screenings of the reaction medium and temperature for the manganese-catalyzed allylation of Trp **221a** with MBH substrate **222b**.

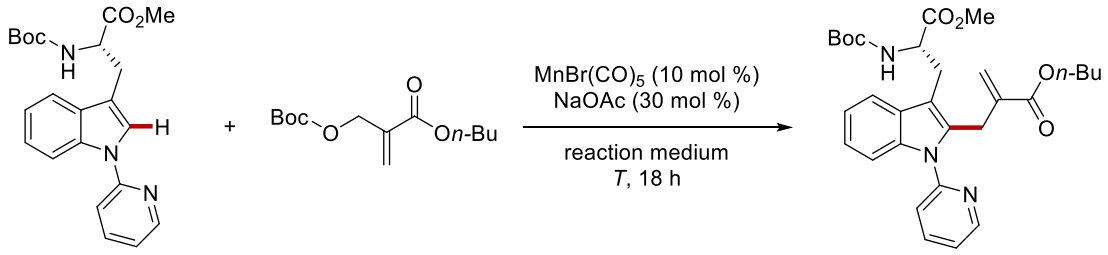

221a 1.0 equiv | **222b** 2.0 equiv | **224ab**

Entry	Reaction Medium	Temperature [°C]	**224ab** [%][a]
1	1,4-dioxane	80	(89)
2	H_2O	80	85 (86)
3	TPGS-750-M (2 wt%)/H_2O	80	(82)
4	PS-750-M (2 wt%)/H_2O	80	(80)
5	1,4-dioxane	100	(94)
6	H_2O	100	86 (88)
7	TPGS-750-M (2 wt%)/H_2O	100	78 (80)
8	PS-750-M (2 wt%)/H_2O	100	(76)

[a] Reaction conditions: **221a** (0.20 mmol), **222b** (0.40 mmol), $MnBr(CO)_5$ (10 mol %), NaOAc (30 mol %), reaction medium (1.5 mL), 80–100 °C, 18 h, under N_2. Yields refer to the isolated products. The conversion in parentheses was determined by LC-MS.

Taking these results into account, water was chosen as the most potent medium. To realize as mild conditions as possible, the temperature was fixed to 80 °C for the further optimization, in which the impact of the substoichiometric base was probed (Table 3.27). Acetate bases as sodium or potassium salts furnished the allylated amino acid **224ab** in excellent yields of approximately 85% (entries 1–2). In stark contrast, the use of the bulkier adamantyl carboxylate salt or Na_2CO_3 as smaller alternative resulted in a significantly less efficient catalysis

(entries 3–4). However, by the addition of $MesCO_2H$ (**38**) to Na_2CO_3, the efficacy was strongly improved, being slightly lower than in case of the acetate bases (entry 5). As a consequence, NaOAc was thereby identified as the base of choice.

Table 3.27: Optimization of the base for the manganese-catalyzed functionalization of Trp **221a** in water.

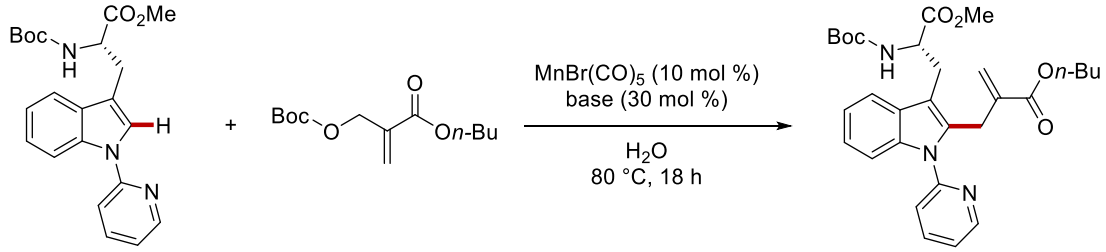

221a 1.0 equiv | **222b** 2.0 equiv | **224ab**

Entry	Base	**224ab** [%][a]
1	KOAc	(84)
2	NaOAc	(86)
3	$NaCO_2Ad$	(65)
4	Na_2CO_3	(26)
5	Na_2CO_3 + $MesCO_2H$ (**38**)	(79)[b]

[a] Reaction conditions: **221a** (0.20 mmol), **222b** (0.40 mmol), $MnBr(CO)_5$ (10 mol %), base (30 mol %), H_2O (1.5 mL), 80 °C, 18 h, under N_2. The conversion in parentheses was determined by LC-MS. [b] Addition of $MesCO_2H$ (**38**, 30 mol %)

Based on the optimal reaction conditions thus far, control experiments were conducted to prove the necessity of the components (Table 3.28). In the absence of the manganese catalyst, the formation of the allylated tryptophan **224ab** was not observed, which highlights the crucial role of the earth-abundant metal catalyst (entries 1–2). In contrast to the previous studies on the allylation with allyl carbonate **129a**, the base had a strongly enhancing effect on the reactivity, as the yield of **224ab** was reduced to roughly the half without the co-catalyst (entry 3). A low catalyst loading of 1.0 mol % still furnished the desired product with 70% conversion (entry 4). In addition, the $Mn_2(CO)_{10}$ complex was employed as a catalyst instead of $MnBr(CO)_5$, but it failed to catalyze the desired modification efficiently (entry 5).

Table 3.28: Control experiments for the manganese-catalyzed allylation of Trp **221a** in water.

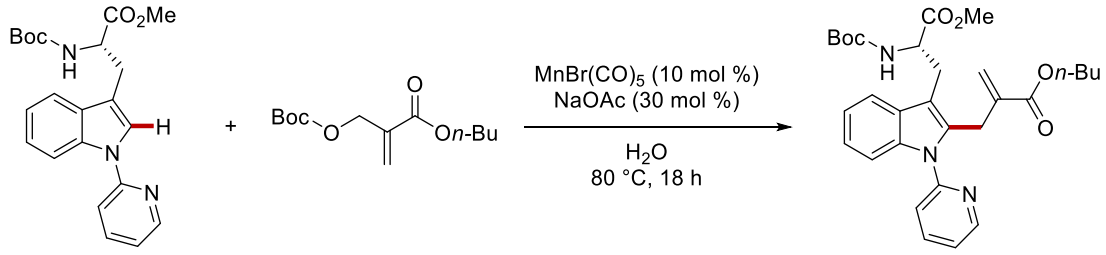

221a
1.0 equiv

222b
2.0 equiv

224ab

Entry	Deviation from Standard Conditions	**224ab** [%][a]
1	none	(86)
2	no catalyst	---
3	no base	(47)
4	$MnBr(CO)_5$ (1.0 mol %)	(70)
5	$Mn_2(CO)_{10}$ (5.0 mol %)	(7)

[a] Reaction conditions: **221a** (0.20 mmol), **222b** (0.40 mmol), $MnBr(CO)_5$ (10 mol %), NaOAc (30 mol %), H_2O (1.5 mL), 80 °C, 18 h, under N_2. The conversion in parentheses was determined by LC-MS.

The aim of the project was not only to develop suitable reaction conditions which enable the manganese-catalyzed allylation of amino acid derivative **221a** with high efficacy, but also to test the limits of the aqueous catalysis with respect to exceedingly sustainable and mild conditions, which would allow for a scale up. To this end, the reduction of the catalyst loading or attempts to perform the reaction at lower reaction temperatures had been of great interest.

First, the robustness of the manganese-catalyzed C–H activation procedure in the aqueous reaction medium was shown in test reactions with a low catalyst loading of 1 mol % (Table 3.29). Noteworthily, the reaction promoted in water showed a remarkable conversion of 65% **224ab** (entry 1). On the contrary, the conversion was decreased by employing the lower loading in the solutions of the vitamine E-derived designer surfactant TPGS-750-M or the more polar PS-750-M surfactant (entries 2–3).

Table 3.29: Test reactions with reduced catalyst loading for the manganese-catalyzed Trp-allylation.

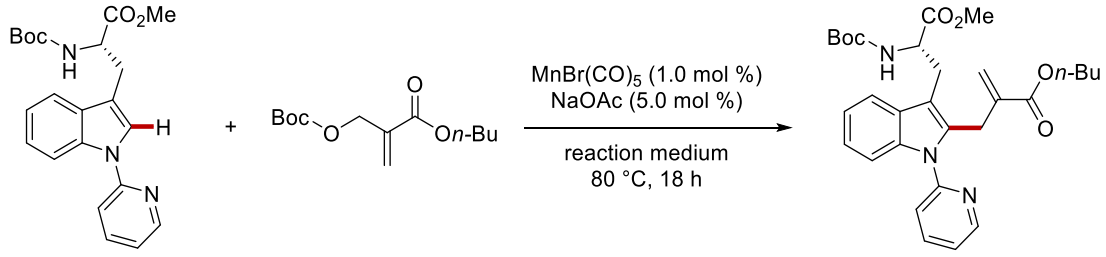

221a
1.0 equiv

222b
2.0 equiv

224ab

Entry	Reaction Medium	**224ab** [%][a]
1	H_2O	(65)
2	TPGS-750-M (2 wt%)/H_2O	(51)
3	PS-750-M (2 wt%)/H_2O	(58)

[a] Reaction conditions: **221a** (0.20 mmol), **222b** (0.40 mmol), $MnBr(CO)_5$ (1 mol %), NaOAc (5.0 mol %), reaction medium (1.5 mL), 80 °C, 18 h, under N_2. The conversion in parentheses was determined by LC-MS.

In addition, the reaction with 10 mol % catalyst loading was carried out in different reaction media at lower temperatures to determine the lowest temperature at which the catalysis can be performed to obtain the modified amino acid **224ab** in synthetically reasonable yields (Table 3.30). The reaction temperature of 40 °C failed in providing the product **224ab** in conversions higher than 25% (entries 1–3). Interestingly, here for the first time an advantageous effect of the surfactant was measurable, as the reaction outcome was about 6% higher for the PS-750-M solution compared to the use of pure water. This can be explained by the fact that the micelle formation is believed to be effected by the temperature.[271] By increasing the reaction temperature to 50 °C, the formation of product **224ab** was more than doubled for all solvent systems (entries 4–6), resulting in conversions above 50% in water as well as in the presence of the PS-750-M surfactant. By elevating the temperature to 60 °C, the manganese catalysis was further enhanced and gave conversions of roughly 60% (entries 7–9). Remarkably, here the use of water was superior to the use of surfactants, as already seen at higher reaction temperatures.

Table 3.30: Reduced temperatures for the manganese-catalyzed modification of Trp **221a**.

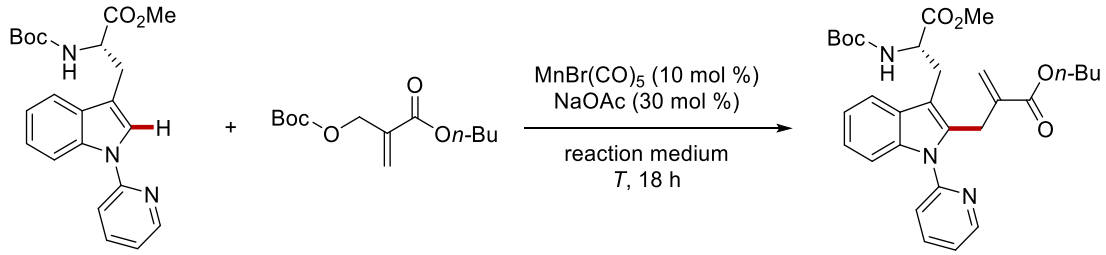

221a 1.0 equiv | **222b** 2.0 equiv | **224ab**

Entry	Reaction Medium	Temperature [°C]	**224ab** [%][a]
1	H_2O	40	(18)
2	TPGS-750-M (2 wt%)/H_2O	40	(17)
3	PS-750-M (2 wt%)/H_2O	40	(24)
4	H_2O	50	(53)
5	TPGS-750-M (2 wt%)/H_2O	50	(43)
6	PS-750-M (2 wt%)/H_2O	50	(52)
7	H_2O	60	(62)
8	TPGS-750-M (2 wt%)/H_2O	60	(57)
9	PS-750-M (2 wt%)/H_2O	60	(56)

[a] Reaction conditions: **221a** (0.20 mmol), **222b** (0.40 mmol), $MnBr(CO)_5$ (10 mol %), NaOAc (30 mol %), reaction medium (1.5 mL), 40–60 °C, 18 h, under N_2. The conversion in parentheses was determined by LC-MS.

To analyze the impact of the reaction time on the reactions at lower temperatures, experiments with long reaction times of 66 h were conducted (Table 3.31). At 40 °C, an increased product formation of 40% was detected in water or TPGS-750-M surfactant solution (entries 1–2). The beneficial influence of the solubilized PS-750-M amphiphile, previously observed for 18 h duration, could be further supported at low temperatures as the product **224ab** was formed in 55% yield with the extended reaction times (entry 3). Moreover, the longer reaction time was key to success to reach excellent reactivity at 60 °C, giving conversions above 80% for all three aqueous reaction media (entries 4–6).

Table 3.31: Test reaction with reduced temperature and long reaction time for the manganese-catalyzed allylation of Trp **221a**.

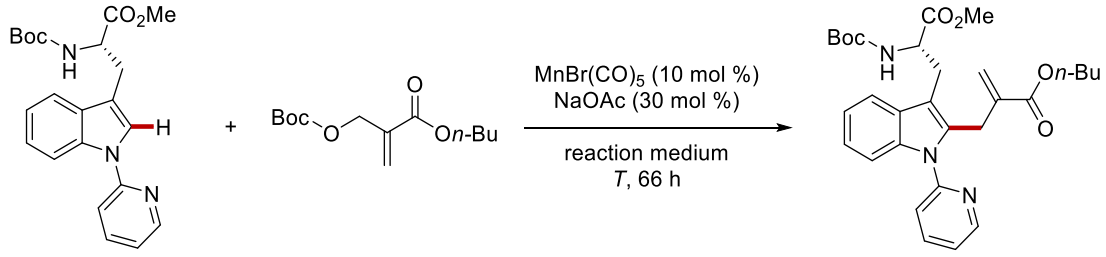

221a 1.0 equiv | **222b** 2.0 equiv | **224ab**

Entry	Reaction Medium	Temperature [°C]	**224ab** [%][a]
1	H_2O	40	(40)
2	TPGS-750-M (2 wt%)/H_2O	40	(38)
3	PS-750-M (2 wt%)/H_2O	40	(55)
4	H_2O	60	(84)
5	TPGS-750-M (2 wt%)/H_2O	60	(81)
6	PS-750-M (2 wt%)/H_2O	60	(82)

[a] Reaction conditions: **221a** (0.20 mmol), **222b** (0.40 mmol), $MnBr(CO)_5$ (10 mol %), NaOAc (30 mol %), reaction medium (1.5 mL), 40–60 °C, 66 h, under N_2. The conversion in parentheses was determined by LC-MS.

3.6.3 Substrate Scope

With the optimized conditions for the diversification of tryptophan **221a** in hand, the generality of the manganese-catalyzed C–H activation in water was analyzed (Scheme 3.48). The C–H allylation with the sterically more demanding *tert*-butyl containing coupling reagent **222c** resulted in a slightly diminished yield of 77%, whereas the more hydrophobic substrate **222d**, bearing a longer alkyl moiety, afforded the corresponding allylation product **224ad** only in moderate yield. Aromatic functionalities, such in benzyl derivative **222e**, were fully tolerated and furnished **224ae** in an excellent yield. Furthermore, the MBH substrate with the heterocyclic tetrahydrofuryl residue **222f** reacted selectively in water to afford the modified amino acid **224af** in a synthetically useful amount.

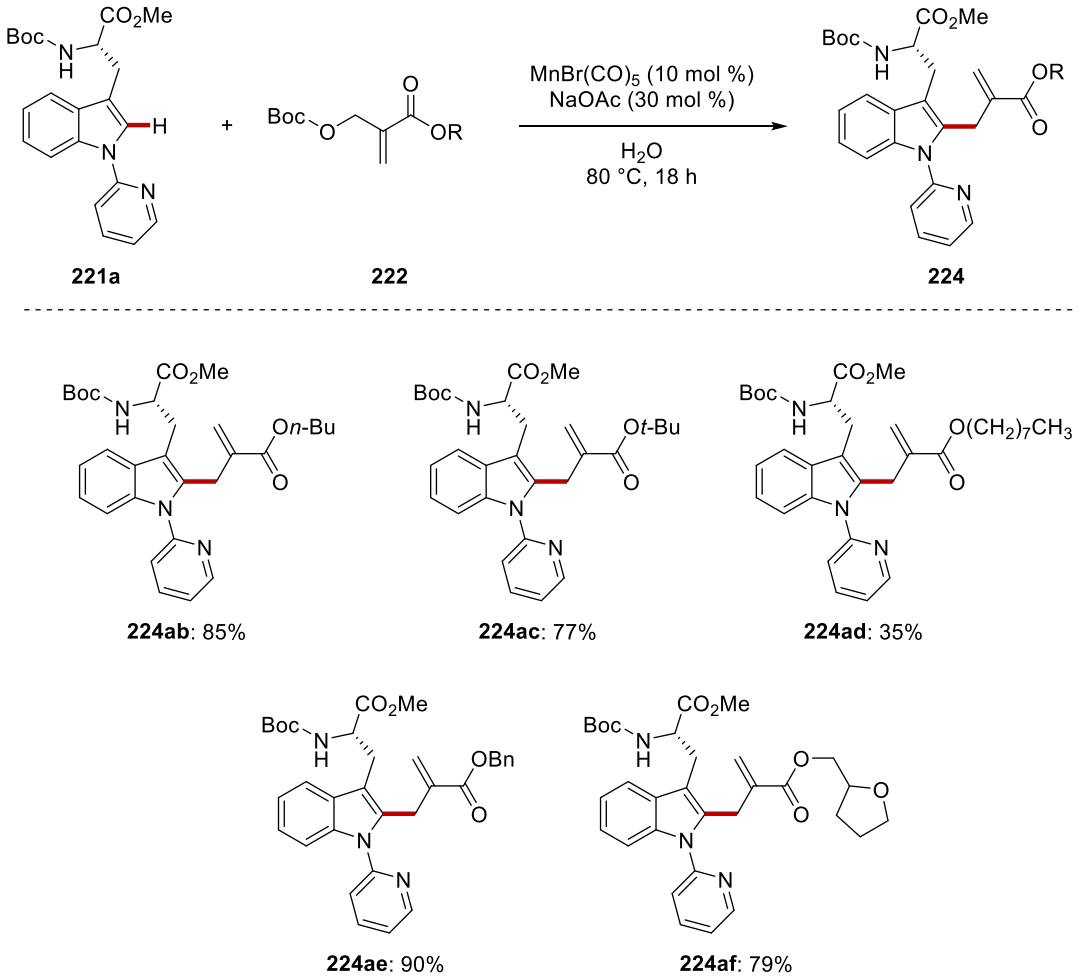

[a] Reaction conditions: **221a** (0.20 mmol), **222** (0.40 mmol), $MnBr(CO)_5$ (10 mol %), NaOAc (30 mol %), H_2O (1.5 mL), 80 °C, 18 h, under N_2.

Scheme 3.48: Manganese-catalyzed allylation of Trp **221a** in water with different MBH substrates **222**.

3.6.4 Kinetic Studies

As already demonstrated during the optimization studies on the manganese-assisted direct C–H activation of amino acid derivative **221a**, the robust allylation with MBH substrate **222b** was achieved under extremely mild reaction conditions. The reaction was conducted with lower catalyst loadings as low as 1.0 mol % at 80 °C or with a catalyst loading of 10 mol % at different reaction temperatures. To further examine these mild and sustainable procedures, kinetic studies were performed to monitor the formation of the desired product **224ab** in the course of the reaction by LC-MS analysis.

A comparison of the reaction profile at different reaction temperatures highlighted the fast conversion of the starting material **221a** to the C–H activated compound **224ab** at elevated temperatures (Figure 3.14). For a reaction temperature of 100 °C, the catalysis was almost

completed within 3 h. After this period, almost 80% of the product **224ab** was formed and the reaction progress was limited afterwards with only small improvement at longer reaction times. In contrast, a plateau was reached much later with lower reaction temperatures. After 7 h at 80 °C and after 10 h at 60 °C, the manganese catalysis became more slowly, resulting in approximately 70% product formation after 21 h.

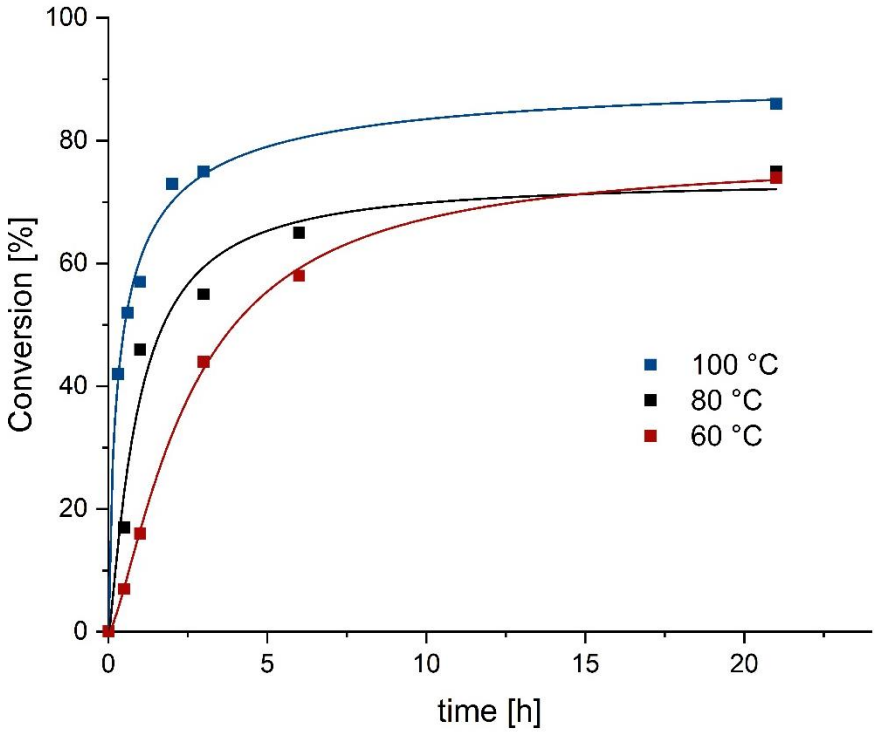

Figure 3.14: Kinetic profile for C–H allylation of Trp **221a** at different temperatures.

Moreover, the catalysis with lower catalyst loadings was monitored to get further insights into the efficacy of the manganese catalysis in water at 80 °C (Figure 3.15). With 10 mol % of the catalyst, the final conversion was reached after 7 h, where the allylation product **224ab** was formed in 70%. With 5.0 mol % catalyst loading, the efficient conversion of amino acid **221a** was finished after comparable reaction times, which resulted in an over-all lower product formation of **224ab** in 50% after 18 h. Remarkably, the whole measured period showed significant reaction progress and formation of the allylated product **224ab** when 1.0 mol % of the manganese catalyst was used. A non-linear dependence on the reaction time was observable, as the catalysis is slightly slowed down during the second half of the period. Nonetheless, the robust system allowed similar high functionalization of tryptophan **221a** as with 5.0 mol %, thereby affording C–H activation product **224ab** with 50% after 18 h without any hints for catalyst decomposition or inactivation in water.

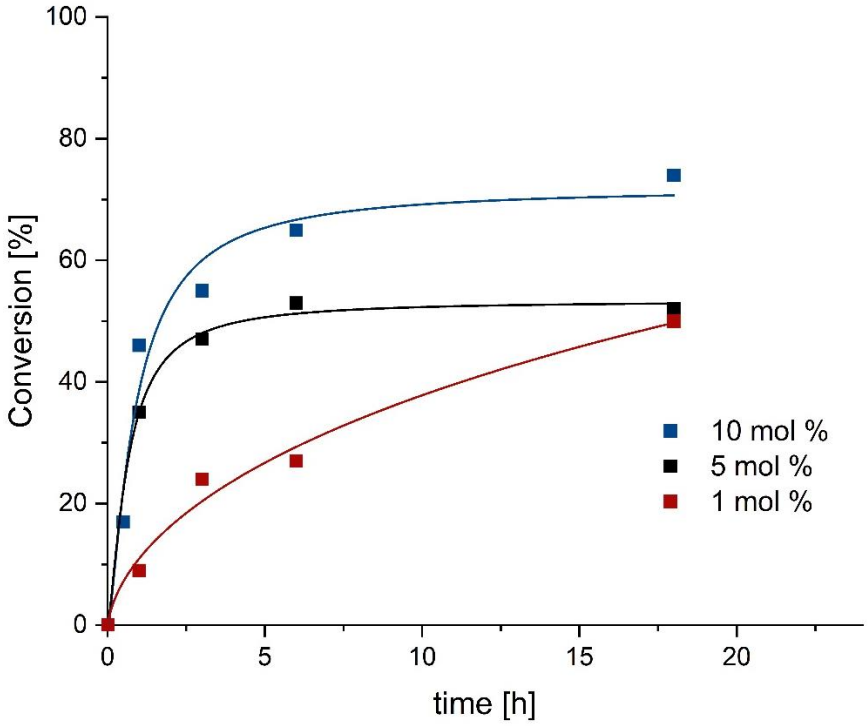

Figure 3.15: Profile for manganese-catalyzed modification of Trp with different catalyst loadings.

4 CONCLUSION AND OUTLOOK

Transition metal-catalyzed C–H activation bears an enormous potential for efficient and selective constructions of C–C and C–Het bonds with widespread applications for crop protection, pharmaceutical chemistry and material science. Precious metals, such as rhodium, but also the more cost-efficient ruthenium, were recognized as powerful catalysts which greatly expand the toolbox of synthetic chemists. In addition, base metals, such as manganese, have been identified as sustainable alternatives. Especially, the merger of the transition metal-catalyzed activation of C–H bonds as well as the undirected functionalization of them with electric current or visible light has gained significant momentum to achieve striking progress towards sustainable and mild reactions. In addition to the development of suitable conditions to realize a synthetic transformation, a detailed understanding of the reaction mechanism is essential to enable further advancement based on this understanding. Within this thesis, a variety of different synthetic catalytic systems was developed and investigated with the focus on sustainable strategies to enable mild reaction conditions following the principles of Green Chemistry.

In the first part of the thesis, a rhodium(III)-catalyzed olefination of benzamides **212** was realized under electrochemical conditions with electricity as the terminal oxidant. The reaction with styrenes **113** was achieved under modified conditions (Scheme 4.1).[235] The metalla-electrocatalyzed Fujiwara-Moritani reaction furnished the product **216** with high functional group tolerance accompanied by hydrogen as the sole side product in a hydrogen evolution reaction (HER). Mechanistic experiments allowed for the proposal of a mechanistic scenario. Despite this undisputable progress, the protocol was restricted to the use of activated olefins, while terminal alkyl alkenes afforded the desired products only in low conversions. Thus, the development of reaction conditions, which allow for the reaction with unactivated olefins, continues to be highly desirable.

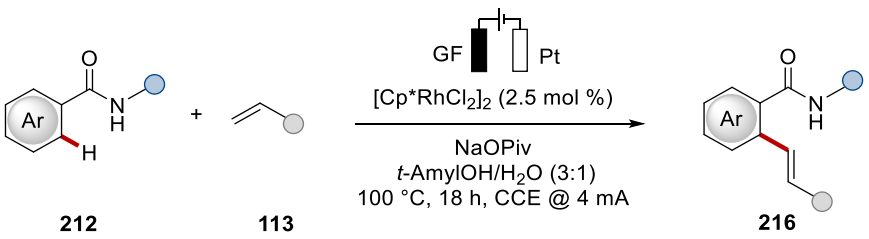

Scheme 4.1: Rhodaelectro-oxidative olefination of benzamide **216**.

Attracted by the observation of an *ortho*-selective alkylation with secondary alkyl bromides **218** under decarboxylative ruthenium catalysis for C–C activation,[232] this so far unprecedented reactivity could be achieved by C–H activation (Scheme 4.2).[232] The regiodivergence of the alkylation turned out to be strongly influenced by the steric hinderance of the alkyl halide and likewise, of the pyrazole directing group. Moreover, the electronic properties of the phenyl ring of the phenylpyrazole **217** had significant impact on the site-selectivity. Mechanistic experiments were conducted, being indicative of two distinct pathways to construct the two different products **219** and **220**. Starting form an arene-free ruthenacycle, which has been identified as the catalytically active species, both products can be accessed. While a concerted oxidative addition/reductive elimination manifold seems likely for the *ortho*-selective alkylation process, a SET event was indicative of the *meta*-functionalization.

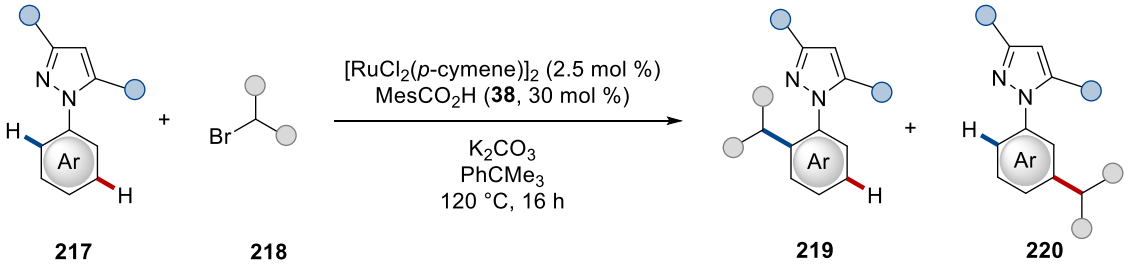

Scheme 4.2: Regiodivergent alkylation of pyrazolyl arenes **217** by ruthenium carboxylate catalysis.

The third project was focused on the combination of ruthenium-catalyzed C–H activation and photoredox catalysis, which allowed *ortho*-arylations of divers arenes **23** under exceedingly mild conditions at ambient temperature (Scheme 4.3).[249] Noteworthily, the addition of an exogenous photoredox catalyst was not required. The mild procedure was reflected in a remarkable high functional group tolerance and rendered the transformation of various valuable heterocyclic compounds, such as triazoles. A detailed comparison of the light-enabled reactivity to thermal conditions at 120 °C highlighted the synthetic utility of the mild protocol, as an improved chemoselectivity was observable. Detailed mechanistic investigations by experiments complemented by computations were suggestive of the formation of the biscyclometalated complex under the reaction conditions, which is photocatalytically active. After excitation, this complex was proposed to undergo a light-induced metal-to-ligand charge transfer followed by intersystem crossing to generate a long-lived triplet species.

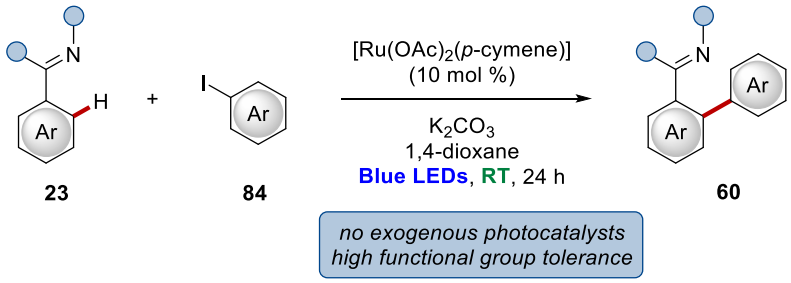

Scheme 4.3: Ruthenium-catalyzed C–H arylation at ambient temperature induced by visible light.

Based on the successful merger of ruthenium catalysis and photochemistry by means of *ortho*-selective C–H arylations, this powerful strategy was applied to an *ortho*-selective benzylation reaction (Scheme 4.4).[258] Under remarkably mild conditions, the efficient synthesis of diarylmethane motifs **91** tolerated a plethora of functional groups and was compatible with the chelating assistance of various heterocycles. The photo-induced conditions enabled the reaction with electrophiles bearing different natural products, such as peptides, triglycerides and carbohydrates, as well as the functionalization of biorelevant purine scaffolds. Remarkably, this reaction was highly efficient in water or surfactant solutions with comparable yields as in the organic solvent. Based on detailed mechanistic studies, a plausible catalytic cycle was proposed.

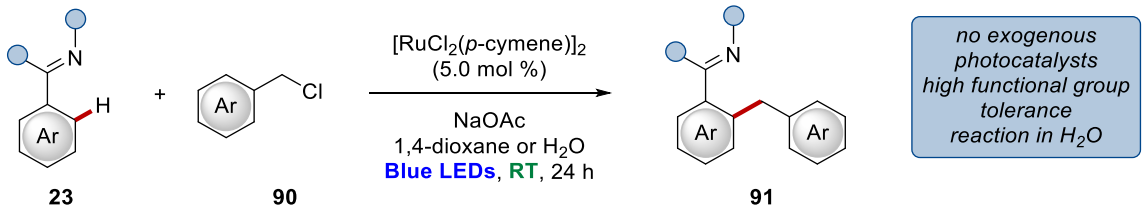

Scheme 4.4: *ortho*-Selective benzylation of arenes **23** by photoredox ruthenium catalysis.

Given the great potential and current interest of electrophotochemical C–H functionalization procedures, a detailed study on the undirected trifluoromethylation of (hetero-)arenes **137** was conducted in continuation of a previous work[157] (Scheme 4.5). The first systematic comparison of more than 12 different (photo)redox catalysts, which was thus far unexplored in electrophoto-catalyzed transformations, was performed for trimethoxybenzene as the model substrate, highlighting that all of them were capable to catalyze the envisioned transformation. To demonstrate the generality of this observation, different arenes and heteroarenes, among those some of biological interest, were subjected to the reaction conditions with two different catalysts, furnishing the corresponding products only with minor differences in efficacy. Among the tested catalysts, the electrophotocatalyst [TAC]ClO_4 showed remarkable beneficial

features in terms of improved selectivity of mono-functionalization and with respect to sensitive arenes, as highlighted in experiments to modify the anticancer pro-drug KAN0438757.

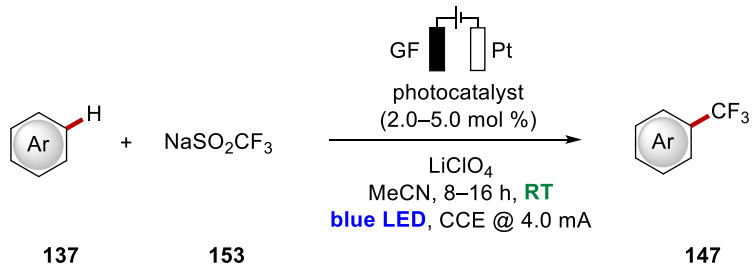

Scheme 4.5: Undirected trifluoromethylation of (hetero)arenes enabled by electrophoto-catalysis.

The last project was conducted in collaboration with Dr. F. Gallou from Novartis Pharma in Basel with a focus on the use of water and micellar catalysis as environmentally-benign reaction medium. The manganese-catalyzed allylation of tryptophan **221a** with allyl carbonates and MBH adducts were investigated, resulting in a highly efficient procedure for the latter one. (Scheme 4.6). Remarkably, among the tested conditions and surfactants, the use of sole water as the reaction medium turned out to be the most suitable one. Kinetic studies were performed to determine the boundaries of efficient catalysis with respect to temperature and catalyst loading. Reduced temperatures of 60 °C allowed efficient turnover in the time frame of 18 h, while the use of only 1 mol % catalyst loading enabled likewise good reactivity at 80 °C. It would be worthwhile to apply this sustainable reaction conditions not only on the protected tryptophan **221**, but also on larger peptides to prove the generality of this catalytic approach. Here, the impact of surfactants beyond pure water would be interesting, as the solubility of di- or tripeptides might be worse than the one from tryptophan, so that the use of an additional surfactant could be beneficial.

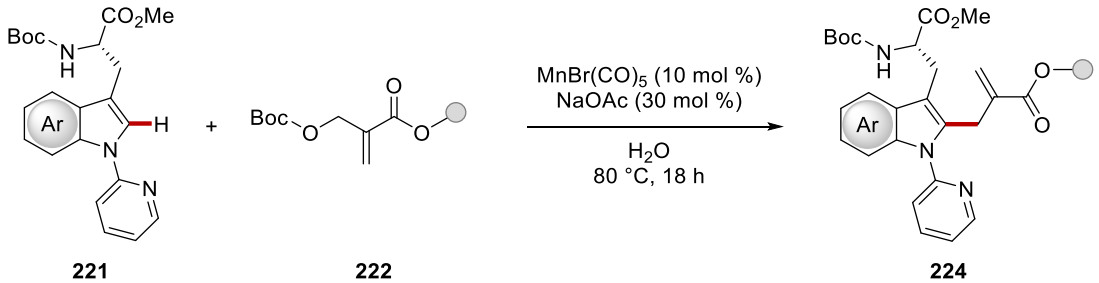

Scheme 4.6: Manganese-catalyzed allylation of tryptophan **221** in water.

5 EXPERIMENTAL SECTION

5.1 GENERAL REMARKS

Air and moisture sensitive reactions were carried out under inert gas atmosphere using standard glovebox or Schlenk technique. The glassware was dried in an oven (120 °C) and heatgun dried (600 °C) under high vacuum prior to use (three times, backflushed with nitrogen. Liquids and solutions were transferred *via* three times nitrogen-flushed syringes by Braun, with oven-dried stainless steel cannulas (predried at 120 °C). Solids were added under counter flow of nitrogen (standard Schlenk technique). Solutions were concentrated under reduced pressure employing rotary evaporation at 40 °C with IKA *RV 10 digital FLEX* efficient. Low volatile products were dried under high vacuum for 8 h (rotary vane pump). Air and moisture sensitive substances were stored in a M. Braun glovebox. Yields refer to isolated compounds, estimated to be >95% pure as determined by ^{1}H-NMR and GC-MS, unless otherwise noted.

5.1.1 Solvents and Chemicals

Solvents

All solvents involved in reactions with air or moisture sensitive reagents were dried before their use and stored under an inert atmosphere of nitrogen. For the drying of the solvents the following standard procedures were employed.

Solvents purified by solvent purification system (SPS-800) from M. Braun: Toluene, dichloromethane, tetrahydrofuran, diethyl ether, acetonitrile, *N*,*N*-dimethylformamide.

Solvents dried and distilled over Na in the presence of benzophenone as indicator: 1,4-dioxane, toluene, *o*-xylene.

Solvents dried and distilled over CaH_2: 1,2-Dichloroethane, *N*,*N*-dimethylacetamide, *N*,*N*-dimethylformamide, dimethyl sulfoxide, *N*-methyl-2-pyrrolidone.

Solvents dried and distilled over $Mg(OMe)_2$: Methanol.

Solvents dried over 4 Å molecular sieves degassed by multiple cycles of freeze-pump-thaw: Acetonitrile, *tert*-amyl alcohol, *tert*-butylbenzene.

Water was degassed by freeze-pump-thaw cycles and degassed with nitrogen directly before its use

Solvents used for work-up and purification were distilled under reduced pressure by rotary evaporation.

Reagents

Reagents which were commercially available with a purity higher than 95% were used without further purification unless stated otherwise. K_2CO_3, NaOAc and Na_2CO_3 were dried at 140 °C and $4 \cdot 10^{-1}$ mbar for 24 h and stored under an inert atmosphere of N_2.

The following substrates were synthesized according to procedures reported in literature: 2-phenylpyridines **44a**–**44e**,[272] phenylpyrazoles **217a**–**217f**,[273] ketimine **247a**,[274] triazoles **253a–253d**,[81] tryptophan **221a**[242b] and MBH substrates **222b**–**222f**.[275]

Moreover, cyclometalated ruthenium complexes were synthesized as described in literature.[87]

The following chemicals were generously provided by the persons named below:

Karsten Rauch: $[Cp^*RhCl_2]_2$, $[Cp^*IrCl_2]_2$, $[RuCl_2(p\text{-cymene})]_2$, $[Ru(OAc)_2(p\text{-cymene})]$ $[Ru(O_2CMes)_2(p\text{-cymene})]$, KAN0438757 and intermediates (**288**–**291**), dried solvents.

Dr. Korkit Korvorapun: Ruthenium complex $[Ru(O_2CAd)_2(p\text{-cymene})]$, $[Ru(NC\textit{t}\text{-Bu})_6](BF_4)_2$, $[Ru(NC\textit{t}\text{-Bu})_6](PF_6)_2$, $[Ru(NC\textit{t}\text{-Bu})_6](SbF_6)_2$, purines **267a**–**267b**, aryliodides **84p**–**84q**, benzyl chlorides **90r**–**90s**.

Dr. Tanumoy Mandal: Styryl pyridines **255a**–**255c**.

Dr. Isaac Choi: Ru@polymer (**273**).

Dr. Valentin Müller: Purine **137m**.

Jiawei Xu: $[Ni(bpy)_3]Br_2$.

Anna Casnati: Oxazoline **246a**–**246b**.

Hanke Spink: $[TAC]ClO_4$, $[Ru(bpy)_3](PF_6)_2$.

Moritz von Geyso: $[Fe(bpy)_3](PF_6)_2$.

5.1.2 Experimental and Analytical Methods

Vaccum

A pressure of approximately $4 \cdot 10^{-1}$ mbar could be achieved with the employed rotary vane pump Vacuubrand RD4.

Liquid Chromatography

Analytic Thin Layer Chromatography (TLC): TLC plates (silica gel 60) on alumina with fluorescence indicator F-254 (Macherey Nagel or Merck) were employed to monitor the reactions and to analyze the column chromatography. The analysis of the TLC plates was done by UV light (λ = 254 nm or 366 nm), if applicable, or by staining solution ($KMnO_4$-solution) followed by gentle heating by heatgun at 300 °C until dryness.

Flash Column Chromatography: Purification of crude products was accomplished by flash column chromatography using silica gel from Macherey-Nagel (Silica 60 M, 0.04–0.063 mm) or Merck (Geduran SI 60, 40–63 µm). The products were loaded in the respective eluent. In case of the cyclometalated complexes, neutral aluminum oxide from Sigma Aldrich was used for column chromatography under a gentle pressure of nitrogen.

Gas Chromatography

Gas chromatographic analysis (GC) was conducted on an Agilent *7890A* GC system or an Agilent *7890B* GC system equipped with an Agilent *HP-5* column (30 m, 0.32 mm diameter, 0.25 µm film thickness) and a flame-ionization detector (FID) using hydrogen as the carrier gas. Gas chromatography coupled to mass spectrometry (GC-MS) was measured on the same instrument equipped with an Agilent *HP-5MS* column (30 m, 0.25 mm diameter, 0.25 µm film thickness) and an Agilent *5875C* Triple-Axis-Detector or alternatively on an Agilent *5977B* MSD. Mass spectra were obtained with electron-ionization (EI) at 70 eV using the positive ion mode.

Gel Permeation Chromatography

For gel permeation chromatographies (GPC or recycling preparative HPLC), a Japan Analytical Industries (JAI) *LC-92XX II NEXT* system equipped with a JAIGEL 2.5HR or JAIGEL 2HH column, was used with chloroform (HPLC-grade) as the solvent.

UV-VIS Spectroscopy

UV-Visible Spectroscopy was measured on a Jasco® V-770 spectrophotometer. Prior to the record of the spectra, a baseline was measured with the corresponding solvent.

Infrared Spectroscopy

Infrared (IR) spectra were detected on a Bruker Alpha-P FT-IR spectrometer with a diamond ATR probe in the range of 4000–400 cm^{-1}. Liquid samples were measured as a film and solid samples neat. Analysis of the spectral data was carried out using Opus 6 software. Absorption is given in wavenumbers (cm^{-1}).

NMR-Spectroscopy

Nuclear magnetic resonance (NMR) spectra were recorded at 300–600 MHz (^{1}H-NMR) and 75–150 MHz (^{13}C-NMR) on Varian *Mercury Plus 300* and Bruker *Avance 300*, *Avance III 300*, *Avance III 400*, *Avance III HD 400*, *Avance Neo 400*, *Avance III HD 500* and *Avance Neo 600* instruments. All measurements were performed at 298 K unless mentioned otherwise. Chemical shifts are reported as δ-values in parts per million (ppm) relative to tetramethylsilane and referenced to the deuterated solvent or its carbon atoms. ^{19}F-NMR spectra were referenced to $CFCl_3$ as external standard, while 85% phosphoric acid was employed for ^{31}P-NMR spectra.

Solvent	^{1}H-NMR	^{13}C-NMR
$CDCl_3$	7.26 ppm	77.2 ppm
MeCN-d_3	1.94 ppm	118.26, 1.32 ppm

Coupling constants *J* are reported in Hertz (Hz), abbreviations used to characterize the signals are s (singlet), d (doublet), t (triplet), q (quartet), quint (quintet), sext (sextet), hept (heptet), dd

(doublet of doublets), dt (doublet of triplets), ddd (doublets of doublets of doublets), td (triplet of doublets), m (multiplet) and s br (broad singlet). All spectra analysis was conducted with *MestReNova* 10.0.2 and 12.0.1 from Mestrelab Research.

Mass spectrometry

Mass spectrometric analysis of the samples was performed with electrospray ionization (ESI) or electron ionization (EI) on instruments equipped with time-of-flight (TOF) analyzers. EI mass spectra were recorded on a Jeol *AccuTOF* instrument. ESI measurement was performed on Bruker *maXis* and *MicrOTOF*. High resolution mass spectrometry (HR-MS) was measured on Bruker *Daltronic maXis Q-TOF*, Bruker *Daltronic MicrOTOF*, Thermo Scietific *LTQ Orbitrap XL*, Thermo Scietific *Exactive GC-Orbitrap-MS* and *Jeol AccuTOF*. The ratio of mass to charge is given with the intensity relative to the base peak (I = 100) in parentheses.

On-Line NMR Monitoring in Flow

^{19}F-NMR spectroscopic measurements in flow were conducted on a *Spinsolve 60Ultra* system from Magritek. A peristatic pump from *Reglo digital MS-2/12* (*ISM 596*) from Isamatec was employed or pumping the solution with a flowrate of 4 mL/min. Analysis was done with the reaction monitoring tool *Wizard* of 12.0.3 from Mestrelab Research.

Melting Points

Melting points were recorded on a *Stuart Melting Point Apparatus SMP3* from Barloworld Scientific. The given values were not corrected.

Cyclic Voltammetry

Cyclic Voltammetry (CV) studies were conducted using a Metrohm Autolab *PGSTAT204* workstation, and the following analysis was performed with the software *Nova 2.0*. For the measurement, a glassy carbon disc electrode (3.0 mm diameter, 99.99%, Chempur) was employed as the working electrode with a coiled platinum wire (1.0 mm diameter, 99.99%, Chempur) as the counter electrode and a saturated calomel electrode (SCE, Hg/Hg_2Cl_2, ceramic frit, OD = 6 mm) as the reference electrode. The measurements were performed with a scan

rate of 100 mV/s. All solutions were degassed prior to use by bubbling nitrogen through the solution for 5 min and a constant flow of dry nitrogen was maintained during the experiment.

Electrochemical Equipment

Electrochemical reactions were conducted with platinum electrodes (10 mm × 15 mm × 0.125 mm, 99.9%, ChemPur Edelmetall-Service), graphite felt electrodes (10 mm × 15 mm × 6.0 mm, *Sigracell® GFA 6 EA*, SGL carbon) or RVC electrodes (10 mm × 15 mm × 5.0 mm, *Duocel® Reticulated Vitreous Carbon RVC100* (100 PPI), ERG Aerospace Corporation), which were connected using stainless steel adapters. Electrocatalysis was performed using an AXIOMET *AX-3003P* potentiostat or a Metrohm *Multi Autolab/M204* system in the constant current mode using the software *Nova* 2.1.

Data Analysis and Plots

Data analysis and the generation of plots was performed using the software *OriginPro 2020*, which was also used for fitting of the data.

5.2 GENERAL PROCEDURES

5.2.1 General Procedure A: Electrochemical Rhodium-Catalyzed Alkenylation of Benzamides with Acrylate

The electrocatalysis was carried out in an undivided cell equipped with a GF anode (10 mm × 15 mm × 6 mm) and a platinum cathode (10 mm × 15 mm). The aromatic amide **212** or **213** (1.00 mmol, 2.0 equiv), *n*-butyl acrylate (**99a**, 71 µL, 0.50 mmol, 1.0 equiv), $[Cp^*RhCl_2]_2$ (7.7 mg, 25 µmol, 2.5 mol %), KPF_6 (50 µmol, 10 mol %), and KOAc (98.2 mg, 1.00 mmol, 2.0 equiv) were dissolved in *t*-AmylOH/H_2O (3:1, 4.0 mL). Electrocatalysis was performed at 100 °C with a constant current of 4.0 mA maintained for 18 h. Afterwards, the electrodes were rinsed with CH_2Cl_2 (3 × 10 mL). Evaporation of the solvent and subsequent column chromatography (SiO_2, *n*-hexane/EtOAc) afforded the corresponding product **214** or **215**.

5.2.2 General Procedure B: Electrochemical Rhodium-Catalyzed Alkenylation of Benzamides with Styrene

The electrocatalysis was carried out in an undivided cell equipped with a GF anode (10 mm × 15 mm × 6 mm) and a platinum cathode (10 mm × 15 mm). The aromatic amide **212** (0.40 mmol, 1.0 equiv), styrene (**113a**, 75 µL, 0.80 mmol, 2.0 equiv), $[Cp^*RhCl_2]_2$ (7.7 mg, 25 µmol, 2.5 mol %) and NaOPiv (98.2 mg, 1.00 mmol, 2.0 equiv) were dissolved in *t*-AmylOH/H_2O (3:1, 4.0 mL). Electrocatalysis was performed at 100 °C with a constant current of 4.0 mA maintained for 18 h. Afterwards, the electrodes were rinsed with CH_2Cl_2 (3 × 10 mL). Evaporation of the solvent and subsequent column chromatography (SiO_2, *n*-hexane/EtOAc) afforded the corresponding product **216**.

5.2.3 General Procedure C: Regiodivergent Ruthenium-Catalyzed C–H Alkylation of Pyrazoles

Pyrazole **217** (0.50 mmol, 1.0 equiv), $[RuCl_2(p\text{-cymene})]_2$ (7.7 mg, 13 µmol, 2.5 mol %), $MesCO_2H$ (**38**, 24.6 mg, 150 µmol, 30 mol %) and K_2CO_3 (138 mg, 1.00 mmol, 2.0 equiv) were placed in a predried 25 mL Schlenk tube. The tube was evacuated and purged with N_2 three times. Alkyl bromide **218** (0.75–1.50 mmol, 1.5–3.0 equiv) and $PhCMe_3$ (1.0 mL) were then added and the mixture was stirred at 120 °C. After 16 h, the resulting mixture was filtered through a pad of silica gel and washed with EtOAc. The filtrate was concentrated *in vacuo*. Purification of the residue by column chromatography (SiO_2, *n*-hexane/EtOAc) yielded the alkylated product **219** or **220**.

5.2.4 General Procedure D: Photo-Induced Ruthenium-Catalyzed ortho-C–H Arylation

Heteroarene **23** (0.50 mmol, 1.0 equiv), $[Ru(OAc)_2(p\text{-cymene})]$ (17.7 mg, 50.0 µmol, 10 mol %) and K_2CO_3 (138 mg, 1.00 mmol, 2.0 equiv) were placed in a 10 mL vial, before the vial was capped with a septum and wrapped with parafilm. The vial was evacuated and purged with N_2 three times. Aryl iodide **84** (0.75 mmol, 1.5 equiv) and 1,4-dioxane (2.0 mL) were added and the mixture was stirred under visible light irradiation (2 × Kessil A360N, temperature was maintained between 30 °C and 33 °C). After 24 h, the resulting mixture was filtered through a pad of silica gel, washed with EtOAc and the filtrate was concentrated *in vacuo*.

Purification of the residue by column chromatography (SiO_2, *n*-hexane/EtOAc) furnished the *ortho*-arylated product **60**.

5.2.5 General Procedure E: Ruthenium-Catalyzed ortho-C–H Arylation under Thermal Condition

Heteroarene **23** (1.1 mmol, 2.20 equiv), [$Ru(OAc)_2$(*p*-cymene)] (17.7 mg, 50.0 µmol, 10 mol %) and K_2CO_3 (276 mg, 2.00 mmol, 4.0 equiv) were placed in a predried 25 mL Schlenk tube, before the tube was capped with a septum. The Schlenk tube was evacuated and purged with N_2 three times. Aryl iodide **84** (0.5 mmol, 1.0 equiv) and 1,4-dioxane (2.0 mL) were added and the septum was wrapped with parafilm. The mixture was stirred at 120 °C for 24 h. The resulting mixture was filtered through a pad of silica gel, washed with EtOAc and the filtrate was concentrated *in vacuo*. Purification of the residue by column chromatography (SiO_2, *n*-hexane/EtOAc) provided the *ortho*-arylated product **60** or side-products.

5.2.6 General Procedure F: Light-Induced Ruthenium-Catalyzed ortho-C–H Benzylation

Heteroarene **23** (0.5 mmol, 1.0 equiv), [$RuCl_2$(*p*-cymene)]$_2$ (15.3 mg, 25.0 µmol, 5.0 mol %) and dry NaOAc (82.0 mg, 1.00 mmol, 2.0 equiv) from the glovebox were placed in a 10 ml vial, before the vial was capped with a septum and wrapped with parafilm. The vial was evacuated and purged with N_2 three times. Benzyl chloride **90** (0.75 mmol, 1.5 equiv) and 1,4-dioxane (2.0 mL) were added and the mixture was stirred under visible light irradiation (2 × Kessil A360N, temperature was maintained between 30 °C and 33 °C). After 24 h, the resulting mixture was filtered through a pad of silica gel and washed with EtOAc. After removal of the solvent under reduced pressure followed by purification of the residue by column chromatography (SiO_2, *n*-hexane/EtOAc) the *ortho*-benzylated product **91** was obtained.

5.2.7 General Procedure G: Electrophotochemical C–H Trifluoromethylation of (Hetero-)Arenes

The electrophotocatalysis was carried out in an undivided cell with a GF anode (10 mm × 15 mm × 6 mm) and a Pt cathode (10 mm × 15 mm × 0.25 mm). Unless in case of volatile substrates, substrate **137** (0.25 mmol, 1.0 equiv), CF_3SO_2Na (**153**, 78 mg, 0.50 mmol,

2.0 equiv), $LiClO_4$ (42 mg, 0.40 mmol) and the photocatalyst (2.0 or 5.0 mol %) were placed into a 10 mL Schlenk tube and closed with a stopper with integrated electrode holders. The vial was evacuated and purged with N_2 three times, before volatile compounds were added and the components were dissolved in CH_3CN (4.0 mL) under N_2. The electrophotocatalysis was performed at ambient temperature with a constant current of 4.0 mA maintained for 8–16 h under visible light irradiation at 450 nm or 390 nm wavelength (2 × Kessil A360N or 2 × Kessil A160WE). After completion of the reaction time, the resulting mixture was transferred into a round bottom flask. The vial was rinsed carefully and the GF anode was washed with CH_2Cl_2 (3 × 10 mL) in an ultrasonic bath. Evaporation of the solvent and subsequent column chromatography on silica gel afforded the corresponding product **147**.

5.2.8 General Procedure H: Manganese-Catalyzed Allylation of Tryptophan

Tryptophan **221a** (63.4 mg, 0.20 mmol, 1.0 equiv), $MnBr(CO)_5$ (5.5 mg, 20 µmol, 10 mol %) and NaOAc (4.9 mg, 60 µmol, 30 mol %) were placed in a 10 mL vial and evacuated and reflushed with N_2 for three times. Afterwards, allyl methyl carbonate (**129a**, 46.4 mg, 0.40 mmol, 2.0 equiv) or MBH adduct **222** (0.40 mmol, 2.0 equiv) and water (1.5 mL) were added and the suspension was stirred at 80 °C for 16 h under N_2. After cooling down to ambient temperature, EtOAc (10 mL) was added, the organic phase was separated, and the aqueous phase was extracted with EtOAc (3 × 10 mL). After drying of the combined organic phases over Na_2SO_4, the crude mixture was concentrated *in vacuo*. Purification by column chromatography (SiO_2, *n*-hexane/EtOAc) afforded the desired product **223** or **224**.

5.3 RHODIUM-CATALYZED ELECTROOXIDATIVE C–H OLEFINATION OF BENZAMIDES

5.3.1 Characterization Data

Butyl-2-(2-methyl-3-oxoisoindolin-1-yl)acetate (214aa)

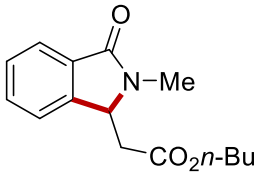

The general procedure **A** was followed using benzamide **212a** (135 mg, 1.00 mmol), acrylate **99a** (71 µL, 0.50 mmol) in *t*-AmylOH/H_2O (3:1, 4.0 mL). After 18 h, purification by column chromatography (*n*-hexane/EtOAc 10:1 + 1% NEt_3) yielded **214aa** (69.2 mg, 53%) as a colourless oil.

^{1}H-NMR (400 MHz, $CDCl_3$): δ = 7.81 (dt, *J* = 7.2, 1.0 Hz, 1H), 7.57–7.37 (m, 3H), 4.84 (t, *J* = 6.2 Hz, 1H), 4.11 (t, *J* = 6.7 Hz, 2H), 3.11 (s, 3H), 2.87 (dd, *J* = 15.9, 5.6 Hz, 1H), 2.67 (dd, *J* = 15.9, 6.8 Hz, 1H), 1.68–1.46 (m, 2H), 1.40–1.19 (m, 2H), 0.90 (t, *J* = 7.3 Hz, 3H).

^{13}C-NMR (100 MHz, $CDCl_3$): δ = 170.6 (C_q), 168.2 (C_q), 144.6 (C_q), 132.2 (C_q), 131.6 (CH), 128.6 (CH), 123.7 (CH), 122.4 (CH), 65.1 (CH_2), 58.5 (CH_3), 37.7 (CH_2), 30.6 (CH_2), 27.6 (CH_3), 19.2 (CH_2), 13.7 (CH_3).

IR (ATR): $\tilde{\nu}$ = 2958, 1729, 1687, 1359, 1245, 1159, 1058, 749, 680 cm^{-1}.

MS (ESI) *m/z* (relative intensity): 545 (100) $[2M+Na]^+$, 284 (100) $[M+Na]^+$, 262 (90) $[M+H]^+$.

HR-MS (ESI): *m/z* calcd for $C_{15}H_{20}NO_3^+$ $[M+H]^+$ 262.1438, found: 262.1436.

The spectral data are in accordance with those reported in the literature.[179]

Butyl (*E*)-3-(2-[*tert*-butylcarbamoyl]phenyl)acrylate (215aa)

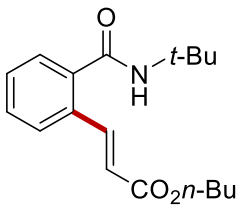

The general procedure **A** was followed using benzamide **213a** (177 mg, 1.00 mmol), acrylate **99a** (71 µL, 0.50 mmol), additive KPF_6 (50 µmol, 10 mol %) with KOAc (98.2 mg, 1.00 mmol) as the base in *t*-AmylOH/H_2O (3:1, 4.0 mL) After 18 h, purification by column chromatography (*n*-hexane/EtOAc 10:1 + 1% NEt_3) yielded **215aa** (91.0 mg, 60%) as a colourless oil.

^{1}H-NMR (400 MHz, $CDCl_3$): δ = 7.94 (d, J = 16.0 Hz, 1H), 7.59–7.54 (m, 1H), 7.46–7.31 (m, 3H), 6.36 (d, J = 16.0 Hz, 1H), 5.63 (s, 1H), 4.17 (t, J = 6.6 Hz, 2H), 1.75–1.57 (m, 2H), 1.46 (s, 9H), 1.44–1.35 (m, 2H), 0.94 (t, J = 7.3 Hz, 3H).

^{13}C-NMR (100 MHz, $CDCl_3$): δ = 168.3 (C_q), 166.6 (C_q), 141.9 (CH), 138.6 (C_q), 132.2 (C_q), 130.0 (CH), 129.9 (CH), 127.6 (CH), 127.0 (CH), 120.7 (CH), 64.6 (CH_2), 52.3 (CH_2), 30.8 (CH_2), 28.8 (CH_3), 19.3 (CH_2), 13.8 (CH_3).

IR (ATR): $\tilde{\nu}$ = 2960, 1708, 1636, 1534, 1312, 1272, 976, 763, 731 cm^{-1}.

MS (EI) *m/z* (relative intensity): 303 (5) $[M]^+$, 202 (50), 146 (100).

HR-MS (EI) *m/z* calcd for $C_{18}H_{26}NO_3^+$ $[M+H]^+$ 303.1834, found: 303.1824.

(*E*)-*N*,5-Dimethyl-2-styrylbenzamide (216ba)

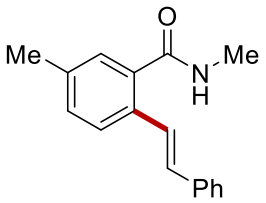

The general procedure **B** was followed using benzamide **212b** (75.1 mg, 0.50 mmol), styrene (**113a**, 75 µL, 1.00 mmol) in *t*-AmylOH/H_2O (3:1, 4.0 mL) After 18 h, purification by column chromatography (*n*-hexane/EtOAc 10:1) yielded **216ba** (81.6 mg, 65%) as a white solid.

^{1}H-NMR (400 MHz, $CDCl_3$): δ = 7.60 (d, J = 8.1 Hz, 1H), 7.54–7.49 (m, 2H), 7.44 (dd, J = 16.2, 3.2 Hz, 1H), 7.40–7.33 (m, 2H), 7.32–7.27 (m, 2H), 7.26–7.22 (m, 1H), 7.02 (d, J = 16.3 Hz, 1H), 5.88 (s, 1H), 3.01 (d, J = 4.9 Hz, 3H), 2.38 (d, J = 3.1 Hz, 3H).

^{13}C-NMR (100 MHz, $CDCl_3$): δ = 170.4 (C_q), 137.6 (C_q), 137.3 (C_q), 135.6 (C_q), 132.7 (C_q), 131.0 (CH), 130.5 (CH), 128.8 (CH), 128.3 (CH), 127.9 (CH), 126.8 (CH), 126.2 (CH), 126.0 (CH), 26.9 (CH_3), 21.2 (CH_3).

IR (ATR): $\tilde{\nu}$ = : 3283, 1629, 1542, 1407, 1323, 950, 817, 698, 683 cm^{-1}.

m.p.: 141–142 °C.

MS (ESI) *m/z* (relative intensity): 274 (100) $[M+Na]^+$, 252 (80) $[M+H]^+$.

HR-MS (ESI): *m/z* calcd for $C_{17}H_{17}NONa^+$ $[M+Na]^+$ 274.1202, found: 274.1204.

5.3.2 Cyclic Voltammetry

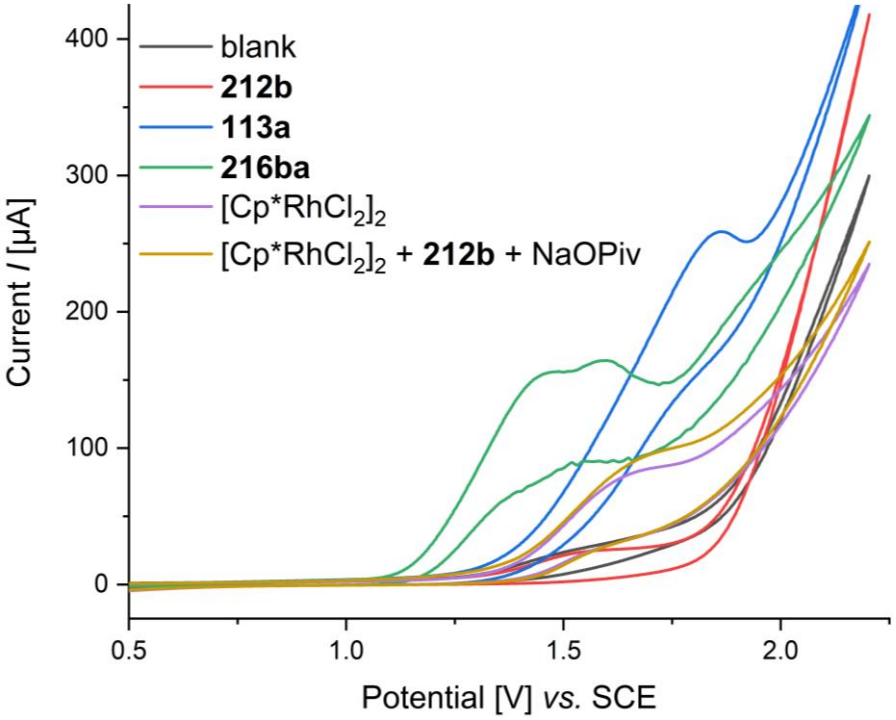

Figure 5.1: Cyclic voltammograms in MeOH with *n*-Bu_4NPF_6 (0.1 M) with a scan rate of 100 mV/s. Blank (black), amide **212b** (red), olefin **113a** (blue), product **216ba** (green), $[Cp^*RhCl_2]_2$ (purple) and $[Cp^*RhCl_2]_2$, **212b** and NaOPiv (yellow). $[Cp^*RhCl_2]_2$ 2.5 mM, all other substrates: 5 mM.

5.4 RUTHENIUM-CATALYZED REGIODIVERGENT ALKYLATIONS OF PYRAZOLES

5.4.1 Characterization Data

1-(2-Cyclohexylphenyl)-1*H*-pyrazole (219aa)

1-(3-Cyclohexylphenyl)-1*H*-pyrazole (220aa)

The general procedure **C** was followed using 1-phenyl-1*H*-pyrazole (**217a**, 72.1 mg, 0.50 mmol) and bromocyclohexane (**218a**, 245 mg, 1.50 mmol). After 16 h, purification by column chromatography (*n*-hexane/EtOAc 30:1) yielded the *ortho*-alkylated product **219aa** (68.0 mg, 60%) as a colorless oil and the *meta*-alkylated product **220aa** (13.1 mg, 12%) as a colorless oil.

1-(2-Cyclohexylphenyl)-1*H*-pyrazole (219aa)

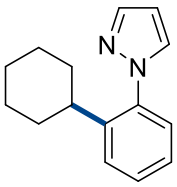

^{1}H-NMR (300 MHz, $CDCl_3$): δ = 7.72 (dd, J = 1.9, 0.7 Hz, 1H), 7.55 (dd, J = 2.3, 0.7 Hz, 1H), 7.42–7.38 (m, 2H), 7.29–7.24 (m, 2H), 6.44 (dd, J = 2.3, 1.9 Hz, 1H), 2.44 (tt, J = 12.0, 3.1 Hz, 1H), 1.82–1.66 (m, 5H), 1.48–1.33 (m, 2H), 1.30–1.16 (m, 3H).

^{13}C-NMR (100 MHz, $CDCl_3$): δ = 144.0 (C_q), 140.0 (CH), 138.9 (C_q), 130.9 (CH), 128.8 (CH), 127.1 (CH), 126.9 (CH), 126.0 (CH), 105.9 (CH), 38.3 (CH), 34.3 (CH_2), 26.8 (CH_2), 26.1 (CH_2).

IR (ATR): $\tilde{\nu}$ = 2924, 2851, 1515, 1448, 1394, 1043, 938, 745, 620 cm^{-1}.

MS (EI) *m*/*z* (relative intensity): 226 (74) $[M]^+$, 225 (100) $[M–H]^+$, 208 (14), 197 (21), 183 (39), 169 (46), 157 (17), 143 (13), 130 (25), 115 (17).

HR-MS (ESI): *m*/*z* calcd for $C_{15}H_{19}N_2^+$ $[M+H]^+$ 227.1543, found 227.1552.

1-(3-Cyclohexylphenyl)-1*H*-pyrazole (220aa)

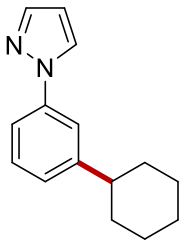

^{1}H-NMR (400 MHz, $CDCl_3$): δ = 7.92 (d, *J* = 2.3 Hz, 1H), 7.72 (d, *J* = 1.9 Hz, 1H), 7.59 (dd, *J* = 2.1, 1.7 Hz, 1H), 7.46 (ddd, *J* = 7.9, 2.1, 1.2 Hz, 1H), 7.36 (dd, *J* = 7.9, 7.8 Hz, 1H), 7.14 (ddd, *J* = 7.8, 1.7, 1.2 Hz, 1H), 6.46 (dd, *J* = 2.3, 1.9 Hz, 1H), 2.58 (tt, *J* = 12.2, 3.7 Hz, 1H), 1.92 (ddd, *J* = 12.5, 3.7, 2.4 Hz, 2H), 1.86 (ddd, *J* = 13.0, 3.5, 3.1 Hz, 2H), 1.76 (dtt, *J* = 12.8, 3.0, 1.5 Hz, 1H), 1.48 (dddd, *J* = 12.6, 12.5, 12.2, 3.1 Hz, 2H), 1.40 (ddddd, *J* = 13.0, 12.8, 12.6, 3.0, 2.4 Hz, 2H), 1.27 (dtt, *J* = 12.8, 12.8, 3.5 Hz, 1H).

^{13}C-NMR (100 MHz, $CDCl_3$): δ = 149.7 (C_q), 140.8 (CH), 140.1 (C_q), 129.1 (CH), 126.7 (CH), 125.0 (CH), 118.0 (CH), 116.6 (CH), 107.3 (CH), 44.7 (CH), 34.4 (CH_2), 26.9 (CH_2), 26.2 (CH_2).

IR (ATR): $\tilde{\nu}$ = 2924, 2851, 1608, 1591, 1519, 1448, 1393, 1044, 950, 748 cm^{-1}.

MS (EI) *m*/*z* (relative intensity): 226 (100) $[M]^+$, 225 (29) $[M–H]^+$, 211 (14), 197 (18), 183 (20), 171 (40), 170 (29), 158 (24), 144 (10) $[M–Cy]^+$, 115 (14), 77 (9).

HR-MS (EI): *m*/*z* calcd for $C_{15}H_{18}N_2^+$ $[M]^+$ 226.1465, found 226.1471.

1-(3-Cycloheptylphenyl)-1*H*-pyrazole (220ad)

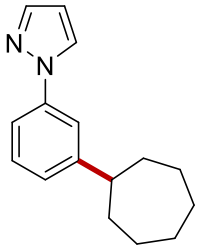

The general procedure **C** was followed using 1-phenyl-1*H*-pyrazole (**217a**, 72.1 mg, 0.50 mmol) and bromocycloheptane (**218d**, 266 mg, 1.50 mmol). After 16 h, purification by column chromatography (*n*-hexane/EtOAc 30:1) yielded the *meta*-alkylated product **220ad** (69.9 mg, 58%) as a colorless oil.

^{1}H-NMR (400 MHz, $CDCl_3$): δ = 7.92 (dd, *J* = 2.5, 0.7 Hz, 1H), 7.72 (dd, *J* = 1.8, 0.7 Hz, 1H), 7.57 (dd, *J* = 2.2, 1.8 Hz, 1H), 7.43 (ddd, *J* = 7.9, 2.2, 1.3 Hz, 1H), 7.34 (dd, *J* = 7.9, 7.7 Hz, 1H), 7.12 (ddd, *J* = 7.7, 1.8, 1.3 Hz, 1H), 6.45 (dd, *J* = 2.5, 1.8 Hz, 1H), 2.74 (tt, *J* = 10.6, 3.6 Hz, 1H), 1.99–1.91 (m, 2H), 1.85–1.77 (m, 2H), 1.76–1.50 (m, 8H).

^{13}C-NMR (100 MHz, $CDCl_3$): δ = 151.7 (C_q), 140.8 (CH), 140.2 (C_q), 129.2 (CH), 126.8 (CH), 124.9 (CH), 117.9 (CH), 116.3 (CH), 107.3 (CH), 47.1 (CH), 36.7 (CH_2), 27.8 (CH_2), 27.2 (CH_2).

IR (ATR): $\tilde{\nu}$ = 2919, 2852, 1607, 1590, 1518, 1392, 1043, 784, 744, 697 cm^{-1}.

MS (EI) *m*/*z* (relative intensity): 240 (100) $[M]^+$, 239 (36) $[M–H]^+$, 225 (10), 211 (17), 197 (26), 183 (29), 171 (53), 158 (61), 144 (14), 130 (15), 115 (23), 77 (12).

HR-MS (EI): *m*/*z* calcd for $C_{16}H_{20}N_2^+$ $[M]^+$ 240.1621, found 240.1633.

1-(3-Cyclooctylphenyl)-1*H*-pyrazole (220ae)

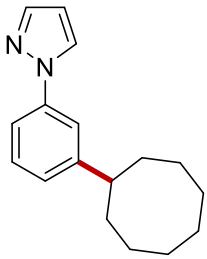

The general procedure **C** was followed using 1-phenyl-1*H*-pyrazole (**217a**, 72.1 mg, 0.50 mmol) and bromocyclooctane (**218e**, 287 mg, 1.50 mmol). After 16 h, purification by column chromatography (*n*-hexane/EtOAc 30:1) yielded the *meta*-alkylated product **220ae** (80.6 mg, 66%) as a yellow oil.

^{1}H-NMR (400 MHz, $CDCl_3$): δ = 7.92 (d, *J* = 2.3 Hz, 1H), 7.73 (d, *J* = 1.9 Hz, 1H), 7.59 (dd, *J* = 2.2, 1.7 Hz, 1H), 7.43 (ddd, *J* = 7.9, 2.2, 1.3 Hz, 1H), 7.34 (dd, *J* = 7.9, 7.7 Hz, 1H), 7.12 (ddd, *J* = 7.7, 1.7, 1.3 Hz, 1H), 6.45 (dd, *J* = 2.3, 1.9 Hz, 1H), 2.85 (tt, *J* = 9.8, 3.6 Hz, 1H), 2.00–1.44 (m, 14H).

^{13}C-NMR (100 MHz, $CDCl_3$): δ = 152.3 (C_q), 140.9 (CH), 140.2 (C_q), 129.3 (CH), 126.9 (CH), 125.2 (CH), 118.3 (CH), 116.4 (CH), 107.4 (CH), 44.8 (CH), 34.7 (CH_2), 26.9 (CH_2), 26.4 (CH_2), 26.1 (CH_2).

IR (ATR): $\tilde{\nu}$ = 2917, 2849, 1606, 1591, 1518, 1392, 1042, 782, 744, 697 cm^{-1}.

MS (ESI) *m*/*z* (relative intensity): 277 (35) $[M+Na]^+$, 255 (100) $[M+H]^+$.

HR-MS (ESI): *m*/*z* calcd for $C_{17}H_{23}N_2^+$ $[M+H]^+$ 255.1859, found: 255.1854.

1-(2-Neopentylphenyl)-1*H*-pyrazole (219af)

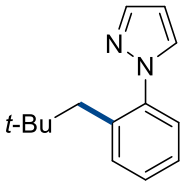

The general procedure **C** was followed using 1-phenyl-1*H*-pyrazole (**217a**, 72.1 mg, 0.50 mmol) and neopentyl bromide (**218f**, 227 mg, 1.50 mmol). After 16 h, purification by column chromatography (*n*-hexane/EtOAc 30:1) yielded the *ortho*-alkylated product **219af** (53.2 mg, 50%) as a colorless oil. In case of using *o*-xylene (1.0 mL) as the solvent, the reaction provided the *ortho*-alkylated product **219af** (67.5 mg, 63%).

^{1}H-NMR (600 MHz, $CDCl_3$): δ = 7.70 (dd, *J* = 2.0, 0.7 Hz, 1H), 7.58 (dd, *J* = 2.2, 0.7 Hz, 1H), 7.34–7.26 (m, 4H), 6.41 (dd, *J* = 2.2, 2.0 Hz, 1H), 2.75 (s, 2H), 0.68 (s, 9H).

^{13}C-NMR (100 MHz, $CDCl_3$): δ = 140.4 (C_q), 140.0 (CH), 135.5 (C_q), 133.0 (CH), 130.9 (CH), 127.6 (CH), 126.8 (CH), 126.7 (CH), 106.1 (CH), 43.9 (CH_2), 32.1 (C_q), 29.3 (CH_3).

IR (ATR): $\tilde{\nu}$ = 2950, 1517, 1476, 1394, 1364, 1044, 939, 748, 718 cm^{-1}.

MS (EI) *m*/*z* (relative intensity): 214 (23) $[M]^+$, 199 (28) $[M–Me]^+$, 158 (100) $[M–t\text{-}Bu]^+$, 157 (74), 130 (55), 103 (9), 77 (11), 57 (15), 41 (13).

HR-MS (EI): *m*/*z* calcd for $C_{14}H_{18}N_2^+$ $[M]^+$ 214.1465, found 214.1470.

The analytical data correspond with those reported in the literature.[64]

1-(4-Methoxy-2-neopentylphenyl)-1*H*-pyrazole (219bf)

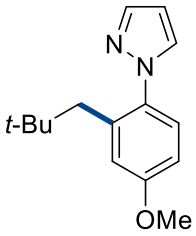

The general procedure **C** was followed using 1-(4-methoxyphenyl)-1*H*-pyrazole (**217b**, 87.1 mg, 0.50 mmol) and neopentyl bromide (**218f**, 227 mg, 1.50 mmol) in *o*-xylene (1.0 mL). After 16 h, purification by column chromatography (*n*-hexane/EtOAc 30:1) yielded the *ortho*-alkylated product **219bf** (80.6 mg, 66%) as a viscous colorless oil.

^{1}H-NMR (400 MHz, $CDCl_3$): δ = 7.67 (d, *J* = 2.0 Hz, 1H), 7.52 (d, *J* = 2.2 Hz, 1H), 7.21–7.16 (m, 1H), 6.83–6.77 (m, 2H), 6.38 (dd, *J* = 2.2, 2.0 Hz, 1H), 3.83 (s, 3H), 2.65 (s, 2H), 0.70 (s, 9H).

^{13}C-NMR (100 MHz, $CDCl_3$): δ = 158.7 (C_q), 139.9 (CH), 137.3 (C_q), 134.1 (C_q), 131.3 (CH), 128.0 (CH), 118.1 (CH), 111.8 (CH), 106.0 (CH), 55.6 (CH_3), 44.3 (CH_2), 32.2 (C_q), 29.6 (CH_3).

IR (ATR): $\tilde{\nu}$ = 2951, 2865, 1518, 1279, 1235, 2047, 747, 612 cm^{-1}.

MS (ESI) *m*/*z* (relative intensity): 267 (100) $[M+Na]^+$, 245 (28) $[M+H]^+$.

HR-MS (ESI): *m*/*z* calcd for $C_{15}H_{20}N_2ONa^+$ $[M+Na]^+$ 267.1468, found 267.1468.

1-(2-Cyclohexyl-4-methylphenyl)-1*H*-pyrazole (219ca)

1-(3-Cyclohexyl-4-methylphenyl)-1*H*-pyrazole (220ca)

The general procedure **C** was followed using 1-(4-methylphenyl)-1*H*-pyrazole (**217c**, 79.0 mg, 0.50 mmol) and bromocyclohexane (**218a**, 245 mg, 1.50 mmol). After 16 h, purification by column chromatography (*n*-hexane/EtOAc 50:1) yielded the *ortho*-alkylated product **219ca**

(74.2 mg, 62%) as a colorless oil and the *meta*-alkylated product **220ca** (30.2 mg, 25%) as a colorless oil.

1-(2-Cyclohexyl-4-methylphenyl)-1*H*-pyrazole (219ca)

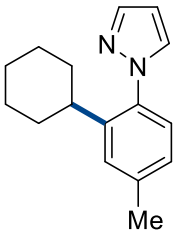

^{1}H-NMR (300 MHz, $CDCl_3$): δ = 7.70 (dd, *J* = 2.0, 0.7 Hz, 1H), 7.52 (dd, *J* = 2.2, 0.7 Hz, 1H), 7.20 (s, 1H), 7.16 (d, *J* = 8.0 Hz, 1H), 7.05 (ddd, *J* = 8.0, 1.9, 0.7 Hz, 1H), 6.41 (dd, *J* = 2.2, 2.0 Hz, 1H), 2.47–2.27 (m, 4H), 1.82–1.59 (m, 5H), 1.49–1.09 (m, 5H).

^{13}C-NMR (100 MHz, $CDCl_3$): δ = 143.9 (C_q), 140.1 (CH), 138.8 (C_q), 136.8 (C_q), 131.2 (CH), 127.8 (CH), 126.9 (CH), 126.9 (CH), 106.0 (CH), 38.3 (CH), 34.4 (CH_2), 26.9 (CH_2), 26.2 (CH_2), 21.5 (CH_3).

IR (ATR): $\tilde{\nu}$ = 1517, 1447, 1395, 1043, 1023, 944, 817, 746, 623 cm^{-1}.

MS (ESI) *m*/*z* (relative intensity): 263 (20) $[M+Na]^+$, 241 (100) $[M+H]^+$.

HR-MS (ESI): *m*/*z* calcd for $C_{16}H_{21}N_2^+$ $[M+H]^+$ 241.1699, found 241.1705.

1-(3-Cyclohexyl-4-methylphenyl)-1*H*-pyrazole (220ca)

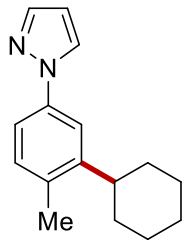

^{1}H-NMR (300 MHz, $CDCl_3$): δ = 7.89 (dd, *J* = 2.5, 0.7 Hz, 1H), 7.71 (dd, *J* = 1.8, 0.7 Hz, 1H), 7.58 (d, *J* = 2.4 Hz, 1H), 7.34 (dd, *J* = 8.2, 2.4 Hz, 1H), 7.19 (d, *J* = 8.2 Hz, 1H), 6.44 (dd, *J* = 2.5, 1.8 Hz, 1H), 2.75 (tt, *J* = 11.5, 3.0 Hz, 1H), 2.35 (s, 3H), 1.91–1.73 (m, 5H), 1.57–1.24 (m, 5H).

^{13}C-NMR (75 MHz, $CDCl_3$): δ = 147.5 (C_q), 140.8 (CH), 138.8 (C_q), 133.7 (C_q), 131.0 (CH), 126.9 (CH), 117.1 (CH), 116.4 (CH), 107.3 (CH), 40.5 (CH), 33.7 (CH_2), 27.2 (CH_2), 26.4 (CH_2), 19.0 (CH_3).

IR (ATR): $\tilde{\nu}$ = 1612, 1519, 1499, 1449, 1393, 1335, 1044, 747 cm^{-1}.

MS (ESI) *m*/*z* (relative intensity): 263 (10) $[M+Na]^+$, 241 (100) $[M+H]^+$.

HR-MS (ESI): *m*/*z* calcd for $C_{16}H_{21}N_2^+$ $[M+H]^+$ 241.1699, found 241.1702.

1-[2-Cyclohexyl-4-(trifluoromethyl)phenyl]-1*H*-pyrazole (219da)

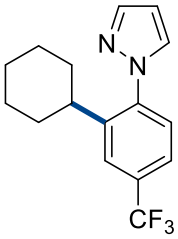

The general procedure **C** was followed using 1-[4-(trifluoromethyl)phenyl]-1*H*-pyrazole (**217d**, 106 mg, 0.50 mmol) and bromocyclohexane (**218a**, 245 mg, 1.50 mmol). After 16 h, purification by column chromatography (*n*-hexane/EtOAc 50:1) yielded the *ortho*-alkylated product **219da** (80.9 mg, 55%) as a colourless solid.

^{1}H-NMR (400 MHz, $CDCl_3$): δ = 7.75 (d, J = 2.1 Hz, 1H), 7.66 (d, J = 2.1 Hz, 1H), 7.58 (d, J = 2.3 Hz, 1H), 7.52 (dd, J = 8.1, 2.1 Hz, 1H), 7.40 (d, J = 8.1 Hz, 1H), 6.48 (dd, J = 2.3, 2.1 Hz, 1H), 2.60 (tt, J = 12.1, 3.0 Hz, 1H), 1.82–1.67 (m, 5H), 1.50–1.34 (m, 2H), 1.33–1.15 (m, 3H).

^{13}C-NMR (100 MHz, $CDCl_3$): δ = 144.9 (C_q), 141.9 (C_q), 141.0 (CH), 131.1 (CH), 131.0 (q, $^2J_{C–F}$ = 33 Hz, C_q), 127.4 (CH), 124.7 (q, $^3J_{C–F}$ = 4 Hz, CH), 124.1 (q, $^1J_{C–F}$ = 272 Hz, C_q), 123.4 (q, $^3J_{C–F}$ = 4 Hz, CH), 106.9 (CH), 38.4 (CH), 34.2 (CH_2), 26.7 (CH_2), 26.0 (CH_2).

^{19}F-NMR (376 MHz, $CDCl_3$): δ = − 62.5 (s).

IR (ATR): $\tilde{\nu}$ = 1520, 1395, 1333, 1274, 1165, 1122, 1101, 939, 749 cm^{-1}.

m.p.: 56–58 °C.

MS (ESI) *m*/*z* (relative intensity): 317 (4) $[M+Na]^+$, 295 (100) $[M+H]^+$.

HR-MS (ESI): *m*/*z* calcd for $C_{16}H_{18}F_3N_2^+$ $[M+H]^+$ 295.1417, found 295.1421.

1-(3-Cyclohexylphenyl)-3,5-dimethyl-1*H*-pyrazole (220ea)

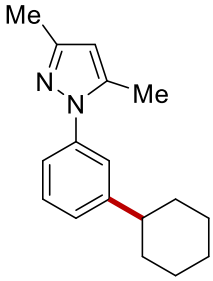

The general procedure **C** was followed using 3,5-dimethyl-1-phenyl-1*H*-pyrazole (**217e**, 86.2 mg, 0.50 mmol) and bromocyclohexane (**218a**, 122 mg, 0.75 mmol). After 16 h, purification by column chromatography (*n*-hexane/EtOAc 30:1) yielded the *meta*-alkylated product **220ea** (79.3 mg, 62%) as a colorless oil.

^{1}H-NMR (300 MHz, $CDCl_3$): δ = 7.34 (dd, J = 7.9, 7.7 Hz, 1H), 7.27 (ddd, J = 2.3, 1.6, 0.6 Hz, 1H), 7.21 (ddd, J = 7.9, 2.3, 1.2 Hz, 1H), 7.19 (dddd, J = 7.7, 1.6, 1.2, 0.6 Hz, 1H), 6.00–5.97 (m, 1H), 2.55 (tt, J = 11.6, 3.3 Hz, 1H), 2.30 (d, J = 0.4 Hz, 3H), 2.29 (d, J = 0.7 Hz, 3H), 1.96–1.71 (m, 5H), 1.52–1.18 (m, 5H).

^{13}C-NMR (125 MHz, $CDCl_3$): δ = 149.1 (C_q), 148.6 (C_q), 139.8 (C_q), 139.2 (C_q), 128.6 (CH), 125.7 (CH), 123.4 (CH), 122.1 (CH), 106.6 (CH), 44.5 (CH), 34.4 (CH_2), 26.9 (CH_2), 26.2 (CH_2), 13.6 (CH_3), 12.4 (CH_3).

IR (ATR): $\tilde{\nu}$ = 2922, 2850, 1605, 1590, 1492, 1446, 1380, 792, 701 cm^{-1}.

MS (EI) *m*/*z* (relative intensity): 254 (100) $[M]^+$, 253 (34) $[M–H]^+$, 239 (8) $[M–Me]^+$, 225 (26), 213 (12), 211 (11), 199 (74), 186 (15), 115 (11), 91 (9), 77 (8), 41 (10).

HR-MS (EI): *m*/*z* calcd for $C_{17}H_{22}N_2^+$ $[M]^+$ 254.1778, found 254.1773.

1-(3-Cyclooctylphenyl)-3,5-dimethyl-1*H*-pyrazole (220ee)

1-(3,5-Dicyclooctylphenyl)-3,5-dimethyl-1*H*-pyrazole (220ee')

The general procedure **C** was followed using 3,5-dimethyl-1-phenyl-1*H*-pyrazole (**217e**, 86.2 mg, 0.50 mmol) and bromocyclooctane (**218e**, 287 mg, 1.50 mmol). After 16 h, purification by column chromatography (*n*-hexane/EtOAc 51:1) yielded the *meta*-alkylated product **220ee** (54.1 mg, 38%) as a viscous colorless oil and the di-*meta*-alkylated product **220ee'** (114 mg, 58%) as a colouless solid.

1-(3-Cyclooctylphenyl)-3,5-dimethyl-1*H*-pyrazole (220ee)

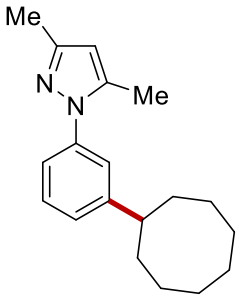

^{1}H-NMR (400 MHz, $CDCl_3$): δ = 7.35 (dd, *J* = 7.8, 7.8 Hz, 1H), 7.28 (dd, *J* = 1.9, 1.9 Hz, 1H), 7.23–7.16 (m, 2H), 6.00 (s, 1H), 2.85 (tt, *J* = 9.7, 3.6 Hz, 1H), 2.33 (s, 3H), 2.31 (s, 3H), 1.90 (ddd, *J* = 13.4, 6.7, 4.0 Hz, 2H), 1.84–1.73 (m, 4H), 1.72–1.54 (m, 8H).

^{13}C-NMR (100 MHz, $CDCl_3$): δ = 151.6 (C_q), 148.8 (C_q), 139.9 (C_q), 139.4 (C_q), 128.8 (CH), 126.0 (CH), 123.7 (CH), 121.9 (CH), 106.8 (CH), 44.6 (CH), 34.7 (CH_2), 26.9 (CH_2), 26.4 (CH_2), 26.1 (CH_2), 13.6 (CH_3), 12.5 (CH_3).

IR (ATR): $\tilde{\nu}$ = 2917, 2850, 1605, 1590, 1445, 1380, 1363, 786, 701 cm^{-1}.

MS (ESI) *m*/*z* (relative intensity): 305 (21) $[M+Na]^+$, 283 (100) $[M+H]^+$.

HR-MS (ESI): *m*/*z* calcd for $C_{19}H_{27}N_2^+$ $[M+H]^+$ 283.2169, found: 283.2170.

1-(3,5-Dicyclooctylphenyl)-3,5-dimethyl-1*H*-pyrazole (220ee')

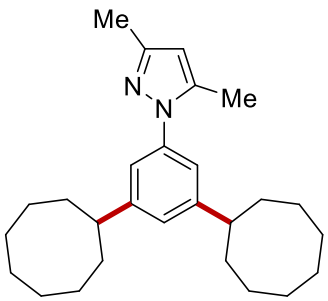

^{1}H-NMR (400 MHz, $CDCl_3$): δ = 7.02 (d, J = 1.7 Hz, 2H), 6.99 (t, J = 1.7 Hz, 1H), 5.97 (s, 1H), 2.78 (tt, J = 9.6, 3.5 Hz, 2H), 2.30 (s, 3H), 2.28 (s, 3H), 1.96–1.51 (m, 28H).

^{13}C-NMR (100 MHz, $CDCl_3$): δ = 151.4 (C_q), 148.6 (C_q), 139.7 (C_q), 139.4 (C_q), 124.9 (CH), 120.8 (CH), 106.5 (CH), 44.8 (CH), 34.8 (CH_2), 27.0 (CH_2), 26.5 (CH_2), 26.1 (CH_2), 13.7 (CH_3), 12.5 (CH_3).

IR (ATR): $\tilde{\nu}$ = 2917, 2849, 1596, 1445, 1383, 978, 876, 729, 710 cm^{-1}.

m.p.: 89–91 °C.

MS (ESI) *m*/*z* (relative intensity): 785 (100) $[2M+H]^+$, 415 (14) $[M+Na]^+$, 393 (75) $[M+H]^+$.

HR-MS (ESI): *m*/*z* calcd for $C_{27}H_{41}N_2^+$ $[M+H]^+$ 393.3264, found: 393.3254.

5.4.2 C–H Alkylation in the Presence of Typical Radical Scavengers

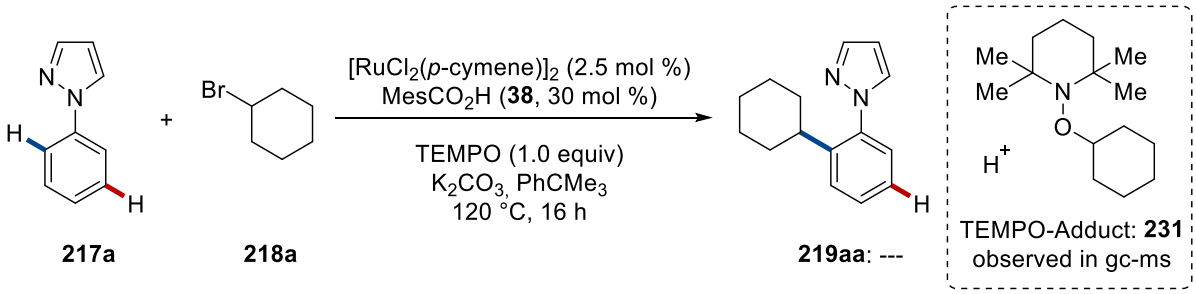

1-Phenyl-1*H*-pyrazole (**217a**, 72.1 mg, 0.50 mmol), $[RuCl_2(p\text{-cymene})]_2$ (7.7 mg, 13 µmol, 2.5 mol %), $MesCO_2H$ (**38**, 24.6 mg, 150 µmol, 30 mol %), K_2CO_3 (138 mg, 1.00 mmol) and TEMPO (78.1 mg, 0.50 mmol) were placed in a predried 25 mL Schlenk tube. The tube was evacuated and purged with N_2 three times. Bromocyclohexane (**218a**, 245 mg, 1.50 mmol) and $PhCMe_3$ (1.0 mL) were added and the mixture was stirred at 120 °C. After 16 h, the resulting mixture was filtered through a pad of silica gel and washed with EtOAc. Product formation was not observed by GC-MS, whereas the formation of the TEMPO-adduct **231** could be confirmed.

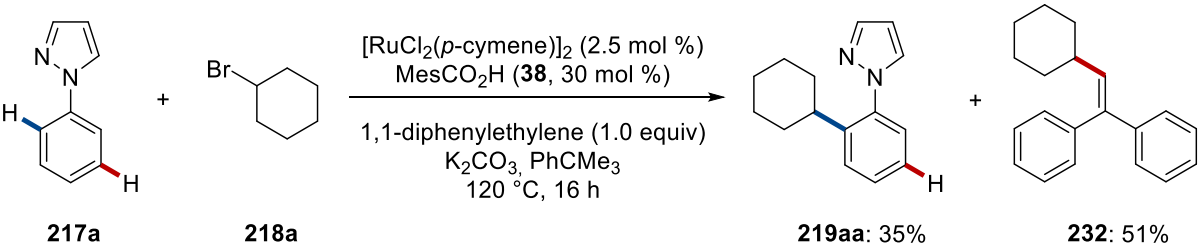

1-Phenyl-1*H*-pyrazole (**217a**, 72.1 mg, 0.50 mmol), $[RuCl_2(p\text{-cymene})]_2$ (7.7 mg, 13 µmol, 2.5 mol %), $MesCO_2H$ (**38**, 24.6 mg, 150 µmol, 30 mol %) and K_2CO_3 (138 mg, 1.00 mmol) were placed in a predried 25 mL Schlenk tube. The tube was evacuated and purged with N_2 three times. Bromocyclohexane (**218a**, 245 mg, 1.50 mmol), 1,1-diphenylethylene (90.1 mg, 0.50 mmol) and $PhCMe_3$ (1.0 mL) were added and the mixture was stirred at 120 °C. After 16 h, the resulting mixture was filtered through a pad of silica gel and washed with EtOAc. The filtrate was concentrated *in vacuo*. Purification of the residue by column chromatography on silica gel (*n*-hexane/EtOAc 100:1 to 50:1) yielded the corresponding product **219aa** (39.6 mg, 35%) as a colorless oil and the adduct **232** (69.2 mg, 51%) as a colorless oil.

(2-Cyclohexylethene-1,1-diyl)dibenzene (232)

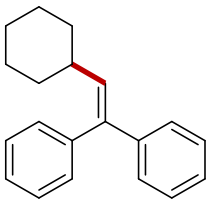

^{1}H-NMR (400 MHz, $CDCl_3$): δ = 7.46–7.33 (m, 3H), 7.33–7.16 (m, 7H), 5.95 (dd, *J* = 10.2, 3.6 Hz, 1H), 2.17 (tdt, *J* = 10.2, 7.2, 3.5 Hz, 1H), 1.80–1.51 (m, 5H), 1.42–1.06 (m, 5H).

^{13}C-NMR (100 MHz, $CDCl_3$): δ = 143.1 (C_q), 140.7 (C_q), 139.7 (C_q), 136.1 (CH), 129.9 (CH), 128.3 (CH), 128.2 (CH), 127.3 (CH), 126.9 (CH), 126.8 (CH), 38.5 (CH), 33.5 (CH_2), 26.1 (CH_2), 25.7 (CH_2).

IR (ATR): $\tilde{\nu}$ = 2921, 1494, 1445, 1073, 1031, 898, 760, 695, 598 cm^{-1}.

MS (EI) *m*/*z* (relative intensity): 262 (100) $[M]^+$, 179 (30).

HR-MS (EI): *m*/*z* calcd for $C_{20}H_{22}^+$ $[M]^+$ 262.1722, found 262.1724.

The analytical data correspond with those reported in the literature.[276]

5.4.3 Detection of Free para-Cymene

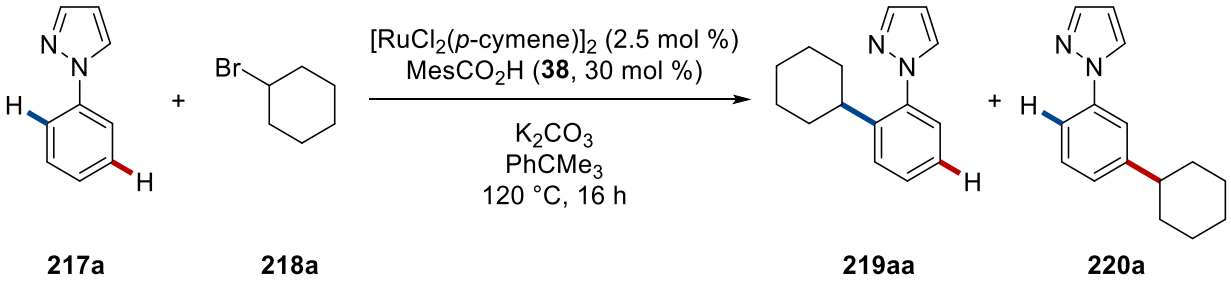

Under an atmosphere of N_2 inside a glovebox, a Schlenk tube was charged with 1-phenyl-1*H*-pyrazole (**217a**, 144 mg, 1.00 mmol), $[RuCl_2(p\text{-cymene})]_2$ (15.4 mg, 25.0 µmol, 2.5 mol %), $MesCO_2H$ (**38**, 49.2 mg, 300 µmol, 30 mol %) and K_2CO_3 (276 mg, 2.00 mmol). Bromocyclohexane (**218a**, 489 mg, 3.00 mmol), *n*-dodecane (40 µL) and $PhCMe_3$ (2.0 mL) were added and the mixture was stirred at 106 °C. During the course of the reaction, an aliquot of 100 µL was removed via syringe after 0.5 h, 1 h, 3 h, 6 h, 9 h, and 24 h. The sample was diluted with EtOAc, filtered through a short plug of silica gel and analyzed by gas chromatography.

Time [h]	**219aa** [%]	**220aa** [%]	*p*-cymene [%]
0.5	11.8	0.1	39.6
1	24.6	2.2	55.7
3	46.0	5.4	63.1
6	55.6	8.3	63.8
9	64.1	11.5	64.8
24	71.0	12.4	64.0

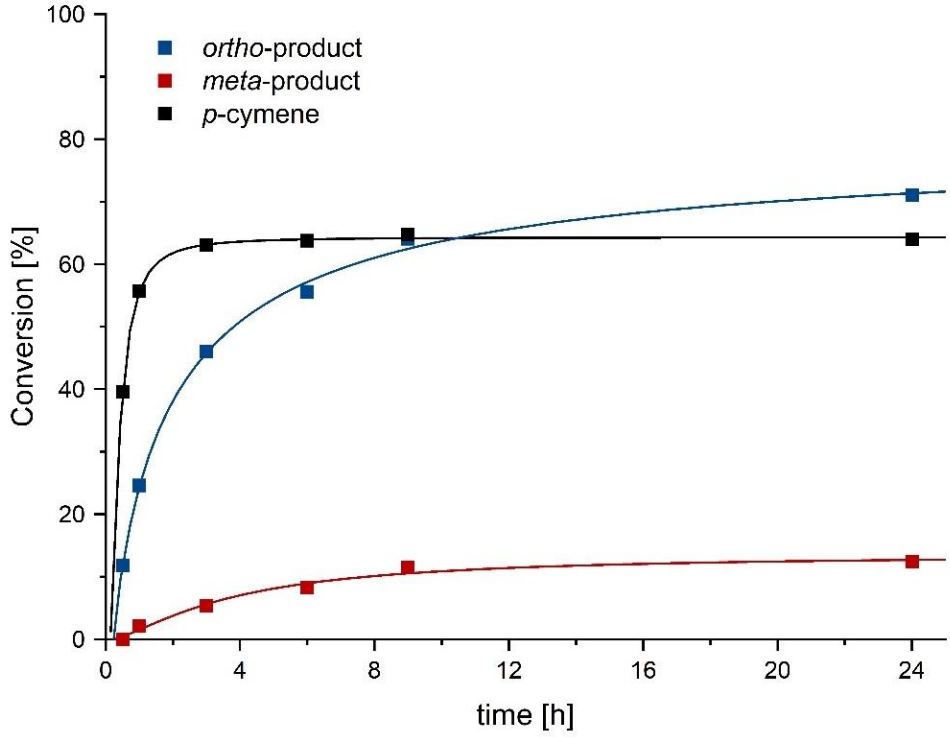

Figure 5.2: Detection of free *para*-cymene is regiodivergent C–H alkylation.

*5.4.4 Synthesis of Cyclometalated Ruthenium Complex **233***

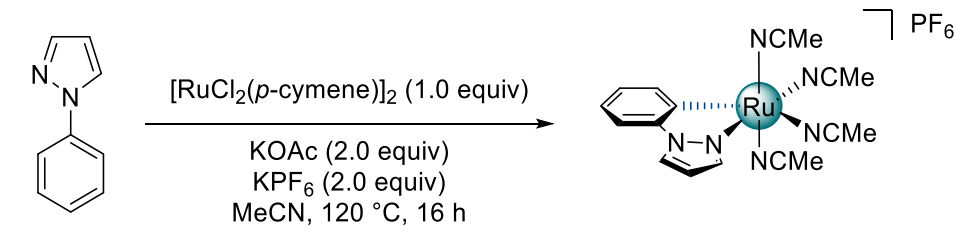

217a (2.0 equiv)

233: 79%

An oven-dried pressure tube was equipped with 1-phenyl-1*H*-pyrazole (**217a**, 144 mg, 1.00 mmol), $[RuCl_2(p\text{-cymene})]_2$ (306 mg, 0.50 mmol), KOAc (196 mg, 2.00 mmol) and KPF_6 (368 mg, 2.00 mmol). After evacuation and refilling with N_2 for three times, MeCN (6.5 mL) was added and the tube was sealed. The reaction mixture was stirred at 120 °C. After 16 h, the reaction was cooled down to ambient temperature. The crude mixture was loaded on an aluminium oxide (Al_2O_3, neutral, conditioned with CH_2Cl_2) column and eluted with MeCN/CH_2Cl_2 (1:1) using N_2 instead of air. The pale green band was collected and the solvent was removed under reduced pressure. The complex was dissolved in MeCN (10 mL) and precipitated with Et_2O, affording the desired complex **233** (435 mg, 79%) as a green solid. The complex **233** was transferred to the glovebox subsequently.

^{1}H-NMR (400 MHz, MeCN-d_3): δ = 8.40–8.20 (m, 1H), 7.96–7.77 (m, 2H), 7.36 (dt, J = 7.6, 1.5 Hz, 1H), 7.10–6.86 (m, 2H), 6.56 (dq, J = 3.3, 1.6 Hz, 1H), 2.51 (s, 3H), 2.03 (s, 6H), 1.96 (s, 3H).

^{13}C-NMR (100 MHz, MeCN-d_3): δ = 164.8 (C_q), 146.7 (C_q), 141.9 (CH), 140.1 (CH), 127.2 (CH), 125.3 (CH), 123.9 (C_q), 122.4 (C_q), 122.2 (CH), 111.6 (CH), 108.3 (CH), 4.4 (CH_3), 3.8 (CH_3).

^{19}F{^{1}H}-NMR (282 MHz, MeCN-d_3): δ = – 72.9 (d, J = 706 Hz).

^{31}P{^{1}H}-NMR (121 MHz, MeCN-d_3): δ = – 144.6 (hept, J = 706 Hz).

IR (ATR): $\tilde{\nu}$ = 2273, 1580, 1471, 1408, 1273, 1242, 1031, 830, 744, 650 cm^{-1}.

m.p.: >180 °C (decomp.).

MS (ESI) *m*/*z* (relative intensity): 368 (100) $[M–MeCN–PF_6]^+$.

HR-MS (ESI): *m*/*z* calcd for $C_{15}H_{16}N_5Ru^+$ $[M–MeCN–PF_6]^+$ 386.0447, found 386.0454.

*5.4.5 C–H Alkylation by Ruthenacycle **233** in Stoichiometric Amounts*

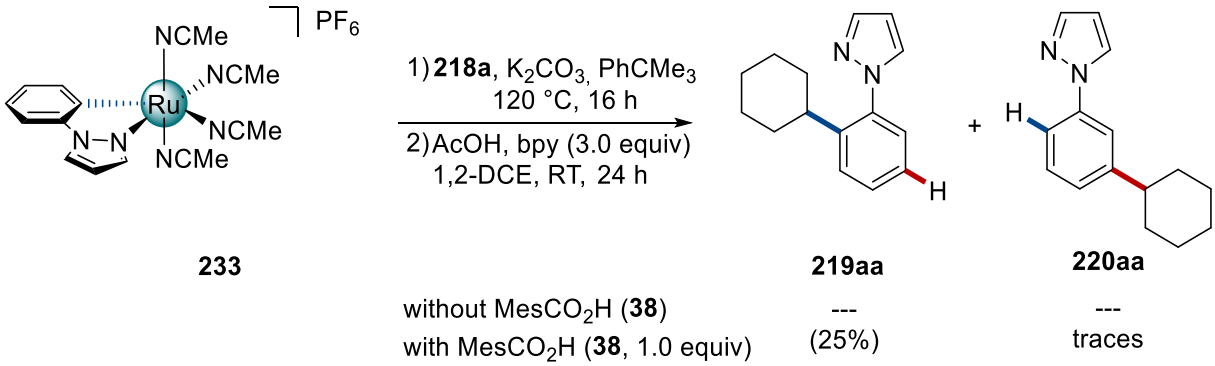

233

	219aa	**220aa**
without $MesCO_2H$ (**38**)	---	---
with $MesCO_2H$ (**38**, 1.0 equiv)	(25%)	traces

Complex **233** (55.2 mg, 0.10 mmol), $MesCO_2H$ (**38**, 16.4 mg, 0.10 mol, 30 mol %) and K_2CO_3 (27.6 mg, 0.20 mmol) were placed in a predried 5 mL Schlenk tube. The tube was evacuated and purged with N_2 three times. Bromocyclohexane (**218a**, 49.3 mg, 0.3 mmol) and $PhCMe_3$ (0.4 mL) were added and the mixture was stirred at 120 °C. After 16 h, the solution was cooled down to room temperature, and AcOH (25 µL), bipyridine (46.9 mg, 0.30 mmol) and 1,2-DCE (0.4 mL) were added, before the mixture was stirred for further 24 h at ambient temperature. Analysis of the crude NMR indicated that the *ortho*-alkylated product **219aa** was formed in 25%, whereas no product formation was observable by omitting the carboxylic acid.

*5.4.6 C–H Alkylation by Ruthenacycle **233** as Catalyst*

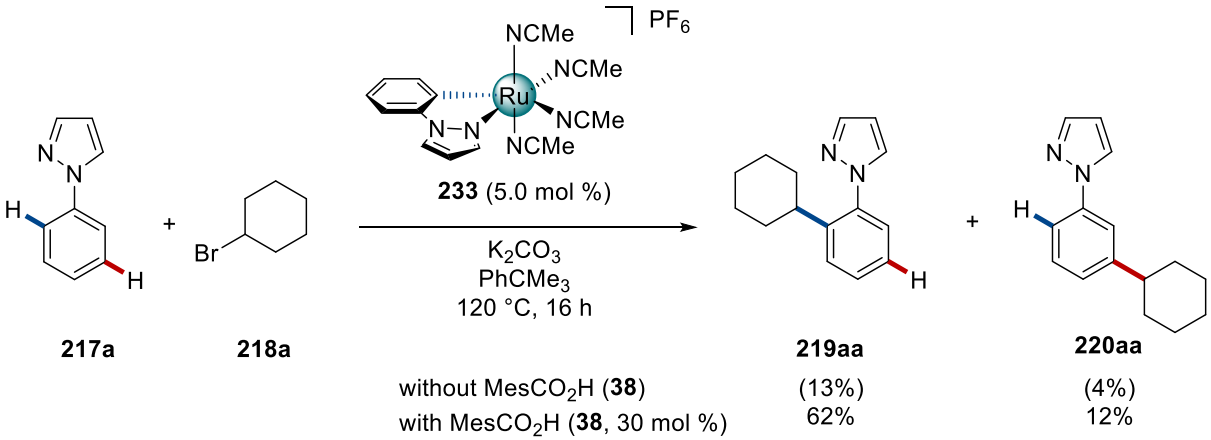

1-Phenyl-1*H*-pyrazole (**217a**, 72.1 mg, 0.50 mmol), complex **233** (13.8 mg, 25 µmol, 5.0 mol %), $MesCO_2H$ (**38**, 24.6 mg, 150 µmol, 30 mol %) and K_2CO_3 (138 mg, 1.00 mmol) were placed in a predried 25 mL Schlenk tube. The tube was evacuated and purged with N_2 three times. Bromocyclohexane (**218a**, 245 mg, 1.50 mmol) and $PhCMe_3$ (1.0 mL) were then added and the mixture was stirred at 120 °C. After 16 h, the resulting mixture was filtered through a pad of silica gel and washed with EtOAc. The filtrate was concentrated *in vacuo*. Purification of the residue by column chromatography on silica gel (*n*-hexane/EtOAc 20:1) yielded the *ortho*-alkylated product **219aa** (70.1 mg, 62%) as a colorless oil and the *meta*-alkylated product **220aa** (13.5 mg, 12%) as a colorless oil.

In case of the reaction without $MesCO_2H$, the crude reaction was determined by ^{1}H-NMR using 1,3,5-trimethoxybenzene as internal standard. 13% of the *ortho*-alkylated product **219aa** and 4% of the *meta*-alkylated product **220aa** were obtained.

5.5 PHOTO-INDUCED RUTHENIUM-CATALYZED C–H ARYLATIONS AT AMBIENT TEMPERATURE

5.5.1 Characterization Data

2-(4'-Methoxy-3-methyl-[1,1'-biphenyl]-2-yl)pyridine (243aa)

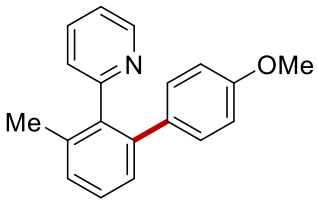

The general procedure **D** was followed using pyridine **44a** (84.6 mg, 0.50 mmol) and aryl iodide **84a** (176 mg, 0.75 mmol). After 24 h, purification by column chromatography (*n*-hexane/EtOAc 7:1) yielded **243aa** (129 mg, 94%) as a viscous colorless oil.

^{1}H-NMR (400 MHz, $CDCl_3$): δ = 8.64 (ddd, *J* = 4.9, 1.9, 1.1 Hz, 1H), 7.46 (ddd, *J* = 7.8, 7.7, 1.9 Hz, 1H), 7.34 (dd, *J* = 7.6, 7.5 Hz, 1H), 7.28–7.23 (m, 2H), 7.09 (ddd, *J* = 7.7, 4.9, 1.2 Hz, 1H), 6.99 (d, *J* = 8.8 Hz, 2H), 6.88 (ddd, *J* = 7.8, 1.2, 1.1 Hz, 1H), 6.68 (d, *J* = 8.8 Hz, 2H), 3.73 (s, 3H), 2.17 (s, 3H).

^{13}C-NMR (100 MHz, $CDCl_3$): δ = 159.8 (C_q), 158.0 (C_q), 148.9 (CH), 140.8 (C_q), 139.3 (C_q), 136.7 (C_q), 135.7 (CH), 134.1 (C_q), 130.7 (CH), 129.0 (CH), 128.0 (CH), 127.6 (CH), 125.6 (CH), 121.2 (CH), 113.1 (CH), 55.1 (CH_3), 20.5 (CH_3).

IR (ATR): $\tilde{\nu}$ = 2954, 2835, 1609, 1585, 1511, 1458, 1244, 1178, 1029, 748 cm^{-1}.

MS (EI) *m*/*z* (relative intensity): 275 (48) $[M]^+$, 274 (100) $[M–H]^+$, 260 (24) $[M–Me]^+$, 231 (20).

HR-MS (ESI): *m*/*z* calcd for $C_{19}H_{18}NO^+$ $[M+H]^+$ 276.1383, found 276.1381.

The spectral data are in accordance with those reported in the literature.[81]

2-(3-Methyl-[1,1'-biphenyl]-2-yl)pyridine (243ab)

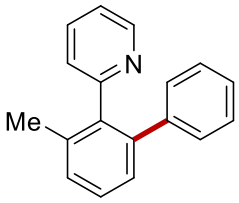

The general procedure **D** was followed using pyridine **44a** (84.6 mg, 0.50 mmol) and aryl iodide **84b** (153 mg, 0.75 mmol). After 24 h, purification by column chromatography (*n*-hexane/EtOAc 7:1) yielded **243ab** (86.8 mg, 71%) as a viscous colorless oil.

^{1}H-NMR (300 MHz, $CDCl_3$): δ = 8.66 (d, *J* = 4.9 Hz, 1H), 7.46 (ddd, *J* = 7.8, 7.7, 1.8 Hz, 1H), 7.38 (dd, *J* = 7.4, 7.4 Hz, 1H), 7.35–7.28 (m, 2H), 7.20–7.07 (m, 6H), 6.91 (d, *J* = 7.8 Hz, 1H), 2.22 (s, 3H).

^{13}C-NMR (100 MHz, $CDCl_3$): δ = 159.6 (C_q), 148.8 (CH), 141.6 (C_q), 141.2 (C_q), 139.3 (C_q), 136.7 (C_q), 135.6 (CH), 129.6 (CH), 129.4 (CH), 128.0 (CH), 127.6 (CH), 127.5 (CH), 126.2 (CH), 125.6 (CH), 121.2 (CH), 20.5 (CH_3).

IR (ATR): $\tilde{\nu}$ = 3059, 2925, 1585, 1562, 1459, 1025, 787, 759, 749, 702 cm^{-1}.

MS (ESI) *m*/*z* (relative intensity): 268 (12) $[M+Na]^+$, 246 (100) $[M+H]^+$.

HR-MS (ESI): *m*/*z* calcd for $C_{18}H_{16}N^+$ $[M+H]^+$ 246.1277, found 246.1280.

The spectral data are in accordance with those reported in the literature.[277]

2-(3,4'-Dimethyl-[1,1'-biphenyl]-2-yl)pyridine (243ac)

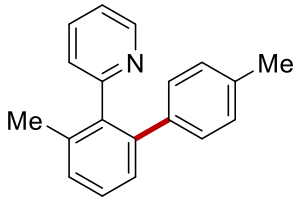

The general procedure **D** was followed using pyridine **44a** (84.6 mg, 0.50 mmol) and aryl iodide **84c** (164 mg, 0.75 mmol). After 24 h, purification by column chromatography (*n*-hexane/EtOAc 7:1) yielded **243ac** (112 mg, 91%) as a viscous colorless oil.

^{1}H-NMR (400 MHz, $CDCl_3$): δ = 8.78–8.61 (m, 1H), 7.47 (tdd, *J* = 7.7, 1.8, 1.0 Hz, 1H), 7.43–7.34 (m, 1H), 7.31 (d, *J* = 7.6 Hz, 2H), 7.12 (ddd, *J* = 7.7, 4.9, 1.1 Hz, 1H), 7.06–6.96 (m, 4H), 6.93 (dt, *J* = 7.8, 1.2 Hz, 1H), 2.29 (s, 3H), 2.23 (s, 3H).

^{13}C-NMR (100 MHz, $CDCl_3$): δ = 159.8 (C_q), 148.9 (CH), 141.2 (C_q), 139.3 (C_q), 138.8 (C_q), 136.7 (C_q), 135.8 (C_q), 135.8 (CH), 129.5 (CH), 129.2 (CH), 128.4 (CH), 128.1 (CH), 127.7 (CH), 125.6 (CH), 121.3 (CH), 21.1 (CH_3), 20.6 (CH_3).

IR (ATR): $\tilde{\nu}$ = 1585, 1562, 1459, 1421, 1024, 823, 782, 746, 578 cm^{-1}.

MS (ESI) *m*/*z* (relative intensity): 541 (5) $[2M+Na]^+$, 282 (18) $[M+Na]^+$, 260 (100) $[M+H]^+$.

HR-MS (ESI): *m*/*z* calcd for $C_{19}H_{18}N^+$ $[M+H]^+$ 260.1434, found 260.1435.

The spectral data are in accordance with those reported in the literature.[278]

3'-Methyl-2'-(pyridin-2-yl)-[1,1'-biphenyl]-4-ol (243ae)

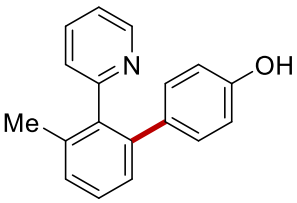

The general procedure **D** was followed using pyridine **44a** (84.6 mg, 0.50 mmol) and aryl iodide **84e** (165 mg, 0.75 mmol) in DMA (2.0 mL). After 24 h, purification by column chromatography

(*n*-hexane/EtOAc 8:1 to 5:1) yielded **243ae** (66.8 mg, 51%) as a white solid.

^{1}H-NMR (300 MHz, $CDCl_3$): δ = 8.58 (ddd, *J* = 5.1, 1.8, 0.9 Hz, 1H), 7.99 (s br, 1H), 7.53 (td, *J* = 7.7, 1.8 Hz, 1H), 7.37–7.27 (m, 1H), 7.27–7.18 (m, 2H), 7.13 (ddd, *J* = 7.5, 5.0, 1.1 Hz, 1H), 6.98 (dt, *J* = 7.6 Hz, 1.0 Hz, 1H), 6.85–6.76 (m, 2H), 6.44–6.37 (m, 2H), 2.14 (s, 3H).

^{13}C-NMR (100 MHz, $CDCl_3$): δ = 159.9 (C_q), 154.7 (C_q), 148.8 (CH), 141.2 (C_q), 139.2 (C_q), 136.8 (C_q), 136.3 (CH), 133.9 (C_q), 131.0 (CH), 129.2 (CH), 128.3 (CH), 127.8 (CH), 126.1 (CH), 121.6 (CH), 114.9 (CH), 20.7 (CH_3).

IR (ATR): $\tilde{\nu}$ = 3062, 1595, 1513, 1458, 1272, 1244, 836, 793, 753 cm^{-1}.

m.p.: 199–201 °C.

MS (ESI) *m*/*z* (relative intensity): 284 (27) $[M+Na]^+$, 262 (100) $[M+H]^+$.

HR-MS (ESI): *m*/*z* calcd for $C_{18}H_{16}NO^+$ $[M+H]^+$ 262.1226, found 262.1227.

3'-Methyl-2'-(pyridin-2-yl)-[1,1'-biphenyl]-4-carbonitrile (243af)

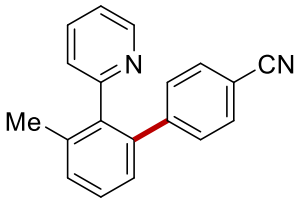

The general procedure **D** was followed using pyridine **44a** (84.6 mg, 0.50 mmol) and aryl iodide **84f** (172 mg, 0.75 mmol) in DMA (2.0 mL). After 48 h, purification by column chromatography (*n*-hexane/EtOAc 7:1) yielded **243af** (28.4 mg, 21%) as a viscous colorless oil.

^{1}H-NMR (400 MHz, $CDCl_3$): δ = 8.66 (ddd, *J* = 4.9, 1.9, 1.0 Hz, 1H), 7.47 (ddd, *J* = 7.7, 7.7, 1.8 Hz, 1H), 7.41–7.24 (m, 3H), 7.11 (ddd, *J* = 7.6, 4.9, 1.2 Hz, 1H), 7.06–6.98 (m, 2H), 6.91 (dt, *J* = 7.8, 1.1 Hz, 1H), 6.75–6.64 (m, 2H), 2.21 (s, 3H).

^{13}C-NMR (100 MHz, $CDCl_3$): δ = 159.8 (C_q), 158.1 (C_q), 148.9 (CH), 140.8 (C_q), 139.4 (C_q), 136.7 (C_q), 135.8 (CH), 134.1 (C_q), 130.7 (CH), 129.1 (CH), 128.0 (CH), 127.6 (CH), 125.6 (CH), 121.3 (CH), 113.1 (CH), 55.1 (CH_3), 20.5 (CH_3).

IR (ATR): $\tilde{\nu}$ = 1585, 1459, 1423, 1266, 1148, 1024, 842, 790, 582 cm^{-1}.

m.p.: 200–201 °C.

MS (ESI) *m*/*z* (relative intensity): 293 (100) $[M+Na]^+$, 271 (89) $[M+H]^+$.

HR-MS (ESI): *m*/*z* calcd for $C_{19}H_{15}N_2^+$ $[M+H]^+$ 271.1230, found 271.1233.

2-(4'-Fluoro-3-methyl-[1,1'-biphenyl]-2-yl)pyridine (243ag)

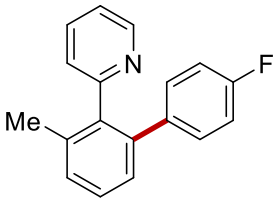

The general procedure **D** was followed using pyridine **44a** (84.6 mg, 0.50 mmol) and aryl iodide **84g** (167 mg, 0.75 mmol). After 24 h, purification by column chromatography (*n*-hexane/EtOAc 7:1) yielded **243ag** (84.6 mg, 67%) as a viscous colorless oil.

^{1}H-NMR (300 MHz, $CDCl_3$): δ = 8.65 (ddd, *J* = 4.9, 1.8, 1.0 Hz, 1H), 7.48 (td, *J* = 7.6, 1.5 Hz, 1H), 7.41–7.18 (m, 3H), 7.11 (dd, *J* = 7.5, 4.7 Hz, 1H), 7.03 (d, *J* = 8.6, 5.5 Hz, 2H), 6.94–6.71 (m, 3H), 2.18 (s, 3H).

^{13}C-NMR (75 MHz, $CDCl_3$): δ = 162.1 (d, $^1J_{C–F}$ = 241 Hz, C_q), 159.5 (C_q), 149.0 (CH), 140.3 (C_q), 139.4 (C_q), 137.6 (d, $^4J_{C–F}$ = 3 Hz, C_q), 136.9 (C_q), 136.0 (CH), 131.1 (d, $^3J_{C–F}$ = 8 Hz, CH), 129.6 (CH), 128.2 (CH), 127.6 (CH), 125.7 (CH), 121.5 (CH), 114.5 (d, $^2J_{C–F}$ = 22 Hz, CH), 20.6 (CH_3).

^{19}F-NMR (282 MHz, $CDCl_3$): δ = − 116.5 (s).

IR (ATR): $\tilde{\nu}$ = 1584, 1507, 1459, 1423, 1218, 1157, 838, 785, 749 cm^{-1}.

MS (ESI) *m*/*z* (relative intensity): 549 (5) $[2M+Na]^+$, 286 (18) $[M+Na]^+$, 264 (100) $[M+H]^+$.

HR-MS (ESI): *m*/*z* calcd for $C_{18}H_{15}FN^+$ $[M+H]^+$ 264.1183, found 264.1185.

The spectral data are in accordance with those reported in the literature.[278]

2-(4'-Bromo-3-methyl-[1,1'-biphenyl]-2-yl)pyridine (243ai)

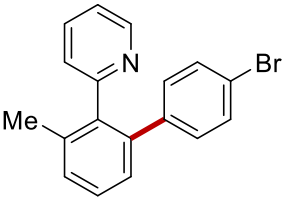

The general procedure **D** was followed using pyridine **44a** (84.6 mg, 0.50 mmol) and aryl iodide **84i** (217 mg, 0.75 mmol). After 24 h, purification by column chromatography (*n*-hexane/EtOAc 7:1) yielded **243ai** (108 mg, 67%) as a viscous colorless oil.

^{1}H-NMR (400 MHz, $CDCl_3$): δ = 8.62 (ddd, *J* = 4.9, 1.9, 1.0 Hz, 1H), 7.47 (td, *J* = 7.7, 1.7 Hz, 1H), 7.39–7.28 (m, 2H), 7.27–7.20 (m, 3H), 7.11 (ddd, *J* = 7.6, 5.0, 1.2 Hz, 1H), 6.95 (dd, *J* = 8.0, 1.2 Hz, 2H), 6.89 (dt, *J* = 7.8, 1.0 Hz, 1H), 2.17 (s, 3H).

^{13}C-NMR (100 MHz, $CDCl_3$): δ = 159.3 (C_q), 149.1 (CH), 140.7 (C_q), 140.0 (C_q), 139.3 (C_q), 137.0 (C_q), 136.0 (CH), 131.3 (CH), 130.8 (CH), 129.8 (CH), 128.2 (CH), 127.5 (CH), 125.6 (CH), 121.6 (CH), 120.7 (C_q), 20.5 (CH_3).

IR (ATR): $\tilde{\nu}$ = 1585, 1457, 1422, 1264, 1010, 786, 736, 702 cm^{-1}.

MS (ESI) *m*/*z* (relative intensity): 348 (100) [M(^{81}Br)+Na]$^+$, 346 (100) [M(^{79}Br)+Na]$^+$, 326 (74) [M(^{81}Br)+H]$^+$, 324 (74) [M(^{79}Br)+H]$^+$.

HR-MS (ESI): *m*/*z* calcd for $C_{18}H_{15}{}^{79}BrN^+$ [M+H]$^+$ 324.0382, found 324.0387.

The spectral data are in accordance with those reported in the literature.[278]

2-[3-Methyl-4'-(trifluoromethyl)-[1,1'-biphenyl]-2-yl]pyridine (243aj)

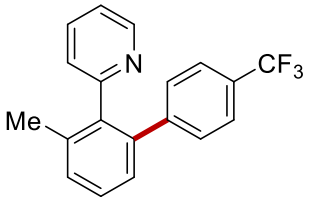

The general procedure **D** was followed using pyridine **44a** (84.6 mg, 0.50 mmol) and aryl bromide **59j** (169 mg, 0.75 mmol). After 24 h, purification by column chromatography (*n*-hexane/EtOAc 7:1) followed by recycling preparative HPLC yielded **243aj** (82.7 mg, 52%) as a viscous colorless oil.

^{1}H-NMR (300 MHz, $CDCl_3$): δ = 8.63 (ddd, *J* = 4.8, 1.5, 1.1 Hz, 1H), 7.48 (ddd, *J* = 7.9, 7.7, 1.5 Hz, 1H), 7.42–7.36 (m, 3H), 7.33 (dd, *J* = 7.8, 1.8 Hz, 1H), 7.25 (dd, *J* = 7.1, 1.8 Hz, 1H), 7.19 (d, *J* = 8.1 Hz, 2H), 7.12 (ddd, *J* = 7.7, 4.8, 1.1 Hz, 1H), 6.90 (ddd, *J* = 7.9, 1.1, 1.1 Hz, 1H), 2.19 (s, 3H).

^{13}C-NMR (100 MHz, $CDCl_3$): δ = 159.0 (C_q), 149.0 (CH), 145.4 (q, $^5J_{C–F}$ = 2 Hz, C_q), 139.8 (C_q), 139.3 (C_q), 137.0 (C_q), 135.9 (CH), 130.1 (CH), 129.8 (CH), 128.4 (q, $^2J_{C–F}$ = 32 Hz, C_q), 128.2 (CH), 127.4 (CH), 125.6 (CH), 124.5 (q, $^3J_{C–F}$ = 4 Hz, CH), 124.2 (q, $^1J_{C–F}$ = 272 Hz, C_q), 121.6 (CH), 20.4 (CH_3).

^{19}F-NMR (282 MHz, $CDCl_3$): δ = – 62.4 (s).

IR (ATR): $\tilde{\nu}$ = 1617, 1585, 1564, 1323, 1163, 1122, 1062, 844, 792, 750 cm^{-1}.

MS (ESI) *m*/*z* (relative intensity): 649 (12) [2M+Na]$^+$, 336 (100) [M+Na]$^+$, 314 (98) [M+H]$^+$.

HR-MS (ESI): *m*/*z* calcd for $C_{19}H_{14}F_3NNa^+$ [M+Na]$^+$ 336.0971, found 336.0976.

The spectral data are in accordance with those reported in the literature.[277]

1-[3'-Methyl-2'-(pyridin-2-yl)-[1,1'-biphenyl]-4-yl]ethan-1-one (243ak)

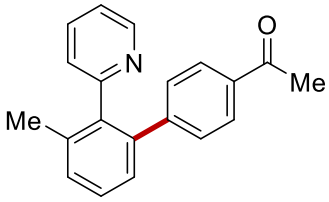

The general procedure **D** was followed using pyridine **44a** (84.6 mg, 0.50 mmol) and aryl iodide **84k** (185 mg, 0.75 mmol). After 48 h, purification by column chromatography (*n*-hexane/EtOAc 7:1 to 3:1) yielded **243ak** (107 mg, 75%) as a white solid.

^{1}H-NMR (300 MHz, $CDCl_3$): δ = 8.62 (ddd, *J* = 4.9, 1.8, 0.9 Hz, 1H), 7.73 (d, *J* = 8.3 Hz, 2H), 7.47 (ddd, *J* = 7.8, 7.7, 1.8 Hz, 1H), 7.39 (dd, *J* = 7.7, 7.3 Hz, 1H), 7.33 (dd, *J* = 7.7, 1.7 Hz, 1H), 7.27 (dd, *J* = 7.3, 1.7 Hz, 1H), 7.17 (d, *J* = 8.3 Hz, 2H), 7.11 (ddd, *J* = 7.7, 4.9, 1.2 Hz, 1H), 6.90 (dd, *J* = 7.8, 1.2 Hz, 1H), 2.53 (s, 3H), 2.19 (s, 3H).

^{13}C-NMR (100 MHz, $CDCl_3$): δ = 197.9 (C_q), 159.1 (C_q), 149.0 (CH), 146.8 (C_q), 140.1 (C_q), 139.3 (C_q), 137.0 (C_q), 135.9 (CH), 134.9 (C_q), 130.1 (CH), 129.8 (CH), 128.2 (CH), 127.7 (CH), 127.4 (CH), 125.5 (CH), 121.6 (CH), 26.6 (CH_3), 20.4 (CH_3).

IR (ATR): $\tilde{\nu}$ = 3344, 1678, 1604, 1400, 1267, 792, 752, 621, 560 cm^{-1}.

m.p.: 94–96 °C.

MS (ESI) *m*/*z* (relative intensity): 597 (25) $[2M+Na]^+$, 310 (38) $[M+Na]^+$, 288 (100) $[M+H]^+$.

HR-MS (ESI): *m*/*z* calcd for $C_{20}H_{18}NO^+$ $[M]^+$ 288.1383, found 288.1386.

The spectral data are in accordance with those reported in the literature.[278]

Methyl 3'-methyl-2'-(pyridin-2-yl)-[1,1'-biphenyl]-4-carboxylate (243al)

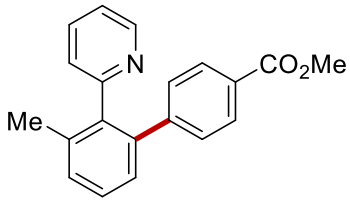

The general procedure **D** was followed using pyridine **44a** (84.6 mg, 0.50 mmol) and aryl iodide **84l** (197 mg, 0.75 mmol). After 24 h, purification by column chromatography (*n*-hexane/EtOAc 9:1 to 5:1) yielded **243al** (109 mg, 72%) as a viscous colorless oil.

^{1}H-NMR (400 MHz, $CDCl_3$): δ = 8.66 (ddd, *J* = 4.9, 1.9, 1.0 Hz, 1H), 7.47 (td, *J* = 7.7, 1.8 Hz, 1H), 7.41–7.24 (m, 3H), 7.11 (ddd, *J* = 7.6, 4.9, 1.2 Hz, 1H), 7.06–6.98 (m, 2H), 6.91 (dt, *J* = 7.8, 1.1 Hz, 1H), 6.75–6.64 (m, 2H), 3.74 (d, *J* = 1.0 Hz, 3H), 2.21 (s, 3H).

^{13}C-NMR (100 MHz, $CDCl_3$): δ = 167.0 (C_q), 159.1 (C_q), 149.0 (CH), 146.6 (C_q), 140.3 (C_q), 139.3 (C_q), 136.9 (C_q), 135.9 (CH), 130.1 (CH), 129.7 (CH), 128.9 (CH), 128.2 (CH), 128.0 (C_q), 127.4 (CH), 125.6 (CH), 121.6 (CH), 52.0 (CH_3), 20.5 (CH_3).

IR (ATR): $\tilde{\nu}$ = 1717, 1585, 1277, 1103, 769, 732, 702 cm^{-1}.

MS (ESI) *m*/*z* (relative intensity): 541 (28) $[2M+Na]^+$, 326 (32) $[M+K]^+$, 326 (32) $[M+Na]^+$, 304 (100) $[M+H]^+$.

HR-MS (ESI): *m*/*z* calcd for $C_{20}H_{18}NO_2^+$ $[M+H]^+$ 304.1332, found 304.1335.

The spectral data are in accordance with those reported in the literature.[278]

3'-Methyl-2'-(pyridin-2-yl)-[1,1'-biphenyl]-4-yl (*Z*)-nonadec-10-enoate (243as)

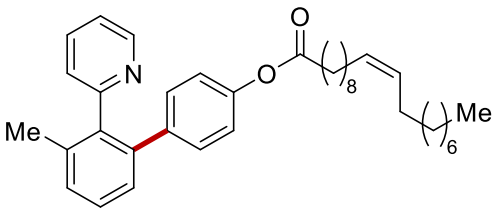

The general procedure **D** was followed using pyridine **44a** (84.6 mg, 0.50 mmol) and aryl iodide **84s** (375 mg, 0.75 mmol). After 24 h, purification by column chromatography (*n*-hexane/EtOAc 10:1) yielded **243as** (111 mg, 41%) as a viscous colorless oil.

^{1}H-NMR (400 MHz, $CDCl_3$): δ = 8.65 (dt, *J* = 5.0, 1.3 Hz, 1H), 7.47 (td, *J* = 7.7, 1.8 Hz, 1H), 7.38 (dd, *J* = 7.5, 7.5 Hz, 1H), 7.35–7.26 (m, 2H), 7.12 (q, *J* = 8.3 Hz, 5H), 7.01–6.80 (m, 1H), 5.48–5.27 (m, 2H), 5.04 (s, 2H), 2.35 (t, *J* = 7.6 Hz, 2H), 2.20 (s, 3H), 2.03 (q, *J* = 6.7 Hz, 3H), 1.65 (quint, *J* = 7.0 Hz, 2H), 1.40–1.18 (m, 20H), 0.90 (t, *J* = 6.8 Hz, 3H).

^{13}C-NMR (100 MHz, $CDCl_3$): δ = 173.1 (C_q), 159.6 (C_q), 149.0 (CH), 149.0 (CH), 141.7 (CH), 140.8 (C_q), 139.4 (C_q), 136.9 (C_q), 135.9 (C_q), 134.1 (CH), 130.1 (C_q), 129.9 (CH), 129.8 (CH), 129.7 (CH), 128.2 (CH), 127.7 (CH), 127.5 (CH), 125.7 (CH), 121.5 (CH), 65.8 (CH_2), 34.4 (CH_2), 32.0 (CH_2), 29.9 (CH_2), 29.8 (CH_2), 29.6 (CH_2), 29.4 (CH_2), 29.3 (CH_2), 29.2 (CH_2), 29.2 (CH_2), 27.3 (CH_2), 27.3 (CH_2), 25.0 (CH_2), 22.8 (CH_3), 20.6 (CH_3).

IR (ATR): $\tilde{\nu}$ = 2923, 2853, 1736, 1585, 1460, 1161, 1024, 785, 748, 578 cm^{-1}.

MS (ESI) *m*/*z* (relative intensity): 562 (4) $[M+Na]^+$, 540 (100) $[M+H]^+$.

HR-MS (ESI): *m*/*z* calcd for $C_{37}H_{50}NO_2^+$ $[M+H]^+$ 540.3836, found 540.3840.

2,2'-(3,3''-Dimethyl-[1,1':4',1''-terphenyl]-2,2''-diyl)dipyridine (244aa)

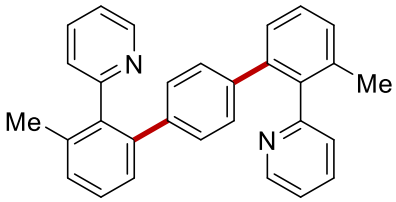

The general procedure **D** was followed using pyridine **84a** (186 mg, 1.10 mmol), diiodide **84t** (165 mg, 0.50 mmol) and K_2CO_3 (276 mg, 2.00 mmol). After 24 h, purification by column chromatography (*n*-hexane/EtOAc 2:1) yielded **244aa** (200 mg, 97%) as a pale yellow solid.

^{1}H-NMR (400 MHz, $CDCl_3$): δ = 8.58 (ddd, *J* = 4.9, 1.9, 1.0 Hz, 2H), 7.42 (td, *J* = 7.7, 1.9 Hz, 2H), 7.32 (t, *J* = 7.5 Hz, 2H), 7.27–7.18 (m, 4H), 7.08 (ddd, *J* = 7.5, 4.9, 1.2 Hz, 2H), 6.82 (s, 6H), 2.15 (s, 6H).

^{13}C-NMR (100 MHz, $CDCl_3$): δ = 159.7 (C_q), 148.9 (CH), 141.0 (C_q), 139.6 (C_q), 139.4 (C_q), 136.8 (C_q), 135.6 (CH), 129.5 (CH), 129.0 (CH), 128.1 (CH), 127.7 (CH), 125.7 (CH), 121.3 (CH), 20.6 (CH_3).

IR (ATR): $\tilde{\nu}$ = 1584, 1562, 1455, 1422, 1023, 840, 784, 748, 596 cm^{-1}.

m.p.: 210–212 °C.

MS (ESI) *m*/*z* (relative intensity): 435 (100) $[M+Na]^+$, 413 (50) $[M+H]^+$.

HR-MS (ESI): *m*/*z* calcd for $C_{30}H_{24}N_2Na^+$ $[M+Na]^+$ 435.1832, found 435.1836.

1-(3,4'-Dimethoxy-[1,1'-biphenyl]-2-yl)ethan-1-one (252aa)

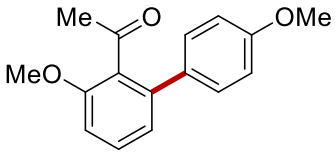

Ketimine **247a** (158 mg, 0.50 mmol), $[Ru(OAc)_2(p\text{-cymene})]$ (17.7 mg, 50.0 µmol, 10 mol %) and K_2CO_3 (138 mg, 1.00 mmol) were placed in a 10 mL vial. The vial was capped with a septum and wrapped with parafilm. The vial was evacuated and purged with N_2 three times. Aryl iodide **84a** (176 mg, 0.75 mmol) and 1,4-dioxane (2.0 mL) were then added and the mixture was stirred under visible light irradiation (2 × Kessil A360N, temperature was maintained between 30 °C and 33 °C) for 24 h. At ambient temperature, HCl (2 N, 3.0 mL) was added, and the resulting mixture was stirred for additional 3 h, before being extracted with EtOAc (3 × 20 mL). The combined organic layers were dried over Na_2SO_4 and concentrated *in vacuo*. Purification of the residue by column chromatography (SiO_2, *n*-hexane/EtOAc 7:1) yielded the *ortho*-arylated product **252aa** (58.4 mg, 46%) as a light yellow solid.

^{1}H-NMR (400 MHz, $CDCl_3$): δ = 7.36 (dd, J = 8.4, 7.7 Hz, 1H), 7.27 (d, J = 8.8 Hz, 2H), 6.95 (dd, J = 7.7, 0.9 Hz, 1H), 6.91 (d, J = 8.8 Hz, 2H), 6.91 (dd, J = 8.4, 0.9 Hz, 1H), 3.85 (s, 3H), 3.83 (s, 3H), 2.14 (s, 3H).

^{13}C-NMR (100 MHz, $CDCl_3$): δ = 205.2 (C_q), 159.2 (C_q), 155.5 (C_q), 139.6 (C_q), 132.0 (C_q), 131.1 (C_q), 130.0 (CH), 129.8 (CH), 122.2 (CH), 113.9 (CH), 109.5 (CH), 55.9 (CH_3), 55.2 (CH_3), 32.4 (CH_3).

IR (ATR): $\tilde{\nu}$ = 2938, 1687, 1566, 1514, 1462, 1247, 1176, 1020, 834, 795 cm^{-1}.

m.p.: 127–129 °C.

MS (ESI) *m*/*z* (relative intensity): 535 (13) $[2M+Na]^+$, 404 (27), 279 (100) $[M+Na]^+$, 257 (11) $[M+H]^+$, 148 (31).

HR-MS (ESI): *m*/*z* calcd for $C_{16}H_{16}O_3Na^+$ $[M+Na]^+$ 279.0992, found 279.0994.

The spectral data are in accordance with those reported in the literature.[279]

4-Butyl-1-(3-methoxy-4'-methyl-[1,1'-biphenyl]-2-yl)-1*H*-1,2,3-triazole (254ac)

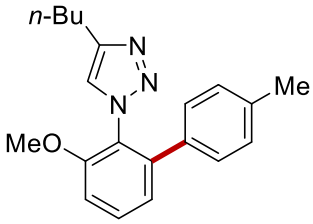

The general procedure **D** was followed using triazole **253a** (116 mg, 0.50 mmol), aryl iodide **84c** (327 mg, 1.50 mmol) and $[Ru(OAc)_2(p\text{-cymene})]$ (35.3 mg, 0.10 mmol, 20 mol %) in DMA (2.0 mL). After 24 h, purification by column chromatography (*n*-hexane/EtOAc 7:1) yielded **254ac** (127 mg, 79%) as a white solid.

^{1}H-NMR (400 MHz, $CDCl_3$): δ = 7.48 (dd, J = 8.1, 8.1 Hz, 1H), 7.08 (dd, J = 7.8, 1.2 Hz, 1H), 7.05–6.92 (m, 6H), 3.80 (s, 3H), 2.66 (t, J = 7.5 Hz, 2H), 2.27 (s, 3H), 1.54 (tt, J = 7.6, 6.5 Hz, 2H), 1.21 (hept, J = 7.4 Hz, 2H), 0.86 (t, J = 7.3 Hz, 3H).

^{13}C-NMR (100 MHz, $CDCl_3$): δ = 155.3 (C_q), 147.5 (C_q), 141.1 (C_q), 137.5 (C_q), 134.6 (C_q), 130.8 (CH), 129.0 (CH), 128.2 (CH), 124.7 (C_q), 123.9 (CH), 122.4 (CH), 110.8 (CH), 56.3 (CH_3), 31.5 (CH_2), 25.2 (CH_2), 22.0 (CH_2), 21.2 (CH_3), 13.9 (CH_3).

IR (ATR): $\tilde{\nu}$ = 2933, 1473, 1313, 1264, 1122, 1016, 790, 731, 702 cm^{-1}.

m.p.: 67–68 °C.

MS (ESI) *m*/*z* (relative intensity): 665 (85) $[2M+Na]^+$, 344 (100) $[M+Na]^+$, 322 (80) $[M+H]^+$.

HR-MS (ESI): *m*/*z* calcd for $C_{20}H_{24}N_3O^+$ $[M+H]^+$ 322.1914, found 322.1916.

4-Butyl-1-(3,4'-dimethoxy-[1,1'-biphenyl]-2-yl)-1*H*-1,2,3-triazole (254aa)

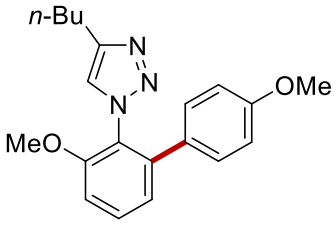

The general procedure **D** was followed using triazole **253a** (116 mg, 0.50 mmol), aryl iodide **84a** (352 mg, 1.50 mmol) and $[Ru(OAc)_2(p\text{-cymene})]$ (35.3 mg, 0.10 mmol, 20 mol %) in DMA (2.0 mL). After 24 h, purification by column chromatography (*n*-hexane/EtOAc 3:1) yielded **254aa** (129 mg, 77%) as a white solid.

^{1}H-NMR (400 MHz, $CDCl_3$): δ = 7.48 (dd, *J* = 8.3, 7.8 Hz, 1H), 7.07 (dd, *J* = 7.8, 1.2 Hz, 1H), 7.03 (t, *J* = 0.7 Hz, 1H), 7.02 (dd, *J* = 8.3, 1.2 Hz, 1H), 6.99 (d, *J* = 8.8 Hz, 2H), 6.73 (d, *J* = 8.8 Hz, 2H), 3.80 (s, 3H), 3.74 (s, 3H), 2.67 (t, *J* = 7.5 Hz, 2H), 1.60–1.51 (m, 2H), 1.28–1.17 (m, 2H), 0.86 (t, *J* = 7.3 Hz, 3H).

^{13}C-NMR (100 MHz, $CDCl_3$): δ = 159.1 (C_q), 155.2 (C_q), 147.4 (C_q), 140.7 (C_q), 130.7 (CH), 129.7 (C_q), 129.4 (CH), 124.5 (C_q), 123.7 (CH), 122.2 (CH), 113.6 (CH), 110.5 (CH), 56.2 (CH_3), 55.1 (CH_3), 31.4 (CH_2), 25.1 (CH_2), 21.9 (CH_2), 13.8 (CH_3).

IR (ATR): $\tilde{\nu}$ = 2932, 1610, 1516, 1471, 1244, 1176, 1122, 1021, 833, 790 cm^{-1}.

m.p.: 60–62 °C.

MS (EI) *m*/*z* (relative intensity): 337 (3) $[M]^+$, 308 (59) $[M–Et]^+$, 294 (40) $[M–Pr]^+$, 278 (13) $[M–Pr–Me]^+$, 266 (100) $[M–Bu–Me]^+$, 251 (61) $[M–Bu–OMe]^+$, 236 (36), 223 (25), 155 (10), 139 (12), 127 (12).

HR-MS (EI): *m*/*z* calcd for $C_{20}H_{23}N_3O_2^+$ $[M]^+$ 337.1785, found 337.1791.

The spectral data are in accordance with those reported in the literature.[92]

4-Butyl-1-(4'-fluoro-3-methoxy-[1,1'-biphenyl]-2-yl)-1*H*-1,2,3-triazole (254ag)

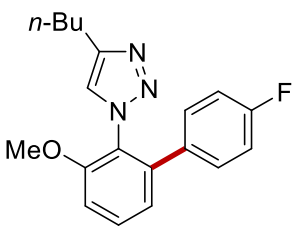

The general procedure **D** was followed using triazole **253a** (116 mg, 0.50 mmol), aryl iodide **84g** (333 mg, 1.50 mmol) and $[Ru(OAc)_2(p\text{-cymene})]$ (35.3 mg, 0.10 mmol, 20 mol %) in DMA (2.0 mL). After 24 h, purification by column chromatography

(*n*-hexane/EtOAc 3:1) yielded **254ag** (93.0 mg, 51%) as a white solid.

^{1}H-NMR (400 MHz, $CDCl_3$): δ = 7.50 (dd, J = 8.1, 8.1 Hz, 1H), 7.08–7.01 (m, 5H), 6.88 (dd, J = 8.7, 8.7 Hz, 2H), 3.80 (s, 3H), 2.66 (t, J = 7.5 Hz, 2H), 1.55 (quint, J = 7.5 Hz, 2H), 1.27–1.16 (m, 2H), 0.86 (t, J = 7.3 Hz, 3H).

^{13}C-NMR (100 MHz, $CDCl_3$): δ = 162.5 (d, $^1J_{C–F}$ = 248 Hz, C_q), 155.3 (C_q), 147.7 (C_q), 140.1 (C_q), 133.5 (d, $^4J_{C–F}$ = 3 Hz, C_q), 131.0 (CH), 130.1 (d, $^3J_{C–F}$ = 8 Hz, CH), 124.7 (C_q), 123.8 (CH), 122.3 (CH), 115.3 (d, $^2J_{C–F}$ = 22 Hz, CH), 111.2 (CH), 56.3 (CH_3), 31.5 (CH_2), 25.2 (CH_2), 22.0 (CH_2), 13.9 (CH_3).

^{19}F-NMR (282 MHz, $CDCl_3$): δ = – 114.4 (s).

IR (ATR): $\tilde{\nu}$ = 2953, 1606, 1512, 1468, 1227, 119, 1045, 838, 792 cm^{-1}.

m.p.: 86–68 °C.

MS (ESI) *m*/*z* (relative intensity): 674 (20) $[2M+Na]^+$, 348 (100) $[M+Na]^+$, 326 (30) $[M+H]^+$.

HR-MS (ESI): *m*/*z* calcd for $C_{19}H_{20}FN_3ONa^+$ $[M+Na]^+$ 348.1483, found 348.1490.

4-Butyl-1-(3,4'-dimethyl-[1,1'-biphenyl]-2-yl)-1*H*-1,2,3-triazole (254bc)

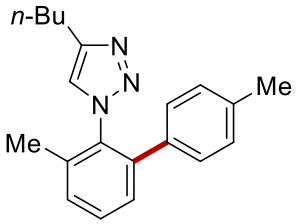

The general procedure **D** was followed using triazole **253b** (108 mg, 0.50 mmol), aryl iodide **84c** (327 mg, 1.50 mmol) and $[Ru(OAc)_2(p\text{-cymene})]$ (35.3 mg, 0.10 mmol, 20 mol %) in DMA (2.0 mL). After 24 h, purification by column chromatography (*n*-hexane/EtOAc 10:1) yielded **254bc** (87.7 mg, 57%) as a pale yellow oil.

^{1}H-NMR (400 MHz, $CDCl_3$): δ = 7.40 (d, J = 7.6, 7.6 Hz, 1H), 7.34–7.26 (m, 2H), 6.98 (d, J = 7.8 Hz, 2H), 6.95–6.88 (m, 3H), 2.62 (t, J = 7.4 Hz, 2H), 2.26 (s, 3H), 2.10 (s, 3H), 1.50 (quint, J = 7.5 Hz, 2H), 1.16 (hept, J = 7.4 Hz, 2H), 0.83 (t, J = 7.3 Hz, 3H).

^{13}C-NMR (100 MHz, $CDCl_3$): δ = 147.7 (C_q), 139.5 (C_q), 137.2 (C_q), 136.1 (C_q), 134.9 (C_q), 129.9 (CH), 129.8 (CH), 128.9 (CH), 128.2 (CH), 128.1 (CH), 123.2 (CH), 31.4 (CH_2), 25.0 (CH_2), 22.5 (CH_2), 21.8 (CH_2), 21.0 (CH_3), 17.7 (CH_3), 13.8 (CH_3).

IR (ATR): $\tilde{\nu}$ = 2933, 1475, 1450, 1373, 1180, 1028, 792, 748, 723 cm^{-1}.

MS (ESI) *m*/*z* (relative intensity): 633 (80) $[2M+Na]^+$, 328 (100) $[M+Na]^+$, 306 (70) $[M+H]^+$.

HR-MS (ESI): *m*/*z* calcd for $C_{20}H_{23}N_3Na^+$ $[M+Na]^+$ 328.1784, found 328.1787.

4-Butyl-1-(4'-methoxy-3-methyl-[1,1'-biphenyl]-2-yl)-1*H*-1,2,3-triazole (254ba)

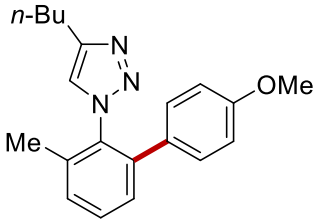

The general procedure **D** was followed using triazole **253b** (108 mg, 0.50 mmol), aryl iodide **84a** (350 mg, 1.50 mmol) and $[Ru(OAc)_2(p\text{-cymene})]$ (35.3 mg, 0.10 mmol, 20 mol %) in DMA (2.0 mL). After 24 h, purification by column chromatography (*n*-hexane/EtOAc 10:1) yielded **254ba** (77.1 mg, 48%) as a pale yellow oil.

^{1}H-NMR (400 MHz, $CDCl_3$): δ = 7.42 (dd, *J* = 7.6, 7.6 Hz, 1H), 7.30 (d, *J* = 7.1 Hz, 2H), 7.04–6.90 (m, 3H), 6.73 (d, *J* = 8.7 Hz, 2H), 3.74 (s, 3H), 2.65 (t, *J* = 7.4 Hz, 2H), 2.12 (s, 3H), 1.54 (q, *J* = 7.4 Hz, 3H), 1.20 (hept, *J* = 7.4 Hz, 3H), 0.85 (t, *J* = 7.3 Hz, 3H).

^{13}C-NMR (100 MHz, $CDCl_3$): δ = 159.1 (C_q), 147.8 (C_q), 139.2 (C_q), 136.1 (C_q), 134.7 (C_q), 130.1 (C_q), 129.8 (CH), 129.7 (CH), 129.4 (CH), 128.2 (CH), 123.1 (CH), 113.7 (CH), 55.1 (CH_3), 31.4 (CH_2), 25.0 (CH_2), 21.8 (CH_2), 17.7 (CH_3), 13.8 (CH_3).

IR (ATR): $\tilde{\nu}$ = 1610, 1515, 1466, 1250, 1178, 1036, 834, 787, 734 cm^{-1}.

MS (ESI) *m*/*z* (relative intensity): 344 (40) $[M+Na]^+$, 322 (100) $[M+H]^+$.

HR-MS (ESI): *m*/*z* calcd for $C_{20}H_{24}N_3O^+$ $[M+H]^+$ 322.1914, found 322.1915.

4-Butyl-1-(3,3'-dimethyl-[1,1'-biphenyl]-2-yl)-1*H*-1,2,3-triazole (254bm)

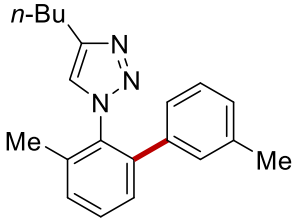

The general procedure **D** was followed using triazole **253b** (108 mg, 0.50 mmol), aryl iodide **84m** (327 mg, 1.50 mmol) and $[Ru(OAc)_2(p\text{-cymene})]$ (35.3 mg, 0.10 mmol, 20 mol %) in DMA (2.0 mL). After 24 h, purification by column chromatography (*n*-hexane/EtOAc 12:1) yielded **254bm** (36.6 mg, 24%) as a pale yellow oil.

^{1}H-NMR (400 MHz, $CDCl_3$): δ = 7.43 (dd, *J* = 7.6, 7.6 Hz, 1H), 7.35–7.29 (m, 2H), 7.08 (dd, *J* = 8.0, 6.8 Hz, 1H), 7.04–6.99 (m, 1H), 6.93 (s, 1H), 6.87–6.82 (m, 2H), 2.63 (t, *J* = 7.4 Hz, 2H), 2.23 (s, 3H), 2.13 (s, 3H), 1.56–1.44 (m, 2H), 1.16 (hept, *J* = 7.3 Hz, 2H), 0.84 (t, *J* = 7.3 Hz, 3H).

^{13}C-NMR (100 MHz, $CDCl_3$): δ = 147.8 (C_q), 139.8 (C_q), 137.9 (C_q), 137.8 (C_q), 136.2 (C_q), 134.8 (C_q), 130.1 (CH), 129.9 (CH), 129.0 (CH), 128.3 (CH), 128.2 (CH), 125.4 (CH), 123.3 (CH), 31.6 (CH_2), 25.1 (CH_2), 21.9 (CH_2), 21.4 (CH_3), 17.9 (CH_3), 13.9 (CH_3).

IR (ATR): $\tilde{\nu}$ = 1467, 1379, 1187, 1038, 987, 777, 753, 704, 414 cm^{-1}.

MS (ESI) *m*/*z* (relative intensity): 633 (10) $[2M+Na]^+$, 328 (100) $[M+Na]^+$, 306 (40) $[M+H]^+$.

HR-MS (ESI): *m*/*z* calcd for $C_{20}H_{23}N_3Na^+$ $[M+Na]^+$ 328.1784, found 328.1787.

4-Butyl-1-(3-methoxy-3'-methyl-[1,1'-biphenyl]-2-yl)-1*H*-1,2,3-triazole (254am)

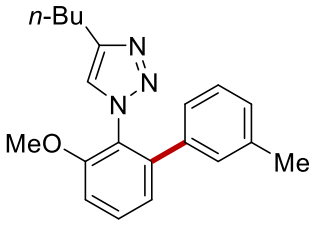

The general procedure **D** was followed using triazole **253a** (116 mg, 0.50 mmol), aryl iodide **84m** (327 mg, 1.50 mmol) and $[Ru(OAc)_2(p\text{-cymene})]$ (35.3 mg, 0.10 mmol, 20 mol %) in DMA (2.0 mL). After 24 h, purification by column chromatography (*n*-hexane/EtOAc 20:1) yielded **254am** (62.6 mg, 39%) as a colourless oil.

^{1}H-NMR (400 MHz, $CDCl_3$): δ = 7.49 (t, *J* = 8.1 Hz, 1H), 7.23–6.94 (m, 5H), 6.87 (dt, *J* = 9.1, 1.7 Hz, 2H), 3.81 (s, 3H), 2.66 (t, *J* = 7.5 Hz, 2H), 2.23 (s, 3H), 1.54 (hept, *J* = 7.4 Hz, 2H), 1.23 (hept, *J* = 7.4 Hz, 2H), 0.86 (t, *J* = 7.4 Hz, 3H).

^{13}C-NMR (100 MHz, $CDCl_3$): δ = 155.3 (C_q), 147.5 (C_q), 141.3 (C_q), 137.9 (C_q), 137.4 (C_q), 130.9 (CH), 129.0 (CH), 128.5 (CH), 128.2 (CH), 125.4 (CH), 124.7 (C_q), 124.0 (CH), 122.4 (CH), 111.0 (CH), 56.4 (CH_3), 31.6 (CH_2), 25.3 (CH_2), 22.0 (CH_2), 21.4 (CH_3), 13.9 (CH_3).

IR (ATR): $\tilde{\nu}$ = 1578, 1469, 1314, 1265, 1120, 1038, 779, 704 cm^{-1}.

MS (ESI) *m*/*z* (relative intensity): 344 (60) $[M+Na]^+$, 322 (100) $[M+H]^+$.

HR-MS (ESI): *m*/*z* calcd for $C_{20}H_{24}N_3O^+$ $[M+H]^+$ 322.1914, found 322.1918.

5-(2-(4-Butyl-1*H*-1,2,3-triazol-1-yl)-3-methoxyphenyl)-1*H*-indole (254ap)

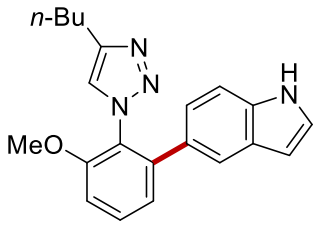

The general procedure **D** was followed using triazole **253a** (116 mg, 0.50 mmol), aryl iodide **84p** (365 mg, 1.50 mmol) and $[Ru(OAc)_2(p\text{-cymene})]$ (35.3 mg, 0.10 mmol, 20 mol %) in DMA (2.0 mL). After 24 h, purification by column chromatography (*n*-hexane/EtOAc 6:1) yielded **254ap** (135 mg, 75%) as a white solid.

^{1}H-NMR (400 MHz, $CDCl_3$): δ = 9.32 (d, J = 6.4 Hz, 1H), 7.52 (dd, J = 8.1, 8.1 Hz, 1H), 7.47–7.43 (m, 1H), 7.25–7.15 (m, 2H), 7.13–6.99 (m, 3H), 6.82 (dd, J = 8.5, 1.7 Hz, 1H), 6.47 (ddd, J = 3.1, 2.0, 0.9 Hz, 1H), 3.82 (s, 3H), 2.62 (t, J = 7.5 Hz, 2H), 1.49 (tt, J = 7.7, 6.5 Hz, 2H), 1.13 (hept, J = 7.4 Hz, 2H), 0.76 (t, J = 7.3 Hz, 3H).

^{13}C-NMR (100 MHz, $CDCl_3$): δ = 155.2 (C_q), 147.4 (C_q), 142.5 (C_q), 135.6 (C_q), 130.8 (CH), 128.8 (C_q), 127.9 (C_q), 125.1 (CH), 124.7 (C_q), 124.2 (CH), 123.1 (CH), 122.1 (CH), 120.5 (CH), 111.1 (CH), 110.2 (CH), 102.3 (CH), 56.3 (CH_3), 31.4 (CH_2), 25.1 (CH_2), 21.9 (CH_2), 13.8 (CH_3).

IR (ATR): $\tilde{\nu}$ = 2930, 1491, 1463, 1264, 1092, 1028, 787, 729, 702 cm^{-1}.

m.p.: 126–128 °C.

MS (ESI) *m*/*z* (relative intensity): 715 (5) $[2M+Na]^+$, 369 (35) $[M+Na]^+$, 347 (100) $[M+H]^+$.

HR-MS (ESI): *m*/*z* calcd for $C_{21}H_{23}N_4O^+$ $[M+H]^+$ 347.1866, found 347.1867.

9-(2'-(4-Butyl-1*H*-1,2,3-triazol-1-yl)-3'-methoxy-[1,1'-biphenyl]-4-yl)-9*H*-carbazole (254aq)

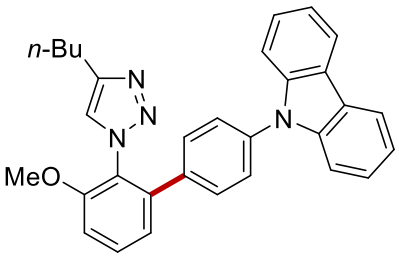

The general procedure **D** was followed using triazole **253a** (116 mg, 0.50 mmol), aryl iodide **84q** (553 mg, 1.50 mmol) and $[Ru(OAc)_2(p\text{-cymene})]$ (35.3 mg, 0.10 mmol, 20 mol %) in DMA (2.0 mL). After 24 h, purification by column chromatography (*n*-hexane/EtOAc 10:1 to 4:1) yielded **254aq** (191 mg, 81%) as a pale yellow solid.

^{1}H-NMR (400 MHz, $CDCl_3$): δ = 8.15 (dq, J = 7.7, 1.0 Hz, 2H), 7.6–7.56 (m, 1H), 7.50–7.27 (m, 10 H), 7.27–7.20 (m, 2H), 7.14 (dd, J = 8.4, 1.2 Hz, 1H), 3.88 (s, 3H), 2.77 (t, J = 7.7 Hz, 2H), 1.74–1.57 (m, 2H), 1.42–1.23 (m, 2H), 0.88 (dd, J = 7.9, 6.8 Hz, 3H).

^{13}C-NMR (100 MHz, $CDCl_3$): δ = 155.4 (C_q), 147.9 (C_q), 140.7 (C_q), 140.3 (C_q), 137.3 (C_q), 136.6 (C_q), 131.2 (CH), 129.9 (CH), 126.8 (CH), 126.1 (CH), 124.8 (C_q), 123.9 (CH), 123.5 (C_q), 122.3 (CH), 120.4 (CH), 120.2 (CH), 111.4 (CH), 109.8 (CH), 56.4 (CH_3), 31.7 (CH_2), 25.3 (CH_2), 22.3 (CH_2), 13.9 (CH_3).

IR (ATR): $\tilde{\nu}$ = 2930, 1519, 1475, 1450, 1315, 1228, 1223, 792, 748, 723 cm^{-1}.

m.p.: 170–172 °C.

MS (ESI) *m*/*z* (relative intensity): 945 (20) $[2M+H]^+$, 495 (40) $[M+Na]^+$, 473 (100) $[M+H]^+$.

HR-MS (ESI): *m*/*z* calcd for $C_{31}H_{29}N_4^+$ $[M+H]^+$ 473.2336, found 473.2339.

1-[2-(Benzo[*d*][1,3]dioxol-5-yl)-6-methoxyphenyl]-4-butyl-1*H*-1,2,3-triazole (254au)

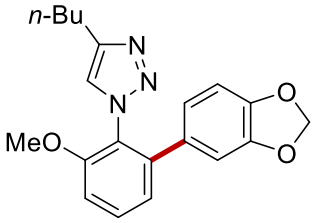

The general procedure **D** was followed using triazole **253a** (116 mg, 0.50 mmol), aryl iodide **84u** (372 mg, 1.50 mmol) and $[Ru(OAc)_2(p\text{-cymene})]$ (35.3 mg, 0.10 mmol, 20 mol %) in DMA (2.0 mL). After 24 h, purification by column chromatography (*n*-hexane/EtOAc 3:1) yielded **254au** (133 mg, 76%) as a white solid.

^{1}H-NMR (400 MHz, $CDCl_3$): δ = 7.46 (dd, *J* = 8.1, 8.1 Hz, 1H), 7.09 (d, *J* = 0.8 Hz, 1H), 7.06–6.99 (m, 2H), 6.63 (d, *J* = 8.7 Hz, 1H), 6.59–6.47 (m, 2H), 5.89 (s, 2H), 3.79 (s, 3H), 2.69 (t, *J* = 7.5 Hz, 2H), 1.68–1.43 (m, 2H), 1.35–1.15 (m, 2H), 0.88 (t, *J* = 7.3 Hz, 3H).

^{13}C-NMR (100 MHz, $CDCl_3$): δ = 155.3 (C_q), 147.6 (C_q), 147.6 (C_q), 147.3 (C_q), 140.8 (C_q), 131.3 (C_q), 130.8 (CH), 124.7 (C_q), 123.9 (CH), 122.4 (CH), 122.1 (CH), 110.9 (CH), 108.8 (CH), 108.2 (CH), 101.2 (CH_2), 56.3 (CH_3), 31.6 (CH_2), 25.3 (CH_2), 22.0 (CH_2), 13.9 (CH_3).

IR (ATR): $\tilde{\nu}$ = 2931, 1580, 1469, 1225, 1091, 1037, 1020, 787 cm^{-1}.

m.p.: 106–108 °C.

MS (ESI) *m*/*z* (relative intensity): 726 (20) $[2M+Na]^+$, 374 (100) $[M+Na]^+$, 352 (35) $[M+H]^+$.

HR-MS (ESI): *m*/*z* calcd for $C_{20}H_{21}N_3O_3Na^+$ $[M+Na]^+$ 374.1475, found 374.1483.

1-[2-(Benzo[*d*][1,3]dioxol-5-yl)-6-methoxyphenyl]-4-propyl-1*H*-1,2,3-triazole (254cu)

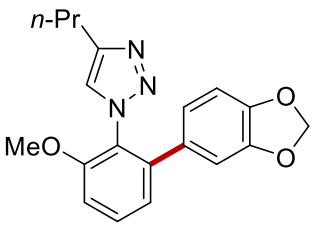

The general procedure **D** was followed using triazole **253c** (109 mg, 0.50 mmol), aryl iodide **84u** (372 mg, 1.50 mmol) and $[Ru(OAc)_2(p\text{-cymene})]$ (35.3 mg, 0.10 mmol, 20 mol %) in DMA (2.0 mL). After 24 h, purification by column chromatography (*n*-hexane/EtOAc 3:1) yielded **254cu** (138 mg, 82%) as a colourless oil.

^{1}H-NMR (400 MHz, $CDCl_3$): δ = 7.40 (dd, J = 8.1, 8.1 Hz, 1H), 7.08 (s, 1H), 7.02–6.85 (m, 2H), 6.57 (dd, J = 8.5, 0.8 Hz, 1H), 6.54–6.42 (m, 2H), 5.80 (s, 2H), 3.72 (s, 3H), 2.61 (t, J = 7.4 Hz, 2H), 1.58 (hept, J = 7.4 Hz, 2H), 0.80 (t, J = 7.4 Hz, 3H).

^{13}C-NMR (100 MHz, $CDCl_3$): δ = 155.0 (C_q), 147.4 (C_q), 147.1 (C_q), 147.1 (C_q), 140.5 (C_q), 131.1 (C_q), 130.7 (CH), 124.4 (C_q), 123.9 (CH), 122.2 (CH), 121.9 (CH), 110.8 (CH), 108.6 (CH), 108.0 (CH), 101.0 (CH_2), 56.1 (CH_3), 27.3 (CH_2), 22.5 (CH_2), 13.3 (CH_3).

IR (ATR): $\tilde{\nu}$ = 1471, 1264, 1228, 1094, 1040, 790, 728, 701 cm^{-1}.

MS (ESI) *m*/*z* (relative intensity): 697 (100) $[2M+Na]^+$, 360 (78) $[M+Na]^+$, 338 (16) $[M+H]^+$.

HR-MS (ESI): *m*/*z* calcd for $C_{19}H_{19}N_3O_3Na^+$ $[M+Na]^+$ 360.1319, found 360.1322.

1-[2-(Benzo[*d*][1,3]dioxol-5-yl)-6-methoxyphenyl]-4-hexyl-1*H*-1,2,3-triazole (254du)

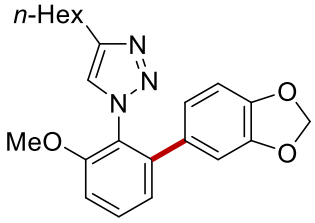

The general procedure **D** was followed using triazole **253d** (129 mg, 0.50 mmol), aryl iodide **84u** (372 mg, 1.50 mmol) and $[Ru(OAc)_2(p\text{-cymene})]$ (35.3 mg, 0.10 mmol, 20 mol %) in DMA (2.0 mL). After 24 h, purification by column chromatography (*n*-hexane/EtOAc 4:1) yielded **254du** (138 mg, 73%) as a colourless oil.

^{1}H-NMR (400 MHz, $CDCl_3$): δ = 7.46 (dd, J = 8.1, 8.1 Hz, 1H), 7.10 (s, 1H), 7.03 (ddd, J = 8.4, 8.1, 1.2 Hz, 2H), 6.63 (d, J = 8.0 Hz, 1H), 6.60–6.47 (m, 2H), 5.88 (s, 2H), 3.79 (s, 3H), 2.68 (t, J = 7.5 Hz, 2H), 1.59 (hept, J = 7.3 Hz, 2H), 1.25 (hept, J = 4.5 Hz, 8H), 0.94–0.77 (m, 3H).

^{13}C-NMR (100 MHz, $CDCl_3$): δ =155.3 (C_q), 147.6 (C_q), 147.6 (C_q), 147.3 (C_q), 140.7 (C_q), 131.3 (CH), 130.8 (C_q), 124.6 (CH), 123.9 (C_q), 122.4 (CH), 122.1 (CH), 110.9 (CH), 108.8 (CH), 108.2 (CH), 101.2 (CH_2), 56.3 (CH_3), 31.7 (CH_2), 29.4 (CH_2), 28.7 (CH_2), 25.6 (CH_2), 22.6 (CH_2), 14.2 (CH_3).

IR (ATR): $\tilde{\nu}$ = 1580, 1443, 1266, 1226, 1093, 1038, 1021, 917, 788 cm^{-1}.

MS (ESI) *m*/*z* (relative intensity): 781 (46) $[2M+Na]^+$, 402 (100) $[M+Na]^+$.

HR-MS (ESI): *m*/*z* calcd for $C_{22}H_{25}N_3O_3Na^+$ $[M+Na]^+$ 402.1788, found 402.1791.

4-Butyl-1-(3,3',4'-trimethoxy-[1,1'-biphenyl]-2-yl)-1*H*-1,2,3-triazole (254av)

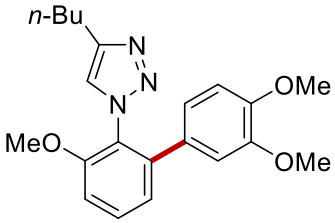

The general procedure **D** was followed using triazole **253a** (116 mg, 0.50 mmol), aryl iodide **84v** (396 mg, 1.50 mmol) and [Ru(OAc)$_2$(*p*-cymene)] (35.3 mg, 0.10 mmol, 20 mol %) in DMA (2.0 mL). After 24 h, purification by column chromatography (*n*-hexane/EtOAc 4:1 to 2:1) yielded **254av** (147 mg, 76%) as a pale brown solid.

^{1}H-NMR (400 MHz, $CDCl_3$): δ = 7.47 (dd, J = 8.1, 8.1 Hz, 1H), 7.08 (dd, J = 7.8, 1.2 Hz, 1H), 7.03–6.98 (m, 2H), 6.73 (d, J = 1.4 Hz, 2H), 6.49 (t, J = 1.1 Hz, 1H), 3.81 (s, 3H), 3.79 (s, 3H), 3.65 (s, 3H), 2.64 (t, J = 7.6 Hz, 2H), 1.63–1.42 (m, 2H), 1.29–1.11 (m, 2H), 0.84 (t, J = 7.4 Hz, 3H).

^{13}C-NMR (100 MHz, $CDCl_3$): δ = 155.4 (C_q), 148.7 (C_q), 148.6 (C_q), 147.7 (C_q), 140.7 (C_q), 130.9 (CH), 130.0 (C_q), 124.5 (C_q), 123.8 (CH), 122.1 (CH), 120.8 (CH), 111.2 (CH), 110.9 (CH), 110.7 (CH), 56.3 (CH_3), 55.8 (CH_3), 55.8 (CH_3), 31.5 (CH_2), 25.2 (CH_2), 22.1 (CH_2), 13.8 (CH_3).

IR (ATR): $\tilde{\nu}$ = 2934, 1519, 1475, 1266, 1249, 1118, 1026, 907, 724 cm^{-1}.

m.p.: 103–105 °C.

MS (ESI) *m*/*z* (relative intensity): 757 (10) $[2M+Na]^+$, 390 (100) $[M+Na]^+$, 368 (98) $[M+H]^+$.

HR-MS (ESI): *m*/*z* calcd for $C_{21}H_{25}N_3O_3Na^+$ $[M+Na]^+$ 390.1788, found 390.1792.

(*Z*)-2-[2-(4-Methoxyphenyl)-2-phenylvinyl]pyridine (256aa)

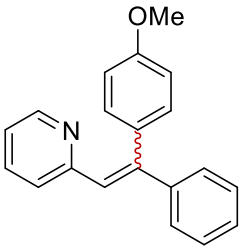

The general procedure **D** was followed using (*E*)-2-styrylpyridine **255a** (90.5 mg, 0.50 mmol), aryl iodide **84a** (175 mg, 0.75 mmol) and Na_2CO_3 (106 mg, 1.00 mmol) in a mixture of DMA and 1,4-dioxane (3:1, 1.5 mL). After 24 h, purification by column chromatography (*n*-hexane/EtOAc 7:1) yielded **256aa** (114 mg, 79%) as a colourless oil in a ratio of *E*/*Z* = 1:4.0.

The general procedure **E** was followed using (*E*)-2-styrylpyridine **255a** (90.5 mg, 0.50 mmol), aryl iodide **84a** (175 mg, 0.75 mmol) and Na_2CO_3 (106 mg, 1.00 mmol) in a mixture of DMA and 1,4-dioxane (3:1, 1.5 mL) stirred at 120 °C. After 24 h, purification by column chromatography (*n*-hexane/EtOAc 7:1) yielded **256aa** (116 mg, 81%) as a colourless oil in a ratio of *E*/*Z* = 1:5.5.

^{1}H-NMR (400 MHz, $CDCl_3$): δ = 8.67–8.53 (m, 1H), 7.47–7.40 (m, 2H), 7.40–7.30 (m, 4H), 7.17 (dd, *J* = 6.9, 1.9 Hz, 3H), 7.01 (ddd, *J* = 7.5, 4.9, 1.1 Hz, 1H), 6.95–6.88 (m, 2H), 6.82 (dt, *J* = 8.2, 1.2 Hz, 1H), 3.86 (d, *J* = 0.6 Hz, 3H).

^{13}C-NMR (100 MHz, $CDCl_3$): δ = 159.3 (C_q), 156.9 (C_q), 149.3 (CH), 145.6 (C_q), 143.0 (C_q), 135.3 (CH), 132.1 (C_q), 131.5 (CH), 128.4 (CH), 128.2 (CH), 128.1 (CH), 127.9 (CH), 123.7 (CH), 121.1 (CH), 114.2 (CH), 55.2 (CH_3).

IR (ATR): $\tilde{\nu}$ = 3055, 1606, 1508, 1460, 1243, 1031, 834, 768, 727, 514 cm^{-1}.

MS (ESI) *m*/*z* (relative intensity): 311 (28) [M+Na], 288 (100) [M+H].

HR-MS (ESI): *m*/*z* calcd for $C_{20}H_{18}NO^+$ $[M+H]^+$ 288.1383, found 288.1386.

The spectral data are in accordance with those reported in the literature.[280]

(*Z*)-2-{2-[4-(*tert*-Butyl)phenyl]-2-phenylvinyl}pyridine (256ba)

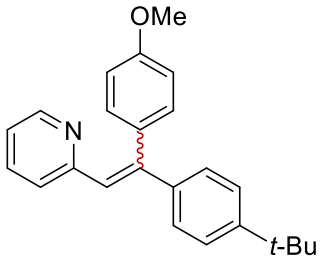

The general procedure **D** was followed using (*E*)-2-styrylpyridine **255b** (119 mg, 0.50 mmol), aryl iodide **84a** (175 mg, 0.75 mmol) and Na_2CO_3 (106 mg, 1.00 mmol) in a mixture of DMA and 1,4-dioxane (3:1, 1.5 mL). After 24 h, purification by column chromatography (*n*-hexane/EtOAc 8:1) yielded **256ba** (68.7 mg, 40%) as a colourless oil in a ratio of *E*/*Z* = 1:5.9.

^{1}H-NMR (400 MHz, $CDCl_3$): δ = 8.59–8.53 (m, 1H), 7.38–7.27 (m, 5H), 7.18–7.09 (m, 3H), 7.03–6.85 (m, 3H), 6.75 (d, *J* = 8.1 Hz, 1H), 3.87 (s, 3H), 1.35 (s, 9H).

^{13}C-NMR (100 MHz, $CDCl_3$): δ = 159.3 (C_q), 157.1 (C_q), 151.2 (C_q), 149.3 (CH), 145.4 (C_q), 139.9 (C_q), 135.4 (CH), 132.3 (C_q), 131.5 (CH), 127.6 (CH), 125.2 (CH), 123.8 (CH), 121.0 (CH), 114.2 (CH), 55.3 (CH_3), 34.7 (C_q), 31.4 (CH_3).

IR (ATR): $\tilde{\nu}$ = 2959, 1606, 1580, 1508, 1461, 1432, 1241, 1028, 830, 738, 577, 405 cm^{-1}.

MS (ESI) *m*/*z* (relative intensity): 366 (20) [M+Na], 344 (100) [M+H].

HR-MS (ESI): *m*/*z* calcd for $C_{24}H_{26}NO^+$ $[M+H]^+$ 344.2009, found 344.2011.

2-[(3*E*)-2-(4-Methoxyphenyl)-4-phenylbuta-1,3-dien-1-yl]pyridine (256ca)

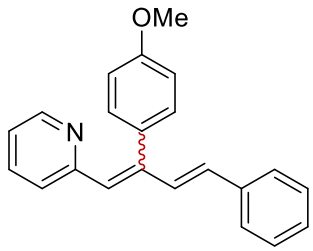

The general procedure **D** was followed using (*E*)-2-styrylpyridine **255c** (119 mg, 0.50 mmol), aryl iodide **84a** (175 mg, 0.75 mmol) and Na_2CO_3 (106 mg, 1.00 mmol) in a mixture of DMA and 1,4-dioxane (3:1, 1.5 mL). After 24 h, purification by column chromatography (*n*-hexane/EtOAc 9:1) yielded **256ca** (75.2 mg, 48%) as a colourless oil in a ratio of *E*/*Z* = 1:2.0.

^{1}H-NMR (400 MHz, $CDCl_3$): δ = 8.67–8.44 (m, 1H), 7.61–7.13 (m, 9H), 7.07–6.81 (m, 4H), 6.62–6.51 (m, 1H), 6.30 (d, *J* = 15.9 Hz, 1H), 3.90 (s, 3H).

^{13}C-NMR (100 MHz, $CDCl_3$): δ = 159.3 (C_q), 156.2 (C_q), 149.4 (C_q), 144.6 (C_q), 137.2 (C_q), 135.4 (CH), 134.1 (CH), 133.2 (CH), 132.7 (CH), 130.7 (CH), 130.6 (CH), 128.7 (CH), 128.7 (CH), 127.9 (CH), 127.1 (CH), 126.8 (CH), 125.3 (CH), 123.6 (CH), 121.2 (CH), 114.6 (CH), 113.7 (CH), 55.4 (CH_3).

IR (ATR): $\tilde{\nu}$ = 1603, 1511, 1246, 1245, 1180, 1031, 832, 696 cm^{-1}.

MS (ESI) *m*/*z* (relative intensity): 312 (100) $[M+H]^+$.

HR-MS (ESI): *m*/*z* calcd for $C_{22}H_{20}NO^+$ $[M+H]^+$ 312.1384, found 312.1383.

5.5.2 Comparision to Thermal Reaction Conditions

2-(3'-Bromo-3-methyl-[1,1'-biphenyl]-2-yl)pyridine (243ay)

2,2'-(3,3''-Dimethyl-[1,1':3',1''-terphenyl]-2,2''-diyl)dipyridine (244ab)

The general procedure **D** was followed using pyridine **44a** (186 mg, 1.10 mmol), aryl iodide **84y** (141 mg, 0.50 mmol) and K_2CO_3 (276 mg, 2.00 mmol). After 24 h, purification by column chromatography (*n*-hexane/EtOAc 7:1) yielded **243ay** (122 mg, 76%) as a colorless oil.

The general procedure **E** was followed using pyridine **44a** (186 mg, 1.10 mmol), aryl iodide **84y** (141 mg, 0.50 mmol) and K_2CO_3 (276 mg, 2.00 mmol). After 24 h, purification by column chromatography (*n*-hexane/EtOAc 7:1 to 3:1) yielded **243ay** (12 mg, 7%) as a colorless oil and **244ab** (159 mg, 77%) as a green solid.

2-(3'-Bromo-3-methyl-[1,1'-biphenyl]-2-yl)pyridine (243ay)

The NMR spectra show a small impurity (<5%) caused by the starting material **44a**.

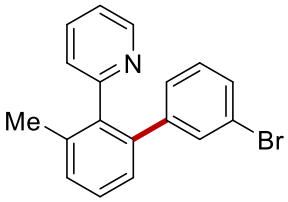

^{1}H-NMR (300 MHz, $CDCl_3$): δ = 8.63 (ddd, *J* = 4.9, 1.9, 1.1 Hz, 1H), 7.48 (ddd, *J* = 7.8, 7.7, 1.9 Hz, 1H), 7.36 (dd, *J* = 7.5, 7.3 Hz, 1H), 7.33–7.27 (m, 2H), 7.27–7.21 (m, 2H), 7.11 (ddd, *J* = 7.7, 4.9, 1.2 Hz, 1H), 6.98–6.95 (m, 2H), 6.91 (ddd, *J* = 7.8, 1.2, 1.1 Hz, 1H), 2.19 (s, 3H).

^{13}C-NMR (100 MHz, $CDCl_3$): δ = 159.2 (C_q), 149.1 (CH), 143.8 (C_q), 139.8 (C_q), 139.4 (C_q), 136.9 (C_q), 135.9 (CH), 132.6 (CH), 130.0 (CH), 129.4 (CH), 129.1 (CH), 128.4 (CH), 128.2 (CH), 127.5 (CH), 125.6 (CH), 121.8 (C_q), 121.6 (CH), 20.5 (CH_3).

IR (ATR): $\tilde{\nu}$ = 1585, 1561, 1456, 1424, 1068, 1025, 775, 747, 694, 665 cm^{-1}.

MS (ESI) *m*/*z* (relative intensity): 348 (19) $[M(^{81}Br)+Na]^+$, 346 (19) $[M(^{79}Br)+Na]^+$, 326 (98) $[M(^{81}Br)+H]^+$, 324 (100) $[M(^{79}Br)+H]^+$.

HR-MS (ESI): *m*/*z* calcd for $C_{18}H_{15}{}^{79}BrN^+$ $[M+H]^+$ 324.0382, found 324.0387.

2,2'-(3,3''-Dimethyl-[1,1':3',1''-terphenyl]-2,2''-diyl)dipyridine (244ab)

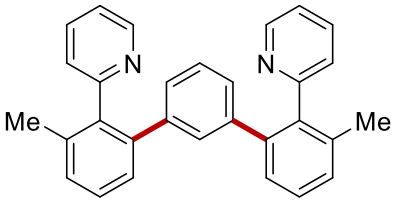

^{1}H-NMR (400 MHz, $CDCl_3$): δ = 8.64 (ddd, *J* = 4.9, 1.8, 1.0 Hz, 2H), 7.43 (ddd, *J* = 7.8, 7.6, 1.8 Hz, 2H), 7.29 (dd, *J* = 7.5, 7.4 Hz, 2H), 7.27–7.23 (m, 2H), 7.11 (ddd, *J* = 7.6, 4.9, 1.2 Hz, 2H), 7.03 (dd, *J* = 7.4, 1.6 Hz, 2H), 7.00 (t, *J* = 1.8 Hz, 1H), 6.81 (dd, *J* = 8.7, 6.2 Hz, 1H), 6.75 (dd, *J* = 6.8, 1.8 Hz, 2H), 6.72 (ddd, *J* = 7.8, 1.2, 1.0 Hz, 2H), 2.16 (s, 6H).

^{13}C-NMR (100 MHz, $CDCl_3$): δ = 159.8 (C_q), 148.9 (CH), 141.2 (C_q), 141.1 (C_q), 139.3 (C_q), 136.7 (C_q), 135.6 (CH), 131.0 (CH), 129.4 (CH), 128.0 (CH), 127.8 (CH), 127.7 (CH), 126.8 (CH), 125.8 (CH), 121.3 (CH), 20.5 (CH_3).

IR (ATR): $\tilde{\nu}$ = 1584, 1455, 1417, 1148, 1024, 987, 780, 744, 711 cm^{-1}.

m.p.: 129–130 °C.

MS (ESI) *m*/*z* (relative intensity): 825 (2) $[2M+H]^+$, 435 (11) $[M+Na]^+$, 413 (100) $[M+H]^+$.

HR-MS (ESI): *m*/*z* calcd for $C_{30}H_{25}N_2^+$ $[M+H]^+$ 413.2012, found 413.2018.

1-[2-(4-Bromo-3-methylphenyl)naphthalen-1-yl]-1*H*-pyrazole (258az)

1-[2-(*m*-Tolyl)naphthalen-1-yl]-1*H*-pyrazole (258az–Br)

The general procedure **D** was followed using pyrazole **257a** (97 mg, 0.50 mmol), aryl iodide **84z** (220 mg, 0.75 mmol) and K_2CO_3 (138 mg, 1.00 mmol) in 1,4-dioxane (1.0 mL). After 24 h, purification by column chromatography (*n*-hexane/EtOAc 20:1 to 10:1) yielded **258az** (125 mg, 69%) as a white solid.

The general procedure **E** was followed using pyrazole **257a** (97 mg, 0.50 mmol), aryl iodide **84z** (220 mg, 0.75 mmol) and K_2CO_3 (138 mg, 1.00 mmol) in 1,4-dioxane (1.0 mL). After 24 h, purification by column chromatography (*n*-hexane/EtOAc 20:1 to 10:1) yielded **258az–Br** (108 mg, 76%) as a colorless oil.

1-[2-(4-Bromo-3-methylphenyl)naphthalen-1-yl]-1*H*-pyrazole (258az)

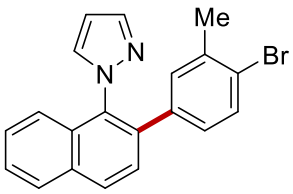

^{1}H-NMR (400 MHz, $CDCl_3$): δ = 8.00 (d, J = 8.5 Hz, 1H), 7.93 (dd, J = 7.7, 1.9 Hz, 1H), 7.80 (dd, J = 2.1, 0.8 Hz, 1H), 7.59 (d, J = 8.5 Hz, 1H), 7.57–7.48 (m, 2H), 7.44–7.38 (m, 2H), 7.27 (dd, J = 2.3, 0.8 Hz, 1H), 7.08 (d, J = 1.9 Hz, 1H), 6.87 (dd, J = 8.2, 2.3 Hz, 1H), 6.35 (dd, J = 2.3, 2.1 Hz, 1H), 2.33 (s, 3H).

^{13}C-NMR (100 MHz, $CDCl_3$): δ = 140.3 (CH), 137.9 (C_q), 137.8 (C_q), 135.8 (C_q), 134.4 (C_q), 133.5 (C_q), 132.9 (CH), 132.2 (CH), 131.5 (C_q), 131.1 (CH), 129.7 (CH), 127.9 (CH), 127.8 (CH), 127.6 (CH), 127.4 (CH), 126.9 (CH), 124.5 (C_q), 123.7 (CH), 106.6 (CH), 23.0 (CH_3).

IR (ATR): $\tilde{\nu}$ = 1597, 1484, 1400, 1193, 1094, 1025, 824, 768, 751 cm^{-1}.

m.p.: 121–123 °C.

MS (ESI) *m*/*z* (relative intensity): 751 (30) [2M(^{81}Br^{81}Br)+Na]$^+$, 749 (60) [2M(^{81}Br^{79}Br)+Na]$^+$, 747 (30) [2M(^{79}Br^{79}Br)+Na]$^+$, 387 (98) [M(^{81}Br)+Na]$^+$, 385 (100) [M(^{79}Br)+Na]$^+$, 365 (96) [M(^{81}Br)+H]$^+$, 363 (96) [M(^{79}Br)+H]$^+$.

HR-MS (ESI): *m*/*z* calcd for $C_{20}H_{15}{}^{79}BrN_2Na^+$ [M+Na]$^+$ 385.0311, found 385.0311.

1-[2-(*m*-Tolyl)naphthalen-1-yl]-1*H*-pyrazole (258az–Br)

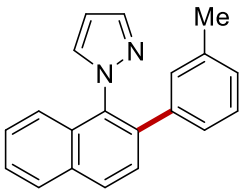

^{1}H-NMR (400 MHz, $CDCl_3$): δ = 8.01 (d, J = 8.7 Hz, 1H), 7.93 (d, J = 8.6 Hz, 1H), 7.79 (d, J = 2.3 Hz, 1H), 7.64 (d, J = 8.7 Hz, 1H), 7.57–7.47 (m, 2H), 7.43 (d, J = 7.7 Hz, 1H), 7.26 (d, J = 2.4 Hz, 1H), 7.17 (dd, J = 7.7, 7.7 Hz, 1H), 7.08 (d, J = 7.7 Hz, 1H), 7.05–6.97 (m, 2H), 6.32 (dd, J = 2.4, 2.3 Hz, 1H), 2.30 (s, 3H).

^{13}C-NMR (100 MHz, $CDCl_3$): δ = 140.2 (CH), 138.6 (C_q), 138.0 (C_q), 137.0 (C_q), 134.4 (C_q), 133.5 (C_q), 132.9 (CH), 131.5 (C_q), 129.5 (CH), 129.5 (CH), 128.3 (CH), 128.2 (CH), 127.9 (CH), 127.8 (CH), 127.7 (CH), 126.7 (CH), 125.8 (CH), 123.8 (CH), 106.4 (CH), 21.5 (CH_3).

IR (ATR): $\tilde{\nu}$ = 2922, 1599, 1514, 1397, 1089, 1042, 916, 780, 746, 705 cm^{-1}.

MS (ESI) *m*/*z* (relative intensity): 591 (5) [2M+Na]$^+$, 307 (69) [M+Na]$^+$, 285 (100) [M+H]$^+$.

HR-MS (ESI): *m*/*z* calcd for $C_{20}H_{17}N_2^+$ [M+H]$^+$ 285.1386, found 285.1389.

5.5.3 *H/D Scrambling Experiments*

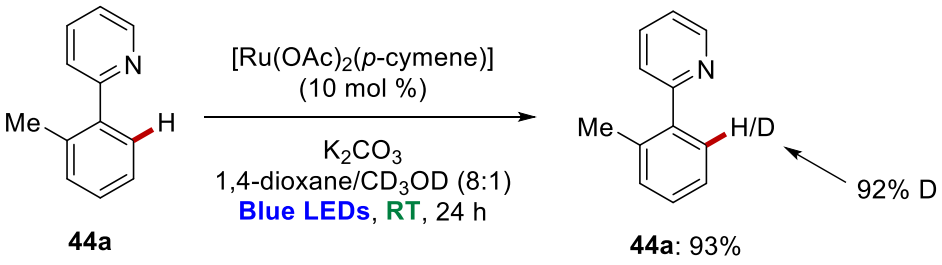

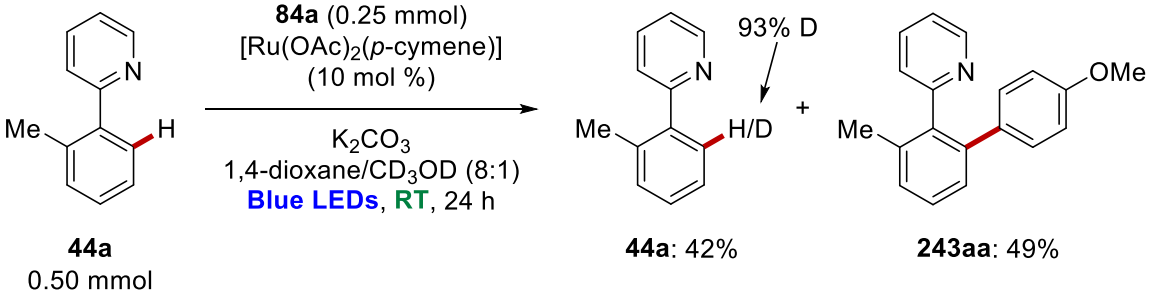

Pyridine **44a** (85.1 mg, 0.50 mmol), [Ru(OAc)$_2$(*p*-cymene)] (17.7 mg, 50.0 µmol, 10 mol %) and K_2CO_3 (138 mg, 1.00 mmol) were placed in a 10 mL vial. The vial was capped with a septum and wrapped with parafilm, before the vial was evacuated and purged with N_2 three times. Aryl iodide **84a** (58.3 mg, 0.25 mmol), CD_3OD (0.2 mL) and 1,4-dioxane (1.6 mL) were added and the mixture was stirred under visible light irradiation (2 × Kessil A360N, temperature was maintained between 30 °C and 33 °C). After 24 h, the resulting mixture was filtered through a pad of silica gel and washed with EtOAc. Afterwards, the solvent was removed under reduced pressure. Purification by column chromatography (*n*-hexane/EtOAc 10:1) yielded **44a** (35.3 mg, 42%) and **243aa** (64.0 mg, 49%). The degree of deuteration was determined to be 93% D by employing ^{1}H-NMR spectroscopy.

By performing the H/D scrambling experiments in the absence of aryl halide **84a**, the reisolated starting material **44a** exhibited a deuteration degree of 92% as determined by ^{1}H-NMR spectroscopy.

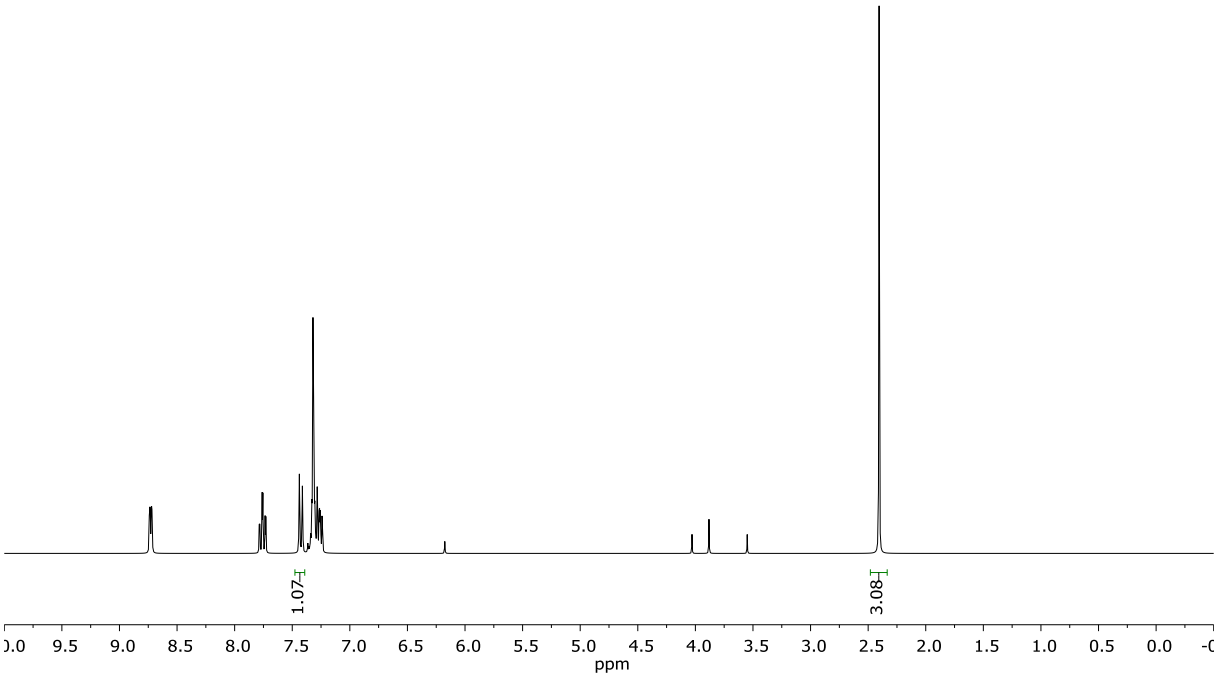

Figure 5.3: ^{1}H-NMR spectrum of deuterated starting material in presence of aryl iodide **84a**.

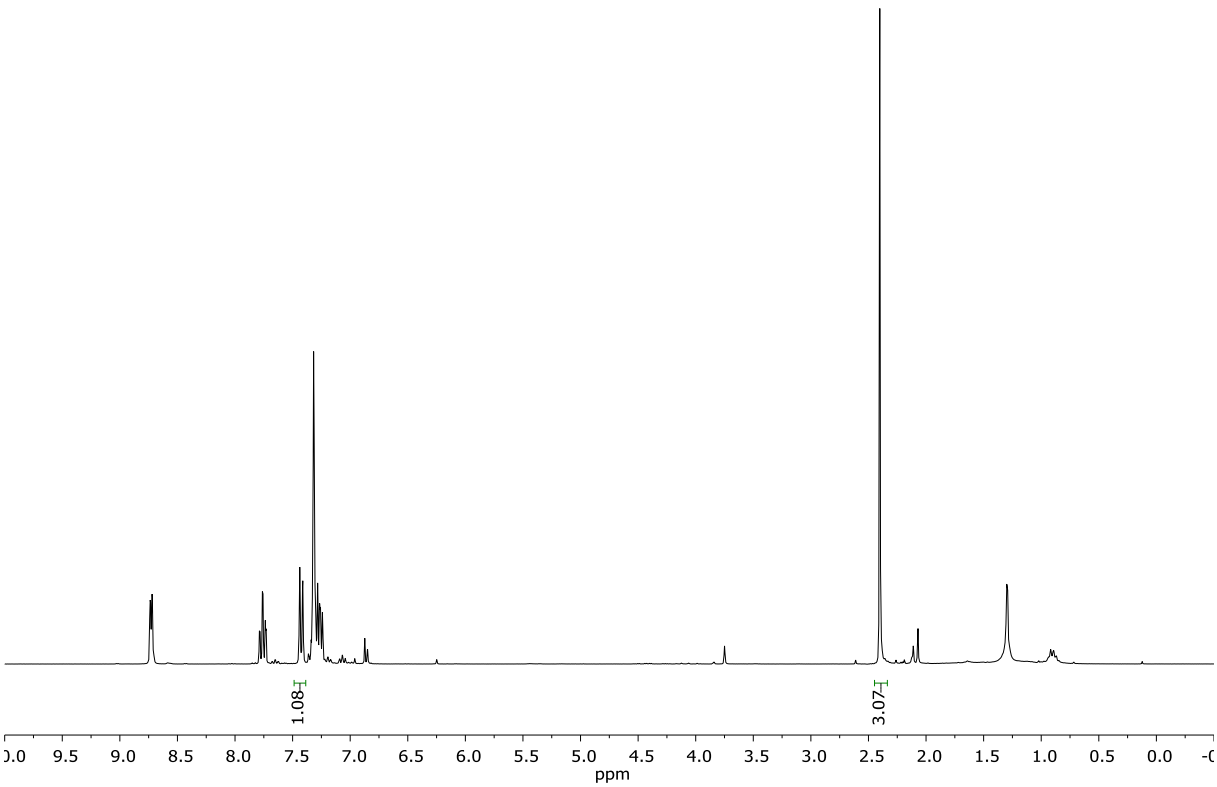

Figure 5.4: ^{1}H-NMR spectrum of deuterated starting material in absence of aryl iodide **84a**.

5.5.4 Competition Experiments

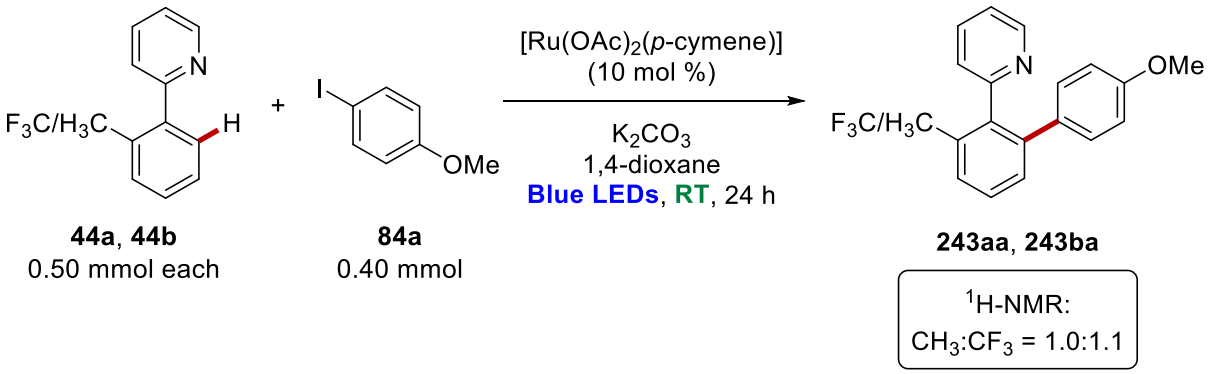

Pyridines **44a** (85.1 mg, 0.50 mmol), **44b** (111 mg, 0.50 mmol), [Ru(OAc)$_2$(*p*-cymene)] (17.7 mg, 50.0 µmol, 10 mol %) and K_2CO_3 (138 mg, 1.00 mmol) were placed in a 10 mL vial. The vial was capped with a septum and wrapped with parafilm. The vial was evacuated and purged with N_2 three times. Aryl iodide **84a** (93.2 mg, 0.40 mmol) and 1,4-dioxane (2.0 mL) were added and the mixture was stirred under visible light irradiation (2 × Kessil A360N, temperature was maintained between 30 °C and 33 °C). After 24 h, the resulting mixture was filtered through a pad of silica gel and washed with EtOAc. The filtrate was concentrated *in vacuo*. The crude mixture was analyzed by ^{1}H-NMR spectroscopy using 1,3,5-trimethoxybenzene (84.1 mg, 0.50 mmol) as internal standard.

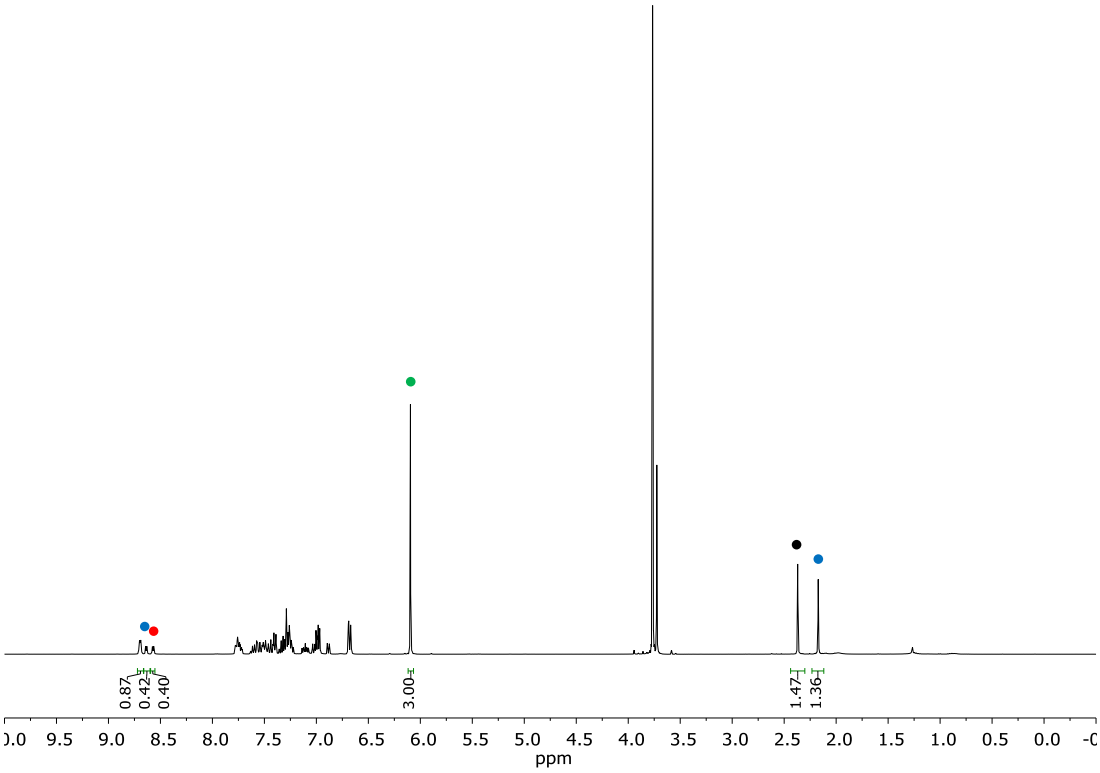

Figure 5.5: ^{1}H-NMR spectrum of competition experiment between **44a** and **44b**. • = **44a** (Me), • = **243aa** (Me), • = **243ba** (CF_3), • = internal standard.

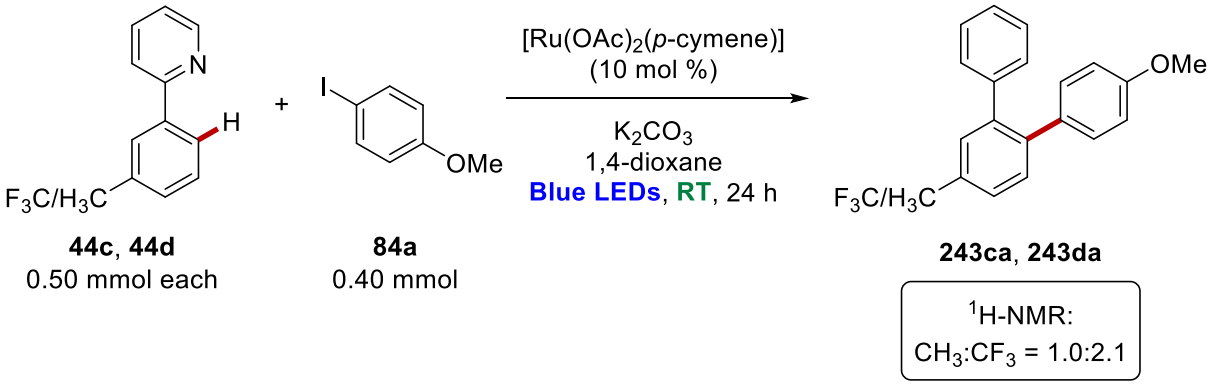

Pyridines **44c** (85.1 mg, 0.50 mmol), **44d** (111 mg, 0.50 mmol), [Ru(OAc)$_2$(*p*-cymene)] (17.7 mg, 50.0 µmol, 10 mol %) and K_2CO_3 (138 mg, 1.00 mmol) were placed in a 10 mL vial. The vial was capped with a septum and wrapped with parafilm. The vial was evacuated and purged with N_2 three times. Aryl iodide **84a** (93.2 mg, 0.40 mmol) and 1,4-dioxane (2.0 mL) were added and the mixture was stirred under visible light irradiation (2 × Kessil A360N, temperature was maintained between 30 °C and 33 °C). After 24 h, the resulting mixture was filtered through a pad of silica gel and washed with EtOAc. The filtrate was concentrated *in vacuo*. The crude mixture was analyzed by ^{1}H-NMR spectroscopy using

1,3,5-trimethoxybenzene (84.1 mg, 0.50 mmol) as internal standard. Purification by column chromatography (*n*-hexane/EtOAc 10:1) and followed by recycling preparative HPLC yielded **243ca** (30.1 mg, 28%) as a viscous colorless oil and **243da** (73.9 mg, 59%) as a viscous colorless oil.

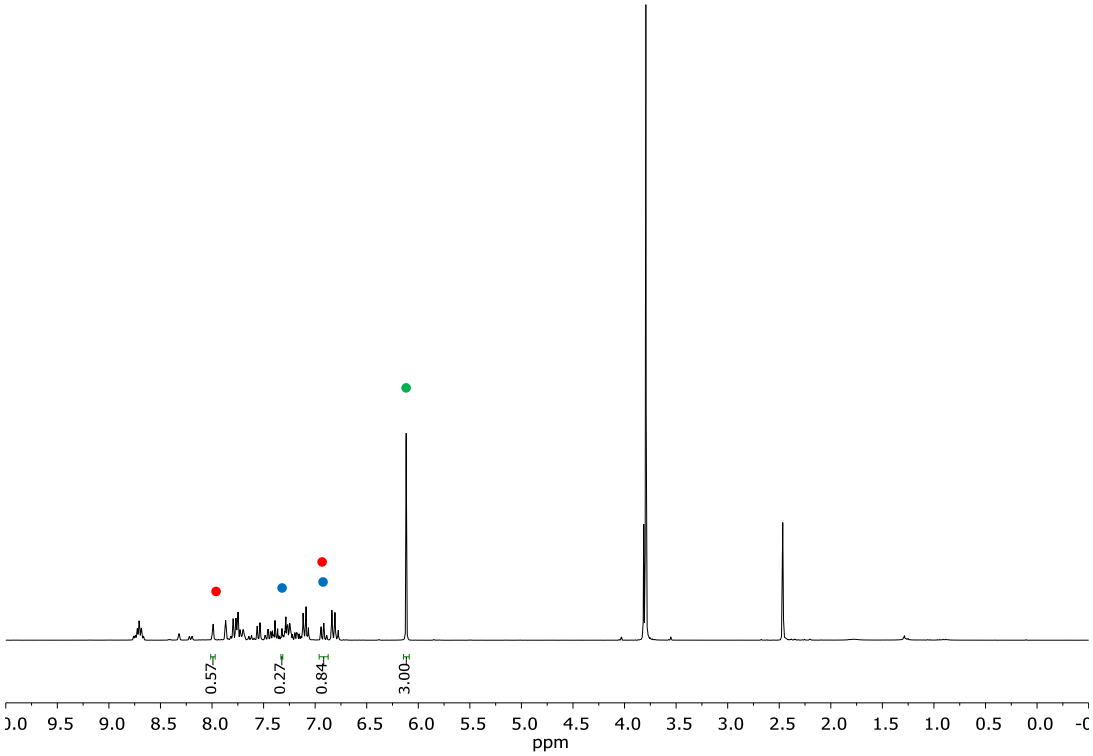

Figure 5.6: ^{1}H-NMR spectrum of competition experiment between **44c** and **44d**. • = **243ca** (Me), • = **243da** (CF_3), • = internal standard.

2-{4'-Methoxy-3-(trifluoromethyl)-[1,1'-biphenyl]-2-yl}pyridine (243ba)

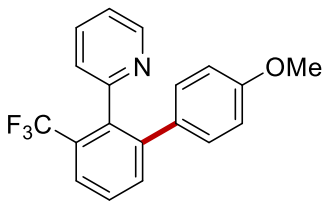

^{1}H-NMR (400 MHz, $CDCl_3$): δ = 8.57 (ddd, J = 4.9, 1.8, 1.1 Hz, 1H), 7.78–7.74 (m, 1H), 7.60–7.52 (m, 2H), 7.49 (ddd, J = 7.8, 7.7, 1.8 Hz, 1H), 7.12 (ddd, J = 7.7, 4.9, 1.2 Hz, 1H), 7.02 (ddd, J = 7.8, 1.2, 1.1 Hz, 1H), 6.97 (d, J = 8.9 Hz, 2H), 6.68 (d, J = 8.9 Hz, 2H), 3.73 (s, 3H).

^{13}C-NMR (100 MHz, $CDCl_3$): δ = 158.4 (C_q), 156.8 (C_q), 148.4 (CH), 142.9 (C_q), 138.3 (q, $^{3}J_{C–F}$ = 2 Hz, C_q), 135.3 (CH), 133.6 (CH), 132.4 (C_q), 130.7 (CH), 129.2 (q, $^{2}J_{C–F}$ = 30 Hz, C_q), 128.2 (CH), 125.6 (q, $^{5}J_{C–F}$ = 2 Hz, CH), 124.9 (q, $^{3}J_{C–F}$ = 5 Hz, CH), 124.0 (q, $^{1}J_{C–F}$ = 274 Hz, C_q), 122.0 (CH), 113.2 (CH), 55.1 (CH_3).

^{19}F-NMR (376 MHz, $CDCl_3$): δ = – 57.1 (s).

IR (ATR): $\tilde{\nu}$ = 2934, 1609, 1517, 1445, 1323, 1247, 1166, 1119, 1025, 748 cm^{-1}.

m.p.: 83–85 °C.

MS (ESI) *m*/*z* (relative intensity): 681 (3) $[2M+Na]^+$, 352 (22) $[M+Na]^+$, 330 (100) $[M+H]^+$.

HR-MS (ESI): *m*/*z* calcd for $C_{19}H_{15}F_3NO^+$ $[M+H]^+$ 330.1100, found 330.1114.

The spectral data are in accordance with those reported in the literature.[82]

2-(4'-Methoxy-4-methyl-[1,1'-biphenyl]-2-yl)pyridine (243ca)

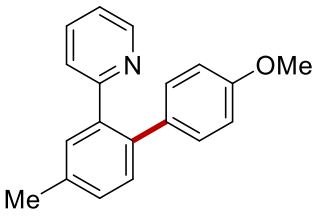

^{1}H-NMR (300 MHz, $CDCl_3$): δ = 8.65 (dt, *J* = 5.1, 1.2 Hz, 1H), 7.55–7.47 (m, 1H), 7.38 (td, *J* = 7.7, 1.8 Hz, 1H), 7.34–7.22 (m, 2H), 7.15–6.97 (m, 3H), 6.88 (d, *J* = 8.0 Hz, 1H), 6.84–6.70 (m, 2H), 3.78 (s, 3H), 2.44 (s, 3H).

^{13}C-NMR (75 MHz, $CDCl_3$): δ = 159.7 (C_q), 158.5 (C_q), 149.5 (CH), 139.2 (C_q), 137.5 (C_q), 137.1 (C_q), 135.3 (CH), 133.8 (C_q), 131.2 (CH), 130.9 (CH), 130.5 (CH), 129.4 (CH), 125.6 (CH), 121.3 (CH), 113.6 (CH), 55.3 (CH_3), 21.2 (CH_3).

IR (ATR): $\tilde{\nu}$ = 2835, 1586, 1491, 1462, 1246, 1177, 1036, 819, 789, 732 cm^{-1}.

MS (ESI) *m*/*z* (relative intensity): 298 (5) $[M+Na]^+$, 276 (100) $[M+H]^+$.

HR-MS (ESI): *m*/*z* calcd for $C_{19}H_{18}NO^+$ $[M+H]^+$ 276.1383, found 276.1384.

The spectral data are in accordance with those reported in the literature.[92]

2-{4'-Methoxy-4-(trifluoromethyl)-[1,1'-biphenyl]-2-yl}pyridine (243da)

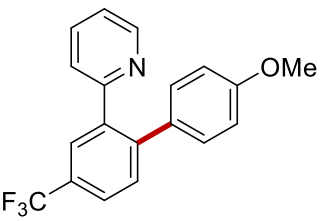

^{1}H-NMR (300 MHz, $CDCl_3$): δ = 8.66 (ddd, *J* = 5.0, 1.8, 0.9 Hz, 1H), 7.97 (d, *J* = 2.0 Hz, 1H), 7.68 (dd, *J* = 8.1, 2.0 Hz, 1H), 7.52 (d, *J* = 8.0 Hz, 1H), 7.45–7.37 (m, 1H), 7.14 (ddd, *J* = 7.6, 4.9, 1.1 Hz, 1H), 7.11–7.03 (m, 2H), 6.90 (dt, *J* = 7.9, 1.0 Hz, 1H), 6.83–6.74 (m, 2H), 3.78 (s, 3H).

^{13}C-NMR (75 MHz, $CDCl_3$): δ = 159.1 (C_q), 158.0 (C_q), 149.7 (CH), 143.7 (C_q), 139.9 (C_q), 135.5 (CH), 132.3 (C_q), 130.9 (CH), 130.7 (CH), 129.5 (q, $^2J_{C–F}$ = 31 Hz, C_q), 127.6 (q, $^3J_{C–F}$ = 4 Hz, CH), 125.3 (CH), 125.1 (q, $^3J_{C–F}$ = 4 Hz, CH), 124.2 (q, $^1J_{C–F}$ = 270 Hz, C_q), 121.9 (CH), 113.8 (CH), 55.2 (CH_3).

^{19}F-NMR (282 MHz, $CDCl_3$): δ = – 62.3 (s).

IR (ATR): $\tilde{\nu}$ = 2839, 1607, 1566, 1336, 1251, 1167, 1116, 1081, 828, 788 cm^{-1}.

MS (ESI) *m*/*z* (relative intensity): 352 (5) $[M+Na]^+$, 330 (100) $[M+H]^+$.

HR-MS (ESI): *m*/*z* calcd for $C_{19}H_{15}F_3NO^+$ $[M+H]^+$ 330.1100, found 330.1100.

The spectral data are in accordance with those reported in the literature.[281]

5.5.5 *C–H Arylation in the Presence of Typical Radical Scavengers*

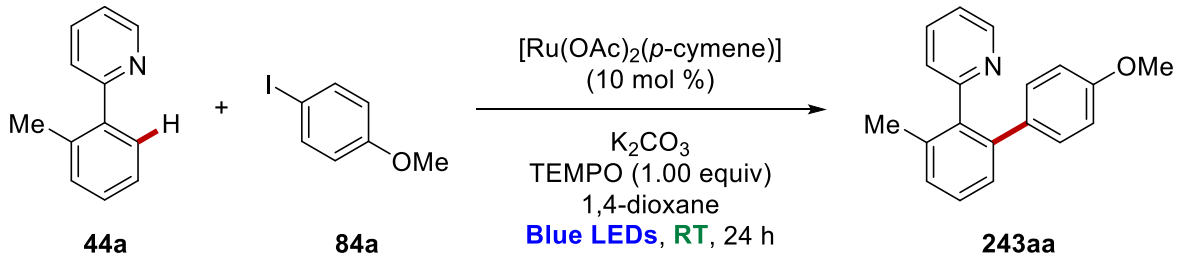

44a **84a** **243aa**

Pyridine **44a** (84.6 mg, 0.50 mmol), [Ru(OAc)$_2$(*p*-cymene)] (17.7 mg, 50.0 µmol, 10 mol %), K_2CO_3 (138 mg, 1.00 mmol) and TEMPO (78.1 mg, 0.50 mmol) were placed in a 10 mL vial. The vial was capped with a septum and wrapped with parafilm. The vial was evacuated and purged with N_2 three times. Aryl iodide **84a** (176 mg, 0.75 mmol) and 1,4-dioxane (2.0 mL) were then added and the mixture was stirred under visible light irradiation (2 × Kessil A360N, temperature was maintained between 30 °C and 33 °C). After 16 h, the resulting mixture was filtered through a pad of silica gel and washed with EtOAc. Product formation was not observed by GC-MS.

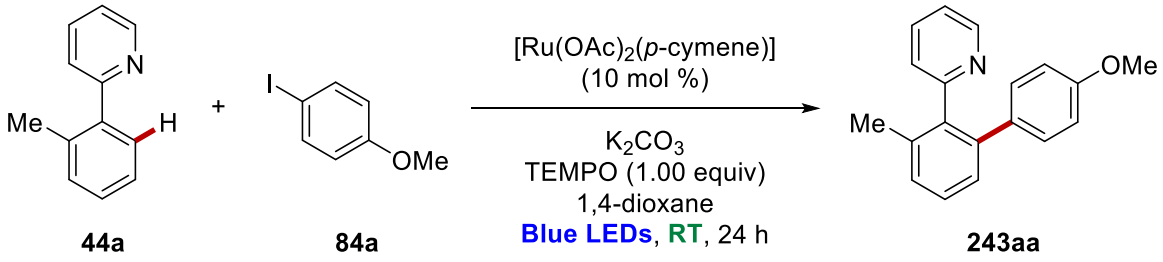

44a **84a** **243aa**

Pyridine **44a** (84.6 mg, 0.50 mmol), [Ru(OAc)$_2$(*p*-cymene)] (17.7 mg, 50.0 µmol, 10 mol %), K_2CO_3 (138 mg, 1.00 mmol) and BHT (110 mg, 0.50 mmol) were placed in a 10 mL. The vial was capped with a septum and wrapped with parafilm. The vial was evacuated and purged with N_2 three times. Aryl iodide **84a** (176 mg, 0.75 mmol) and 1,4-dioxane (2.0 mL) were then added and the mixture was stirred under visible light irradiation (2 × Kessil A360N, temperature was maintained between 30 °C and 33 °C). After 16 h, the resulting mixture was filtered through a pad of silica gel and washed with EtOAc. Product **243aa** (83.9 mg, 61%) was formed in a diminished yield and was isolated by column chromatography as a viscous oil.

5.5.6 On-Off Experiment

Pyridine **44a** (84.6 mg, 0.50 mmol), [Ru(OAc)$_2$(*p*-cymene)] (17.7 mg, 50.0 µmol, 10 mol %) and K_2CO_3 (138 mg, 1.00 mmol) were placed in a 10 mL vial. The vial was capped with a septum and wrapped with parafilm. The vial was evacuated and purged with N_2 three times. Aryl iodide **84a** (176 mg, 0.75 mmol), *n*-dodecane (40 µL) and 1,4-dioxane (2.0 mL) were then added and the mixture was stirred with a N_2 ballon sequentially under visible light irradiation (2 × Kessil A360N, temperature was maintained between 30 °C and 33 °C) and in the absence of light. Every two hours, an aliquot of 100 µL was removed *via* syringe, diluted with EtOAc, filtered through a short plug of silica gel and analyzed by gas chromatography.

Time [h]	**243aa** [%]
0	0.078
2	20.559
4	22.320
6	50.738
8	52.913

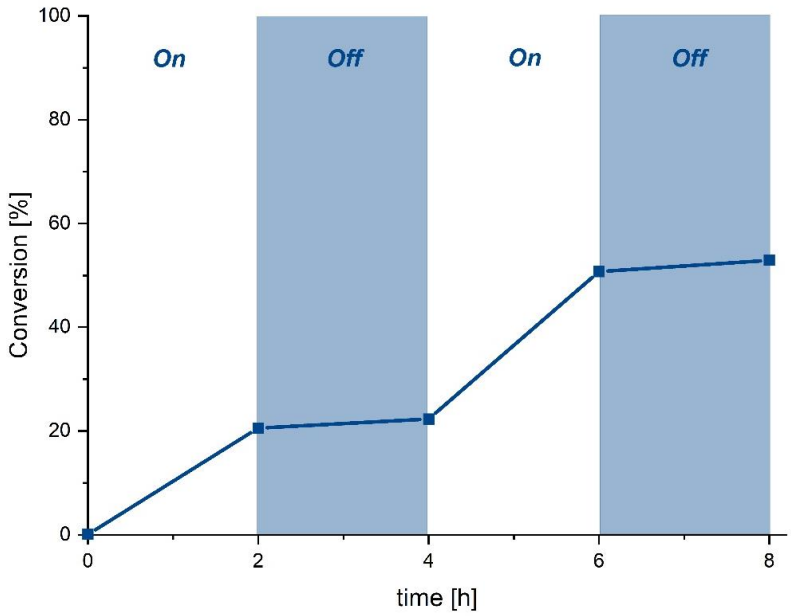

Figure 5.7: On-Off experiment for photo-induced C–H arylation.

5.5.7 *Detection of Free para-Cymene in Photo-Induced Arylation*

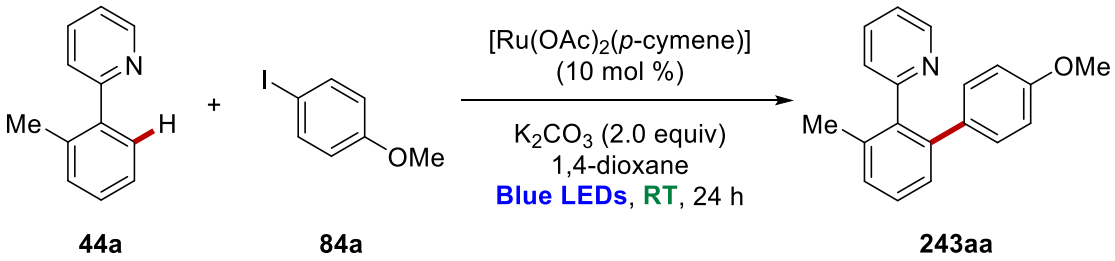

44a **84a** **243aa**

Pyridine **44a** (169 mg, 1.00 mmol), [Ru(OAc)$_2$(*p*-cymene)] (35.4 mg, 100.0 µmol, 10 mol %) and K_2CO_3 (276 mg, 2.00 mmol) were placed in a 10 mL vial. The vial was capped with a septum and wrapped with parafilm. The vial was evacuated and purged with N_2 three times. Aryl iodide **84a** (351 mg, 1.50 mmol), *n*-dodecane (80 µL) and 1,4-dioxane (4.0 mL) were then added and the mixture was stirred with a N_2 ballon under visible light irradiation (2 × Kessil A360N, temperature was maintained between 30 °C and 33 °C). During the course of the reaction an aliquot of 100 µL was removed *via* syringe after 5 min, 15 min, 30 min, 1 h, 4 h, 8 h and 24 h. The sample was diluted with EtOAc, filtered through a short plug of silica gel and analyzed by gas chromatography.

Time [h]	**243aa** [%]	*p*-cymene [%]
0.08	–0.07	2.92
0.25	–0.07	11.48
0.5	0.98	16.26
1	3.01	23.08
4	52.82	63.32
8	89.02	69.26
24	96.56	76.43

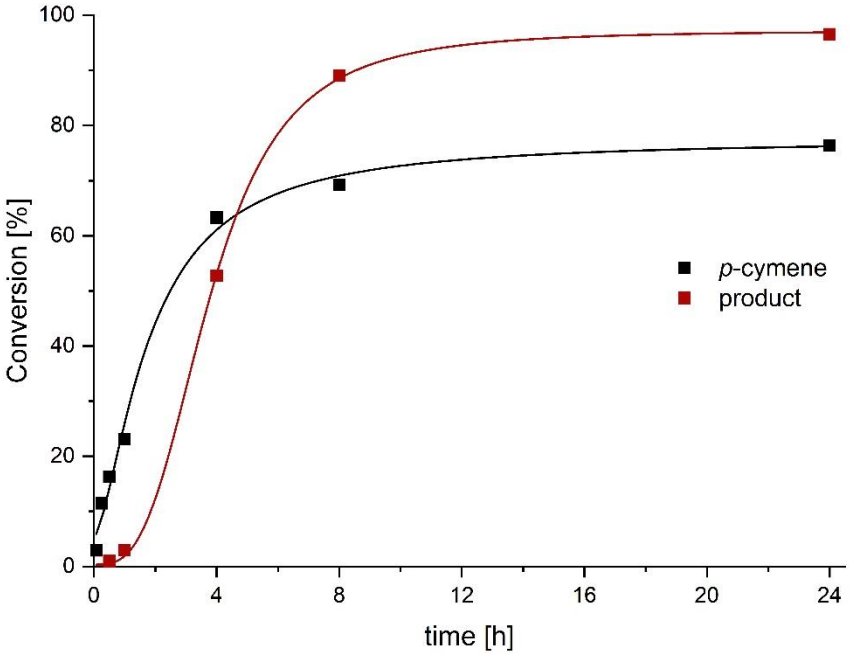

Figure 5.8: Detection of free *para*-cymene.

5.5.8 Determination of Quantum Yield

The quantum yield was determined in slight variation to the literature.[282]

Preparation of potassium ferrioxalate solution:

118 mg of solid potassium ferrioxalate, and 56 µL of H_2SO_4 were diluted with H_2O to a final volume of 20 mL.

Preparation of buffer solution:

2.48 g of NaOAc and 0.5 ml of H_2SO_4 were diluted with H_2O to a finale volume of 50 mL.

Using the same setup as for catalytic reactions, 2.0 mL of the potassium ferrioxalate solution was irradiated for 10 sec. The sample solution was added to 4.0 mL of the buffer solution containing 2.0 mg 1,10-phenanthroline and diluted with H_2O to a finale volume of 10 mL. Subsequently the absorbance of this solution was determined at 510 nm. The same procedure was followed for an unirradiated sample.

Calculation Number of Photons:

Abs of Fe^{2+} (at 510 nm) = 2.7844 (after irradiation of 10 sec)

Abs of Fe^{2+} (at 510 nm) = 0.0137 (no irradiation)

Abs of Fe^{2+} (at 510 nm) = 2.7844−0.0137 = 2.7707

$$[Fe^{2+}] = \frac{\text{Abs of } Fe^{2+} (\text{at } 510 \text{ nm})}{\varepsilon_{510\text{ nm}} \times l}$$

$$[Fe^{2+}] = \frac{2.7707}{11100\ M^{-1} \cdot cm^{-1} \times 1cm} = 2.496 \times 10^{-4}\ M$$

$$n_{(Fe^{2+})} = (2.496 \times 10^{-4}) M \times 0.010\ L = 2.496 \times 10^{-6}\ mol$$

with quantum yield of 0.805 for the absorption of Fe^{3+}:

$$n_{(photons)} = 3.101 \times 10^{-6}\ mol$$

$$n_{(photons/s)} = 3.101 \times 10^{-7}\ mol \cdot s^{-1}$$

The initial rate of the alkylation was determined to be 2.698×10^{-8} mol/s.

$$\text{Quantum Yield} = \frac{n_{product}/s}{photons/s} = \frac{2.698 \times 10^{-8}\ mol/s}{3.101 \times 10^{-7}\ mol/s} = 0.087$$

5.6 PHOTO-INDUCED RUTHENIUM-CATALYZED C–H BENZYLATIONS AND ALLYLATIONS AT AMBIENT TEMPERATURE

5.6.1 Characterization Data

2-[2-(4-Fluorobenzyl)-6-methylphenyl]pyridine (265aa)

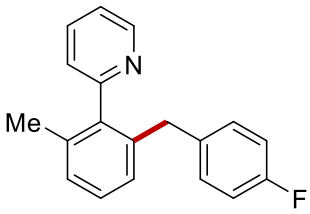

The general procedure **F** was followed using 2-(*o*-tolyl)pyridine (**44a**, 84.6 mg, 0.50 mmol) and benzyl chloride **90a** (108 mg, 0.75 mmol). After 24 h, purification by column chromatography (*n*-hexane/EtOAc 10:1) yielded **265aa** (152 mg, 81%) as a colorless oil. Using H_2O (138 mg, 74%) or Brij-35 (10 wt%)/H_2O (143 mg, 77%) as reaction medium, yielded the product **265aa** in similar yields.

^{1}H-NMR (400 MHz, $CDCl_3$): δ = 8.69 (ddd, *J* = 4.9, 1.8, 0.9 Hz, 1H), 7.63 (ddd, *J* = 7.7, 7.7, 1.8 Hz, 1H), 7.26–7.20 (m, 2H), 7.15 (ddd, *J* = 7.7, 1.3, 0.9 Hz, 1H), 7.07–7.01 (m, 2H), 6.87–6.79 (m, 4H), 3.72 (s, 2H), 2.04 (s, 3H).

^{13}C-NMR (100 MHz, $CDCl_3$): δ = 161.3 (d, $^1J_{C–F}$ = 243 Hz, C_q), 159.5 (C_q), 149.7 (CH), 140.6 (C_q), 138.9 (C_q), 136.9 (d, $^4J_{C–F}$ = 3 Hz, C_q), 136.3 (C_q), 136.1 (CH), 130.2 (d, $^3J_{C–F}$ = 8 Hz, CH), 128.4 (CH), 128.2 (CH), 127.7 (CH), 125.0 (CH), 121.9 (CH), 114.9 (d, $^2J_{C–F}$ = 21 Hz, CH), 38.8 (CH_2), 20.4 (CH_3).

^{19}F-NMR (376 MHz, $CDCl_3$): δ = – 117.9 (s).

IR (ATR): $\tilde{\nu}$ = 3063, 2918, 1584, 1506, 1459, 1218, 1157, 1026, 784, 749 cm^{-1}.

MS (EI) *m*/*z* (relative intensity): 277 (62) $[M]^+$, 276 (100) $[M–H]^+$, 261 (19) $[M–Me]^+$, 180 (26).

HR-MS (EI): *m*/*z* calcd for $C_{19}H_{16}FN^+$ $[M]^+$ 277.1261, found 277.1260.

2-(2-Benzyl-6-methylphenyl)pyridine (265ab)

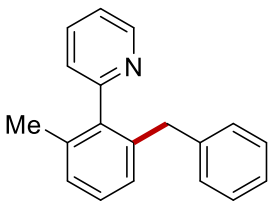

The general procedure **F** was followed using 2-(*o*-tolyl)pyridine (**44a**, 84.6 mg, 0.50 mmol) and benzyl chloride (**90b**, 94.9 mg, 0.75 mmol). After 24 h, purification by column chromatography (*n*-hexane/EtOAc 15:1 to 10:1) yielded **265ab** (105 mg, 81%) as a viscous colorless oil.

^{1}H-NMR (400 MHz, $CDCl_3$): δ = 8.76 (ddd, J = 4.9, 1.8, 1.0 Hz, 1H), 7.66 (ddd, J = 7.7, 7.7, 1.4 Hz, 1H), 7.36–7.05 (m, 8H), 7.04–6.90 (m, 2H), 3.83 (s, 2H), 2.12 (s, 3H).

^{13}C-NMR (100 MHz, $CDCl_3$): δ = 159.4 (C_q), 149.6 (CH), 141.1 (C_q), 140.5 (C_q), 138.9 (C_q), 136.1 (C_q), 135.9 (CH), 128.9 (CH), 128.1 (CH), 128.1 (CH), 128.0 (CH), 127.6 (CH), 125.7 (CH), 124.9 (CH), 121.7 (CH), 39.4 (CH_2), 20.3 (CH_3).

IR (ATR): $\tilde{\nu}$ = 1585, 1494, 1452, 1423, 1265, 1027, 791, 751, 730, 699 cm^{-1}.

MS (ESI) *m*/*z* (relative intensity): 282 (12) $[M+Na]^+$, 260 (100) $[M+H]^+$.

HR-MS (ESI): *m*/*z* calcd for $C_{19}H_{18}N^+$ $[M+H]^+$ 260.1434, found 260.1430.

The spectral data is in accordance with those reported in the literature.[94]

2-[2-Methyl-6-(4-methylbenzyl)phenyl]pyridine (265ac)

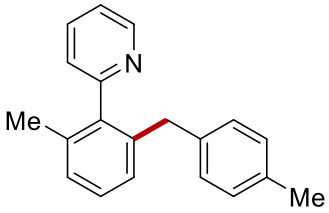

The general procedure **F** was followed using 2-(*o*-tolyl)pyridine (**44a**, 84.6 mg, 0.50 mmol) and benzyl chloride **90c** (105 mg, 0.75 mmol). After 24 h, purification by column chromatography (*n*-hexane/EtOAc 10:1) yielded **265ac** (103 mg, 75%) as a viscous colorless oil. The product was obtained as a mixture of regioisomers (*ortho*:others 94:6).

^{1}H-NMR (400 MHz, $CDCl_3$): δ = 8.70 (ddd, J = 4.9, 1.8, 0.9 Hz, 1H), 7.65 (ddd, J = 7.7, 7.7, 1.8 Hz, 1H), 7.32–7.18 (m, 2H), 7.16–7.02 (m, 3H), 6.98 (d, J = 7.7 Hz, 2H), 6.82 (d, J = 7.7 Hz, 2H), 3.68 (s, 2H), 2.27 (s, 3H), 2.04 (s, 3H).

^{13}C-NMR (100 MHz, $CDCl_3$): δ = 159.6 (C_q), 149.7 (CH), 140.6 (C_q), 139.2 (C_q), 138.1 (C_q), 136.1 (C_q), 136.1 (CH), 135.3 (C_q), 128.9 (CH), 128.9 (CH), 128.1 (CH), 128.1 (CH), 127.6 (CH), 125.0 (CH), 121.8 (CH), 39.0 (CH_2), 21.1 (CH_3), 20.5 (CH_3).

IR (ATR): $\tilde{\nu}$ = 1583, 1513, 1458, 1423, 1147, 1026, 789, 750, 620, 486 cm^{-1}.

MS (ESI) *m*/*z* (relative intensity): 569 (14) $[2M+Na]^+$, 547 (2) $[2M+H]^+$, 296 (65) $[M+Na]^+$, 274 (100) $[M+H]^+$.

HR-MS (ESI): *m*/*z* calcd for $C_{20}H_{20}N^+$ $[M+H]^+$ 274.1590, found 274.1596.

2-[2-(4-Methoxybenzyl)-6-methylphenyl]pyridine (265ad)

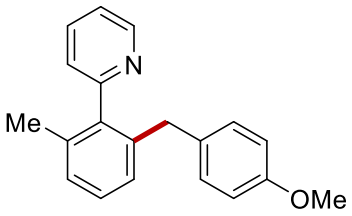

The general procedure **F** was followed using 2-(*o*-tolyl)pyridine (**44a**, 84.6 mg, 0.50 mmol) and benzyl chloride **90d** (118 mg, 0.75 mmol). After 24 h, purification by column chromatography (*n*-hexane/EtOAc 12:1) yielded **265ad** (104 mg, 72%) as a viscous colorless oil.

^{1}H-NMR (400 MHz, $CDCl_3$): δ = 8.73 (dd, J = 4.0, 0.9 Hz, 1H), 7.67 (dd, J = 7.6, 1.9 Hz, 1H), 7.32–7.22 (m, 2H), 7.20–7.15 (m, 1H), 7.14–7.02 (m, 2H), 6.88 (d, J = 8.0 Hz, 2H), 6.75 (d, J = 8.1 Hz, 2H), 3.77 (s, 3H), 3.69 (s, 2H), 2.07 (s, 3H).

^{13}C-NMR (100 MHz, $CDCl_3$): δ = 159.5 (C_q), 157.7 (C_q), 149.6 (CH), 140.5 (C_q), 139.3 (C_q), 136.1 (C_q), 136.0 (CH), 133.3 (C_q), 129.8 (CH), 128.1 (CH), 128.1 (CH), 127.5 (CH), 125.0 (CH), 121.7 (CH), 113.6 (CH), 55.3 (CH_3), 38.5 (CH_2), 20.4 (CH_3).

IR (ATR): $\tilde{\nu}$ = 1538, 1510, 1462, 1245, 1037, 1026, 908, 780, 725, 513 cm^{-1}.

MS (ESI) *m*/*z* (relative intensity): 312 (7) $[M+Na]^+$, 290 (100) $[M+H]^+$.

HR-MS (ESI): *m*/*z* calcd for $C_{20}H_{20}NO^+$ $[M+H]^+$ 290.1539, found 290.1540.

The spectral data are in accordance with those reported in the literature.[94]

2-{2-Methyl-6-[4-(trifluoromethyl)benzyl]phenyl}pyridine (265ae)

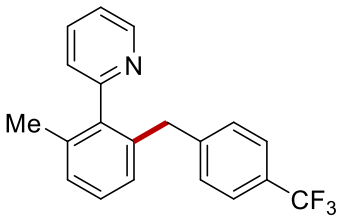

The general procedure **F** was followed using 2-(*o*-tolyl)pyridine (**44a**, 84.6 mg, 0.50 mmol) and benzyl chloride **90e** (145 mg, 0.75 mmol). After 24 h, purification by column chromatography (*n*-hexane/EtOAc 10:1) yielded **265ae** (127 mg, 78%) as a viscous colorless oil. The product was obtained as a mixture of regioisomers (*ortho*:others 92:8).

^{1}H-NMR (400 MHz, $CDCl_3$): δ = 8.67 (ddd, J = 4.9, 1.7, 0.9 Hz, 1H), 7.63 (ddd, J = 7.7, 7.7, 1.8 Hz, 1H), 7.39 (d, J = 8.0 Hz, 2H), 7.31–7.13 (m, 3H), 7.10–6.89 (m, 4H), 3.81 (s, 2H), 2.04 (s, 3H).

^{13}C-NMR (100 MHz, $CDCl_3$): δ = 159.2 (C_q), 149.7 (CH), 145.3 (C_q), 140.6 (C_q), 137.9 (C_q), 136.4 (C_q), 136.1 (CH), 129.1 (q, $^2J_{C–F}$ = 36 Hz, C_q), 129.1 (CH), 128.6 (CH), 128.3 (CH),

127.7 (CH), 125.0 (q, $^{3}J_{C–F}$ = 4 Hz, CH), 124.9 (CH), 124.4 (q, $^{1}J_{C–F}$ = 275 Hz, C_q), 121.9 (CH), 39.4 (CH_2), 20.3 (CH_3).

^{19}F-NMR (282 MHz, $CDCl_3$): δ = – 62.3 (s).

IR (ATR): $\tilde{\nu}$ = 1564, 1428, 1321, 1159, 1108, 1065, 1018, 779, 750 cm^{-1}.

MS (ESI) *m*/*z* (relative intensity): 677 (7) $[2M+Na]^+$, 655 (1) $[2M+H]^+$, 350 (25) $[M+Na]^+$, 328 (100) $[M+H]^+$.

HR-MS (ESI): *m*/*z* calcd for $C_{20}H_{17}NF_3^+$ $[M+H]^+$ 328.1308, found 328.1311.

2-[2-(4-Chlorobenzyl)-6-methylphenyl]pyridine (265af)

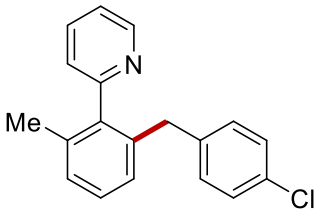

The general procedure **F** was followed using 2-(*o*-tolyl)pyridine (**44a**, 84.6 mg, 0.50 mmol) and benzyl chloride **90f** (121 mg, 0.75 mmol). After 24 h, purification by column chromatography (*n*-hexane/EtOAc 10:1) yielded **265af** (123 mg, 82%) as a viscous colorless oil.

^{1}H-NMR (400 MHz, $CDCl_3$): δ = 8.68 (ddd, *J* = 4.9, 1.8, 1.0 Hz, 1H), 7.64 (ddd, *J* = 7.7, 7.7, 1.8 Hz, 1H), 7.30–7.19 (m, 2H), 7.18–7.09 (m, 3H), 7.04 (ddd, *J* = 7.8, 2.2, 1.2 Hz, 2H), 6.91–6.73 (m, 2H), 3.71 (s, 2H), 2.04 (s, 3H).

^{13}C-NMR (100 MHz, $CDCl_3$): δ = 159.4 (C_q), 149.7 (CH), 140.6 (C_q), 139.7 (C_q), 138.5 (C_q), 136.4 (C_q), 136.2 (CH), 131.6 (C_q), 130.2 (CH), 128.5 (CH), 128.3 (CH), 128.3 (CH), 127.7 (CH), 125.0 (CH), 121.9 (CH), 38.9 (CH_2), 20.4 (CH_3).

IR (ATR): $\tilde{\nu}$ = 1584, 1489, 1423, 1265, 1089, 1014, 773, 734, 485 cm^{-1}.

MS (ESI) *m*/*z* (relative intensity): 316 (38) $[M(^{35}Cl)+Na]^+$, 294 (100) $[M(^{35}Cl)+H]^+$.

HR-MS (ESI): *m*/*z* calcd for $C_{19}H_{17}{}^{35}ClN^+$ $[M+H]^+$ 294.1044, found 294.1047.

The spectral data are in accordance with those reported in the literature.[94]

2-[2-(4-Bromobenzyl)-6-methylphenyl]pyridine (265ag)

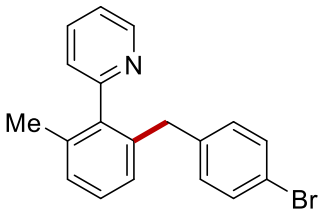

The general procedure **F** was followed using 2-(*o*-tolyl)pyridine (**44a**, 84.6 mg, 0.50 mmol) and benzyl chloride **90g** (154 mg, 0.75 mmol). After 24 h, purification by column chromatography

(*n*-hexane/EtOAc 10:1) yielded **265ag** (107 mg, 63%) as a viscous yellow oil. Using H_2O (104 mg, 61%) or Brij-35 (10 wt%)/H_2O (107 mg, 63%) as reaction medium, yielded the product **265ag** in similar yields.

^{1}H-NMR (400 MHz, $CDCl_3$): δ = 8.70 (ddd, J = 4.9, 1.8, 0.9 Hz, 1H), 7.66 (ddd, J = 7.7, 7.7, 1.8 Hz, 1H), 7.34–7.22 (m, 4H), 7.22–7.16 (m, 1H), 7.11–7.00 (m, 2H), 6.87–6.68 (m, 2H), 3.72 (s, 2H), 2.06 (s, 3H).

^{13}C-NMR (100 MHz, $CDCl_3$): δ = 159.4 (C_q), 149.8 (CH), 140.6 (C_q), 140.2 (C_q), 138.4 (C_q), 136.4 (C_q), 136.2 (CH), 131.3 (CH), 130.7 (CH), 128.5 (CH), 128.3 (CH), 127.7 (CH), 125.0 (CH), 121.9 (CH), 119.7 (C_q), 39.0 (CH_2), 20.4 (CH_3).

IR (ATR): $\tilde{\nu}$ = 1583, 1562, 1485, 1423, 1069, 1010, 789, 770, 748 cm^{-1}.

MS (ESI) *m*/*z* (relative intensity): 360 (27) [M(^{79}Br)+Na]$^+$, 338 (100) [M(^{79}Br)+H]$^+$.

HR-MS (ESI): *m*/*z* calcd for $C_{19}H_{17}{}^{79}BrN^+$ [M+H]$^+$ 338.0539, found 338.0541.

Ethyl 4-[3-methyl-2-(pyridin-2-yl)benzyl]benzoate (265ah)

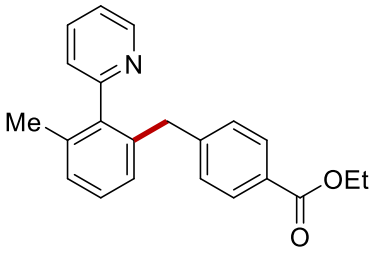

The general procedure **F** was followed using 2-(*o*-tolyl)pyridine (**44a**, 84.6 mg, 0.50 mmol) and benzyl chloride **90h** (149 mg, 0.75 mmol). After 24 h, purification by column chromatography (*n*-hexane/EtOAc 10:1 to 5:1) yielded **265ah** (111 mg, 67%) as a viscous yellow oil.

^{1}H-NMR (400 MHz, $CDCl_3$): δ = 8.69 (ddd, J = 4.9, 1.8, 1.0 Hz, 1H), 7.90–7.77 (m, 2H), 7.62 (ddd, J = 7.7, 7.7, 1.8 Hz, 1H), 7.30–7.14 (m, 3H), 7.12–7.01 (m, 2H), 6.97 (d, J = 8.0 Hz, 2H), 4.35 (q, J = 7.1 Hz, 2H), 3.82 (s, 2H), 2.05 (s, 3H), 1.37 (t, J = 7.1 Hz, 3H).

^{13}C-NMR (100 MHz, $CDCl_3$): δ = 166.6 (C_q), 159.1 (C_q), 149.6 (CH), 146.5 (C_q), 140.5 (C_q), 138.0 (C_q), 136.3 (C_q), 136.1 (CH), 129.4 (CH), 128.7 (CH), 128.5 (CH), 128.2 (CH), 128.0 (C_q), 127.7 (CH), 124.9 (CH), 121.8 (CH), 60.7 (CH_2), 39.5 (CH_2), 20.3 (CH_3), 14.3 (CH_3).

IR (ATR): $\tilde{\nu}$ = 1714, 1705, 1272, 1177, 1105, 1022, 906, 725, 707, 645 cm^{-1}.

MS (ESI) *m*/*z* (relative intensity): 354 (12) [M+Na]$^+$, 332 (100) [M+H]$^+$.

HR-MS (ESI): *m*/*z* calcd for $C_{22}H_{22}NO_2^+$ [M+H]$^+$ 332.1645, found 332.1646.

2-[2-(3-Fluorobenzyl)-6-methylphenyl]pyridine (265ai)

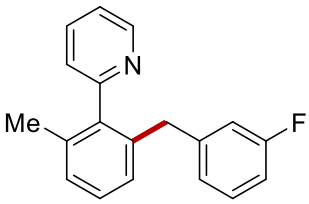

The general procedure **F** was followed using 2-(*o*-tolyl)pyridine (**44a**, 84.6 mg, 0.50 mmol) and benzyl chloride **90i** (108 mg, 0.75 mmol). After 24 h, purification by column chromatography (*n*-hexane/EtOAc 10:1) yielded **265ai** (109 mg, 79%) as a viscous yellow oil.

^{1}H-NMR (400 MHz, $CDCl_3$): δ = 8.73 (ddd, J = 4.8, 1.9, 1.0 Hz, 1H), 7.65 (ddd, J = 7.7, 7.7, 1.8 Hz, 1H), 7.31–7.19 (m, 3H), 7.17–7.03 (m, 3H), 6.82 (ddd, J = 8.3, 2.7, 0.9 Hz, 1H), 6.72 (ddt, J = 7.5, 1.6, 0.8 Hz, 1H), 6.67–6.60 (m, 1H), 3.79 (s, 2H), 2.09 (s, 3H).

^{13}C-NMR (100 MHz, $CDCl_3$): δ = 162.8 (d, $^{1}J_{C–F}$ = 245 Hz, C_q), 159.3 (C_q), 149.7 (CH), 143.7 (d, $^{3}J_{C–F}$ = 7 Hz, C_q), 140.6 (C_q), 138.2 (C_q), 136.3 (C_q), 136.0 (CH), 129.5 (d, $^{3}J_{C–F}$ = 8 Hz, CH), 128.5 (CH), 128.2 (CH), 127.7 (CH), 124.9 (CH), 124.5 (CH), 121.8 (CH), 115.7 (d, $^{2}J_{C–F}$ = 21 Hz, CH), 112.6 (d, $^{2}J_{C–F}$ = 21 Hz, CH), 39.2 (CH_2), 20.4 (CH_3).

^{19}F-NMR (282 MHz, $CDCl_3$): δ = – 113.9 (s).

IR (ATR): $\tilde{\nu}$ = 1586, 1486, 1447, 1423, 1245, 1135, 908, 776, 750, 730 cm^{-1}.

MS (ESI) *m*/*z* (relative intensity): 300 (4) $[M+Na]^+$, 278 (100) $[M+H]^+$.

HR-MS (ESI): *m*/*z* calcd for $C_{19}H_{17}FN^+$ $[M+H]^+$ 278.1340, found 278.1343.

2-[2-Methyl-6-(2-methylbenzyl)phenyl]pyridine (265aj)

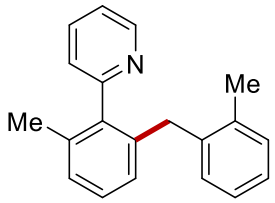

The general procedure **F** was followed using 2-(*o*-tolyl)pyridine (**44a**, 84.6 mg, 0.50 mmol) and benzyl chloride **90j** (106 mg, 0.75 mmol). After 24 h, purification by column chromatography (*n*-hexane/EtOAc 10:1 to 7:1) yielded **265aj** (104 mg, 76%) as a viscous colorless oil.

^{1}H-NMR (400 MHz, $CDCl_3$): δ = 8.78 (dd, J = 5.0, 2.1 Hz, 1H), 7.70 (ddd, J = 7.7, 7.7, 1.8 Hz, 1H), 7.30–7.17 (m, 4H), 7.16–7.10 (m, 3H), 7.01 (dd, J = 6.4, 1.8 Hz, 1H), 6.95–6.84 (m, 1H), 3.76 (s, 2H), 2.13 (s, 3H), 2.11 (s, 3H).

^{13}C-NMR (100 MHz, $CDCl_3$): δ = 159.6 (C_q), 149.7 (CH), 140.5 (C_q), 139.0 (C_q), 138.2 (C_q), 136.5 (C_q), 136.1 (CH), 135.9 (C_q), 129.9 (CH), 129.9 (CH), 128.0 (CH), 128.0 (CH), 126.8 (CH), 126.1 (CH), 125.8 (CH), 124.6 (CH), 121.7 (CH), 37.0 (CH_2), 20.3 (CH_3), 19.6 (CH_3).

IR (ATR): $\tilde{\nu}$ = 1638, 1460, 1422, 1027, 907, 792, 765, 723, 645, 620 cm^{-1}.

MS (ESI) *m*/*z* (relative intensity): 296 (3) $[M+Na]^+$, 274 (100) $[M+H]^+$.

HR-MS (ESI): *m*/*z* calcd for $C_{20}H_{20}N^+$ $[M+H]^+$ 274.1590, found 274.1594.

2-{2-Methyl-6-[2-(trifluoromethyl)benzyl]phenyl}pyridine (265ak)

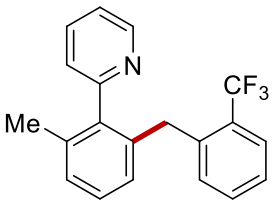

The general procedure **F** was followed using 2-(*o*-tolyl)pyridine (**44a**, 84.6 mg, 0.50 mmol) and benzyl chloride **90k** (146 mg, 0.75 mmol). After 24 h, purification by column chromatography (*n*-hexane/EtOAc 10:1 to 5:1) yielded **265ak** (142 mg, 87%) as a viscous yellow oil.

^{1}H-NMR (400 MHz, $CDCl_3$): δ = 8.69 (ddd, *J* = 4.8, 1.9, 0.9 Hz, 1H), 7.65 (dd, *J* = 7.7, 1.3 Hz, 1H), 7.57 (d, *J* = 7.8 Hz, 1H), 7.40 (dd, *J* = 7.6, 7.6 Hz, 1H), 7.30–7.09 (m, 6H), 6.99–6.92 (m, 1H), 3.97 (s, 2H), 2.11 (s, 3H).

^{13}C-NMR (100 MHz, $CDCl_3$): δ = 159.2 (C_q), 149.7 (CH), 140.8 (C_q), 139.7 (C_q), 137.5 (C_q), 136.3 (C_q), 136.1 (CH), 131.7 (q, $^4J_{C–F}$ = 2 Hz, CH), 131.6 (CH), 128.4 (CH), 128.3 (q, $^2J_{C–F}$ = 33 Hz, C_q), 128.1 (CH), 127.8 (CH), 125.9 (CH), 125.5 (q, $^3J_{C–F}$ = 6 Hz, CH), 124.6 (CH), 124.4 (q, $^1J_{C–F}$ = 277 Hz, C_q), 121.8 (CH), 35.4 (CH_2), 20.3 (CH_3).

^{19}F-NMR (282 MHz, $CDCl_3$): δ = – 60.3 (s).

IR (ATR): $\tilde{\nu}$ = 1585, 1432, 1424, 1154, 1123, 1105, 1037, 907, 765, 656 cm^{-1}.

MS (ESI) *m*/*z* (relative intensity): 350 (5) $[M+Na]^+$, 328 (100) $[M+H]^+$.

HR-MS (ESI): *m*/*z* calcd for $C_{20}H_{17}F_3N^+$ $[M+H]^+$ 328.1308, found 328.1313.

2-{2-Methyl-6-[(perfluorophenyl)methyl]phenyl}pyridine (265an)

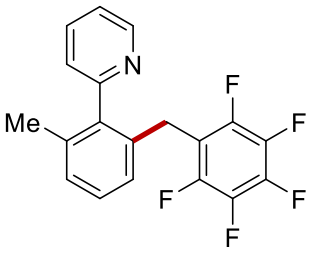

The general procedure **F** was followed using 2-(*o*-tolyl)pyridine (**44a**, 84.6 mg, 0.50 mmol) and benzyl bromide **90n** (196 mg, 0.75 mmol). After 24 h, purification by column chromatography (*n*-hexane/EtOAc 12:1 to 9:1) yielded **265an** (121 mg, 69%) as a viscous brown oil. The product was obtained as a mixture of regioisomers (*ortho*:others 92:8).

^{1}H-NMR (500 MHz, $CDCl_3$): δ = 8.70 (ddd, *J* = 4.9, 1.8, 1.0 Hz, 1H), 7.75 (ddd, *J* = 7.7, 7.7, 1.8 Hz, 1H), 7.30–7.12 (m, 4H), 6.95 (d, *J* = 7.6 Hz, 1H), 3.79 (s, 2H), 2.01 (s, 3H).

^{13}C-NMR (125 MHz, $CDCl_3$): δ = 159.0 (C_q), 150.0 (CH), 145.3 (dddd, J = 247, 15, 8, 4 Hz, C_q), 140.3 (C_q), 139.9 (ddd, J = 275, 15, 7 Hz, C_q), 137.5 (ddd, J = 280, 15, 6 Hz, C_q), 136.5 (C_q), 136.6 (CH), 135.0 (C_q), 129.0 (CH), 128.3 (CH), 126.4 (CH), 124.7 (CH), 122.2 (CH), 114.1 (dddd, J = 18, 18, 4, 4 Hz, C_q), 26.3 (CH_2), 20.4 (CH_3).

^{19}F-NMR (476 MHz, $CDCl_3$): δ = – 142.1 (dd, J = 22.4, 8.1 Hz, 2F), – 157.3 (dd, J = 20.8, 20.8 Hz, 1F), – 163.0 (ddd, J = 22.3, 20.2, 8.1 Hz, 2F).

IR (ATR): $\tilde{\nu}$ = 1520, 1502, 1423, 1265, 1121, 1000, 959, 735, 707 cm^{-1}.

MS (ESI) *m*/*z* (relative intensity): 372 (2) $[M+Na]^+$, 350 (100) $[M+H]^+$.

HR-MS (ESI): *m*/*z* calcd for $C_{19}H_{13}F_5N^+$ $[M+H]^+$ 350.0963, found 350.0967.

2-[2-Methyl-6-(naphthalen-1-ylmethyl)phenyl]pyridine (265ao)

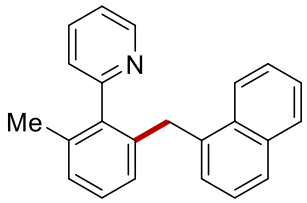

The general procedure **F** was followed using 2-(*o*-tolyl)pyridine (**44a**, 84.6 mg, 0.50 mmol) and 1-(chloromethyl)naphthalene (**90o**, 133 mg, 0.75 mmol). After 24 h, purification by column chromatography (*n*-hexane/EtOAc 10:1) yielded **265ao** (124 mg, 80%) as a white solid.

^{1}H-NMR (300 MHz, $CDCl_3$): δ = 8.76 (dd, J = 4.9, 1.6 Hz, 1H), 7.89–7.79 (m, 2H), 7.73 (d, J = 8.3 Hz, 1H), 7.71–7.62 (m, 1H), 7.49–7.33 (m, 3H), 7.30–7.11 (m, 5H), 6.84 (dd, J = 6.6, 2.3 Hz, 1H), 4.17 (s, 2H), 2.12 (s, 3H).

^{13}C-NMR (100 MHz, $CDCl_3$): δ = 159.7 (C_q), 150.0 (CH), 140.5 (C_q), 138.5 (C_q), 136.9 (C_q), 136.3 (CH), 136.1 (C_q), 133.9 (C_q), 132.2 (C_q), 128.6 (CH), 128.2 (CH), 127.6 (CH), 127.1 (CH), 127.0 (CH), 126.0 (CH), 125.6 (CH), 125.5 (CH), 124.7 (CH), 124.5 (CH), 121.9 (CH), 36.7 (CH_2), 20.5 (CH_3).

IR (ATR): $\tilde{\nu}$ = 3044, 1582, 1562, 1460, 1422, 1397, 1026, 770, 748, 621 cm^{-1}.

m.p.: 75–77 °C.

MS (ESI) *m*/*z* (relative intensity): 332 (2) $[M+Na]^+$, 310 (100) $[M+H]^+$.

HR-MS (ESI): *m*/*z* calcd for $C_{23}H_{20}N^+$ $[M+H]^+$ 310.1590, found 310.1592.

2-{2-[4-(Chloromethyl)benzyl]-6-methylphenyl}pyridine (265ap)

1,4-Bis[3-methyl-2-(pyridin-2-yl)benzyl]benzene (266aa)

The general procedure **F** was followed using 2-(*o*-tolyl)pyridine (**44a**, 186 mg, 1.1 mmol) and 1,4-bis(chloromethyl)benzene (**90p**, 88.2 mg, 0.5 mmol). After 24 h, purification by column chromatography (*n*-hexane/EtOAc 15:1 to 2:1) yielded **265ap** (7.2 mg, 5%) as a viscous colorless oil and **266aa** (158 mg, 72%) as white solid.

2-{2-[4-(Chloromethyl)benzyl]-6-methylphenyl}pyridine (265ap)

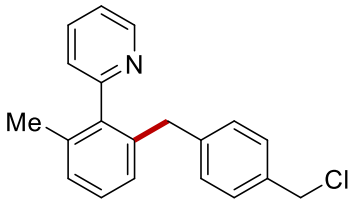

^{1}H-NMR (400 MHz, $CDCl_3$): δ = 8.68 (ddd, *J* = 4.9, 1.8, 0.9 Hz, 1H), 7.63 (ddd, *J* = 7.7, 7.7, 1.8 Hz, 1H), 7.25–7.19 (m, 2H), 7.19–7.12 (m, 3H), 7.05 (ddt, *J* = 7.8, 2.2, 1.3 Hz, 2H), 6.93–6.87 (m, 2H), 4.52 (s, 2H), 3.74 (s, 2H), 2.04 (s, 3H).

^{13}C-NMR (100 MHz, $CDCl_3$): δ = 159.5 (C_q), 149.7 (CH), 141.7 (C_q), 140.7 (C_q), 138.7 (C_q), 136.3 (C_q), 136.1 (CH), 135.0 (C_q), 129.3 (CH), 128.6 (CH), 128.4 (CH), 128.2 (CH), 127.8 (CH), 125.0 (CH), 121.9 (CH), 46.4 (CH_2), 39.3 (CH_2), 20.5 (CH_3).

IR (ATR): $\tilde{\nu}$ = 1618, 1512, 1463, 1422, 1264, 770, 739, 724, 696 cm^{-1}.

MS (ESI) *m*/*z* (relative intensity): 330 (4) $[M(^{35}Cl)+Na]^+$, 308 (100) $[M(^{35}Cl)+H]^+$.

HR-MS (ESI): *m*/*z* calcd for $C_{20}H_{19}{}^{35}ClN^+$ $[M+H]^+$ 308.1201, found 308.1203.

1,4-Bis[3-methyl-2-(pyridin-2-yl)benzyl]benzene (266aa)

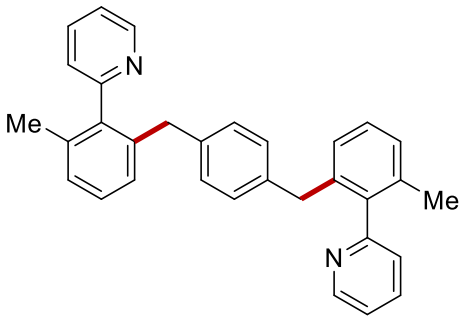

^{1}H-NMR (400 MHz, $CDCl_3$): δ = 8.92–8.57 (m, 2H), 7.62 (ddd, *J* = 7.6, 7.6, 1.8 Hz, 2H), 7.30–7.15 (m, 6H), 7.10–7.03 (m, 4H), 6.79 (s, 4H), 3.72 (s, 4H), 2.08 (s, 6H).

^{13}C-NMR (100 MHz, $CDCl_3$): δ = 159.3 (C_q), 149.4 (CH), 140.3 (C_q), 139.0 (C_q), 138.3 (C_q), 138.3 (C_q), 135.9 (CH), 128.6 (CH), 127.9 (CH), 127.9 (CH), 127.4 (CH), 124.8 (CH), 121.6 (CH), 38.8 (CH_2), 20.3 (CH_3).

IR (ATR): $\tilde{\nu}$ = 1822, 1511, 1459, 1422, 1264, 1025, 791, 731, 701 cm^{-1}.

m.p.: 141–142 °C.

MS (ESI) *m*/*z* (relative intensity): 363 (3) $[M+Na]^+$, 441 (100) $[M+H]^+$.

HR-MS (ESI): *m*/*z* calcd for $C_{32}H_{29}N_2^+$ $[M+H]^+$ 441.2325, found 441.2327.

(*R*)-2-({4-[3-Methyl-2-(pyridin-2-yl)benzyl]benzoyl}oxy)propane-1,3-diyl didodecanoate (265ar)

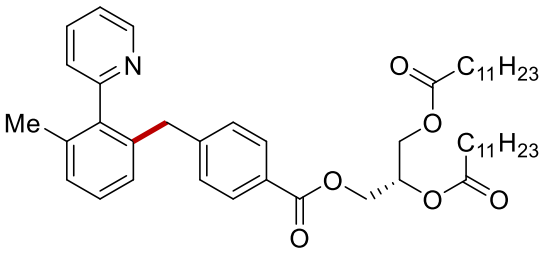

The general procedure **F** was followed using 2-(*o*-tolyl)pyridine (**44a**, 84.6 mg, 0.50 mmol) and benzyl chloride **90r** (457 mg, 0.75 mmol). After 24 h, purification by column chromatography (*n*-hexane/EtOAc 20:1 to 10:1) followed by recycling preparative HPLC yielded **265ar** (330 mg, 89%) as a viscous colorless oil. The product was obtained as a mixture of regioisomers (*ortho*:others 92:8).

^{1}H-NMR (400 MHz, $CDCl_3$): δ = 8.70 (dd, *J* = 5.0, 1.6 Hz, 1H), 7.81 (d, *J* = 8.0 Hz, 2H), 7.64 (ddd, *J* = 7.7, 7.7, 1.8 Hz, 1H), 7.31–7.17 (m, 3H), 7.12–6.91 (m, 4H), 5.52–5.33 (m, 1H), 4.49 (dd, *J* = 11.9, 4.4 Hz, 1H), 4.39 (dd, *J* = 12.0, 5.1 Hz, 2H), 4.23 (dd, *J* = 11.9, 6.0 Hz, 1H), 3.82 (s, 2H), 2.34 (t, *J* = 7.5 Hz, 4H), 2.06 (s, 3H), 1.61 (q, *J* = 7.2 Hz, 4H), 1.35–1.21 (m, 32H), 0.89 (t, *J* = 6.5 Hz, 6H).

^{13}C-NMR (100 MHz, $CDCl_3$): δ = 173.4 (C_q), 173.0 (C_q), 166.1 (C_q), 159.3 (C_q), 149.7 (CH), 147.2 (C_q), 140.6 (C_q), 137.9 (C_q), 136.4 (C_q), 136.1 (CH), 129.7 (CH), 129.0 (CH), 128.6 (CH), 128.3 (CH), 127.8 (CH), 127.1 (C_q), 125.0 (CH), 121.9 (CH), 69.0 (CH), 62.8 (CH_2), 62.3 (CH_2), 39.6 (CH_2), 34.3 (CH_2), 34.2 (CH_2), 32.0 (CH_2), 29.7 (CH_2), 29.6 (CH_2), 29.6 (CH_2), 29.4 (CH_2), 29.4 (CH_2), 29.2 (CH_2), 29.2 (CH_2), 25.0 (CH_2), 25.0 (CH_2), 22.8 (CH_2), 20.4 (CH_3), 14.2 (CH_3).

IR (ATR): $\tilde{\nu}$ = 1745, 1721, 1269, 1177, 1106, 1020, 908, 750, 732 cm^{-1}.

MS (ESI) *m*/*z* (relative intensity): 1485 (68) $[2M+H]^+$, 743 (100) $[M+H]^+$.

HR-MS (ESI): *m*/*z* calcd for $C_{47}H_{68}NO_6^+$ $[M+H]^+$ 742.5041, found 742.5043.

Methyl {4-[3-methyl-2-(pyridin-2-yl)benzyl]benzoyl}-L-valinate (265as)

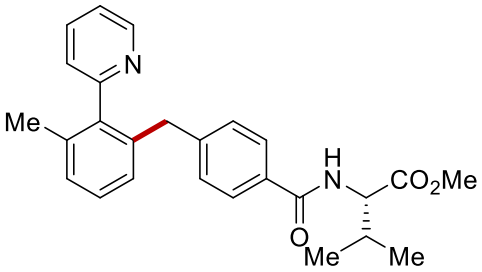

The general procedure **F** was followed using 2-(*o*-tolyl)pyridine (**44a**, 84.6 mg, 0.50 mmol) and benzyl chloride **90s** (212 mg, 0.75 mmol). After 24 h, purification by column chromatography (*n*-hexane/EtOAc 4:1 to 2:1) and recycling preparative HPLC yielded **265as** (165 mg, 79%) as a viscous colorless oil. The product was obtained as a mixture of regioisomers (*ortho*:others 98:2).

^{1}H-NMR (400 MHz, $CDCl_3$): δ = 8.65 (ddd, J = 5.0, 1.9, 0.9 Hz, 1H), 7.63–7.55 (m, 3H), 7.25–7.10 (m, 3H), 7.06–6.98 (m, 2H), 6.94 (d, J = 8.0 Hz, 2H), 6.59 (d, J = 8.7 Hz, 1H), 4.73 (dd, J = 8.6, 4.9 Hz, 1H), 3.77 (s, 2H), 3.73 (s, 3H), 2.29–2.12 (hept, J = 6.9 Hz, 1H), 2.02 (s, 3H), 0.96 (d, J = 7.0, 3H), 0.95 (d, J = 7.0, 3H).

^{13}C-NMR (100 MHz, $CDCl_3$): δ = 172.7 (C_q), 167.2 (C_q), 159.1 (C_q), 149.6 (CH), 145.3 (C_q), 140.5 (C_q), 138.0 (C_q), 136.3 (C_q), 136.1 (CH), 131.6 (C_q), 129.0 (CH), 128.4 (CH), 128.1 (CH), 127.6 (CH), 126.9 (CH), 124.9 (CH), 121.8 (CH), 57.4 (CH_3), 52.2 (CH), 39.3 (CH_2), 31.6 (CH), 20.3 (CH_3), 19.0 (CH_3), 18.0 (CH_3).

IR (ATR): $\tilde{\nu}$ = 1728, 1639, 1522, 1495, 1436, 1206, 1156, 908, 772, 726 cm^{-1}.

MS (ESI) *m*/*z* (relative intensity): 833 (20) $[2M+H]^+$, 439 (5) $[M+Na]^+$, 417 (100) $[M+H]^+$.

HR-MS (ESI): *m*/*z* calcd for $C_{26}H_{29}N_2O_3^+$ $[M+H]^+$ 417.2173, found 417.2174.

2-[2-(4-Fluorobenzyl)phenyl]pyridine (265ea)

2-[2,6-Bis(4-fluorobenzyl)phenyl]pyridine (265ea')

The general procedure **F** was followed using pyridine **44e** (77.6 mg, 0.50 mmol) and benzyl chloride **90a** (108 mg, 0.75 mmol). After 24 h, purification by column chromatography (*n*-hexane/EtOAc 10:1) yielded **265ea** (27.6 mg, 21%) as a viscous colorless oil and the di-functionalized product **265ea'** (113 mg, 61%) as a white solid.

2-[2-(4-Fluorobenzyl)phenyl]pyridine (265ea)

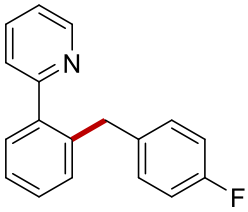

^{1}H-NMR (300 MHz, $CDCl_3$): δ = 8.70 (dt, J = 4.2, 1.7 Hz, 1H), 7.69 (ddd, J = 7.7, 7.7, 1.8 Hz, 1H), 7.50–7.18 (m, 6H), 7.03–6.74 (m, 4H), 4.12 (s, 2H).

^{13}C-NMR (75 MHz, $CDCl_3$): δ = 161.5 (d, $^{1}J_{C–F}$ = 245 Hz, C_q), 159.7 (C_q), 149.2 (CH), 140.7 (C_q), 138.9 (C_q), 137.1 (d, $^{4}J_{C–F}$ = 3 Hz, C_q), 136.4 (CH), 130.7 (CH), 130.3 (d, $^{3}J_{C–F}$ = 8 Hz, CH), 130.1 (CH), 128.6 (CH), 126.6 (CH), 124.3 (CH), 122.0 (CH), 115.0 (d, $^{2}J_{C–F}$ = 21 Hz, CH), 38.2 (CH_2).

^{19}F-NMR (282 MHz, $CDCl_3$): δ = – 117.8 (s).

IR (ATR): $\tilde{\nu}$ = 1585, 1506, 1469, 1425, 1218, 1156, 811, 749, 499 cm^{-1}.

MS (ESI) *m*/*z* (relative intensity): 286 (64) $[M+Na]^+$, 264 (100) $[M+H]^+$.

HR-MS (ESI): *m*/*z* calcd for $C_{18}H_{15}FN^+$ $[M+H]^+$ 264.1183, found: 264.1187.

2-[2,6-Bis(4-fluorobenzyl)phenyl]pyridine (265ea')

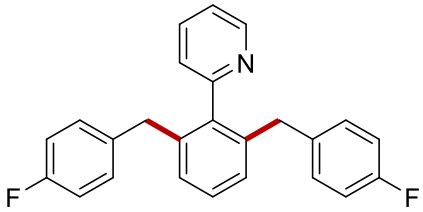

^{1}H-NMR (300 MHz, $CDCl_3$): δ = 8.68 (ddd, J = 4.9, 1.9, 1.0 Hz, 1H), 7.55 (ddd, J = 7.7, 7.7, 1.8 Hz, 1H), 7.35–7.25 (m, 1H), 7.22 (ddd, J = 7.6, 4.9, 1.2 Hz, 1H), 7.12 (d, J = 7.6 Hz, 2H), 6.90–6.79 (m, 9H), 3.73 (s, 4H).

^{13}C-NMR (75 MHz, $CDCl_3$): δ = 160.9 (d, $^{1}J_{C–F}$ = 245 Hz, C_q), 159.7 (C_q), 149.6 (CH), 140.5 (C_q), 139.3 (C_q), 136.6 (d, $^{4}J_{C–F}$ = 3 Hz, C_q), 135.9 (CH), 130.3 (d, $^{3}J_{C–F}$ = 8 Hz, CH), 128.5 (CH), 128.4 (CH), 125.4 (CH), 122.0 (CH), 115.0 (d, $^{2}J_{C–F}$ = 21 Hz, CH), 38.8 (CH_2).

^{19}F-NMR (282 MHz, $CDCl_3$): δ = – 117.7 (s).

IR (ATR): $\tilde{\nu}$ = 1507, 1425, 1265, 1219, 1157, 804, 732, 703 cm^{-1}.

MS (ESI) *m*/*z* (relative intensity): 394 (56) $[M+Na]^+$, 372 (100) $[M+H]^+$.

HR-MS (ESI): *m*/*z* calcd for $C_{25}H_{10}F_2N^+$ $[M+H]^+$ 372.1558, found 372.1560.

2-[2-(4-Fluorobenzyl)-6-(trifluoromethyl)phenyl]pyridine (265ba)

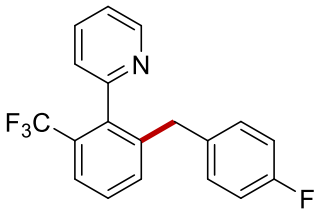

The general procedure **F** was followed using pyridine **44b** (112 mg, 0.50 mmol) and benzyl chloride **90a** (108 mg, 0.75 mmol). After 24 h, purification by column chromatography (*n*-hexane/EtOAc 10:1 to 6:1) yielded **265ba** (144 mg, 87%) as a viscous colorless oil.

^{1}H-NMR (400 MHz, $CDCl_3$): δ = 8.71 (ddd, J = 4.9, 1.8, 0.9 Hz, 1H), 7.64 (ddd, J = 7.4, 1.7 Hz, 2H), 7.50–7.36 (m, 2H), 7.27 (ddd, J = 7.6, 4.9, 1.1 Hz, 1H), 7.10 (d, J = 7.8 Hz, 1H), 6.87 (d, J = 7.1 Hz, 4H), 3.74 (d, J = 2.5 Hz, 2H).

^{13}C-NMR (100 MHz, $CDCl_3$): δ = 161.4 (d, $^{1}J_{C–F}$ = 244 Hz, C_q), 156.4 (C_q), 149.1 (CH), 141.3 (C_q), 139.0 (q, $^{3}J_{C–F}$ = 4 Hz, C_q), 135.7 (C_q), 135.7 (CH), 133.6 (d, $^{4}J_{C–F}$ = 2 Hz, CH), 130.3 (d, $^{3}J_{C–F}$ = 8 Hz, CH), 129.3 (q, $^{2}J_{C–F}$ = 27 Hz, C_q), 128.4 (CH), 125.2 (q, $^{4}J_{C–F}$ = 2 Hz, CH), 124.2 (q, $^{3}J_{C–F}$ = 5 Hz, CH), 124.0 (q, $^{1}J_{C–F}$ = 276 Hz, C_q), 122.5 (CH), 115.1 (d, $^{2}J_{C–F}$ = 21 Hz, CH), 38.2 (CH_2).

^{19}F-NMR (377 MHz, $CDCl_3$): δ = – 117.0 (s), – 57.2 (s).

IR (ATR): $\tilde{\nu}$ = 1586, 1508, 1427, 1312, 1219, 1157, 1112, 809, 789, 748 cm^{-1}.

MS (ESI) *m*/*z* (relative intensity): 354 (8) $[M+Na]^+$, 332 (100) $[M+H]^+$.

HR-MS (ESI): *m*/*z* calcd for $C_{19}H_{14}F_4N^+$ $[M+H]^+$ 332.1057, found 332.1059.

2-[2-(4-Fluorobenzyl)-5-methylphenyl]pyridine (265ca)

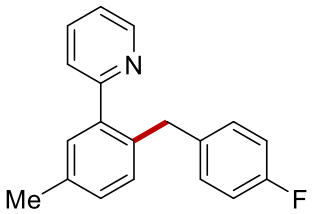

The general procedure **F** was followed using pyridine **44c** (84.6 mg, 0.50 mmol) and benzyl chloride **90a** (108 mg, 0.75 mmol). After 24 h, purification by column chromatography (*n*-hexane/EtOAc 10:1 to 8:1) yielded **265ca** (131 mg, 94%) as a viscous colorless oil.

^{1}H-NMR (400 MHz, $CDCl_3$): δ = 8.69 (s, 1H), 7.68 (s, 1H), 7.41–7.06 (m, 5H), 7.06–6.73 (m, 4H), 4.10 (s, 2H), 2.42 (s, 3H).

^{13}C-NMR (100 MHz, $CDCl_3$): δ = 161.1 (d, $^{1}J_{C–F}$ = 244 Hz, C_q), 149.1 (CH), 140.3 (C_q), 137.1 (C_q), 137.1 (C_q), 136.0 (CH), 135.6 (CH), 130.5 (CH), 130.3 (CH), 130.2 (CH), 130.1 (d, $^{3}J_{C–F}$ = 7 Hz, CH), 129.2 (CH), 124.1 (C_q), 121.7 (C_q), 114.8 (d, $^{2}J_{C–F}$ = 21 Hz, CH), 37.6 (CH_2), 21.0 (CH_3).

^{19}F-NMR (282 MHz, $CDCl_3$): δ = – 117.8 (s).

IR (ATR): $\tilde{\nu}$ = 1587, 1506, 1471, 1156, 1092, 839, 815, 769, 747, 586 cm^{-1}.

MS (ESI) *m*/*z* (relative intensity): 300 (4) [M+Na]$^+$, 278 (100) [M+H]$^+$.

HR-MS (ESI): *m*/*z* calcd for $C_{19}H_{17}FN^+$ [M+H]$^+$ 278.1340, found 278.1347.

2-[2-(4-Fluorobenzyl)-5-(trifluoromethyl)phenyl]pyridine (265da)

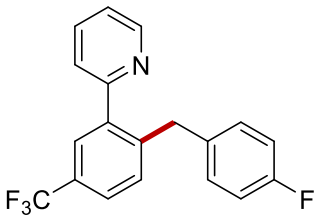

The general procedure **F** was followed using pyridine **44d** (112 mg, 0.50 mmol) and benzyl chloride **90a** (108 mg, 0.75 mmol). After 24 h, purification by column chromatography (*n*-hexane/EtOAc 10:1) yielded **265da** (161 mg, 97%) as a viscous colorless oil.

^{1}H-NMR (400 MHz, $CDCl_3$): δ = 8.78–8.67 (m, 1H), 7.77–7.67 (m, 2H), 7.65–7.56 (m, 1H), 7.37 (d, *J* = 8.1 Hz, 1H), 7.33–7.23 (m, 2H), 7.00–6.83 (m, 4H), 4.18 (s, 2H).

^{13}C-NMR (100 MHz, $CDCl_3$): δ = 161.4 (d, $^1J_{C–F}$ = 244 Hz, C_q), 158.5 (C_q), 149.4 (CH), 143.2 (C_q), 141.2 (C_q), 136.7 (CH), 135.9 (d, $^4J_{C–F}$ = 3 Hz, C_q), 131.1 (CH), 130.3 (d, $^3J_{C–F}$ = 8 Hz, CH), 128.9 (q, $^2J_{C–F}$ = 33 Hz, C_q), 126.9 (q, $^3J_{C–F}$ = 4 Hz, CH), 125.2 (q, $^3J_{C–F}$ = 4 Hz, CH), 124.2 (CH), 124.2 (q, $^1J_{C–F}$ = 272 Hz, C_q), 122.5 (CH), 115.2 (d, $^2J_{C–F}$ = 21 Hz, CH), 38.1 (CH_2).

^{19}F-NMR (282 MHz, $CDCl_3$): δ = – 62.3 (s), – 117.0 (s).

IR (ATR): $\tilde{\nu}$ = 1508, 1410, 1336, 1260, 1220, 1167, 1114, 1076, 824, 798 cm^{-1}.

MS (ESI) *m*/*z* (relative intensity): 354 (2) [M+Na]$^+$, 332 (100) [M+H]$^+$.

HR-MS (ESI): *m*/*z* calcd for $C_{19}H_{14}F_4N^+$ [M+H]$^+$ 332.1057, found 332.1063.

1-[2-(4-Fluorobenzyl)phenyl]-5-methyl-1*H*-pyrazole (268ga)

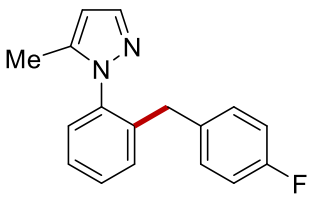

The general procedure **F** was followed using pyrazole **217g** (79.1 mg, 0.50 mmol) and benzyl chloride **90a** (108 mg, 0.75 mmol). After 24 h, purification by column chromatography (*n*-hexane/EtOAc 20:1 to 10:1) yielded **268ga** (99.8 mg, 75%) as a viscous colorless oil.

^{1}H-NMR (400 MHz, $CDCl_3$): δ = 7.63 (d, *J* = 1.8 Hz, 1H), 7.47–7.26 (m, 3H), 7.21 (d, *J* = 7.4 Hz, 1H), 6.98–6.75 (m, 4H), 6.12 (d, *J* = 2.2 Hz, 1H), 3.80 (s, 2H), 1.83 (s, 3H).

^{13}C-NMR (100 MHz, $CDCl_3$): δ = 161.3 (d, $^1J_{C–F}$ = 244 Hz, C_q), 139.7 (C_q), 139.6 (CH), 139.4 (C_q), 138.3 (C_q), 135.4 (d, $^4J_{C–F}$ = 3 Hz, C_q), 130.8 (CH), 130.2 (d, $^3J_{C–F}$ = 8 Hz, CH), 129.3 (CH), 128.1 (CH), 127.1 (CH), 114.9 (d, $^2J_{C–F}$ = 21 Hz, CH), 105.2 (CH), 36.5 (CH_2), 11.0 (CH_3).

^{19}F-NMR (282 MHz, $CDCl_3$): δ = – 117.1 (s).

IR (ATR): $\tilde{\nu}$ = 1712, 1507, 1500, 1392, 1359, 1219, 764, 529, 502 cm^{-1}.

MS (ESI) *m*/*z* (relative intensity): 289 (10) $[M+Na]^+$, 267 (100) $[M+H]^+$.

HR-MS (ESI): *m*/*z* calcd for $C_{17}H_{16}FN_2^+$ $[M+H]^+$ 267.1992, found 267.1993.

1-[2-(4-Fluorobenzyl)phenyl]-3,5-dimethyl-1*H*-pyrazole (268ea)

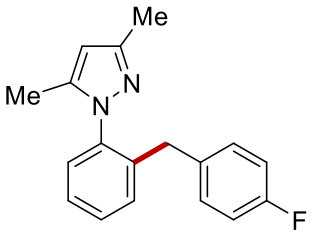

The general procedure **F** was followed using pyrazole **217e** (86.1 mg, 0.50 mmol) and benzyl chloride **90a** (108 mg, 0.75 mmol). After 24 h, purification by column chromatography (*n*-hexane/EtOAc 12:1 to 6:1) yielded **268ea** (105 mg, 75%) as a viscous colorless oil. The product was obtained as a mixture of regioisomers (*ortho*:others 92:8). Using H_2O (109 mg, 78%) or Brij-35 (10 wt%)/H_2O (112 mg, 80%) as reaction medium, yielded the product **268ea** in similar yields.

^{1}H-NMR (400 MHz, $CDCl_3$): δ = 7.42–7.34 (m, 1H), 7.34–7.27 (m, 2H), 7.20 (dd, *J* = 8.1, 1.4 Hz, 1H), 6.95–6.84 (m, 4H), 5.91 (d, *J* = 0.9 Hz, 1H), 3.82 (s, 2H), 2.34 (s, 3H), 1.80 (s, 3H).

^{13}C-NMR (100 MHz, $CDCl_3$): δ = 161.4 (d, $^1J_{C–F}$ = 245 Hz, C_q), 148.7 (C_q), 140.5 (C_q), 139.6 (C_q), 138.5 (C_q), 135.7 (d, $^4J_{C–F}$ = 3 Hz, C_q), 130.8 (CH), 130.4 (d, $^3J_{C–F}$ = 7.8 Hz, CH), 129.2 (CH), 128.4 (CH), 127.2 (CH), 114.9 (d, $^2J_{C–F}$ = 21 Hz, CH), 105.1 (CH), 36.7 (CH_2), 13.7 (CH_3), 11.2 (CH_3).

^{19}F-NMR (282 MHz, $CDCl_3$): δ = – 117.3 (s).

IR (ATR): $\tilde{\nu}$ = 1555, 1504, 1416, 1218, 1157, 842, 811, 774, 735, 503 cm^{-1}.

m.p.: 81–82 °C.

MS (ESI) *m*/*z* (relative intensity): 303 (20) $[M+Na]^+$, 281 (100) $[M+H]^+$.

HR-MS (ESI): *m*/*z* calcd for $C_{18}H_{18}FN_2^+$ $[M+H]^+$ 281.1449, found 281.1449.

1-[2-(4-Bromobenzyl)phenyl]-3,5-dimethyl-1*H*-pyrazole (268eg)

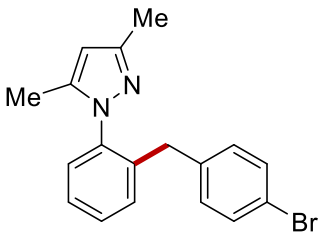

The general procedure **F** was followed using pyrazole **217e** (86.1 mg, 0.50 mmol) and benzyl chloride **90g** (154 mg, 0.75 mmol). After 24 h, purification by column chromatography (*n*-hexane/EtOAc 12:1 to 8:1) yielded **268eg** (123 mg, 72%) as a viscous colorless oil. The product was obtained as a mixture of regioisomers (*ortho*:others 93:7). Using H_2O (116 mg, 68%) or Brij-35 (10 wt%)/H_2O (123 mg, 72%) as reaction medium, yielded the product **268eg** in similar yields.

^{1}H-NMR (400 MHz, $CDCl_3$): δ = 7.47–7.24 (m, 5H), 7.24–7.16 (m, 1H), 6.87–6.77 (m, 2H), 5.91 (s, 1H), 3.79 (s, 2H), 2.33 (s, 3H), 1.81 (s, 3H).

^{13}C-NMR (100 MHz, $CDCl_3$): δ = 148.7 (C_q), 140.5 (C_q), 139.1 (C_q), 139.0 (C_q), 138.5 (C_q), 131.2 (CH), 130.8 (CH), 130.7 (CH), 129.2 (CH), 128.3 (CH), 127.2 (CH), 119.9 (C_q), 105.2 (CH), 36.8 (CH_2), 13.7 (CH_3), 11.2 (CH_3).

IR (ATR): $\tilde{\nu}$ = 1555, 1502, 1486, 1455, 1365, 1069, 1011, 792, 775, 743 cm^{-1}.

MS (ESI) *m*/*z* (relative intensity): 363 (20) $[M(^{79}Br)+Na]^+$, 341 (100) $[M(^{79}Br)+H]^+$.

HR-MS (ESI): *m*/*z* calcd for $C_{18}H_{18}{}^{79}BrN_2^+$ $[M+H]^+$ 341.0648, found 341.0650.

4-Butyl-1-[2-(4-fluorobenzyl)-6-methoxyphenyl]-1*H*-1,2,3-triazole (296aa)

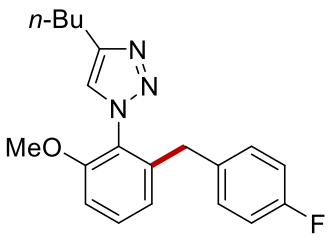

The general procedure **F** was followed using triazole **253a** (116 mg, 0.50 mmol) and benzyl chloride **90a** (108 mg, 0.75 mmol). After 24 h, purification by column chromatography (*n*-hexane/EtOAc 8:1 to 5:1) yielded **269aa** (109 mg, 64%) as a viscous colorless oil.

^{1}H-NMR (400 MHz, $CDCl_3$): δ = 7.37 (dd, *J* = 8.1, 8.1 Hz, 1H), 7.08 (d, *J* = 0.9 Hz, 1H), 6.94–6.80 (m, 6H), 3.74 (s, 2H), 3.71 (s, 3H), 2.82–2.64 (m, 2H), 1.65 (quint, *J* = 7.5 Hz, 2H), 1.38 (hept, *J* = 7.3 Hz, 2H), 0.94 (t, *J* = 7.3 Hz, 3H).

^{13}C-NMR (100 MHz, $CDCl_3$): δ = 161.5 (d, $^1J_{C–F}$ = 244 Hz, C_q), 154.9 (C_q), 147.6 (C_q), 140.0 (C_q), 135.2 (d, $^4J_{C–F}$ = 3 Hz, C_q), 130.9 (CH), 130.2 (d, $^3J_{C–F}$ = 8 Hz, CH), 125.7 (C_q), 123.9 (CH), 122.6 (CH), 115.1 (d, $^2J_{C–F}$ = 21 Hz, CH), 110.2 (CH), 56.1 (CH_2), 36.6 (CH_2), 31.6 (CH_2), 25.4 (CH_2), 22.4 (CH_2), 13.9 (CH_3).

^{19}F-NMR (282 MHz, $CDCl_3$): δ = – 117.0 (s).

IR (ATR): $\tilde{\nu}$ = 1508, 1476, 1274, 1220, 1068, 1039, 823, 795, 733, 508 cm^{-1}.

MS (ESI) *m*/*z* (relative intensity): 701 (10) $[2M+Na]^+$, 679 (18) $[2M+H]^+$, 262 (3) $[2M+Na]^+$, 340 (100) $[M+H]^+$.

HR-MS (ESI): *m*/*z* calcd for $C_{20}H_{23}FN_3O^+$ $[M+H]^+$ 340.1820, found 340.1817.

2-[2,6-Bis(4-fluorobenzyl)phenyl]-4,5-dihydrooxazole (270ba')

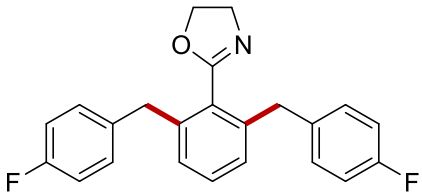

The general procedure **F** was followed using oxazoline **246b** (73.6 mg, 0.50 mmol) and benzyl chloride **90a** (108 mg, 0.75 mmol). After 24 h, purification by column chromatography (*n*-hexane/EtOAc 10:1 to 1:1) yielded **270ba'** (122 mg, 67%) as a pale brown solid.

^{1}H-NMR (400 MHz, $CDCl_3$): δ = 7.25 (dd, *J* = 7.7, 7.7 Hz, 1H), 7.12 (dd, *J* = 8.3, 5.5 Hz, 4H), 7.04–6.92 (m, 6H), 4.15 (t, *J* = 9.4 Hz, 2H), 4.03 (s, 4H), 3.95 (t, *J* = 9.5 Hz, 2H).

^{13}C-NMR (100 MHz, $CDCl_3$): δ = 163.5 (C_q), 161.5 (d, $^1J_{C–F}$ = 244 Hz, C_q), 140.5 (C_q), 136.3 (d, $^4J_{C–F}$ = 3 Hz, C_q), 130.5 (d, $^3J_{C–F}$ = 8 Hz, CH), 129.9 (CH), 129.0 (C_q), 128.2 (CH), 115.2 (d, $^2J_{C–F}$ = 21 Hz, CH), 67.1 (CH_2), 55.2 (CH_2), 38.8 (CH_2).

^{19}F-NMR (282 MHz, $CDCl_3$): δ = – 117.2 (s).

IR (ATR): $\tilde{\nu}$ = 1667, 1600, 1575, 1508, 1461, 1349, 1215, 1155, 1092, 936 cm^{-1}.

m.p.: 118–119 °C.

MS (ESI) *m*/*z* (relative intensity): 386 (4) $[M+Na]^+$, 364 (100) $[M+H]^+$.

HR-MS (ESI): *m*/*z* calcd for $C_{23}H_{20}F_2NO^+$ $[M+H]^+$ 364.1507, found 364.1508.

6-[2-(4-Fluorobenzyl)-4-methoxyphenyl)]-9-*iso*-propyl-9*H*-purine (271aa)

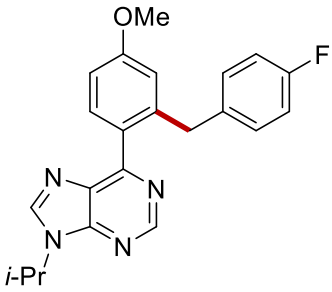

The general procedure **F** was followed using purine **267a** (67.1 mg, 0.25 mmol) and benzyl chloride **90a** (54.1 mg, 0.375 mmol) in 1,2-DCE (1.0 mL). After 24 h, purification by column chromatography (*n*-hexane/EtOAc 1:1) yielded **271aa** (64.2 mg, 67%) as a viscous colorless oil. The product was obtained as a mixture of regioisomers (*ortho*:others 98:2).

^{1}H-NMR (400 MHz, $CDCl_3$): δ = 8.94 (s, 1H), 8.08 (s, 1H), 7.73 (d, J = 8.5 Hz, 1H), 6.95–6.88 (m, 3H), 6.84–6.65 (m, 3H), 4.92 (hept, J = 6.6 Hz, 1H), 4.25 (s, 2H), 3.79 (s, 3H), 1.64 (d, J = 6.8 Hz, 6H).

^{13}C-NMR (100 MHz, $CDCl_3$): δ = 161.0 (d, $^{1}J_{C–F}$ = 245 Hz, C_q), 160.7 (C_q), 158.4 (C_q), 151.7 (CH), 151.3 (C_q), 142.1 (C_q), 142.0 (CH), 136.6 (d, $^{4}J_{C–F}$ = 4 Hz, C_q), 132.9 (CH), 132.6 (C_q), 130.4 (d, $^{3}J_{C–F}$ = 4 Hz, CH), 127.7 (C_q), 117.0 (CH), 114.7 (d, $^{2}J_{C–F}$ = 23 Hz, CH), 111.4 (CH), 55.3 (CH_3), 47.4 (CH), 38.6 (CH_2), 22.6 (CH_3).

^{19}F-NMR (282 MHz, $CDCl_3$): δ = – 117.9 (s).

IR (ATR): $\tilde{\nu}$ = 1606, 1576, 1504, 1329, 1282, 1213, 1157, 1061, 806, 727 cm^{-1}.

MS (ESI) *m*/*z* (relative intensity): 399 (18) $[M+Na]^+$, 377 (100) $[M+H]^+$.

HR-MS (ESI): *m*/*z* calcd for $C_{22}H_{22}FN_4O^+$ $[M+H]^+$ 377.1772, found 377.1775.

(2*R*,3*R*,4*S*,5*R*)-2-(Acetoxymethyl)-5-{6-[2-(4-fluorobenzyl)phenyl]-9*H*-purin-9-yl}tetrahydrofuran-3,4-diyl diacetate (271ba)

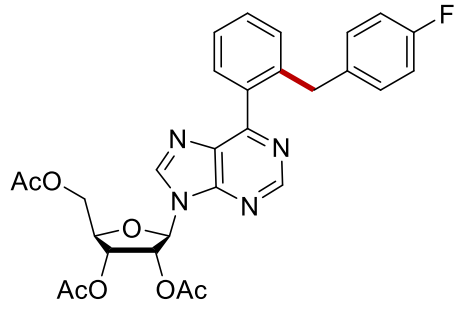

The general procedure **F** was followed using purine **267b** (113 mg, 0.25 mmol) and benzyl chloride **90a** (54.1 mg, 0.375 mmol) in 1,2-DCE (1.0 mL). After 24 h, purification by column chromatography (*n*-hexane/EtOAc 1:1 to 1:2) yielded **271ba** (106 mg, 76%) as a viscous colorless oil.

^{1}H-NMR (400 MHz, $CDCl_3$): δ = 8.99 (s, 1H), 8.19 (s, 1H), 7.66 (dd, J = 6.7, 2.4 Hz, 1H), 7.48–7.33 (m, 2H), 7.27–7.23 (m, 1H), 6.90–6.81 (m, 2H), 6.77–6.68 (m, 2H), 6.24 (d, J = 5.1 Hz, 1H), 6.00 (dd, J = 5.4, 5.4 Hz, 1H), 5.76–5.58 (m, 1H), 4.52–4.42 (m, 2H), 4.38 (dd, J = 12.9, 5.3 Hz, 1H), 4.22–4.14 (m, 2H), 2.14 (s, 3H), 2.10 (s, 3H), 2.09 (s, 3H).

^{13}C-NMR (100 MHz, $CDCl_3$): δ = 170.3 (C_q), 169.6 (C_q), 169.4 (C_q), 161.0 (d, $^1J_{C–F}$ = 245 Hz, C_q), 159.2 (C_q), 152.4 (CH), 151.3 (C_q), 143.0 (CH), 140.1 (C_q), 136.5 (d, $^4J_{C–F}$ = 2 Hz, C_q), 134.7 (C_q), 132.9 (C_q), 131.0 (CH), 130.9 (CH), 130.3 (d, $^3J_{C–F}$ = 7 Hz, CH), 130.0 (CH), 126.5 (CH), 114.7 (d, $^2J_{C–F}$ = 21 Hz, CH), 86.6 (CH), 80.4 (CH), 73.1 (CH), 70.6 (CH), 63.1 (CH_2), 38.4 (CH_2), 20.8 (CH_3), 20.6 (CH_3), 20.5 (CH_3).

^{19}F-NMR (282 MHz, $CDCl_3$): δ = – 117.7 (s).

IR (ATR): $\tilde{\nu}$ = 1744, 1582, 1507, 1204, 1093, 1044, 909, 761, 724, 645 cm^{-1}.

MS (ESI) *m*/*z* (relative intensity): 1125 (12) $[2M+H]^+$, 585 (10) $[M+Na]^+$, 563 (100) $[M+H]^+$.

HR-MS (ESI): *m*/*z* calcd for $C_{29}H_{28}FN_4O_7^+$ $[M+H]^+$ 563.1937, found 563.1936.

5.6.2 Late-Stage Diversification by Ozonolysis

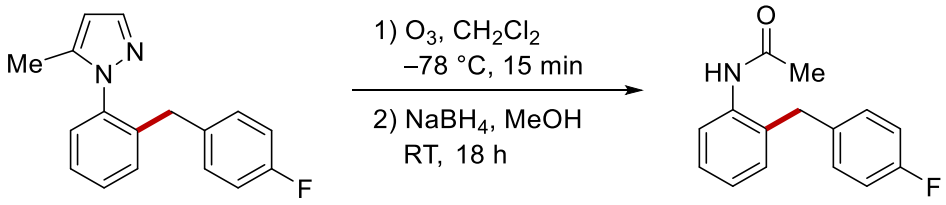

268ga **272ga**: 56%

A solution of pyrazole **268ga** (53.2 mg, 0.20 mmol) in CH_2Cl_2 (20 mL) was cooled down to –78 °C. Ozone (initial current 250 mA, flow 50 L/h) was passed through the solution for 15 min. Afterwards, the reaction was allowed to warm up to ambient temperature. Subsequently, a solution of $NaBH_4$ (30.3 mg, 0.80 mmol) in MeOH (10 mL) was added, and the reaction was stirred for 18 h. To quench the reaction, H_2O (10 mL) and brine (10 mL) were added and the aqueous phase was extracted with CH_2Cl_2 (3 × 10 mL). After drying of the organic phase over Na_2SO_4, purification by column chromatography on silica gel (*n*-hexane/EtOAc 4:1) yielded anilide **272ga** (27.3 mg, 56%) as colourless oil

^{1}H-NMR (400 MHz, $CDCl_3$): δ = 7.59 (s, 1H), 7.45–7.37 (m, 1H), 7.38–7.30 (m, 2H), 7.19–7.14 (m, 1H), 6.86 (d, J = 5.6 Hz, 3H), 3.77 (s, 2H), 1.73 (s, 3H).

^{13}C-NMR (100 MHz, $CDCl_3$): δ =161.6 (d, $^1J_{C–F}$ = 244 Hz, C_q), 139.5 (C_q), 138.3 (C_q), 137.9 (CH), 137.0 (C_q), 135.3 (d, $^4J_{C–F}$ = 3 Hz, C_q), 131.2 (CH), 130.3 (d, $^3J_{C–F}$ = 8 Hz, CH), 128.2 (CH), 127.5 (CH), 115.1 (d, $^2J_{C–F}$ = 21 Hz, CH), 36.7 (CH_2), 9.2 (CH_3).

^{19}F-NMR (377 MHz, $CDCl_3$): δ = – 116.9 (s).

IR (ATR): $\tilde{\nu}$ = 1506, 1395, 1218, 1157, 1074, 930, 841, 809, 764, 496 cm^{-1}.

MS (ESI) *m*/*z* (relative intensity): 266 (10) $[M+Na]^+$, 243 (100) $[M+H]^+$.

HR-MS (ESI): *m*/*z* calcd for $C_{15}H_{15}FN_2O_2^+$ $[M+H]^+$ 244.1059, found 244.1060.

5.6.3 H/D Scrambling Experiments

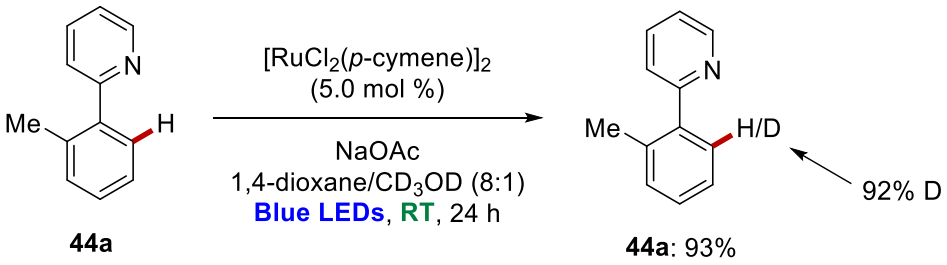

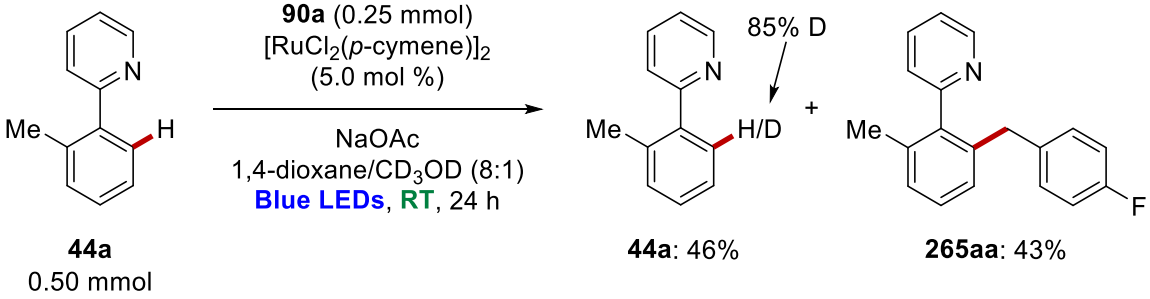

Phenylpyridine **44a** (84.6 mg, 0.50 mmol), $[RuCl_2(p\text{-cymene})]_2$ (15.3 mg, 25.0 µmol, 5.0 mol %) and NaOAc (82.0 mg, 1.00 mmol) were placed in a 10 mL vial. The vial was capped with a septum and wrapped with parafilm, before the vial was evacuated and purged with N_2 three times. Benzyl chloride **90a** (36.1 mg, 0.25 mmol), CD_3OD (0.2 mL) and 1,4-dioxane (1.6 mL) were added and the mixture was stirred under visible light irradiation (2 × Kessil A360N, temperature was maintained between 30 °C and 33 °C). After 24 h, the resulting mixture was filtered through a pad of silica gel and washed with EtOAc. Afterwards, the solvent was removed under reduced pressure. Purification by column chromatography (*n*-hexane/EtOAc 10:1) yielded **44a** (38.5 mg, 46%) and **265aa** (59.5 mg, 43%). The degree of deuteration was determined to be 85% D by employing ^{1}H-NMR spectroscopy.

By performing the H/D scrambling experiments in the absence of benzyl chloride **90a**, the reisolated starting material **44a** exhibited a deuteration degree of 92% as determined by ^{1}H-NMR spectroscopy.

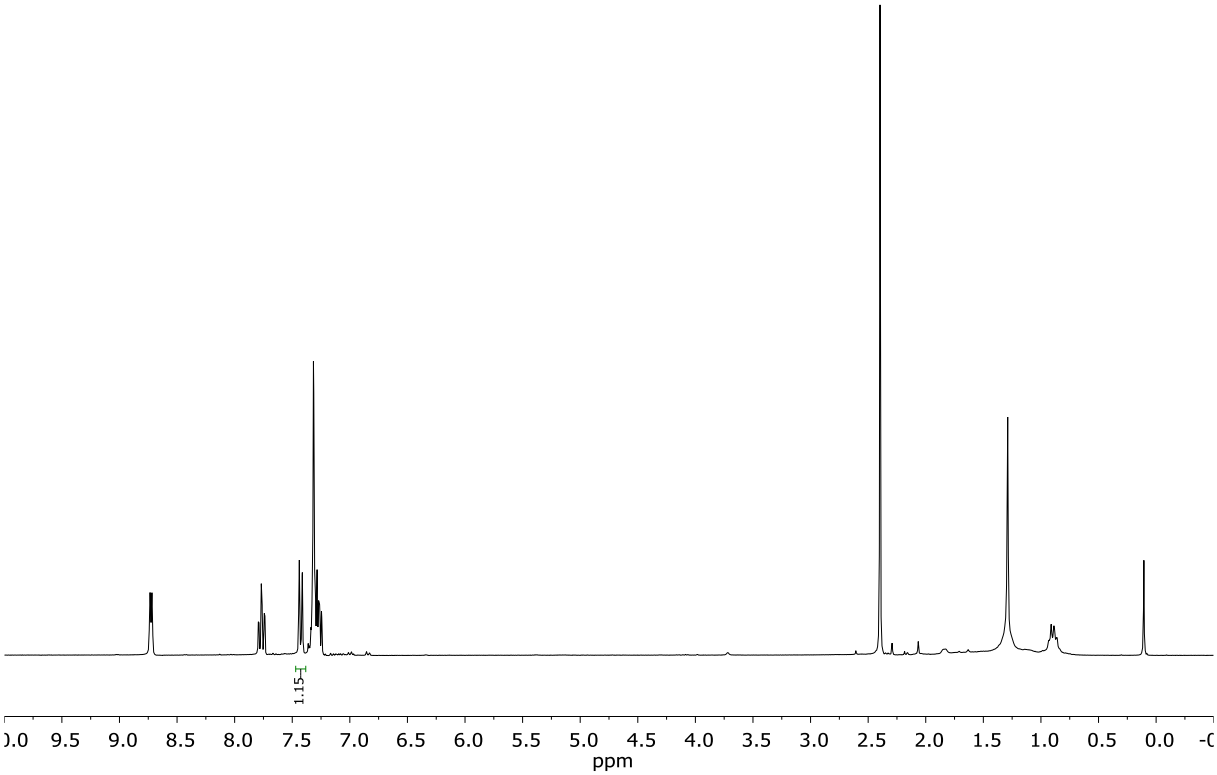

Figure 5.9: ^{1}H-NMR spectrum of deuterated starting material in presence of electrophile **90a**.

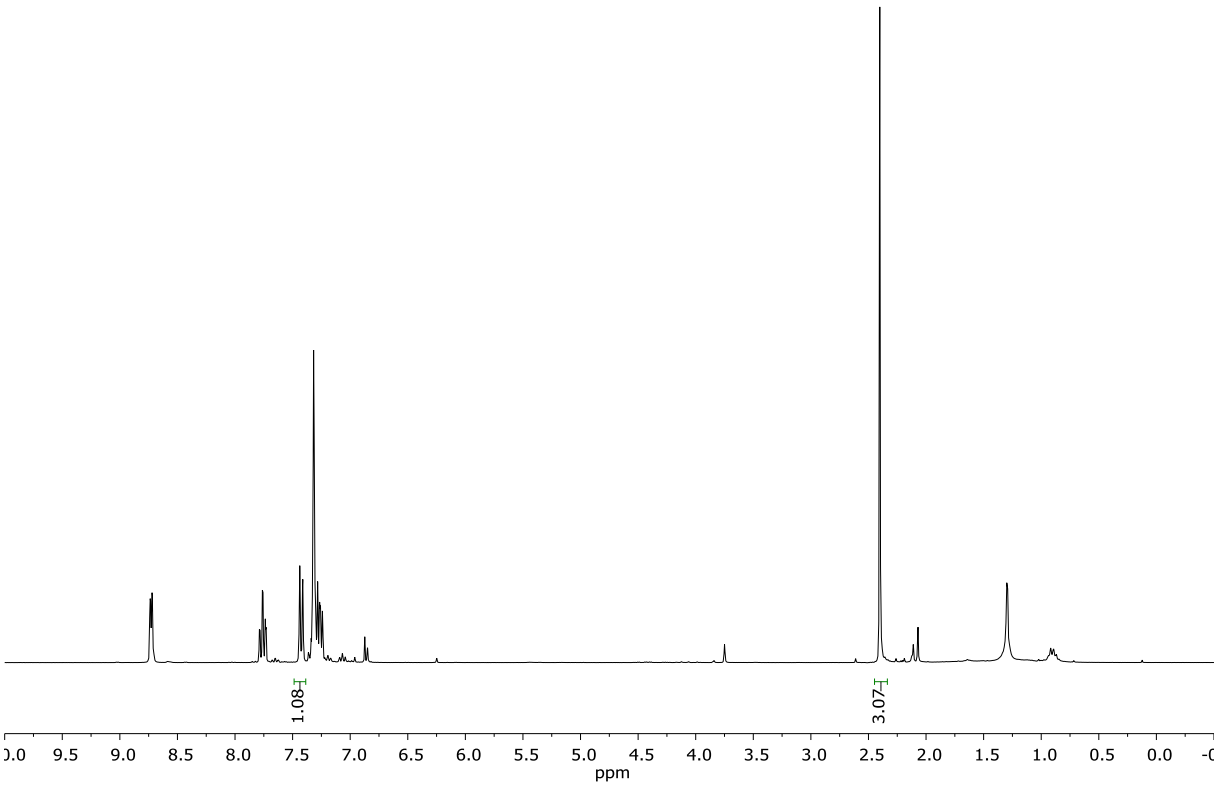

Figure 5.10: ^{1}H-NMR spectrum of deuterated starting material in absence of electrophile **90a**.

5.6.4 Competition Experiments

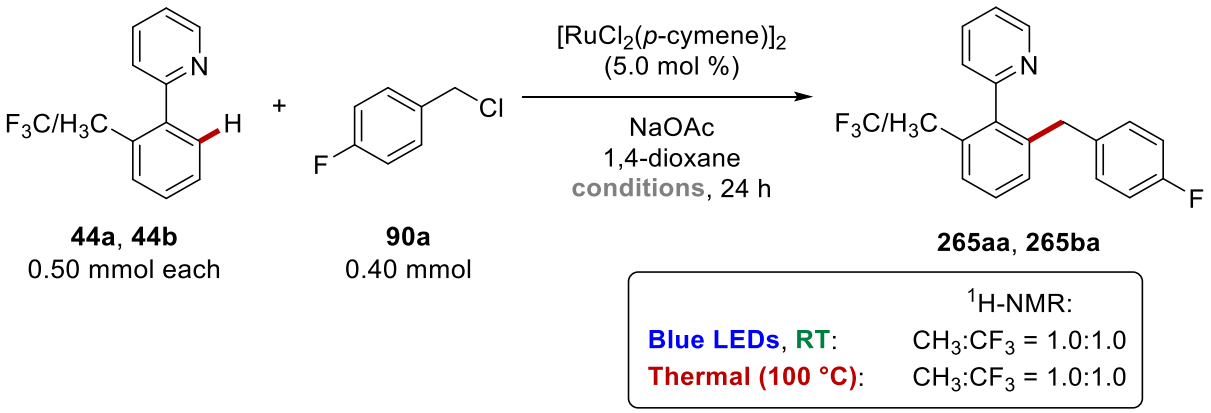

Ortho-substituted pyridines **44a** (84.6 mg, 0.50 mmol), **44b** (111 mg, 0.50 mmol), $[RuCl_2(p\text{-cymene})]_2$ (15.3 mg, 25.0 µmol, 5.0 mol %) and NaOAc (82.0 mg, 1.00 mmol) were placed in a 10 mL vial. The vial was capped with a septum and wrapped with parafilm, before the vial was evacuated and purged with N_2 three times. Benzyl chloride **90a** (57.8 mg, 0.40 mmol) and 1,4-dioxane (2.0 mL) were added and the mixture was stirred under visible light irradiation (2 × Kessil A360N, temperature was maintained between 30 °C and 33 °C) by following the General procedure **F**. After 24 h, the resulting mixture was filtered through a pad of silica gel and washed with EtOAc. Afterwards, the solvent was removed under reduced pressure. The crude mixture was analyzed by ^{1}H-NMR spectroscopy using 1,3,5-trimethoxybenzene (84.1 mg, 0.50 mmol) as internal standard and based on the NMR-data of the pure compound. The conversion of **265ba** was identified to be 40.04%, while the one of **265aa** was 39.98%. Under thermal conditions at 100 °C instead of the irradiation the ratio of **265ba** to **265aa** was determined as 41.01% to 41.00%.

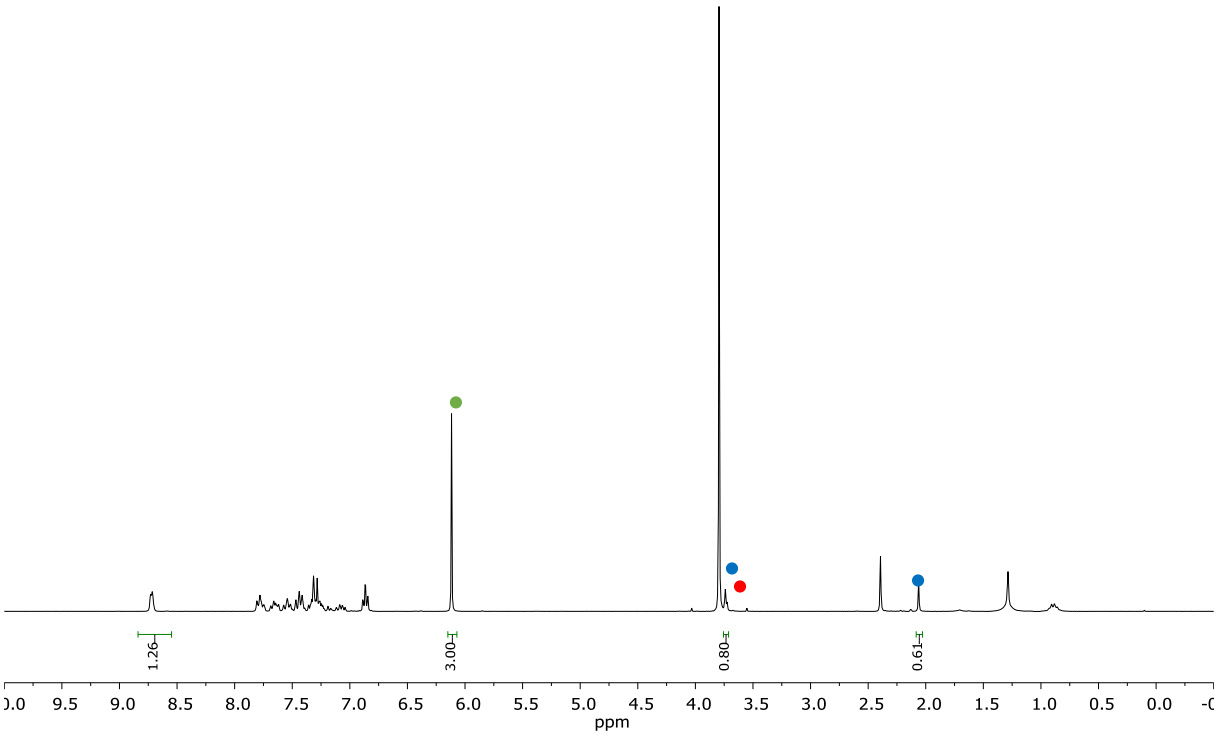

Figure 5.11: ^{1}H-NMR spectrum of competition experiment between **44a** and **44b** under visible light irradiation. • = **265aa** (Me), • = **265ba** (CF_3), • = internal standard.

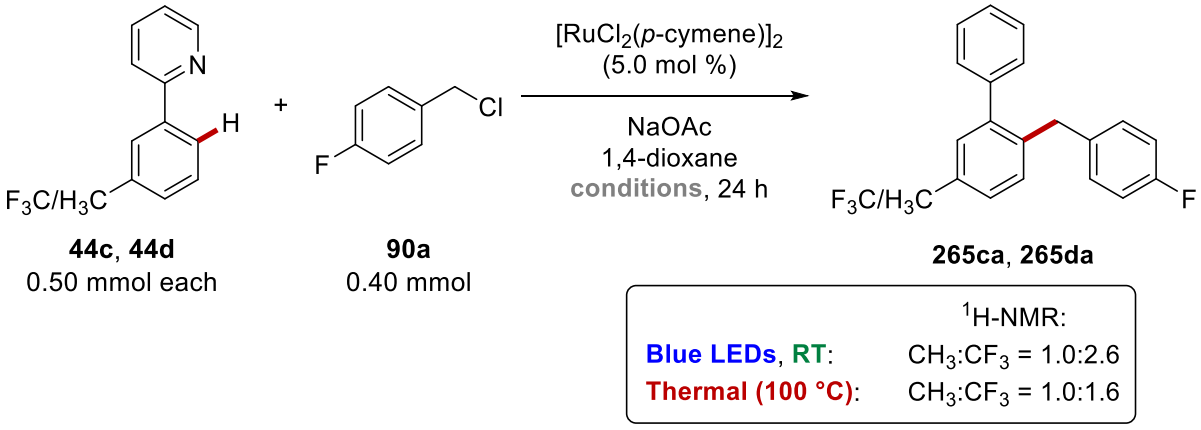

Meta-substituted pyridines **44c** (84.6 mg, 0.50 mmol), **44d** (111 mg, 0.50 mmol), $[RuCl_2(p\text{-cymene})]_2$ (15.3 mg, 25.0 µmol, 5.0 mol %) and NaOAc (82.0 mg, 1.00 mmol) were placed in a 10 mL vial. The vial was capped with a septum and wrapped with parafilm, before the vial was evacuated and purged with N_2 three times. Benzyl chloride **90a** (57.8 mg, 0.40 mmol) and 1,4-dioxane (2.0 mL) were added and the mixture was stirred under visible light irradiation (2 × Kessil A360N, temperature was maintained between 30 °C and 33 °C) by following the General procedure **F**. After 24 h, the resulting mixture was filtered through a pad

of silica gel and washed with EtOAc. Afterwards, the solvent was removed under reduced pressure. The crude mixture was analyzed by ^{1}H-NMR spectroscopy using 1,3,5-trimethoxybenzene (84.1 mg, 0.50 mmol) as internal standard and based on the NMR-data of the pure compound. The conversion of **265ca** was identified to be 19.66%, while the one of **265da** was 51.27%. Under thermal conditions at 100 °C instead of the irradiation the ratio of **265ca** to **265da** was determined as 28.21% to 44.21%.

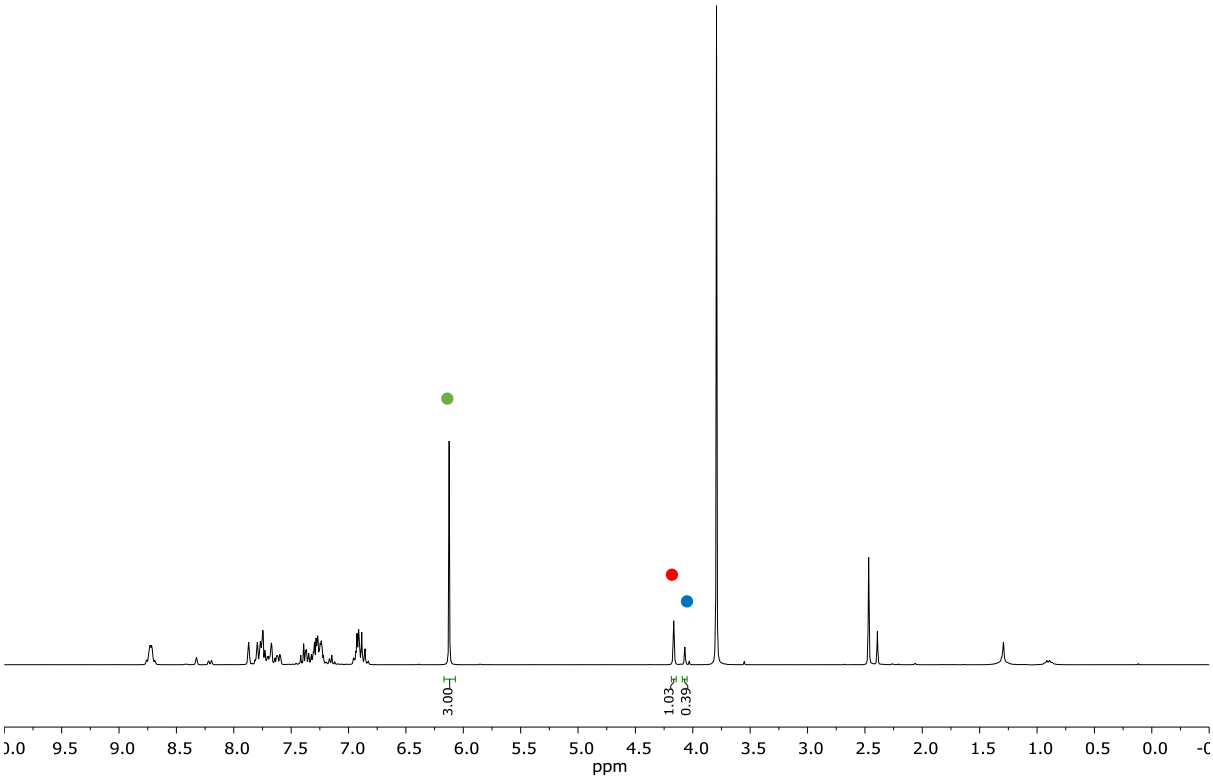

Figure 5.12: ^{1}H-NMR spectrum of competition experiment between **44c** and **44d** under visible light irradiation. • = **265ca** (Me), • = **265da** (CF_3), • = internal standard.

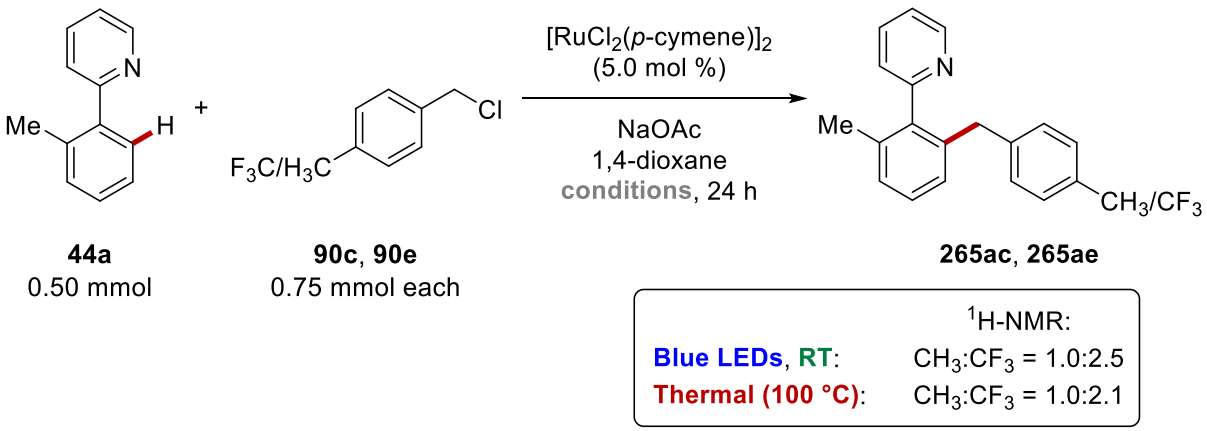

2-(*o*-Tolyl)pyridine (**44a**, 84.6 mg, 0.50 mmol), $[RuCl_2(p\text{-cymene})]_2$ (15.3 mg, 25.0 µmol, 5.0 mol %) and NaOAc (82.0 mg, 1.00 mmol) were placed in a 10 mL vial. The vial was capped with a septum and wrapped with parafilm, before the vial was evacuated and purged with N_2 three times. Benzyl chlorides **90c** (105 mg, 0.75 mmol) and **90e** (145 mg, 0.75 mmol) as well as 1,4-dioxane (2.0 mL) were added and the mixture was stirred under visible light irradiation (2 × Kessil A360N, temperature was maintained between 30 °C and 33 °C) by following the General Procedure **F**. After 24 h, the resulting mixture was filtered through a pad of silica gel and washed with EtOAc. Afterwards, the solvent was removed under reduced pressure. The crude mixture was analyzed by ^{1}H-NMR spectroscopy using 1,3,5-trimethoxybenzene (84.1 mg, 0.50 mmol) as internal standard and based on the NMR-data of the pure compound. The conversion of **265ac** was identified to be 20.20%, while the one of **265ae** was 50.81%. Under thermal conditions at 100 °C instead of the irradiation the ratio of **265ac** to **265ae** was determined as 25.32% to 54.16%.

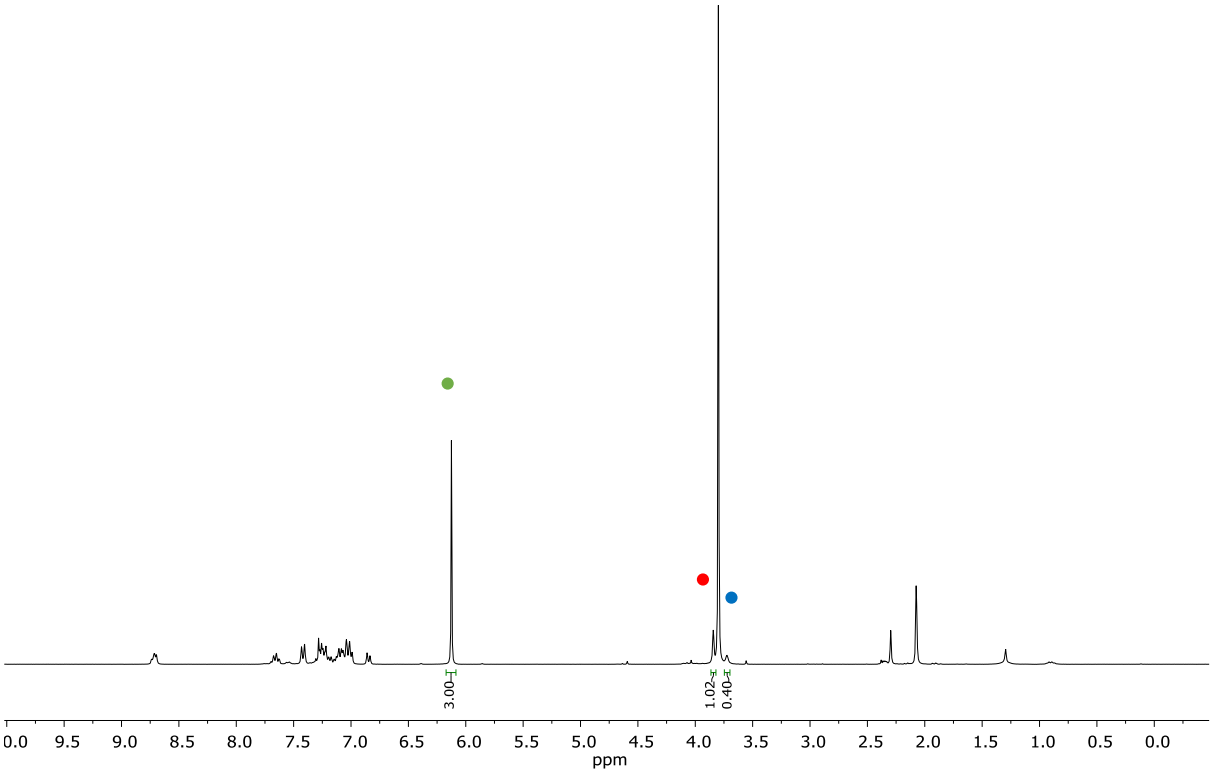

Figure 5.13: ^{1}H-NMR spectrum of competition experiment between **90c** and **90e** under visible light irradiation. • = **265ac** (Me), • = **265ae** (CF_3), • = internal standard.

*5.6.5 Photo-Induced C–H Benzylation by Ruthenacycle **276** in Stoichiometric Amounts*

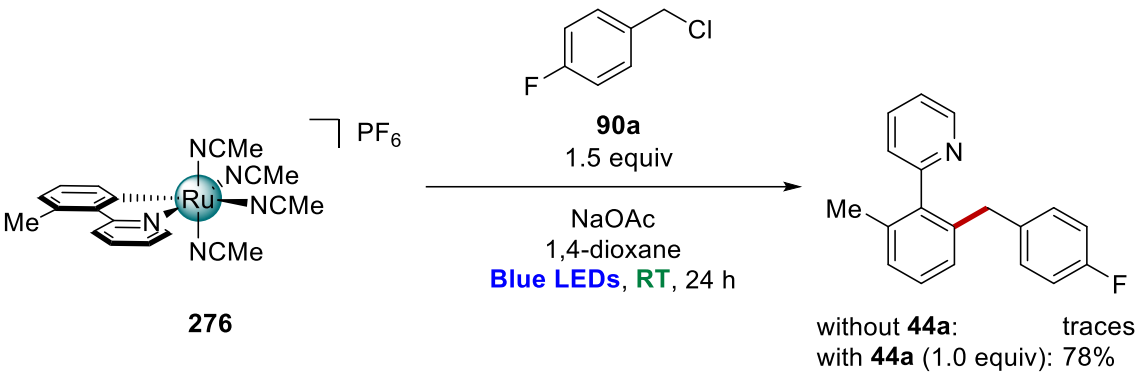

Cyclometalated complex **276** (57.6 mg, 0.10 mmol) and NaOAc (16.4 mg, 0.20 mmol) were placed in a 10 mL vial. The vial was capped with a septum and wrapped with parafilm, before the vial was evacuated and purged with N_2 three times. Benzyl chloride **90a** (17.8 mg, 0.15 mmol) and 1,4-dioxane (2.0 mL) were added and the mixture was stirred under visible light irradiation (2 × Kessil A360N, temperature was maintained between 30 °C and 33 °C). After 24 h, the resulting mixture was filtered through a pad of silica gel and washed with EtOAc. Afterwards, the filtrate was concentrated *in vacuo*, The crude mixture was analyzed by ^{1}H-NMR spectroscopy using 1,3,5-trimethoxybenzene (84.1 mg, 0.50 mmol) as internal standard. Only trace amounts of the desired product **265aa** were observed.

When the reaction was performed in the presence of arene **44a** (18.4 mg, 0.10 mmol), the product formation of **265aa** was determined to be 78%.

*5.6.6 Photo-Induced C–H Benzylation by Ruthenacycle **276** as Catalyst*

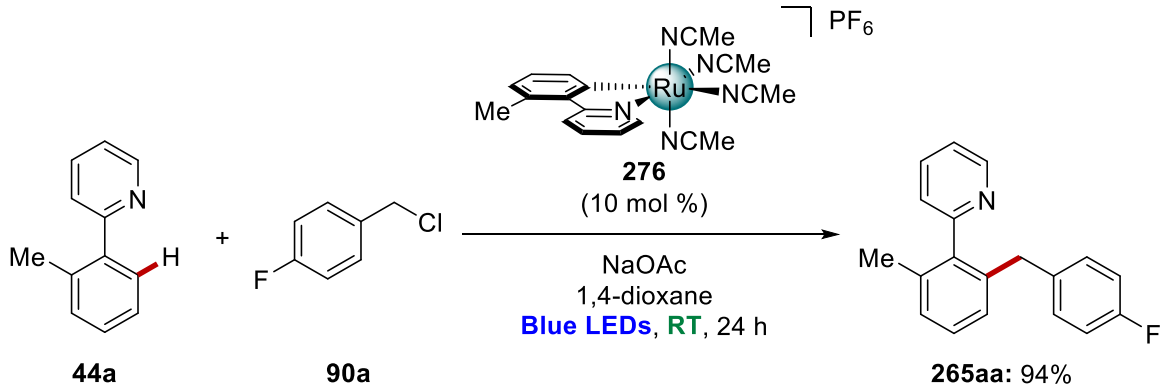

Pyridine **44a** (84.6 mg, 0.50 mmol), ruthenacycle **276** (28.9 mg, 50.0 µmol, 10 mol %) and NaOAc (82 mg, 1.00 mmol) were placed in a 10 mL vial. The vial was capped with a septum and wrapped with parafilm, before the vial was evacuated and purged with N_2 three times. Benzyl chloride **90a** (108 mg, 0.75 mmol) and 1,4-dioxane (2.0 mL) were added and the mixture was stirred under visible light irradiation (2 × Kessil A360N, temperature was maintained between 30 °C and 33 °C). After 24 h, the resulting mixture was filtered through a pad of silica gel and washed with EtOAc. Afterwards, the filtrate was concentrated *in vacuo* and purification of the residue by column chromatography (SiO_2, *n*-hexane/EtOAc 10:1) yielded *ortho*-benzylated product **265aa** (130 mg, 94%) as a viscous colorless oil.

5.6.7 Photo-Induced Benzylation in Presence of TEMPO

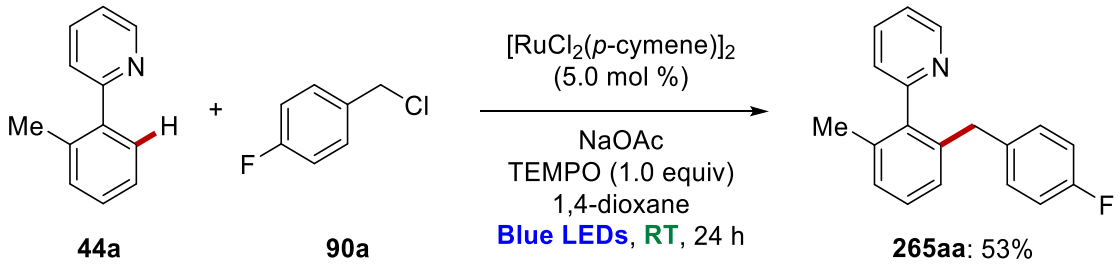

44a **90a** **265aa**: 53%

The general procedure **F** was followed using 2-(*o*-tolyl)pyridine (**44a**, 84.6 mg, 0.50 mmol), 4-fluorobenzyl chloride (**90a**, 108 mg, 0.75 mmol) and TEMPO (82.1 mg, 0.50 mmol). After 24 h, the crude reaction was analyzed by HR-MS, where the TEMPO-adduct peak was observable (**HR-MS** (ESI): *m*/*z* calcd for $C_{16}H_{15}FNO^+$ $[M+H]^+$ 266.1915, found 266.1917). The crude mixture was filtered through a pad of silica gel and washed with EtOAc. Afterwards, the filtrate was concentrated *in vacuo* and purification of the residue by column chromatography (SiO_2, *n*-hexane/EtOAc 10:1) yielded the *ortho*-benzylated product **265aa** (73.4 mg, 53%) as a viscous colorless oil.

5.6.8 On-Off Experiment in Benzylation Reaction

Pyridine **44a** (84.6 mg, 0.50 mmol), $[RuCl_2(p\text{-cymene})]_2$ (15.3 mg, 25.0 µmol, 5.0 mol %) and NaOAc (82.0 mg, 1.00 mmol) were placed in a 10 mL vial. The vial was capped with a septum and wrapped with parafilm, before the vial was evacuated and purged with N_2 three times. Benzyl chloride **90a** (108 mg, 0.75 mmol), fluorobenzene (48.1 mg, 0.50 mmol) as internal standard and 1,4-dioxane (2.0 mL) were added and the mixture was stirred with a N_2 ballon sequentially under visible light irradiation (2 × Kessil A360N, temperature was maintained between 30 °C and 33 °C) and in the absence of light. Every two hours, an aliquot of 50 µL was removed *via* syringe, diluted with $CDCl_3$, filtered through a short plug of silica gel and analyzed by ^{19}F-NMR spectrometry.

Time [h]	**265aa** [%]
0	0.01
2	31.02
4	34.15
6	77.68
8	82.21

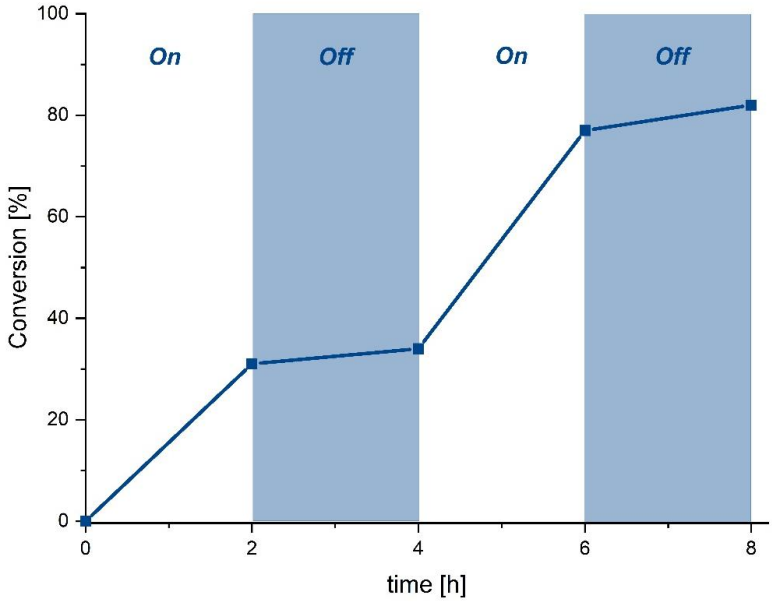

Figure 5.14: Effect of visible light irradiation on the product formation of **265aa**.

5.7 ELECTROPHOTOCHEMICAL UNDIRECTED TRIFLUOROMETHYLATION OF (HETERO-)ARENES

5.7.1 Characterization Data

1,3,5-Trimethoxy-2-(trifluoromethyl)benzene (147b)

1,3,5-Trimethoxy-2,4-bis(trifluoromethyl)benzene (147b')

The general procedure **G** was followed using 1,3,5-trimethoxybenzene (**137b**, 0.25 mmol, 42.0 mg). After electrolysis at 4 mA under blue light irradiation for 8 h, purification by column chromatography (*n*-hexane/EtOAc 10:1) yielded **147b** and **147b'** as white solids. When [Mes-Acr]ClO_4 was used as the photocatalyst, the mono-functionalized product **147b** was obtained in 72% (42.3 mg) and the di-functionalized product **147b'** in 16% (8.4 mg), while the use of [TAC]ClO_4 gave **147b** in 78% (46.0 mg) and **147b'** in 9% (6.8 mg).

1,3,5-Trimethoxy-2-(trifluoromethyl)benzene (147b)

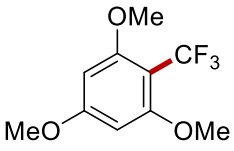

^{1}H-NMR (400 MHz, $CDCl_3$): δ = 6.14 (s, 2H), 3.83 (s, 9H).

^{13}C-NMR (100 MHz, $CDCl_3$): δ = 163.7 (C_q), 160.5 (q, $^3J_{C–F}$ = 2 Hz, C_q), 124.3 (q, $^1J_{C–F}$ = 273 Hz, C_q), 100.5 (q, $^2J_{C–F}$ = 30 Hz, C_q), 91.4 (CH), 56.4 (CH_3), 55.5 (CH_3).

^{19}F-NMR (377 MHz, $CDCl_3$): δ = – 54.2 (s).

IR (ATR): $\tilde{\nu}$ = 1589, 1459, 1417, 1278, 1232, 1207, 1161, 1092, 1024, 814 cm^{-1}.

m.p.: 63–64 °C.

MS (ESI) *m*/*z* (relative intensity): 259 (100) $[M+Na]^+$, 237 (90) $[M+H]^+$.

HR-MS (ESI): *m*/*z* calcd for $C_{10}H_{12}F_3O_3^+$ $[M+H]^+$ 237.0733, found 237.0735.

The spectral data is in accordance with those reported in the literature.[157]

1,3,5-Trimethoxy-2,4-bis(trifluoromethyl)benzene (147b')

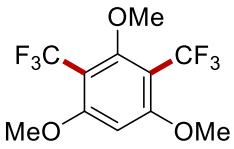

^{1}H-NMR (400 MHz, $CDCl_3$): δ = 6.35 (s, 1H), 3.96 (s, 6H), 3.82 (s, 3H).

^{13}C-NMR (100 MHz, $CDCl_3$): δ = 162.5 (C_q), 160.7 (C_q), 123.6 (q, $^{1}J_{C–F}$ = 274 Hz, C_q), 106.3 (q, $^{2}J_{C–F}$ = 30 Hz, C_q), 92.7 (CH), 64.9 (CH_3), 56.5 (CH_3).

^{19}F-NMR (377 MHz, $CDCl_3$): δ = – 55.5 (s).

IR (ATR): $\tilde{\nu}$ = 1604, 1577, 1311, 1257, 1218, 1105, 1059, 731 cm^{-1}.

m.p.: 98–100 °C.

MS (ESI) *m*/*z* (relative intensity): 327 (100) $[M+Na]^+$, 305 (10) $[M+H]^+$.

HR-MS (ESI): *m*/*z* calcd for $C_{11}H_{11}F_6O_3^+$ $[M+H]^+$ 305.0607, found 305.0609.

The spectral data is in accordance with those reported in the literature.[283]

1,3,5-Triethyl-2-(trifluoromethyl)benzene (147c)

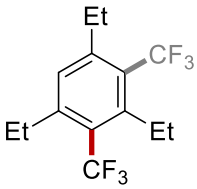

The general procedure **G** was followed using 1,3,5-triethylbenzene (**137c**, 0.25 mmol, 40.6 mg). After electrolysis at 4 mA under blue light irradiation for 8 h, purification by column chromatography (*n*-pentane) yielded **147c** as a colourless oil. When [Mes-Acr]ClO_4 was used as the photocatalyst, the product **147c** was obtained in 63% (36.8 mg), while the use of [TAC]ClO_4 gave 57% (32.7 mg). In both cases, the product was obtained as a mixture with a minor amount of the di-functionalized product **147c'** in a ratio of 3.6:1. The ratio was determined based on the ^{1}H-NMR of the isolated product.

^{1}H-NMR (300 MHz, $CDCl_3$): δ = 6.97 (s, 2H), 2.90–2.77 (m, 4H), 2.63 (q, *J* = 7.7 Hz, 2H), 1.24 (td, *J* = 7.7, 3.4 Hz, 9H).

^{13}C-NMR (100 MHz, $CDCl_3$): δ = 147.4 (C_q), 144.1 (q, $^{3}J_{C–F}$ = 2 Hz, C_q), 128.7 (CH), 126.3 (q, $^{1}J_{C–F}$ = 276 Hz, C_q), 123.8 (q, $^{2}J_{C–F}$ = 28 Hz, C_q), 28.6 (CH_2), 28.1 (CH_2), 16.7 (CH_3), 15.3 (CH_3).

^{19}F-NMR (377 MHz, $CDCl_3$): δ = – 52.4 (s).

IR (ATR): $\tilde{\nu}$ = 2968, 1609, 1575, 1459, 1294, 1199, 1144, 1105, 1062, 1038 cm^{-1}.

MS (EI) *m*/*z* (relative intensity): 230 (10) $[M]^+$, 215 (100) $[M–CH_3]^+$.

HR-MS (EI): *m*/*z* calcd for $C_{13}H_{17}F_3^+$ $[M]^+$ 230.1277, found 230.1279.

The spectral data is in accordance with those reported in the literature.[157]

4-Methyl-8-(trifluoromethyl)quinoline (147d)

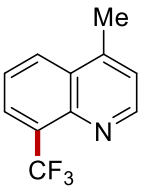

The general procedure **G** was followed using 4-methylquinoline (**137d**, 0.25 mmol, 37.1 mg). After electrolysis at 4 mA under blue light irradiation for 16 h, purification by column chromatography (*n*-hexane/EtOAc 10:1) yielded **147d** as a colourless oil. When [Mes-Acr]ClO_4 was used as the photocatalyst, the product **147d** was obtained in 52% (27.9 mg), while the use of [TAC]ClO_4 gave 60% (31.6 mg).

^{1}H-NMR (400 MHz, $CDCl_3$): δ = 8.92 (d, *J* = 4.4 Hz, 1H), 8.21 (d, *J* = 8.4 Hz, 1H), 8.07 (d, *J* = 7.3 Hz, 1H), 7.66–7.55 (m, 1H), 7.33 (d, *J* = 4.4 Hz, 1H), 2.73 (s, 3H).

^{13}C-NMR (100 MHz, $CDCl_3$): δ = 151.0 (CH), 144.7 (q, $^3J_{C–F}$ = 3 Hz, C_q), 144.7 (C_q), 128.9 (C_q), 128.5 (CH), 128.1 (q, $^2J_{C–F}$ = 30 Hz, C_q), 127.7 (q, $^3J_{C–F}$ = 6 Hz, CH), 124.4 (q, $^1J_{C–F}$ = 275 Hz, C_q), 125.0 (CH), 122.8 (CH), 19.1 (CH_3).

^{19}F-NMR (377 MHz, $CDCl_3$): δ = – 60.0 (s).

IR (ATR): $\tilde{\nu}$ = 1600, 1315, 1294, 1120, 1092, 1079, 1047, 838, 762, 713 cm^{-1}.

MS (ESI) *m*/*z* (relative intensity): 234 (12) $[M+Na]^+$, 212 (100) $[M+H]^+$.

HR-MS (ESI): *m*/*z* calcd for $C_{11}H_9NF_3^+$ $[M+H]^+$ 212.0682, found 212.0684.

The spectral data is in accordance with those reported in the literature.[157]

4,7-Dichloro-8-(trifluoromethyl)quinoline (147e)

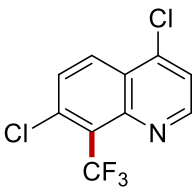

The general procedure **G** was followed using 4,7-dichloroquinoline (**137e**, 0.25 mmol, 49.5 mg). After electrolysis at 4 mA under blue light irradiation for 16 h, purification by column chromatography (*n*-hexane/EtOAc 20:1) and purification by recycling preparative HPLC yielded **147e** as a white solid. When [Mes-Acr]ClO_4 was used as the photocatalyst, the product **147e** was obtained in 31% (20.7 mg), while the use of [TAC]ClO_4 gave 35% (23.3 mg).

^{1}H-NMR (300 MHz, $CDCl_3$): δ = 8.93 (d, *J* = 4.7 Hz, 1H), 8.30 (d, *J* = 9.1 Hz, 1H), 7.69 (d, *J* = 9.1 Hz, 1H), 7.59 (d, *J* = 4.7 Hz, 1H).

^{13}C-NMR (100 MHz, $CDCl_3$): δ = 151.1 (CH), 147.5 (C_q), 142.9 (C_q), 136.6 (q, $^3J_{C–F}$ = 5 Hz, C_q), 131.1 (CH), 128.6 (CH), 125.6 (C_q), 125.5 (q, $^2J_{C–F}$, = 32 Hz, C_q), 123.4 (q, $^1J_{C–F}$ = 275 Hz, C_q) 122.2 (CH).

^{19}F-NMR (377 MHz, $CDCl_3$): δ = – 53.0 (s).

IR (ATR): $\tilde{\nu}$ = 1586, 1561, 1485, 1405, 1263, 1204, 1151, 1129, 895, 788 cm^{-1}.

m.p.: 113–116 °C.

MS (ESI) *m*/*z* (relative intensity): 268 (75) $[M(^{37}Cl)+H]^+$, 266 (100) $[M(^{35}Cl)+H]^+$.

HR-MS (ESI): *m*/*z* calcd for $C_{10}H_5NF_3{}^{35}Cl_2{}^+$ $[M+H]^+$ 265.9946, found 265.9947.

4,6-Dimethoxy-5-(trifluoromethyl)pyrimidine (147f)

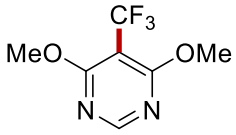

The general procedure **G** was followed using 4,6-dimethoxy pyrimidine (**137f**, 0.25 mmol, 35.0 mg). After electrolysis at 4 mA under blue light irradiation for 16 h, purification by column chromatography (*n*-hexane/EtOAc 30:1 to 20:1) yielded **147f** as a white solid. When [Mes-Acr]ClO_4 was used as the photocatalyst, the product **147f** was obtained in 68% (35.4 mg), while the use of [TAC]ClO_4 gave 61% (31.7 mg).

^{1}H-NMR (400 MHz, $CDCl_3$): δ = 8.46 (s, 1H), 4.03 (s, 6H).

^{13}C-NMR (100 MHz, $CDCl_3$): δ = 168.1 (C_q), 159.1 (CH), 123.0 (q, $^1J_{C–F}$ = 273 Hz, C_q), 95.6 (q, $^2J_{C–F}$ = 34 Hz, C_q), 55.1 (CH_3).

^{19}F-NMR (377 MHz, $CDCl_3$): δ = – 57.0 (s).

IR (ATR): $\tilde{\nu}$ = 1573, 1475, 1414, 1324, 1247, 1107, 1035, 733, 703 cm^{-1}.

m.p.: 94–96 °C.

MS (ESI) *m*/*z* (relative intensity): 231 (50) $[M+Na]^+$, 209 (100) $[M+H]^+$.

HR-MS (ESI): *m*/*z* calcd for $C_7H_8F_3N_2O_2N^+$ $[M+H]^+$ 209.0538, found 209.0541.

The spectral data is in accordance with those reported in the literature.[157]

3-Methyl-2-(trifluoromethyl)benzofuran (147g)

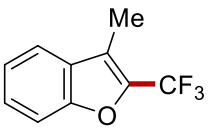

The general procedure **G** was followed using 3-methylbenzofurane (**137g**, 0.25 mmol, 33.0 mg). After electrolysis at 4 mA under blue light irradiation for 8 h, purification by column chromatography (*n*-hexane) yielded **147g** as a colourless oil. When [Mes-Acr]ClO_4 was used as the photocatalyst, the product **147g** was obtained in 71% (35.5 mg), while the use of [TAC]ClO_4 gave 72% (36.0 mg).

^{1}H-NMR (300 MHz, $CDCl_3$): δ = 7.61 (dd, J = 7.7, 1.2 Hz, 1H), 7.52 (dd, J = 8.3, 0.9 Hz, 1H), 7.47–7.40 (m, 1H), 7.33 (dd, J = 7.5, 1.1 Hz, 1H), 2.42 (s, 3H).

^{13}C-NMR (100 MHz, $CDCl_3$): δ = 154.2 (C_q), 138.6 (q, $^2J_{C–F}$ = 39 Hz, C_q), 128.5 (C_q), 127.1 (CH), 123.5 (CH), 120.8 (CH), 120.4 (q, $^1J_{C–F}$ = 269 Hz, C_q), 118.4 (q, $^3J_{C–F}$ = 3 Hz, C_q), 112.0 (CH), 7.8 (q, $^4J_{C–F}$ = 2 Hz, CH_3).

^{19}F-NMR (282 MHz, $CDCl_3$): δ = – 62.0 (s).

IR (ATR): $\tilde{\nu}$ = 1635, 1395, 1383, 1301, 1367, 1179, 1111, 1082, 1038, 743 cm^{-1}.

MS (EI) *m*/*z* (relative intensity): 200 (100) $[M]^+$.

HR-MS (EI): *m*/*z* calcd for $C_{10}H_7F_3O$ $[M]^+$ 200.0444, found 200.0448.

The spectral data is in accordance with those reported in the literature.[157]

***N*-Methyl-5-(trifluoromethyl)furan-3-carboxamide (147h)**

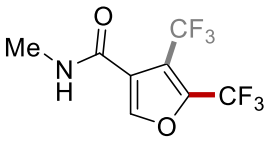

The general procedure **G** was followed using *N*-methylfuran-3-carboxamide (**137h**, 0.25 mmol, 31.2 mg). After electrolysis at 4 mA under blue light irradiation for 16 h, purification by column chromatography (*n*-hexane/EtOAc 1:1 to 1:2) yielded **147h** as a pale yellow oil. When [Mes-Acr]ClO_4 was used as the photocatalyst, the product **147h** was obtained in 69% (33.3 mg), while the use of [TAC]ClO_4 gave 74% (35.7 mg) in both cases as mixture of isomers in a ratio of 3.0:1 as determined based on the ^{1}H-NMR of the isolated product.

^{1}H-NMR (400 MHz, $CDCl_3$): δ = 7.46 (s, 1H), 6.70 (s, 1H), 6. 35 (s br, 1H), 2.94 (d, J = 4.9 Hz, 3H).

^{13}C-NMR (100 MHz, $CDCl_3$): δ = 161.6 (C_q), 143.9 (q, $^3J_{C–F}$ = 2 Hz, CH), 139.8 (q, $^2J_{C–F}$ = 42 Hz, C_q), 123.6 (C_q), 118.9 (q, $^1J_{C–F}$ = 269 Hz, C_q), 111.6 (CH), 26.7 (CH_3).

^{19}F-NMR (282 MHz, $CDCl_3$): δ = – 61.2 (s).

IR (ATR): $\tilde{\nu}$ = 1406, 1304, 1266, 1175, 1131, 1105, 935, 894, 734, 702 cm^{-1}.

MS (ESI) *m*/*z* (relative intensity): 216 (100) $[M+Na]^+$, 194 (12) $[M+H]^+$.

HR-MS (EI): *m*/*z* calcd for $C_7H_6NO_2F_3Na$ $[M+Na]^+$ 216.0243, found 216.0253.

N-Methyl-5-(trifluoromethyl)thiophene-3-carboxamide (147i)

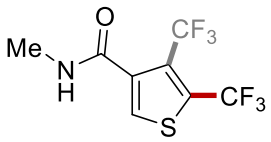

The general procedure **G** was followed using *N*-methylthiophen-3-carboxamide (**137i**, 0.25 mmol, 35.2 mg). After electrolysis at 4 mA under blue light irradiation for 16 h, purification by column chromatography (*n*-hexane/EtOAc 2:1 to 1:1) yielded **147i** as a white solid. When [Mes-Acr]ClO_4 was used as the photocatalyst, the product **147i** was obtained in 65% (33.8 mg), while the use of [TAC]ClO_4 gave 68% (35.8 mg) in both cases as mixture of isomers in a ratio of 2.7:1 as determined based on the ^{1}H-NMR of the isolated product.

^{1}H-NMR (400 MHz, $CDCl_3$): δ = 7.43 (dd, *J* = 3.2, 2.3 Hz, 1H), 7.32–7.03 (m, 1H), 6.16 (s br, 1H), 3.19–2.89 (m, 3H).

^{13}C-NMR (100 MHz, $CDCl_3$): δ = 163.5 (C_q), 137.6 (C_q), 129.9 (q, $^2J_{C–H}$ = 37 Hz, C_q), 129.1 (CH), 127.1 (q, $^3J_{C–H}$ = 6 Hz, CH), 122.0 (q, $^1J_{C–H}$ = 270 Hz, C_q), 27.0 (CH_3).

^{19}F-NMR (377 MHz, $CDCl_3$): δ = – 52.8 (s).

IR (ATR): $\tilde{\nu}$ = 1638, 1562, 1523, 1431, 1276, 1159, 1119, 1019, 1007 cm^{-1}.

MS (ESI) *m*/*z* (relative intensity): 232 (100) $[M+Na]^+$, 210 (9) $[M+H]^+$.

HR-MS (ESI): *m*/*z* calcd for $C_7H_6SNOF_3Na$ $[M+Na]^+$ 232.0014, found 232.0018.

N-[*tert*-Butyl]-3,4,5-trimethoxy-2-(trifluoromethyl)benzamide (147j)

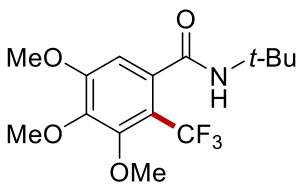

The general procedure **G** was followed using *N*-(*tert*-butyl)-3,4,5-trimethoxybenzamide (**137j**, 0.25 mmol, 42.0 mg). After electrolysis at 4 mA under blue light irradiation for 16 h, purification by column chromatography (*n*-hexane/EtOAc 4:1 to 2:1) yielded **147j** as a white solid. When [Mes-Acr]ClO_4 was used as the photocatalyst, the product **147j** was obtained in 56% (46.9 mg), while the use of [TAC]ClO_4 gave 53% (44.4 mg). The obtained product shows in the ^{1}H- and ^{13}C-NMR in $CDCl_3$ a splitting of the signals in two sets as a consequence of the limited rotation along the amide bond.

^{1}H-NMR (400 MHz, $CDCl_3$): δ = 6.65 (s, 1H), 5.45 (s br, 1H), 3.92 (s, 3H), 3.90 (s, 3H), 3.86 (s, 3H), 1.42 (s, 9H).

^{13}C-NMR (100 MHz, $CDCl_3$): δ = 167.4 (C_q), 156.2 (C_q), 153.2 (C_q), 143.4 (C_q), 133.7 (q, $^{3}J_{C–F}$ = 3 Hz, C_q), 123.5 (q, $^{1}J_{C–F}$ = 274 Hz, C_q), 113.6 (q, $^{2}J_{C–F}$ = 31 Hz, C_q), 106.8 (CH), 61.9 (CH_3), 61.0 (CH_3), 56.4 (CH_3), 52.3 (C_q), 28.6 (CH_3).

^{19}F-NMR (377 MHz, $CDCl_3$): δ = – 55.6 (s).

IR (ATR): $\tilde{\nu}$ = 1641, 1580, 1496, 1453, 1403, 1302, 1116, 1009, 930 cm^{-1}.

m.p.: 107–108 °C.

MS (ESI) *m*/*z* (relative intensity): 358 (100) $[M+Na]^+$, 336 (5) $[M+H]^+$.

HR-MS (ESI): *m*/*z* calcd for $C_{15}H_{20}NO_4F_3Na$ $[M+Na]^+$ 358.1237, found 358.1237.

The spectral data is in accordance with those reported in the literature.[284]

1,3,7-Trimethyl-8-(trifluoromethyl)-3,7-dihydro-1*H*-purine-2,6-dione (147k)

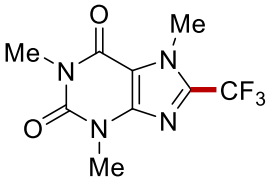

The general procedure **G** was followed using caffeine (**137k**, 0.25 mmol, 48.5 mg). After electrolysis at 4 mA under blue light irradiation for 8 h, purification by column chromatography (*n*-hexane/EtOAc 3:1) yielded **147k** as a white solid. When $[Mes\text{-}Acr]ClO_4$ was used as the photocatalyst, the product **147k** was obtained in 71% (46.5 mg), while the use of $[TAC]ClO_4$ gave 70% (45.8 mg).

^{1}H-NMR (400 MHz, $CDCl_3$): δ = 4.13 (s, 3H), 3.56 (s, 3H), 3.38 (s, 3H).

^{13}C-NMR (100 MHz, $CDCl_3$): δ = 155.5 (C_q), 151.4 (C_q), 146.6 (C_q), 138.9 (q, $^{2}J_{C–F}$ = 40 Hz, C_q), 118.2 (q, $^{1}J_{C–F}$ = 270 Hz, C_q), 109.7 (C_q), 33.3 (q, $^{4}J_{C–F}$ = 2 Hz, CH_3), 30.0 (CH_3), 28.3 (CH_3).

^{19}F-NMR (377 MHz, $CDCl_3$): δ = – 62.4 (s).

IR (ATR): $\tilde{\nu}$ = 1709, 1665, 1548, 1247, 1202, 1178, 1098, 973, 745 cm^{-1}.

m.p.: 129–130 °C.

MS (ESI) *m*/*z* (relative intensity): 285 (80) $[M+Na]^+$, 263 (100) $[M+H]^+$.

HR-MS (ESI): *m*/*z* calcd for $C_9H_{10}N_4F_3O_2^+$ $[M+H]^+$ 263.0750, found 263.2754.

The spectral data is in accordance with those reported in the literature.[157]

3,7-Dimethyl-1-[5-oxohexyl]-8-(trifluoromethyl)-3,7-dihydro-1*H*-purine-2,6-dione (147l)

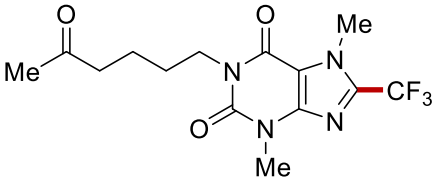

The general procedure **G** was followed using Pentoxifylline (**137l**, 0.25 mmol, 69.5 mg). After electrolysis at 4 mA under blue light irradiation for 16 h, purification by column chromatography (*n*-hexane/EtOAc 1:1) yielded **147l** as a white solid. When [Mes-Acr]ClO_4 was used as the photocatalyst, the product **147l** was obtained in 73% (63.1 mg), while the use of [TAC]ClO_4 gave 72% (62.2 mg).

^{1}H-NMR (400 MHz, $CDCl_3$): δ = 4.13 (t, J = 1.6 Hz, 3H), 3.99 (t, J = 8.0 Hz, 2H), 3.56 (s, 3H), 2.49 (t, J = 6.9 Hz, 2H), 2.13 (s, 3H), 1.67–1.56 (m, 4H).

^{13}C-NMR (100 MHz, $CDCl_3$): δ = 208.7 (C_q), 155.4 (C_q), 151.2 (C_q), 146.7 (C_q), 139.0 (q, $^2J_{C–F}$ = 40 Hz, C_q), 118.3 (q, $^1J_{C–F}$ = 271 Hz, C_q), 109.8 (C_q), 43.2 (CH_2), 41.2 (CH_2), 33.3 (q, $^4J_{C–F}$ = 2 Hz, CH_3), 30.1 (CH_3), 30.0 (CH_3), 27.4 (CH_2), 21.0 (CH_2).

^{19}F-NMR (282 MHz, $CDCl_3$): δ = – 62.4 (s).

IR (ATR): $\tilde{\nu}$ = 1705, 1656, 1546, 1468, 1248, 1170, 1128, 1099, 766 cm^{-1}.

m.p.: 70–72 °C.

MS (ESI) *m*/*z* (relative intensity): 369 (100) $[M+Na]^+$, 347 (10) $[M+H]^+$.

HR-MS (ESI): *m*/*z* calcd for $C_{14}H_{17}F_3N_4O_3Na^+$ $[M+Na]^+$ 369.1145, found 369.1149.

The spectral data is in accordance with those reported in the literature.[157]

4-(9-Isopropyl-8-(trifluoromethyl)-9*H*-purin-6-yl)morpholine (147m)

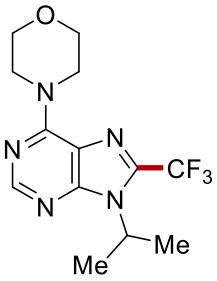

The general procedure **G** was followed using 4-(9-isopropyl-9*H*-purin-6-yl)morpholine (**137m**, 0.25 mmol, 61.8 mg). After electrolysis at 4 mA under blue light irradiation for 16 h, purification by column chromatography (*n*-hexane/EtOAc 3:1) yielded **147m** as a white solid. When [Mes-Acr]ClO_4 was used as the photocatalyst, the product **147m** was obtained in 49% (38.6 mg), while the use of [TAC]ClO_4 gave 56% (44.1 mg).

^{1}H-NMR (400 MHz, $CDCl_3$): δ = 8.39 (s, 1H), 4.84 (hept, J = 6.9 Hz, 1H), 4.32 (s br, 4H), 3.84 (t, J = 4.6 Hz, 4H), 1.75 (d, J = 6.8 Hz, 6H).

^{13}C-NMR (100 MHz, $CDCl_3$): δ = 154.7 (C_q), 153.4 (CH), 152.5 (C_q), 135.9 (q, $^2J_{C–F}$ = 39 Hz, C_q), 119.4 (C_q), 119.1 (q, $^1J_{C–F}$ = 271 Hz, C_q), 67.2 (CH_2), 67.2 (CH_2), 50.6 (CH), 21.1 (CH_3).

^{19}F-NMR (377 MHz, $CDCl_3$): δ = – 62.1 (s).

IR (ATR): $\tilde{\nu}$ = 1588, 1496, 1441, 1263, 1181, 1163, 1112, 1053, 1009, 930 cm^{-1}.

m.p.: 99–101 °C.

MS (ESI) *m*/*z* (relative intensity): 316 (100) $[M+H]^+$.

HR-MS (ESI): *m*/*z* calcd for $C_{13}H_{17}F_3N_5O^+$ $[M+H]^+$ 316.380, found 316.1385.

Methyl (*S*)-2-[(*tert*-butoxycarbonyl)amino]-3-{1-(pyridin-2-yl)-2-(trifluoromethyl)-1*H*-indol-3-yl}propanoate (147n)

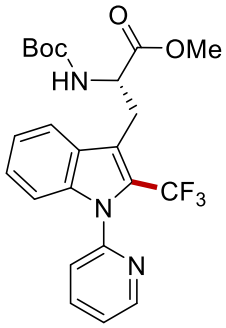

The general procedure **G** was followed using tryptophan derivative **137n** (0.25 mmol, 98.8 mg). After electrolysis at 4 mA under blue light irradiation for 16 h, purification by column chromatography (*n*-hexane/EtOAc 4:1) yielded **147n** as a white solid. When $[Mes\text{-}Acr]ClO_4$ was used as photocatalyst, the product **147n** was obtained in 49% (56.7 mg), while the use of $[TAC]ClO_4$ gave 53% (61.3 mg).

^{1}H-NMR (400 MHz, $CDCl_3$): δ = 8.79–8.50 (m, 1H), 7.91 (ddd, *J* = 7.7, 7.7, 1.7 Hz, 1H), 7.76 (d, *J* = 7.8 Hz, 1H), 7.51–7.39 (m, 2H), 7.35–7.03 (m, 3H), 5.23 (s, 1H), 4.69 (t, *J* = 7.1 Hz, 1H), 3.66 (s, 3H), 3.48 (d, *J* = 6.6 Hz, 2H), 1.40 (s, 9H).

^{13}C-NMR (100 MHz, $CDCl_3$): δ = 172.4 (C_q), 155.1 (C_q), 150.6 (C_q), 149.8 (CH), 138.7 (CH), 138.2 (C_q), 127.1 (C_q), 125.8 (CH), 124.3 (q, $^2J_{C–F}$ = 34 Hz, C_q), 123.7 (CH), 122.4 (CH), 121.9 (q, $^1J_{C–F}$ = 273 Hz, C_q), 121.8 (CH), 120.5 (CH), 115.8 (C_q), 111.4 (CH), 79.9 (C_q), 54.1 (CH), 52.4 (CH_3), 28.4 (CH_3), 27.9 (CH_2).

^{19}F-NMR (377 MHz, $CDCl_3$): δ = – 53.5 (s).

IR (ATR): $\tilde{\nu}$ = 1746, 1714, 1590, 1469, 1438, 1367, 1276, 1162, 1113, 1059 cm^{-1}.

m.p.: 108–109 °C.

MS (ESI) *m*/*z* (relative intensity): 486 (100) $[M+Na]^+$, 464 (100) $[M+H]^+$.

HR-MS (ESI): *m*/*z* calcd for $C_{23}H_{24}F_3N_3O_4Na^+$ $[M+Na]^+$ 486.1611, found 486.1617.

Methyl 4-amino-2-hydroxy-3-(trifluoromethyl)benzoate (293a)

Methyl 4-amino-2-hydroxy-5-(trifluoromethyl)benzoate (293b)

Methyl 4-amino-2-hydroxy-3,5-bis(trifluoromethyl)benzoate (293c)

The general procedure **G** was followed using methyl 4-amino-2-hydroxybenzoate (**286**, 0.50 mmol, 84.3 mg). After electrolysis at 4 mA under blue light irradiation for 8 h, purification by column chromatography (*n*-hexane/EtOAc 9:1) yielded **293a**, **293b** and **293c** as white solids. When [Mes-Acr]ClO_4 was used as the photocatalyst, the mono-functionalized product **293a** was obtained in 28% (33.8 mg), **293b** in 11% (12.8 mg) and the di-functionalized **293c** in 3% (4.8 mg), while the use of [TAC]ClO_4 gave **293a** in 50% (58.5 mg), **293b** in 15% (17.9 mg) and **293c** in 9% (14.1 mg).

Methyl 4-amino-2-hydroxy-3-(trifluoromethyl)benzoate (293a)

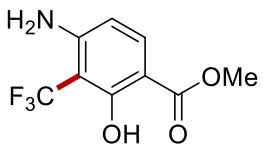

^{1}H-NMR (400 MHz, $CDCl_3$): δ = 12.05 (s, 1H), 7.67 (d, J = 8.9 Hz, 1H), 6.12 (d, J = 8.9 Hz, 1H), 4.83 (s, 2H), 3.89 (s, 3H).

^{13}C-NMR (100 MHz, $CDCl_3$): δ = 170.5 (C_q), 163.5 (q, $^3J_{C–F}$ = 2 Hz, C_q), 151.3 (C_q), 133.6 (CH), 125.4 (q, $^1J_{C–F}$ = 274 Hz, C_q), 108.4 (CH), 102.4 (C_q), 100.1 (q, $^2J_{C–F}$ = 29 Hz, C_q), 52.2 (CH_3).

^{19}F-NMR (377 MHz, $CDCl_3$): δ = – 55.1 (s).

IR (ATR): $\tilde{\nu}$ = 1627, 1575, 1505, 1441, 1352, 1272, 1105, 1070, 969, 759 cm^{-1}.

m.p.: 73–75 °C.

MS (ESI) *m*/*z* (relative intensity): 258 (100) $[M+Na]^+$, 236 (90) $[M+H]^+$.

HR-MS (ESI): *m*/*z* calcd for $C_9H_9F_3O_3^+$ $[M+H]^+$ 236.0529, found 236.0522.

Methyl 4-amino-2-hydroxy-5-(trifluoromethyl)benzoate (293b)

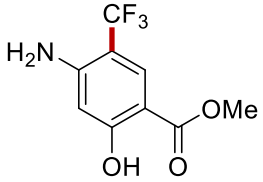

^{1}H-NMR (400 MHz, $CDCl_3$): δ = 11.05 (s, 1H), 7.96 (s, 1H), 6.20 (s, 1H), 4.56 (s, 2H), 3.91 (s, 3H).

^{13}C-NMR (100 MHz, $CDCl_3$): δ = 169.9 (C_q), 165.1 (C_q), 150.6 (q, $^4J_{C–F}$ = 1 Hz, C_q), 130.5 (q, $^3J_{C–F}$ = 5 Hz, CH), 124.6 (q, $^1J_{C–F}$ = 271 Hz, C_q), 106.5 (q, $^2J_{C–F}$ = 31 Hz, C_q), 103.0 (C_q), 102.5 (CH), 52.2 (CH_3).

^{19}F-NMR (377 MHz, $CDCl_3$): δ = – 61.6 (s).

IR (ATR): $\tilde{\nu}$ = 1671, 1638, 1331, 1255, 1234, 1211, 1076, 786, 683 cm^{-1}.

m.p.: 93–95 °C.

MS (ESI) *m*/*z* (relative intensity): 234 (100) $[M–H]^-$.

HR-MS (ESI): *m*/*z* calcd for $C_9H_7F_3O_3^-$ $[M–H]^-$ 234.0384, found 234.0374.

Methyl 4-amino-2-hydroxy-3,5-bis(trifluoromethyl)benzoate (293c)

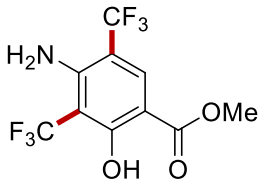

^{1}H-NMR (400 MHz, $CDCl_3$): δ = 12.29 (s, 1H), 8.09 (s, 1H), 5.38 (s, 2H), 3.94 (s, 3H).

^{13}C-NMR (100 MHz, $CDCl_3$): δ = 169.9 (C_q), 165.1 (C_q), 149.0 (C_q), 132.7 (q, $^3J_{C–F}$ = 6 Hz, CH), 124.7 (q, $^1J_{C–F}$ = 275 Hz, C_q), 124.7 (q, $^1J_{C–F}$ = 272 Hz, C_q), 106.8 (q, $^2J_{C–F}$ = 31 Hz, C_q), 101.9 (C_q), 101.3 (q, $^2J_{C–F}$ = 29 Hz, C_q), 52.7 (CH_3).

^{19}F-NMR (377 MHz, $CDCl_3$): δ = – 55.1 (s), – 62.1 (s).

IR (ATR): $\tilde{\nu}$ = 1648, 1591, 1489, 1438, 1232, 1069, 968, 801, 643 cm^{-1}.

m.p.: 112–113 °C.

MS (ESI) *m*/*z* (relative intensity): 302 (100) $[M–H]^-$.

HR-MS (ESI): *m*/*z* calcd for $C_{10}H_6F_6O_3^-$ $[M–H]^-$ 302.0257, found 302.0260.

*5.7.2 Kinetic Studies of Caffeine (**137k**) In Situ Flow NMR*

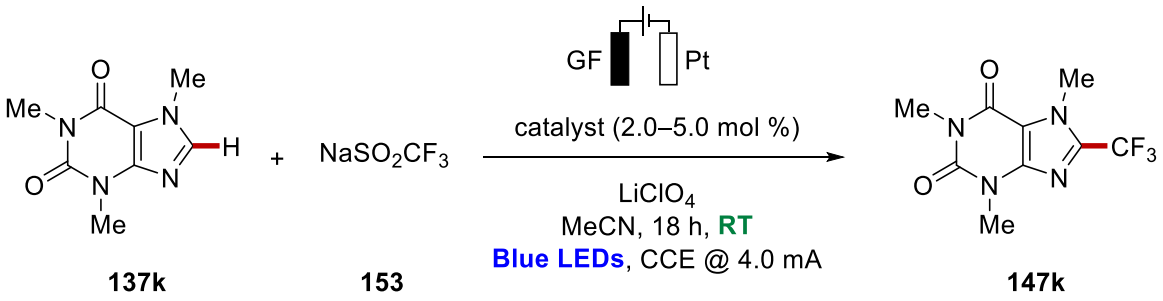

A 10 mL Schlenk tube was charged with caffeine (**137k**, 116 mg, 0.6 mmol), CF_3SO_2Na (**153**, 187 mg, 1.20 mmol), $LiClO_4$ (62 mg, 0.60 mmol) and the photocatalyst (2.0 or 5.0 mol %). The Schlenk tube and closed with a stopper with integrated electrode holders equipped with a RVC anode and a platinum cathode. The vial was evacuated and purged with N_2 three times, before CH_3CN (6.0 mL) and HFIP (0.2 mL) as internal standard were added. The electrophotocatalysis was performed at ambient temperature with a constant current of 4.0 mA maintained for 18 h under visible light irradiation (2 × Kessil A360N) and the conversion was monitored.

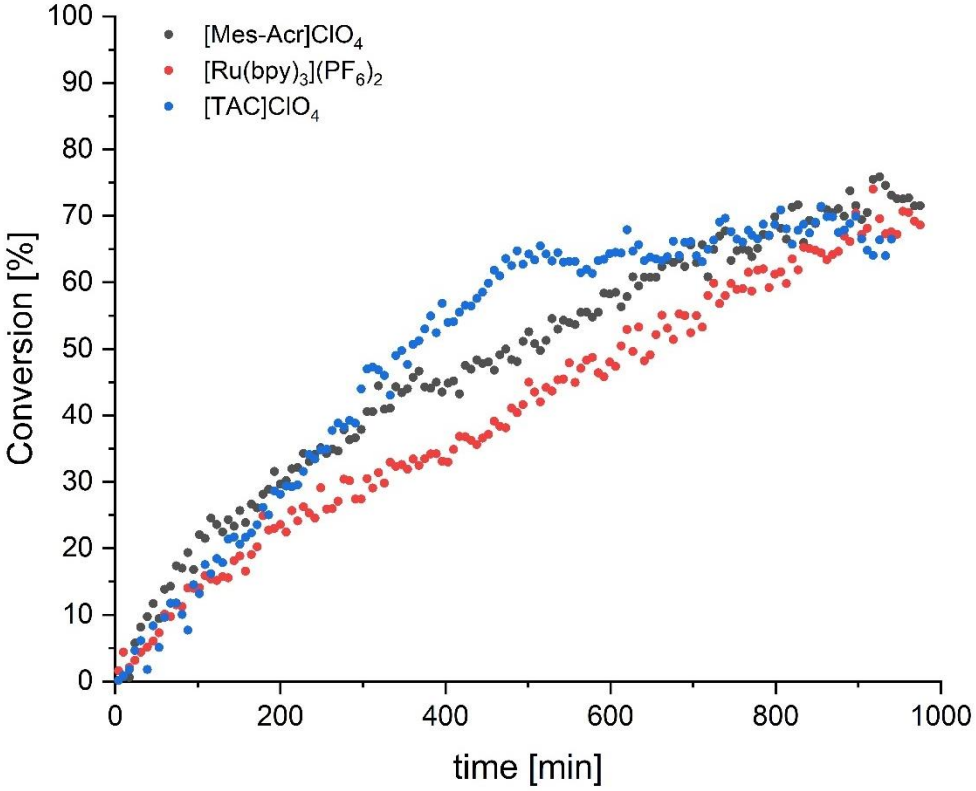

Figure 5.15: Reaction monitoring with *in situ* NMR studies with different catalysts.

5.8 MANGANESE(I)-CATALYZED TRYPTOPHAN FUNCTIONALIZATION IN WATER

5.8.1 Characterization Data

Methyl (*S*)-3-(2-allyl-1-(pyridin-2-yl)-1*H*-indol-3-yl)-2-((*tert*-butoxycarbonyl)amino)-propanoate (223aa)

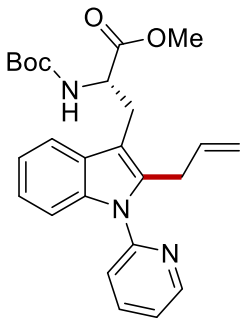

The general procedure **H** was followed using tryptophan **221a** (63.4 mg, 0.20 mmol) and allyl carbonate **129a** (46.2 mg, 0.40 mmol) in degassed water (0.6 mL). After stirring at 100 °C for 18 h, purification by column chromatography (*n*-hexane/EtOAc 4:1) yielded **223aa** (47.0 mg, 53%) as a colourless oil.

^{1}H-NMR (400 MHz, $CDCl_3$): δ = 8.72–8.52 (m, 1H), 7.85 (ddd, *J* = 7.7, 7.7, 2.0 Hz, 1H), 7.65–7.49 (m, 1H), 7.40 (dt, *J* = 8.1, 1.0 Hz, 1H), 7.33–7.27 (m, 2H), 7.14 (dt, *J* = 5.0, 3.6 Hz, 2H), 5.68 (ddt, *J* = 16.4, 10.9, 5.9 Hz, 1H), 5.16 (d, *J* = 8.1 Hz, 1H), 4.81 (d, *J* = 10.2 Hz, 1H), 4.78–4.70 (m, 1H), 4.64 (q, *J* = 6.6 Hz, 1H), 3.76–3.57 (m, 5H), 3.30 (dd, *J* = 6.2, 2.4 Hz, 2H), 1.41 (s, 9H).

^{13}C-NMR (100 MHz, $CDCl_3$): δ = 173.0 (C_q), 155.2 (C_q), 151.5 (C_q), 149.6 (CH), 138.3 (CH), 136.9 (C_q), 136.0 (C_q), 135.0 (CH), 128.7 (C_q), 122.4 (CH), 122.2 (CH), 121.4 (CH), 120.7 (CH), 118.6 (CH), 116.1 (C_q), 110.2 (CH_2), 109.4 (CH), 79.8 (C_q), 60.5 (CH), 52.4 (CH_3), 29.2 (CH_2), 28.4 (CH_3), 27.6 (CH_2).

IR (ATR): $\tilde{\nu}$ = 1746, 1713, 1471, 1436, 1366, 1283, 1248, 1148, 1017, 911 cm^{-1}.

MS (ESI) *m*/*z* (relative intensity): 895 (72) $[2M+Na]^+$, 458 (100) $[M+Na]^+$.

HR-MS (ESI): *m*/*z* calcd for $C_{25}H_{29}N_3O_4Na$ $[M+Na]^+$ 458.2050, found 458.2050.

Butyl (*S*)-2-((3-(2-((*tert*-butoxycarbonyl)amino)-3-methoxy-3-oxopropy)-1-(pyridin-2-yl)-1*H*-indol-2-ylmethyl) acrylate) (224ab)

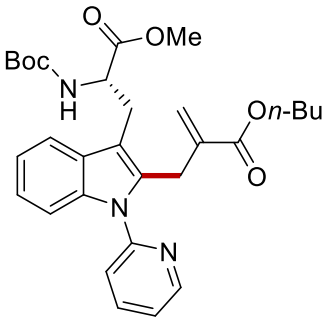

The general procedure **H** was followed using tryptophan **221a** (63.4 mg, 0.20 mmol) and MBH substrate **222b** (103 mg, 0.40 mmol) in degassed water (1.5 mL). After stirring at 80 °C for 18 h, purification by column chromatography (*n*-hexane/EtOAc 4:1) yielded **224ab** (91.1 mg, 85%) as a colourless oil.

^{1}H-NMR (400 MHz, $CDCl_3$): δ = 8.57 (d, J = 4.6 Hz, 1H), 7.82 (dt, J = 7.8, 1.5 Hz, 1H), 7.57 (dd, J = 3.9, 3.9 Hz, 1H), 7.38–7.22 (m, 3H), 7.19–7.09 (m, 2H), 5.97 (d, J = 2.0 Hz, 1H), 5.18 (d, J = 8.1 Hz, 1H), 5.02 (d, J = 2.2 Hz, 1H), 4.65 (q, J = 6.6 Hz, 1H), 4.07 (td, J = 6.7, 1.3 Hz, 2H), 3.96 (s, 2H), 3.66 (d, J = 1.3 Hz, 3H), 3.30 (d, J = 5.1 Hz, 2H), 1.58 (q, J = 6.9 Hz, 2H), 1.40 (s, 9H), 1.35–1.27 (m, 2H), 0.90 (t, J = 7.4 Hz, 3H).

^{13}C-NMR (100 MHz, $CDCl_3$): δ = 172.9 (C_q), 166.5 (C_q), 155.3 (C_q), 151.4 (C_q), 149.6 (CH), 138.4 (CH), 137.8 (C_q), 136.9 (C_q), 134.6 (C_q), 128.7 (C_q), 126.0 (C_q), 122.6 (CH), 122.2 (CH), 121.0 (CH), 120.8 (CH), 118.8 (CH), 110.7 (CH_2), 110.3 (CH), 79.8 (C_q), 64.8 (CH_2), 62.6 (CH_2), 54.1 (CH), 52.4 (CH_3), 30.7 (CH_2), 28.4 (CH_3), 27.0 (CH_2), 19.2 (CH_2), 13.8 (CH_3).

IR (ATR): $\tilde{\nu}$ = 1713, 1586, 1471, 1436, 1366, 1250, 1159, 1061, 1017, 783 cm^{-1}.

MS (ESI) *m*/*z* (relative intensity): 1093 (60) $[2M+Na]^+$, 558 (100) $[M+Na]^+$, 536 (8) [M+H].

HR-MS (ESI): *m*/*z* calcd for $C_{30}H_{37}N_3O_6Na$ $[M+Na]^+$ 558.2575, found 558.2575.

***tert*-Butyl (*S*)-2-((3-(2-((*tert*-butoxycarbonyl)amino)-3-methoxy-3-oxopropyl)-1 (pyridin-2-yl)-1*H*-indol-2-yl)methyl)acrylate) (224ac)**

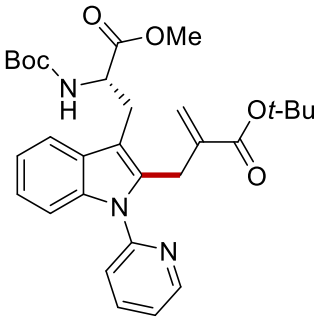

The general procedure **H** was followed using tryptophan **221a** (63.4 mg, 0.20 mmol) and MBH substrate **222c** (103 mg, 0.40 mmol) in degassed water (1.5 mL). After stirring at 80 °C for 18 h, purification by column chromatography (*n*-hexane/EtOAc 4:1) yielded **224ac** (82.4 mg, 77%) as a colourless oil.

^{1}H-NMR (400 MHz, $CDCl_3$): δ = 8.62 (d, J = 6.9 Hz, 1H), 7.86 (dd, J = 7.8, 1.7 Hz, 1H), 7.64–7.56 (m, 1H), 7.37 (dd, J = 7.0, 7.0 Hz, 2H), 7.35–7.27 (m, 1H), 7.24–7.13 (m, 2H), 5.94 (s, 1H), 5.21 (d, J = 8.0 Hz, 1H), 5.02 (d, J = 2.1 Hz, 1H), 4.96 (q, J = 6.7 Hz, 1H), 3.95 (s, 2H), 3.71 (s, 3H), 3.34 (d, J = 5.6 Hz, 2H), 1.47–1.40 (m, 18H).

^{13}C-NMR (100 MHz, $CDCl_3$): δ = 172.9 (C_q), 165.6 (C_q), 155.3 (C_q), 151.4 (C_q), 149.6 (CH), 139.1 (C_q), 138.3 (CH), 136.9 (C_q), 135.0 (C_q), 128.7 (C_q), 125.2 (C_q), 122.6 (CH), 122.1 (CH), 121.0 (CH), 120.8 (CH), 118.8 (CH), 110.6 (CH_2), 110.3 (CH), 80.9 (C_q), 62.8 (C_q), 60.5 (C_q), 54.2 (CH), 52.4 (CH_3), 28.4 (CH_3), 28.1 (CH_3), 26.8 (CH_2).

IR (ATR): $\tilde{\nu}$ = 1701, 1586, 1472, 1437, 1367, 1253, 1135, 1017, 784 cm^{-1}.

MS (ESI) *m*/*z* (relative intensity): 1093 (2) $[2M+Na]^+$, 558 (100) $[M+Na]^+$, 536 (22) [M+H].

HR-MS (ESI): *m*/*z* calcd for $C_{30}H_{37}N_3O_6Na$ $[M+Na]^+$ 558.2775, found 558.2774.

Octyl (*S*)-2-((3-(2-((*tert*-butoxycarbonyl)amino)-3-methoxy-3-oxopropyl)-1-(pyridin-2-yl)-1*H*-indol-2-yl)methyl)acrylate) (224ad)

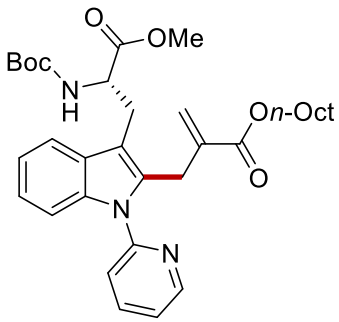

The general procedure **H** was followed using tryptophan **221a** (63.4 mg, 0.20 mmol) and MBH substrate **222d** (126 mg, 0.40 mmol) in degassed water (1.5 mL). After stirring at 80 °C for 18 h, purification by column chromatography (*n*-hexane/EtOAc 3:1) yielded **224ad** (42.8 mg, 35%) as a colourless oil.

^{1}H-NMR (400 MHz, $CDCl_3$): δ = 8.62 (d, *J* = 4.7 Hz, 1H), 7.87 (td, *J* = 7.6, 1.7 Hz, 1H), 7.67–7.57 (m, 1H), 7.42–7.29 (m, 3H), 7.25–7.15 (m, 2H), 6.02 (s, 1H), 5.22 (d, *J* = 8.1 Hz, 1H), 5.08 (s, 1H), 4.70 (d, *J* = 7.1 Hz, 1H), 4.14–4.07 (m, 2H), 4.00 (s, 2H), 3.71 (d, *J* = 1.4 Hz, 3H), 3.36 (q, *J* = 6.9, 4.8 Hz, 2H), 1.45 (s, 9H), 1.40–1.26 (m, 12H), 0.93 (t, *J* = 6.4 Hz, 3H).

^{13}C-NMR (100 MHz, $CDCl_3$): δ = 172.9 (C_q), 166.5 (C_q), 155.3 (C_q), 151.4 (C_q), 149.6 (CH), 138.4 (CH), 137.8 (C_q), 136.9 (C_q), 134.6 (C_q), 128.7 (C_q), 126.0 (C_q), 122.6 (CH), 122.2 (CH), 121.0 (CH), 120.8 (CH), 118.8 (CH), 110.7 (CH_2), 110.3 (CH), 79.9 (C_q), 65.1 (CH_2), 62.6 (C_q), 54.2 (CH), 52.4 (CH_3), 31.9 (CH_2), 29.3 (CH_2), 29.3 (CH_2), 28.7 (CH_3), 28.4 (CH_2), 27.0 (CH_2), 26.0 (CH_2), 22.8 (CH_2), 14.2 (CH_3).

IR (ATR): $\tilde{\nu}$ = 1713, 1585, 1471, 1436, 1366, 1250, 1061, 1017, 783 cm^{-1}.

MS (ESI) *m*/*z* (relative intensity): 614 (100) $[M+Na]^+$, 592 (18) $[M+H]^+$.

HR-MS (ESI): *m*/*z* calcd for $C_{34}H_{45}N_3O_6Na$ $[M+Na]^+$ 614.3201, found 614.3193.

Benzyl (*S*)-2-((3-(2-((*tert*-butoxycarbonyl)amino)-3-methoxy-3-oxopropyl)-1-(pyridin-2-yl)-1*H*-indol-2-yl)methyl)acrylate (224ae)

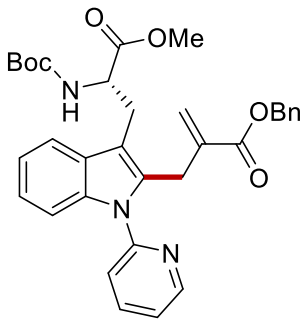

The general procedure **H** was followed using tryptophan **221a** (63.4 mg, 0.20 mmol) and MBH substrate **222e** (117 mg, 0.40 mmol) in degassed water (1.5 mL). After stirring at 80 °C for 18 h, purification by column chromatography (*n*-hexane/EtOAc 4:1) yielded **224ae** (102 mg, 90%) as a colourless oil.

^{1}H-NMR (400 MHz, $CDCl_3$): δ = 8.56 (ddd, J = 4.9, 2.0, 0.8 Hz, 1H), 7.83 (dd, J = 7.7, 2.0 Hz, 1H), 7.71–7.52 (m, 1H), 7.40–7.30 (m, 8H), 7.25–7.17 (m, 2H), 6.07 (q, J = 1.3 Hz, 1H), 5.17 (s, 3H), 4.69 (q, J = 6.6 Hz, 1H), 4.04 (s, 2H), 3.70 (s, 3H), 3.33 (q, J = 6.9, 5.3 Hz, 2H), 1.44 (s, 9H).

^{13}C-NMR (100 MHz, $CDCl_3$): δ = 172.9 (C_q), 166.2 (C_q), 155.3 (C_q), 151.4 (C_q), 149.6 (CH), 138.4 (CH), 137.5 (C_q), 136.9 (C_q), 136.0 (C_q), 134.5 (C_q), 128.7 (C_q), 128.6 (CH), 128.3 (CH), 128.2 (CH), 126.6 (C_q), 122.7 (CH), 122.2 (CH), 121.0 (CH), 120.8 (CH), 118.9 (CH), 110.8 (CH_2), 110.3 (CH), 79.9 (C_q), 66.6 (CH_2), 54.2 (CH), 52.4 (CH_3), 28.4 (CH_3), 27.6 (CH_2), 27.1 (CH_2).

IR (ATR): $\tilde{\nu}$ = 1745, 1472, 1454, 1436, 1366, 1252, 1165, 1017 cm^{-1}.

MS (ESI) *m*/*z* (relative intensity): 592 (100) $[M+Na]^+$.

HR-MS (ESI): *m*/*z* calcd for $C_{33}H_{35}N_3O_6Na$ $[M+Na]^+$ 592.2418, found 592.2422.

(Tetrahydrofuran-2-yl)methyl 2-((3-((*S*)-2-((*tert*-butoxycarbonyl)amino)-3-methoxy-3-oxopropyl)-1-(pyridin-2-yl)-1*H*-indol-2-yl)methyl)acrylate (224af)

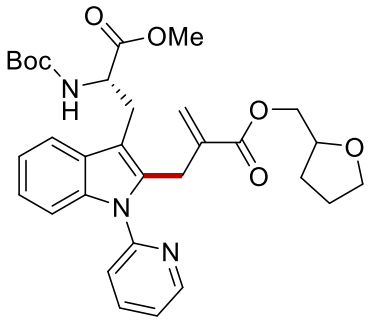

The general procedure **H** was followed using tryptophan **221a** (63.4 mg, 0.20 mmol) and MBH substrate **222f** (114 mg, 0.40 mmol) in degassed water (1.5 mL). After stirring at 80 °C for 18 h, purification by column chromatography (*n*-hexane/EtOAc 3:1 to 2:1) yielded **224af** (89.4 mg, 79%) as a colourless oil.

^{1}H-NMR (400 MHz, $CDCl_3$): δ = 8.61 (d, J = 5.0 Hz, 1H), 7.93–7.70 (m, 1H), 7.68–7.52 (m, 1H), 7.42–7.27 (m, 3H), 7.23–7.05 (m, 2H), 6.05 (s, 1H), 5.25 (d, J = 8.2 Hz, 1H), 5.10 (s, 1H), 4.67 (q, J = 6.7 Hz, 1H), 4.25–4.06 (m, 4H), 4.00 (s, 2H), 3.89–

3.77 (m, 2H), 3.69 (s, 3H), 1.90 (quint, J = 6.8 Hz, 2H), 1.61 (dt, J = 11.1, 7.0 Hz, 1H), 1.43 (s, 10H).

^{13}C-NMR (100 MHz, $CDCl_3$): δ = 172.8 (C_q), 166.2 (C_q), 155.2 (C_q), 151.3 (C_q), 149.6 (CH), 138.4 (CH), 137.4 (CH), 136.9 (C_q), 134.4 (C_q), 128.6 (C_q), 126.4 (C_q), 122.6 (CH), 122.2 (CH), 121.0 (CH), 120.7 (CH), 118.8 (CH), 110.7 (CH_2), 110.2 (CH), 79.8 (C_q), 76.4 (CH), 68.5 (C_q), 66.8 (CH_2), 62.2 (CH_2), 54.1 (CH), 52.3 (CH_3), 28.3 (CH_3), 28.0 (CH_2), 26.9 (CH_2), 25.7 (CH_2).

IR (ATR): $\tilde{\nu}$ = 1745, 1583, 1472, 1452, 1366, 1250, 1172, 1060, 1017, 784 cm^{-1}.

MS (ESI) m/z (relative intensity): 586 (100) $[M+Na]^+$, 564 (12) $[M+H]^+$.

HR-MS (ESI): m/z calcd for $C_{31}H_{37}N_3O_7Na$ $[M+Na]^+$ 586.2524, found 586.2513.

5.8.2 Kinetic Studies: Temperature

Tryptophan **221a** (63.4 mg, 0.20 mmol), $MnBr(CO)_5$ (5.5 mg, 20 µmol, 10 mol %) and NaOAc (4.9 mg, 60 µmol, 30 mol %) were placed in a 10 mL vial and evacuated and reflushed with N_2 for three times. Afterwards, MBH adduct **222b** (0.40 mmol) and water (1.5 mL) were added and the reaction was stirred at 60, 80 or 100 °C for 21 h under N_2 with a ballon. After certain durations, a small sample of 20 µL was taken with a mechanical pipet and the conversion was determined by LC-MS.

Time [h]	**244ab** [%] 60 °C	**244ab** [%] 80 °C	**244ab** [%] 100 °C
0	0.0	0.0	0.0
0.3	---	---	42.2
0.5	7.1	17.8	---
0.6	---	---	52.1
1	16.3	45.7	57.4
2	---	---	62.8
3	44.2	55.4	75.3
6	57.9	65.2	---
21	73.9	75.3	86.2

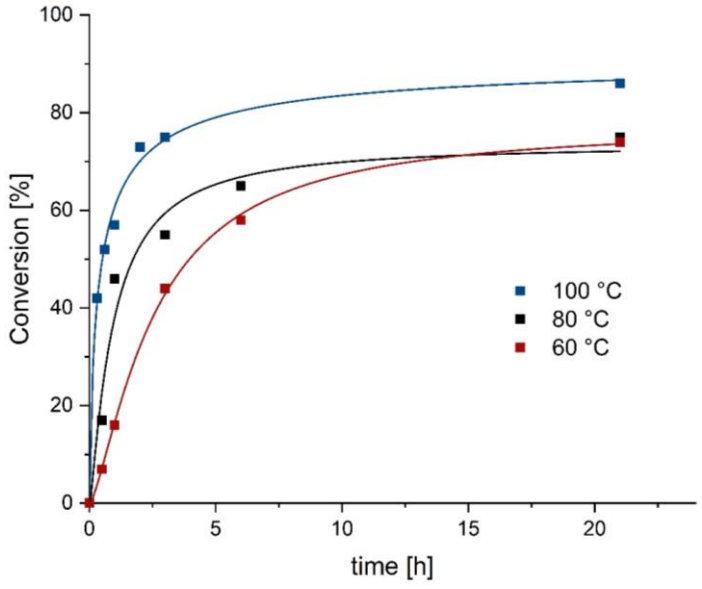

Figure 5.16: Kinetic studies for different reaction temperatures.

5.8.3 Kinetic Studies: Catalyst Loading

Tryptophan **221a** (63.4 mg, 0.20 mmol), $MnBr(CO)_5$ (1.0 mol %, 5.0 mol %, 10 mol %) and NaOAc (3.0 mol %, 10 mol %, 30 mol %) were placed in a 10 mL vial and evacuated and reflushed with N_2 for three times. Afterwards, MBH adduct **222b** (0.40 mmol) and water (1.5 mL) were added and the reaction was strirred at 80 °C for 18 h under N_2 with a ballon. After certain durations, a small sample of 20 µL was taken with a mechanical pipet and the conversion was determined by LC-MS.

Time [h]	**224ab** [%] 1.0 mol %	**224ab** [%] 5.0 mol %	**224ab** [%] 10 mol %
0	0.0	0.0	0.0
0.5	---	---	17.4
1	9.2	34.8	46.3
3	24.1	47.4	55.4
6	27.3	53.0	65.1
18	50.2	52.7	74.2

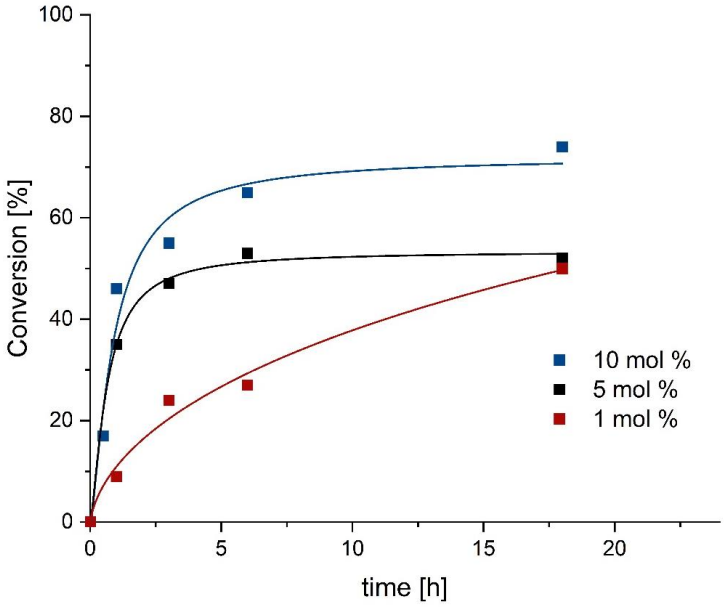

Figure 5.17: Kinetic studies with different catalyst loadings.

6 REFERENCES

[1] F. Wöhler, *Ann. Phys.* **1828**, *88*, 253–256.

[2] K. C. Nicolaou, *Angew. Chem. Int. Ed.* **2013**, *52*, 131–146.

[3] a) D. G. Brown, J. Boström, *J. Med. Chem.* **2016**, *59*, 4443–4458; b) M. Colombo, I. Peretto, *Drug Discov. Today.* **2008**, *13*, 677–684; c) M. MacCoss, T. A. Baillie, *Science* **2004**, *303*, 1810–1813.

[4] The Nobel Prize Hompage: https://www.nobelprize.org/prizes/chemistry/ (accessed: 28.01.2023)

[5] P. Anastas, J. C. Warner, *Green Chemistry: Theory and Practice*, Oxford University Press, **1998**.

[6] a) J. B. Zimmerman, P. T. Anastas, H. C. Erythropel, W. Leitner, *Science* **2020**, *367*, 397–400; b) P. Anastas, N. Eghbali, *Chem. Soc. Rev.* **2010**, *39*, 301–312; c) C.-J. Li, B. M. Trost, *Proc. Natl. Acad. Sci.* **2008**, *105*, 13197–13202; d) I. T. Horváth, P. T. Anastas, *Chem. Rev.* **2007**, *107*, 2169–2173; e) P. T. Anastas, M. M. Kirchhoff, *Acc. Chem. Res.* **2002**, *35*, 686–694.

[7] a) U. B. Kim, D. J. Jung, H. J. Jeon, K. Rathwell, S.-g. Lee, *Chem. Rev.* **2020**, *120*, 13382–13433; b) C. Zhong, X. Shi, *Eur. J. Org. Chem.* **2010**, 2999–3025.

[8] a) D. Wang, D. Astruc, *Chem. Soc. Rev.* **2017**, *46*, 816–854; b) M. S. Holzwarth, B. Plietker, *ChemCatChem* **2013**, *5*, 1650–1679.

[9] a) L. Lin, Y. Ge, H. Zhang, M. Wang, D. Xiao, D. Ma, *JACS Au* **2021**, *1*, 1834–1848; b) S. Gisbertz, B. Pieber, *ChemPhotoChem* **2020**, *4*, 456–475; c) C. M. Friend, B. Xu, *Acc. Chem. Res.* **2017**, *50*, 517–521; d) I. Fechete, Y. Wang, J. C. Védrine, *Cata. Today* **2012**, *189*, 2–27.

[10] a) I. Choi, V. Müller, G. Lole, R. Köhler, V. Karius, W. Viöl, C. Jooss, L. Ackermann, *Chem. Eur. J.* **2020**, *26*, 3509–3514; b) L.-C. Lee, J. He, J.-Q. Yu, C. W. Jones, *ACS Catal.* **2016**, *6*, 5245–5250; c) T. Iwai, T. Harada, K. Hara, M. Sawamura, *Angew. Chem. Int. Ed.* **2013**, *52*, 12322–12326; d) K. M. Chepiga, Y. Feng, N. A. Brunelli, C. W. Jones, H. M. L. Davies, *Org. Lett.* **2013**, *15*, 6136–6139.

[11] a) T. Shen, S. Zhou, J. Ruan, X. Chen, X. Liu, X. Ge, C. Qian, *Adv. Colloid Interface Sci.* **2021**, *287*, 102299; b) A. Steven, *Synthesis* **2019**, *51*, 2632–2647.

[12] a) N. Kaplaneris, M. Vilches-Herrera, J. Wu, L. Ackermann, *ACS Sustain. Chem. Eng.* **2022**, *10*, 6871–6888; b) M. Tobiszewski, S. Tsakovski, V. Simeonov, J. Namieśnik, F. Pena-Pereira, *Green Chem.* **2015**, *17*, 5206–5206; c) D. Prat, J. Hayler, A. Wells, *Green Chem.* **2014**, *16*, 4546–4551; d) R. K. Henderson, C. Jiménez-González, D. J. C. Constable, S. R. Alston, G. G. A. Inglis, G. Fisher, J. Sherwood, S. P. Binks, A. D. Curzons, *Green Chem.* **2011**, *13*, 854–862.

[13] a) P. K. Mohan, G. Nakhla, E. K. Yanful, *Water Res.* **2006**, *40*, 533–540; b) M. Franska, R. Franski, A. Szymanski, Z. Lukaszewski, *Water Res.* **2003**, *37*, 1005–1014; c) A. Jiménez-González, M. Salazar-González, M. Gutiérrez-Rojas, O. Monroy, *Water Sci. Technol.* **2001**, *44*, 175–181.

[14] a) T. Lorenzetto, G. Berton, F. Fabris, A. Scarso, *Catal. Sci. Technol.* **2020**, *10*, 4492–4502; b) F. Gallou, N. A. Isley, A. Ganic, U. Onken, M. Parmentier, *Green Chem.* **2016**, *18*, 14–19.

[15] a) P. Klumphu, B. H. Lipshutz, *J. Org. Chem.* **2014**, *79*, 888–900; b) B. H. Lipshutz, S. Ghorai, *Aldrichimica Acta* **2012**, *45*, 3–16.

[16] For selected examples for micellar catalysis, see: a) Y. Hu, M. J. Wong, B. H. Lipshutz, *Angew. Chem. Int. Ed.* **2022**, e202209784; b) B. S. Takale, R. R. Thakore, G. Casotti, X. Li, F. Gallou, B. H. Lipshutz, *Angew. Chem. Int. Ed.* **2021**, *60*, 4158–4163; c) A. B. Wood, S. Plummer, R. I. Robinson, M. Smith, J. Chang, F. Gallou, B. H. Lipshutz, *Green Chem.* **2021**, *23*, 7724–7730; d) T. N. Ansari, A. Taussat, A. H. Clark, M. Nachtegaal, S. Plummer, F. Gallou, S. Handa, *ACS Catal.* **2019**, *9*, 10389–10397; e) R. R. Thakore, B. S. Takale, F. Gallou, J. Reilly, B. H. Lipshutz, *ACS Catal.* **2019**, *9*, 11647–11657.

[17] a) X. Li, K. S. Iyer, R. R. Thakore, D. K. Leahy, J. D. Bailey, B. H. Lipshutz, *Org. Lett.* **2021**, *23*, 7205–7208; b) X. Li, R. R. Thakore, B. S. Takale, F. Gallou, B. H. Lipshutz, *Org. Lett.* **2021**, *23*, 8114–8118; c) F. Gallou, *Chimia* **2020**, *74*, 538–548; d) M. Cortes-Clerget, N. R. Lee, B. H. Lipshutz, *Nat. Protoc.* **2019**, *14*, 1108–1129.

[18] B. S. Takale, F.-Y. Kong, R. R. Thakore, *Organics* **2022**, *3*, 1–21.

[19] M. P. Andersson, *J. Colloid. Interface Sci.* **2022**, *628*, 819–828.

[20] a) T. Fantoni, S. Bernardoni, A. Mattellone, G. Martelli, L. Ferrazzano, P. Cantelmi, D. Corbisiero, A. Tolomelli, W. Cabri, F. Vacondio, F. Ferlenghi, M. Mor, A. Ricci, *ChemSusChem* **2021**, *14*, 2591–2600; b) M. Cortes-Clerget, J. Yu, J. R. A. Kincaid, P. Walde, F. Gallou, B. H. Lipshutz, *Chem. Sci.* **2021**, *12*, 4237–4266; c) S. Handa, Y. Wang, F. Gallou, B. H. Lipshutz, *Science* **2015**, *349*, 1087–1091.

[21] N. Suzuki, S. Koyama, R. Koike, N. Ebara, R. Arai, Y. Takeoka, M. Rikukawa, F.-Y. Tsai, *Polymers* **2021**, *13*, 2717–2736.

[22] a) U. Dhawa, N. Kaplaneris, L. Ackermann, *Org. Chem. Front.* **2021**; b) T. H. Meyer, I. Choi, C. Tian, L. Ackermann, *Chem* **2020**, *6*, 2484–2496; c) L. Guillemard, J. Wencel-Delord, *Beilstein J. Org. Chem.* **2020**, *16*, 1754–1804.

[23] a) D. Basu, S. Kumar, S. S. V, R. Bandichhor, *J. Chem. Sci.* **2018**, *130*, 71; b) D. J. Abrams, P. A. Provencher, E. J. Sorensen, *Chem. Soc. Rev.* **2018**, *47*, 8925–8967; c) Z. Dong, Z. Ren, S. J. Thompson, Y. Xu, G. Dong, *Chem. Rev.* **2017**, *117*, 9333–9403; d) Y. Park, Y. Kim, S. Chang, *Chem. Rev.* **2017**, *117*, 9247–9301; e) W. R. Gutekunst, P. S. Baran, *Chem. Soc. Rev.* **2011**, *40*, 1976–1991; f) L. Ackermann, *Modern Arlyation Methods*, Wiley VCH, Weinheim, **2009**.

[24] F. Ullmann, J. Bielecki, *Ber. Dtsch. Chem. Ges.* **1901**, *34*, 2174–2185.

[25] I. Goldberg, *Ber. Dtsch. Chem. Ges.* **1906**, *39*, 1691–1692.

[26] a) K. Tamao, K. Sumitani, M. Kumada, *J. Am. Chem. Soc.* **1972**, *94*, 4374–4376; b) R. J. P. Corriu, J. P. Masse, *J. Chem. Soc., Chem. Commun.* **1972**, 144a.

[27] a) H. A. Dieck, R. F. Heck, *J. Am. Chem. Soc.* **1974**, *96*, 1133–1136; b) R. F. Heck, J. P. Nolley, *J. Org. Chem.* **1972**, *37*, 2320–2322; c) T. Mizoroki, K. Mori, A. Ozaki, *Bull. Chem. Soc. Jpn.* **1971**, *44*, 581–581.

[28] K. Sonogashira, Y. Tohda, N. Hagihara, *Tetrahedron Lett.* **1975**, *16*, 4467–4470.

[29] a) N. Miyaura, A. Suzuki, *Chem. Rev.* **1995**, *95*, 2457–2483; b) N. Miyaura, T. Yano, A. Suzuki, *Tetrahedron Lett.* **1980**, *21*, 2865–2868; c) N. Miyaura, K. Yamada, A. Suzuki, *Tetrahedron Lett.* **1979**, *20*, 3437–3440.

[30] E. Negishi, A. O. King, N. Okukado, *J. Org. Chem.* **1977**, *42*, 1821–1823.

[31] a) Y. Hatanaka, T. Hiyama, *J. Org. Chem.* **1988**, *53*, 918–920; b) J. K. Stille, *Angew. Chem. Int. Ed.* **1986**, *25*, 508–524; c) D. Milstein, J. K. Stille, *J. Am. Chem. Soc.* **1978**, *100*, 3636–3638.

[32] a) A. S. Guram, S. L. Buchwald, *J. Am. Chem. Soc.* **1994**, *116*, 7901–7902; b) F. Paul, J. Patt, J. F. Hartwig, *J. Am. Chem. Soc.* **1994**, *116*, 5969–5970.

[33] a) C. C. C. Johansson Seechurn, M. O. Kitching, T. J. Colacot, V. Snieckus, *Angew. Chem. Int. Ed.* **2012**, *51*, 5062−5085; b) E.-i. Negishi, *Angew. Chem. Int. Ed.* **2011**, *50*, 6738–6764; c) A. Suzuki, *Angew. Chem. Int. Ed.* **2011**, *50*, 6722–6737.

[34] For selected reviews on C–H activation, see: a) T. Rogge, N. Kaplaneris, N. Chatani, J. Kim, S. Chang, B. Punji, L. L. Schafer, D. G. Musaev, J. Wencel-Delord, C. A. Roberts, R. Sarpong, Z. E. Wilson, M. A. Brimble, M. J. Johansson, L. Ackermann, *Nature Rev. Methods Primer* **2021**, *1*, 43; b) S. M. Khake, N. Chatani, *Trends Chem.* **2019**, *1*, 524–539; c) P. Gandeepan, T. Müller, D. Zell, G. Cera, S. Warratz, L. Ackermann, *Chem. Rev.* **2019**, *119*, 2192–2452; d) K. Murakami, S. Yamada, T. Kaneda, K. Itami, *Chem. Rev.* **2017**, *117*, 9302–9332.

[35] a) R. A. Sheldon, *Pure Appl. Chem.* **2000**, *72*, 1233–1246; b) B. M. Trost, *Angew. Chem. Int. Ed.* **1995**, *34*, 259–281.

[36] H. Yi, G. Zhang, H. Wang, Z. Huang, J. Wang, A. K. Singh, A. Lei, *Chem. Rev.* **2017**, *117*, 9016–9085.

[37] a) K. M. Altus, J. A. Love, *Commun. Chem.* **2021**, *4*, 173; b) L. Ackermann, *Chem. Rev.* **2011**, *111*, 1315–1345; c) D. H. Ess, W. A. Goddard, R. A. Periana, *Organometallics* **2010**, *29*, 6459–6472; d) D. Balcells, E. Clot, O. Eisenstein, *Chem. Rev.* **2010**, *110*, 749–823; e) Y. Boutadla, D. L. Davies, S. A. Macgregor, A. I. Poblador-Bahamonde, *Dalton Trans.* **2009**, 5820–5831; f) J. A. Labinger, J. E. Bercaw, *Nature* **2002**, *417*, 507–514.

[38] V. I. Sokolov, L. L. Troitskaya, O. A. Reutov, *J. Organomet. Chem.* **1979**, *182*, 537–546.

[39] a) D. L. Davies, S. A. Macgregor, C. L. McMullin, *Chem. Rev.* **2017**, *117*, 8649–8709; b) B. Biswas, M. Sugimoto, S. Sakaki, *Organometallics* **2000**, *19*, 3895–3908.

[40] a) D. Lapointe, K. Fagnou, *Chem. Lett.* **2010**, *39*, 1118–1126; b) S. I. Gorelsky, D. Lapointe, K. Fagnou, *J. Am. Chem. Soc.* **2008**, *130*, 10848–10849.

[41] Y. Boutadla, D. L. Davies, S. A. Macgregor, A. I. Poblador-Bahamonde, *Dalton Trans.* **2009**, 5887–5893.

[42] a) D. Zell, M. Bursch, V. Müller, S. Grimme, L. Ackermann, *Angew. Chem. Int. Ed.* **2017**, *56*, 10378–10382; b) W. Ma, R. Mei, G. Tenti, L. Ackermann, *Chem. Eur. J.* **2014**, *20*, 15248–15251.

[43] a) D. García-Cuadrado, P. de Mendoza, A. A. C. Braga, F. Maseras, A. M. Echavarren, *J. Am. Chem. Soc.* **2007**, *129*, 6880–6886; b) D. García-Cuadrado, A. A. C. Braga, F. Maseras, A. M. Echavarren, *J. Am. Chem. Soc.* **2006**, *128*, 1066–1067.

[44] M. Lafrance, C. N. Rowley, T. K. Woo, K. Fagnou, *J. Am. Chem. Soc.* **2006**, *128*, 8754–8756.

[45] J. F. Hartwig, M. A. Larsen, *ACS Cent. Sci.* **2016**, *2*, 281–292.

[46] X.-S. Xue, P. Ji, B. Zhou, J.-P. Cheng, *Chem. Rev.* **2017**, *117*, 8622–8648.

[47] J. F. Hartwig, *Chem. Soc. Rev.* **2011**, *40*, 1992–2002.

[48] a) S. Rej, Y. Ano, N. Chatani, *Chem. Rev.* **2020**, *120*, 1788–1887; b) C. Sambiagio, D. Schönbauer, R. Blieck, T. Dao-Huy, G. Pototschnig, P. Schaaf, T. Wiesinger, M. F. Zia, J. Wencel-Delord, T. Besset, B. U. W. Maes, M. Schnürch, *Chem. Soc. Rev.* **2018**, *47*, 6603–6743; c) Z. Chen, B. Wang, J. Zhang, W. Yu, Z. Liu, Y. Zhang, *Org. Chem. Front.* **2015**, *2*, 1107–1295.

[49] W. Ma, P. Gandeepan, J. Li, L. Ackermann, *Org. Chem. Front.* **2017**, *4*, 1435–1467.

[50] a) P. Gandeepan, L. Ackermann, *Chem* **2018**, *4*, 199–222; b) F. Zhang, D. R. Spring, *Chem. Soc. Rev.* **2014**, *43*, 6906–6919.

[51] a) M. T. Mihai, G. R. Genov, R. J. Phipps, *Chem. Soc. Rev.* **2018**, *47*, 149–171; b) L. Ackermann, J. Li, *Nat. Chem.* **2015**, *7*, 686–687; c) J. Yang, *Org. Biomol. Chem.* **2015**, *13*, 1930–1941; d) J. Schranck, A. Tlili, M. Beller, *Angew. Chem. Int. Ed.* **2014**, *53*, 9426–9428.

[52] a) A. Mondal, H. Chen, L. Flämig, P. Wedi, M. van Gemmeren, *J. Am. Chem. Soc.* **2019**, *141*, 18662–18667; b) C. Cheng, J. F. Hartwig, *Science* **2014**, *343*, 853–857; c) D. W. Robbins, J. F. Hartwig, *Angew. Chem. Int. Ed.* **2013**, *52*, 933–937; d) I. A. I. Mkhalid, J. H. Barnard, T. B. Marder, J. M. Murphy, J. F. Hartwig, *Chem. Rev.* **2010**, *110*, 890–931; e) J.-Y. Cho, M. K. Tse, D. Holmes, R. E. Maleczka, M. R. Smith, *Science* **2002**, *295*, 305–308.

[53] a) M. Font, A. R. A. Spencer, I. Larrosa, *Chem. Sci.* **2018**, *9*, 7133–7137; b) N. Y. P. Kumar, A. Bechtoldt, K. Raghuvanshi, L. Ackermann, *Angew. Chem. Int. Ed.* **2016**, *55*, 6929–6932; c) J. Luo, S. Preciado, I. Larrosa, *J. Am. Chem. Soc.* **2014**, *136*, 4109–4112.

[54] a) A. Dey, S. K. Sinha, T. K. Achar, D. Maiti, *Angew. Chem. Int. Ed.* **2019**, *58*, 10820–10843; b) H.-J. Xu, Y.-S. Kang, H. Shi, P. Zhang, Y.-K. Chen, B. Zhang, Z.-Q. Liu, J. Zhao, W.-Y. Sun, J.-Q. Yu, Y. Lu, *J. Am. Chem. Soc.* **2019**, *141*, 76–79; c) U. Dutta, A. Modak, B. Bhaskararao, M. Bera, S. Bag, A. Mondal, D. W. Lupton, R. B. Sunoj, D. Maiti, *ACS Catal.* **2017**, *7*, 3162–3168; d) D. Leow, G. Li, T.-S. Mei, J.-Q. Yu, *Nature* **2012**, *486*, 518–522.

[55] Y. Kuninobu, H. Ida, M. Nishi, M. Kanai, *Nat. Chem.* **2015**, *7*, 712–717.

[56] a) M. Catellani, E. Motti, N. Della Ca', *Acc. Chem. Res.* **2008**, *41*, 1512–1522; b) M. Catellani, F. Frignani, A. Rangoni, *Angew. Chem. Int. Ed.* **1997**, *36*, 119–122.

[57] a) L.-Y. Liu, J. X. Qiao, K.-S. Yeung, W. R. Ewing, J.-Q. Yu, *J. Am. Chem. Soc.* **2019**, *141*, 14870–14877; b) J. Ye, M. Lautens, *Nat. Chem.* **2015**, *7*, 863–870; c) X.-C. Wang, W. Gong, L.-Z. Fang, R.-Y. Zhu, S. Li, K. M. Engle, J.-Q. Yu, *Nature* **2015**, *519*, 334–338.

[58] a) K. Korvorapun, R. C. Samanta, T. Rogge, L. Ackermann, *Synthesis* **2021**, *53*, 2911–2946; b) J. A. Leitch, C. G. Frost, *Chem. Soc. Rev.* **2017**, *46*, 7145–7153; c) M. Gagliardo, D. J. M. Snelders, P. A. Chase, R. J. M. Klein Gebbink, G. P. M. van Klink, G. van Koten, *Angew. Chem. Int. Ed.* **2007**, *46*, 8558–8573.

[59] J. Chatt, J. M. Davidson, *J. Chem. Soc.* **1965**, 843–855.

[60] L. N. Lewis, J. F. Smith, *J. Am. Chem. Soc.* **1986**, *108*, 2728–2735.

[61] a) K. A. Pittard, J. P. Lee, T. R. Cundari, T. B. Gunnoe, J. L. Petersen, *Organometallics* **2004**, *23*, 5514–5523; b) M. Lail, B. N. Arrowood, T. B. Gunnoe, *J. Am. Chem. Soc.* **2003**, *125*, 7506–7507.

[62] S. Murai, F. Kakiuchi, S. Sekine, Y. Tanaka, A. Kamatani, M. Sonoda, N. Chatani, *Nature* **1993**, *366*, 529–531.

[63] T. Matsubara, N. Koga, D. G. Musaev, K. Morokuma, *Organometallics* **2000**, *19*, 2318–2329.

[64] L. Ackermann, P. Novák, R. Vicente, N. Hofmann, *Angew. Chem. Int. Ed.* **2009**, *48*, 6045–6048.

[65] L. Ackermann, N. Hofmann, R. Vicente, *Org. Lett.* **2011**, *13*, 1875–1877.

[66] M. Wheatley, M. T. Findlay, R. López-Rodríguez, D. M. Cannas, M. Simonetti, I. Larrosa, *Chem Catal.* **2021**, *1*, 691–703.

[67] M. Pfeffer, E. P. Urriolabeitia, J. Fischer, *Inorg. Chem.* **1995**, *34*, 643–650.

[68] N. Hofmann, L. Ackermann, *J. Am. Chem. Soc.* **2013**, *135*, 5877–5884.

[69] J. Li, S. Warratz, D. Zell, S. De Sarkar, E. E. Ishikawa, L. Ackermann, *J. Am. Chem. Soc.* **2015**, *137*, 13894–13901.

[70] A. J. Paterson, S. St John-Campbell, M. F. Mahon, N. J. Press, C. G. Frost, *Chem. Commun.* **2015**, *51*, 12807–12810.

[71] G. Li, X. Ma, C. Jia, Q. Han, Y. Wang, J. Wang, L. Yu, S. Yang, *Chem. Commun.* **2017**, *53*, 1261–1264.

[72] G. Li, P. Gao, X. Lv, C. Qu, Q. Yan, Y. Wang, S. Yang, J. Wang, *Org. Lett.* **2017**, *19*, 2682–2685.

[73] B. Zhao, T. Rogge, L. Ackermann, Z. Shi, *Chem. Soc. Rev.* **2021**, *50*, 8903–8953.

[74] S. Oi, S. Fukita, N. Hirata, N. Watanuki, S. Miyano, Y. Inoue, *Org. Lett.* **2001**, *3*, 2579–2581.

[75] S. Oi, Y. Ogino, S. Fukita, Y. Inoue, *Org. Lett.* **2002**, *4*, 1783–1785.

[76] S. Oi, E. Aizawa, Y. Ogino, Y. Inoue, *J. Org. Chem.* **2005**, *70*, 3113–3119.

[77] L. Ackermann, M. Mulzer, *Org. Lett.* **2008**, *10*, 5043–5045.

[78] S. G. Ouellet, A. Roy, C. Molinaro, R. Angelaud, J. F. Marcoux, P. D. O'Shea, I. W. Davies, *Synfacts* **2011**, 0579–0579.

[79] L. Ackermann, A. Althammer, R. Born, *Synlett* **2007**, 2833–2836.

[80] L. Ackermann, A. Althammer, R. Born, *Tetrahedron* **2008**, *64*, 6115–6124.

[81] L. Ackermann, R. Vicente, A. Althammer, *Org. Lett.* **2008**, *10*, 2299–2302.

[82] L. Ackermann, R. Vicente, H. K. Potukuchi, V. Pirovano, *Org. Lett.* **2010**, *12*, 5032–5035.

[83] a) L. Ackermann, J. Pospech, H. K. Potukuchi, *Org. Lett.* **2012**, *14*, 2146–2149; b) L. Ackermann, A. Althammer, R. Born, *Angew. Chem. Int. Ed.* **2006**, *45*, 2619–2622.

[84] J. Hubrich, L. Ackermann, *Eur. J. Org. Chem.* **2016**, 3700–3704.

[85] a) L. Ackermann, *Org. Process Res. Dev.* **2015**, *19*, 260–269; b) E. Diers, N. Y. Phani Kumar, T. Mejuch, I. Marek, L. Ackermann, *Tetrahedron* **2013**, *69*, 4445–4453.

[86] T. Rogge, T. Müller, H. Simon, X. Hou, S. Wagschal, D. Broggini, L. Ackermann, *Synlett* **2021**, *33*, 346–350.

[87] M. Simonetti, D. M. Cannas, X. Just-Baringo, I. J. Vitorica-Yrezabal, I. Larrosa, *Nat. Chem.* **2018**, *10*, 724–731.

[88] M. T. Findlay, P. Domingo-Legarda, G. McArthur, A. Yen, I. Larrosa, *Chem. Sci.* **2022**, *13*, 3335–3362.

[89] M. Simonetti, D. M. Cannas, A. Panigrahi, S. Kujawa, M. Kryjewski, P. Xie, I. Larrosa, *Chem. Eur. J.* **2017**, *23*, 549–553.

[90] R. Mei, C. Zhu, L. Ackermann, *Chem. Commun.* **2016**, *52*, 13171–13174.

[91] A. Biafora, T. Krause, D. Hackenberger, F. Belitz, L. J. Gooßen, *Angew. Chem. Int. Ed.* **2016**, *55*, 14752–14755.

[92] S. R. Yetra, T. Rogge, S. Warratz, J. Struwe, W. Peng, P. Vana, L. Ackermann, *Angew. Chem. Int. Ed.* **2019**, *58*, 7490–7494.

[93] M. Simonetti, G. J. P. Perry, X. C. Cambeiro, F. Juliá-Hernández, J. N. Arokianathar, I. Larrosa, *J. Am. Chem. Soc.* **2016**, *138*, 3596–3606.

[94] L. Ackermann, P. Novák, *Org. Lett.* **2009**, *11*, 4966–4969.

[95] G. Li, D. Li, J. Zhang, D.-Q. Shi, Y. Zhao, *ACS Catal.* **2017**, *7*, 4138–4143.

[96] B. Li, S.-L. Fang, D.-Y. Huang, B.-F. Shi, *Org. Lett.* **2017**, *19*, 3950–3953.

[97] K. Korvorapun, R. Kuniyil, L. Ackermann, *ACS Catal.* **2020**, *10*, 435–440.

[98] a) J. A. Osborn, F. H. Jardine, J. F. Young, G. Wilkinson, *J. Chem. Soc. A* **1966**, 1711–1732; b) J. F. Young, J. A. Osborn, F. H. Jardine, G. Wilkinson, *Chem. Commun.* **1965**, 131–132.

[99] a) G. Song, F. Wang, X. Li, *Chem. Soc. Rev.* **2012**, *41*, 3651–3678; b) T. Satoh, M. Miura, *Chem. Eur. J.* **2010**, *16*, 11212–11222.

[100] Y.-G. Lim, Y. H. Kim, J.-B. Kang, *J. Chem. Soc., Chem. Commun.* **1994**, 2267–2268.

[101] a) D. A. Colby, A. S. Tsai, R. G. Bergman, J. A. Ellman, *Acc. Chem. Res.* **2012**, *45*, 814–825; b) D. A. Colby, R. G. Bergman, J. A. Ellman, *Chem. Rev.* **2010**, *110*, 624–655.

[102] a) T. Matsumoto, R. A. Periana, D. J. Taube, H. Yoshida, *J. Catal.* **2002**, *206*, 272–280; b) T. Matsumoto, H. Yoshida, *Chem. Lett.* **2000**, *29*, 1064–1065.

[103] a) K. Ueura, T. Satoh, M. Miura, *J. Org. Chem.* **2007**, *72*, 5362–5367; b) K. Ueura, T. Satoh, M. Miura, *Org. Lett.* **2007**, *9*, 1407–1409.

[104] a) A. Bechtoldt, M. E. Baumert, L. Vaccaro, L. Ackermann, *Green Chem.* **2018**, *20*, 398–402; b) S. Warratz, C. Kornhaaß, A. Cajaraville, B. Niepötter, D. Stalke, L. Ackermann, *Angew. Chem. Int. Ed.* **2015**, *54*, 5513–5517; c) L. Ackermann, J. Pospech, K. Graczyk, K. Rauch, *Org. Lett.* **2012**, *14*, 930–933; d) L. Ackermann, J. Pospech, *Org. Lett.* **2011**, *13*, 4153–4155.

[105] L. Li, W. W. Brennessel, W. D. Jones, *J. Am. Chem. Soc.* **2008**, *130*, 12414–12419.

[106] D. R. Stuart, M. Bertrand-Laperle, K. M. N. Burgess, K. Fagnou, *J. Am. Chem. Soc.* **2008**, *130*, 16474–16475.

[107] N. Guimond, K. Fagnou, *J. Am. Chem. Soc.* **2009**, *131*, 12050–12051.

[108] T. Fukutani, N. Umeda, K. Hirano, T. Satoh, M. Miura, *Chem. Commun.* **2009**, 5141–5143.

[109] S. Mochida, M. Shimizu, K. Hirano, T. Satoh, M. Miura, *Chem. Asian J.* **2010**, *5*, 847–851.

[110] N. Umeda, K. Hirano, T. Satoh, N. Shibata, H. Sato, M. Miura, *J. Org. Chem.* **2011**, *76*, 13–24.

[111] K. Morimoto, K. Hirano, T. Satoh, M. Miura, *Org. Lett.* **2010**, *12*, 2068–2071.

[112] N. Umeda, H. Tsurugi, T. Satoh, M. Miura, *Angew. Chem. Int. Ed.* **2008**, *47*, 4019–4022.

[113] S. Mochida, N. Umeda, K. Hirano, T. Satoh, M. Miura, *Chem. Lett.* **2010**, *39*, 744–746.

[114] T. K. Hyster, T. Rovis, *J. Am. Chem. Soc.* **2010**, *132*, 10565–10569.

[115] F. W. Patureau, F. Glorius, *J. Am. Chem. Soc.* **2010**, *132*, 9982–9983.

[116] F. W. Patureau, T. Besset, F. Glorius, *Angew. Chem. Int. Ed.* **2011**, *50*, 1064–1067.

[117] S. Miriyala, I. Spasojevic, A. Tovmasyan, D. Salvemini, Z. Vujaskovic, D. St. Clair, I. Batinic-Haberle, *Biochim. Biophys. Acta - Mol. Basis Dis.* **2012**, *1822*, 794–814.

[118] Y. Hu, B. Zhou, C. Wang, *Acc. Chem. Res.* **2018**, *51*, 816–827.

[119] a) A. S. Borovik, *Chem. Soc. Rev.* **2011**, *40*, 1870–1874; b) A. Gunay, K. H. Theopold, *Chem. Rev.* **2010**, *110*, 1060–1081.

[120] M. I. Bruce, M. Z. Iqbal, F. G. A. Stone, *J. Chem. Soc. A* **1970**, 3204–3209.

[121] a) J.-P. Djukic, A. Maisse, M. Pfeffer, *J. Organomet. Chem.* **1998**, *567*, 65–74; b) G. J. Depree, L. Main, B. K. Nicholson, *J. Organomet. Chem.* **1998**, *551*, 281–291; c) R. C. Cambie, M. R. Metzler, P. S. Rutledge, P. D. Woodgate, *J. Organomet. Chem.* **1992**, *429*, 41–57; d) L. S. Liebeskind, J. R. Gasdaska, J. S. McCallum, S. J. Tremont, *J. Org. Chem.* **1989**, *54*, 669–677.

[122] Y. Kuninobu, Y. Nishina, T. Takeuchi, K. Takai, *Angew. Chem. Int. Ed.* **2007**, *46*, 6518–6520.

[123] B. Zhou, H. Chen, C. Wang, *J. Am. Chem. Soc.* **2013**, *135*, 1264–1267.

[124] S. Tang, O. Eisenstein, Y. Nakao, S. Sakaki, *Organometallics* **2017**, *36*, 2761–2771.

[125] L. Shi, X. Zhong, H. She, Z. Lei, F. Li, *Chem. Commun.* **2015**, *51*, 7136–7139.

[126] Z. Ruan, N. Sauermann, E. Manoni, L. Ackermann, *Angew. Chem. Int. Ed.* **2017**, *56*, 3172–3176.

[127] N. Kaplaneris, F. Kaltenhäuser, G. Sirvinskaite, S. Fan, T. De Oliveira, L.-C. Conradi, L. Ackermann, *Sci. Adv.* **2021**, *7*, eabe6202.

[128] B. B. Jei, L. Yang, L. Ackermann, *Chem. Eur. J.* **2022**, *28*, e202200811.

[129] W. Liu, S. C. Richter, Y. Zhang, L. Ackermann, *Angew. Chem. Int. Ed.* **2016**, *55*, 7747–7750.

[130] T. Brückl, R. D. Baxter, Y. Ishihara, P. S. Baran, *Acc. Chem. Res.* **2012**, *45*, 826–839.

[131] Y. Fujiwara, I. Moritani, S. Danno, R. Asano, S. Teranishi, *J. Am. Chem. Soc.* **1969**, *91*, 7166–7169.

[132] J. D. Lasso, D. J. Castillo-Pazos, C.-J. Li, *Chem. Soc. Rev.* **2021**, *50*, 10955–10982.

[133] X.-F. Wu, H. Neumann, M. Beller, *Chem. Asian J.* **2012**, *7*, 1744–1754.

[134] P. Shah, A. D. Westwell, *J. Enzyme Inhib. Med. Chem.* **2007**, *22*, 527–540.

[135] a) H. Xiao, Z. Zhang, Y. Fang, L. Zhu, C. Li, *Chem. Soc. Rev.* **2021**, *50*, 6308–6319; b) A. Studer, *Angew. Chem. Int. Ed.* **2012**, *51*, 8950–8958.

[136] M. Hamzehloo, A. Hosseinian, S. Ebrahimiasl, A. Monfared, E. Vessally, *J. Fluor. Chem.* **2019**, *224*, 52–60.

[137] L. M. Yagupolskii, N. V. Kondratenko, G. N. Timofeeva, *J. Org. Chem. USSR* **1984**, *20*, 103–106.

[138] T. Umemoto, S. Ishihara, *J. Am. Chem. Soc.* **1993**, *115*, 2156–2164.

[139] J.-J. Yang, R. L. Kirchmeier, J. M. Shreeve, *J. Org. Chem.* **1998**, *63*, 2656–2660.

[140] a) K. Stanek, R. Koller, A. Togni, *J. Org. Chem.* **2008**, *73*, 7678–7685; b) P. Eisenberger, S. Gischig, A. Togni, *Chem. Eur. J.* **2006**, *12*, 2579–2586.

[141] a) P. Eisenberger, I. Kieltsch, N. Armanino, A. Togni, *Chem. Commun.* **2008**, 1575–1577; b) I. Kieltsch, P. Eisenberger, A. Togni, *Angew. Chem. Int. Ed.* **2007**, *46*, 754–757.

[142] a) T. Liu, Q. Shen, *Eur. J. Org. Chem.* **2012**, 6679–6687; b) O. A. Tomashenko, V. V. Grushin, *Chem. Rev.* **2011**, *111*, 4475–4521.

[143] a) Y. Kobayashi, I. Kumadaki, *Tetrahedron Lett.* **1969**, *10*, 4095–4096; b) V. C. R. McLoughlin, J. Thrower, *Tetrahedron* **1969**, *25*, 5921–5940.

[144] H. Urata, T. Fuchikami, *Tetrahedron Lett.* **1991**, *32*, 91–94.

[145] T. Schareina, X.-F. Wu, A. Zapf, A. Cotté, M. Gotta, M. Beller, *Top. Catal.* **2012**, *55*, 426–431.

[146] K. Matsui, E. Tobita, M. Ando, K. Kondo, *Chem. Lett.* **1981**, *10*, 1719–1720.

[147] Y. Li, T. Chen, H. Wang, R. Zhang, K. Jin, X. Wang, C. Duan, *Synlett* **2011**, 1713–1716.

[148] S. Seo, J. B. Taylor, M. F. Greaney, *Chem. Commun.* **2013**, *49*, 6385–6387.

[149] K. Natte, R. V. Jagadeesh, L. He, J. Rabeah, J. Chen, C. Taeschler, S. Ellinger, F. Zaragoza, H. Neumann, A. Brückner, M. Beller, *Angew. Chem. Int. Ed.* **2016**, *55*, 2782–2786.

[150] H. Jia, A. P. Häring, F. Berger, L. Zhang, T. Ritter, *J. Am. Chem. Soc.* **2021**, *143*, 7623–7628.

[151] B. R. Langlois, E. Laurent, N. Roidot, *Tetrahedron Lett.* **1991**, *32*, 7525–7528.

[152] Y. Ji, T. Brueckl, R. D. Baxter, Y. Fujiwara, I. B. Seiple, S. Su, D. G. Blackmond, P. S. Baran, *Proc. Natl. Acad. Sci.* **2011**, *108*, 14411–14415.

[153] Y. Fujiwara, J. A. Dixon, F. O'Hara, E. D. Funder, D. D. Dixon, R. A. Rodriguez, R. D. Baxter, B. Herlé, N. Sach, M. R. Collins, Y. Ishihara, P. S. Baran, *Nature* **2012**, *492*, 95–99.

[154] J. Shen, J. Xu, L. He, C. Liang, W. Li, *Chin. Chem. Lett.* **2022**, *33*, 1227–1235.

[155] For selected examples, see:a) F. Xiao, J.-H. Lin, F. Hao, X. Zheng, Y. Guo, J.-C. Xiao, *Org. Chem. Front.* **2022**, *9*, 1982–1985; b) I. Ghosh, J. Khamrai, A. Savateev, N. Shlapakov, M. Antonietti, B. König, *Science* **2019**, *365*, 360–366; c) F. Ye, F. Berger,

H. Jia, J. Ford, A. Wortman, J. Börgel, C. Genicot, T. Ritter, *Angew. Chem. Int. Ed.* **2019**, *58*, 14615–14619; d) C. Bottecchia, R. Martín, I. Abdiaj, E. Crovini, J. Alcazar, J. Orduna, M. J. Blesa, J. R. Carrillo, P. Prieto, T. Noël, *Adv. Synth. Catal.* **2019**, *361*, 945–950; e) Y. Ouyang, X.-H. Xu, F.-L. Qing, *Angew. Chem. Int. Ed.* **2018**, *57*, 6926–6929; f) I. Abdiaj, C. Bottecchia, J. Alcazar, T. Noël, *Synthesis* **2017**, *49*, 4978–4985; g) Joel W. Beatty, James J. Douglas, R. Miller, Rory C. McAtee, Kevin P. Cole, Corey R. J. Stephenson, *Chem* **2016**, *1*, 456–472; h) J. W. Beatty, J. J. Douglas, K. P. Cole, C. R. J. Stephenson, *Nat. Commun.* **2015**, *6*, 7919; i) L. Cui, Y. Matusaki, N. Tada, T. Miura, B. Uno, A. Itoh, *Adv. Synth. Catal.* **2013**, *355*, 2203–2207.

[156] For selected referecnes, see: a) E. Leclercq, A. Moncomble, C. Debavelaere, M. Beaucamp, M. Penhoat, L. Chausset-Boissarie, *Green Chem.* **2022**, *24*, 7388–7394; b) Z. Zou, W. Zhang, Y. Wang, Y. Pan, *Org. Chem. Front.* **2021**, *8*, 2786–2798; c) C. M. Kisukuri, V. A. Fernandes, J. A. C. Delgado, A. P. Häring, M. W. Paixão, S. R. Waldvogel, *Chem. Rec.* **2021**, *21*, 2502–2525; d) R. P. Bhaskaran, B. P. Babu, *Adv. Synth. Catal.* **2020**, *362*, 5219–5237; e) G.-Y. Dou, Y.-Y. Jiang, K. Xu, C.-C. Zeng, *Org. Chem. Front.* **2019**, *6*, 2392–2397; f) A. G. O'Brien, A. Maruyama, Y. Inokuma, M. Fujita, P. S. Baran, D. G. Blackmond, *Angew. Chem. Int. Ed.* **2014**, *53*, 11868–11871.

[157] Y. Qiu, A. Scheremetjew, L. H. Finger, L. Ackermann, *Chem. Eur. J.* **2020**, *26*, 3241–3246.

[158] X. Wang, L. Truesdale, J.-Q. Yu, *J. Am. Chem. Soc.* **2010**, *132*, 3648–3649.

[159] X.-G. Zhang, H.-X. Dai, M. Wasa, J.-Q. Yu, *J. Am. Chem. Soc.* **2012**, *134*, 11948–11951.

[160] M. Miura, C.-G. Feng, S. Ma, J.-Q. Yu, *Org. Lett.* **2013**, *15*, 5258–5261.

[161] M. Shang, S.-Z. Sun, H.-L. Wang, B. N. Laforteza, H.-X. Dai, J.-Q. Yu, *Angew. Chem. Int. Ed.* **2014**, *53*, 10439–10442.

[162] A. Hafner, S. Bräse, *Angew. Chem. Int. Ed.* **2012**, *51*, 3713–3715.

[163] a) A. Y. Chan, I. B. Perry, N. B. Bissonnette, B. F. Buksh, G. A. Edwards, L. I. Frye, O. L. Garry, M. N. Lavagnino, B. X. Li, Y. Liang, E. Mao, A. Millet, J. V. Oakley, N. L. Reed, H. A. Sakai, C. P. Seath, D. W. C. MacMillan, *Chem. Rev.* **2022**, *122*, 1485–1542; b) J. Twilton, C. Le, P. Zhang, M. H. Shaw, R. W. Evans, D. W. C. MacMillan, *Nat. Rev. Chem.* **2017**, *1*, 0052; c) J. M. R. Narayanam, C. R. J. Stephenson, *Chem. Soc. Rev.* **2011**, *40*, 102–113.

[164] a) A. Wiebe, T. Gieshoff, S. Möhle, E. Rodrigo, M. Zirbes, S. R. Waldvogel, *Angew. Chem. Int. Ed.* **2018**, *57*, 5594–5619; b) M. Yan, Y. Kawamata, P. S. Baran, *Chem. Rev.* **2017**, *117*, 13230–13319.

[165] H. Huang, K. A. Steiniger, T. H. Lambert, *J. Am. Chem. Soc.* **2022**, *144*, 12567–12583.

[166] M. Faraday, *Ann. Phys.* **1834**, *109*, 433–451.

[167] a) H. Kolbe, *Liebigs Ann. Chem.* **1849**, *69*, 257–294; b) H. C. Kolb, *Liebigs Ann. Chem.* **1848**, *64*, 339–341.

[168] For selected reviews on electrosynthesis, see: a) X. Cheng, A. Lei, T.-S. Mei, H.-C. Xu, K. Xu, C. Zeng, *CCS Chem.* **2022**, *4*, 1120–1152; b) J. E. Nutting, J. B. Gerken, A. G. Stamoulis, D. L. Bruns, S. S. Stahl, *J. Org. Chem.* **2021**, *86*, 15875–15885; c) S. B. Beil, D. Pollok, S. R. Waldvogel, *Angew. Chem. Int. Ed.* **2021**, *60*, 14750–14759; d) T. Wu, K. D. Moeller, *Angew. Chem. Int. Ed.* **2021**, *60*, 12883–12890; e) S. Möhle, M. Zirbes,

E. Rodrigo, T. Gieshoff, A. Wiebe, S. R. Waldvogel, *Angew. Chem. Int. Ed.* **2018**, *57*, 6018–6041; f) R. Francke, R. D. Little, *Chem. Soc. Rev.* **2014**, *43*, 2492–2521; g) J.-i. Yoshida, K. Kataoka, R. Horcajada, A. Nagaki, *Chem. Rev.* **2008**, *108*, 2265–2299.

[169] a) M. Dörr, J. L. Röckl, J. Rein, D. Schollmeyer, S. R. Waldvogel, *Chem. Eur. J.* **2020**, *26*, 10195–10198; b) T. H. Meyer, L. H. Finger, P. Gandeepan, L. Ackermann, *Trends Chem.* **2019**, *1*, 63–76; c) N. Sauermann, T. H. Meyer, Y. Qiu, L. Ackermann, *ACS Catal.* **2018**, *8*, 7086–7103; d) M. D. Kärkäs, *Chem. Soc. Rev.* **2018**, *47*, 5786–5865.

[170] a) P. Alfonso-Súarez, A. V. Kolliopoulos, J. P. Smith, C. E. Banks, A. M. Jones, *Tetrahedron Lett.* **2015**, *56*, 6863–6867; b) A. M. Jones, C. E. Banks, *Beilstein J. Org. Chem.* **2014**, *10*, 3056–3072; c) T. Shono, H. Hamaguchi, Y. Matsumura, *J. Am. Chem. Soc.* **1975**, *97*, 4264–4268.

[171] X. Tan, L. Massignan, X. Hou, J. Frey, J. C. A. Oliveira, M. N. Hussain, L. Ackermann, *Angew. Chem. Int. Ed.* **2021**, *60*, 13264–13270.

[172] C. Amatore, C. Cammoun, A. Jutand, *Adv. Synth. Catal.* **2007**, *349*, 292–296.

[173] For selected examples, see: a) J. Frey, X. Hou, L. Ackermann, *Chem. Sci.* **2022**, *13*, 2729–2734; b) U. Dhawa, C. Tian, T. Wdowik, J. C. A. Oliveira, J. Hao, L. Ackermann, *Angew. Chem. Int. Ed.* **2020**, *59*, 13451–13457; c) A. Shrestha, M. Lee, A. L. Dunn, M. S. Sanford, *Org. Lett.* **2018**, *20*, 204–207; d) Q.-L. Yang, Y.-Q. Li, C. Ma, P. Fang, X.-J. Zhang, T.-S. Mei, *J. Am. Chem. Soc.* **2017**, *139*, 3293–3298; e) H. Aiso, T. Kochi, H. Mutsutani, T. Tanabe, S. Nishiyama, F. Kakiuchi, *J. Org. Chem.* **2012**, *77*, 7718–7724.

[174] L. Ackermann, *Acc. Chem. Res.* **2020**, *53*, 84–104.

[175] For selected examples, see: a) X. Hou, N. Kaplaneris, B. Yuan, J. Frey, T. Ohyama, A. M. Messinis, L. Ackermann, *Chem. Sci.* **2022**, *13*, 3461–3467; b) Y. Qiu, C. Tian, L. Massignan, T. Rogge, L. Ackermann, *Angew. Chem. Int. Ed.* **2018**, *57*, 5818–5822; c) F. Xu, Y.-J. Li, C. Huang, H.-C. Xu, *ACS Catal.* **2018**, *8*, 3820–3824; d) R. Mei, J. Koeller, L. Ackermann, *Chem. Commun.* **2018**, *54*, 12879–12882.

[176] Y. Qiu, C. Zhu, M. Stangier, J. Struwe, L. Ackermann, *CCS Chem.* **2020**, *3*, 1529–1552.

[177] M. Stangier, A. M. Messinis, J. C. A. Oliveira, H. Yu, L. Ackermann, *Nat. Commun.* **2021**, *12*, 4736.

[178] Y. Qiu, J. Struwe, L. Ackermann, *Synlett* **2019**, *30*, 1164–1173.

[179] Y. Qiu, W.-J. Kong, J. Struwe, N. Sauermann, T. Rogge, A. Scheremetjew, L. Ackermann, *Angew. Chem. Int. Ed.* **2018**, *57*, 5828–5832.

[180] W.-J. Kong, L. H. Finger, J. C. A. Oliveira, L. Ackermann, *Angew. Chem. Int. Ed.* **2019**, *58*, 6342–6346.

[181] W.-J. Kong, Z. Shen, L. H. Finger, L. Ackermann, *Angew. Chem. Int. Ed.* **2020**, *59*, 5551–5556.

[182] W.-J. Kong, L. H. Finger, A. M. Messinis, R. Kuniyil, J. C. A. Oliveira, L. Ackermann, *J. Am. Chem. Soc.* **2019**, *141*, 17198–17206.

[183] Y.-K. Xing, X.-R. Chen, Q.-L. Yang, S.-Q. Zhang, H.-M. Guo, X. Hong, T.-S. Mei, *Nat. Commun.* **2021**, *12*, 930.

[184] Y. Wang, J. C. A. Oliveira, Z. Lin, L. Ackermann, *Angew. Chem. Int. Ed.* **2021**, *60*, 6419–6424.

[185] B. Sadowski, B. Yuan, Z. Lin, L. Ackermann, *Angew. Chem. Int. Ed.* **2022**, *61*, e202117188.

[186] a) G. Ciamician, *Science* **1912**, *36*, 385–394; b) G. Ciamician, P. Silber, *Ber. Dtsch. Chem. Ges.* **1900**, *33*, 2911–2913.

[187] Günther, O. Schenck, K. Ziegler, *Sci. Nat.* **1944**, *32*, 157–157.

[188] N. Holmberg-Douglas, D. A. Nicewicz, *Chem. Rev.* **2022**, *122*, 1925–2016.

[189] D. C. Fabry, M. Rueping, *Acc. Chem. Res.* **2016**, *49*, 1969–1979.

[190] M. Osawa, H. Nagai, M. Akita, *Dalton Trans.* **2007**, 827–829.

[191] D. Kalyani, K. B. McMurtrey, S. R. Neufeldt, M. S. Sanford, *J. Am. Chem. Soc.* **2011**, *133*, 18566–18569.

[192] H. Cano-Yelo, A. Deronzier, *J. Chem. Soc. Perkin Trans.* **1984**, 1093–1098.

[193] a) L. Huang, D. Hackenberger, L. J. Gooßen, *Angew. Chem. Int. Ed.* **2015**, *54*, 12607–12611; b) K. Shin, S.-W. Park, S. Chang, *J. Am. Chem. Soc.* **2015**, *137*, 8584–8592.

[194] A. Polley, K. Varalaxmi, R. Jana, *ACS Omega* **2018**, *3*, 14503–14516.

[195] L. Liang, M.-S. Xie, H.-X. Wang, H.-Y. Niu, G.-R. Qu, H.-M. Guo, *J. Org. Chem.* **2017**, *82*, 5966–5973.

[196] a) J. Jiang, W.-M. Zhang, J.-J. Dai, J. Xu, H.-J. Xu, *J. Org. Chem.* **2017**, *82*, 3622–3630; b) M. K. Sahoo, S. P. Midya, V. G. Landge, E. Balaraman, *Green Chem.* **2017**, *19*, 2111–2117.

[197] S. R. Neufeldt, M. S. Sanford, *Adv. Synth. Catal.* **2012**, *354*, 3517–3522.

[198] V. Gauchot, D. R. Sutherland, A. L. Lee, *Chem. Sci.* **2017**, *8*, 2885–2889.

[199] Y.-F. Liang, R. Steinbock, L. Yang, L. Ackermann, *Angew. Chem. Int. Ed.* **2018**, *57*, 10625–10629.

[200] F. Yang, J. Koeller, L. Ackermann, *Angew. Chem. Int. Ed.* **2016**, *55*, 4759–4762.

[201] a) S. Santoro, F. Ferlin, L. Ackermann, L. Vaccaro, *Chem. Soc. Rev.* **2019**, *48*, 2767–2782; b) D. Cambié, C. Bottecchia, N. J. W. Straathof, V. Hessel, T. Noël, *Chem. Rev.* **2016**, *116*, 10276–10341.

[202] a) U. K. Sharma, H. P. L. Gemoets, F. Schröder, T. Noël, E. V. Van der Eycken, *ACS Catal.* **2017**, *7*, 3818–3823; b) N. Xu, P. Li, Z. Xie, L. Wang, *Chem. Eur. J.* **2016**, *22*, 2236–2242; c) C. Zhou, P. Li, X. Zhu, L. Wang, *Org. Lett.* **2015**, *17*, 6198–6201.

[203] a) H. J. Kim, D. C. Fabry, S. Mader, M. Rueping, *Org. Chem. Front.* **2019**, *6*, 2319–2323; b) D. Kalsi, S. Dutta, N. Barsu, M. Rueping, B. Sundararaju, *ACS Catal.* **2018**, *8*, 8115–8120; c) K. Liu, M. Zou, A. Lei, *J. Org. Chem.* **2016**, *81*, 7088–7092; d) J. Zoller, D. C. Fabry, M. A. Ronge, M. Rueping, *Angew. Chem. Int. Ed.* **2014**, *53*, 13264–13268.

[204] a) S. K. Kariofillis, A. G. Doyle, *Acc. Chem. Res.* **2021**, *54*, 988–1000; b) Y.-Y. Gui, L. Sun, Z.-P. Lu, D.-G. Yu, *Org. Chem. Front.* **2016**, *3*, 522–526; c) J. C. Tellis, C. B. Kelly, D. N. Primer, M. Jouffroy, N. R. Patel, G. A. Molander, *Acc. Chem. Res.* **2016**, *49*, 1429–1439; d) J. C. Tellis, D. N. Primer, G. A. Molander, *Science* **2014**, *345*, 433–436; e) Z. Zuo, D. T. Ahneman, L. Chu, J. A. Terrett, A. G. Doyle, D. W. C. MacMillan, *Science* **2014**, *345*, 437–440.

[205] Y. Shen, Y. Gu, R. Martin, *J. Am. Chem. Soc.* **2018**, *140*, 12200–12209.

[206] C. Le, Y. Liang, R. W. Evans, X. Li, D. W. C. MacMillan, *Nature* **2017**, *547*, 79–83.

[207] X. Chen, Z. Tan, Q. Gui, L. Hu, J. Liu, J. Wu, G. Wang, *Chem. Eur. J.* **2016**, *22*, 6218–6222.

[208] J. Koeller, P. Gandeepan, L. Ackermann, *Synthesis* **2019**, *51*, 1284–1292.

[209] P. Gandeepan, J. Koeller, K. Korvorapun, J. Mohr, L. Ackermann, *Angew. Chem. Int. Ed.* **2019**, *58*, 9820–9825.

[210] A. Sagadevan, M. F. Greaney, *Angew. Chem. Int. Ed.* **2019**, *58*, 9826–9830.

[211] J. Thongpaen, R. Manguin, V. Dorcet, T. Vives, C. Duhayon, M. Mauduit, O. Baslé, *Angew. Chem. Int. Ed.* **2019**, *58*, 15244–15248.

[212] D. C. Fabry, M. A. Ronge, J. Zoller, M. Rueping, *Angew. Chem. Int. Ed.* **2015**, *54*, 2801–2805.

[213] D. C. Fabry, J. Zoller, S. Raja, M. Rueping, *Angew. Chem. Int. Ed.* **2014**, *53*, 10228–10231.

[214] J. Galczynski, H. Huang, T. H. Lambert, *Electrophotocatalysis* in *Science of Synthesis: Electrochemistry in Organic Synthesis* (Ed.: L. Ackermann), Thieme, Stuttgart, **2021**, p. 325–362.

[215] R. M. Wilson, T. H. Lambert, *Acc. Chem. Res.* **2022**, *55*, 3057–3069.

[216] J.-C. Moutet, G. Reverdy, *Tetrahedron Lett.* **1979**, *20*, 2389–2392.

[217] J.-C. Moutet, G. Reverdy, *J. Chem. Soc., Chem. Commun.* **1982**, 654–655.

[218] R. Scheffold, R. Orlinski, *J. Am. Chem. Soc.* **1983**, *105*, 7200–7202.

[219] H. Yan, Z.-W. Hou, H.-C. Xu, *Angew. Chem. Int. Ed.* **2019**, *58*, 4592–4595.

[220] H. Huang, Z. M. Strater, M. Rauch, J. Shee, T. J. Sisto, C. Nuckolls, T. H. Lambert, *Angew. Chem. Int. Ed.* **2019**, *58*, 13318–13322.

[221] F. Wang, S. S. Stahl, *Angew. Chem. Int. Ed.* **2019**, *58*, 6385–6390.

[222] C.-Y. Cai, X.-L. Lai, Y. Wang, H.-H. Hu, J. Song, Y. Yang, C. Wang, H.-C. Xu, *Nat. Catal.* **2022**.

[223] a) H. Huang, T. H. Lambert, *J. Am. Chem. Soc.* **2022**, *144*, 18803–18809; b) S. Wu, J. Žurauskas, M. Domański, P. S. Hitzfeld, V. Butera, D. J. Scott, J. Rehbein, A. Kumar, E. Thyrhaug, J. Hauer, J. P. Barham, *Org. Chem. Front.* **2021**, *8*, 1132–1142; c) T. Shen, T. H. Lambert, *J. Am. Chem. Soc.* **2021**, *143*, 8597–8602; d) T. Shen, T. H. Lambert, *Science* **2021**, *371*, 620–626; e) H. Huang, T. H. Lambert, *Angew. Chem. Int. Ed.* **2021**, *60*, 11163–11167; f) W. Zhang, K. L. Carpenter, S. Lin, *Angew. Chem. Int. Ed.* **2020**, *59*, 409–417; g) L. Zhang, L. Liardet, J. Luo, D. Ren, M. Grätzel, X. Hu, *Nat. Catal.* **2019**, *2*, 366–373.

[224] H. Huang, T. H. Lambert, *Angew. Chem. Int. Ed.* **2020**, *59*, 658–662.

[225] a) X. Tian, T. A. Karl, S. Reiter, S. Yakubov, R. de Vivie-Riedle, B. König, J. P. Barham, *Angew. Chem. Int. Ed.* **2021**, *60*, 20817–20825; b) Y.-J. Chen, T. Lei, H.-L. Hu, H.-L. Wu, S. Zhou, X.-B. Li, B. Chen, C.-H. Tung, L.-Z. Wu, *Matter* **2021**, *4*, 2354–2366; c) C. P. Chernowsky, A. F. Chmiel, Z. K. Wickens, *Angew. Chem. Int. Ed.* **2021**, *60*, 21418–21425; d) H. Kim, H. Kim, T. H. Lambert, S. Lin, *J. Am. Chem. Soc.* **2020**, *142*, 2087–2092; e) N. G. W. Cowper, C. P. Chernowsky, O. P. Williams, Z. K. Wickens, *J. Am. Chem. Soc.* **2020**, *142*, 2093–2099.

[226] X.-L. Lai, X.-M. Shu, J. Song, H.-C. Xu, *Angew. Chem. Int. Ed.* **2020**, *59*, 10626–10632.

[227] P. Xu, P.-Y. Chen, H.-C. Xu, *Angew. Chem. Int. Ed.* **2020**, *59*, 14275–14280.

[228] L. Capaldo, L. L. Quadri, D. Merli, D. Ravelli, *Chem. Commun.* **2021**, *57*, 4424–4427.

[229] H. Huang, Z. M. Strater, T. H. Lambert, *J. Am. Chem. Soc.* **2020**, *142*, 1698–1703.

[230] P. B. Arockiam, C. Bruneau, P. H. Dixneuf, *Chem. Rev.* **2012**, *112*, 5879–5918.

[231] T. Naota, H. Takaya, S.-I. Murahashi, *Chem. Rev.* **1998**, *98*, 2599–2660.

[232] K. Korvorapun, M. Moselage, J. Struwe, T. Rogge, A. M. Messinis, L. Ackermann, *Angew. Chem. Int. Ed.* **2020**, *59*, 18795–18803.

[233] a) N. A. McGrath, M. Brichacek, J. T. Njardarson, *J. Chem. Educ.* **2010**, *87*, 1348–1349; b) University of Arizona, Top 200 Pharmaceuticals by Retail Sails in 2021: https://www.pharmaexcipients.com/news/top-2200-drugs-2021-the-poster/ (accessed: 01.02.2023).

[234] J. Struwe, *Electrochemical C–H Functionalization*, Master Thesis, Georg-August Universität Göttingen **2018**.

[235] Y. Zhang, J. Struwe, L. Ackermann, *Angew. Chem. Int. Ed.* **2020**, *59*, 15076–15080.

[236] D. Aynetdinova, M. C. Callens, H. B. Hicks, C. Y. X. Poh, B. D. A. Shennan, A. M. Boyd, Z. H. Lim, J. A. Leitch, D. J. Dixon, *Chem. Soc. Rev.* **2021**, *50*, 5517–5563.

[237] a) J. A. Leitch, C. L. McMullin, A. J. Paterson, M. F. Mahon, Y. Bhonoah, C. G. Frost, *Angew. Chem. Int. Ed.* **2017**, *56*, 15131–15135; b) C. Yuan, L. Zhu, C. Chen, X. Chen, Y. Yang, Y. Lan, Y. Zhao, *Nat. Commun.* **2018**, *9*, 1189.

[238] G.-W. Wang, M. Wheatley, M. Simonetti, D. M. Cannas, I. Larrosa, *Chem* **2020**, *6*, 1459–1468.

[239] J. Hassan, M. Sévignon, C. Gozzi, E. Schulz, M. Lemaire, *Chem. Rev.* **2002**, *102*, 1359–1470.

[240] S. G. Ouellet, A. Roy, C. Molinaro, R. Angelaud, J.-F. Marcoux, P. D. O'Shea, I. W. Davies, *J. Org. Chem.* **2011**, *76*, 1436–1439.

[241] M. Seki, *ACS Catal.* **2014**, *4*, 4047–4050.

[242] a) A. Schischko, N. Kaplaneris, T. Rogge, G. Sirvinskaite, J. Son, L. Ackermann, *Nat. Commun.* **2019**, *10*, 3553; b) A. Schischko, H. Ren, N. Kaplaneris, L. Ackermann, *Angew. Chem. Int. Ed.* **2017**, *56*, 1576–1580.

[243] a) V. Gayakhe, Y. S. Sanghvi, I. J. S. Fairlamb, A. R. Kapdi, *Chem. Commun.* **2015**, *51*, 11944–11960; b) M. K. Lakshman, A. C. Deb, R. R. Chamala, P. Pradhan, R. Pratap, *Angew. Chem. Int. Ed.* **2011**, *50*, 11400–11404.

[244] For selected references, see: a) L.-N. Wang, P.-T. Tang, M. Li, J.-W. Li, Y.-J. Liu, M.-H. Zeng, *Adv. Synth. Catal.* **2021**, *363*, 2843–2849; b) A. M. Spiewak, D. J. Weix, *J. Org. Chem.* **2019**, *84*, 15642–15647; c) R. Boyaala, R. Touzani, T. Roisnel, V. Dorcet, E. Caytan, D. Jacquemin, J. Boixel, V. Guerchais, H. Doucet, J.-F. Soulé, *ACS Catal.* **2019**, *9*, 1320–1328; d) J.-W. Li, L.-N. Wang, M. Li, P.-T. Tang, X.-P. Luo, M. Kurmoo, Y.-J. Liu, M.-H. Zeng, *Org. Lett.* **2019**, *21*, 2885–2889; e) M. Drev, U. Grošelj, B. Ledinek, F. Perdih, J. Svete, B. Štefane, F. Požgan, *Org. Lett.* **2018**, *20*, 5268–5273; f) F. Hu, M. Szostak, *Org. Lett.* **2016**, *18*, 4186–4189; g) J. Hubrich, T. Himmler, L. Rodefeld, L. Ackermann, *ACS Catal.* **2015**, *5*, 4089–4093; h) B. Li, C. Darcel, P. H. Dixneuf, *ChemCatChem* **2014**, *6*, 127–130; i) L. Ackermann, E. Diers, A.

Manvar, *Org. Lett.* **2012**, *14*, 1154–1157; j) W. Li, P. B. Arockiam, C. Fischmeister, C. Bruneau, P. H. Dixneuf, *Green Chem.* **2011**, *13*, 2315–2319; k) L. Ackermann, A. V. Lygin, *Org. Lett.* **2011**, *13*, 3332–3335.

[245] a) T. Dalton, T. Faber, F. Glorius, *ACS Cent. Sci.* **2021**, *7*, 245–261; b) C.-S. Wang, P. H. Dixneuf, J.-F. Soulé, *Chem. Rev.* **2018**, *118*, 7532–7585.

[246] P. Natarajan, N. Kumar, M. Sharma, *Org. Chem. Front.* **2016**, *3*, 1265–1270.

[247] a) J. Ma, S. Chen, P. Bellotti, T. Wagener, C. Daniliuc, K. N. Houk, F. Glorius, *Nat. Catal.* **2022**, *5*, 405–413; b) X. Zhang, D. W. C. MacMillan, *J. Am. Chem. Soc.* **2017**, *139*, 11353–11356; c) D. R. Heitz, J. C. Tellis, G. A. Molander, *J. Am. Chem. Soc.* **2016**, *138*, 12715–12718.

[248] a) P. Bellotti, H.-M. Huang, T. Faber, R. Laskar, F. Glorius, *Chem. Sci.* **2022**, *13*, 7855–7862; b) T. J. Steiman, J. Liu, A. Mengiste, A. G. Doyle, *J. Am. Chem. Soc.* **2020**, *142*, 7598–7605.

[249] K. Korvorapun, J. Struwe, R. Kuniyil, A. Zangarelli, A. Casnati, M. Waeterschoot, L. Ackermann, *Angew. Chem. Int. Ed.* **2020**, *59*, 18103–18109.

[250] A. Sagadevan, A. Charitou, F. Wang, M. Ivanova, M. Vuagnat, M. F. Greaney, *Chem. Sci.* **2020**, *11*, 4439–4443.

[251] a) L. Ackermann, H. K. Potukuchi, *Org. Biomol. Chem.* **2010**, *8*, 4503–4513; b) M. Meldal, C. W. Tornøe, *Chem. Rev.* **2008**, *108*, 2952–3015; c) H. C. Kolb, M. G. Finn, K. B. Sharpless, *Angew. Chem. Int. Ed.* **2001**, *40*, 2004–2021; d) R. Huisgen, *Angew. Chem. Int. Ed.* **1963**, *2*, 565–598.

[252] T. Mandal, J. Struwe, M. Gieuw, L. Ackermann, *unpublished results.*

[253] For selected referecnes, see: a) R. A. Forsch, S. F. Queener, A. Rosowsky, *Bioorganic Med. Chem. Lett.* **2004**, *14*, 1811–1815; b) Y.-Q. Long, X.-H. Jiang, R. Dayam, T. Sanchez, R. Shoemaker, S. Sei, N. Neamati, *J. Med. Chem.* **2004**, *47*, 2561–2573; c) S. Borngraeber, M.-J. Budny, G. Chiellini, S. T. Cunha-Lima, M. Togashi, P. Webb, J. D. Baxter, T. S. Scanlan, R. J. Fletterick, *Proc. Natl. Acad. Sci.* **2003**, *100*, 15358–15363; d) C. Rose, O. Vtoraya, A. Pluzanska, N. Davidson, M. Gershanovich, R. Thomas, S. Johnson, J. J. Caicedo, H. Gervasio, G. Manikhas, F. Ben Ayed, S. Burdette-Radoux, H. A. Chaudri-Ross, R. Lang, *Eur. J. Cancer* **2003**, *39*, 2318–2327; e) H. Juteau, Y. Gareau, M. Labelle, C. F. Sturino, N. Sawyer, N. Tremblay, S. Lamontagne, M.-C. Carrière, D. Denis, K. M. Metters, *Bioorg. Med. Chem.* **2001**, *9*, 1977–1984; f) M. Graffner-Nordberg, K. Kolmodin, J. Åqvist, S. F. Queener, A. Hallberg, *J. Med. Chem.* **2001**, *44*, 2391–2402; g) K. L. McPhail, D. E. A. Rivett, D. E. Lack, M. T. Davies-Coleman, *Tetrahedron* **2000**, *56*, 9391–9396.

[254] For selected examples, see: a) M. Bandini, M. Tragni, *Org. Biomol. Chem.* **2009**, *7*, 1501–1507; b) A. Prades, R. Corberán, M. Poyatos, E. Peris, *Chem. Eur. J.* **2009**, *15*, 4610–4613; c) D. Stadler, T. Bach, *Angew. Chem. Int. Ed.* **2008**, *47*, 7557–7559; d) M. Rueping, B. J. Nachtsheim, W. Ieawsuwan, *Adv. Synth. Catal.* **2006**, *348*, 1033–1037; e) I. Iovel, K. Mertins, J. Kischel, A. Zapf, M. Beller, *Angew. Chem. Int. Ed.* **2005**, *44*, 3913–3917; f) T. Kondo, S. Kajiya, S. Tantayanon, Y. Watanabe, *J. Organomet. Chem.* **1995**, *489*, 83–91; g) T. Kondo, S. Tantayanon, Y. Tsuji, Y. Watanabe, *Tetrahedron Lett.* **1989**, *30*, 4137–4140.

[255] a) S. Afewerki, C. Palo-Nieto, A. Córdova, *Synthesis* **2020**, *52*, 2330–2336; b) H. Fang, M. Oestreich, *Angew. Chem. Int. Ed.* **2020**, *59*, 11394–11398; c) J. Li, Q. Liu, H. Shen, R. Huang, X. Zhang, Y. Xiong, C. Chen, *RSC Adv.* **2015**, *5*, 85291–85295; d) J.

Barluenga, M. Tomás-Gamasa, F. Aznar, C. Valdés, *Nat. Chem.* **2009**, *1*, 494–499; e) N. L'Hermite, A. Giraud, O. Provot, J.-F. Peyrat, M. Alami, J.-D. Brion, *Tetrahedron* **2006**, *62*, 11994–12002.

[256] For selected referecnes, see: a) J. Luo, B. Hu, W. Wu, M. Hu, T. L. Liu, *Angew. Chem. Int. Ed.* **2021**, *60*, 6107–6116; b) C. Zhao, G.-F. Zha, W.-Y. Fang, K. P. Rakesh, H.-L. Qin, *Eur. J. Org. Chem.* **2019**, 1801–1807; c) M. Nambo, E. C. Keske, J. P. G. Rygus, J. C. H. Yim, C. M. Crudden, *ACS Catal.* **2017**, *7*, 1108–1112; d) Y. Aihara, J. Wuelbern, N. Chatani, *Bull. Chem. Soc. Jpn.* **2015**, *88*, 438–446; e) P. Zhang, J. Xu, Y. Gao, X. Li, G. Tang, Y. Zhao, *Synlett* **2014**, *25*, 2928–2932; f) X. Wang, L.-H. Liu, J.-H. Shi, J. Peng, H.-Y. Tu, A.-D. Zhang, *Eur. J. Org. Chem.* **2013**, 6870–6877; g) R. B. Bedford, M. Huwe, M. C. Wilkinson, *Chem. Commun.* **2009**, 600–602; h) Y.-H. Chen, M. Sun, P. Knochel, *Angew. Chem. Int. Ed.* **2009**, *48*, 2236–2239; i) B. Liégault, J.-L. Renaud, C. Bruneau, *Chem. Soc. Rev.* **2008**, *37*, 290–299; j) M. J. Burns, I. J. S. Fairlamb, A. R. Kapdi, P. Sehnal, R. J. K. Taylor, *Org. Lett.* **2007**, *9*, 5397–5400; k) F. O. Arp, G. C. Fu, *J. Am. Chem. Soc.* **2005**, *127*, 10482–10483.

[257] I. Choi, V. Müller, Y. Wang, K. Xue, R. Kuniyil, L. B. Andreas, V. Karius, J. G. Alauzun, L. Ackermann, *Chem. Eur. J.* **2020**, *26*, 15290–15297.

[258] J. Struwe, K. Korvorapun, A. Zangarelli, L. Ackermann, *Chem. Eur. J.* **2021**, *27*, 16237–16241.

[259] A. Abula, Z. Xu, Z. Zhu, C. Peng, Z. Chen, W. Zhu, H. A. Aisa, *J. Chem. Inf. Model.* **2020**, *60*, 6242–6250.

[260] M. Inoue, Y. Sumii, N. Shibata, *ACS Omega* **2020**, *5*, 10633–10640.

[261] a) T. De Oliveira, T. Goldhardt, M. Edelmann, T. Rogge, K. Rauch, N. D. Kyuchukov, K. Menck, A. Bleckmann, J. Kalucka, S. Khan, J. Gaedcke, M. Haubrock, T. Beissbarth, H. Bohnenberger, M. Planque, S.-M. Fendt, L. Ackermann, M. Ghadimi, L.-C. Conradi, *Cancers* **2021**, *13*, 1011–1033; b) N. M. S. Gustafsson, K. Färnegårdh, N. Bonagas, A. H. Ninou, P. Groth, E. Wiita, M. Jönsson, K. Hallberg, J. Lehto, R. Pennisi, J. Martinsson, C. Norström, J. Hollers, J. Schultz, M. Andersson, N. Markova, P. Marttila, B. Kim, M. Norin, T. Olin, T. Helleday, *Nat. Commun.* **2018**, *9*, 3872.

[262] J. L. Lau, M. K. Dunn, *Bioorg. Med. Chem.* **2018**, *26*, 2700–2707.

[263] K. Fosgerau, T. Hoffmann, *Drug Discov. Today.* **2015**, *20*, 122–128.

[264] L. Wang, N. Wang, W. Zhang, X. Cheng, Z. Yan, G. Shao, X. Wang, R. Wang, C. Fu, *Signal Transduct. Target. Ther.* **2022**, *7*, 48.

[265] a) A. F. B. Räder, M. Weinmüller, F. Reichart, A. Schumacher-Klinger, S. Merzbach, C. Gilon, A. Hoffman, H. Kessler, *Angew. Chem. Int. Ed.* **2018**, *57*, 14414–14438; b) M. A. T. Blaskovich, *J. Med. Chem.* **2016**, *59*, 10807–10836.

[266] a) K. Kubota, P. Dai, B. L. Pentelute, S. L. Buchwald, *J. Am. Chem. Soc.* **2018**, *140*, 3128–3133; b) E. V. Vinogradova, C. Zhang, A. M. Spokoyny, B. L. Pentelute, S. L. Buchwald, *Nature* **2015**, *526*, 687–691.

[267] a) C. Bottecchia, T. Noël, *Chem. Eur. J.* **2019**, *25*, 26–42; b) W. Wang, M. M. Lorion, J. Shah, A. R. Kapdi, L. Ackermann, *Angew. Chem. Int. Ed.* **2018**, *57*, 14700–14717; c) X. Lu, S.-J. He, W.-M. Cheng, J. Shi, *Chin. Chem. Lett.* **2018**, *29*, 1001–1008.

[268] W. Wang, J. Wu, R. Kuniyil, A. Kopp, R. N. Lima, L. Ackermann, *Chem* **2020**, *6*, 3428–3439.

[269] a) J. Wu, N. Kaplaneris, S. Ni, F. Kaltenhäuser, L. Ackermann, *Chem. Sci.* **2020**, *11*, 6521–6526; b) W. Wang, M. M. Lorion, O. Martinazzoli, L. Ackermann, *Angew. Chem. Int. Ed.* **2018**, *57*, 10554–10558; c) M. Bauer, W. Wang, M. M. Lorion, C. Dong, L. Ackermann, *Angew. Chem. Int. Ed.* **2018**, *57*, 203–207; d) Y. Zhu, M. Bauer, L. Ackermann, *Chem. Eur. J.* **2015**, *21*, 9980–9983.

[270] a) M. M. Lorion, N. Kaplaneris, J. Son, R. Kuniyil, L. Ackermann, *Angew. Chem. Int. Ed.* **2019**, *58*, 1684–1688; b) N. Kaplaneris, T. Rogge, R. Yin, H. Wang, G. Sirvinskaite, L. Ackermann, *Angew. Chem. Int. Ed.* **2019**, *58*, 3476–3480.

[271] A. Khoshnood, B. Lukanov, A. Firoozabadi, *Langmuir* **2016**, *32*, 2175–2183.

[272] V. P. W. Böhm, T. Weskamp, C. W. K. Gstöttmayr, W. A. Herrmann, *Angew. Chem. Int. Ed.* **2000**, *39*, 1602–1604.

[273] a) H. Wang, X. Sun, S. Zhang, G. Liu, C. Wang, L. Zhu, H. Zhang, *Synlett* **2018**, *29*, 2689–2692; b) A. Correa, C. Bolm, *Adv. Synth. Catal.* **2007**, *349*, 2673–2676.

[274] M. Periasamy, G. Srinivas, P. Bharathi, *J. Org. Chem.* **1999**, *64*, 4204–4205.

[275] B. Jiang, M. Zhao, S.-S. Li, Y.-H. Xu, T.-P. Loh, *Angew. Chem. Int. Ed.* **2018**, *57*, 555–559.

[276] a) X. Jiang, M.-M. Zhang, W. Xiong, L.-Q. Lu, W.-J. Xiao, *Angew. Chem. Int. Ed.* **2019**, *58*, 2402–2406; b) C. Pan, Y. Chen, S. Song, L. Li, J.-T. Yu, *J. Org. Chem.* **2016**, *81*, 12065–12069.

[277] T. Rogge, L. Ackermann, *Angew. Chem. Int. Ed.* **2019**, *58*, 15640–15645.

[278] Q. Wu, C. Du, Y. Huang, X. Liu, Z. Long, F. Song, J. You, *Chem. Sci.* **2015**, *6*, 288–293.

[279] I. Suzuki, H. Kondo, T. Kochi, F. Kakiuchi, *J. Org. Chem.* **2019**, *84*, 12975–12982.

[280] D. Zell, S. Warratz, D. Gelman, S. J. Garden, L. Ackermann, *Chem. Eur. J.* **2016**, *22*, 1248–1252.

[281] W. Song, L. Ackermann, *Angew. Chem. Int. Ed.* **2012**, *51*, 8251–8254.

[282] a) A. Sagadevan, V. P. Charpe, A. Ragupathi, K. C. Hwang, *J. Am. Chem. Soc.* **2017**, *139*, 2896–2899; b) M. A. Cismesia, T. P. Yoon, *Chem. Sci.* **2015**, *6*, 5426–5434.

[283] L. Li, X. Mu, W. Liu, Y. Wang, Z. Mi, C.-J. Li, *J. Am. Chem. Soc.* **2016**, *138*, 5809–5812.

[284] X. Lu, R. Kawazu, J. Song, Y. Yoshigoe, T. Torigoe, Y. Kuninobu, *Org. Lett.* **2021**, *23*, 4327–4331.

7 APPENDIX

NACHHALTIGE METHODEN IN DER C–H FUNKTIONALISIERUNG

ZUSAMMENFASSUNG

Kreuzkupplungsreaktionen haben sich als attraktive Möglichkeiten der Knüpfung von C–C und C–Het Bindungen etablieren können. Dennoch sind sie mit einigen Nachteilen verbunden, allen voran mit Hinblick auf die Nachhaltigkeit, die durch die Notwendigkeit einer Präfunktionalisierung der Edukte stark beeinträchtigt wird. Im Gegensatz dazu bieten die entwickelten Methoden der übergangsmetallkatalysierten direkten Funktionalisierung allgegenwärtiger C–H Bindungen eine nachhaltigere Alternative für den Aufbau komplexer molekularer Strukturen. Auch wenn dieser Ansatz durch eine verbesserte Atom- und Stufenökonomie einen wichtigen Beitrag zur Grünen Chemie und umweltbewussten Synthese leistet, sind typischerweise harsche Reaktionsbedingungen und hohe Temperaturen für die Umsetzungen erforderlich, was die angestrebte breite Anwendbarkeit einschränkt.

In Rahmen unseres Forschungsprogramms zur nachhaltigen Katalyse konzentrieren wir uns darauf, milde und nachhaltige Strategien zu entwickeln, was auch der Kern dieser Doktorarbeit ist. Als wichtige Strategien, um den Umwelteinfluss der Reaktion zu verringern, sollten hier besonders die Verwendung von kostengünstigen 3d-Metallen als Katalysatoren oder das Durchführen der Reaktion in grünen Lösungsmitteln erwähnt werden. Das in großen Mengen der Erdkruste vorkommende Mangan ist besonders attraktiv als Katalysator aufgrund der geringen Toxizität, sodass es für die Funktionalisierung von Tryptophanderivaten untersucht wurde. Zentraler Aspekt war dabei der Einsatz von Wasser und micellarer Katalyse, um die Reaktion unter umweltfreundlichen Bedingungen zu ermöglichen. Andere Projekte zielten auf neuartige Methoden und ein nachhaltiges Reaktionsdesign ab. Neben dem bedeutungsvollen Einsatz von Elektrokatalyse anstelle von toxischen Metalloxidantien, wurde vor allem auch die Verwendung von Licht als elegante Möglichkeit für milde Reaktionsbedingungen untersucht. In Kombination mit Übergangsmetallkatalyse durch Ruthenium konnte der positive Effekt des Lichts hervorgehoben werden, der die Synthese kleiner Moleküle mit potentieller Anwendbarkeit als Wirkstoffe im medizinischen Bereich bei außergewöhnlich milden Bedingungen bei Raumtemperatur ermöglichte, wobei die Chemoselektivität durch das Vermeiden von Nebenprodukten verbessert werden konnte. Gleichermaßen ist das recht neue Feld der elektrophotokatalysierten Funktionalisierung bedeutsam, in welchem interessante Erkenntnisse bezüglich des Katalysators gewonnen werden konnten.

SUSTAINABLE METHODS IN C–H FUNCTIONALIZATION

SUMMARY

Cross-coupling chemistry has matured in an attractive tool in synthetic organic chemistry to realized efficient formation of C–C and C–Het bonds. However, these transformations are also associated with certain drawbacks, especially with respect to the sustainability of the reactions, which is significantly reduced by the requirement of the prefunctionalization of the substrates. Contrary to this, the developed methods in the transition metal-catalyzed direct functionalization of omnipresent C–H bonds presents a sustainable alternative for the construction of complex molecular scaffolds. Although the use of the direct C–H functionalization approach is an important contribution towards Green Chemistry and environmentally-benign synthesis due to an improved atom- and step-economy, it is associated with certain limitations. These transformations typically require harsh reaction conditions with high temperatures, thus restricting an intendent broad applicability.

Within our program on sustainable catalysis, the research is focused on the development of mild and sustainable strategies, which is also the central aspect of this thesis. Important strategies allowing for improved environmental aspects consist in the use of cost-efficient earth-abundant transition metal catalysts or the selection of green solvents to promote transformations. Especially, the employment of abundant manganese as catalyst is of great interest due to its low toxicity, for this reason, it was used for the functionalization of tryptophan derivatives. Here, the use of water and micellar catalysis was investigated to achieve mild and environmentally responsible conditions. Other projects were focused on new technologies and a sustainable reaction design. Besides the important application of electrocatalysis instead of the use of toxic metal salts as chemical oxidants, the irradiation with visible light was recognized as an elegant strategy to achieve mild reaction conditions. The beneficial effect of the blue LED light was further substantiated for ruthenium-catalyzed C–H activation chemistry, as the synthesis of small molecules with a potential applicability as pharmaceutically active compounds was achieved at room temperature with an improved chemoselectivity and the avoidance of byproducts. Moreover, the new field of electrophotocatalysis is of great importance, where interesting findings were made with respect to different employed (photo)redox mediators.

ACKNOWLEDGEMENTS

Zuallererst möchte ich mich ganz herzlich bei meinem Doktorvater Prof. L. Ackermann für die Möglichkeit bedanken, meine Promotion in seinem Team unter wirklich exzellenten Bedingungen durchführen zu können. Nicht nur die Ausstattung und das internationale Arbeitsumfeld haben das Arbeiten hier zu etwas ganz Besonderem gemacht, sondern vor allem stets freundliche Betreuung, die wertvollen Ratschläge, und das entgegengebrauchte Vertrauen in verschiedenen Kooperationen mitwirken zu dürfen.

I am grateful to Prof. Dr. K. Koszinowski and Dr. S. Das for accepting to be my second supervisor or third supervisor, respectively, and for all the helpful discussions we had. Moreover, I want to acknowledge Prof. Dr. Dr. h.c. L. F. Tietze, Jun.-Prof. Dr. J. Walker, PD Dr. M. John and Dr. H. Frauendorf for agreeing to take part of the examination board.

Für die finanzielle Unterstützung der Universität Göttingen, aber vor allem auch des DZHK (Deutsches Zentrum für Herz- und Kreislaufforschung) möchte ich mich ganz herzlich bedanken.

Likewise, the financial support of Novartis during my research stay in Basel is warmly acknowledged. In this context, I would like to thank the whole Department of Chemical and Analytical Development for an exciting experience, and the possibility to learn so much. My thankfulness is especially offered to Dr. F. Gallou for initializing this and his kind supervision during my time in Basel, as well as my lab colleague Adnan for his patience in getting me used to the lab and the campus and for the great working atmosphere.

Auch bei den analytischen Abteilungen des Instituts, der NMR-Abteilung unter Leitung von Dr. M. John sowie der massenspektrometrischen Abteilung unter Leitung von Dr. H. Frauendorf, möchte ich mich ganz herzlich für das zuverlässige und schnelle Messen von Proben und ihre Unterstützung bedanken.

Mein Dank gebührt außerdem den verschiedenen Werkstätten der chemischen Institute der Universität Göttingen, die mit ihrer zuverlässigen Umsetzung von Ideen und Aufträgen immer eine große Hilfe waren.

Gabi, Bianca und Sabine möchte ich ganz herzlich für die Unterstützung bei allen bürokratischen Anliegen danken. Auch bei Svenja möchte ich mich gern bedanken, die sowohl in organisatorischen als auch wissenschaftlichen Fragen immer eine große Hilfe war und immer ein offenes Ohr hatte. Stefan danke ich sehr für seine umfassende Unterstützung bei Problemen

aller Art, und die gründliche Betreuung der Geräte, ohne die das wissenschaftliche Arbeiten nur schwer möglich wäre. Auch Karsten gilt mein Dank für die Bereitstellung verschiedener Katalysatoren und Verbindungen, trockner Lösungsmittel, sowie des Laborequipments.

In addition, I would like to sincerely thank all the colleagues which whom I had the opportunity to collaborate. Many thanks to Youai, Benz, Rositha, Torben, Marc, Ramesh, Kun, Agnese Cong and Isaac among many others for the inspiring and successful collaboration in many different projects during my PhD.

Furthermore, I would like to thank Joao, Lina, Takuya, Matthew, Sven, Tristan, Tsuyoshi, Agnese, Hendrik, Simon, Philipp, Xioayan and Lin for their careful proofreading. Thank you for your time and conscientious support.

I particularly thank all current and former members of the Ackermann group for the nice working atmosphere and memorable activities, such as the trip to Cuxhaven, many BBQs and PhD parties. Among all my lab mates during the PhD, I want to thank especially Max, Sven and Tristan for all the advices, but also all the fun, the chats and the friendship. I really enjoyed working and spending all the day with you. Besides them, I would like to thank also a few other colleagues with those I have spend a lot time and who made my PhD time likewise very precious: Lina, Torben, Benz, Julia, Joao and Valentin.

Desweiteren möchte ich mich bei meinen Studenten Anna Casnati, Adelina Kopp, Hanke Spinck, Moritz von Geyso und Sven Trienes für die motivierte Mitarbeit und ihre Unterstützung bei verschiedenen Projekten bedanken.

Abschließend möchte ich meiner Familie noch den größten Dank aussprechen, die mir nicht nur das Studium ermöglicht hat sondern mich auch in jedem meiner Schritte bedingungslos unterstützt hat. Auch meinen Freunden aus Schul- und Studienzeiten möchte ich für den uneingeschränkten Rückhalt danken, dafür, dass sie immer aufmunternde Worte hatten und mir viel Kraft auch in stressigen Phasen gegeben haben.

NMR SPECTRA

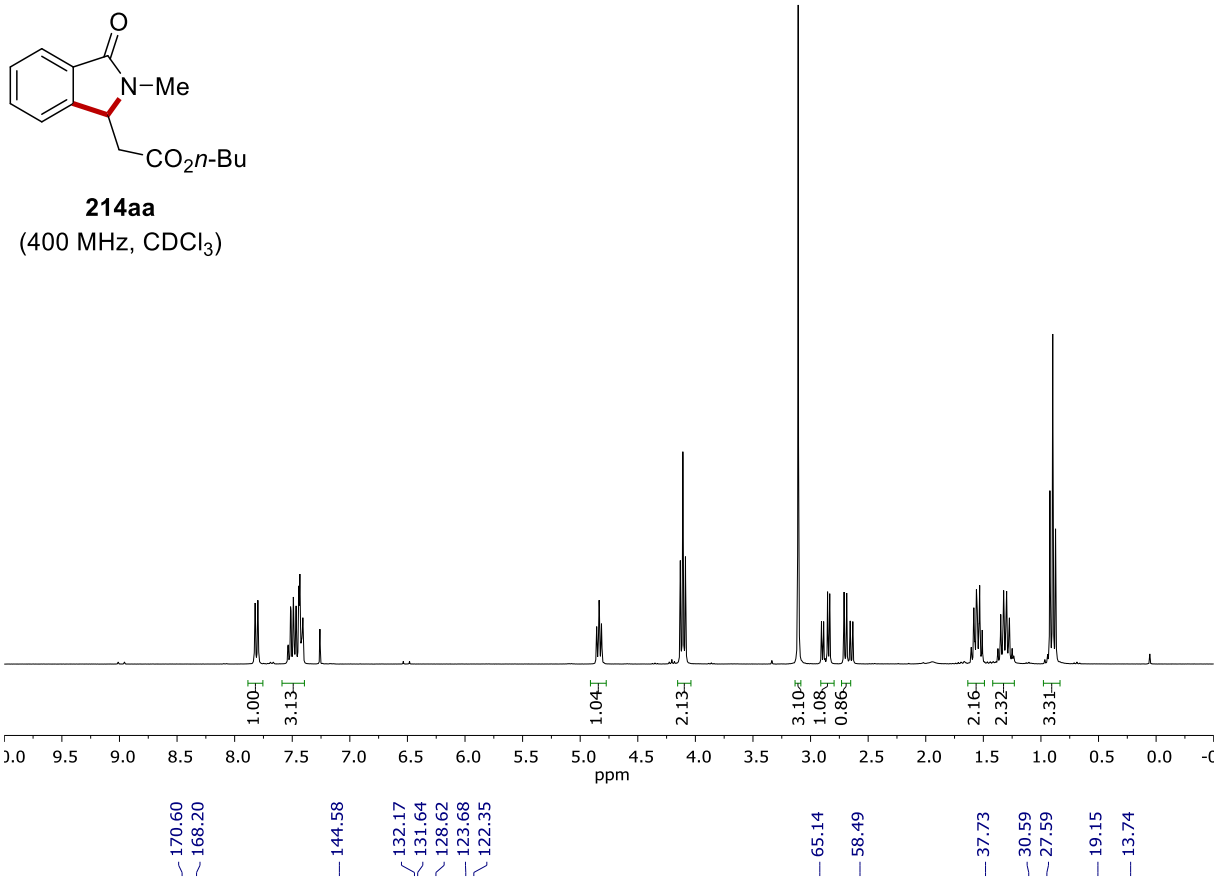
O
N−Me
CO2n-Bu
214aa
(400 MHz, CDCl3)
1.00
3.13
1.04
2.13
3.10
1.08
0.86
2.16
2.32
3.31
ppm
170.60
168.20
144.58
132.17
131.64
128.62
123.68
122.35
65.14
58.49
37.73
30.59
27.59
19.15
13.74

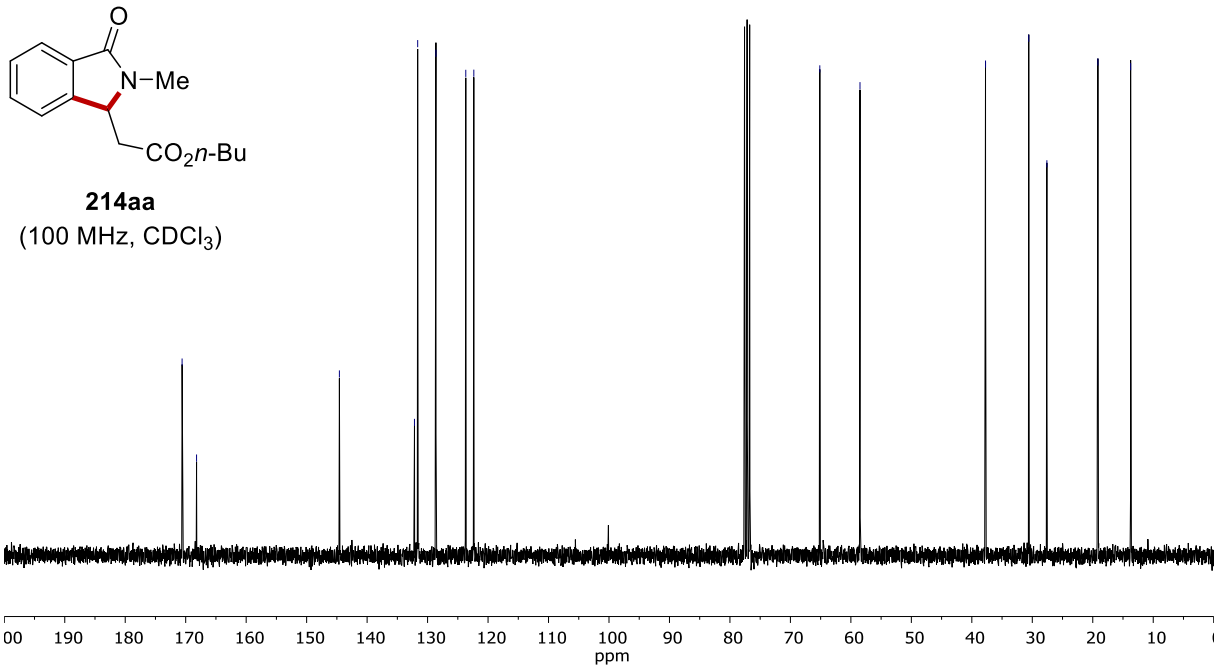
O
N−Me
CO2n-Bu
214aa
(100 MHz, CDCl3)
ppm

215aa
(400 MHz, $CDCl_3$)

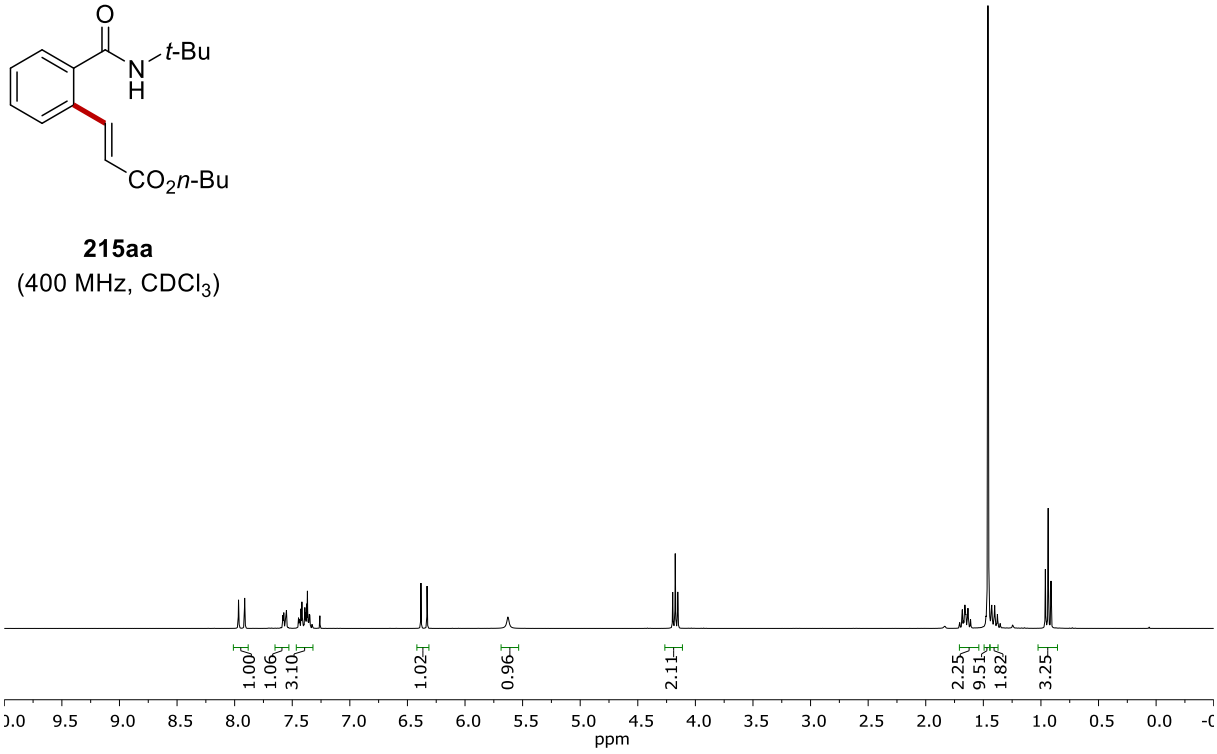

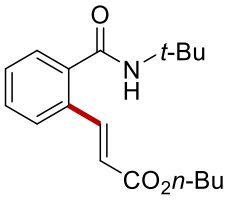

215aa
(100 MHz, $CDCl_3$)

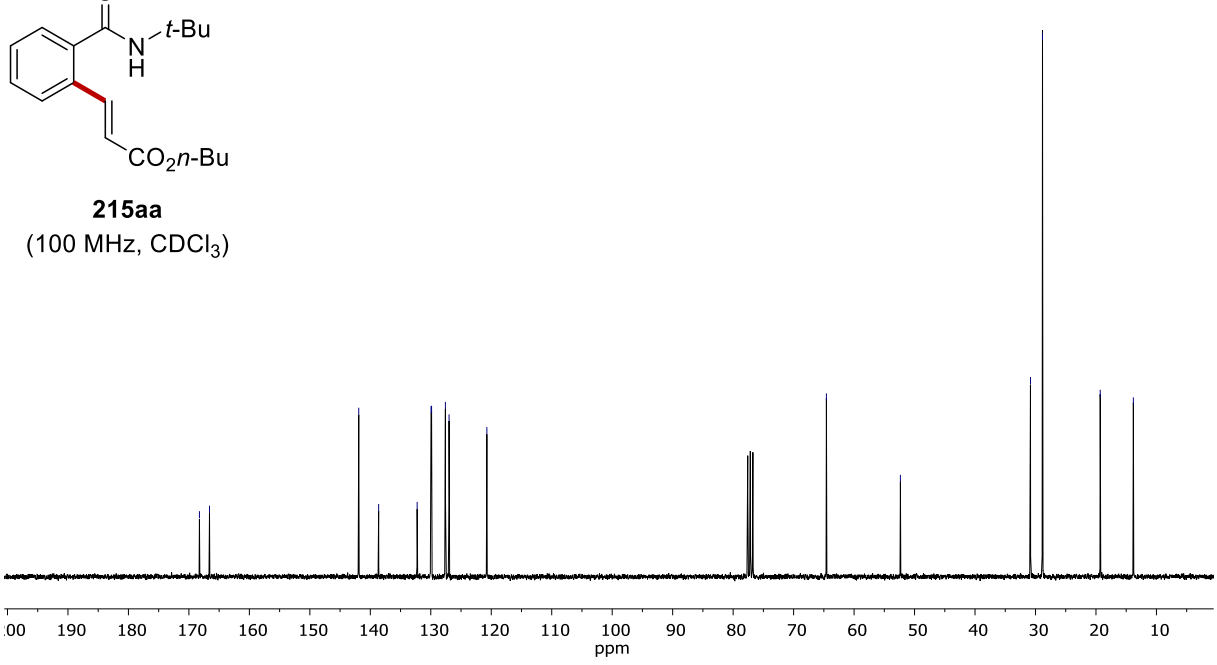

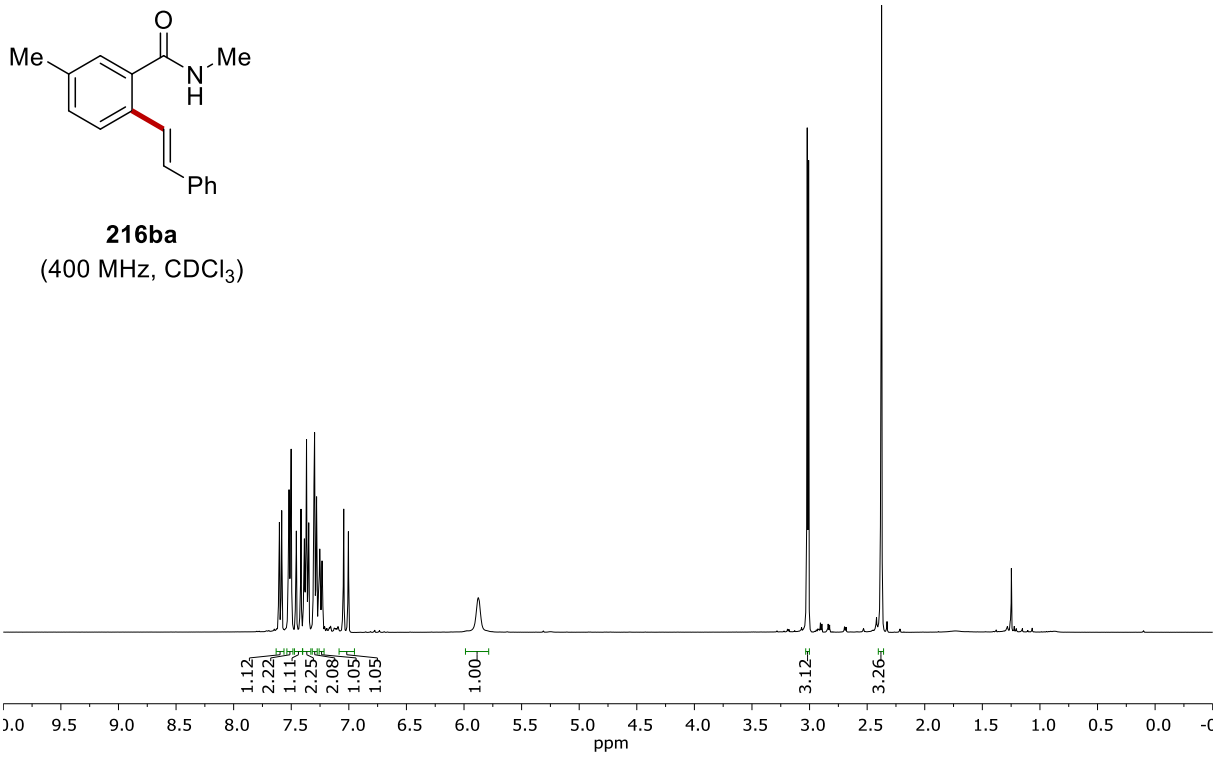

216ba
(400 MHz, $CDCl_3$)

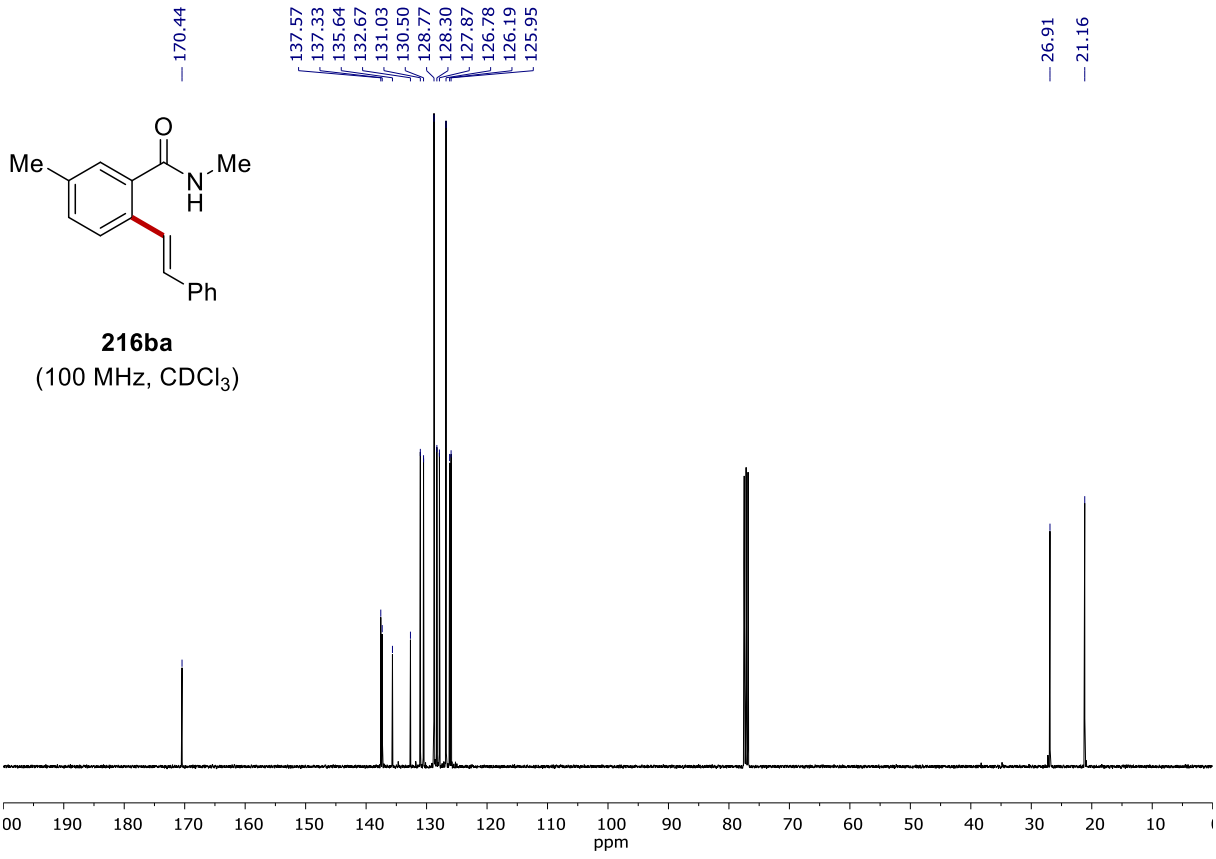

216ba
(100 MHz, $CDCl_3$)

219aa
(300 MHz, $CDCl_3$)

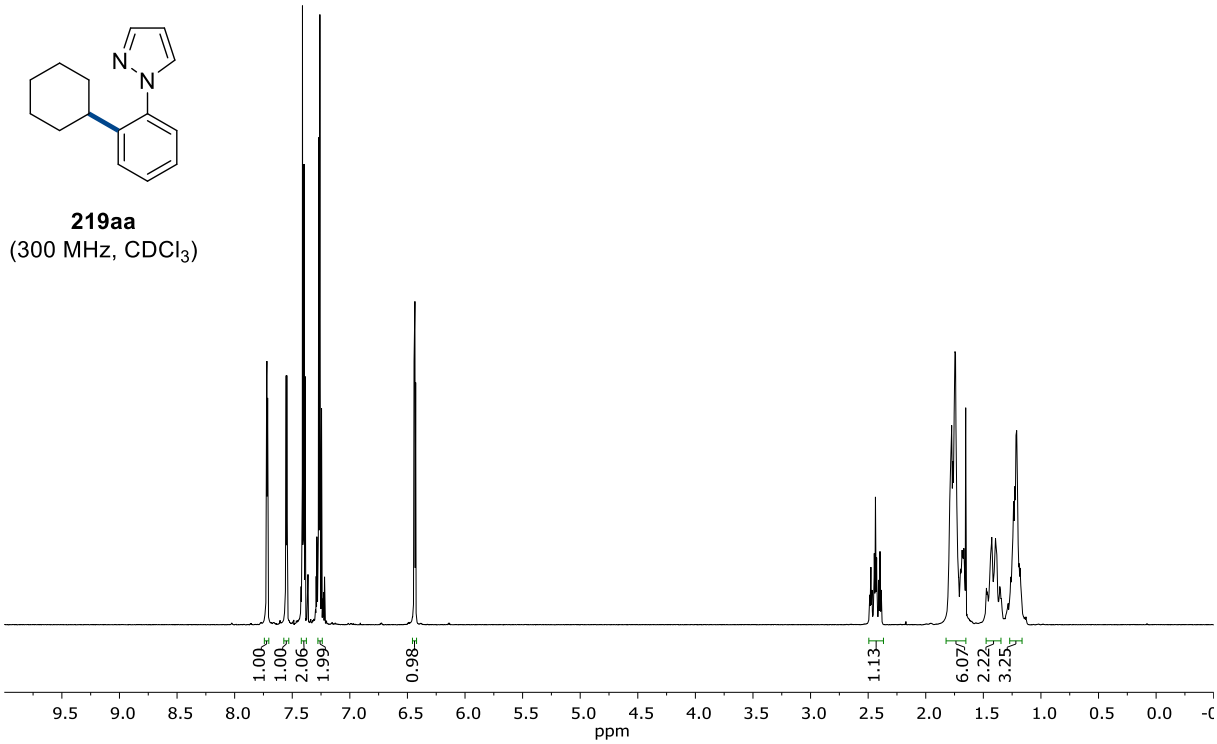

219aa
(100 MHz, $CDCl_3$)

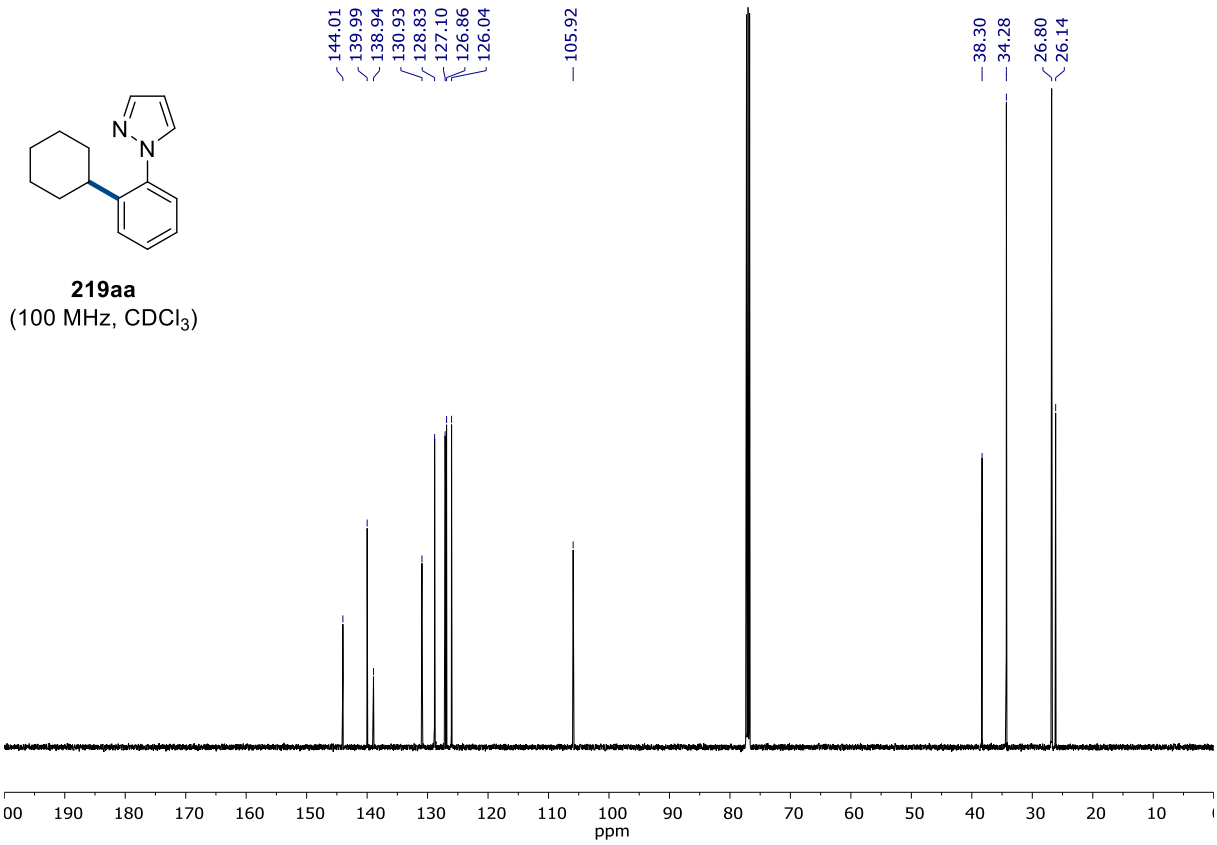

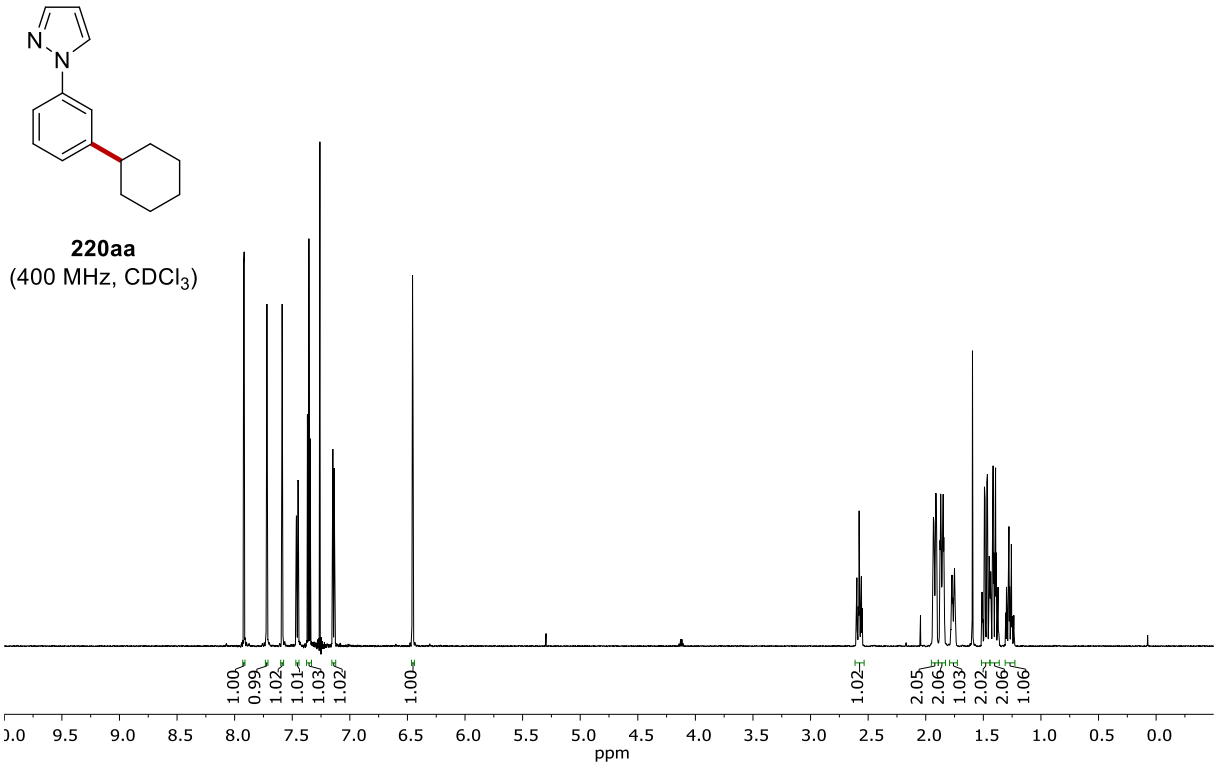
220aa
(400 MHz, CDCl3)
1.00
0.99
1.02
1.01
1.03
1.02
1.00
1.02
2.05
2.06
1.03
2.02
2.06
1.06
ppm

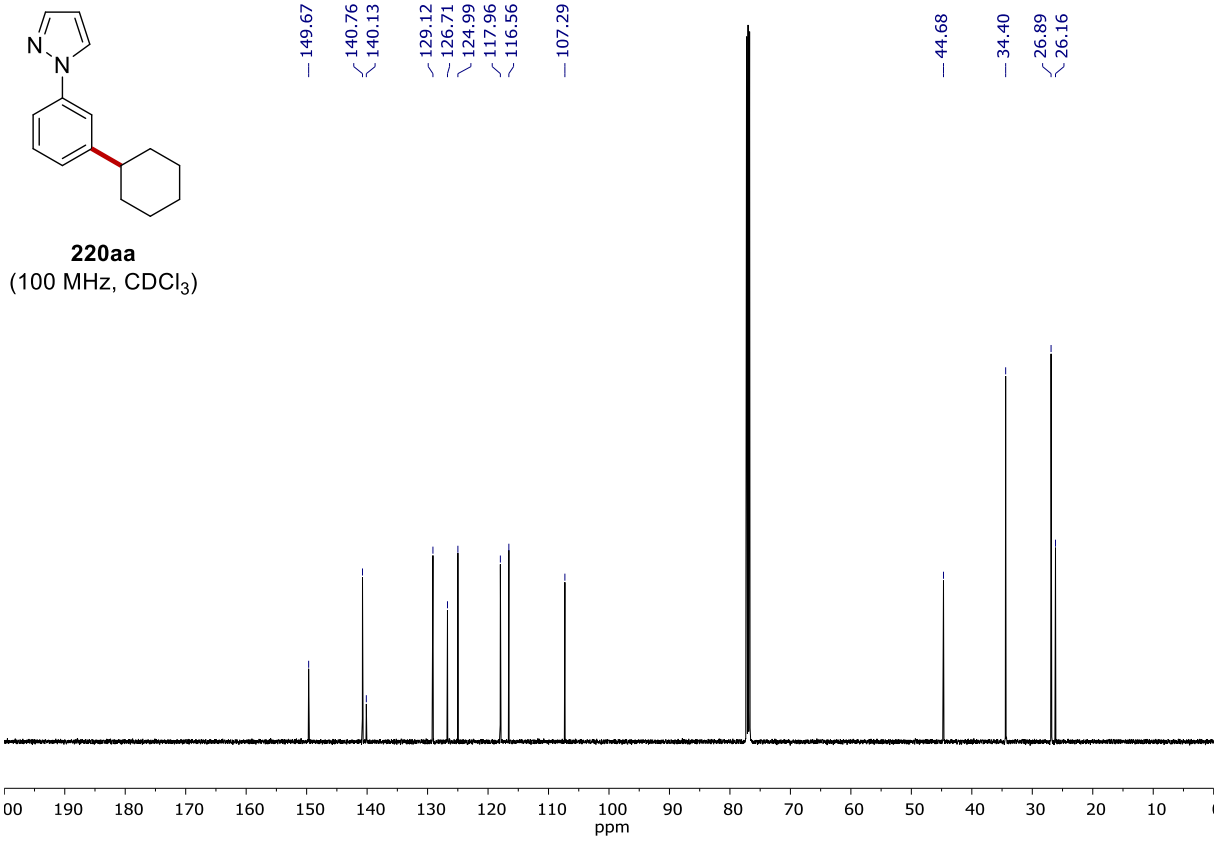
220aa
(100 MHz, CDCl3)
149.67
140.76
140.13
129.12
126.71
124.99
117.96
116.56
107.29
44.68
34.40
26.89
26.16
ppm

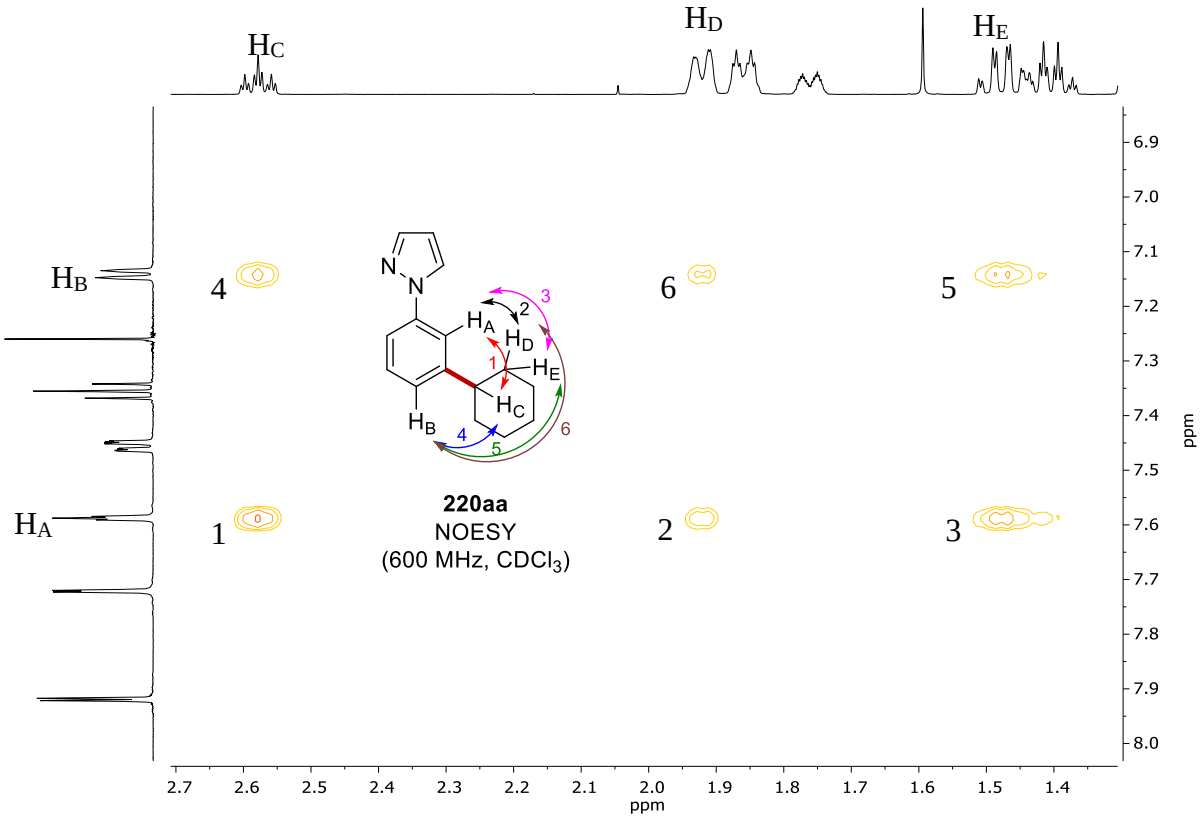
HC
HD
HE
HB
HA
4
6
5
1
2
3
220aa
NOESY
(600 MHz, CDCl3)
ppm

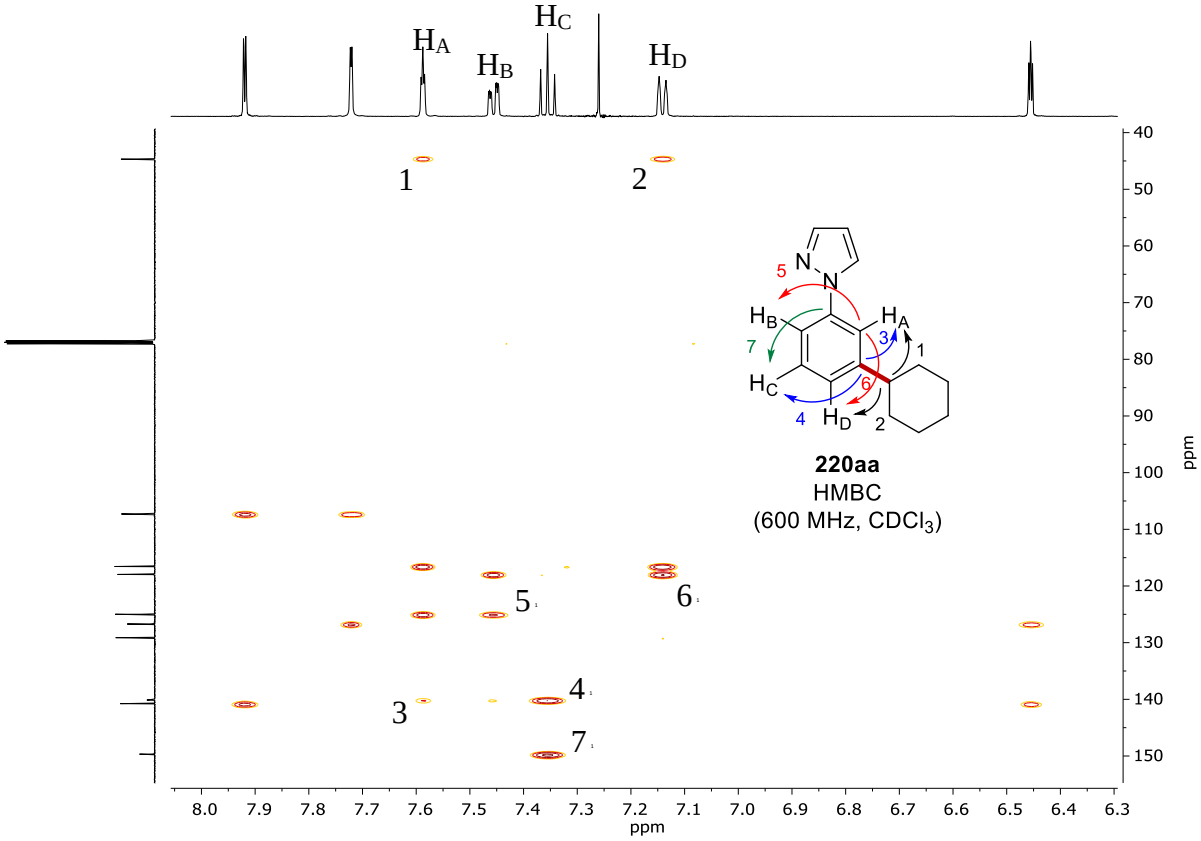
HA
HB
HC
HD
1
2
5
6
3
4
7
220aa
HMBC
(600 MHz, CDCl3)
ppm

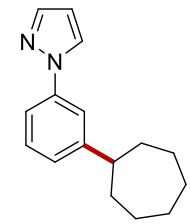

220ad
(400 MHz, $CDCl_3$)

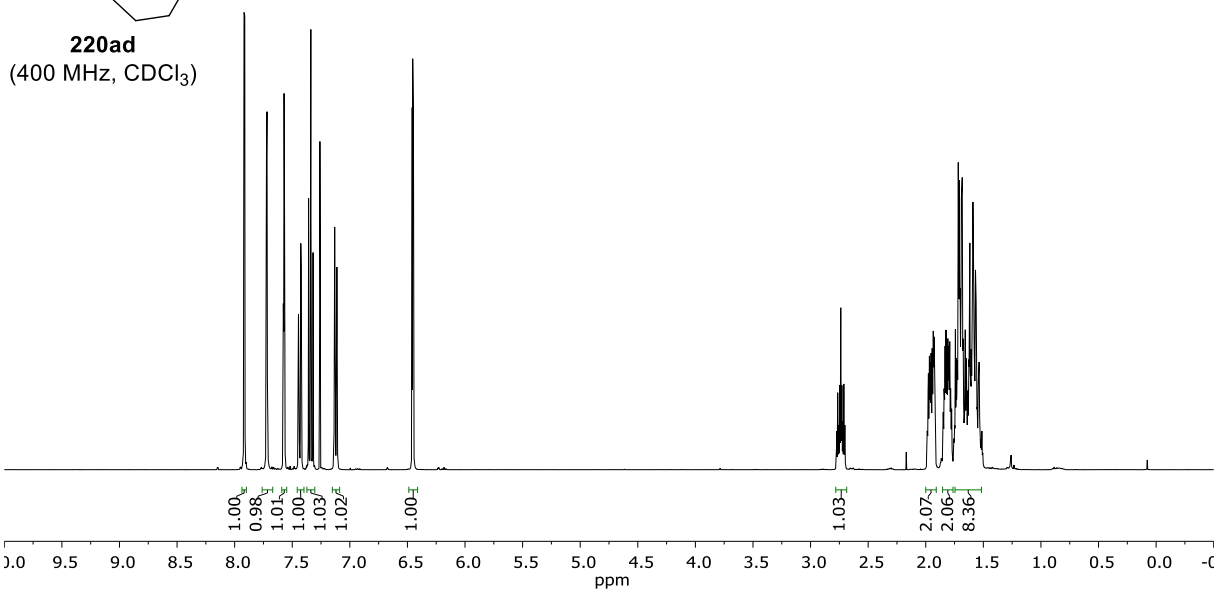

220ad
(100 MHz, $CDCl_3$)

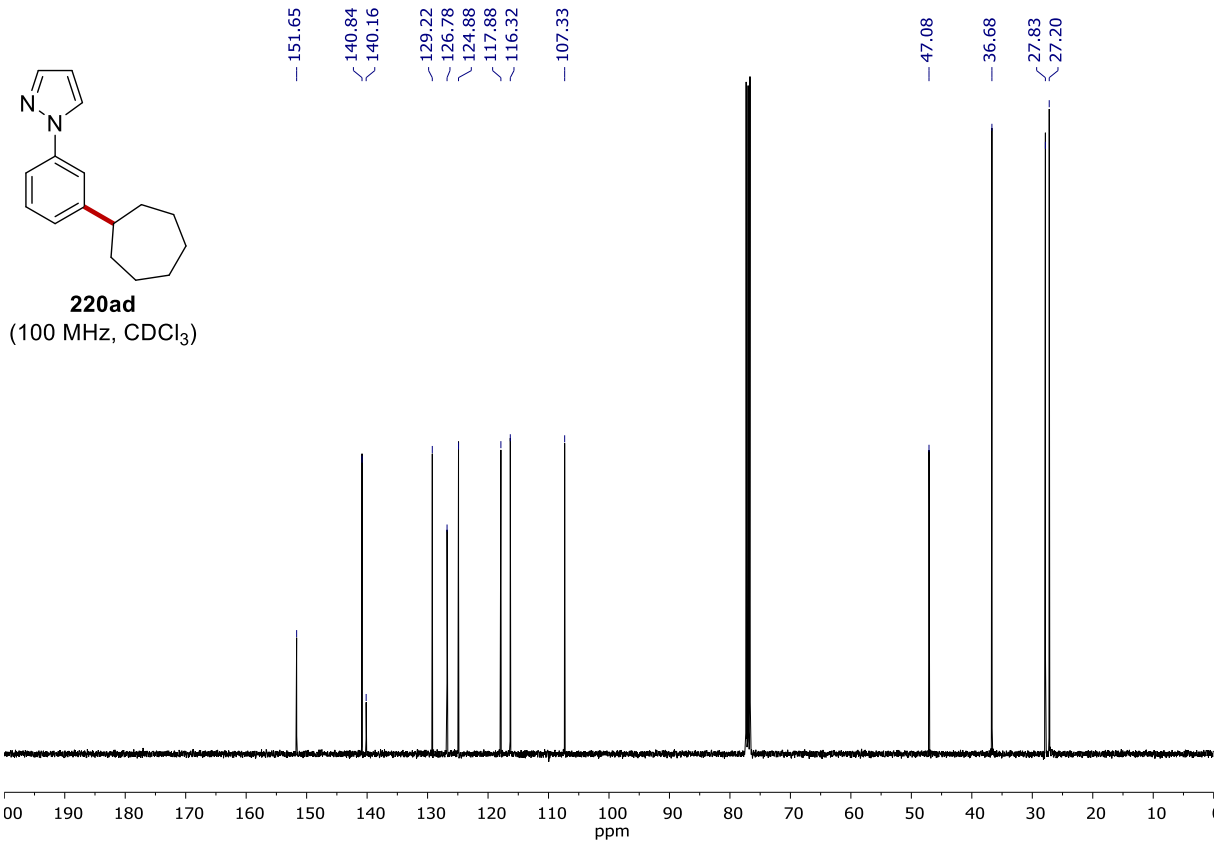

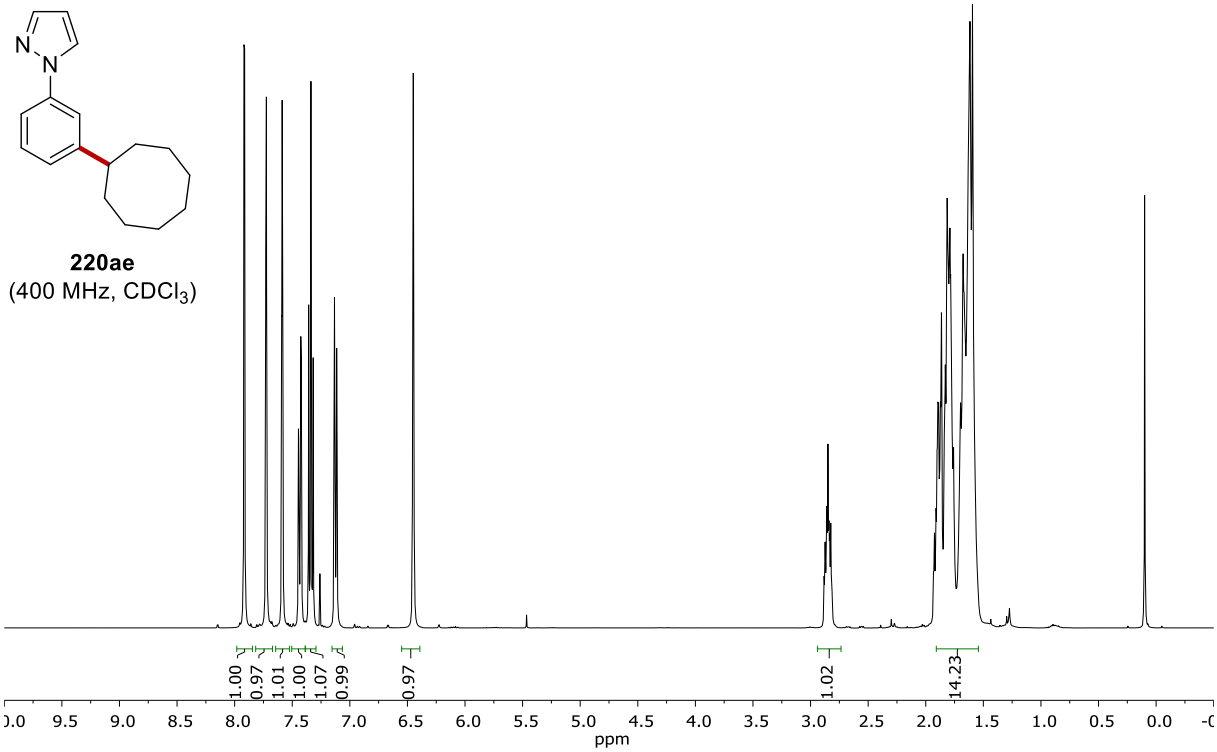
220ae
(400 MHz, CDCl3)
1.00
0.97
1.01
1.00
1.07
0.99
0.97
1.02
14.23
ppm

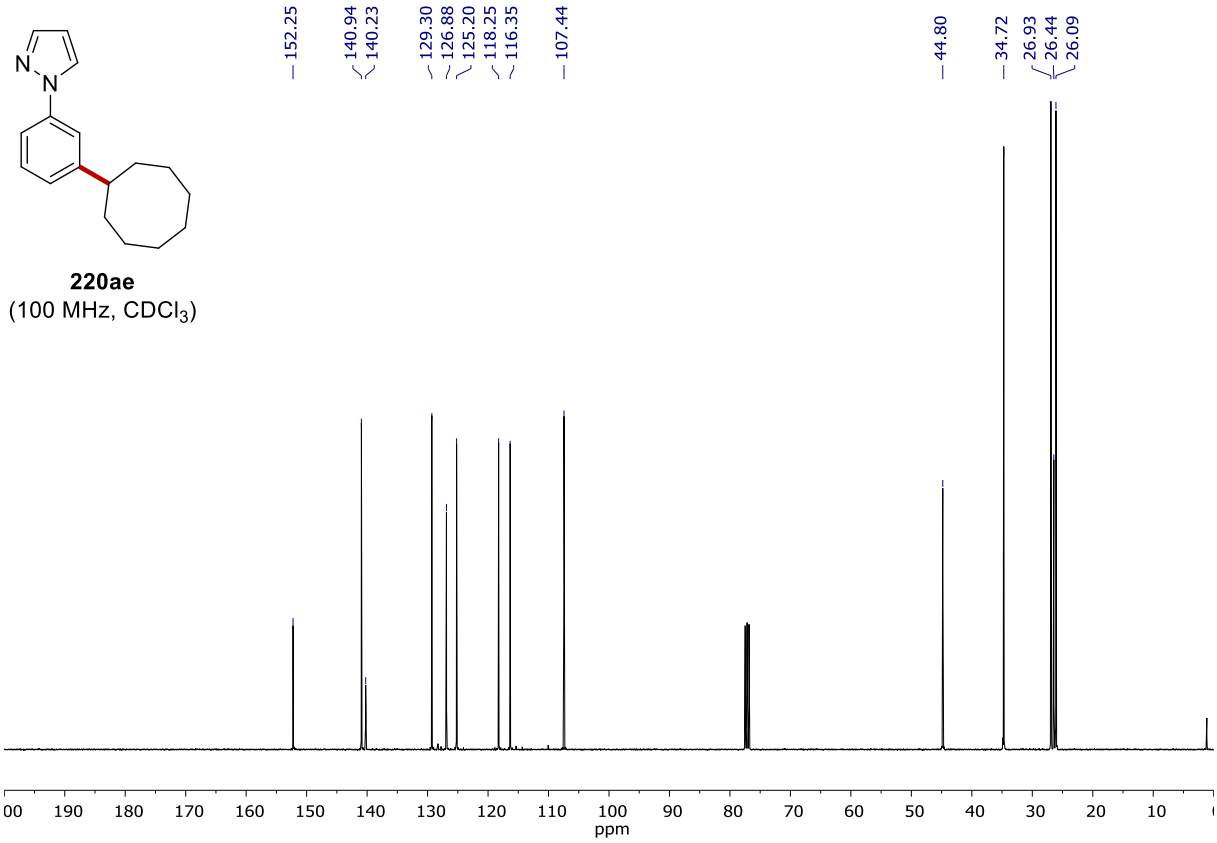
220ae
(100 MHz, CDCl3)
152.25
140.94
140.23
129.30
126.88
125.20
118.25
116.35
107.44
44.80
34.72
26.93
26.44
26.09
ppm

219af
(600 MHz, $CDCl_3$)

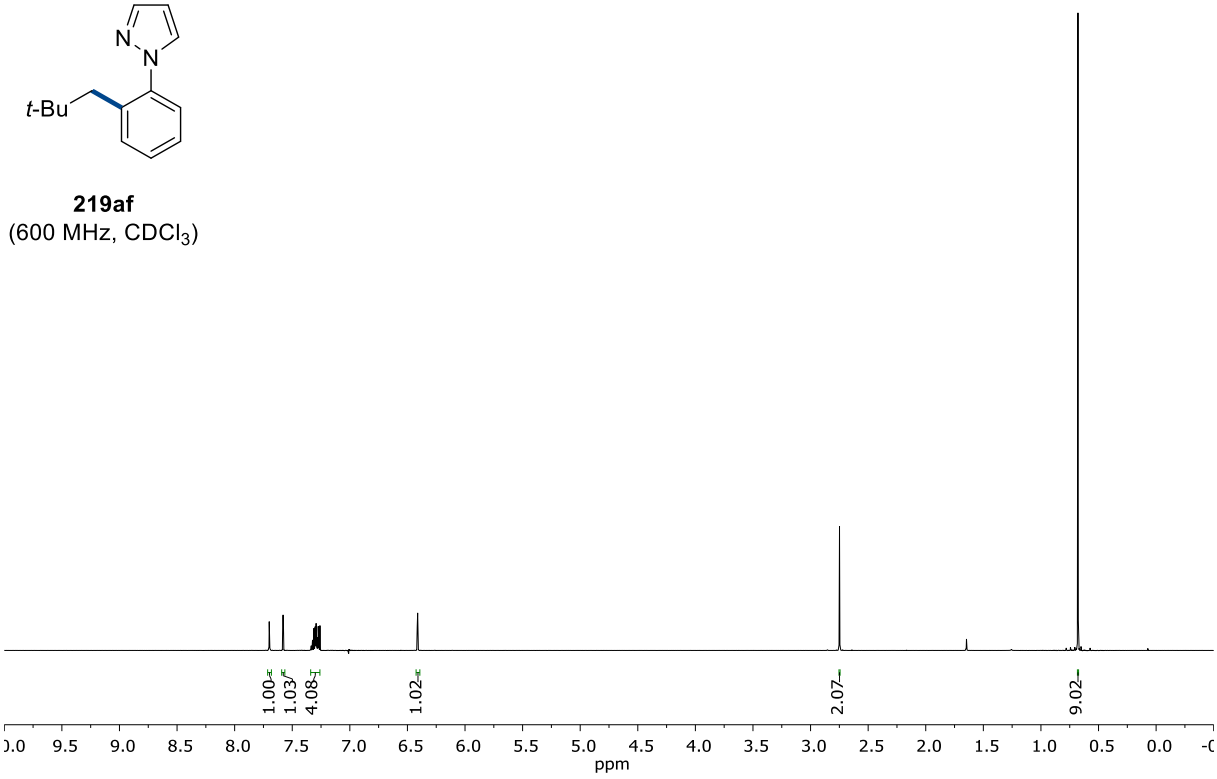

219af
(100 MHz, $CDCl_3$)

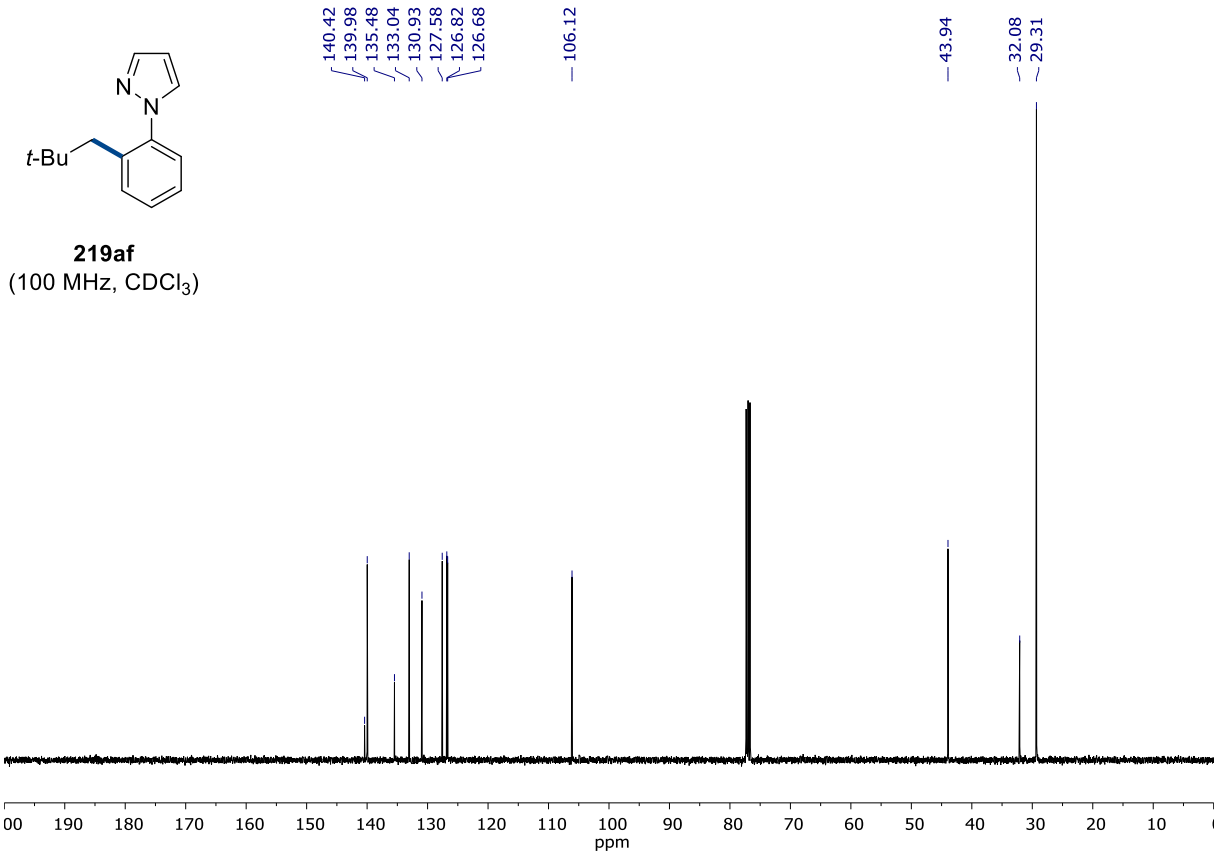

219bf
(400 MHz, $CDCl_3$)

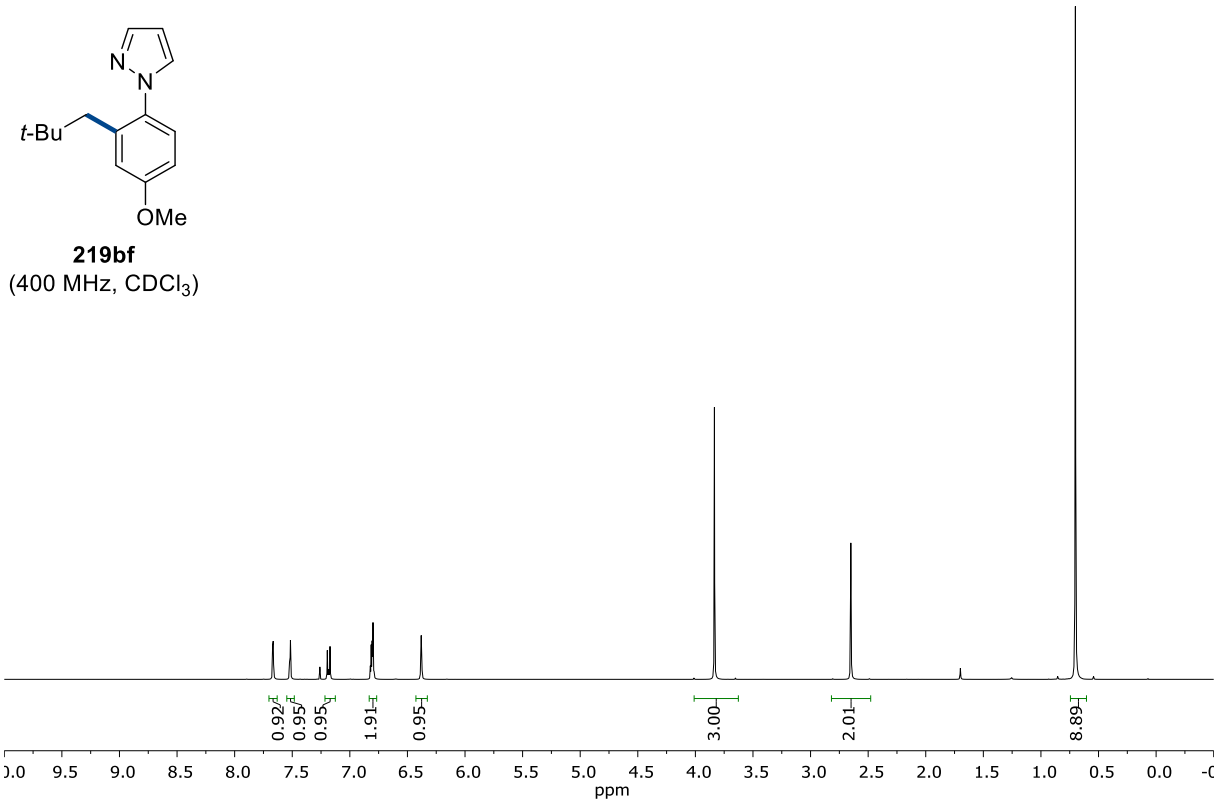

219bf
(100 MHz, $CDCl_3$)

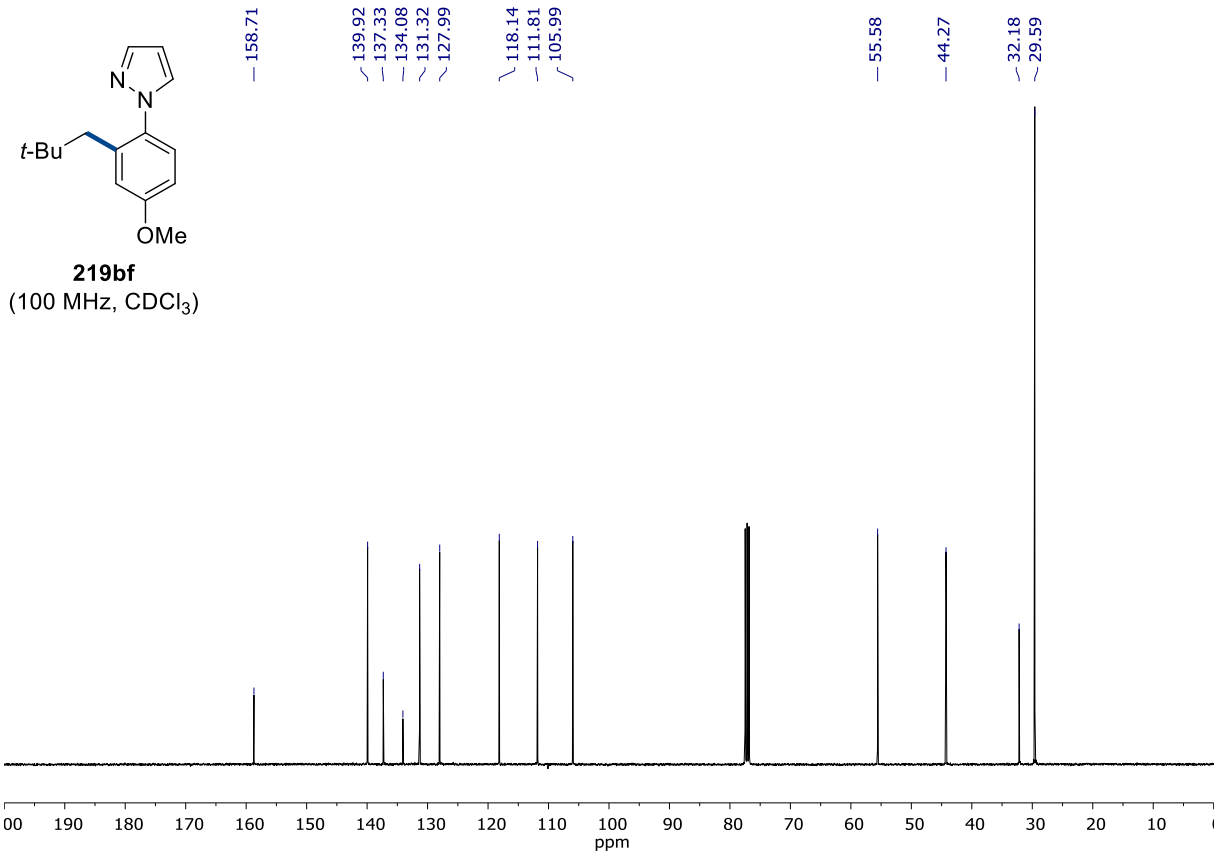

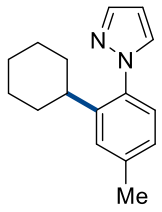

219ca
(300 MHz, $CDCl_3$)

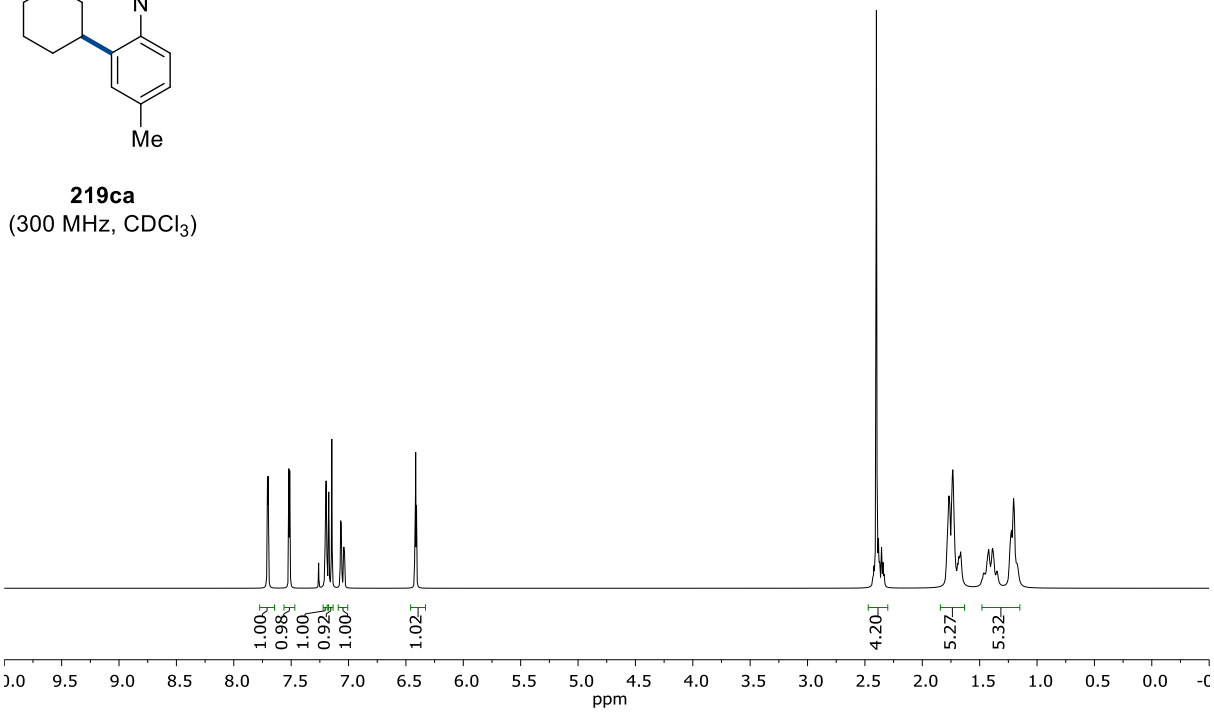

219ca
(100 MHz, $CDCl_3$)

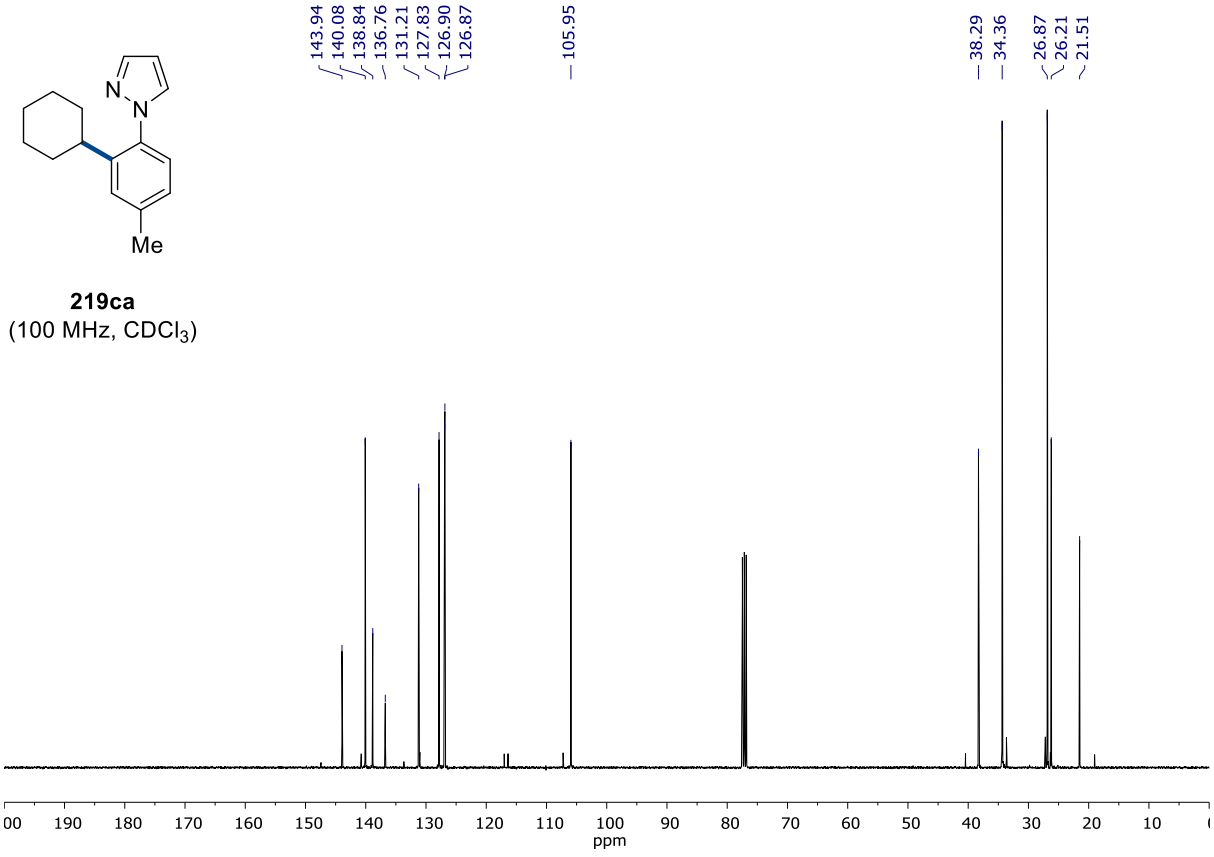

220ca
(300 MHz, $CDCl_3$)

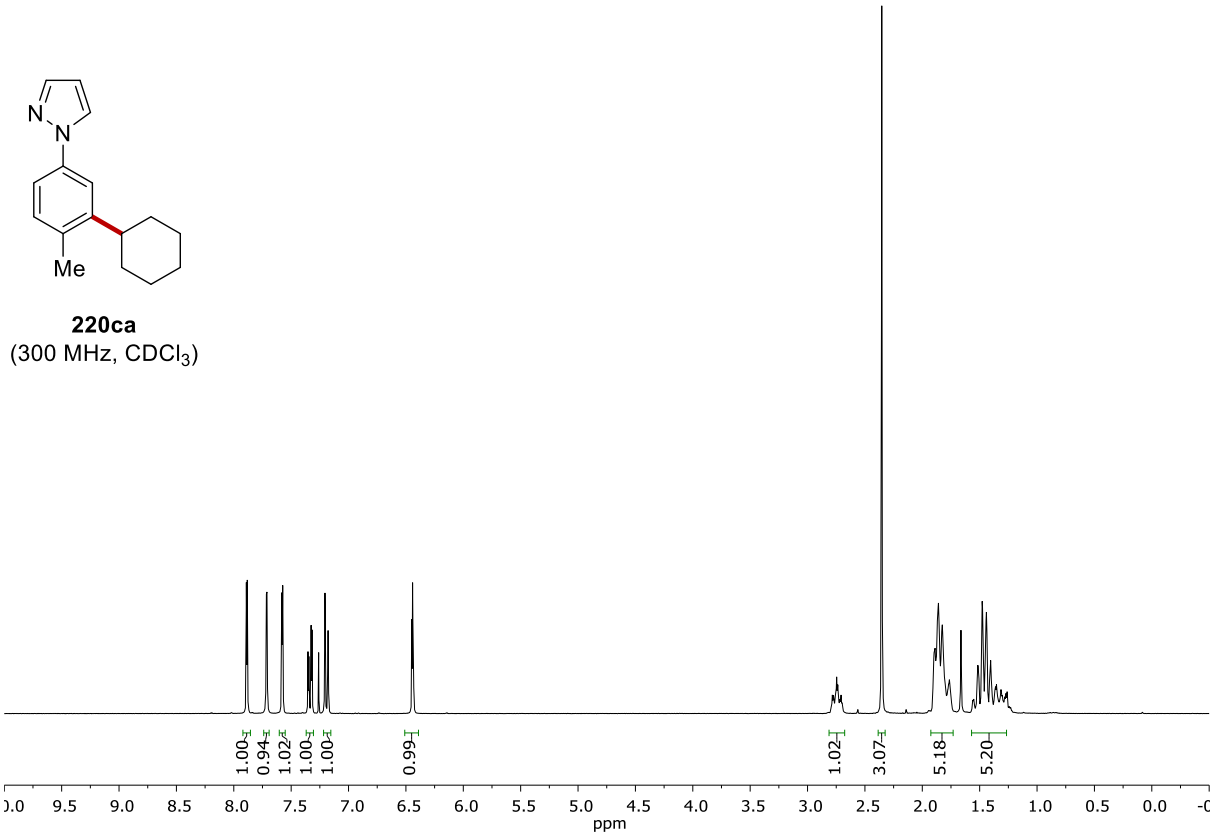

220ca
(75 MHz, $CDCl_3$)

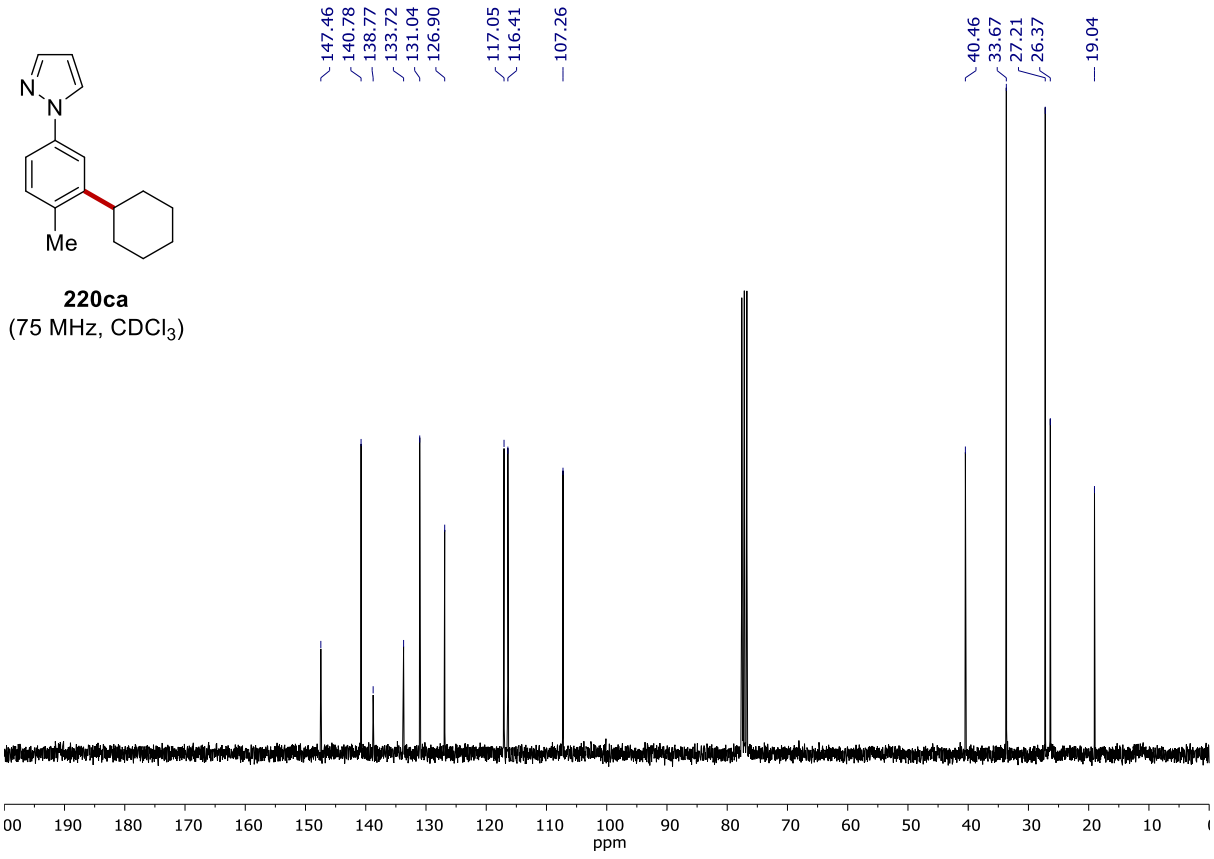

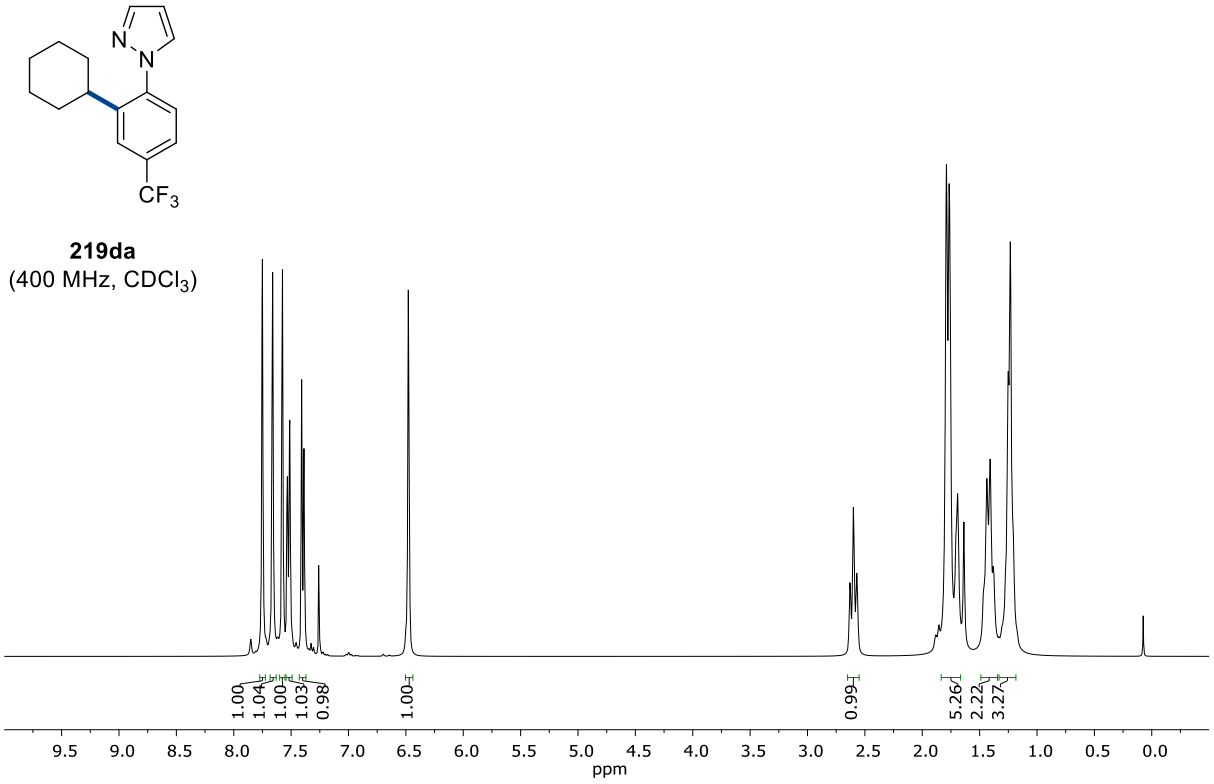
N
N
CF3
219da
(400 MHz, CDCl3)
1.00
1.04
1.00
1.03
0.98
1.00
0.99
5.26
2.22
3.27
9.5 9.0 8.5 8.0 7.5 7.0 6.5 6.0 5.5 5.0 4.5 4.0 3.5 3.0 2.5 2.0 1.5 1.0 0.5 0.0
ppm

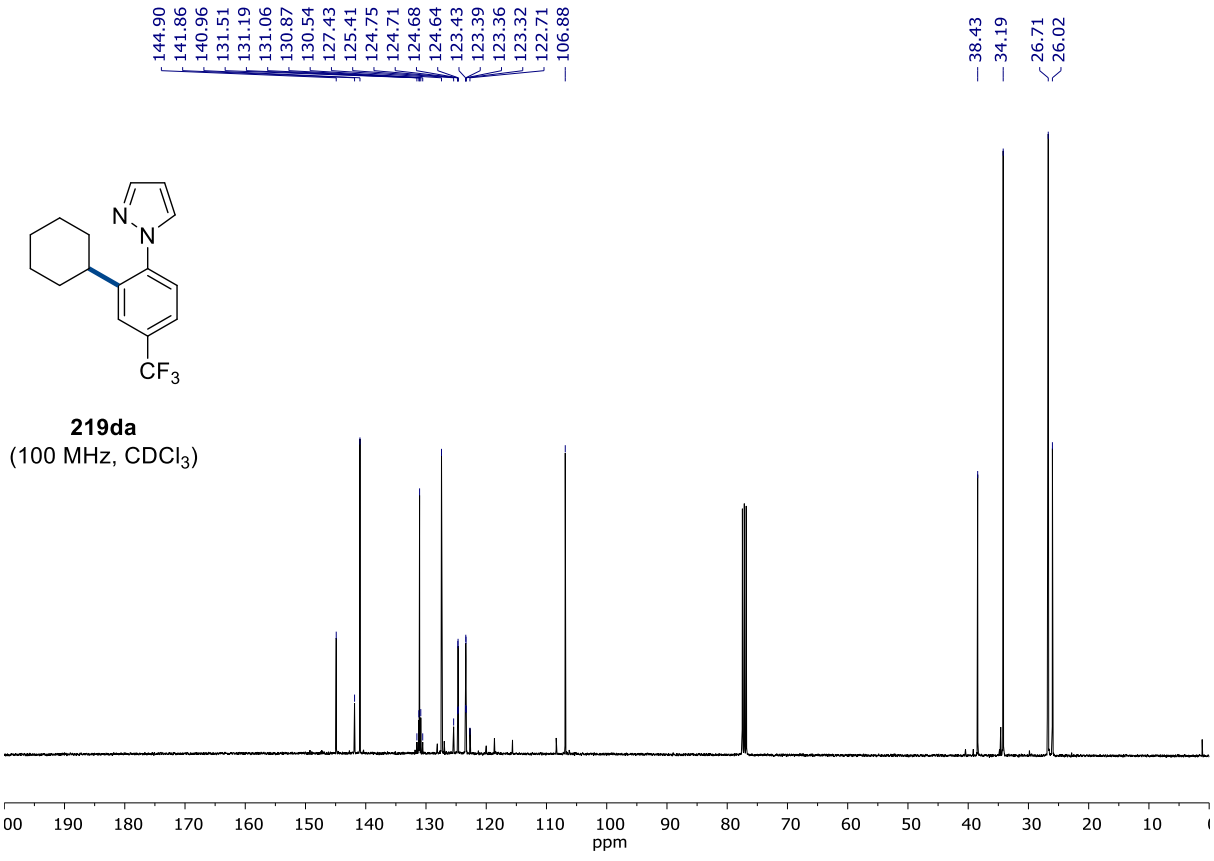
144.90
141.86
140.96
131.51
131.19
131.06
130.87
130.54
127.43
125.41
124.75
124.71
124.68
124.64
123.43
123.39
123.36
123.32
122.71
106.88
38.43
34.19
26.71
26.02
N
N
CF3
219da
(100 MHz, CDCl3)
00 190 180 170 160 150 140 130 120 110 100 90 80 70 60 50 40 30 20 10
ppm

219da
^{19}F
(376 MHz, $CDCl_3$)

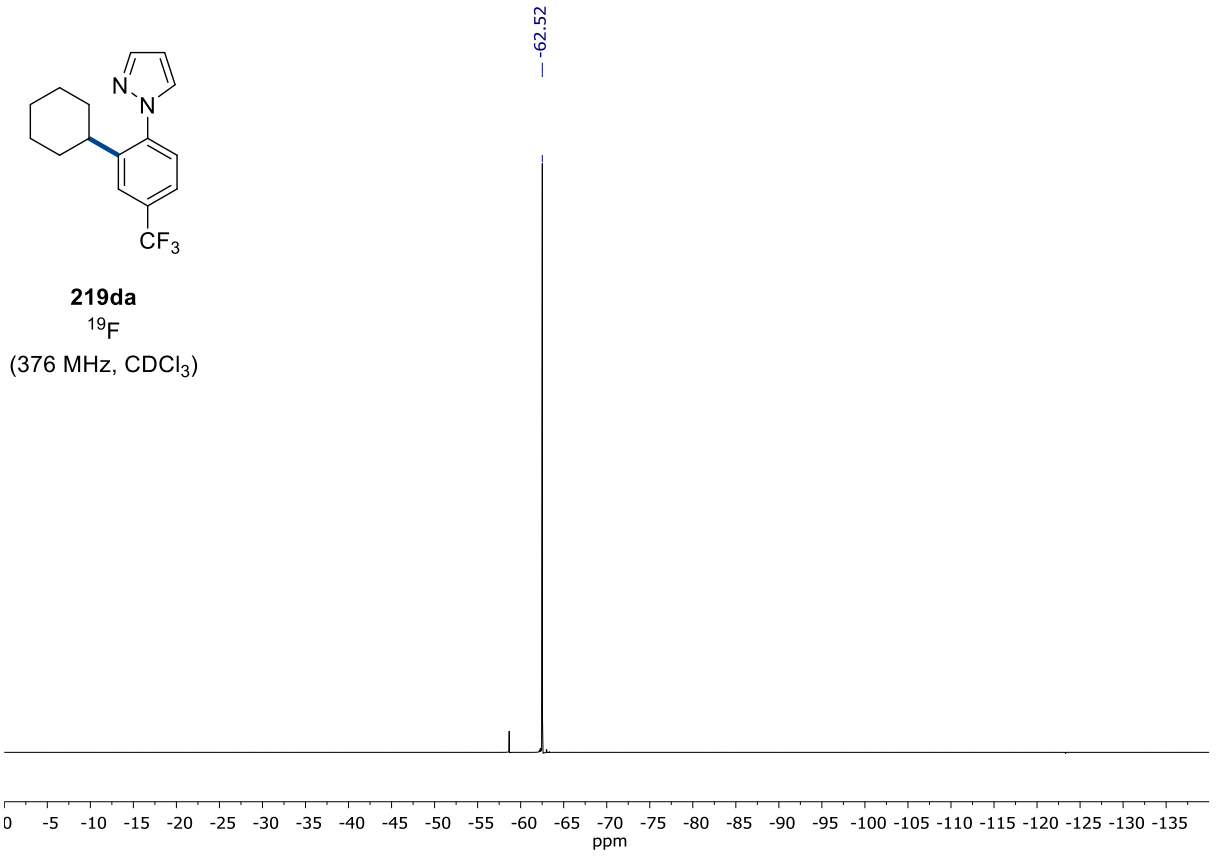

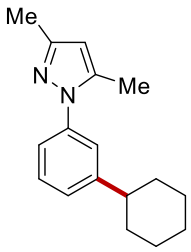

220ea
(300 MHz, $CDCl_3$)

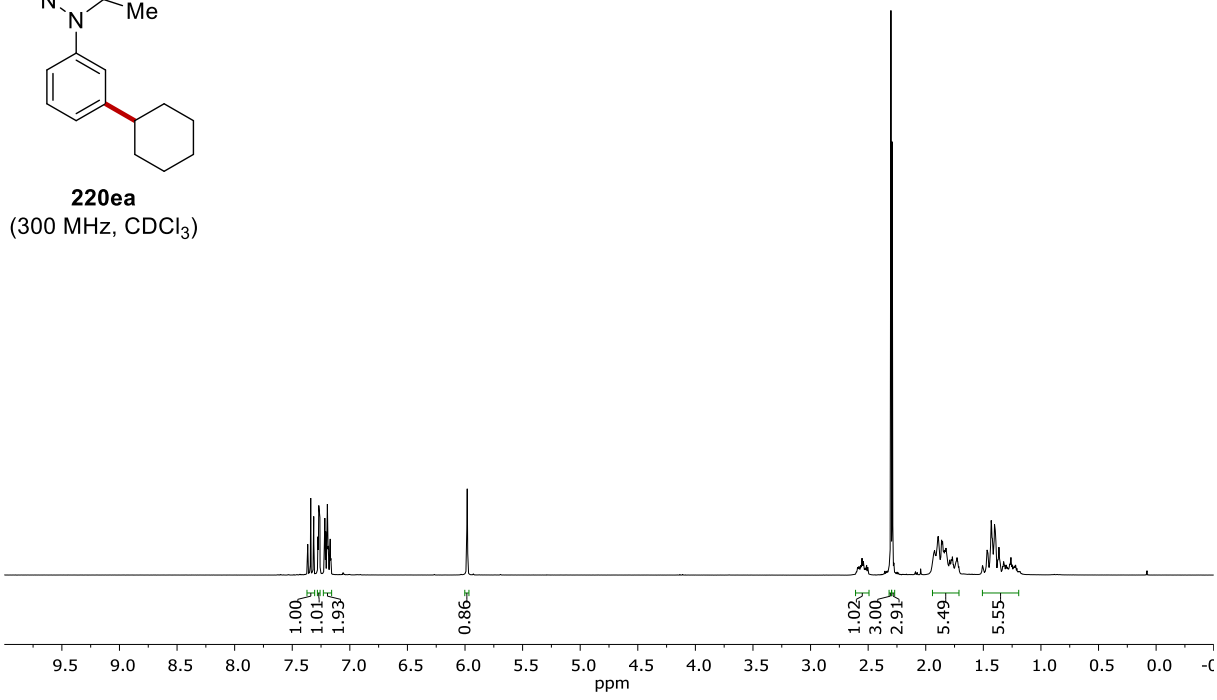

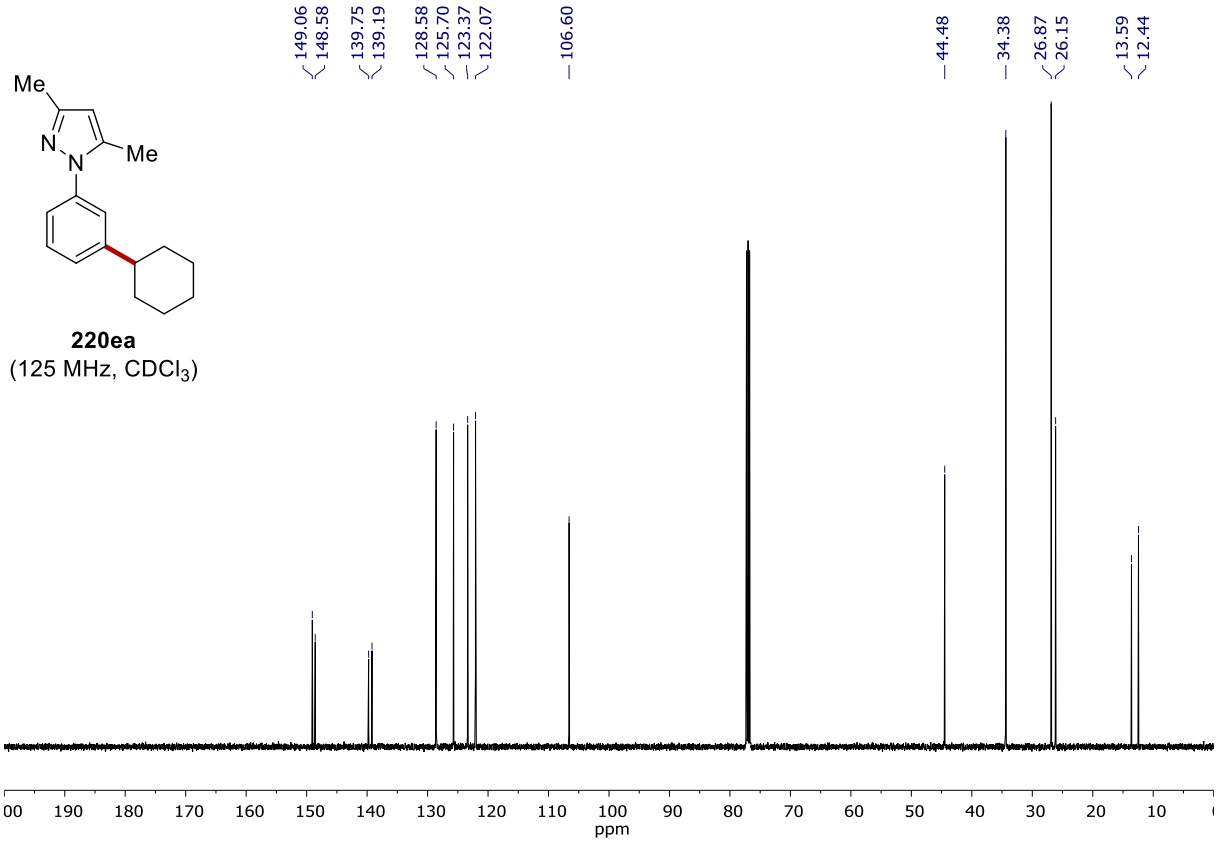

220ea
(125 MHz, $CDCl_3$)

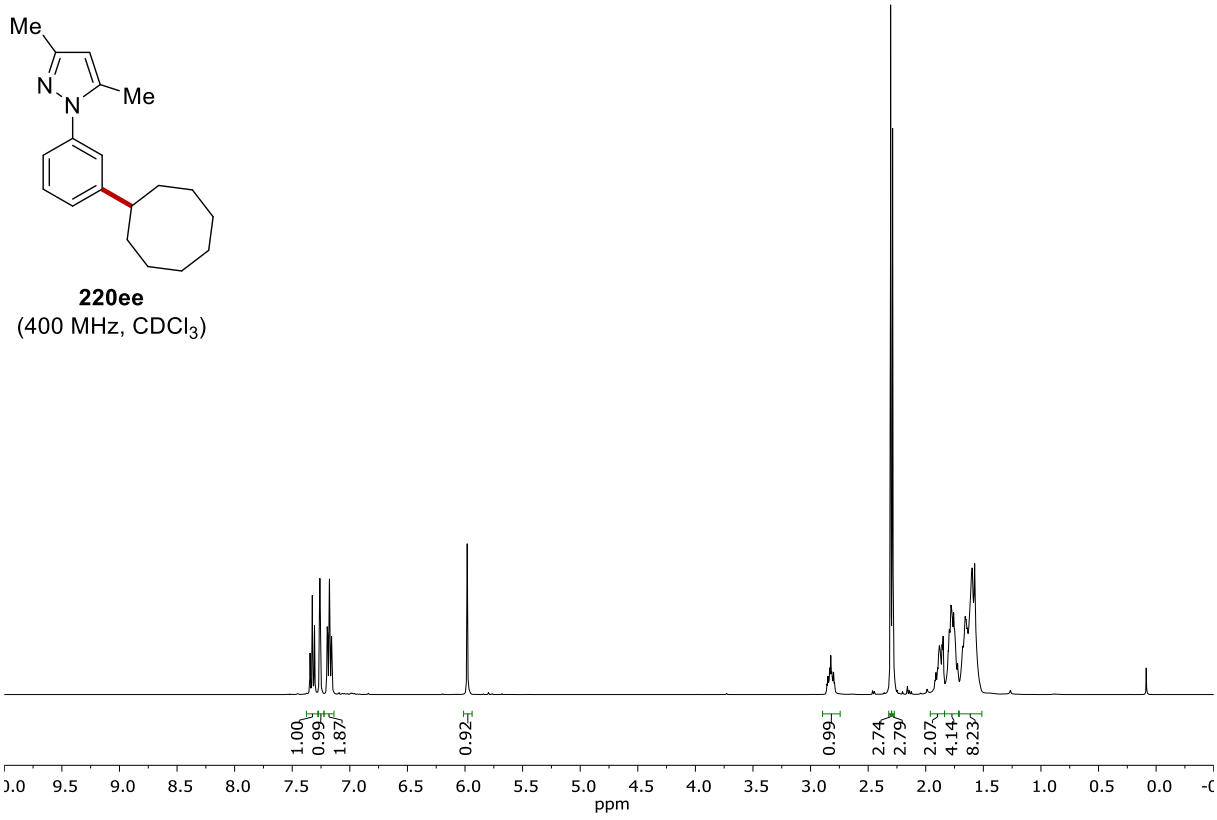

220ee
(400 MHz, $CDCl_3$)

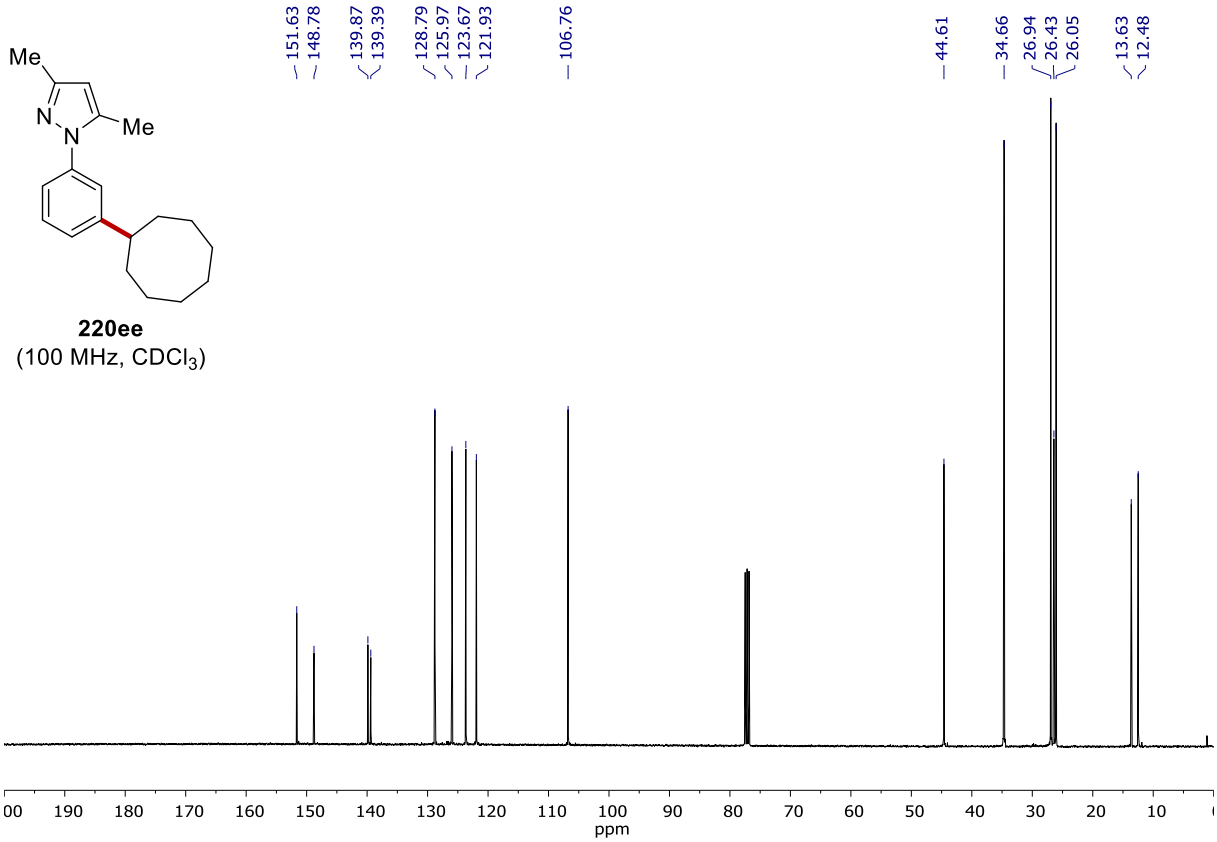

220ee
(100 MHz, $CDCl_3$)

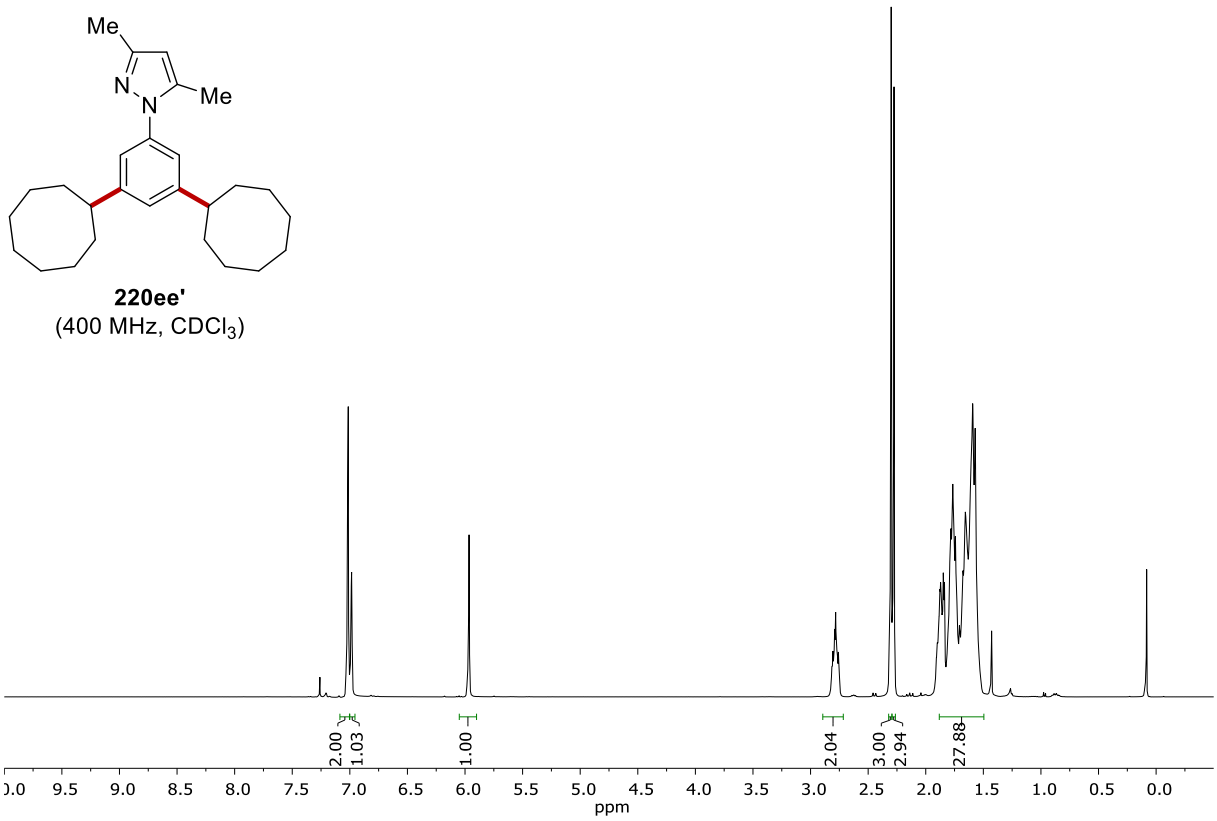

220ee'
(400 MHz, $CDCl_3$)

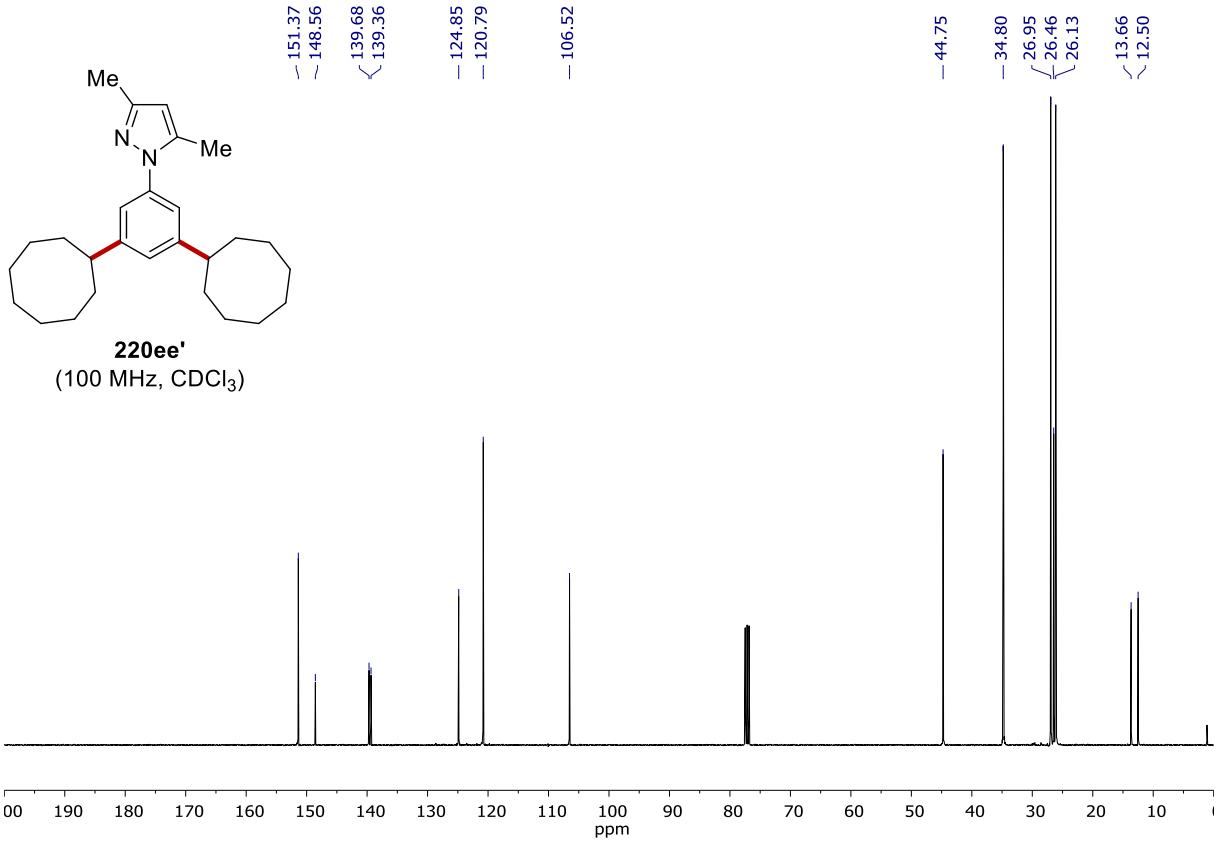

220ee'
(100 MHz, $CDCl_3$)

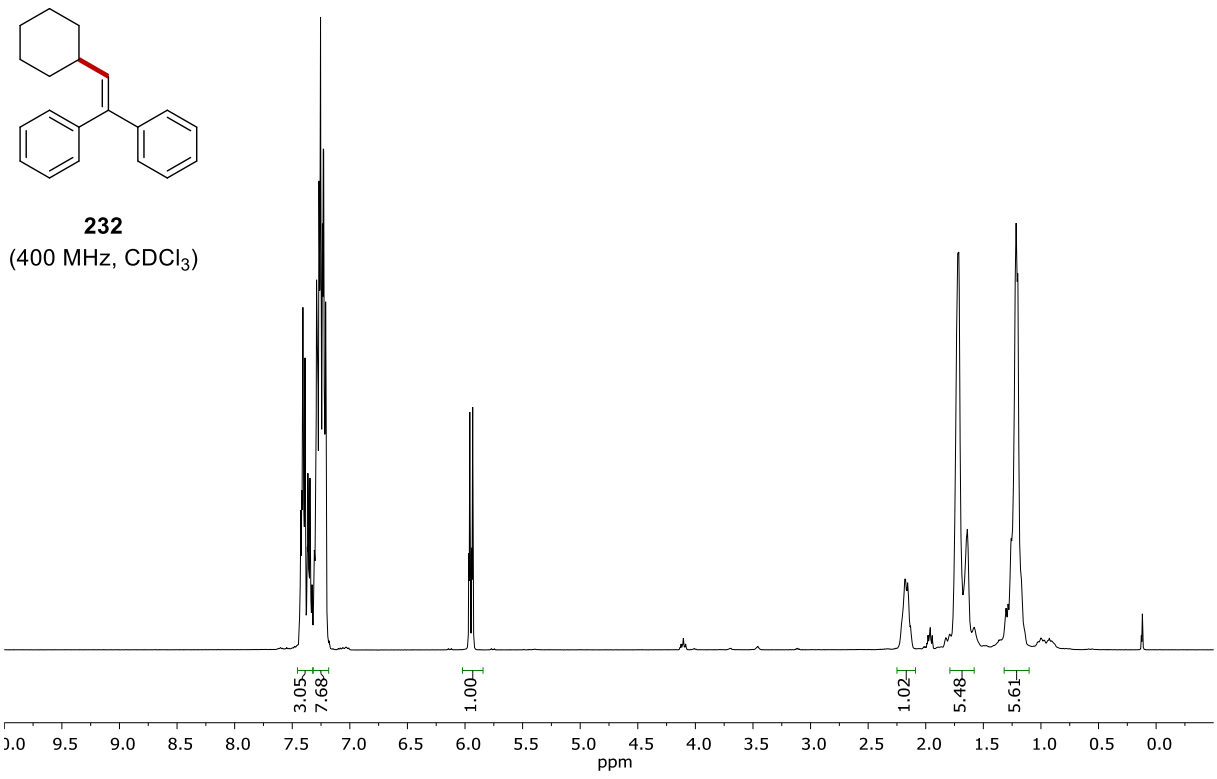

232
(400 MHz, $CDCl_3$)

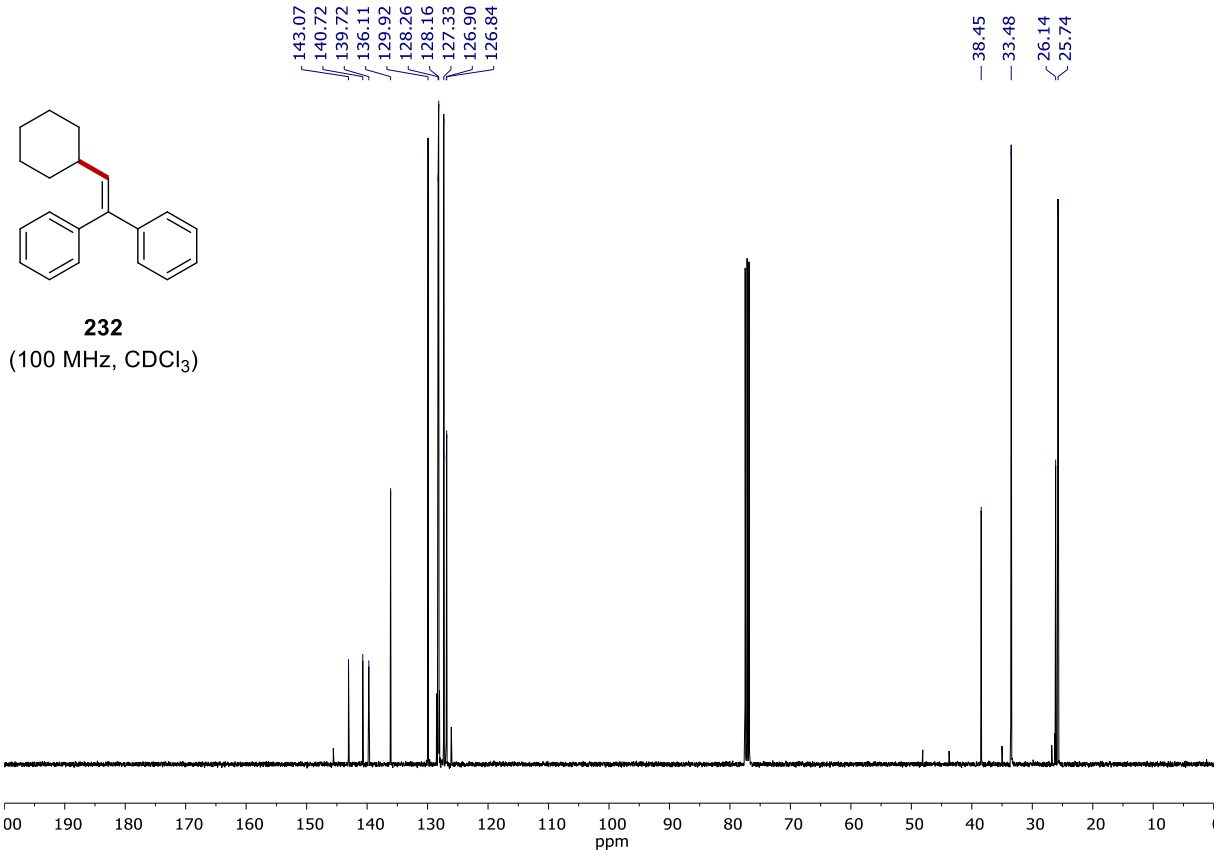

232
(100 MHz, $CDCl_3$)

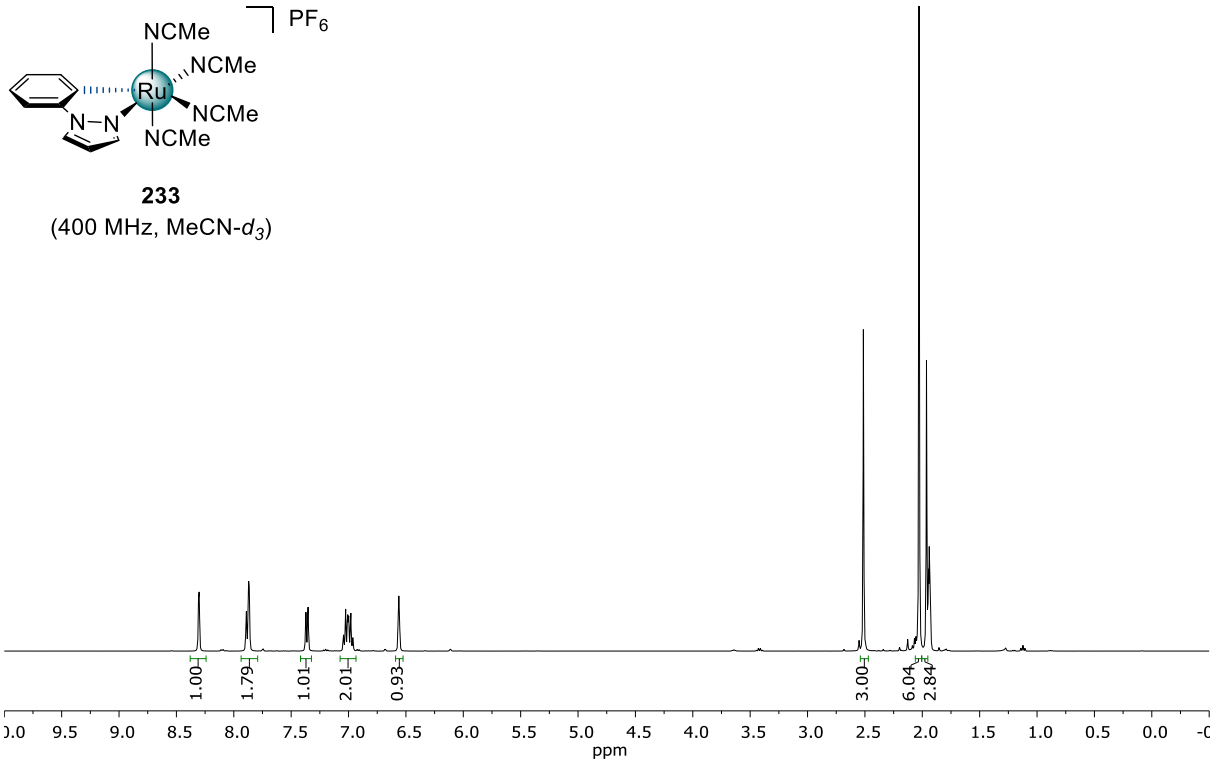

233
(400 MHz, MeCN-d_3)

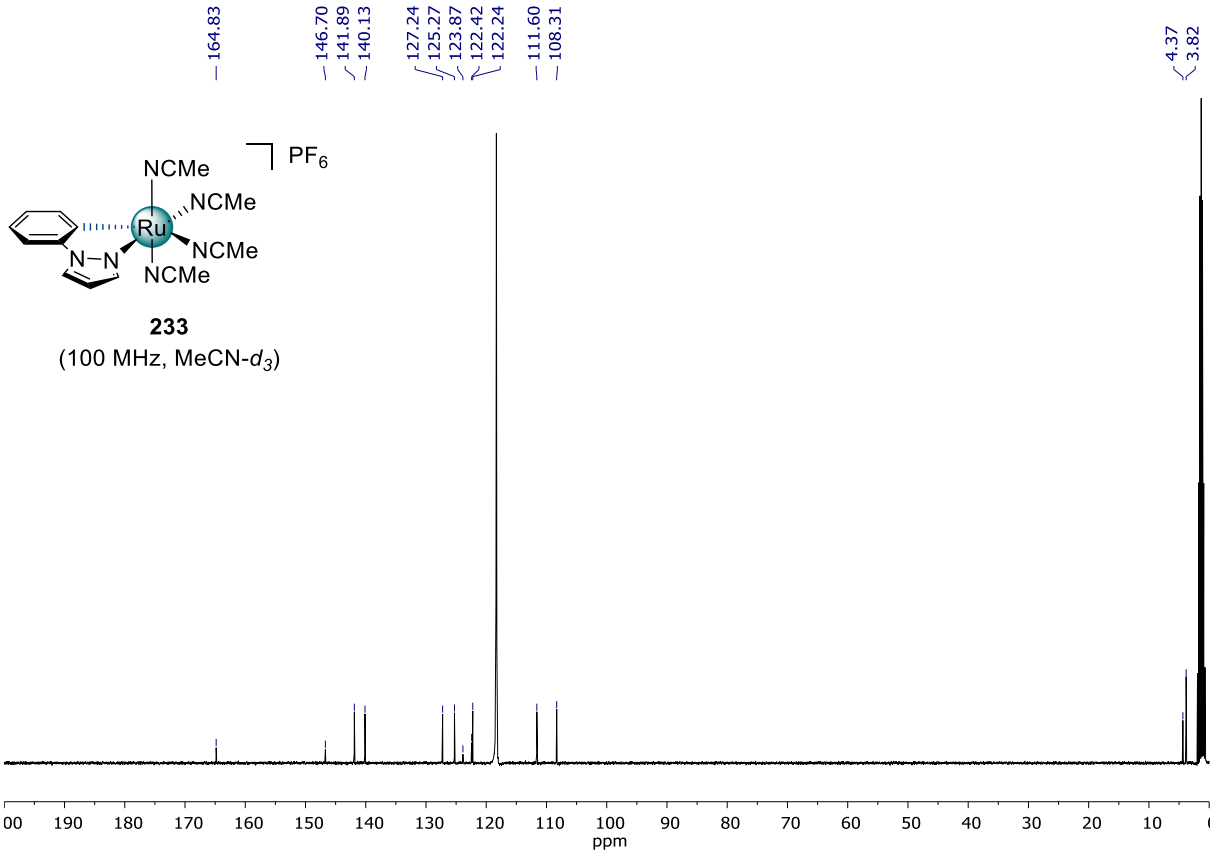
164.83
146.70
141.89
140.13
127.24
125.27
123.87
122.42
122.24
111.60
108.31
4.37
3.82
PF6
NCMe
NCMe
NCMe
NCMe
NCMe
Ru
N–N
233
(100 MHz, MeCN-d3)
ppm

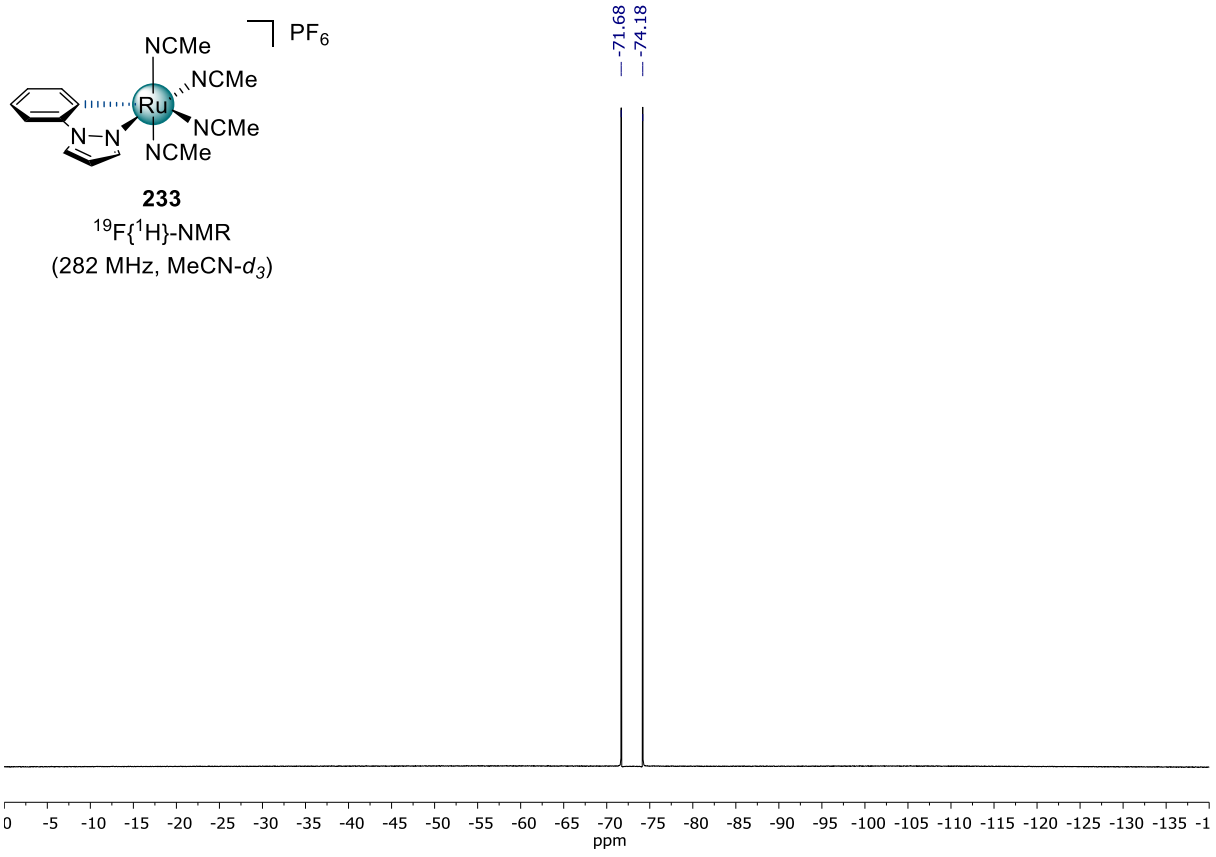
-71.68
-74.18
PF6
NCMe
NCMe
NCMe
NCMe
NCMe
Ru
N–N
233
19F{1H}-NMR
(282 MHz, MeCN-d3)
ppm

233

$^{31}P\{^{1}H\}$-NMR

(121 MHz, MeCN-d_3)

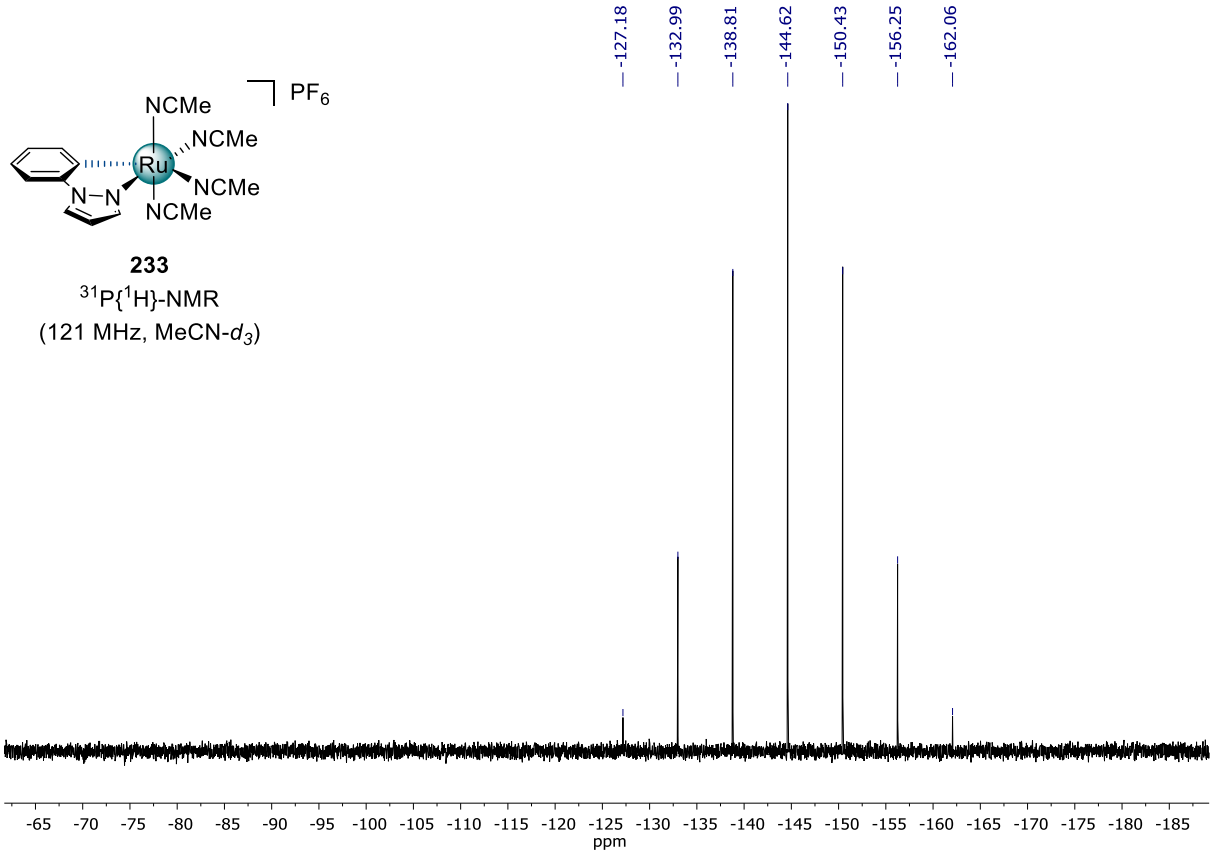

243aa

(400 MHz, $CDCl_3$)

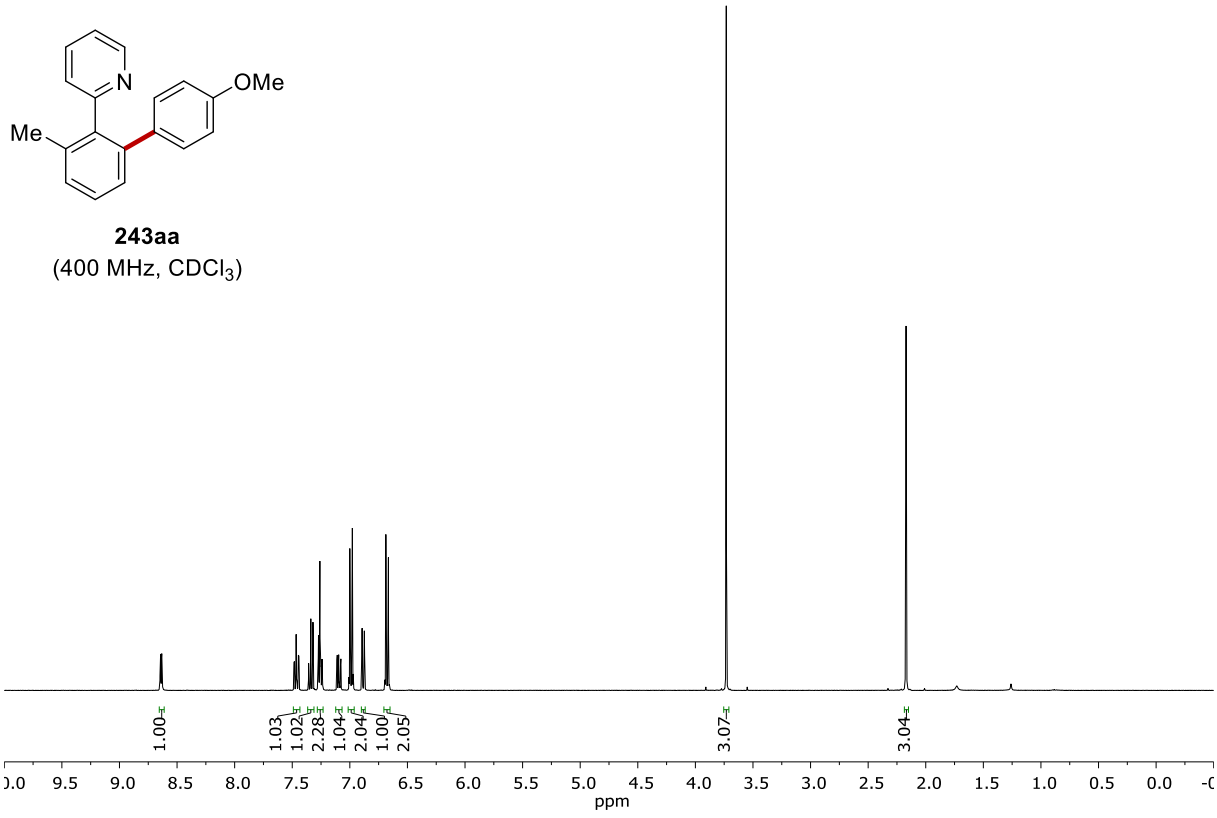

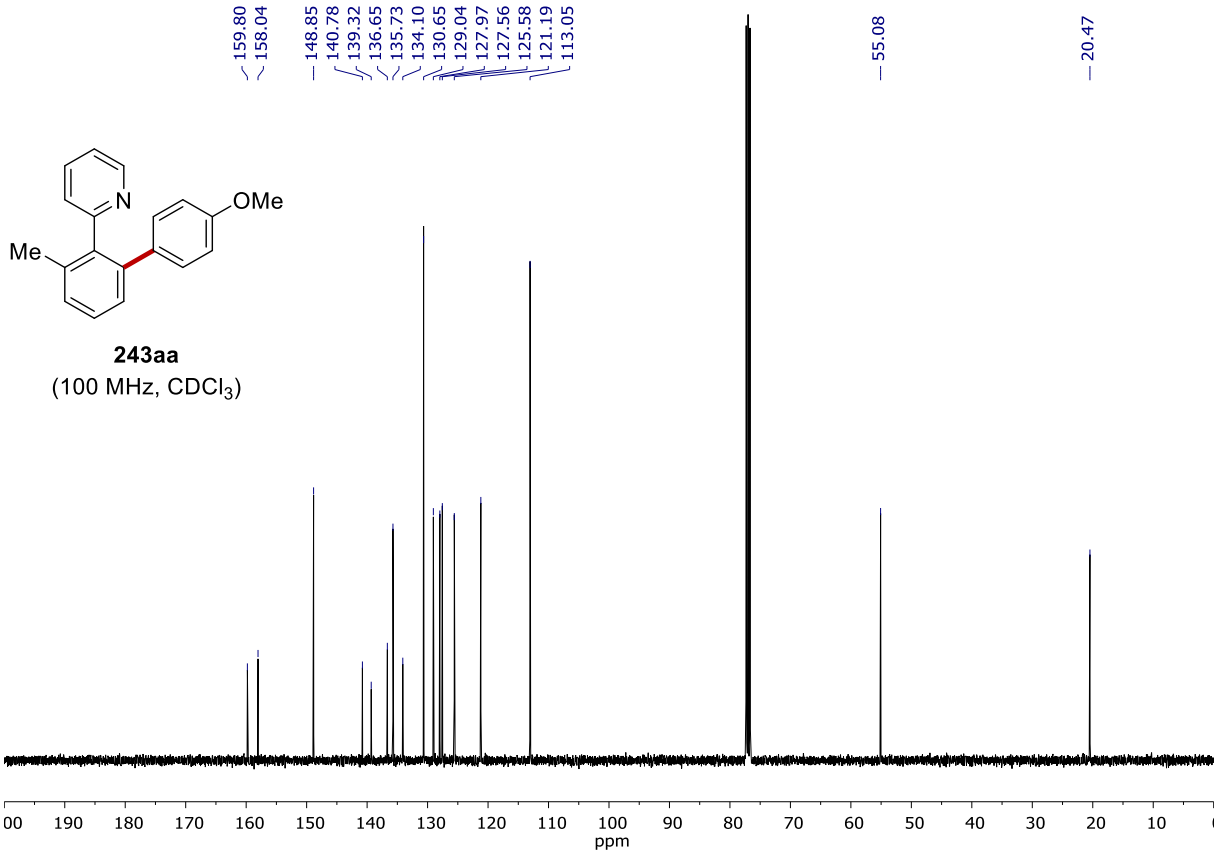

243aa
(100 MHz, $CDCl_3$)

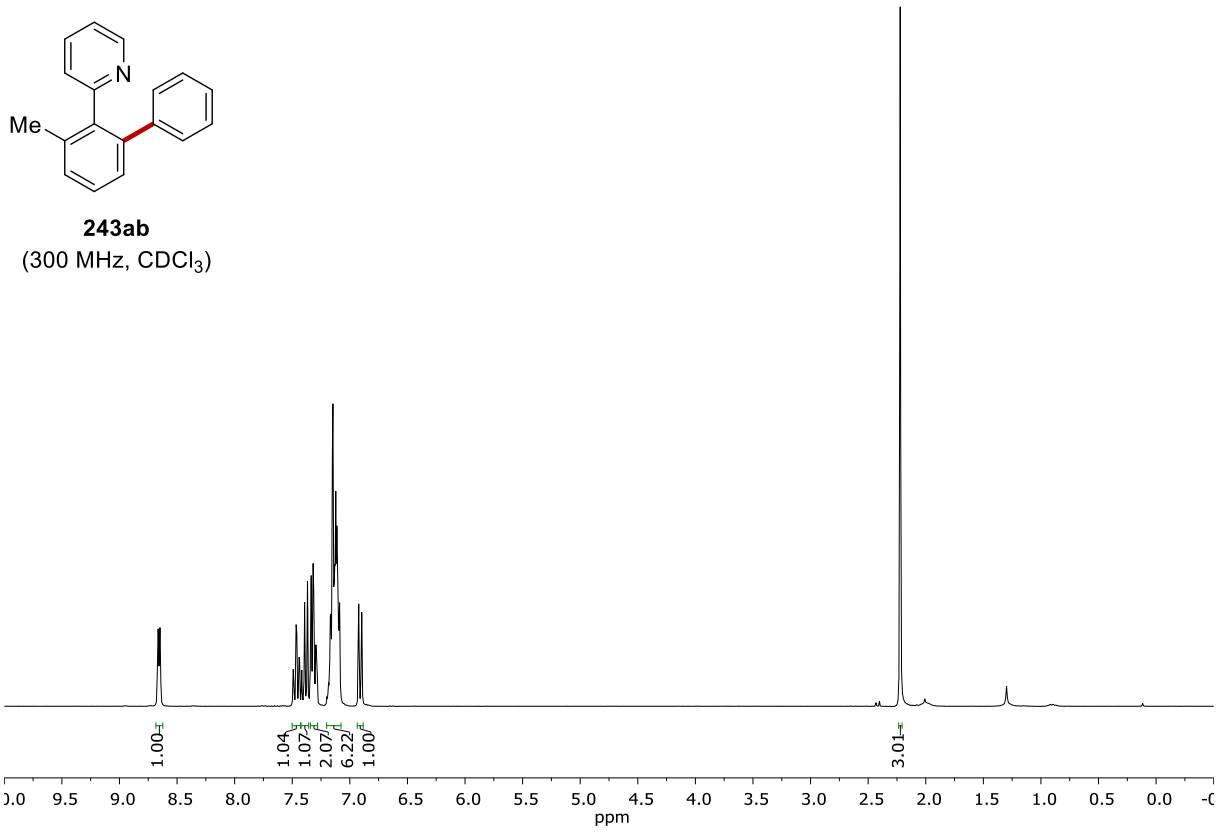

243ab
(300 MHz, $CDCl_3$)

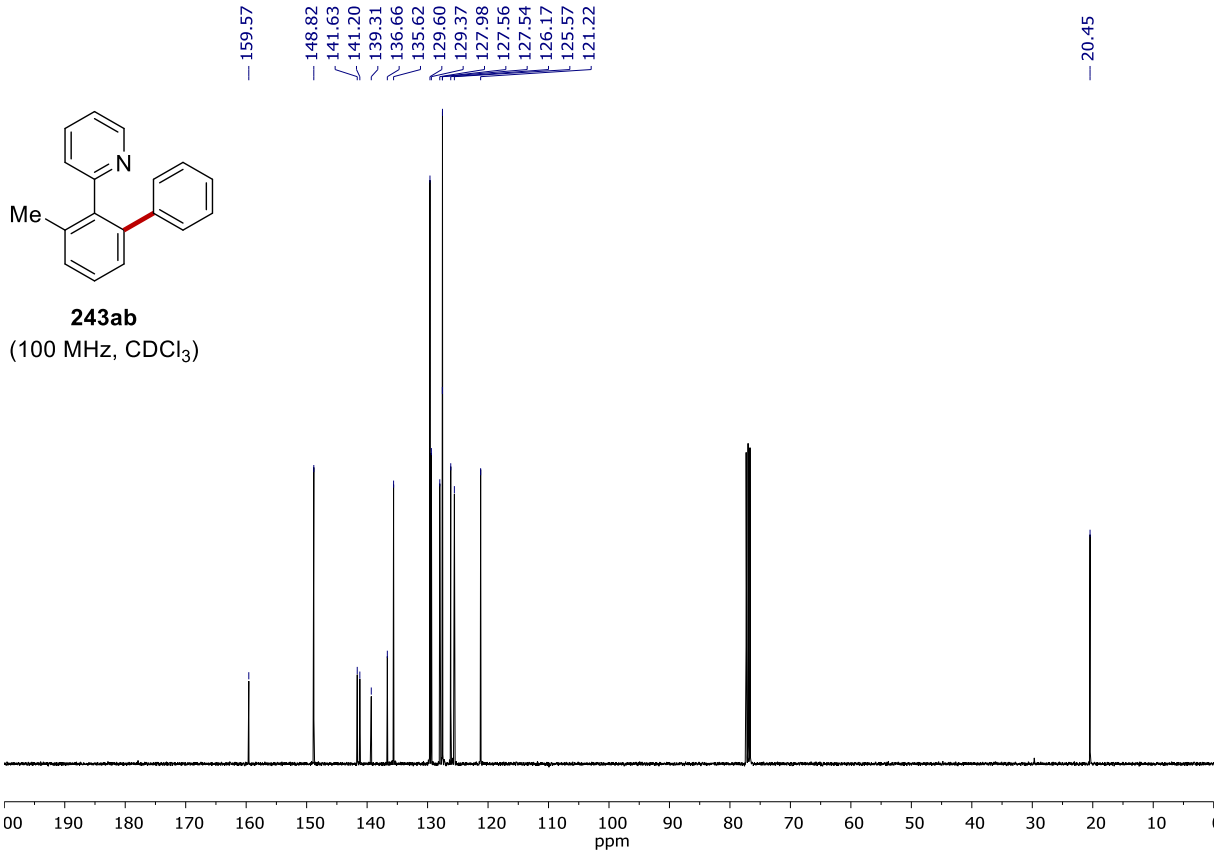

243ab
(100 MHz, $CDCl_3$)

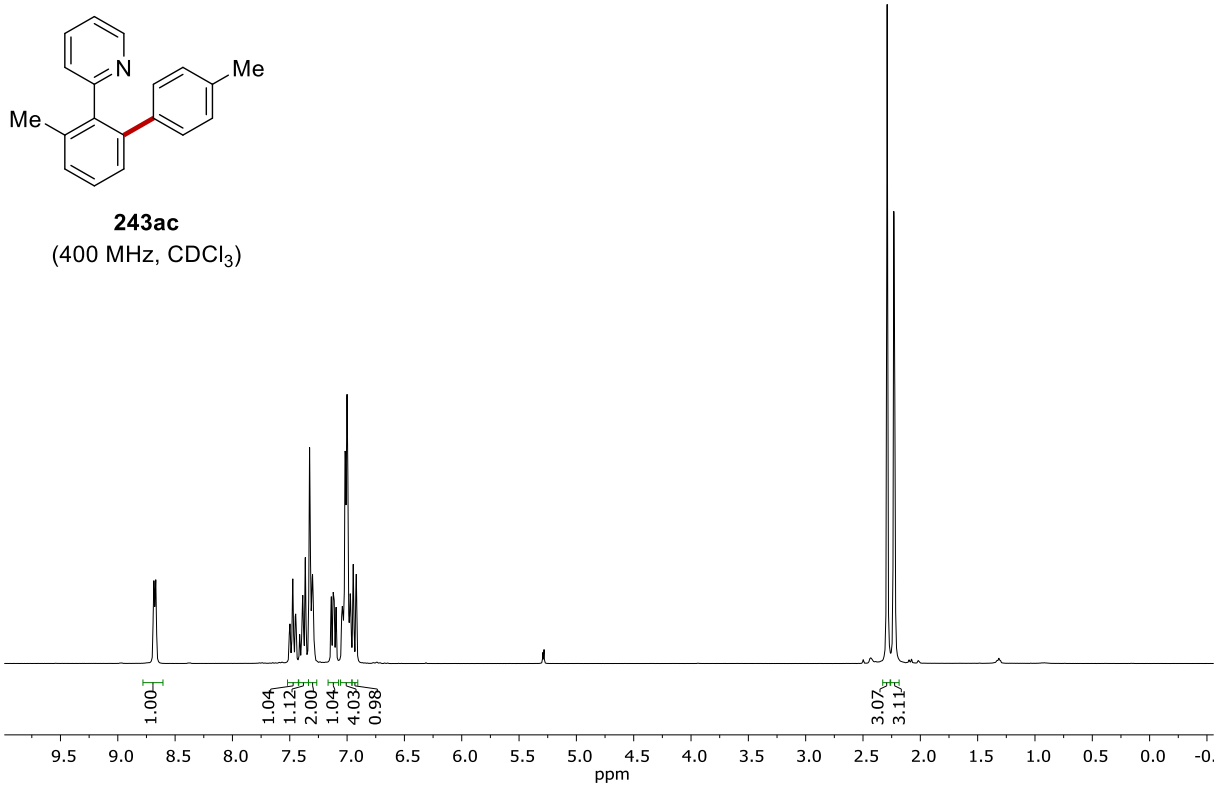

243ac
(400 MHz, $CDCl_3$)

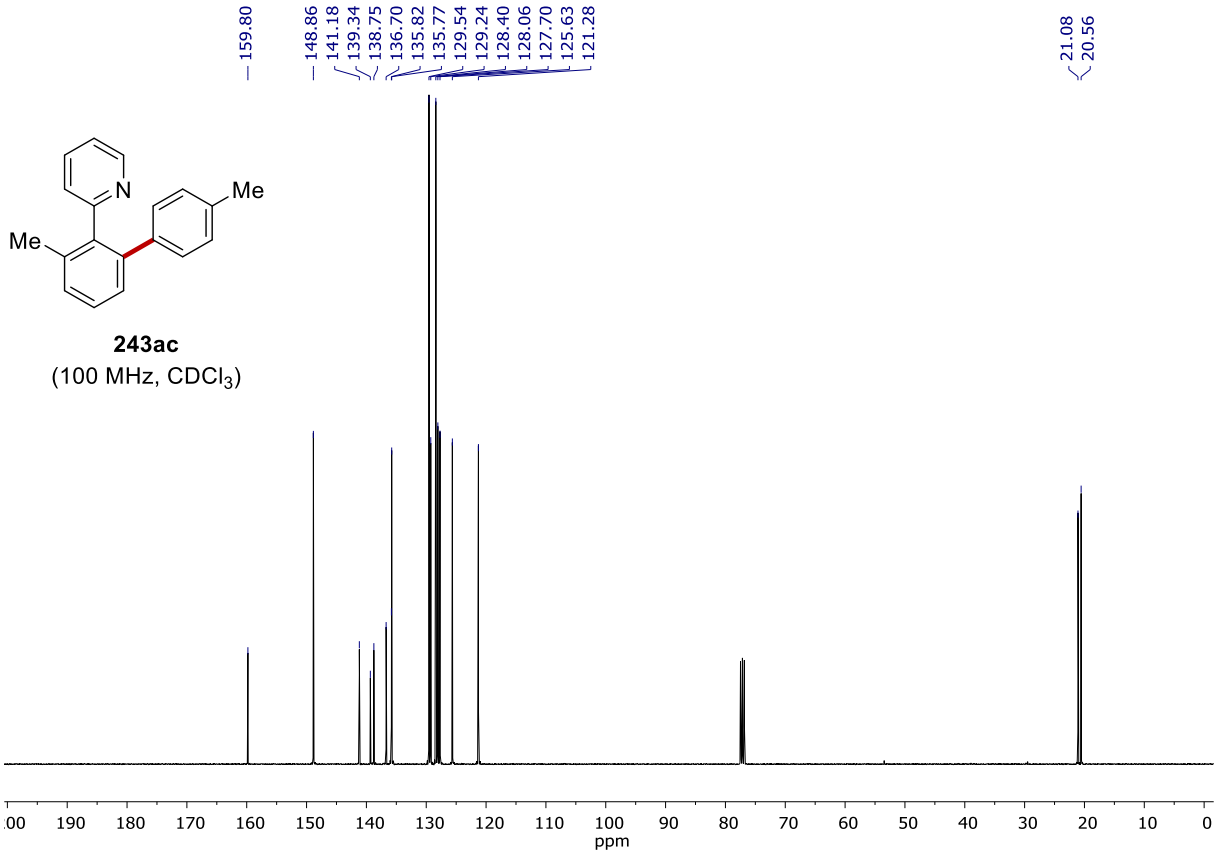

243ac
(100 MHz, $CDCl_3$)

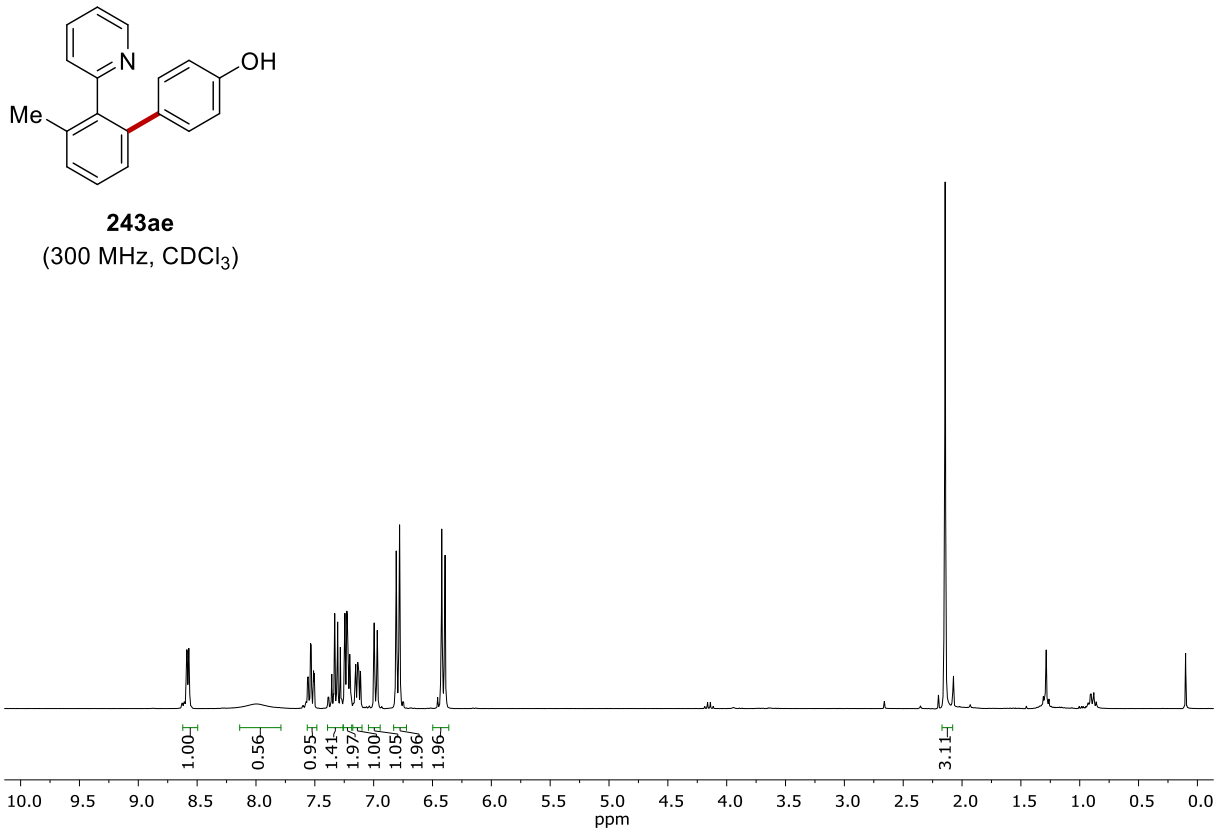

243ae
(300 MHz, $CDCl_3$)

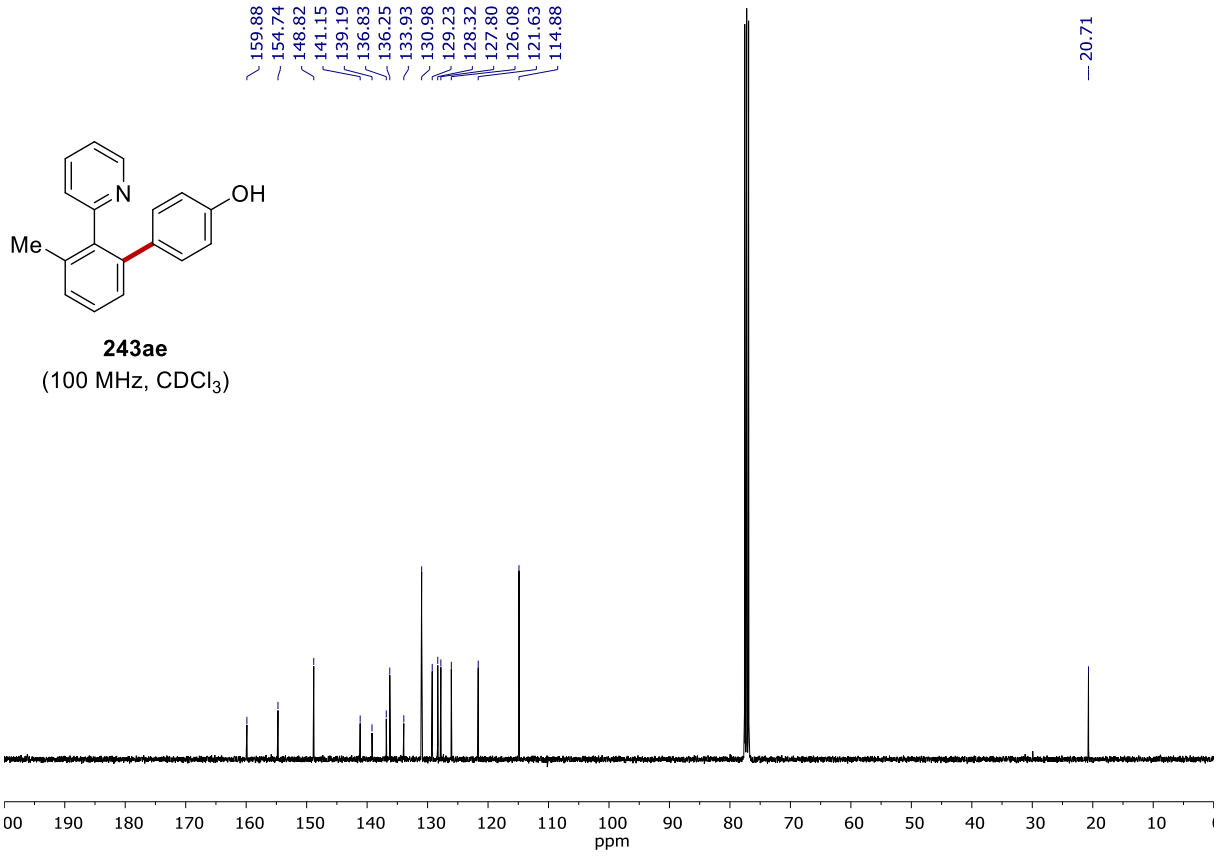

243ae
(100 MHz, $CDCl_3$)

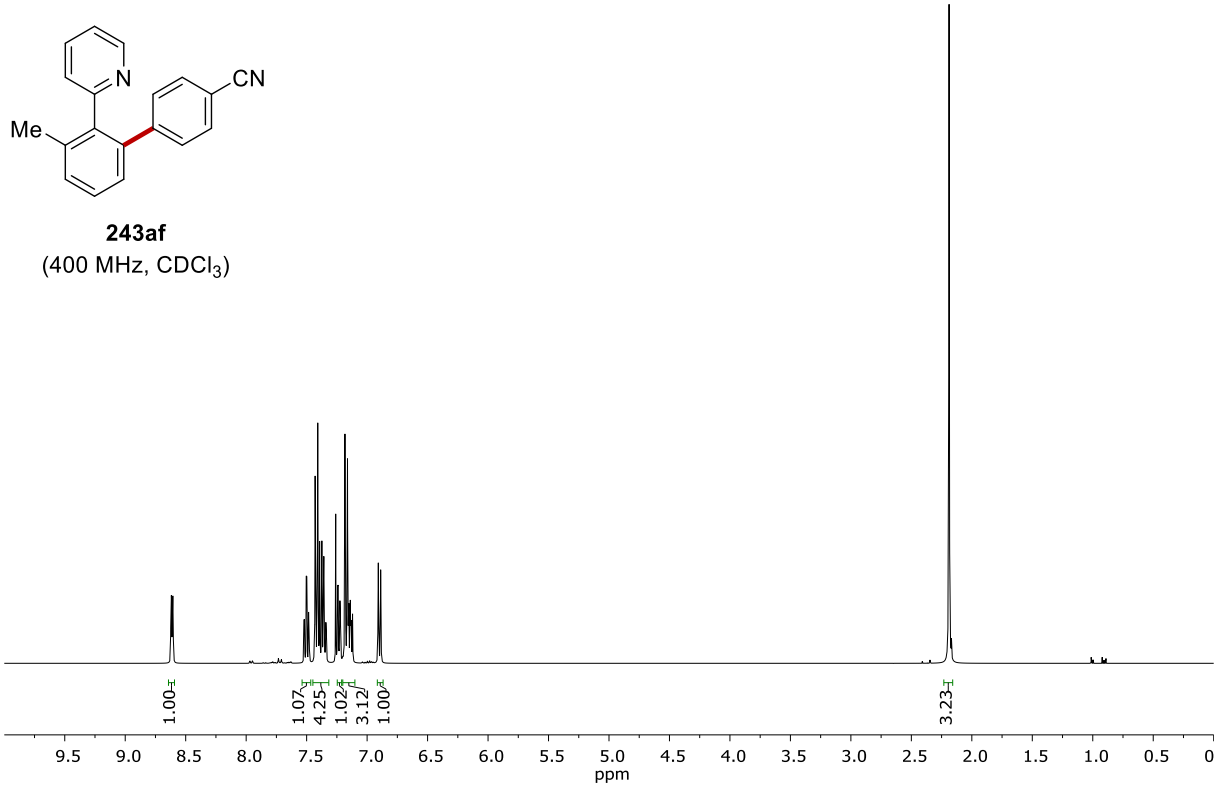

243af
(400 MHz, $CDCl_3$)

243af
(100 MHz, $CDCl_3$)

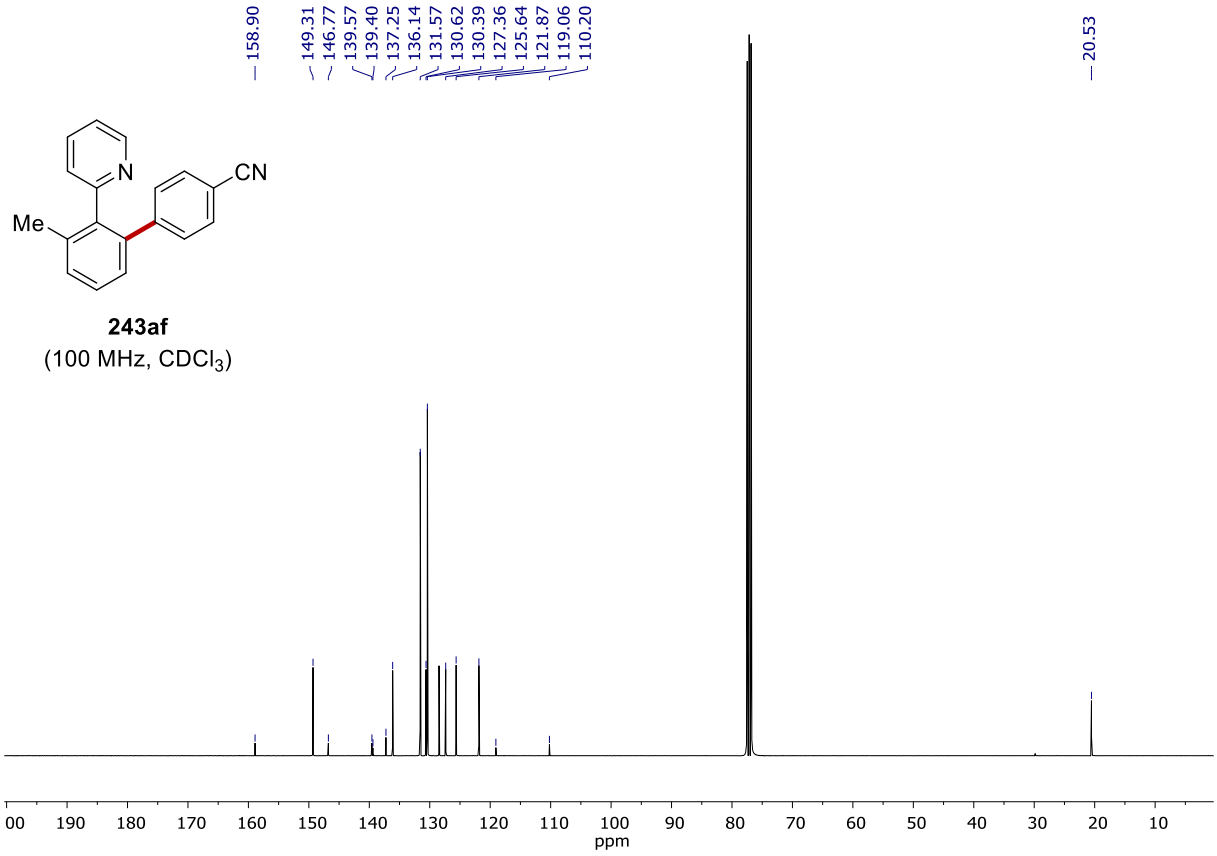

243ag
(300 MHz, $CDCl_3$)

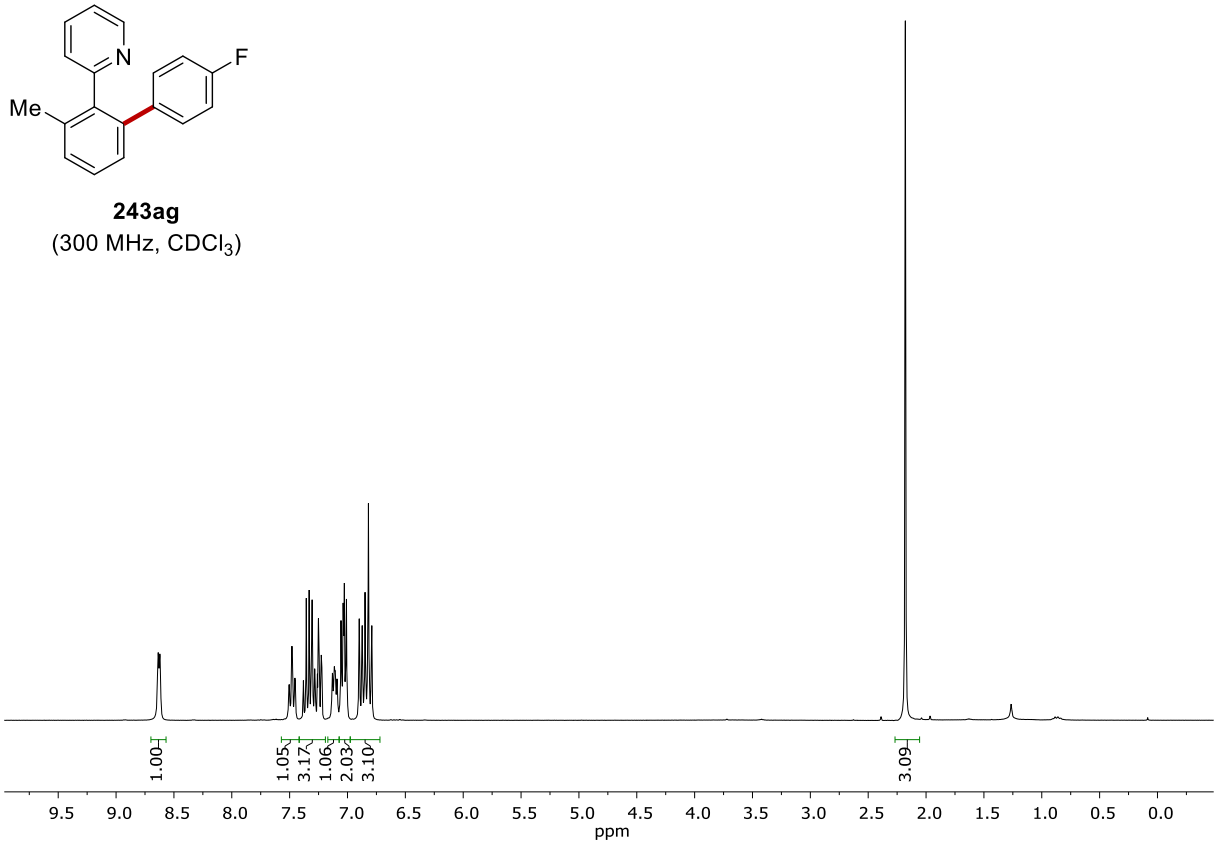

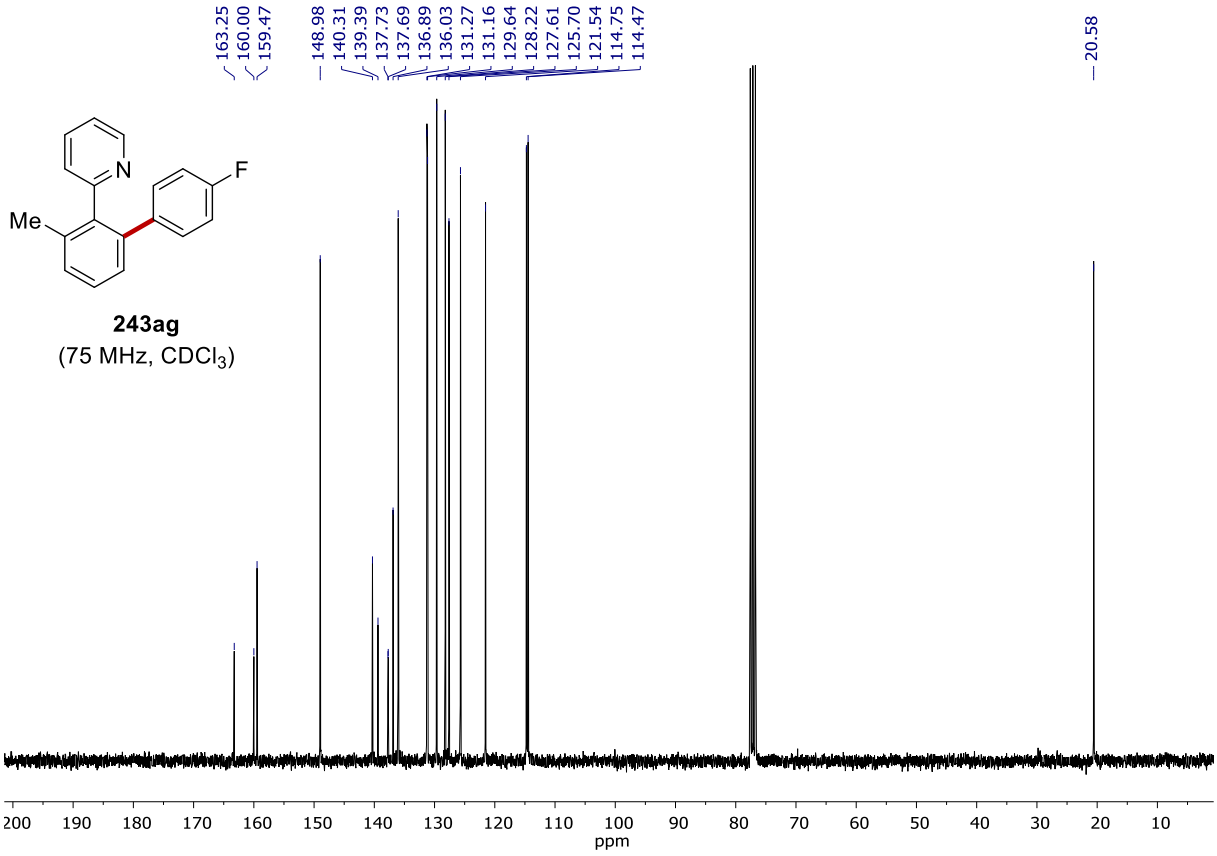

243ag
(75 MHz, $CDCl_3$)

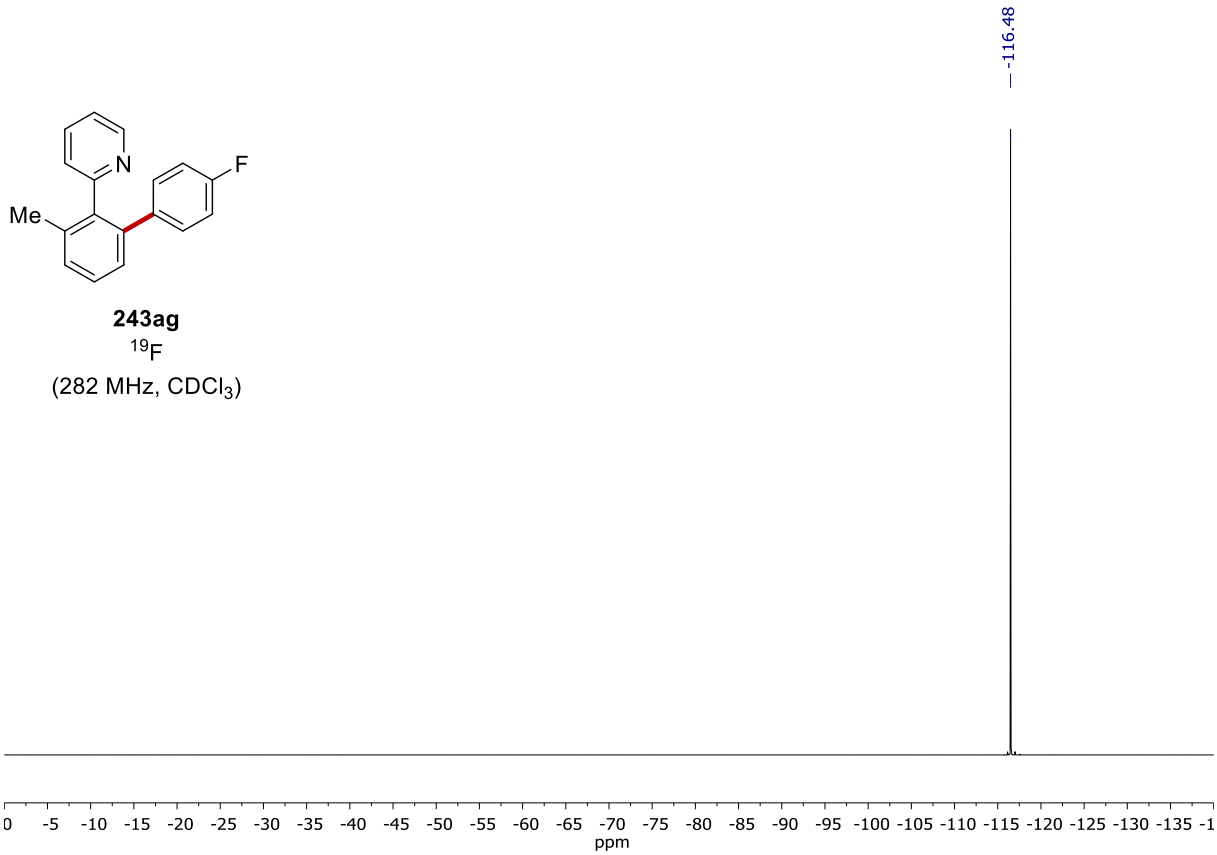

243ag
^{19}F
(282 MHz, $CDCl_3$)

243ai
(400 MHz, $CDCl_3$)

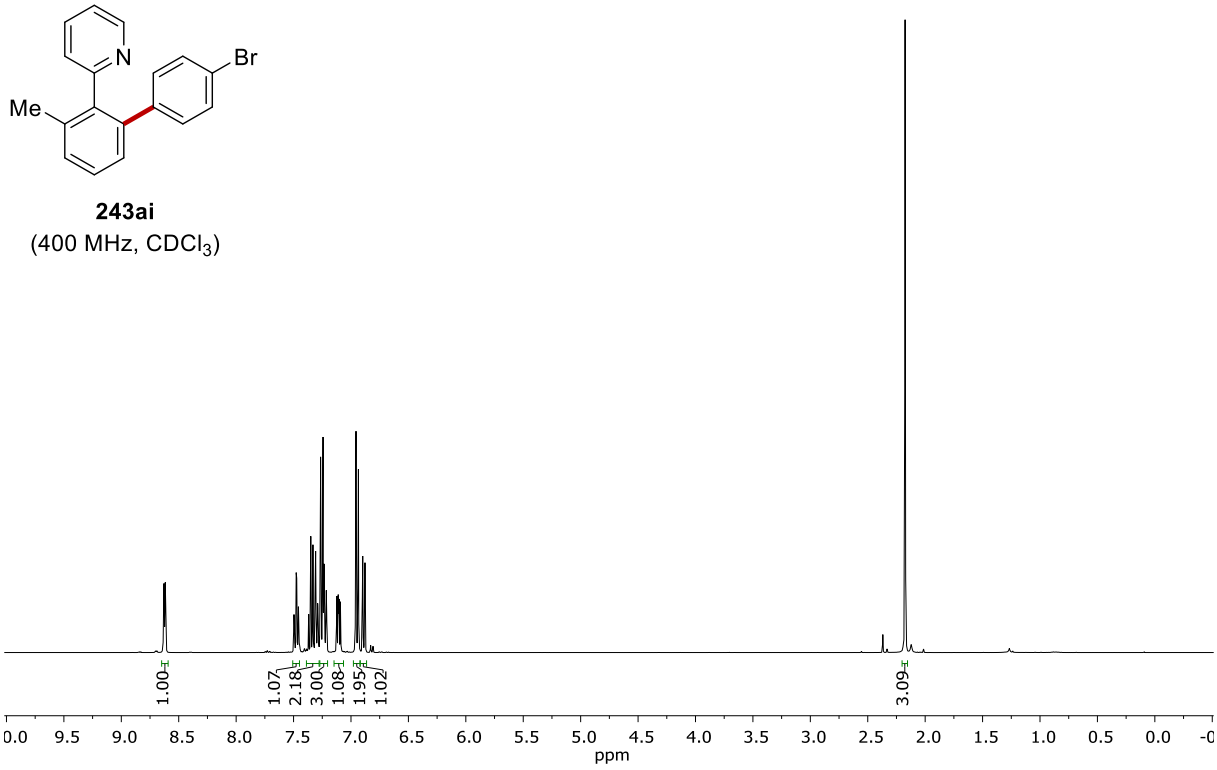

243ai
(100 MHz, $CDCl_3$)

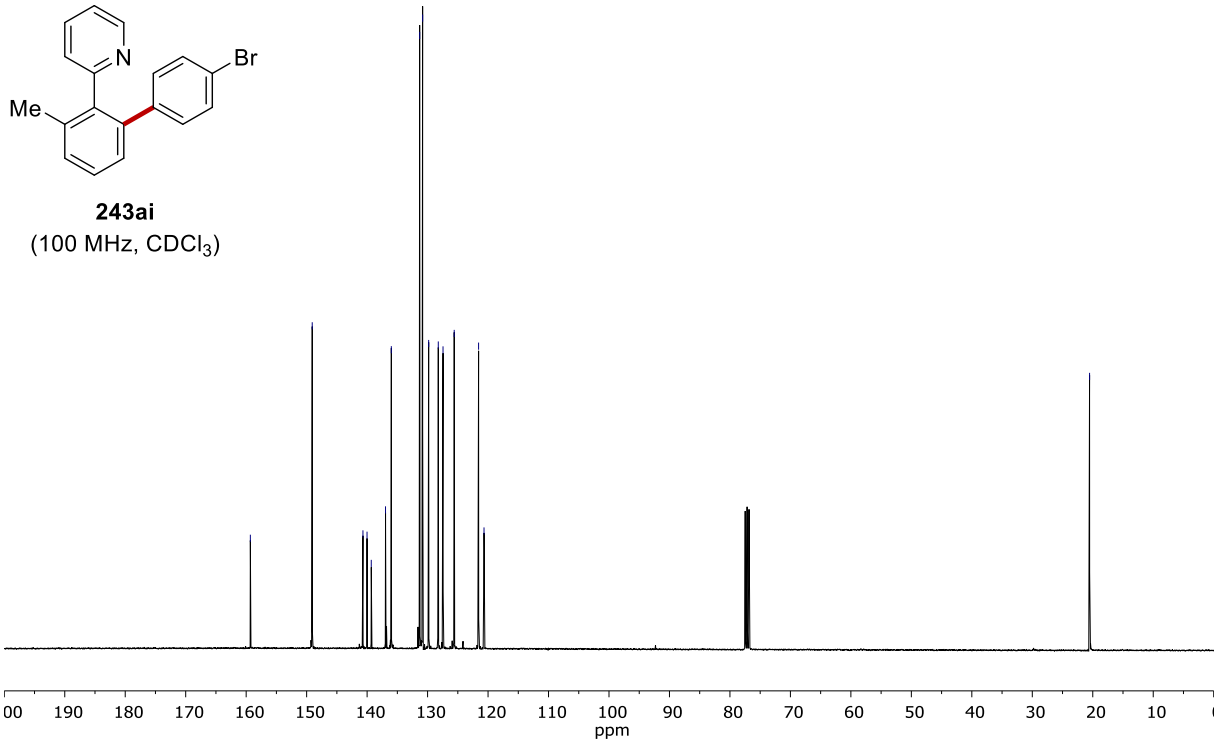

243aj
(300 MHz, $CDCl_3$)

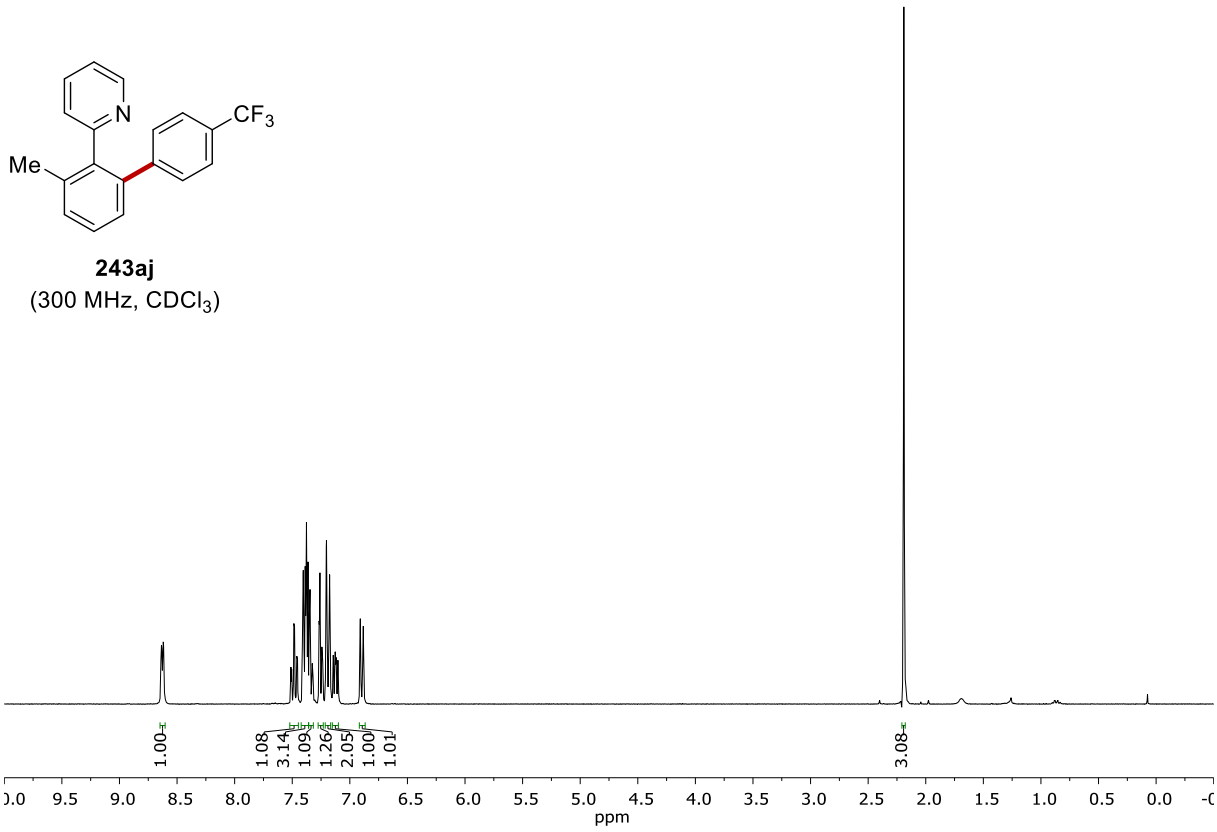

243aj
(100 MHz, $CDCl_3$)

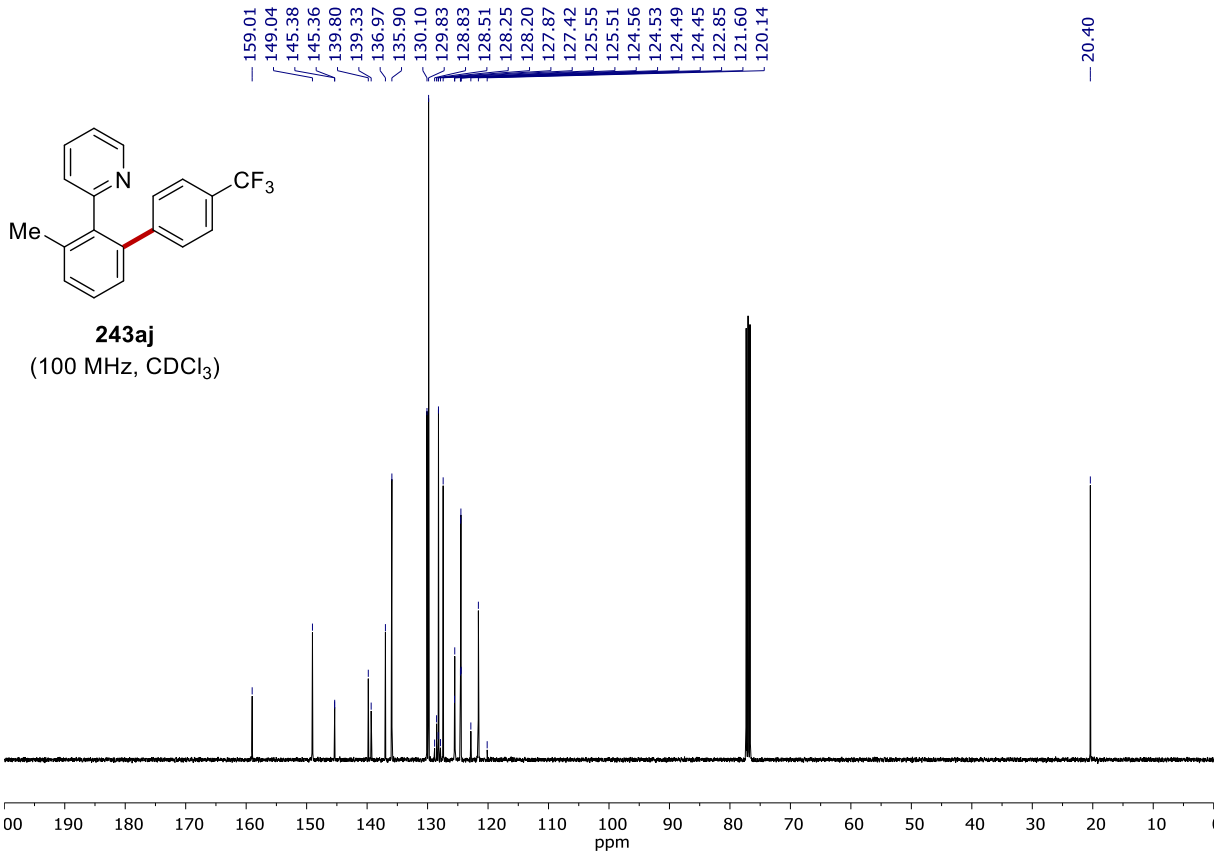

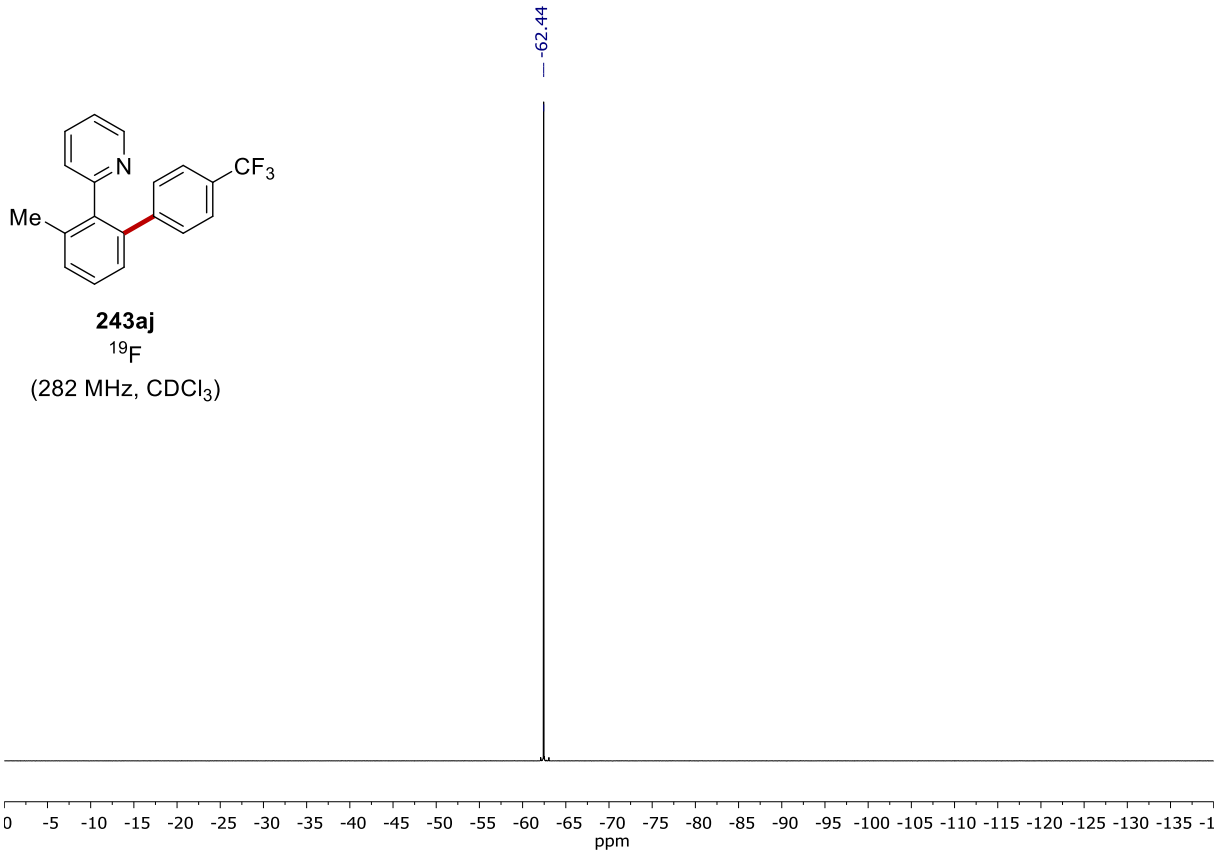

243aj

^{19}F

(282 MHz, $CDCl_3$)

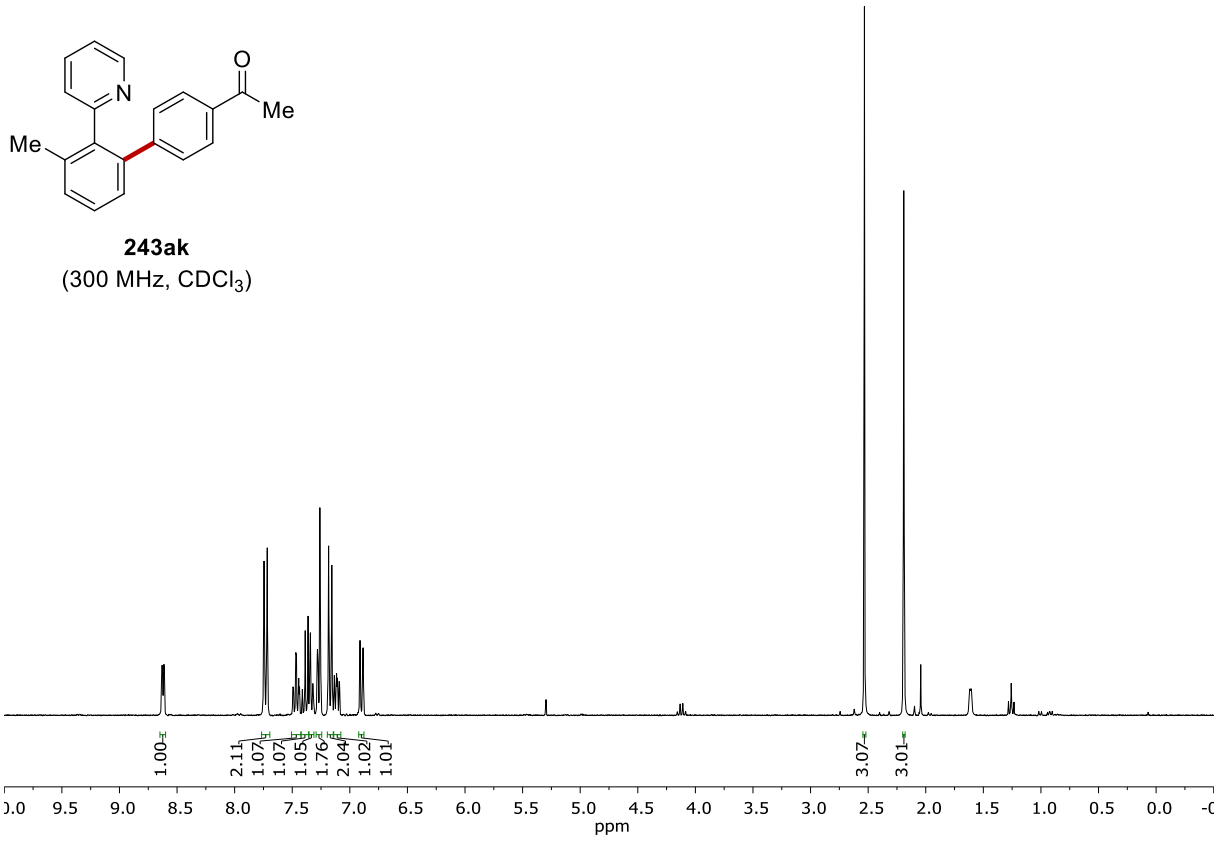

243ak

(300 MHz, $CDCl_3$)

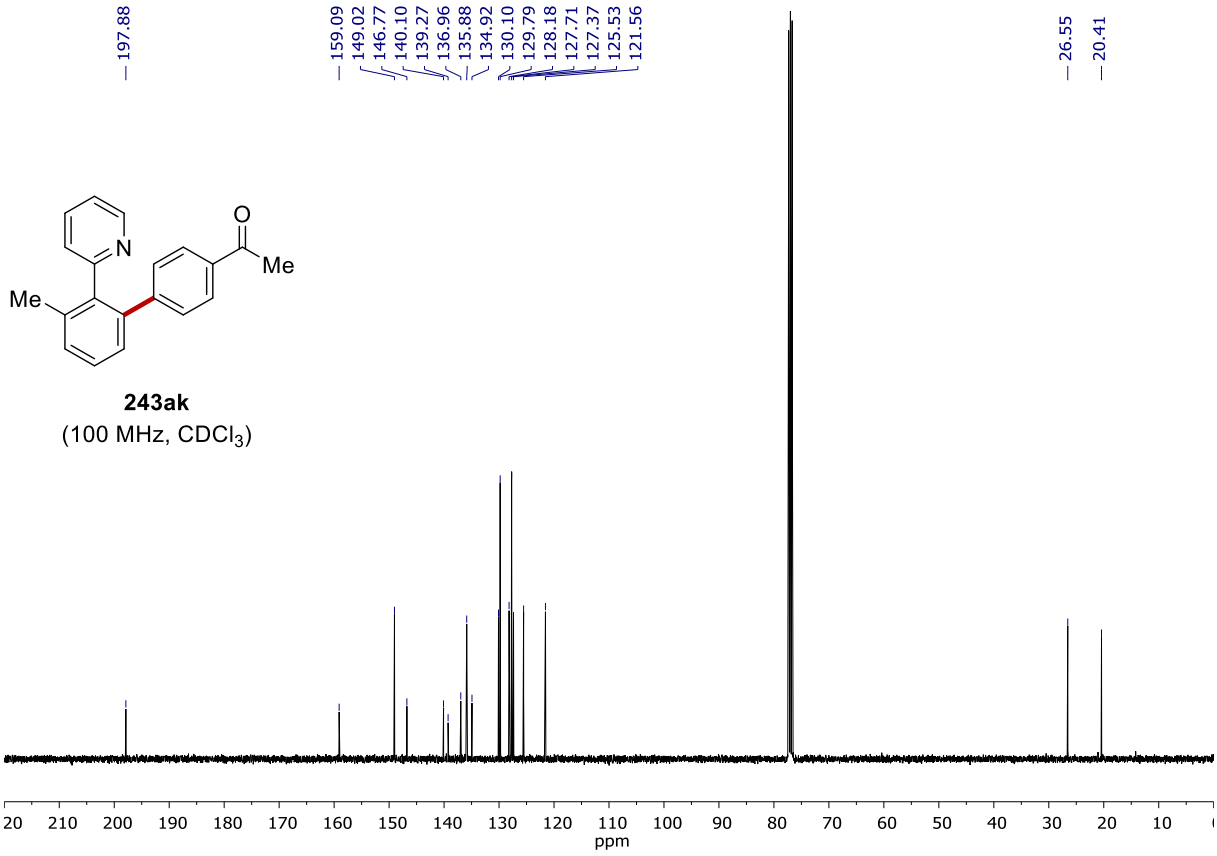

243ak
(100 MHz, $CDCl_3$)

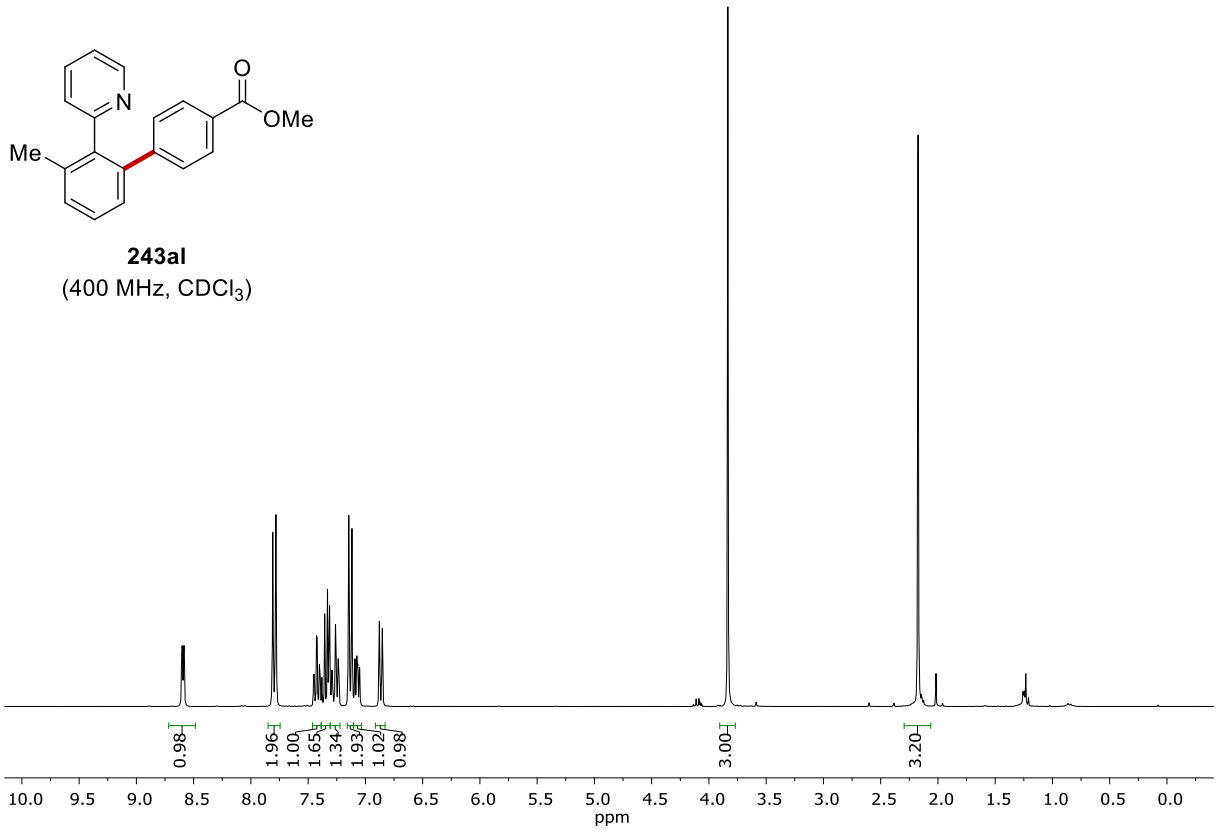

243al
(400 MHz, $CDCl_3$)

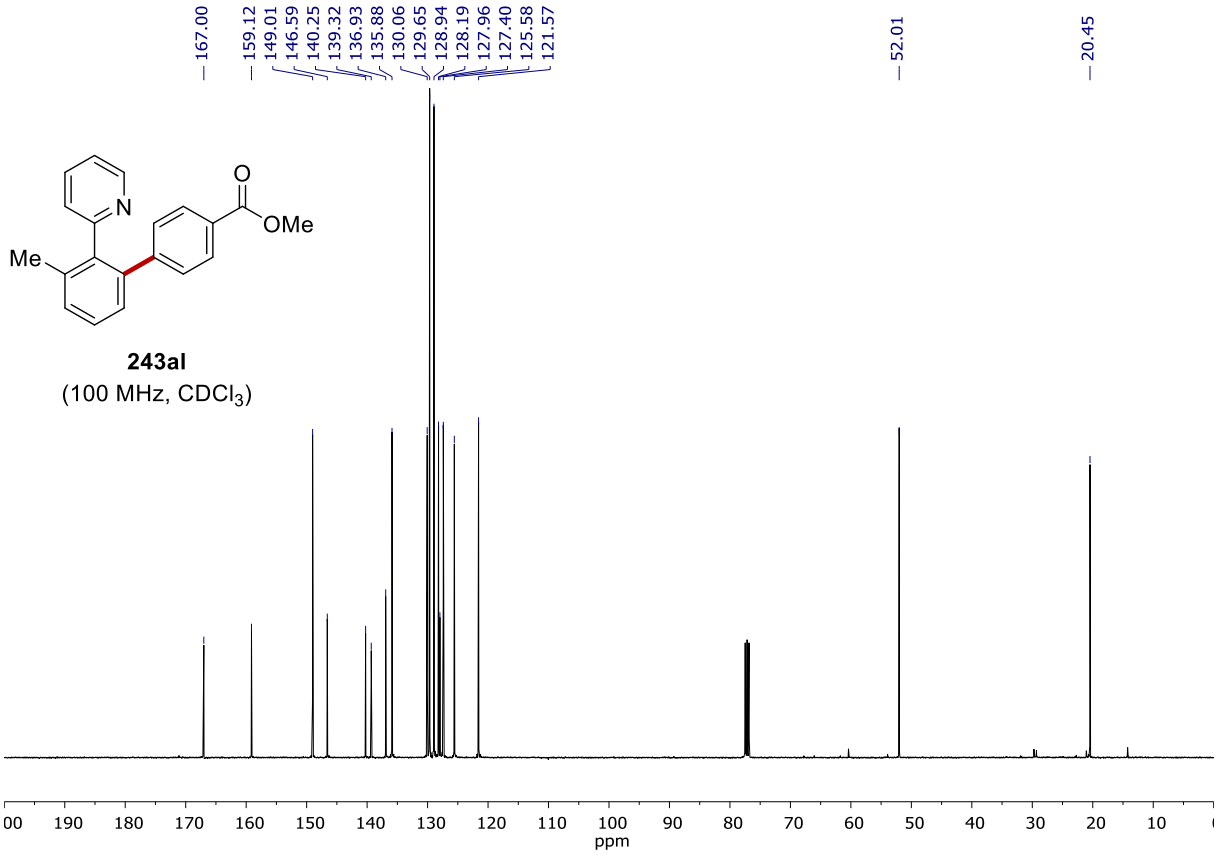

243al
(100 MHz, $CDCl_3$)

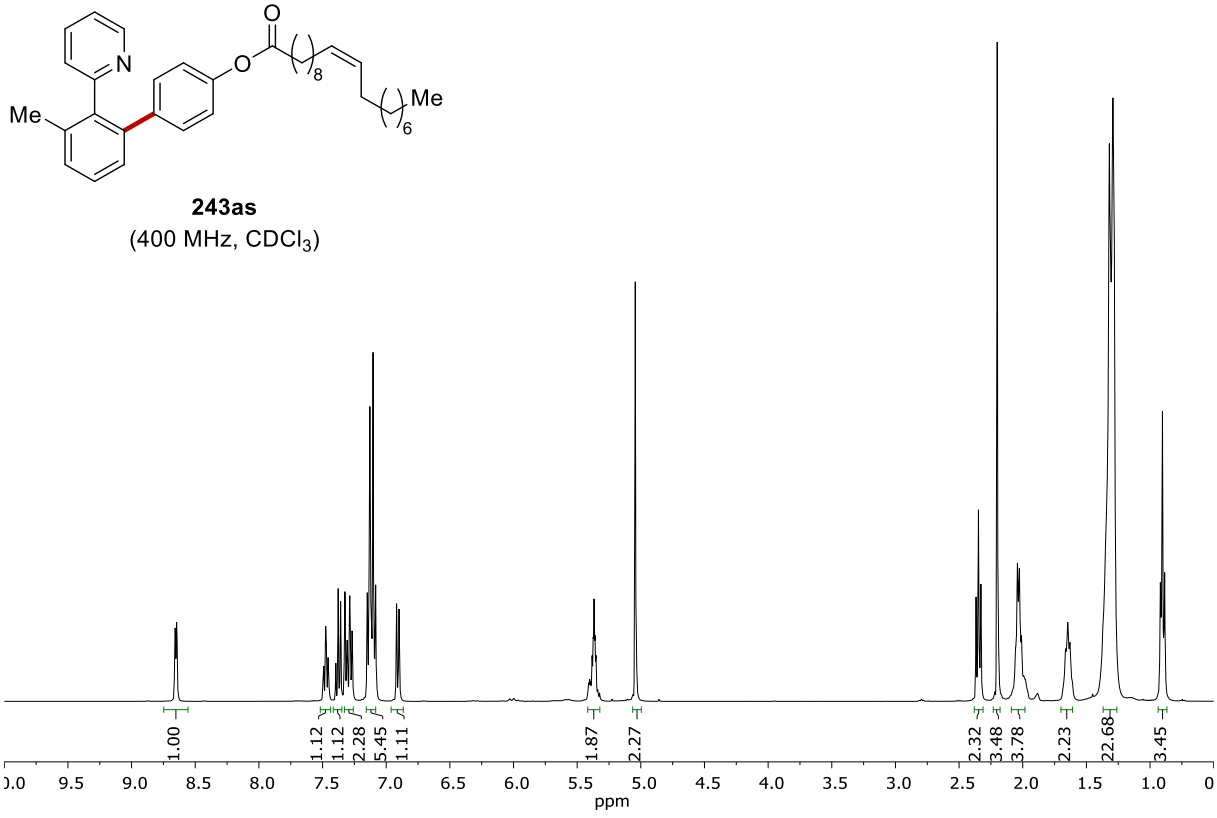

243as
(400 MHz, $CDCl_3$)

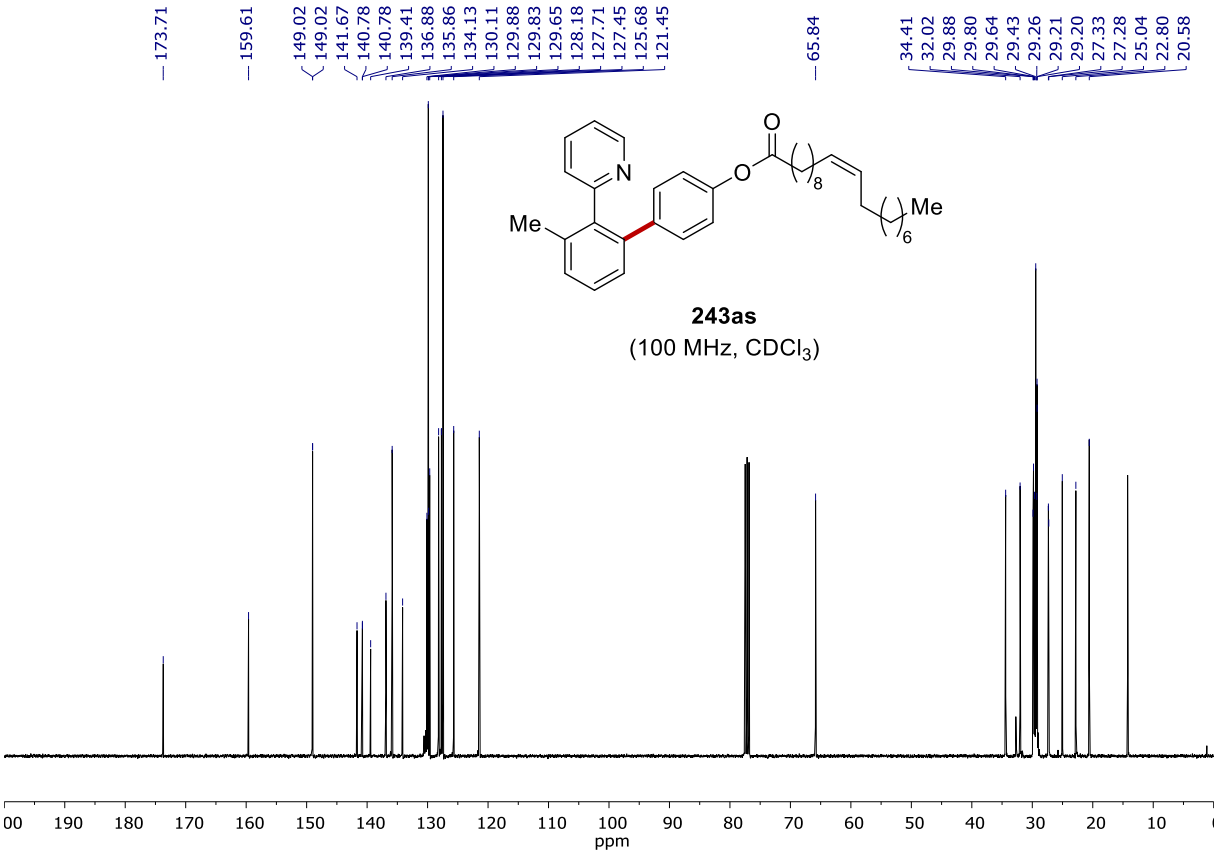
173.71
159.61
149.02
149.02
141.67
140.78
140.78
139.41
136.88
135.86
134.13
130.11
129.88
129.83
129.65
128.18
127.71
127.45
125.68
121.45
65.84
34.41
32.02
29.88
29.80
29.64
29.43
29.26
29.21
29.20
27.33
27.28
25.04
22.80
20.58
N
O
O
8
Me
Me
6
243as
(100 MHz, CDCl3)
00 190 180 170 160 150 140 130 120 110 100 90 80 70 60 50 40 30 20 10
ppm

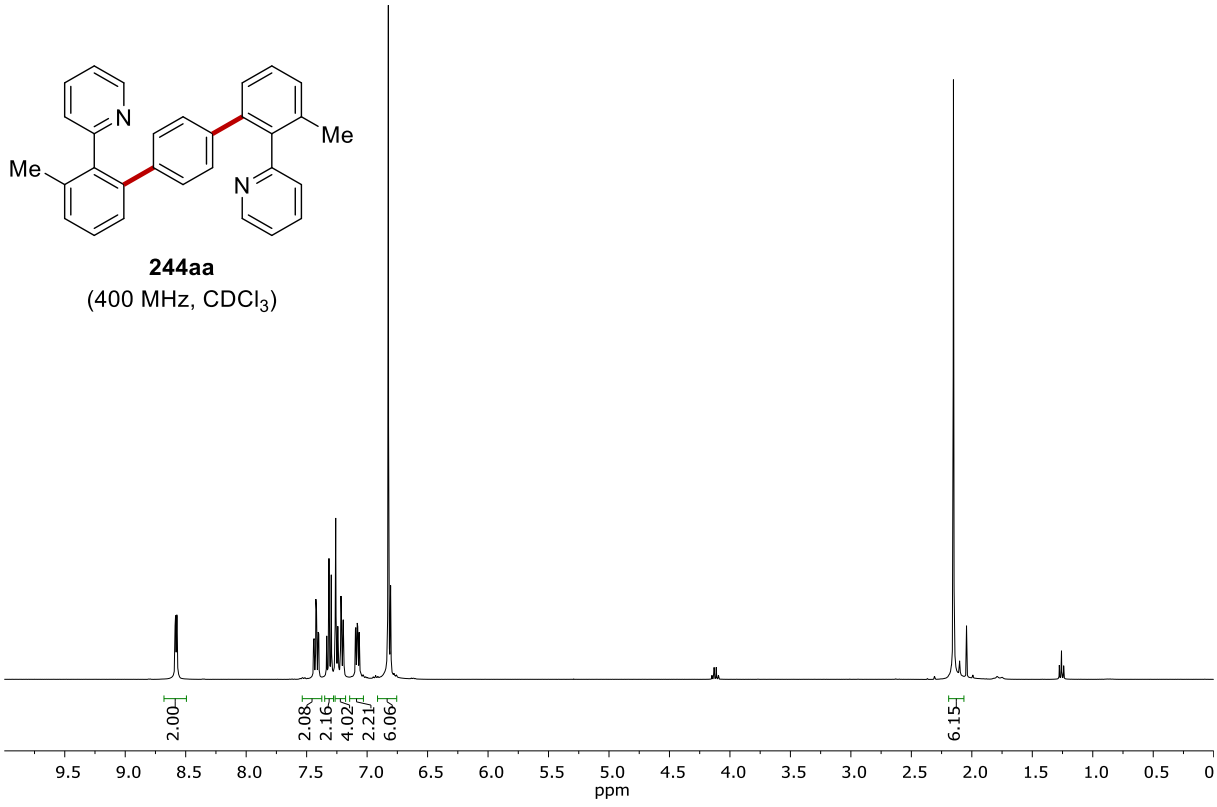
N
Me
Me
N
244aa
(400 MHz, CDCl3)
2.00
2.08
2.16
4.02
2.21
6.06
6.15
9.5 9.0 8.5 8.0 7.5 7.0 6.5 6.0 5.5 5.0 4.5 4.0 3.5 3.0 2.5 2.0 1.5 1.0 0.5 0
ppm

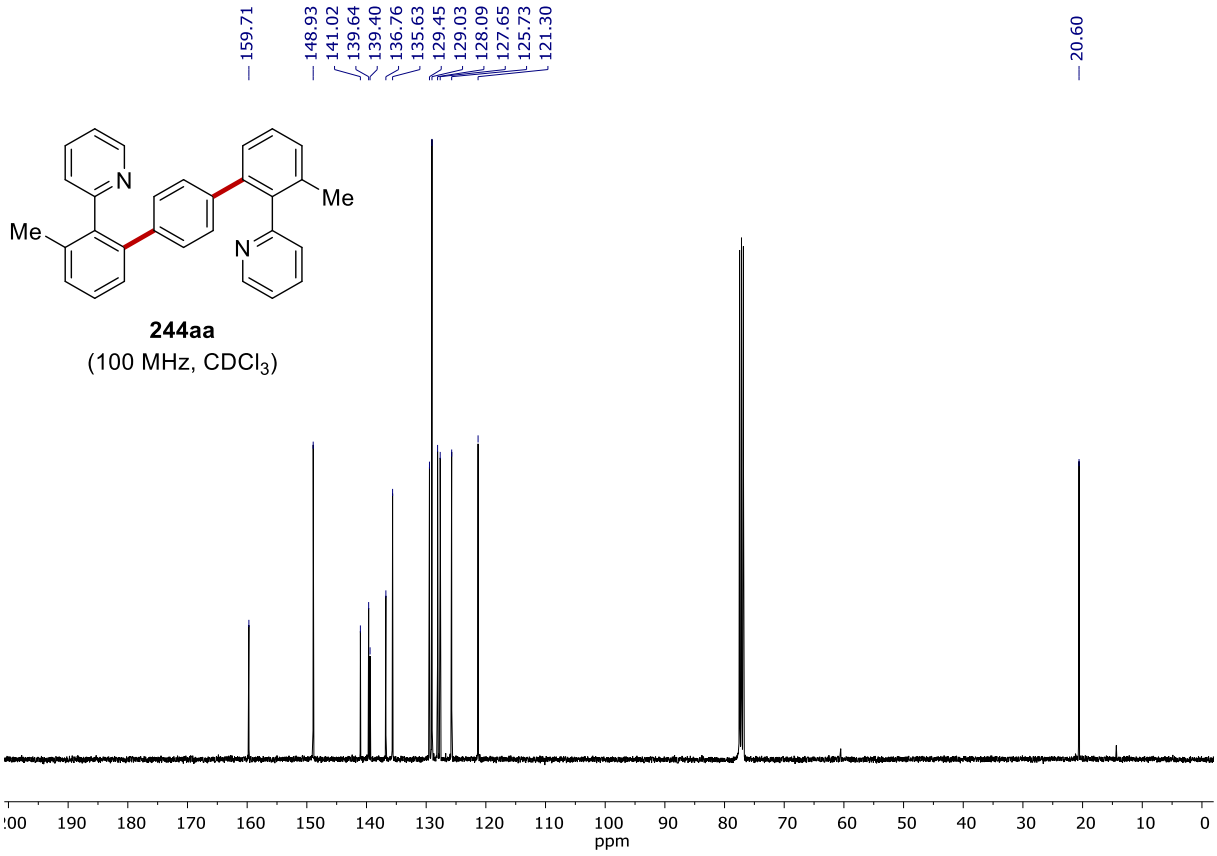
159.71
148.93
141.02
139.64
139.40
136.76
135.63
129.45
129.03
128.09
127.65
125.73
121.30
20.60
N
Me
Me
N
244aa
(100 MHz, CDCl3)
ppm

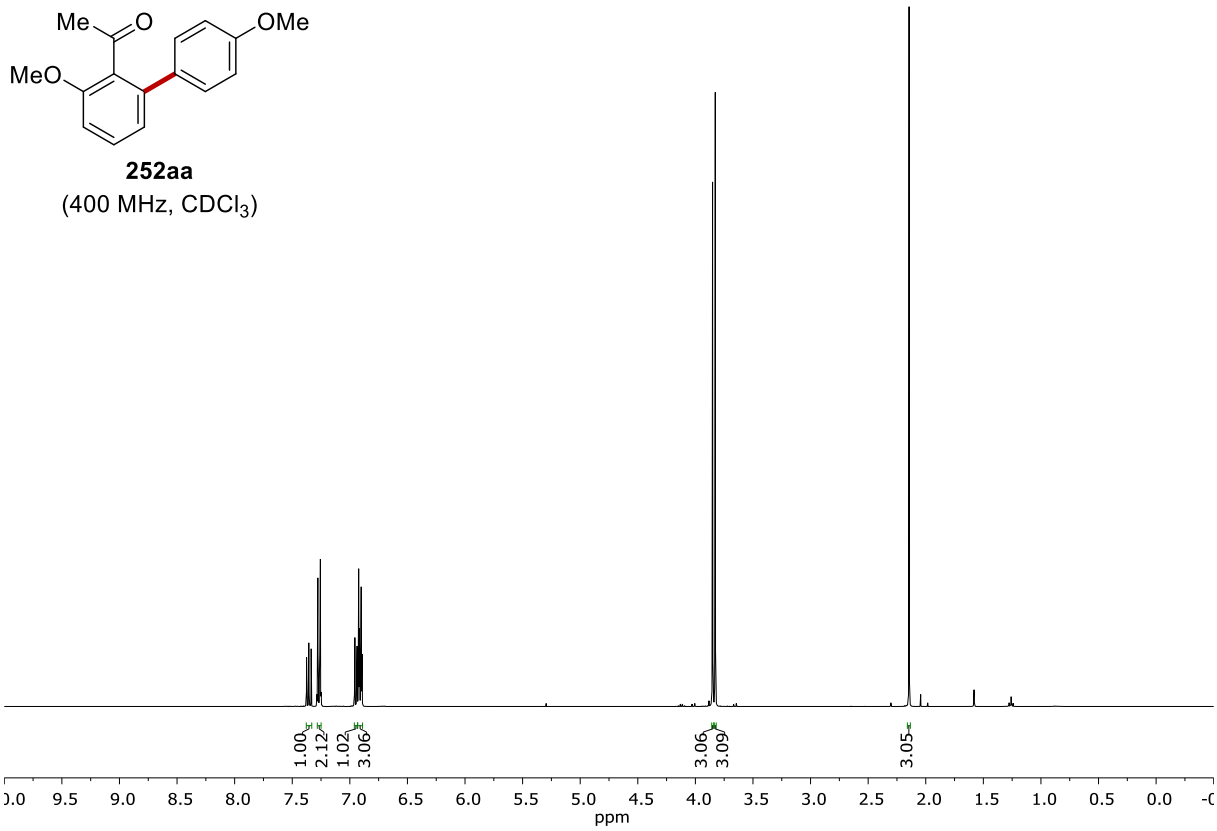
Me
O
OMe
MeO
252aa
(400 MHz, CDCl3)
1.00
2.12
1.02
3.06
3.06
3.09
3.05
ppm

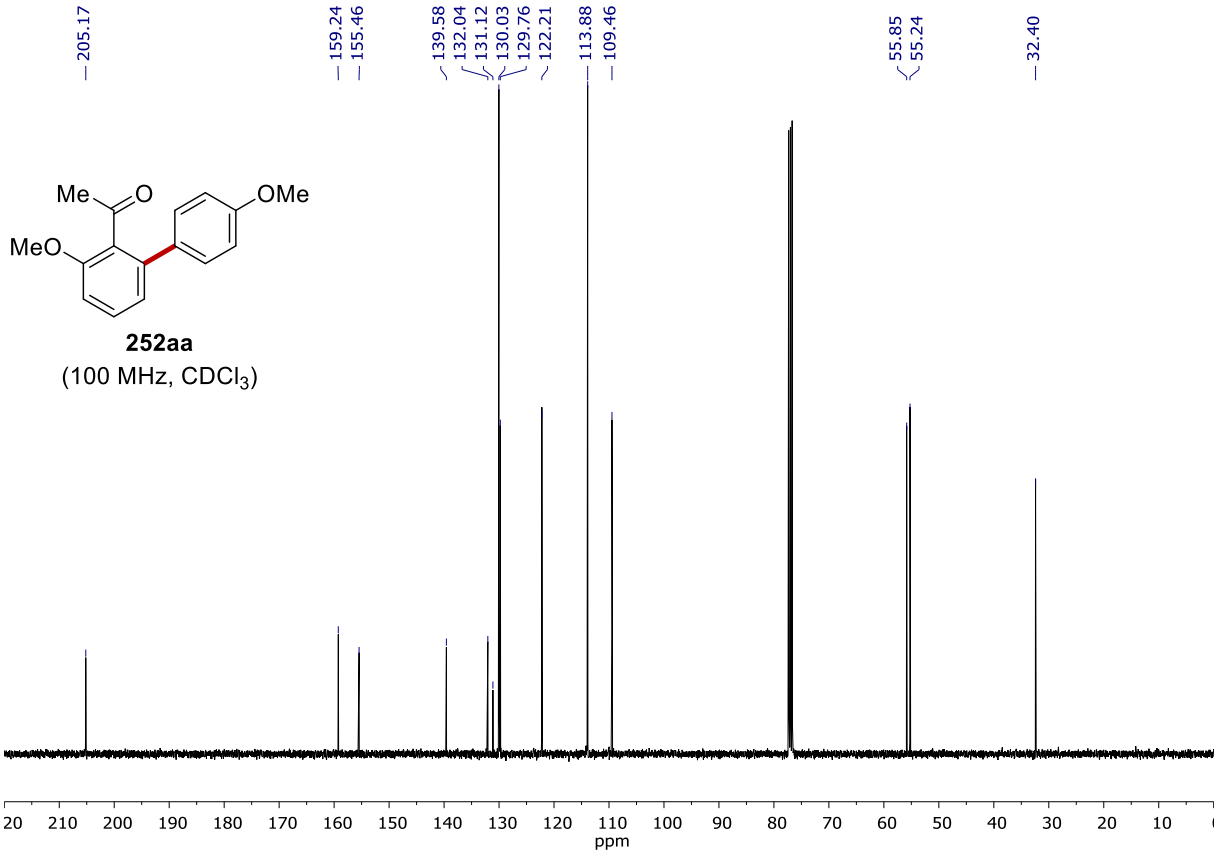

252aa
(100 MHz, $CDCl_3$)

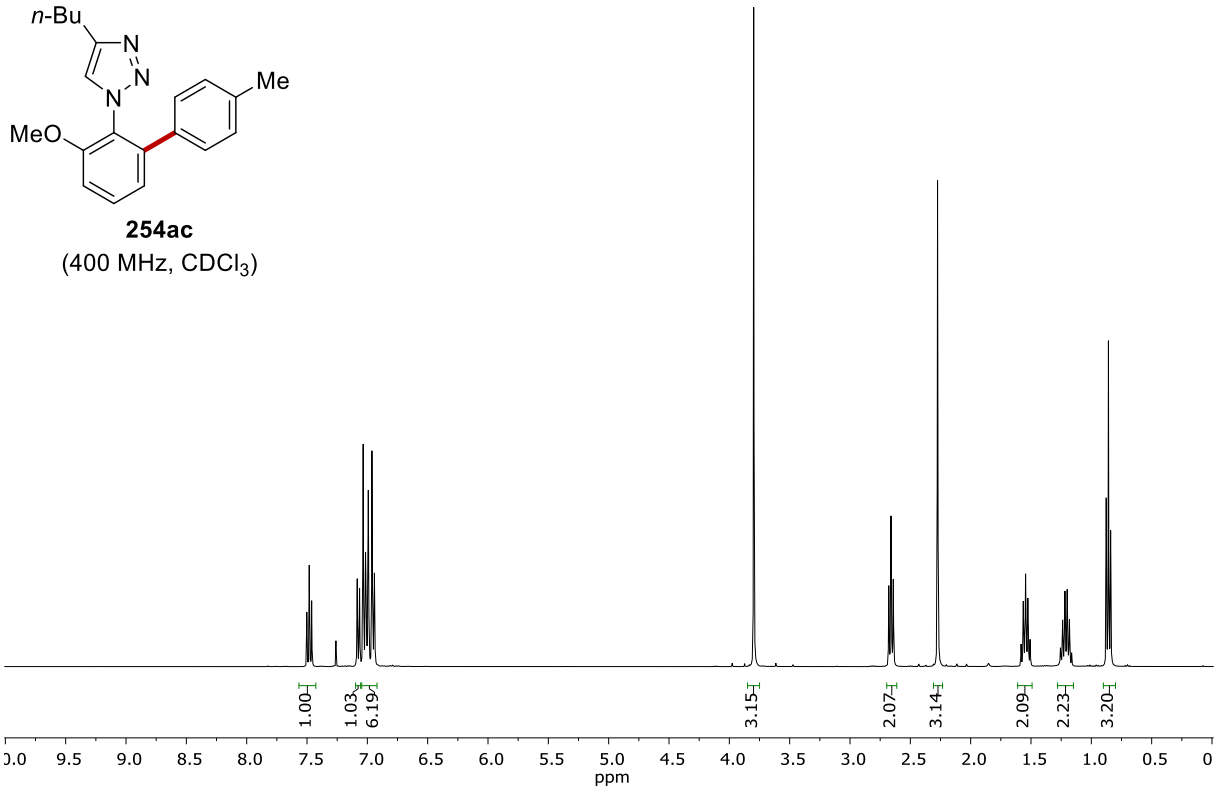

254ac
(400 MHz, $CDCl_3$)

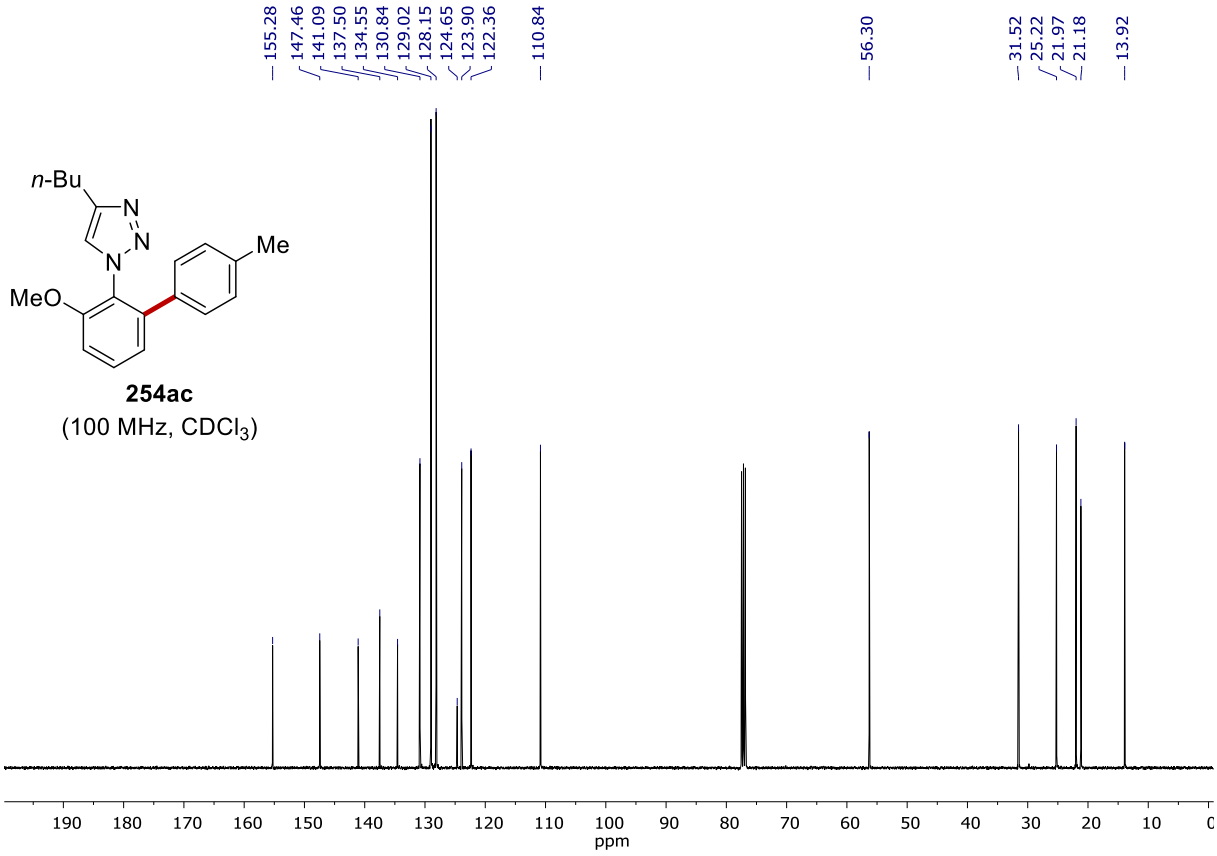

254ac
(100 MHz, $CDCl_3$)

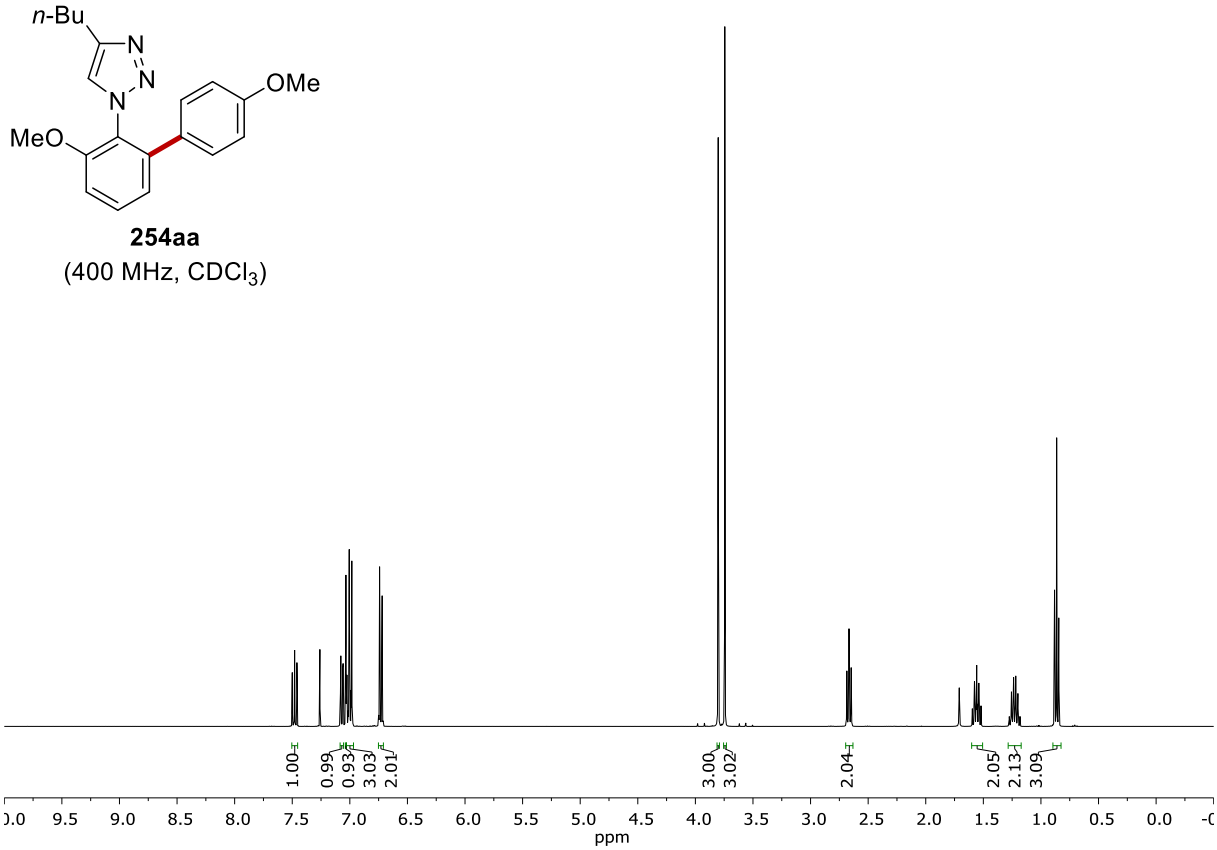

254aa
(400 MHz, $CDCl_3$)

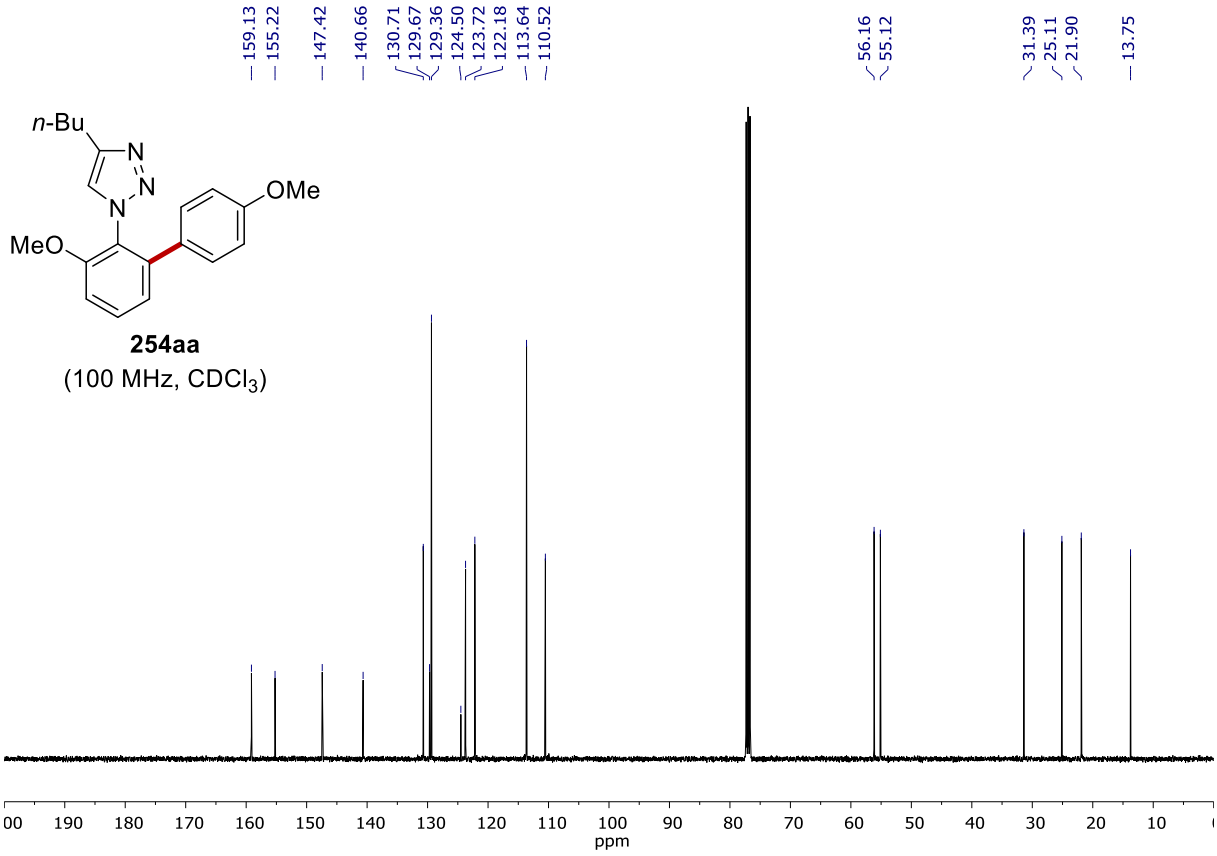

254aa
(100 MHz, $CDCl_3$)

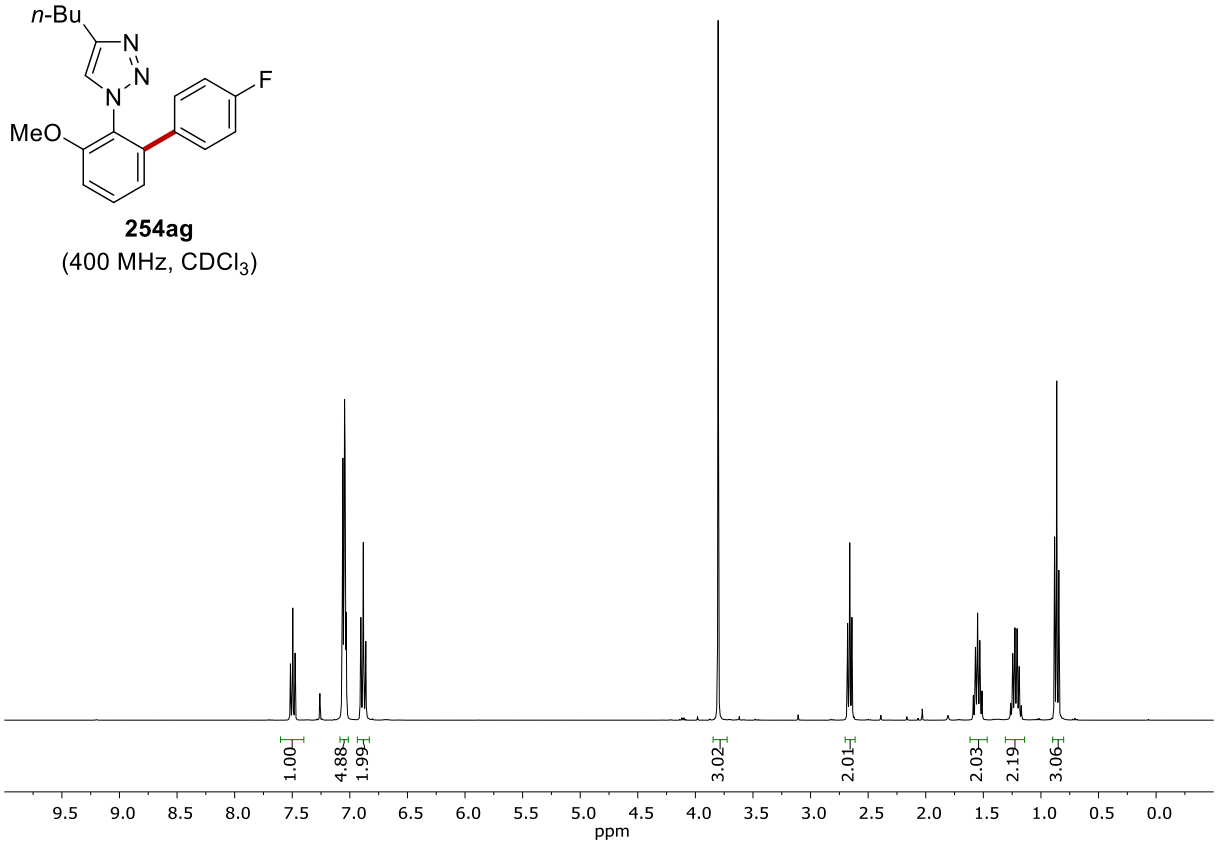

254ag
(400 MHz, $CDCl_3$)

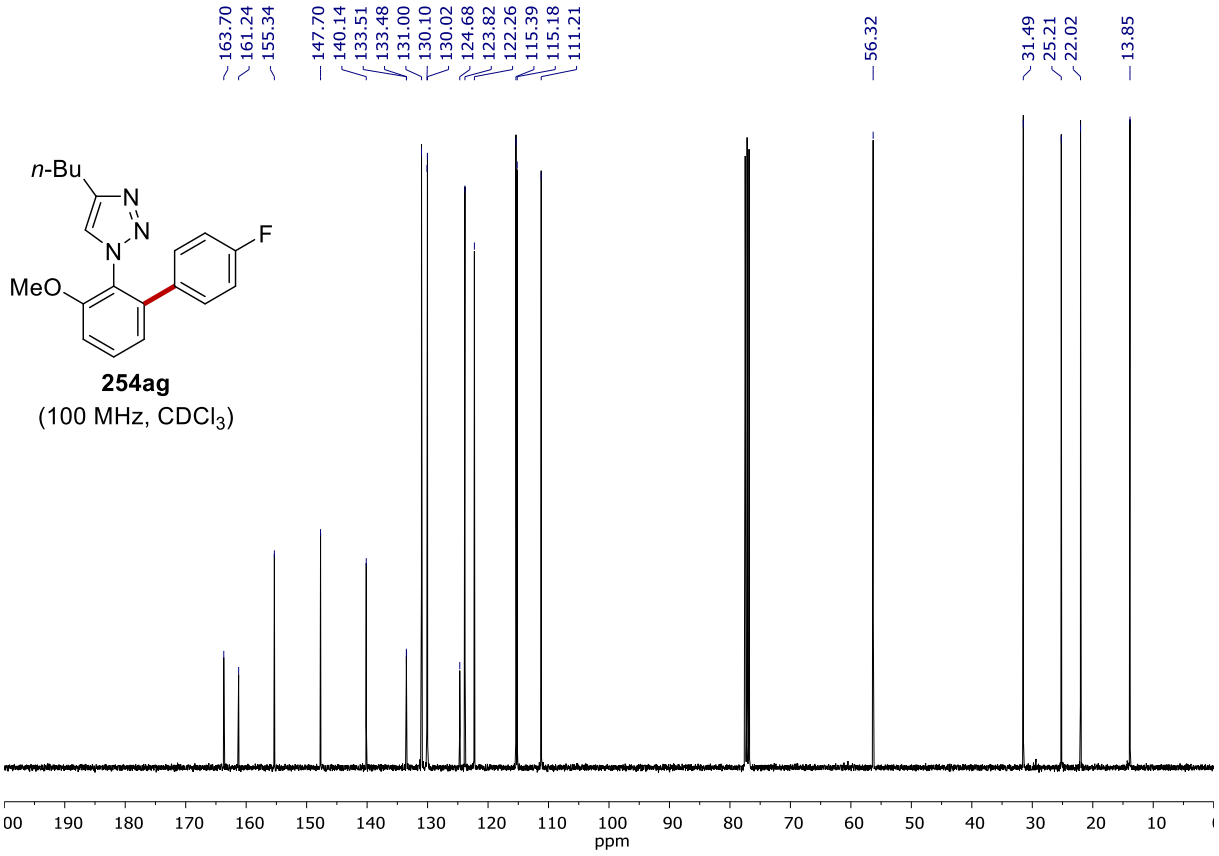

254ag
(100 MHz, $CDCl_3$)

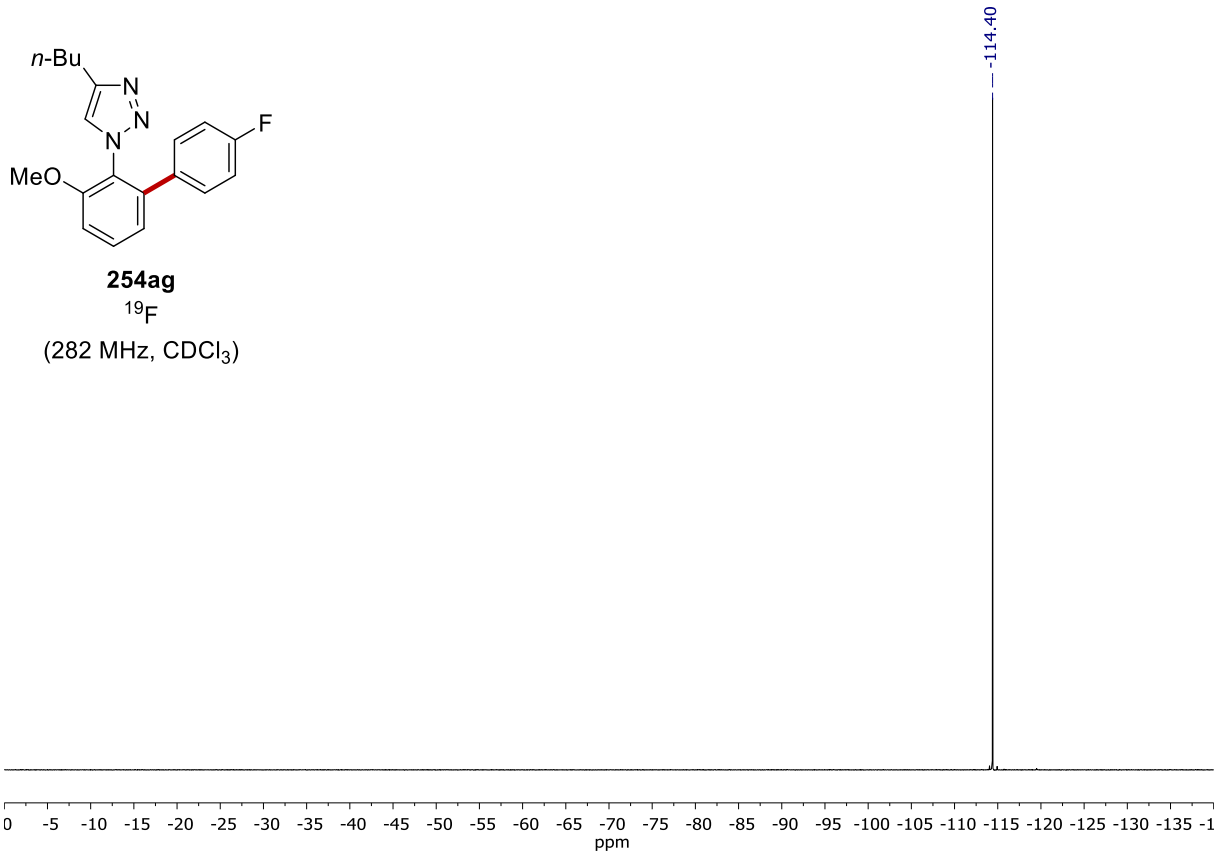

254ag
^{19}F
(282 MHz, $CDCl_3$)

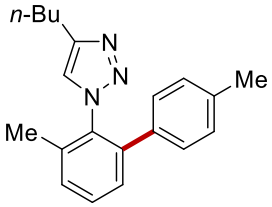

254bc
(400 MHz, $CDCl_3$)

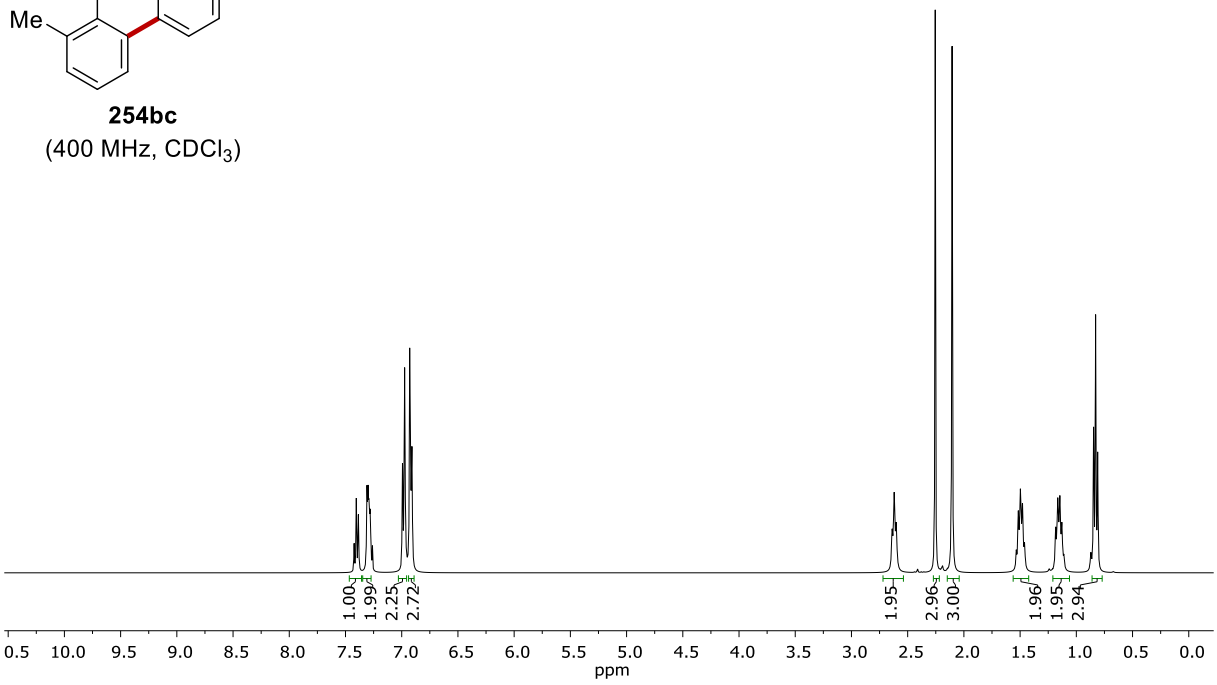

254bc
(100 MHz, $CDCl_3$)

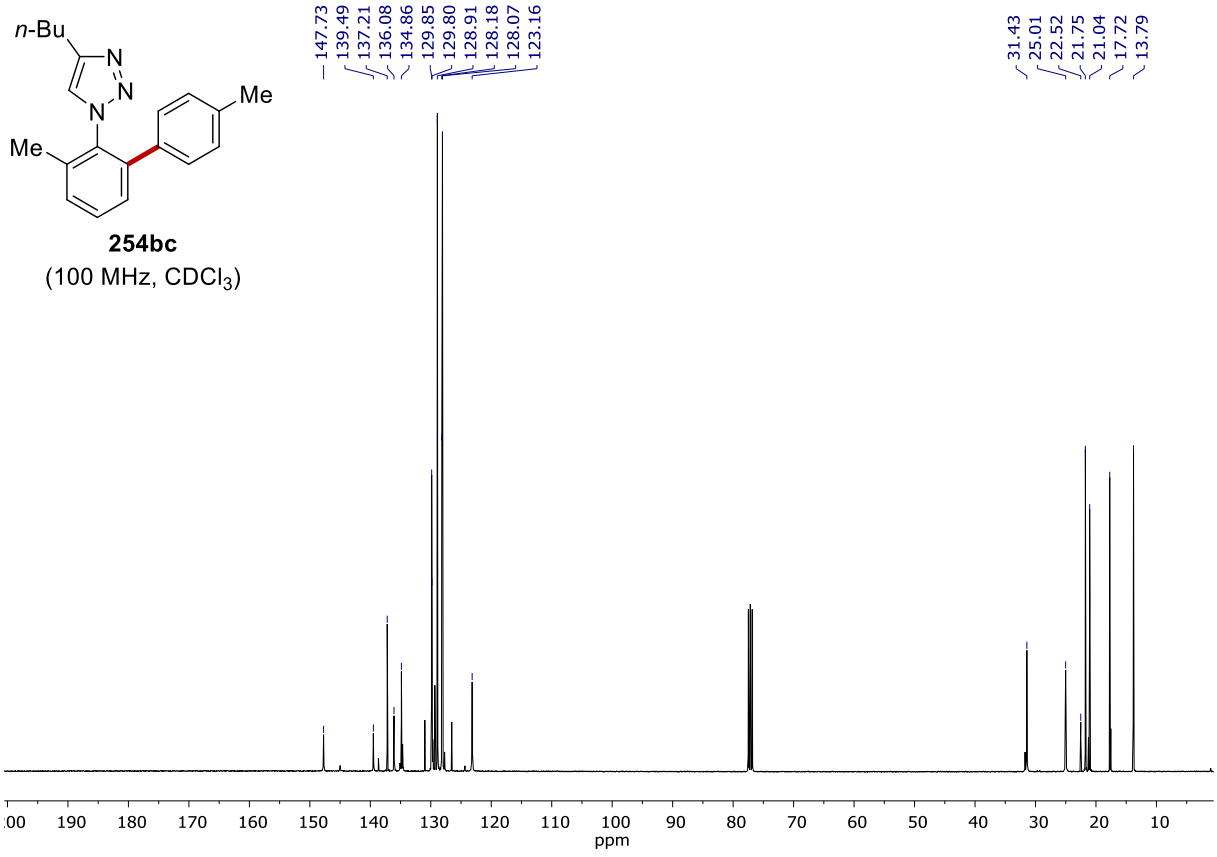

254ba

(400 MHz, $CDCl_3$)

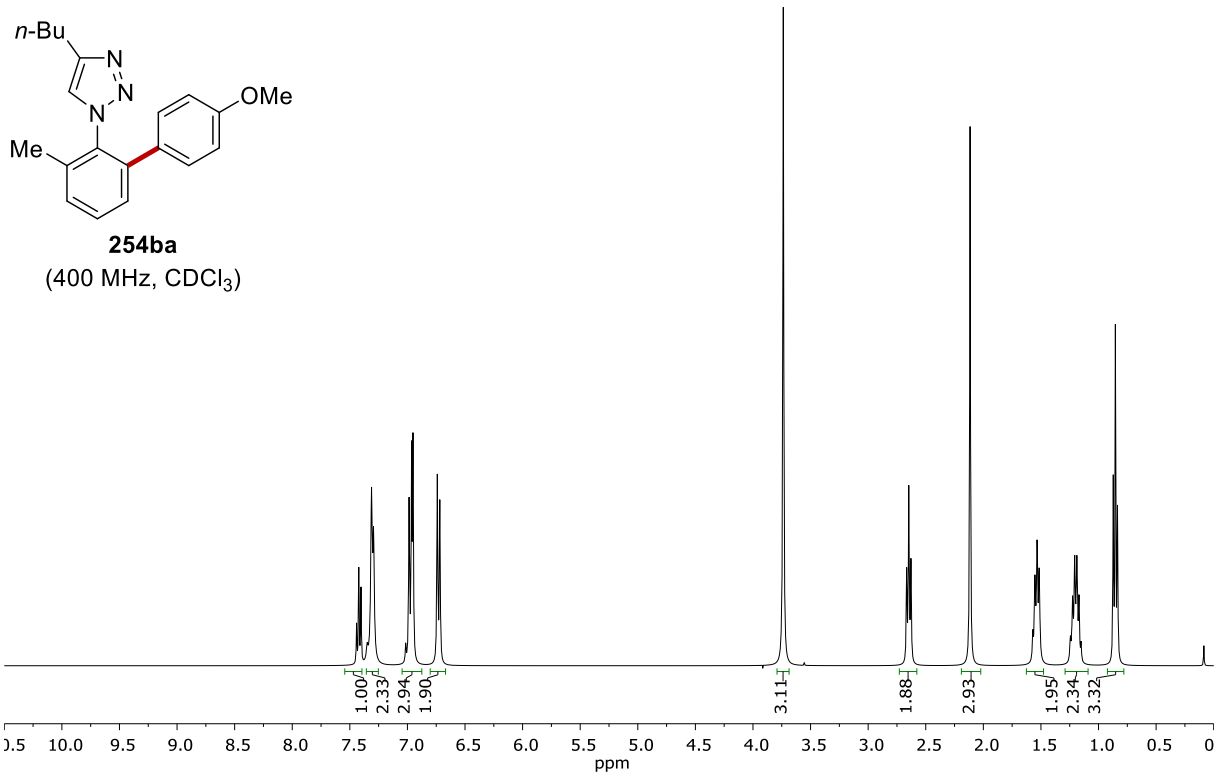

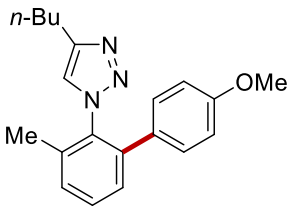

254ba

(100 MHz, $CDCl_3$)

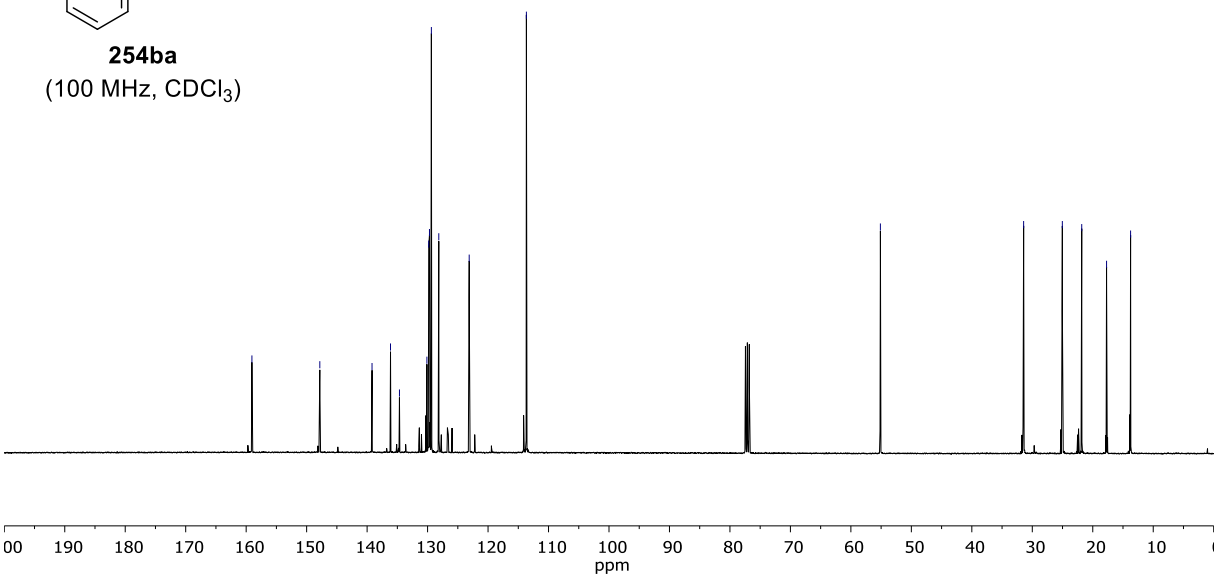

254bm
(400 MHz, $CDCl_3$)

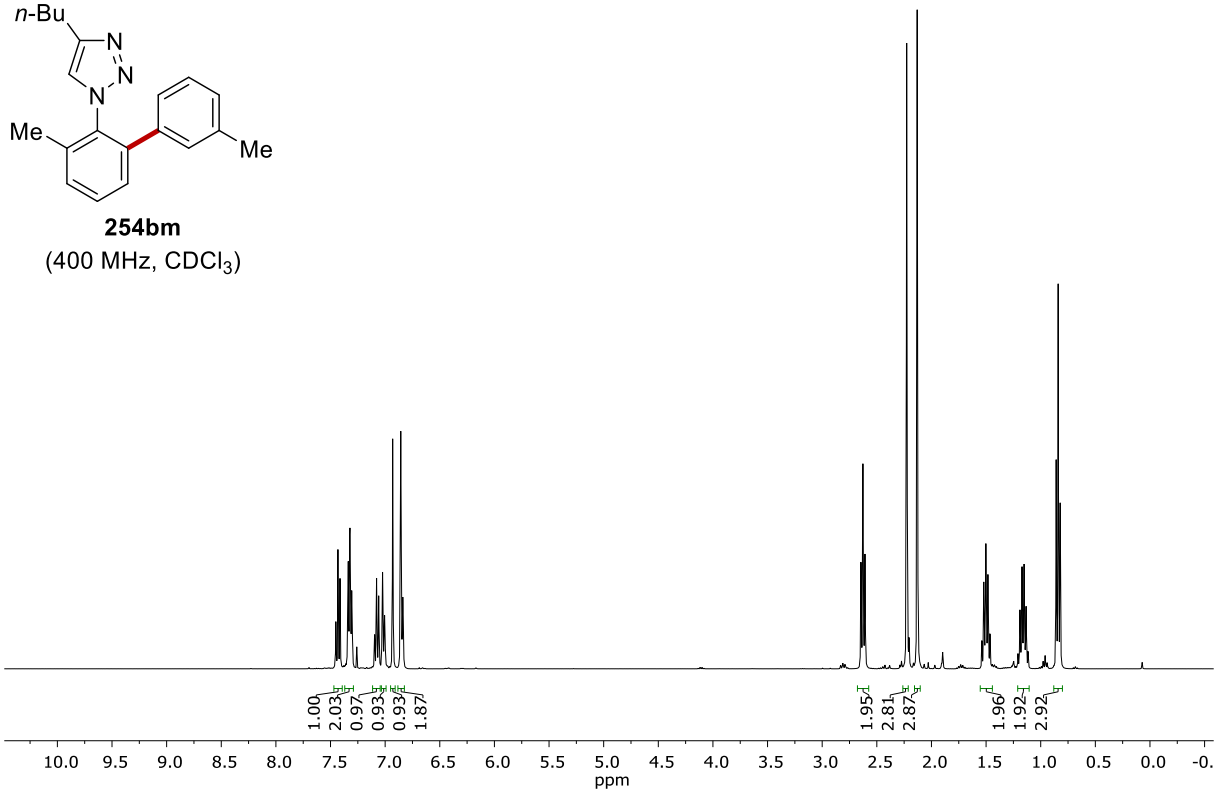

254bm
(100 MHz, $CDCl_3$)

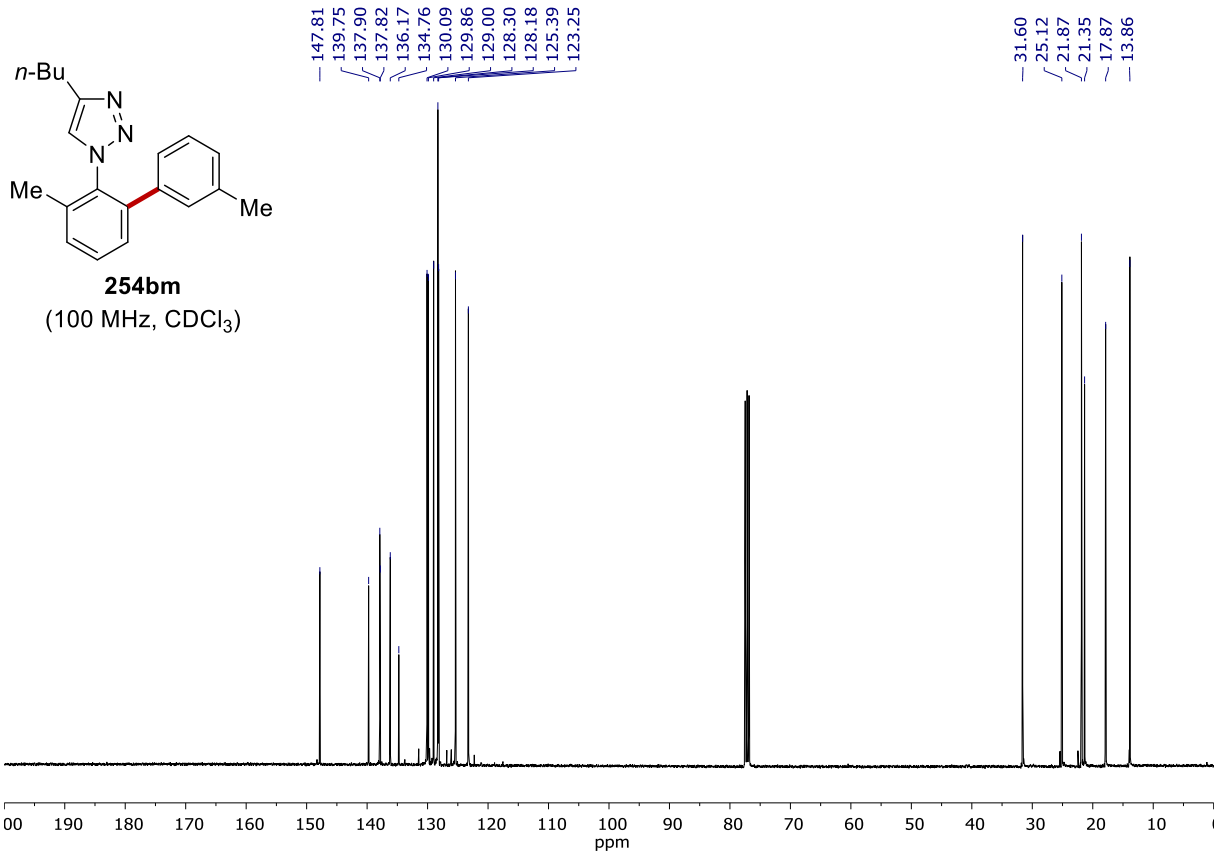

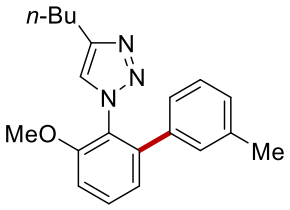

254am

(400 MHz, $CDCl_3$)

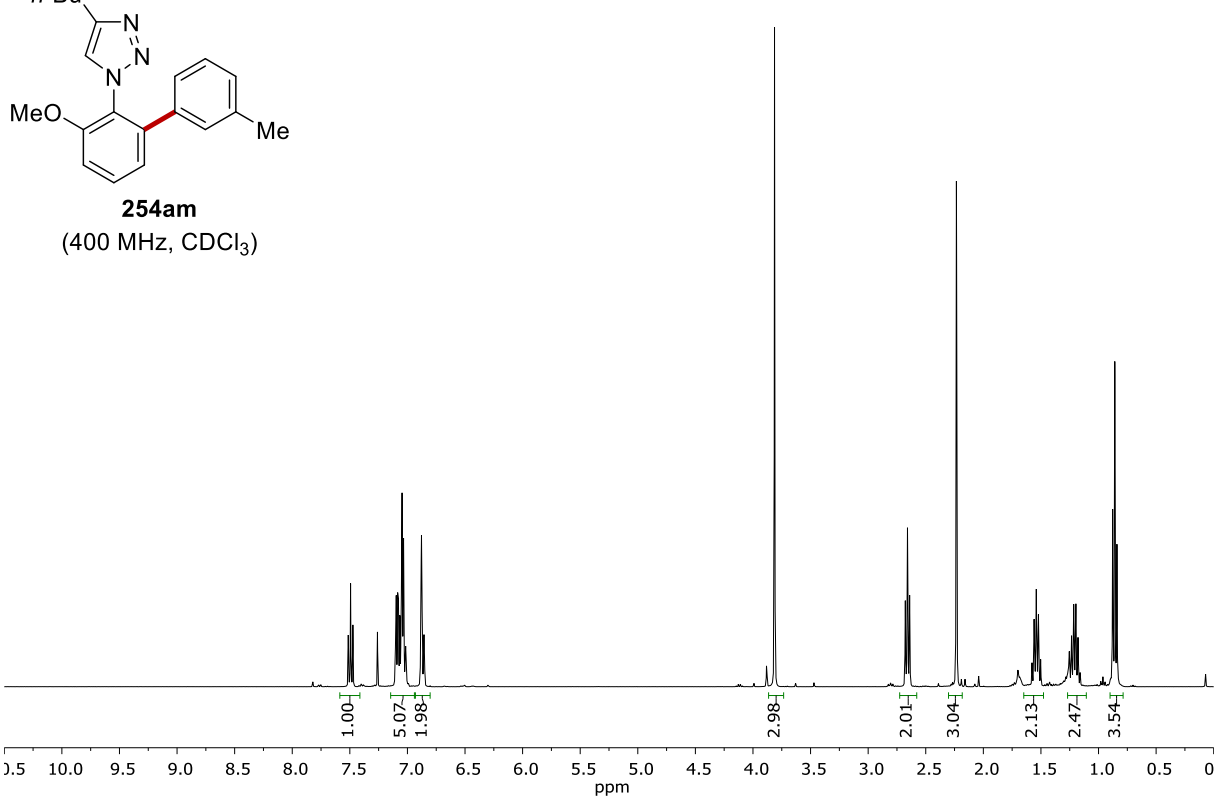

254am

(100 MHz, $CDCl_3$)

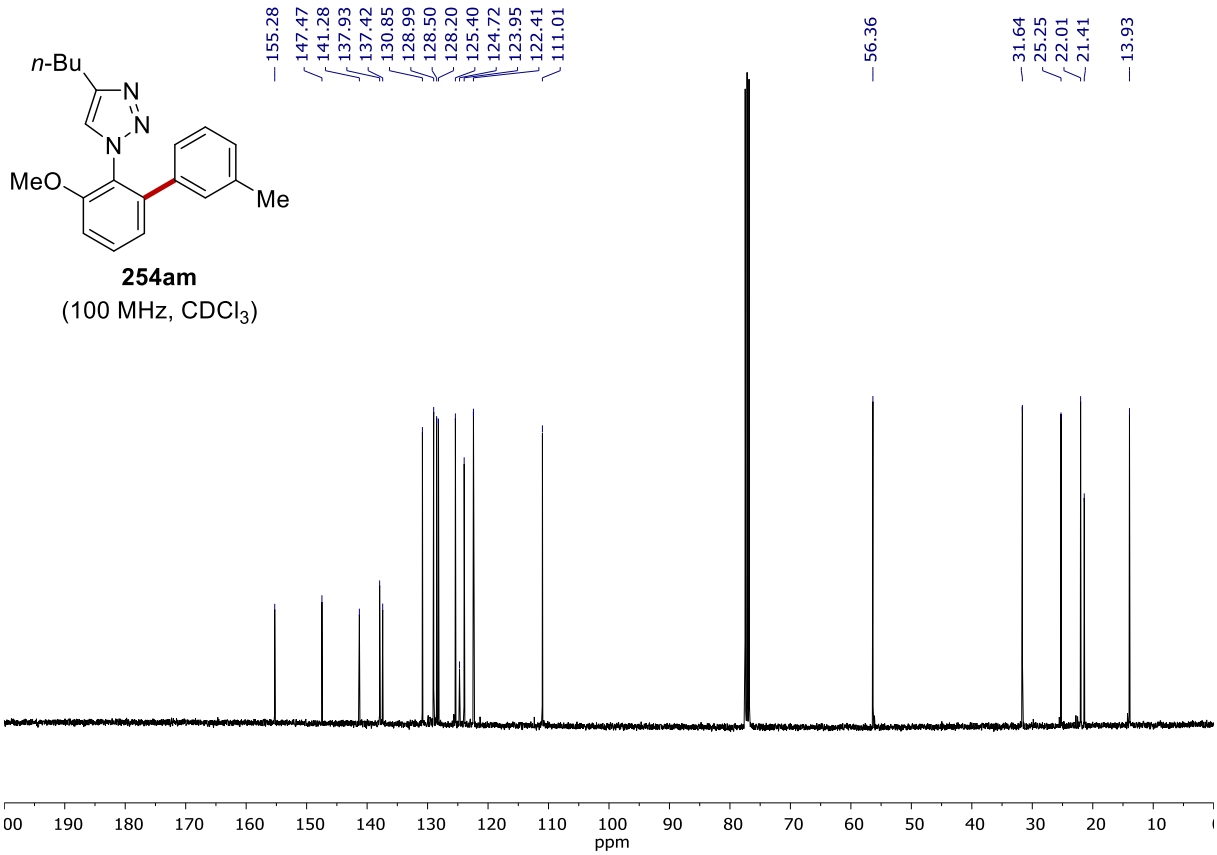

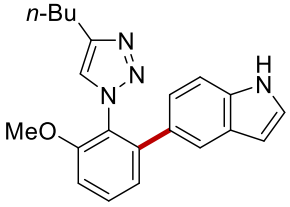

254ap
(100 MHz, $CDCl_3$)

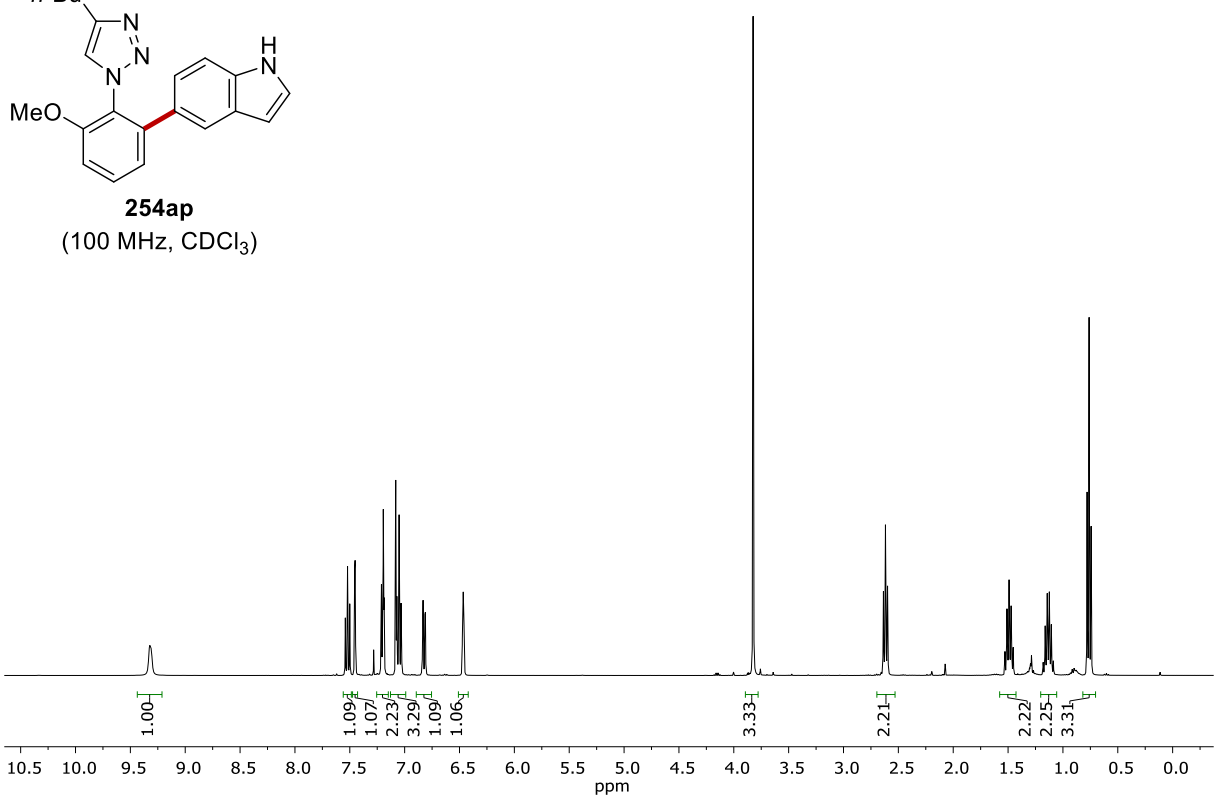

254ap
(100 MHz, $CDCl_3$)

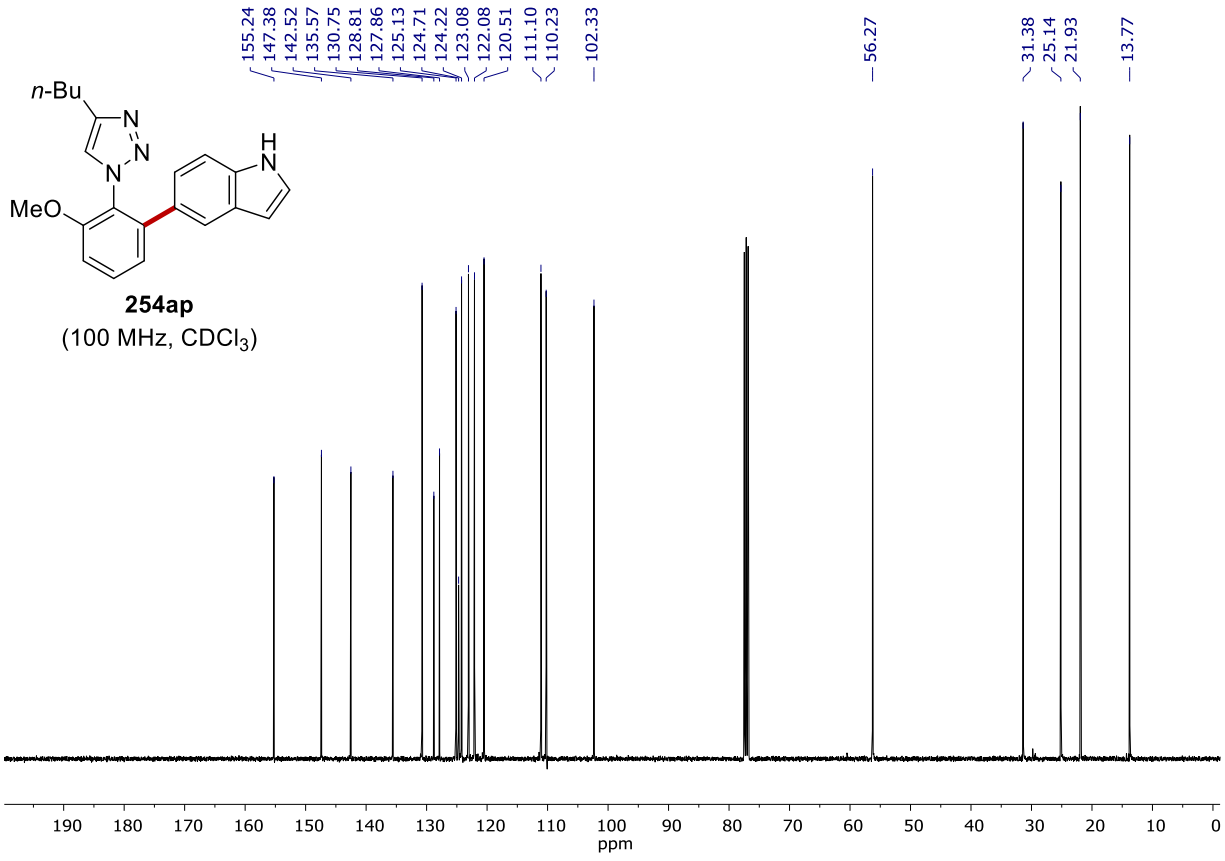

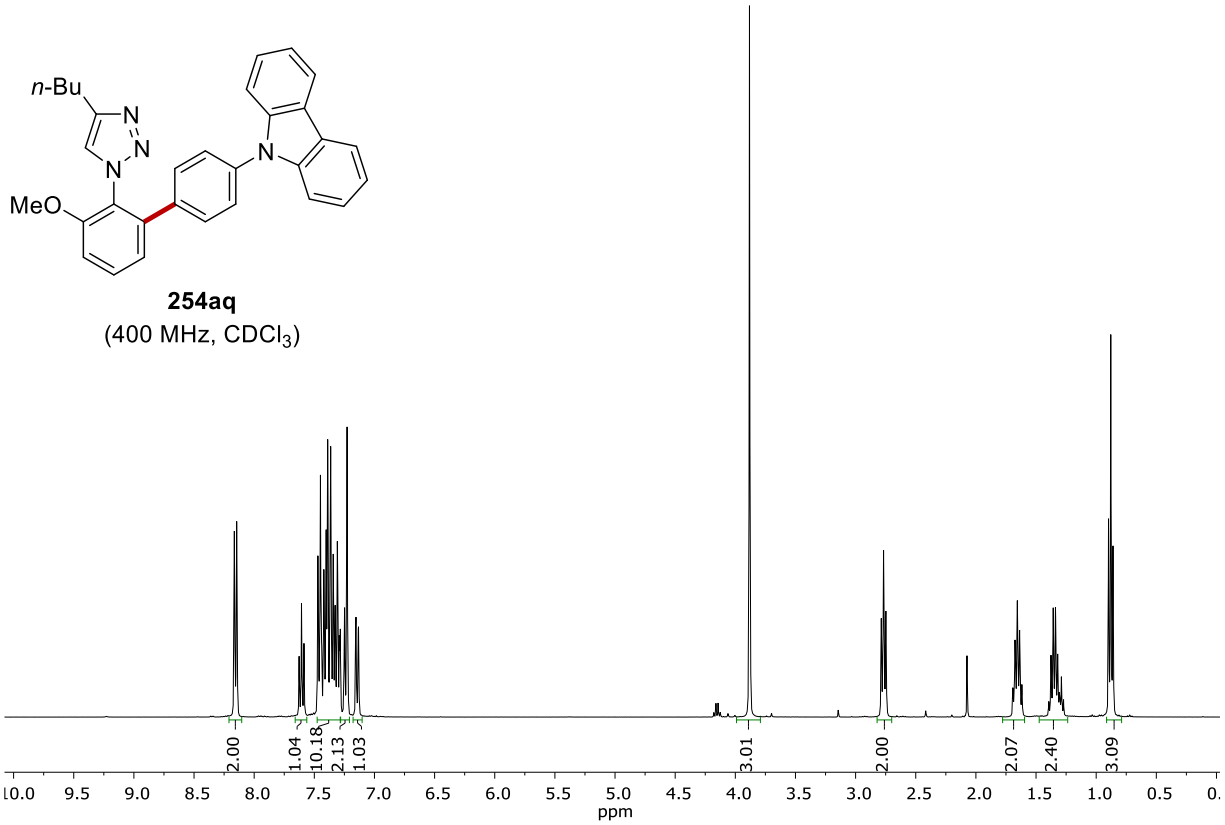

254aq
(400 MHz, $CDCl_3$)

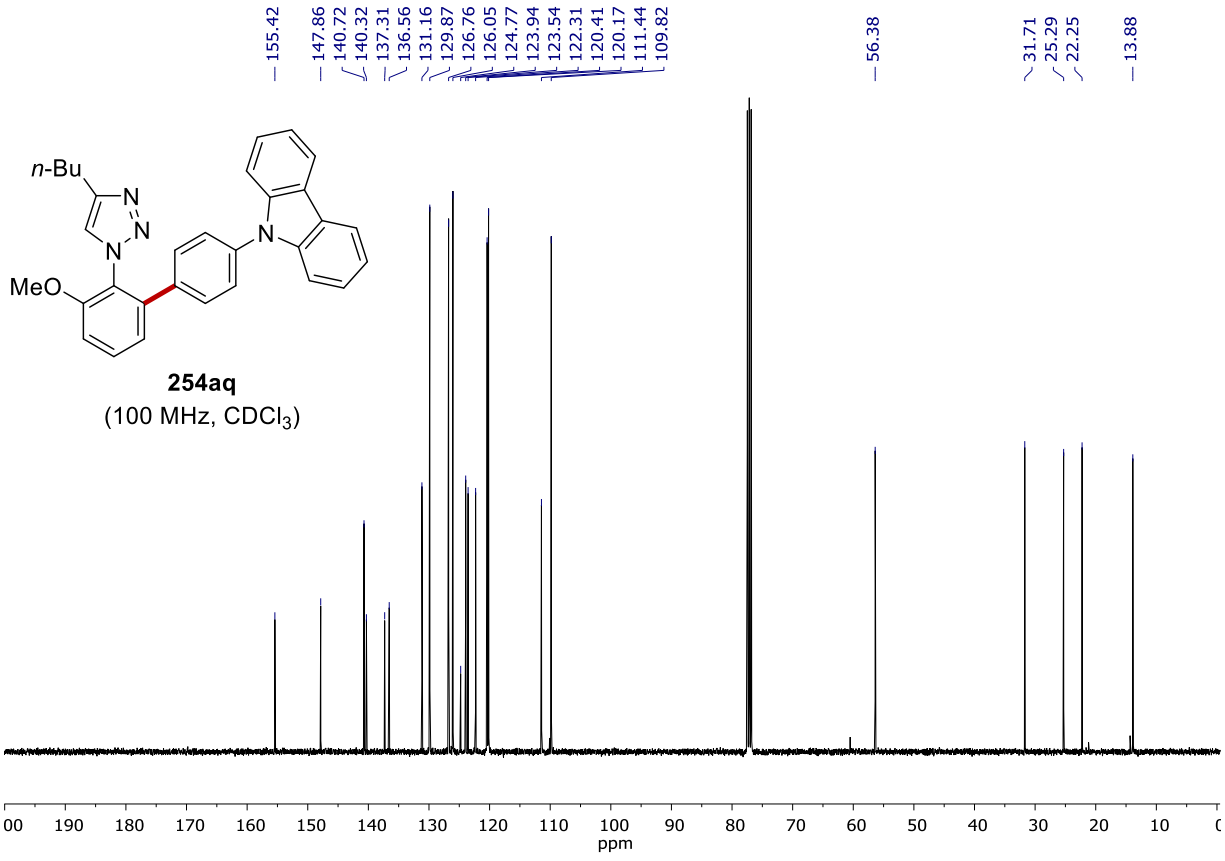

254aq
(100 MHz, $CDCl_3$)

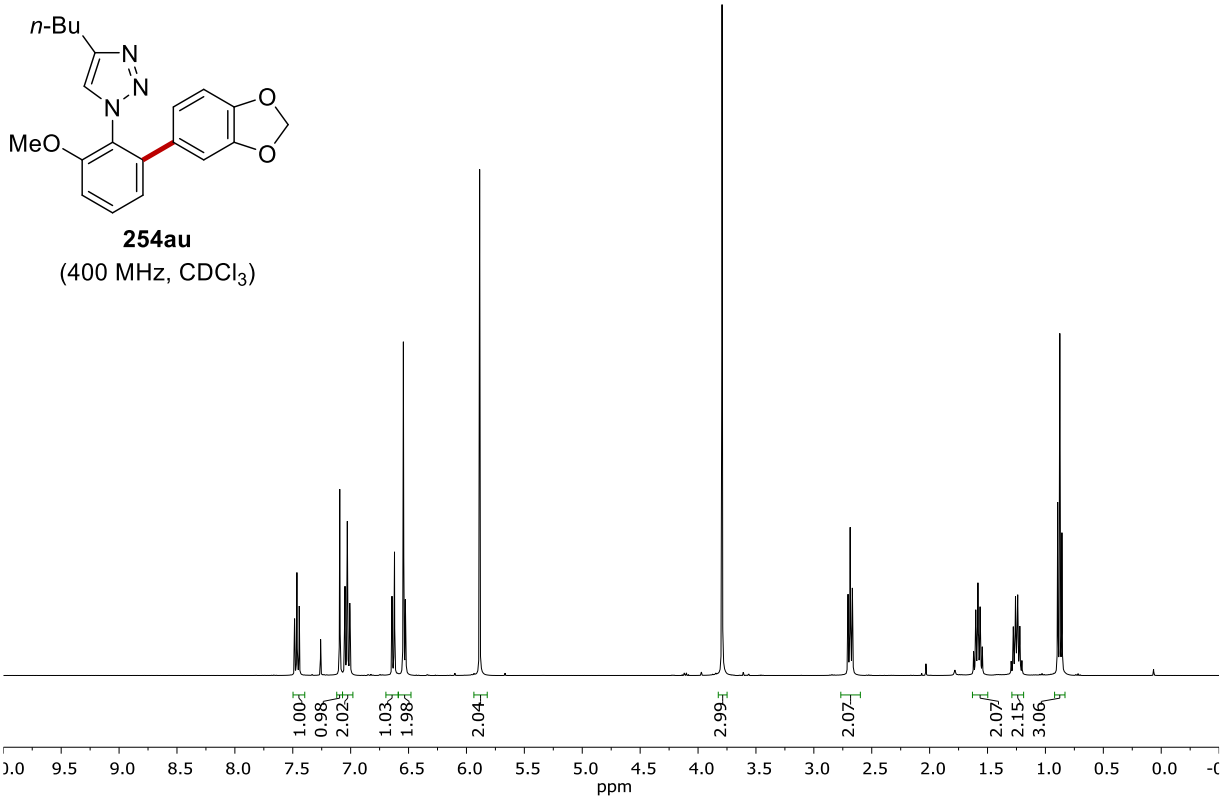

254au
(400 MHz, $CDCl_3$)

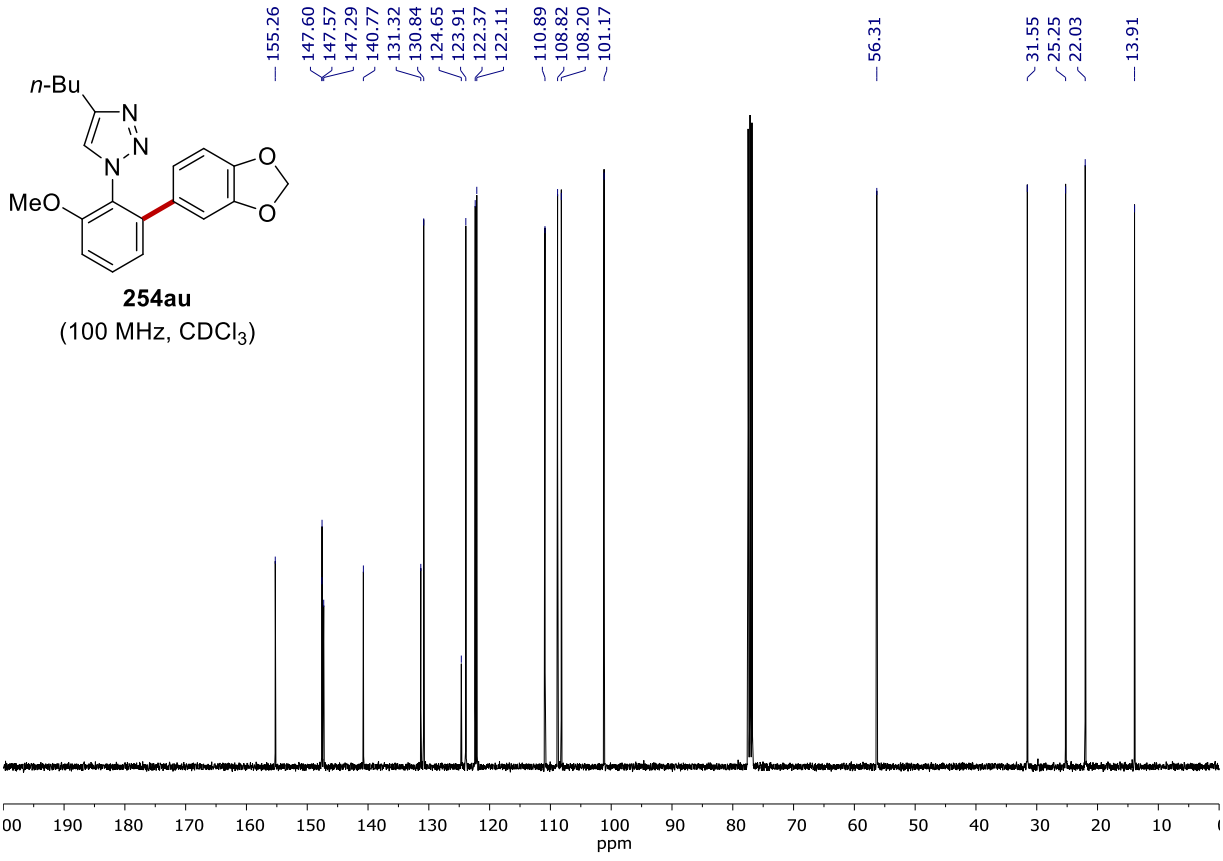

254au
(100 MHz, $CDCl_3$)

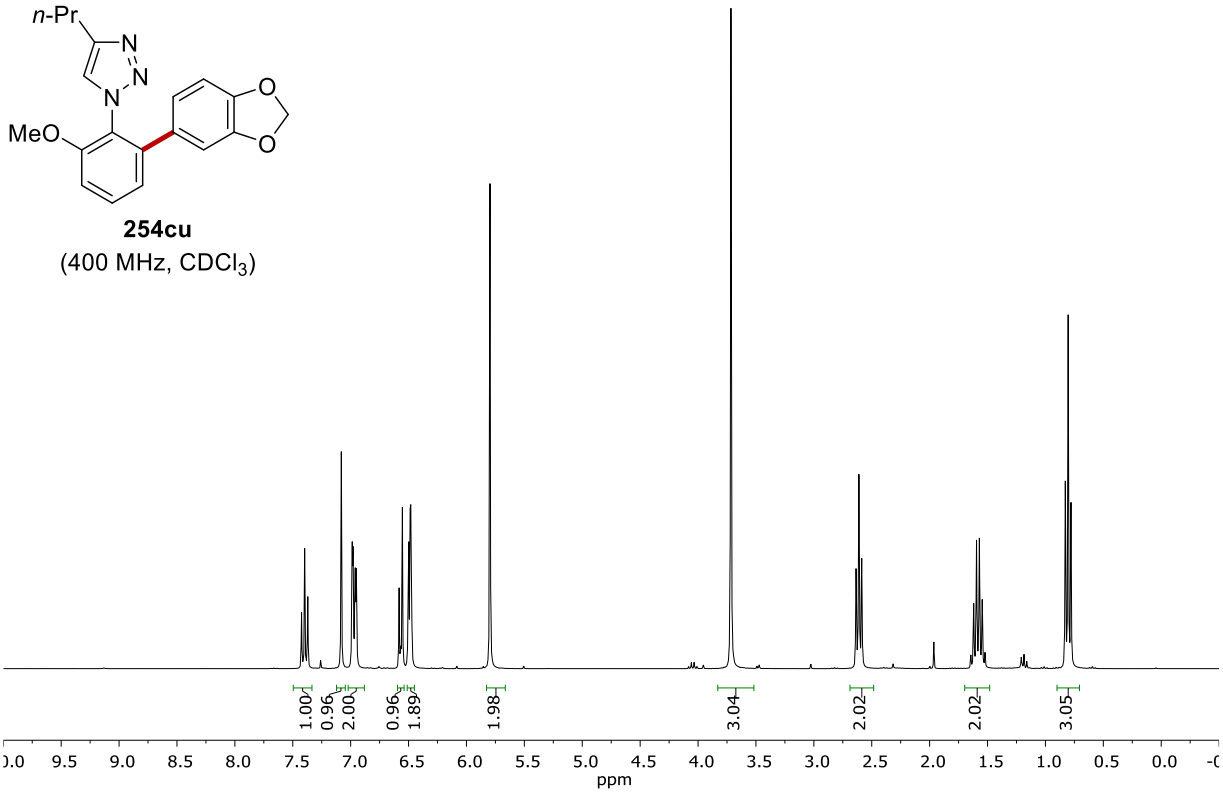

254cu
(400 MHz, $CDCl_3$)

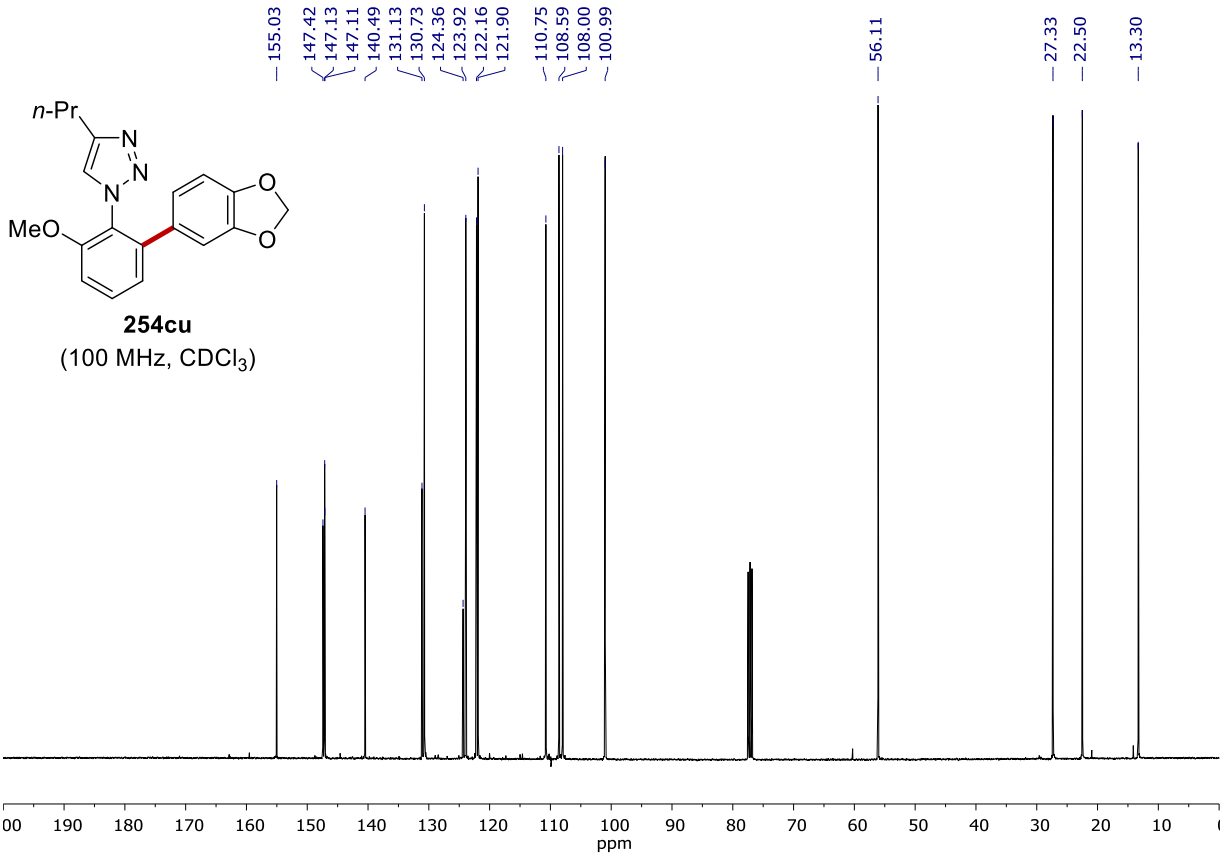

254cu
(100 MHz, $CDCl_3$)

254du
(400 MHz, $CDCl_3$)

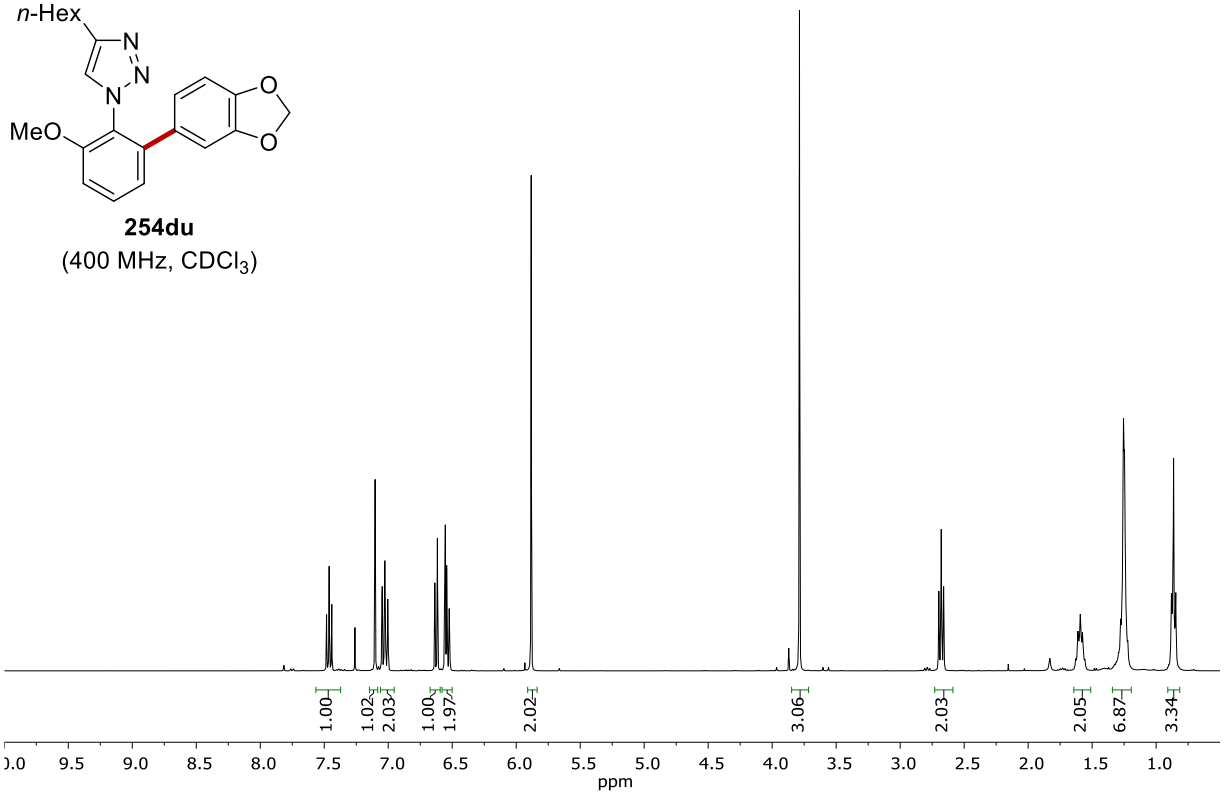

254du
(100 MHz, $CDCl_3$)

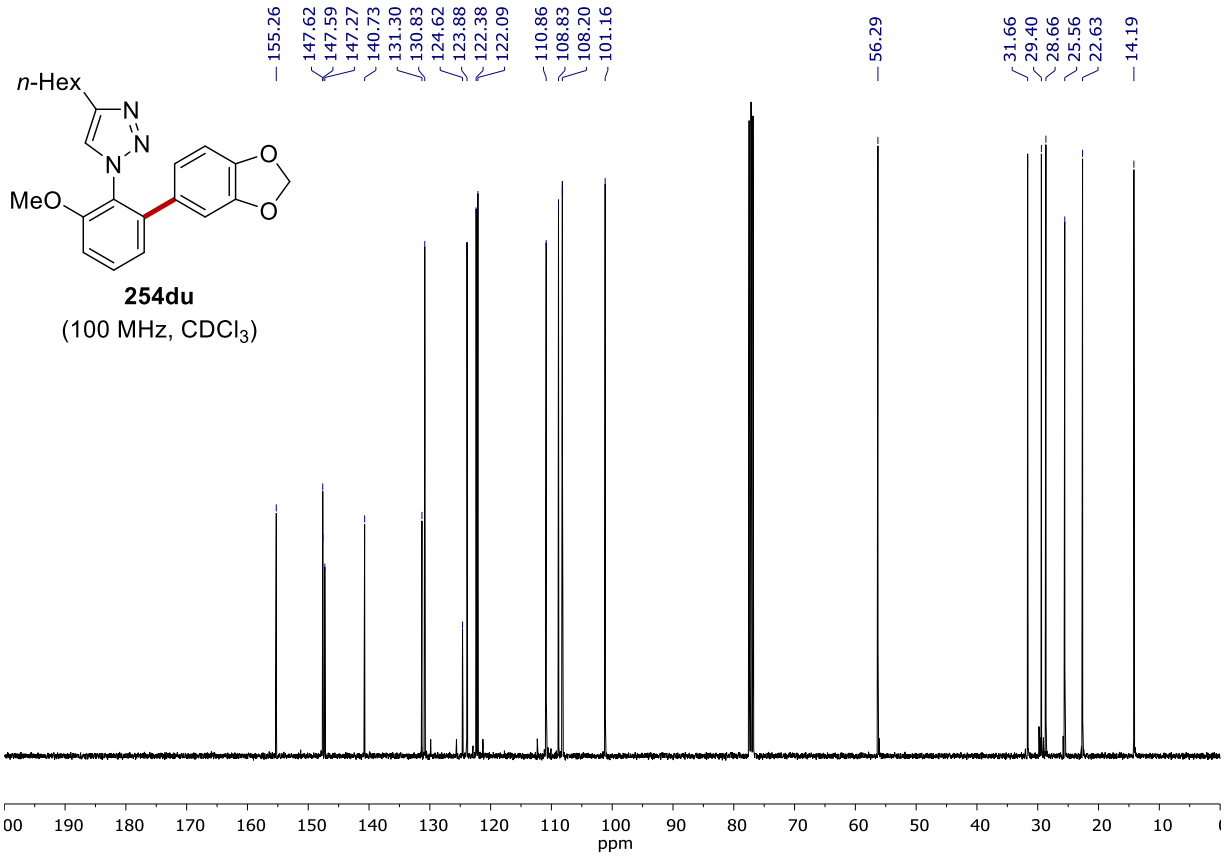

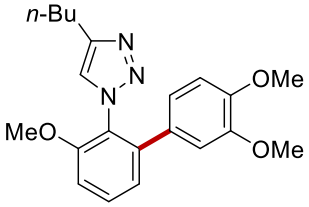

254av
(400 MHz, $CDCl_3$)

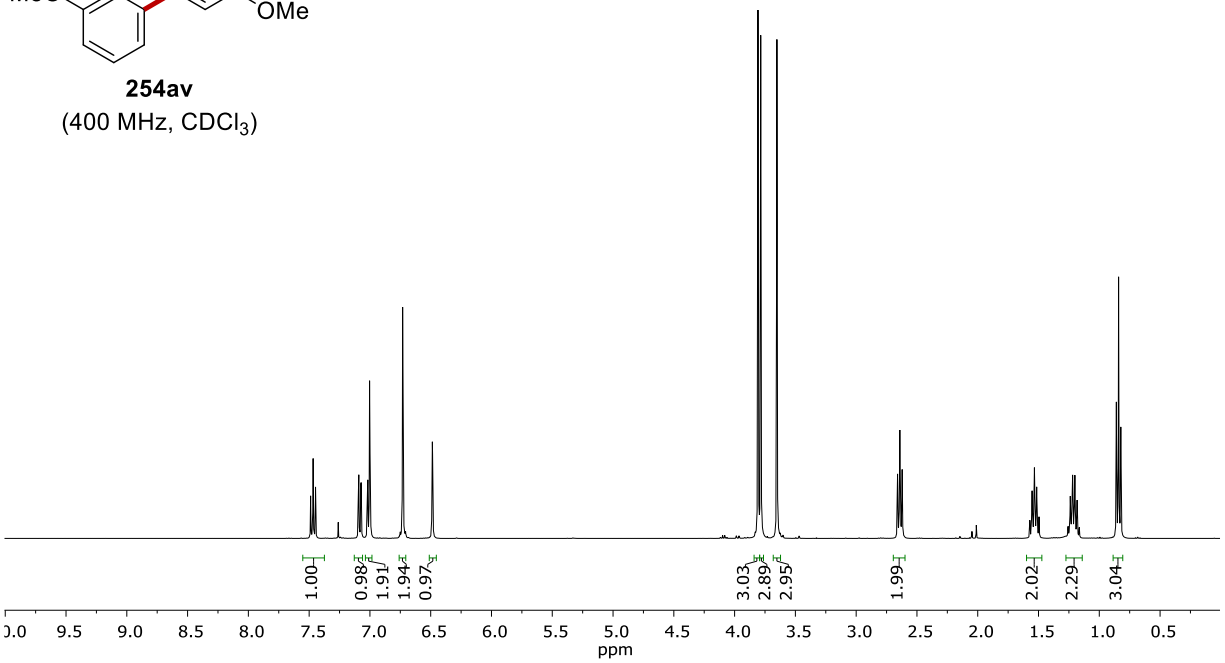

254av
(100 MHz, $CDCl_3$)

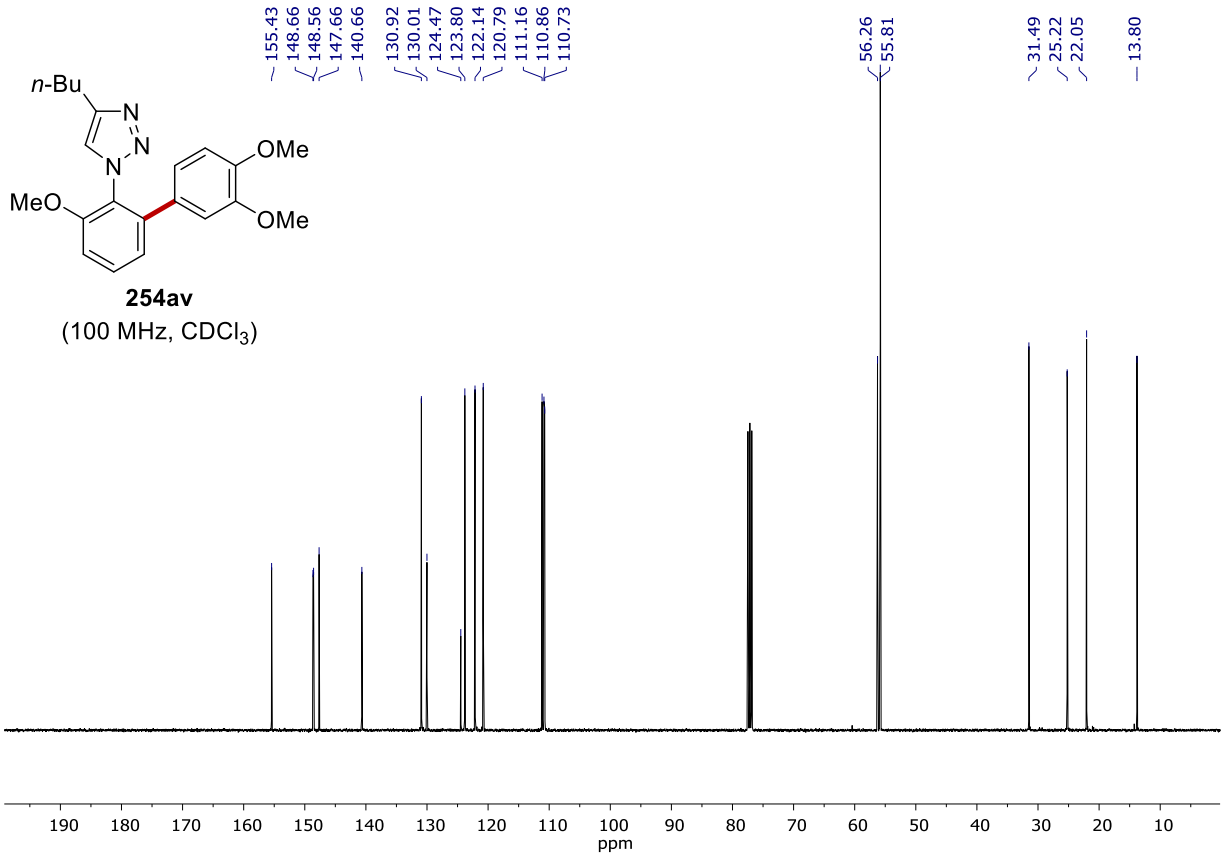

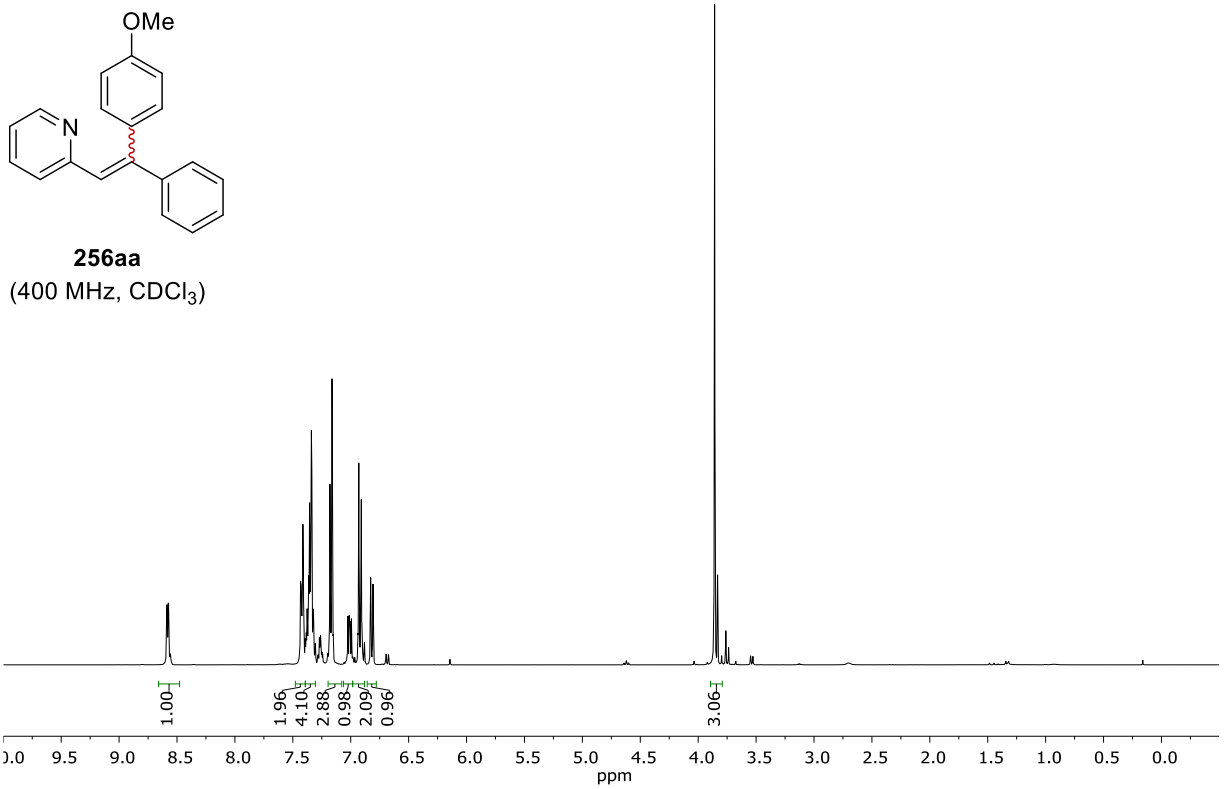

256aa
(400 MHz, $CDCl_3$)

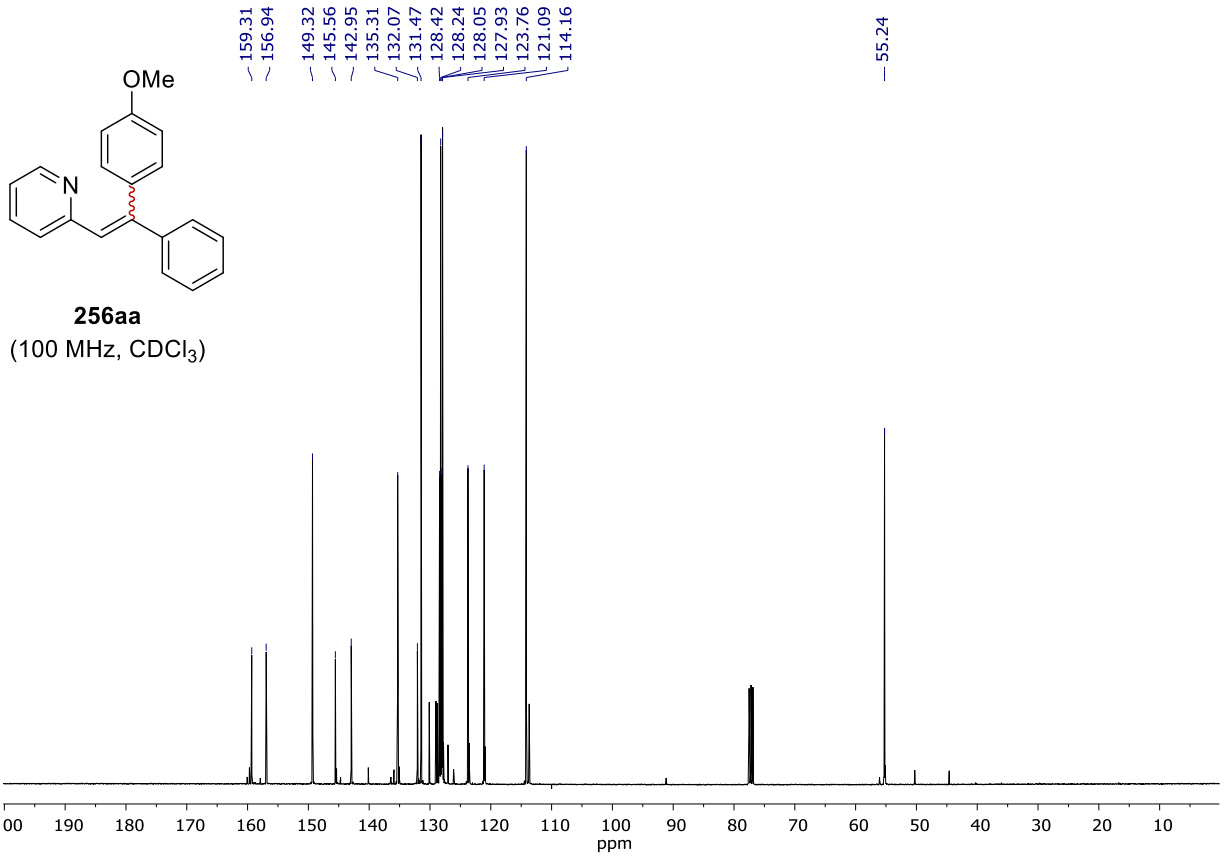

256aa
(100 MHz, $CDCl_3$)

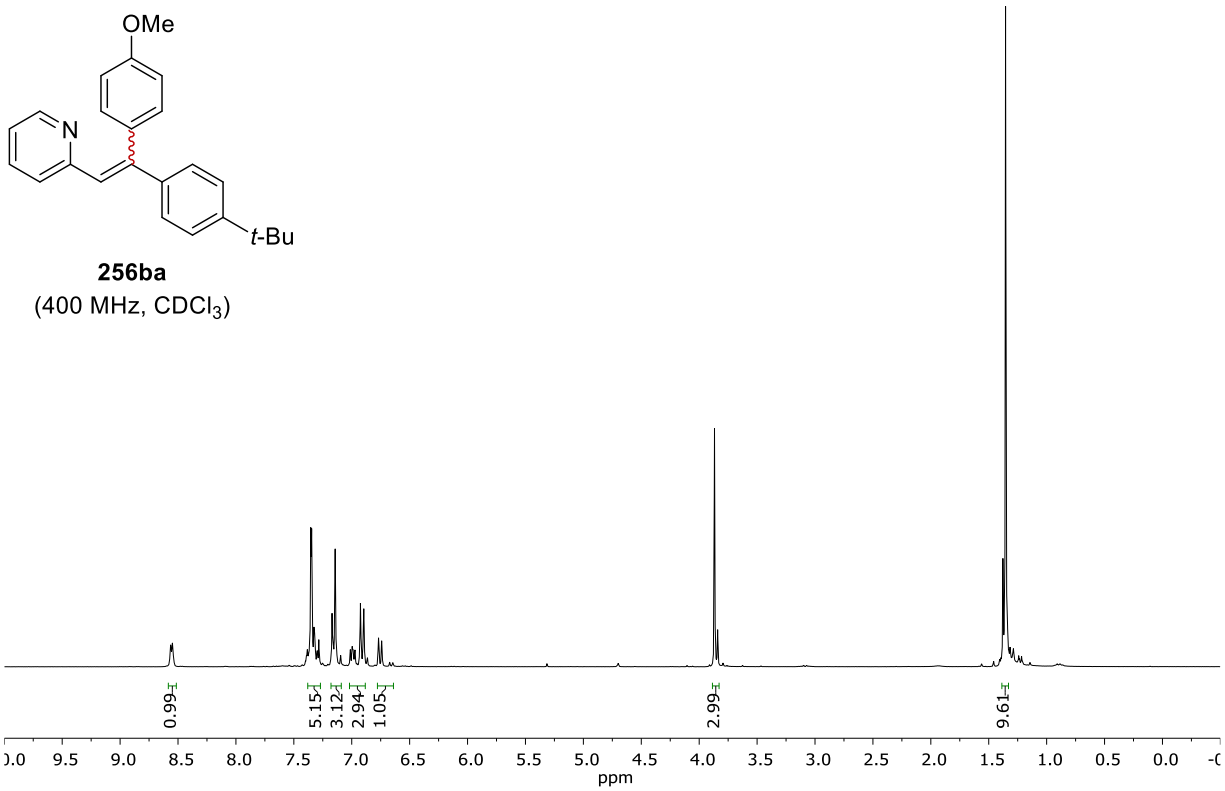

256ba
(400 MHz, $CDCl_3$)

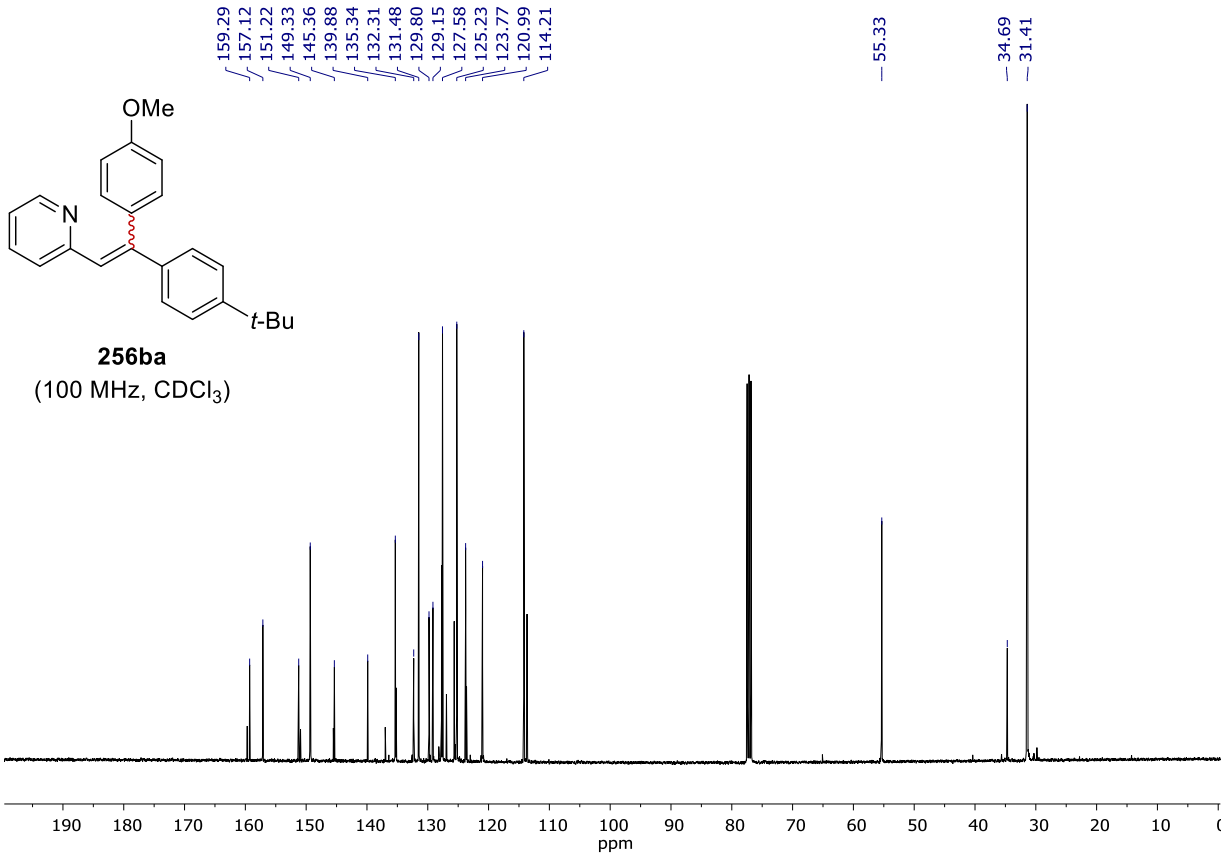

256ba
(100 MHz, $CDCl_3$)

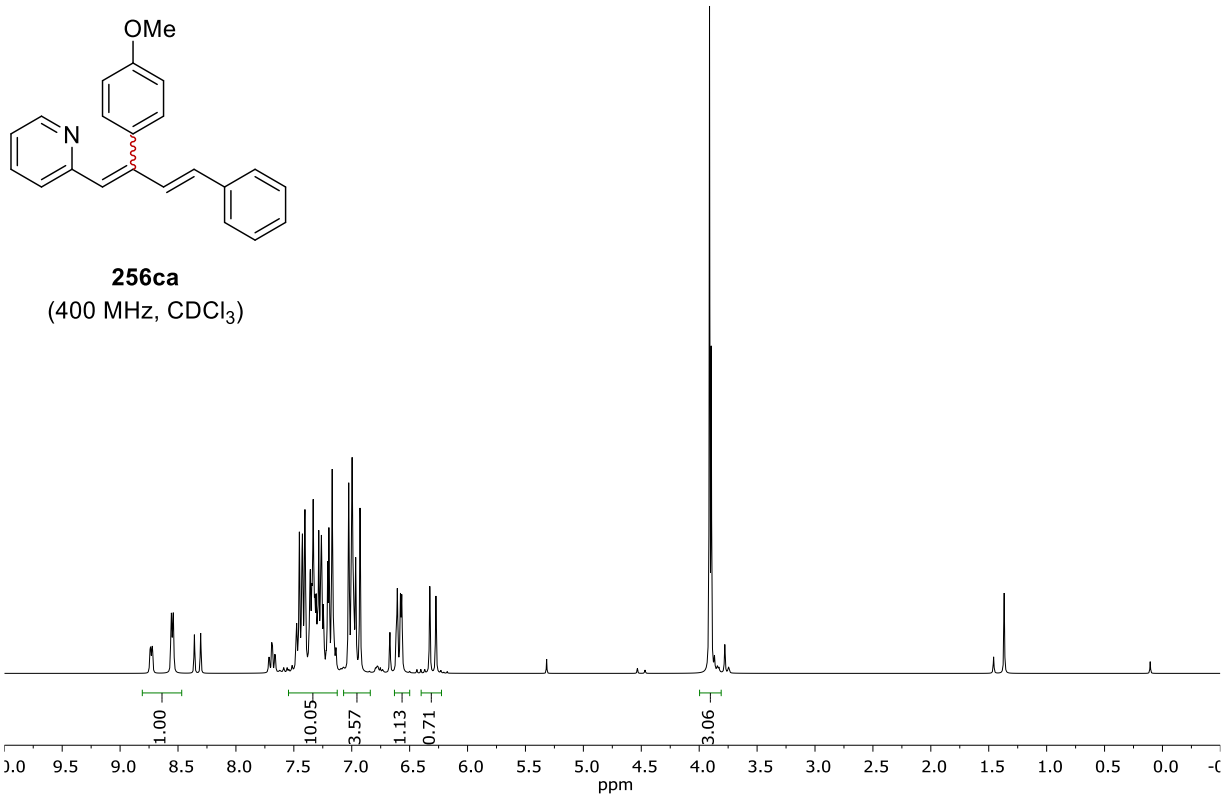

256ca
(400 MHz, $CDCl_3$)

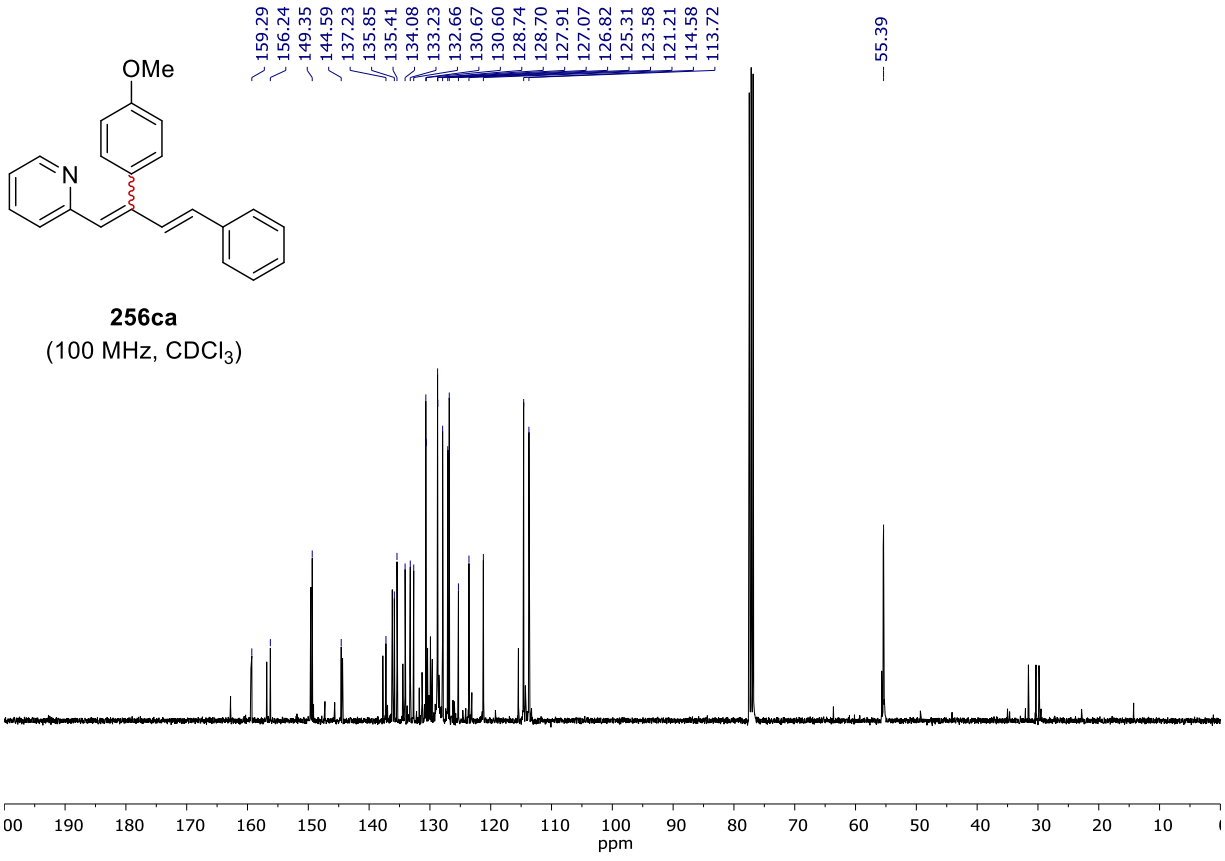

256ca
(100 MHz, $CDCl_3$)

243ay
(300 MHz, $CDCl_3$)

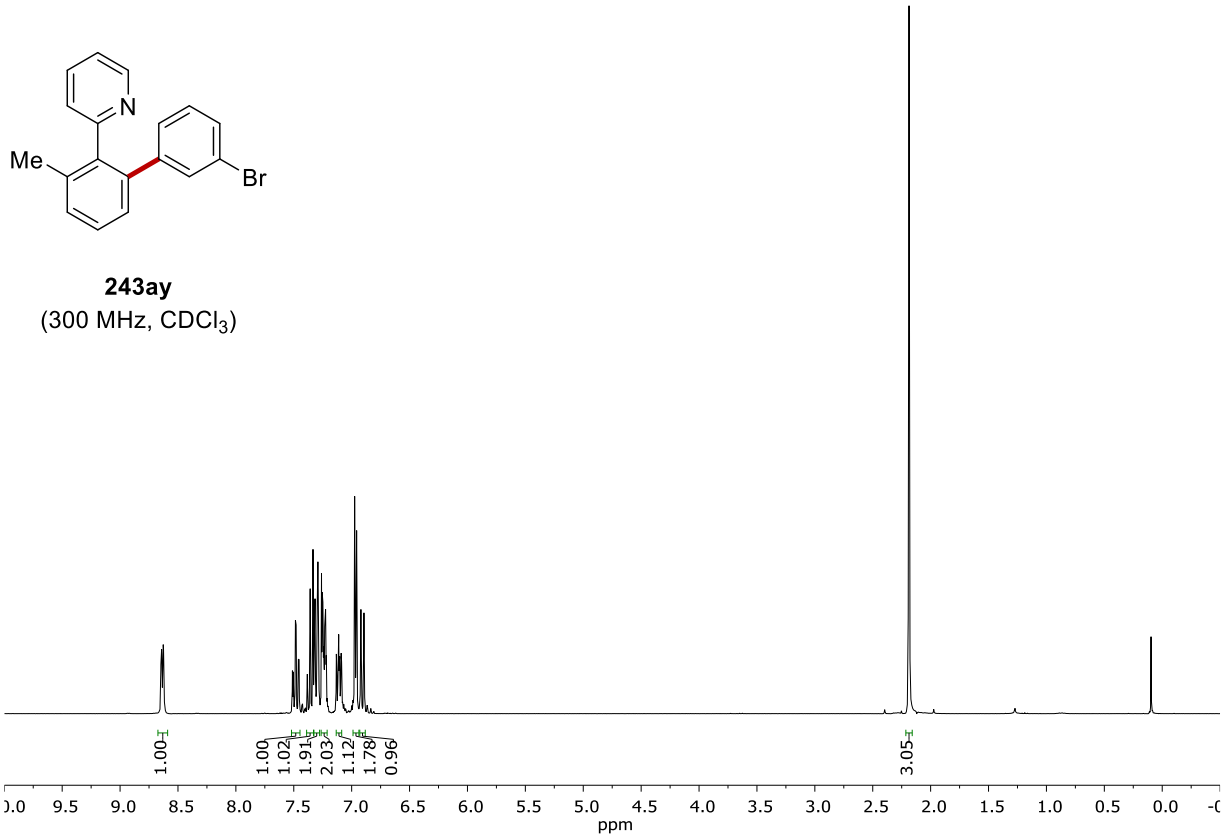

243ay
(100 MHz, $CDCl_3$)

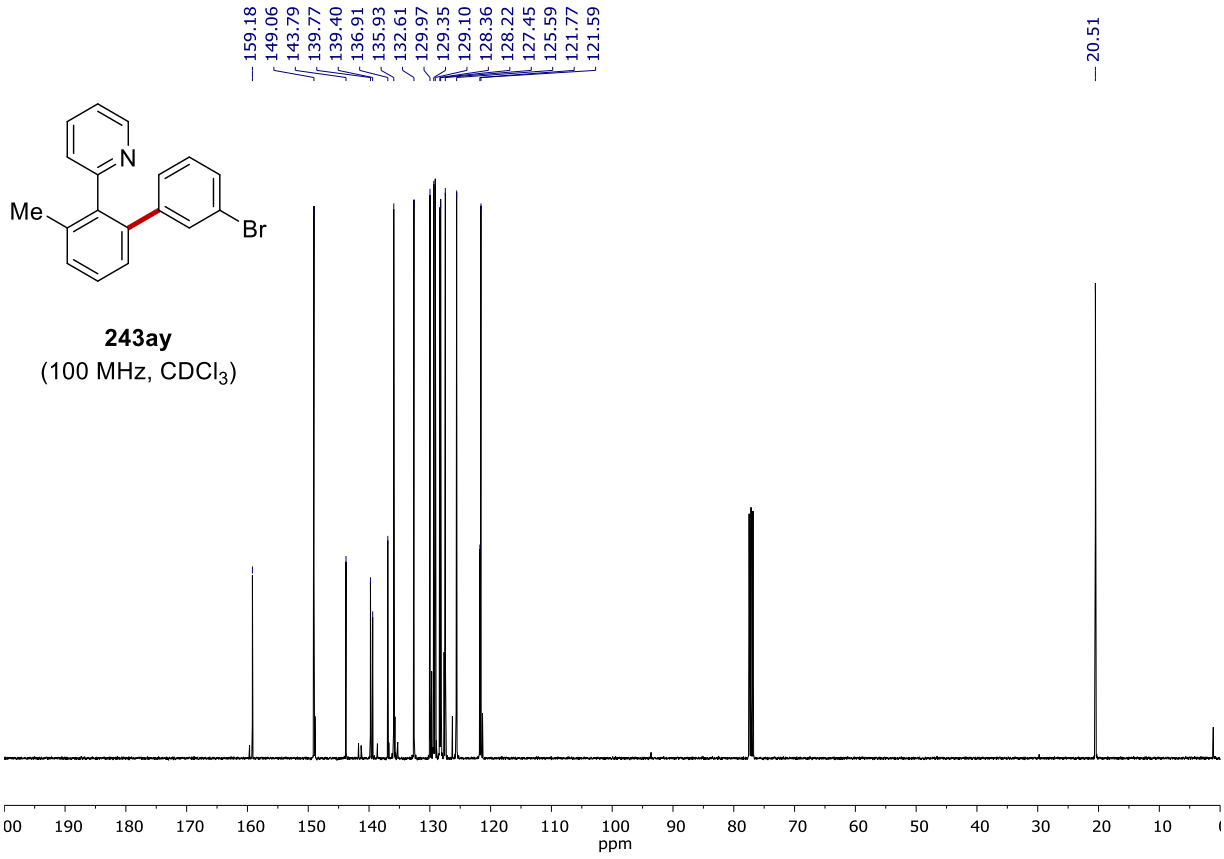

244ab
(400 MHz, $CDCl_3$)

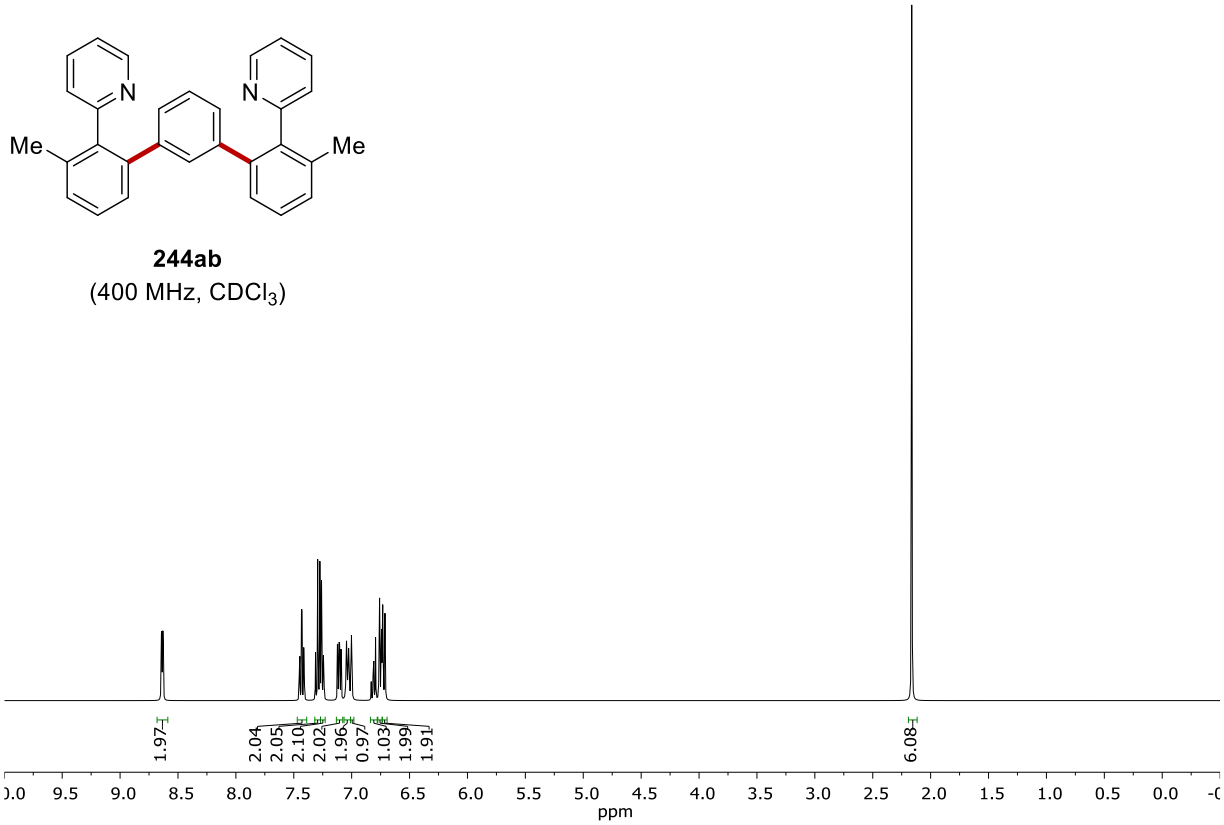

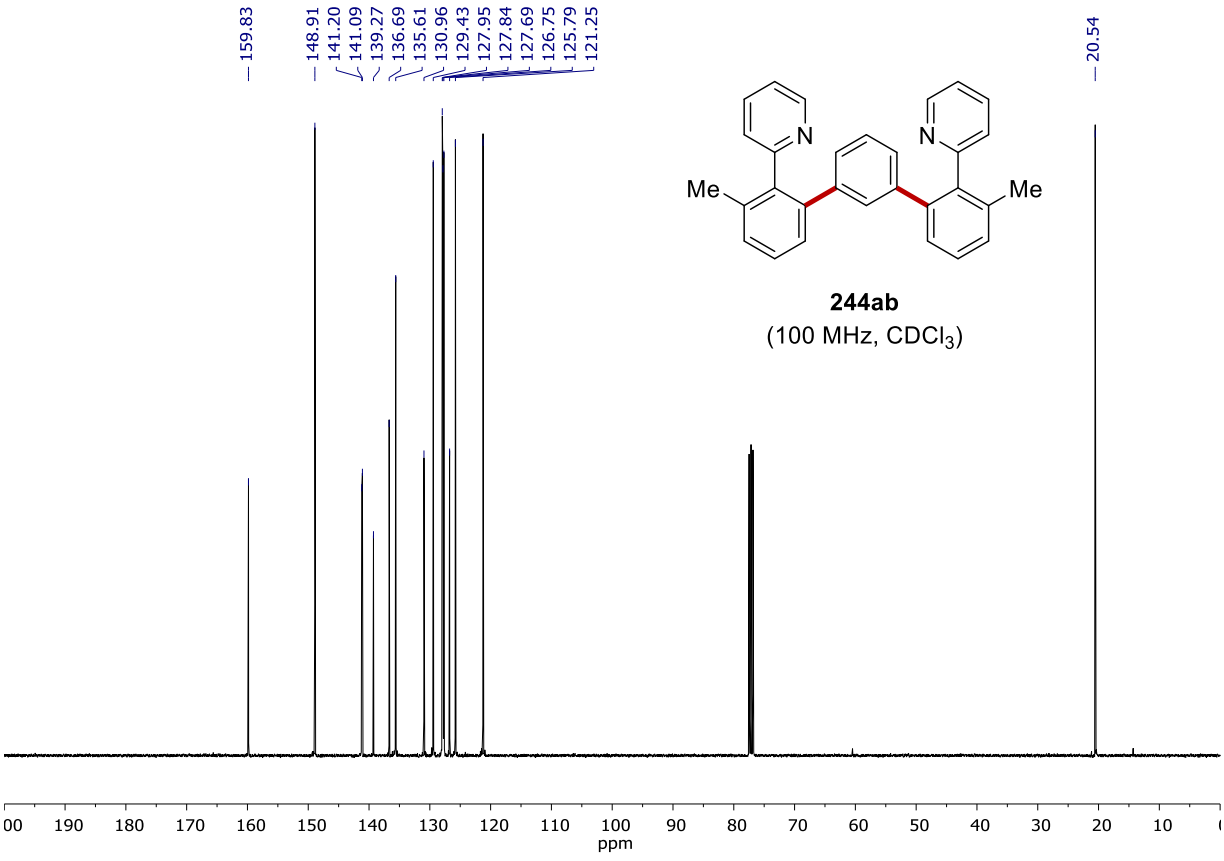

244ab
(100 MHz, $CDCl_3$)

258az
(400 MHz, $CDCl_3$)

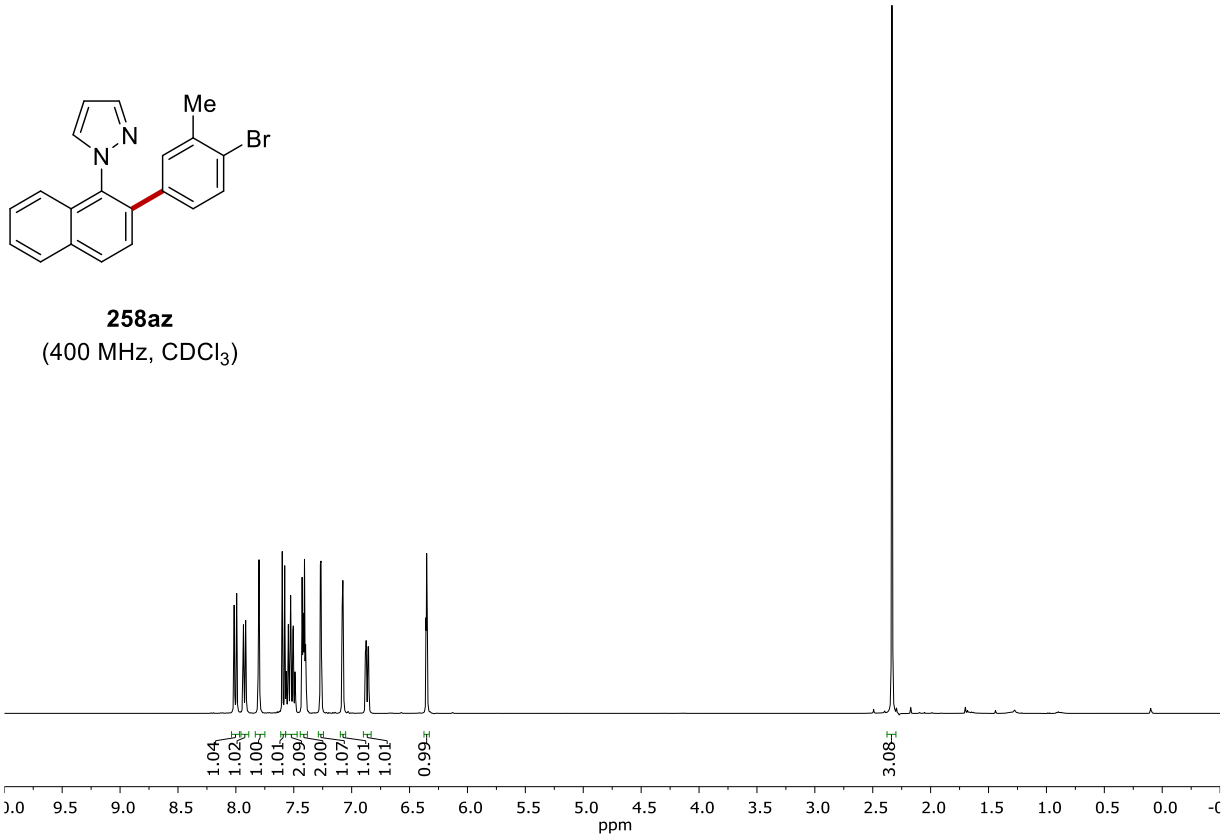

258az
(100 MHz, $CDCl_3$)

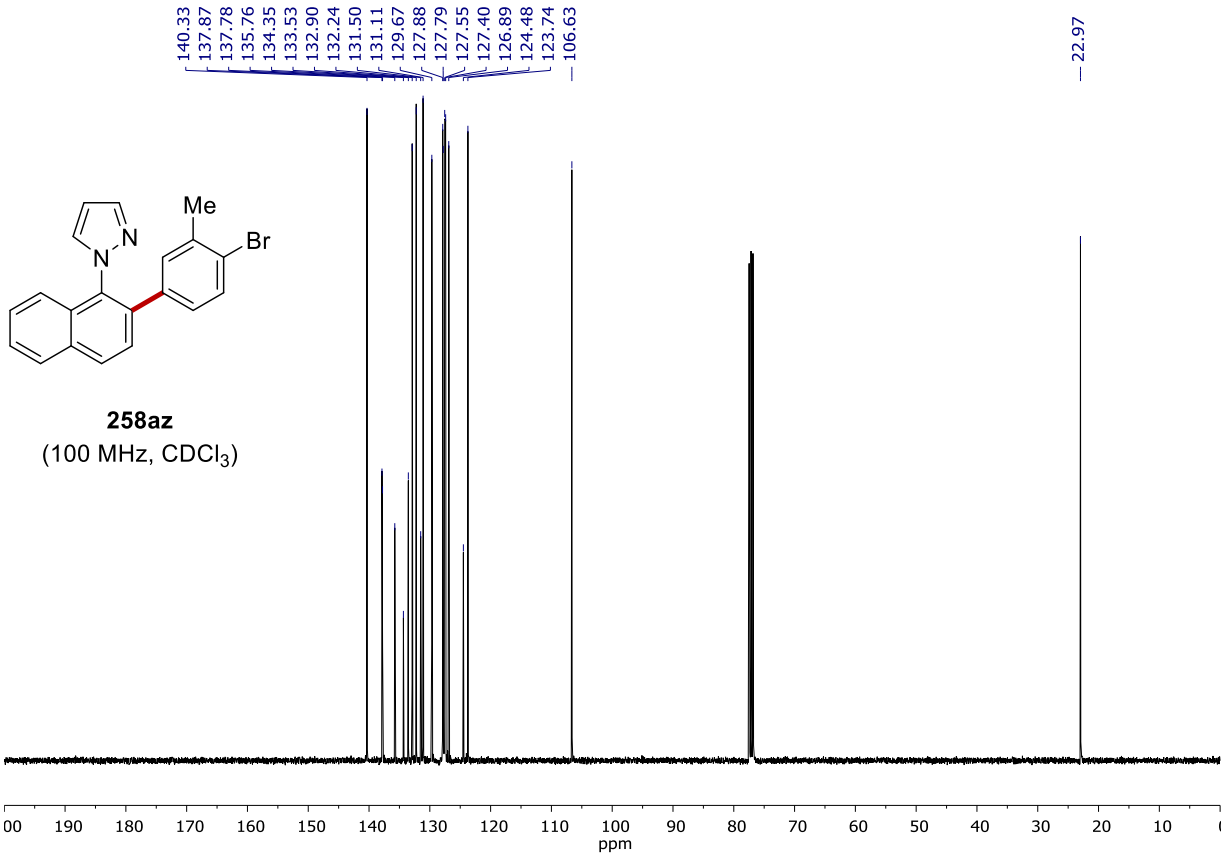

258az–Br
(400 MHz, $CDCl_3$)

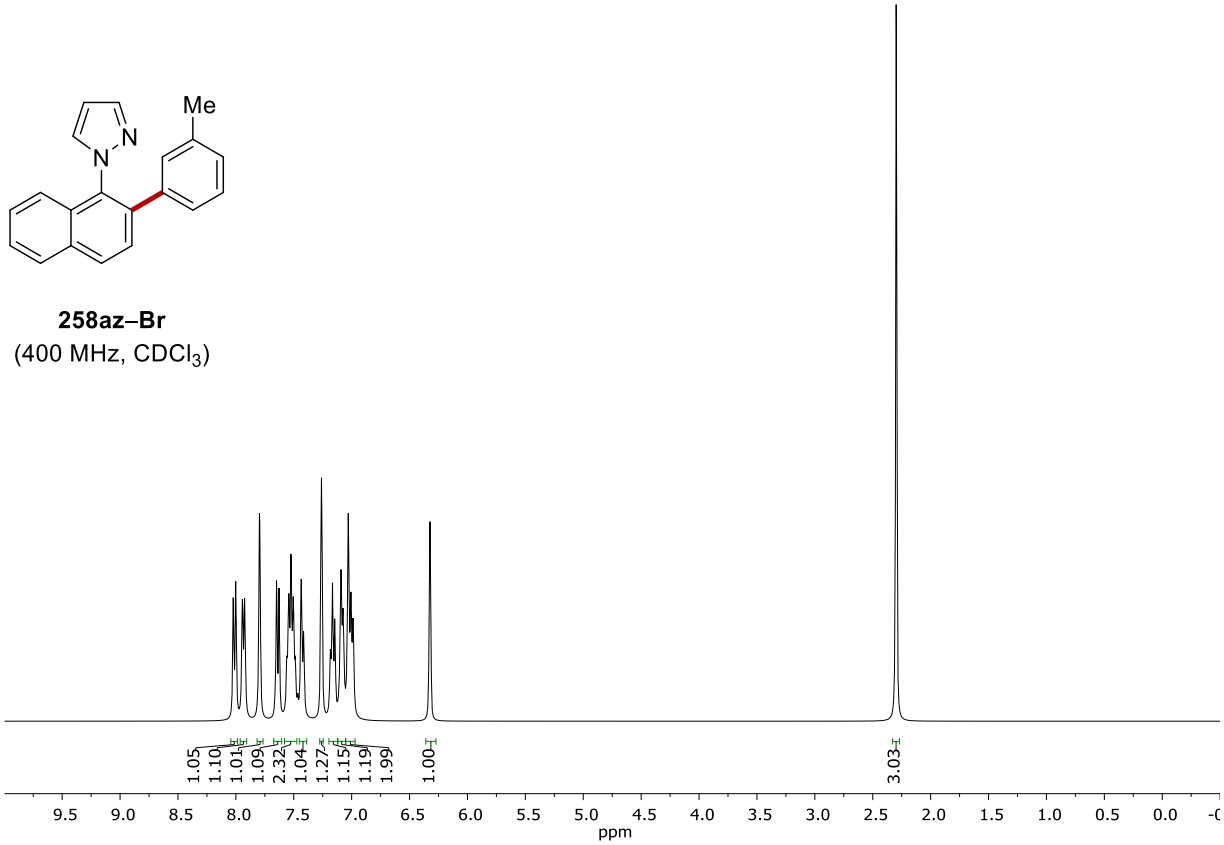

258az–Br
(100 MHz, $CDCl_3$)

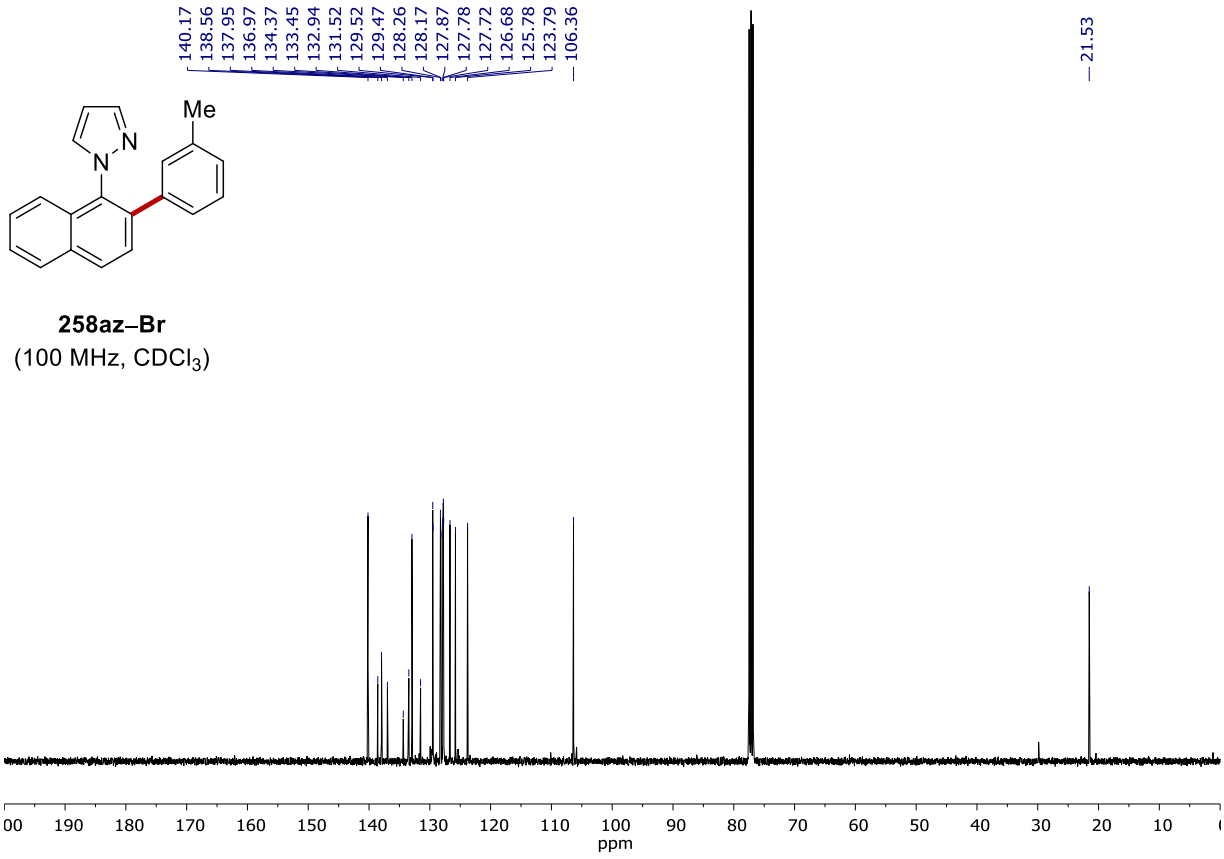

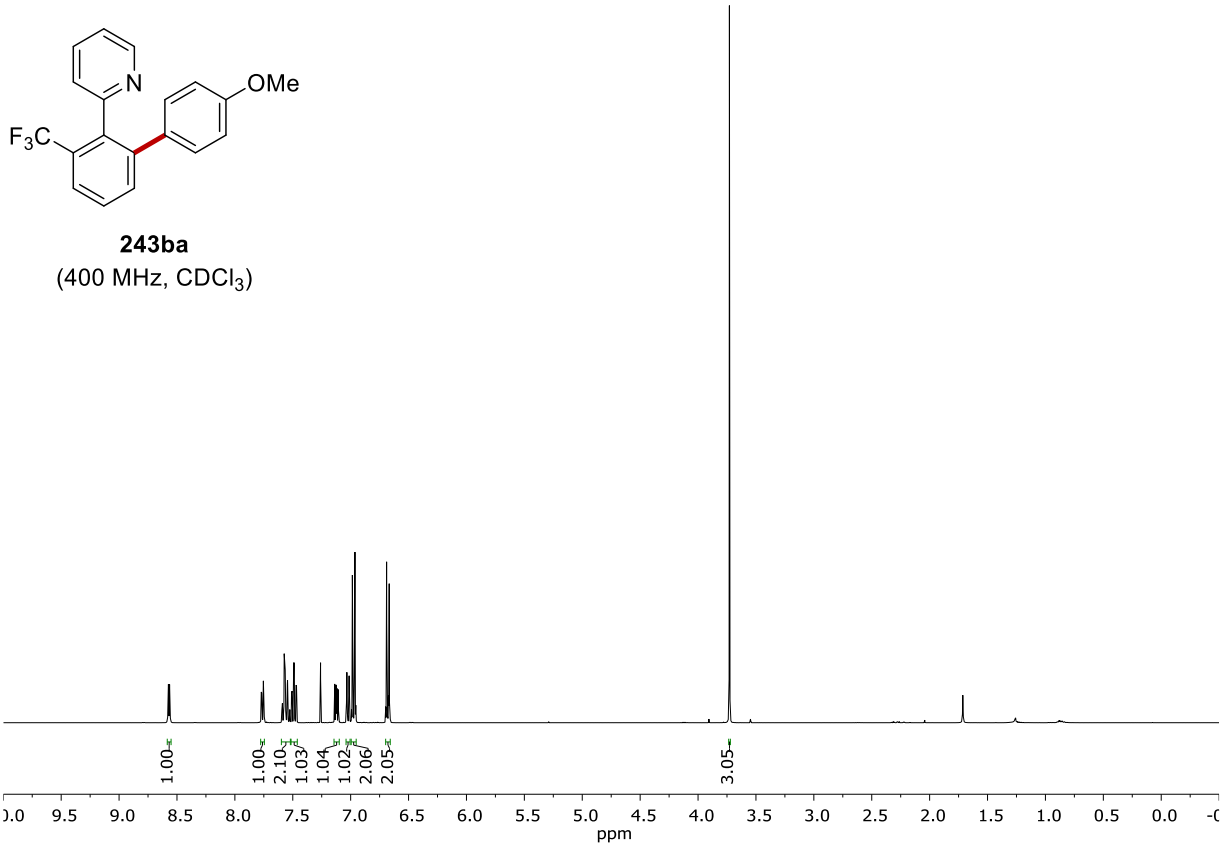

243ba
(400 MHz, $CDCl_3$)

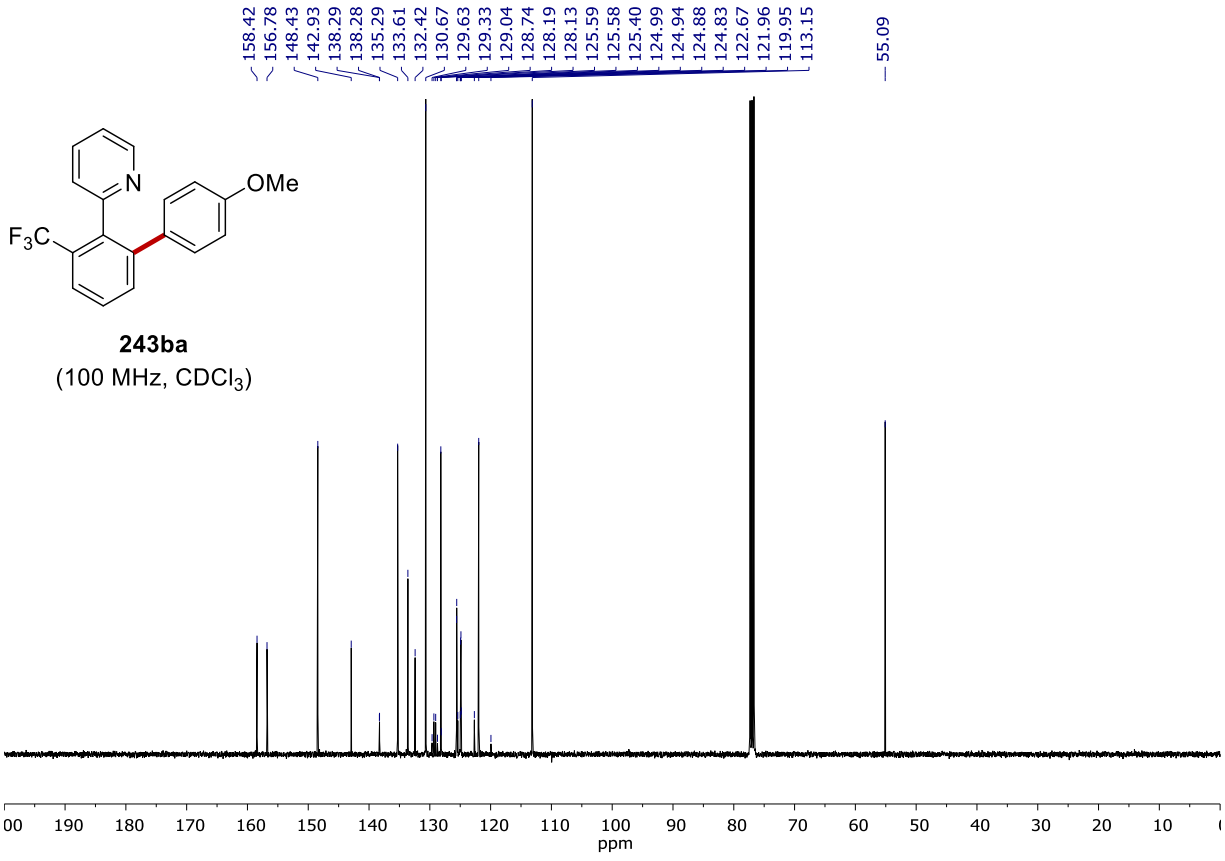

243ba
(100 MHz, $CDCl_3$)

243ba

^{19}F

(376 MHz, $CDCl_3$)

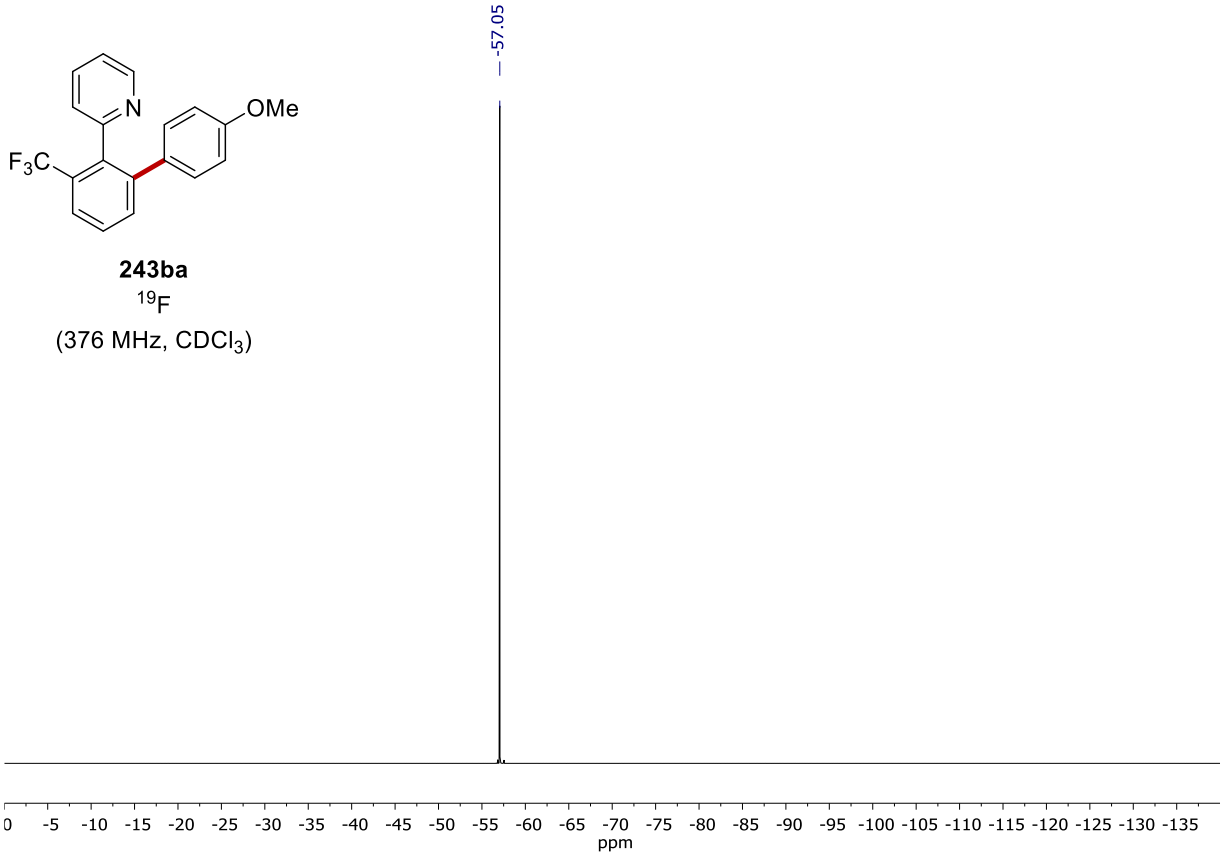

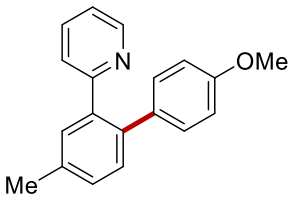

243ca

(300 MHz, $CDCl_3$)

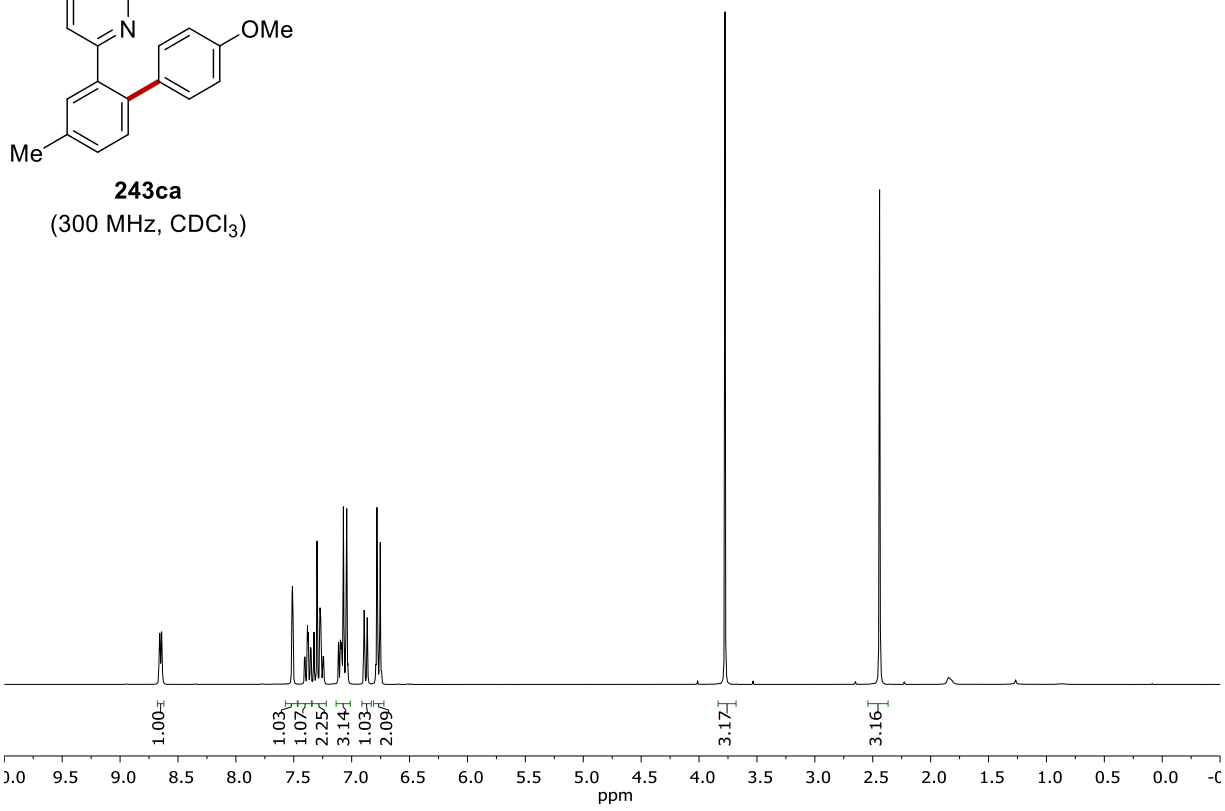

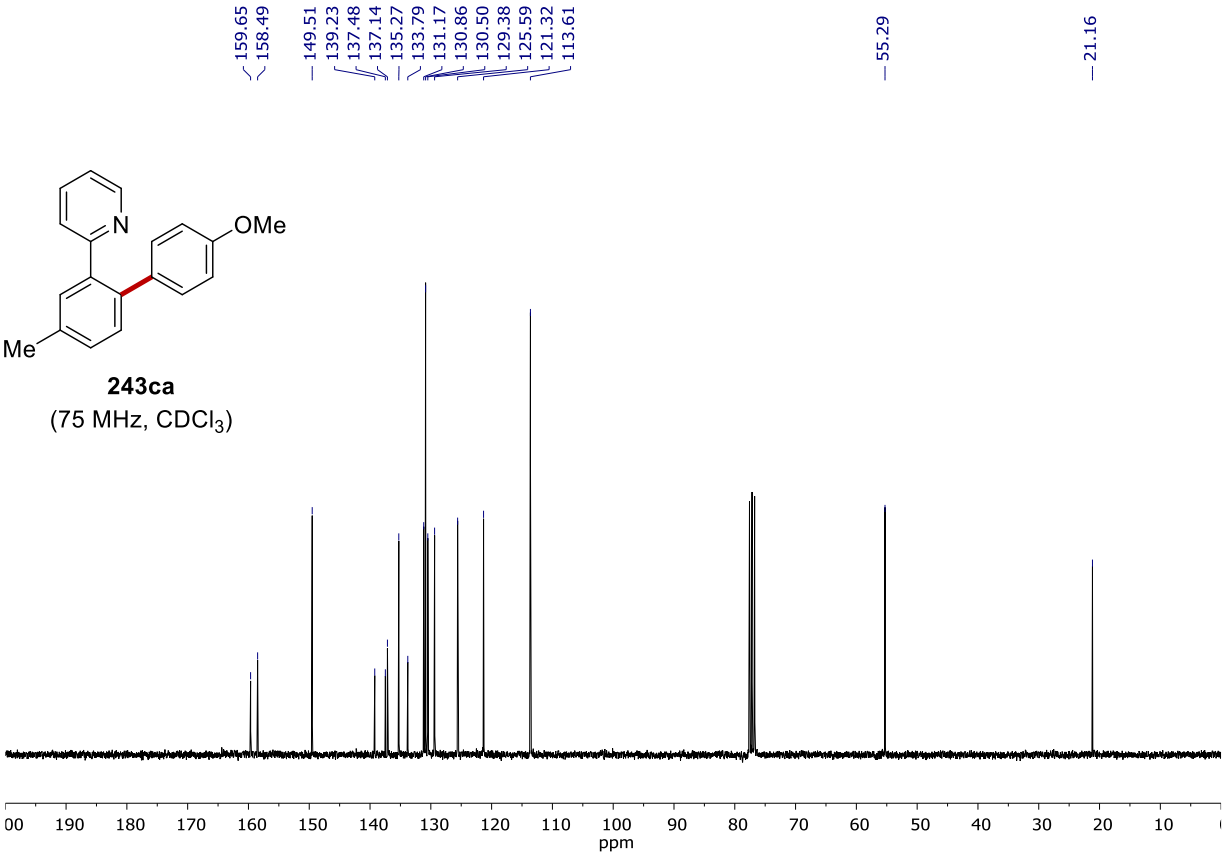
159.65
158.49
149.51
139.23
137.48
137.14
135.27
133.79
131.17
130.86
130.50
129.38
125.59
121.32
113.61
55.29
21.16
N
OMe
Me
243ca
(75 MHz, CDCl3)
ppm

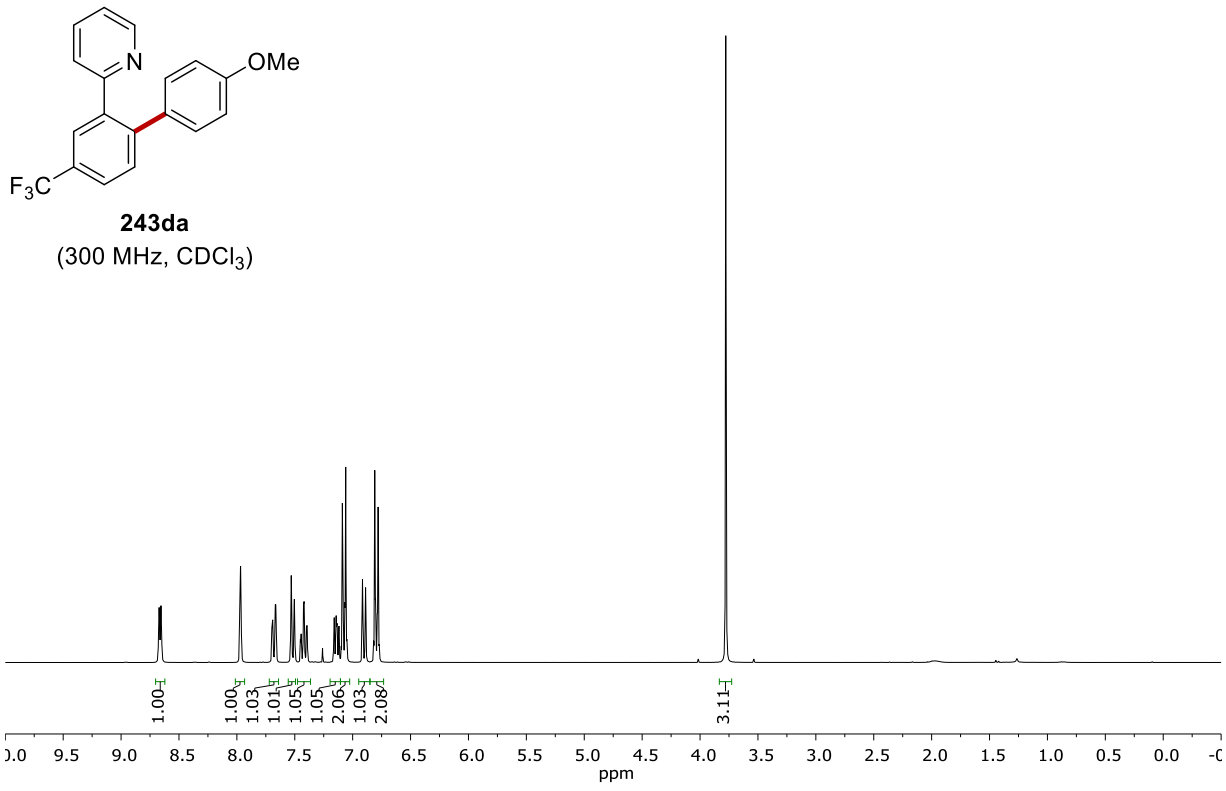
N
OMe
F3C
243da
(300 MHz, CDCl3)
1.00
1.00
1.03
1.01
1.05
1.05
2.06
1.03
2.08
3.11
ppm

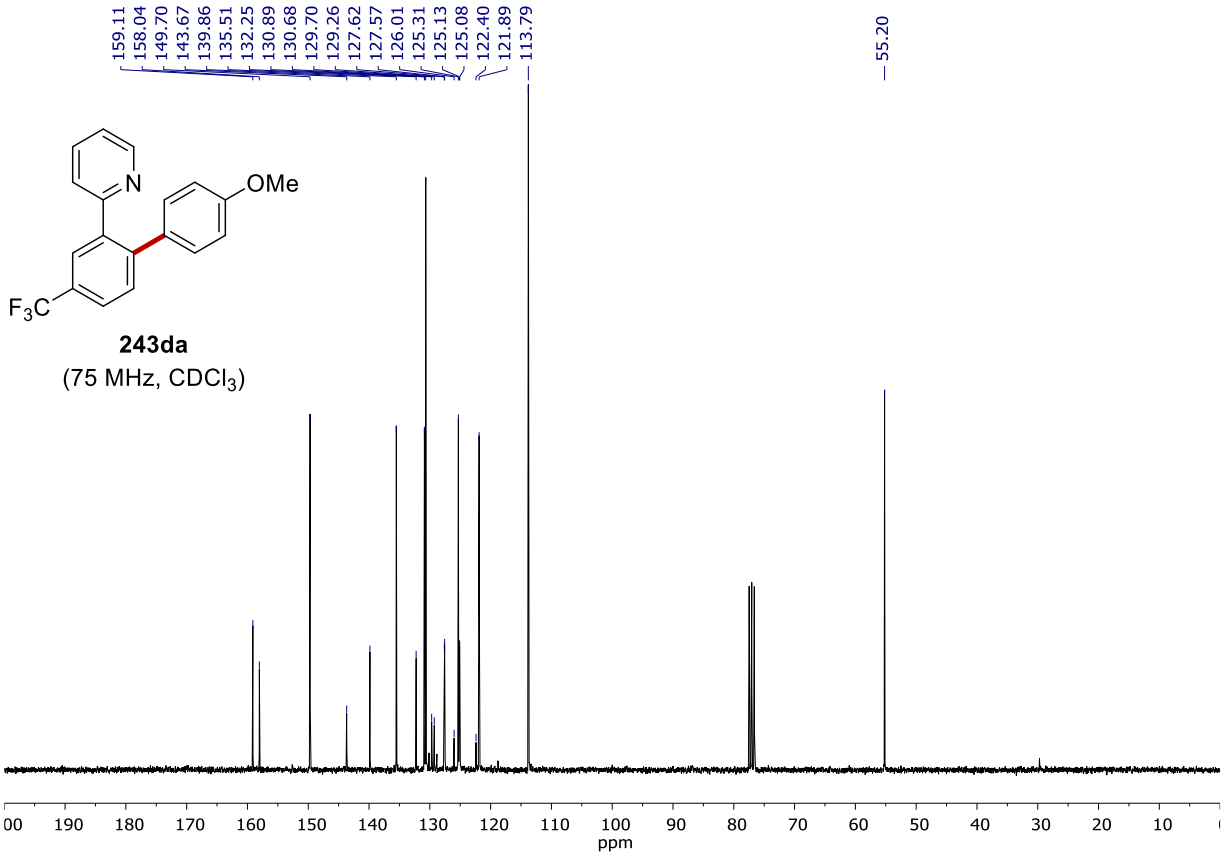
159.11
158.04
149.70
143.67
139.86
135.51
132.25
130.89
130.68
129.70
129.26
127.62
127.57
126.01
125.31
125.13
125.08
122.40
121.89
113.79
55.20
N
OMe
F3C
243da
(75 MHz, CDCl3)
ppm

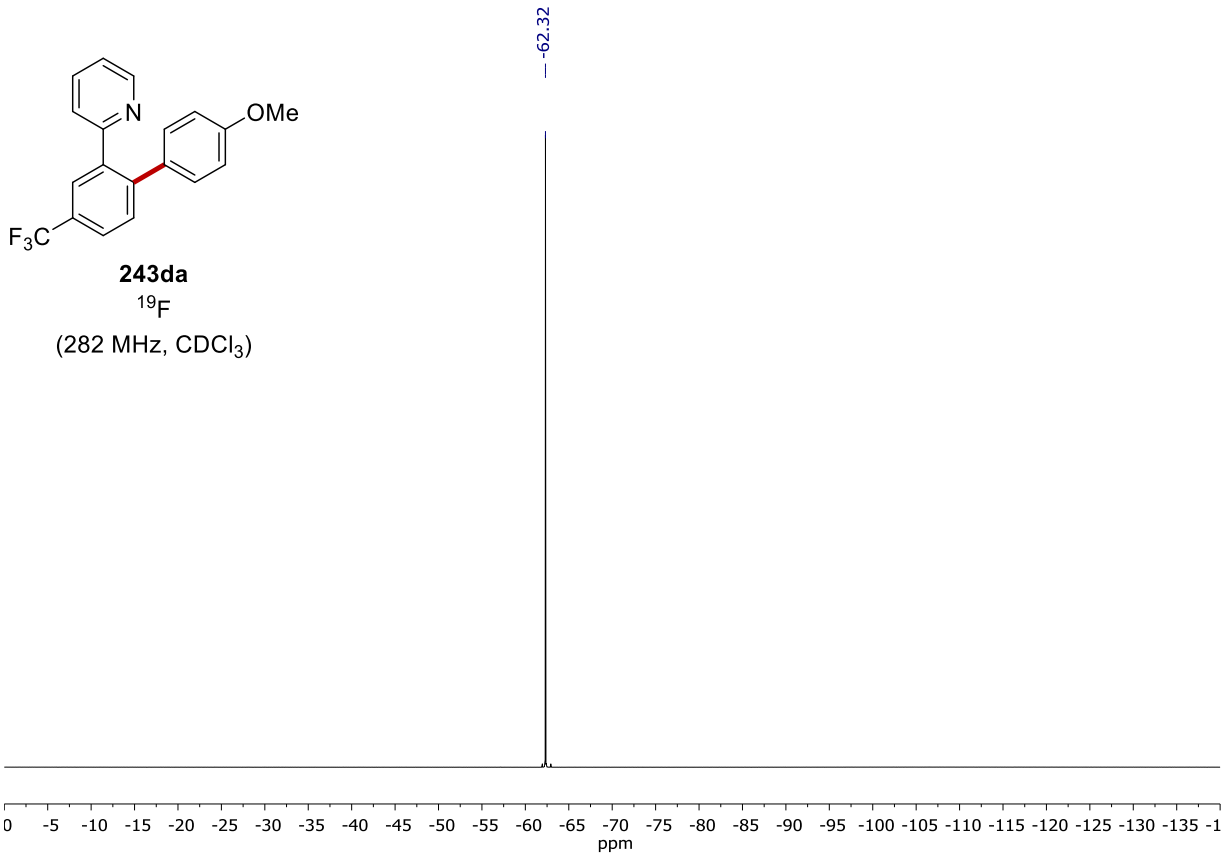
-62.32
N
OMe
F3C
243da
19F
(282 MHz, CDCl3)
ppm

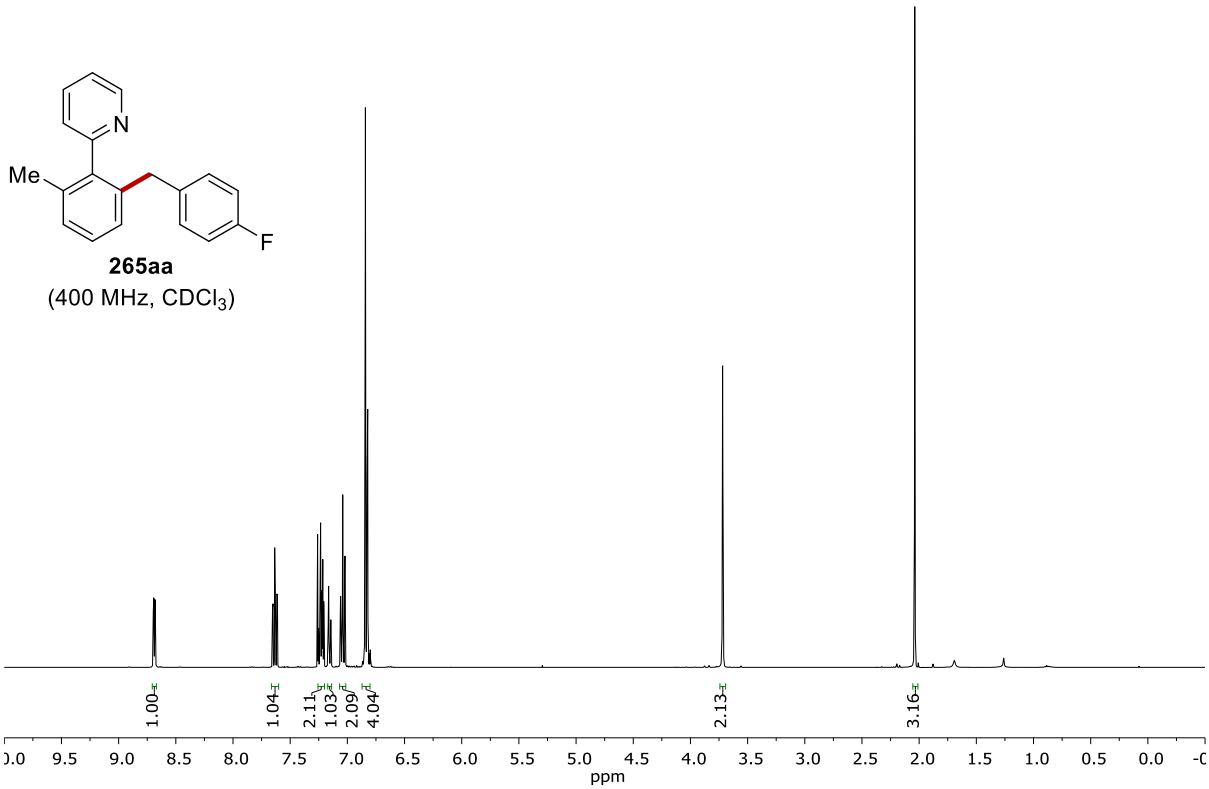
N
Me
F
265aa
(400 MHz, CDCl3)
1.00
1.04
2.11
1.03
2.09
4.04
2.13
3.16
ppm

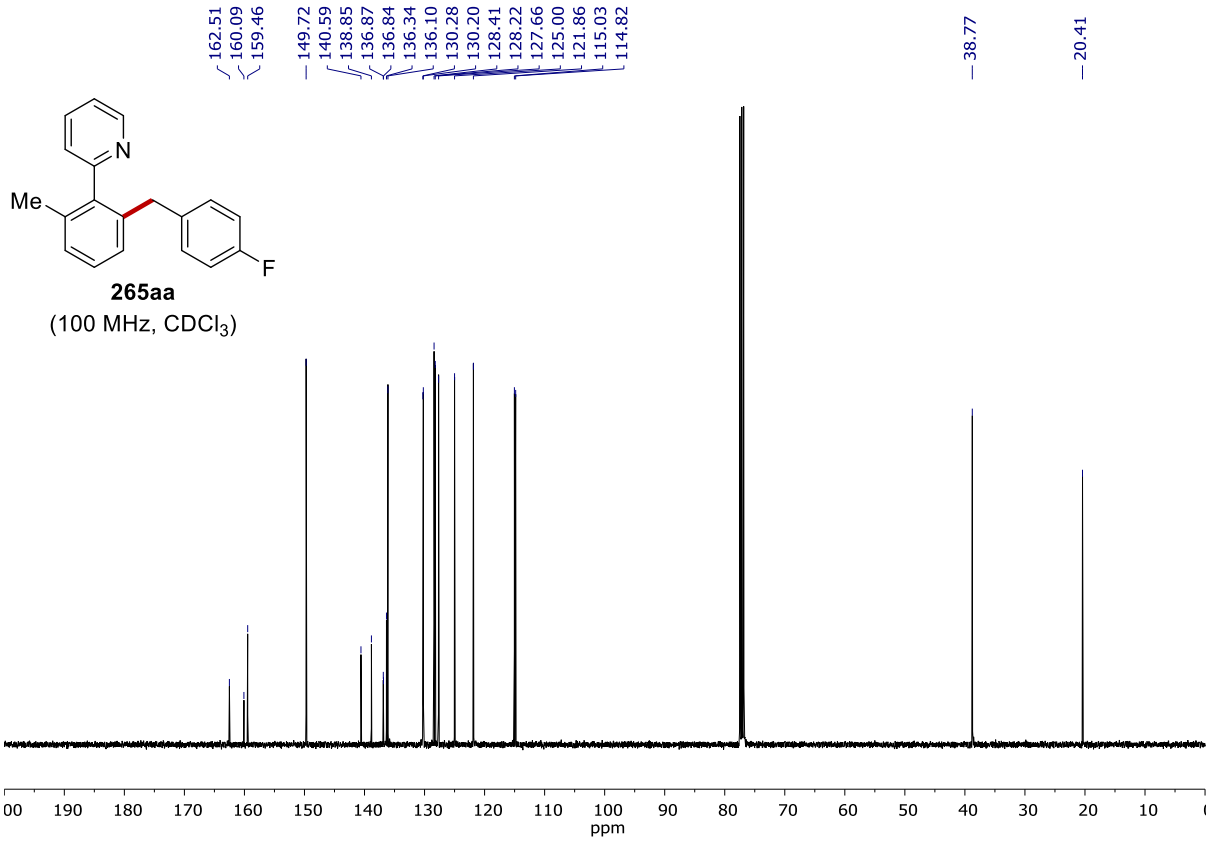
162.51
160.09
159.46
149.72
140.59
138.85
136.87
136.84
136.34
136.10
130.28
130.20
128.41
128.22
127.66
125.00
121.86
115.03
114.82
38.77
20.41
N
Me
F
265aa
(100 MHz, CDCl3)
ppm

265aa

^{19}F-NMR

(376 MHz, $CDCl_3$)

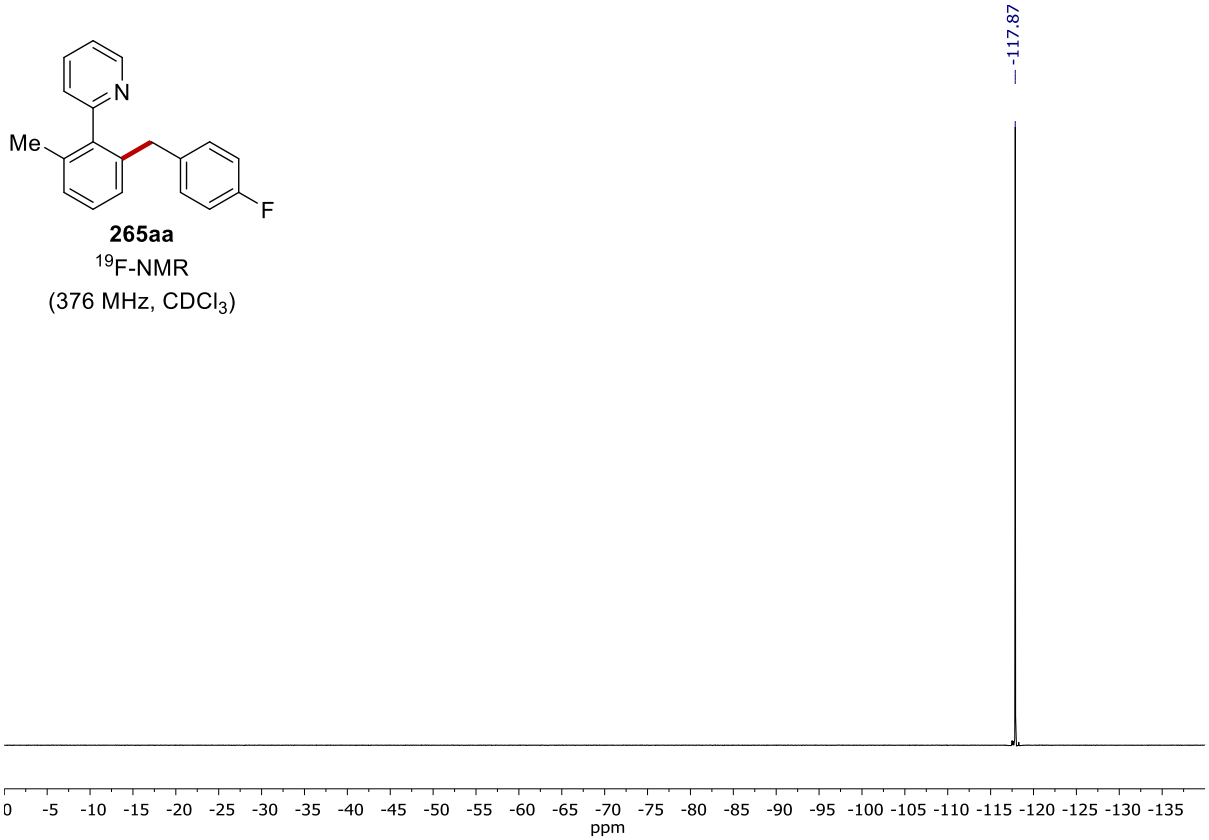

265ab

(400 MHz, $CDCl_3$)

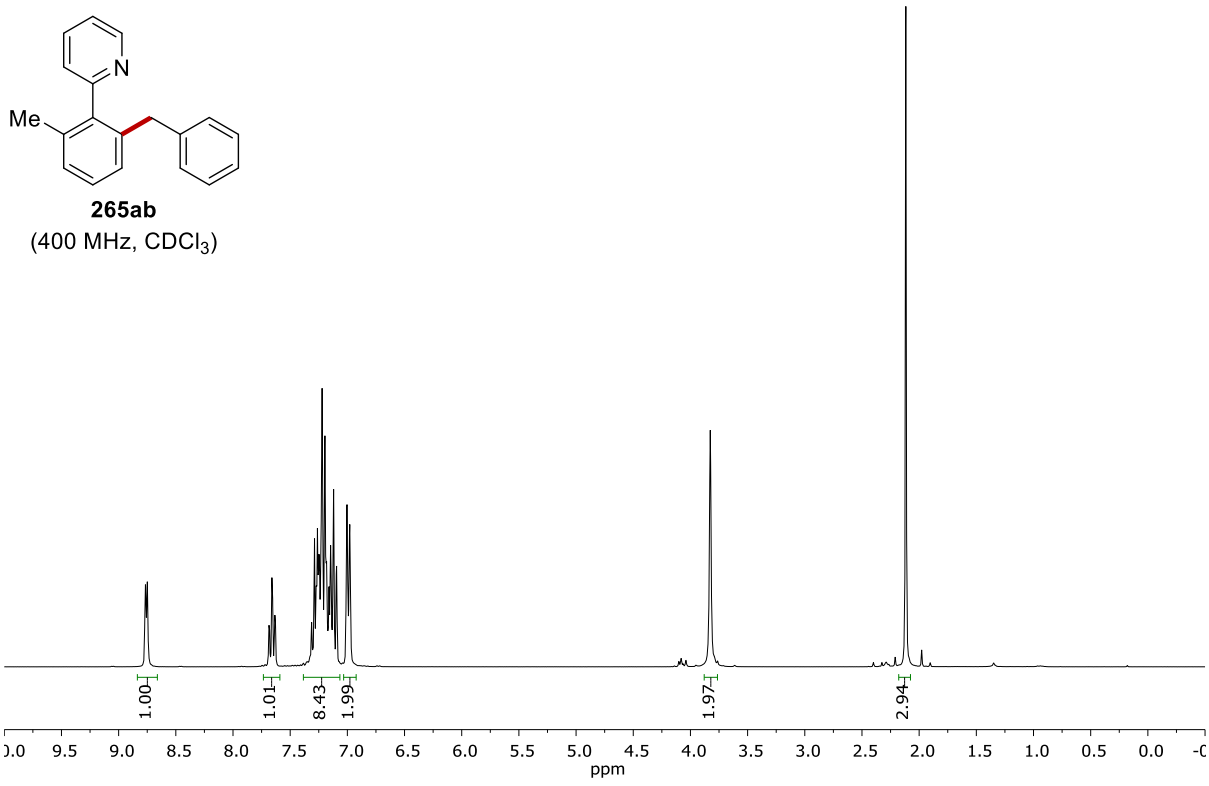

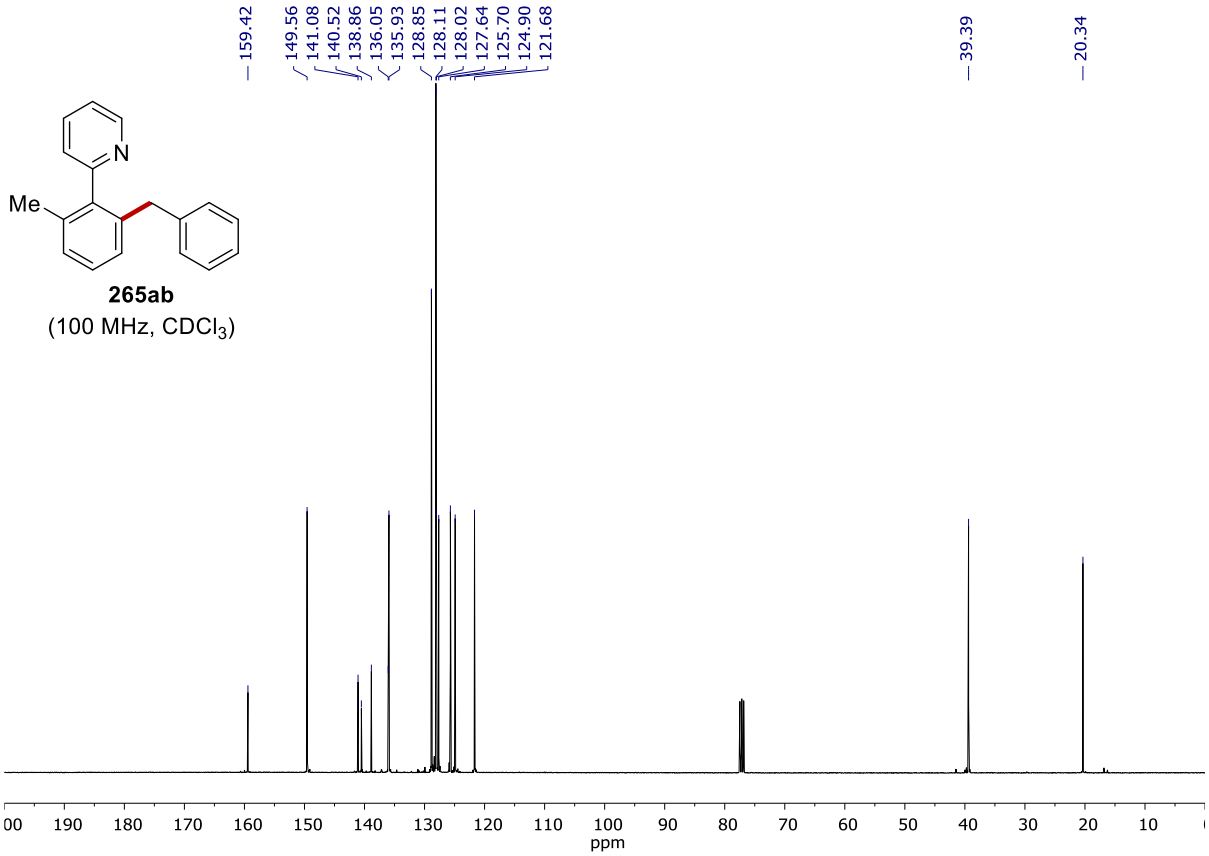

265ab
(100 MHz, $CDCl_3$)

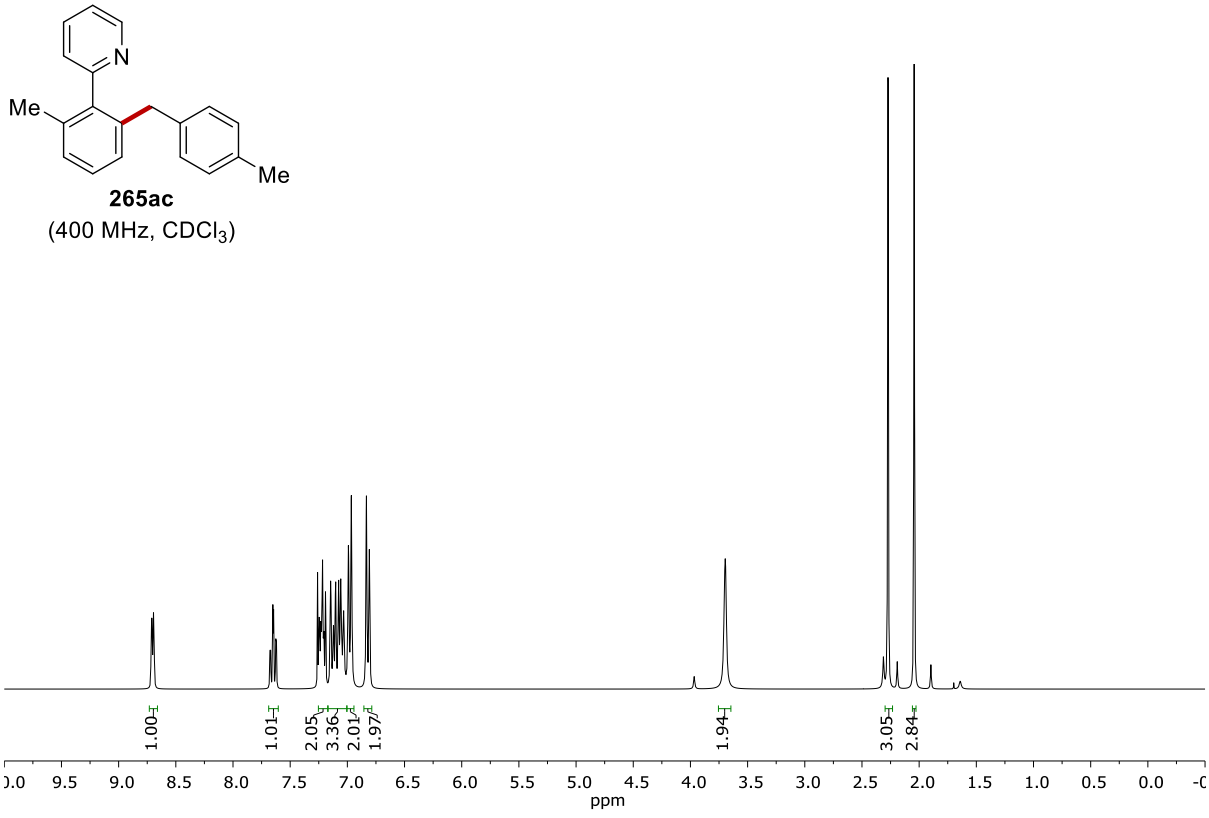

265ac
(400 MHz, $CDCl_3$)

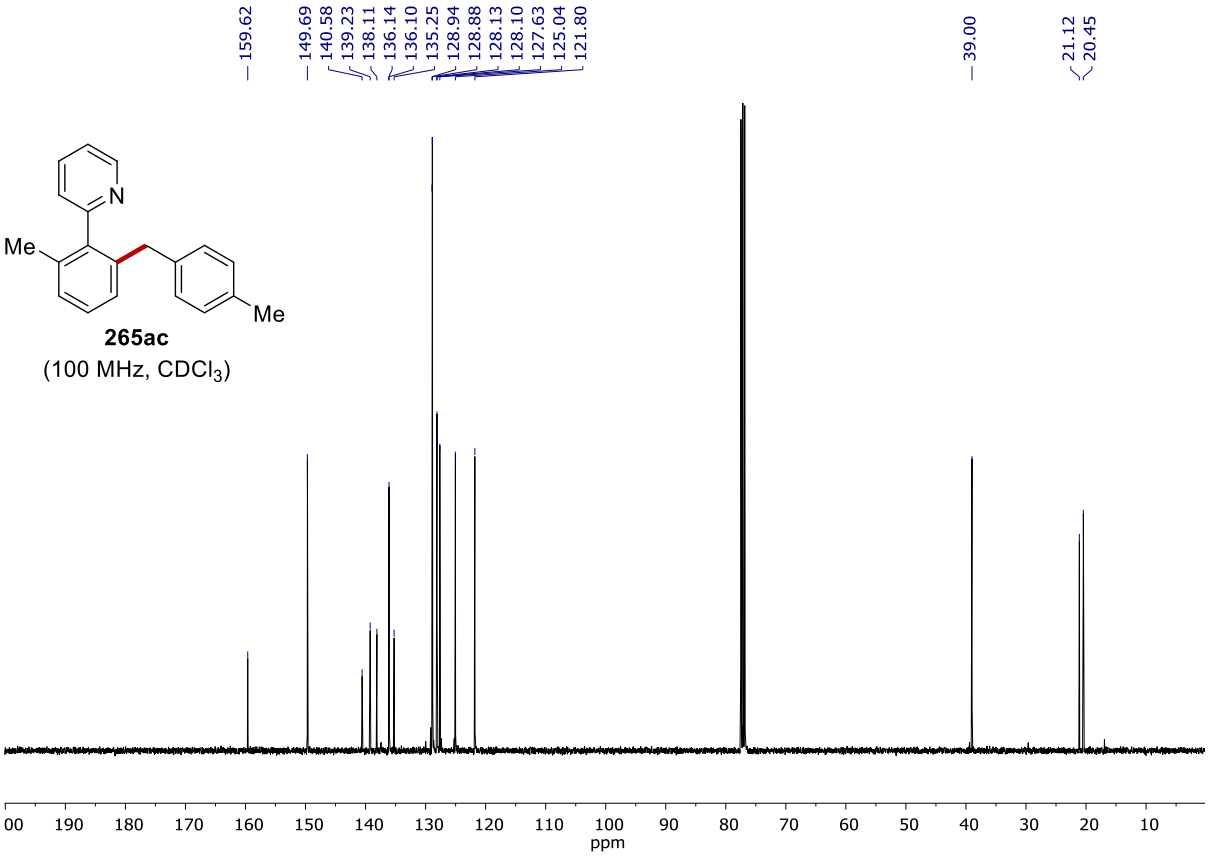
159.62
149.69
140.58
139.23
138.11
136.14
136.10
135.25
128.94
128.88
128.13
128.10
127.63
125.04
121.80
39.00
21.12
20.45
N
Me
Me
265ac
(100 MHz, CDCl3)
ppm

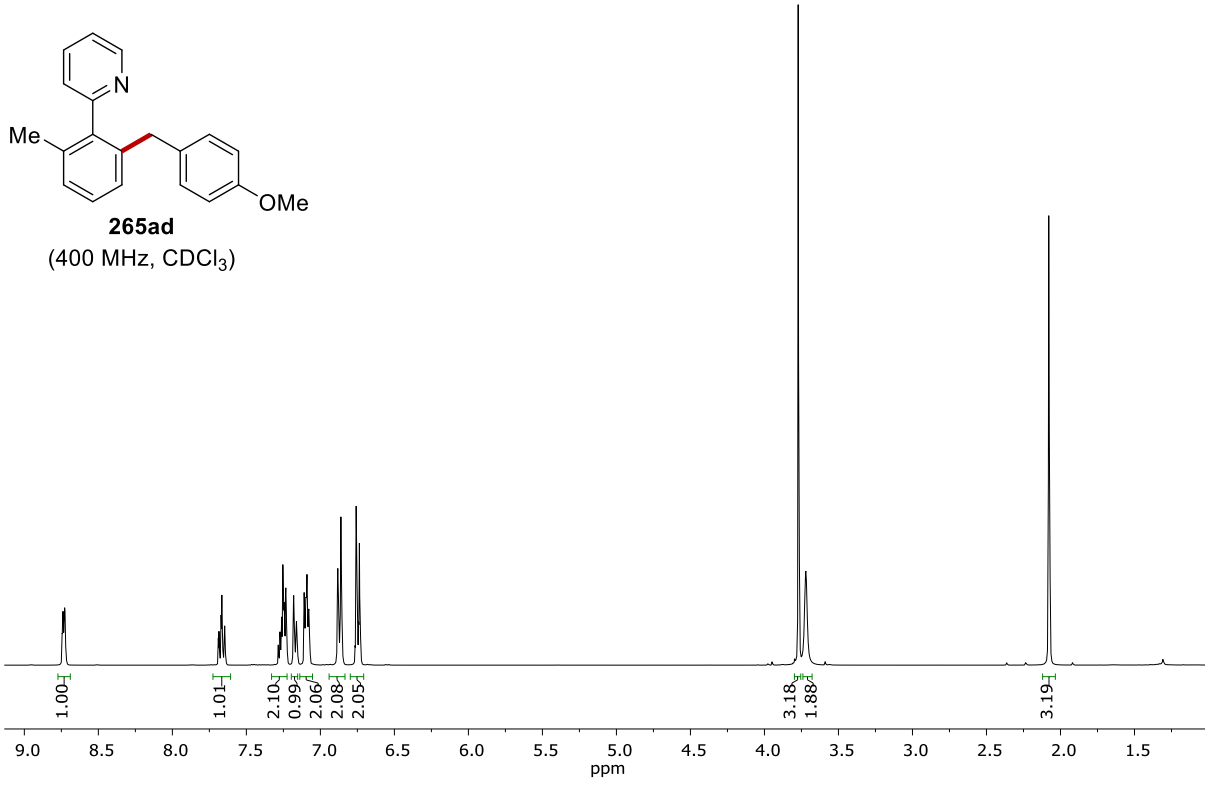
N
Me
OMe
265ad
(400 MHz, CDCl3)
1.00
1.01
2.10
0.99
2.06
2.08
2.05
3.18
1.88
3.19
ppm

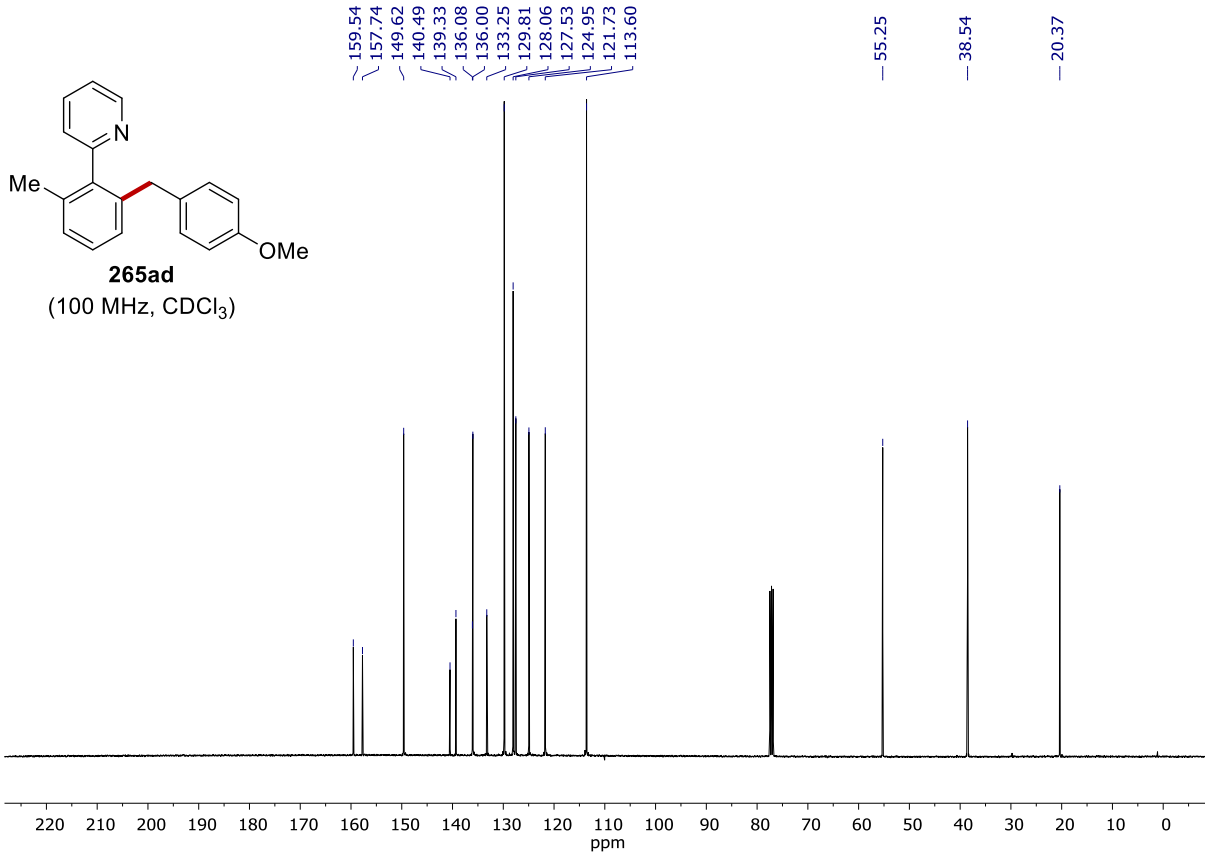

265ad
(100 MHz, $CDCl_3$)

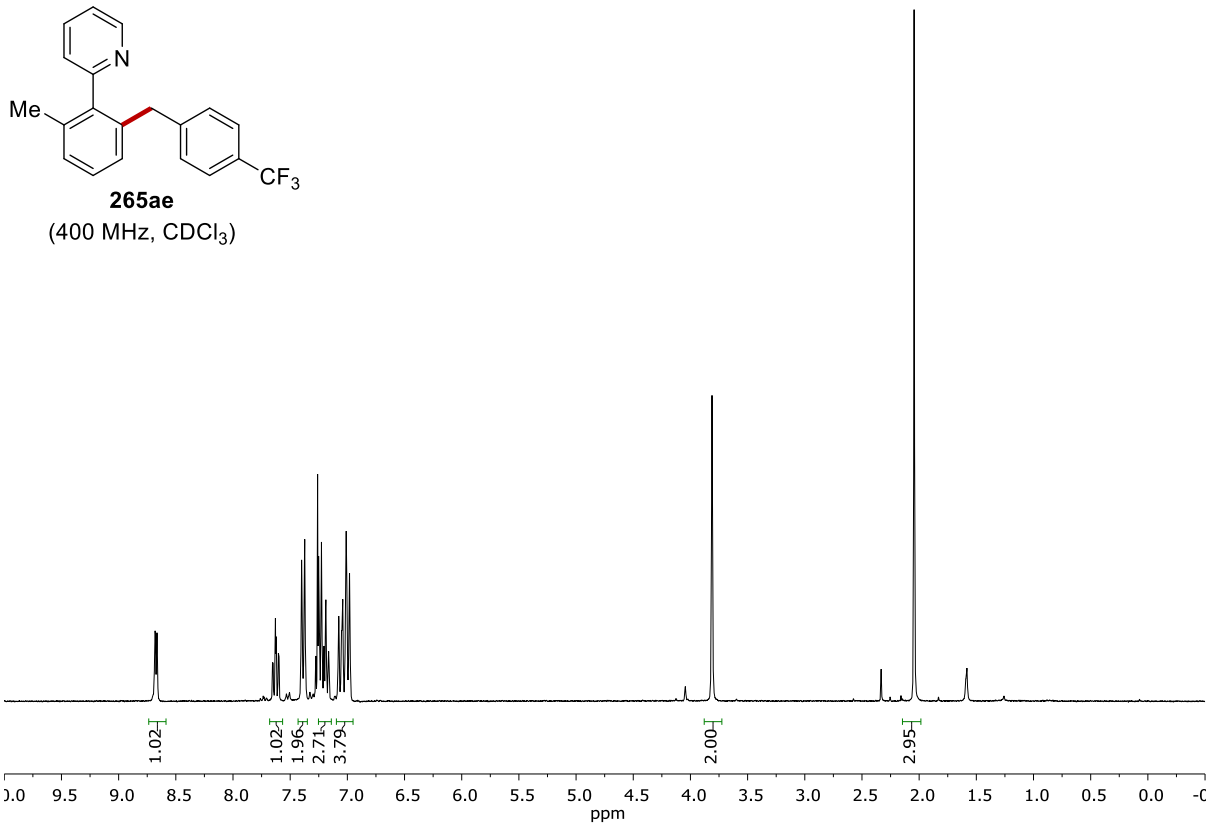

265ae
(400 MHz, $CDCl_3$)

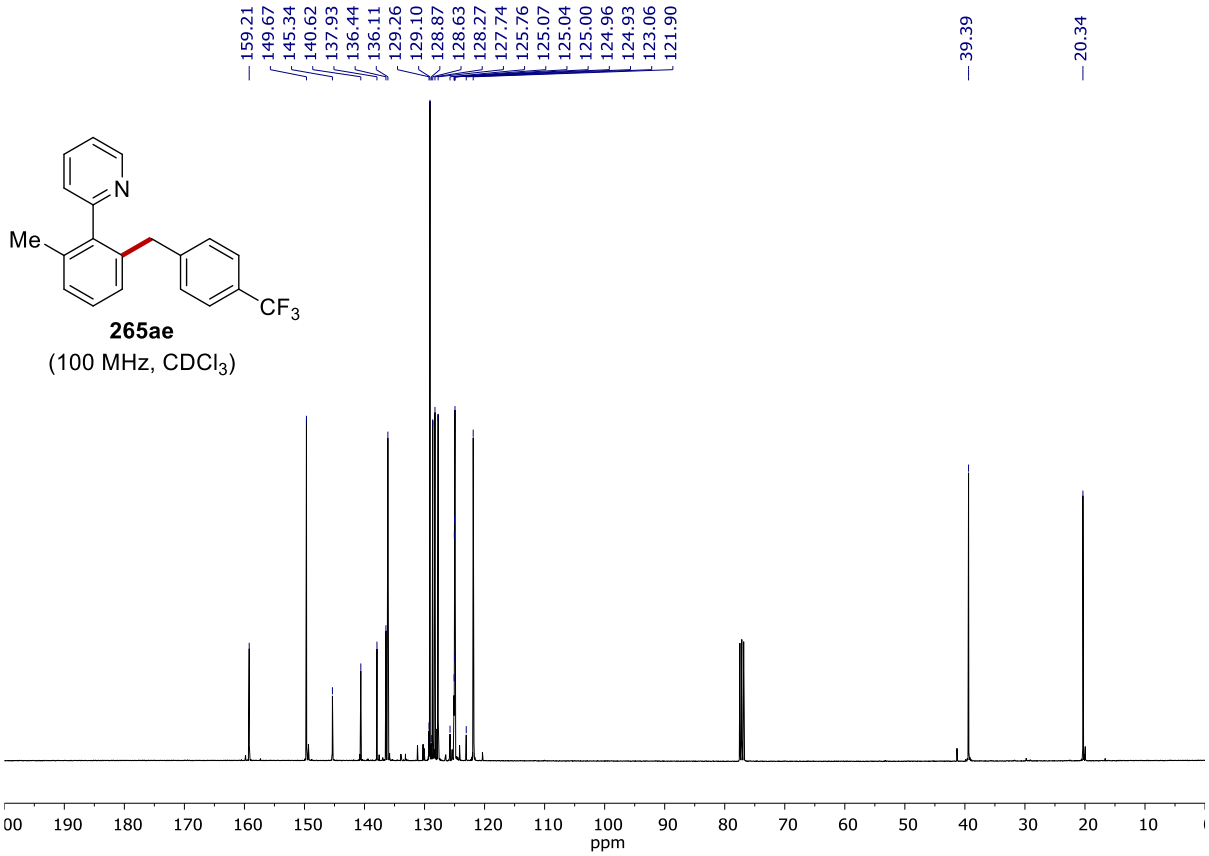
159.21
149.67
145.34
140.62
137.93
136.44
136.11
129.26
129.10
128.87
128.63
128.27
127.74
125.76
125.07
125.04
125.00
124.96
124.93
123.06
121.90
39.39
20.34
N
Me
CF3
265ae
(100 MHz, CDCl3)
ppm

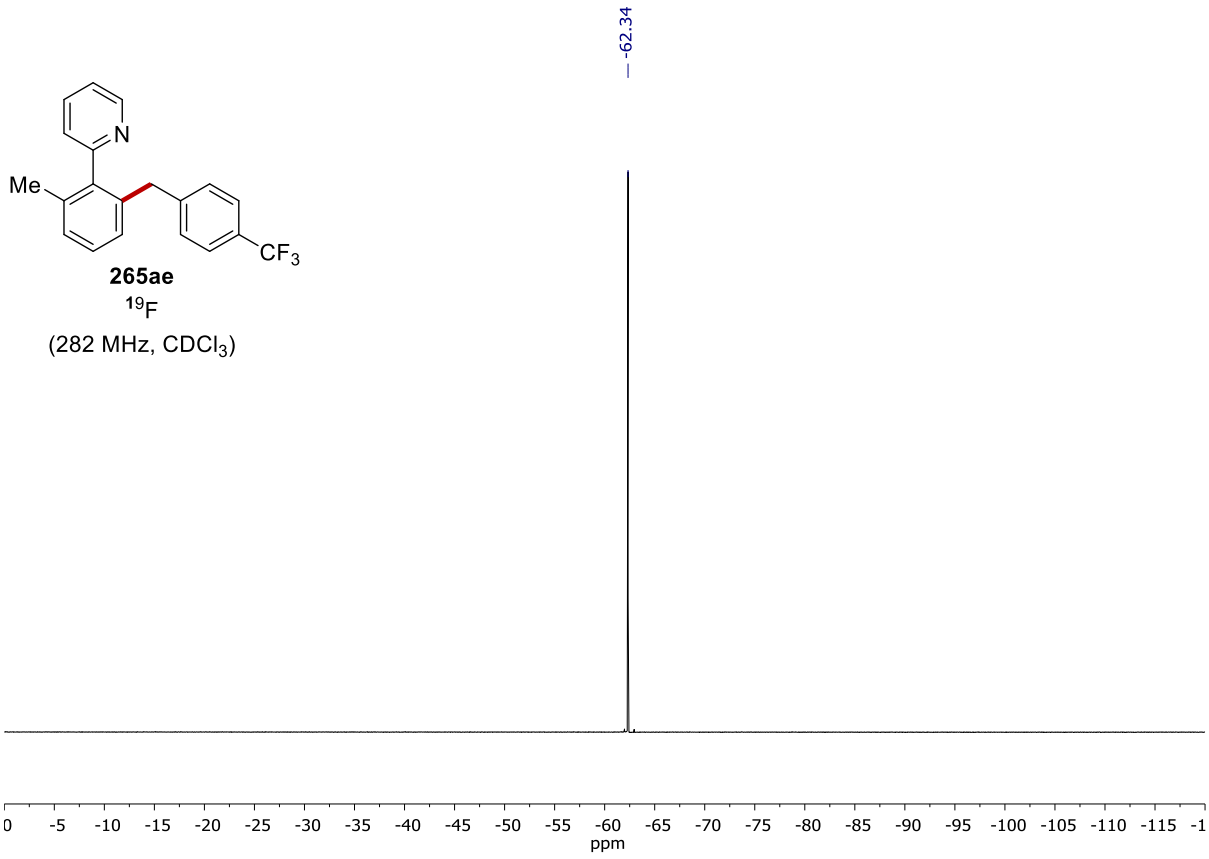
-62.34
N
Me
CF3
265ae
19F
(282 MHz, CDCl3)
ppm

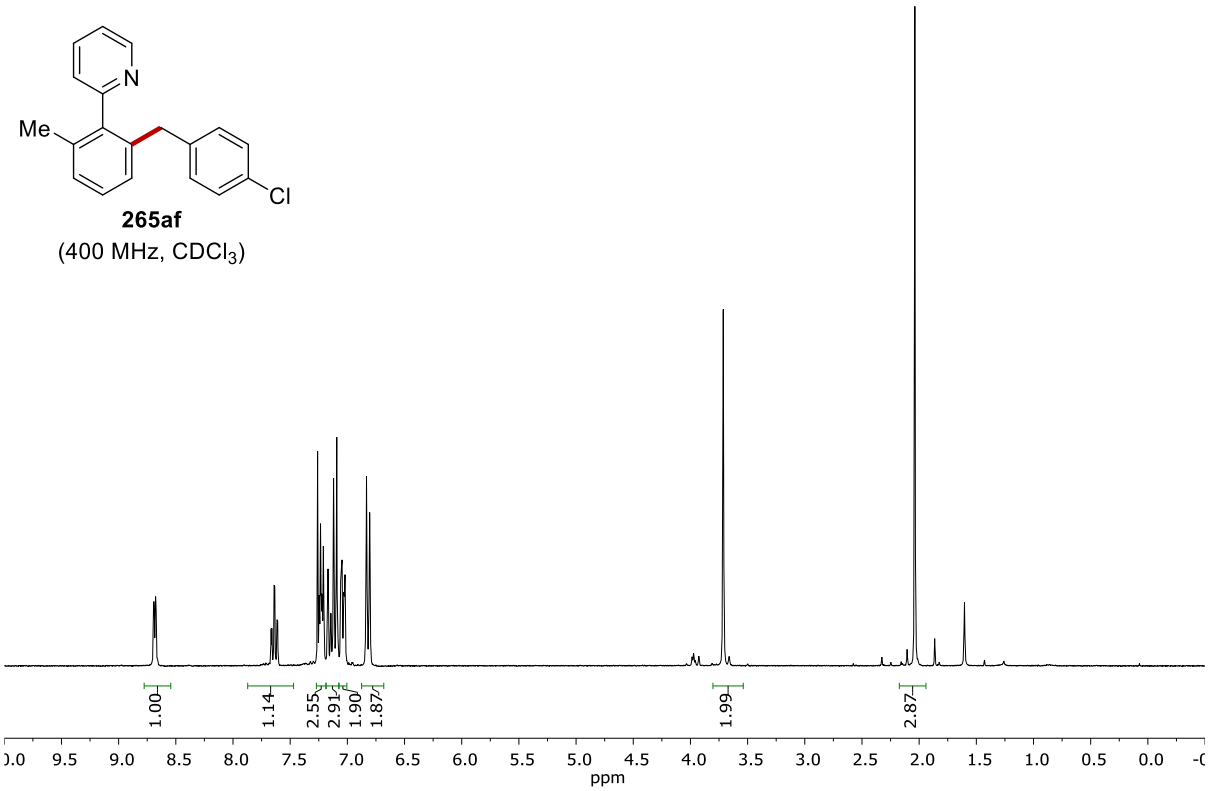
N
Me
Cl
265af
(400 MHz, CDCl3)
1.00
1.14
2.55
2.91
1.90
1.87
1.99
2.87
ppm

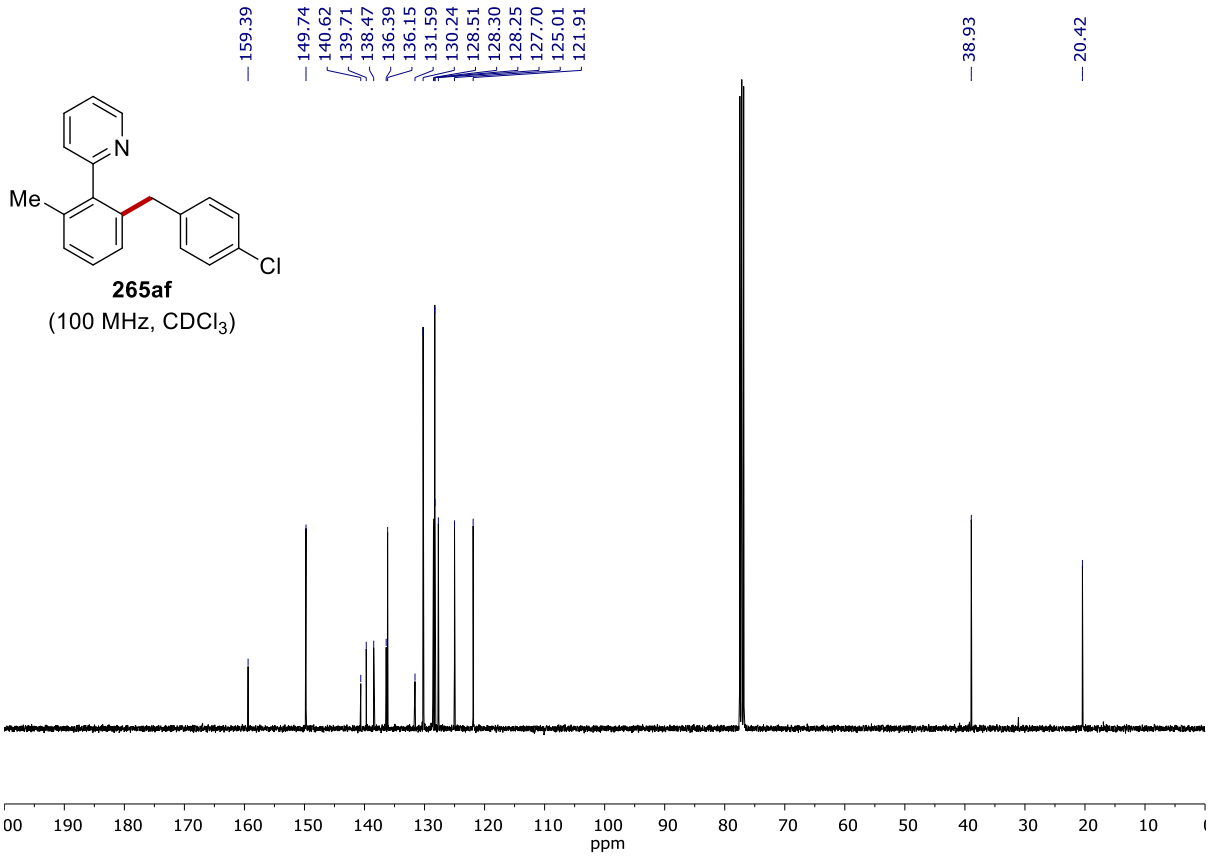
159.39
149.74
140.62
139.71
138.47
136.39
136.15
131.59
130.24
128.51
128.30
128.25
127.70
125.01
121.91
38.93
20.42
N
Me
Cl
265af
(100 MHz, CDCl3)
ppm

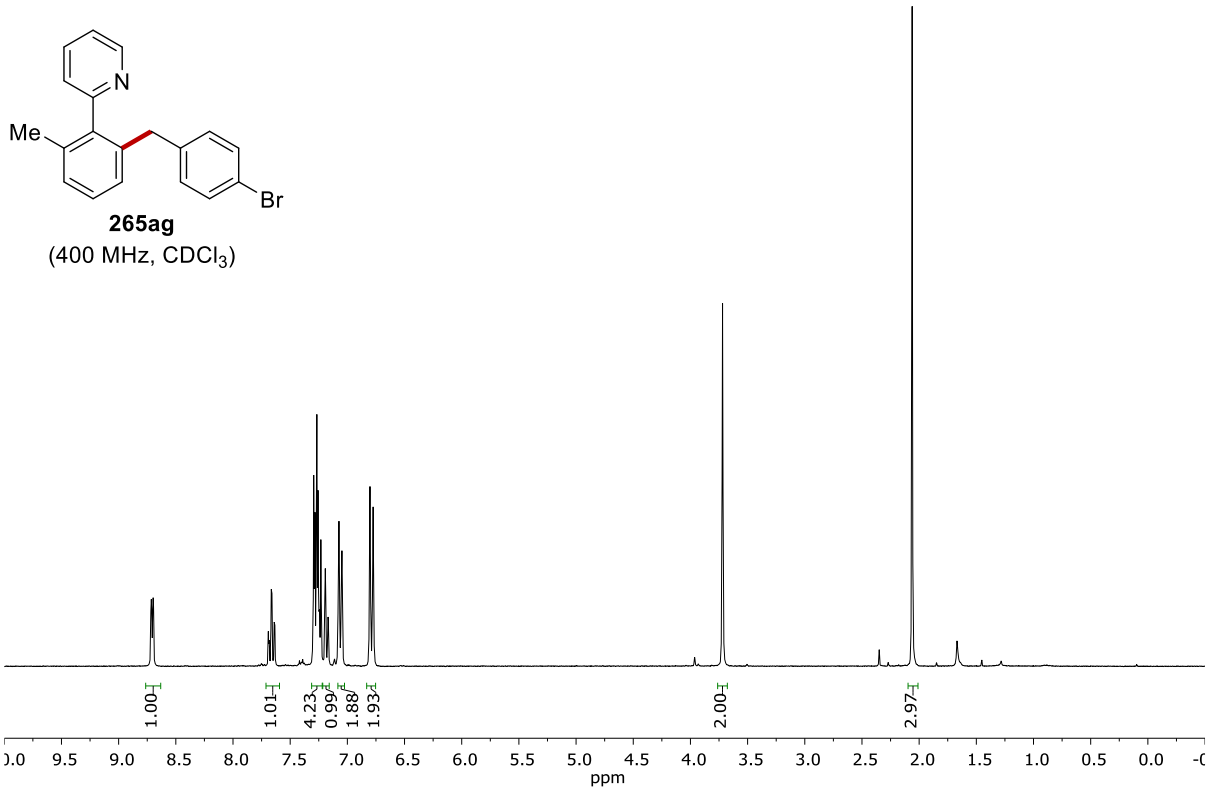
N
Me
Br
265ag
(400 MHz, CDCl3)
1.00
1.01
4.23
0.99
1.88
1.93
2.00
2.97
ppm

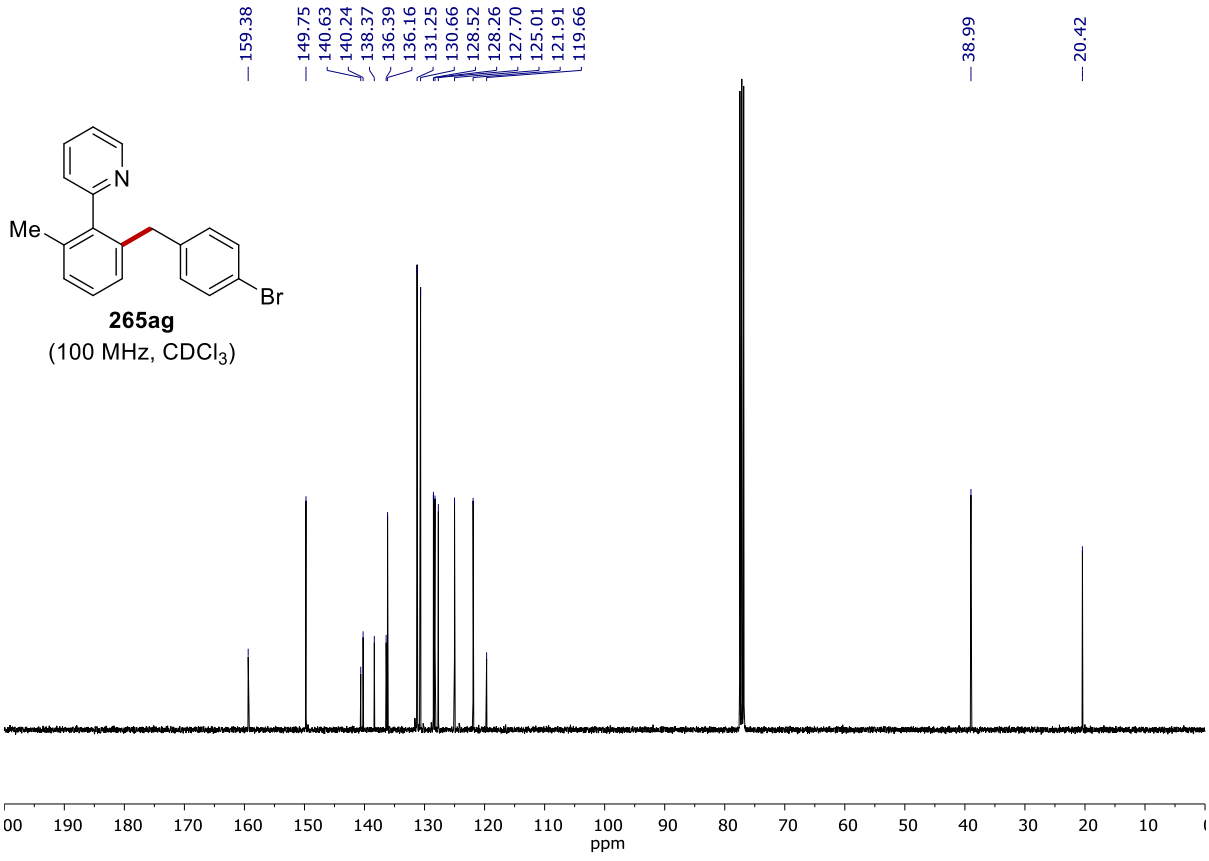
159.38
149.75
140.63
140.24
138.37
136.39
136.16
131.25
130.66
128.52
128.26
127.70
125.01
121.91
119.66
38.99
20.42
N
Me
Br
265ag
(100 MHz, CDCl3)
ppm

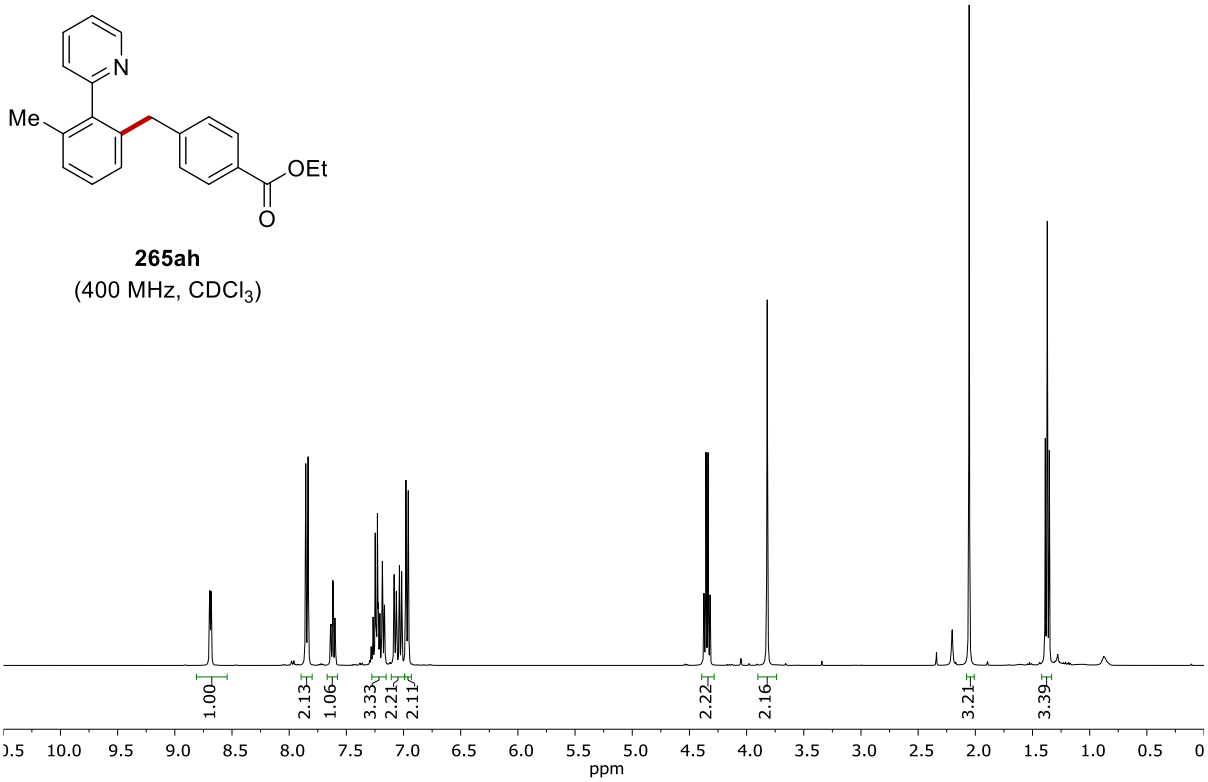

265ah
(400 MHz, $CDCl_3$)

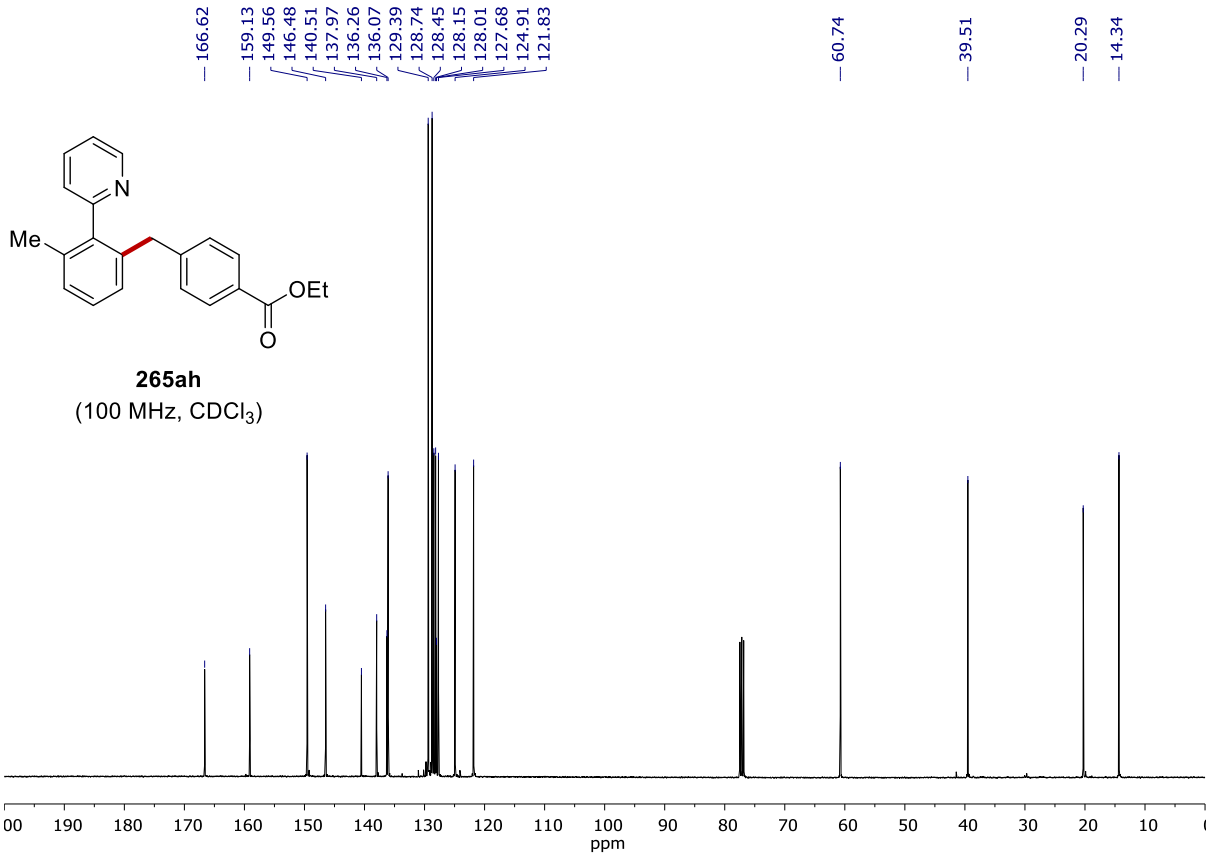

265ah
(100 MHz, $CDCl_3$)

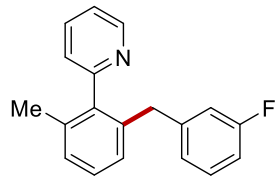

265ai
(400 MHz, $CDCl_3$)

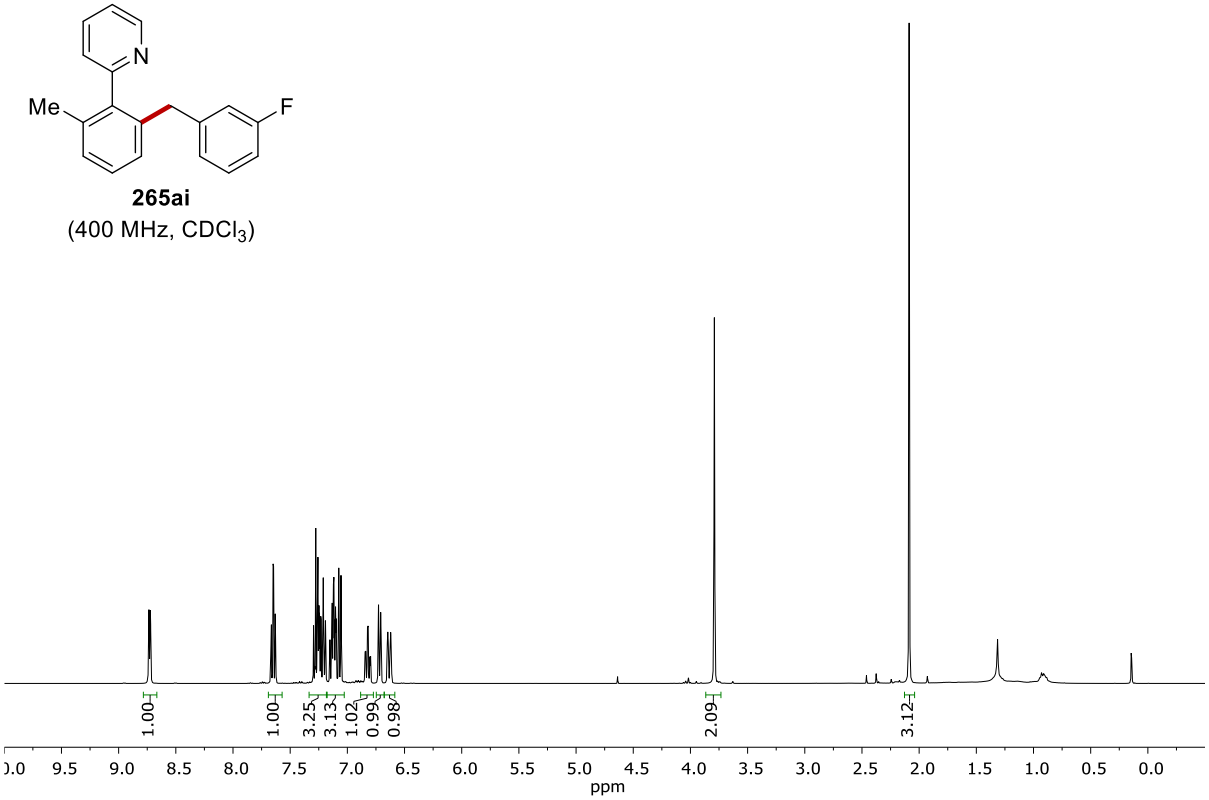

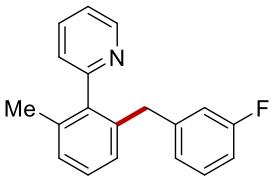

265ai
(100 MHz, $CDCl_3$)

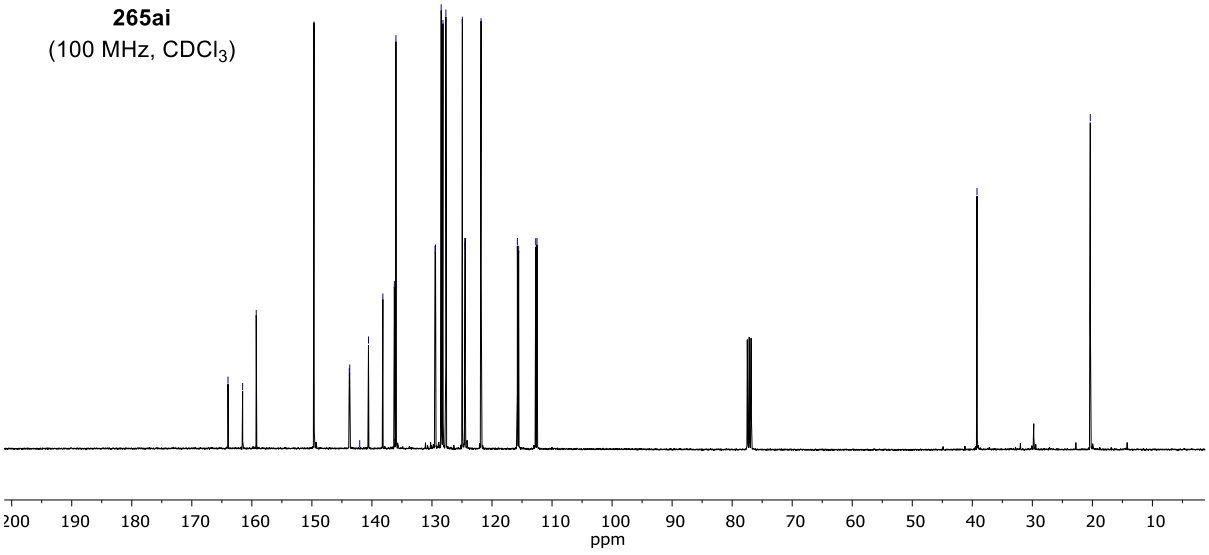

265ai

^{19}F

(282 MHz, $CDCl_3$)

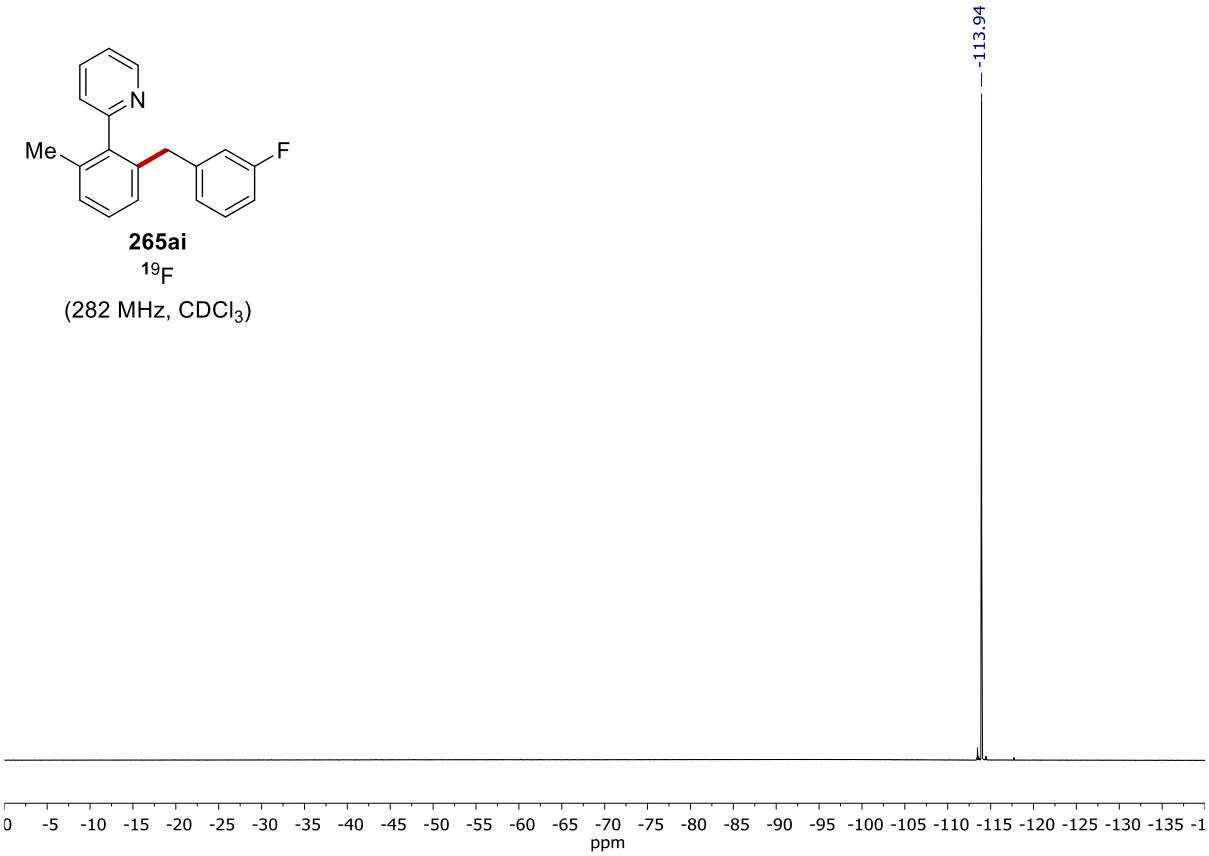

265aj

(400 MHz, $CDCl_3$)

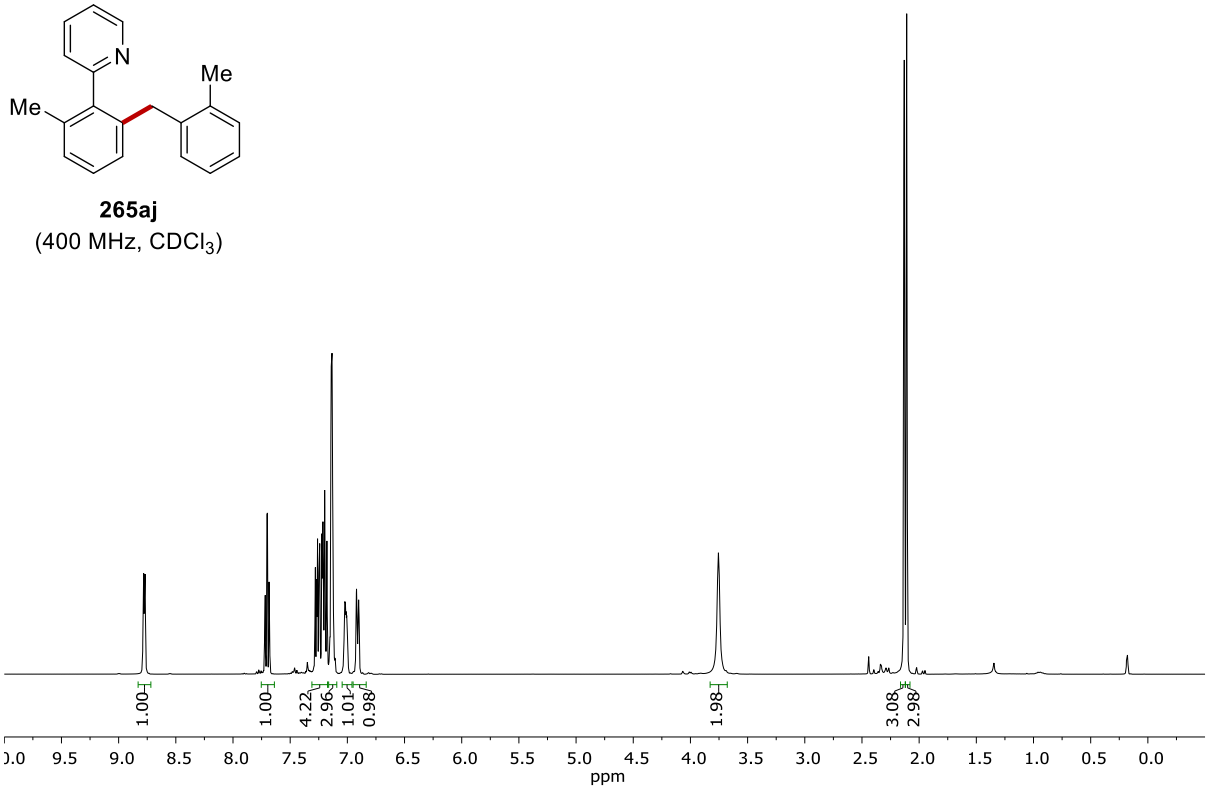

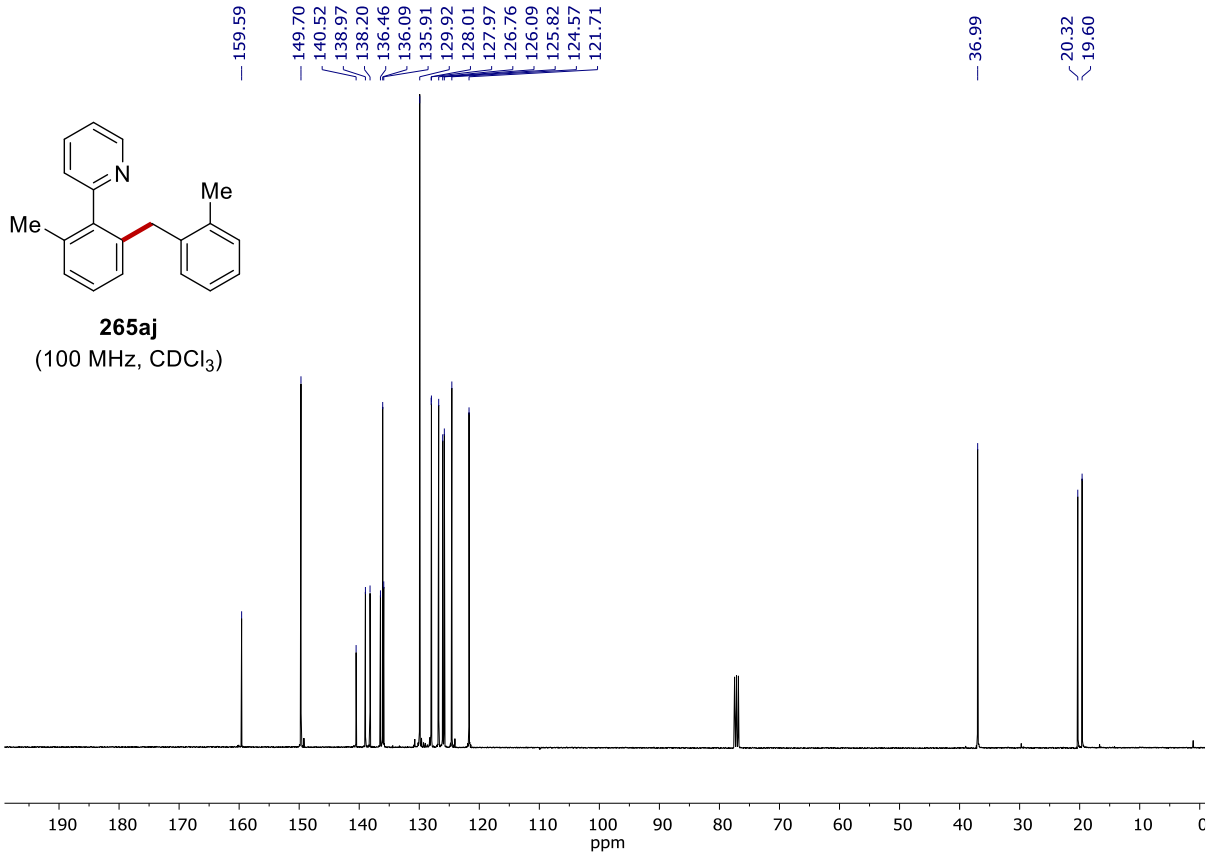

265aj
(100 MHz, $CDCl_3$)

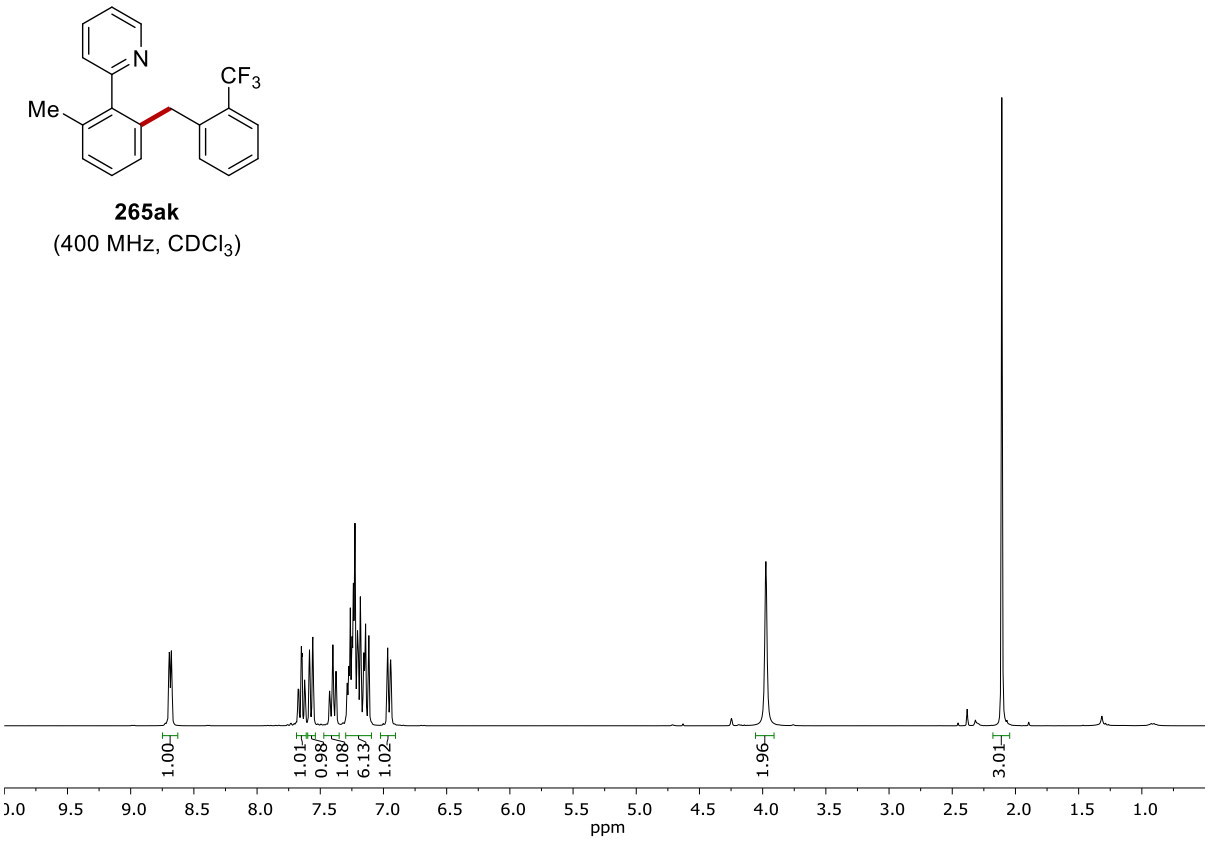

265ak
(400 MHz, $CDCl_3$)

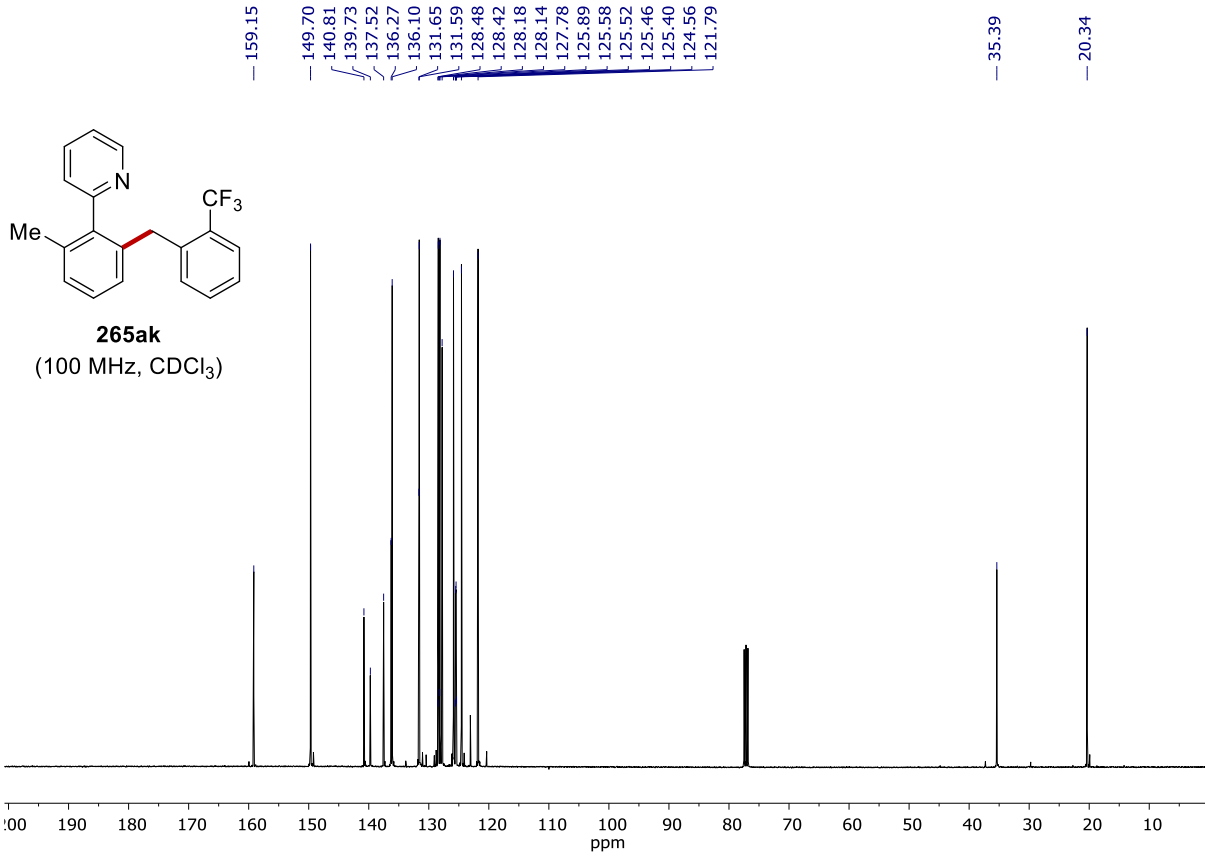

265ak
(100 MHz, $CDCl_3$)

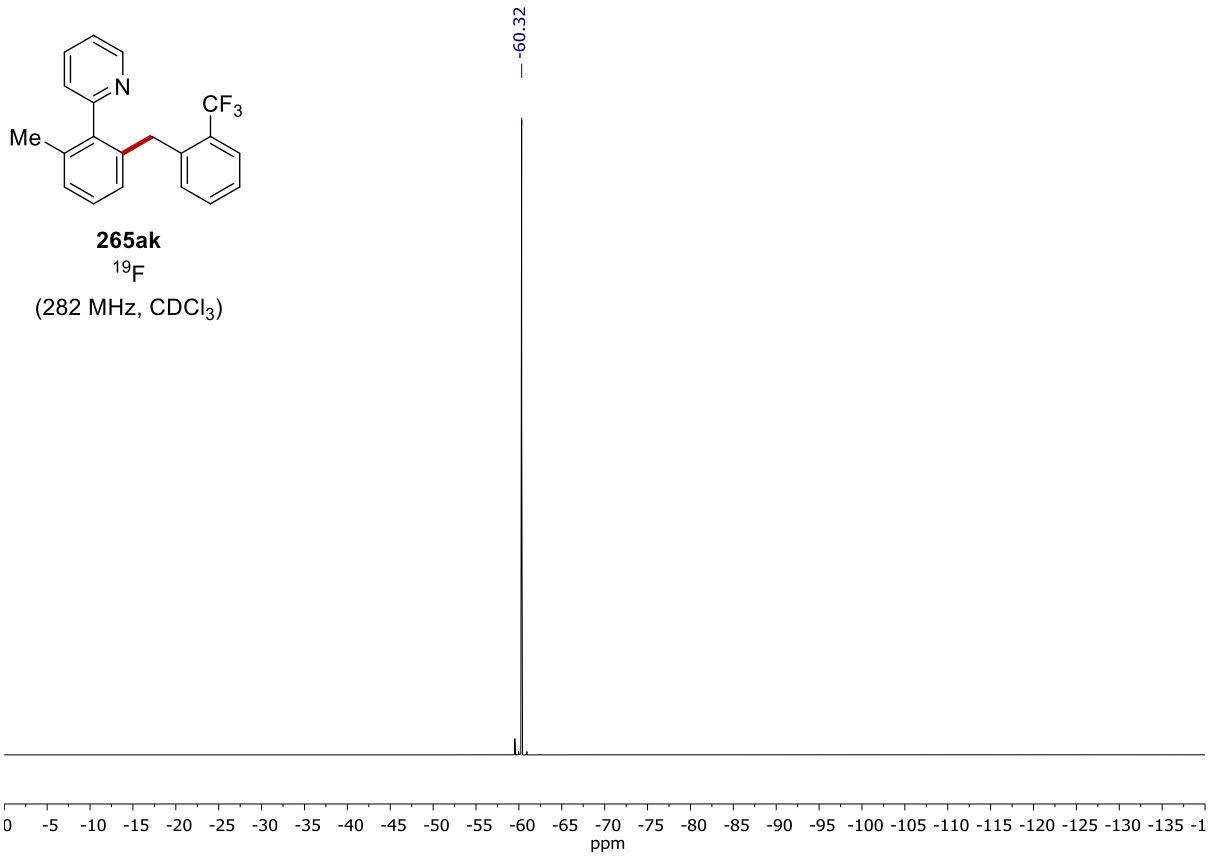

265ak
^{19}F
(282 MHz, $CDCl_3$)

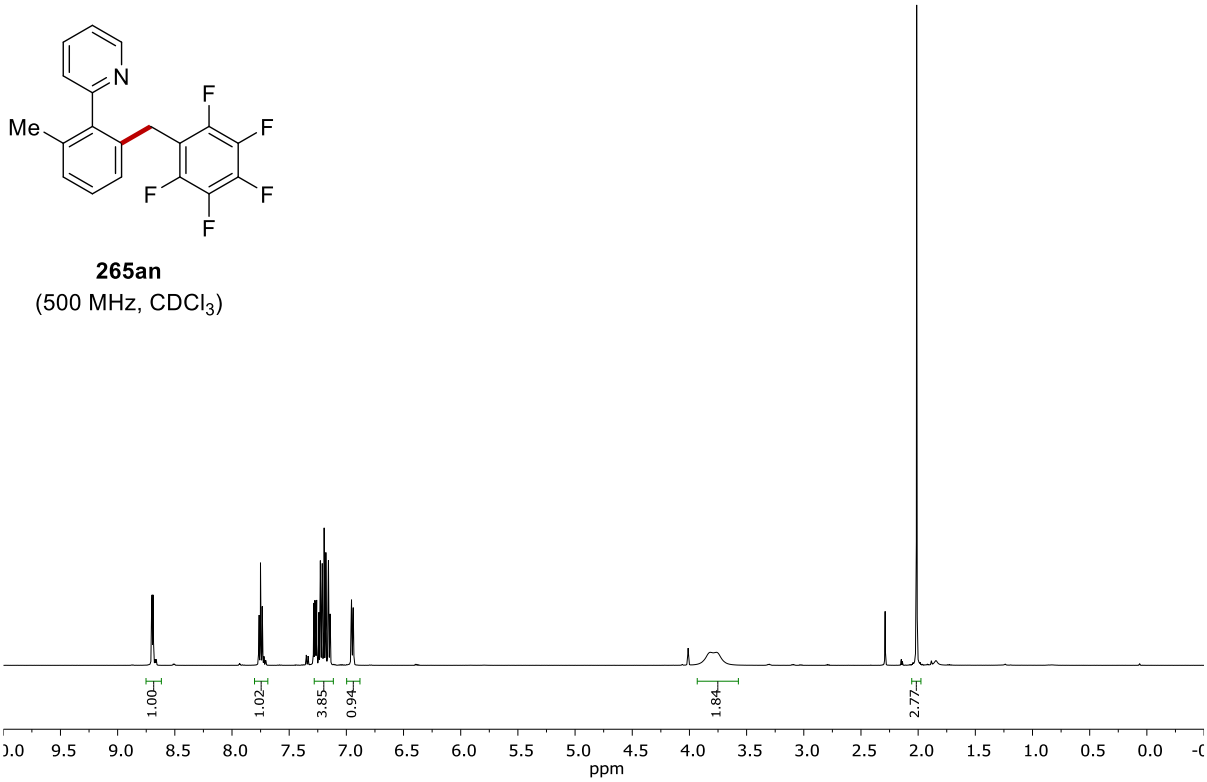
N
Me
F
F
F
F
F
265an
(500 MHz, CDCl3)
1.00
1.02
3.85
0.94
1.84
2.77
ppm

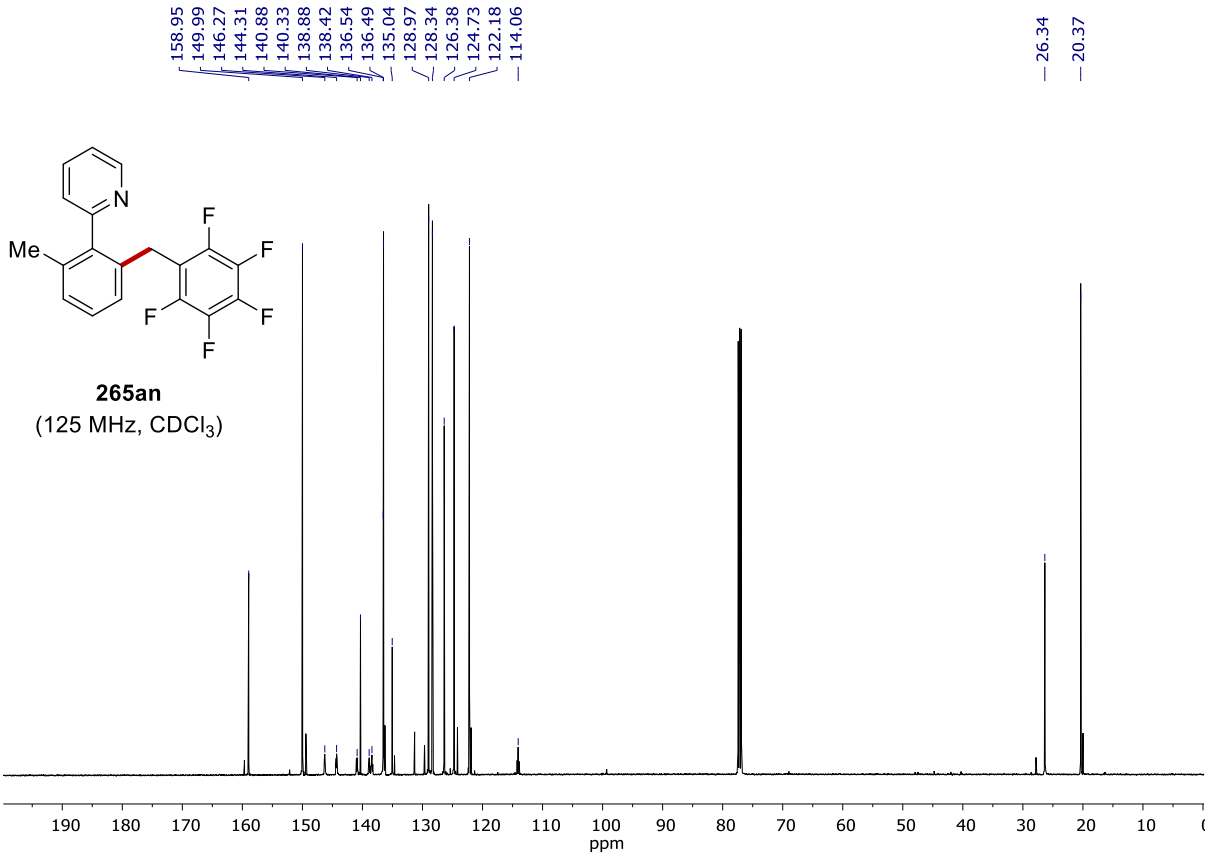
158.95
149.99
146.27
144.31
140.88
140.33
138.88
138.42
136.54
136.49
135.04
128.97
128.34
126.38
124.73
122.18
114.06
26.34
20.37
N
Me
F
F
F
F
F
265an
(125 MHz, CDCl3)
ppm

265an

^{19}F

(476 MHz, $CDCl_3$)

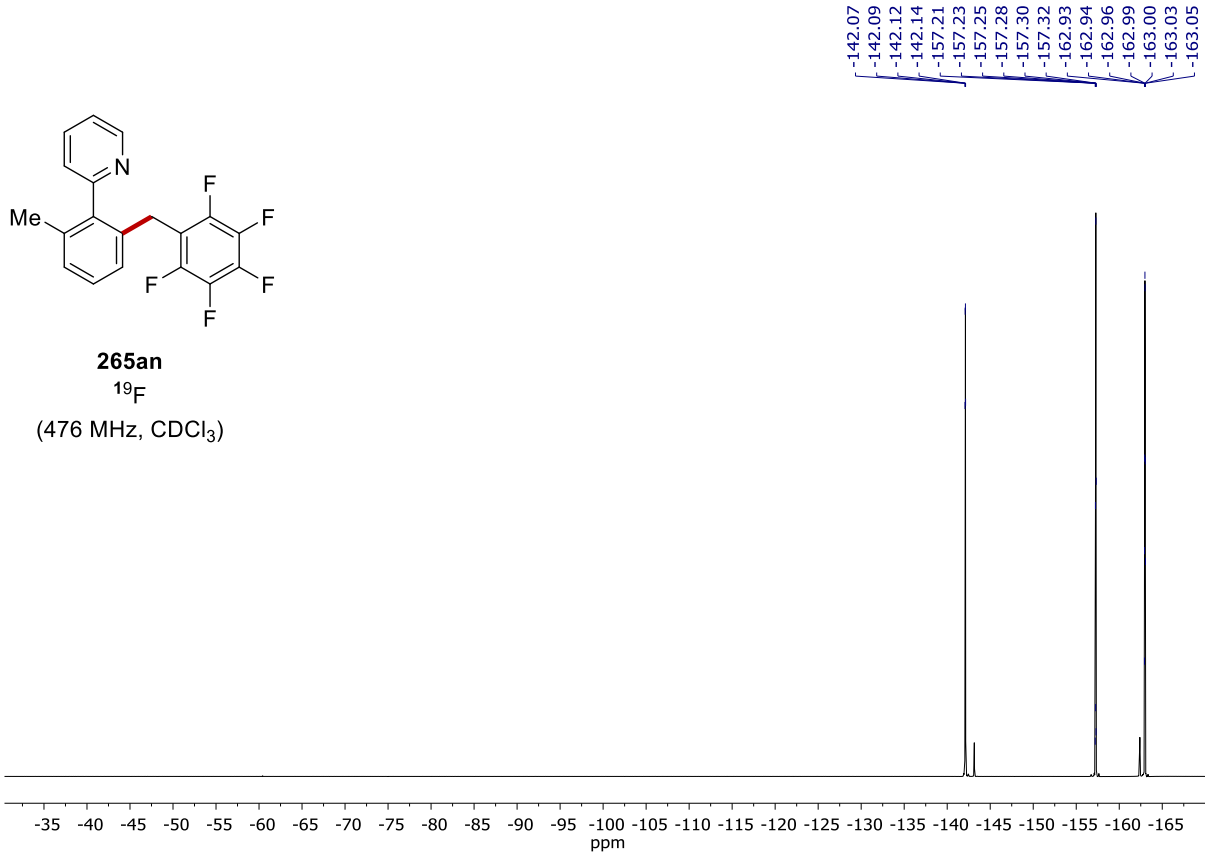

265ao

(300 MHz, $CDCl_3$)

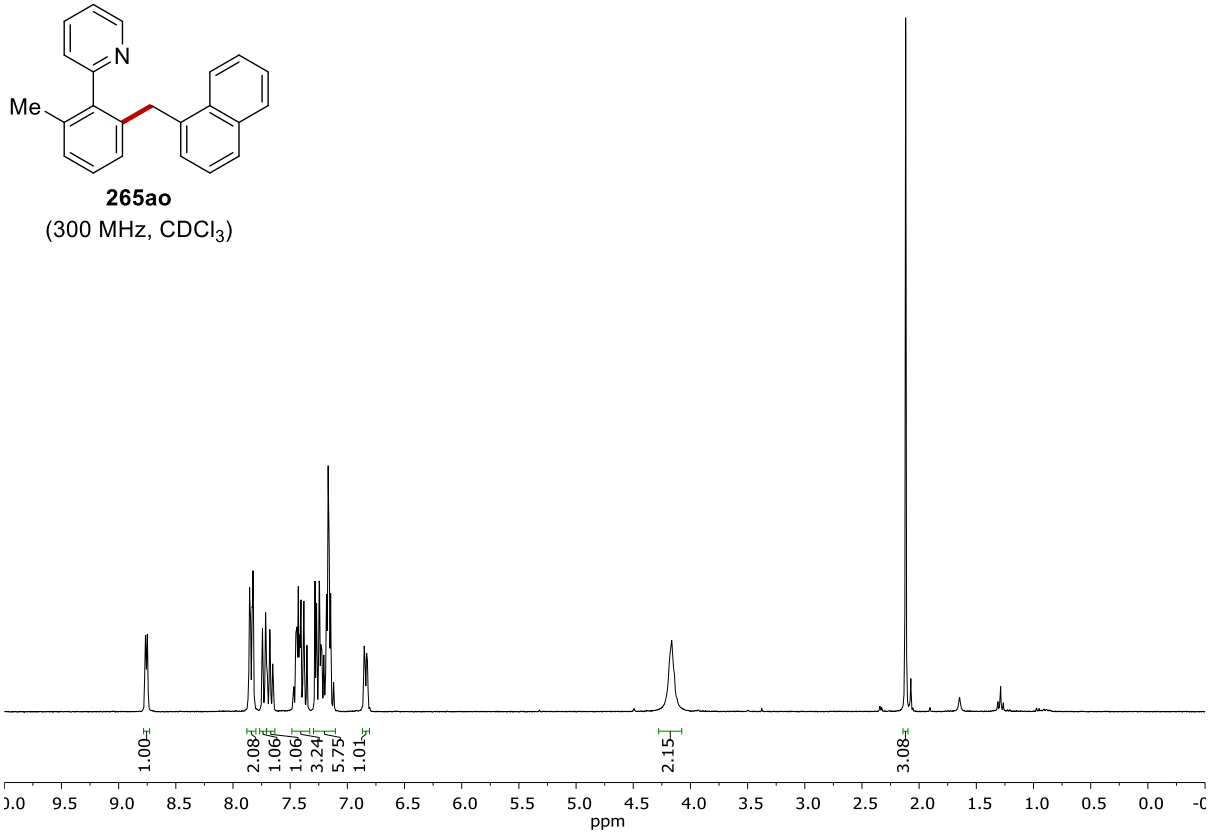

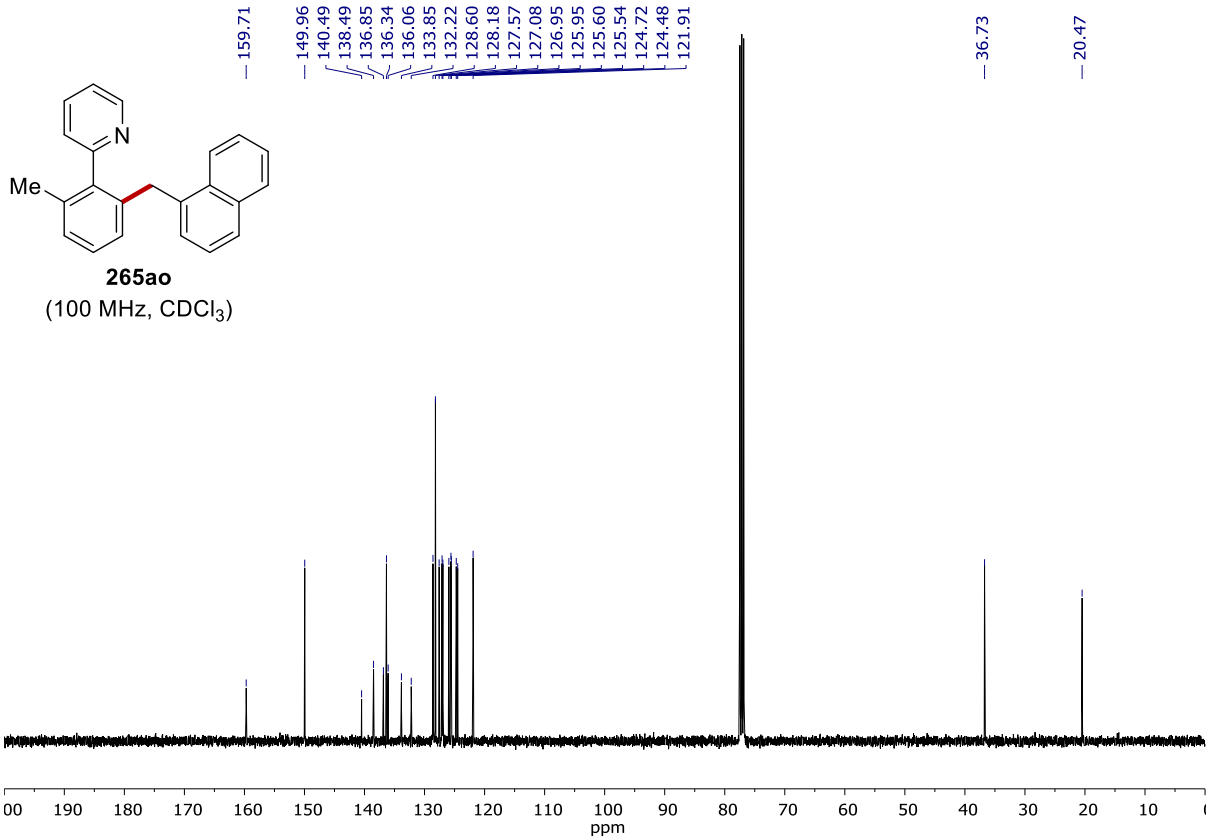
159.71
149.96
140.49
138.49
136.85
136.34
136.06
133.85
132.22
128.60
128.18
127.57
127.08
126.95
125.95
125.60
125.54
124.72
124.48
121.91
36.73
20.47
N
Me
265ao
(100 MHz, CDCl3)
ppm

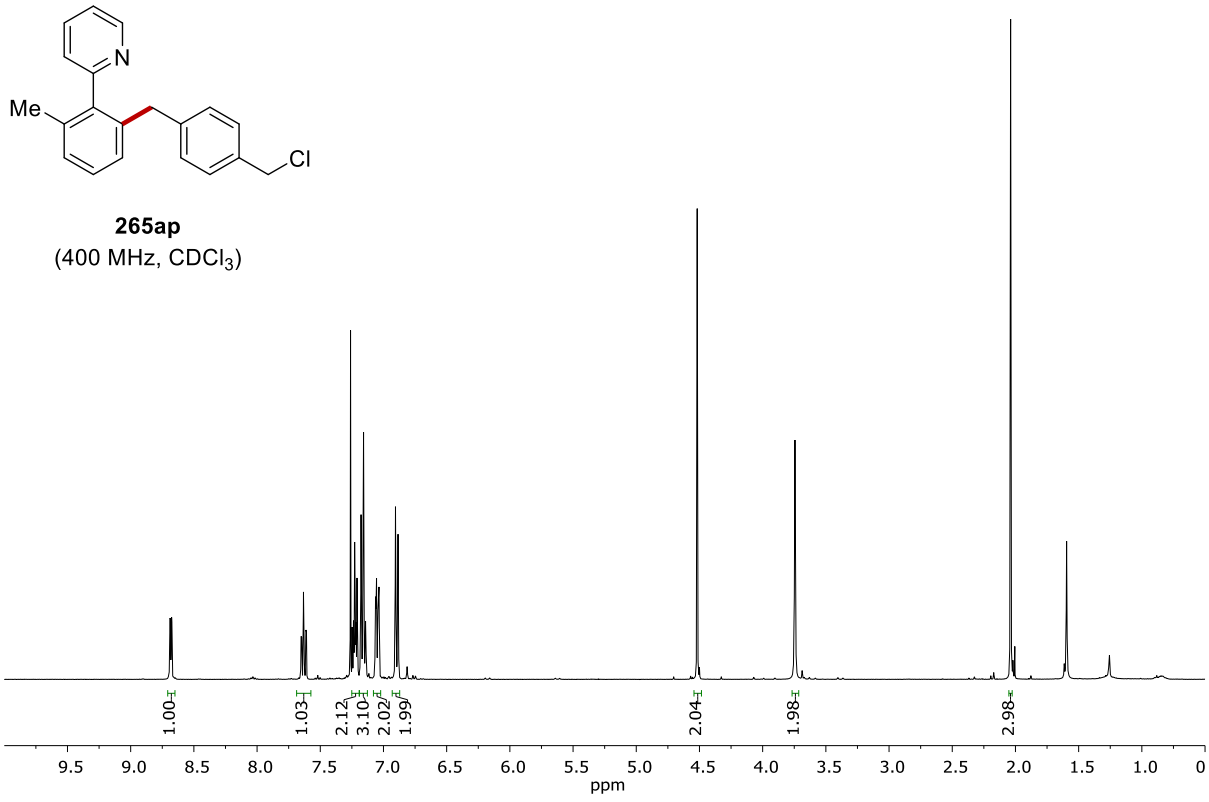
N
Me
Cl
265ap
(400 MHz, CDCl3)
1.00
1.03
2.12
3.10
2.02
1.99
2.04
1.98
2.98
ppm

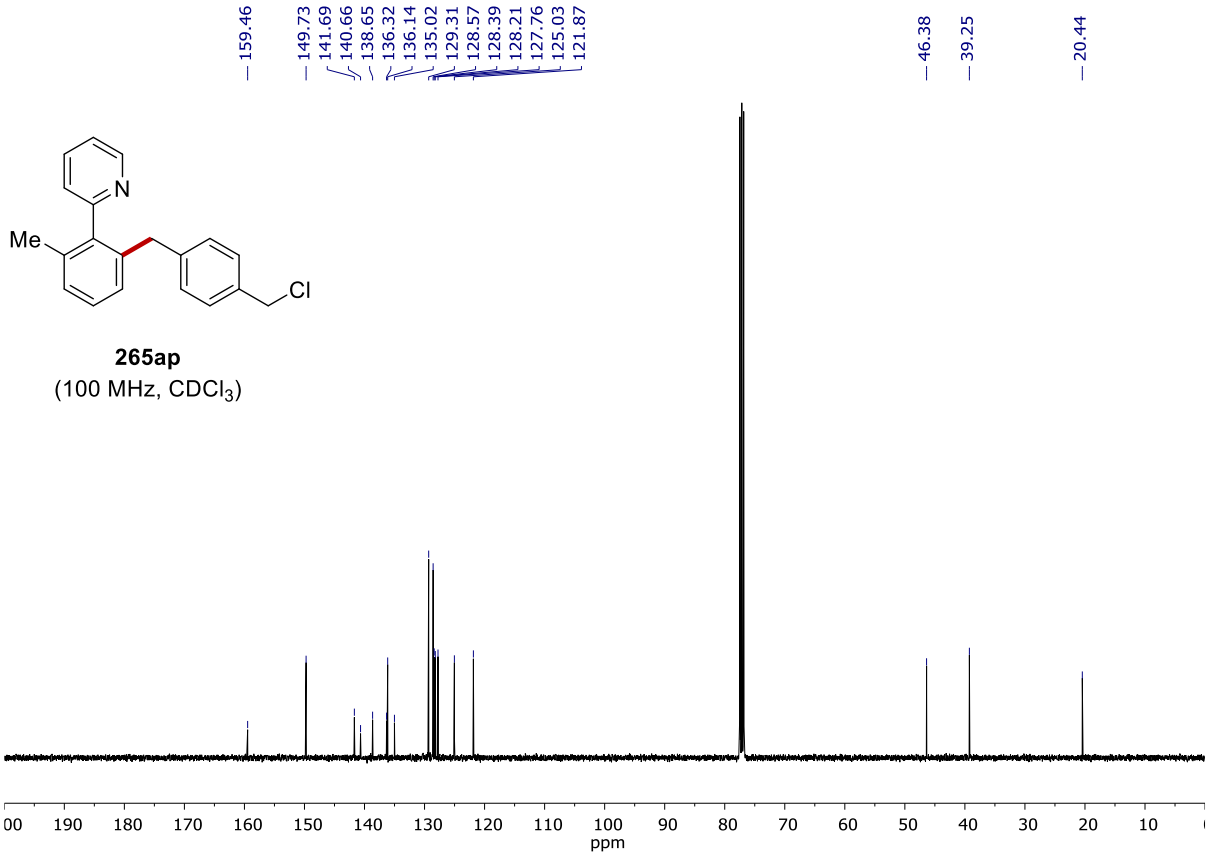

265ap
(100 MHz, $CDCl_3$)

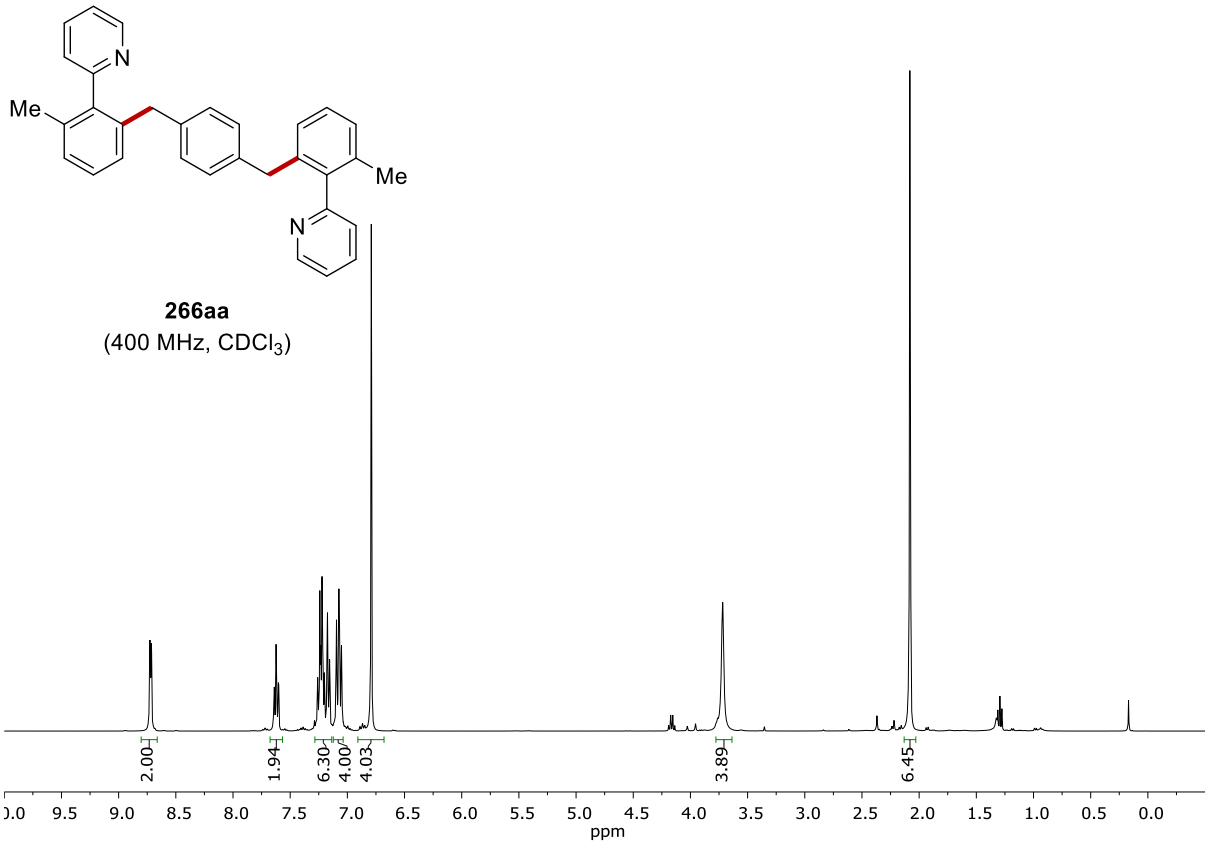

266aa
(400 MHz, $CDCl_3$)

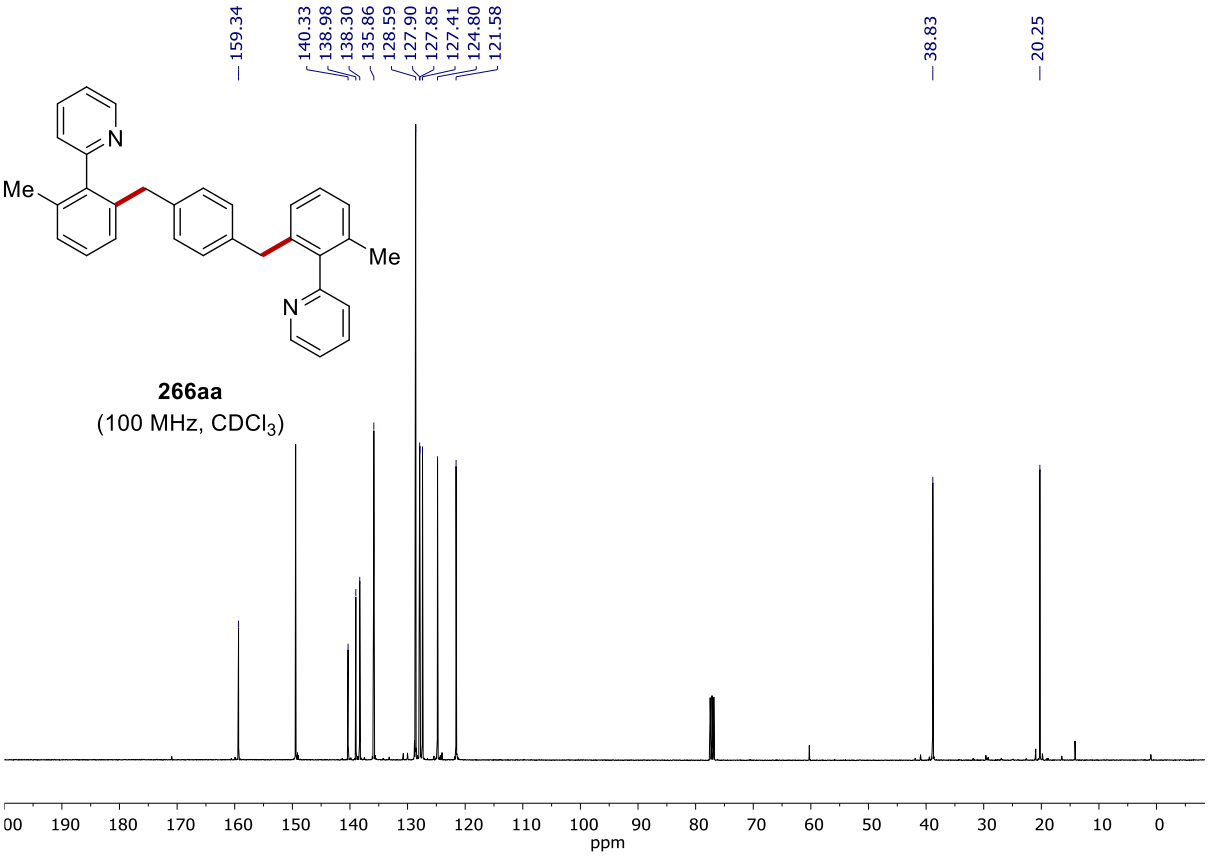

266aa
(100 MHz, $CDCl_3$)

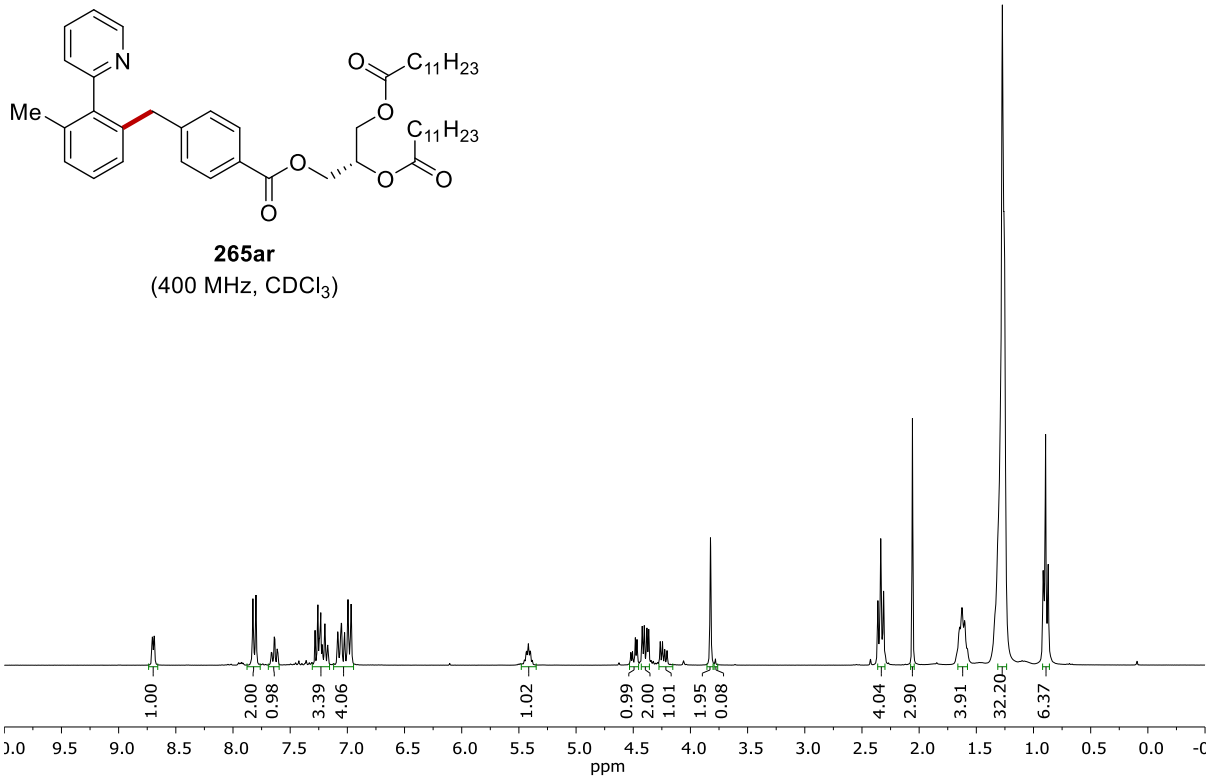

265ar
(400 MHz, $CDCl_3$)

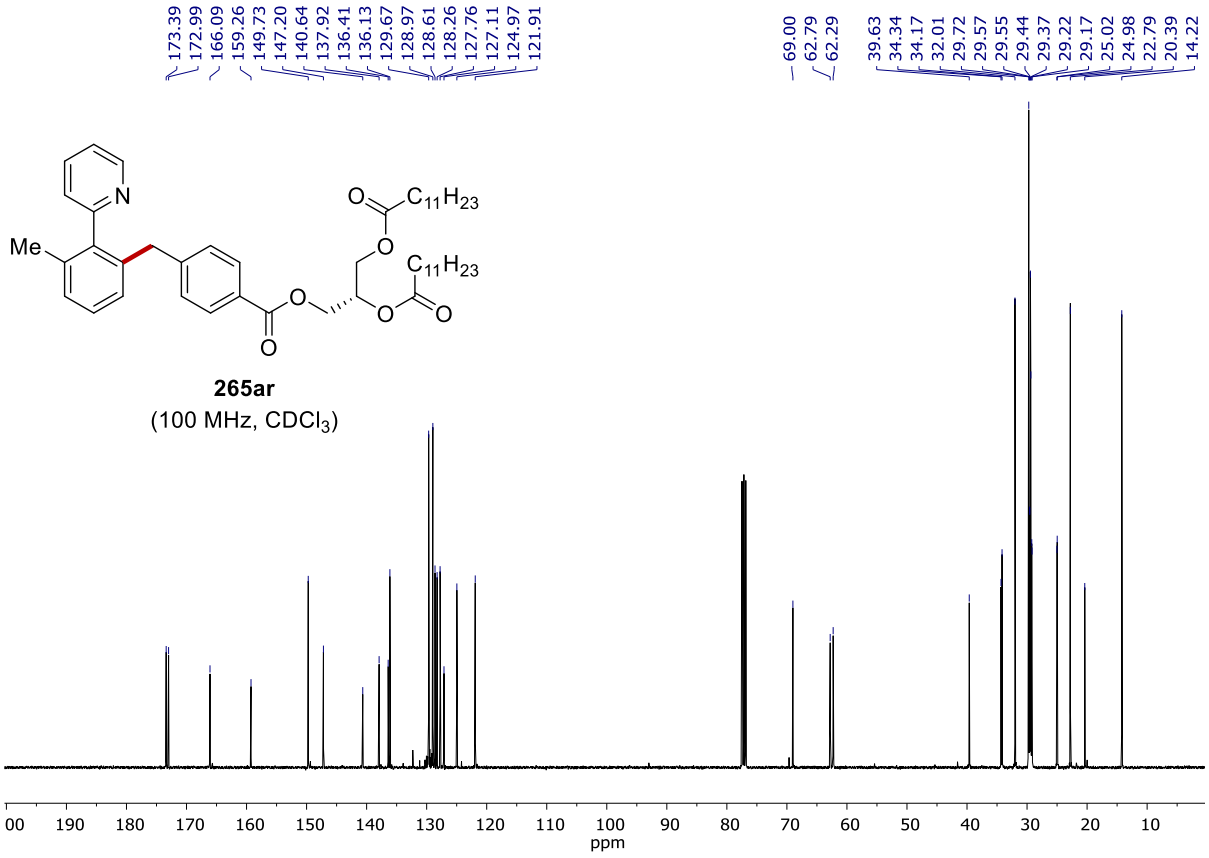

265ar
(100 MHz, $CDCl_3$)

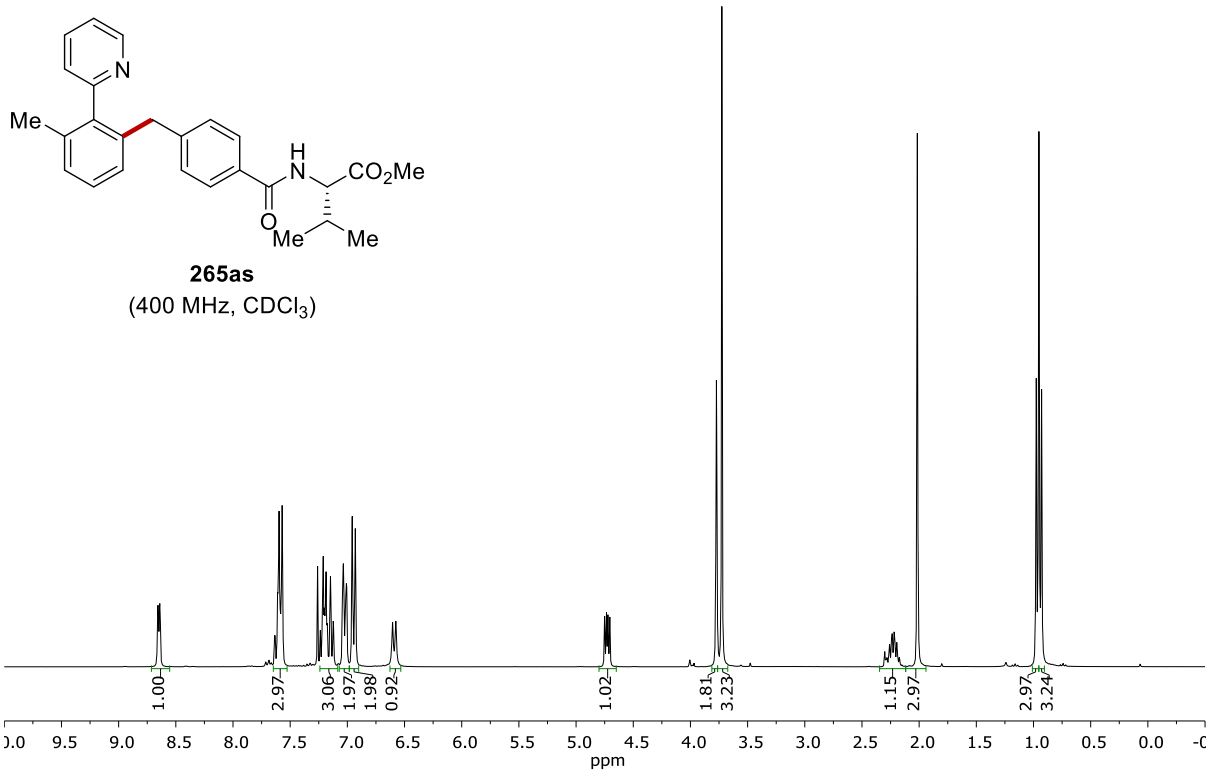

265as
(400 MHz, $CDCl_3$)

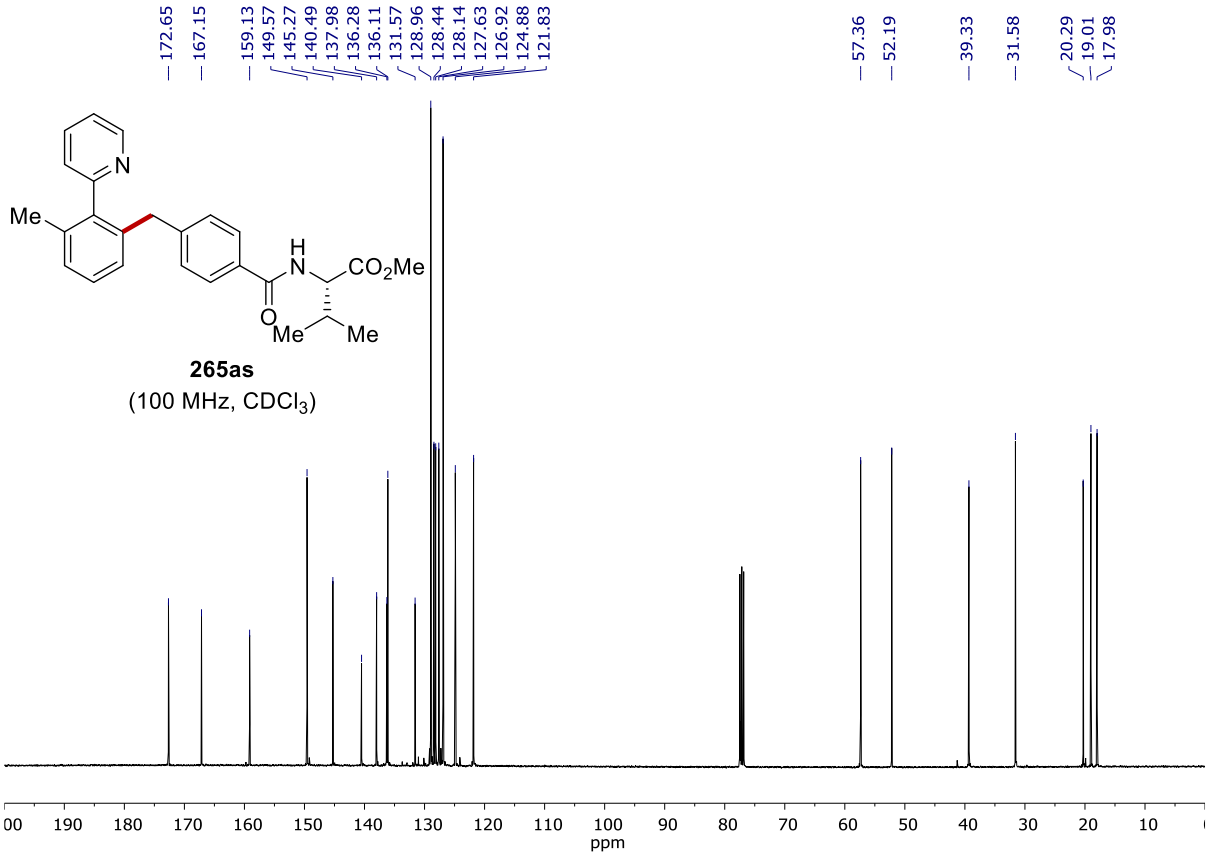
172.65
167.15
159.13
149.57
145.27
140.49
137.98
136.28
136.11
131.57
128.96
128.44
128.14
127.63
126.92
124.88
121.83
57.36
52.19
39.33
31.58
20.29
19.01
17.98
N
Me
H
N
CO2Me
O
Me
Me
265as
(100 MHz, CDCl3)
ppm

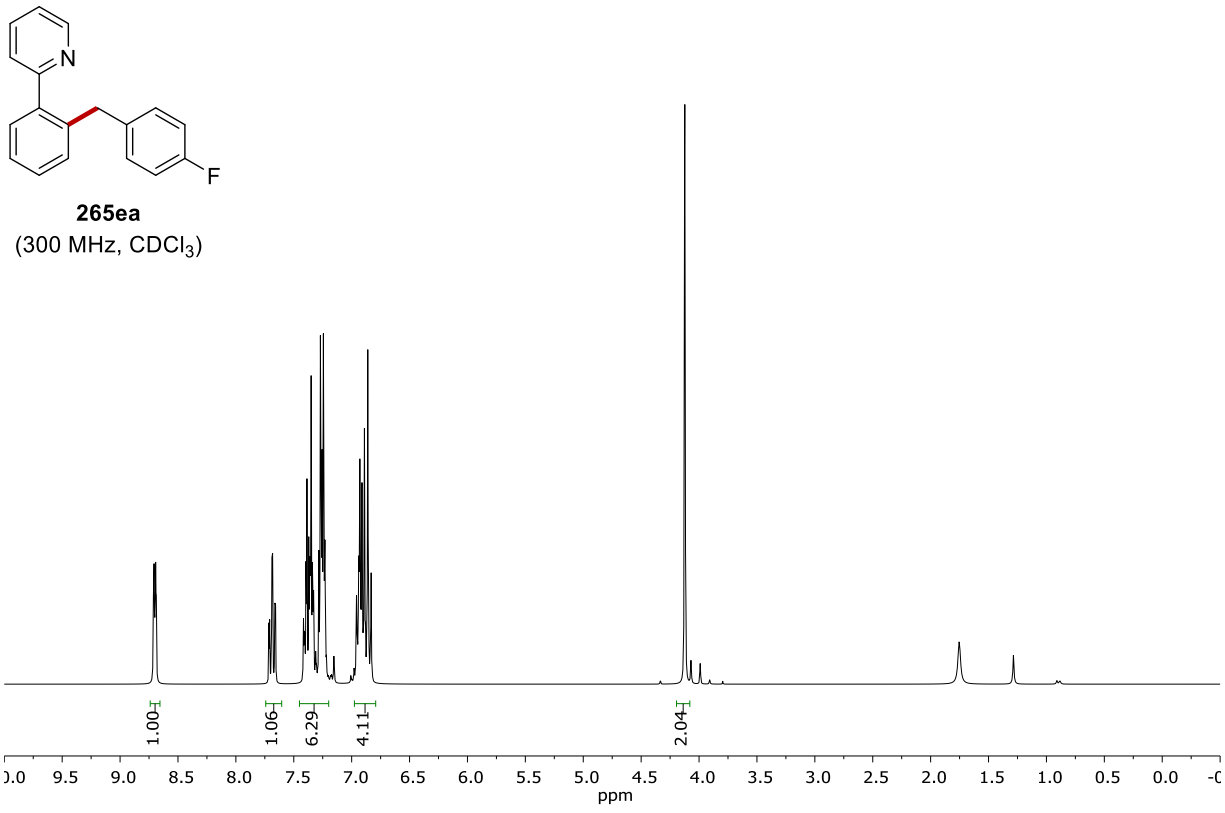
N
F
265ea
(300 MHz, CDCl3)
1.00
1.06
6.29
4.11
2.04
ppm

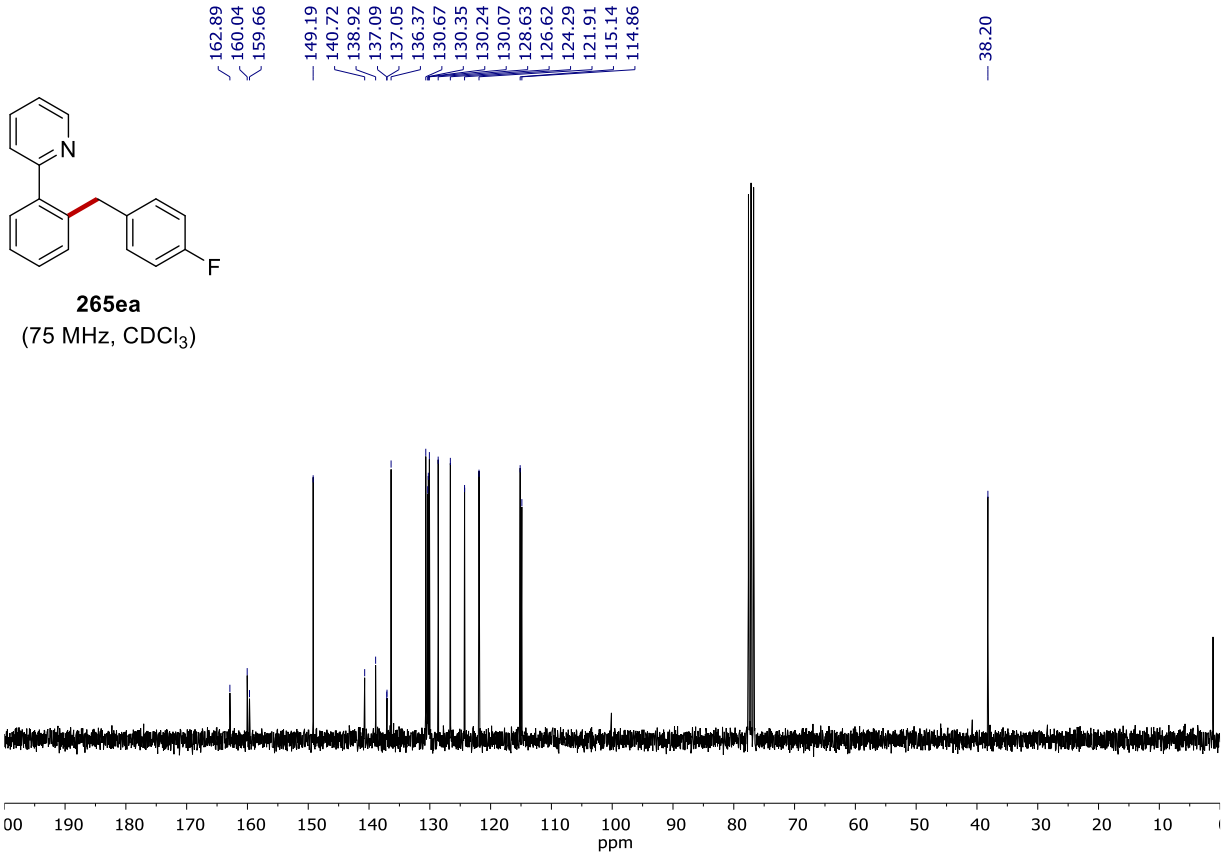
162.89
160.04
159.66
149.19
140.72
138.92
137.09
137.05
136.37
130.67
130.35
130.24
130.07
128.63
126.62
124.29
121.91
115.14
114.86
38.20
N
F
265ea
(75 MHz, CDCl3)
ppm

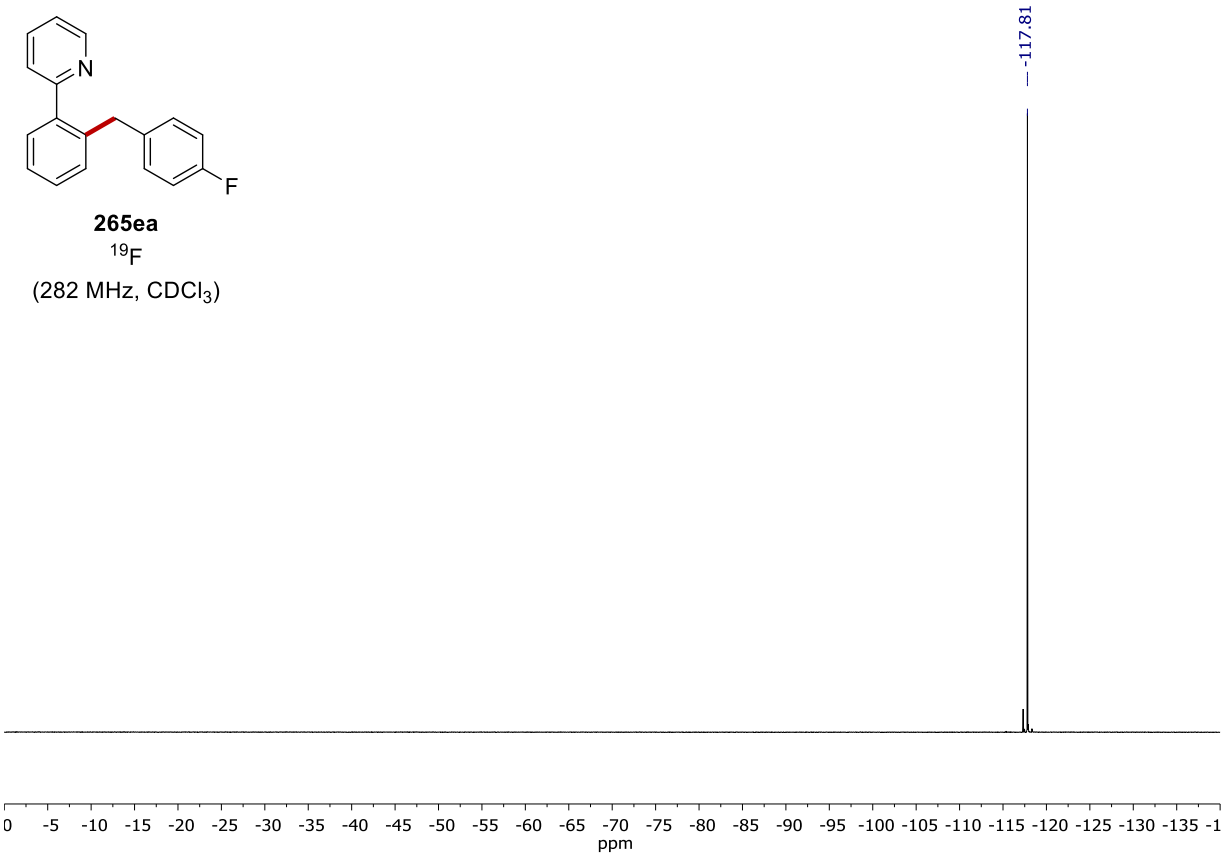
-117.81
N
F
265ea
19F
(282 MHz, CDCl3)
ppm

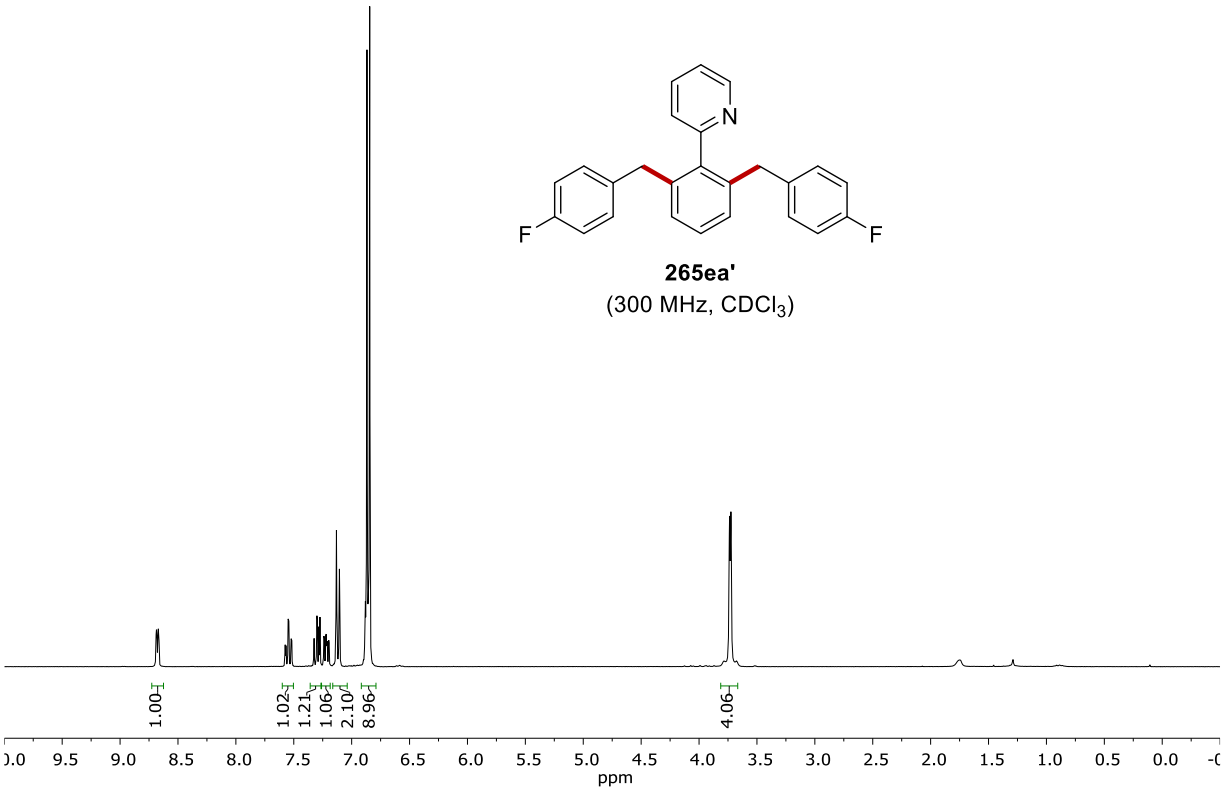
N
F
F
265ea'
(300 MHz, CDCl3)
1.00
1.02
1.21
1.06
2.10
8.96
4.06
ppm

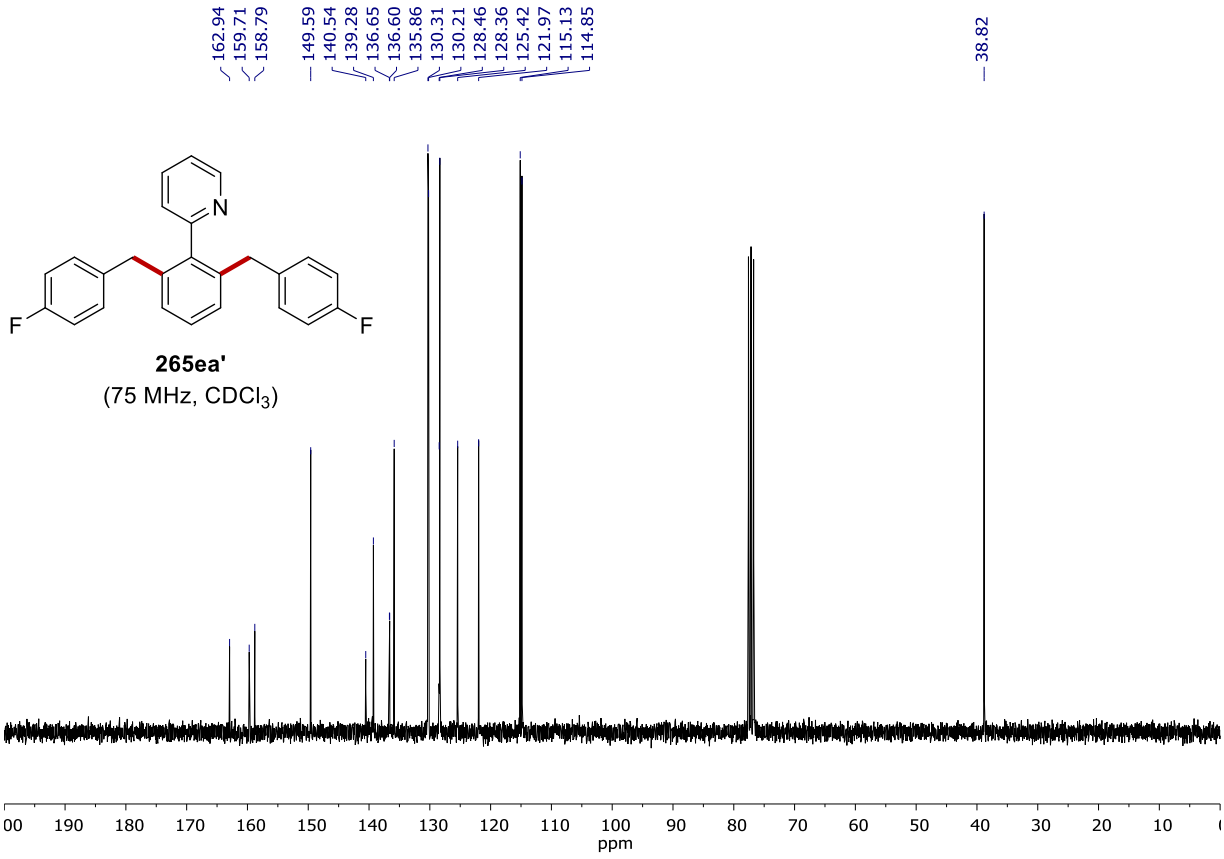
162.94
159.71
158.79
149.59
140.54
139.28
136.65
136.60
135.86
130.31
130.21
128.46
128.36
125.42
121.97
115.13
114.85
38.82
N
F
F
265ea'
(75 MHz, CDCl3)
ppm

265ea'
(282 MHz, $CDCl_3$)

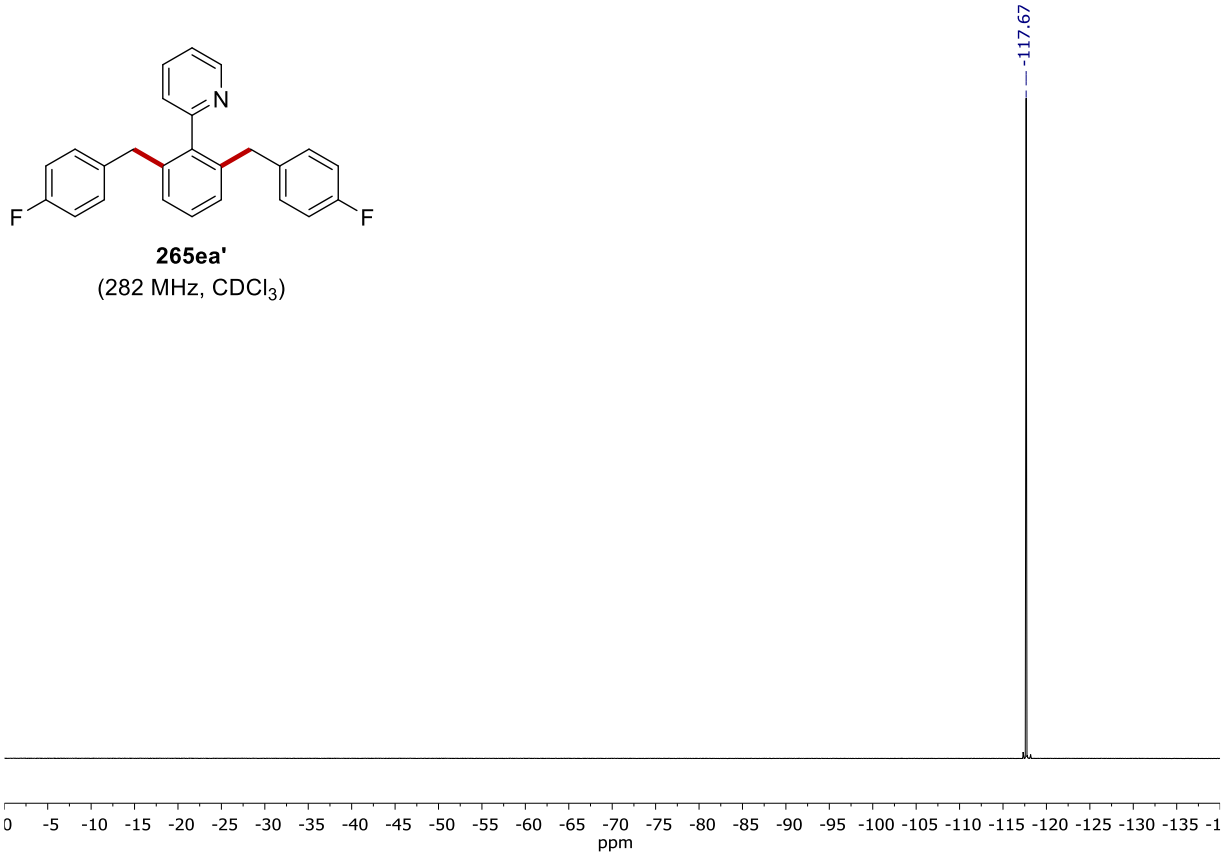

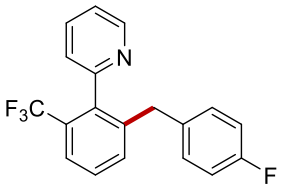

265ba
(400 MHz, $CDCl_3$)

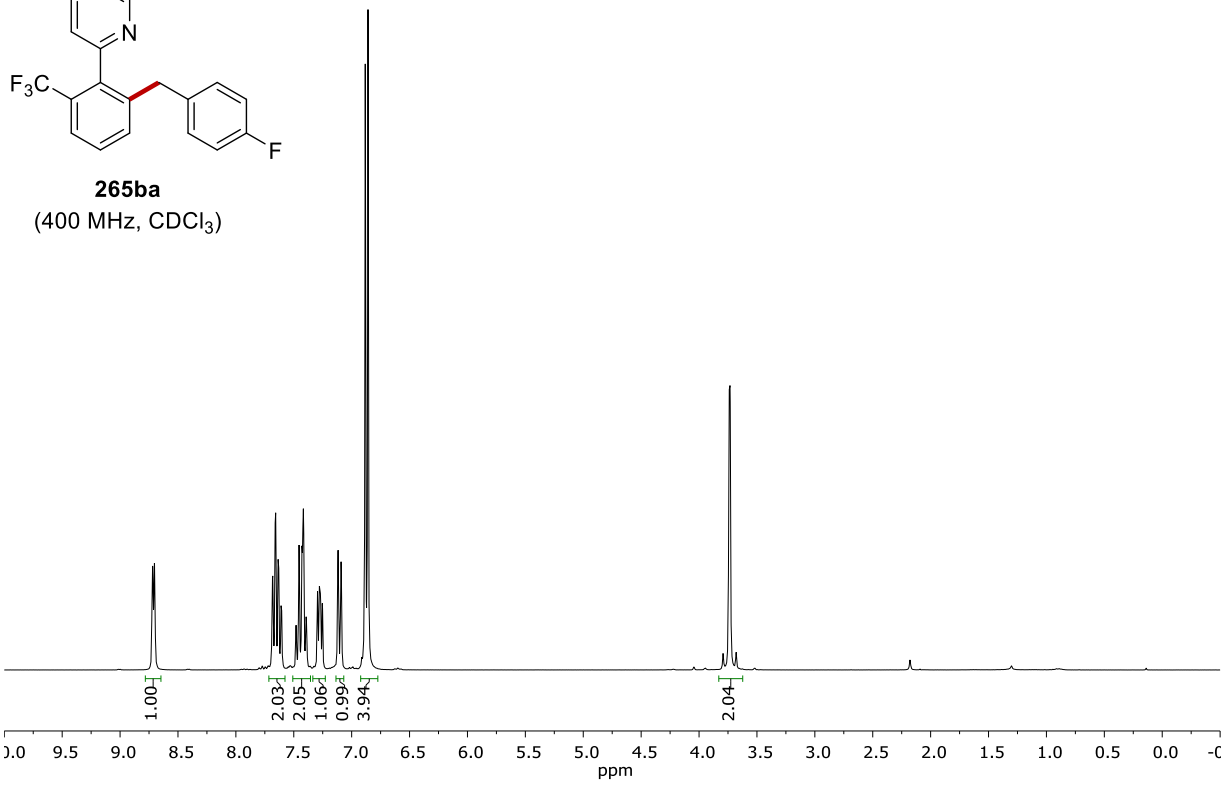

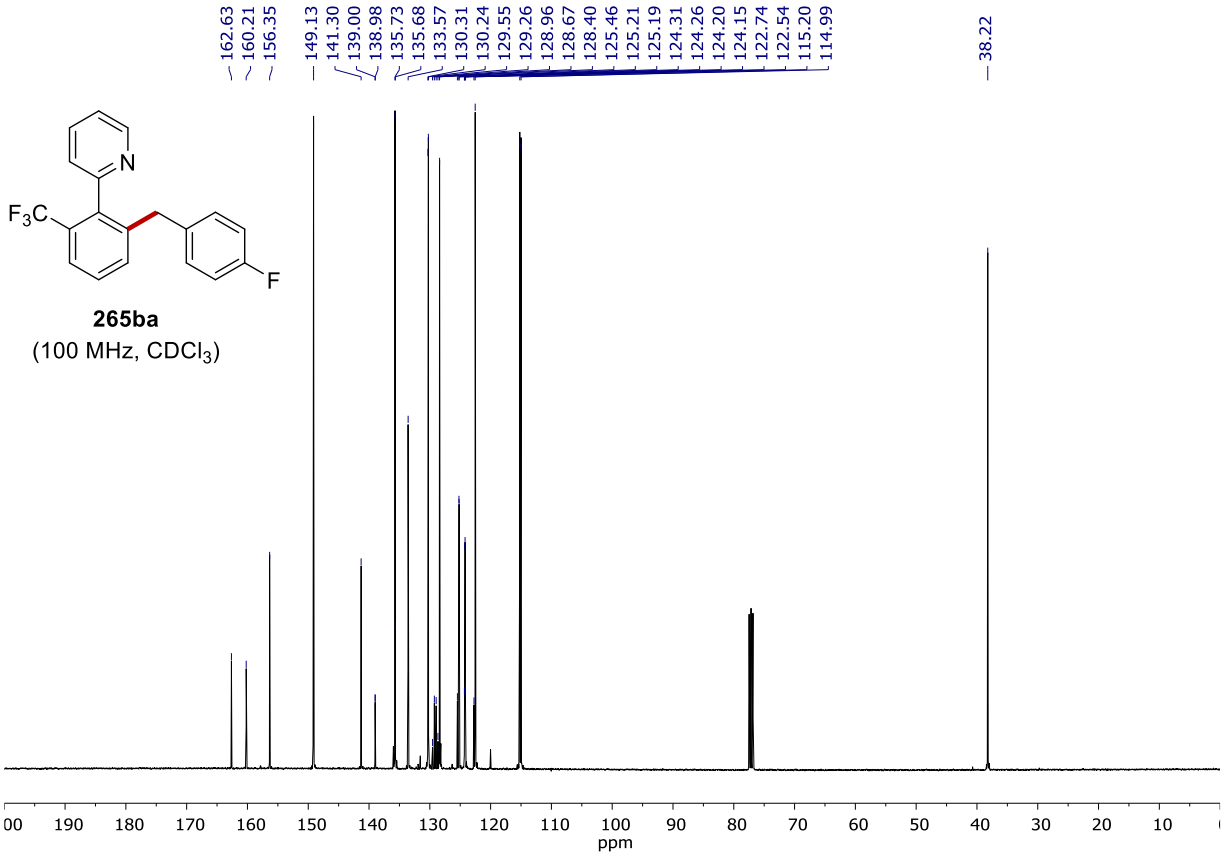
162.63
160.21
156.35
149.13
141.30
139.00
138.98
135.73
135.68
133.57
130.31
130.24
129.55
129.26
128.96
128.67
128.40
125.46
125.21
125.19
124.31
124.26
124.20
124.15
122.74
122.54
115.20
114.99
38.22
N
F3C
F
265ba
(100 MHz, CDCl3)
ppm

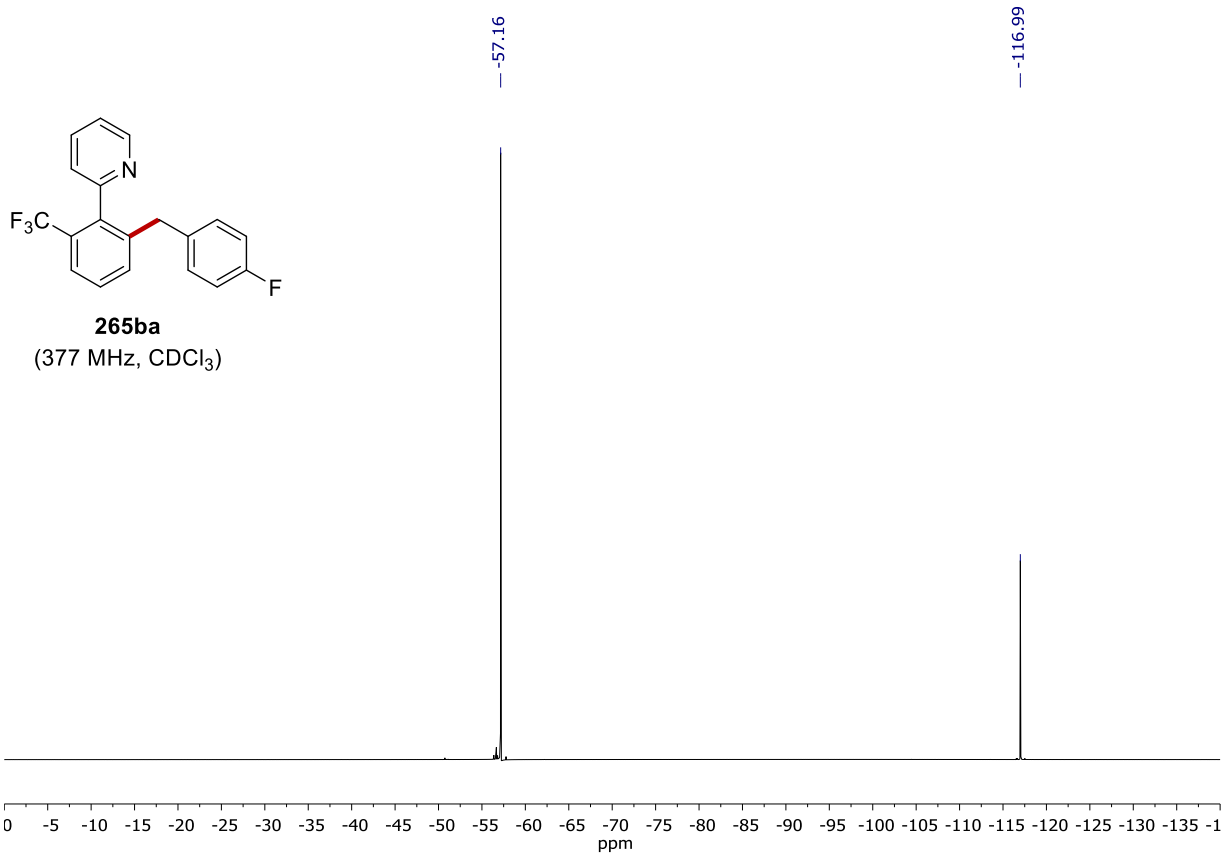
-57.16
-116.99
N
F3C
F
265ba
(377 MHz, CDCl3)
ppm

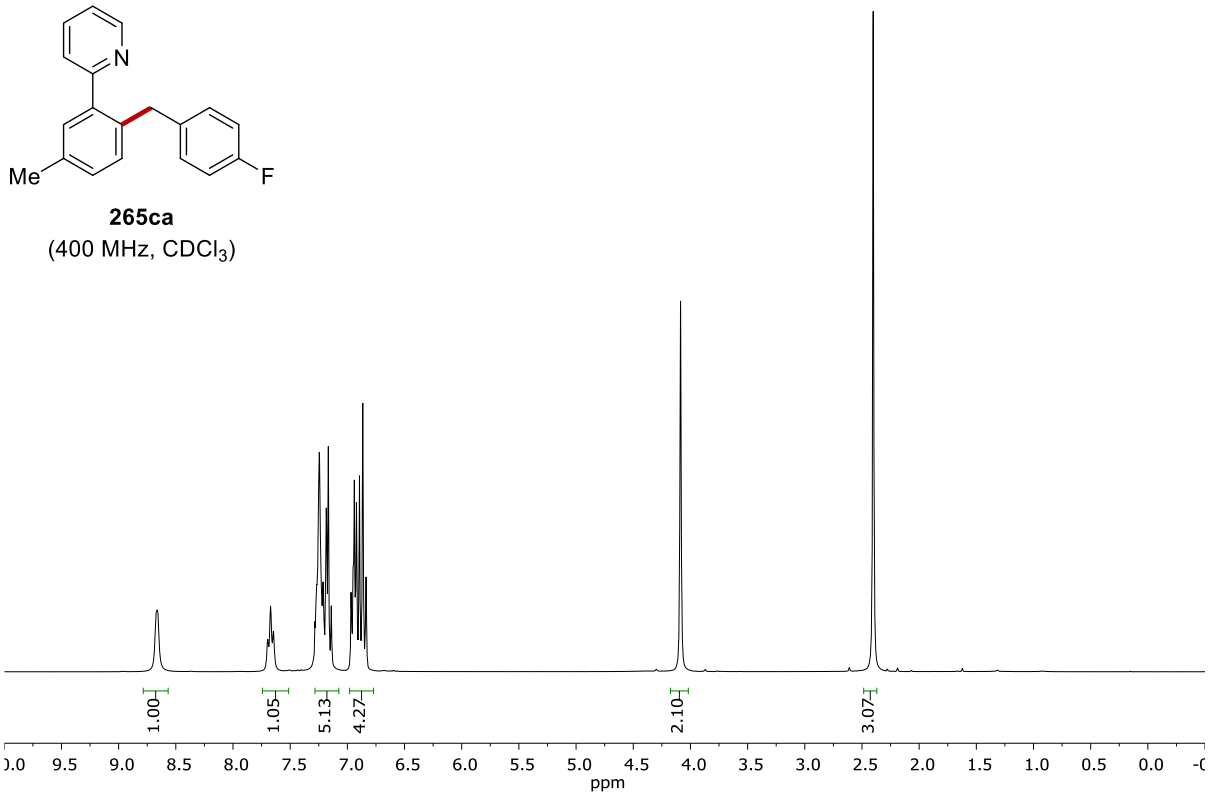
N
Me
F
265ca
(400 MHz, CDCl3)
1.00
1.05
5.13
4.27
2.10
3.07
ppm

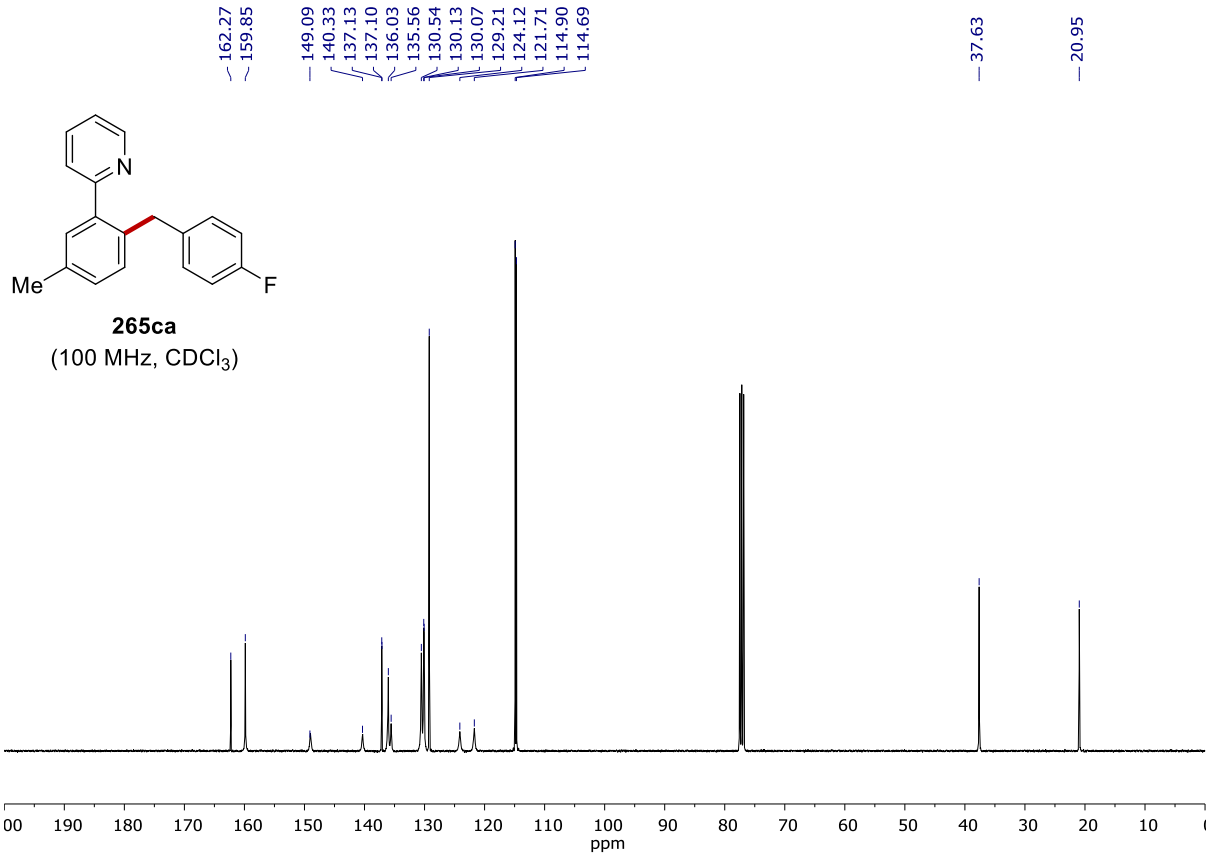
162.27
159.85
149.09
140.33
137.13
137.10
136.03
135.56
130.54
130.13
130.07
129.21
124.12
121.71
114.90
114.69
37.63
20.95
N
Me
F
265ca
(100 MHz, CDCl3)
ppm

265ca

^{19}F

(282 MHz, $CDCl_3$)

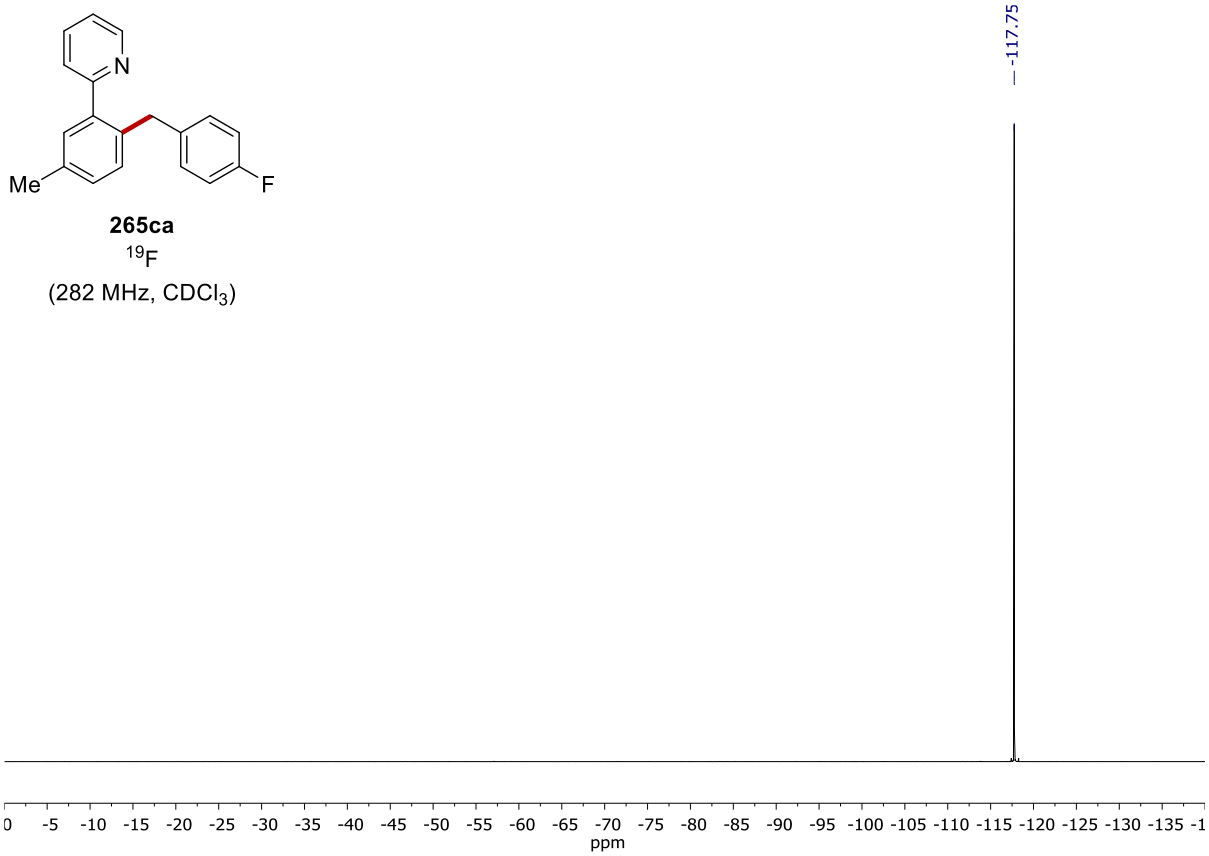

265da

(400 MHz, $CDCl_3$)

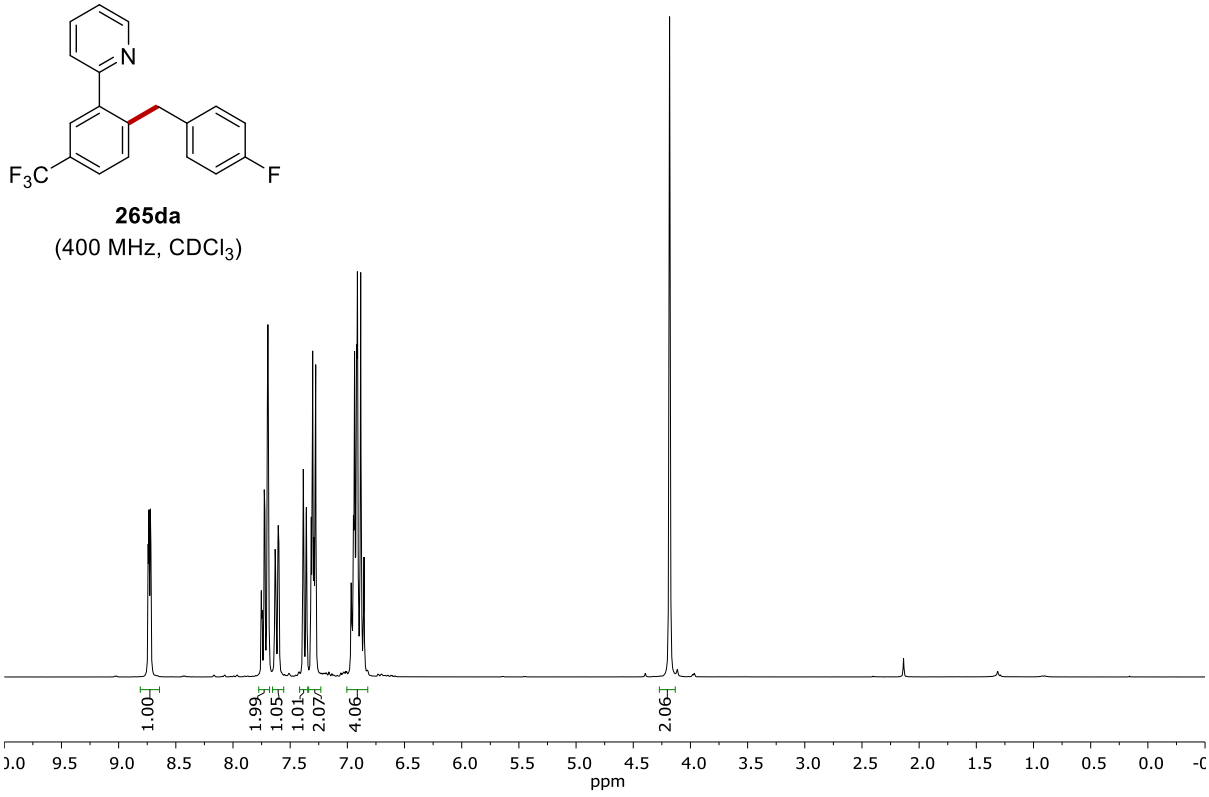

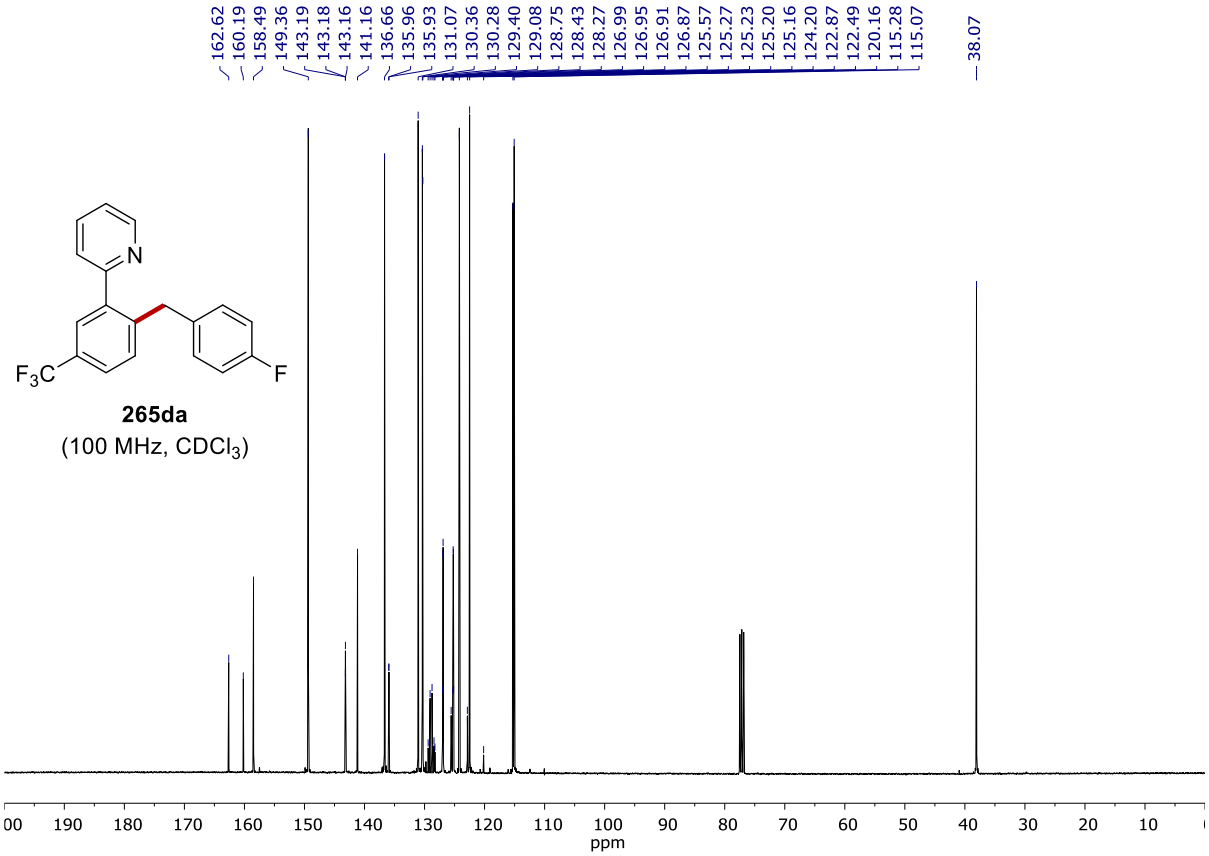
162.62
160.19
158.49
149.36
143.19
143.18
143.16
141.16
136.66
135.96
135.93
131.07
130.36
130.28
129.40
129.08
128.75
128.43
128.27
126.99
126.95
126.91
126.87
125.57
125.27
125.23
125.20
125.16
124.20
122.87
122.49
120.16
115.28
115.07
38.07
N
F3C
F
265da
(100 MHz, CDCl3)
ppm

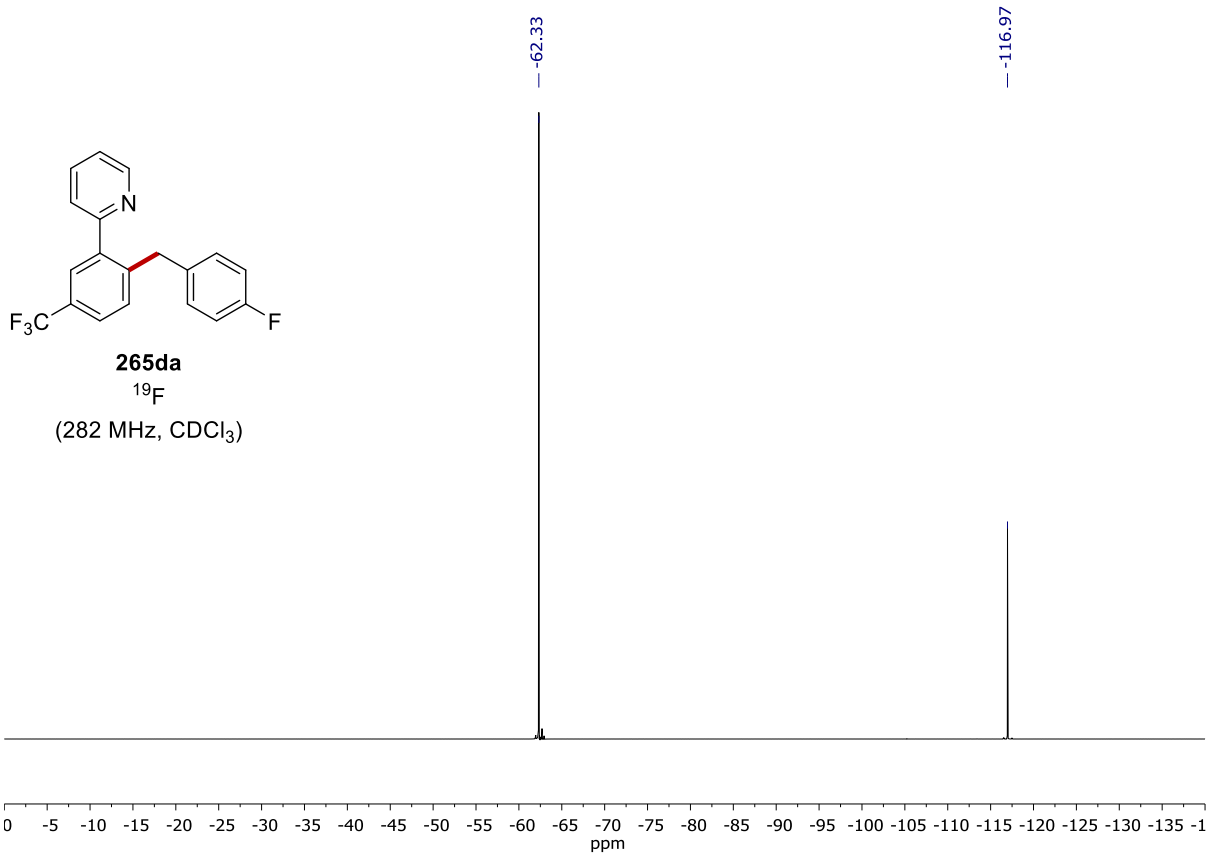
-62.33
-116.97
N
F3C
F
265da
19F
(282 MHz, CDCl3)
ppm

268ga
(400 MHz, $CDCl_3$)

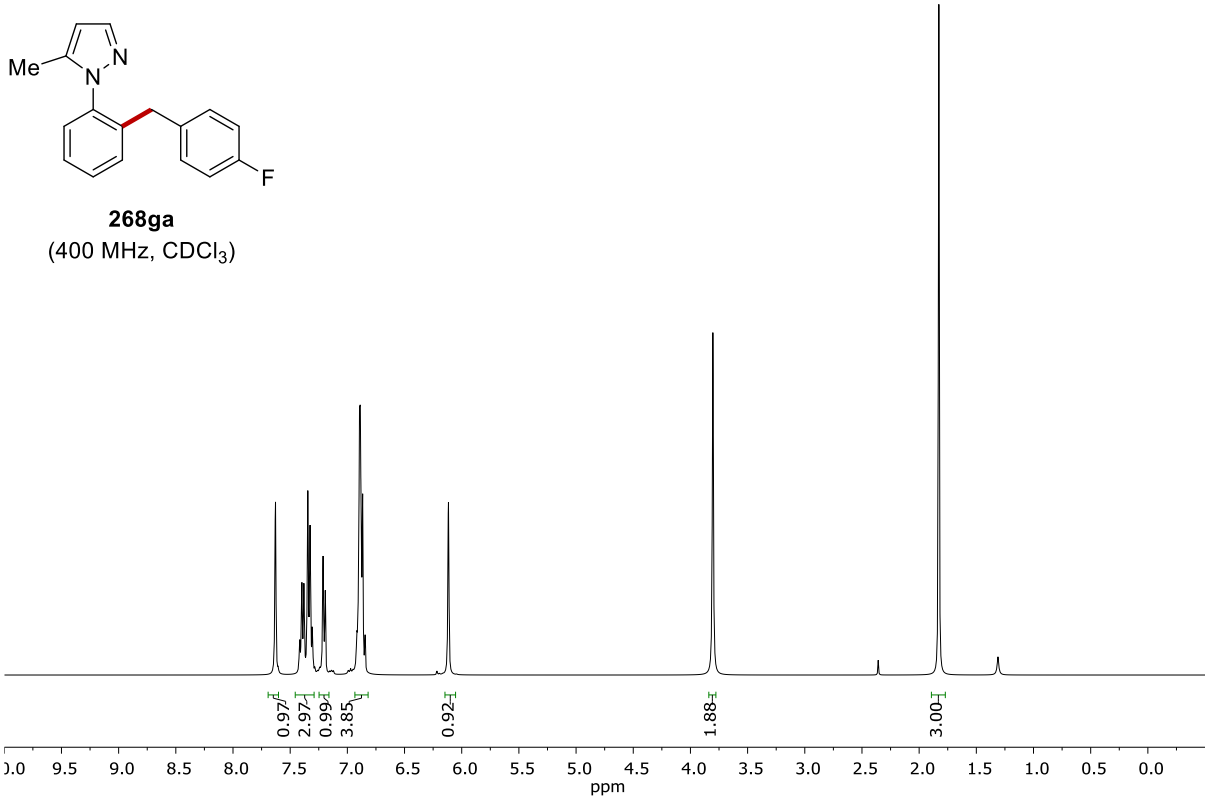

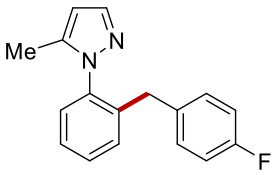

268ga
(100 MHz, $CDCl_3$)

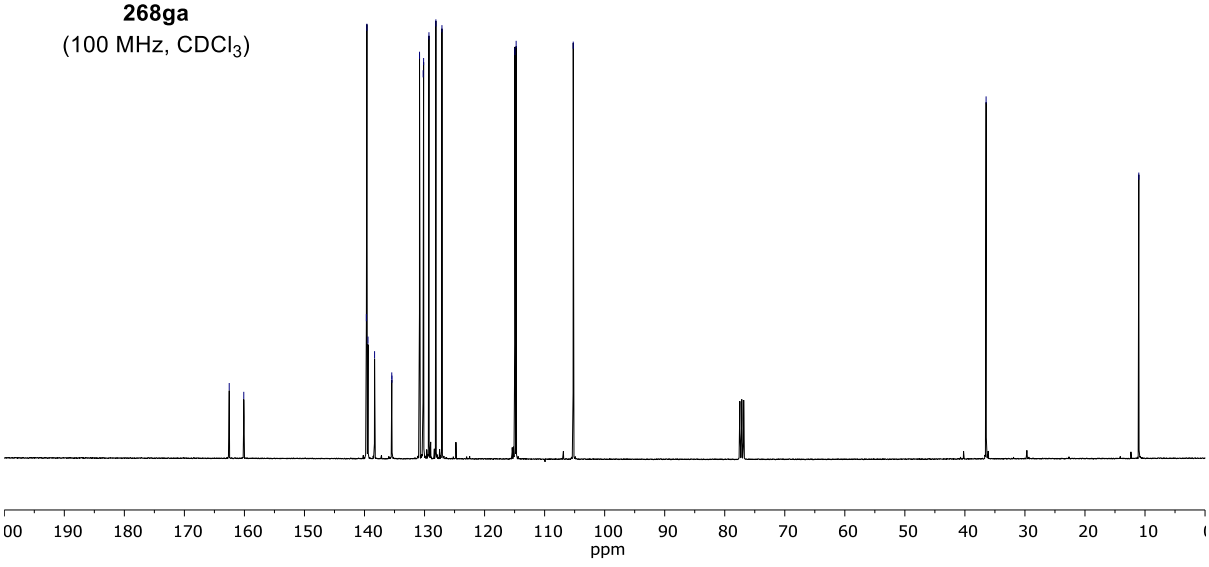

268ga

^{19}F

(282 MHz, $CDCl_3$)

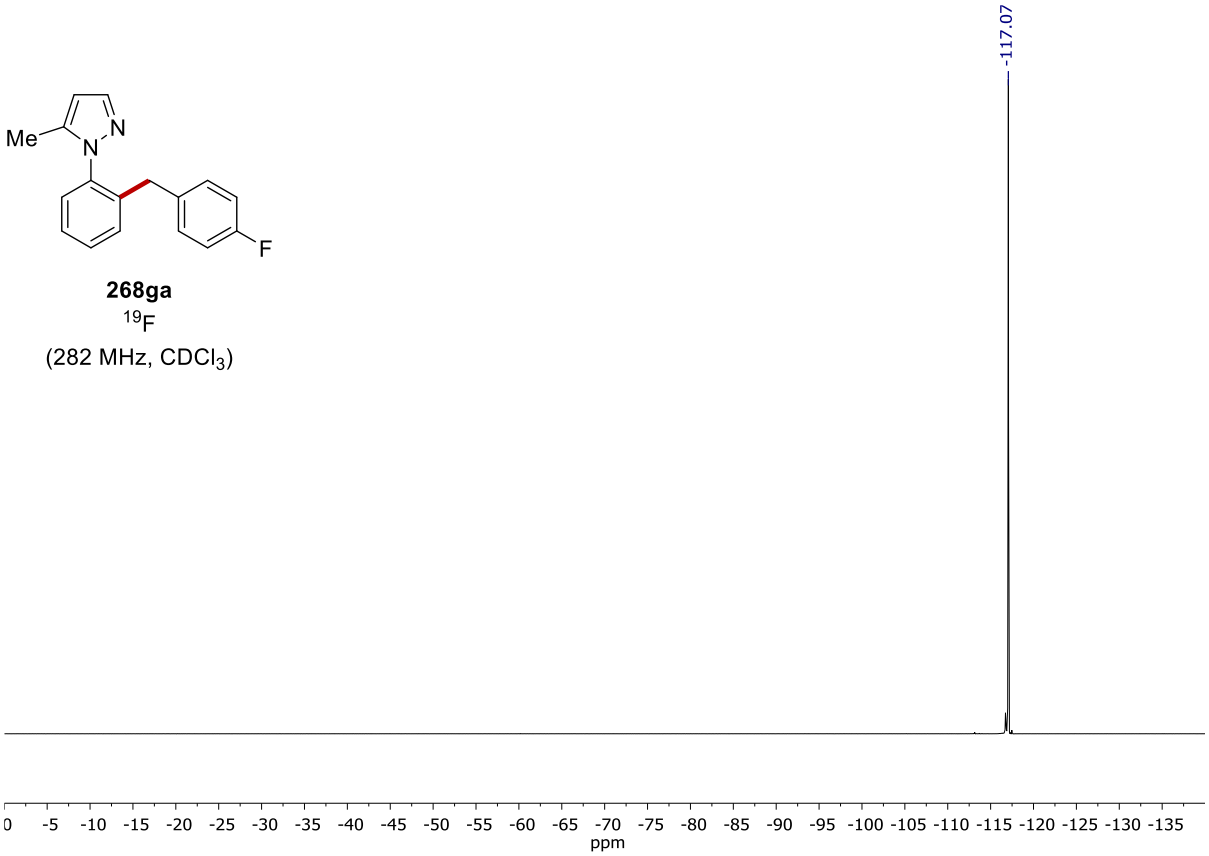

268ea

(400 MHz, $CDCl_3$)

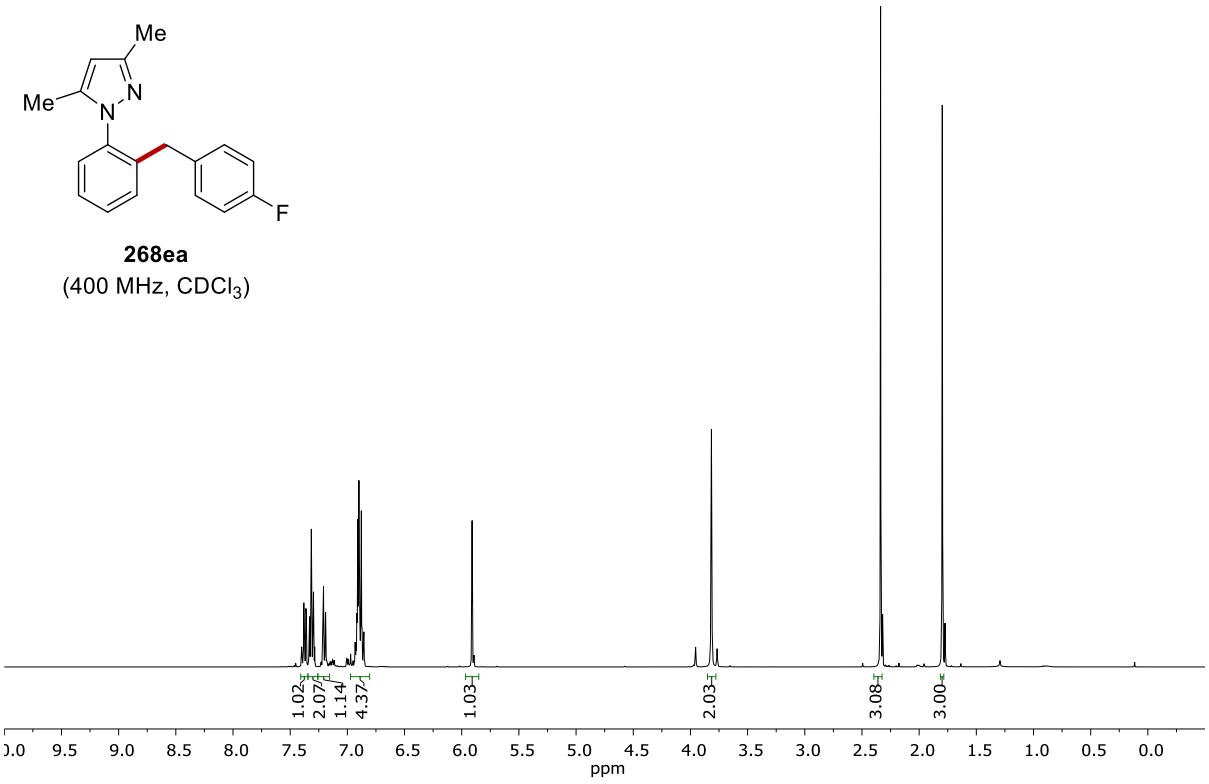

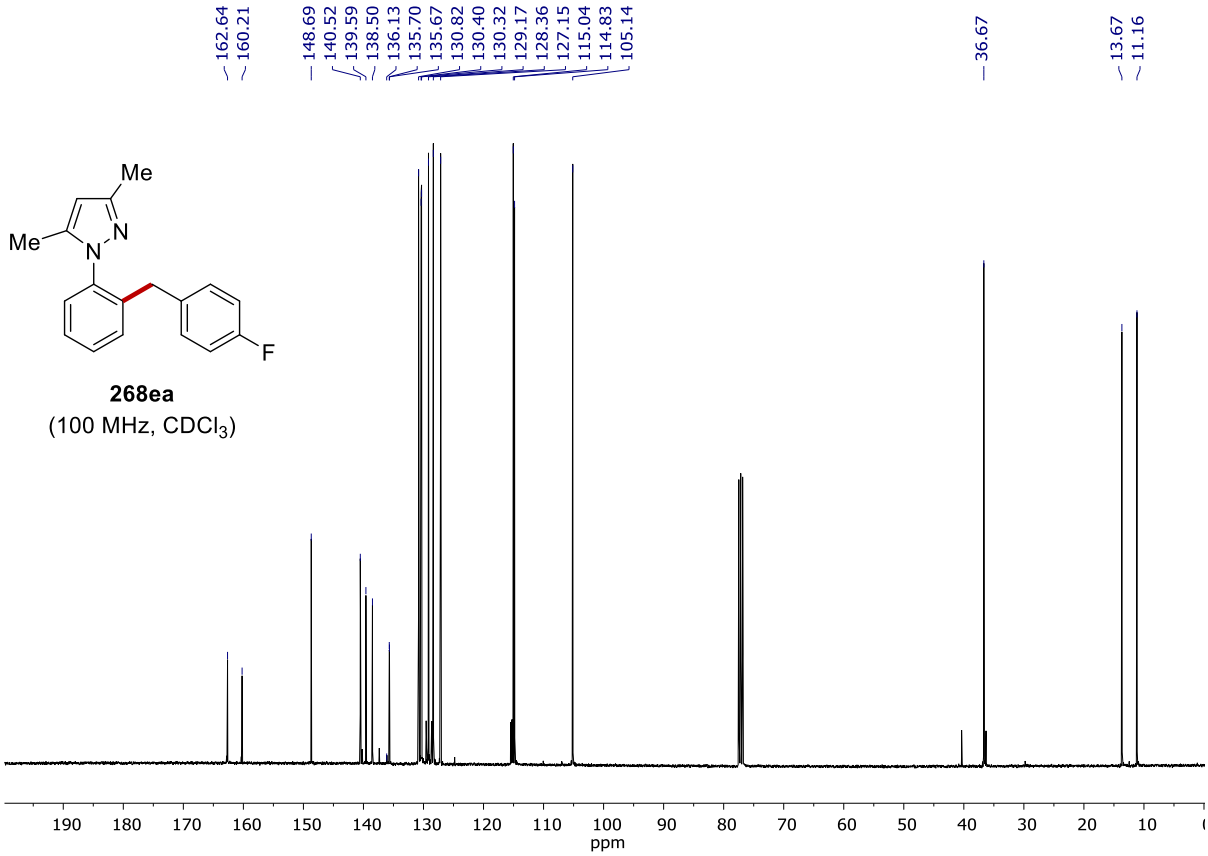

268ea
(100 MHz, $CDCl_3$)

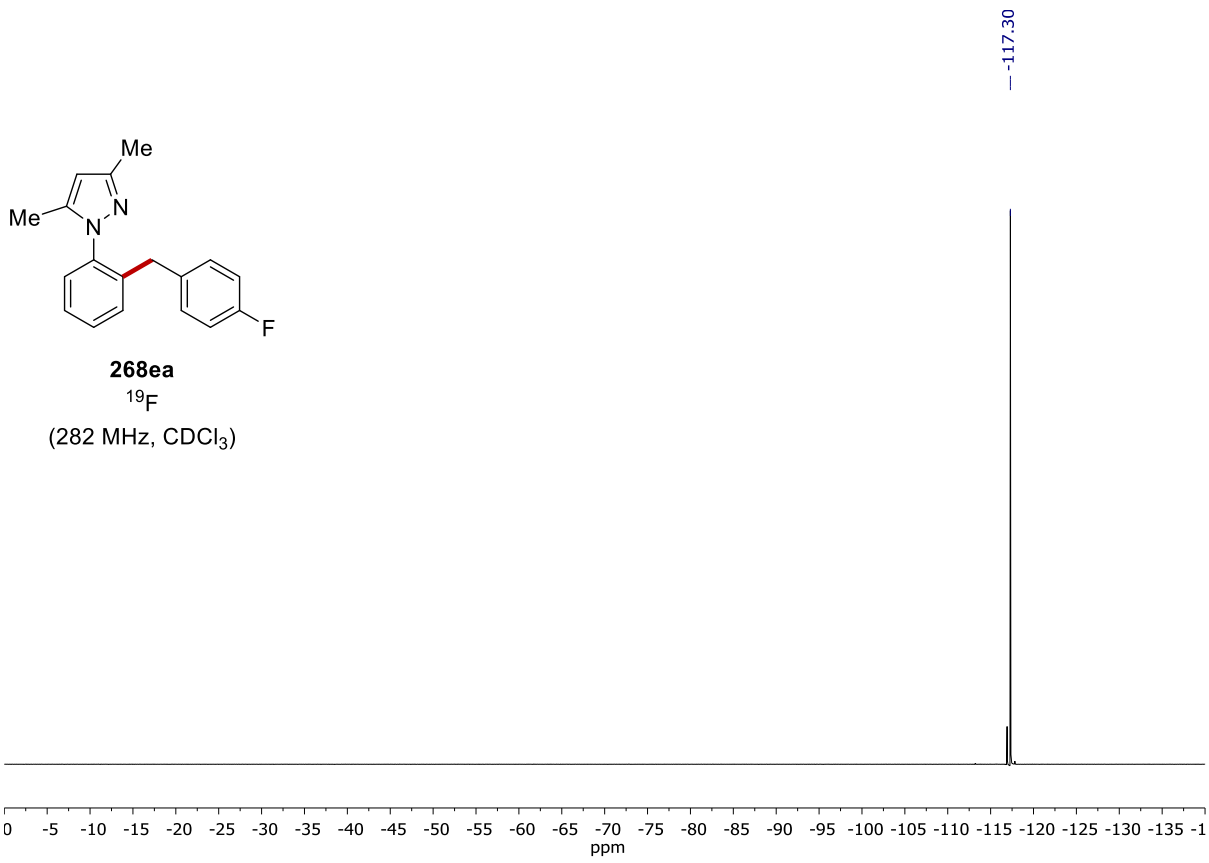

268ea
^{19}F
(282 MHz, $CDCl_3$)

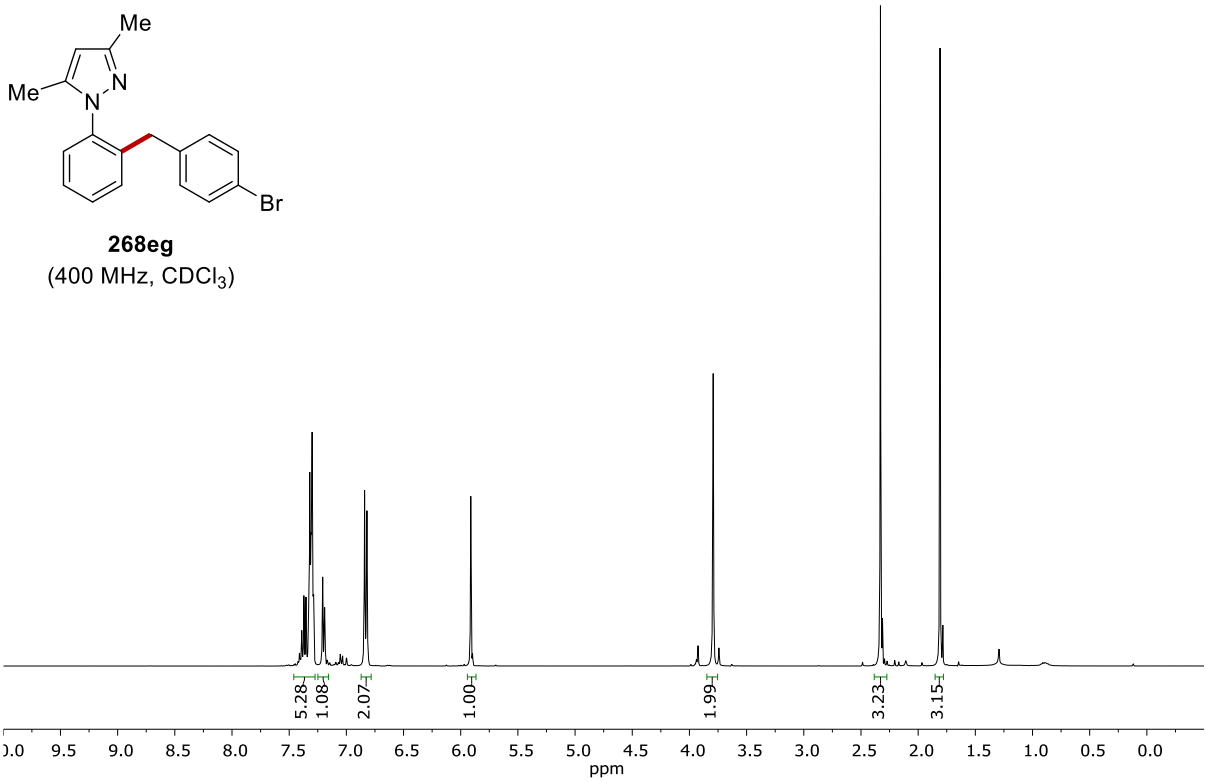

268eg
(400 MHz, $CDCl_3$)

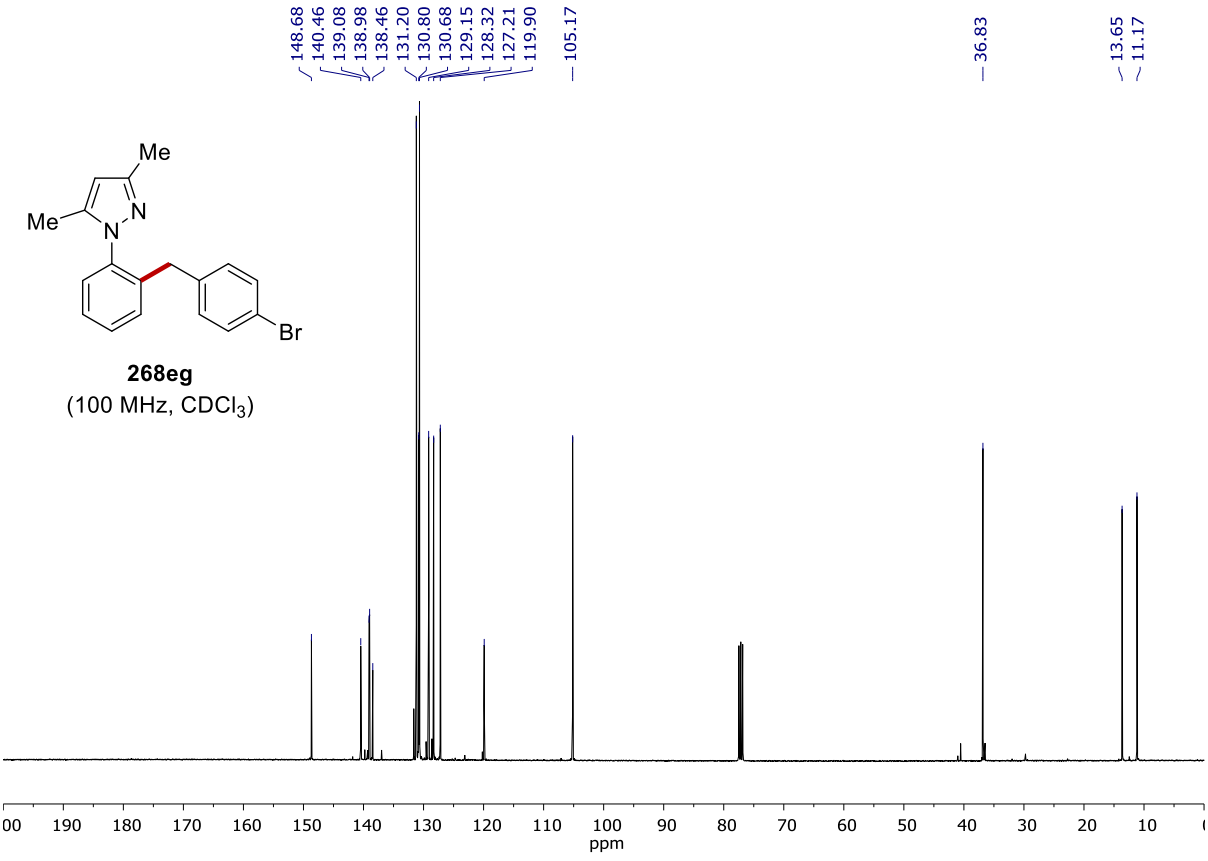

268eg
(100 MHz, $CDCl_3$)

269aa
(400 MHz, $CDCl_3$)

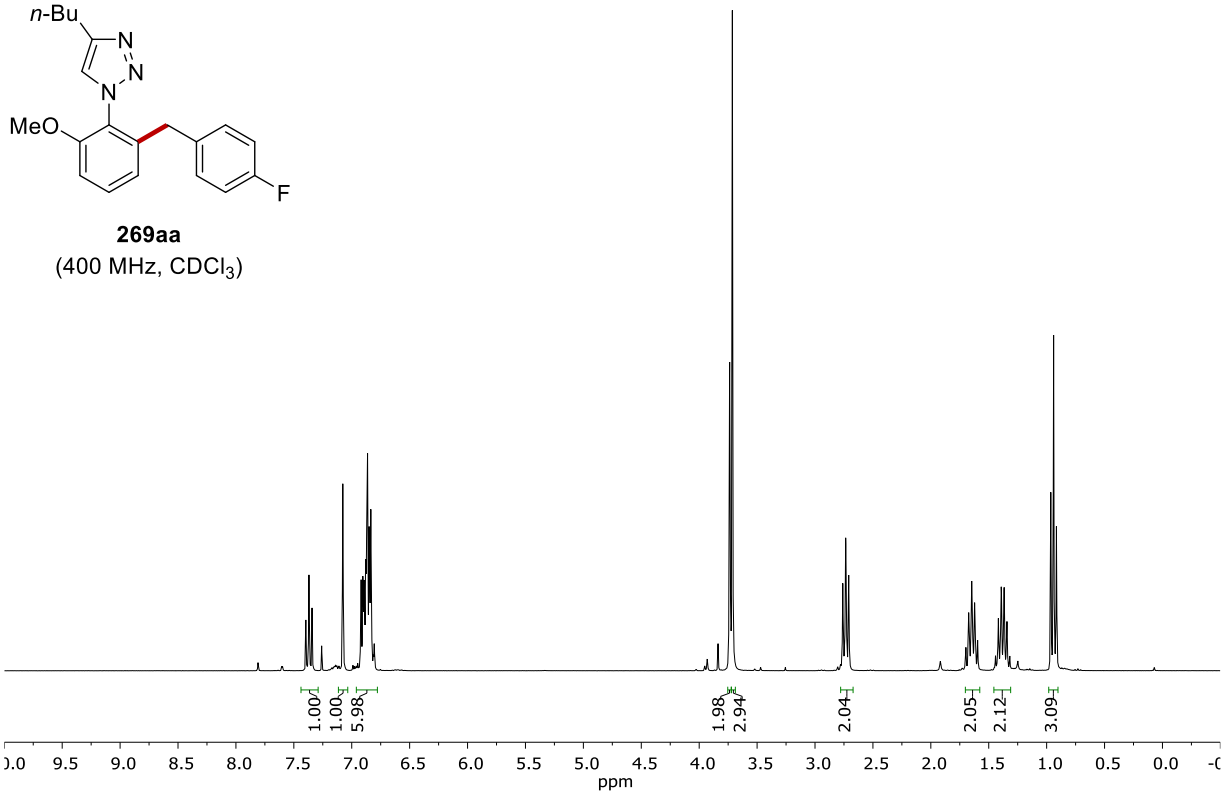

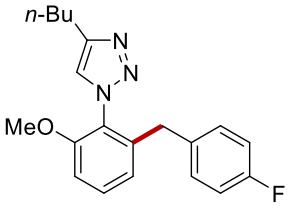

269aa
(100 MHz, $CDCl_3$)

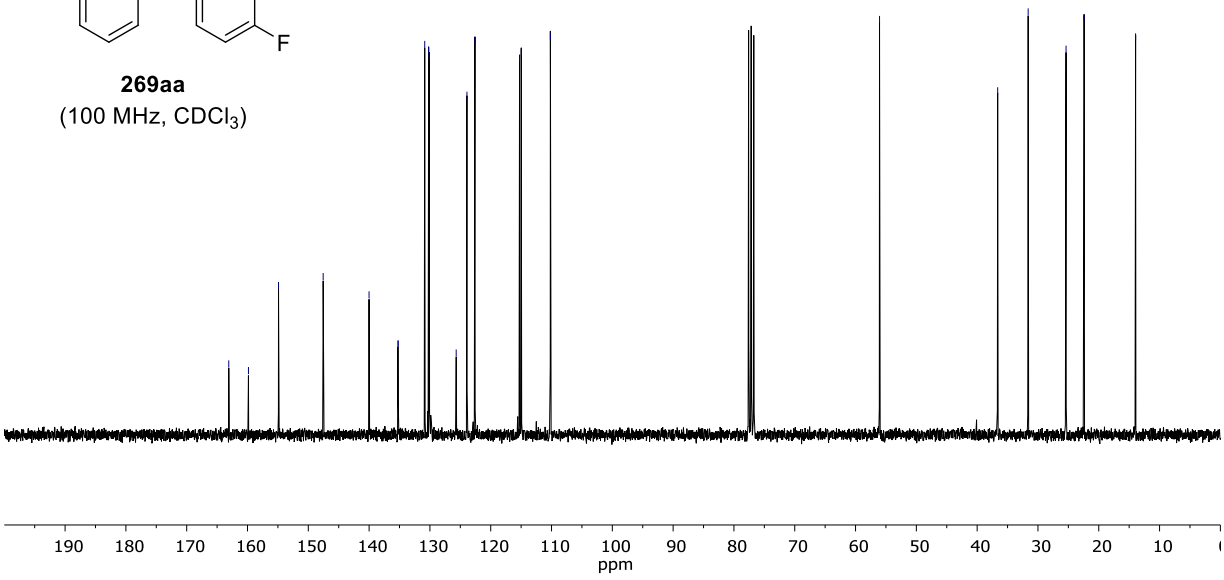

269aa

^{19}F

(282 MHz, $CDCl_3$)

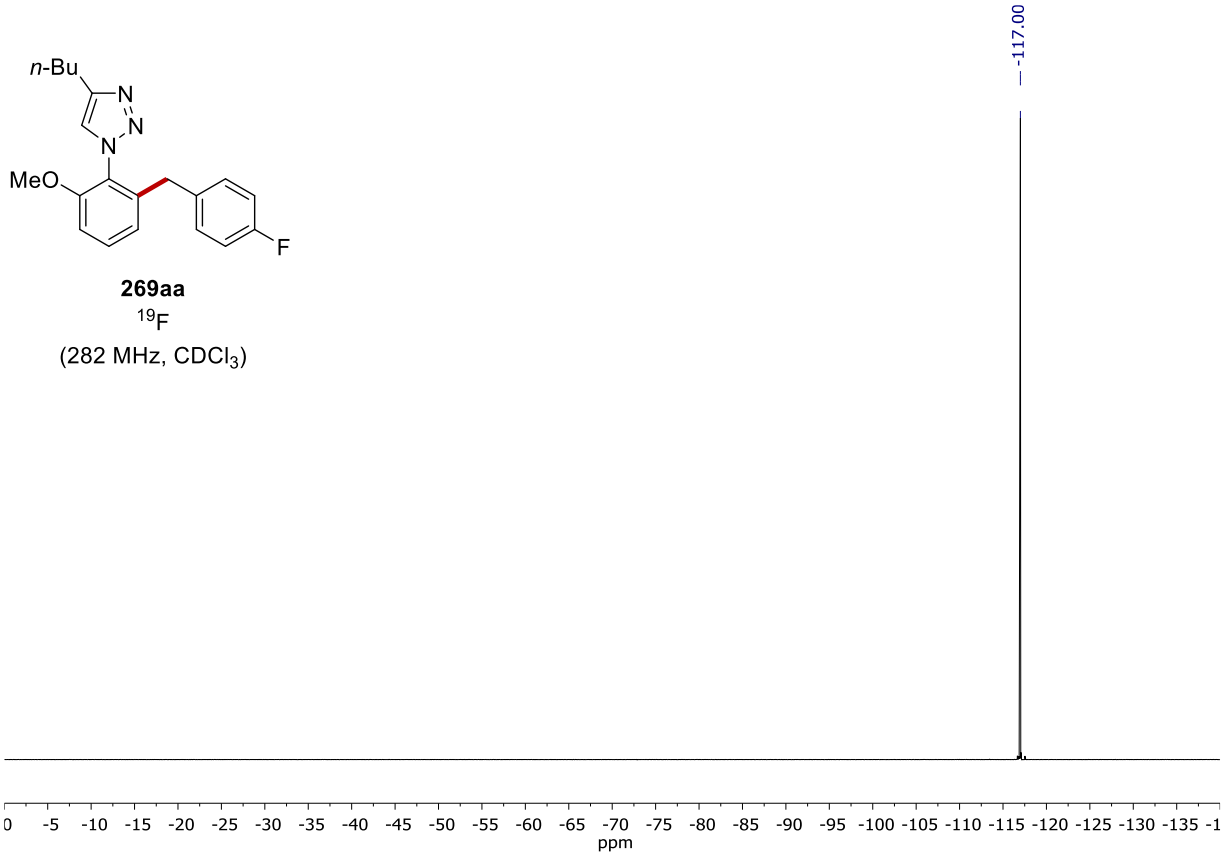

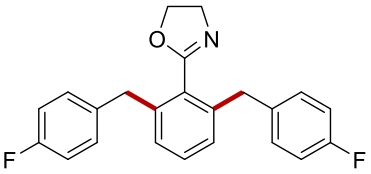

270ba'

(400 MHz, $CDCl_3$)

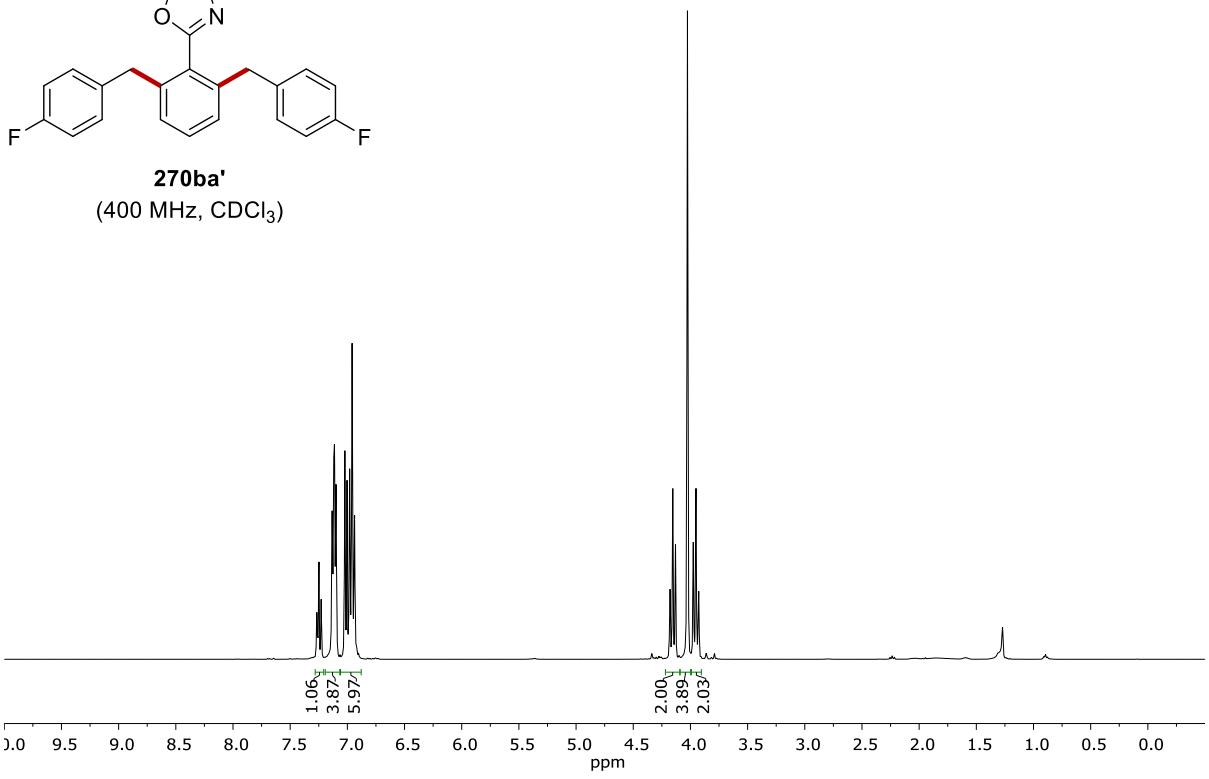

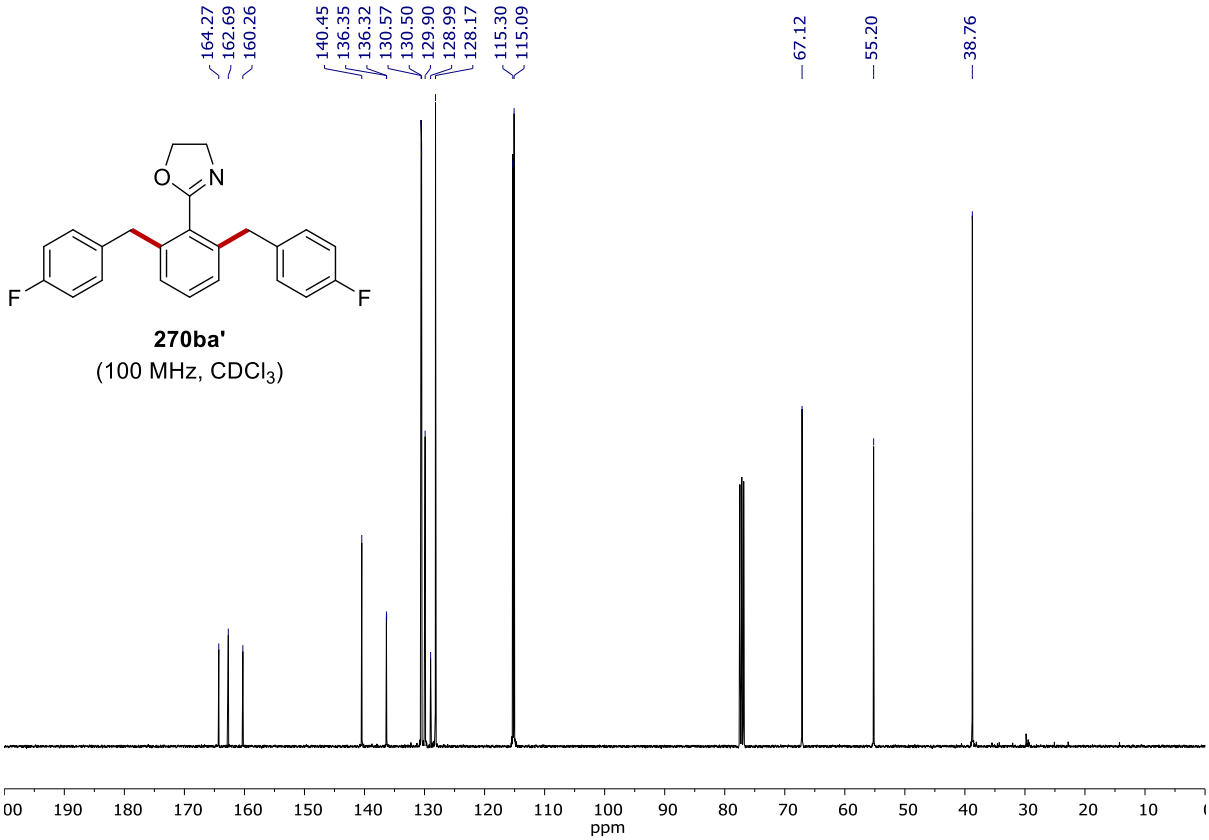
164.27
162.69
160.26
140.45
136.35
136.32
130.57
130.50
129.90
128.99
128.17
115.30
115.09
67.12
55.20
38.76
O
N
F
F
270ba'
(100 MHz, CDCl3)
ppm

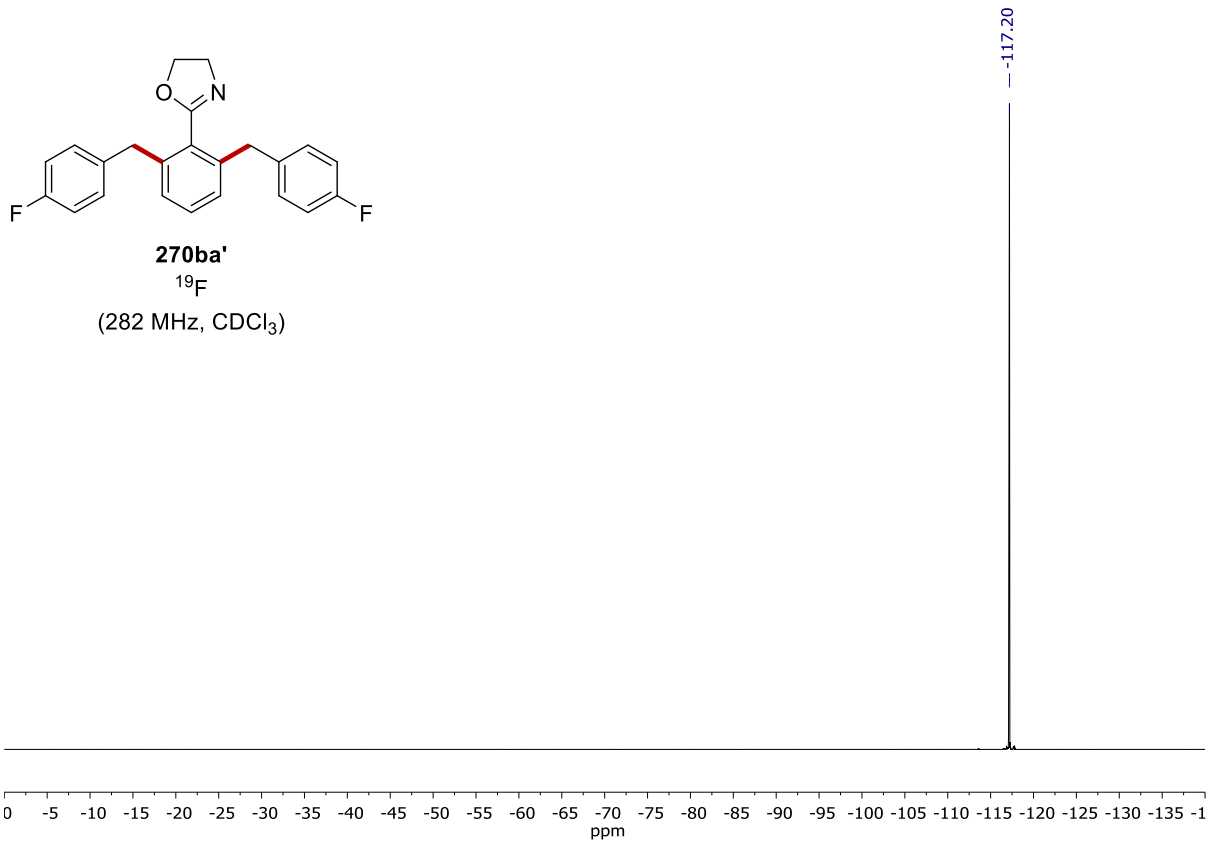
-117.20
O
N
F
F
270ba'
19F
(282 MHz, CDCl3)
ppm

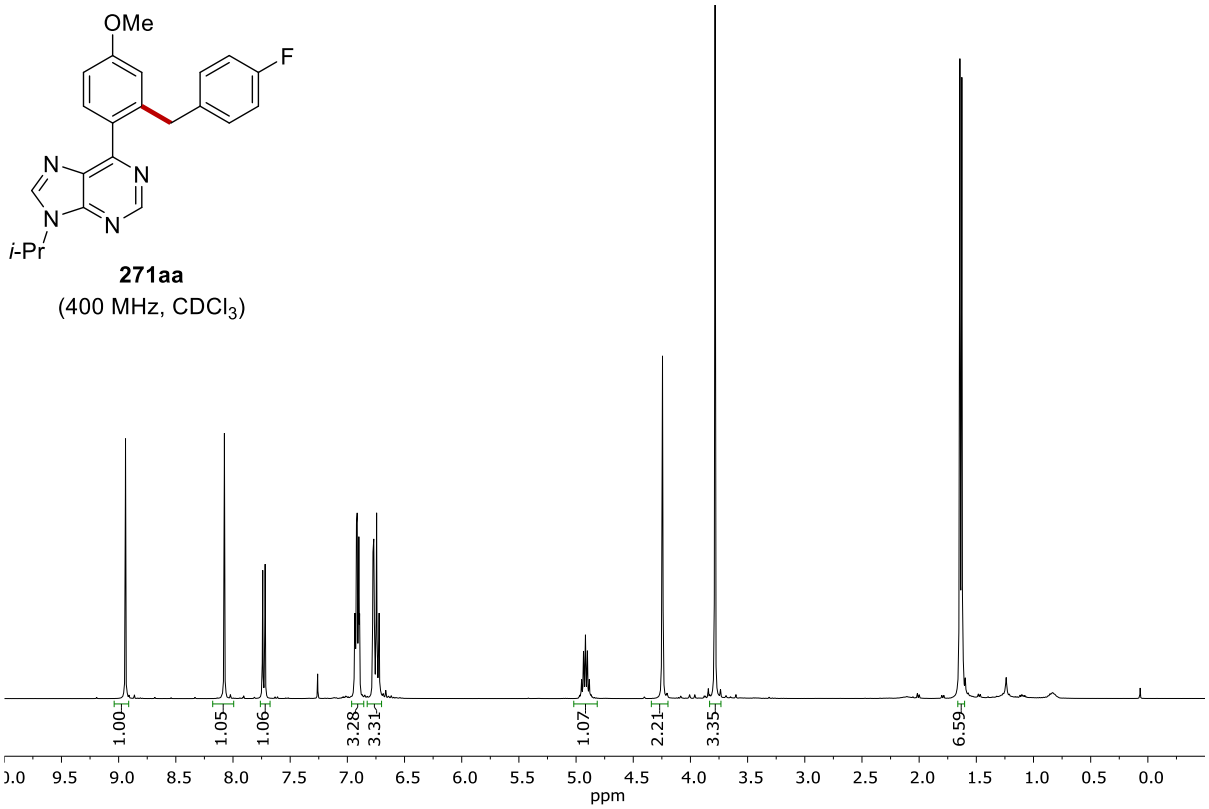
OMe
F
N
N
N
N
i-Pr
271aa
(400 MHz, CDCl3)
1.00
1.05
1.06
3.28
3.31
1.07
2.21
3.35
6.59
ppm

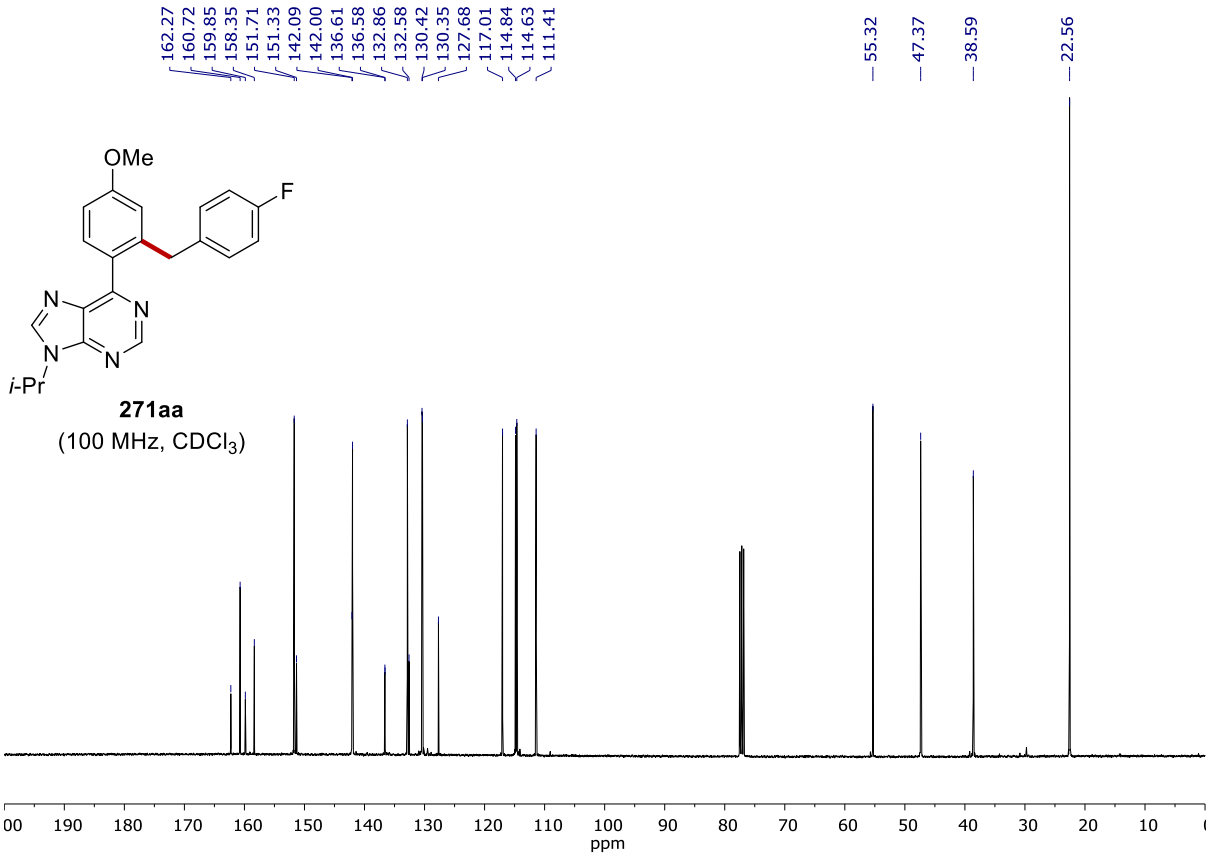
162.27
160.72
159.85
158.35
151.71
151.33
142.09
142.00
136.61
136.58
132.86
132.58
130.42
130.35
127.68
117.01
114.84
114.63
111.41
55.32
47.37
38.59
22.56
OMe
F
N
N
N
N
i-Pr
271aa
(100 MHz, CDCl3)
ppm

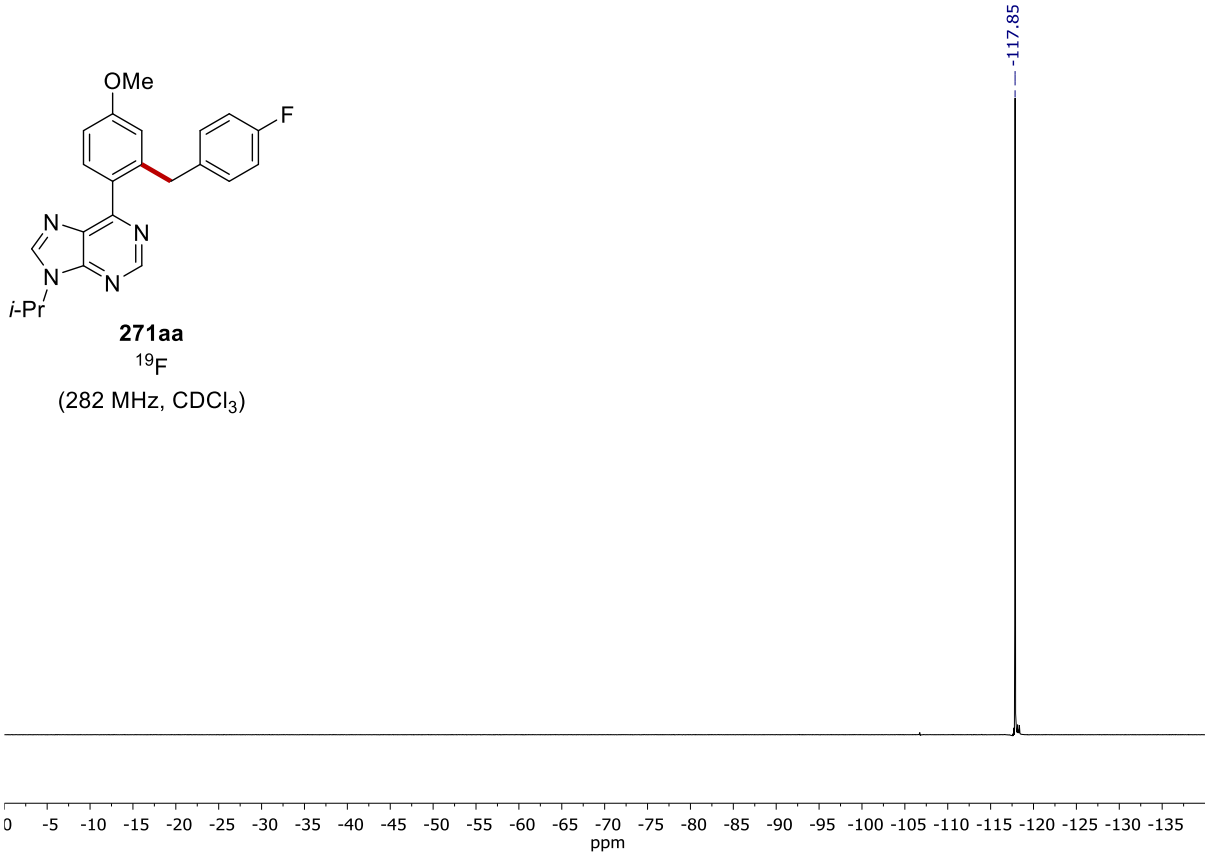

271aa

^{19}F

(282 MHz, $CDCl_3$)

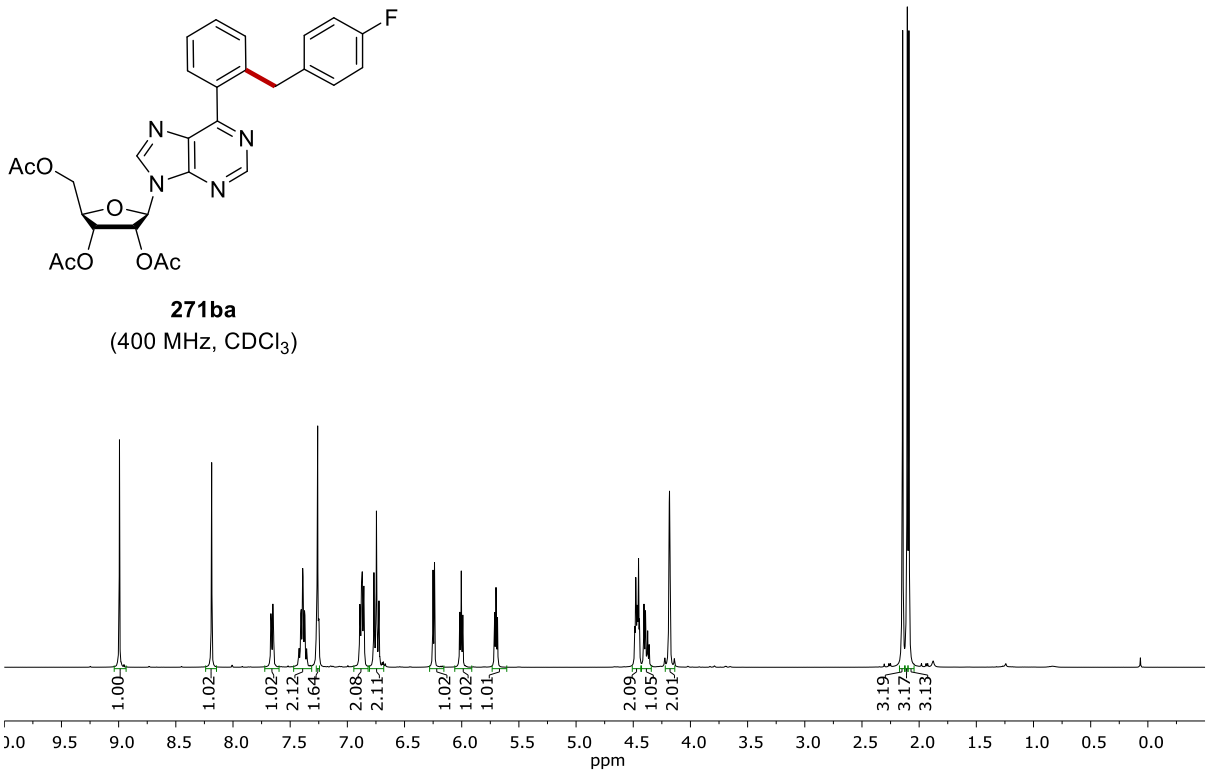

271ba

(400 MHz, $CDCl_3$)

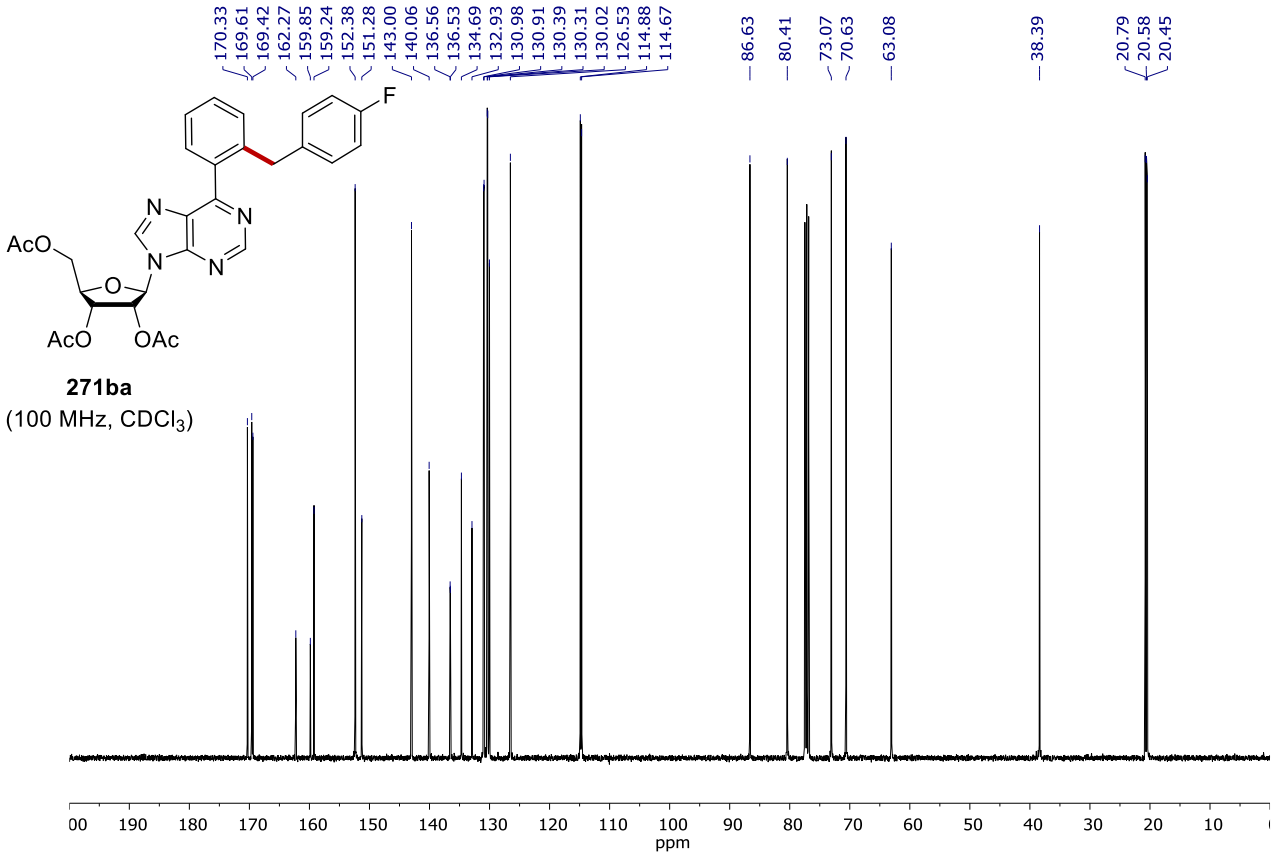

271ba
(100 MHz, $CDCl_3$)

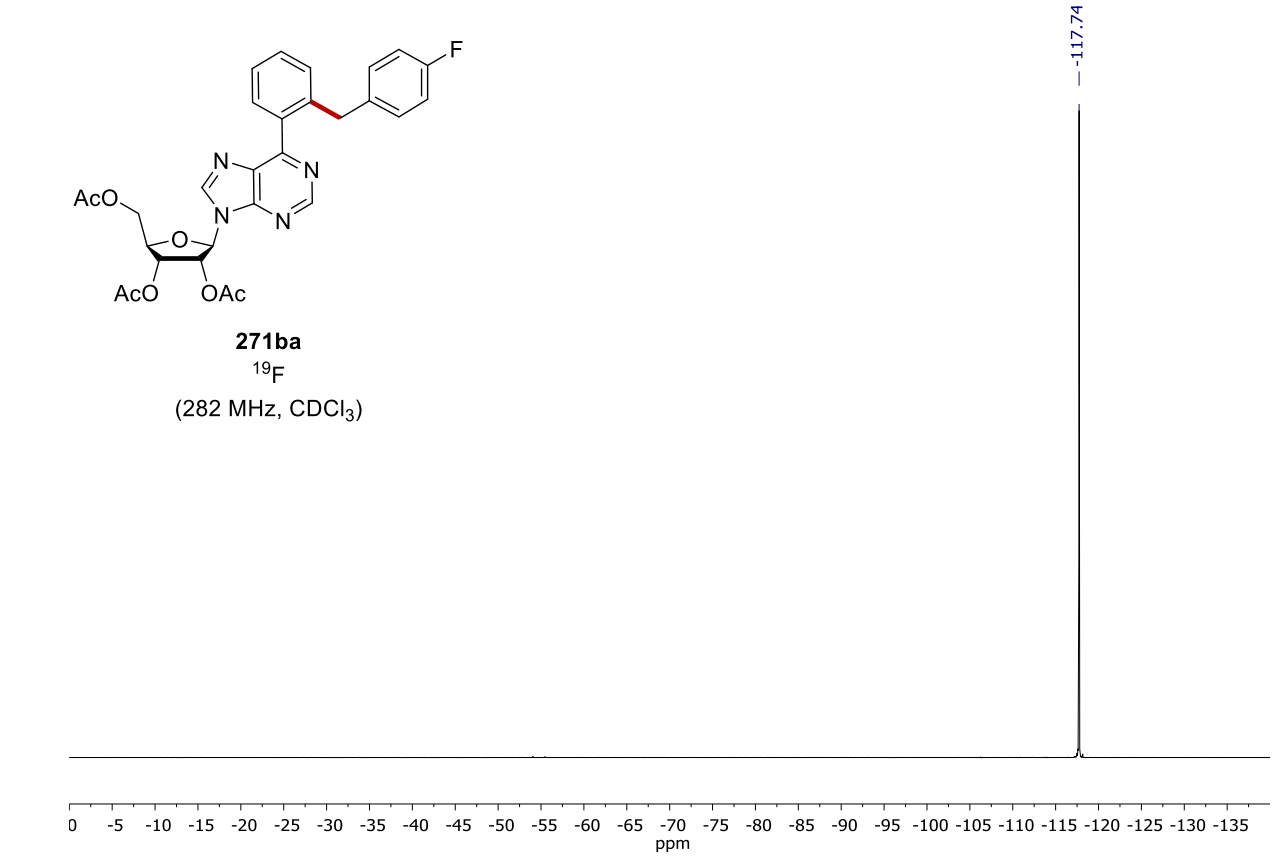

271ba
^{19}F
(282 MHz, $CDCl_3$)

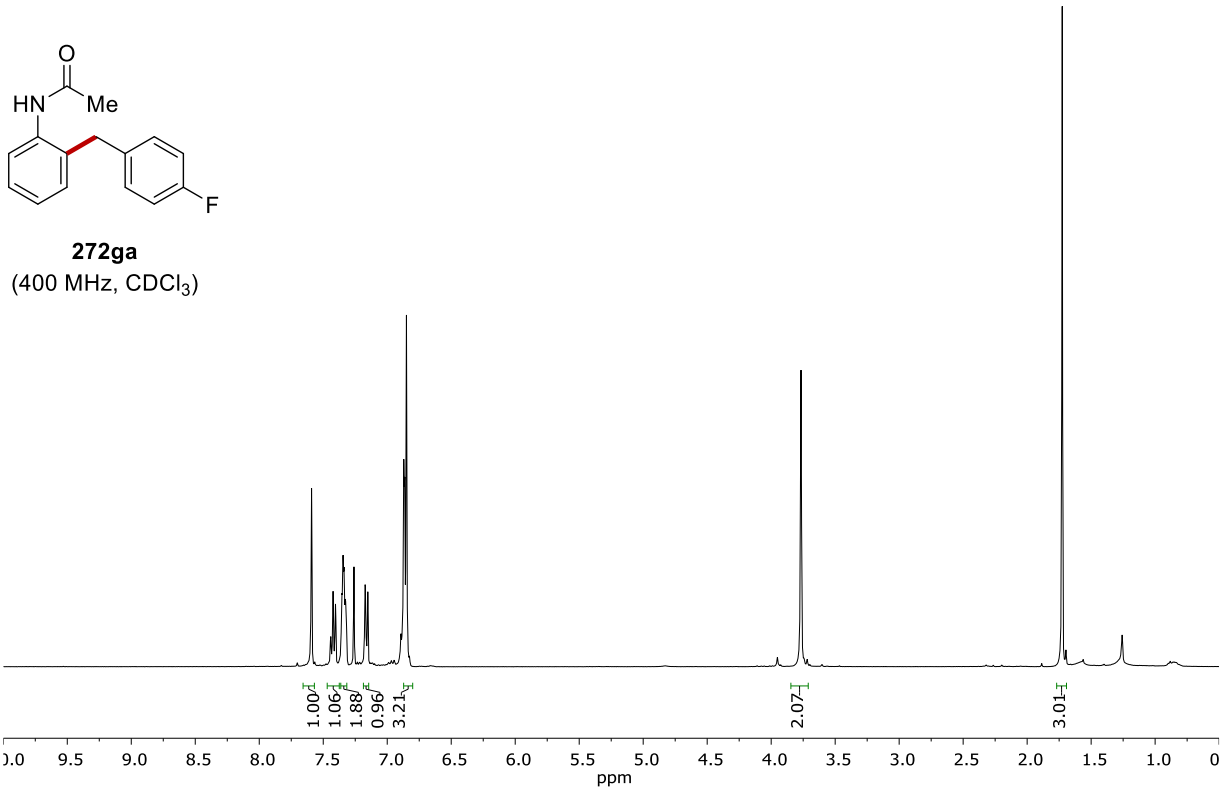
O
HN
Me
F
272ga
(400 MHz, CDCl3)
1.00
1.06
1.88
0.96
3.21
2.07
3.01
ppm

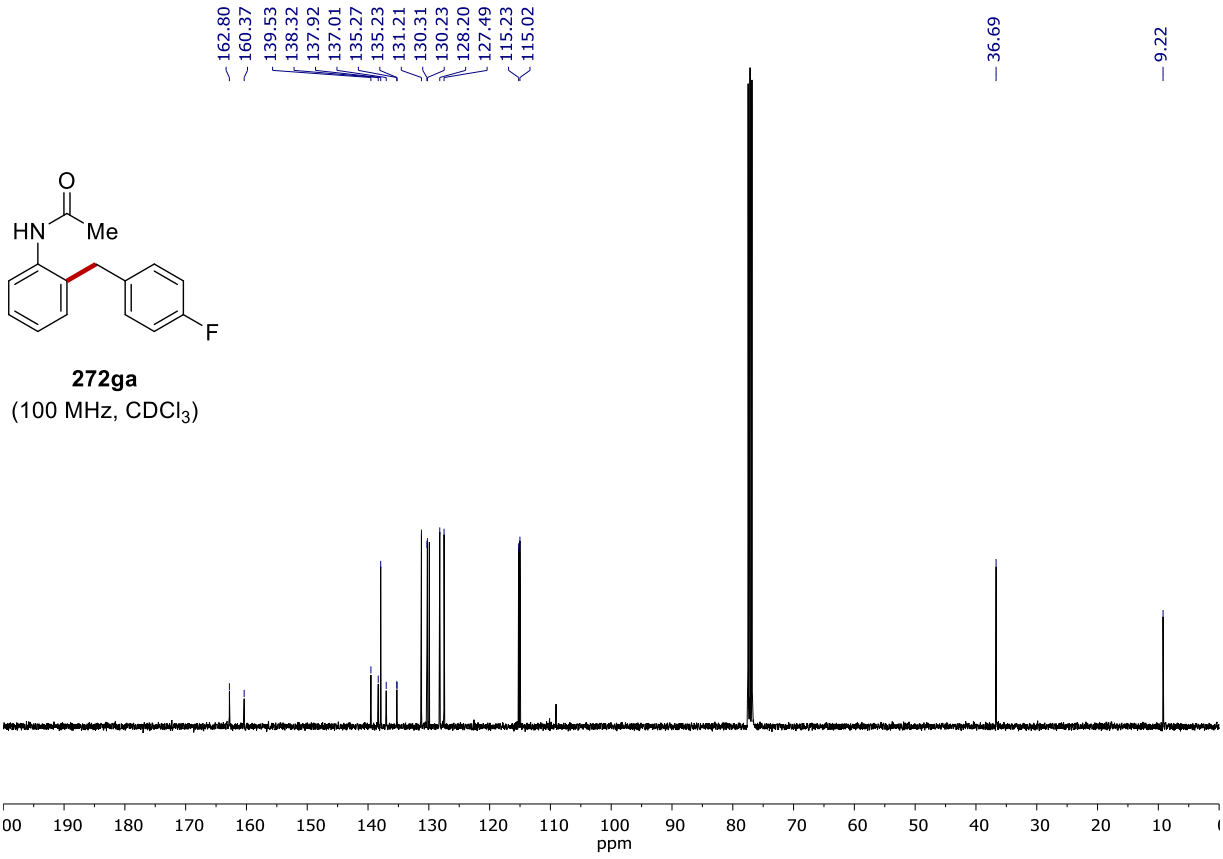
162.80
160.37
139.53
138.32
137.92
137.01
135.27
135.23
131.21
130.31
130.23
128.20
127.49
115.23
115.02
36.69
9.22
O
HN
Me
F
272ga
(100 MHz, CDCl3)
ppm

272ga
(377 MHz, $CDCl_3$)

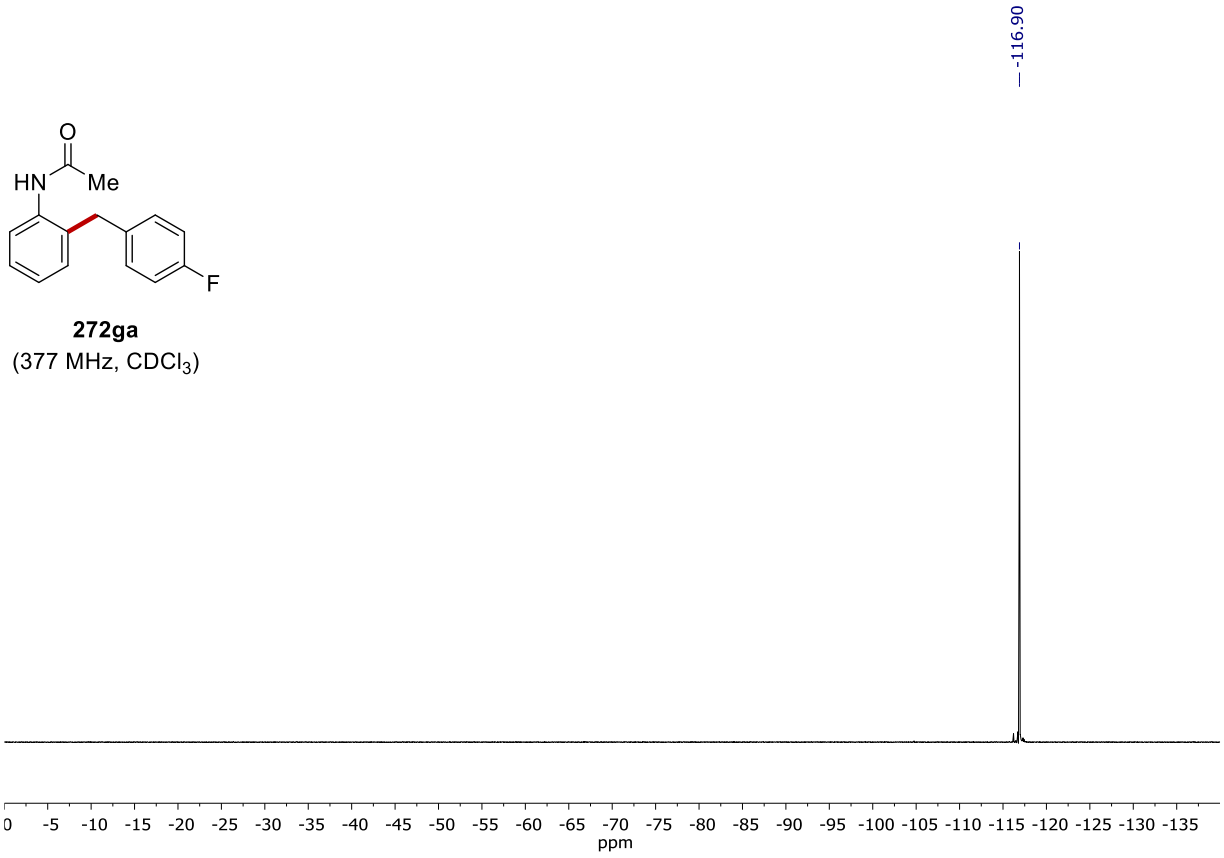

147b
(400 MHz, $CDCl_3$)

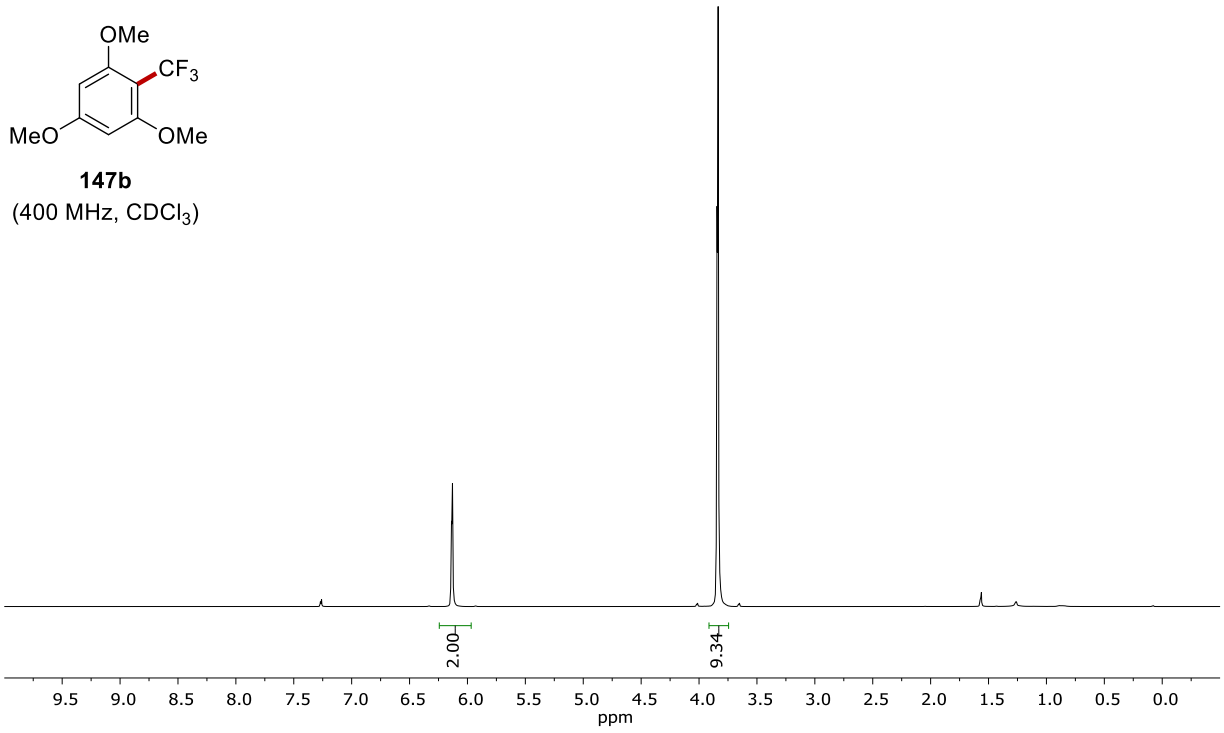

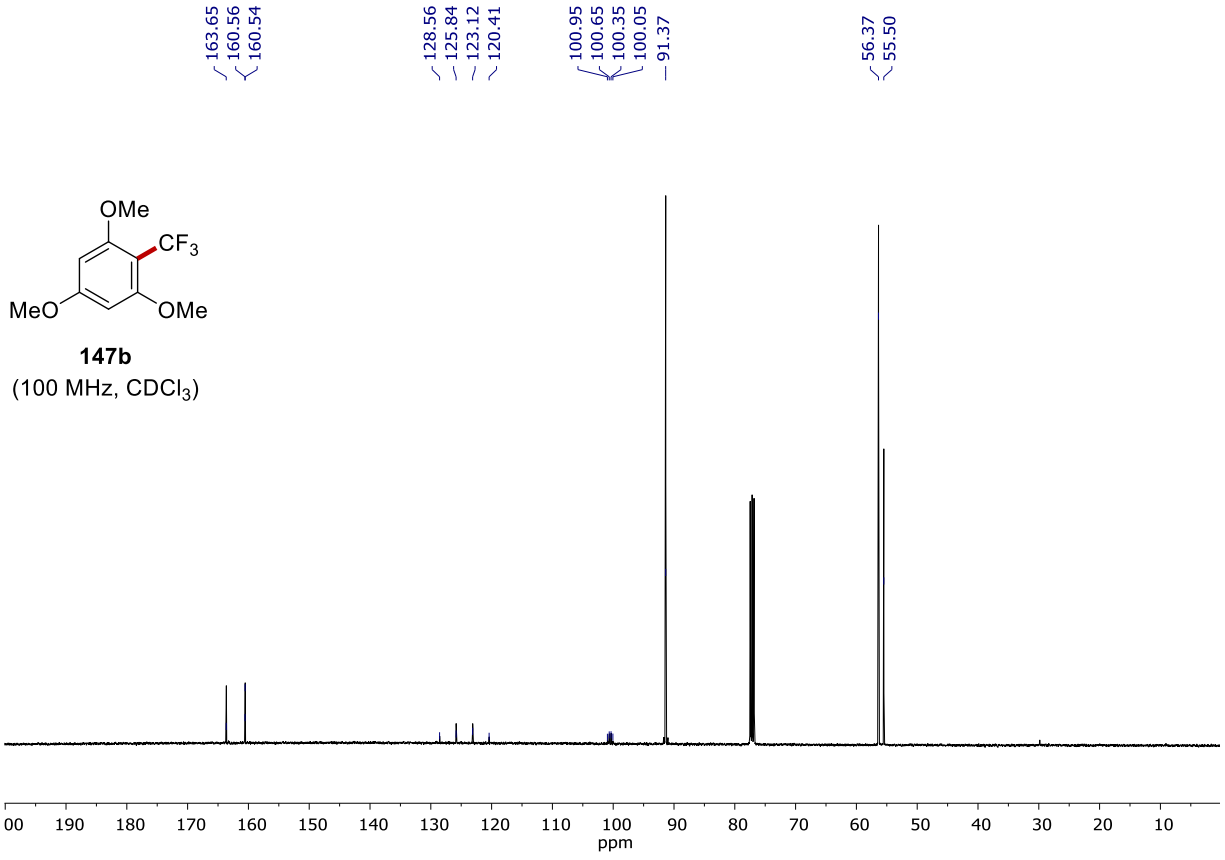
163.65
160.56
160.54
128.56
125.84
123.12
120.41
100.95
100.65
100.35
100.05
91.37
56.37
55.50
OMe
CF3
MeO
OMe
147b
(100 MHz, CDCl3)
ppm

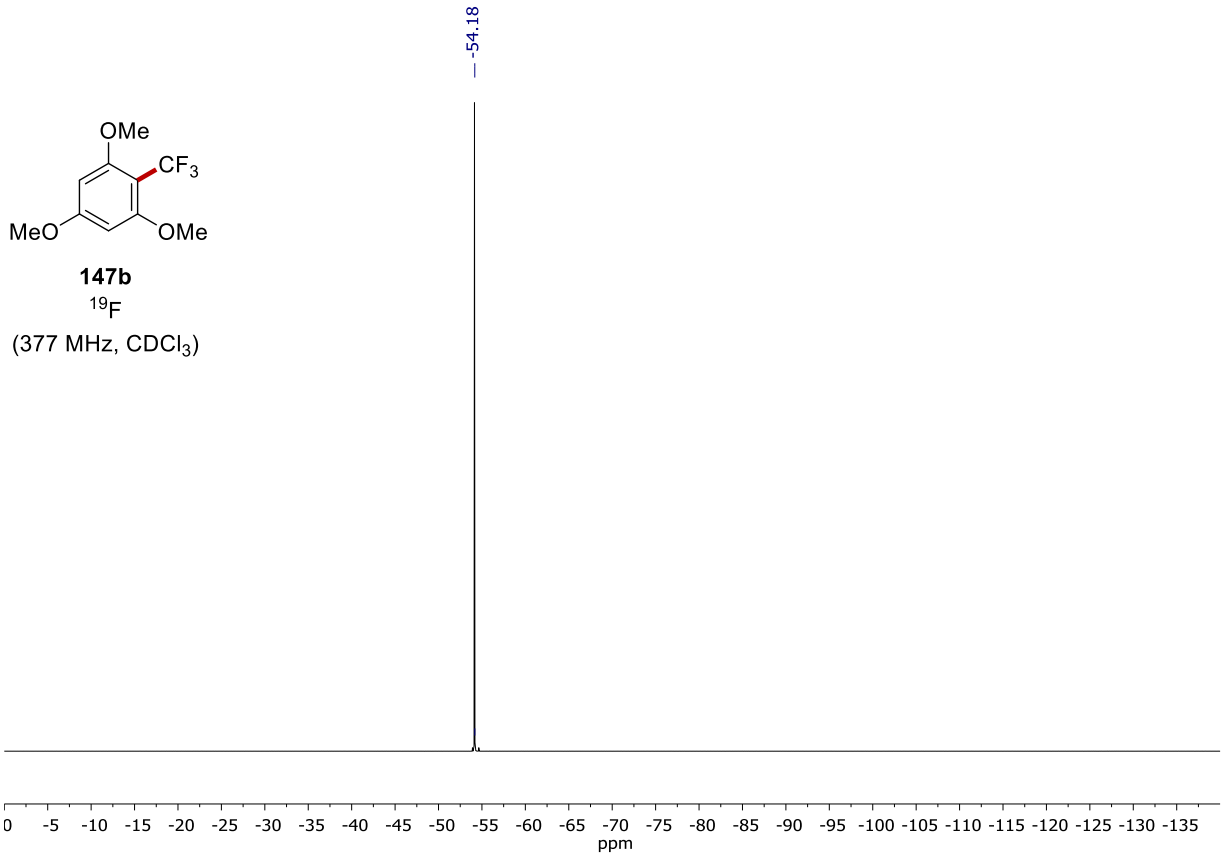
-54.18
OMe
CF3
MeO
OMe
147b
19F
(377 MHz, CDCl3)
ppm

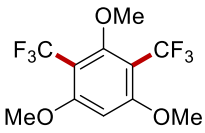

147b'
(400 MHz, $CDCl_3$)

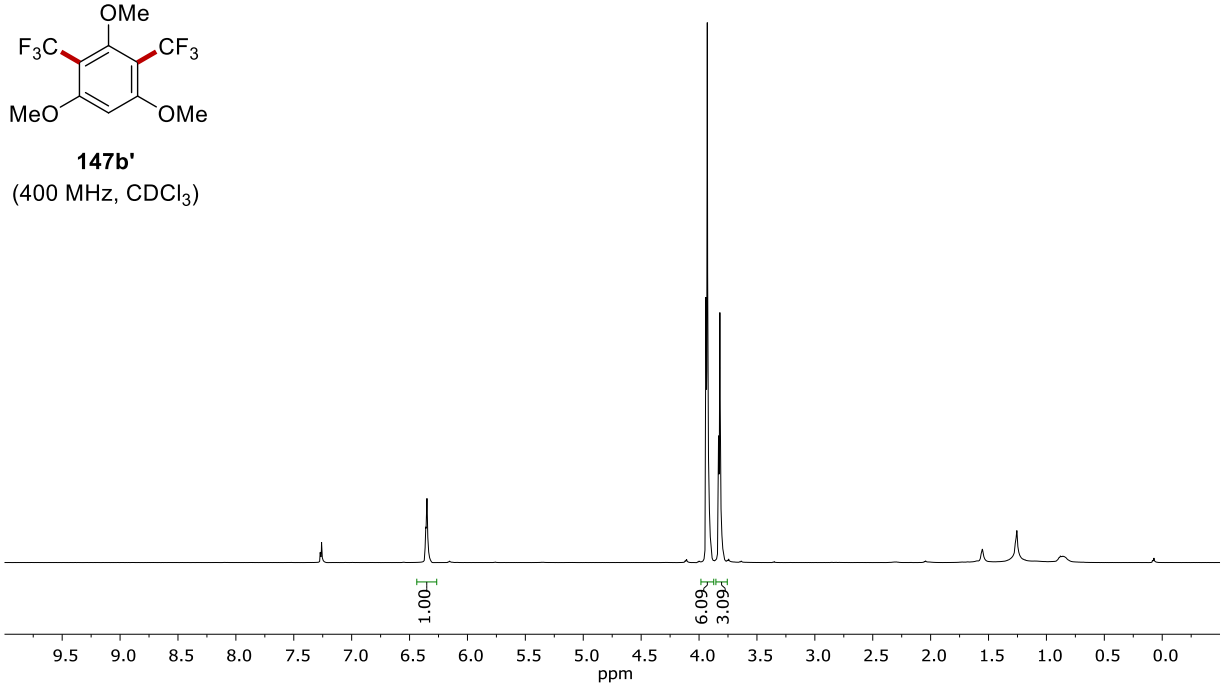

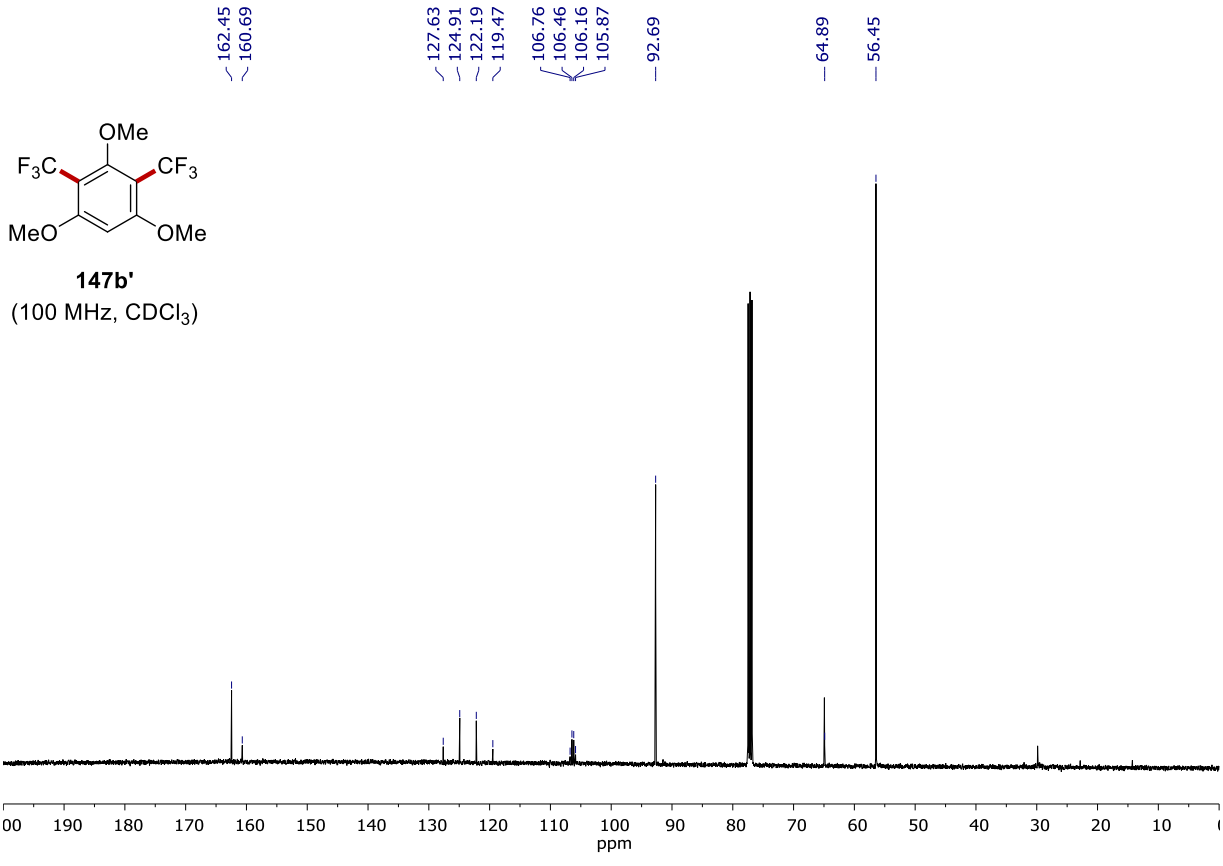

147b'
(100 MHz, $CDCl_3$)

147b'

^{19}F

(377 MHz, $CDCl_3$)

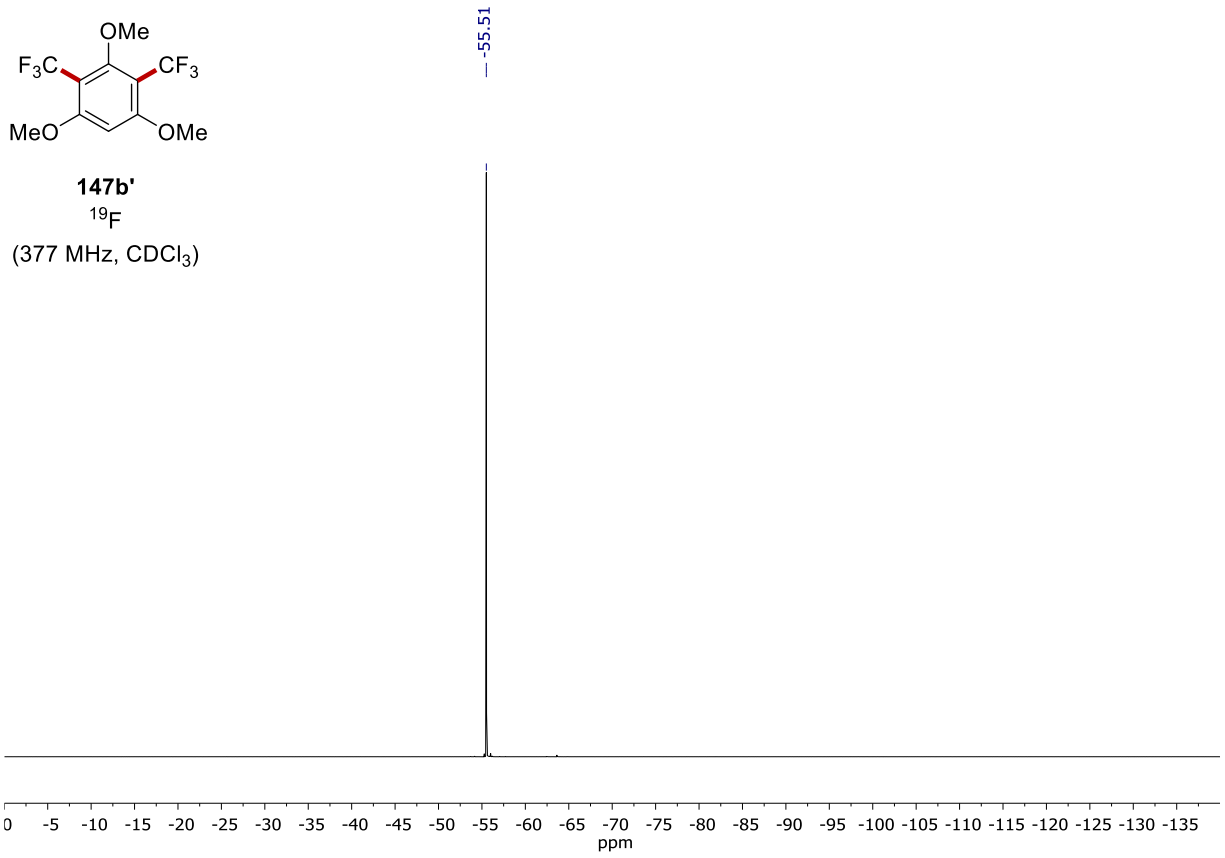

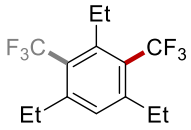

147c

(300 MHz, $CDCl_3$)

Ratio mono/di: 3.6:1

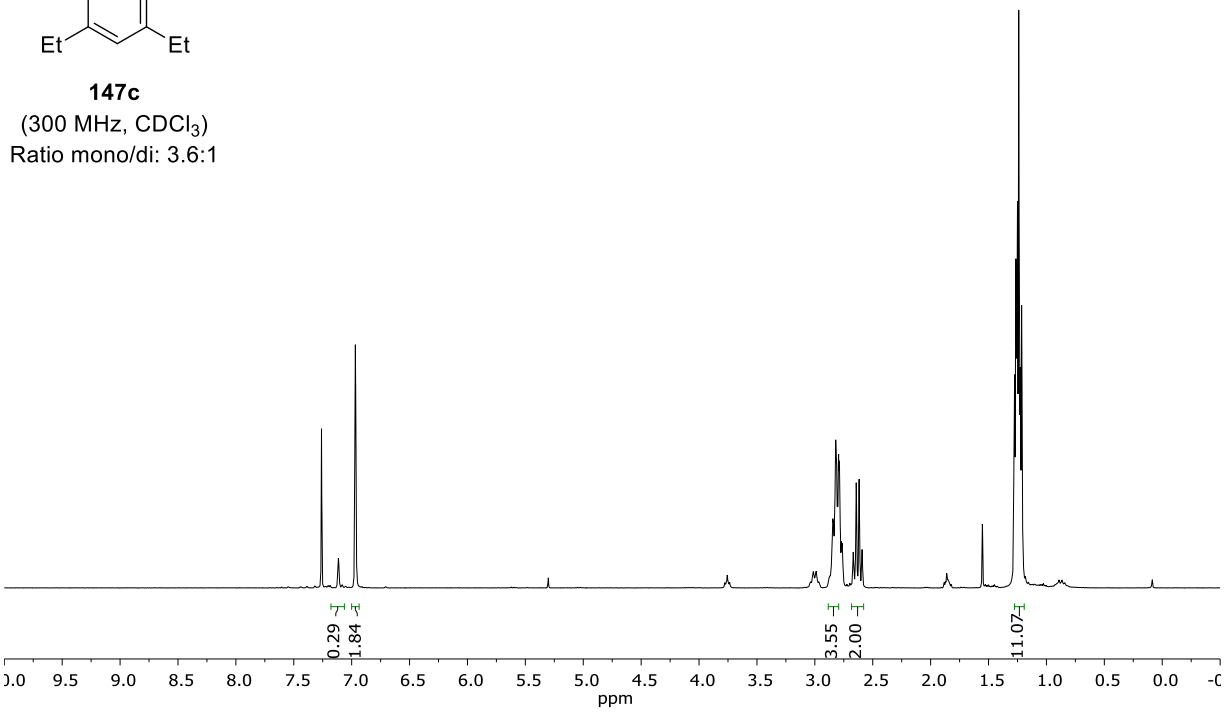

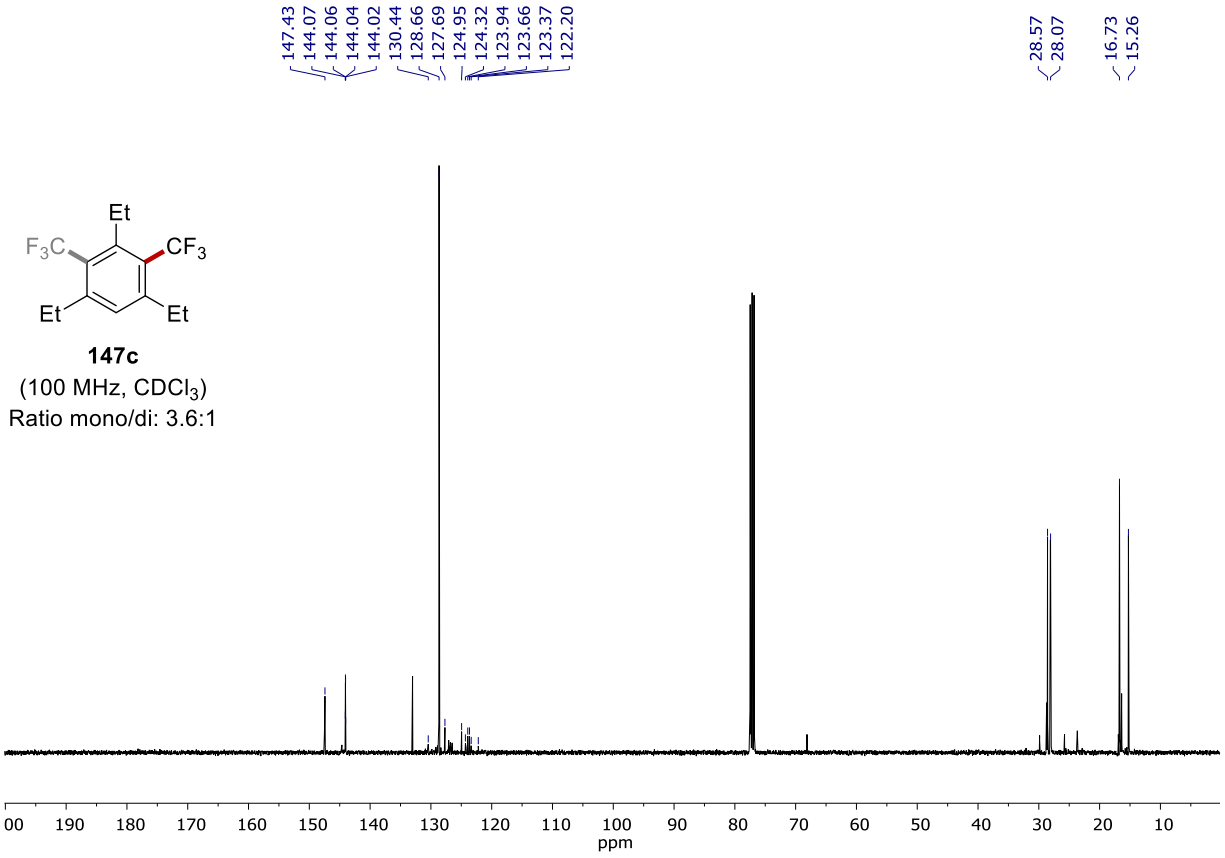
147.43
144.07
144.06
144.04
144.02
130.44
128.66
127.69
124.95
124.32
123.94
123.66
123.37
122.20
28.57
28.07
16.73
15.26
Et
F3C
CF3
Et
Et
147c
(100 MHz, CDCl3)
Ratio mono/di: 3.6:1
00 190 180 170 160 150 140 130 120 110 100 90 80 70 60 50 40 30 20 10
ppm

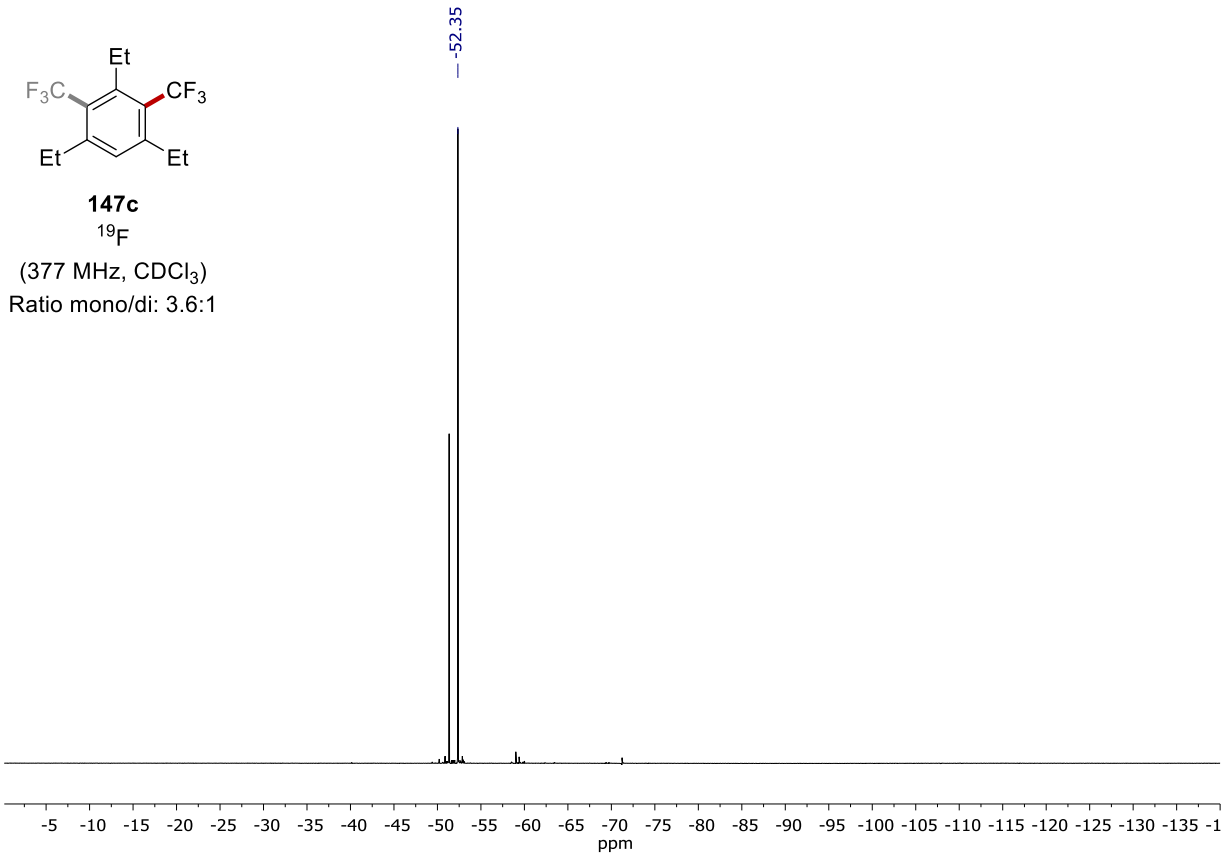
-52.35
Et
F3C
CF3
Et
Et
147c
19F
(377 MHz, CDCl3)
Ratio mono/di: 3.6:1
-5 -10 -15 -20 -25 -30 -35 -40 -45 -50 -55 -60 -65 -70 -75 -80 -85 -90 -95 -100 -105 -110 -115 -120 -125 -130 -135 -1
ppm

147d
(400 MHz, $CDCl_3$)

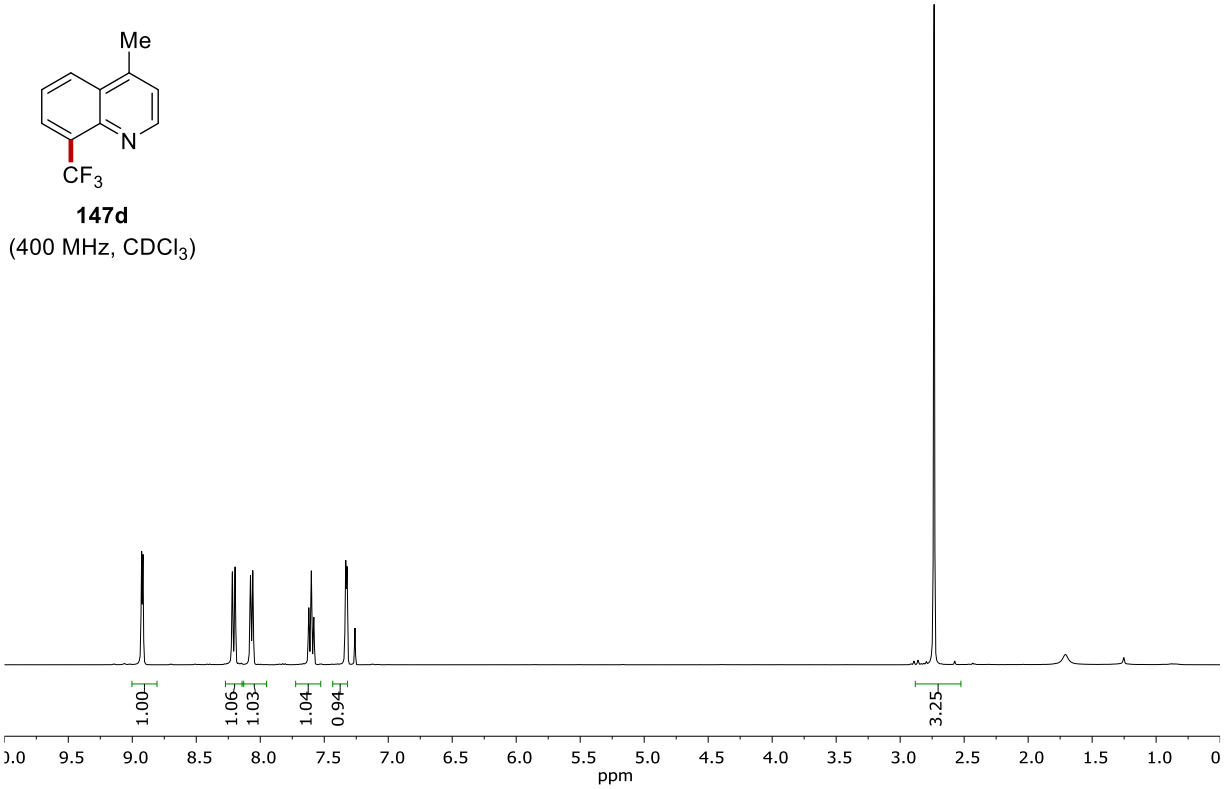

147d
(100 MHz, $CDCl_3$)

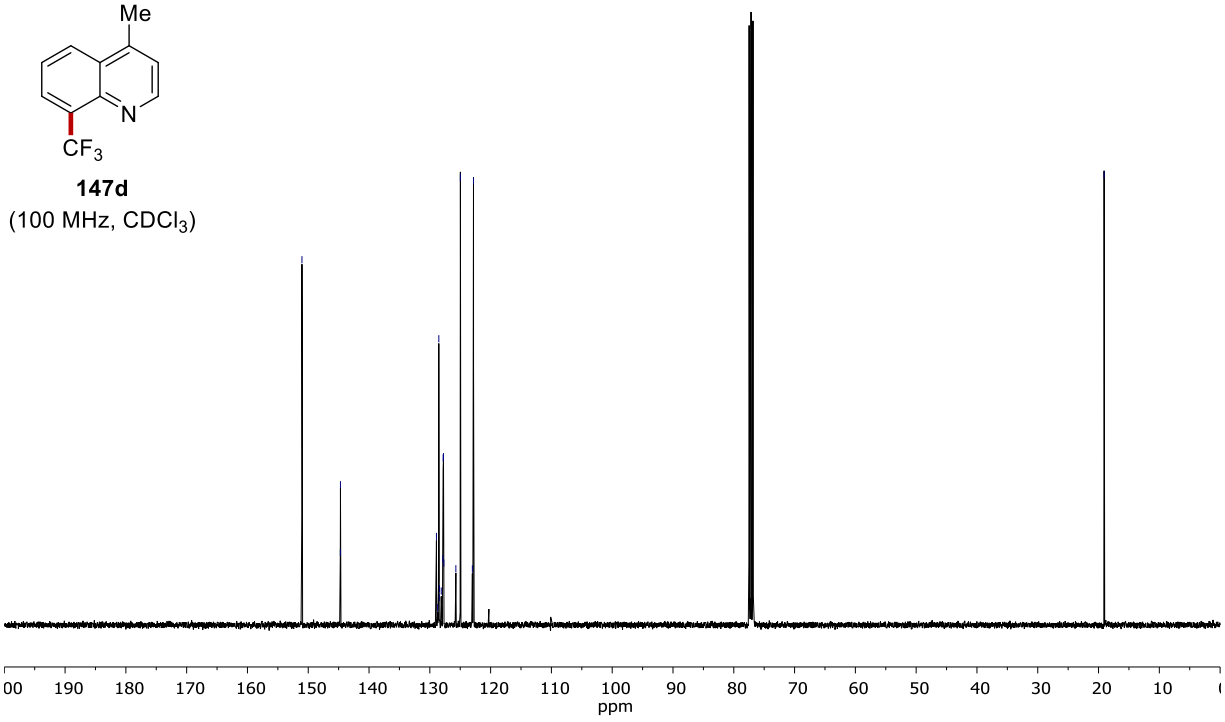

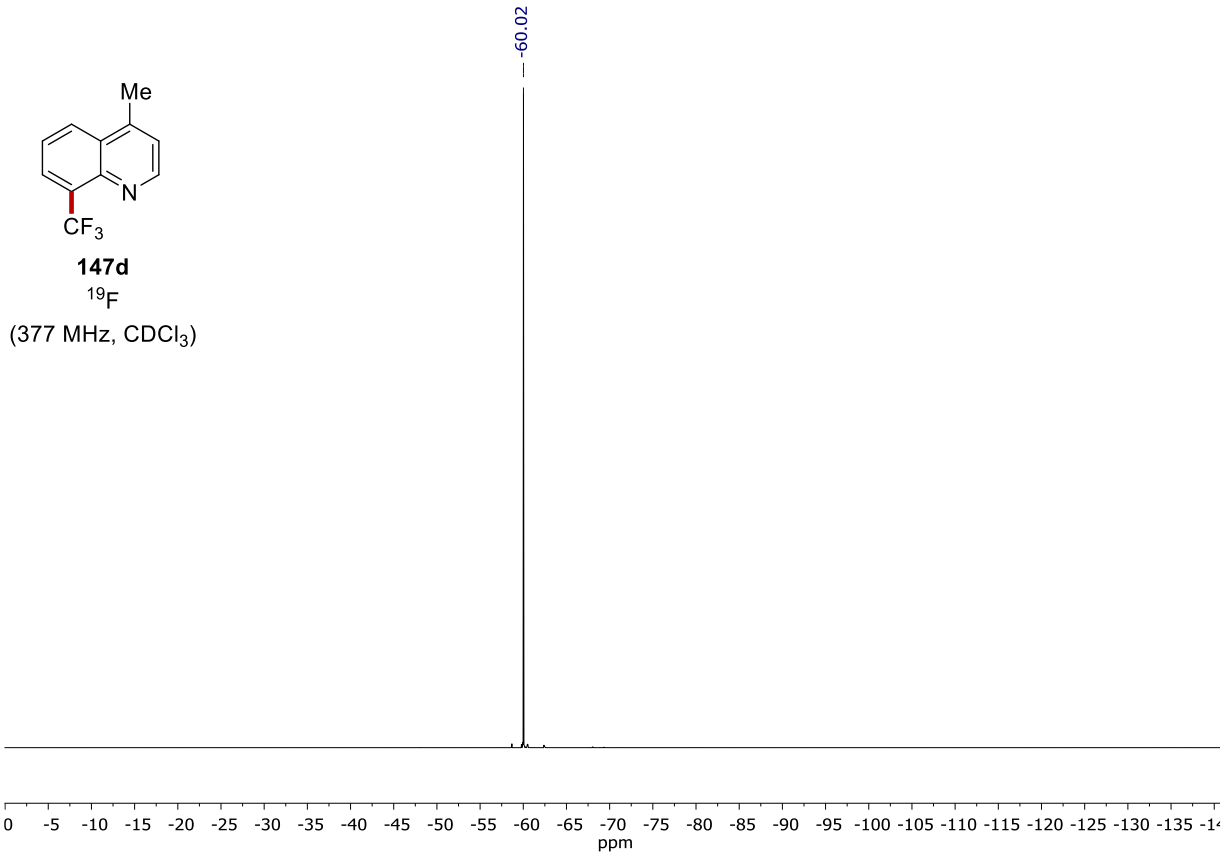

147d

^{19}F

(377 MHz, $CDCl_3$)

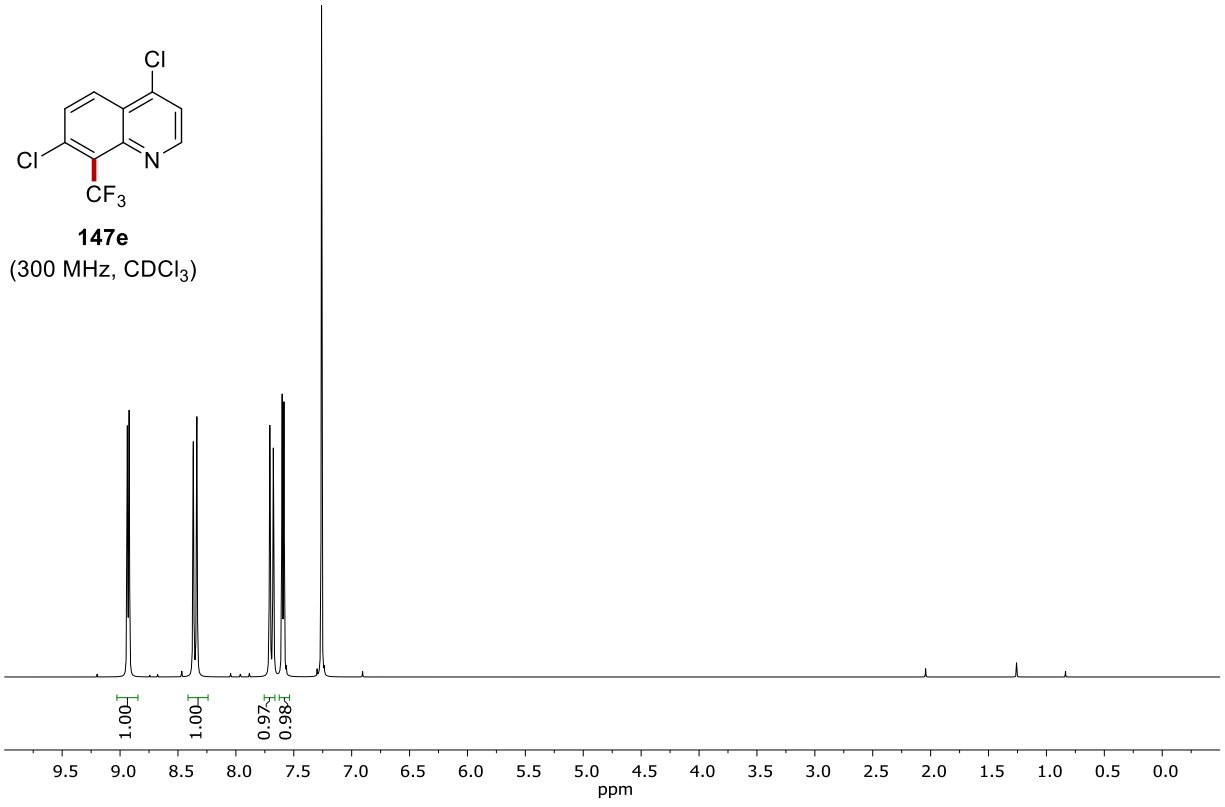

147e

(300 MHz, $CDCl_3$)

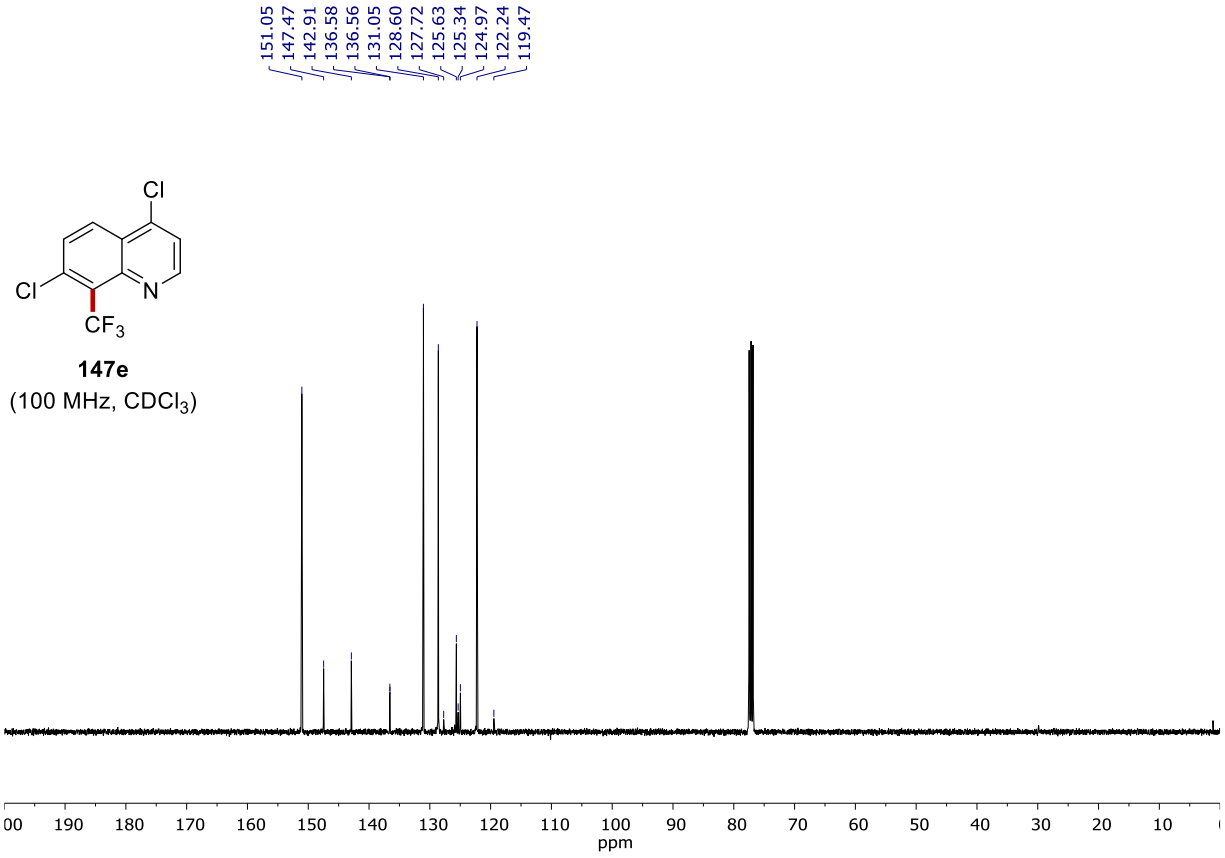
151.05
147.47
142.91
136.58
136.56
131.05
128.60
127.72
125.63
125.34
124.97
122.24
119.47
Cl
Cl
N
CF3
147e
(100 MHz, CDCl3)
ppm

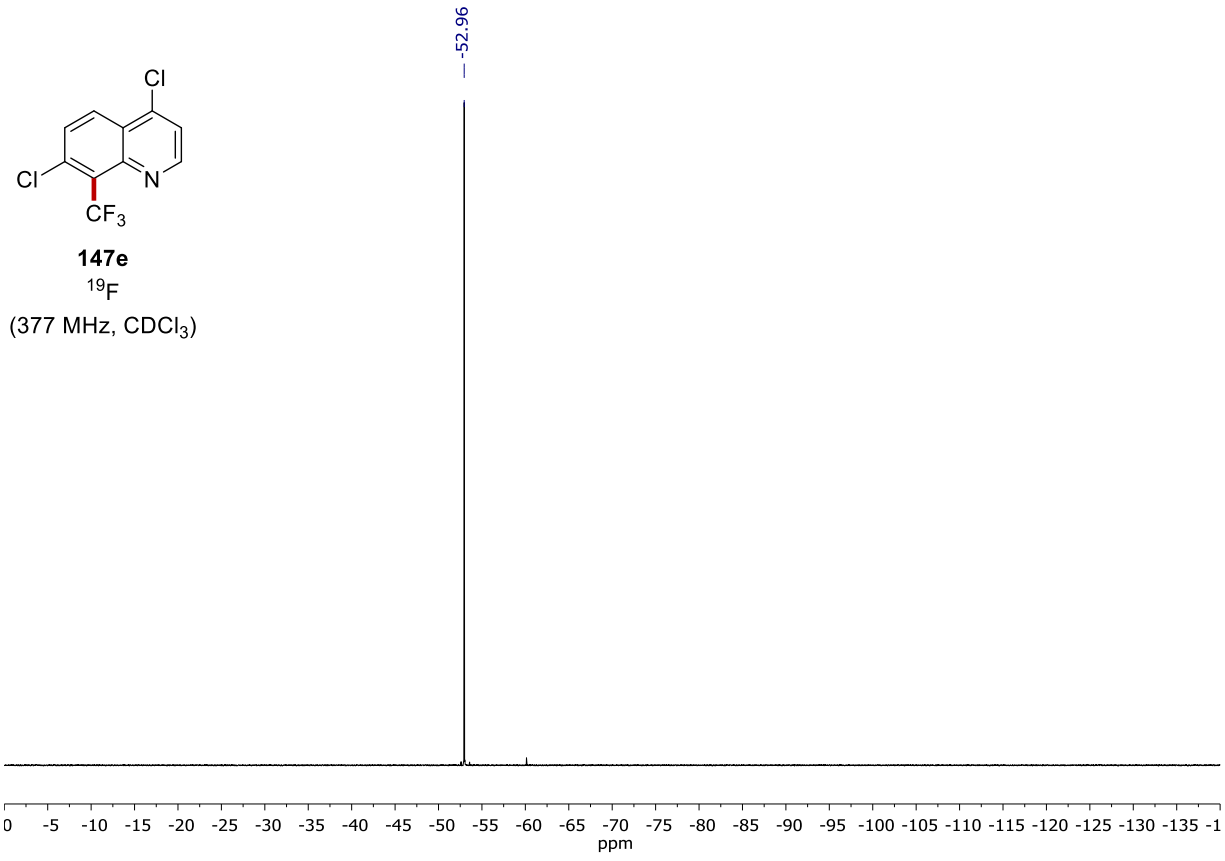
-52.96
Cl
Cl
N
CF3
147e
19F
(377 MHz, CDCl3)
ppm

247f
(400 MHz, $CDCl_3$)

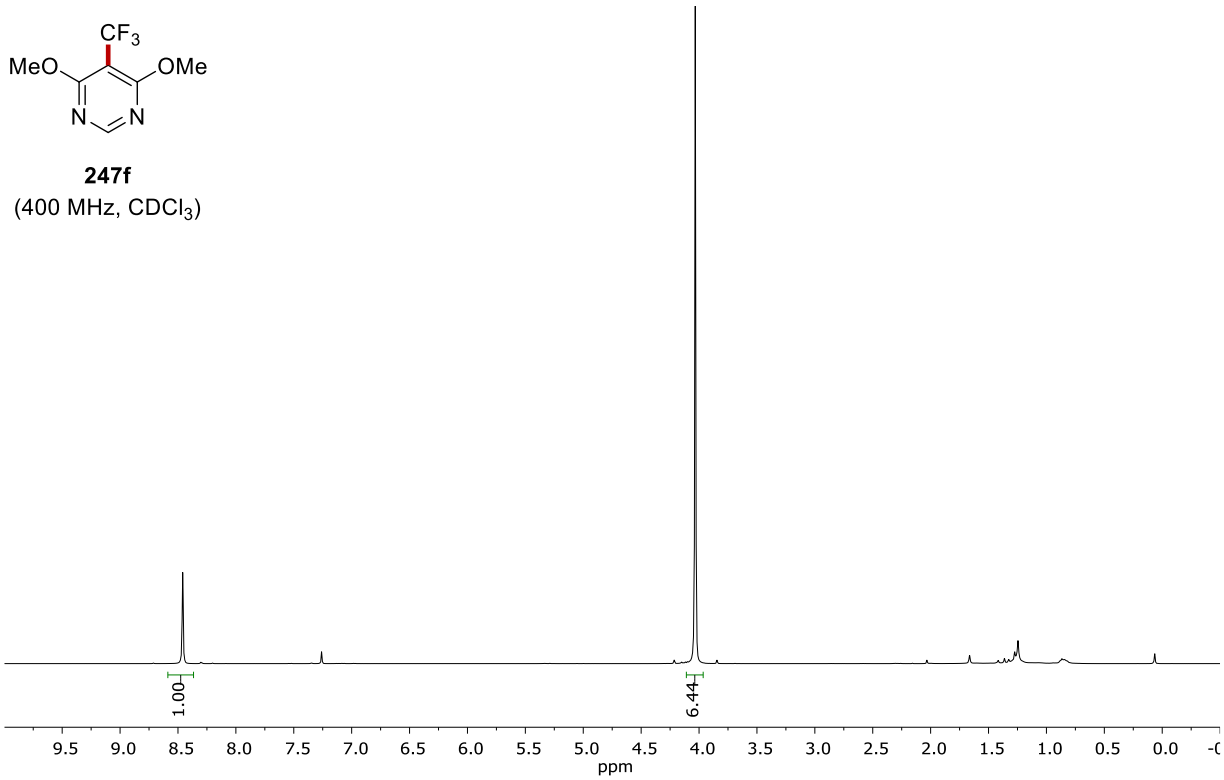

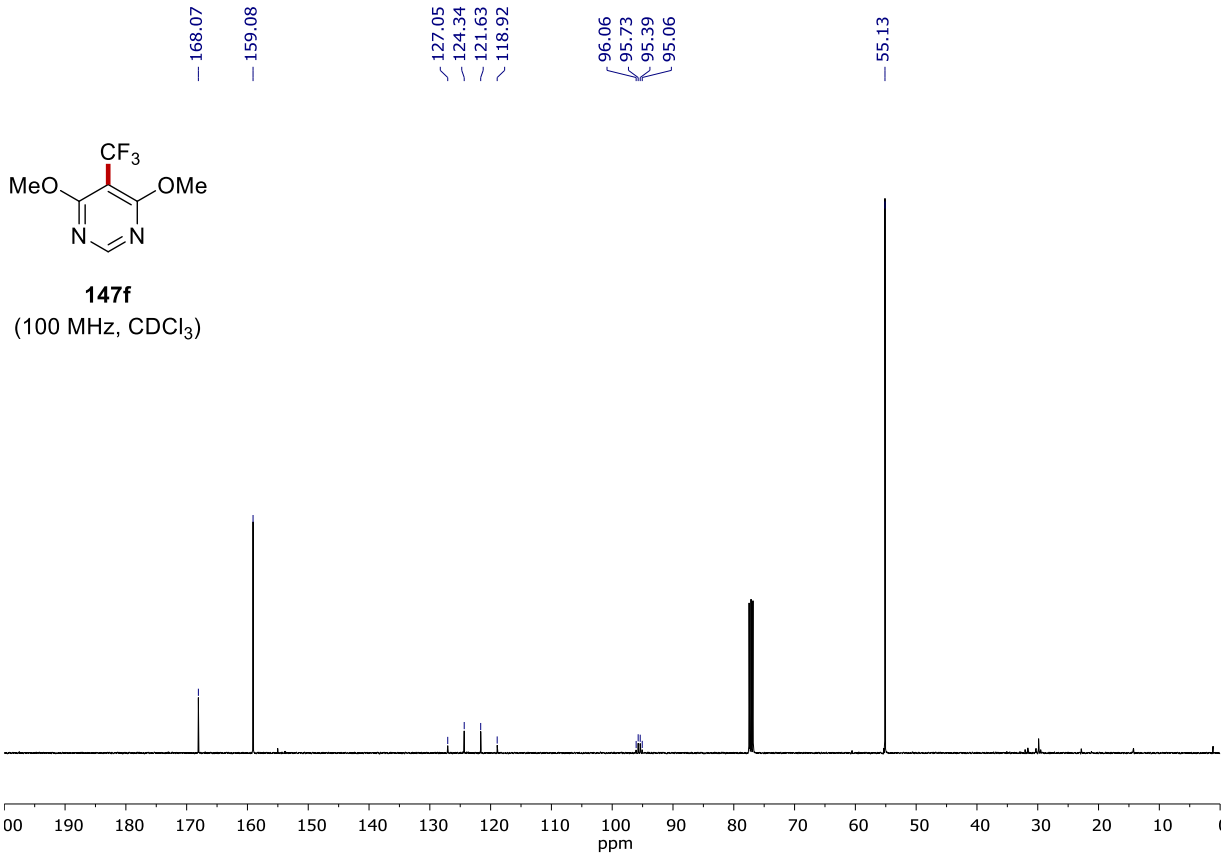

147f
(100 MHz, $CDCl_3$)

147f

^{19}F

(377 MHz, $CDCl_3$)

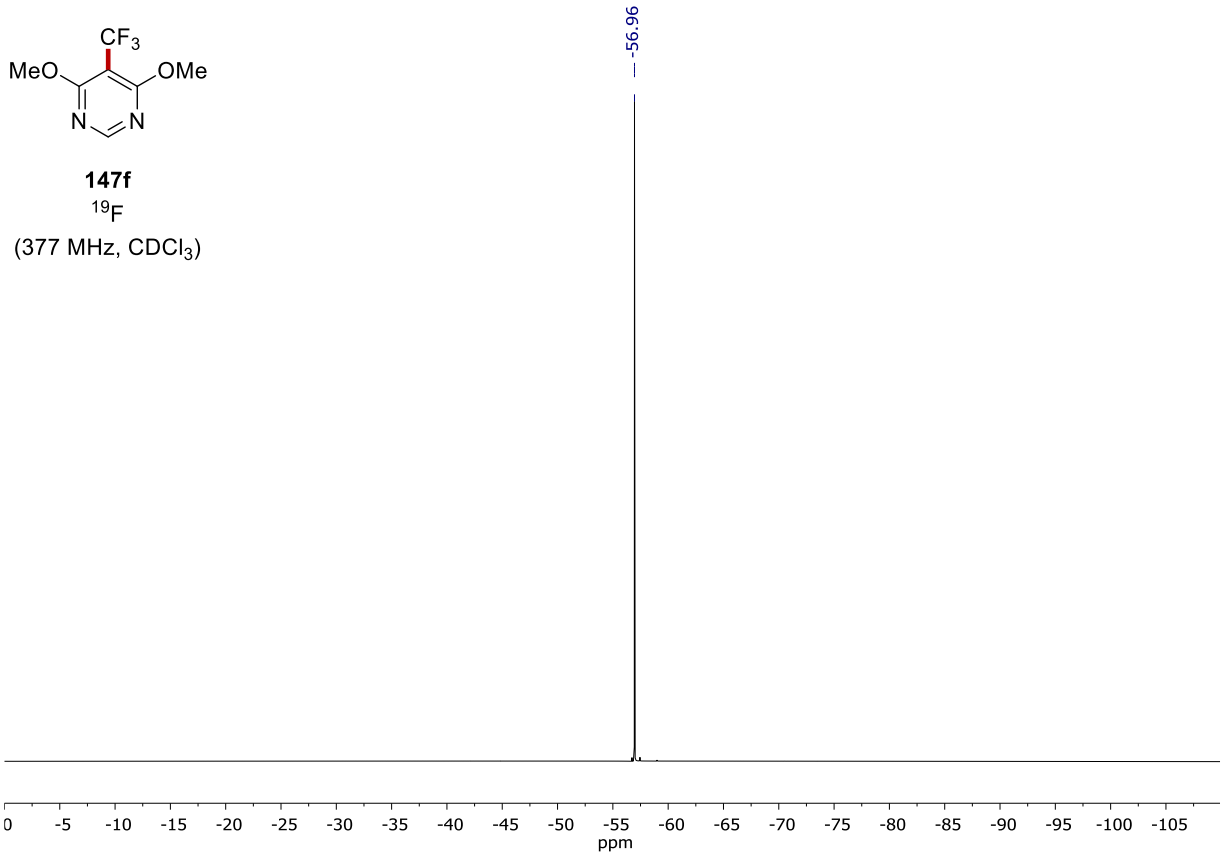

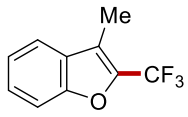

147g

(300 MHz, $CDCl_3$)

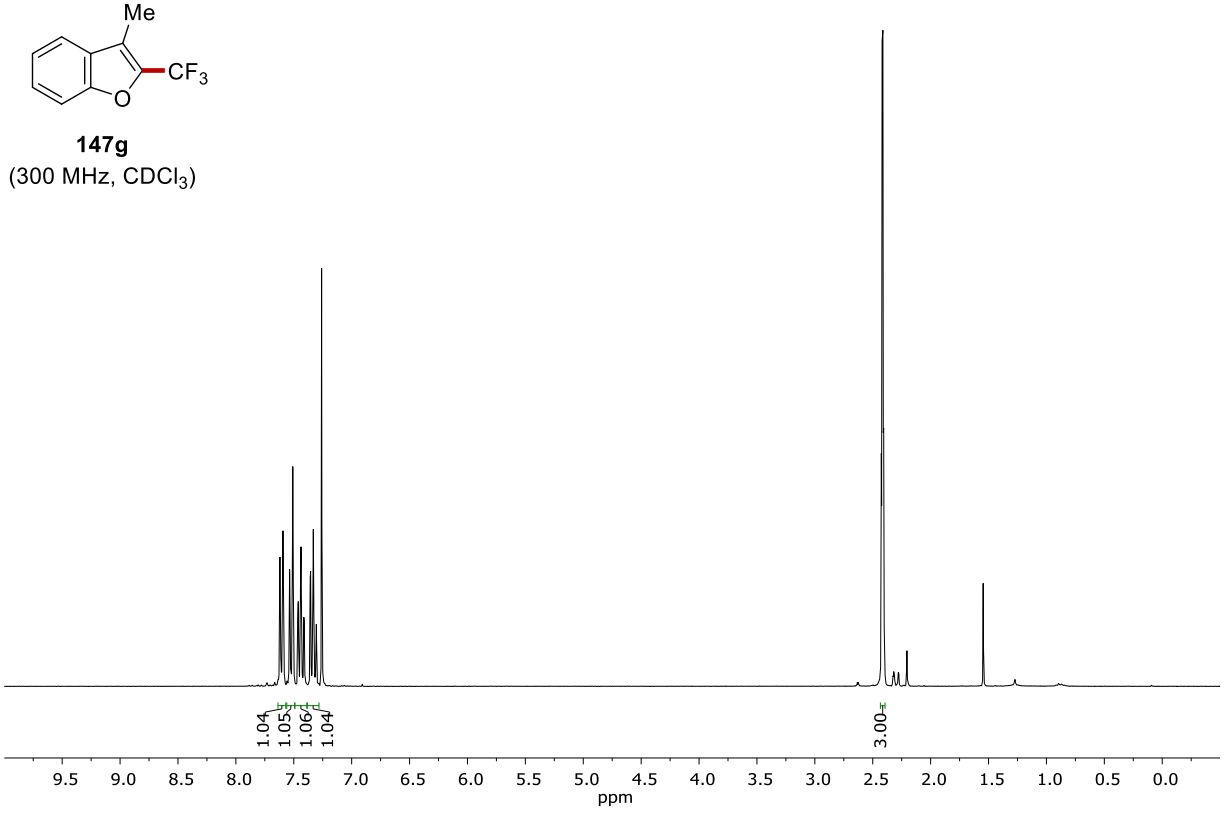

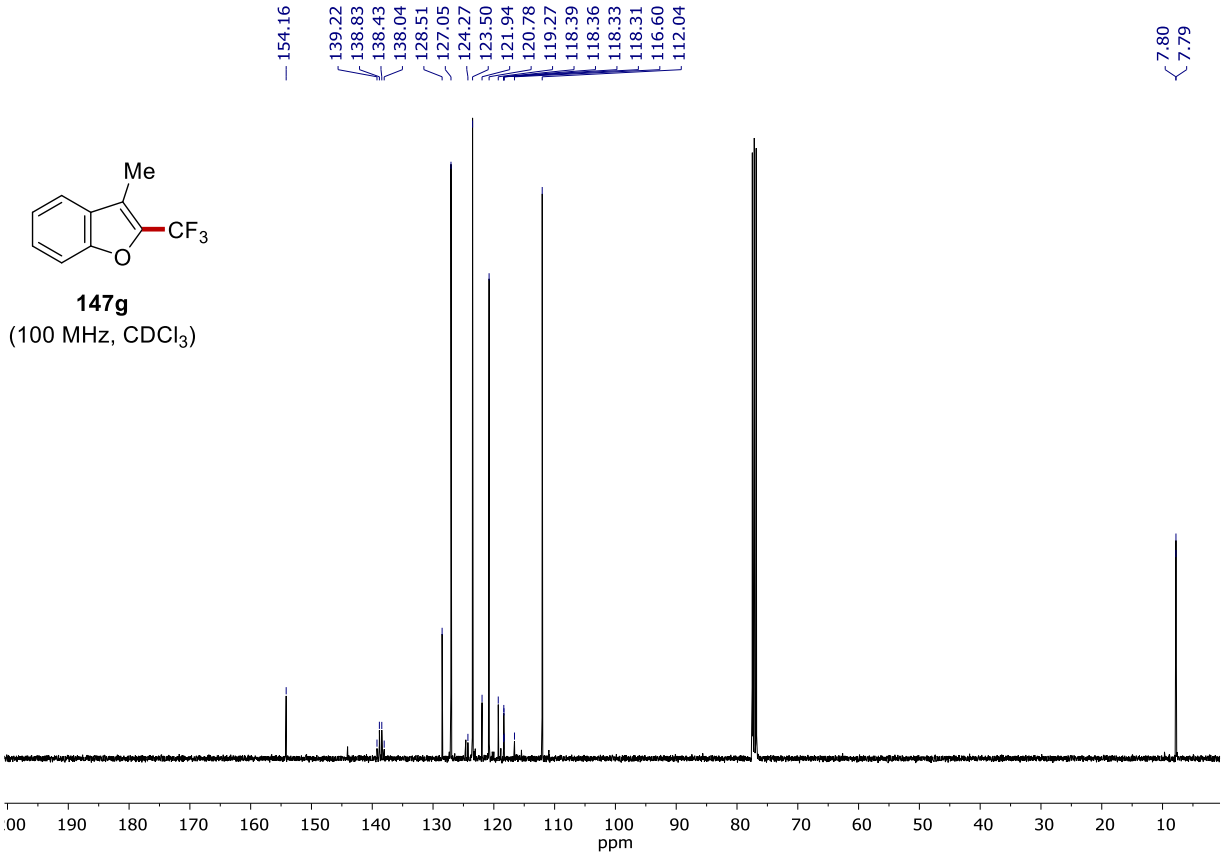
154.16
139.22
138.83
138.43
138.04
128.51
127.05
124.27
123.50
121.94
120.78
119.27
118.39
118.36
118.33
118.31
116.60
112.04
7.80
7.79
Me
CF3
O
147g
(100 MHz, CDCl3)
ppm

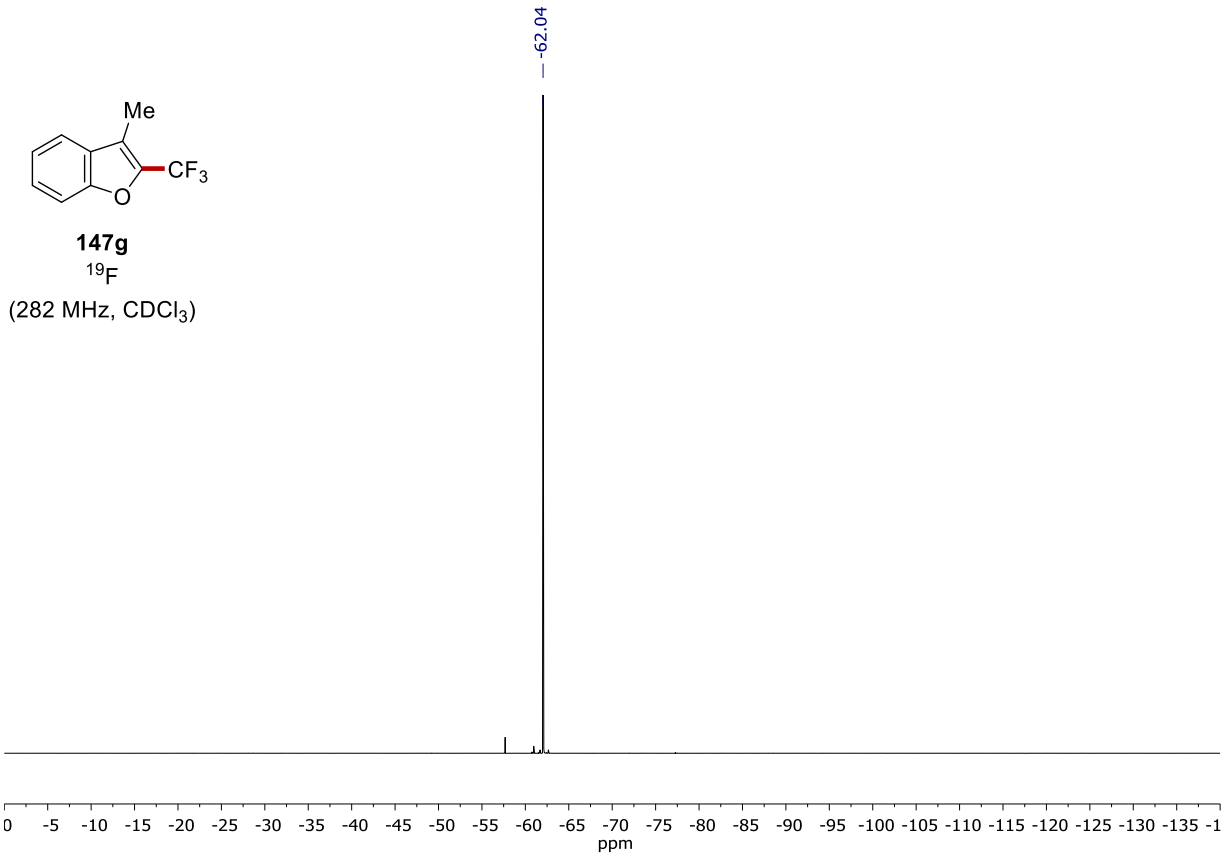
-62.04
Me
CF3
O
147g
19F
(282 MHz, CDCl3)
ppm

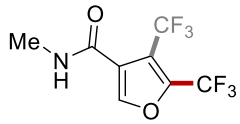

147h
(400 MHz, $CDCl_3$)
Ratio of the isomers: 3.0:1

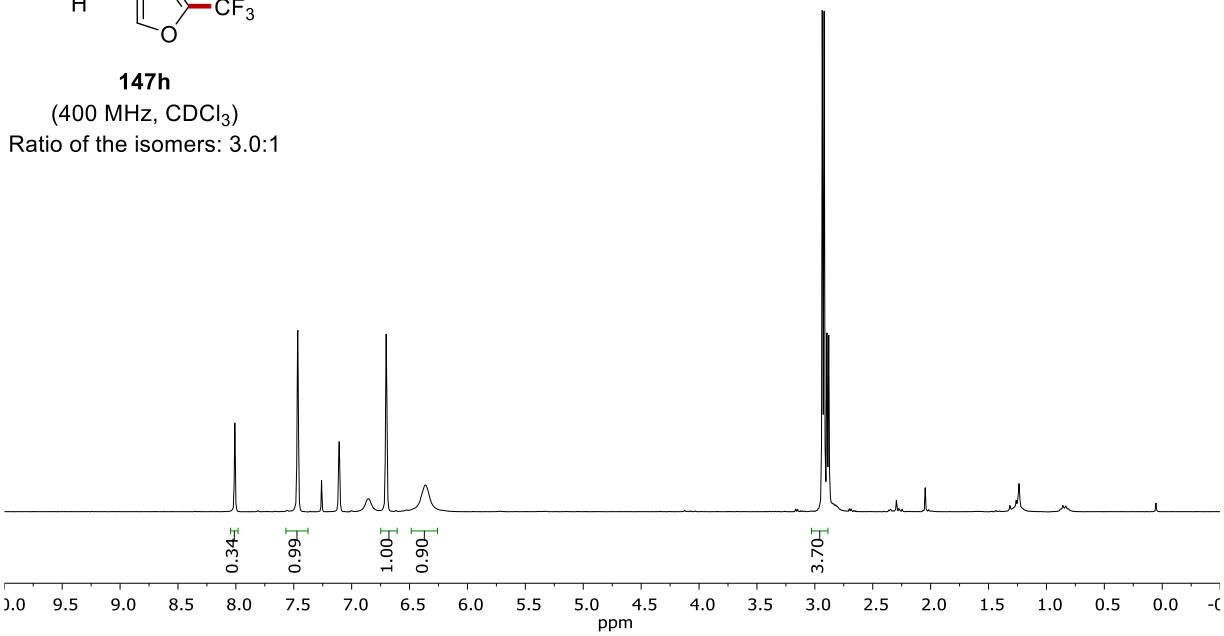

147h
(100 MHz, $CDCl_3$)
Ratio of the isomers: 3.0:1

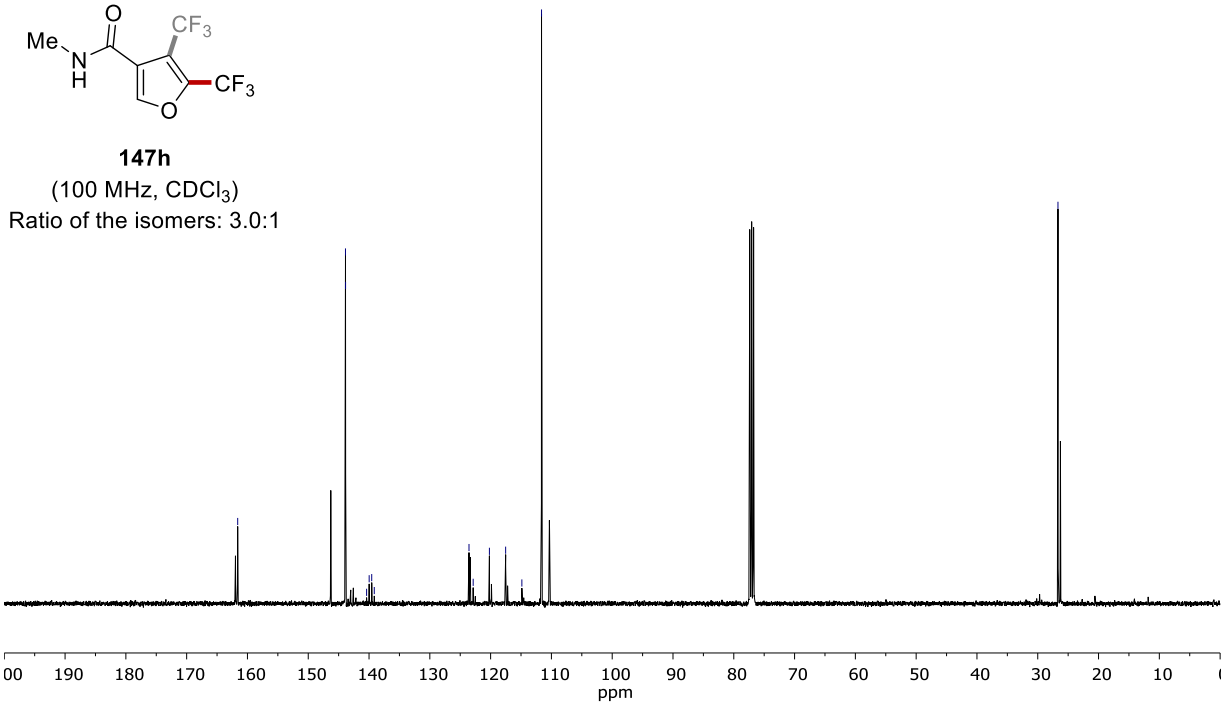

147h

^{19}F

(282 MHz, $CDCl_3$)

Ratio of the isomers: 3.0:1

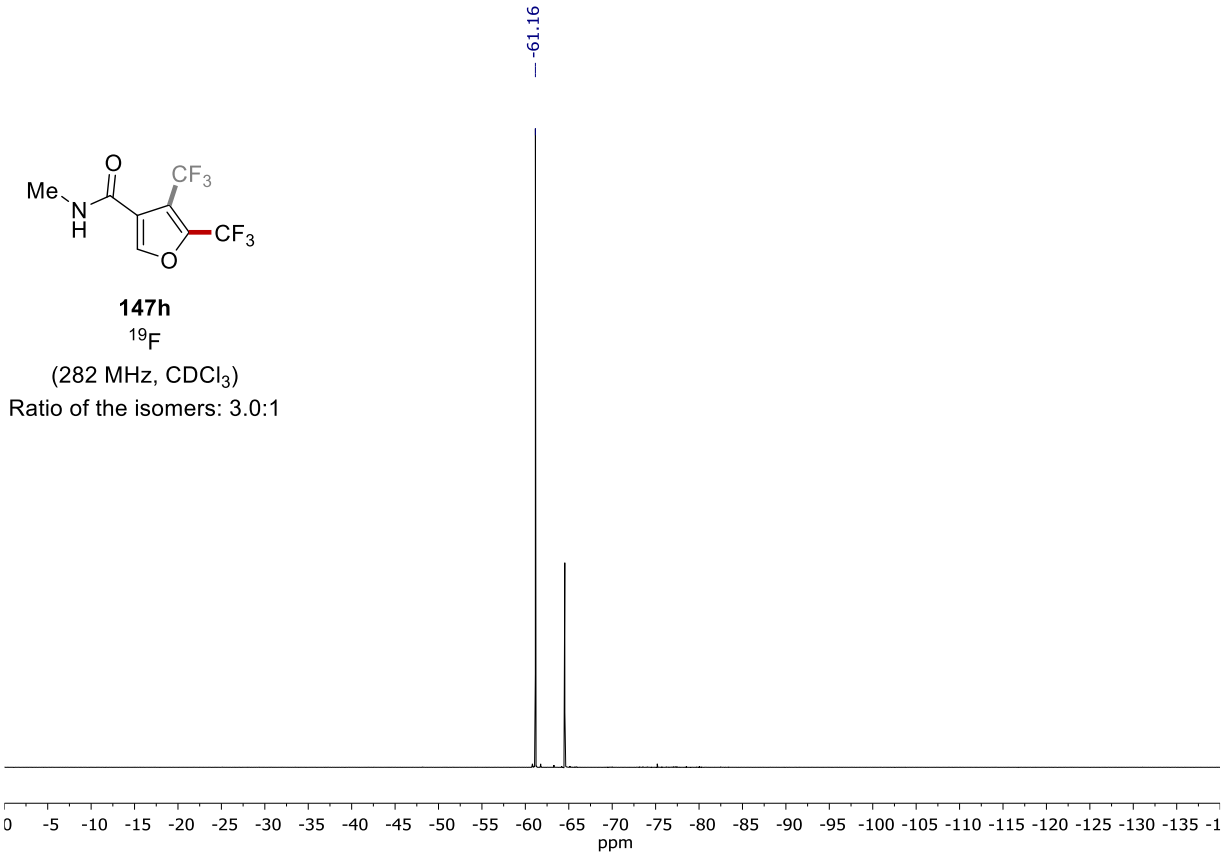

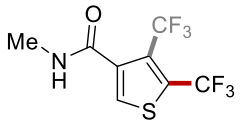

147i

(400 MHz, $CDCl_3$)

Ratio of the isomers: 2.7:1

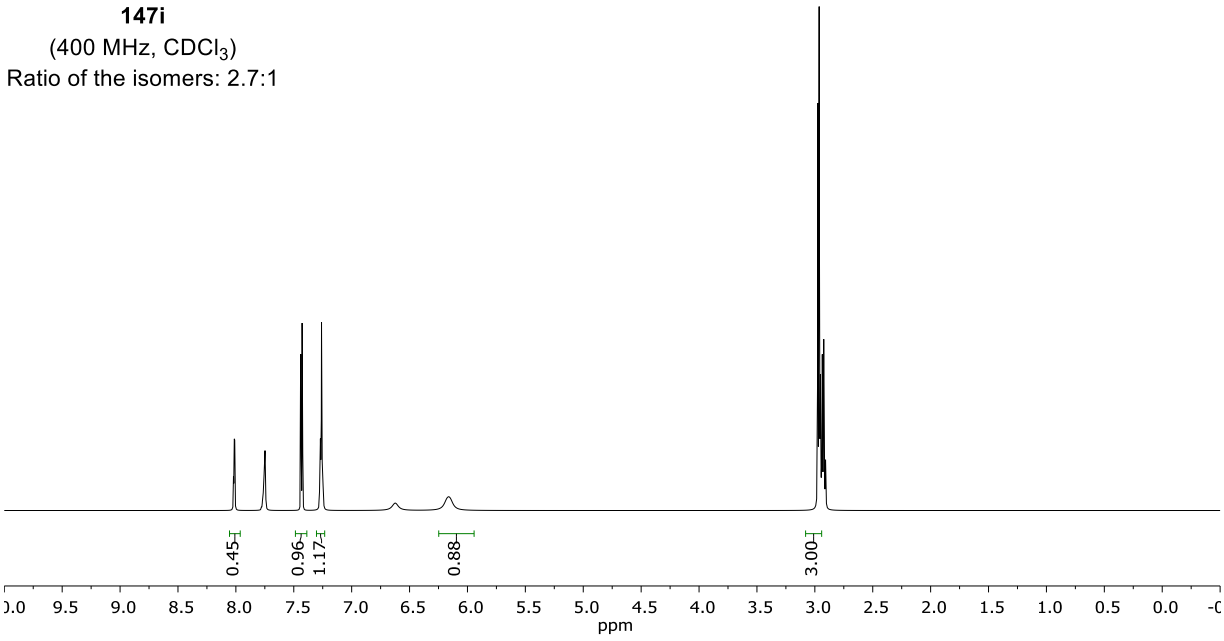

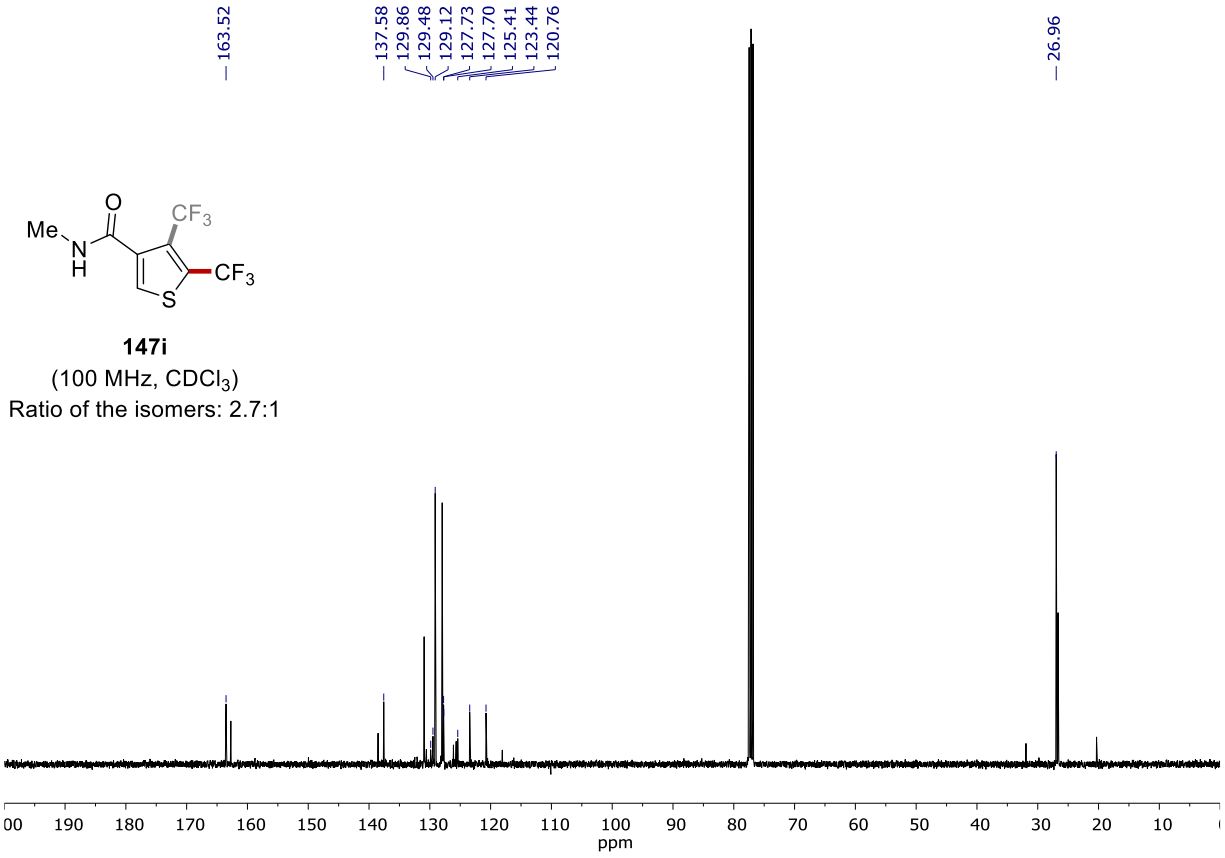

147i

(100 MHz, $CDCl_3$)

Ratio of the isomers: 2.7:1

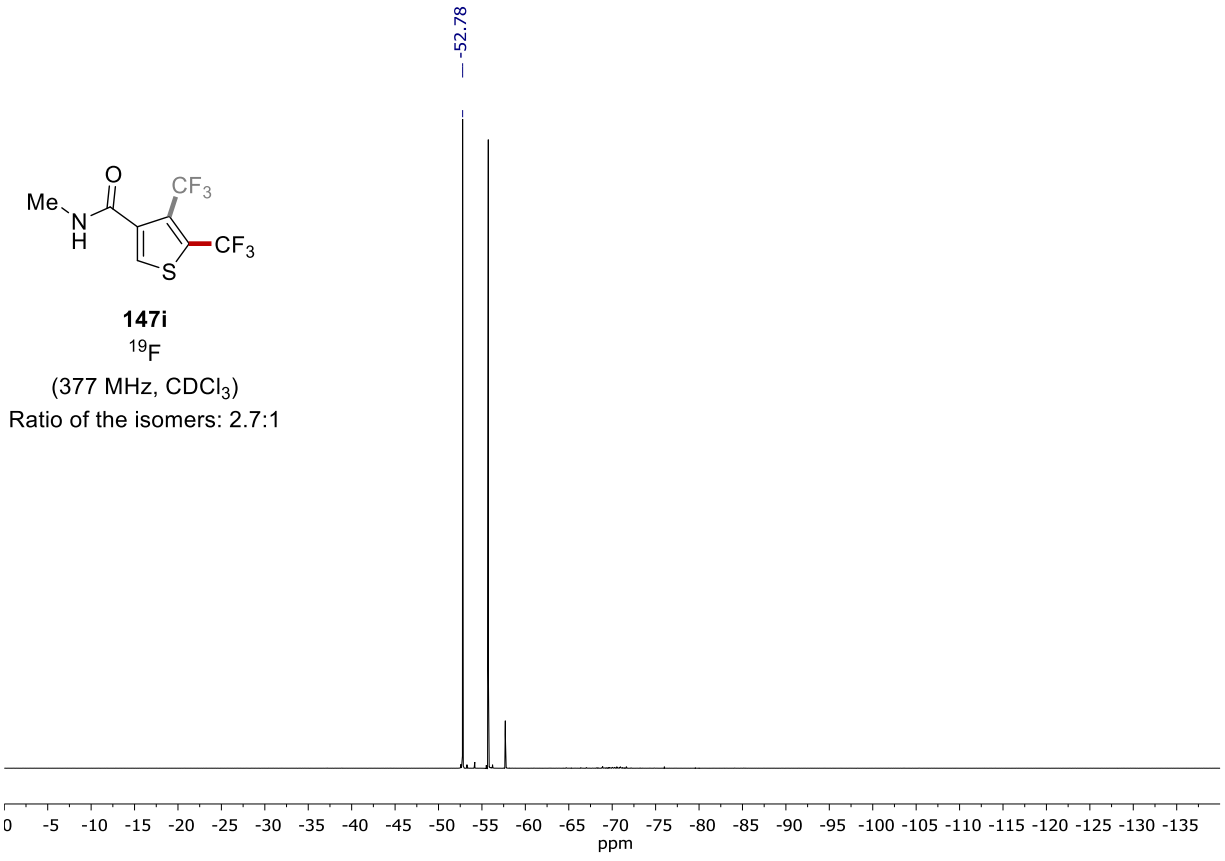

147i

^{19}F

(377 MHz, $CDCl_3$)

Ratio of the isomers: 2.7:1

147j
(400 MHz, $CDCl_3$)

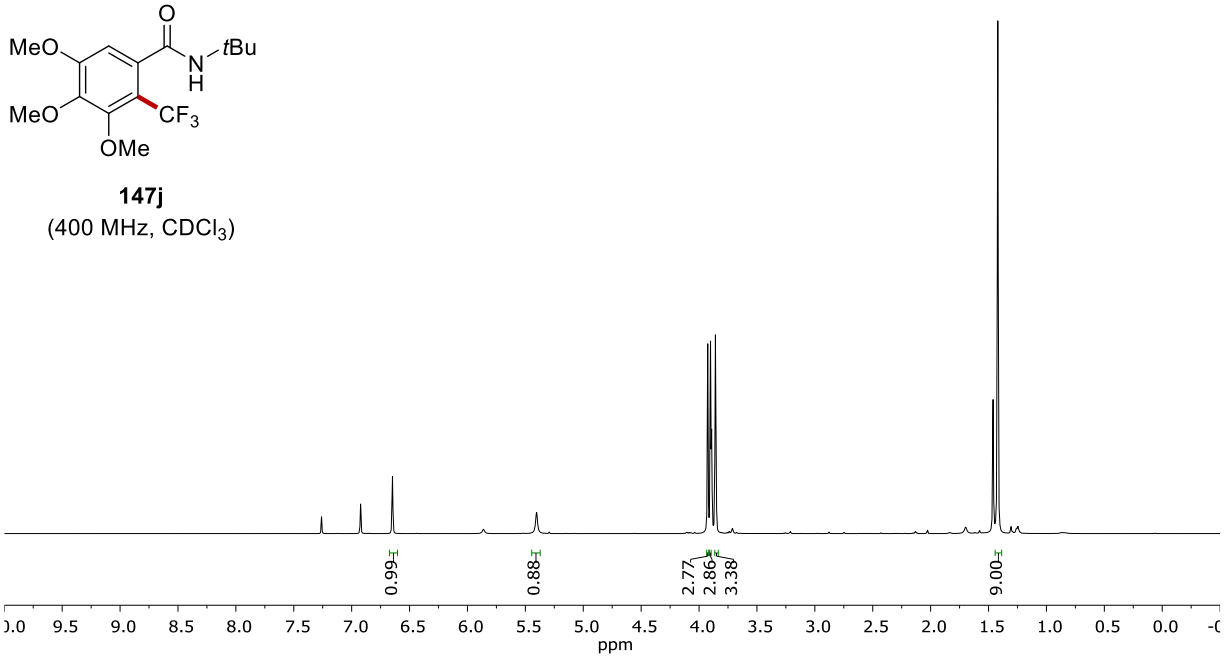

167.41
156.18
153.23
143.42
133.75
133.73
133.70
133.68
127.61
124.89
122.17
119.45
114.03
113.73
113.43
113.12
106.82
61.94
60.98
56.38
52.34
28.62

147j
(100 MHz, $CDCl_3$)

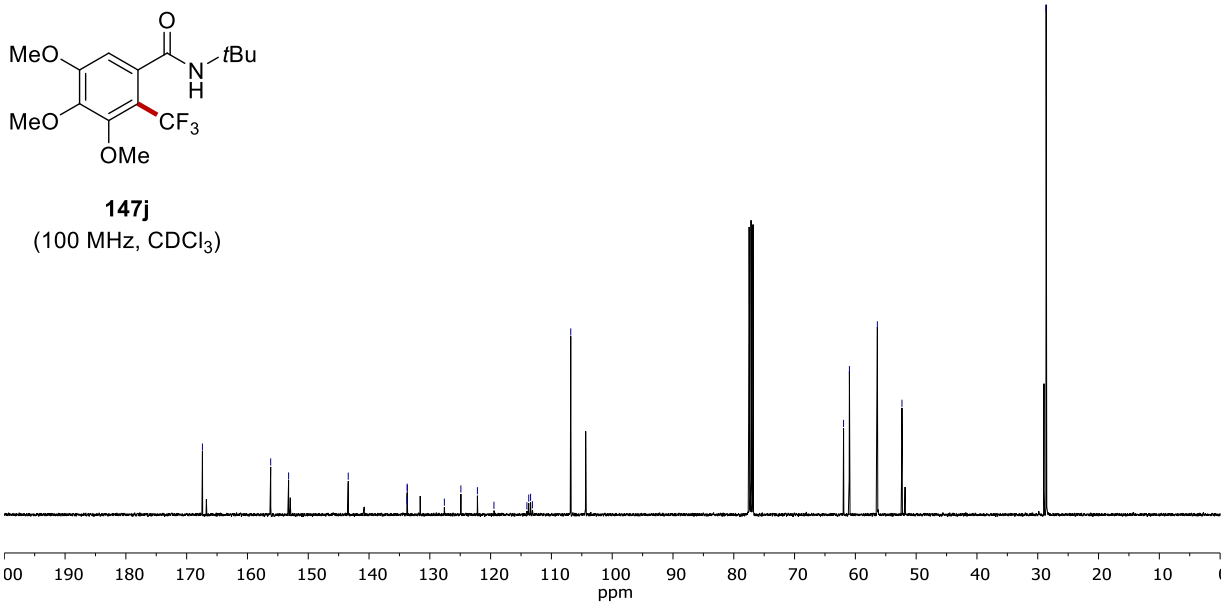

147j

^{19}F

(377 MHz, $CDCl_3$)

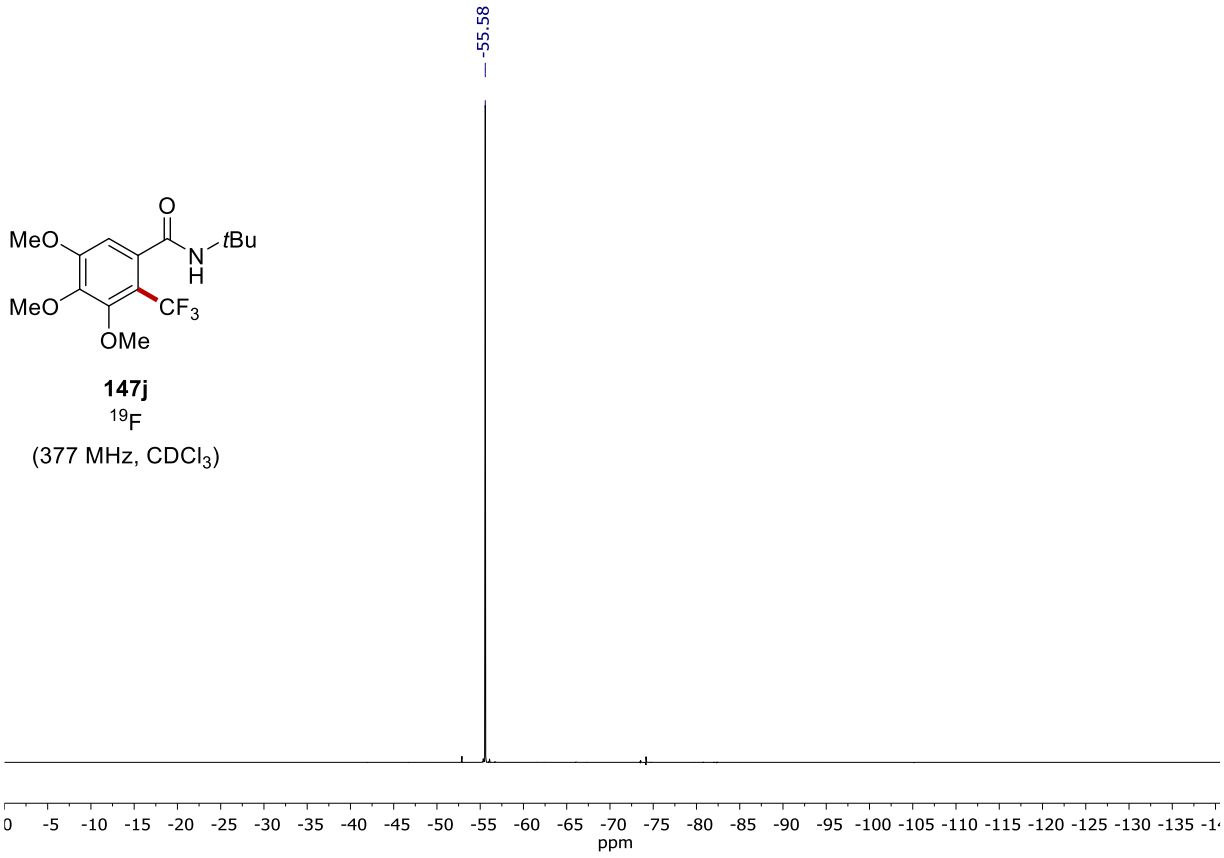

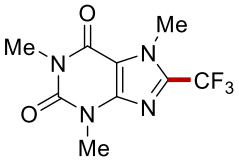

147k

(400 MHz, $CDCl_3$)

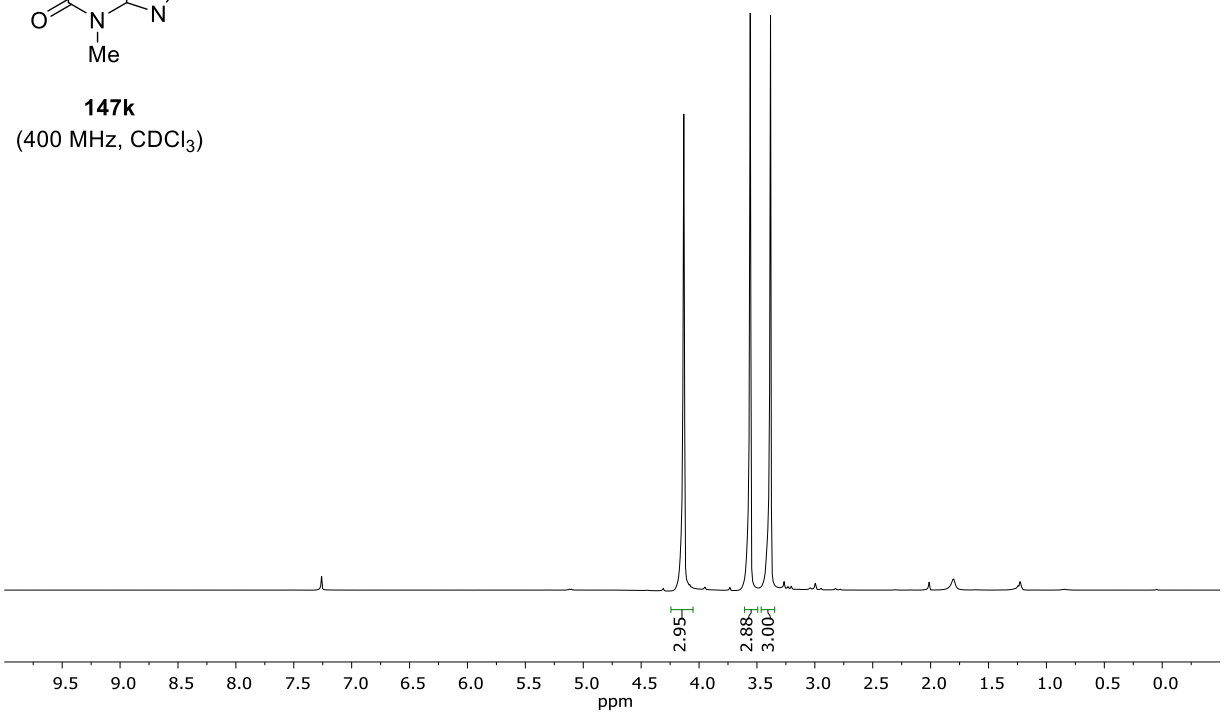

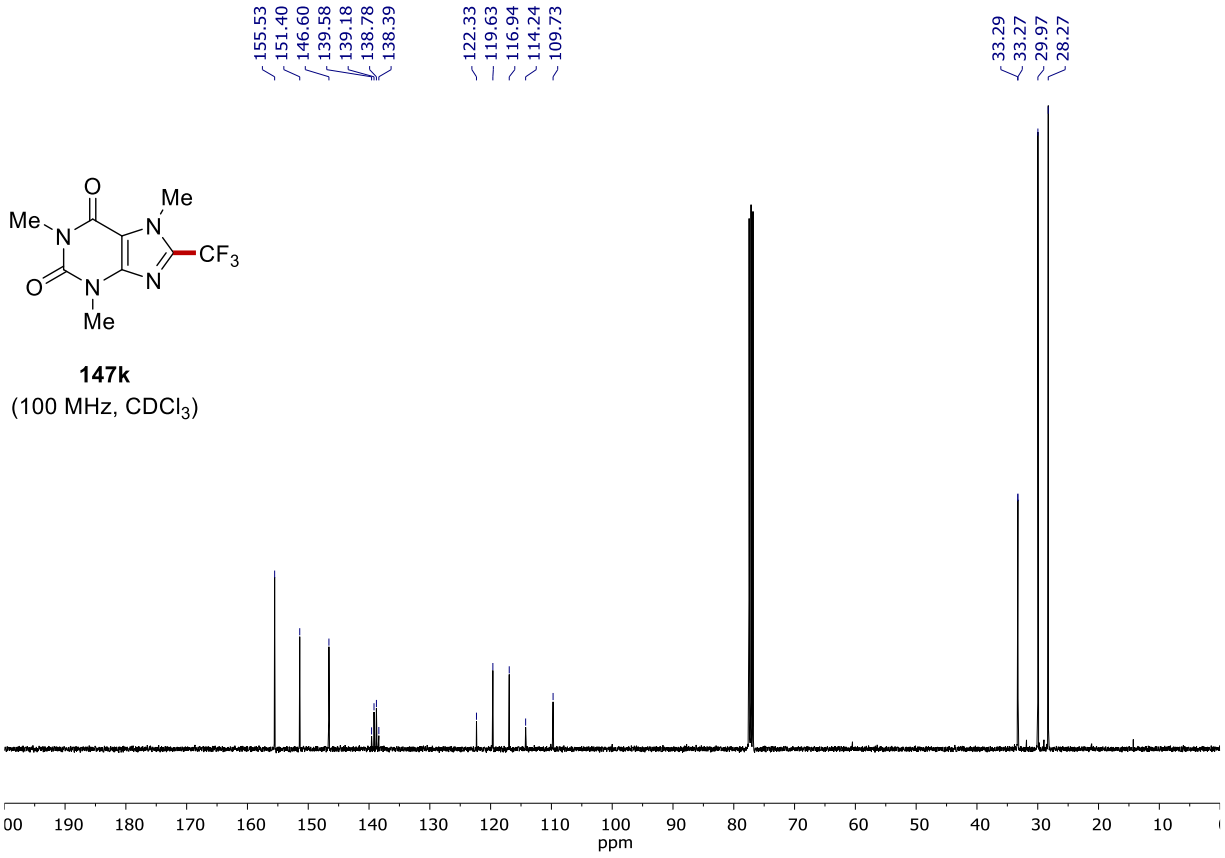

147k
(100 MHz, $CDCl_3$)

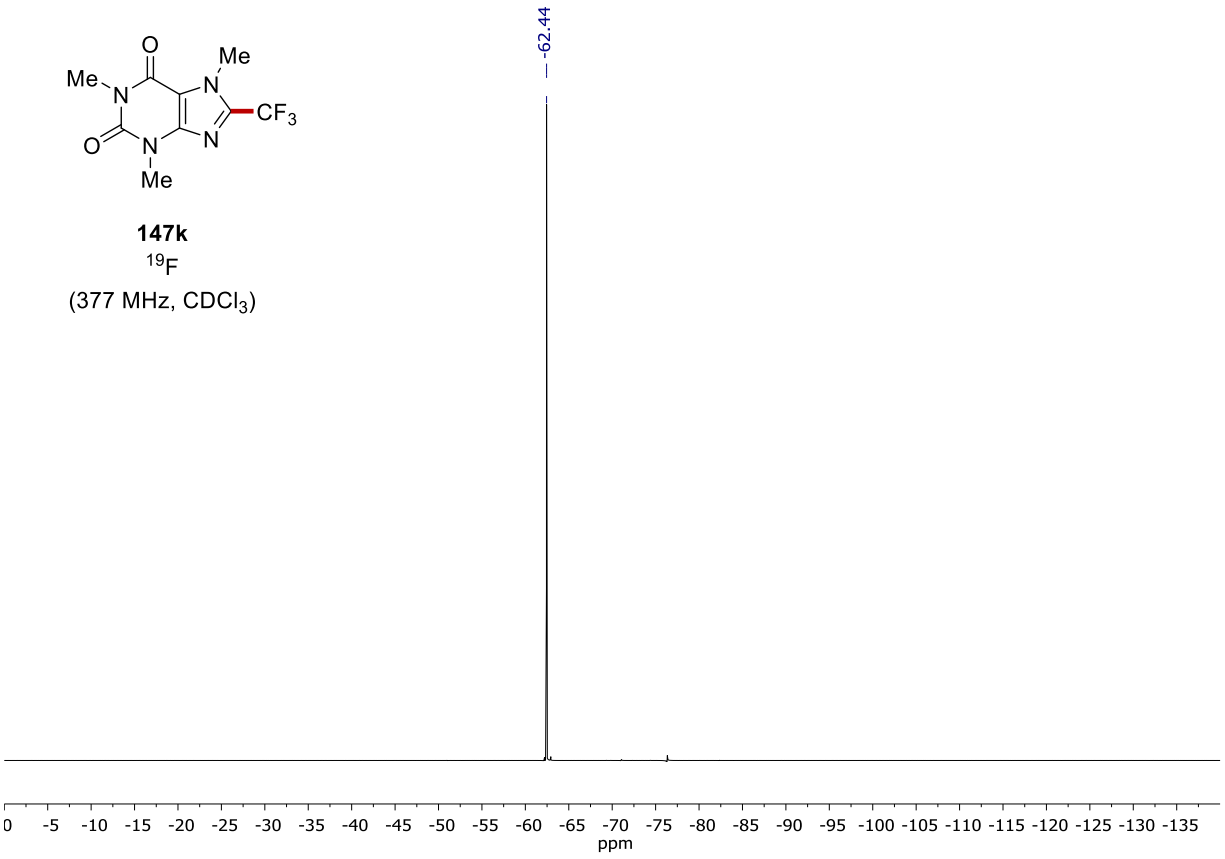

147k
^{19}F
(377 MHz, $CDCl_3$)

147l
(400 MHz, $CDCl_3$)

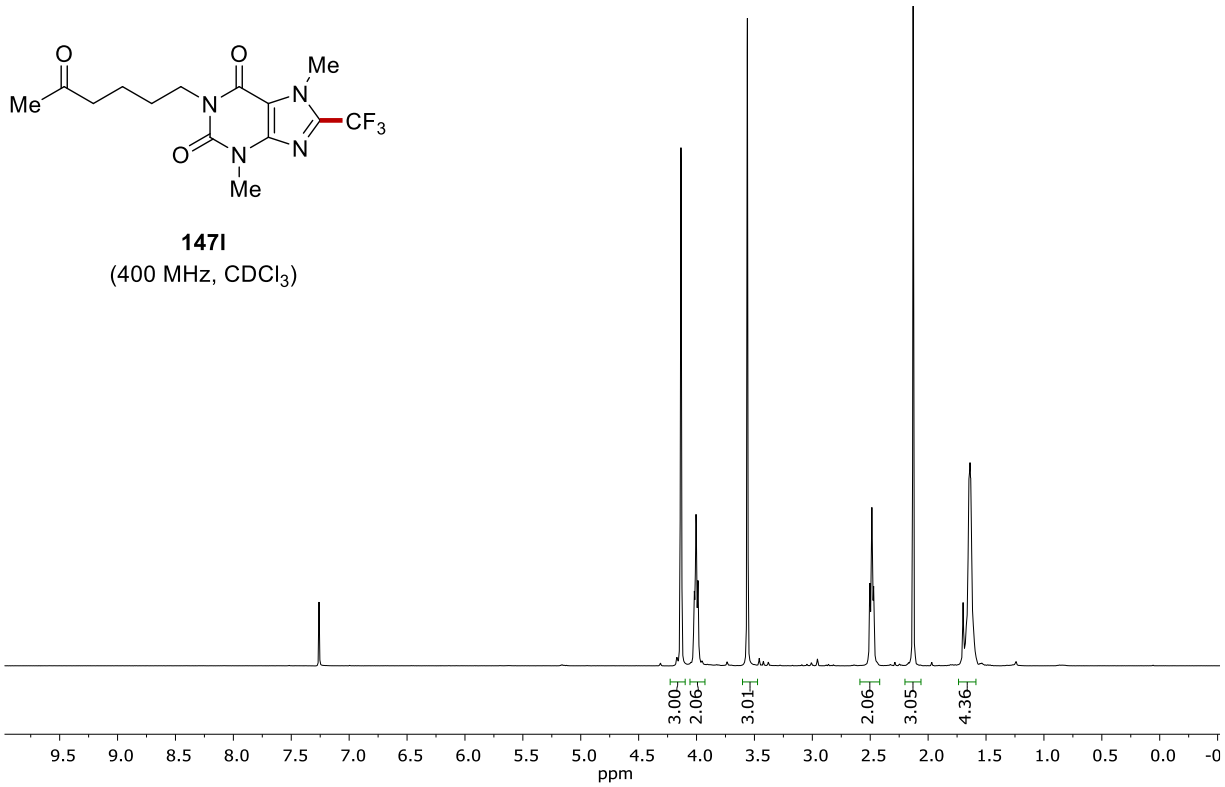

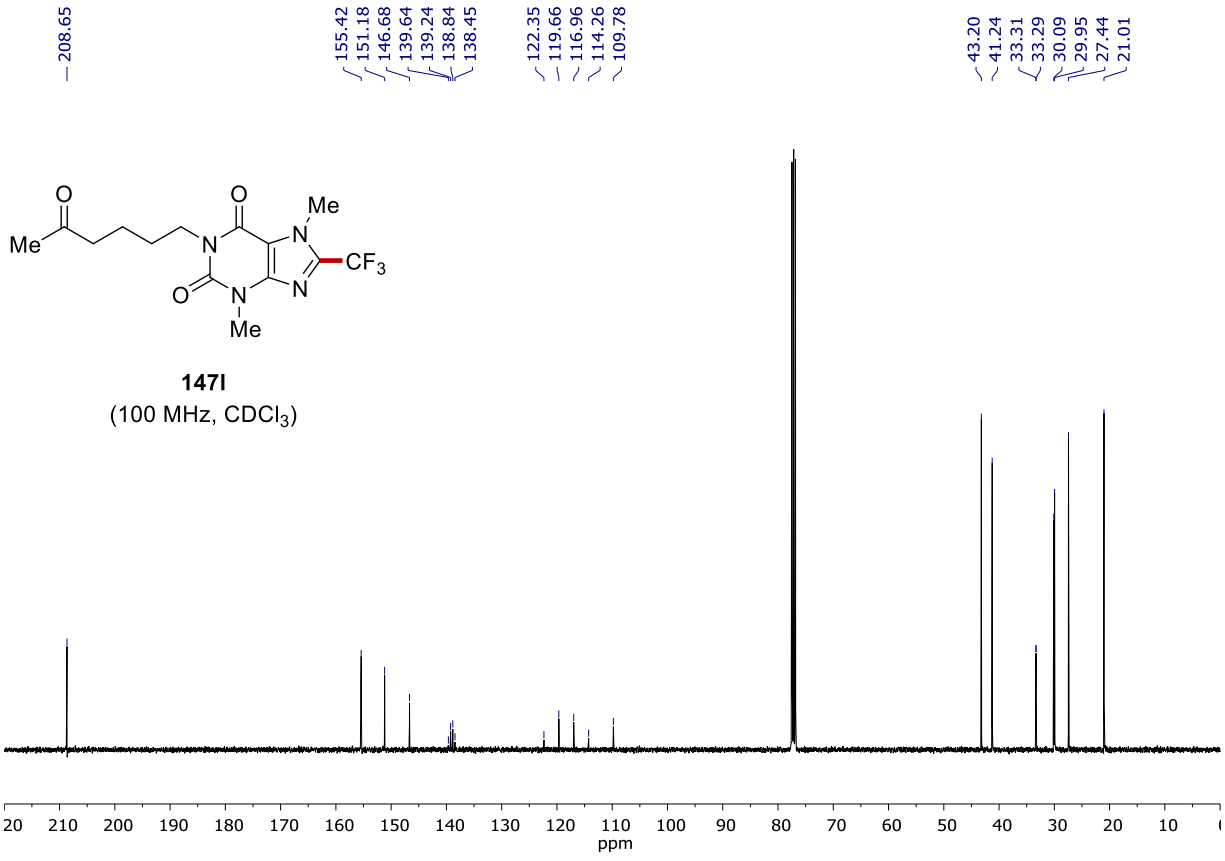

147l
(100 MHz, $CDCl_3$)

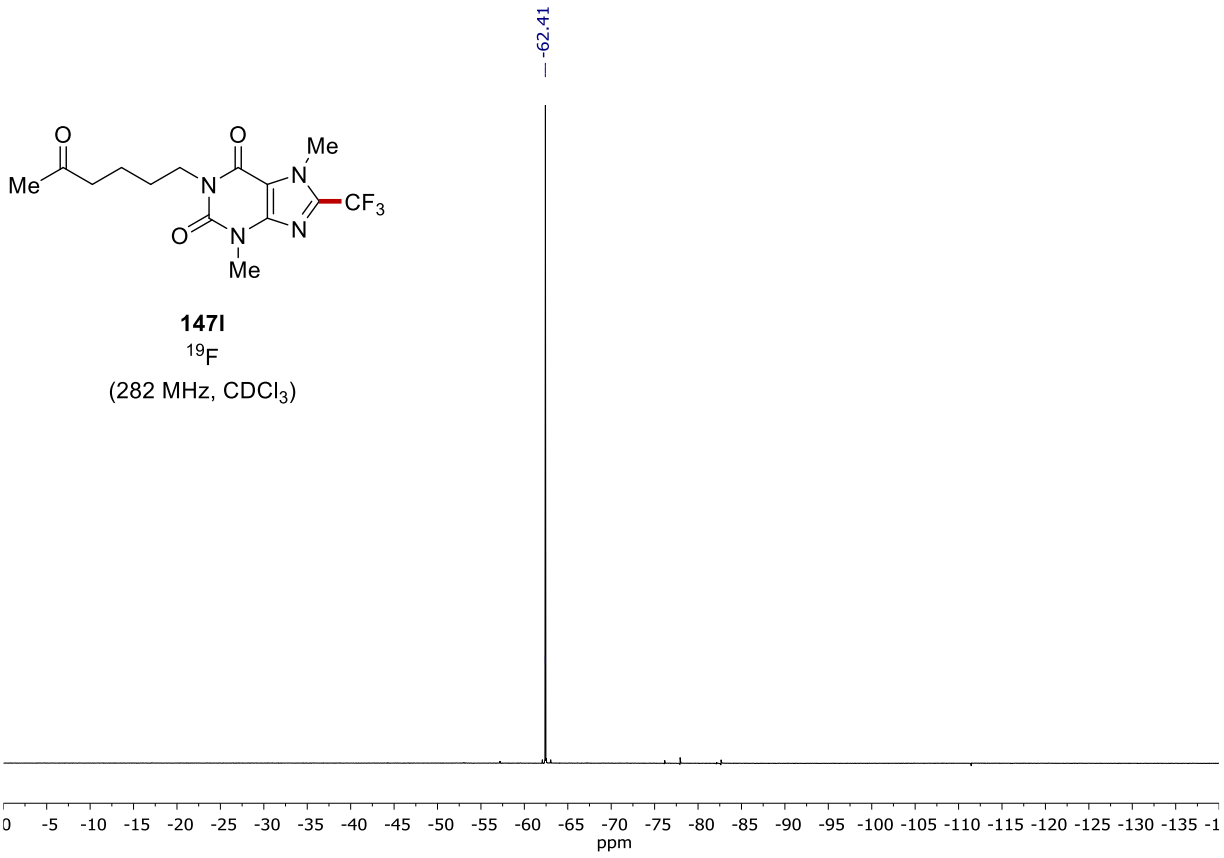

147l

^{19}F

(282 MHz, $CDCl_3$)

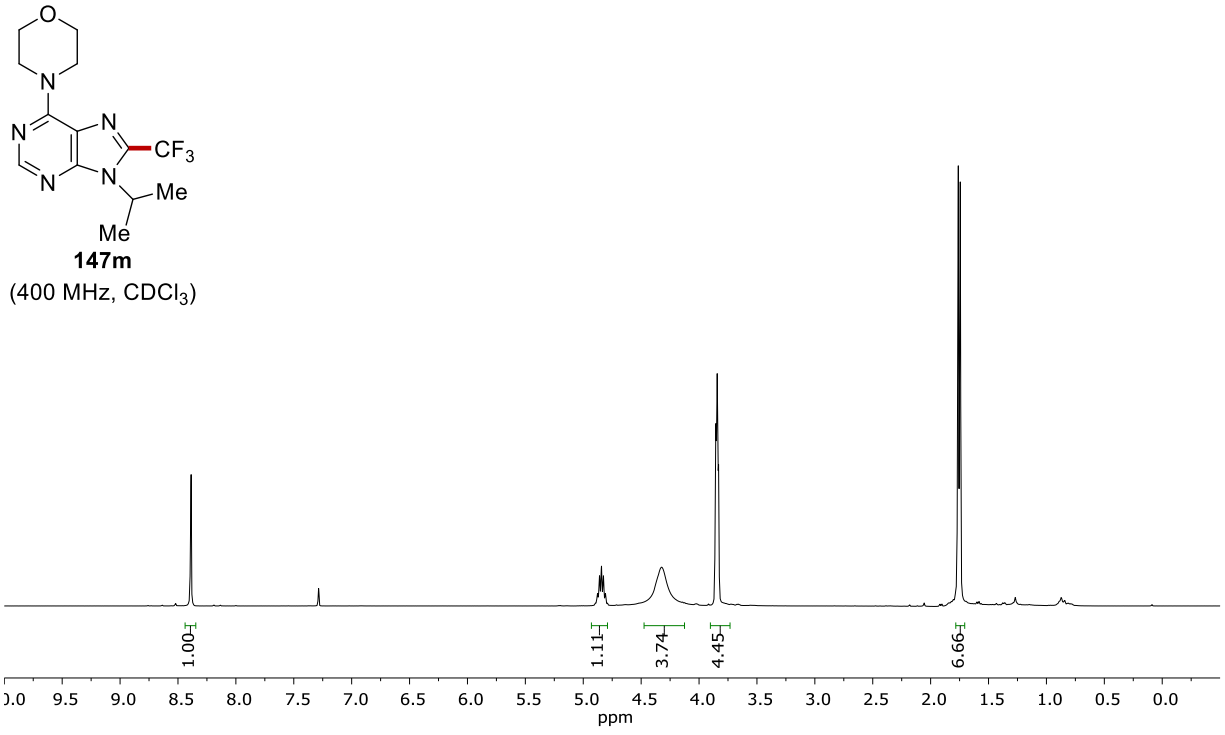

147m

(400 MHz, $CDCl_3$)

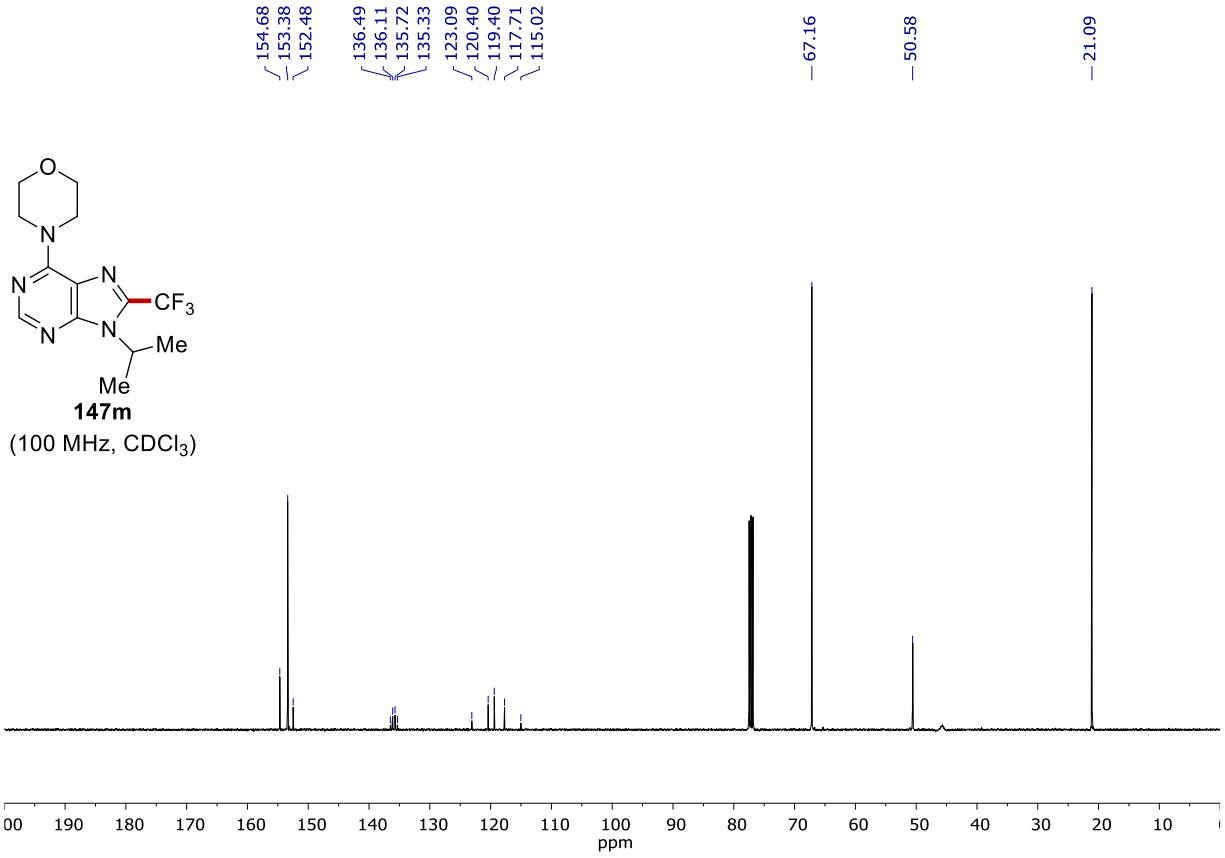
154.68
153.38
152.48
136.49
136.11
135.72
135.33
123.09
120.40
119.40
117.71
115.02
67.16
50.58
21.09
O
N
N
N
N
N
CF3
Me
Me
147m
(100 MHz, CDCl3)
00 190 180 170 160 150 140 130 120 110 100 90 80 70 60 50 40 30 20 10
ppm

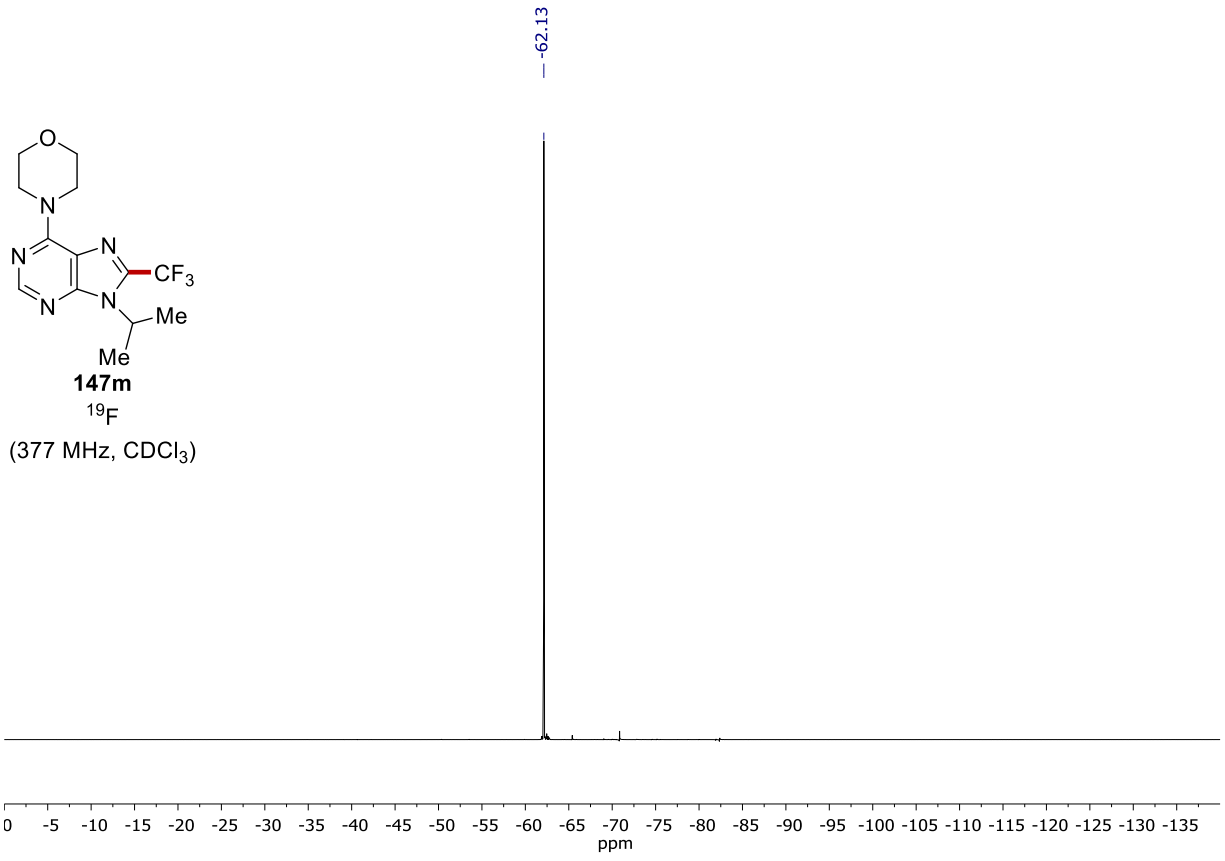
-62.13
O
N
N
N
N
N
CF3
Me
Me
147m
19F
(377 MHz, CDCl3)
0 -5 -10 -15 -20 -25 -30 -35 -40 -45 -50 -55 -60 -65 -70 -75 -80 -85 -90 -95 -100 -105 -110 -115 -120 -125 -130 -135
ppm

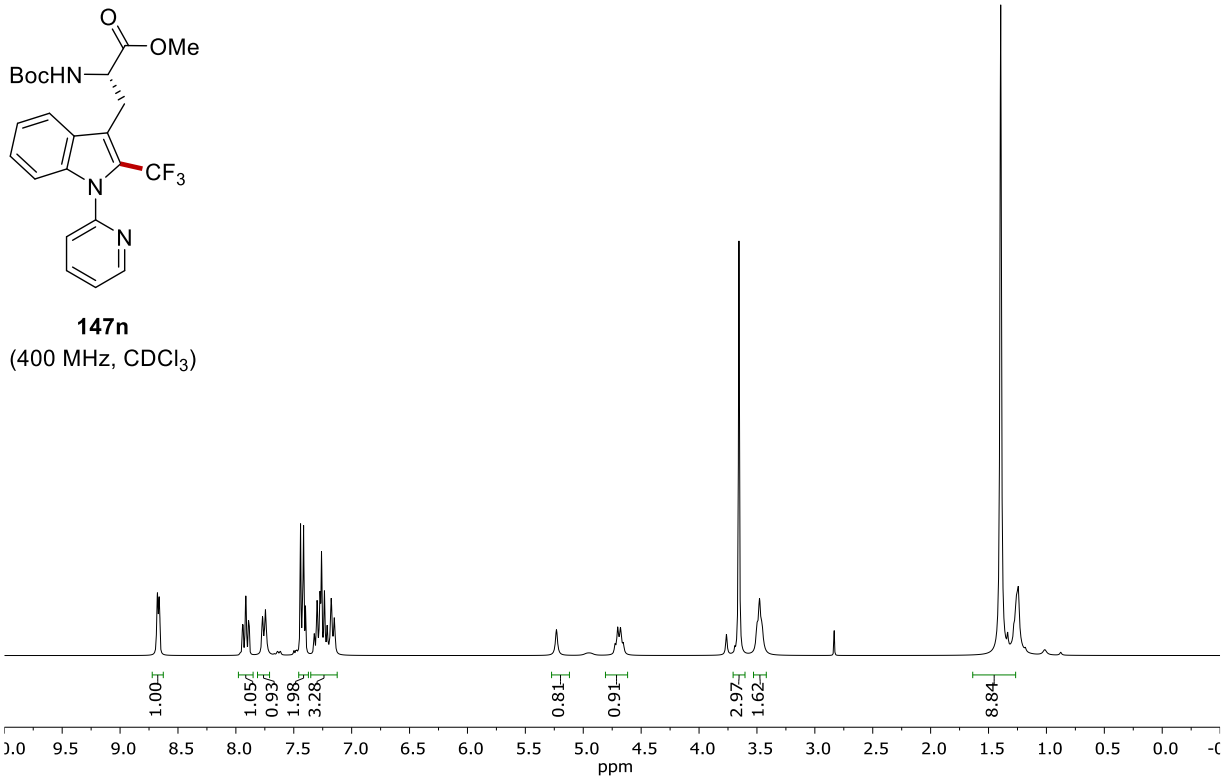

147n
(400 MHz, $CDCl_3$)

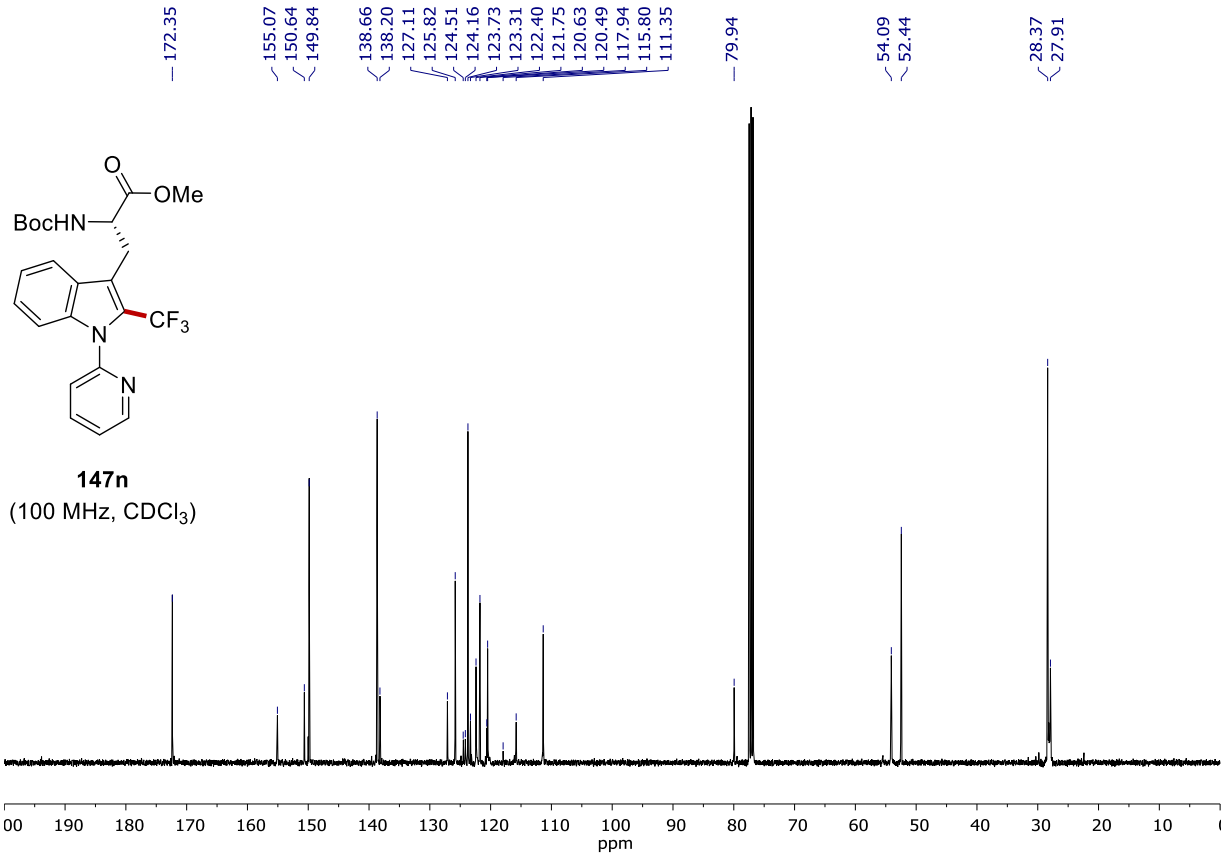

147n
(100 MHz, $CDCl_3$)

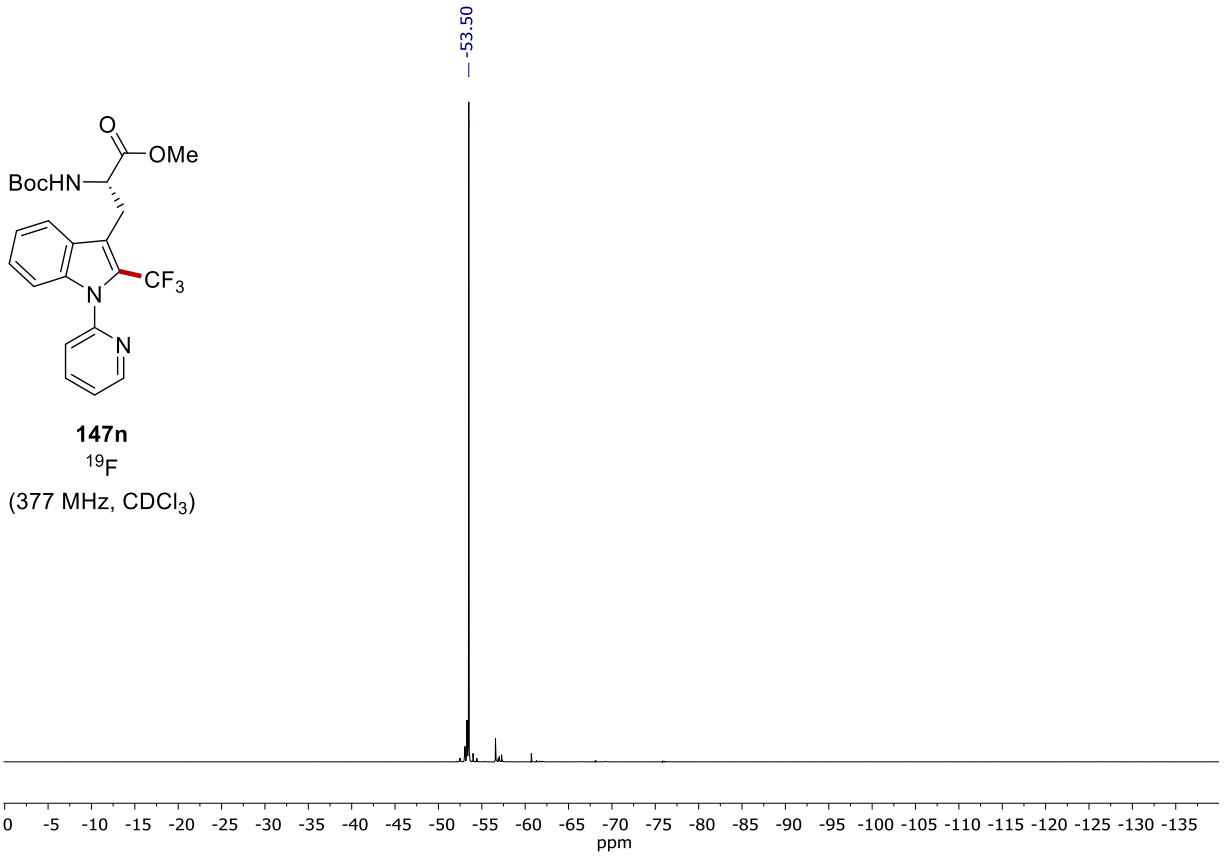

147n

^{19}F

(377 MHz, $CDCl_3$)

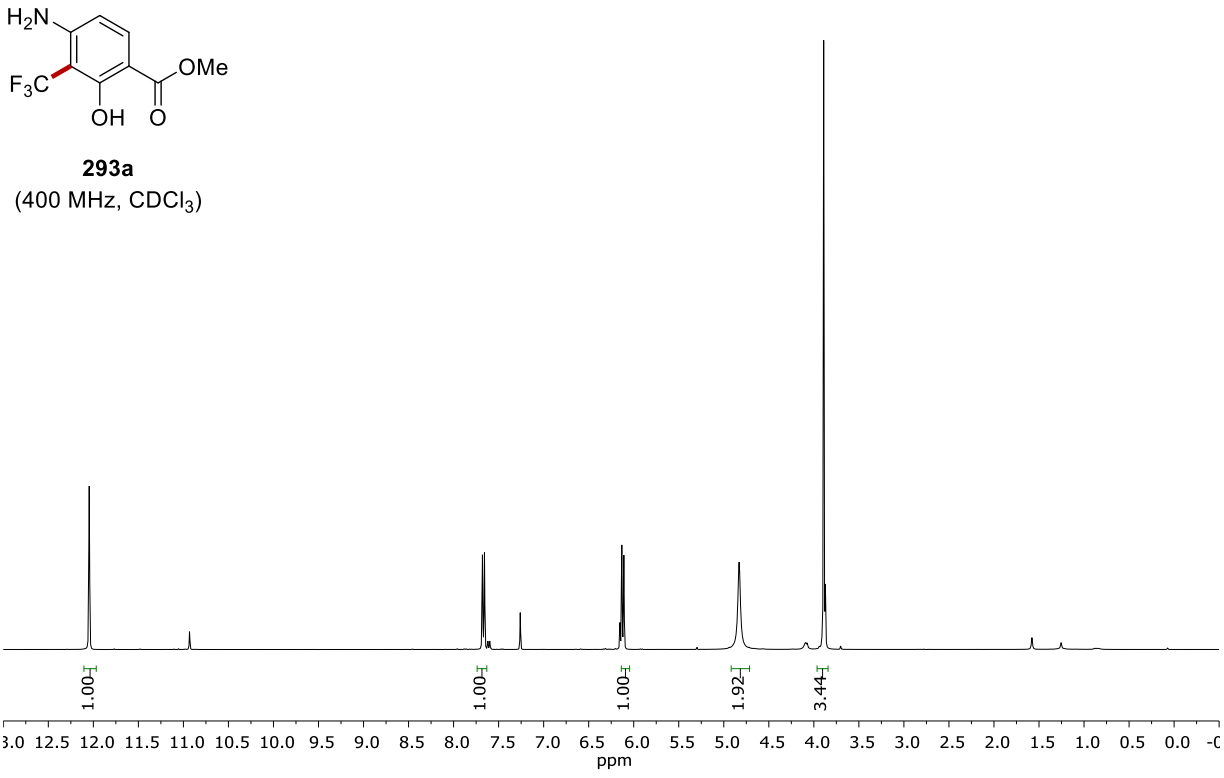

293a

(400 MHz, $CDCl_3$)

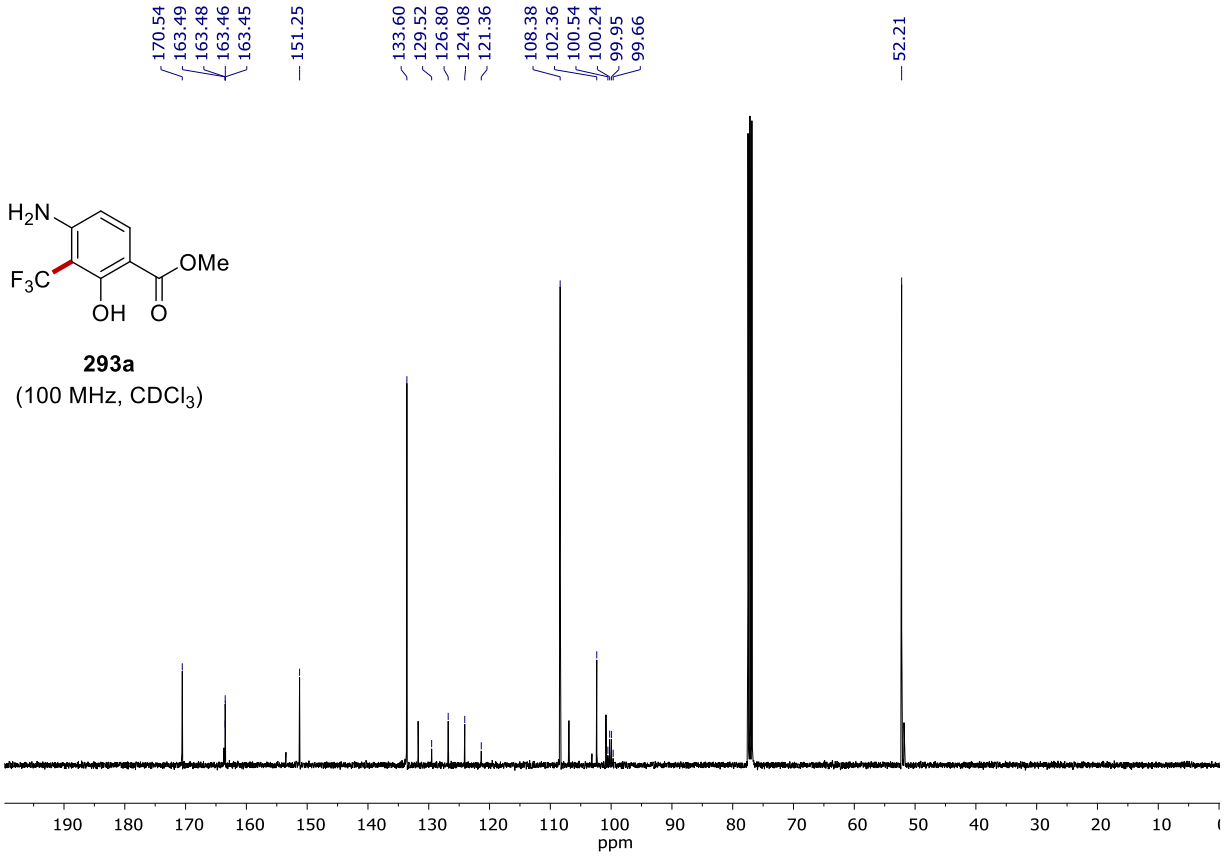

293a
(100 MHz, $CDCl_3$)

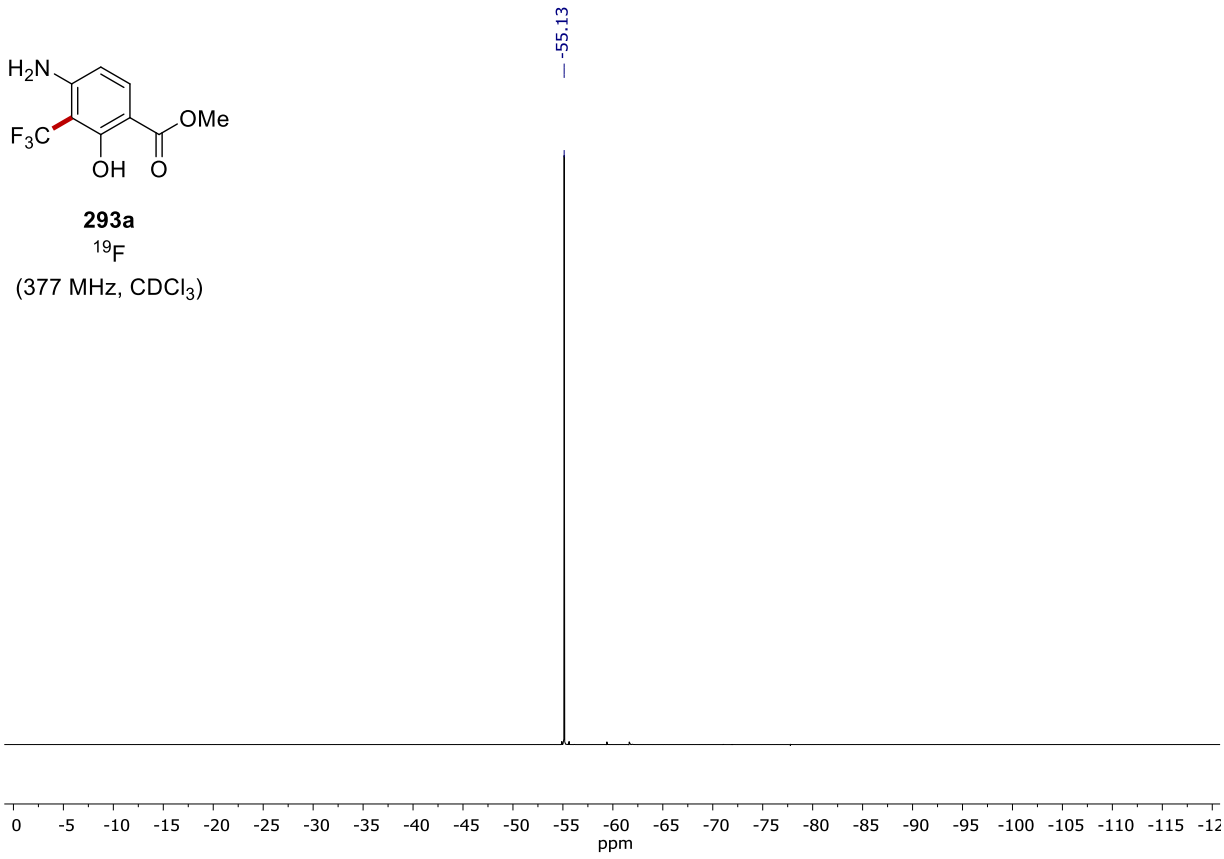

293a
^{19}F
(377 MHz, $CDCl_3$)

293b
(400 MHz, $CDCl_3$)

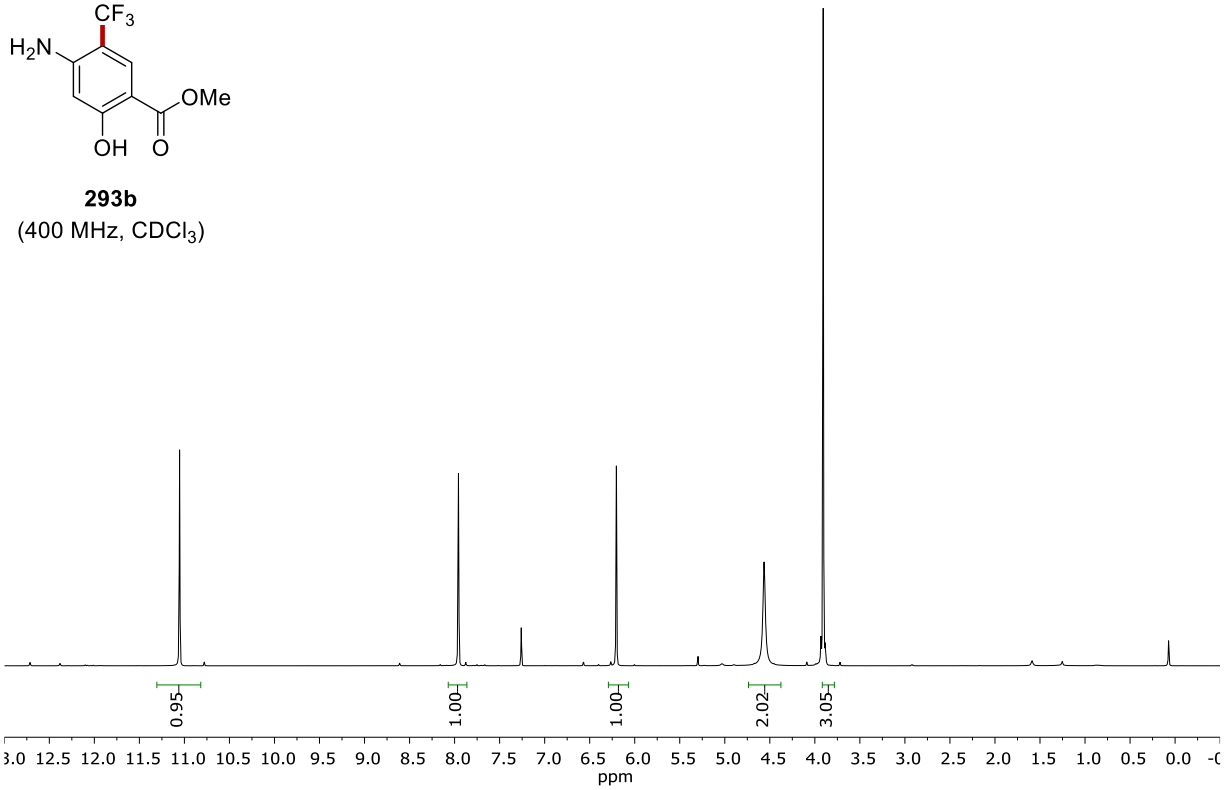

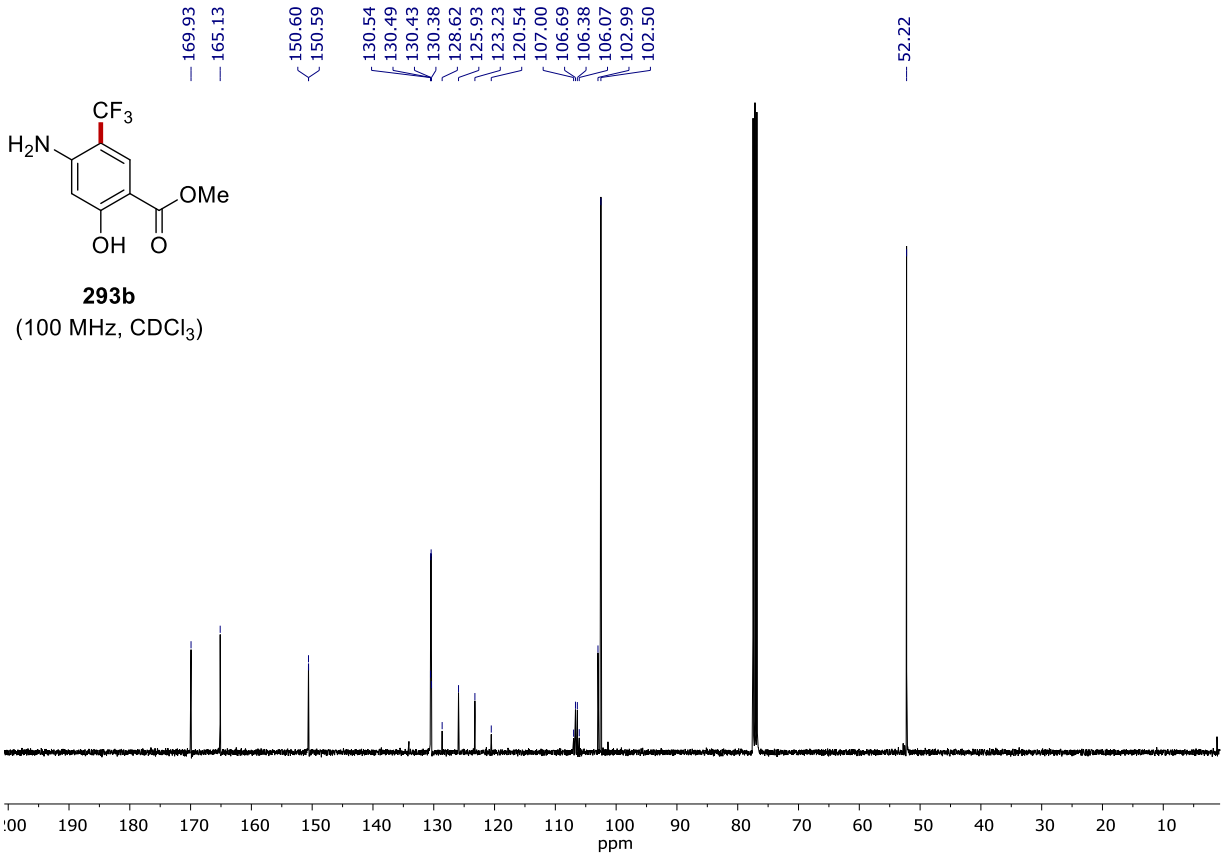

293b
(100 MHz, $CDCl_3$)

293b

^{19}F

(377 MHz, $CDCl_3$)

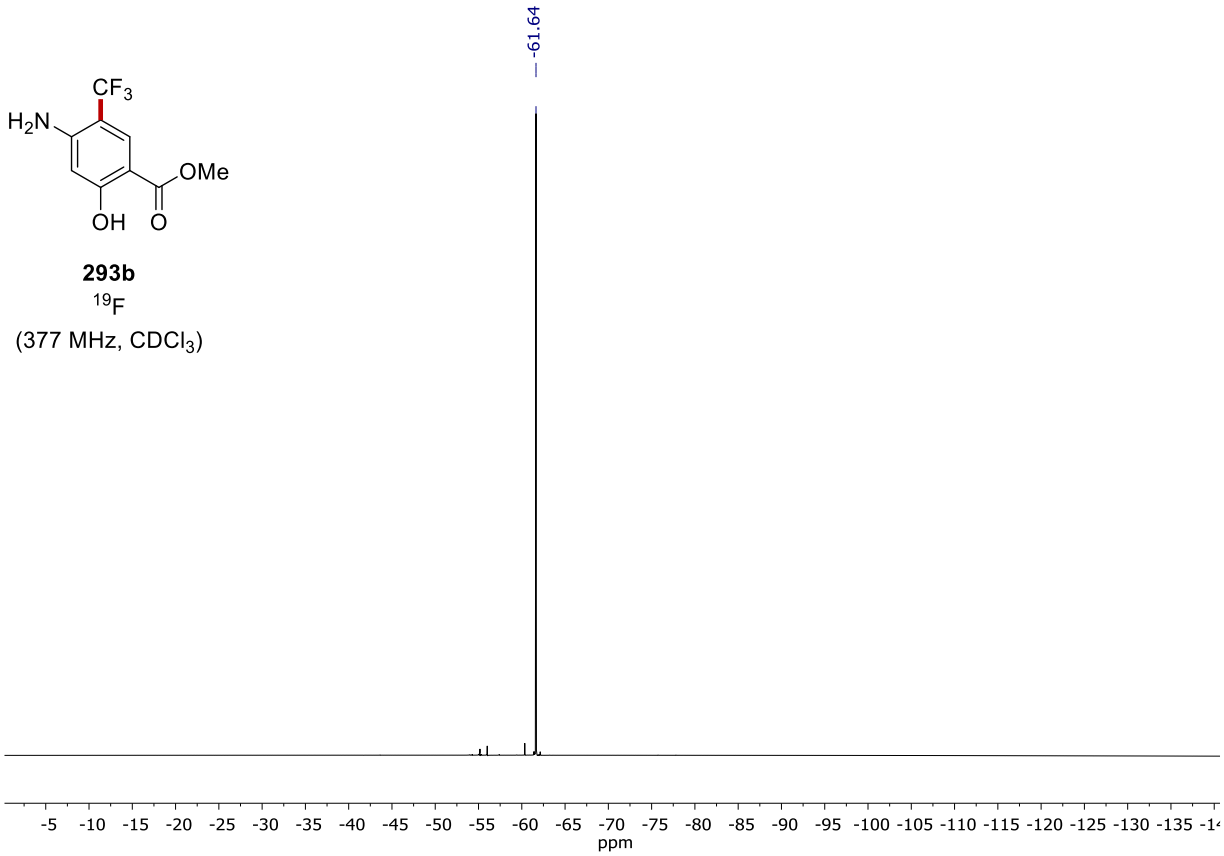

293c

(400 MHz, $CDCl_3$)

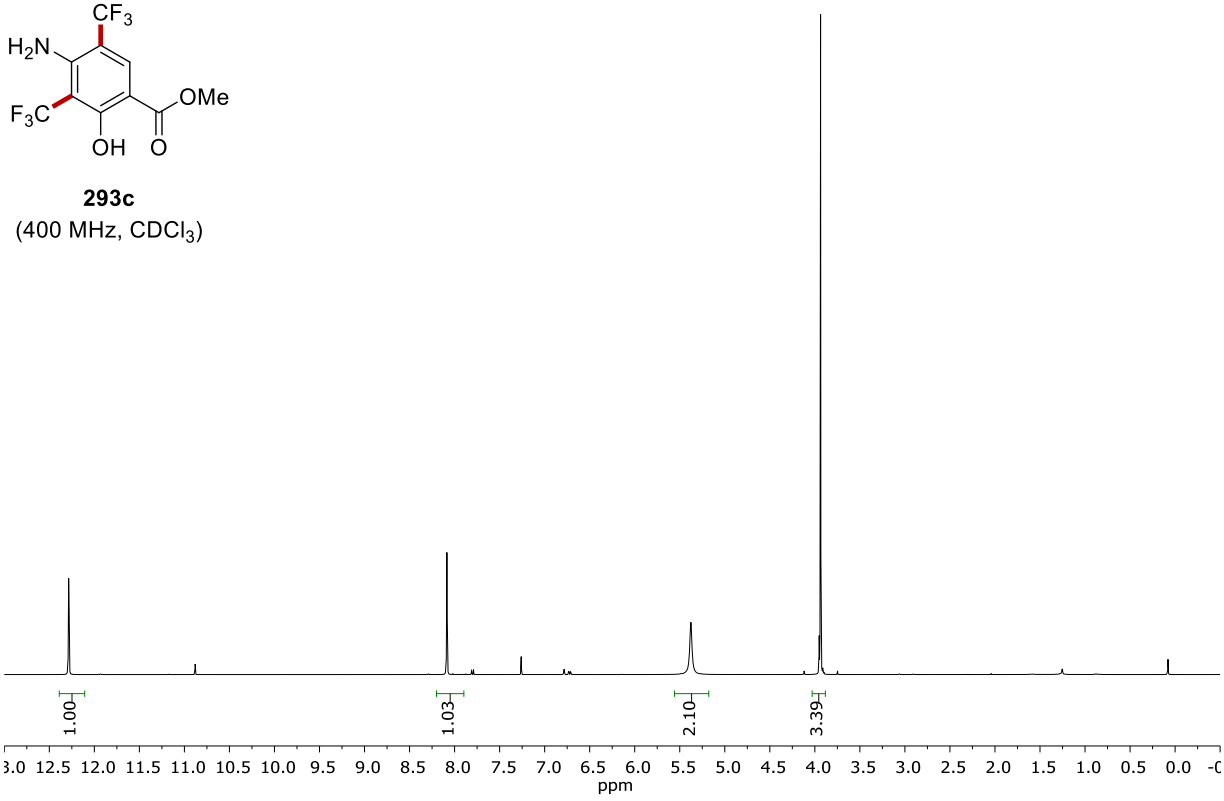

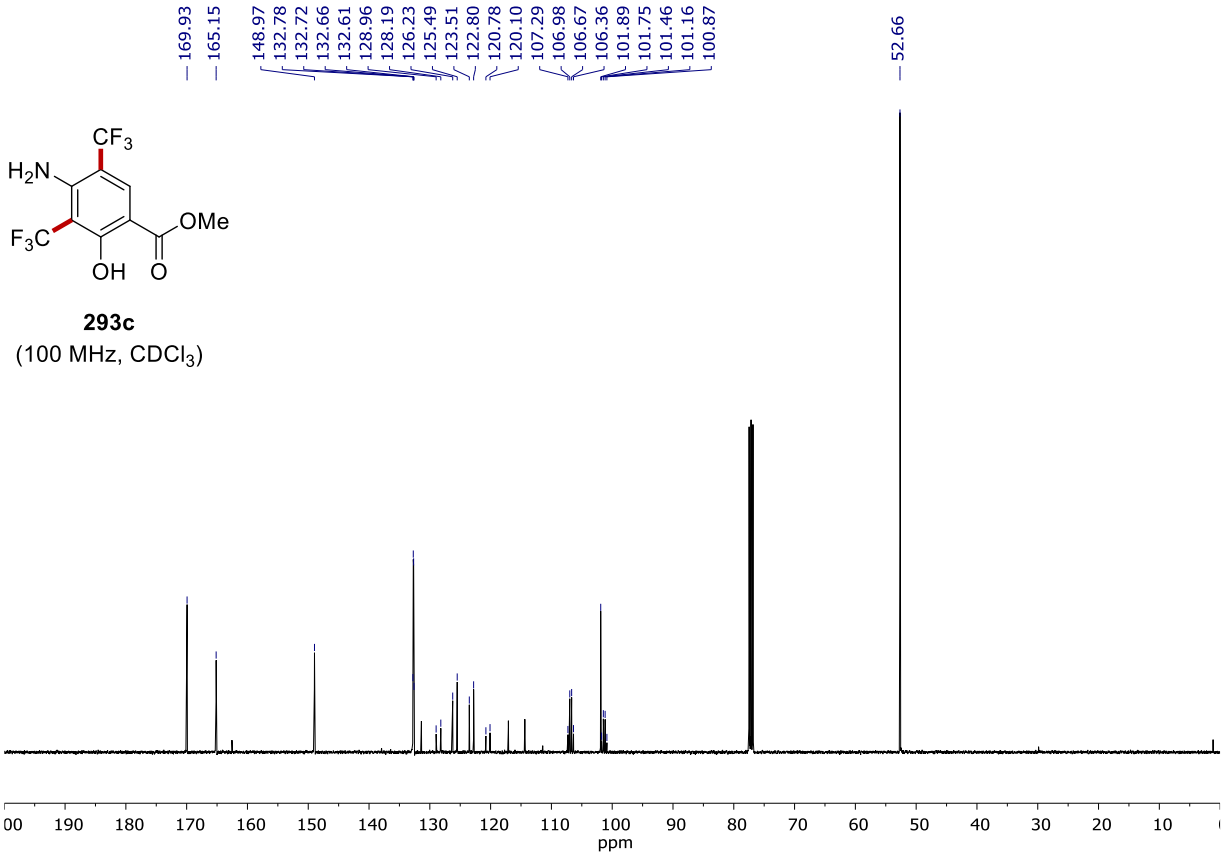

293c
(100 MHz, $CDCl_3$)

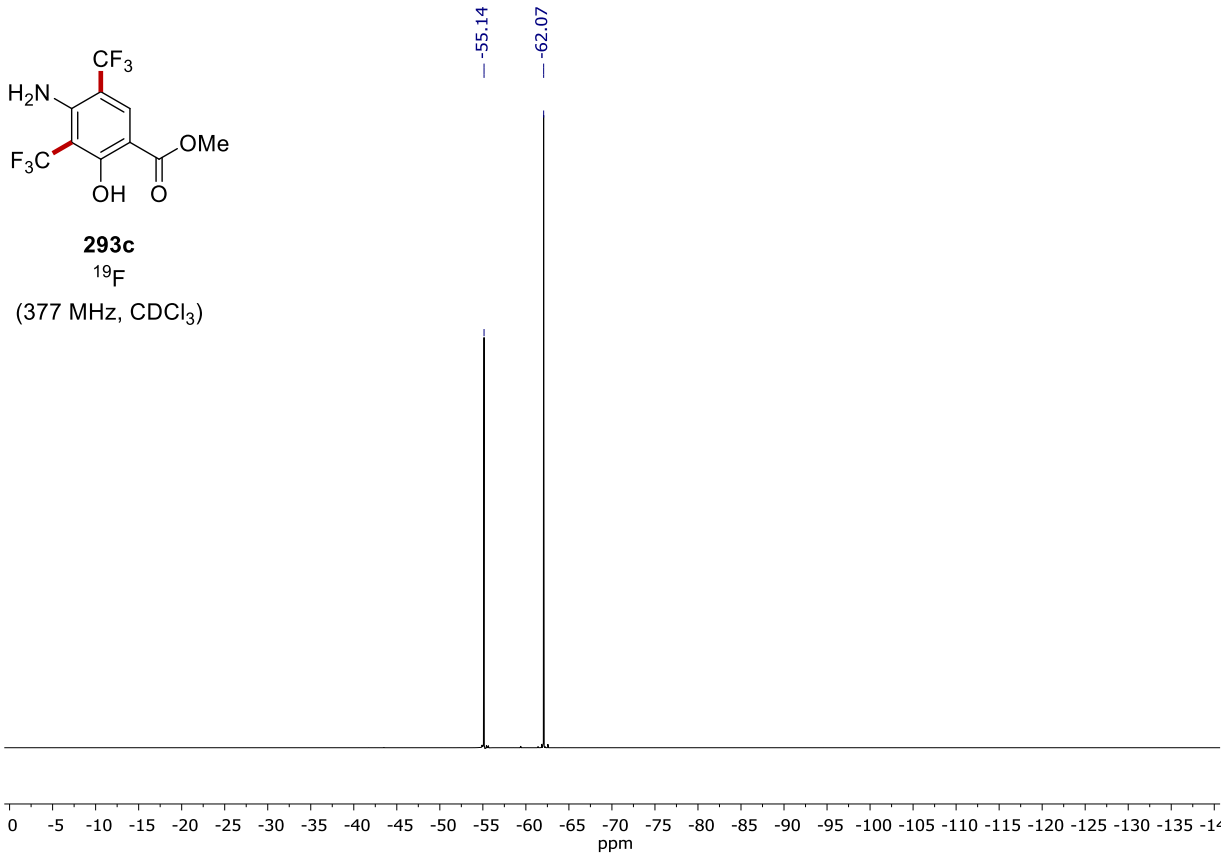

293c
^{19}F
(377 MHz, $CDCl_3$)

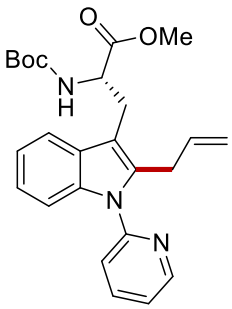

223aa
(400 MHz, $CDCl_3$)

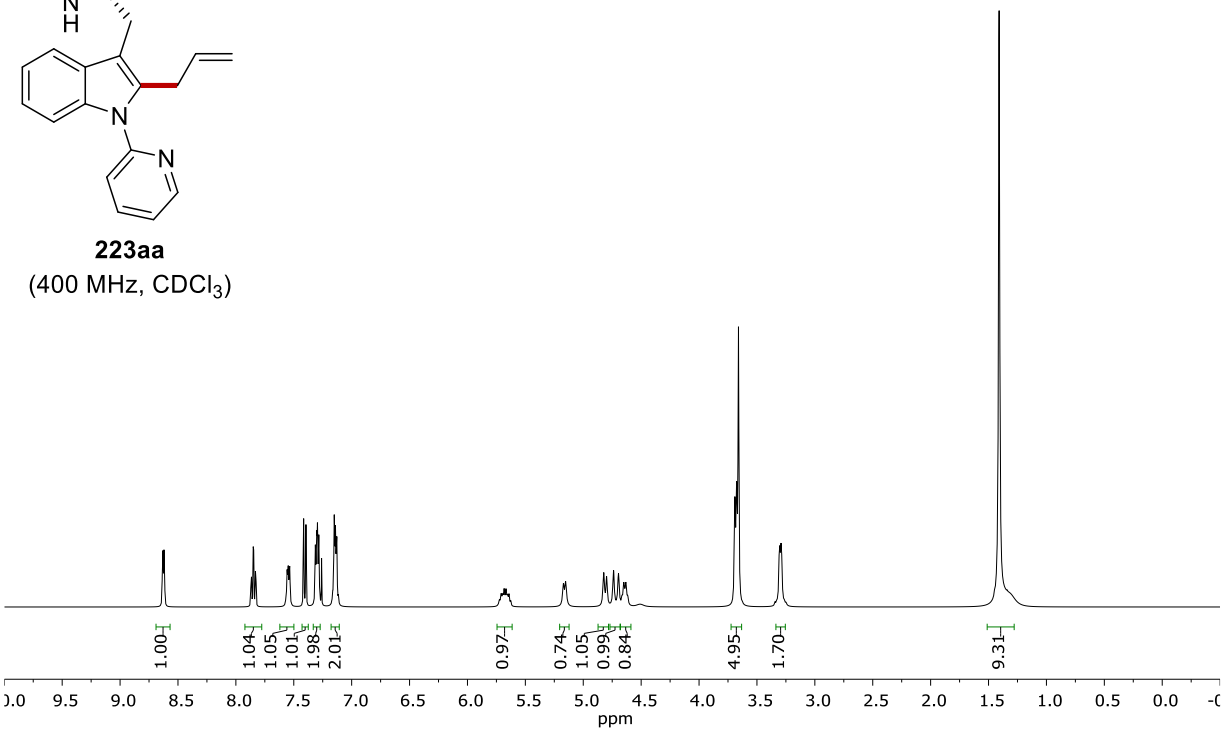

223aa
(100 MHz, $CDCl_3$)

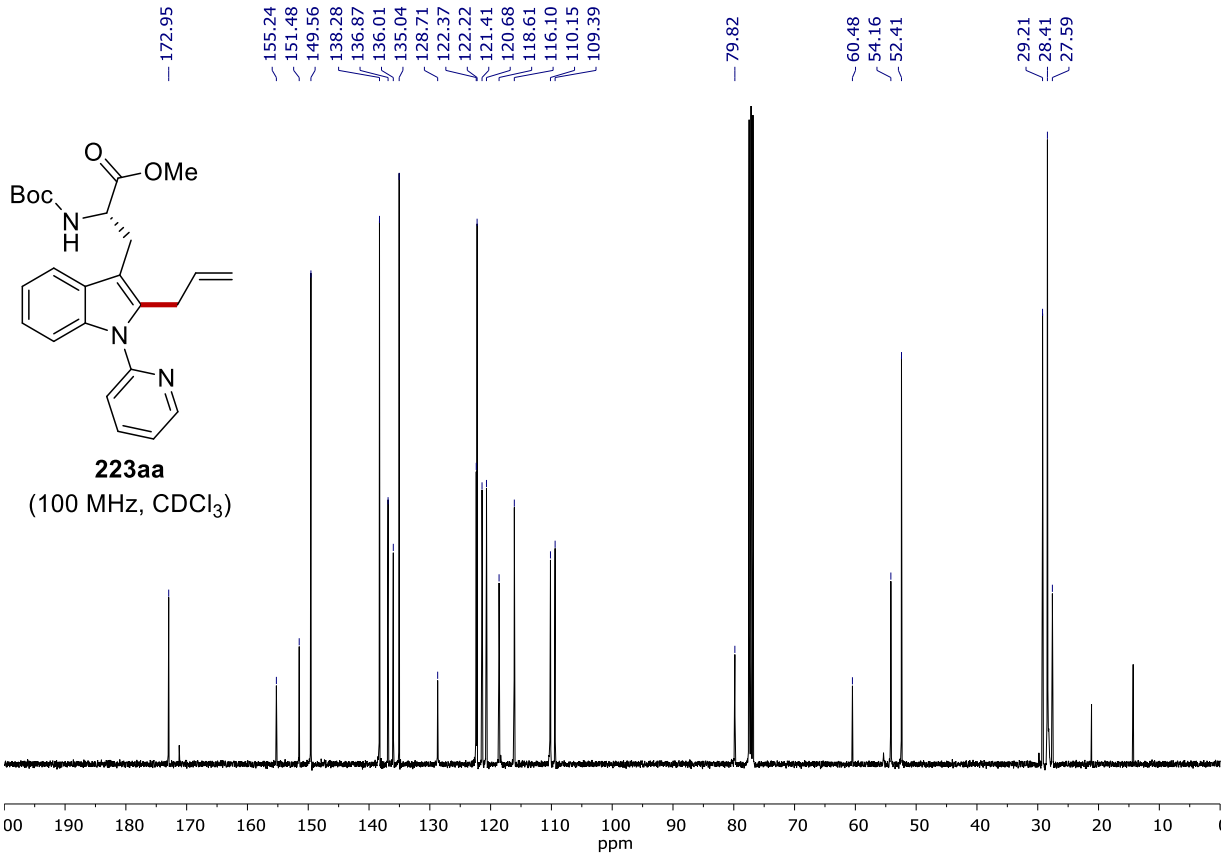

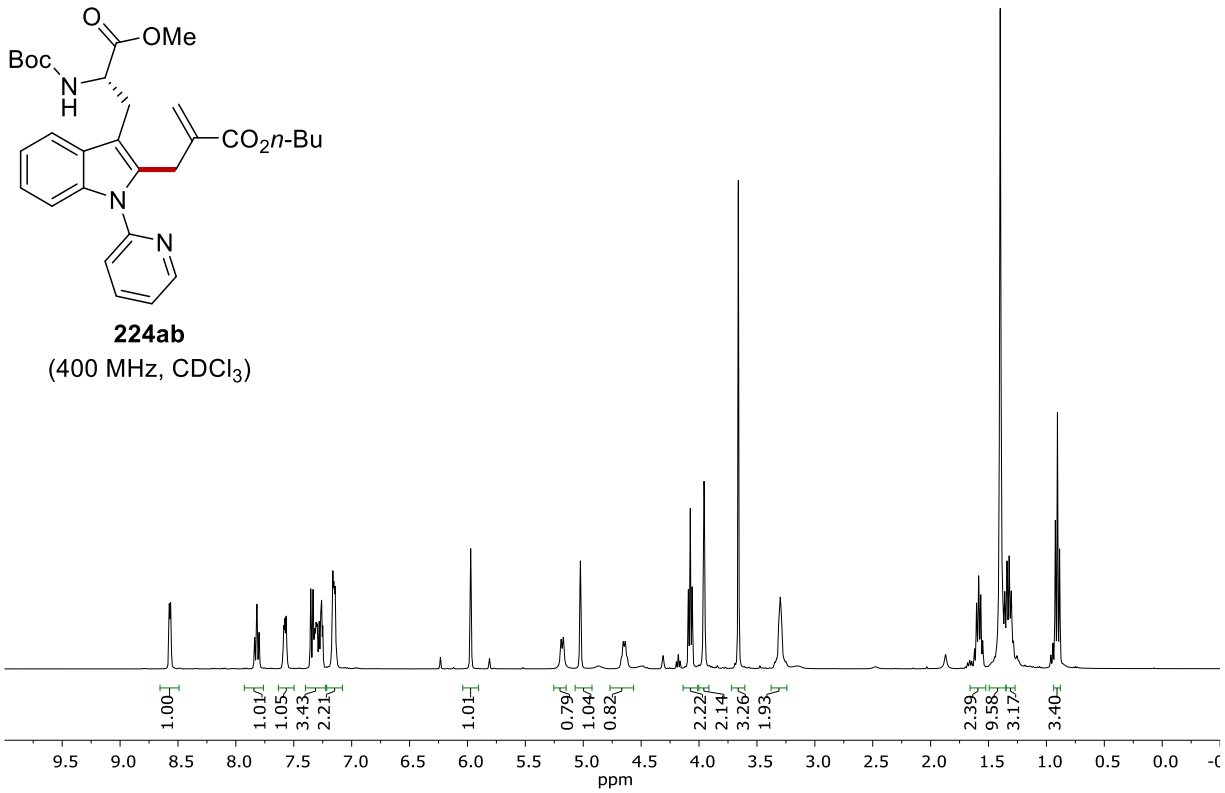
Boc
N
H
O
OMe
CO2n-Bu
N
N
224ab
(400 MHz, CDCl3)
1.00
1.01
1.05
3.43
2.21
1.01
0.79
1.04
0.82
2.22
2.14
3.26
1.93
2.39
9.58
3.17
3.40
9.5 9.0 8.5 8.0 7.5 7.0 6.5 6.0 5.5 5.0 4.5 4.0 3.5 3.0 2.5 2.0 1.5 1.0 0.5 0.0
ppm

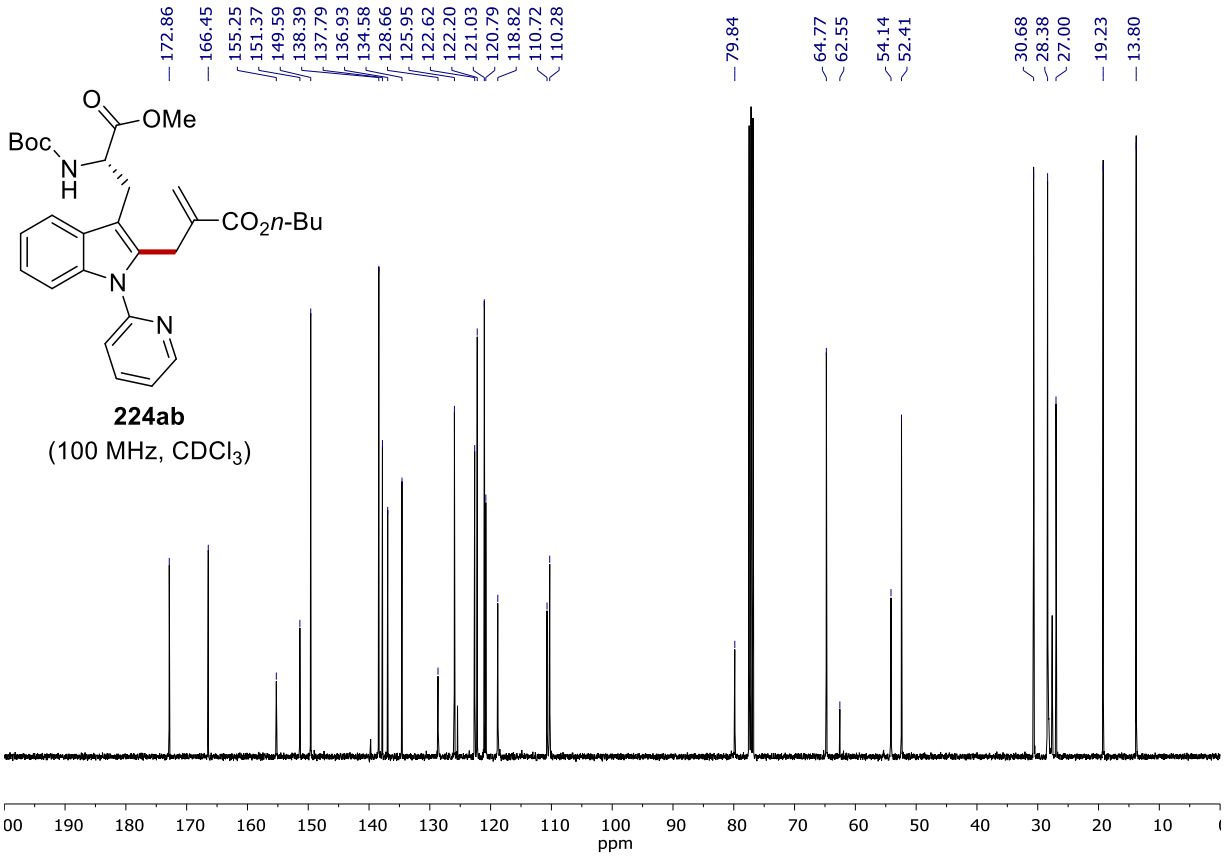
172.86
166.45
155.25
151.37
149.59
138.39
137.79
136.93
134.58
128.66
125.95
122.62
122.20
121.03
120.79
118.82
110.72
110.28
79.84
64.77
62.55
54.14
52.41
30.68
28.38
27.00
19.23
13.80
Boc
N
H
O
OMe
CO2n-Bu
N
N
224ab
(100 MHz, CDCl3)
190 180 170 160 150 140 130 120 110 100 90 80 70 60 50 40 30 20 10
ppm

224ac
(400 MHz, $CDCl_3$)

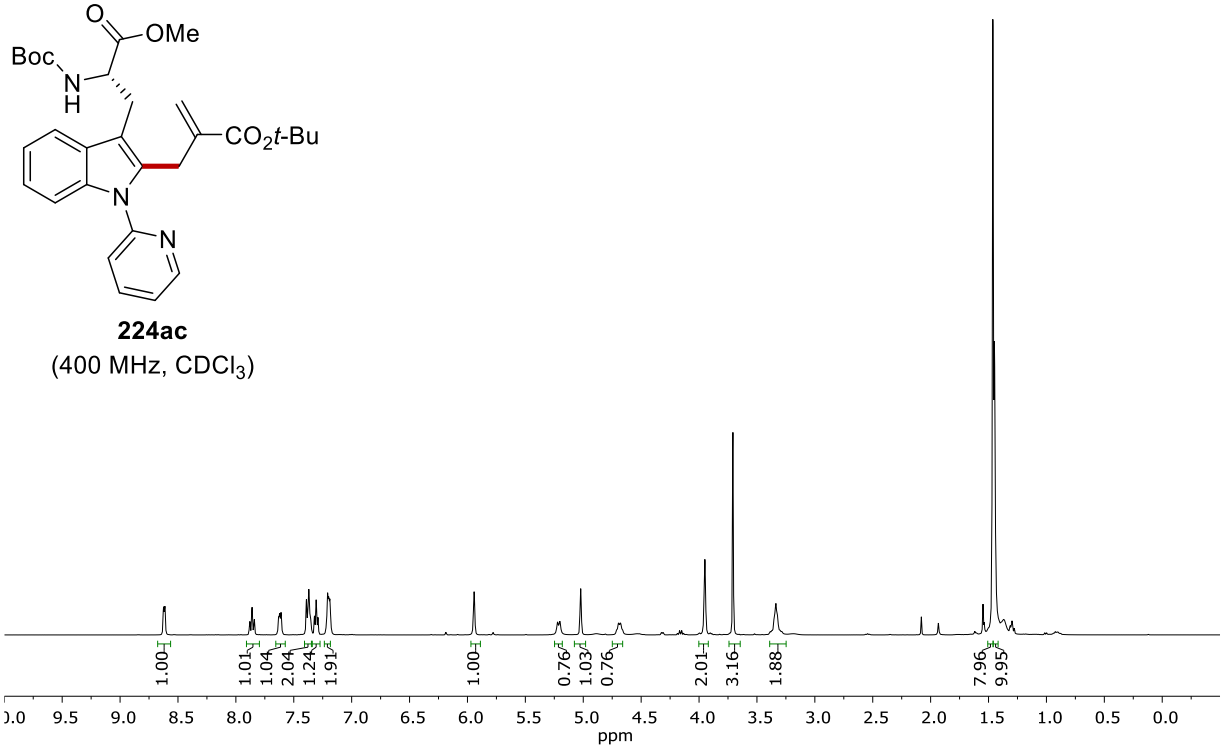

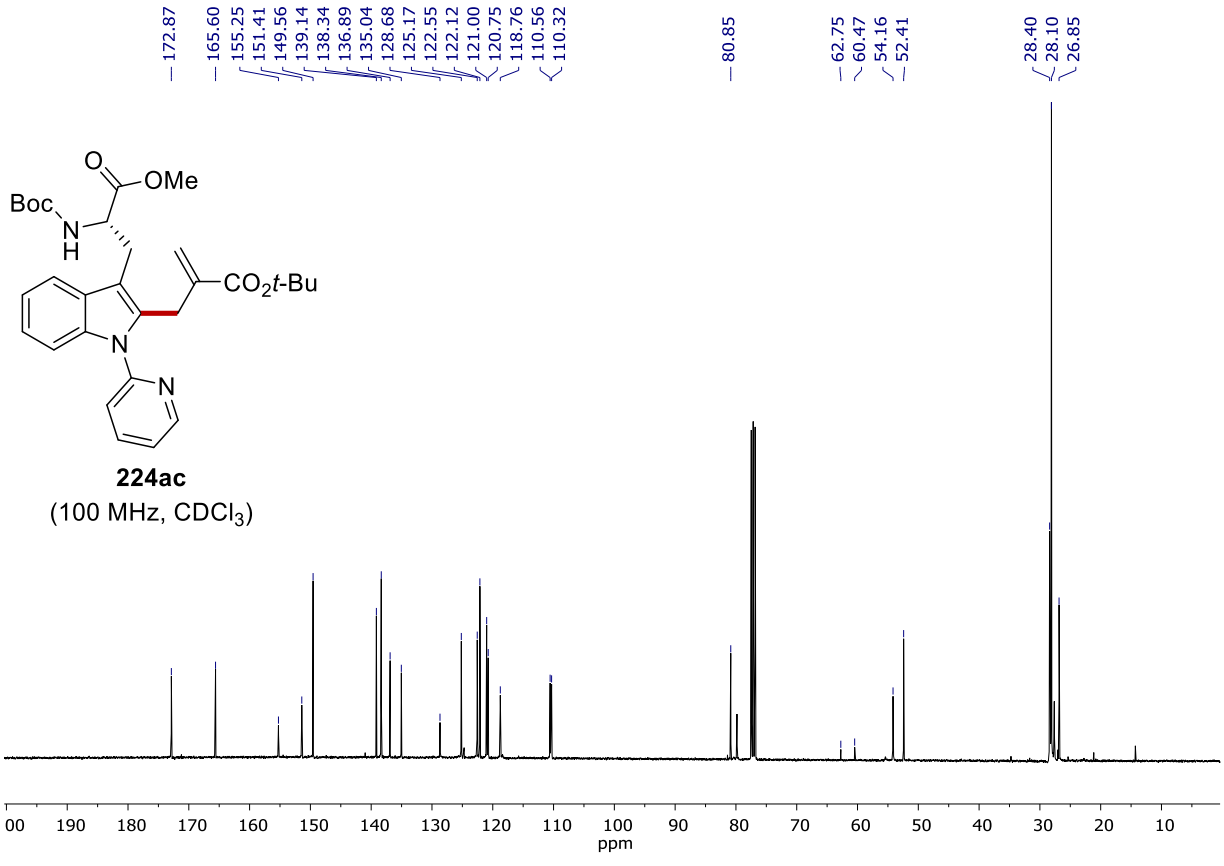

224ac
(100 MHz, $CDCl_3$)

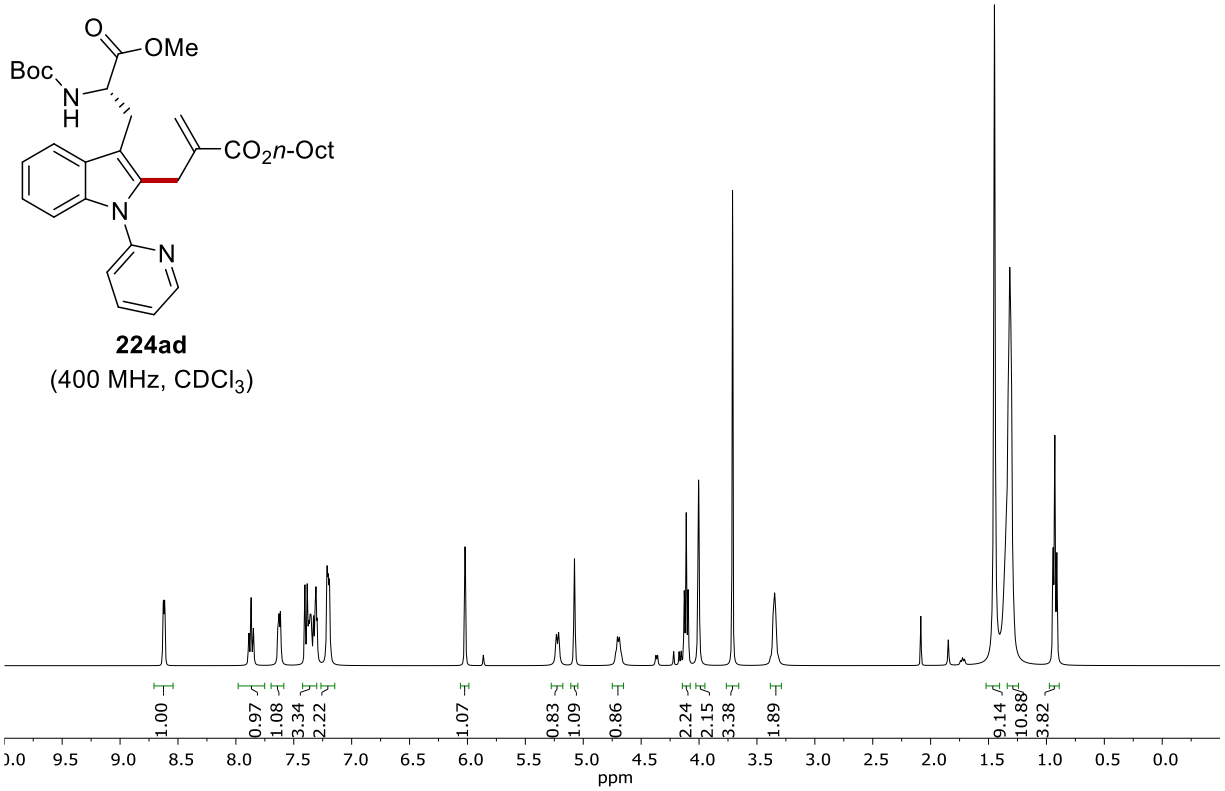

224ad
(400 MHz, $CDCl_3$)

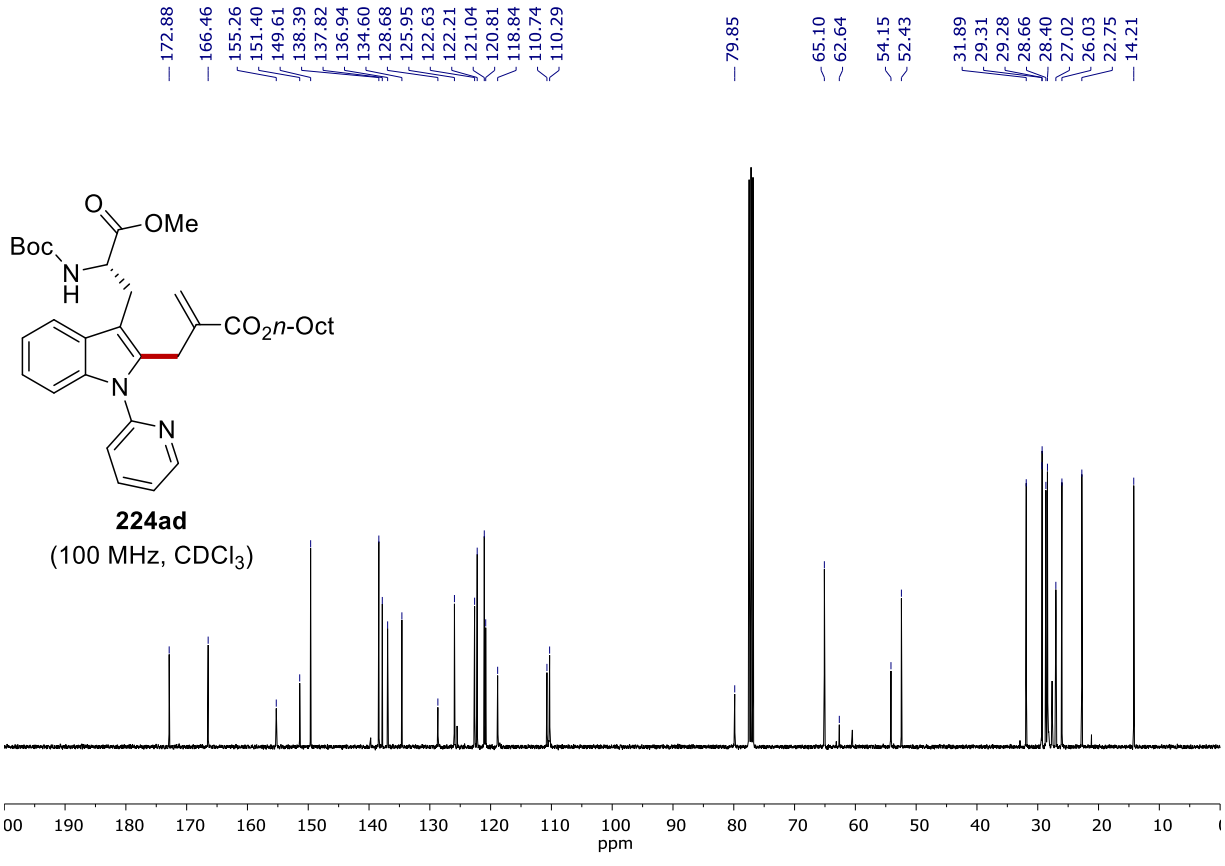

224ad
(100 MHz, $CDCl_3$)

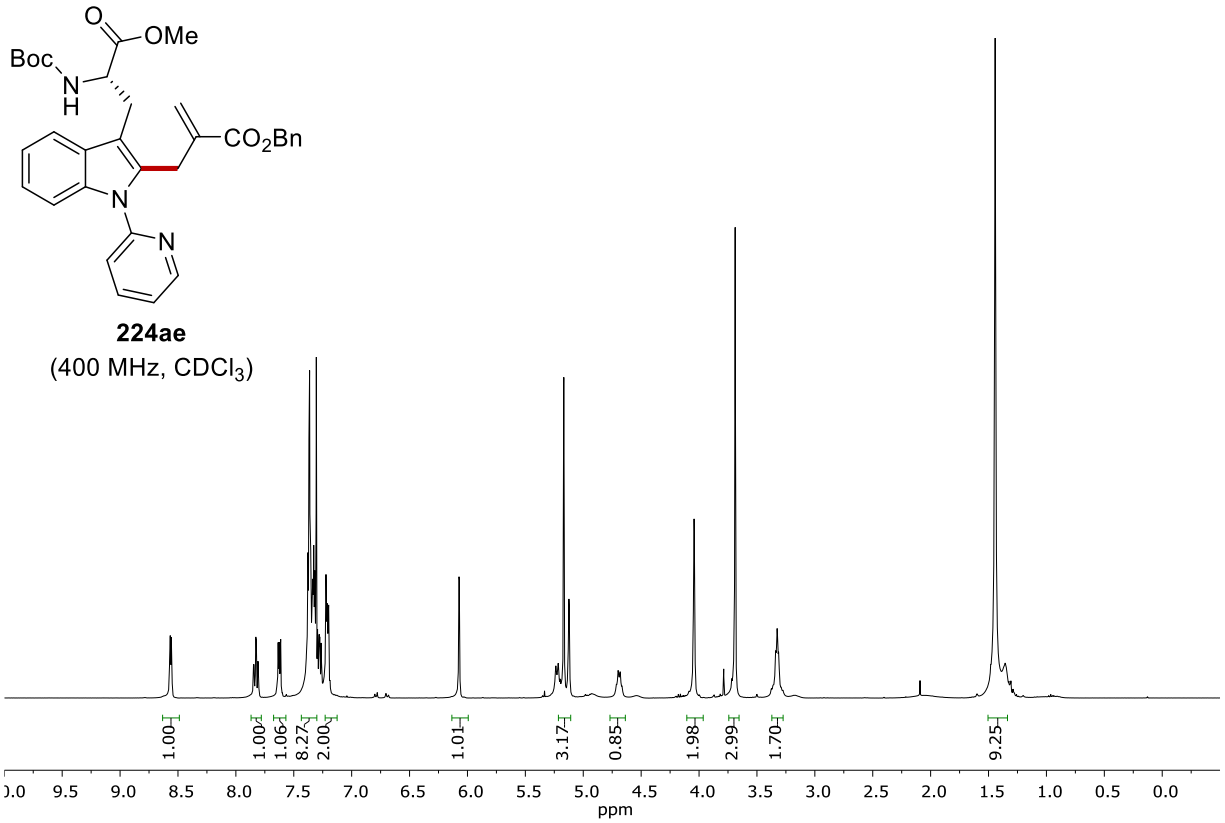

224ae
(400 MHz, $CDCl_3$)

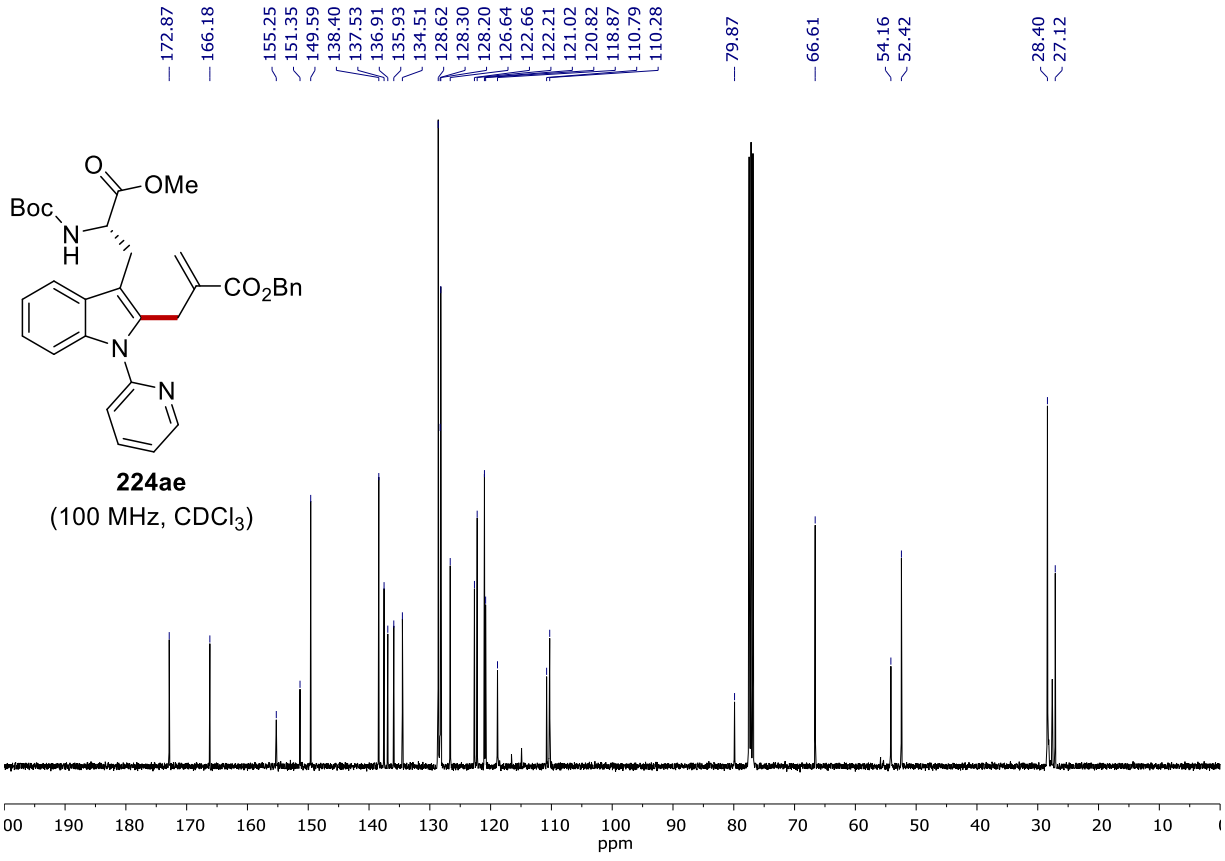

224ae
(100 MHz, $CDCl_3$)

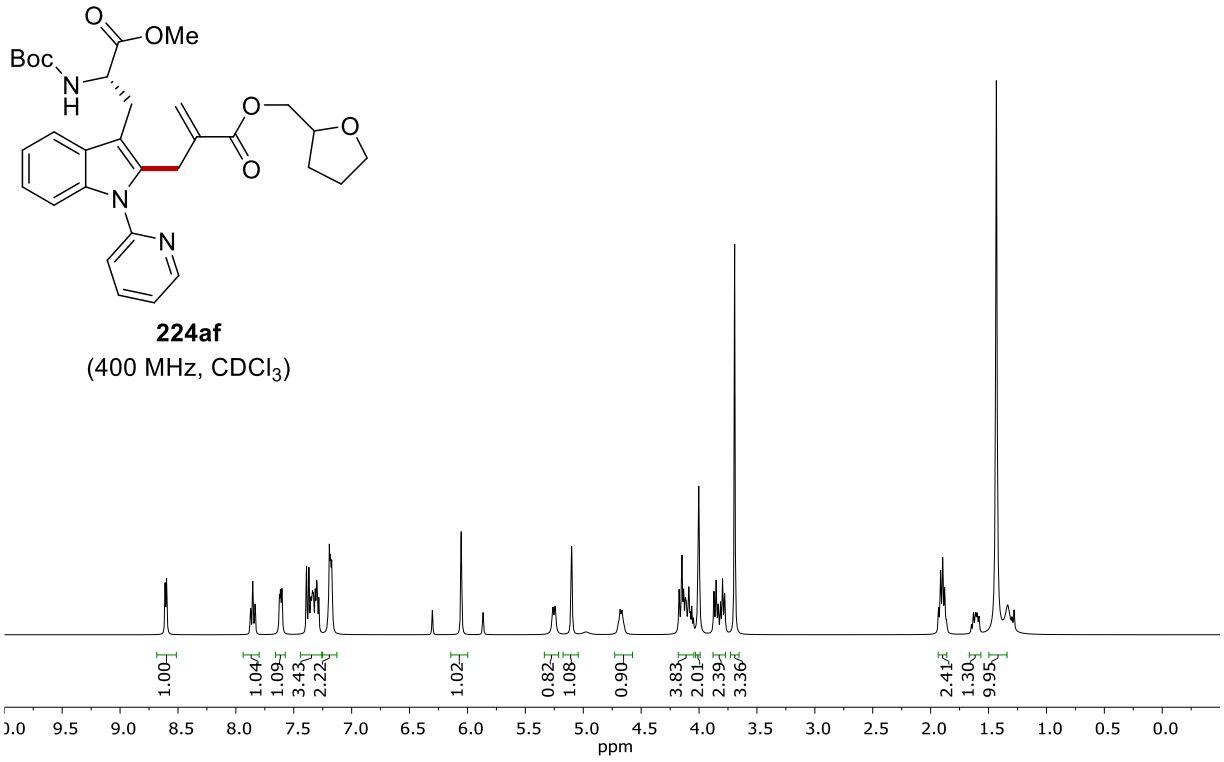

224af
(400 MHz, $CDCl_3$)

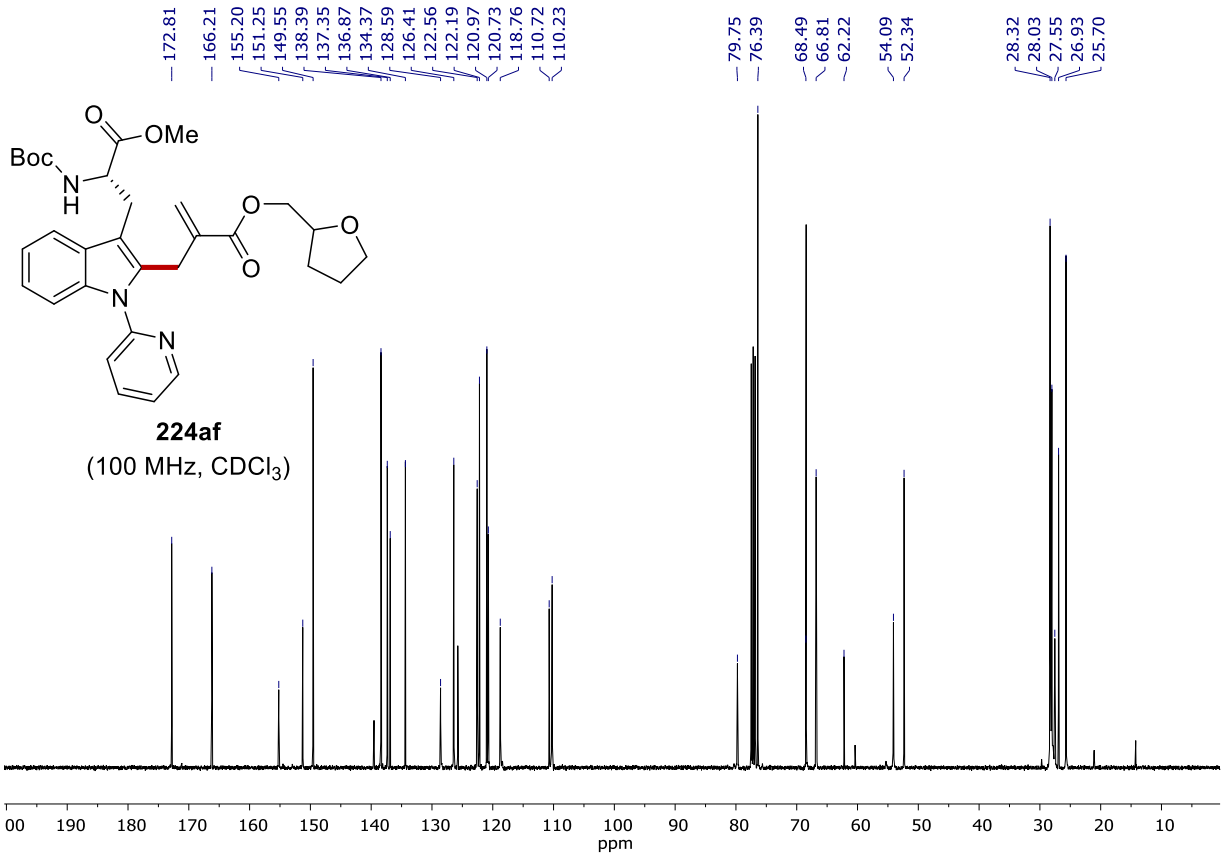

224af
(100 MHz, $CDCl_3$)